IAEA-TECDOC-1861

IAEA TECDOC SERIES

IAEA-TECDOC-1861

Quantitative and Spatial Evaluations of Undiscovered Uranium Resources

IAEA

International Atomic Energy Agency

QUANTITATIVE AND SPATIAL EVALUATIONS OF UNDISCOVERED URANIUM RESOURCES

The following States are Members of the International Atomic Energy Agency:

AFGHANISTAN
ALBANIA
ALGERIA
ANGOLA
ANTIGUA AND BARBUDA
ARGENTINA
ARMENIA
AUSTRALIA
AUSTRIA
AZERBAIJAN
BAHAMAS
BAHRAIN
BANGLADESH
BARBADOS
BELARUS
BELGIUM
BELIZE
BENIN
BOLIVIA, PLURINATIONAL STATE OF
BOSNIA AND HERZEGOVINA
BOTSWANA
BRAZIL
BRUNEI DARUSSALAM
BULGARIA
BURKINA FASO
BURUNDI
CAMBODIA
CAMEROON
CANADA
CENTRAL AFRICAN REPUBLIC
CHAD
CHILE
CHINA
COLOMBIA
CONGO
COSTA RICA
CÔTE D'IVOIRE
CROATIA
CUBA
CYPRUS
CZECH REPUBLIC
DEMOCRATIC REPUBLIC OF THE CONGO
DENMARK
DJIBOUTI
DOMINICA
DOMINICAN REPUBLIC
ECUADOR
EGYPT
EL SALVADOR
ERITREA
ESTONIA
ESWATINI
ETHIOPIA
FIJI
FINLAND
FRANCE
GABON
GEORGIA
GERMANY
GHANA
GREECE
GRENADA
GUATEMALA
GUYANA
HAITI
HOLY SEE
HONDURAS
HUNGARY
ICELAND
INDIA
INDONESIA
IRAN, ISLAMIC REPUBLIC OF
IRAQ
IRELAND
ISRAEL
ITALY
JAMAICA
JAPAN
JORDAN
KAZAKHSTAN
KENYA
KOREA, REPUBLIC OF
KUWAIT
KYRGYZSTAN
LAO PEOPLE'S DEMOCRATIC REPUBLIC
LATVIA
LEBANON
LESOTHO
LIBERIA
LIBYA
LIECHTENSTEIN
LITHUANIA
LUXEMBOURG
MADAGASCAR
MALAWI
MALAYSIA
MALI
MALTA
MARSHALL ISLANDS
MAURITANIA
MAURITIUS
MEXICO
MONACO
MONGOLIA
MONTENEGRO
MOROCCO
MOZAMBIQUE
MYANMAR
NAMIBIA
NEPAL
NETHERLANDS
NEW ZEALAND
NICARAGUA
NIGER
NIGERIA
NORWAY
OMAN
PAKISTAN
PALAU
PANAMA
PAPUA NEW GUINEA
PARAGUAY
PERU
PHILIPPINES
POLAND
PORTUGAL
QATAR
REPUBLIC OF MOLDOVA
ROMANIA
RUSSIAN FEDERATION
RWANDA
SAINT VINCENT AND THE GRENADINES
SAN MARINO
SAUDI ARABIA
SENEGAL
SERBIA
SEYCHELLES
SIERRA LEONE
SINGAPORE
SLOVAKIA
SLOVENIA
SOUTH AFRICA
SPAIN
SRI LANKA
SUDAN
SWEDEN
SWITZERLAND
SYRIAN ARAB REPUBLIC
TAJIKISTAN
THAILAND
THE FORMER YUGOSLAV REPUBLIC OF MACEDONIA
TOGO
TRINIDAD AND TOBAGO
TUNISIA
TURKEY
TURKMENISTAN
UGANDA
UKRAINE
UNITED ARAB EMIRATES
UNITED KINGDOM OF GREAT BRITAIN AND NORTHERN IRELAND
UNITED REPUBLIC OF TANZANIA
UNITED STATES OF AMERICA
URUGUAY
UZBEKISTAN
VANUATU
VENEZUELA, BOLIVARIAN REPUBLIC OF
VIET NAM
YEMEN
ZAMBIA
ZIMBABWE

The Agency's Statute was approved on 23 October 1956 by the Conference on the Statute of the IAEA held at United Nations Headquarters, New York; it entered into force on 29 July 1957. The Headquarters of the Agency are situated in Vienna. Its principal objective is "to accelerate and enlarge the contribution of atomic energy to peace, health and prosperity throughout the world".

IAEA-TECDOC-1861

QUANTITATIVE AND SPATIAL EVALUATIONS OF UNDISCOVERED URANIUM RESOURCES

SELECTED PAPERS
FROM TECHNICAL AND TRAINING MEETINGS
ORGANIZED BY THE IAEA
AND HELD IN FUZHOU (2014), REGINA (2015),
DENVER (2015), VIENNA (2015–2016),
BUENOS AIRES (2016) AND NANCHANG (2017)

INTERNATIONAL ATOMIC ENERGY AGENCY
VIENNA, 2018

Marketing and Sales Unit, Publishing Section
International Atomic Energy Agency
Vienna International Centre
PO Box 100
1400 Vienna, Austria
fax: +43 1 26007 22529
tel.: +43 1 2600 22417
email: sales.publications@iaea.org
www.iaea.org/books

For further information on this publication, please contact:

Nuclear Fuel Cycle and Materials Section
International Atomic Energy Agency
Vienna International Centre
PO Box 100
1400 Vienna, Austria
Email: Official.Mail@iaea.org

Printed by the IAEA in Austria
December 2018

IAEA Library Cataloguing in Publication Data

Names: International Atomic Energy Agency.
Title: Quantitative and spatial evaluations of undiscovered uranium resources / International Atomic Energy Agency.
Description: Vienna : International Atomic Energy Agency, 2018. | Series: IAEA TECDOC series, ISSN 1011–4289 ; no. 1861 | Includes bibliographical references.
Identifiers: IAEAL 18-01211 | ISBN 978–92–0–109518–3 (paperback : alk. paper)
Subjects: LCSH: Uranium ores. | Mines and mineral resources. | Uranium industry. | Geology, Economic.

FOREWORD

An important aspect of IAEA support to Member States is the global assessment of supply and demand relationships for identified and potential uranium resources. Various recent analyses indicate that there is enough supply to satisfy a high demand scenario for several decades. However, initial exploration resulting in discovery and production of new resources often requires similar frames, indicating a current need for a broad understanding of what potential resources remain and where they may be located. Apart from identified uranium resources, very few Member States publish information about additional undiscovered resources, and it is unknown how the data were generated and therefore how internally consistent, reliable and comparable they are. The IAEA has not compiled information on potential additional resources that may exist globally since the International Uranium Resources Evaluation Project (IUREP) during the late 1970s and early 1980s, for which semi-quantitative country scale estimates of potential uranium resources were provided based on subjective expert opinion. Since that time, knowledge of global geology and uranium deposit geology has increased dramatically.

Techniques for analysis of undiscovered resources for mineral commodities have become a robust statistical procedure in the past 20 years but have never been systematically applied to uranium. More recently, new studies integrating spatial assessment techniques and non-spatial quantitative techniques for non-uranium resources offer new opportunities to provide insight into not just how much but also where uranium is potentially yet to be discovered. At the request of Member States, experts have contributed case studies on speculative or undiscovered uranium resource potential in various forums, including technical cooperation activities, Technical Meetings and consultancy meetings held in Member States and at the IAEA's Headquarters in Vienna.

This publication is intended to serve as a record of the work presented by those experts over the period from 2014 to 2016. As the work was updated during that period, the title and authorship of the majority of the papers may vary slightly from the original presentation. Individual contributions have been technically reviewed by other contributing authors to this publication, and the entire volume has been reviewed for technical consistency by E.J.M. Carranza. A detailed technical summary of the project and contributions was provided by V. Lisitsin. Some figures were drafted by J. Wallis.

The IAEA officer responsible for this publication was M. Fairclough of the Division of Nuclear Fuel Cycle and Waste Technology.

CONTENTS

SUMMARY

1. GENERAL

This collection of papers has the common theme of assessing the potential for speculative or undiscovered uranium resources beyond the current supply limits of low cost identified resources. They were presented at several IAEA Meetings over a period of four years. The collection provides a valuable opportunity to record and disseminate information presented at meetings for which insufficient manuscripts are available to justify stand-alone proceedings. As such, an outline of the meeting at which the paper was first presented will be provided, and a summary of the included papers is given. Due to the similar purposes of the meetings, their summaries are aggregated. Papers presented here may vary slightly in title and compared to the corresponding presentation(s), due to the review and editing process, as well as invitations for additional material and papers being requested at some meetings. In the majority of cases the information in the papers has been updated compared to the original presentation, which has also led to some changes of authorship and title.

2. SUMMARY OF MEETINGS

A National Workshop on Uranium Modelling was undertaken in Fuzhou, China, from 3 to 9 November 2014. 16 presentations were given by 5 experts. Respectively hosted by the East China Institute (now University) of Technology. The purpose of the workshop was to assess the current state of techniques in modelling uranium mineral systems in comparison to the recent studies undertaken in China. A. Porwal (India) presented on “A Continent-Wide Uranium Prospectivity Modelling of Australia: GIS Based and Manual Analyses” and on “A Fuzzy Inference System Based Model for Surficial Uranium Prospectivity Modelling of the Yeelirrie Area, Western Australia”. The former presentation outlined one of the first known contemporary studies of Geographic Information Systems (GIS) analysis for uranium, particularly at a large continental scale. The later presentation presented a more detailed study using a wider range of GIS techniques for a particular style of surficial uranium deposit. S. Jaireth (Australia) presented an “Introduction to Uranium Mineral Systems” and on a “National Scale Mineral Potential Assessment of Calcite-Uranium Deposits”. The first presentation outlined an enhanced approach to the inputs to GIS modelling, as applied in the second presentation. J. Royer (France) gave a presentation on “Log Normal Distribution of Uranium Deposits in France” Experts and participants agreed at the meeting that there was some interest in pursuing the idea of national scale assessments of potential or undiscovered uranium resources.

A Consultancy Meeting on “Mineral Economics and Exploration for Uranium” was held in Regina, Canada, on 18–21 May 2015, hosted by the Geological Survey of Saskatchewan. The purpose of this meeting was to assess the impact of the then-current significant downturn in the uranium production cycle industry and in particular managing the effects of decreased exploration on future supply beyond currently identified resources. A. Wilde demonstrated an example of the current situation while speaking on “Impediments to Discovery: Lessons Learned from Exploration in Africa”. Presentations by R. Schodde (Australia) on “Long Term Discovery Performance of The World Uranium Exploration Industry: 1950-2014” and “Outlook for Uranium Exploration and Discoveries: Possible Scenarios: 2015-2060” indicated a lack for future uranium supply in the future due to the historically low discovery rates and long lead in times from exploration through to discover and production. These conclusions were further supported by a presentation showing the company perspective from J. Marlatt (Canada) concerning “Forty-Years, One Discovery: A Uranium Exploration Geologist’s View of the Impact of Industry Cycles on Discovery Rate” and a potential solution to the problem in a subsequent presentation on “Is there a Future for Mathematical Geology: Reflections on the Potential to Improve Uranium Deposit Discovery Rates through Quantitative and Semi-Quantitative Mineral Potential Assessments”. Examples of such assessments were given by O. Kreuzer (Australia) when presenting on “Surficial Uranium Systems in Western Australia: Prospective Tracts and Undiscovered Endowment”. It was agreed at this meeting that a need was identified to develop tools and case studies for undiscovered uranium resources at an international scale, and in particular from both a spatial and quantitative viewpoint to assist Member States in addressing the questions of ‘where’ and ‘how much’.

The ideas presented at the above meeting in Regina were acted upon at a Consultancy Meeting on Methods of Spatial and Quantitative Uranium Resource Assessments in Denver, United States of America, from 6 to 10 July 2015. The meeting was hosted by the United States Geological Survey (USGS), which had developed robust tools for the assessment of undiscovered future resources of copper, gold and other commodities, with a recent interest in modifying such techniques for applications in uranium resources, particularly for supplying undiscovered resource assessments for the joint OECD-NEA/IAEA Uranium: Resources, Production and Demand (Red Book) publication. The USGS indicated that the biggest hurdle to implementing such studies outside of the USA was the lack of internally consistent datasets. IAEA presentations showed that significant progress had been made on the IAEA Uranium Deposit Database (UDEPO) and the related deposit classification scheme, which when published would provide a framework for future assessments. S. Jaireth (Australia) provided some insights into the range of possible approaches that can be used when data is available while speaking on “Methods of Mineral Potential Assessment: A Review with Geological Emphasis”. J. Carranza (Philippines) provided a detailed example of one of these techniques by presenting “Geospatial-Based Assessment Methods 1 Level and integration”. D. Singer (United States of America) provided a preliminary case study using USGS techniqueds entitled “A Three-Part Assessment of Undiscovered Uranium Deposits in the Pine Creek Region, Australia”. The meeting concluded with agreements from several participants to provide case studies for publication, while IAEA worked in parallel to enhance its current databases to make them amenable for future use by Member States wishing to embark on similar country-scale studies. USGS participants further indicated that a longer-term plan should include additional economic follow up studies and some attention paid to mapping existing resource classification to the derived estimates.

A Technical Meeting on Spatial and Quantitative Uranium Resource Assessments was held in Vienna, on 9-11 November 2015. The purpose of these meetings was to show the current state of the propose case studies to be published, as well as solicit additional contributions from participating Member States. Presentations by D. Singer on “Introduction to Quantitative Mineral Resource Assessments” and A. Porwal on “Spatial Mineral Potential Modelling Methods: An Overview” provided outlines of the possible techniques that could be used by participants. Both presenters also outline application case studies when presenting “A Three-part Assessment of Undiscovered Uranium in The Pine Creek Region, Australia” and “Quantitative Assessments of Calcrete-Hosted Surficial Uranium Systems in Western Australia” respectively. Advances in available preliminary data from IAEA were shown by S. Thakur (“Grade-Tonnage Modeling of Global Uranium Deposits”) and applied by B. Chudasama (“Genetic Modelling and Prospectivity Mapping of Calcrete-Hosted Surficial Uranium Systems in Western Australia”). Additional contributions for future publication were provided by F. Bierlein by presenting “GIS-based Fuzzy Logic Mineral Prospectivity Analysis of Sandstone-hosted Uranium Deposits”, A. Wilde: “Mt Isa Uranium Prospectivity” and by C. Bello and L. Lopez for “Uranium Potential Assessment of Argentina Using Quantitative and Qualitative Approaches”. It was agreed at the meeting that there were sufficient proposed contributions to plan an IAEA publication entitled Quantitative and Spatial Evaluations of Undiscovered Uranium Resources.

Additional contributions were received by V. Lisitsin (Australia) in a meeting of authors during the Consultancy Meeting on Consultancy Meeting to Prepare a Report on Undiscovered Uranium Resource Calculations Vienna, Austria, on 20 June–24 June 2016, concerning a summary of all papers as well as providing additional data to other papers.

A Meeting and Consultancy on Evaluation of Undiscovered Uranium Resources was held in Buenos Aires, Argentina, 24–28 October 2016. The purpose of this meeting was to provide a first test of the submitted manuscripts as potential training material for Member States. In particular, an extended training exercise was presented by M. Bruce on “Frome Embayment: Fuzzy Logic Practical Exercise” with additional supporting material given during presentations by D. Singer (“Overview of Quantitative Assessments of Undiscovered Resources” and “How to Estimate Numbers of Deposits”), S. Jaireth (“Mineral System Approach, Critical Features”) and J. Carranza (” Fuzzy and Evidential Belief Modeling of Mineral Potential”). The training workshop indicated that a good range of techniques and case studies had been gathered and that the proposed publication would indeed provide a valuable platform for other Member States to embark on their own uranium modelling projects.

A final meeting was held in Nanchang, China, in December 2017, hosted by the East China University of Technology (ECUT) to demonstrate the progress made since the first workshop in the nearby Fuzhou campus of UCUT during 2014. The workshop was given by A. Porwal and J. Carranza using only previously presented material from the project. Once again, the future plan of advancing the assessment techniques to include economic parameters was discussed.

SELECTED PAPERS

ASSESSING UNDISCOVERED URANIUM RESOURCES – OVERVIEW OF THE CURRENT STATUS AND PROJECT SUMMARY

V. LISITSIN
Geological Survey of Queensland,
Brisbane, QLD, Australia

1. INTRODUCTION

The total identified uranium resources of the world, potentially economic at the current uranium prices, are technically sufficient to satisfy at least the projected cumulative global demand for uranium over the next 20-30 years [1]. However, various geopolitical, socio-economic and technological factors could prevent the economic development of a significant proportion of these identified resources. Security of long-term uranium supply could thus also require timely discoveries of significant new economic resources. As most of the known well-endowed uranium provinces in the world are reaching exploration maturity, the discovery rates of major uranium deposits comparable to those currently dominating the global uranium supply have significantly decreased, despite escalating exploration costs [2]. Adequate assessments of likely locations and grade and tonnage properties of undiscovered uranium deposits are warranted, both to inform decision makers on the availability and possible geographic distribution of future uranium supply and to assist the exploration industry in initial area selection. Such information is not generally available, and standard universally accepted procedures currently do not exist for consistent assessment of undiscovered uranium endowment at a province or global scale.

This volume aims to assist readers in addressing this information gap. The volume contains a collection of 12 individual contributions. It provides a broad overview of identified global uranium endowment, investigates aspects of global uranium supply and demand dynamics and exploration strategies, and illustrates methods that could be used to assess uranium resource potential of mineral districts, provinces and continents. Methods of assessment of undiscovered mineral resources are a particular focus of this volume.

The contributions in this volume involve the following:

1) An overview of the uranium exploration business and its historical trends and analysis of exploration strategies to ensure uninterrupted long-term supply of uranium to the global markets [2];
2) Case studies of modeling the prospectivity for certain types of uranium deposits [3, 4];
3) Case studies of modeling the distribution of grades and tonnages of uranium deposits [5-7];
4) A review [8] and case studies of quantitative methods for assessment of undiscovered uranium resources [9, 10];
5) Case studies of linking the modeling of prospectivity for certain types of uranium deposits to the quantitative assessment of undiscovered uranium resources [11, 12, 13].

The methods of prospectivity modelling and quantitative assessment of undiscovered mineral endowment illustrated by the case studies (including the first published quantitative assessment of undiscovered uranium resources in parts of Australia) can be readily applied, following appropriate modifications, to other regions and deposit types. Four case studies focus on prospectivity of large regions in Australia for various uranium deposit types: sandstone-hosted

U deposits in Australia [4], unconformity-related uranium deposits in Northern Territory [9], albitite sub-type of metasomatic U deposits in Queensland [11] and calcrete-hosted U deposits in Western Australia [12]. Carranza [3] discusses prospectivity of British Columbia (Canada) for surficial U deposits, and Royer and Cuney [6] describe a statistical assessment of undiscovered granite-related uranium deposits in Europe.

2. SUMMARY OF SELECTED INDIVIDUAL CONTRIBUTIONS

2.1. Long-term trends and outlook for uranium exploration: are we finding enough uranium? (R. Schodde) [2]

This contribution [2] attempts, by assessing of the long-term trends in discovery performance of the world's uranium industry from 1945 to 2016, to answer the key question: is the industry finding enough new metal to meet its future needs? The analysis shows that there is a strong correlation between the rate of discovery and exploration expenditures, and between expenditures and the uranium price (lagged by one year). The analysis also shows that, at the current level of exploration activity, the effective discovery rate of mineable metal is estimated to be around 29 kt U per annum. Considering these findings vis-à-vis the IAEA's Low / High Case forecast for uranium demand of 67 / 105 kt U by 2035, this contribution argues that there is insufficient uranium reserve to replace current mine production or to meet any future growth in demand and that the industry will face a major shortage of new projects to develop. Therefore, this contribution recommends that, given the very long lead time between discovery and development, government and industry need to develop new strategies now to increase and make exploration more efficient; otherwise, the industry faces a real risk of uranium supply disruption in the longer term.

2.2. The business of exploration: discovering the next generation of economic uranium deposits (J. Marlatt) [3]

This contribution [3] provides a comprehensive analysis of the uranium exploration process and factors likely to affect the discovery and development of new uranium deposits. The analysis highlights a strongly non-linear nature of uranium exploration and mine development, affected by various technological and socio-economic factors. Examples from Australia and Canada, countries with the largest reasonably assured uranium resources in the world, illustrate that larger uranium deposits are commonly discovered at relatively early stages of an exploration cycle. The majority of discovered deposits do not progress to mine development or cease operation, rendered uneconomic by their geological characteristics or precluded from development for social and political reasons. As the near-surface 'search space' in a province reaches exploration maturity, new significant discoveries are made at increasing depths and often require major innovative developments of exploration technology. This contribution concludes that the next generation of new economic discoveries would rely on effective collaborations between geological surveys, industry and applied academic researchers. Major discoveries would result from successful applications of innovative exploration techniques in prospective areas identified through quantitative and qualitative economic mineral potential assessments.

2.3. Regional-scale prospectivity mapping for surficial uranium deposits in Southern British Columbia, Canada (E.J.M. Carranza) [4]

This contribution [4] illustrates knowledge-driven fuzzy logic prospectivity modeling at a province scale using the mineral system approach. The study tested various spatial proxies for conceptual critical processes of the surficial uranium mineral system in British Columbia and several data aggregation models. A non-linear weighted function of proximity to felsic igneous rocks enriched in uranium was used as a proxy for uranium source, proximity to paleo-channels – as a proxy for fluid transport and uranium content in surface waters – as a proxy for chemical trapping. Prospectivity maps generated by combining the proxy maps for uranium source, transport and trapping using the fuzzy AND operator captured more than 80% of the known uranium occurrences in less than 10% of the total study area with the highest prospectivity rankings. This case study illustrates that using spatial distribution of known uranium deposits and occurrences for validation of both the conceptually defined spatial proxies and final prospectivity maps can identify the most appropriate spatial proxies and data aggregation models to minimize bias of prospectivity maps.

2.4. A continent-scale gis-based assessment of the distribution and potential for sandstone-hosted uranium deposits (F.P. Bierlein, M.D. Bruce) [5]

This contribution [5] describes the process and results of fuzzy logic mineral prospectivity modeling of sandstone-hosted uranium deposits in Australia. The study illustrates a simple GIS-based implementation of knowledge-driven prospectivity mapping using publically available regional-scale datasets. Complex theoretical and empirical considerations of the uranium geochemistry in sedimentary environments are first systematically compiled and simplified using the conceptual mineral system framework. This is done to identify the major first-order controls on the formation and preservation of sandstone-hosted uranium deposits evidence of which could be extracted as mappable criteria from readily available regional datasets.

This contribution describes modifications and re-classification of the relevant datasets to extract mappable targeting criteria relevant at the continental scale of analysis. Expert judgment has been used to define relative weights of the input evidential maps and design of an inference system, with the intent of replicating the current understanding of the operation of the sandstone-hosted uranium mineral system at the continental scale. Prospective regions delineated by GIS outputs of the study highlighted the known uranium provinces but also identified other regions which could be prospective despite a lack of known sandstone-hosted uranium mineralization. The first-pass regional modeling outputs could be used for more detailed province-scale analysis and ground selection for reconnaissance exploration. Modeling results strongly depend on expert knowledge and rely on consistency and quality of the regional datasets used in modeling. Both of these critical factors are common for any knowledge-driven GIS prospectivity modeling.

This contribution suggests that prospectivity modeling results can provide a framework for the consistent definition of permissive tracts that have a potential to host sandstone-hosted uranium deposits. Permissive tracts defined based on prospectivity modeling outputs could be used as an input into a quantitative mineral resource assessment. The general approach and specific procedures discussed in this contribution can be used for a comparable continental scale prospectivity analysis elsewhere in the world.

2.5. Are world uranium resources lognormal distributed? (J.J. Royer) [6]

This contribution [6] discusses the process and results of a statistical analysis of uranium grade and tonnage data contained in the IAEA database of uranium deposits. He concludes that grades and tonnages of uranium deposits are characterized by a log-normal distribution, both for individual uranium deposit types and for the total set of uranium deposits. This conclusion is consistent with similar observations for grade and tonnage models for various other commodities and deposit types, including results of [8] for global uranium deposits which are also discussed in this volume.

2.6. Statistical distribution of the uranium resources in the variscan hydrothermal uranium deposits of Western Europe (J.J. Royer, M. Cuney) [7]

This contribution presents a statistical analysis of uranium originally contained in known granite-related uranium deposits in five European countries (Spain, Germany, Czech Republic, France and Bulgaria) and the fitted statistical models were used to assess undiscovered uranium endowment [7]. They concluded that frequency distributions of deposits' contained uranium in each individual country and Europe overall fit log-uniform distributions. The fitted log-uniform distributions were used to quantify undiscovered uranium endowment for each country. Statistical estimates of the total undiscovered uranium endowment of Europe strongly depend on the estimation procedure (such as including or excluding statistical outliers) and vary from <15,000 t U to >150,000 t U. Results are especially strongly influenced by a decision on whether to use a single log-uniform distribution fitted to all known deposits in Europe, or to estimate endowment of each individual country and then calculate the total for Europe by summation of the individual country estimates (e.g., excluding outliers, 14750 t U and 89800 t U, respectively). The log-uniform distributions fitted to empirical frequency distributions of known deposits are only adequate approximations of corresponding log-normal distributions – possibly better corresponding to the underlying distribution of contained uranium in all uranium deposits in Europe. Notably, many known deposits have only been evaluated to reasonably shallow depths, while others (in eastern Europe) were mined to much deeper levels. Such inconsistent definitions of deposit endowments could significantly affect statistical properties of uranium content of known deposits – and corresponding prediction results.

2.7. Global grade and tonnage modeling of uranium deposits (S. Thakur, B. Chudasama, A. Porwal) [8]

This contribution reviews the IAEA database of global uranium deposits (UDEPO) and analyzed goodness of fit of grade and tonnage distributions for uranium deposits grouped by deposit type to lognormal distributions [8]. For sandstone-hosted uranium deposits, analysis was also performed for individual sub-types (roll-front, tabular, basal channel and tectonic lithologic) and country (USA, Kazakhstan, Uzbekistan and Niger). This contribution concludes that for most uranium deposit types and sub-types both grade and tonnage distributions do not significantly deviate from log-normality. Results indicate that the global grade and tonnage distributions of the tectonic lithologic sub-type are significantly different from those of the other sub-types of sandstone-hosted deposits. Also, roll-front uranium deposits in Kazakhstan and Uzbekistan are shown to generally have much larger tonnages but significantly lower grades than roll-front deposits in USA.

2.8. Quantitative methods of assessment of undiscovered uranium resources: A review (S. Jaireth) [9]

This contribution presents a comprehensive overview of the historic and modern methods for assessing undiscovered mineral resources in general, with a particular focus on uranium resources [9]. It includes an extensive list of relevant references, making it a convenient starting point for the readers to further explore the history and the current state of play in delineating and ranking prospective areas and quantitative assessment of undiscovered mineral resources.

The paper highlights limitations of the existing methods and proposes recommendations for key focus areas further developments of which could help to significantly improve effectiveness of quantitative mineral resource assessments in the future. The practical recommendations for improvements are: (1) the mineral system approach can improve practical usability of traditional mineral deposit models in geologically permissive and prospective areas, particularly at more regional district to province scales of analysis; (2) grade and tonnage models are critical for quantitative mineral resource assessments (QMRA) and developing robust global and province models for different uranium deposit styles is essential; (3) spatial deposit density models can greatly assist in estimating the number of undiscovered deposits and such models need to be developed for uranium deposits; and (4) consistent principles for delineation of permissive tracts at different scales need to be developed.

2.9. A three-part quantitative assessment of undiscovered unconformity-related uranium deposits in the Pine Creek Region of Australia (D.A. Singer, S. Jaireth, I. Roche) [10]

This contribution [10] illustrates a practical application of the versatile and widely used 3-part quantitative assessment approach [14] to uranium resources. It presents an updated global descriptive model of unconformity-related uranium±gold-PGE deposits (which could be used to delineate permissive tracts in other parts of the world where such deposits might exist) and a corresponding grade and tonnage model for deposits in the Pine Creek region (Northern Territory, Australia). A probabilistic estimate of the number of undiscovered deposits was produced using the global regression deposit density model [15]. This method is based on strong empirical evidence that the size of a permissive tract and the median ore tonnage for a corresponding grade and tonnage model are very good predictors of the total number of deposits within the tract. The study estimates that in the Pine Creek region there is a 90% chance of at least 9 and 50% chance of at least 25 undiscovered unconformity-related uranium deposits. The expected (mean) estimate of the total uranium contained in the undiscovered deposits is 0.8 Mt, with a 50% chance of at least 0.5 Mt.

2.10. Undiscovered uranium resource assessment of Argentina (C. Bello, L. López, P. Ferreyra) [11]

This paper [11] discusses the process and results of quantitative assessment of undiscovered uranium endowment in five regions in Argentina: Salta Group Basin, Pampean Ranges, Paganzo Basin, San Rafael Basin and Chubut Group Basin. The assessment followed a method of weighted geological analogy, which has been previously used for assessing undiscovered uranium endowment since the 1980-s [16, 17, 18, 19]. In this method, an assessment region is first subdivided into a series of areas classified as favourable, unfavorable or uncertain for a particular uranium deposit type. Then, a well explored control area is defined, preferably within the assessment region, which contains known uranium deposits of the type under consideration with identified grades and tonnages. The control area is used as an analogue for assessing undiscovered uranium endowment in the favourable areas within the assessment region, weighted by estimated geological similarity between the control and favourable areas and a ratio of their sizes. The subdivision, classification and definition of weighting parameters are done subjectively by an expert team, taking into account all the available geological information.

The assessment process was briefly illustrated by a description of an assessment for the San Rafael Basin. 60% of the total area of the Basin was classified as unfavorable and excluded from the assessment. The remaining area of 2,739 km^2 classified as favourable for volcanic-related uranium deposits was subdivided into 12 favourable areas with varying degrees of geological prospectivity. For each of the 12 favourable areas, the assessment team quantitatively estimated undiscovered uranium endowment at the cut-off grades of 0.01% U and 0.05% U on the basis of their deemed metallogenic similarity with the selected control area in the Rafael Basin (131 km^2) containing 12 known uranium deposits with identified ore grades and ore tonnages. The total undiscovered uranium endowment of the Rafael Basin was calculated by adding up the estimates for the individual favourable areas. The total undiscovered endowment was thus estimated as 7204 t U (a median estimate, within a range between 3010 and 80393 t U) at the 0.01% U cut-off grade and 3020 t U (median, within a range between 1367 and 61898 t U) at the 0.05% U cut-off grade. This compares with the total combined identified resources of 15973 t contained U estimated, at an average cut-off grade of 0.03% U, for the 12 known deposits in the control area.

The combined estimates of undiscovered uranium endowment contained within favourable areas delineated in the Salta Group, Paganzo, San Rafael and Chubut Group basins and Pampean Ranges are 246800 t U at the 0.01% U cut-off grade and 56100 t U at the 0.05% U cut-off grade. These estimates exceed the total identified uranium endowment within the control areas, re-calculated to the same cut-off grades, by a factor of 7.6 and 2.4, respectively.

2.11. Fuzzy logic mineral prospectivity analysis of the Mount Isa Region (Queensland, Australia) for metasomatite-type (albitite-type) uranium (A.R. Wilde, M. Bruce, C. Knox-Robinson, F.P. Bierlein, V. Lisitsin) [12]

This contribution [12] discusses the process and results of prospectivity modeling and quantitative assessment of undiscovered uranium endowment of albitite-type metasomatic uranium deposits in the Mt Isa North region (north-west Queensland, Australia). The contribution presents a compilation of the latest estimates of all identified uranium resources in the region and a conceptual mineral system model for albitite-type uranium deposits. Based on the conceptual model, two different implementations of fuzzy logic GIS prospectivity modeling were used to delineate and rank prospective areas. One model was limited to the central district containing all the known uranium deposits with identified mineral resources and almost all documented albitite-type uranium occurrences, while the other covered a larger region. Both models produced generally similar prospectivity maps for the central district, successfully capturing all six largest and three smaller known deposits in the 10% of the area with the highest prospectivity scores, thus suggesting significant predictive power of the models.

This contribution also presents results of the first quantitative assessment of undiscovered uranium endowment in this region. Two independent statistical models were used for the purpose – a rank-size statistical model (based on 'Zipf's law') and a global regression spatial deposit and endowment density model [15]. Both models rely on a grade and tonnage model for known uranium deposits in the region. In particular, the rank-size statistical model strongly depends on an estimate of total contained uranium in the largest known deposit, while the regression model uses the medium ore tonnage as one of two major inputs. While compilation of identified uranium resources presented in this contribution can be used directly in both models, there is uncertainty of interpretation whether some adjacent known deposits represent parts of the same larger deposits – in which case their endowments should be aggregated. The study investigates effects of this uncertainty on quantitative results.

The rank-size model using resource estimates for the individual deposits suggests that the region's total undiscovered uranium endowment contained in significant deposits (each containing >1,500 t U) is 49,000 t U, while the model based on spatially aggregated resource estimates predicts 80,000 t U. These estimates are comparable with the total identified uranium resources of 59,000 t U. The global regression model of Singer and Kouda (2011) [15] probabilistically estimates total ore tonnage in a permissive tract based on its size and the median ore tonnage of a deposit type under consideration. The permissive tract was delineated on the basis of the regional fuzzy logic prospectivity map, generalizing an outline of the area above the 5% relative favorability cut-off. Using the spatially aggregated grade and tonnage model, the entire permissive tract is estimated to contain approximately 132 Mt of undiscovered ore tonnage (mean), with a 90% probability of at least 20 Mt of ore. The estimates based on the original model of individual deposits are the mean of 83 Mt, with a 90% probability of at least 13 Mt of ore. These estimates are generally comparable with the total identified ore tonnage of 106 Mt.

2.12. Surficial uranium systems in Western Australia: prospective tracts and undiscovered endowment (B. Chudasama, O.P. Kreuzer, S. Thakur, A.K. Porwal, A.J. Buckingham) [13]

This contribution presents a detailed case study assessing prospectivity and undiscovered endowment of calcrete-hosted uranium deposits in Western Australia [13]. It provides an extensive discussion of a genetic model for calcrete-hosted uranium mineral system in Western Australia and illustrates the process of translating the conceptual model into a series of predictor maps which were then used in prospectivity modeling. Three different prospectivity models implemented in the study (weights-of-evidence, neural networks and fuzzy inference system) produced generally similar results. This contribution also presents a compilation of current mineral resource estimates for 20 Western Australian calcrete-hosted uranium deposits (thus creating a local grade and tonnage model) and discusses uranium exploration history in the region and relevant aspects of mineral economics.

This contribution describes applications of three significantly different statistical models to quantify undiscovered uranium endowment of calcrete-hosted deposits in Western Australia. The discussed applications are based on: a rank-size endowment model ('Zipf's law'), a local regression spatial deposit and endowment density model, and the USGS 3-part form of assessment. The applied Zipf's law endowment model assumed that Yeeliree was the largest calcrete-hosted uranium deposit in Western Australia and its current resource estimate was an adequate measure of its total endowment. The Zipf's model suggested that the total undiscovered endowment of deposits with>300 t U was 180 kt U. Local spatial endowment and deposit density models were based on findings of significant correlations between logarithms of the number of known uranium deposits and amounts of contained uranium per km^2 of well-explored calcrete areas, on the one hand, and the logarithms of sizes of the calcrete bodies, on the other. The models were created by fitting log-linear regression models to the plots of uranium endowment and deposit density against the sizes of the control calcrete bodies. It is assumed in this contribution that the regression models created for the well-explored control areas were also applicable for the rest of calcrete bodies classified as prospective by prospectivity modeling and applied them to estimate the number of undiscovered uranium deposits and contained endowment. Probabilistic estimates of the total U endowment of the undiscovered calcrete-hosted uranium deposits indicate a 50% probability of at least 48 kt of contained U and a 10% probability of >2.1 Mt U. Following the USGS 3-part form of assessment, using mapped calcrete bodies classified as prospective as permissive tracts, the local grade and tonnage model and probabilistic estimates of the number of undiscovered deposits based on the local regression deposit density model, indicated a 90% probability of at least 102,000 t U, 50% probability of 387,000 kt U and 10% probability of at least 908,000 t U.

Results of all three statistical models of undiscovered endowment are generally comparable. They jointly indicate that the total undiscovered endowment of calcrete-hosted uranium deposits in Western Australia can exceed the total known uranium endowment in the state, but a significant uncertainty is associated with this estimate.

3. DISCUSSION

Although massive uranium endowment has already been identified around the world [1], new reviews of its properties and exploration and development trends discussed in this volume indicate likely long-term supply disruptions unless the rate of major new economic discoveries significantly accelerated in the next 10-20 years [2, 3]. This further increases the need for more comprehensive and objective information about the scale and general spatial distribution of undiscovered endowment which could conceivably compensate the future supply deficit. Also, more detailed information about likely locations of undiscovered uranium deposits within known and potential uranium provinces is probably needed to improve efficiency of uranium exploration. Methods of obtaining such information and examples of their practical applications comprise the main part of this volume.

The methodology review [9] and the case studies included in this volume [5, 4, 13, 7, 10, 12] describe a wide range of existing methods which could be used to delineate and rank prospective areas with a relatively high probability of occurrence of undiscovered uranium deposits and quantitatively estimate undiscovered uranium endowment. All the presented case studies of prospectivity mapping [5, 4, 13], and [12] used the fuzzy logic method. This consistent choice was probably largely due to its universal applicability (including under-explored terranes with few known uranium deposits and occurrences) and a relative simplicity of implementation in a GIS environment. In contrast, multiple alternative statistical models and approaches were used for quantitative assessments of undiscovered uranium resources [13, 7, 10, 12, 11].

A major challenge for prospectivity mapping is unbiased identification and ranking of exploration targets. Modeling results can be strongly biased by arbitrary selection of input datasets and inadequate conceptual and mathematical models. To reduce the risk of bias, the case studies in this volume illustrating fuzzy logic prospectivity modeling used the mineral system approach [5, 4, 13], and [12]. This approach imposes an explicit systematic framework, guiding consistent definition of a conceptual data integration model and data collection and analysis. It is particularly important in cases/examples of few or no existing targets of mineral deposits, such that statistical relationships with evidential classes cannot be effectively used as a basis for data integration. In this approach, a conceptual model is constructed to define the critical processes (or components) of a natural system, all of which would be required to produce target mineral deposits. The general principles of mineral system analysis and its practical applications are further discussed in a recent special issue of *Ore Geology Reviews* on Australian Mineral Systems and key references therein [16].

All methods of prospectivity mapping and quantitative mineral resource assessment rely on certain critical assumptions (such as, geological or statistical analogy). Modeling outputs are therefore, to a variable degree, sensitive to violations of the critical assumptions and, invariably, have significant associated uncertainty. Explicitly assessing and presenting uncertainty of modeling results, in addition to a single ‘preferred’ output, can be of a significant importance for informed decision making. This can be achieved by using probabilistic methods – such as in the three-part form of quantitative mineral resource assessment, as illustrated in this volume [13, 10, 12], or implementing a probabilistic fuzzy logic model for prospectivity mapping [17].

Additionally, multiple modeling techniques and approaches, based on alternative plausible critical assumptions, can be used in a prospectivity assessment, both for internal cross-validation of analysis results and to provide another measure of uncertainty of the outputs, as illustrated in [13, 12].

The USGS Three-Part form of assessment [14], assisted by spatial density regression modelling (e.g. [15]), represents a versatile generally applicable approach to quantitative assessment of undiscovered uranium endowment. In this approach, a size of a permissive tract is a critical input parameter affecting assessment results of undiscovered endowment within that tract. Delineation of permissive tracts is commonly a subjective expert-driven process, driven by an appropriate descriptive deposit model. Tract delineation can be assisted by GIS-based prospectivity modeling using the mineral system approach, as illustrated in [12]. However, a potential lack of consistency in delineating permissive tracts in different studies remains an ongoing challenge.

Statistical models of uranium deposit grades, tonnages and contained uranium form the basis for all the methods of quantitative assessment of undiscovered uranium endowment illustrated by the case studies in this volume. While the IAEA global database of uranium deposits (UDEPO) is a comprehensive source of relevant information, quality assurance of deposit grade and tonnage information remains a significant ongoing task. For the purposes of assessing undiscovered global uranium endowment, this task is particularly important for the key uranium deposit types of the highest current and potential future economic significance. A likely current problem of the global deposit database is a lack of consistency in the spatial definition of uranium deposits represented in the database. So, some of the records could represent individual orebodies within larger composite deposits, with others corresponding to clusters of adjacent discrete deposits – or even more spatially extensive mining districts.

Mixing past production and current resources in assessing original pre-mining deposit endowment represents another potential quality problem for grade and tonnage models. This can be further exacerbated by potential effects of variable socio-economic and political environments over time and in different jurisdictions; impacts of different mining methods – in turn affecting economic cut-off grades (and, consequently, estimated deposit grades and tonnages), dilution and recoveries. It is generally advisable to use consistent definitions and consistently estimate pre-mining endowment based on production statistics and resource estimates – rather than simply arithmetically adding up past production and remaining resources.

Case studies of quantitative assessments of undiscovered uranium endowment presented in this volume focused only on a few individual mineral districts or geographic regions. Their main utility is to illustrate applications of various statistical models. However, because of significant differences in the methodology and underlying assumptions, their outputs can only be used to compare relative resource potentials of individual regions with extreme caution. Nor can the presented results be used to make reasonable inferences about any potential impact of the estimated undiscovered endowment on long-term uranium supply. Such tasks would require a systematic global program of quantitative assessment of undiscovered uranium endowment, using robust and internally consistent methodology and covering all the major known and potential uranium provinces of the world.

Further work is required to improve the quality and consistency of databases of global uranium deposits. Also, more robust, consistent and transparent techniques are needed for uranium prospectivity modelling and quantitative resource assessment which would be less susceptible to subjectivity and bias. This volume reflects the current state of knowledge and methodology. As such, it represents only an important step towards the future state of predictive modelling of undiscovered uranium resources which could significantly assist practical decision making for their more effective discovery and development.

REFERENCES

[1] OECD-NEA & IAEA, Uranium 2014: resources, production and demand, NEA no. 7209, A joint report by the Organization for Economic Co-operation and Development Nuclear Energy Agency (OECD-NEA) and the International Atomic Energy Agency (IAEA), 508p (2014).

[2] SCHODDE, R., Long-term trends and outlook for uranium exploration: are we finding eough uranium?, in this volume.

[3] MARLATT, J., The business of exploration: discovering the next generation of economic uranium deposits, in this volume.

[4] CARRANZA, E.J.M., Regional-scale prospectivity mapping for surficial uranium deposits in southern British Columbia, Canada, in this volume.

[5] BIERLEIN, F.P., BRUCE, M.D., A Continent-scale GIS-based Assessment of the Distribution and Potential for Sandstone-hosted Uranium Deposits, in this volume.

[6] ROYER, J.J., Are World Uranium Resources Lognormal Distributed?, in this volume.

[7] ROYER, J.J., CUNEY, M., Statistical distribution of the uranium resources in the Variscan hydrothermal uranium deposits of Western Europe, in this volume.

[8] THAKUR, S., CHUDASAMA, B., PORWAL, A., Global grade and tonnage modelling of uranium deposits, in this volume.

[9] JAIRETH, S., Quantitative methods of assessment of undiscovered uranium resources: A Review, in this volume.

[10] SINGER, D.A., JAIRETH, S., ROCHE, I., A three-part quantitative assessment of undiscovered unconformity-related uranium deposits in the Pine Creek Region of Australia, in this volume.

[11] BELLO, C., LÓPEZ, L., FERREYRA P., Undiscovered uranium resource assessment of Argentina, in this volume.

[12] WILDE, A.R., BRUCE, M., KNOX-ROBINSON, C., BIERLEIN, F.P., LISITSIN, V., Fuzzy logic mineral prospectivity analysis of the Mount Isa region (Queensland, Australia) for metasomatite-type (albitite-type) uranium, in this volume.

[13] CHUDASAMA, B., KREUZER, O.P., THAKUR, S., PORWAL, A.K., BUCKINGHAM, A.J., Surficial uranium mineral systems in Western Australia: Permissive tracts and undiscovered endowment, in this volume.

[14] SINGER, D.A., MENZIE, W.D., Quantitative mineral resource assessments - An integrated approach, Oxford University Press, New York (2010) 219 pp.

[15] SINGER, D.A., KOUDA, R., Probabilistic estimates of number of undiscovered deposits and their total tonnages in permissive tracts using deposit densities. Natural Resources Research **20** (2011) 89–93.

[16] HUSTON, D.L., HAGEMANN, S.G., LISITSIN, V.A., Preface: Special edition on Australian mineral systems, Ore Geology Reviews 76 (2016) 163-167.

[17] LISITSIN, V.A., PORWAL, A., MCCUAIG, T.C., Probabilistic fuzzy logic modelling – Quantifying uncertainty of mineral prospectivity models using Monte Carlo simulations. Mathematical Geosciences **46** (2014) 747-769.

[18] McCAMMON, R., Uranium Resources/ Reserves Lecture, United States of the Interior, Geological Survey, Open File Report 97-701 (1997) 38.
[19] MCCAMMON, R.C., FINCH, W.I., PIERSON, C.T., BRIDGES, N.J., The micro-computer program TENDOWG for estimating undiscovered uranium endowment, United States Department of the Interior – Geological Survey, Open File Report 88-653 (1988).

LONG-TERM TRENDS AND OUTLOOK FOR URANIUM EXPLORATION: ARE WE FINDING ENOUGH URANIUM?

R. SCHODDE
MinEx Consulting,
Melbourne, Victoria
Australia

Abstract

This study assesses the long-term trends in discovery performance of the world's uranium industry since its inception in the 1940s. Based on this, it attempts to answer the following key question – is the industry finding enough new metal to meet its future needs? Looking back over the last seven decades (from 1945 to 2016) governments and industry spent a total of $72 billion (in constant US 2017 Dollars) exploring for uranium. To date 11.14 Mt of uranium has been found[1] in 1230 primary uranium deposits larger than >200 t U. These are spread across 70 countries around the World. This equates to an average unit discovery cost of $6.49 per kg U. Over half of these deposits were found by government agencies. Analysis shows that there is a strong correlation between the rate of discovery and exploration expenditures, and between expenditures and the uranium price (lagged by one year). At the prevailing low price, the current level of exploration spend is only ~40% of what it was in 2011 and only ~16% of its historic high back in 1978. This has led to a corresponding decline in the discovery rate to around 10 new deposits per year containing a total of 65 kt U. By comparison, the industry produced 62 kt of uranium in 2016. However, the reality is that not all discoveries turn into mines, and for those that do there is a long delay between discovery and development. Furthermore, not all of the uranium that is mined is recovered. As a result, the effective discovery rate is estimated to only be~ 45% of the headline figure. Half of this production will become available within 15-20 years, and the remaining half 30-35 years later. At the current level of exploration activity, the effective discovery rate of mineable metal is estimated to be around 29 kt U per annum. This is not enough to replace current mine production, let alone meet any future growth in demand. The IAEA's Low / High Case forecast is for uranium demand of 67.0 / 104.7 kt U by 2035. If so, the industry will face a major shortage of new projects to develop. For the industry to be sustainable in the longer term it needs to either get smarter /more efficient in how it explores and develops projects, or it has to spend more on exploration. In practical terms, the effective rate of discovery & development needs to increase by a factor of 2.3 to 3.6x over the next two decades. Alternatively, the uranium price will need to increase from $60/kg at present to $156 or $252/kg U (in constant 2017 US Dollars) by 2035. Given the very long lead time between discovery and development, increased exploration efforts need to start now; otherwise the industry faces a real risk of a supply disruption in the longer term. To avoid this, government and industry need to develop new strategies now.

1. INTRODUCTION

This study is based on a database of 1230 primary uranium deposits containing >200 t U. The total amount of contained[2] metal is 11.14 Mt U. The source data for this study were compiled by the author (MinEx Consulting) from company reports, articles in technical and trade journals, Nuclear Energy Agency (NEA) and International Atomic Energy Agency (IAEA) publications [1, 2] and databases [3], and the author's own estimates. Best efforts were made to ensure that the coverage on deposits containing >5000 t U was as complete and up-to-date as possible.

Notwithstanding the above, it should be noted that while MinEx's database is comprehensive, it is by no means complete. For comparison, the IAEA's database of uranium deposits [3], which used a minimum size threshold of 300 t U up to 2016, has information on 2008 individual deposits containing around 31 Mt U. As of 2016, even though it is larger, the IAEA database is not well suited for analyzing discovery trends because:

---

[1] These figures exclude by-product uranium associated with other metal deposits – such as base metals, rare earths, phosphates and coal. This was done on the basis that money spent finding these deposits was assigned to the primary metal and, in most cases (due to the low grades) the contained uranium is generally not recovered during mining.

[2] Unless otherwise specified all quoted resource figures in this study are on reported on a pre-mined resource. This is defined as the "the current reported resource plus any historical production and associated mining and processing losses".

— It does not include information on the discovery dates and development history;
— In most cases it does not report actual tonnes and grades; instead, it states a general size range for each deposit – such as 10,001 to 25,000 t u, which makes it difficult to carry out a meaningful analysis of the actual unit discovery performance;
— It includes several deposits where uranium is not the primary metal.

With regard to this last point, the author has identified 247 deposits in IAEA's database where the primary metal is copper, rare earth, coal, phosphate or metals other than uranium. While the total amount of contained uranium is large (estimated by the author to be around 18 Mt U), in most cases the grades are too low for the uranium to be economically recovered[3]. Consequently, unless there is a dramatic increase in the price of uranium, these deposits are unlikely to be a significant source of metal in the future – and so should be left out of the analysis. Furthermore, general industry practice is that the exploration expenditures associated with discovering deposits is assigned to the primary metal. Consequently, adding in by-product uranium to the analysis will result in the unit discovery costs being under-estimated. Leaving out these secondary deposits, reduces the total number of uranium deposits in IAEA's database to 1761 containing around 13 Mt U.

Figure 1 compares the cumulative size frequency of primary uranium deposits in MinEx's database with that reported in IAEA's database. It shows that the IAEA database contains several hundred more deposits at the smaller size ranges. Part of the reason is differences in the methodology used to compile the data. The IAEA database has individual entries for each deposit. In MinEx's database, information on individual deposits within a mining camp were consolidated into a single total figure – thereby significantly reducing the number of deposits reported. Notwithstanding this, it appears that both databases do not capture all of the smaller deposits[4]. As discussed later, adjustments were made to the MinEx database to compensate for this. MinEx's database has information on the discovery dates for 874 deposits (~73% of the total by number) containing a total 10.63 Mt U (or ~95% of the total metal by mass). On this basis, the author believes that MinEx's database is sufficiently comprehensive to be of use in assessing the discovery performance of the world's uranium industry.

[3] Historically, uranium extraction has only incurred in a handful of these deposits (such as the Olympic Dam copper mine, and the Witwatersrand gold operations in South Africa in the 1950s)
[4] Evidence for this can be seen in Fig. 1 – which shows that the cumulative frequency curve 'rolls-over' in the smaller size ranges. Instead it should be a straight-line.

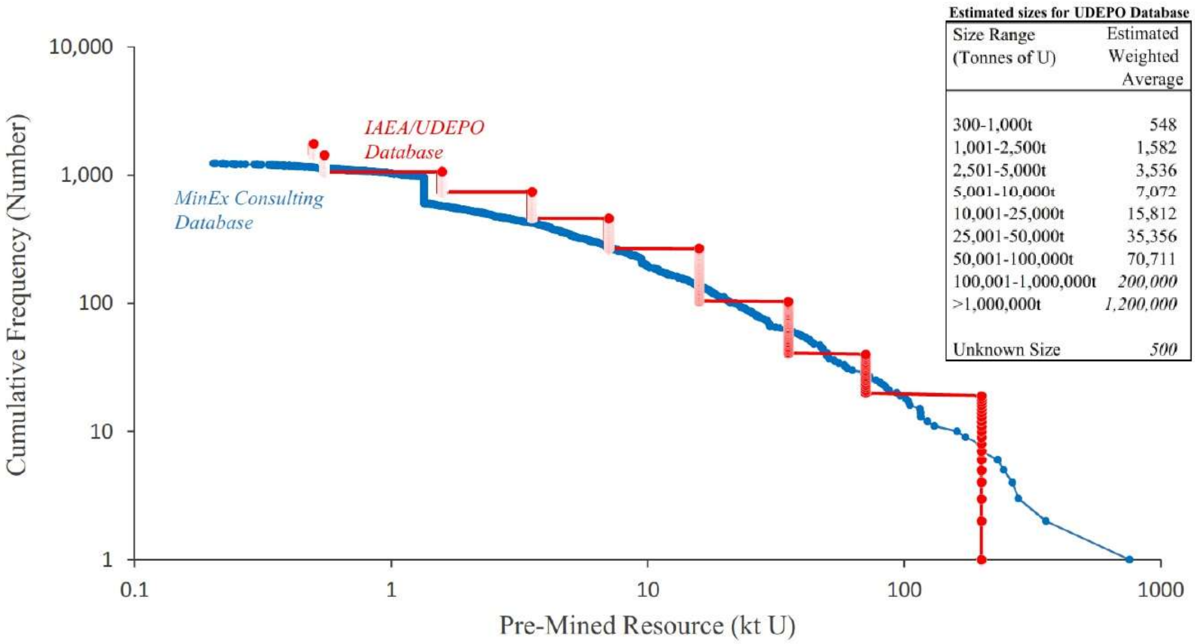

FIG. 1. Cumulative frequency curves for the IAEA/UDEPO and MinEx Consulting uranium database −primary uranium deposits only. Note: The table embedded in the figure contains the author's estimate of the weighted average size of a given deposit for the nominated size-ranges used by the IAEA.

2. OVERVIEW OF URANIUM DEPOSITS

2.1. Location

Fig. 2 shows the location of 1230 primary uranium deposits in 70 countries around the world. The three largest deposits are the Alum Shale deposit camp in Sweden (756 kt U), Elkon in Russia (357 kt U) and Imouraren in Kazakhstan (279 kt U).

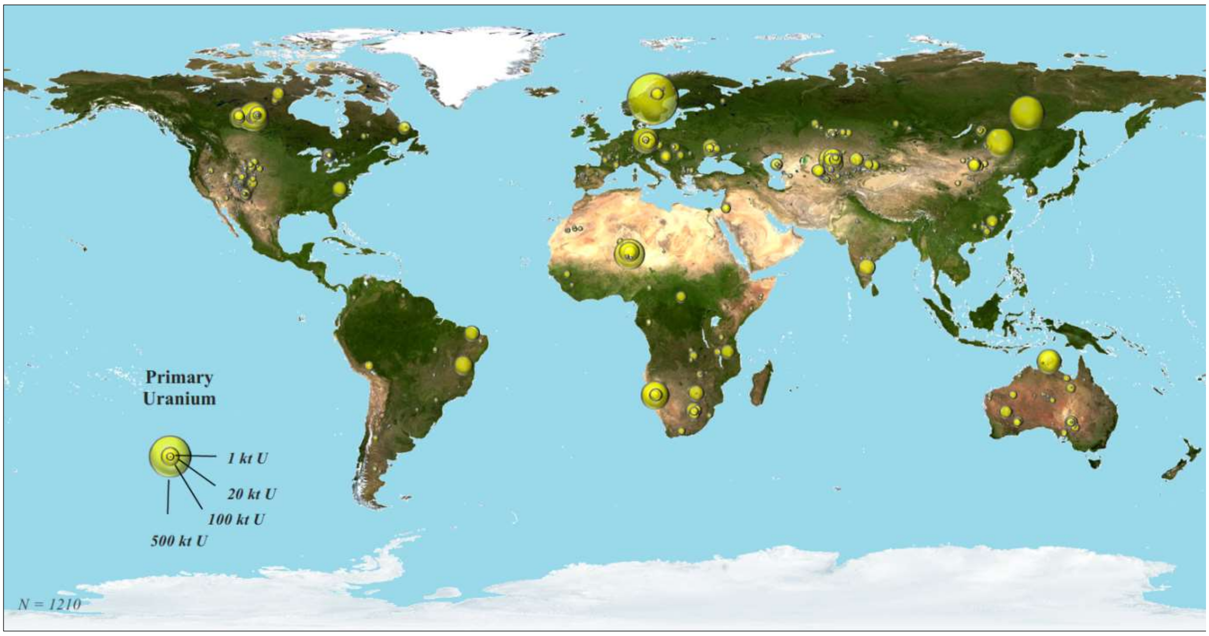

FIG. 2. Location of primary uranium deposits in the World that contain >200 t U.

Table 1 gives a breakdown by key country and region. The top three countries are Canada, Kazakhstan and USA. Between them, they account for ~36% of the known primary uranium resources. It should be noted that these figures include historic production. The current available resource will be smaller than this.

TABLE 1. PRE-MINED URANIUM RESOURCES BY COUNTRY / REGION

Country / Region	Number		kt U	
Australia	92	7.5%	844	7.6%
Canada	100	8.1%	1572	14.1%
USA	400	32.5%	1213	10.9%
Russian Federation	18	1.5%	759	6.8%
Kazakhstan	85	6.9%	1223	11.0%
Uzbekistan	38	3.1%	277	2.5%
China	52	4.2%	300	2.7%
Latin America	48	3.9%	332	3.0%
Pacific SE Asia	13	1.1%	30	0.3%
Africa	93	7.6%	2060	18.5%
Western Europe*	76	6.2%	990	8.9%
Eastern Europe	115	9.3%	1024	9.2%
Rest of Former Soviet Union	35	2.8%	72	0.6%
Rest of World	65	5.3%	450	4.0%
World	1230	100.0%	11149	100.0%

* Including 11 deposits in Sweden containing 818 kt U

2.2. Tonnage and grade distribution

Fig. 3 shows the tonnage and grade characteristics of the 10 main types of uranium deposits. These vary in sizes from <0.1 to >1000 Mt of ore. Similarly, grades can vary by four orders of magnitude from <0.01 to >10% U. Notwithstanding the large range for individual deposits, each deposit style tends to have its own fundamental characteristics (Table 2). In detail, unconformity-related deposits, while small in size, are exceptionally high grades[5]. In contrast, black shale deposits, are the opposite – namely large tonnage but very low grades[6].

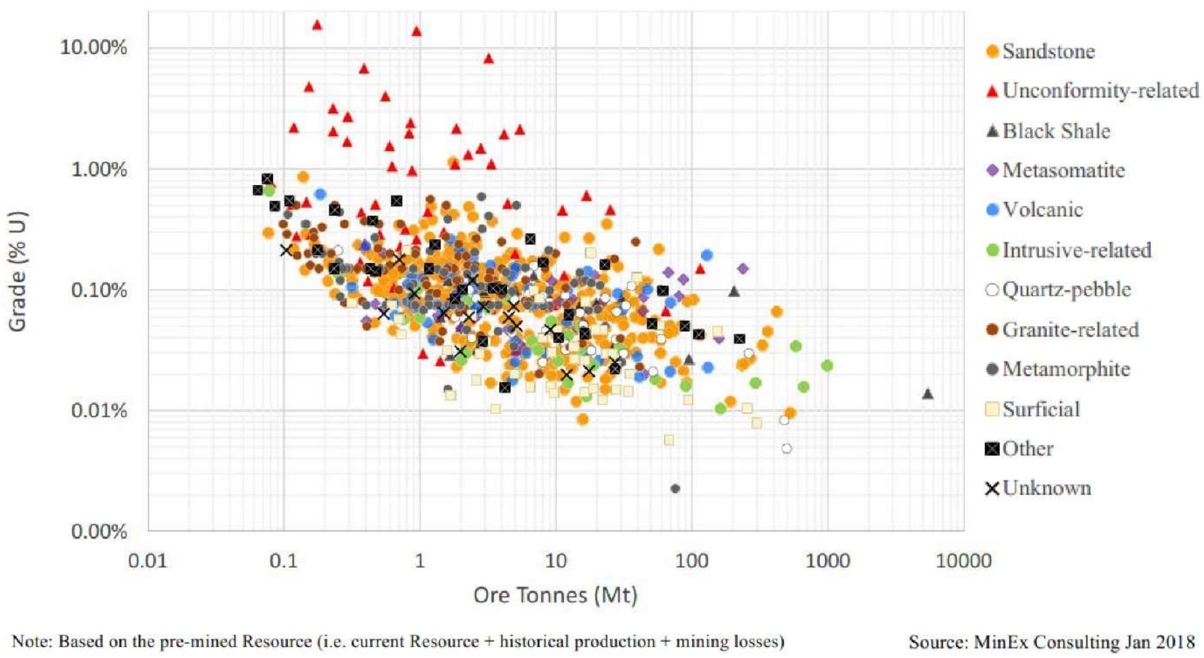

FIG. 3. Tonnage and grade of primary uranium deposits by deposit-style.

In terms of the number of deposits, the most common is the sandstone-type. As shown in Table 2, these account for 564 out of 1230 (or ~46% of the) known deposits in the world. In terms of contained metal, sandstone-type deposits account for 3960 kt out of 11,149 kt (or ~36%) of the world's known pre-mined primary uranium resources. Table 2 also shows that each deposit type has a different likelihood of being developed into a mine. This is discussed in more detail in section 4.

[5] Cigar Lake (which contains 0.94 Mt @ 13.92% U = 132 kt U) is an example of an unconformity-related deposit.
[6] The Viken camp in Sweden (which contains 5412 Mt @ 0.014% U = 756 kt U) is an example of a black shale deposit.

TABLE 2. AVERAGE SIZE AND CURRENT STATUS OF VARIOUS URANIUM DEPOSIT TYPES

Deposit type	No. of deposits	Tonnage (kt U)	Weighted average size			Current status (as % of total number of projects for each deposit type)			
			Mt ore	Grade (% U)	kt U	Un-developed	Pre-Feas / Feas	Developed	Unknown
Sandstone	564	3,960	20.1	0.051%	10.3	30	7	53	10
Unconformity-related	61	1,549	6.0	0.453%	27.1	51	21	28	0
Black Shale	24	1,101	279.0	0.019%	51.8	71	8	21	0
Metasomatite	41	938	24.8	0.096%	23.8	61	12	24	2
Volcanic	93	702	13.0	0.079%	10.3	37	11	34	18
Intrusive-related	30	686	100.0	0.023%	22.9	53	20	27	0
Quartz-pebble	33	455	53.3	0.026%	13.8	33	6	61	0
Granite-related	95	410	3.9	0.117%	4.6	19	5	76	0
Metamorphite	88	393	5.7	0.088%	5.0	57	3	40	0
Surficial	48	383	32.1	0.027%	8.6	69	19	13	0
Other	38	404	20.8	0.058%	12.1	55	0	45	0
Unknown	115	169	5.9	0.039%	2.3	22	0	27	51
Total	1230	11,149	26.8	0.046%	12.4	37	8	45	11

3. DISCOVERY HISTORY

3.1. Trend in the rate of discovery

Figs 4 and 5 show the number of deposits (874) and total amount of uranium discovered (10.53 Mt U) in the world since 1940, that most of these were found in the four decades between 1945 and 1985, and that most of the metal found is contained in a handful of giant deposits. It should be noted that there is often a delay between a deposit being first discovered and it being publicly reported. Furthermore, it can take several years to drill-out a deposit and its true size being fully recognized. Based on past experience, the author has made an estimate of the likely number of unreported discoveries (and associated metal) found. This boosts the reported numbers for the last decade.

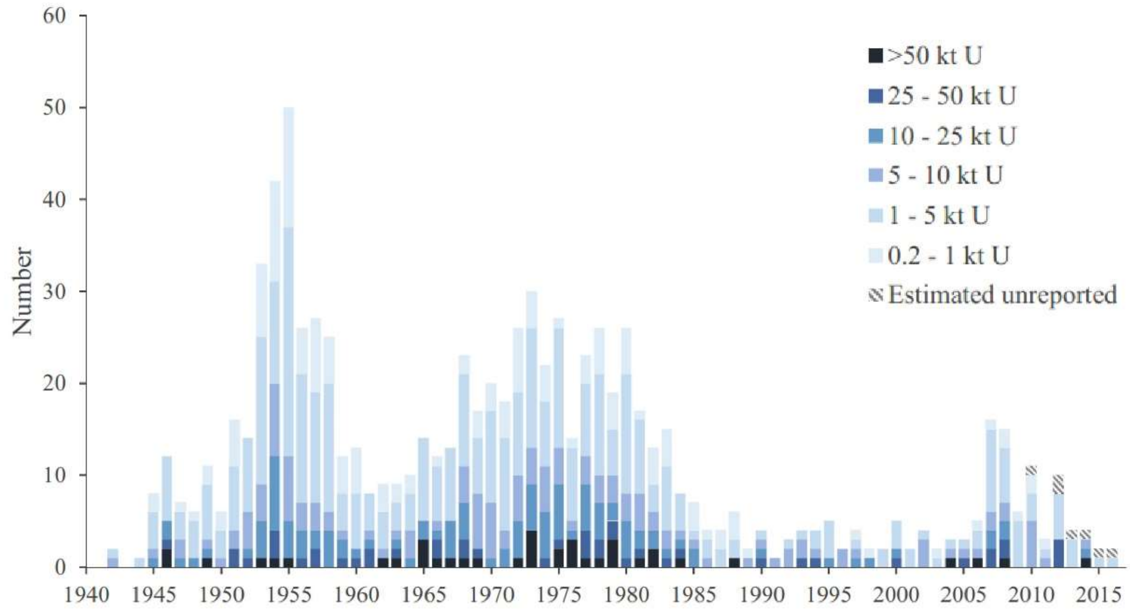

Note: Excludes by-product uranium in other deposits
(such as copper and phosphate etc)

Source: MinEx Consulting January 2018

FIG. 4. Number of primary uranium deposits (>200 t U) found in the world: 1940–2016.

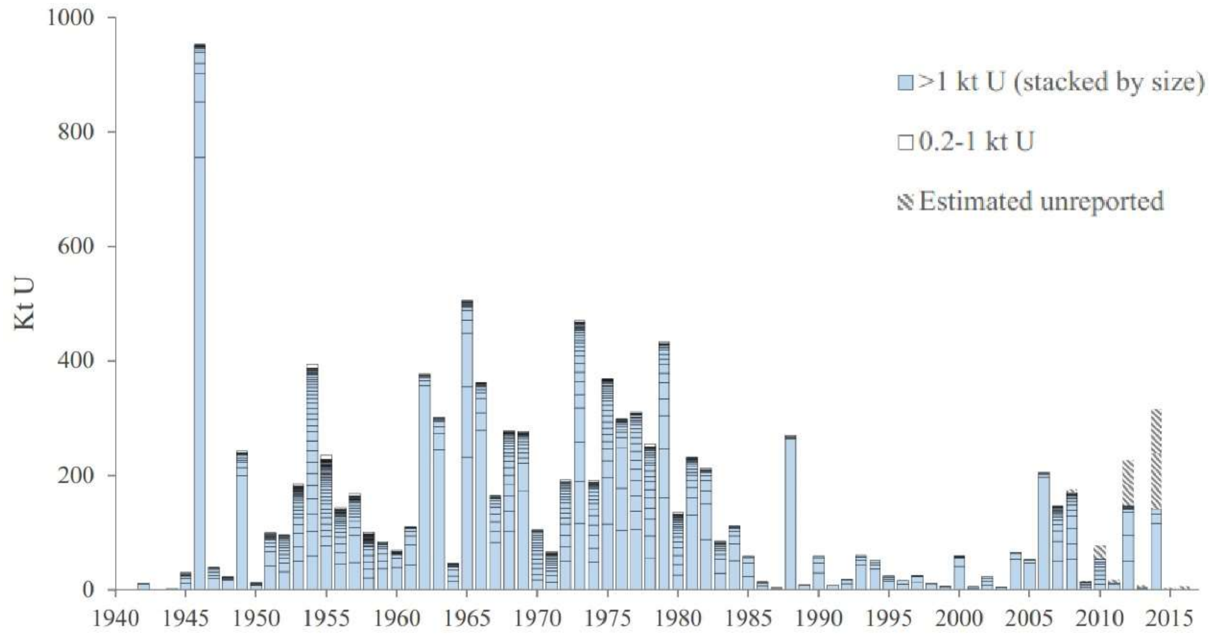

Note: Excludes by-product uranium in other deposits
(such as copper and phosphate etc)

Source: MinEx Consulting January 2018

FIG. 5. Total amount of uranium metal (in primary uranium deposits >200 t U) found in the world: 1940–2016.

Table 3 gives details on the size and status for those discoveries with >100 kt U. These 18 deposits account for ~34% of the world's total primary uranium resource. It is significant to note that six of these have not been mined, even though many of them were discovered several decades ago.

TABLE 3. SIZE, DISCOVERY HISTORY AND CURRENT STATUS OF PRIMARY URANIUM DEPOSITS >100 KT

Deposit name	Country	Pre-mined resource			Key dates			Current status
		Mt ore	% U	kt U	Discovery	Startup	Closure	
Alum Shale U Camp	Sweden	5412.0	0.014%	756.2	post 1946			Feasibility study
Elkon U Camp	Russian Fed.	238.1	0.150%	357.1	ca. 1962			Pre-feas/scoping
Imouraren	Niger	419.1	0.067%	279.2	1966			Feasibility study
McArthur River	Canada	3.2	8.264%	264.4	1988	2000	2017	Care & maintenance
Priargunsky U Camp	Russian Fed.	127.7	0.192%	244.7	1963	1969		Operating mine
Rossing	Namibia	987.8	0.023%	231.6	ca. 1965	1978		Operating mine
Ronneburg U Camp	Germany	202.3	0.099%	200.2	1949	1950	1990	Closed mine
Husab	Namibia	583.2	0.034%	197.3	2006	2016		Dev't/construction
Ranger U Camp	Australia	114.9	0.151%	173.5	1969	1981		Operating mine
Inkai	Kazakhstan	358.2	0.045%	160.8	1979	2008		Operating mine
Cigar Lake	Canada	0.9	13.918%	131.2	1981	2010, 2013	2010	Operating mine
Somair U Camp	Niger	56.9	0.217%	123.2	1965	1970		Operating mine
Jabiluka U Camp	Australia	25.1	0.463%	116.3	1973			Stalled
Arrow	Canada	5.4	2.138%	116.1	2014			Pre-feas/scoping
Mynkuduk	Kazakhstan	330.3	0.035%	115.3	1975	1987		Operating mine
Lagoa Real	Brazil	86.3	0.122%	105.3	1977	1999		Operating mine
Etango	Namibia	658.9	0.016%	104.1	1976	2020		Dev't/construction
Rabbitt Lake U Camp	Canada	16.8	0.606%	101.6	1968	1975, 2002	1999, 2016	Care & maintenance
Total		9627.1	0.039%	3778.0				

Table 3 shows that many of the large deposits were found several decades ago. This raises the general concern for industry over whether or not all the best deposits have been found, i.e., “all the big fish have now been caught”. On closer analysis this does not appear to be the case. Fig. 6 plots the cumulative size-frequency of 87 known discoveries (>200 t U) made in the last 20 years and compares it against the distribution for the total of all known discoveries (previously shown in Fig. 1). While the curve for the most recent period is lower[7] than the total, what is significant is that the angle of the slope for the two curves is the same. This can be seen in the dotted-line that refers to the most recent period multiplied by 8. In other words, the frequency of finding a giant deposit relative to that for major- or moderate-sized deposit has not changed. Instead, the apparent lack of giant discoveries in recent years is simply due to a lack of

[7] Mathematically this is not surprising – as the last 20 years only covers part of the total time period for the industry. By definition, the latter will always be bigger.

exploration effort. In other words, we simply have not ‘rolled-the-dice’ enough times to find them.

Embedded in Fig. 6 is a table showing the number and size of discoveries made in the last two decades. For example, it shows that 4 out of 87 (i.e., ~5%) of the discoveries by number were deposits with >50 kt U. These discoveries contained ~37% (or 420.7 out of 1147.9 kt U) of the total metal found. In contrast, deposits in the size range 1000–5000 t U accounted for ~55% (48 out 87) by number but only 10% by metal content of all discoveries made in this time period. In other words, most discoveries made were small in size, and collectively these do not contain much metal. However, these size-frequency distributions are used later in Section 7 to predict the likely size distribution of future discoveries.

3.2. Trend in deposit size

Related to the generally held perception that the best deposits have already been found, it is the author’s view that the quality of deposits found is getting worse over time. Fig. 7 shows that trend in the average size of discoveries since 1940; it shows that there has been an apparent downward trend in the maximum size of deposit being found. In detail, the largest discovery made in recent years (Husab deposit in Namibia, which was found in 2006) contains 196 kt U. This is one-quarter of the size of the largest known primary uranium deposit, namely the Alum Shale camp in Sweden, with 756 kt U. This deposit was found back in 1946. As noted in the previous section, this may simply be an artefact of the lack of exploration effort in recent years. A more meaningful metric is to look at the trend line for the weighted average size of the discoveries. Surprisingly, this has remained relatively constant over time; varying between 7000 t and 25 kt, with an average of 9000 t U. In other words, the recent average size of discoveries is the same as that 50 years ago[8].

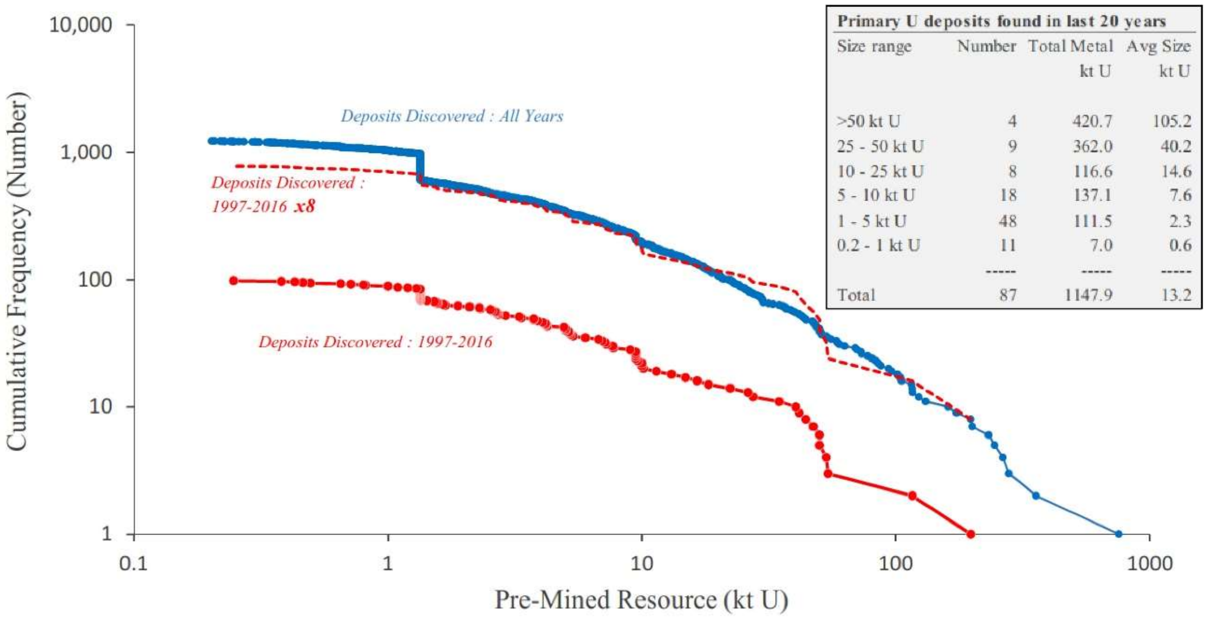

Primary U deposits found in last 20 years			
Size range	Number	Total Metal kt U	Avg Size kt U
>50 kt U	4	420.7	105.2
25 - 50 kt U	9	362.0	40.2
10 - 25 kt U	8	116.6	14.6
5 - 10 kt U	18	137.1	7.6
1 - 5 kt U	48	111.5	2.3
0.2 - 1 kt U	11	7.0	0.6
	-----	-----	-----
Total	87	1147.9	13.2

Note: Pre-Mined Resource = Current Resource + Historical Production + Mining Losses   Source: MinEx Consulting

FIG. 6. Cumulative size-frequency curves for primary uranium deposits found in 1997–2016 versus all-years.

[8] It could also be argued that the reason why the weighted average size has stayed constant this may simply be due to fewer small-size discoveries are being reported. Such deposits still exist, but companies have no incentive to drill them out / report them – as they are unlikely to be economic to develop.

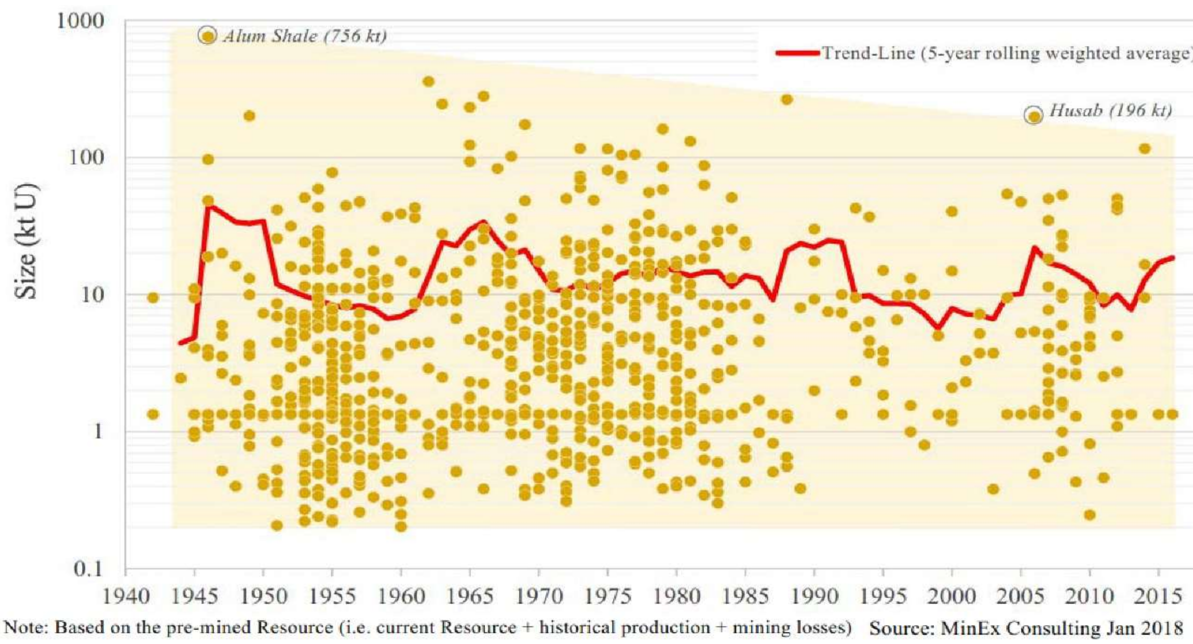

FIG. 7. Trend in the size of primary uranium discoveries found in the World: 1940-2016.

3.3. Trend in deposit grade

Fig. 8 shows the grades of primary uranium deposits found since 1940. Surprisingly, the maximum grade achieved appears to have risen over time, from <1% U in the 1960s to >10% in recent years. One such discovery is the Phoenix deposit found in 2002 in Saskatchewan. This deposit has a resource of 0.18 Mt @ 15.67% U = 27.4 kt U. As noted in Fig. 3, these high-grades are often associated with unconformity-related style deposits.A more meaningful metric is to look at the trend line for the weighted average grade of the discoveries. As seen in Fig. 8, the weighted average grade of discoveries made in the last decade is ~0.034% U. This is less than half of that observed for discoveries made in the 1960s (~0.077% U). Notwithstanding the wide spread in results for individual deposits, there does appear to be slow downward trend in grade over time. As a general rule, lower grade deposits tend to be less economic and so are less likely to be developed into mines.

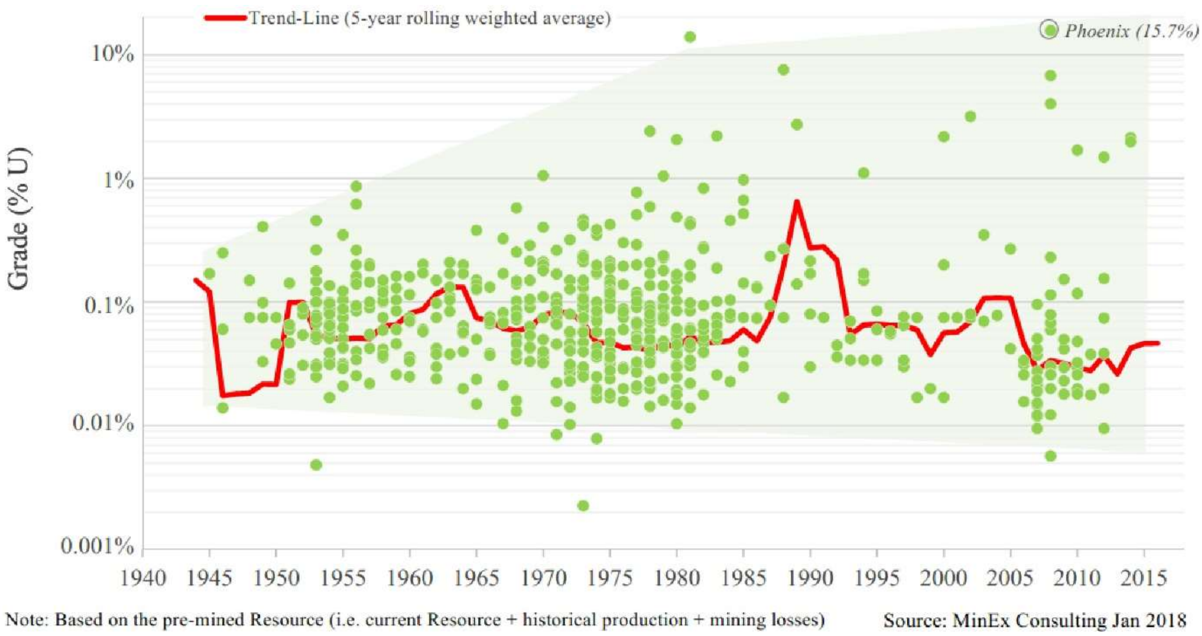

FIG. 8. Trend in the ore grade of primary uranium discoveries found in the world: 1940–2016.

3.4. Trend in the companies making discoveries

Fig. 9 shows the types of companies associated with the 873 known primary uranium deposits (>200 t U) found in the world since 1940 in 5-year increments. Fig. 10 shows the relative importance of each company type for each increment of time. As can be seen from these figures, the relative importance of the various groups (majors, junior explorers, prospectors and state-owned companies, etc.) varied significantly over time.

In the first decade (1940-49), 46 discoveries were made: ~22% by prospectors and ~75% by state-owned companies. The high-level of discoveries from the latter reflects the strategic nature of the industry prevailing at the time[9]. In the 1950s, 251 deposits were found in the world; ~51% of these were by state-owned companies, ~15% by prospectors and ~17% by junior explorers while mining companies only played a peripheral role – finding only ~4% of the deposits. By the late 1950s, military requirements for uranium were largely met, and government agencies cut back on their purchases and exploration efforts. The uranium price correspondingly dropped and less exploration was carried out (see Fig. 14 in Section 5). This led to a fall in the rate of discovery – with only 128 deposits being found in 1960–1969; ~69% of these were by state-owned companies, as private industry abandoned the sector. In the early 1970s, uranium prices rebounded due to the rapid growth in demand from nuclear power stations. The major and moderate-sized mining companies became much more active – and discovered ~20% of the 225 deposits found in that decade. The 1970s were also a time of upheaval in oil market – and many of the major oil companies made a strategic decision to diversify into the energy minerals sector (namely coal and uranium) – leading them to find 1~3% of the uranium deposits. The 1980s was a period of decline. Uranium and oil prices fell, and the oil companies unwound their investments in the mineral sector. Mining companies also cut-back on their exploration efforts; ~56% of the 102 discoveries made that decade were made

[9] This trend continues through to the present for the Centrally Planned Economies (of the FSU, Eastern Europe, China and North Korea). In these countries, virtually all uranium exploration and mine production is controlled by the State. Similar restrictions apply in many of the open-economy countries (such as India, Indonesia and Brazil).

by government geologists. The 1990s was a decade in hibernation. Very low uranium prices led to minimal exploration efforts by private industry. State-owned companies in the former Soviet Union (FSU) and in Eastern Europe were in disarray due to the collapse of the Soviet Union, and very little exploration was done. Only 31 discoveries were made in the world in that decade; ~90% of these were by state-owned companies – mainly in emerging markets in Asia (such as Mongolia and Vietnam). The decade 2000–2009 was a time of rising uranium prices, which led to a substantial increase in exploration efforts by private industry – especially the junior exploration companies. The junior sector accounted for ~57% of the 61 discoveries made in that decade. State-owned companies only played a minor role – accounting for 26% of all discoveries. This trend has continued into the most recent period (2010–2016) – with ~70% of all the discoveries coming from the junior sector. Major mining companies and government agencies now only play a small role in the discovery process.

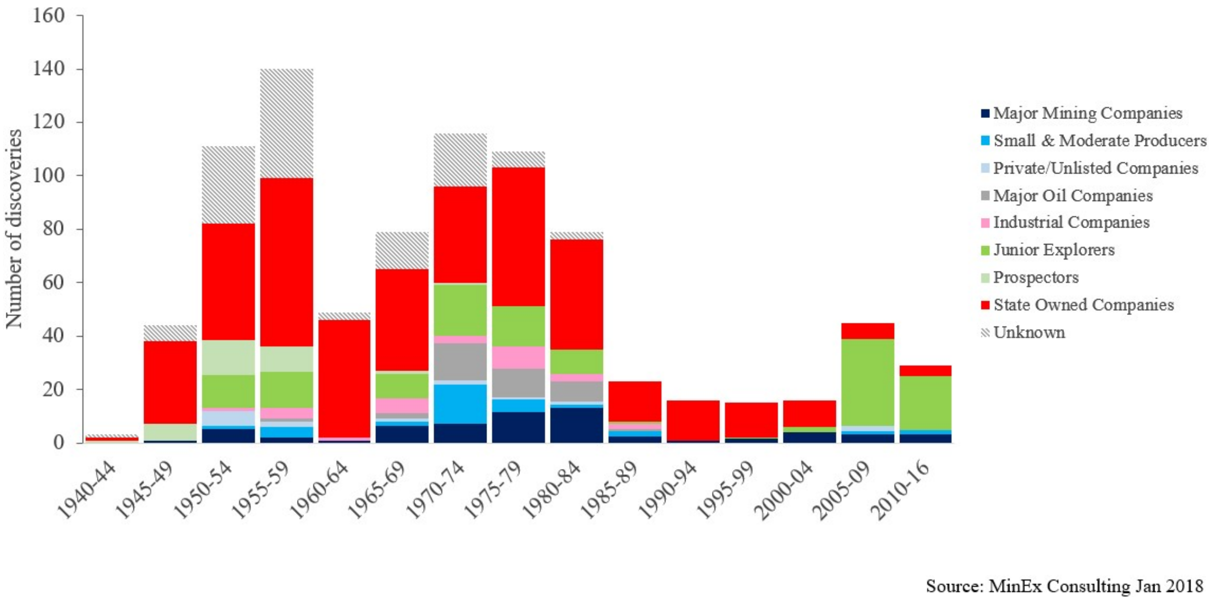

FIG. 9. Number of uranium deposits found in the world by company type: 1940–2016.

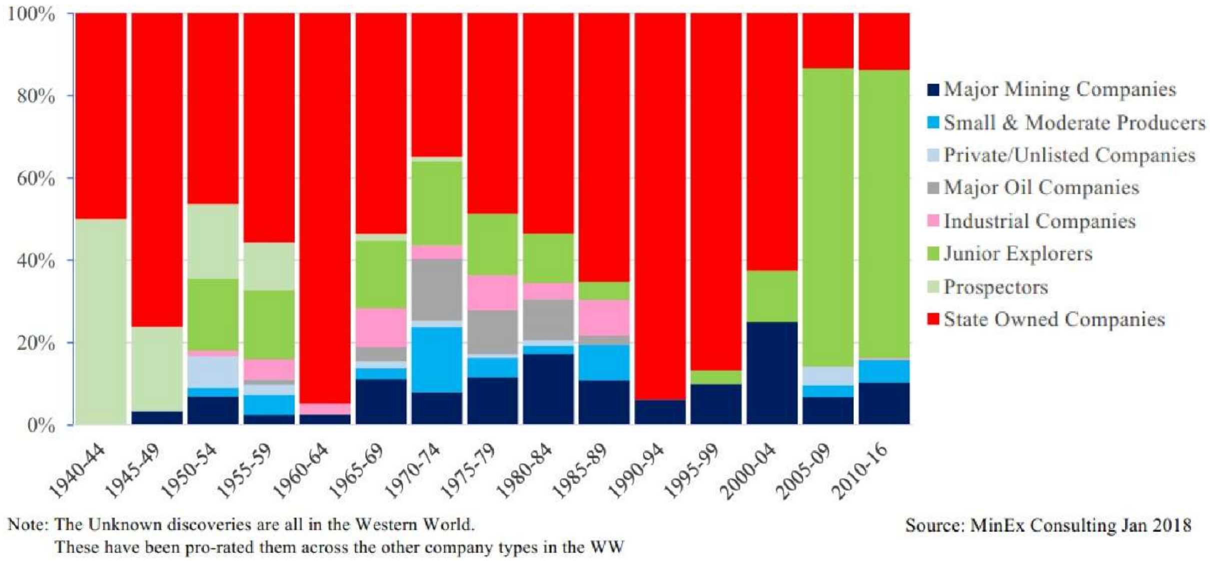

FIG. 10. Percentage of uranium deposits found in the world by company type: 1940–2016.

4. TRENDS IN CONVERSION RATES

It should be noted that not all discoveries turn into mines, and for those that do, the delay between discovery and development can be several decades. Fig. 11 shows the overall percentage of deposits mined versus years after discovery. The individual curves refer to the decade in which the discovery was made. As can be seen, of those deposits found in the period 1946–1955, ~81% by number have now turned into mines. Collectively these account for ~60% of the total metal found in that decade. Most of these occurred very quickly. In detail, in the first 10 years after discovery, ~70% of the deposits by number and ~53% by metal content had gone into production.

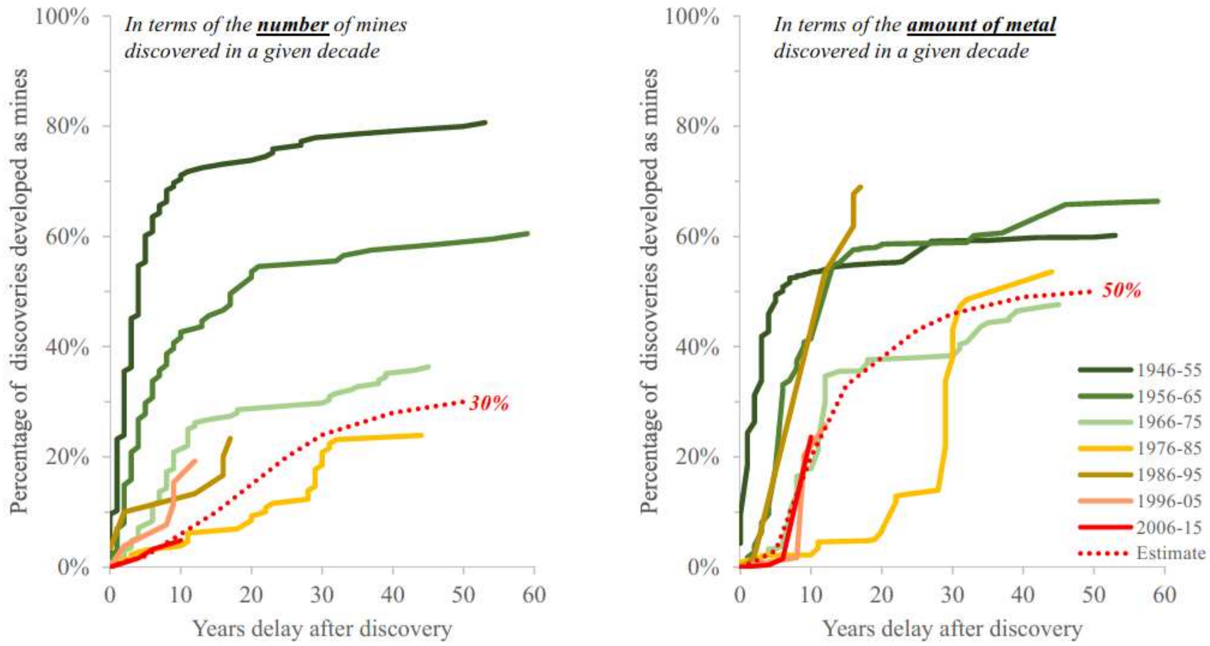

FIG. 11. Cumulative percentage of primary uranium discoveries (by number and total contained metal) in the world that are developed into mines.

Of particular significance and concern is the fact that both the overall speed and overall level of conversion has slowed down over time. For example, for those deposits found in 1996-2005, only ~16% by number and ~24% by contained metal had gone into production in the first 10 years after discovery. The dramatic slowdown in the conversion rate reflects the industry's transition from strategic to commercial priorities. It also reflects increasing difficulties associated with social and environmental issues.

For modelling purposes, the author notionally estimates that in the future only ~30% by number and ~50% by contained-metal in discoveries will ultimately be mined[10]. For those deposits that do get developed, the median delay between discovery and production is around 15–20 years. By comparison, the median time to build a nuclear power station is ~8 years [4]. In other words, it takes twice as long to find and build a new uranium mine as it takes to build a new nuclear power station. As a consequence, there is a real risk that exploration/mine development steps could hold back rapid growth in future nuclear power supplies.

The two key factors affecting the conversion rates are the quality of the deposits and the mining methods used. As a first-pass, quality can be measured in terms of the tonnage and grade of a given deposit. As highlighted in Fig. 12 below, large / high-grade deposits are more likely to be developed than small / low-grade deposits. With regard to mining methods, these include open pit, underground mines and in-situ leaching. Each has different costs, and the preferred method used is driven by ore body geometry and mineralogy – both of which are strongly influenced by the deposit-style.

Table 2 shows that ~45% (by number) of the 1230 known uranium deposits in the world have been developed into mines. However, the conversion rate varies from ~13% for surficial-style deposits to ~53% for sandstone-style deposits and ~76% for granite-style deposits. Surprisingly, in spite of their much higher grade, only ~28% of the unconformity-style deposits have been developed so far. The low conversion rate is largely due to their high mining costs[11].

[10] The relative difference in percentage conversion between the amounts of metal developed versus number of deposits simply reflects that fact that most of the small discoveries (which contain less metal) are not economically viable – and so are not developed.

[11] Many of the unconformity-style deposits are deeply buried and have difficult ground conditions. The very high grades also create special problems during mining – requiring special (and very expensive) mining methods.

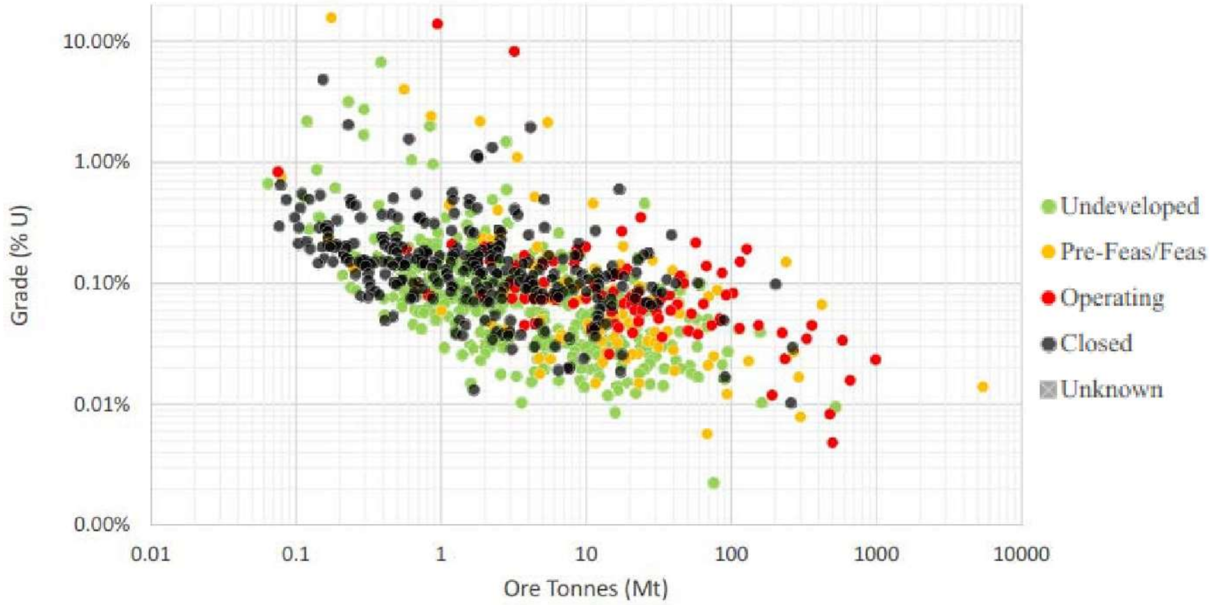

Note: Based on the pre-mined Resource (i.e. current Resource + historical production + mining losses) Source: MinEx Consulting Jan 2018

FIG. 12. Current status of various primary uranium deposits.

5. TRENDS IN EXPLORATION EXPENDITURE

Fig. 13 shows the general trend in expenditures on uranium exploration by country/region since 1945. The primary source of this data was compiled from past editions of the 'Red Book', as jointly prepared by the OECD Nuclear Energy Agency and the International Atomic Energy Agency [1, 2]. With regard to Canada and Australia, the data were adjusted to match that reported by their respective government statistical agencies (ABS [5] and NRCAN [6]). The 2016 expenditure numbers are the author's estimates based, in part, from industry survey data from SNL [7].

It should be noted that the expenditures for the period 1945–1970 are approximate only. This due to incomplete data. In detail, the Red Book data for the FSU and Eastern Europe were reported in 5-year increments (NEA/OECD, 2006). The author has smoothed this out to generate the underlying trend over time. Furthermore, for completeness, the author has notionally assumed that total expenditures in the western world were twice that reported for the United States. Notwithstanding these qualifications, it is clear that most of the global effort exploring for uranium occurred in the period 1945–1980 and that exploration activities effectively ceased during the 1990s and early 2000s. After adjusting for inflation, the recent boom in exploration in 2007–2012 was less than half of that experienced in the late 1970s. All up, from 1945 to 2016, a total of $72 billion (in constant 2017 US Dollars) was spent exploring for uranium.

In the early years of the industry, exploration efforts were largely driven by strategic concerns by governments to find sufficient uranium (at any cost) for weapon production. In the late 1960s, this transitioned to a more commercial focus on meeting needs for power generation. As evidenced in Fig. 14, from the early 1970s onwards, the level of exploration expenditures has been strongly linked to the spot uranium price. Based on the various peaks and troughs, it appears that expenditures lag the uranium price by 1–2 years. Based on this, a simple linear regression model was built – showing the relationship between price (lagged by 1 year) and exploration expenditures for the period 1970–2016. Fig. 15 shows that the trend line has a R^2 value of 0.85 – confirming the strong linkage between the two. This formula is used in Section 7 to predict the likely future level of exploration spend based on a range of projected uranium prices.

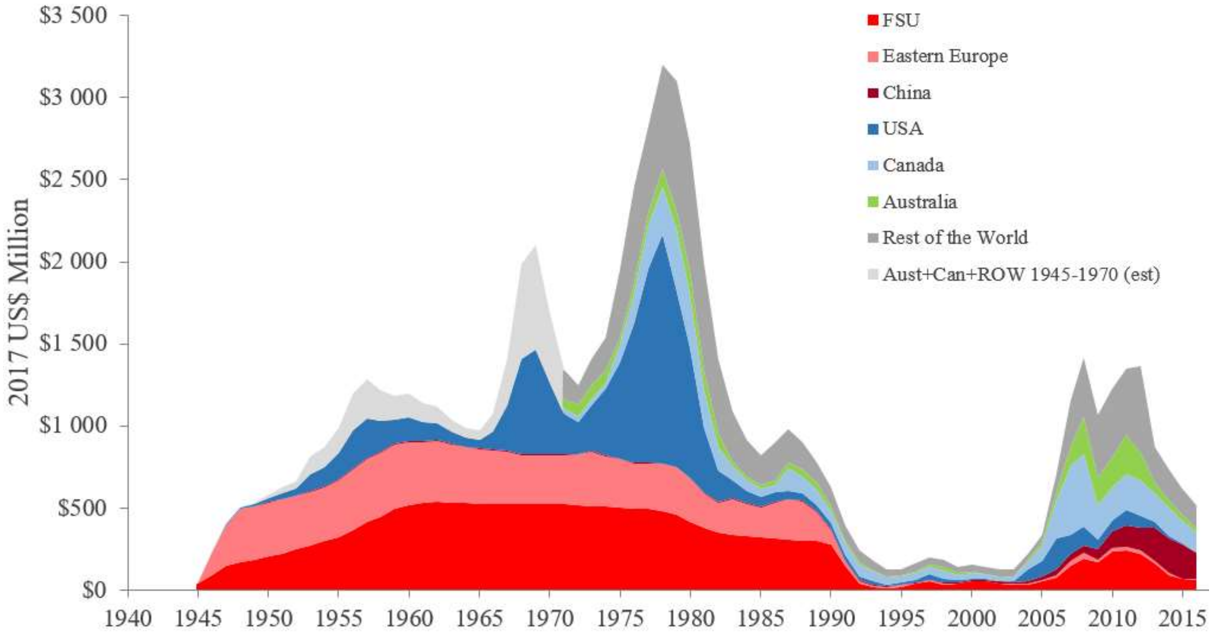

Note: Expenditures for Australia + Canada + ROW for 1945-70 are estimates only. Have assumed that they are collectively the same size as the USA.

Sources: MinEx Consulting estimates based on data from IAEA Red Book, ABS (Australia) and NRCan (Canada)

FIG. 13. Estimated annual expenditures on uranium exploration: 1945–2016.

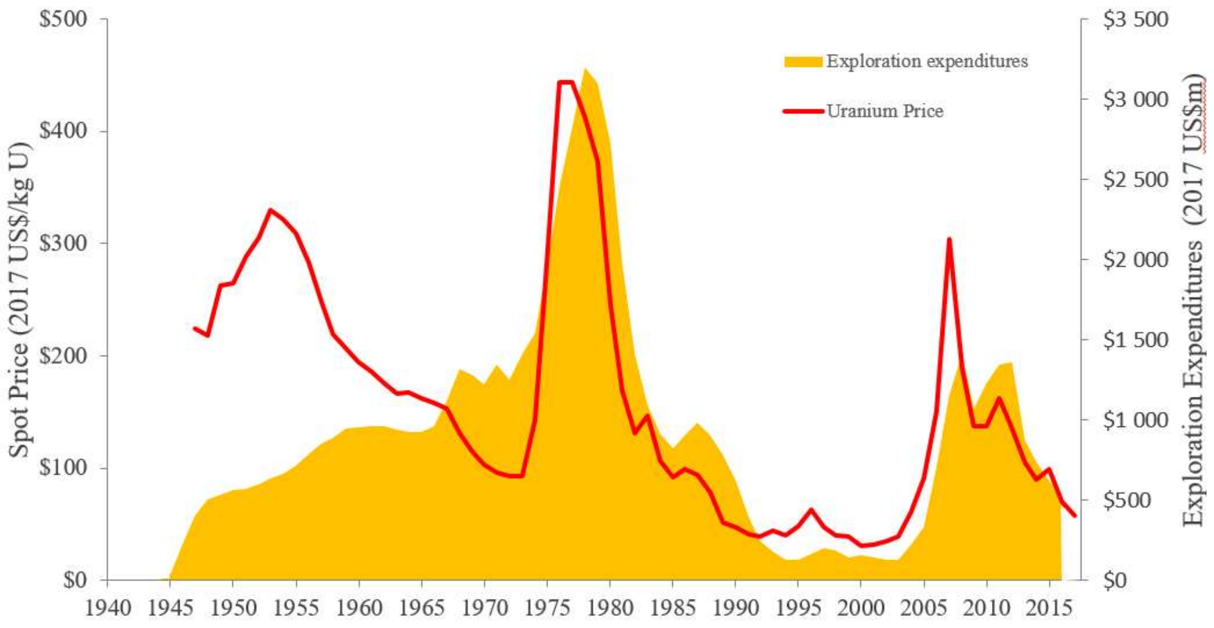

Source: MinEx Consulting estimates

FIG. 14. Uranium price and estimated annual expenditures on uranium exploration: 1945–2016.

6. TRENDS IN DISCOVERY PERFORMANCE

Fig. 16 compares the amount of uranium found in the world versus exploration expenditures. Dividing one by the other gives the average unit discovery cost (see Fig. 17). From this, it is clear that from the 1950s through to the 1980s discovery costs steadily rose from \$2 to around \$8/kg U (in constant 2017 US Dollars) and has fluctuated around this level since then. For purpose of this study, the author forecasts that unit discovery costs will remain at \$8/kg U (within a range of \$6 -10/kg U) into the future.

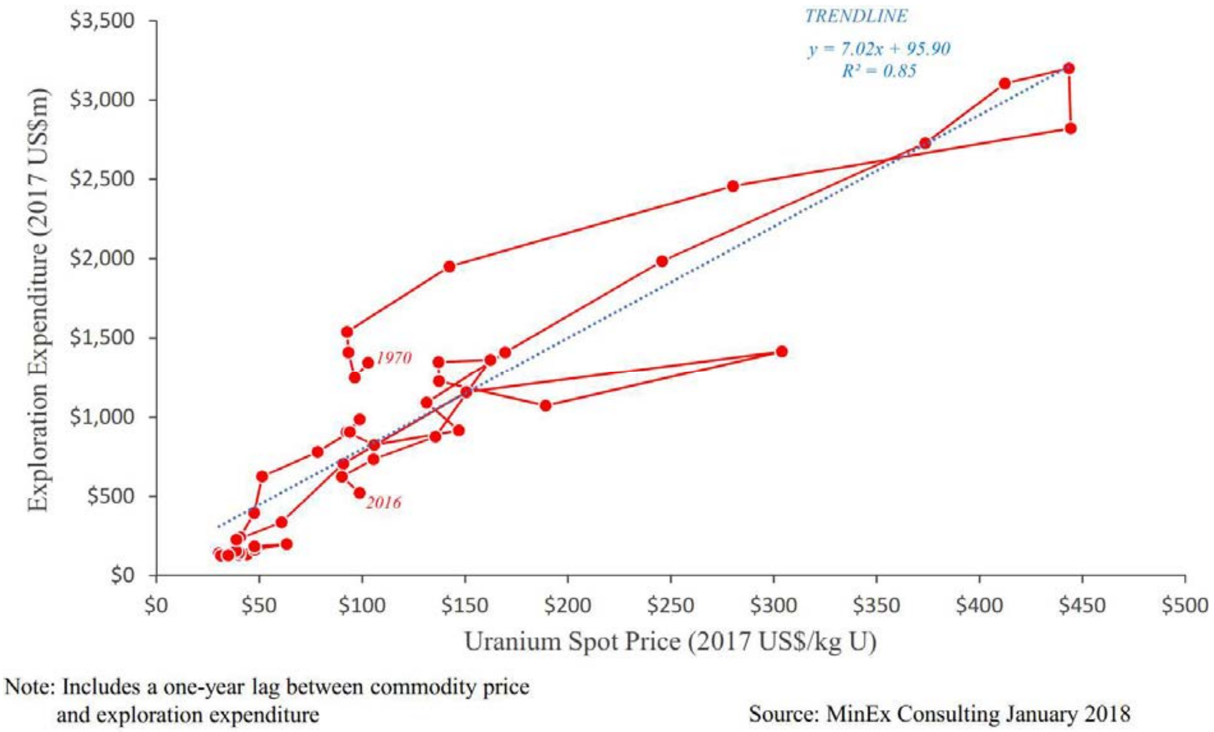

FIG. 15. Relationship between spot uranium price and world exploration expenditures: 1970–2016.

Another way to assess discovery performance is to look at the overall number and size of deposits per billion Dollars spent on exploration. Fig. 18 shows the actual and adjusted[12] size distribution for the period 1997–2016. In detail it shows that, on average, industry found 19.2 deposits of >200 t U containing a total of 125 kt U per everyone billion US dollars spent. Most of these were in the smaller size range. For example, it is estimated that 11.19 of these deposits (containing a total of 5000 t U) were in the size range 200–1000 t U. In contrast, for the same amount of money spent, only 0.81 deposits of >50 kt U were found. The total contained metal in this size range was 68 kt U. In other words, most of the metal discovered was in a small handful of giant deposits.

[12] The adjustments were made to offset missing data (especially for deposits below 1000 t U in size) plus the general issue that the number and size of recent discoveries are often under-estimated. This is because it takes time for companies to report their discoveries and fully drill them out.

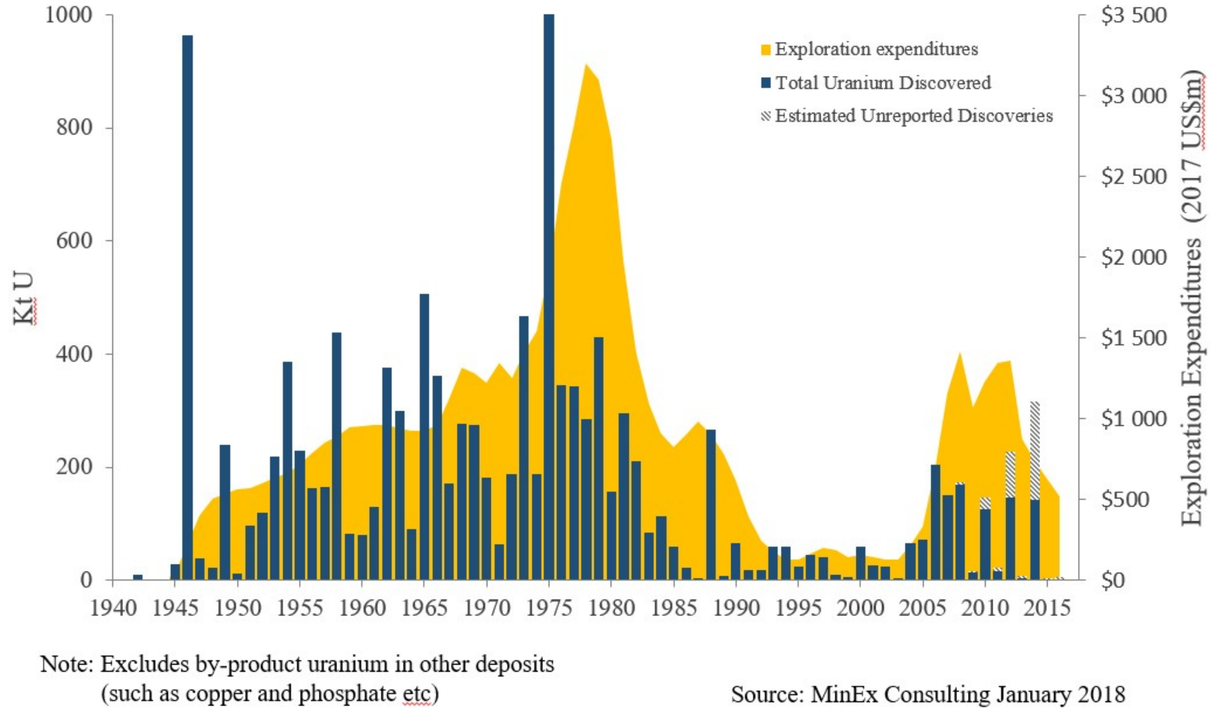

FIG. 16. Exploration expenditures and the amount of primary uranium found in the world: 1940–2016.

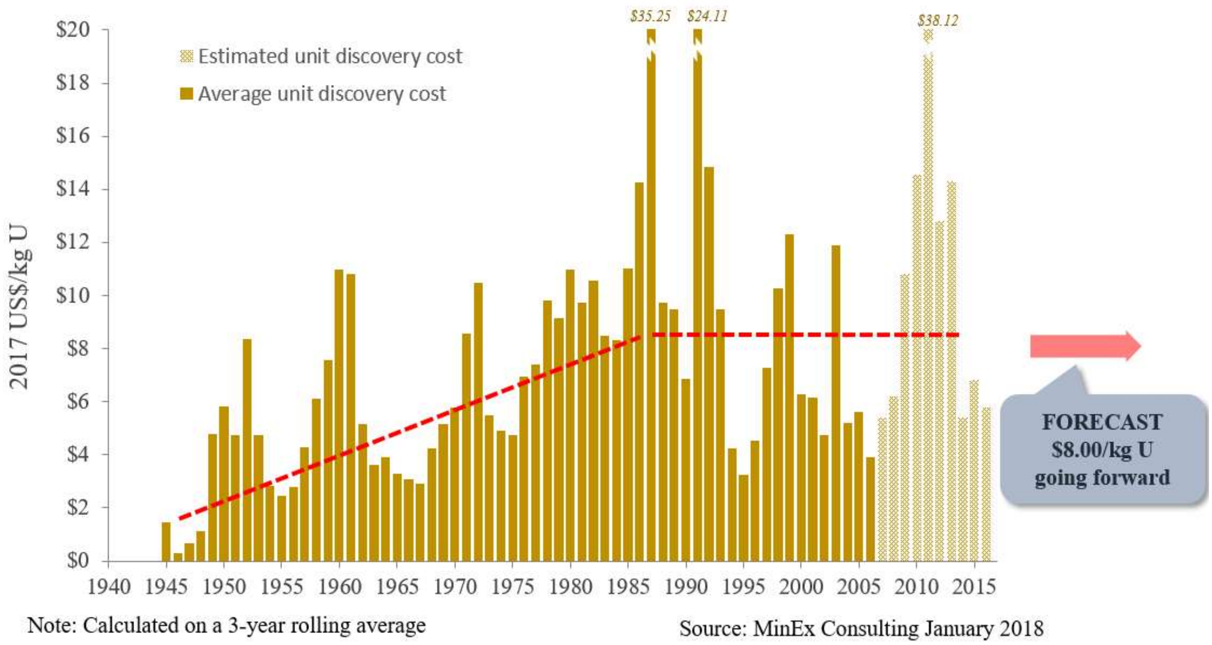

FIG. 17. Trend in unit discovery cost for uranium: world 1945–2016.

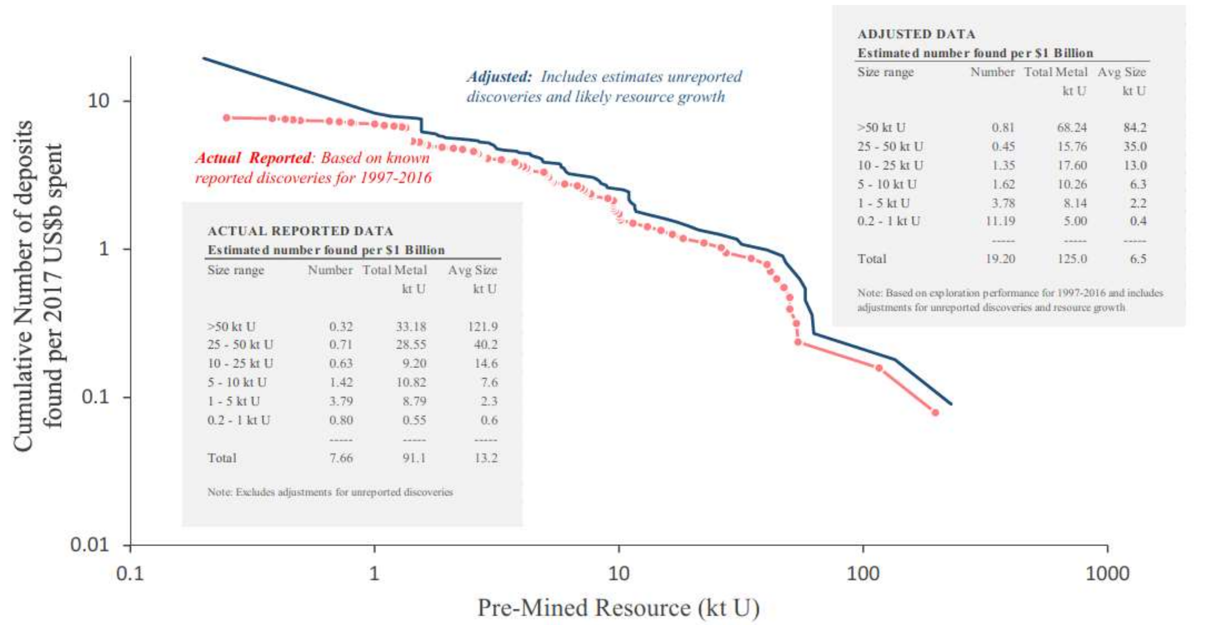

Note: Based on expenditures and reported discoveries in the World for 1997-2016.
Estimated data assumes a 31% increase in total available Resources as more discoveries are reported and from additional drilling on known deposits

Source: MinEx Consulting Jan 2018

FIG. 18. Actual and estimated size-frequency distribution of uranium deposits found per billion dollars spent on exploration: world 1997–2016.

7. FORECAST DISCOVERY RATE

7.1. Current situation

In 2016, the spot price for uranium was \$70/kg U and an estimated \$521 million (in constant 2017 US Dollars) was spent on uranium exploration. Based on a unit discovery cost of \$8/kg U, this level of exploration activity should result in around (521 / 8 =) 65 kt of primary uranium being found each year[13]. Assuming that the size-frequency for future discoveries matches that found per dollar spent in the last two decades (see Fig. 18), the author estimates that, on average, (19.2 x 521/1000 =) 10 discoveries of >200 t U could be made each year. Over half of these (by number) will be less than 1000 t U in size.

As per Fig. 11, the author estimates that the only ~50% of the discovered metal will eventually be mined, and that the average delay between discovery and development is around 15–20 years. Furthermore, not all of the metal mined will be recovered. Depending on the ore grade and processing method around 5 to 20% will be lost during mining and processing. Assuming (say) ~10% losses, at current levels of exploration, the likely amount of new metal supplied from new discoveries will only be (50% x 90% =) 45% of the total reported discovery rate. Given this, the current effective discovery rate for the industry is (65 x 45% =) 29 kt U per annum. By comparison, the world produced 62.4 kt of uranium in 2016.

Given the above, industry's exploration efforts for uranium are currently only replacing half what it mines. For the industry to be sustainable in the longer term it needs (at the very least) to double its output of discoveries. The three main ways of achieving this are:

[13] Exploration expenditure data for 2017 is currently not available. However, given that the spot uranium price dropped to \$60/kg in 2017 the current level of exploration is likely to be correspondingly less.

— Be more effective at exploration. For example, develop tools and concepts that increase the chance of making a significant discovery in a given exploration project. It could also include finding new districts where the mineral endowment is much higher;
— Be more efficient at exploration. For example, developing tools that lower the cost of finding and testing targets – down from the $8/kg U at present;
— Increase the overall level of expenditure.

The first two options require substantial investment in research & development by industry and government. The last option requires either direct financial support from government and/or higher uranium prices.

7.2. Future scenarios for exploration success

Table 4 estimates the likely number of uranium deposits and contained metal found under a range of different unit discovery costs and uranium prices. The Base Case supply scenario assumes a unit discovery cost of $8/kg U and a uranium price of $130/kg U (all in constant 2017 US Dollars). At this price, the industry is forecast to spend $1009M per annum on uranium exploration. Based on this level of expenditure, it is projected to find (1009/8 =) 126 kt U per annum contained in 19.4 deposits of varying sizes[14]. Using different discovery costs (varying from $6 to $10/kg U) and uranium prices (varying from ($60 to $260/kg U) the overall amount of uranium found each year could range from 52 to 320 kt U per annum. As noted before, only half of the uranium found will be mined, and of that, a further ~10% will be lost during mining and processing. Consequently, under the Base Case supply scenario, the effective annual discovery rate for the industry is (126 x 45% =) 57 kt U of recovered metal.

Fig. 19 shows the total amount of uranium discovered in the world each year since 1940. It also shows which discoveries have been developed and the associated amount of metal lost during mining and processing. The forecast Base Case supply scenario assumes that the uranium price progressively rises from $60 (in 2017) to $130/kg U by 2026 then remains constant thereafter. Fig. 19 also includes data on the historic trend in mine production over time. The forward projections are based on Low and High Case demand scenarios published in the latest Red Book [8] – which forecasts that primary uranium demand (sourced from mine production) will reach 66.9 kt (Low Case) to 104.7 kt (High Case) by 2035. In both cases, they exceed the likely effective amount of new supply (57 kt U per annum) from exploration success.

7.3. Discovery perforance/ uranium price required to sustain the industry

For the industry to be sustainable (i.e. find sufficient new metal to replace what it mines), discovery performance needs to dramatically improve and/or the price of uranium needs to rise. Fig. 20 and Table 5 show the general trade-off between the two options. Based on a unit discovery cost of $8/kg U, the industry needs a uranium price of $156/kg U under the Low Case scenario, or $252/kg U under the High Case demand scenario[15].

---

[14] These figures are averages only. In any given year the number and size could be higher/lower. On average 11.4 of the deposits will be in the size range 200–1000 t and 0.8 deposits will be >50 kt U. In other words, it assumes that there is an 80% chance of finding a deposit >50 kt U in any given year.

[15] Caution: These projected prices are simply based on the need to find sufficient new deposits to meet future needs. It assumes that only half to the metal found is mined – and that this factor will not change over time. In practice the conversion rate is sensitive to the uranium price (which impact on the project economics). It is also affected by changes in environmental

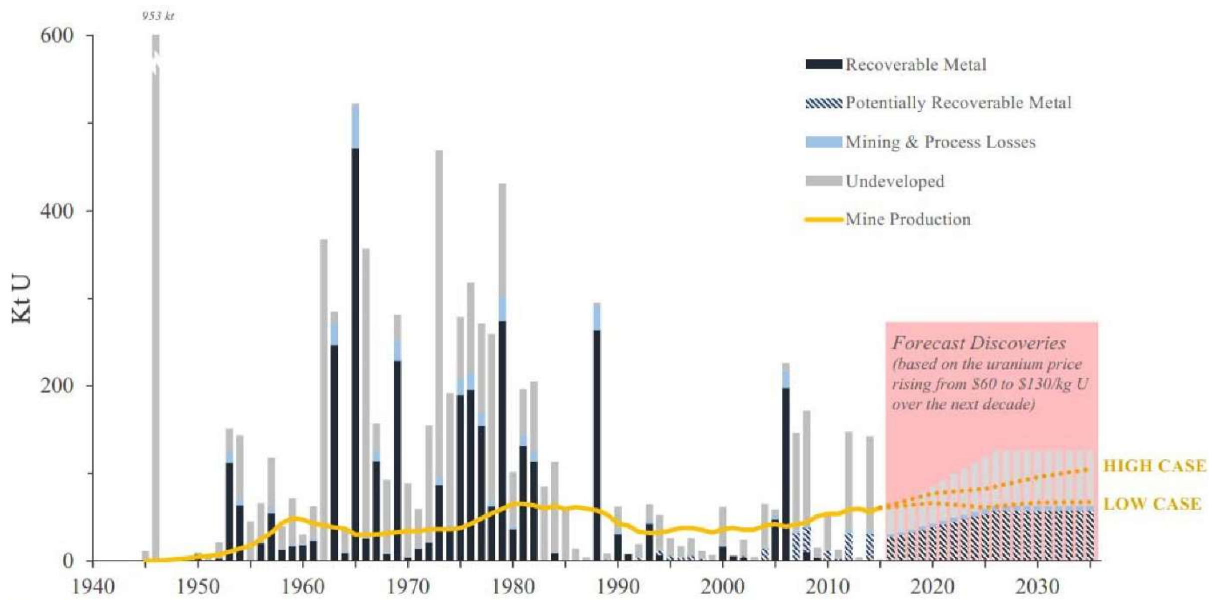

Note: Excludes discoveries of by-product uranium
Potentially recovered metal (from 1997 onwards) assumes that 50% of the discovered resource is developed.
Assumes mining & processing losses are 10% of total metal developed
Forecast discovery rate is indicative only, and assumes a unit discovery cost of $8/kg U

Source: MinEx Consulting Jan 2018

FIG. 19. Total amount of uranium available for discoveries versus current mine production and forecast demand.

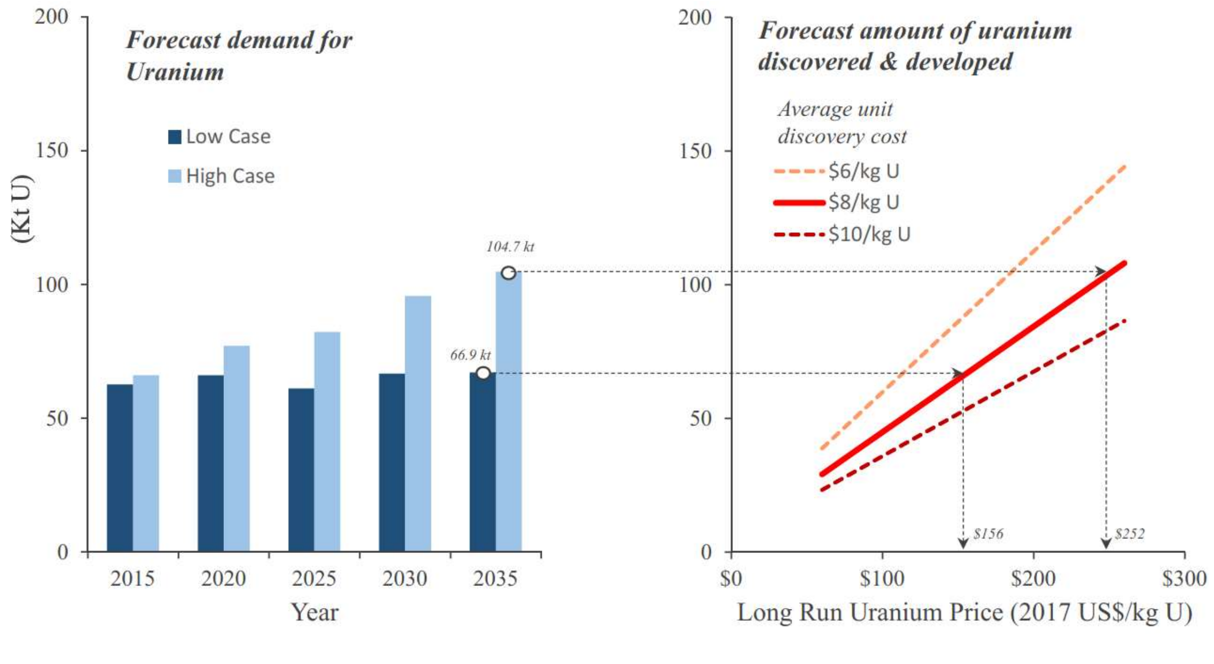

Source: NEA/IAEA Redbook 2016

Source: MinEx Consulting Jan 2018

FIG. 20. Forecast amount of uranium discovered and developed (under a range of price and discovery scenarios) to meet future industry needs.

---

regulations and community acceptance. Predicting such changes is beyond the scope of the current study.

TABLE 4. ESTIMATED LIKELY NUMBER AND AMOUNT OF URANIUM TO BE DISCOVERED IN THE WORLD UNDER A RANGE OF DIFFERENT PRICE FORECASTS AND FUTURE UNIT DISCOVERY COSTS

		Uranium Price (2017 US$/kg U)				
		$60	$80	$130	$200	$260
Forecast exploration expenditures per year (2017 US$ million)		$517	$658	$1,009	$1,500	$1,921
Unit Discovery Cost (2017 US$/kg U)	Deposit Size					
Estimated number of uranium deposits found per year by size, based on a given unit discovery cost						
$6.00 $/kg U	>50 kt U	0.6	0.7	1.1	1.6	2.1
	25 - 50 kt U	0.3	0.4	0.6	0.9	1.2
	10 - 25 kt U	0.9	1.2	1.8	2.7	3.5
	5 - 10 kt U	1.1	1.4	2.2	3.2	4.2
	1 - 5 kt U	2.6	3.3	5.1	7.6	9.7
	0.2 - 1 kt U	7.7	9.8	15.0	22.4	28.7
		----	----	----	----	----
	Total (>1 kt U)	13.2	16.8	25.8	38.4	49.2
$8.00 $/kg U	>50 kt U	0.4	0.5	0.8	1.2	1.6
	25 - 50 kt U	0.2	0.3	0.5	0.7	0.9
	10 - 25 kt U	0.7	0.9	1.4	2.0	2.6
	5 - 10 kt U	0.8	1.1	1.6	2.4	3.1
	1 - 5 kt U	2.0	2.5	3.8	5.7	7.3
	0.2 - 1 kt U	5.8	7.4	11.3	16.8	21.5
		----	----	----	----	----
	Total (>1 kt U)	9.9	12.6	19.4	28.8	36.9
$10.00 $/kg U	>50 kt U	0.3	0.4	0.7	1.0	1.2
	25 - 50 kt U	0.2	0.2	0.4	0.5	0.7
	10 - 25 kt U	0.6	0.7	1.1	1.6	2.1
	5 - 10 kt U	0.7	0.9	1.3	1.9	2.5
	1 - 5 kt U	1.6	2.0	3.1	4.5	5.8
	0.2 - 1 kt U	4.6	5.9	9.0	13.4	17.2
		----	----	----	----	----
	Total (>1 kt U)	7.9	10.1	15.5	23.0	29.5
Estimated amount of uranium found (kt U) per year by deposit size, based on a given unit discovery cost						
$6.00 $/kg U	>50 kt U	47	60	92	136	175
	25 - 50 kt U	11	14	21	32	40
	10 - 25 kt U	12	15	24	35	45
	5 - 10 kt U	7	9	14	21	26
	1 - 5 kt U	6	7	11	16	21
	0.2 - 1 kt U	3	4	7	10	13
		-----	-----	-----	-----	-----
	Total (>1 kt U)	86	110	168	250	320
$8.00 $/kg U	>50 kt U	35	45	69	102	131
	25 - 50 kt U	8	10	16	24	30
	10 - 25 kt U	9	12	18	26	34
	5 - 10 kt U	5	7	10	15	20
	1 - 5 kt U	4	5	8	12	16
	0.2 - 1 kt U	5	7	10	15	20
		-----	-----	-----	-----	-----
	Total (>1 kt U)	65	82	126	187	240
$10.00 $/kg U	>50 kt U	28	36	55	82	105
	25 - 50 kt U	7	8	13	19	24
	10 - 25 kt U	7	9	14	21	27
	5 - 10 kt U	4	5	8	12	16
	1 - 5 kt U	3	4	7	10	13
	0.2 - 1 kt U	2	3	4	6	8
		-----	-----	-----	-----	-----
	Total (>1 kt U)	52	66	101	150	192

TABLE 5. ESTIMATED URANIUM PRICE REQUIRED TO STIMULATE SUFFICIENT EXPLORATION TO

	Prodn (kt U)	Unit Discovery Cost (2017 US$/kg U) $6	$8	$10
Low Demand Case				
2020	66.0	$112	$153	$195
2025	61.0	$102	$141	$180
2030	66.6	$113	$155	$197
2035	67.0	$114	$156	$198
High Demand Case				
2020	77.0	$133	$181	$230
2025	82.2	$142	$194	$247
2030	95.6	$168	$229	$289
2035	104.7	$185	$252	$318

Source: MinEx Consulting January 2018

Note: Forecast Low/High Demand uranium demand as per by IAEA 2016 RedBook
Assumes that only 50% of metal discovered is mined, and that 10% is lost in processing.

8. SUMMARY / CONCLUSIONS

It can be said that uranium is truly a metal of the Modern Age. Prior to the invention of the atomic bomb in 1942, demand was very limited and no formal effort was made to find new mines. In the years after the end of World War II, demand quickly grew and immense efforts were made around the world to find new deposits. Demand was further boosted in the 1960s with the wide scale construction of nuclear power stations. Assessing the discovery history of uranium mining industry provides a unique insight into the dynamics of mineral exploration – as it is the only metal that boasts historical records dating back to day "zero" with regard to the price paid for uranium, the amount of money spent on exploration and the resulting amount of metal found.

Over the period 1945 to 2016, governments and industry spent a total of $72 billion (in constant US 2017 Dollars) exploring for uranium. To date, 11.14 Mt of uranium have been found[16] in 1230 primary uranium deposits with >200 t U. These are spread across 70 countries around the world. Almost all of it was found since 1945. On this basis, the average unit discovery cost over the seven decades was (72/11.14 =) $6.49 per kg U. Over half of these deposits were found by government agencies. Detailed analysis shows that, in the early years, unit discovery was very low (~$2/kg U) but progressively rose to $8/kg by 1985. Since then, average unit discovery costs have remained relatively constant.

While it is true to say that the largest deposits were found early-on in the history of the industry, detailed analysis indicates that, since the 1950s, the weighted average size of discovery has remained relatively constant at ~9000 t U. However, over the same time, the weighted average grade of these deposits has halved – from 0.10% in 1950 to 0.05% U in 2016. This clearly suggests that the quality of discoveries is declining over time.

In the early years, because of the strategic importance of uranium, almost all of the discoveries

[16] These figures exclude by-product uranium associated with other metal deposits – such as base metals, rare earths, phosphates and coal. This was done on the basis that money spent finding these deposits was assigned to the primary metal and, in most cases (due to the low grades) the contained uranium is generally not recovered during mining.

made were quickly developed into mines. However, in recent decades the conversion rate has subsequently declined and the speed of mine development has slowed down. Based on this, the author estimates that, in the future, only ~30% of new uranium discoveries (by number) will eventually be developed. These contain ~50% of all metal found. For those deposits that do get mined, the median[17] time between discovery and development is projected to be 15–20 years. By comparison, the median time to build a nuclear power station is 8 years. In other words, it takes twice as long to find and build a new uranium mine as it takes to build a new power plant. Consequently, the industry's ability to rapidly expand the nuclear power sector is severely constrained by the time lag required to ramp up exploration and build new mines.

Analysis shows that there is a strong correlation between the rate of discovery and exploration expenditures, and between expenditures and the uranium price (lagged by one year). In 2016, the average spot price for uranium price was $70/kg U and $521 million was spent on exploration. This is <40% of the rate spent back in 2012 and only ~16% of the historic peak in spent back in 1978. The author estimates that this level of effort will, on average, deliver around 10 new discoveries each year containing a total of 65 kt U. It is also estimated that, on average, only 3 of these discoveries will ultimately get developed and (after processing losses) deliver 29 kt of uranium to market. By comparison, in 2016 the industry produced 62 kt of uranium.

Given the above, the industry is not finding enough new deposits to replace the metal it mines. The current shortfall is set to get worse over time. Based on the latest Low / High forecasts from the IAEA, demand is set to rise to between 67 kt and 104.7 kt by 2035. In the short-term, the industry will continue to operate its existing mines. However, as these progressively get depleted, new mines will need to be developed. In the first instance, this will be met by developing known projects; however, the current inventory of low cost projects (in jurisdictions where development is acceptable) is limited. In the longer term, several new discoveries need to be made. For the industry to be sustainable in the longer term, the current effective rate of discovery needs to increase by a factor of 2.3 to 3.6x over the next two decades. To achieve this, either require an equivalent improvement in discovery performance (i.e., reduce the unit discovery cost from $8.00/kg down to $2.22 to $3.50/kg U) or the price of uranium needs to rise to stimulate additional exploration efforts.

Any major improvement in discovery performance will require a substantial investment in research and development (R&D). While in the past government agencies and (to a lesser extent) large mining companies were the main players in the exploration process, in the last decade this role has now been taken on by the junior exploration sector – who now account for ~70% of all the discoveries made in the world. The challenge for the industry is that the junior sector does not have the funds, technical capabilities or the patience to heavily invest in R&D efforts. The only way out is for the uranium price to rise to stimulate additional exploration. Assuming no improvement in unit discovery costs, the price of uranium in 2035 will need to increase to $156 or $252/kg U (in constant 2017 US Dollars) under the Low- and High-Case demand scenarios, respectively. Given the very long lead time between discovery and development (of 15–20 years), exploration efforts need to start now; otherwise, the industry faces a real risk of a supply disruption in the longer term. To avoid, this government and industry need to develop new strategies now.

[17] The median time of 15-20 years refers to the time taken for half of the mines to be developed. The author estimates that it will take at least 50 years to achieve the final conversion factor of 30% (by number) and 50% (by metal).

REFERENCES

[1] NEA/IAEA, "Uranium Resources, Production and Demand", or the so-called "Red Book", various years, jointly published by the Nuclear Energy Agency of the OECD and the International Atomic Energy Agency, Vienna.

[2] NEA/IAEA, 2006 "Forty Years of Uranium Resources, Production and Demand in Perspective – The Red Book Perspective", jointly published by the Nuclear Energy Agency of the OECD and the International Atomic Energy Agency, Vienna (2006).

[3] IAEA, 2018, World Distribution of Uranium Deposits Database (UDEPO), compiled by the International Atomic Energy Agency. This database is available online and a copy was downloaded on 31 January 2018 from https://infcis.iaea.org/UDEPO/Deposits, Vienna (2018).

[4] IAEA PRIS Database, 2018, "Power Reactor Information System (PRIS) Database, compiled by the International Atomic Energy Agency. This database is available online and a copy was downloaded on 31 January 2018 from https://www.iaea.org/pris/, Vienna (2018).

[5] ABS, "Mineral and Petroleum Exploration", 8412.0, various years published by the Australian Bureau of Statistics (ABS), Canberra. Data can be downloaded from: http://www.abs.gov.au/ausstats/abs@.nsf/mf/8412.0

[6] NRCAN, "Overview of Trends in Canadian Mineral Exploration", Canadian Intergovernmental Working Group on the Mineral Industry, various years published by Natural Resources Canada, Ottawa. Data for recent years can be downloaded from: http://www.nrcan.gc.ca/mining-materials/statistics/8854

[7] SNL, "Corporate Exploration Strategies" annual survey as published by SNL Metals & Mining, an offering of S&P Global Market Intelligence, Halifax (2017)

[8] NEA/IAEA, "Uranium 2016: Resources, Production and Demand", jointly published by the Nuclear Energy Agency of the OECD and the International Atomic Energy Agency, Vienna (2017).

THE BUSINESS OF EXPLORATION: DISCOVERING THE NEXT GENERATION OF ECONOMIC URANIUM DEPOSITS

J. MARLATT
GeoTotal Group Ltd.,
Qualicum Beach, BC
Canada

Abstract

Uranium exploration is a complex high-risk high-reward business activity at the front end of the nuclear fuel cycle. The uranium exploration process involves the effective use of geoscientific knowledge and exploration technologies for the discovery of economic uranium deposits. On a global basis, historical uranium exploration has led to the discovery of uranium deposits. However, there is significant uncertainty associated with the economic potential illustrated in the global inventory of uranium resources. The exploration process is relatively inefficient and the conversion rate of significant discoveries to producing mining operations is estimated to be approximately fifty percent, due to technical, economic, social and environmental factors. The business drivers of exploration include factors related to uranium supply and demand and attitudes toward investment. The technical drivers of exploration include the optimal selection of geographical areas for exploration based upon an assessment of prospectivity and explorability. The optimization of human, organization and technology factors for discovery is another factor. The quantitative and qualitative estimation of economic mineral potential is an important area of focus for understanding the investment worth of uranium exploration. The key stakeholders in the exploration process are governments, geological survey organizations, consultants, researchers, exploration service providers, and exploration company managers and workers. Geological survey organizations play an important role in attracting investment. They support the establishment of a favourable business environment, provide easy access to pre-competitive geoscientific information, and initiate economic mineral potential assessments, among other activities. Geological survey organizations contribute to significant long-term economic development within their jurisdictions by attracting investment from the uranium exploration and mining sector. Exploration frontiers can be classified as geographical, technological, depth-related, and data-related in nature. Next-generation undiscovered economic deposits are predicted to exist within under explored frontier localities that have received limited historical exploration expenditure. However, a technology leap is indicated as a requirement for these new economic discoveries. This leap could come in the form of innovations associated with geological, geochemical, geophysical, drilling, and mining methods or deposit models, and their deployment in terrains identified through quantitative and qualitative economic mineral potential assessments. Rapid and cost effective innovative evidence-based approaches to assessing the investment worth of uranium exploration in frontier project areas with limited data provide an alternative to more conventional approaches. Innovative approaches rely on the development of collaborations with company and organizational experts, consultants and applied academic researchers, with a focus on the exchange of knowledge for better exploration decision-making and the development of technological innovations.

1. INTRODUCTION

Uranium exploration is a complex high-risk, high-reward business activity within the nuclear fuel cycle. This chapter focuses on the description of aspects of uranium exploration program management and business development for the discovery of the next generation of economic deposits. It includes an overview of the uranium exploration process, the identification of exploration risk factors, and the description of some approaches for understanding the investment worth of uranium exploration.

The exploration process involves many stakeholders, who take on different roles to support the activities of exploration and mining companies. The key stakeholders in the exploration process are governments, geological survey organizations, consultants, researchers, exploration service providers, and exploration company managers and workers. Geological survey organizations play an important role in attracting investment in the exploration and mining sector. They support the establishment of a favorable business environment, initiate economic mineral potential assessments and provide easy access to pre-competitive geoscientific information, among other activities. Survey organizations can promote significant long-term economic development as a service provider.

Long lead times are required from the start of exploration to the discovery of economic uranium deposits and mining production. On a global basis, historical uranium exploration programs have been successful in discovering deposits through prospector-driven and deposit-model-driven approaches. However, there is significant uncertainty associated with the economic potential illustrated in the global inventory of uranium resources. The exploration process is relatively inefficient and the conversion rate of significant discoveries to producing mining operations is estimated to be ~50%, due to technical, economic, social, and environmental factors.

Additional undiscovered economic resources are predicted to exist in under-explored frontier localities that have received limited historical exploration expenditure. A technology leap is indicated as a requirement for the discovery of the next generation of economic uranium deposits. This leap could come in the form of innovations associated with geological, geochemical, geophysical, drilling, and mining methods or deposit models.

Exploration companies make investment decisions based upon a variety of risk assessments. The qualitative and quantitative estimation of economic mineral potential is also an important area of focus for understanding investment worth. The endowment of economic uranium deposits in a geological setting can be inferred through an evaluation of prospectivity. The effectiveness of exploration technologies can be inferred through a study of explorability.

In Part 2 of this chapter, the role of uranium exploration in the nuclear fuel cycle is illustrated. The global distribution of economic uranium resources is identified according to the certainty of their occurrence. Unconformity-related and sandstone-hosted deposits are recognized as significant sources of economic uranium deposits.

In Part 3, the exploration process is reviewed with reference to the mining production cost curve and the long lead-times required to advance from discovery to production. The conversion of significant exploration discoveries to economic mining operations is identified as an inefficient process, as have been more recent exploration investments focused on the search for new economic discoveries. Stakeholders need to be realistic in their assessment of the potential for the mining of identified resources, the expansion of existing resources, and the discovery of new resources.

In Part 4, the relationship between economic resource depletion and future discovery is examined through learning curve models for Australian and Canadian discoveries. The assessment suggests that a technological leap will be required for the discovery and development of the next generation of economic uranium deposits.

Part 5 focuses on the nature of uranium exploration cycles and uranium exploration business development with reference to the correlation of uranium sales price, exploration fund raising and exploration activities. Parts 6, 7, and 8 focus on the description of risk factors in uranium exploration. The role of prospectivity and explorability in evaluating the potential for undiscovered economic uranium resources is reviewed. The role of agencies, governments, geological survey agencies, consultants and academia in attracting investment and supporting exploration is reviewed in Part 9. In Part 10, the management of exploration is reviewed from a human and organizational perspective. Poor management can contribute to the effectiveness of uranium exploration programs. The contribution of qualitative and quantitative approaches to understanding the investment worth of uranium exploration is examined in Part 11.

The chapter ends with Part 12, describing innovative and cost-effective approaches to the assessment of geographical, geological, and technological frontiers for their economic uranium potential. A comparison of conventional and innovative and approaches is presented.

The information within this chapter will be useful to:

- Managers, consultants, researchers, and other workers in the field of uranium exploration who would like to understand their role in the development of uranium exploration programs;
- Government and geological survey organizations interested in developing programs to attract investment in the uranium exploration and mining sector;
- Any other stakeholders who would like to understand how to more effectively participate in decisions related to the management of uranium exploration and business development.

2. EXPLORATION AND THE NUCLEAR FUEL CYCLE

Uranium exploration comprises a critical activity at the front end of the nuclear fuel cycle but it is often poorly understood compared to other capital-intensive activities (Fig. 1). Exploration is a high-risk, high-reward business activity that is akin to a research-and-development process. Exploration can lead to the identification of economic mineral resources that are developed through mining. Refined metal is subsequently converted, and enriched, for fuel fabrication and the generation of electricity in nuclear power reactors.

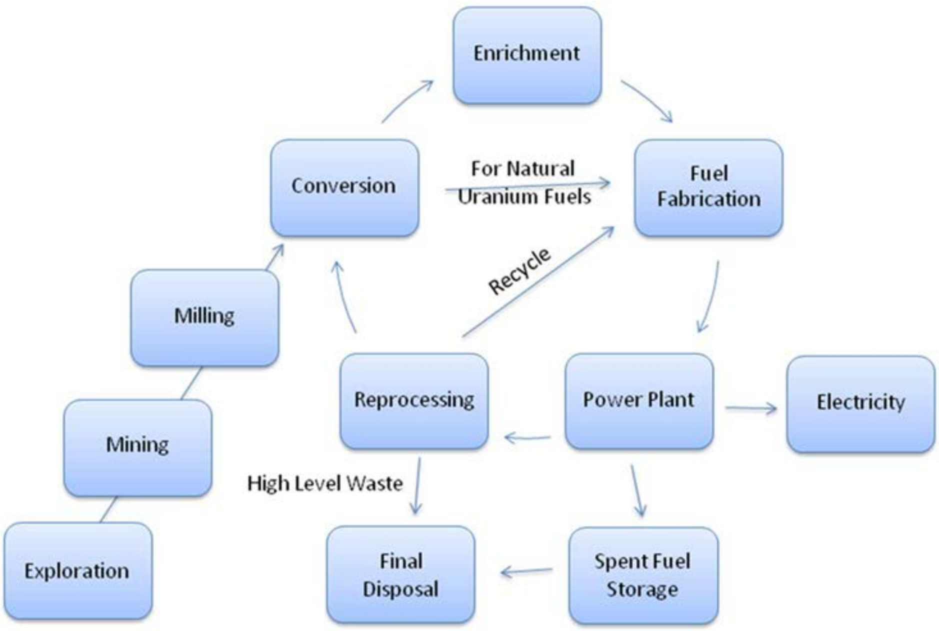

FIG. 1. Situating exploration in the nuclear fuel cycle. Adapted from [3].

The Nuclear Energy Agency (NEA) and the International Atomic Energy Agency (IAEA) co-publish a description of the global distribution of uranium resources in what is informally known as the 'Red Book'. The 'Red Book' published in 2016 indicates that the total identified (reasonably assured and inferred) resources are 5,718,400 tonnes of uranium metal (t U) in the

< US$130/kg U category. This estimate includes 3,458,400 tonnes of reasonably assured resources. Identified resources increased by only 0.1% since publication of the 2014 'Red Book'. The 2016 report attributes the lack of growth in identified resources to lower levels of investment and associated exploration activity under depressed uranium market conditions. In addition, the majority of exploration expenditures during this period were related to the development of the Cigar Lake and Husab uranium mines in Canada and Namibia, respectively. Annual global uranium production has declined by 4% since 2013, to 55,975 t U as of 1 January 2015. Current levels of production satisfy about 99% of world reactor requirements [1, 2].

Future production of uranium resources is anticipated to be more than adequate to meet the high demand case for nuclear power generation through to 2035 if mine developments proceed as planned. However, several factors could impede the production of new uranium resources including significant capital investments, a paucity of technical expertise, geopolitical risk factors, government regulations, a relatively sparse network of production facilities, and weak uranium market prices in the face of rising mining costs. In the face of these challenges, the perception of robust resource estimates available for the industry can be scrutinized to understand if more precise measures are warranted [1, 2].

The distribution of the 2014 'Red Book' uranium resources is presented in Fig. 2. The IAEA classifies resources into reasonably assured resources (RARs), inferred resources (IRs), prognosticated resources (PRs), and speculative resources (SRs), recoverable at various production cost categories. The RARs include economic, sub-economic, and uneconomic resources. The IRs include implied and unverified economic, sub-economic, and uneconomic resources. The PRs and SRs include inconsistently reported, dated, and unreliable information of limited utility. In the 2014 'Red Book', some countries have declined to report on these categories given the level of uncertainty associated with these measures. In addition, the levels of uncertainty in resource estimates are not clearly described in the IAEA classification framework.

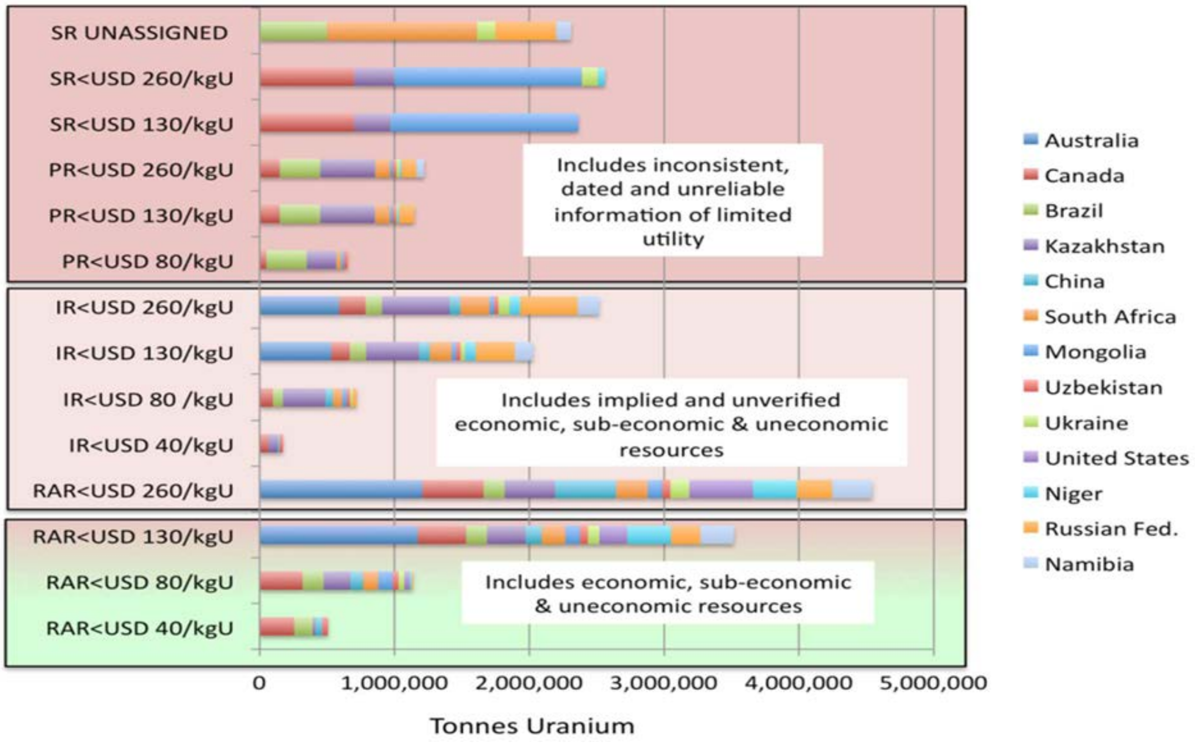

FIG. 2. Country-wise distribution of global uranium resources using data from the 'Red Book'. Adapted

from [1].
The United Nations (UN) framework classification for mineral resources (UNFC-2009) is another framework for portraying mineral resources in a tri-axial format informed by geological knowledge, project feasibility, and socio-economic viability [4]. This framework offers an alternative way to understand uranium resources (Fig. 3). Economic deposits are characterized by robust ore reserves, sound mining economics, and acceptance from environmental safeguard and social license perspectives. When the IAEA classification scheme is mapped onto the UN scheme, the IAEA SRs and PRs fall in the high uncertainty realm. The IAEA has considered the merit of the application of this framework classification to nuclear fuel resources [5].

At a fundamental level, the exploration process involves the discovery of significant indications of uranium mineralization in the geosphere through the drill testing of geological, geochemical and geophysical anomalies defined by exploration experts. Follow-up drilling programs are used to define the grade of mineralization and physical dimensions of the deposit and to collect samples for geo-metallurgical studies. Based on the results of drilling programs, the grade and tonnage of the deposit can be defined with some degree of confidence, providing one of the most important indications of the economic potential of the deposit. With an increase in geological knowledge, one aspect of the risk associated with the economic viability of developing the deposit into a mine is reduced.

Reducing the economic uncertainty from a mining project feasibility, social license, and sustainable development perspective, is a complimentary objective to ore deposit definition. Information on the establishment of uranium mining operations in the context of sustainable development can be found in [6].

Countries that have a significant amount of reasonably assured uranium resources are illustrated in Fig. 4. The 2014 “Red Book” indicates that Australia ceased to report resources at <US$80/kg U pointing to a trend away from the lower cost production category previously reported. A significant portion of Australia’s resource base is drawn from by-product uranium resources indicated at the Olympic Dam copper deposit.

Global reasonably assured uranium resources by production method are illustrated in Fig. 5. Open-pit mining, underground mining, and in-situ acid leach mining are leading methods. A future emphasis on the in-situ-recovery (ISR) method, as a lower cost mode of production for sandstone-hosted uranium deposits, is indicated. Methods of exploitation of different types of uranium deposits are described in [7].

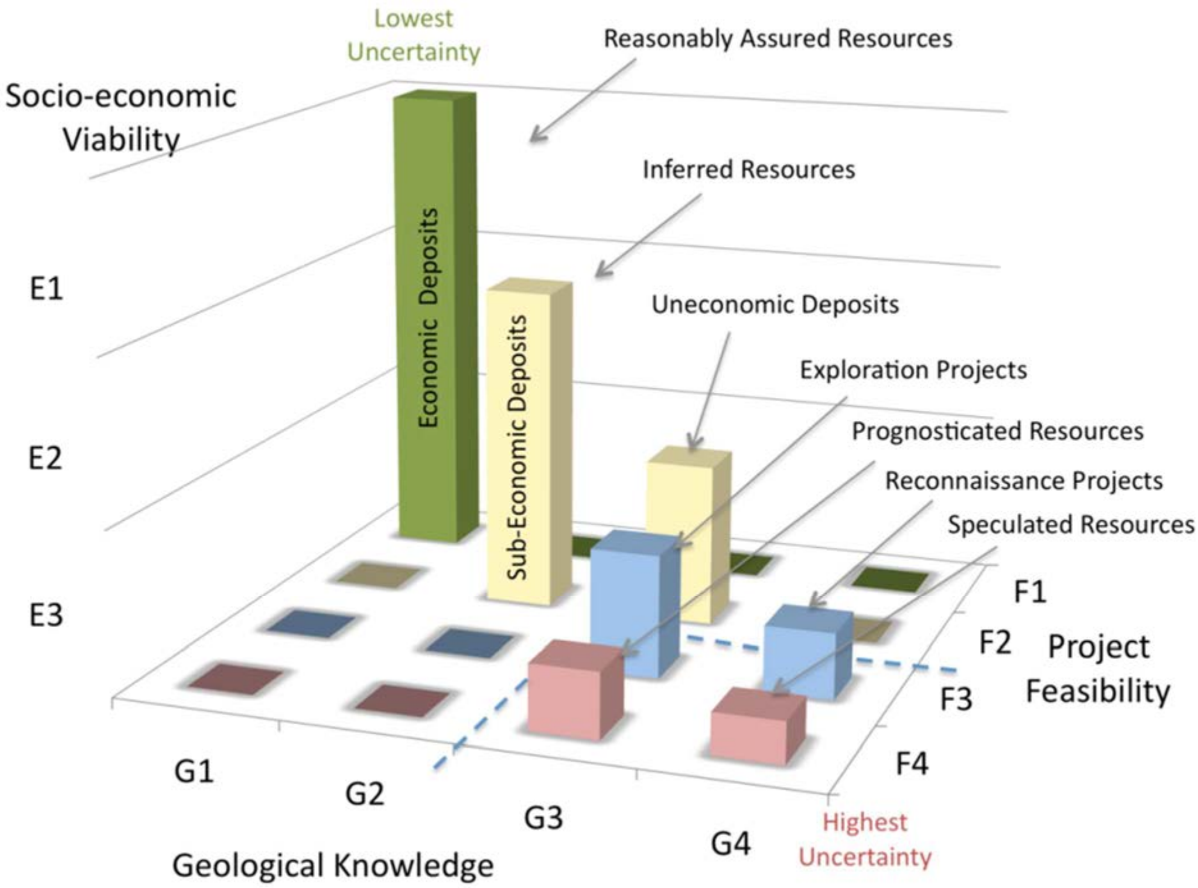

FIG. 3. United Nations framework classification for resources. Adapted from [3].

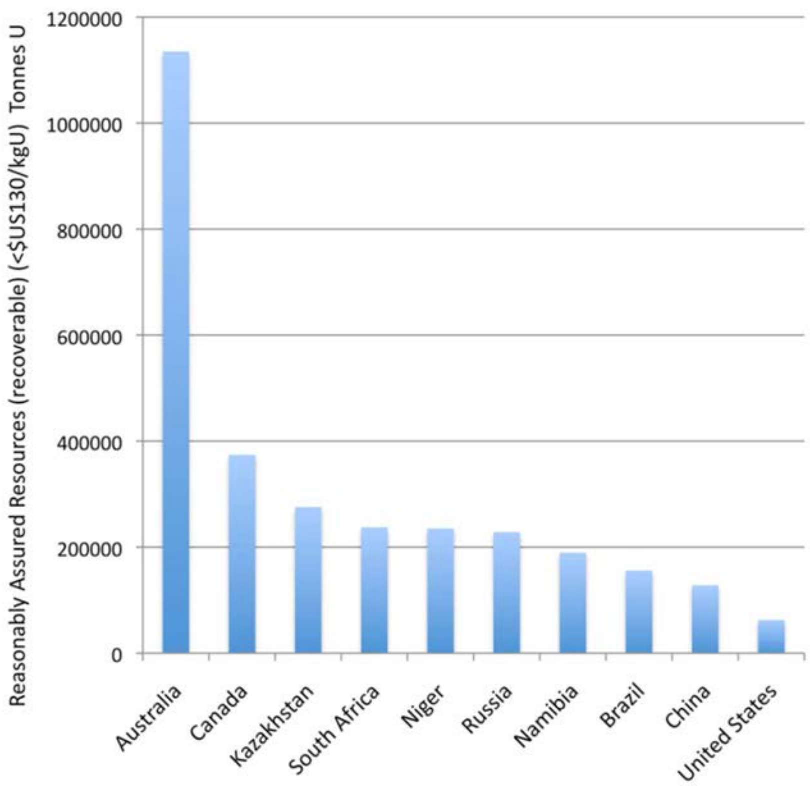

FIG. 4. Reasonably assured uranium resources by countries with significant resources. After [2].

Global reasonably assured uranium resources by deposit type are illustrated in Fig. 6. The RARs are dominated by the sandstone-hosted and unconformity-related deposit types; with a large contribution from the Olympic Dam iron-oxide breccia type deposit. Sandstone-hosted deposits contribute the largest proportion of inferred resources [1]. Uranium deposit types are described by [8] and [9].An historical profile of the world uranium industry between 1965 and 2004 is presented in the 'Red Book Retrospective' report [10], which includes an assessment of uranium resources, exploration, and production. Data related to this publication were updated to include information from more recent 'Red Book' publications, up to and including the 2016 report (Figs 7–9).

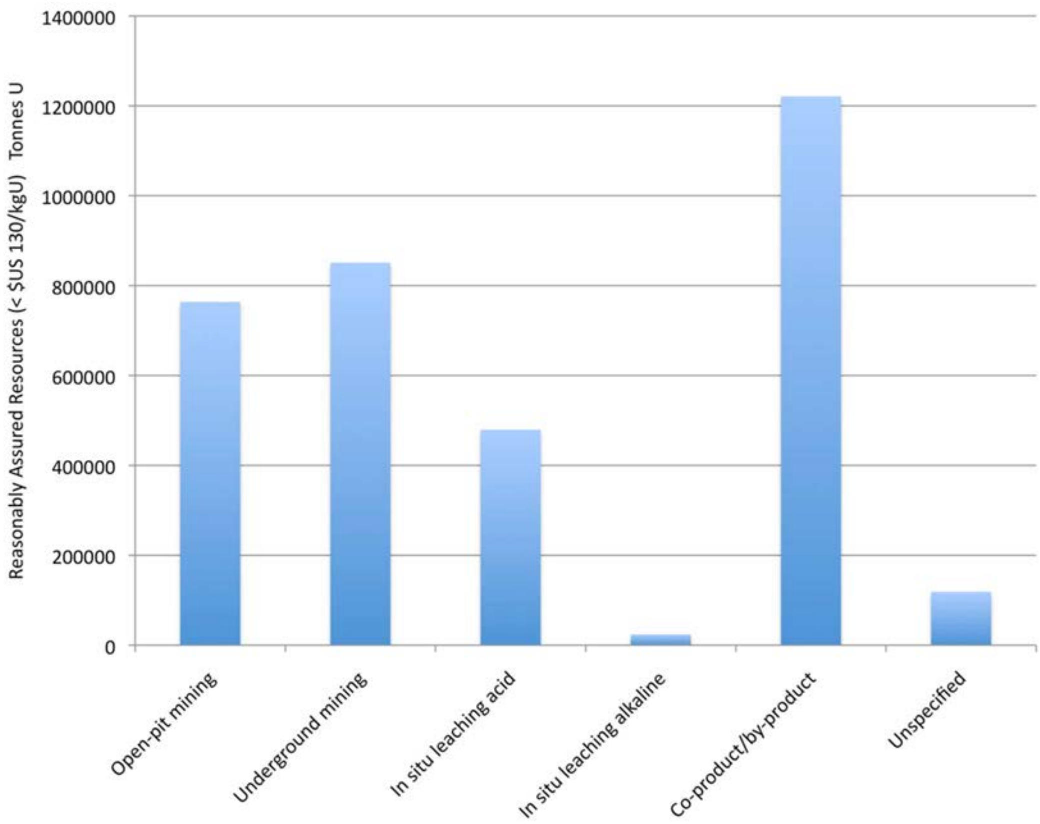

FIG. 5. Reasonably assured uranium resources by production method. After [2].

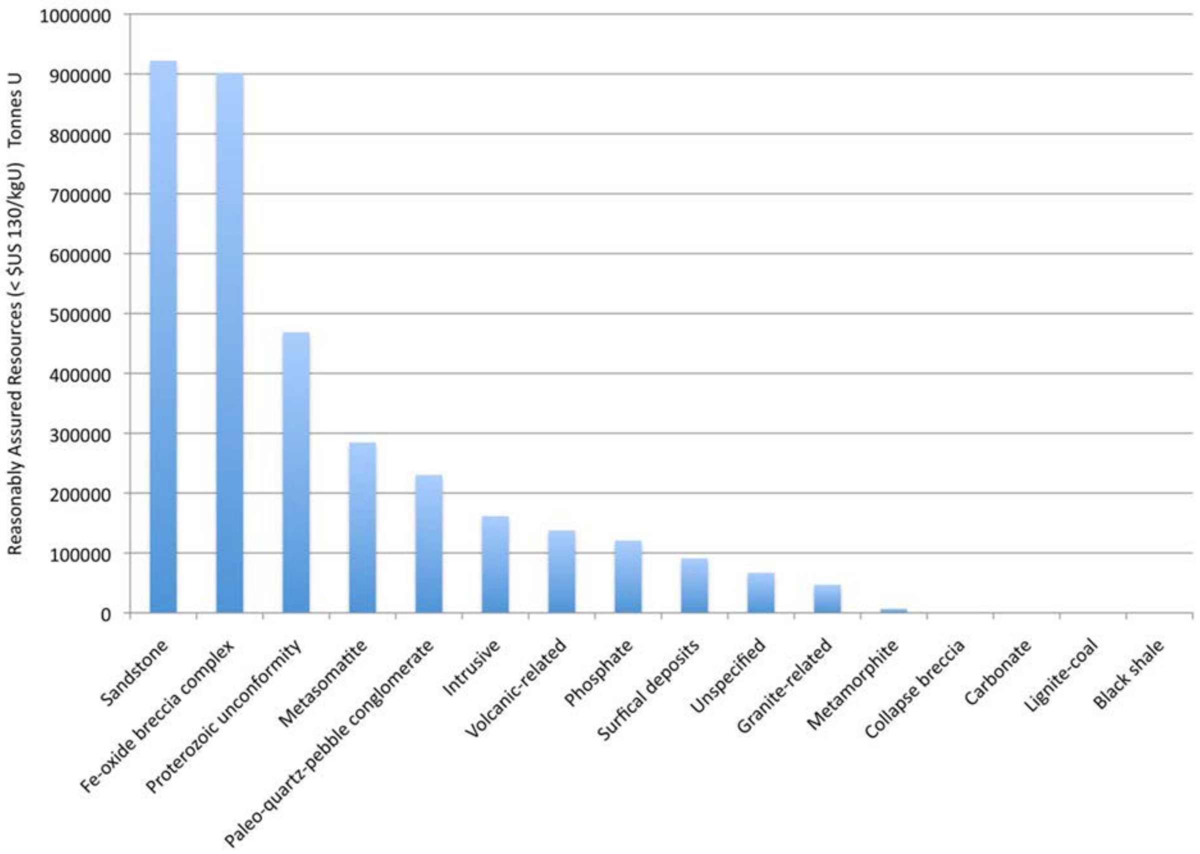

FIG. 6. Reasonably assured uranium resources by deposit type. After [2].

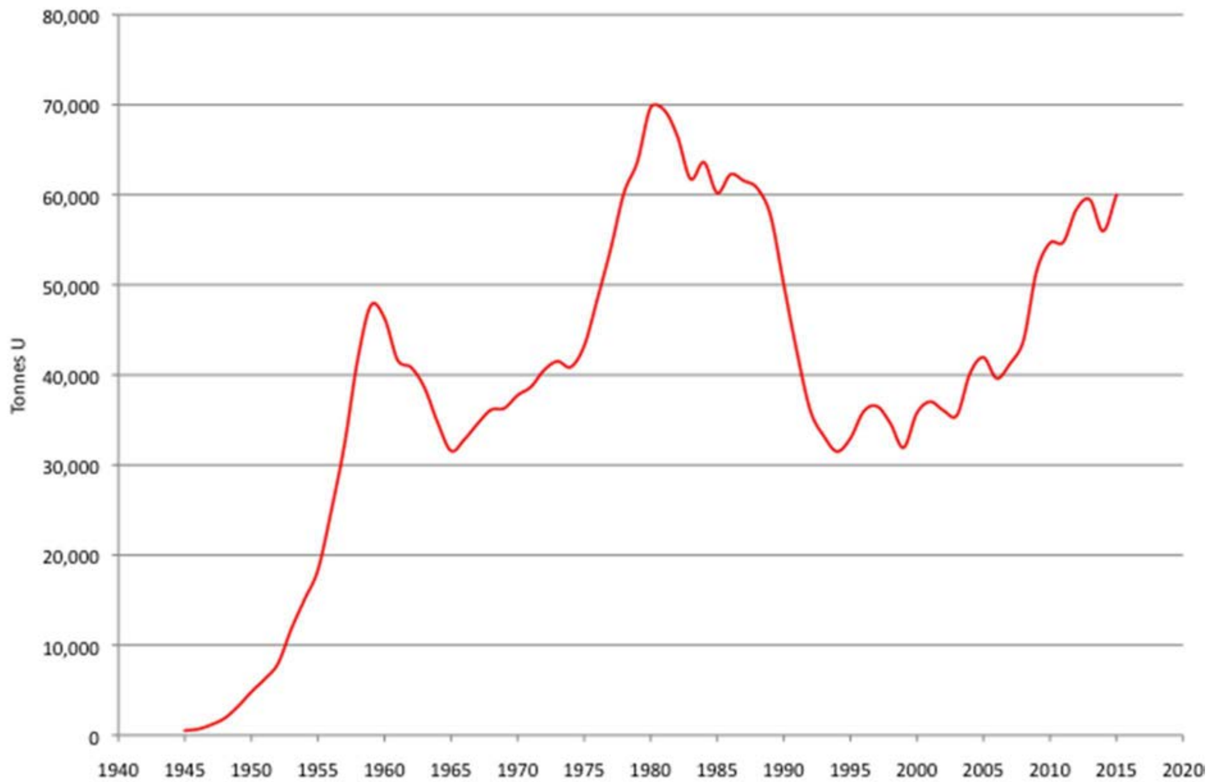

FIG. 7. Global uranium production (1945–2015).

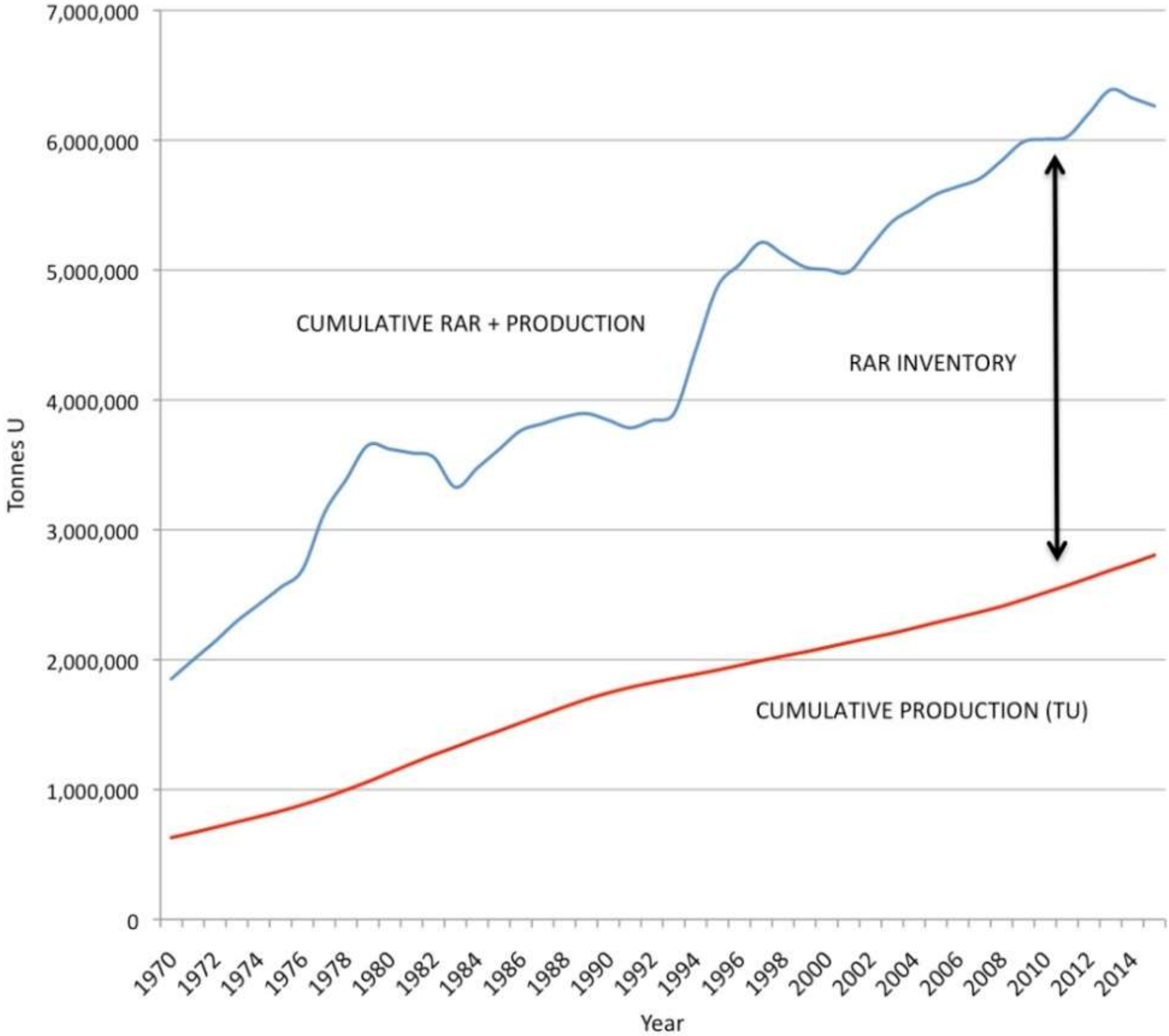

FIG. 8. Global cumulative historical uranium production and historical cumulative reasonably assured resources (US$<130/kg U) 1970–2015.

Historical annual global production of uranium (1945-2016) reached a peak of ~70,000 t U around 1980, decreased to ~30,000 t U around 1995, and recovered to current levels of ~60,000 t U (Fig. 7).

The historical inventory of global recoverable reasonably assured uranium resources (< US$130 kg U) including the production of uranium is estimated to be 6,263,532 t U as of 2015 (Fig. 8). The total historical global production of uranium is estimated to be 2,805,132 t U. This leaves an inventory of recoverable RAR (<US$130 kg U) available for production of 3,458,400 t U (2015). It is unlikely that all of these resources will be ultimately mined and that actual production levels will be lower. The extrapolation of statistics for Canadian and Australian uranium deposits (presented in Part 3) suggests that less than one half of these RARs will be converted to production (< 1,729,000 t U). This is equivalent to ~30 years of production from reasonably assured resources at a rate of ~60,000 t U/year.

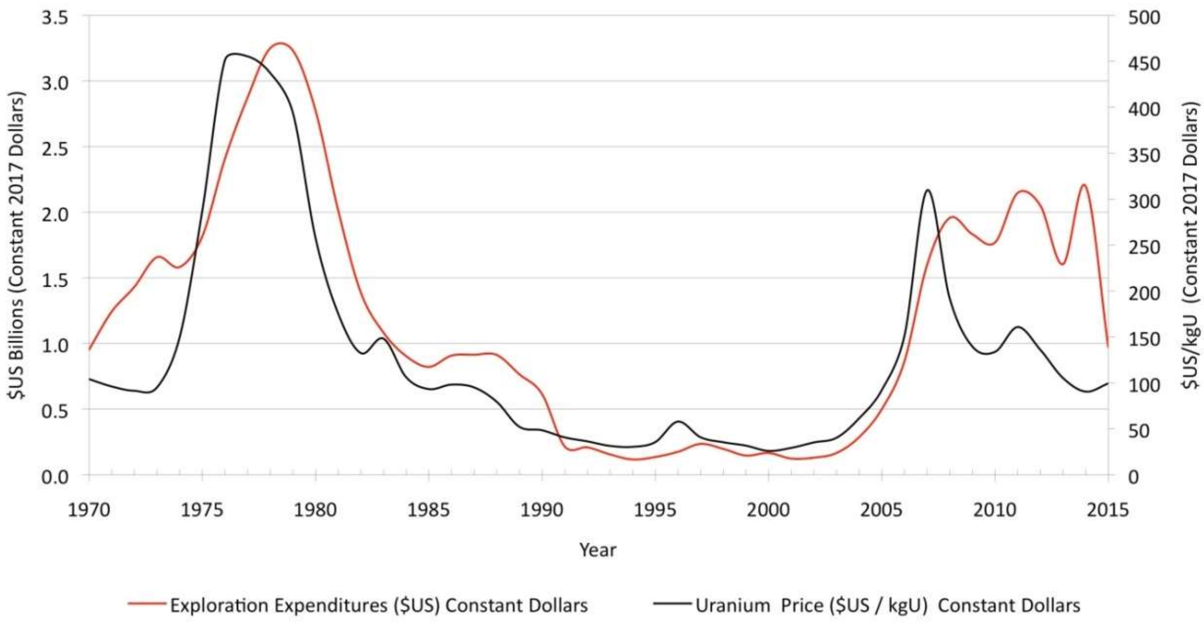

FIG. 9. Global uranium exploration expenditures and uranium price (constant 2017 dollars) 1970–2015.

Annual global uranium exploration expenditures reached levels of over US$3 billion around 1976, declined to less than US$500 million during the 1990's, recovered to around US$2 billion starting in 2007, and as of 2016 are in decline (Fig. 9). Levels are reported in constant 2017 dollars. Uranium exploration expenditure is sympathetic to the price of uranium. Total global uranium exploration expenditures from 1970-2015 are estimated to be US$53.5 billion (constant dollars). About 4,410,991 t U of RARs (< US$130/kg U) were added to the world inventory from 1970-2015 at an estimated cost of > US$12.13/kg U (equivalent to > US$4.66/lb U_3O_8).

A global uranium exploration learning curve for RARs (< US$130/kg U) was developed based upon updated data related to the 'Red Book Retrospective' to provide additional insight into the efficiency of the historical uranium exploration process (Fig. 10). A learning curve is a mathematical model that correlates learning with experience. Learning was defined as the cumulative identification of RAR (including historical production) and was correlated with experience (the effort to identify these resources) recorded as cumulative exploration expenditure. The data was plotted graphically and modeled as two logistic functions (learning curves) that map an exponential rise to a limit. The limit is of critical interest as it defines the maximum RAR that can be anticipated on each learning curve, given exploration expenditure.

For the global exploration learning curve, the shift from the first to the second learning curve is demarcated by an 'innovation' (Fig. 10). The 'innovation' is primarily attributed in the introduction of Russian resources and Kazakhstan ISR amenable resources to the 'Red Book' inventory in the mid-1990's following the dissolution of the Soviet Union. For other cases presented in Part 4, 'innovation' can be attributed to the adoption of a new technology. Another disruptive 'innovation' will be required to take the industry to a third learning curve.

For the current interpretation the shift to the second global exploration learning curve is interpreted to demarcate the ISR dominant mining era from the conventional mining era. Although the data is sparse, the limit of the second global learning curve is postulated to occur (conservatively) at around 7,000,000 t U. This estimate suggests that < 750,000 t U RAR is available for exploitation on the second learning curve given additional exploration expenditure. Incorporating this estimate into the overall analysis suggests that <35 years of production of RAR (< US$130/kg U) remains available for the industry assuming a RAR to production conversion rate of <50% and annual production of 60,000 t U.

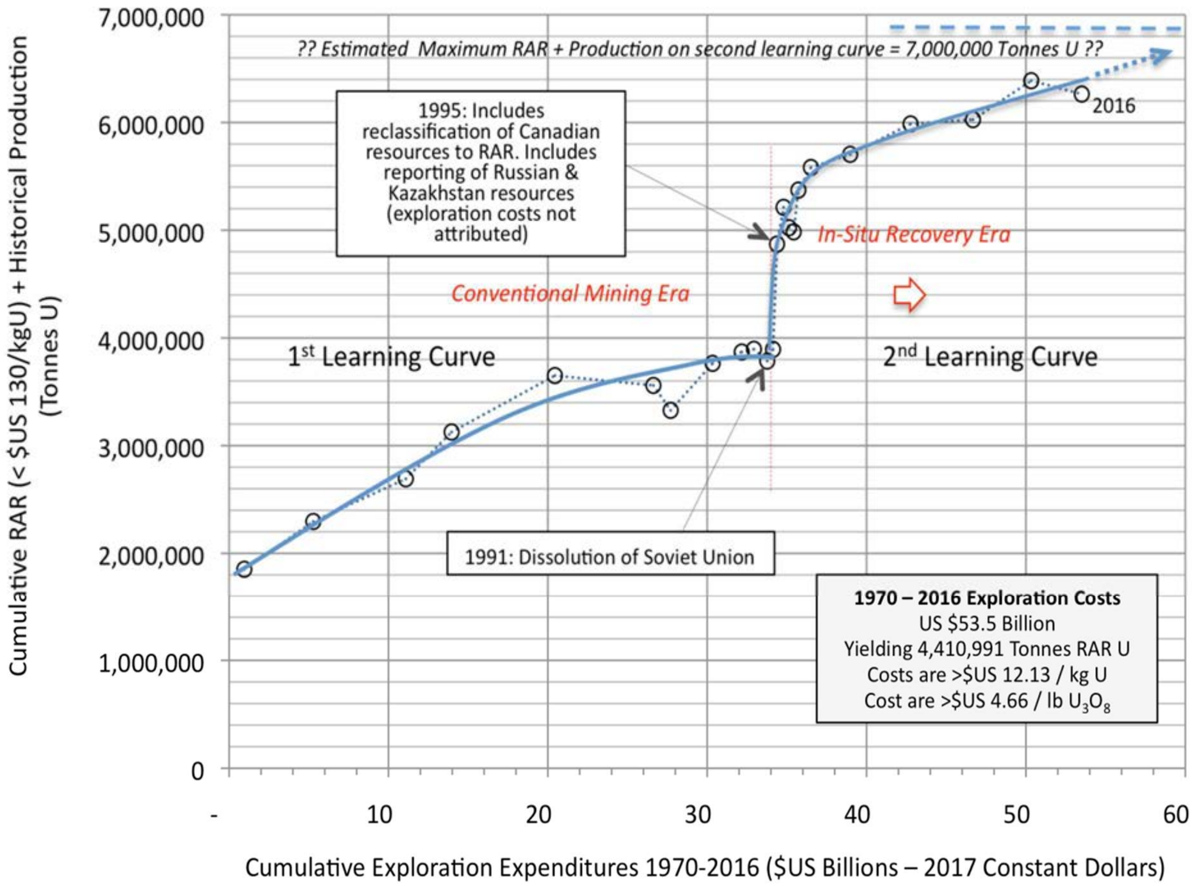

FIG. 10. Global learning curve for reasonably assured resources (US$<130/kg U).

The preceding analysis represents a contrarian view, suggesting the possibility of a constraint on the availability of RARs (< US$130/kg U) for the nuclear industry in the mid-term. This constraint also points to the utility of ongoing investment in exploration and innovative technologies to ensure the availability of future RARs. More conventional logic accepts that higher cost RARs and IRs will be brought into production to mediate any potential production shortfall. Market conditions, relatively low conversion rates of existing RARs to production, the quality of resources (grade and tonnage), increasing long time frames to bring RARs into production, and the many social, political, environmental, and economic factors that constrain development point to many risk factors associated with resource development. The analysis of future ‘Red Book’ data should continue with the goal of developing a robust model of the second learning curve. The quantitative modeling of the probability of identifying RAR given future exploration effort (expenditure) is a goal.

3. THE EXPLORATION PROCESS

Uranium exploration is a business activity that is focused on identifying economic concentrations of mineralization that can be economically exploited through mining. Exploration begins with an evaluation of the investment worth of conducting exploration within a particular political jurisdiction and geographical area. This includes desktop study of historical, geological, and other technical information. A technical objective is the identification of the potential for the occurrence of economic concentrations of uranium within the geological setting under investigation. Another objective is the selection of suitable exploration technologies.

Once a geographical area has been selected, field programs are designed relying on well-known geological, geochemical, geophysical exploration methods [11]. These programs can be conducted over a decade or longer depending upon results. The programs typically involve both regional and detailed exploration components and culminate in the drill testing of promising targets. On rare occasions, economic concentrations of uranium mineralization are encountered and some of these discoveries are developed into ore bodies through more intensive follow-up work. Descriptions of the exploration process and exploration methods can be found in [12].

The typical exploration process is depicted in Fig. 11. Following research and the selection of a project area, exploration moves from regional or reconnaissance surveys, to detailed exploration follow-up, and culminates in drill testing. It is estimated that approximately one in 1,000 exploration projects will lead to the discovery of an economic uranium deposit, and that the probability of success is one in three, that these projects will advance through the feasibility study to the mining stage.

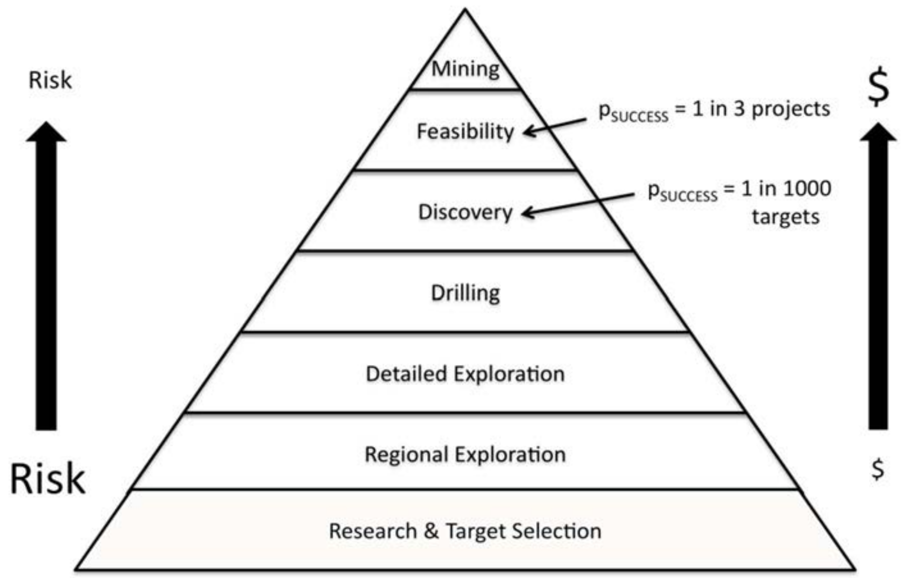

FIG. 11. The exploration process.

Expenditures increase from the exploration to mining stage as the program advances from project generation through to exploration, discovery, and beyond. Pre-development, development, production, and ultimately decommissioning phases associated with mining involve larger investments (Fig. 12).

The sequence of uranium project generation, exploration, discovery, evaluation of deposits to determine their economic viability, and mining project development, involves increasing levels of expenditure and decreasing levels of investment risk. A return on investment is realized only after production starts and after lead times that can be decades long. Upon depletion of a mine's uranium reserves, additional costs are associated with reclamation and environmental monitoring.

The economic viability of uranium deposits depends upon many factors at the mining stage. Some of these factors are ranked in a survey by [14]. Risks associated with the definition of economic reserves, political and country risk, social and environmental risk, metal price, and operating costs are identified as being more significant (Fig. 13).

The world's lowest cost primary uranium producers can be found in the in-situ-acid-recovery amenable sandstone-hosted roll-front uranium deposits of Kazakhstan, and the unconformity-related uranium deposits of Saskatchewan. The long-term viability of producing mines can be impacted by depressed fuel prices leading to the curtailing of production, mine closure, the deferral of mining developments, and the deferral of investments in uranium exploration.

The economic viability of uranium mining operations is related to the sales price of uranium. A uranium production cost curve is presented in Fig. 14. Producing mines are illustrated by geological deposit type relative to short- and long-term uranium fuel price indicators. A global annual uranium production capacity of ~80 million pounds U_3O_8 (~30,000 t U) is available at < US$30/lb, and ~120 million pounds U_3O_8 (~45,000 t U) is available at < US$40/lb [15].

The economic viability of uranium deposits discovered through the exploration process is dictated by uranium grade, and tonnage, among many other factors previously depicted in Fig. 13. To illustrate this, the size distribution of primary Australian and Canadian uranium deposits by contained uranium, is presented in Fig. 15.

Many deposits may never meet an economic size threshold considering the uranium sales price, and social, and political factors. Examples include the sub-economic Kintyre and Millennium deposits, which appear to be sub-economic at current price, based upon public announcements. These deposits provide a rule-of-thumb for a deposit size threshold that economic deposits must exceed. Another example includes the mature Rabbit Lake mine, which closed in response to the depressed uranium market. Another example relates to the challenges associated with committing to mine expansion at Ranger concomitant with low sales price and the timing of the extension of mining agreements.

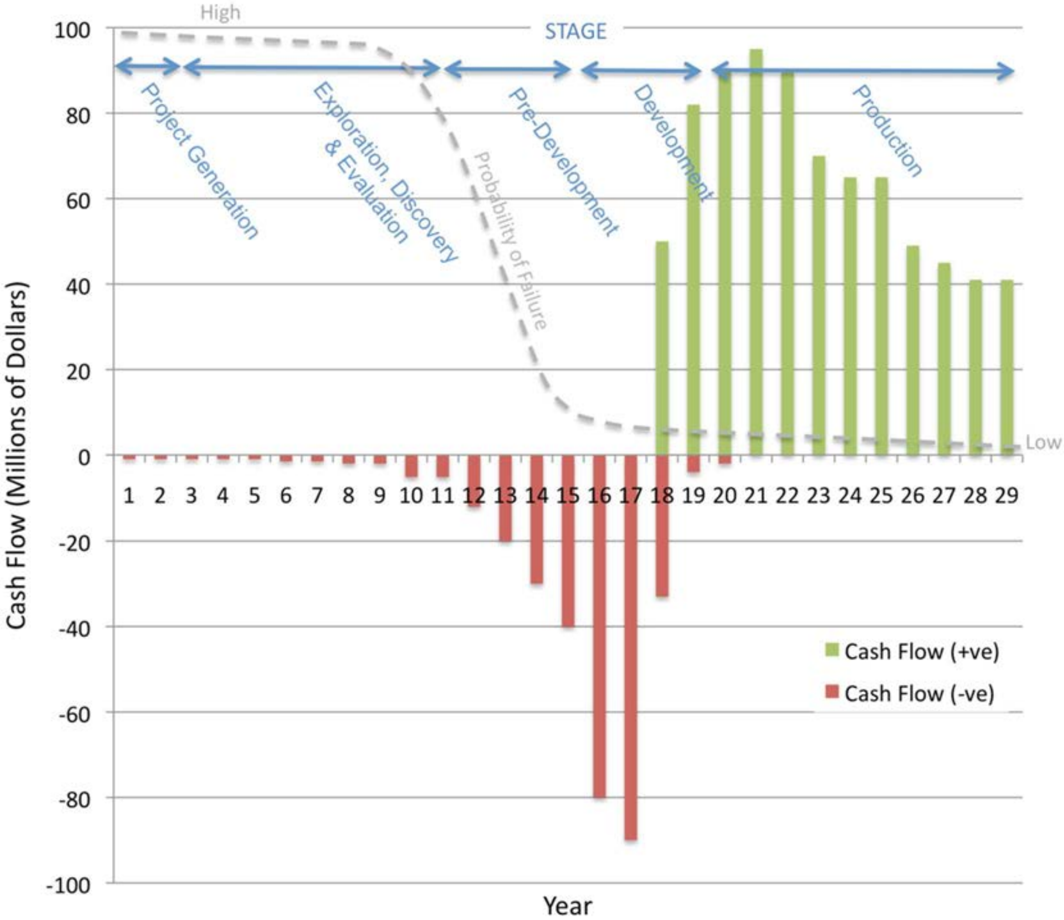

FIG. 12. Hypothetical cash flow linked with exploration and mining development. After [13].

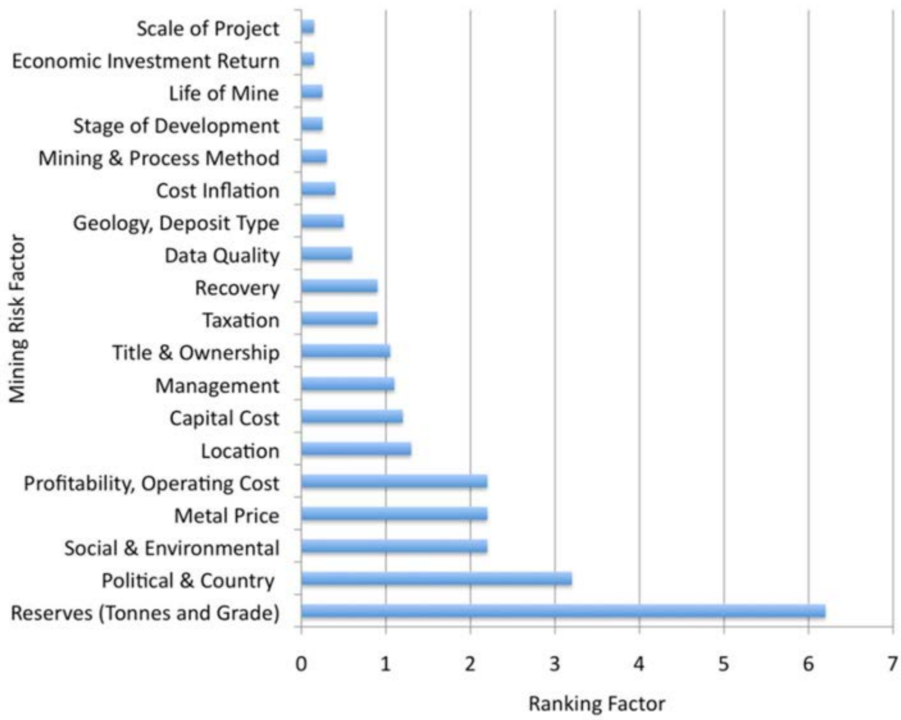

FIG. 13. Ranking of principal mining project risks. After [14].

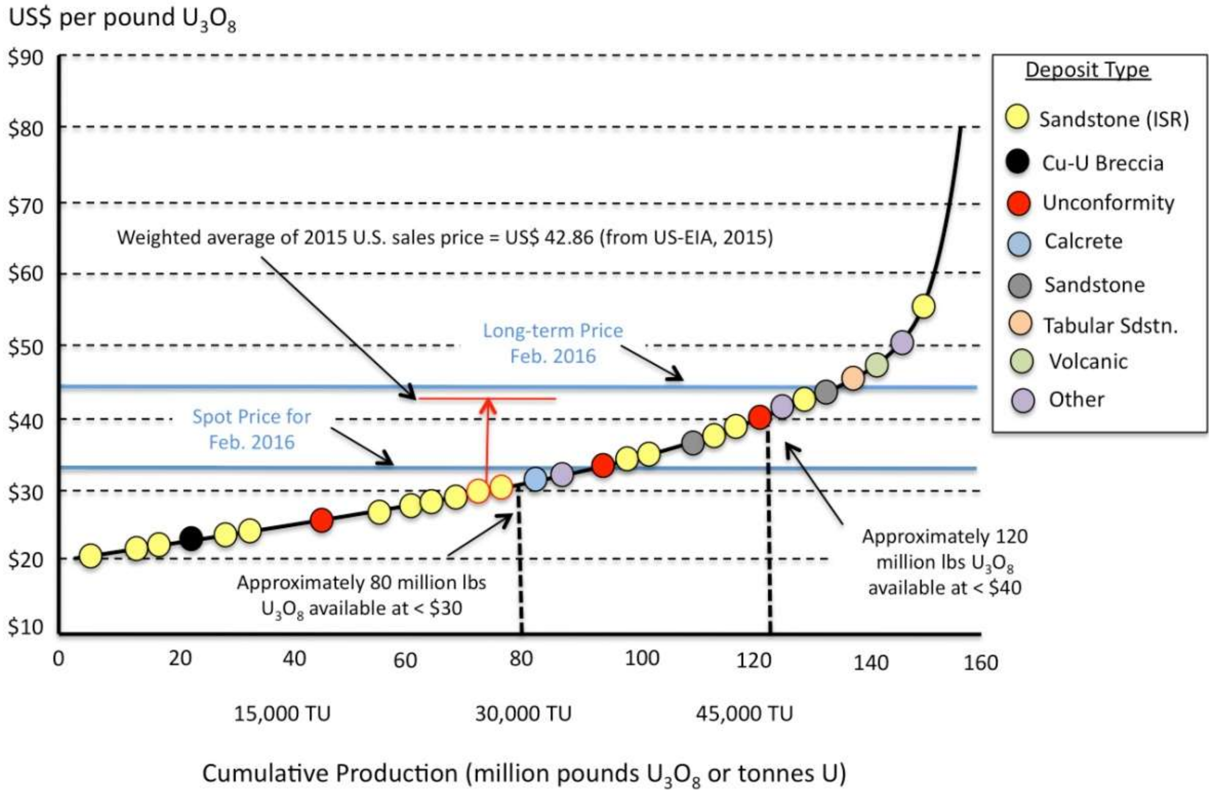

FIG. 14. Uranium mining production cost curve. After [15–17].

In Australia, the inclusion of the Koongarra deposit into the Kakadu National Park means that it may never be developed. This is an example of sovereign risk that has contributed to the withdrawal of uranium exploration and mining investments from the region. The Quebec government moratorium on uranium development is a similar example. Jabiluka, one of the world's largest undeveloped uranium deposits, was discovered in 1971. It has been on long-term care and maintenance for many years due to socio–political factors. Fig. 16 is an illustration of the time from discovery to production for significant Canadian and Australian [18] uranium deposits. The time to production ranges up to 33 years for economic deposits. Many of the other deposits classified in the sub-economic category have been inventoried for over 30 years to over 60 years, despite significant expenditures to expand resources by successive exploration and mining companies. The large 'economic' Jabiluka uranium deposit is also represented in this category. The statistics for Canadian and Australian deposits indicate that less than one half of the significant deposits that have been discovered have been brought into production (Fig. 17).

The IAEA World Distribution of Uranium Deposit Database (UDEPO) is an inventory of the global distribution of uranium deposits [19]. An estimate of the number of economic uranium deposits suggested by their size threshold is presented in Fig. 18. While recognizing that the UDEPO database also includes information on mined out deposits, ~37 economic deposits exist assuming a rule-of-thumb economic cut-off of 50,000 t U. Assuming that one-half of these deposits will be producers, this analysis yields ~30 deposits in this category, or ~2% of the global inventory of deposits.

A comparison of success rates for uranium exploration in the Athabasca Basin and for the USA manufacturing sector is presented in Table 1 for added clarity, where ~100 uranium showings have resulted in one economic discovery [18]. Uranium exploration can be compared to any other research-and-development activity, with comparable rates of conversion of concepts to economic outcomes.

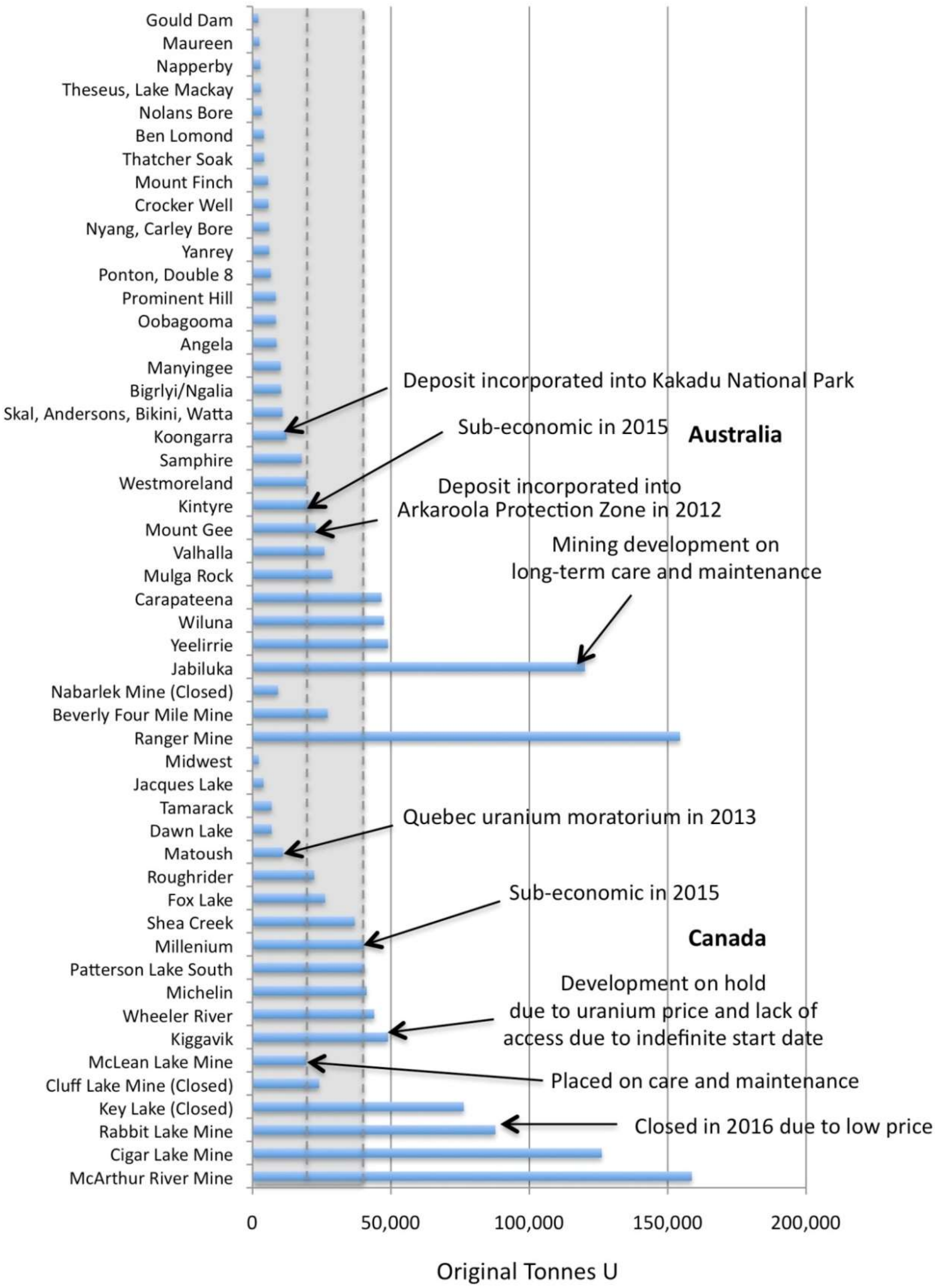

FIG. 15. Status and size distribution of uranium deposits in Australia and Canada. Australia size data from [18]. 'Sub-economic' deposits fall in gray shaded area.

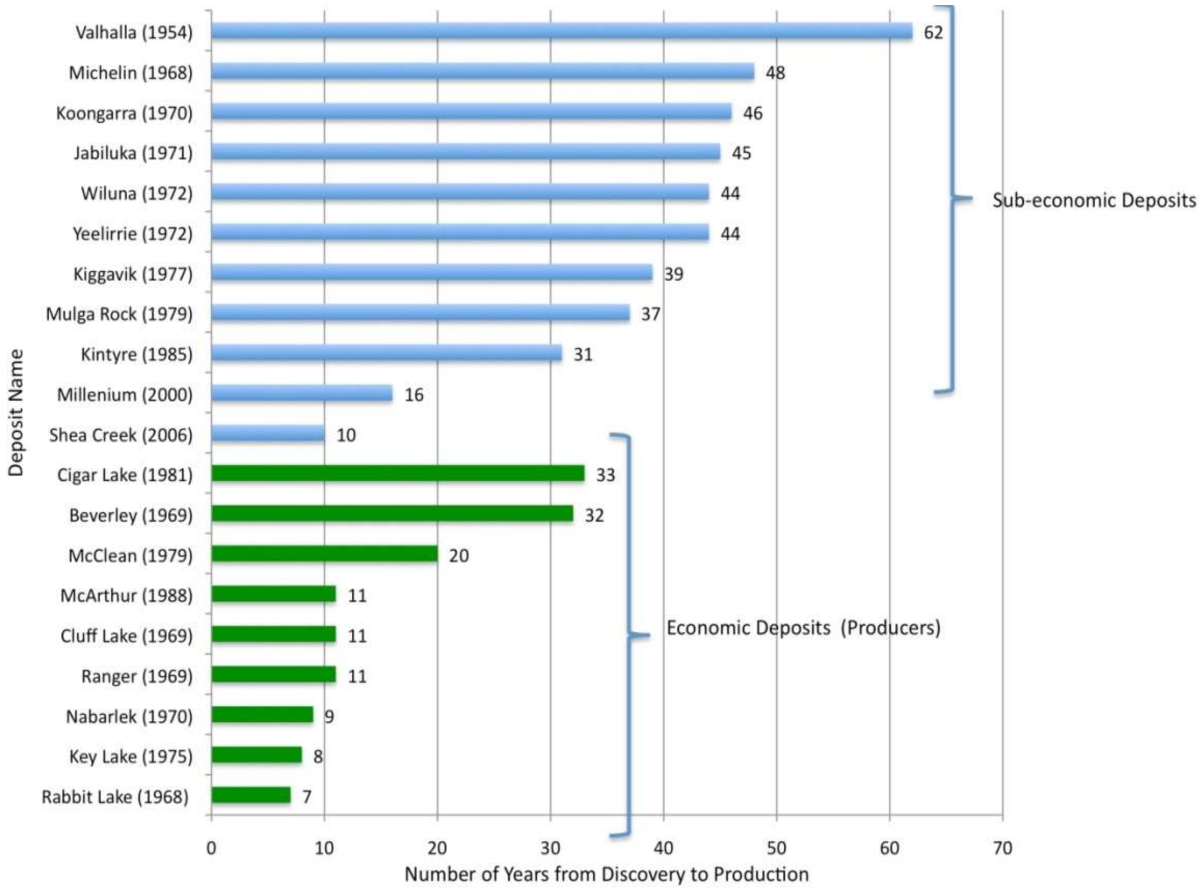

FIG. 16. Number of years from discovery to production for selected Australian and Canadian uranium deposits. Australian data from [18].

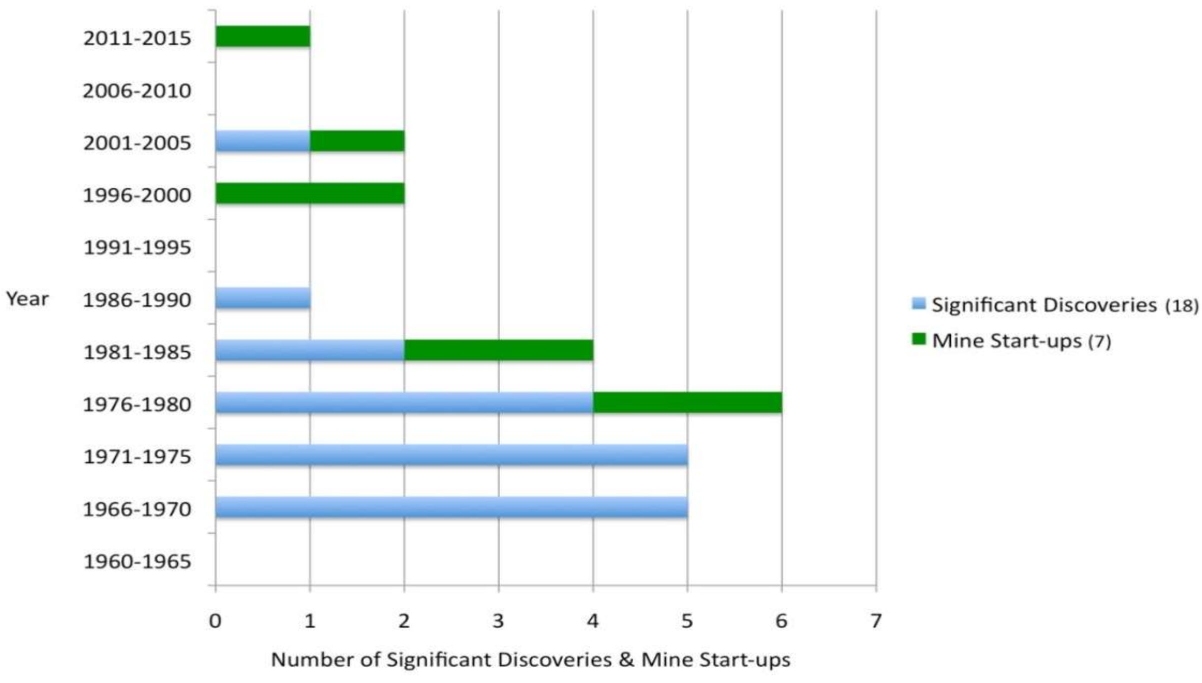

FIG. 17. Conversion of significant discoveries to mines for Australian and Canadian uranium deposits.

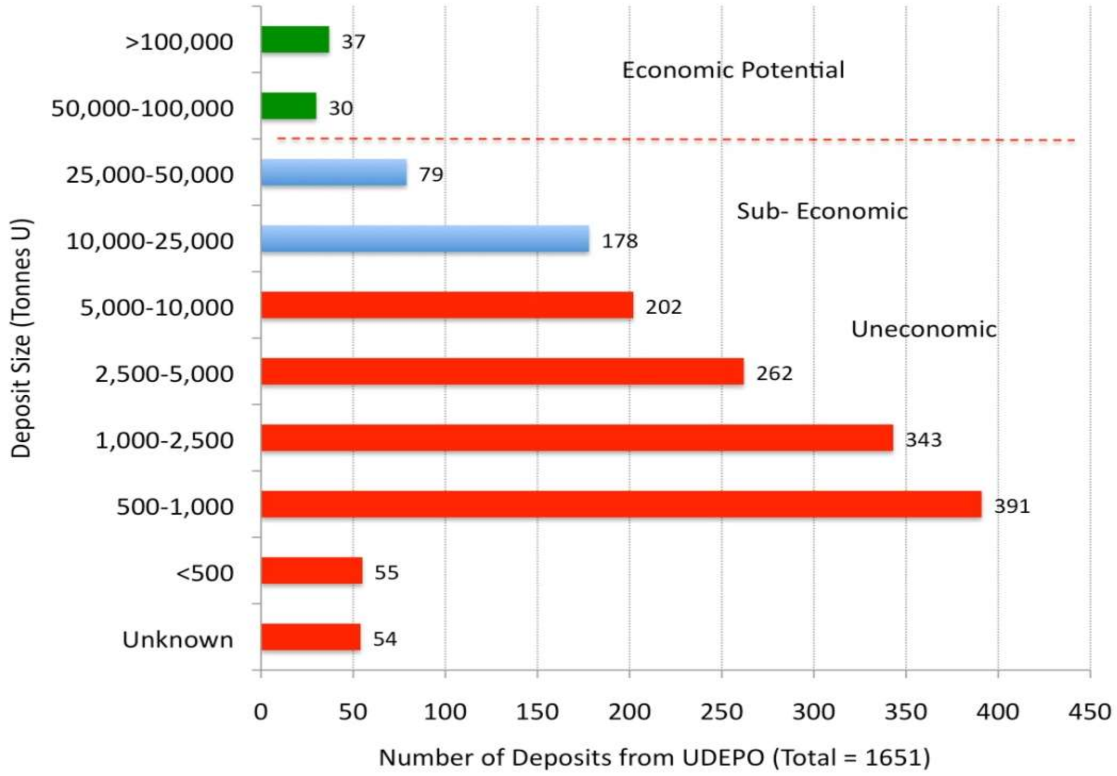

FIG. 18. Estimated number of uranium deposits in the world with economic potential based on size. Data from [19].

TABLE 1: COMPARISON OF USA MANUFACTURING SUCCESS RATES WITH ATHABASCA BASIN DISCOVERY RATES (USA MANUFACTURING DATA FROM [20]. ATHABASCA DISCOVERY RATES AFTER [21])

USA Manufacturing 1 in 3,000 success rate		Athabasca Basin 1 in 10,000 success rate	
Raw ideas	3000	Conceptual drill targets and	10000
Ideas submitted	300	Reconnaissance drill targets	1000
Small projects	125	Showings	100
Significant development	9	Advanced projects	10
Major development	4	Prefeasibility	3
Launches	1.7	Feasibility	1.5
Commercial success	1	Economic deposits	1

4. ECONOMIC RESOURCE DEPLETION AND FUTURE DISCOVERY

The availability of uranium resources will not impede the nuclear power industry for the foreseeable future [22]. Economic uranium resources will be continuously replenished through new discoveries or by moving existing deposits into economic categories. Replenishment occurs in response to supply and demand, price, new exploration and mining technologies, the development of new deposit models [21, 23], and substitution among other factors [24]. Some of the mechanisms that inform the process of replenishing the pool of economic deposits from an exploration perspective are described below.

A core activity of exploration program management involves reducing exploration discovery risk and slowing the rise in average discovery costs that are typically realized as an exploration area matures. This can be achieved through the application of knowledge that equates to the development of innovative approaches to exploration management.

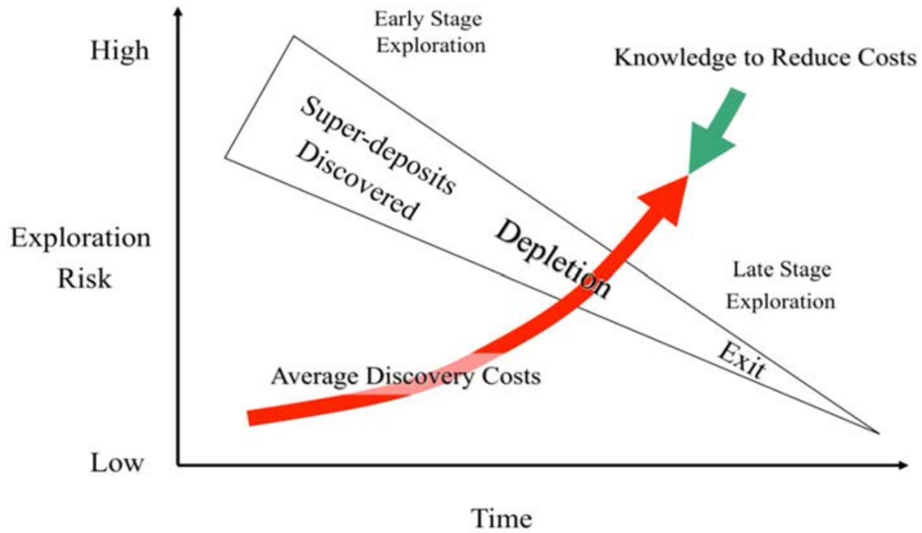

FIG. 19. Relationship of exploration risk of failure, average discovery costs, and time linked with exploration.

Economic uranium mineral resource depletion relates to the fact that there are only so many economic deposits available in the natural environment to be discovered. After each economic discovery, the number of available economic deposits is reduced (depleted).

The history of exploration also suggests that in a virgin geological setting that is prospective for economic uranium deposits, large economic deposits will typically be discovered earlier in the exploration process than later. The risk of failure of an exploration program at this stage in a fertile environment is relatively lower, compared to a mature exploration play that has received intense exploration effort over time (Fig. 19).

Average discovery costs will also increase with time as the probability of economic discovery decreases. At some time in the history of the exploration region, the discovery rate will become so low that explorers will abandon exploration and invest in other project areas. Innovations in exploration geophysics and geochemistry have contributed to extending the life of exploration regions in some instances.

The relationship between exploration effort, the quantum of economic discovery, and the role of technology in reaching discovery can be understood through a model know as the ‘learning curve.’ A learning curve can be developed for an exploration region where economic deposits have been discovered and where the history of exploration expenditure, or other measures of effort, has been documented. The curve is constructed by plotting the cumulative exploration expenditure versus cumulative discovery of economic uranium. It is also possible to predict the magnitude of future discovery given future exploration expenditure using this model.

A learning curve for Canada's Athabasca Basin is illustrated in Fig. 20, based upon prior work [25]. An analysis of the learning curve suggests that the basin has experienced two periods of exploration correlated with a prospector-driven, and a deposit model-driven technology phase. Large high-grade deposits were discovered earlier in the history of each cycle. The absence of discoveries on the second learning curve, given more recent expenditure, suggests that a technological breakthrough will be required to drive future economic discovery. That is, future discoveries will likely occur on a third learning curve. Reliance on existing modes of exploration will not likely be efficient or effective. A discussion of the Athabasca learning curve can be found in [21].

A learning curve for 'economic' uranium deposits discovered in Australia is depicted in Fig. 21. Seven deposits discovered during 1969–1985 define the curve. The Olympic Dam deposit is excluded from this analysis. Over 3.5 billion dollars was spent on uranium exploration across Australia during 1967–2015, yielding ~400,000 t U. One-half of that resource is reasonably assumed to be mineable at this time due to the marginal nature of economics or political constraints. The Kintyre deposit is included in the analysis even though it was discovered during a diamond exploration program. Less than one-half of the deposits have reached production.

The Australian learning curve is analogous to the first learning curve for the Athabasca Basin that was similarly dominated by prospector discoveries using radiometric exploration methods. The absence of discoveries in response to more recent expenditure (and the long-time frame since the last discovery) suggests that the current technology is not effective and that additional discoveries using this technology will be limited. Additional exploration using the current technology will be a value-destroying activity. The learning curve analysis is a call for innovation for new discoveries on a second learning curve.

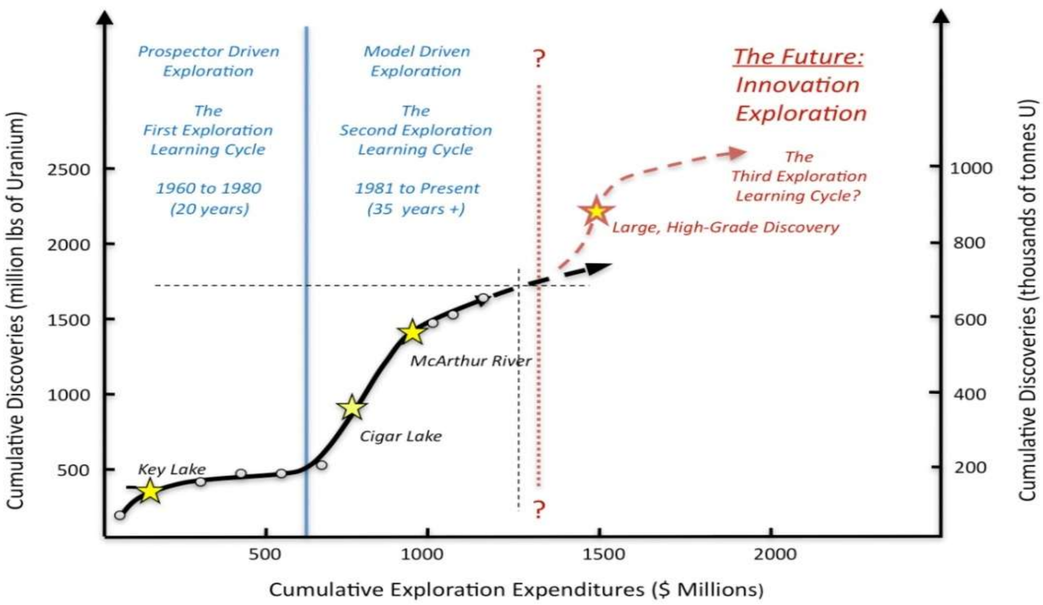

FIG. 20. Athabasca Basin learning curve for the discovery of economic uranium deposits (constant dollars). Adapted from [21].

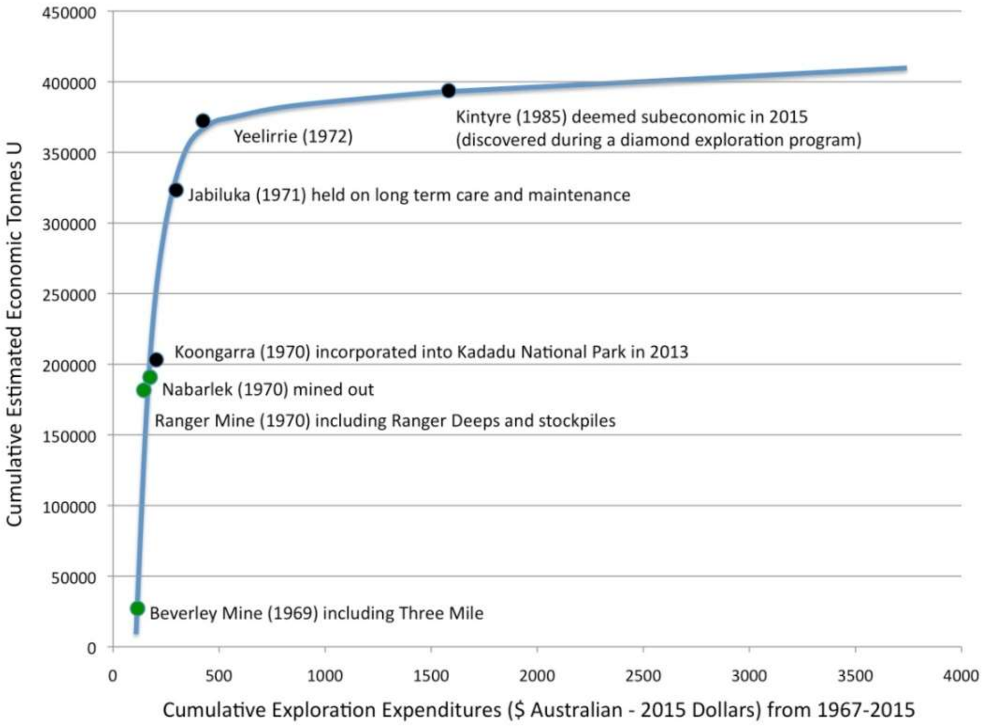

FIG. 21. Australia learning curve for the discovery of economic uranium deposits (excluding Olympic Dam). Based on data from [18] and [26].

An assessment of the impact of exploration expenditures on the frequency of Australian economic uranium resource discoveries supports the learning curve analysis (Fig. 22). More recent exploration expenditures have not resulted in new economic discoveries, and economic and geopolitical factors have likely removed significant resources from the pool of deposits that will reach production.

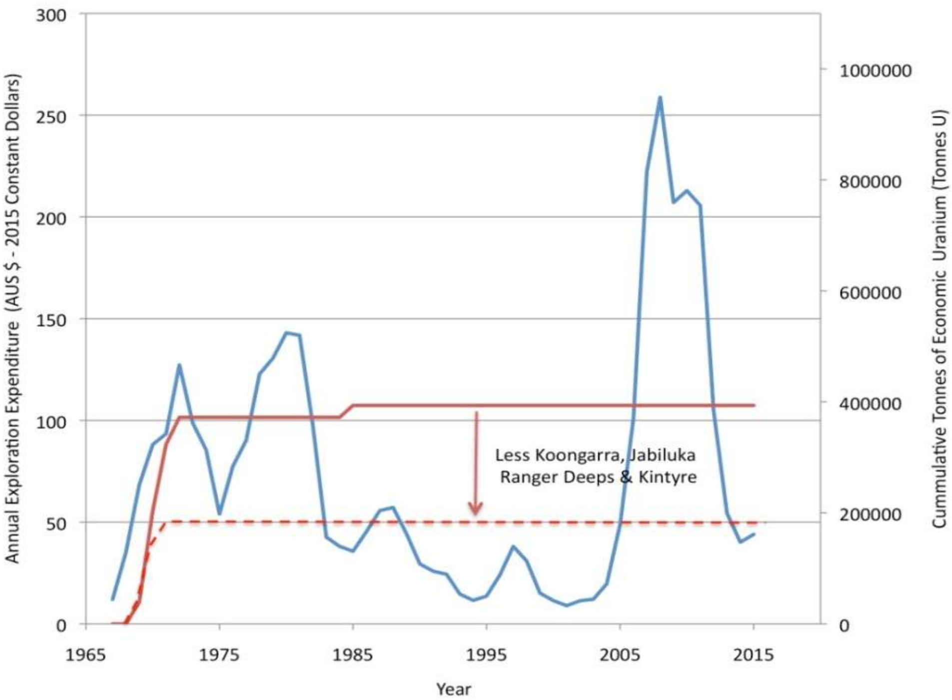

FIG. 22. Impact of exploration expenditures on the frequency of Australian economic uranium resource discovery. Expenditure data from [26]. Resources from the Olympic Dam deposit are excluded.

The history of the discovery of significant uranium deposits in the Athabasca Basin is represented in Fig. 23. Discoveries made during the period from the late 1960's through to the mid-2000s are characterized by increasing depth of initial discovery. The discoveries can be divided into two phases that also correspond to the Athabasca Basin learning curve analysis. Generally speaking, earlier discoveries in the Athabasca Basin were made near surface, through the follow-up of radioactive boulder trains identified by radiometric prospecting methods. Later discoveries can generally be attributed to innovations in ground and airborne geophysical technology given the recognition of a close spatial relationship between the occurrence of uranium deposits and electromagnetic features. Exploration at greater depths in the basin is currently restricted by some limits related to capacity of geophysical technology to resolve targets, and by the high cost and longer time frames to drill to these depths. New geochemical technologies have been offered as an innovative approach to identifying deep, blind, deposits [11]. A breakthrough in the development of a more efficient drilling or other geoscientific technology could be a catalyst for discoveries on the third learning curve.

Deposit grade-and-tonnage models can be used to characterize the statistical distribution of uranium deposits per type [27]. These models provide a guide for predicting the occurrence of economic deposits. A plot of grade versus ore tonnage for selected Canadian and Australian economic and sub-economic uranium deposits is presented in Fig. 24. The isolines define several thresholds of contained metal. In this example, the largest Canadian deposits are characterized by their high grade and their relatively low ore tonnage. In contrast, the largest Australian deposits are characterized by their relative low grade and high ore tonnage. In this example, many uneconomic deposits fall below the lower isoline for contained metal. Only a few deposits are large enough to be deemed economic within the grade-tonnage spectrum (Fig. 25).

5. BUSINESS DEVELOPMENT AND EXPLORATION CYCLES

The uranium exploration process involves the effective use of geoscientific knowledge and exploration technologies, with long time frames required for the discovery and development of economic mineral deposits. Long-term funding of the business of exploration is required. The availability of exploration funding can be linked to the market price of uranium that varies in response to uranium supply and demand and other geopolitical factors that can be mapped as business cycles.

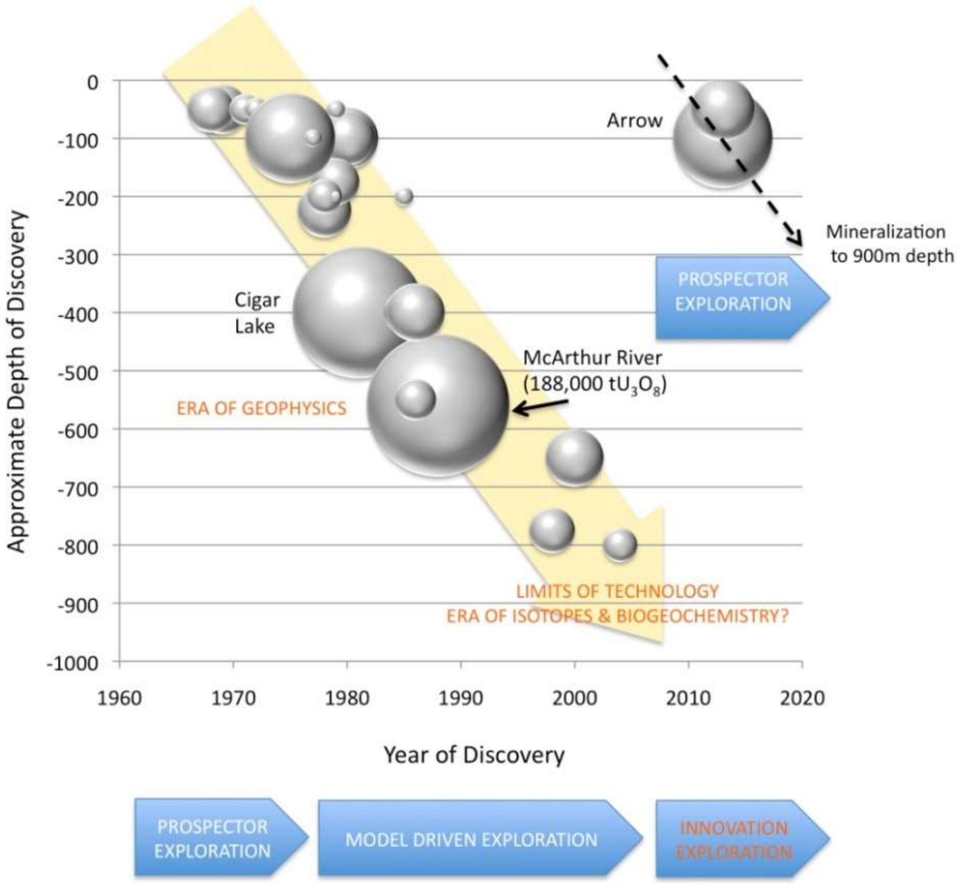

FIG. 23. History of Athabasca Basin uranium deposit discoveries by year of discovery, size, and depth.

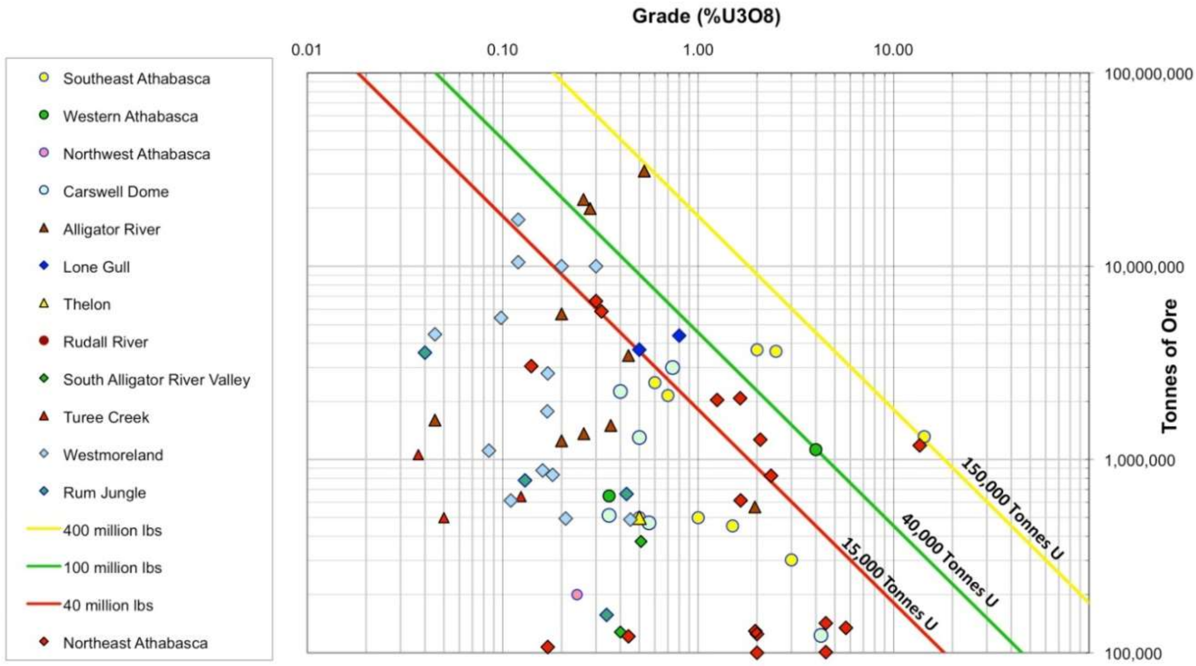

FIG. 24. Grade-tonnage plot for Australian and Canadian unconformity-related uranium deposits by locality (isolines show thresholds for contained t U).

Participants in the uranium exploration business environment can have different motivations for their involvement (Fig. 26). Governmental organizations can support exploration directly or indirectly with a focus on securing uranium resources for strategic reasons. This can include the support of domestic nuclear energy programs, and economic development in the domestic mining sector through the generation of royalties and employment opportunities.

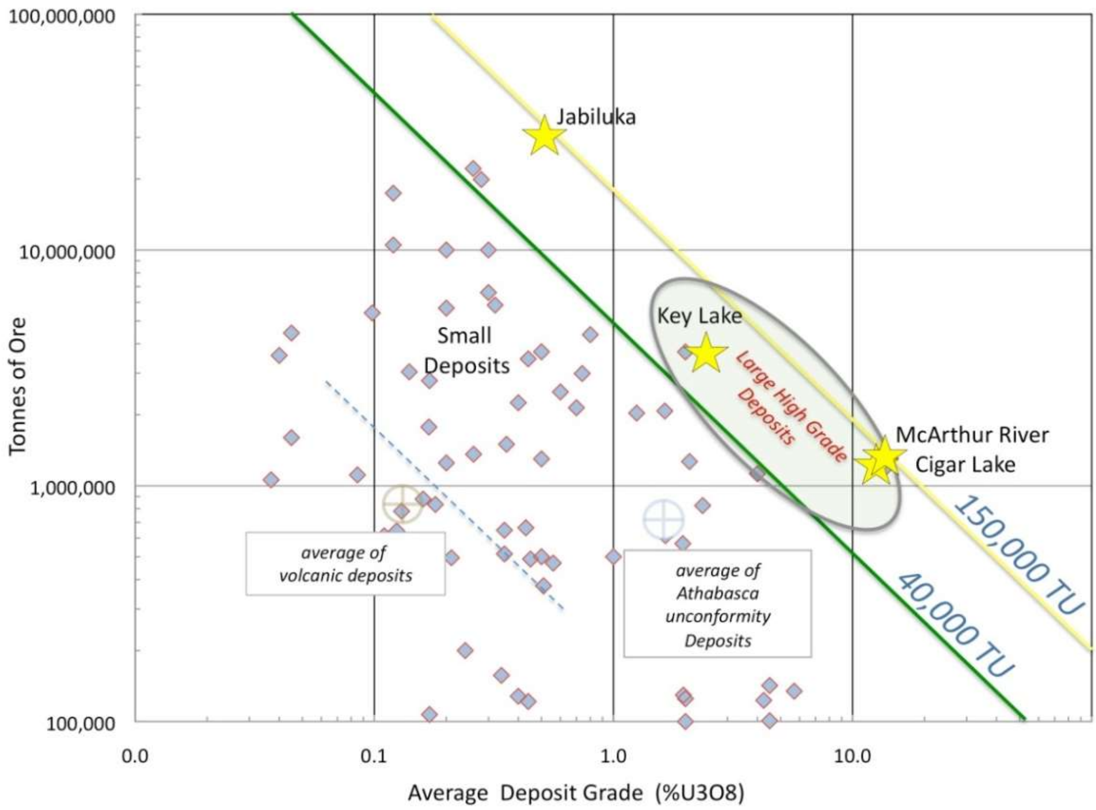

FIG. 25. Grade-tonnage plot for Australian and Canadian unconformity-related uranium deposits showing some of the large economic deposits. The isolines show the approximate thresholds for contained t U.

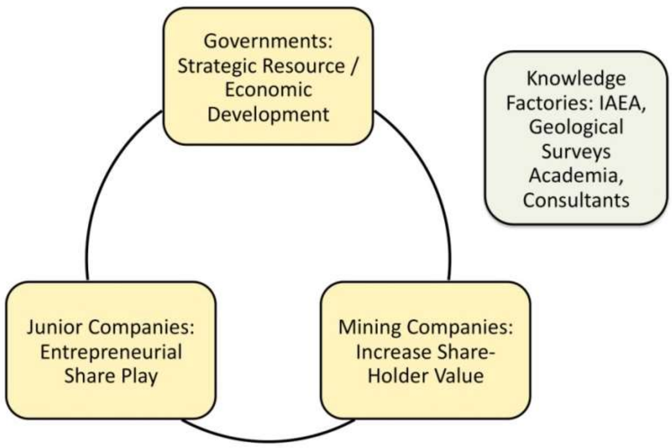

FIG. 26. Rational for uranium exploration

Major mining companies focus on the exploration and mining of uranium deposits with an objective of generating corporate profits and increasing shareholder value in a sustainable manner. Junior exploration companies are generally focused on increasing company share price through entrepreneurial and promotional activities in the stock market. A common ambition of junior companies is the identification of an economic deposit or highly prospective property and its eventual sale to major mining company. Other forms of agreements between junior and major mining companies are also common, including joint exploration ventures and strategic alliances, with major companies funding junior exploration activities as their surrogates.

Another group of participants in the uranium exploration business include international agencies such as the IAEA, federal and provincial/state geological survey organizations, pure and applied university researchers, consultants/specialists, and contractors. These knowledge brokers have different motivations that include the promotion of peaceful and sustainable uses of nuclear energy, the attraction of investment in countries and provinces/states, the development of innovative geoscience and exploration technologies, and the provision of expert advice and a wide variety of exploration services, respectively. In addition, major exploration and mining companies often employ internal exploration departments to support their business activities.

The business of uranium exploration can be very competitive. Major and junior exploration companies with limited funding must select the jurisdictions where investment is warranted. The business case for investment is driven by the selection of the geographical area for exploration, the assessment of the economic mineral potential of the area and the selection of exploration technologies that are suited for the environment. Other risk factors that could impact the sale of a resource or the economic viability of a future mining operation are also considered. Exploration funding over long-time frames is fundamental to discovery success. Junior exploration companies are particularly susceptible to the challenge of raising money through private and public avenues in the share market to sustain their exploration initiatives. The availability of funding as reflected in exploration expenditure is generally sympathetic with the price of uranium.

The sales price of uranium changes as a result of the perception of its scarcity. The price will not stay below the cost of production for extended periods of time, and it will not stay above the cost of production, as new production will eventually enter the market causing prices to drop in response to the additional supply [28]. Emerging situations can also impact perceptions of scarcity that can impact price. These include nuclear incidents, accidents and catastrophes, perceptions of impacts from de-weaponization and secondary supply, financial bubbles, credit crises, and the economics of alternatives to nuclear power generation, among others. A simple model of how major and junior companies and knowledge brokers react to shifts in uranium sales price is presented in Fig. 27. In this model, junior and major companies and researchers and consultants engage or disengage in a logical sequence as funding opportunities become available, or grow scarce with time.

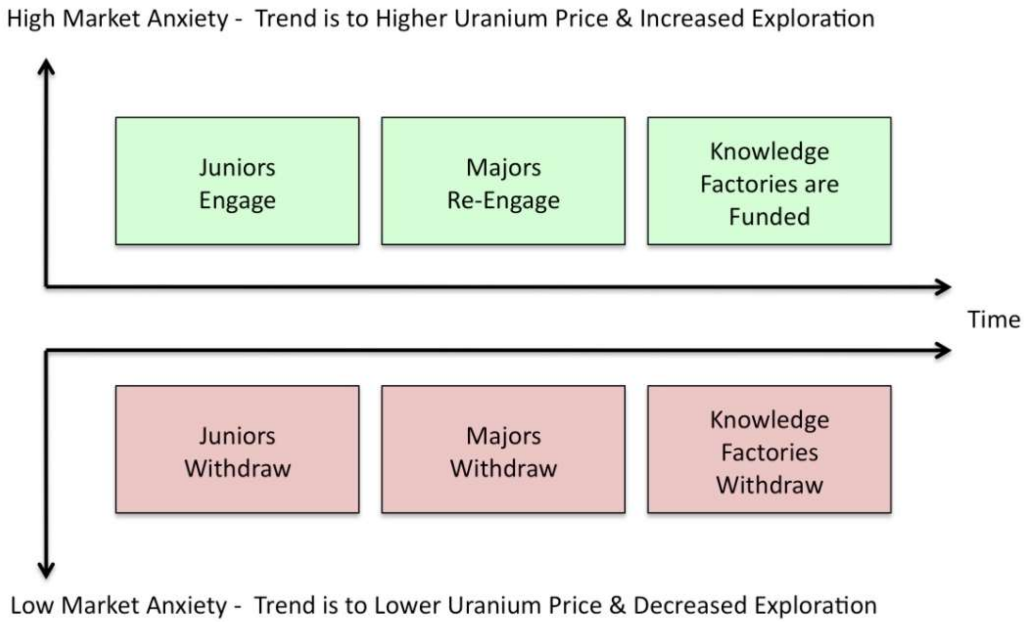

FIG. 27. Model of the impact of uranium price on exploration activity.

Future discovery is very dependent upon junior exploration activity given that that there are only a few major mining companies currently focusing on the exploration for uranium. Geological survey organizations must actively market their jurisdictions from both a geopolitical, geoscientific, and technological perspective to attract investment from uranium exploration companies. During exploration booms money is available to support intensive exploration activities that are commonly focused on the re-evaluation of historical prospects and sub-economic deposits in hope of developing previously identified resources into economic deposits. Junior company shareholders are often rewarded through stock transactions as share prices escalate in sympathy with increases in uranium sales price, and in response to promotional announcements about new discoveries and rediscoveries.

The impact of depressed price on uranium exploration can be more pronounced as a lack of funding disrupts exploration strategies because of the flight of venture capital. This can result in reduced or refocused exploration budgets, and the effective demise or mothballing of junior companies. The stifling of frontier exploration (political, physiographic, and technological) is also a common outcome as companies withdraw to historically productive jurisdictions. During times of severe downturn, staff lay-offs can be associated with an irrevocable loss of expertise and with a decrease or elimination of research-and-development activities.

The history of exploration in the Athabasca Basin, Canada is illustrated in Fig. 28. Exploration investment cycles are mapped relative to metal price, the timing of discovery and production, uranium mining investment (including exploration expenditures) and events influencing the market. Exploration investments can lead to significant capital investments in mining infrastructure and on-going operations, supporting economic development and providing revenue streams to governments in the form of royalties.

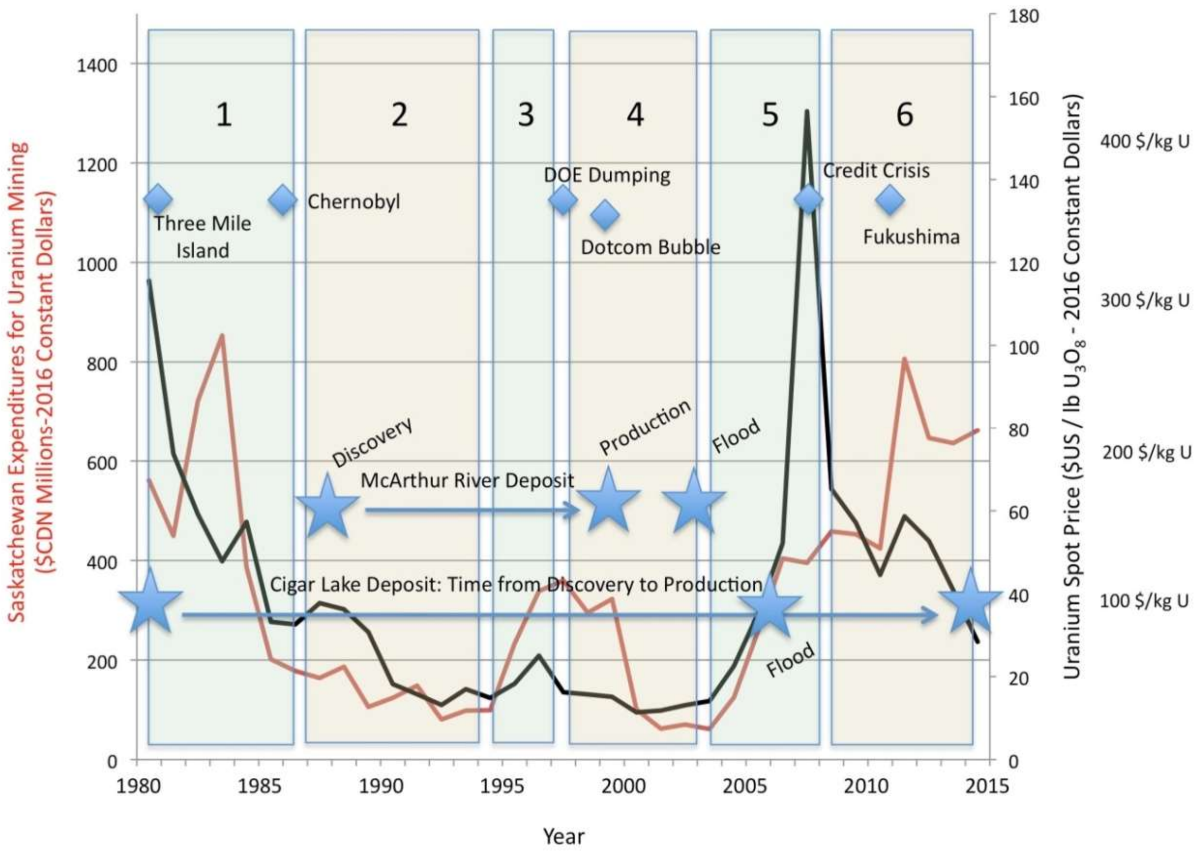

FIG. 28. Exploration cycles and Saskatchewan uranium mining investments relative to events influencing the market. Cycles 1, 2 and 3 correlate with increased exploration investments. Mining investments include capital and exploration investments and exclude operating costs. Mining investment data sourced from [29].

A description of the various roles and interests of the various players in the uranium exploration business is presented in Table 2. Factors influencing uranium exploration and mining investment decisions are illustrated from the perspective of various stakeholders. Within this framework, one of the roles of governments, agencies, geological survey organizations, and consultants is to reduce geopolitical and technical risk for major and junior companies interested in conducting exploration in countries of interest.

Governments and geological survey organizations can promote their country as a good place to conduct exploration by understanding the interests and risk tolerance of exploration companies. At the exploration stage the role of governments is to attract investors through the development of favorable uranium exploration and mining policies, and the development of a reliable mineral tenure system.

Geological survey organizations can also attract investment by providing access to free or low cost, high-quality, pre-competitive geoscientific datasets. Governmental support for the development of a business environment that is not impacted by corruption is another factor in attracting investment, among many others.

The business case for the development of pre-competitive datasets by geological survey organizations is strong. Organizations that are engaged in the marketing of their particular jurisdiction through the assembly, maintenance, and distribution of relevant information, datasets, reports, and mineral potential assessments, help exploration companies to understand the mineral potential and make decisions about the efficacy of investing in exploration programs within the jurisdiction.Governments and geological survey agencies can also understand their competitive position relative to other countries through global rankings related to exploration and mining. These include perceptions of investment attractiveness, mineral policy effectiveness, corruption, expert judgment about prospectivity, and other factors more specifically related to uranium exploration and mining investment decisions.

TABLE 2: FACTORS INFLUENCING URANIUM EXPLORATION AND MINING INVESTMENT DECISIONS. FACTORS ADAPTED FROM [31]

Factors Influencing Investment Decisions in Various Jurisdictions	Role of Governments & Ministries	Role of Agencies, & Geological Survey Organizations	Role & Needs of Consultants / Academics Involved in Supporting Uranium Exploration	Needs of Junior Uranium Exploration Companies	Needs of Uranium Exploration & Mining Companies	Needs of Multi-Commodity Exploration & Mining Companies
Motivation of Organizations, Consultants & Academics	Attract Investors	Provide Information and Expertise	Provide Specialist Expertise	Share Price Escalation	Increase Shareholder Value	Increase Shareholder Value
Exploration Investment Risk Tolerance	Risk Mitigation Role	Risk Mitigation Role	Technical Risk Mitigation Role	Higher	Moderate	Lower
At the Exploration Stage						
Higher level of security	x				?	x
Favourable uranium exploration & mining policies	x	x		x	x	x
Lower level of corruption	x	x		?	?	x
Advocate for Best Practice	x	x				x
Availability of local logistical experts		x		x	x	
Safe working conditions				?	x	x
Access to senior government officials	x	x		x	x	x
Easy/free access to high-quality geoscientfic databases	x	x	x	x	?	?
Availability of local geoscientific experts/consultants/academics		x	x	x	?	
Advice on uranium prospectivity and explorability		x	x	x		
Certainty around the application of regulations*	x	x		?	x	
Cost effective land tenure and reporting system*	x	x		x	x	
Timely granting of exploration land holdings	x	x		x	x	
Ability to import scientific equipment	x	x	x	x	x	
Ability to export rock, soil, vegetation, water and other samples	x	x	x	x	x	
Reporting on the status of mineral resources (i.e. 43-101)			x			
Exploration agreements with consultants, experts, & academics				?	?	x
Exploration agreements with junior exploration companies					x	x
Development of stakeholder relationships	x	x	x	x	x	x
At the Mining Stage						
Higher level of security	x			A common strategy is to develop a resource and sell the company to a major mining company.	x	x
Lower level of corruption	x				x	x
Political stability*	x				x	x
Fair legal system*	x				x	x
Clear taxation regime*	x				x	x
Understanding trade barriers*	x				x	x
Certainty around the application of regulations*	x	x			x	x
Minimal regulatory duplication and inconsistency*	x	x			x	x
Certainty around environmental regulations*	x	x			x	x
Clear understanding of socioeconomic stakeholder agreements*	x	x			x	x
Clear land claim dispute mechanism*	x	x			x	x
Infrastructure to support mining development*	x				x	x
Understanding labour regulations*	x				x	x
Availability of labour/skills*	x				x	x
Worker health & safety	x				x	x

Competitive benchmarks that can be used by governments and geological survey organizations to benchmark competitiveness include the Fraser Institute annual rankings on perceptions of investment attractiveness and policy perceptions, Transparency International's anti-corruption index, and measures of annual exploration expenditures, meters of exploration drilling, and the number of deposits discovered, among others (Table 3) [30, 31].

Governments and survey agencies can also rely on the IAEA as a source of education and training opportunities, baseline data, and value-added products, including methodologies for the development of mineral potential assessments for uranium.

TABLE 3: A COMPARISON OF URARNIUM EXPLORATION AND MINING INVESTMENT ATTRACTIVENESS BY COUNTRY (RANKINGS AFTER [30] AND [31]. HIGHER VALUES ARE MORE FAVORABLE)

Country	State / Province	Economic Deposit Models	Economic Uranium Prospectivity Ranking	Transparency International Corruption Index (2015)	Fraser Institute Investment Attractiveness Index (2015) [not specific to urarnium]	Fraser Institute Policy Perception Index (2015) [not specific to uranium]	Factors impacting Uranium Exploration and Mining Investment Decisions
Uzbekistan		ISR Sandstone	moderate	19	?	?	
Ukraine		ISR Sandstone	depleted	27	?	?	
Kazakhstan		ISR sandstone	high	28	75	70	State controlled; acid leach permitted
Guyana		Unconformity-related?	low (under-explored)	29	51	60	permitting timelines
Russia		Various	moderate	29	66	52	
Niger		Sandstone	high	34	46	30	Threat of terrorism.
Gabon		Unconformity-related?	low	34	?	?	Under-cover exploration in a tropical environment.
China		ISR Sandstone	moderate	37	58	46	State controlled
Brazil		BY-product	by-product	38	61	57	
Mongolia		Sandstone	low	39	50	37	
South Africa		By-product	low	44	58	52	Permitting challenges; no new discoveries.
Namibia		Calcrete	moderate	53	70	30	Namibian state firm has exclusive rights to future uranium developments
United States	New Mexico	ISR Sandstone	low	76	61	77	Permitting challenges
United States	Wyoming	ISR Sandstone	moderate	76	78	97	Acid leach prohibited
Australia	Queensland	Volcanic	low	79	78	79	History of back-flipping on uranium mining policy/ Uranium exploration permitted but mining is not.
Australia	South Australia	ISR Sandstone; By-product	high	79	80	86	High level of government support. Excellent pre-competitive databases.
Australia	Northern Territory	Unconformity-related	moderate	79	82	85	Koongarra deposit incorporated into Kakadu National Park; Jabiluka mine on care and maintenance; NT government opposes Angela-Pamela uranium mine.
Australia	Western Australia	Calcrete	high	79	87	92	History of back-flipping on uranium mining policy
Canada	Northwest Territories	Unconformity-related	low	83	69	65	Remote, expensive, exploration, and permitting challenges.
Canada	Nunavut	Unconformity-related?	low	83	74	69	Uranium mining developments impeded by process
Canada	Newfoundland / Labrador	Volcanic-related	low	83	74	88	New deposits have not been discovered.
Canada	Quebec	Dyke-related	low	83	81	85	Uranium exploration and mining prohibited
Canada	Saskatchewan	Unconformity-related	moderate (depleted)	83	86	95	Economic deposits are taking longer to find.
Finland		U-Au and hydrothermal vein type	low	90	84	95	Anti-uranium politics. Uranium-specific permitting requirements.

6. EXPLORATION RISK FACTOR FRAMEWORK

The business drivers of exploration include the nature of uranium supply and demand that is linked to investment attitudes and return on investment, including share prices. The technical drivers of exploration for the discovery of economic uranium deposits include the selection of geographical areas for exploration based upon an assessment of prospectivity and explorability.

Additional strategic risk factors impacting investment decisions by uranium exploration companies include sovereign risk, risks at the mining stage, as well social and environmental risks. Operational risk factors include the availability of talent, and the capacity of the exploration team members to innovate and conduct exploration in a safe manner (Fig. 29).

A definition of some of these risk factors follows along with some examples is presented below. Exploration companies have different risk appetites and consider these risk factors, to varying degrees, when making investment decisions.

PROSPECTIVITY: This refers to the likelihood that economic mineral deposits will be found (by prospecting) in a project area. Things to consider when assessing prospectivity include the economic mineral potential of the project area. The term mineral prospectivity is synonymous with mineral potential, which refers to the likelihood that economic mineral deposits are contained in a project area. Associated factors of mineral prospectivity or mineral potential include available deposit models and the expected value of discovery, the history of exploration and discovery, mineral resource depletion, the stage of exploration and estimated discovery costs, and the availability of prospective lands. An assessment of mineral prospectivity can be made, in part, through the ranking of geoscientific factors in an exploration project area that are indicative of favorable ore-forming processes as defined by descriptive or genetic deposit models. Estimates of mineral potential can also be made through more quantitative assessments.

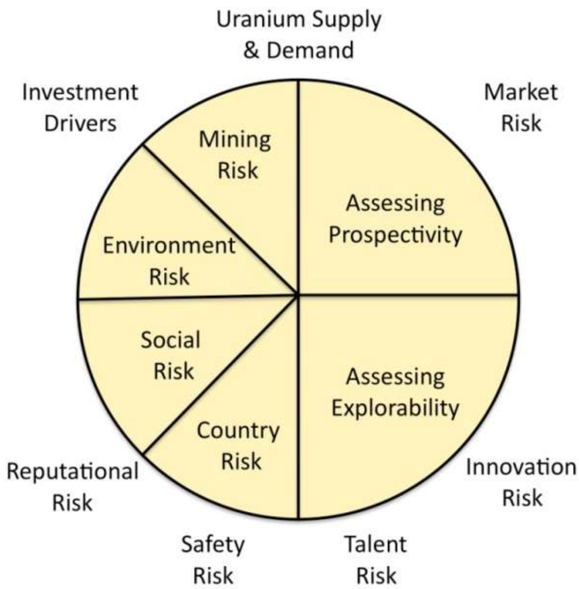

FIG. 29. Uranium exploration risk factors.

General examples of risk: Exploring in high-risk frontier terrains with a poor technical knowledge base. Deploying the wrong deposit model. Working in mature exploration environments facing economic mineral resource depletion.

EXPLORABILTY: This refers to the likelihood that a project area can be explored in an economical and efficient fashion using existing exploration technology, or technology under development. Technology includes both the ‘hardware’ and ‘software’ of exploration. Exploration methods include geology, geochemistry, geophysics, and drilling tools—the ‘hardware.’ The ‘software’ refers to innovative thinking to support better exploration decision-making.

Examples of risk: Exploring for blind deep deposits and exploring in jungles and deserts, where access is difficult and where standard geochemical and geophysical approaches may not work.

MINING RISK: This refers to changes in the business environment that can impact the likelihood that the mineral deposit will be developed considering economic, geopolitical, and geo-environmental factors (Fig. 11) [30]. These changes can adversely affect operating profits as well as the value of assets. The social impact on the business environment of working in countries where AIDS/HIV is endemic is included in this risk category. Sovereign risk is also included in this category.

COUNTRY RISK: This refers to changes in the business (political, economic, and financial) environment that could increase the cost of doing exploration in a country or prohibit exploration [32]. Special planning is required when there is the potential for political instability and violence that could affect the exploration team and operations [33]. Countries may have particular stances on the exploration and mining of uranium. This risk is included in this category. Risks associated with the security of mineral and land tenure are also included in this category.

Examples of risk: Changes in government stability, socioeconomic conditions, internal conflict, external conflict, corruption, military-in-politics, religion-in-politics, inflation, exchange rate stability, and terrorism [34].

ENVIRONMENTAL RISK: This refers to environmental issues that could lead to changes in the business environment that will increase the cost of doing exploration in a country or prohibit exploration. These risks include those associated with legislation, working in environmentally sensitive lands, and working near parks or reserves. Interventions by governments, national or international organizations, agencies or parties, and interventions by first nations or other indigenous people are also included in this category. Uranium politics are entwined with environmental issues

Examples of risk: Declaration or expansion of parks, reserves and heritage sites. Increased monitoring, regulatory and relationship burden.

SOCIAL RISK: This refers to the likelihood that changes in the political environment will occur and will lead to increases in the cost of exploration or the prohibition of exploration. This can include issues related to land rights or uranium project development. Industry can “manage the business processes to produce an overall positive impact on society [through a] continuing commitment by businesses to behave ethically and contribute to economic development while improving the quality of life of the workforce and their families as well as of the local community and society at large” [35].

Examples of risk: Fluid (and often intergenerational) uranium exploration and development stances by Traditional Aboriginal Owners. Increased regulatory and relationship burdens.

REPUTATIONAL RISK: This refers to the likelihood that exploration and mining activities will reflect poorly on the organization.

Examples of risk: Working in countries known for corrupt business practices. Working in environmentally or ecologically sensitive areas. Working in countries governed by dictatorial regimes.

7. ASSESSING PROSPECTIVITY

The assessment of the investment worth of uranium exploration involves a number of activities including gaining an understanding of prospectivity. A basic framework for assessing prospectivity is presented in Fig. 30. Activities include assessment of strategic risks, assessment of existing mineral occurrences, selection of appropriate uranium deposit models, assessment of economic mineral potential, development of conceptual targets for exploration, and acquisition of exploration permits.

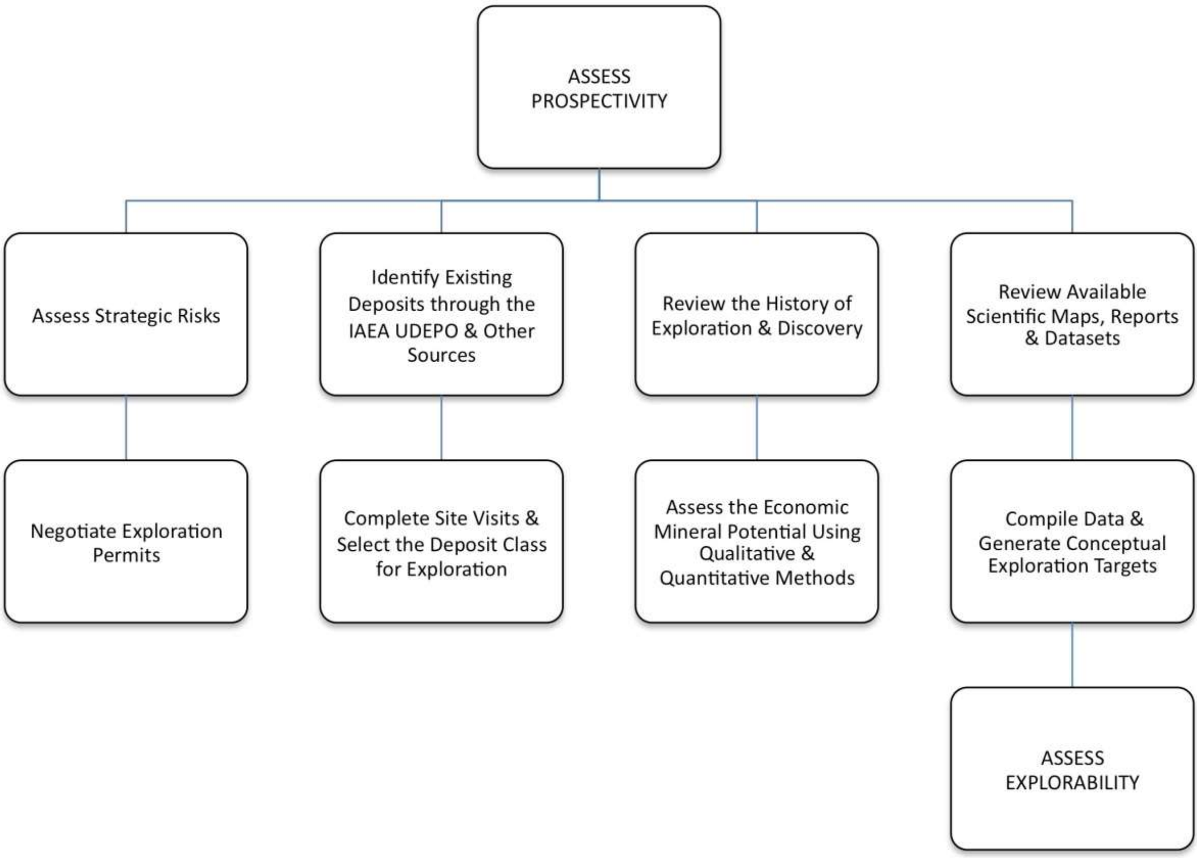

FIG. 30. A basic framework for assessing prospectivity.

Explorers assess the prospectivity of a geographical area in different ways and with different levels of rigor. Assessments can include gauging the likelihood of discovering economic deposits through the analysis of geological maps, reports and geological, geochemical, and geophysical datasets. This work often includes visits to historical mineralized showings with a focus on validating physical patterns known to characterize uranium deposits.

An evaluation of prospectivity can include the qualitative, spatial and quantitative assessment of mineral potential on regional and more localized scales, such as those presented in this publication. Some of these approaches are informed by an understanding of the type of uranium deposit anticipated to occur in an area, and anticipated deposit grades and tonnages.

Data reviews can also focus on understanding mineral potential from an ore genesis perspective. These assessments involve gaining an understanding of geological processes in time and space that are indicated in the project area. The geological processes involve the sourcing, transport, trap, and preservation of mineralizing fluids in the form of ore deposits.

Government and geological survey agencies can assist potential investors through the provision of easily access to free, or low cost, pre-competitive data. This information includes deposit location databases and geoscientific base maps – typically topographical, geological, magnetic, and radiometric maps, drillhole locations, geological sample archives, and mineral potential assessment reports.

8. ASSESSING EXPLORABILITY

Technologies for assessing explorability include both the 'hardware' related to the survey methods and tools, and the 'software' or knowledge residing with industry experts. A basic framework for assessing explorability is presented in Fig. 31. This assessment includes an evaluation of physical access and logistics associated with working within the permit area, determining if service providers are available to support activities in the field, evaluating geoscientific baseline data and historical reports by exploration companies to understand past successes and failures, estimating the depth to targets, and holding discussions with resident experts.

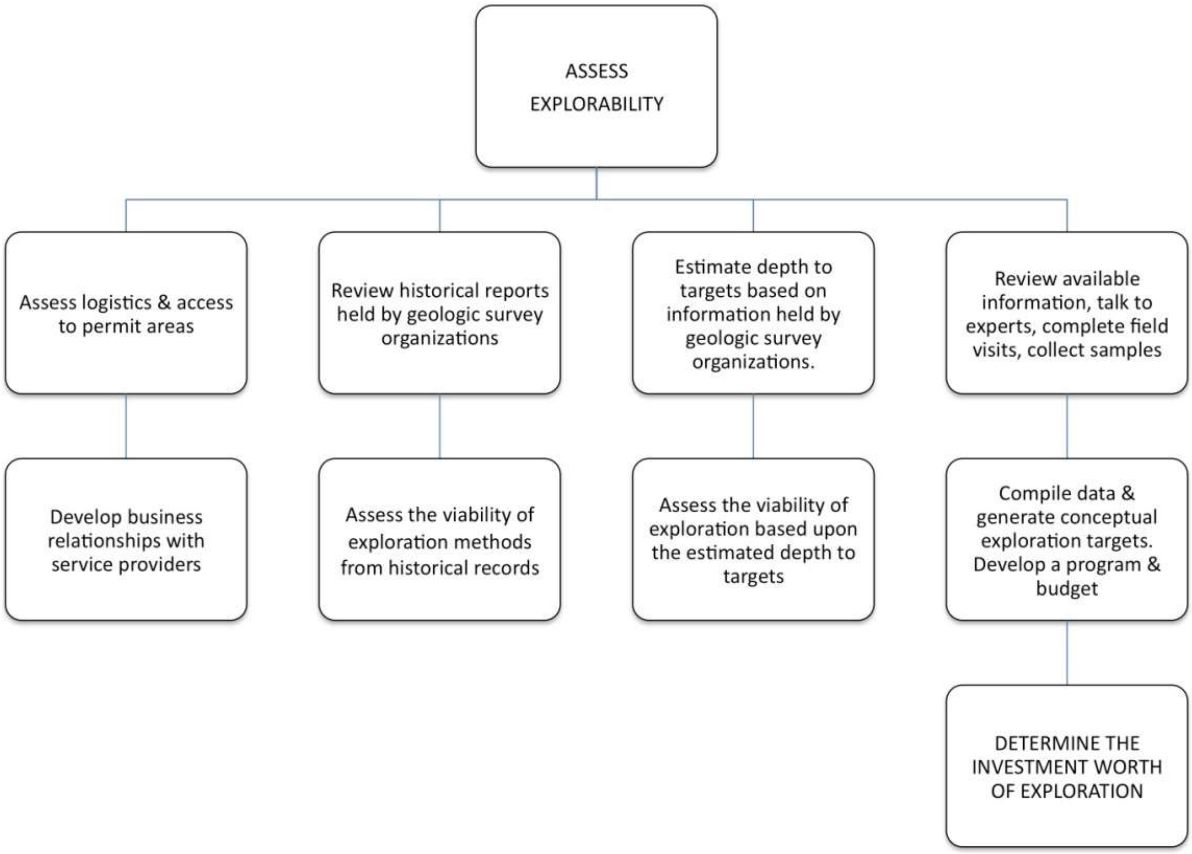

FIG. 31. A basic framework for assessing explorability.

The availability of low cost baseline geoscientific data from geological survey organizations in the form of maps, samples, drill cores, reports, and historical records of exploration company activities, is an important factor in assessing explorability. Exploration companies will compile the information, develop conceptual exploration targets, develop a program and budget, and determine if it is worthwhile to invest in exploration.

There are a wide variety of exploration survey methods available to explorers. These methods are deployed in various combinations depending upon the type of uranium deposit being explored for, the scale of exploration (regional or detailed), and available funding.

Exploration programs are designed to identify anomalous physical signatures that are analogous to those associated with known economic uranium deposits. The technical literature on descriptive and genetic uranium deposit models and other reports describe some of these signatures [9]. Targets for testing by diamond or rotary drilling techniques are developed through an iterative and increasingly detailed series of surveys from reconnaissance to detailed scales (Fig. 11).

A selection of exploration methods used in uranium exploration is listed in Fig. 32, along with an estimate of their cost. The survey methods can be divided in geological, geochemical, geophysical, and drilling categories. Geophysical methods can be further sub-divided into magnetic, gravimetric, electromagnetic, radiometric, and seismic methods. Remote sensing data from satellites are also used in uranium exploration. Exploration managers must carefully assess the value of deploying exploration methods given their cost and utility. More detailed information about exploration methods can be found in several IAEA publications such as a recent publication on innovations in geophysical methods [36].

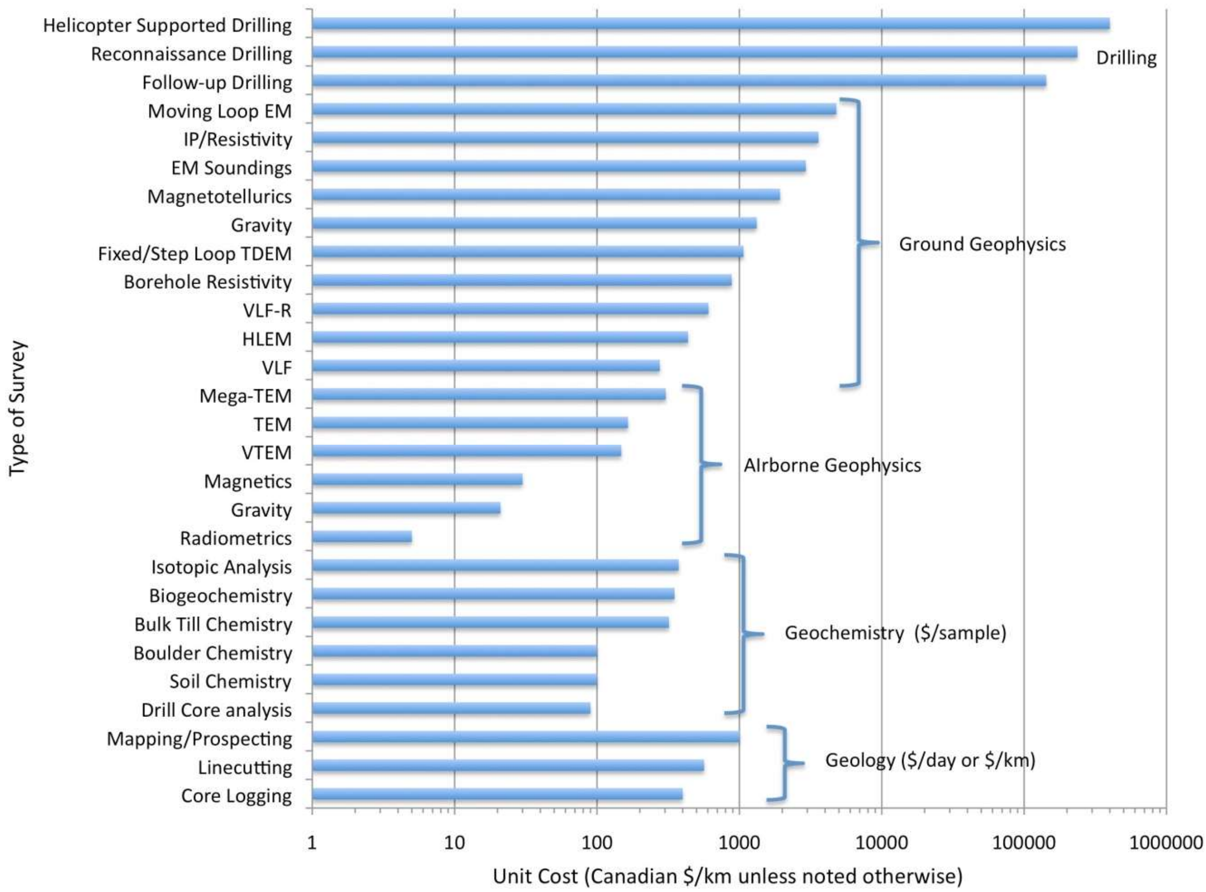

FIG. 32. Approximate unit cost of exploration by type of survey.

Many of the survey methods are offered by consulting companies that specialize in ground-based and airborne geophysical surveying, and rock, soil and botanical sample analysis at geochemical laboratories. Exploration companies also contract geological consultants to support their exploration programs in addition to developing their own exploration teams. Some companies also develop research and development with universities and other organizations to develop innovative exploration technologies with a goal of increasing economic discovery success rates.

The physical geography of an exploration project area can also dictate the choice of exploration survey methods. For example, characteristics of geomorphology, hydrology, pedology, and glaciology can impact their selection. Different combinations of methods are used for programs conducted in tropical vs. temperate vs. desert environments.

Innovations in exploration technology have occurred in response to the discovery of economic deposits at increasing depths below surface (Fig. 23). Geophysical technologies have evolved to map targets at increasing depths. The developments of biogeochemical and isotopic methods for exploration are more recent examples of the industry response to the search for blind deposits [11].

9. THE ROLE OF AGENCIES, GOVERNMENTS, CONSULTANTS AND ACADEMIA

In the broadest sense, uranium exploration technology consists of the system of experts, techniques and program managers involved in supporting the business of uranium exploration (Fig. 33). Experts take on different support roles depending upon their individual mandates. Exploration program managers assess investment worth and organizations make investment decisions. Exploration programs and budgets are developed and implemented using a variety of exploration methods, with the support of contractors. The IAEA, geological survey organizations, independent consultants, internal consultants employed by exploration companies, and researchers in university and government organizations, will continue to play a critical role in the discovery of the next generation of economic uranium deposits.

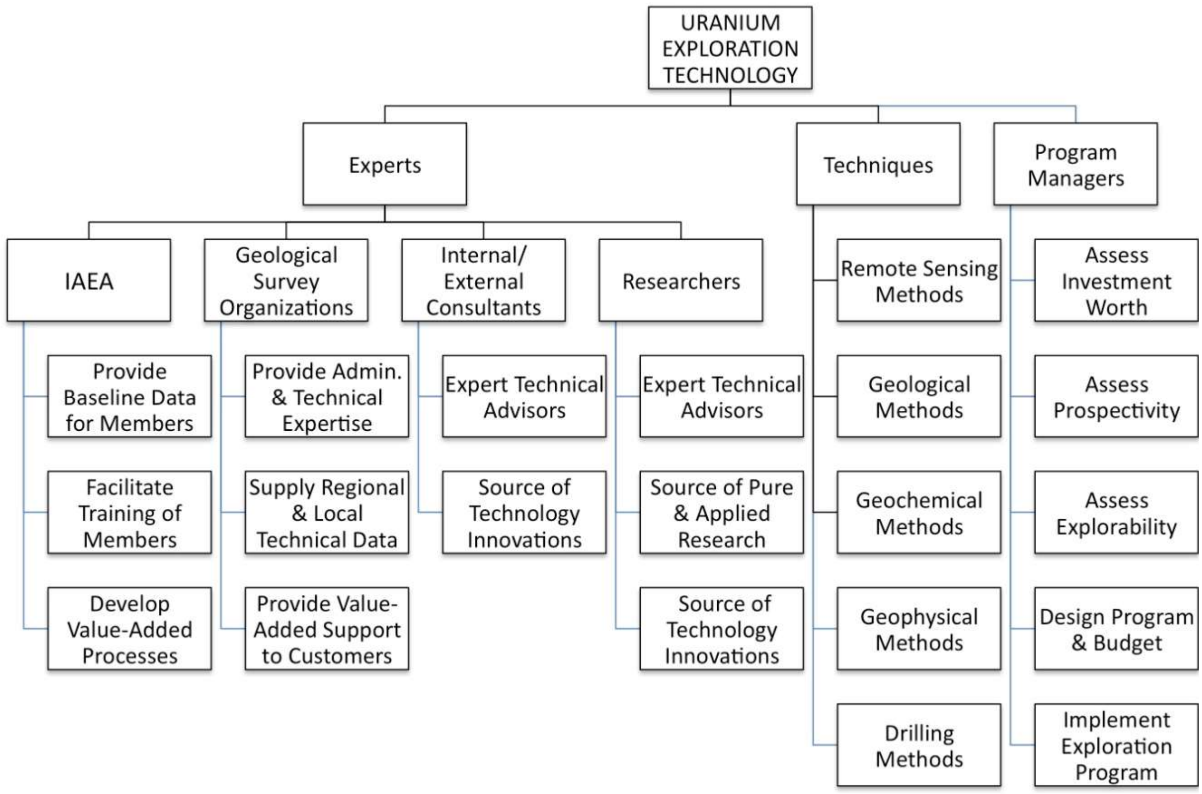

FIG. 33. The uranium exploration technology system.

The IAEA provides baseline data and education and training opportunities, including programs in the field of uranium exploration and mining, with a goal of promoting the peaceful and sustainable use of nuclear energy. The IAEA also engages experts in the field of exploration to add additional value to the IAEA programs. Geological survey organizations play a critical role in the uranium exploration process as sources of administrative and technical expertise and suppliers of pre-competitive technical datasets to their customers, the exploration companies. As described earlier, effective geological survey organizations act to attract exploration investment by providing easy and low-cost access to information that exploration companies can use to support investment decisions. Some exemplar state- and country-based geological survey organizations that have a history of uranium exploration can be found in South Australia, Saskatchewan, and Finland, among others. Independent external consultants can offer unique managerial and technical experience in the uranium field and can act as advisors or experts. They support the IAEA and member states through participation in education and training programs and as contributors to technical publications. Independent consultants can also provide advice and specialized services to exploration companies. Some consultants work with researchers to develop innovative methods in uranium exploration. Geological survey organizations in developing countries could benefit from the expert knowledge that consultants have to offer. Some university researchers focus on pure and applied research projects in the field of uranium metallogeny and innovation in uranium exploration technology. Their work is funded through government grants, university–company–government collaboration programs, and through contracts with exploration companies. Many researchers also act as independent consultants in tandem with their positions at universities. Some governments also fund research and innovation in the field of exploration through dedicated governmental organizations. Researchers can also organize and provide education and training to new graduates and industry. Geological survey organizations in developing countries could benefit from the authoritative knowledge that some researchers have to offer. Specialist contractors are responsible for the innovation, development and sale of an array of exploration services to exploration companies. These services include the acquisition, interpretation and reporting on survey data collected for clients. Remote sensing, geological, geochemical, geophysical and drilling methods are included in this category. Exploration company program managers develop, implement and assess their exploration programs and budgets. Exploration teams can range in size and experience and sophistication. Large multi-commodity and major uranium mining companies often employ large experienced exploration teams. Junior exploration companies employ smaller teams led by exploration managers of varying experience levels. Multinational and junior companies may not have the same depth of experience with uranium exploration and sometimes engage independent uranium consultants to support their exploration programs.

Significant competitive advantage could likely be achieved by optimizing the degree of collaboration between the disparate participants in the uranium exploration technology system for the discovery of the next generation of economic uranium deposits.

10. OPTIMIZING HUMAN, ORGANIZATION AND TECHNOLOGY FACTORS

While much attention is given to technology innovation as a key to discovery, less attention is given to addressing how human and organizational elements contribute to success, or the lack of success, in the management of the exploration process. The exploration project management cycle involves the optimization of human, organization and technology factors for discovery. Success can be related to efforts to reduce exploration risk, optimizing plans and budgets, optimizing project portfolios, and developing human and organizational resources and schemes for innovation management in the exploration program management cycle (Fig. 34).

Economic discoveries are sometimes promoted as exemplars of effective technology deployment and effective teams when in reality elements of serendipity and individual achievement situated in more dysfunctional organizations may be more evident. One view is that the exploration process is a value creating activity. That is, discoveries result from the deployment of exacting technologies through the actions of high performing exploration teams operating within effective and efficient organizations. An alternative view is that the exploration process is more of a value-destroying activity related to a suspected failure of leadership, a failure to manage, a failure to innovate, or a failure to learn (Tables 4 and 5).

There is room to debate these viewpoints while acknowledging opportunities for improvement of the exploration process in the search for the next generation of economic ore deposits—optimizing human, organization and technology factors to increase discovery rates. Key success factors for exploration involve the development of effective leadership and teams, technology, and knowledge transfer mechanisms, within an organization supported by collaborative research and development activities.

Some additional resources related to the business of mineral exploration include a comprehensive publication on the management of mineral exploration by [37]. Innovation in exploration is described by [21]. A description of factors that have impacted the discovery of economic uranium deposits in the Athabasca Basin is documented by [38, 39]. This is in addition to the vast literature on business, organization and leadership development that is also applicable to the business of exploration.

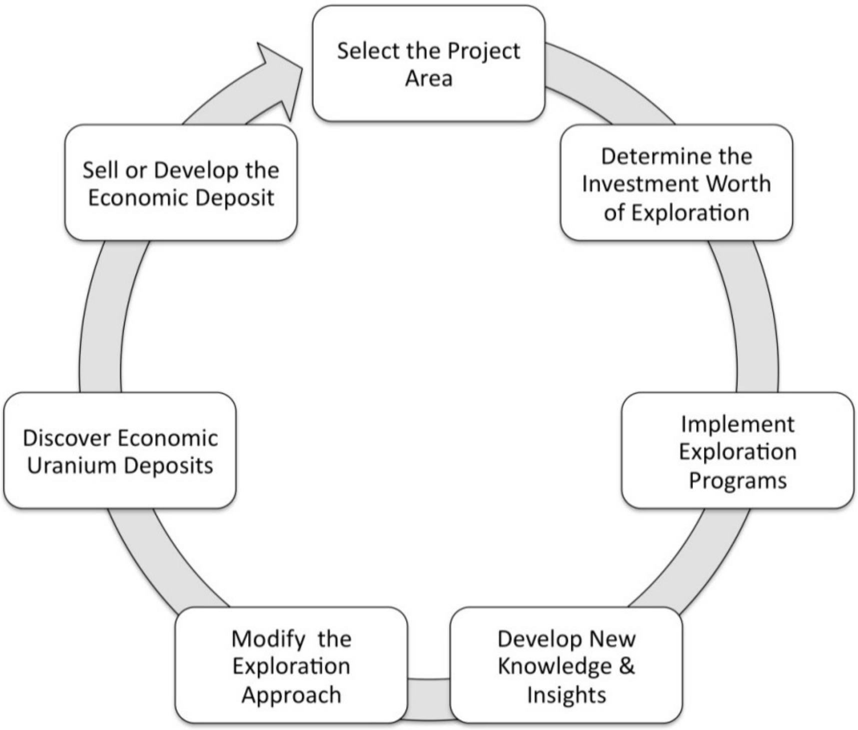

FIG. 34. The exploration program management cycle.

TABLE 4: OPPOSING VIEWS OF THE MANAGEMENT OF MINERAL EXPLORATION

Exploration and discovery is viewed as a value creating activity	Exploration and discovery is viewed as a value-destroying activity
- It's all about skill. - It's all about applying good science and technology. - It's all about great people. - It's all about great organizations. - It's about great leadership. - It's about adequate funding and resources. - It's the effort of a high-performing team.	- It's about luck. - Spend enough money and it will happen. - It's the "heroic" effort of one individual. - It's about success despite factors working against success such as: • 'Bad' science; • Inadequate funding; • Management deficiency; • Organization deficiency; • Inadequate training; • Inadequate equipment and infrastructure; • Politics (organizational dark side); • Poor morale.

11. PREDICTIVE APPROACHES TO UNDERSTANDING INVESTMENT WORTH

Geological survey organizations, consultants, researchers, and project managers can help to improve economic discovery success rates through the use of deposit models. A variety of uranium deposit models are available to support mineral exploration investment decisions. The models include economic (grade-tonnage), descriptive and genetic deposit models and other predictive models that rely on probabilistic and spatial recognition methods. The modeling of ore-forming processes is another category.

The potential exists to improve uranium deposit discovery rates through the quantitative estimation of the endowment of economic mineral deposits in a particular geologic environment using a combination of these models. It is also possible to estimate the exploration investment worth of exploration in a more quantitative fashion using models. A framework for deposit models is presented that depicts model classes, sub-classes and related technologies for their implementation (Fig. 35). An alternative model framework is described by Cox and Singer along with detailed descriptions and examples [27].

TABLE 5: SOME EXAMPLES OF VALUE-DESTROYING EXPLORATION ACTIVITIES

Some examples of value-destroying exploration activities at the strategic level
- 'Bad' science: Misidentification of key uranium occurrences by government geologists catalyzing successive multi-million dollar staking rushes. An example of using the wrong deposit model; - Knowledge hoarding: Companies who are reluctant to publish critical scientific data from deposits, despite the competitive advantage of doing so, leading other companies to explore for the wrong deposit model; - Ostrich principal: Companies focusing exploration on, and promoting a particular exploration deposit model, despite contrary evidence; - Premature exit from the exploration play: Companies failing to adequately plan and fund for economic discoveries through sustained investment over long term.
Some examples of value-destroying exploration activities at the managerial level
- Poor leadership: Failure to maintain employee engagement and retain talent through the implementation of effective organization systems (strategic planning, on-boarding, rewards, succession planning, and leadership development); - Inefficient project management: Inefficient allocation of funds between prospector–, model–, and information–driven exploration; - Ineffective promotional funding of drilling programs that are focused on drilling out uneconomic mineralized intersections for publicity and self-promotion; - Failure to Learn: Failure to leverage existing exploration science, failure to innovate, poor training, and failure to collaborate.
Some examples of value-destroying exploration activities at the operational level
- Ineffective exploration team dynamics: Poor competency, dysfunctional teams, inadequate leadership and inadequate organizational support, leading to an inefficient and ineffective exploration process; - Ineffective knowledge transfer: Failure to understand lessons learned reducing exploration success rates. Failure to develop a learning organization. Failure to develop knowledge brokers; - Poor employee engagement and motivation: Failure to provide meaningful work, empower staff, provide adequate resources, and develop technical and leadership competency.

Descriptive models are used as frameworks for interpreting geological observations collected during exploration programs. Models are developed through the description of geological settings and identifying specific characteristics such as tectonic settings, rock type, ages of deposit formation, and geochemical and geophysical signatures, among other factors [27]. Genetic models involve the development of explanations of mineralizing fluid sources, modes of fluid transportation, and trapping and preservation mechanisms in the geosphere. Descriptive models evolve into genetic models, as ore formation processes are understood through the iterative cycle of exploration practice and research. Some aspects of the economic potential of deposits can also be understood through the analysis of mathematical distribution of their grade and tonnage characteristics.

Descriptive models for uranium deposits are described by [8]. The IAEA combined a uranium deposit classification scheme used for the 'Red Book' publication since 1991, with Dahlkamp's classification scheme [40]. The revised scheme defines 15 types of uranium deposits worldwide (Table 6). An example of a descriptive and grade-tonnage model for a uranium deposit can be found in [27]. Sources of information related to genetic models for uranium deposits can be found in publications by [41, 42].

Probabilistic and spatial recognition models have evolved in response to the demand for more reliable approaches for the assessment of the economic mineral potential of exploration areas. Some examples can be found in this publication. The development of these models relies upon specialists in mathematical geology and geographic information systems. Spatial modeling relies on the availability of datasets defining topography, geology, geochemistry, geophysics, and drilling results, at relevant scales suiting the stage of exploration, and an understanding of deposit models.

An example of a sophisticated quantitative investment worth model for uranium exploration appears in a publication by [25]. The sophisticated model estimates the economic value of an exploration program in response to exploration program expenditure. It involves the combined use of descriptive and genetic deposit models, grade-tonnage models, probability distributions and simulations, engineering costs estimates, stochastic price forecasts, and discounted cash flow and risk adjustment techniques, guided by expert judgments (Fig. 36).

Another example is the qualitative data-process-criteria predictive model that can be used to identify exploration potential through the recognition of geological data, genetic processes and the criteria that are most likely to be favorable for the occurrence of economic deposits. This type of model can be used at regional to local scales that are represented by general to specific geological factors, and categorized as necessary for the occurrence of a deposit through to sufficient to permit the occurrence of a deposit. An example of a data–process–criteria model for sandstone roll-type uranium deposits can be found in the work of [43] as represented in Fig. 37. These models are useful in assessing the uranium potential of frontier environments where spatial and other data may be limited, making qualitative assessments more problematic.

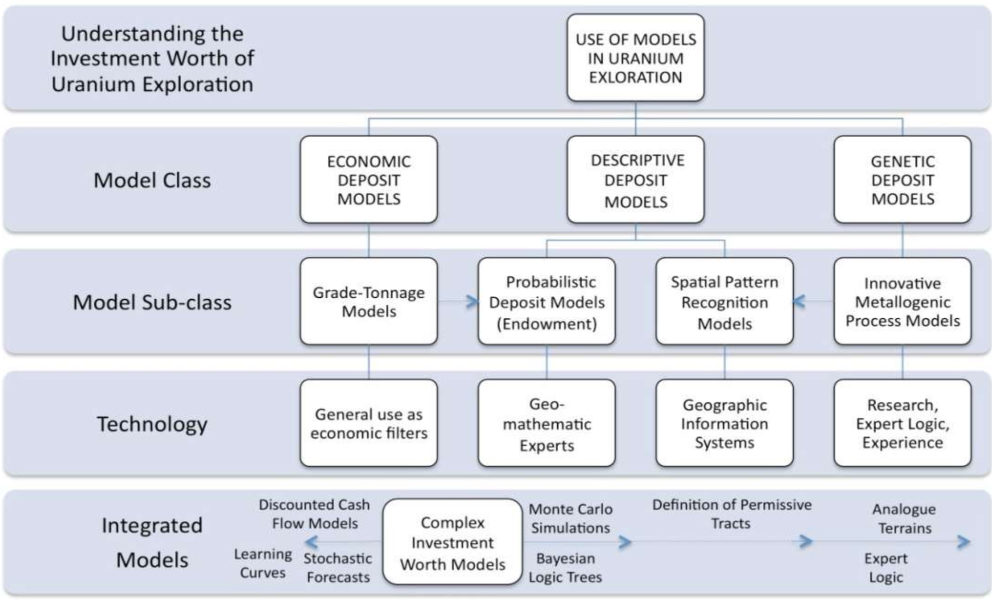

FIG. 35. Deposit models used in uranium exploration.

TABLE 6: IAEA URANIUM DEPOSIT CLASSIFICATION SCHEME (AFTER [9])

Worldwide uranium deposit types
1. Intrusive
2. Granite-related
3. Polymetallic hematite breccia complex
4. Volcanic-related
5. Metasomatite
6. Metamorphite
7. Proterozoic unconformity
8. Collapse breccia pipe
9. Sandstone
10. Paleo-quartz pebble conglomerate
11. Surficial
12. Coal-lignite
13. Carbonate
14. Phosphate
15. Black shales

Qualitative models also extend to the generation of assessments based on the judgment of experts in the field of uranium metallogeny and exploration. Experts can create qualitative mineral potential assessments through the compilation of available information, reports and interviews with other technical specialists in an efficient manner. The World Uranium Geology and Uranium Potential report is an example of an assessment of uranium potential at a country level that that is still relevant [44]. Consultants and researchers play a critical role in the development of quantitative and qualitative models to support uranium exploration. They provide expert advice from practical and technical perspectives, scrutinize information used to construct the models, validate output from the models, and comment on the efficacy of resulting decisions. Models can only provide an estimate of mineral potential as a guide for field exploration programs. Testing hypotheses that arise from the modeling is the art, craft and science of exploration.

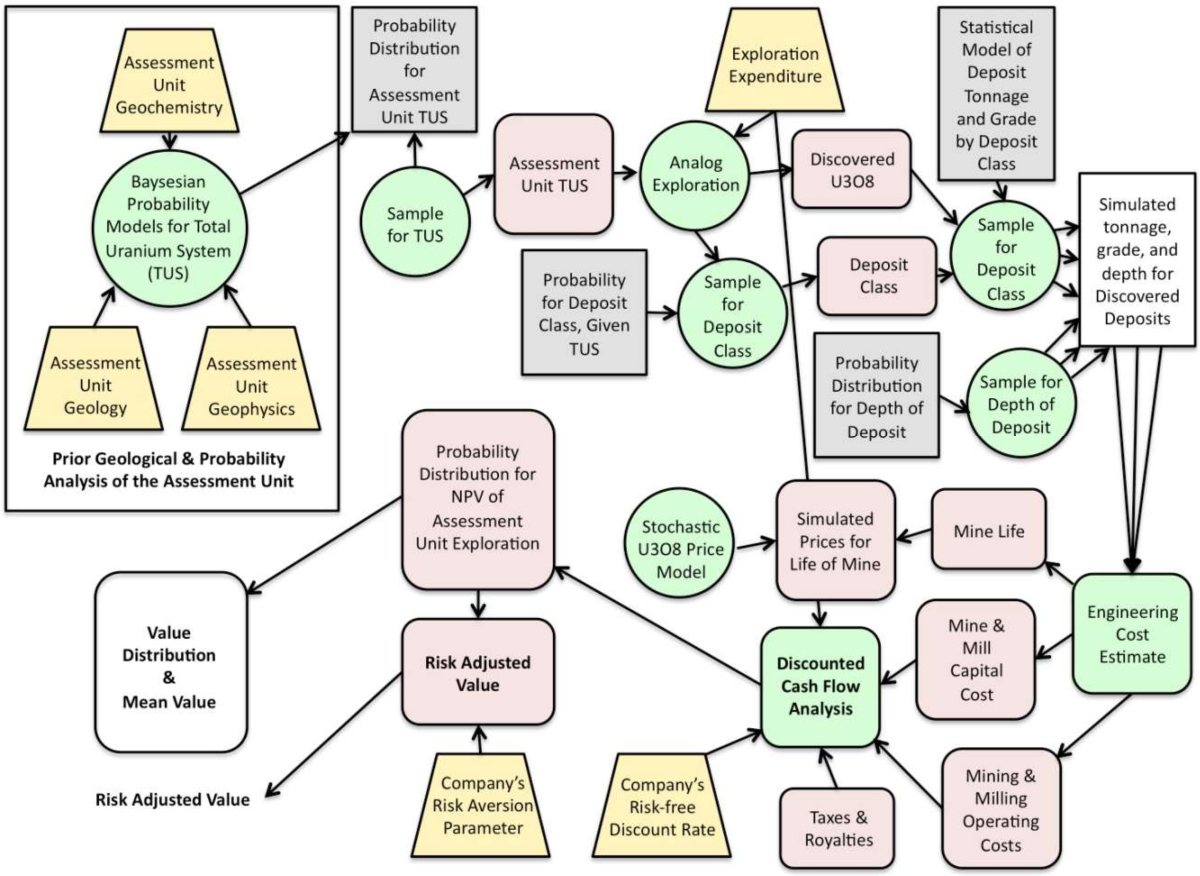

FIG. 36. An investment worth model for uranium exploration (adapted from [25]).

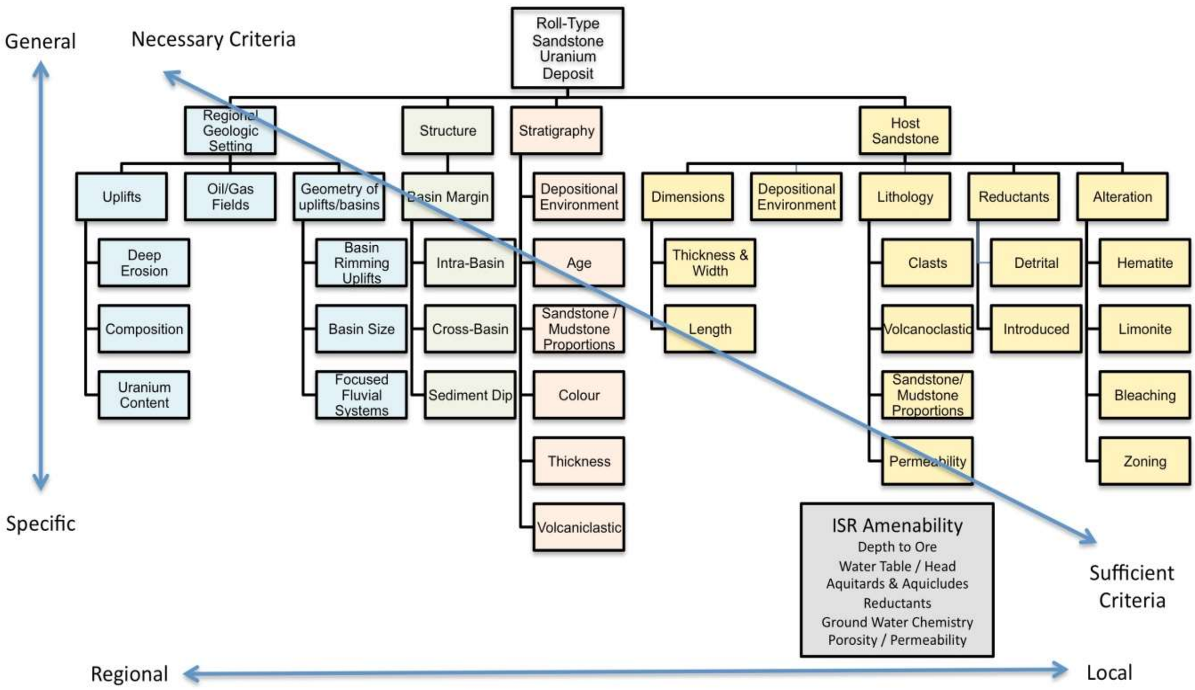

FIG. 37. Data–process–criteria model for sandstone roll-type uranium deposits (after [43]).

12. INNOVATIVE APPROACHES TO FRONTIER EXPLORATION

The next generation of undiscovered economic deposits resources is predicted to exist within some of the under-explored frontier localities that have received limited historical exploration expenditure or where efforts have been focused on near-surface exploration. Implementing programs in frontier areas is the riskiest form of exploration because of the uncertainty associated with explorability and prospectivity. Investments in exploration within these environments can be classified as very high-risk and high-reward. An approach to assessing the investment worth of exploration in frontier project areas with limited data and few or no discoveries follows.

Exploration frontiers can be classified as geographical, technological, depth-related, and data-related in nature (Table 7). The nature of the first three frontiers informs explorability, the fourth informs prospectivity. Assessing the uranium potential of frontier exploration environments in a rapid and low-cost way is particularly challenging, especially when baseline data are unavailable and historical discoveries are absent or sparse. The adoption of more systematic approaches to assessing uranium potential can lead to more robust decision-making.

TABLE 7: TYPES OF EXPLORATION FRONTIERS

Frontiers	Description	Example
Geographical	Exploration project areas are difficult to access and explore.	Working in remote equatorial rainforest or desert environments with poor infrastructure and logistics.
Technological	Exploration targets are difficult to identify or resolve by existing exploration methods.	Geochemical haloes over economic unconformity uranium deposits may not be detectable at >1000 m.
Depth	Exploration targets are anticipated to be too deep and expensive to explore.	Drilling program for targets >1000 m is too expensive and takes too long to complete.
Data	Datasets, reports and drill cores are not available to companies considering exploration investment.	Some geological survey organizations do not have adequate regional data and do not offer easy and low-cost access to historical data submitted by explorers.

An example of a geographical frontier would be an exploration project area in rainforest-covered area that cannot be easily accessed by road, or air, or foot and where limited and highly weathered bedrock and dense vegetation makes geological mapping and sampling difficult. The area may also be classified as a technological frontier if ‘classic’ geochemical methods do not work, or if current geophysical methods cannot resolve targets adequately due to contrasts in the physical properties of rocks postulated to host undiscovered deposits. The same area may also be classified as a depth frontier due to the presence of cover rocks suggesting that the depth to exploration target may be too deep to explore in an economical fashion with exiting technology.

Frontier uranium exploration areas can also exist in mature exploration environments that host economic deposits. An example would be exploration in the deeper parts of the Athabasca sandstone basin (Canada) where geochemical and geophysical technologies cannot adequately resolve targets at depths in excess of 1,000 m. The cost of testing targets at these depths is not economical due to the high cost of drilling and the long-time frames required for testing targets with typical exploration program budgets. Technological and economic risks associated with mining at greater depths are another consideration that can impact exploration investment decisions.

Exploration investments decisions are fundamentally driven by an assessment of available geoscientific data that exploration companies use to evaluate the prospectivity of a project area. Useful regional datasets typically consist of geological maps, and topographic, cadastral, aeromagnetic, radiometric, gravimetric, and multi-element geochemical surveys, among other information. Exploration companies also rely on access to historical drill cores and samples for examination. Geological survey organizations commonly curate these samples through core storage facilities. Most geological survey organizations require exploration companies to file activity reports as evidence of their fulfillment of obligations set out in exploration permits. These reports commonly contain copies of the exploration data collected during the program that are publicized. As a best practice, geological survey organizations organize all of this information so that it is easily available to potential exploration investors through Internet portals according to certain protocols.

However, many frontiers are often characterized as being data-poor. This situation can arise for several reasons including insufficiently funded geological survey organizations that have not invested in the acquisition of regional baseline datasets, the development of data libraries, and technical staff and infrastructure to support exploration investment. In some instances, useful historical geologic baseline information collected during the colonial era, resides in other countries, and cannot be accessed in an efficient manner by exploration companies due to information transfer agreements. In addition, the sheer remoteness of some geographical areas and preconceptions about their prospectivity may have resulted in limited investment by exploration companies. An example would be false assessments about the uranium potential of ancient sandstone basins before the discovery of the unconformity uranium deposit class in the late 1960's. Up until that time the perception was that many of these basins had a very low potential to host uranium and other types of deposits leading to low levels of exploration investment.

Assessing the investment worth of exploration in frontier project areas with limited data and few or no discoveries is very challenging. In the absence of local data, quantitative models can be developed that make use of analogies with other areas that have yielded economic deposits. Probabilistic estimates of the likelihood and magnitude of economic discovery in response to exploration expenditures can be derived, based upon geological and probability analysis [25]. However, the application of these methods is still its infancy. Qualitative approaches are also available that are more easily accessible and that leverage research and development as a core activity.

A comparison of conventional and rapid, innovative, approaches to assessing the investment worth of uranium exploration in a frontier project area with limited data is presented in Fig. 38. Conventional approaches to evaluating frontier project areas typically involve an initial assessment of existing spatial datasets provided by geological survey organizations with a particular deposit model in mind. The goal is to identify general target areas that warrant exploration based on what is known from descriptive deposit models. This approach is fundamentally a pattern recognition exercise. A series of follow-up regional, local, and detailed geophysical, geochemical and geological survey program are designed, completed, and reviewed, and typically result in drilling programs to test significant anomalies. A typical uranium exploration program could involve the expenditure of US$5 million over four or five years. Decisions to continue or abandon the project are typical, after a few drilling programs, and are based upon the presence or absence of significant geoscientific signatures associated with mineralization, among other factors.

In contrast, an alternative approach to evaluating frontier project areas focuses on the rapid and cost effective qualitative assessment of economic uranium potential relying on expert knowledge. One goal is to evaluate prospectivity through a holistic evidence-based geoscientific analysis. A second goal is the assessment of prospectivity and the identification and development of uranium exploration technologies that are best suited to the local geological setting. This approach relies on the development of collaborations with company experts, consultants and applied academic researchers, with a focus on the exchange of knowledge for better decision-making. This approach includes a dialogue around critical questions surrounding uranium exploration, the further development of genetic deposit models, the refinement of approaches to holistic prospectivity analysis, and the development of next generation exploration technologies. Information about critical questions in uranium exploration and holistic analysis of sandstone basins for their uranium potential can be in a paper by [45]. A typical program could involve expenditures of US$2 million over two to three years to determine the investment worth of exploration prior to proceeding with more conventional approaches to identify specific drilling targets.

An example of a rapid frontier basin assessment of the potential for economic unconformity–related deposits in Roraima sandstone basin (Guyana) is presented in a publication by [46]. The frontier environment can be classified as extremely challenging from the perspective of logistics, geography, technology, target depth and the availability of baseline data. The exploration team (exploration manager, researchers, and geophysical technology consultants) used an evidence-based approach founded on holistic basin analysis that relied on expert judgment. The team concluded that it was unlikely that the basin will host unconformity–related uranium deposits from both a prospectivity and explorability perspective. The program was characterized by the extensive exchange of knowledge and was conducted at lower cost and within a short time frame than a conventional program. Further investment was halted and reallocated to other projects.

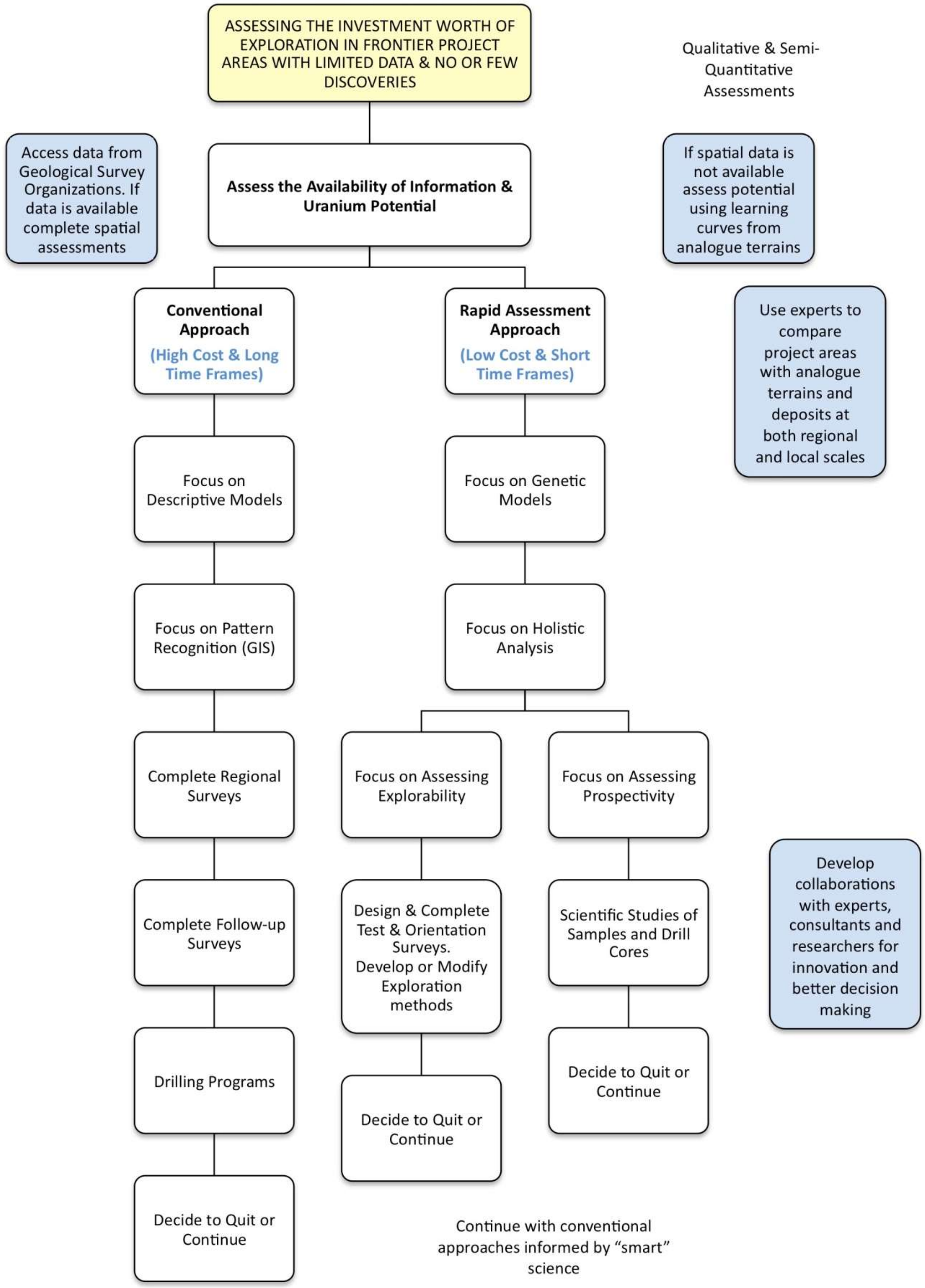

FIG. 38. A comparison of conventional and rapid approaches to assessing the investment worth of uranium exploration in frontier project areas with limited data.

13. CONCLUSIONS

Uranium exploration is a complex high-risk, high-reward business activity at the front end of the nuclear fuel cycle. The uranium exploration process involves the effective use of geoscientific knowledge and exploration technologies for the discovery of economic uranium deposits. The quantitative and qualitative estimation of economic mineral potential is an important area of focus for understanding the investment worth of uranium exploration.

The business drivers of exploration include factors related to uranium supply and demand and attitudes toward investment. The technical drivers of exploration include the optimal selection of geographical areas for exploration based upon an assessment of prospectivity and explorability. The optimization of human, organization and technology factors for discovery is another factor.

The key stakeholders in the exploration process are governments, geological survey organizations, consultants, researchers, exploration service providers, and exploration company managers and workers. Geological survey organizations play an important role in attracting investment. They support the establishment of a favorable business environment, provide easy access to pre-competitive geoscientific information, and initiate economic mineral potential assessments, among other activities. Survey organizations contribute to significant long-term economic development within their jurisdictions by attracting investment from the uranium exploration and mining sector.

On a global basis, historical uranium exploration has led to the discovery of uranium deposits. However, there is significant uncertainty associated with the economic potential illustrated in the global inventory of uranium resources. The exploration process is relatively inefficient and the conversion rate of significant discoveries to producing mining operations is estimated to be approximately fifty percent, due to technical, economic, social and environmental factors.

Rapid and cost-effective evidence-based approaches to assessing the investment worth of uranium exploration in frontier project areas with limited data provide an alternative to more conventional approaches. Exploration frontiers can be classified as geographical, technological, depth-related, and data-related in nature. Innovative approaches rely on the development of collaborations with company and organizational experts, consultants and applied academic researchers, with a focus on the exchange of knowledge for better exploration decision-making and the development of technological innovations.

Next-generation undiscovered economic deposits are predicted to exist within under explored frontier localities that have received limited historical exploration expenditure. However, a technology leap is indicated as a requirement for these new economic discoveries. This leap could come in the form of innovations associated with geological, geochemical, geophysical, drilling, and mining methods or deposit models, and their deployment in terrains identified through quantitative and qualitative economic mineral potential assessments.

REFERENCES

[1] OECD-NEA & IAEA, Uranium 2014: resources, production and demand, NEA no. 7209, A joint report by the Organization for Economic Co-operation and Development Nuclear Energy Agency (OECD-NEA) and the International Atomic Energy Agency (IAEA), 508p (2014).

[2] OECD-NEA & IAEA, Uranium 2016: Resources, Production and Demand, OECD NEA (2016).
[3] INTERNATIONAL ATOMIC ENERGY AGENCY, The Nuclear Fuel Cycle, IAEA, Vienna (2011). https://www.iaea.org/sites/default/files/nfc0811.pdf
[4] UNITED NATIONS ECONOMIC COMMISSION FOR EUROPE, United Nations Framework Classification for Fossil Energy and Mineral Reserves and Resources 2009, UNECE Energy Series No. 42, United Nations, New York (2013).
[5] TULSIDAS, H., LI, S., VAN GOSEN, B., VILLES-BOAS, R., CARSON, L., GRIFFITHS, C., ROSS, J., MACDONALD, D., BANKES, P., HANLY, A., MIEZITIS, Y., HALL, S., VANCE, R., MUKUSHER, A., Application of United Nations Framework Classification 2009 (UNFC-2009) to Nuclear Fuel Resources, paper presented at the IAEA URAM 2014 symposium, IAEA, Vienna (2014).
[6] INTERNATIONAL ATOMIC ENERGY AGENCY, Establishment of Uranium Mining and Processing Operations in the Context of Sustainable Development, IAEA Nuclear Energy Series No. NF-T-1.1, IAEA, Vienna (2009).
[7] INTERNATIONAL ATOMIC ENERGY AGENCY, Parameters to be Considered When Assessing a Uranium Ore Deposit, IAEA-TECDOC-1174, IAEA, Vienna (2000).
[8] DALHKAMP, F., Uranium Deposit Models, Springer-Verlag, Berlin, (1993) 460 pp.
[9] BRUNETON, P., CUNEY M., DAHLKAMP, F., ZALUSKI, G., IAEA geological classification of uranium deposits. URAM 2014, IAEA Vienna (2014).
[10] OECD NUCLEAR ENERGY AGENCY, Forty Years of Uranium Resources, Production and Demand in Perspective, NEA, Paris (2006).
[11] KYSER, T.K., Exploration for Uranium, in: Hore-Lacey, I. (Ed.) Uranium for Nuclear Power, Woodhead, Swaston, 468p (2016).
[12] INTERNATIONAL ATOMIC ENERGY AGENCY, Uranium Exploration Planning and Practice, IAEA-TECDOC-583, IAEA, Vienna (1991).
[13] SMITH, A., TAUCHID, M., Uranium Exploration Planning and Practice, in: Uranium Exploration Planning and Strategy, IAEA-TECDOC-583, IAEA, Vienna (1991).
[14] CANADIAN INSTITUTE OF MINING AND METALLURGY, Survey of Principal Mining Risks, CIMM, Toronto (2000).
[15] CARTER, N., A Market in Transition, paper presented at the IAEA International Symposium on Uranium Raw Material for the Nuclear Fuel Cycle, Vienna (2014).
[16] BOYSTOV, A., Worldwide ISL Uranium Mining Outlook, paper presented at the URAM 2014 symposium, IAEA, Vienna (2014).
[17] U.S. ENERGY INFORMATION ADMINISTRATION, 2015 Domestic Uranium Production Report, U.S. Department of Energy, Washington, 15p (2016).
[18] MCKAY, A., MIEZITIS, Y., Australia's Uranium Resources, Geology and Development of Deposits, AGSO - Geoscience Australia, 184p (2001).
[19] INTERNATIONAL ATOMIC ENERGY AGENCY, World Distribution of Uranium Deposits, IAEA, Vienna (2016). https://infcis.iaea.org/UDEPO/About.cshtml
[20] STEVEN, G., BURLEY, J., 3000 Raw Ideas = 1 Commercial Success, Research Technology Management 1997, 16p (1997).
[21] MARLATT, J., KYSER, T.K. Paradigmatic Shifts in the Uranium Exploration Process: Knowledge Brokers and the Athabasca Learning Curve, Society of Economic Geologists Newsletter 84, 1 (2011).
[22] POOL, T.C., Uranium Supply to 2060, paper presented at IAEA URAM 2014 symposium, IAEA, Vienna (2014).

[23] CRANSTONE, D., WHILLANS, R., The Analysis of Uranium Discovery in Canada, 1930-1983: Rates of Discovery, Exploration Expenditures, Discovery Costs and Geological Deposit Types, In: Uranium Resources and Geology of North America, IAEA-TECDOC-500, IAEA, Vienna (1989).
[24] MACDONALD, C., Uranium: Sustainable Resource or Limit to Growth? 2003 WNA Symposium, World Nuclear Association, London (2003).
[25] HARRIS, D., ZALUSKI, G., MARLATT, J., A Method for the Selection of Exploration Areas for Unconformity Uranium Deposits, Natural Resources Research (2009).
[26] AUSTRALIAN BUREAU OF STATISTICS, Mineral and Petroleum Exploration, Statistics Report 8412.0, ABS, Australia (2015).
[27] COX, D., SINGER, D., Mineral Deposit Models, U.S. Geological Survey Bulletin 1693, United States Government Printing Office, Washington (1986).
[28] WORLD NUCLEAR ASSOCIATION, Uranium Market (updated February 2015), WNA (2015). http://www.world-nuclear.org/information-library/nuclear-fuel-cycle/uranium-resources/uranium-markets.aspx
[29] SASKATCHEWAN MINING ASSOCIATION, Expenditures for Uranium Mining 1980-2014, SMA (2016). http://www.saskmining.ca/commodity-info/Commodities/24/uranium.html
[30] TRANSPARENCY INTERNATIONAL, Corruptions Perceptions Index 2015, TI (2015). http://www.transparency.org/
[31] JACKSON, T., GREEN, K., Annual Survey of Mining Companies, Fraser Institute, Toronto (2016).
[32] SMITH, L., Discounted Cash Flow Analysis Methodology and Discount Rates, Mineral Valuation Proceedings, Mining Millenium 2000 Symposium, Canadian Institute of Mining, Metallurgy and Petroleum, Toronto (2000).
[33] THE PRS GROUP INC., Country Risk, International Country Risk Guide, XXI, 9, (2001).
[34] CENTER FOR STRATEGIC AND INTERNATONAL STUDIES, High Country Risk Definition (2012) http://www.csis.org/energy/ga120601mamae/sld004.htm
[35] WORLD BUSINESS COUNCIL FOR SUSTAINABLE DEVELOPMENT, Corporate Social Responsibility Definition (2002). http://www.wbcsd.org/
[36] INTERNATIONAL ATOMIC ENERGY AGENCY, Advances in Airborne and Ground Geophysical Methods of Uranium Exploration, IAEA Nuclear Energy Series No. NF-T-1.5, IAEA, Vienna (2013).
[37] WHITE, A., Management of Mineral Exploration, 2nd ed., James Cook University of Earth & Environmental Sciences, 335p (2009).
[38] WALLIS, R., KERR, W., Facts and Fallacies: A Personal Commentary on 45 Years of Uranium Exploration and Development in the Athabasca Basin of Northern Saskatchewan, paper presented to the Toronto Geological Discussion Group, Toronto (2014).
[39] KERR, W., WALLACE, R., "Real-World" Economics of the Uranium Deposits of the Athabasca Basin, Northern Saskatchewan: Why Grade is Not Always King!, Society of Economic Geologists Newsletter, 99 (2014).
[40] INTERNATIONAL ATOMIC ENERGY AGENCY, World Distribution of Uranium Deposits (UDEPO) with Uranium Deposit Classification, IAEA-TECDOC-1629, IAEA, Vienna (2009).
[41] CUNEY, M., Geology of Uranium Deposits, in: Hore-Lacey, I. (Ed.), Uranium for Nuclear Power, Woodhead, Swatson, 468p (2016).

[42] CUNEY, M., KYSER, T.K., Recent and Not-So-Recent Developments in Uranium Deposits and Implications for Exploration, Mineral Association of Canada Short Course Series, Vol. 39, Mineral Association of Canada, Quebec, 258p (2009).

[43] ADAMS, S., CRAMER, R., Data-Process-Criteria Model for Roll-Front Deposits, in: Geological Environments for Sandstone Uranium Deposits, IAEA-TECDOC-328, IAEA, Vienna (1985).

[44] NUCLEAR ENERGY AGENCY, OECD, World Uranium Geology and Resource Potential, Miller Freeman, San Francisco, 524p (1980).

[45] KYSER, T.K., Fluids, Basin Analysis, and Mineral Deposits, Geofluids 7, 238 (2007).

[46] BEYER, S., HIATT, E., KYSER, K., DREVER, G., MARLATT, J., Stratigraphy, Diagenesis and Geological Evolution of the Paleoproterozoic Roraima Basin, Guyana: Links to Tectonic Events on the Amazon Craton and Assessment for Uranium Mineralization, Precambrian Research 267, 227-249 (2015).

REGIONAL-SCALE PROSPECTIVITY MAPPING FOR SURFICIAL URANIUM DEPOSITS IN SOUTHERN BRITISH COLUMBIA, CANADA

E.J.M. CARRANZA
University of KwaZulu-Natal,
Westville, South Africa

Abstract

This chapter presents a case study of GIS-based mineral systems approach to mapping of prospectivity for surficial uranium mineralization in the central part of southernmost British Columbia. The surficial U mineralization in this region is different from the ones in well known provinces such as Western Australia or Namibia. Therefore, the GIS-based approach described here is adapted from a seminal previous work to map prospectivity for surficial uranium mineralization in Western Australia. In particular, this case study demonstrates how to use data on content of labile uranium in potential source rocks in the analysis and synthesis of uranium source spatial proxies. In addition, this case study strives to analyze the spatial proxies' efficiency for outlining of areas that are prospective for surficial uranium mineralization in the study area.

1. INTRODUCTION

Surficial uranium (U) deposits represent only ~4% of the world's U resources [1]. However, because such deposits occur near the surface they are relatively inexpensive to mine and so they are appealing to the mining industry. Surficial U mineralization in the central part of southernmost British Columbia of Canada (Fig. 1) is represented by a few surficial U deposits (n=4) and many small prospects and showings (n=32). The few surficial U deposits in the region (with tonnages varying from 24 to 629 kt, and U grades varying from 0.01 to 0.5%) are described in [2, 3] whereas information about each of the small prospects and showings (with U grades varying from 0.007 to 0.297%) can be found in the MINFILE mineral inventory of British Columbia (http://minfile.gov.bc.ca/). The prospectivity of the region for the same type of deposits has not been assessed fully yet.

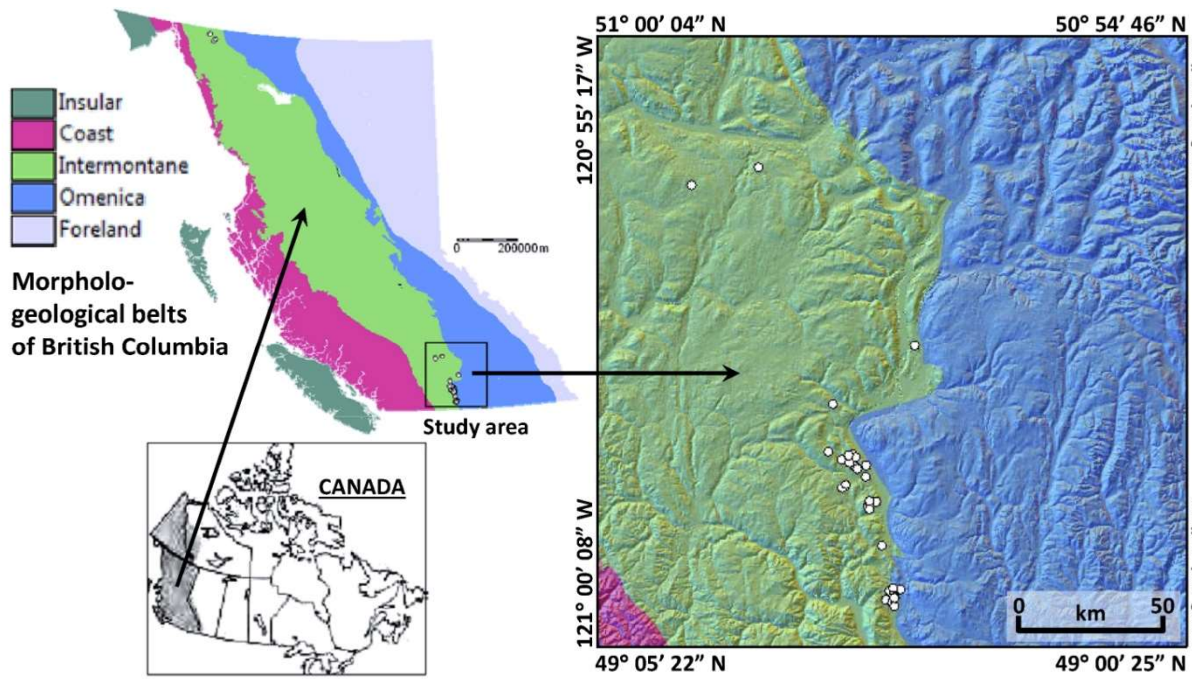

FIG. 1. Surficial U occurrences (white dots) in south-central British Columbia (Canada).

Two possible options exist for mapping, with the aid of a geographical information system (GIS), the prospectivity of a region for mineral deposits of the type sought [4, 5]. One option is to follow the data-driven approach, whereby the spatial associations of known mineral deposits/occurrences of the type sought with various geological features representing mineralization controls are quantified and used to develop a probabilistic model, portrayed as a map, depicting locations where undiscovered mineral deposits/occurrences of the same type are likely to exist. Very recent examples of data-driven prospectivity mapping for certain types of mineral deposits can be found in [6−8]. The alternate option is to follow the knowledge-driven approach, whereby expert opinions about geological features that are genetically and, thus, spatially associated with mineral deposits of the type sought are synthesized into a favorability model, portrayed as a map, depicting locations where undiscovered mineral deposits/occurrences of the same type may exist. Very recent examples of knowledge-driven prospectivity mapping for certain types of mineral deposits can be found in [9−11]. Very recent studies that compare the efficiency of data- and knowledge-driven approaches to mineral prospectivity mapping can be found in [12−14]. Essentially, data-driven prospectivity mapping is suitable only in regions where mineral deposits are known to exist whereas knowledge-driven prospectivity mapping is suitable in regions where minerals deposits are either known or not known to exist. Therefore, either data- or knowledge-driven approach to prospectivity mapping can be applied to delineate exploration targets for surficial U deposits in the central part of southernmost British Columbia of Canada.

Many researchers have argued, however, that expert opinions about geological features that are genetically and, thus, spatially associated with mineral deposits of the type sought are highly subjective and impart systemic uncertainty in knowledge-driven prospectivity mapping whereas inadequate or poor quality evidential data and insufficient data on mineral deposit locations impart stochastic uncertainty in either knowledge- or data-driven prospectivity mapping. Systemic uncertainty also derives from 'black-box' data-driven methods of prospectivity mapping. Obviously, adequate and good quality evidential data are needed for either knowledge- or data-driven prospectivity mapping. However, in recent years, many researchers have proposed to adopt a mineral systems approach to prospectivity mapping in order to minimize mainly systemic uncertainty [15, 20]. A seminal work on the application of mineral systems approach to prospectivity analysis for six models of U systems is described by [21], whereas a seminal work on the application of mineral systems approach to prospectivity analysis for surficial U system is described by [22].

The mineral systems approach to prospectivity mapping requires understanding of the source-transport-trap system of mineralization of interest and its application to derive and integrate spatial proxies (or evidential maps) from suitable geoscience spatial data. Porwal et al. [22] were the first to demonstrate a mineral systems approach using GIS to map prospectivity for surficial U deposits in Yeelirrie area (Western Australia). In that area, surficial U mineralization occurs as carnotite hosted in calcretes [23]. However, surficial U mineralization in the central part of southernmost British Columbia differs from the ones in Western Australia and Namibia in that the former is still in progress and no typical U minerals have been formed yet because U is tied loosely to sediments, from which it is remobilized easily, because no appropriate material (e.g., calcrete) exist there that could as act both as a trap and host to mineralization [2, 3]. Therefore, the system of surficial U mineralization in the central part of southernmost British Columbia is different from the ones in well known areas such as Western Australia or Namibia. It follows that the GIS-based approach described by [22] to map prospectivity for surficial U on a regional in Yeelirrie needs to be adapted for application in south-central British Columbia.

An essential element in the central part of southernmost British Columbia is that data on content of labile U in potential source rocks are available [2, 3]. Therefore, this case study focuses on how to use such data in the analysis and synthesis of U source spatial proxies. In addition, this case study strives to analyze the spatial proxies' efficiency for outlining of areas that are prospective for surficial U mineralization in south-central British Columbia.

2. SYSTEM OF SURFICIAL URANIUM MINERALIZATION

The oldest rocks underlying most of the region belong to the Shuswap metamorphic complex, containing gneisses, quartzites, schists and limestones (Fig. 2) [24]. Mesozoic metavolcanic-metasedimentary rocks overlie the Shuswap metamorphic terrane. These older rocks are intruded by Jurassic to Early Cretaceous granitoids, comprised mostly by the Okanagan Highlands intrusive complex consisting of granodiorite, diorite, granite, monzonite and pegmatite. Late Cretaceous to Paleocene granitoids (quartz monzonite, porphyritic granite and pegmatite) intruded into the pre-existing rocks. Early Tertiary (Paleocene–Oligocene) volcanic-sedimentary rocks (trachytes, rhyodacites, rhyolites, andesites, basalts, shales, mudstones, sandstones and conglomerates) formed in isolated basins over the pre-existing rocks. Coeval with the Early Tertiary volcanics are the Eocene granitoid intrusions.

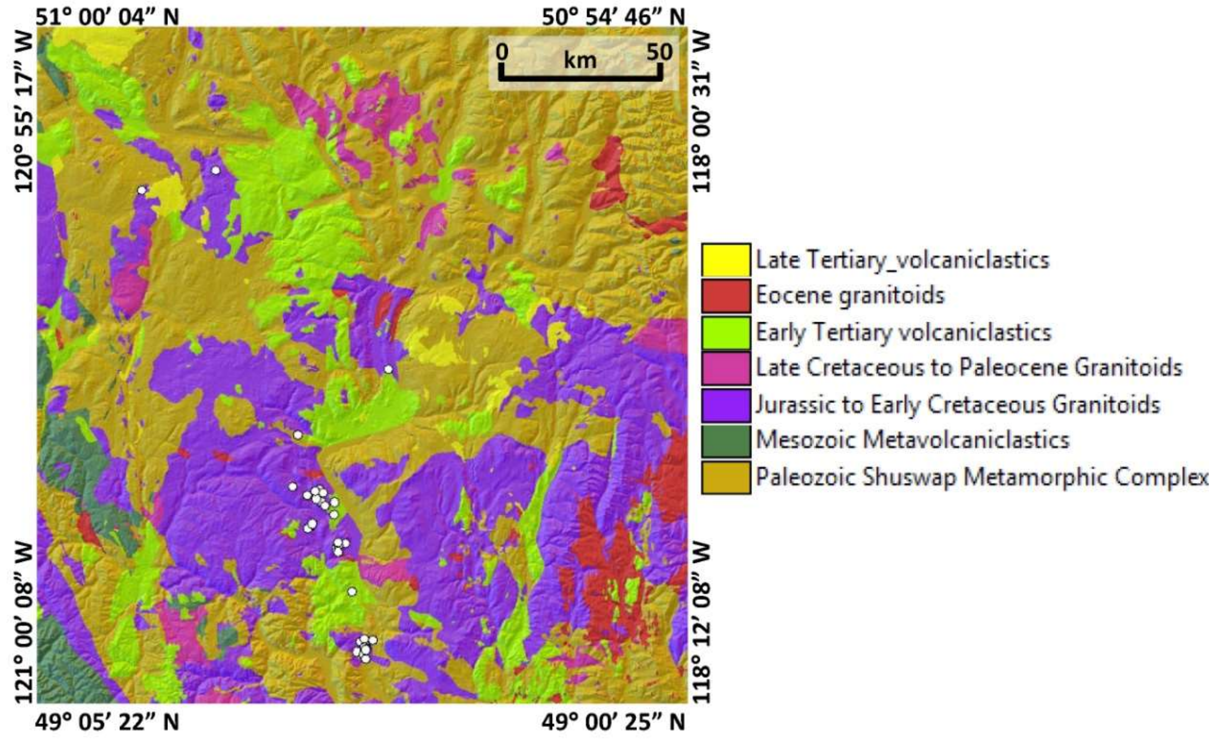

FIG. 2. Simplified lithostratigraphic units and locations of surficial U deposits/occurrences (white dots), south-central British Columbia, Canada (adapted from [24])

The lacustrine/playa and/or fluviatile U mineralization in the south-central British Columbia, which occurs within loose, permeable Late Miocene fluvial sediments along (paleo)channels or (paleo)depressions [2], is probably younger than 10,000 years [3], [25], [26]. Uranium mineralization is characterized mainly by uranyl carbonates ($UO_2(CO_3)$) [3] and/or uranous phosphate minerals like saleeite ($Mg(UO_2)_2(PO_4)_2 \cdot 8\text{-}10H_2O$), ningoyite $(U,Ca)_2(PO_4) \cdot 1\text{-}2H_2O$)

and autunite ($Ca(UO_2)_2(PO_4)_2 \cdot 8\text{-}10H_2O$) [2]. No typical U ore minerals (e.g., uraninite (UO_2), carnotite ($K_2(UO_2)_2(VO_4)_2 \cdot 3H_2O$)) have been identified yet in the region.

2.1. Source of uranium

The typical sources of U for surficial as well as other types of U mineralization are felsic intrusive or volcanic rocks with labile U [27]. This is apparently true in the south-central British Columbia, as the known U deposits/occurrences exhibit strong spatial association with Jurassic to Early Cretaceous granitoids as well as Early Tertiary volcanics (Fig. 2).

The possible source rocks of U in the region are Eocene volcanics (trachyte and rhyolite), Eocene-Oligocene intrusions (Coryell Monzonite), Jurassic to Early Cretaceous granitoids, and Paleozoic Shuswap Metamorphic Complex (which includes small units of uraniferous pegmatites) [2, 3]. As can be seen from Table 1, the Coryell Monzonite seems to the greatest donor of U but considering the percent labile U the Okanagan granites and pegmatites are major sources of U in south-central British Columbia.

Aside from availability of labile U, the ease with which U is released from the source is an important source factor. Recurring tectonic and multiphase intrusive activities that have affected south-central British Columbia fabric-loosened intrusive bodies cut by interconnected faults/fractures, which favored the release of U from the source rocks [2].

TABLE 1. LABILE URANIUM CONTENT OF POTENTIAL SOURCE ROCKS OF URANIUM IN SOUTH-CENTRAL BRITISH COLUMBIA (*1)

Rock type	Average U in rock (ppb)	Average labile U (ppb)	% of labile U (*2)
Eocene-Oligocene Coryell Monzonite	6200	43	0.69
Eocene trachyte/rhyolite	5600	12	0.21
Jurassic-Cretaceous Okanagan Granite	5400	59	1.09
Jurassic-Cretaceous Okanagan Granodiorite	2300	9	0.39
Jurassic-Cretaceous Okanagan Pegmatite	5200	192	3.69
Paleozoic Shuswap Gneiss	1600	?	?

(*1) Data in the first three columns are from [2]. (*2) Values in the last column were obtained by dividing the values in the third column by those in the second column and then multiplying the quotient by 100.

2.2. Transport of uranium

The fabric-loosened intrusive bodies cut by interconnected faults/fractures also favored widely-distributed and deep-seated flow of U-bearing groundwater that eventually infiltrated permeable sediments along (paleo)channels or (paleo)depressions [3]. In these near-surface environments, U is transported by oxygenated alkaline groundwater in the form of soluble uranyl carbonate complexes [28]. Water flow is focused through permeable (paleo)topographic lows occupied by porous fluviatile sediments. Driver of fluid flow is mainly hydrological gradient along the system of (paleo)topographic lows.

2.3. Deposition of uranium

As groundwater carrying soluble U complexes enter trap areas, U minerals may precipitate and accumulate through various mechanisms depending on the type of surficial environment of the trap areas. In lacustrine/playa environments, lake sediments provide both physical and chemical traps, and U precipitates/accumulates mainly by evaporation and/or by reduction due to organic-rich lake sediments or bacteria [3]. In permeable zones of fluviatile (or channel) environments, U minerals precipitate and accumulate as upwelling groundwater encounter organic-rich sediments or soils. As no typical U minerals have been identified in the region, U precipitates/accumulates likely due to adsorption, reduction or evaporation [3], [26]. However, geochemical calculations by [26] suggest that the role of evaporation is limited because groundwater has not reach saturation with respect to common U phosphates. It has also been argued by [26] that the role of reduction cannot be assessed because no U minerals have been identified although groundwater show changed in Eh. Therefore, the mostly likely dominant factor of U mineralization in fluviatile (or channel) systems in the study region is adsorption, followed by reduction [26].

3. TARGETING CRITERIA AND SPATIAL PROXIES FOR SURFICIAL URANIUM MINERALIZATION

The surficial U system in south-central British Columbia is similar to but is different from the most important surficial U deposits in the world, which are in the form of carnotite ($K2(UO2)2(VO4)2•3H2O$) hosted in calcrete [29–32]. This means that targeting criteria and spatial proxies for mapping of prospectivity for surficial U in south-central British Columbia will differ somewhat from those defined/used by [22] for mapping of prospectivity for surficial U in the Yeelirrie area (Australia).

3.1. Uranium source

Two U source targeting criteria are suitable for regional-scale mapping of prospectivity for surficial U deposits in the study region (Table 2).

TABLE 2. REGIONAL-SCALE TARGETING CRITERIA AND SPATIAL PROXIES FOR URANIUM SOURCE IN SURFICIAL URANIUM MINERALIZATION, SOUTH-CENTRAL BRITISH COLUMBIA

Targeting criteria	Spatial proxy	Data source	Rationale
Felsic rocks (intrusives or volcanics) with labile U	Presence of or proximity to felsic rocks with labile U	1) Regional-scale lithologic map [33] 2) Total and labile U contents of felsic rocks [2]	Felsic rocks (intrusives or volcanics) are typically enriched in U and are widely considered as the main sources of U for most U mineral systems, but not all felsic rocks are capable of releasing large quantities of labile U
Fabric-loosened source rocks for ease of release of U	Proximity to major faults	Regional-scale fault map [33]	The ease of U released from source rock is an important source factor. Presence of fabric-loosened source rocks is thus important for surficial U mineralization. Fabric of source rocks cut by or proximal to major faults are likely loosened due to recurrent tectonic activities.

Porwal et al. [22] used proximity (i.e., Euclidean distance) to U-enriched granites as spatial proxy of U-rich Archean granites as targeting criterion for surficial U systems in Yeelirrie area. The use of proximity to U-enriched rocks as spatial proxy of source rocks for surficial U mineralization is intuitive because labile U is carried, by groundwater, away from source rocks and surficial U mineralization may form not only on areas underlain by source rocks but on areas proximal to such rocks. However, here, we convert Euclidean distance into fuzzy proximity depicting pseudo-probability values (i.e., nearest distance being equal or nearly equal to 1 and farthest distance in a map being equal or nearly equal to 0). That is because, like in [22], we will use in this case study the fuzzy set theory for prospectivity mapping. To convert Euclidean distance into fuzzy proximity we use not a linear but a non-linear function, because mineral prospectivity is a non-linear function of proximity to geological features that are genetically as well as spatially associated with mineral deposits. A non-linear function that is commonly used to model spatial proxies of mineral prospectivity is the logistic function [5], [34], [35], [36], [37], [38]. The form of logistic function used here is:

$$\textit{fuzzy score} = 1/(1 + e^{s(x - m)}) \tag{1}$$

where e is the mathematical constant or Euler number, s is the slope of the function, x is a value (e.g., distance) to be transformed in the [0,1] range, and m is the chosen inflexion point of the function (or curve).

For modeling of proximity to U-source rocks in this case study, m is chosen to be 10 km to portray that in areas within 10 km of a source (a pathway, or a trap) there is 0.5 to 1.0 likelihood of surficial U mineralization whereas in areas beyond 10 km of a source (a pathway, or a trap) there is less than 0.5 likelihood of surficial U mineralization. The choice of m is arbitrary and certainly requires expert knowledge and the example of 10 km for m here for modeling of proximity to U-source rocks in this case study is meant for demonstrating the method but not a submission of expert opinion. Fig.s 3 to 5 show the maps of fuzzy proximity to mapped potential U-source rock units derived from the respective maps of Euclidean distance to those lithologic units.

Porwal et al. [22] generated their map of U-enriched granite by integrating lithologic map, geochemical map of U concentration, and radiometric data. However, this procedure is redundant in this case study because the available lithologic map (Fig. 2) is the result of integration of bedrock geology, surficial geology, and geophysical and geochemical interpretations [24]. Nevertheless, there are data on total and labile U content of felsic rocks [2] and these present challenges for spatial data integration in this context as the seminal works of [21] and [22] have not dealt with the same type of data.

Although total and labile U data are available for different certain potential U-source rocks (Table 1) the available regional-scale lithological map [33] depicts only the: (a) Coryell Plutonic Suite, which includes felsic rocks other than monzonite, (b) Eocene volcanics, which consist felsic volcanics other than trachyte/rhyolite, and (c) Okanagan Batholith or intrusive complex, which consists of felsic intrusives other than granite, granodiorite, and pegmatite. However, considering that the specific rocks for which labile U data are available are representative of the afore-mentioned lithologic units, it is demonstrated here how labile U data may be used as spatial weights for proximity to potential U-source lithologic units. Thus, the % of labile U data of Coryell monzonite are used for the Coryell Plutonic Suite, % of labile U data of Eocene trachyte/rhyolite for the Eocene Volcanics, and average of % of labile U data of Okanagan granite, granodiorite and pegmatite (Table 1) for the Okanagan Batholith (Table 3). The spatial weights were then obtained as normalized values of the % of labile U values of the lithologic units (Table 3).

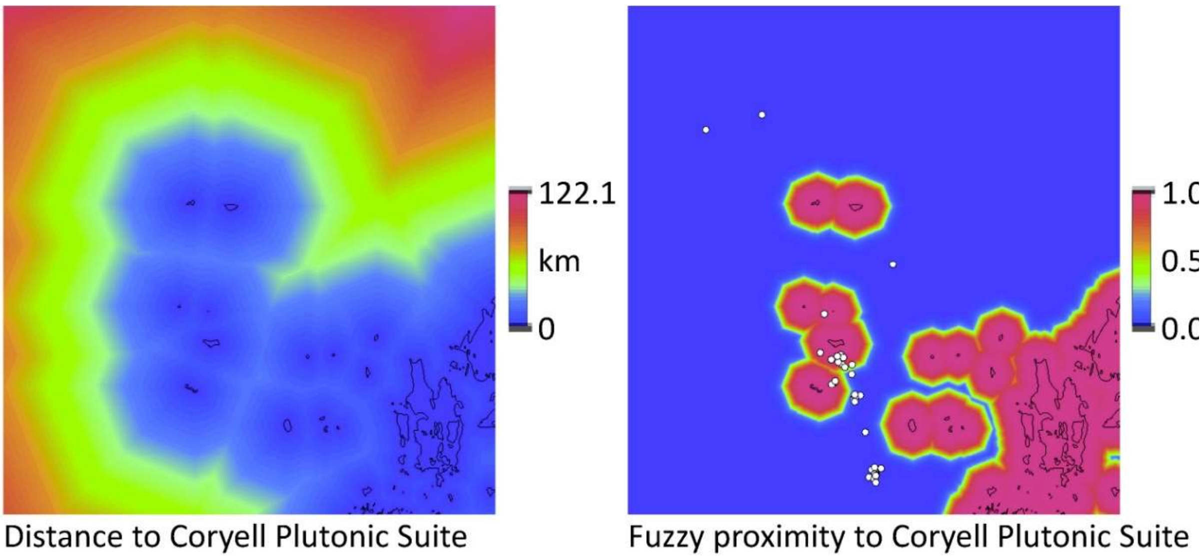

FIG. 3. Map of Euclidean distance to Coryell Plutonic Suite in the study region converted to a map of fuzzy proximity to lithologic unit using Equation 1. Black polylines are margins of the Coryell Plutonic Suite. White dots are surficial U deposits/occurrences. For map coordinates, see Fig. 1 or 2.

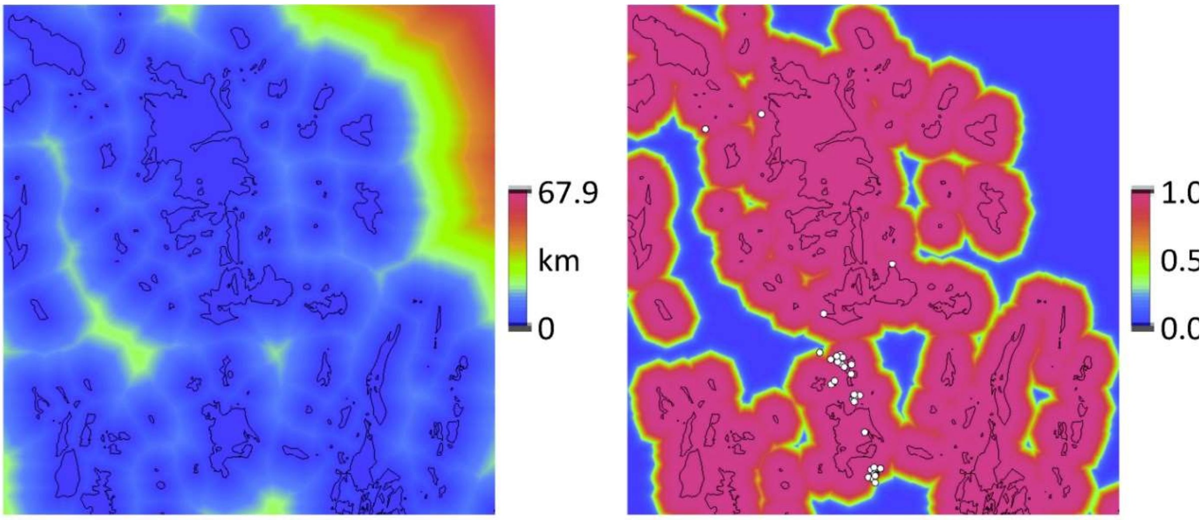

FIG. 4. Map of Euclidean distance to Eocene Volcanics in the study region converted to a map of fuzzy proximity to Eocene Volcanics using Equation 1. Black polylines are margins of the Eocene Volcanics. White dots are surficial U deposits/occurrences. For map coordinates, see Fig. 1 or 2.

Now that we have three maps of fuzzy proximity to individual potential U-source rocks (Figs. 3, 4 and 5) and the weights (Table 3), the next challenge is how to combine these maps, using the weights, into a single map of fuzzy proximity to all potential U-source rocks. That is intuitive because the labile U leached from various source rocks eventually gets mixed together in groundwater. For this purpose, the fuzzy algebraic sum (*FAS*) is the most suitable among the five commonly used fuzzy operators (see Appendix I) because according to [4] the *FAS* is suitable when at least two layers of evidence (in this case maps of proximity to potential U-source rocks) that support a proposition (in this case prospectivity for surficial U deposits) reinforce each other and the integrated layer of evidence is stronger than each of the individual layers of evidence. However, the result of using the *FAS* equation (Appendix I), shown in Fig. 6 (left panel), is apparently unsatisfactory because the map resembles mainly the map of fuzzy proximity to Eocene Volcanics (Fig. 4, right panel) suggesting that the Eocene Volcanics are most important sources of U. Although rhyolites are known to be important sources of U [39–46], this general knowledge is inconsistent with the labile U information about the potential U-source rocks (see Tables 1 and 3). In order to use the weights (denoted as w) in combining the three maps of fuzzy proximity to individual potential U-source rocks (denoted as μ_i, i=1, …, n), it is proposed here to modify the *FAS* equation in Appendix I to a weighted *FAS*, thus:

$$\mu_i = 1 - \prod_i^n (1 - w\mu_i) \tag{2}$$

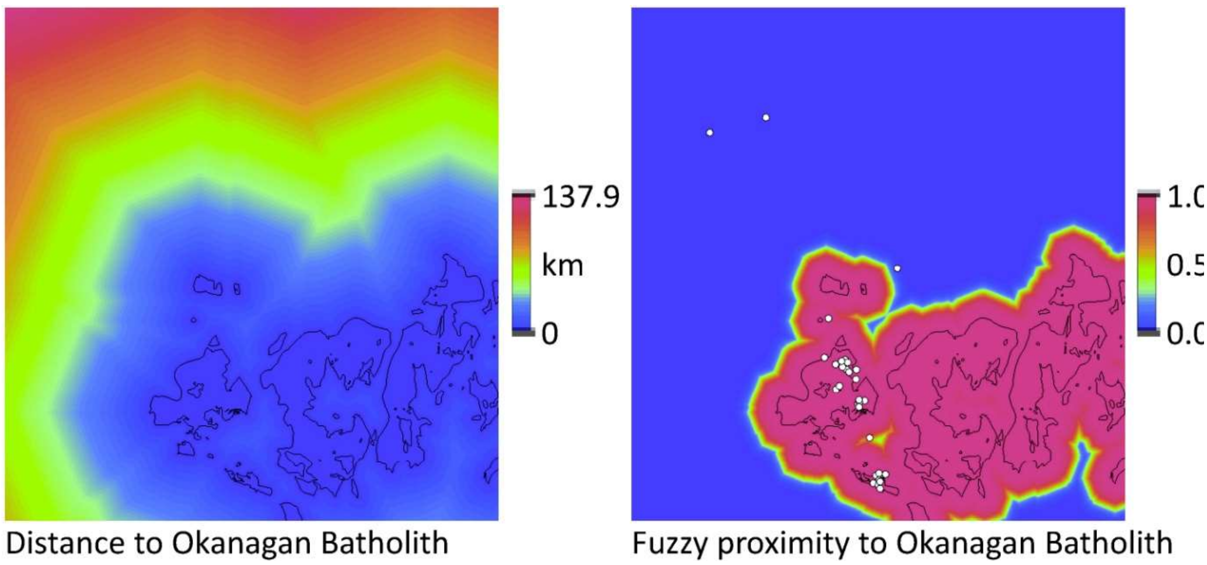

FIG. 5. Map of Euclidean distance to Okanagan Batholith converted to a map of fuzzy proximity to Okanagan Batholith using Equation 1. Black polylines are margins of the Okanagan Batholith. White dots are surficial U deposits/occurrences. For map coordinates, see Fig. 1 or 2.

TABLE 3. SPATIAL WEIGHTS OF PROXIMITY TO LITHOLOGIC UNITS AS POTENTIAL SOURCES OF LABILE URANIUM FOR SURFICIAL URANIUM MINERALIZATION

Rock type	% of labile U (*1)	weight (*3)
Coryell Plutonic Suite (monzonite)	0.69	0.28
Eocene Volcanics (trachyte/rhyolite)	0.21	0.08
Okanagan Batholith (granite, granodiorite, pegmatite)	1.72 (*2)	0.66

(*1) Values in this column are derived from the last column of Table 1, except where indicated.
(*2) Average % of labile U for Okanagan granite, granodiorite and pegmatite, given in Table 1.
(*3) Values in the last column were obtained by dividing (or normalizing) each value in the second column by the sum of those values.

The result of using Equation 2 (Fig. 6, right panel) is apparently satisfactory because the map portrays that the Okanagan Batholith is the most important potential U-source rock (cf. Fig. 5 (right panel), Table 3), whereas the Coryell Plutonic Suite and Eocene Volcanics have lesser importance. However, if the spatial association of each of the maps in Fig. 6 is quantified (see Appendix II for method of spatial association analysis), it seems that both maps are equally good as spatial predictors of areas prospective for surficial U mineral deposits (Fig. 7). Fig. 7 tells us that, based on both maps, 25% of the study region underlain by or proximal to potential U-source rocks contains 89% of the known surficial U deposits/occurrences. Therefore, it seems that using weights based on labile U data are trivial for representation of spatial proxy of potential U-source rocks. Because there is no precedent research on this aspect, this initial evaluation of the generated (non-weighted and weighted) U-source spatial proxies' efficiency for outlining of areas that are prospective surficial U deposits in the study region will be revisited in the next chapter wherein all the spatial proxies were integrated to map areas prospective for surficial U deposits.

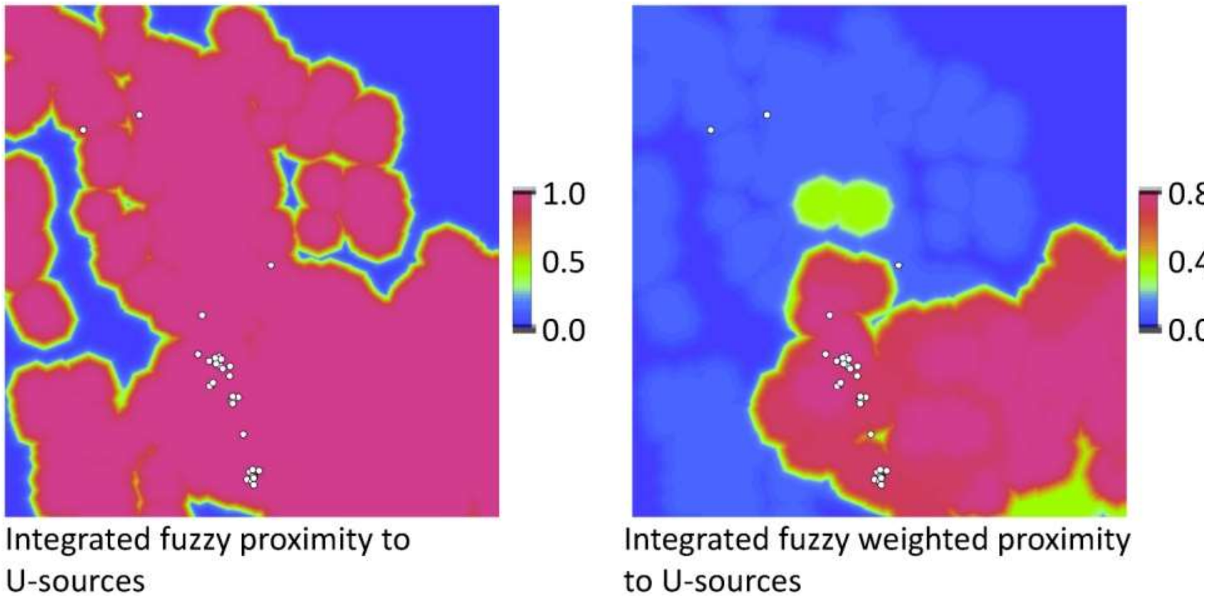

FIG. 6. Map of integrated fuzzy proximity to potential U-source rocks (left; using Equation I.6 in Appendix I) and integrated fuzzy weighted proximity to potential U-source rocks (right; using Equation 2). White dots are surficial U deposits/occurrences. For map coordinates, see Fig. 1 or 2.

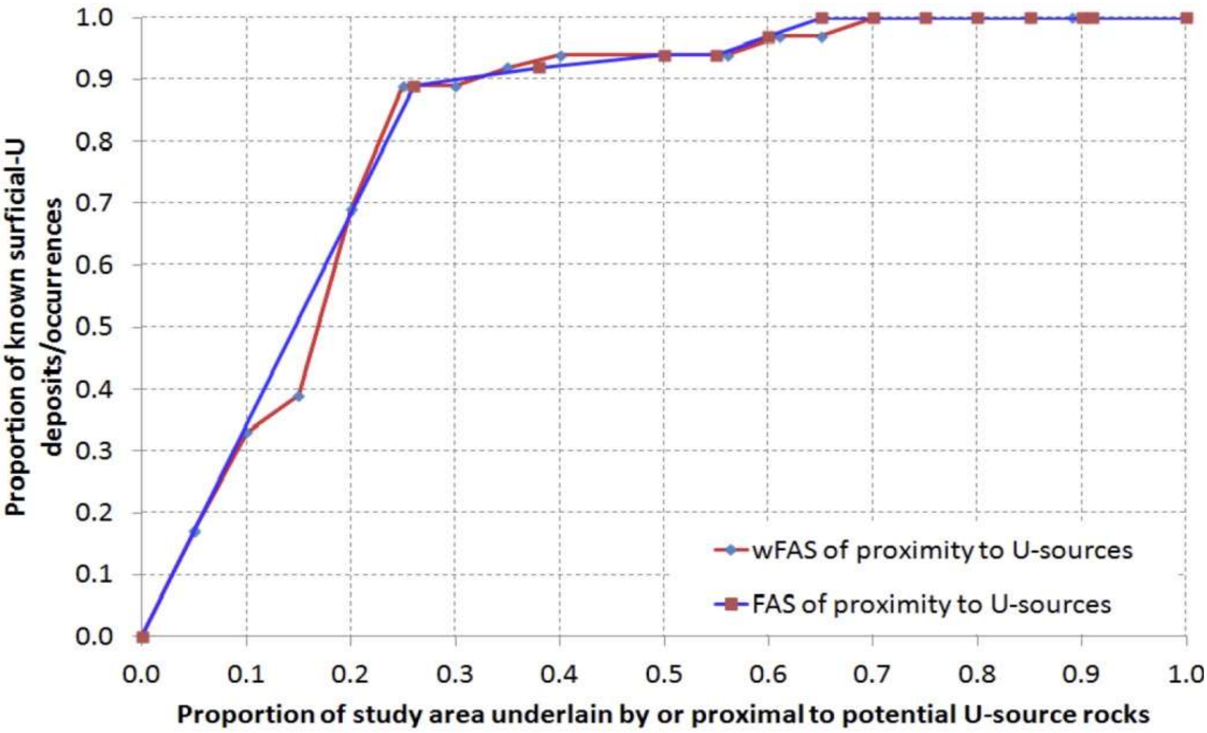

FIG. 7. Graphs depicting the spatial association of the known surficial U deposits in the study region with the map of integrated fuzzy proximity to potential U-source rocks (Fig. 6, left panel) and with the map of integrated fuzzy weighted proximity to potential U-source rocks (Fig. 6, right panel). The procedure for deriving these graphs is explained in Appendix II.

3.2. Pathways

Following [22], a single criterion is suitable for regional-scale mapping of prospectivity for surficial U deposits in the study region (Table 4).

With the use of night-time ASTER (Advanced Spaceborne Thermal Emission and Reflection Radiometer) thermal infrared data and a digital elevation model (DEM), it is possible to interpret/map subsurface topographic features (e.g., paleo-channels). Details of this method can be found in [47] and/or [48]. ASTER data can be obtained freely from NASA Jet Propulsion Laboratory (http://asterweb.jpl.nasa.gov/data.asp), whereas ASTER DEM or SRTM (Shuttle Radar Topography Mission) DEM can be obtained freely from USGS (http://gdex.cr.usgs.gov/gdex/). Because of the regional-scale of the work described here, SRTM DEM with 90-m (or 3 arc sec) spatial resolution was used instead of ASTER DEM with 30-m spatial resolution. A map of Euclidean distance to interpreted paleo-channels is then generated, which is converted using Equation 1 (with m = 10 km) into a map of fuzzy proximity to paleo-channels as spatial proxy of pathways. Apparently, most of the known surficial U deposits/occurrences exist in close proximity to paleo-channels (Fig. 8). However, Fig. 9 tells us that surficial U mineralization is almost absent within 20% of the study region's locations that are the most proximal to (i.e., within ~2 km of) interpreted paleo-channels whereas most (10–90%) of the known surficial U deposits/occurrences are found within the next 20-50% of the study region's locations that are the most proximal to (i.e., within 2 to 5 km of) interpreted paleo-channels.

TABLE 4. REGIONAL-SCALE TARGETING CRITERIA AND SPATIAL PROXIES FOR PATHWAYS IN SURFICIAL URANIUM MINERALIZATION, SOUTH-CENTRAL BRITISH COLUMBIA

Targeting criterion	Spatial proxy	Data source	Rationale
Tertiary to recent paleo-channels	Proximity to paleo-channels	1) SRTM digital elevation model; 2) ASTER thermal infrared data.	Near-surface groundwater (carrying U) flows, due to gravity, through porous soils or sediments in (paleo)topographic lows; A map of drainage network can also be used as proxy for pathways if large drainage systems are now inactive.

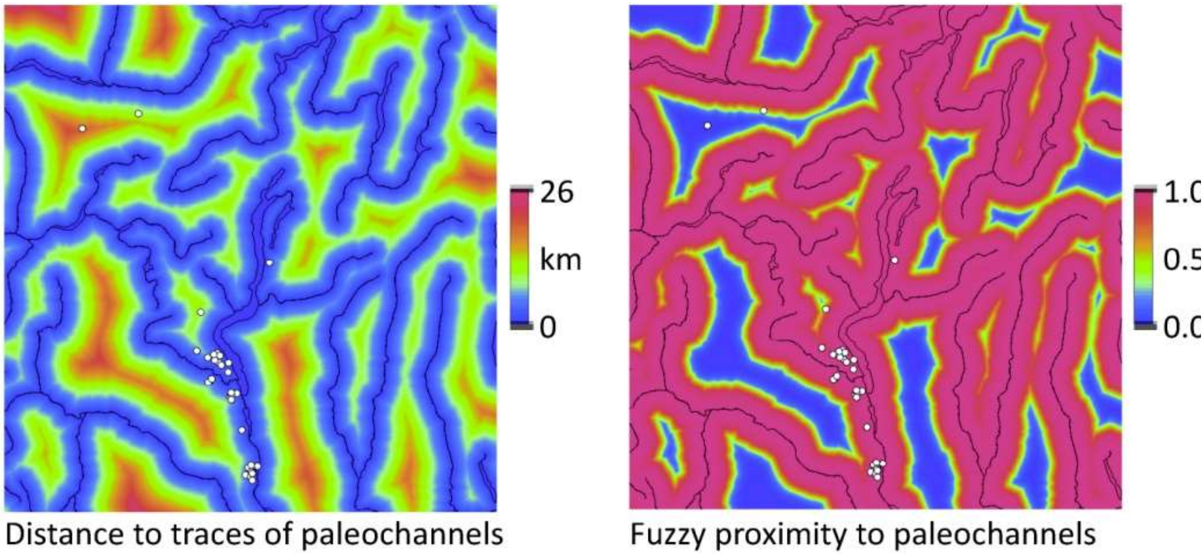

FIG. 8. Map of Euclidean distance to traces/outlines of interpreted paleo-channels (black lines) in the study region converted to a map of fuzzy proximity to paleo-channels using Equation 1. White dots are surficial U deposits/occurrences. For map coordinates, see Fig. 1 or 2.

There are three plausible explanations for the quantified spatial association between known surficial U deposits/occurrences and interpreted paleo-channels in the study region illustrated in Fig. 9. Firstly, because surficial U mineralization in the study region is probably younger than 10,000 years [3], [25], [26] and is apparently still in progress and, thus, U is remobilized easily, it is likely that the known surficial U deposits have "migrated from their original locations at/near paleo-channels to their existing locations". Secondly, the surficial U deposit/occurrence data [2], [3], [25], [26], [27], [28], [49] are not up-to-date, but the ASTER and DEM data used to interpret paleo-channels are accurate. Thirdly, the interpreted paleo-channels are inaccurate. Because the second and third plausible explanations are more verifiable and are rectifiable, further/future attempts at regional-scale prospectivity mapping for surficial U deposits in the region should nevertheless strive at generating more accurate interpretation/mapping of paleo-channels. That is because sediment-fills in paleo-channels provide the aquifers required for transporting U.

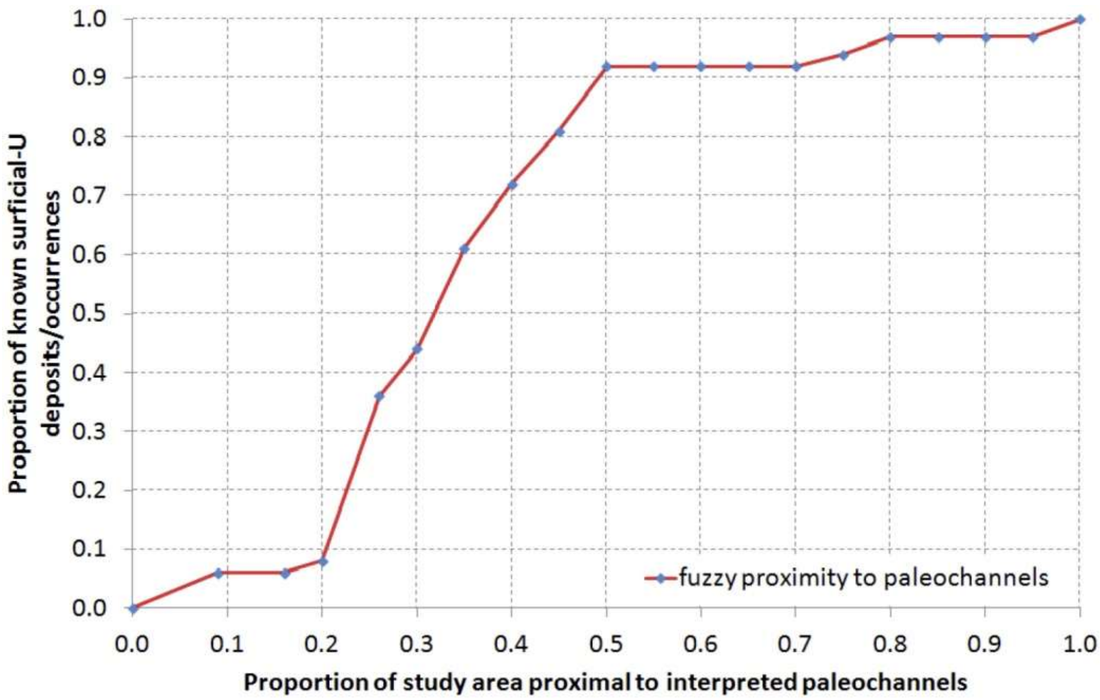

FIG. 9. Graphs depicting the spatial association of the known surficial U deposits in the study region with the map of fuzzy proximity to interpreted paleo-channels (Fig. 7, right panel). The procedure for deriving these graphs is explained in Appendix II.

3.3. Traps

Surficial U mineralization requires both chemical and physical traps. Chemical traps provide the favorable chemical conditions for the concentration and enrichment of U and for the precipitation and formation of U deposits. Physical traps constrain where formation of surficial U deposits take place.

3.3.1. Chemical traps

As the mapping of prospectivity for surficial U deposits in this case study is regional in scale, no distinction between fluviatile or lacustrine sub-type of deposits is made and, therefore, only the mineralization control by reduction that is common to both of these sub-types of surficial U mineralization [3, 26] is considered here. For more detailed (e.g., district to local) scale prospectivity mapping, it is imperative to consider adsorption for fluviatile systems [26] and evaporation for lacustrine systems [3].

For regional-scale mapping of prospectivity for surficial U deposits in the study region, spatial proxies for two chemical trap targeting criteria can be modeled considering the regional-scale data that are available (Table 5). Both of the spatial proxies used here for prospectivity analysis – alkalinity of stream waters and U-richness of stream waters (Table 5) – basically point to the enrichment of aqueous uranyl complexes in surface waters, and so one would argue that these spatial proxies are probably more indicative of the presence of good sources of U and complexing ligands rather than chemical traps (i.e., alkaline waters at near surface temperatures would carry U as soluble uranyl phosphate and uranyl carbonate complexes). However, although stream waters represent mixed sources upslope/upstream of any sampling site, physico-chemical properties of stream waters captured during sampling would reflect physico-chemical conditions at sampling sites. Therefore, alkalinity of stream waters and U-richness of stream waters can be considered products of chemical trapping processes at sampling sites. Nevertheless, a detailed soil classification map/data would have been a better source of spatial proxies for chemical traps relevant to surficial U mineralization although such map/data were unavailable for this study.

Data on pH and U concentrations of stream waters [50] were used herein to derive spatial proxies for variations in, respectively, bicarbonate and U contents of stream waters in the study region. The pH and U stream water data for the study region were obtained from 3338 samples [47], (Fig. 10a), representing an average of 1 sample per 13 km^2 that is typical for regional-scale geochemical surveys. The semi-variograms of the stream water pH and U datasets exhibit the very strong spatial autocorrelations of these variables (Figs. 10b, c), meaning that it is justifiable to interpolate each of these point datasets to portray their spatial distributions as continuous variables (Figs. 11 left panel, 12 left panel).

TABLE 5. REGIONAL-SCALE TARGETING CRITERIA AND SPATIAL PROXIES FOR CHEMICAL TRAPS IN SURFICIAL URANIUM MINERALIZATION, SOUTH-CENTRAL BRITISH COLUMBIA

Targeting criteria	Spatial proxy	Data source	Rationale
Bicarbonate contents of stream waters	Alkalinity stream waters	pH of stream waters [50]	Bicarbonate contents of highly alkaline waters are generally of the order of 50–600 ppm, which significantly enhance the ability of sediments/soils along (paleo)topographic lows to concentrate U [3].
U-rich groundwater	U-richness of stream waters	U content of stream waters [50]	Dispersion of U from sources and its concentration in surficial and groundwater allows great amounts of this metal to reach traps by which and in which surficial U deposits form.

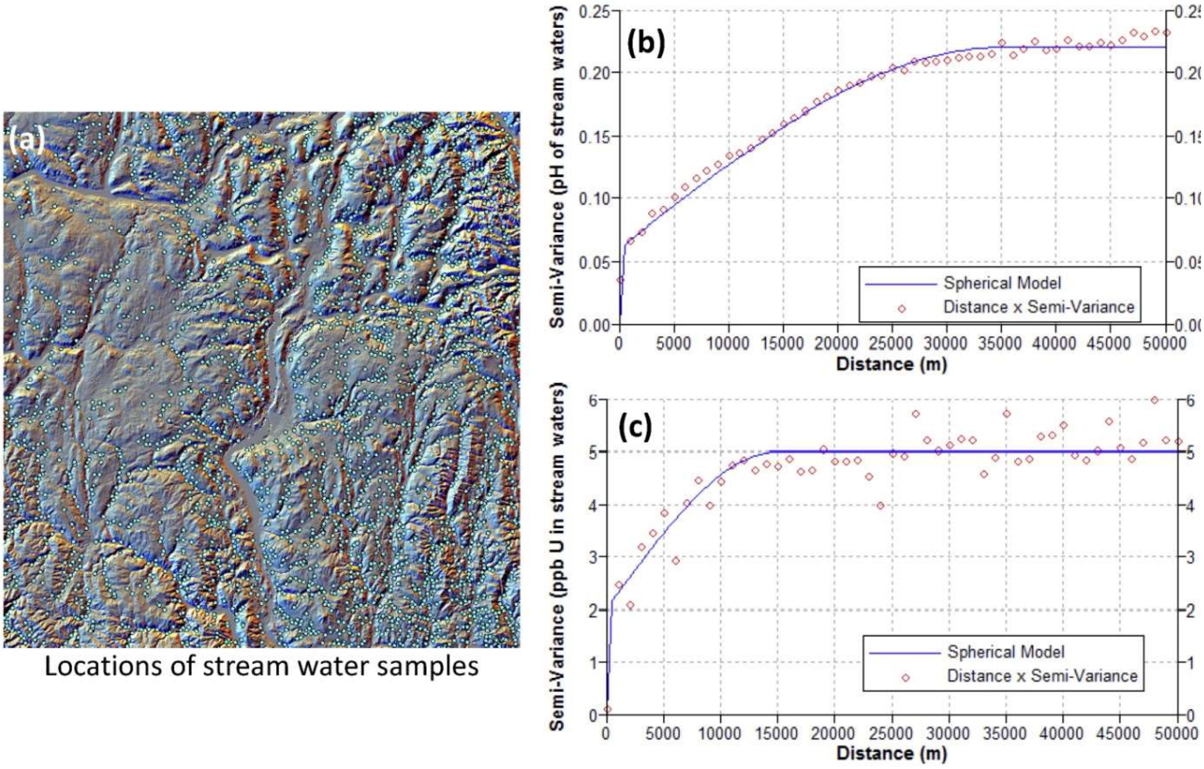

FIG. 10. (a) Locations of stream water samples (cyan dots) and semi-variograms of (b) pH of stream waters and (c) U content of stream waters. For map coordinates, see Fig. 1 or 2.

It is clear in Figs 11 and 12 that the known surficial U deposits/occurrences exist along areas with alkaline and U-rich stream waters. These areas more-or-less coincide with areas that are proximal to interpreted paleo-channels (Fig. 8). However, according to Fig. 13, the map of fuzzy U-richness of stream waters is a better spatial proxy of chemical trap than the map of fuzzy alkalinity of stream waters. This is likely true because, although there may be several areas in the study region where alkaline stream waters exist, especially in the western part of the study region (Fig. 11, left panel), the most important source rocks of labile U that is carried by stream waters exist mainly in the south-central to south-eastern areas of the study region (Fig. 6, right panel).

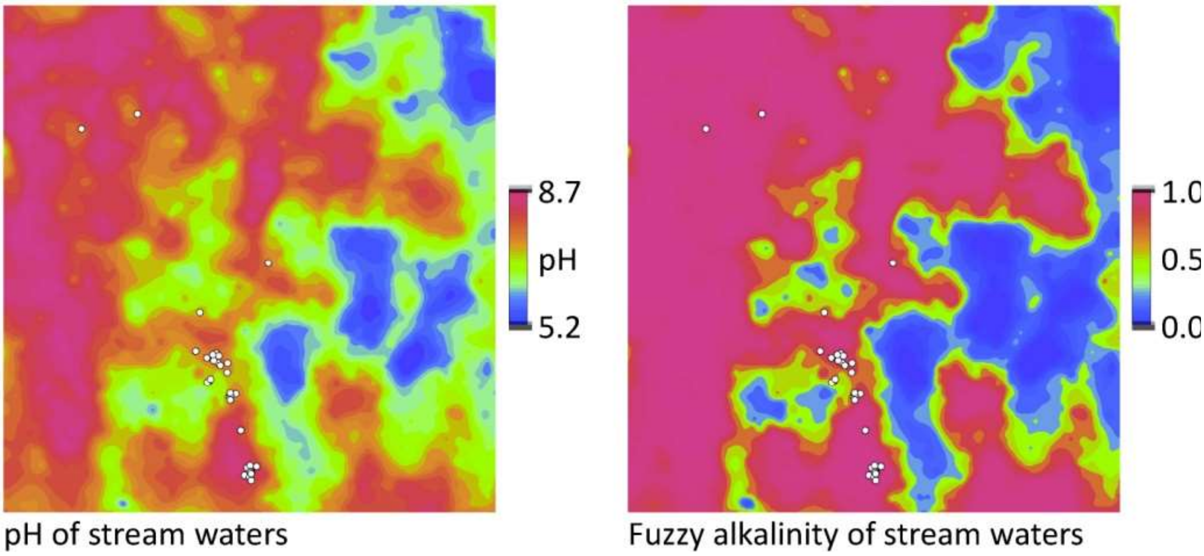

FIG. 11. Map of pH of stream waters in the study region converted to a map of fuzzy alkalinity of stream waters using Equation 1 with a negative value for s and a ph=7 for m. White dots are surficial U deposits/occurrences. For map coordinates, see Fig. 1 or 2.

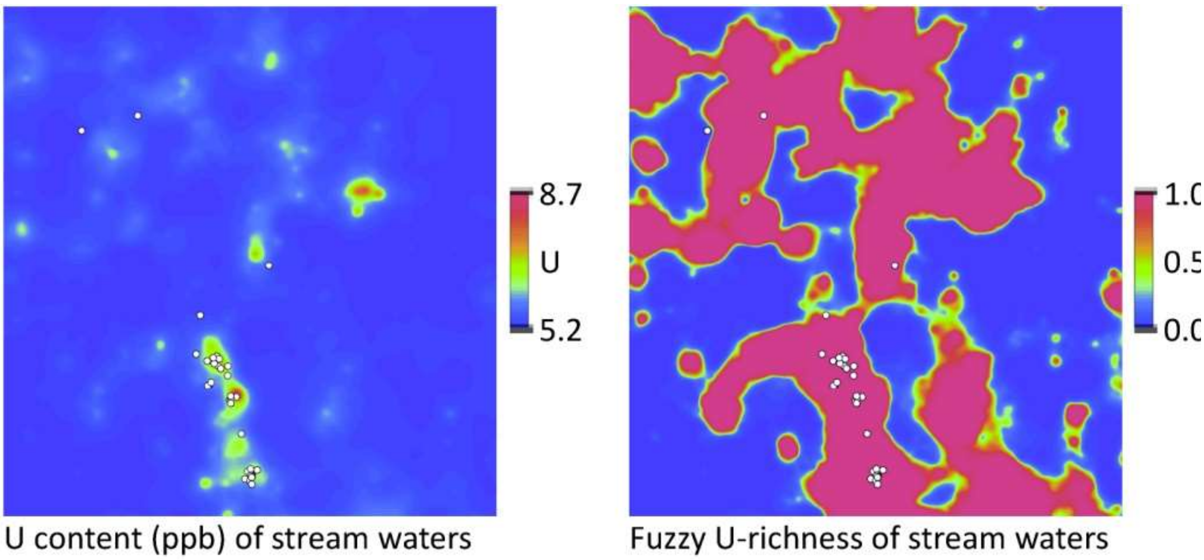

FIG. 12. Map of U content (ppb) of stream waters in the study region converted to a map of fuzzy U-richness of stream waters using Equation 1 with a negative value for s and a value of 2 ppb for m. White dots are surficial U deposits/occurrences. For map coordinates, see Fig. 1 or 2.

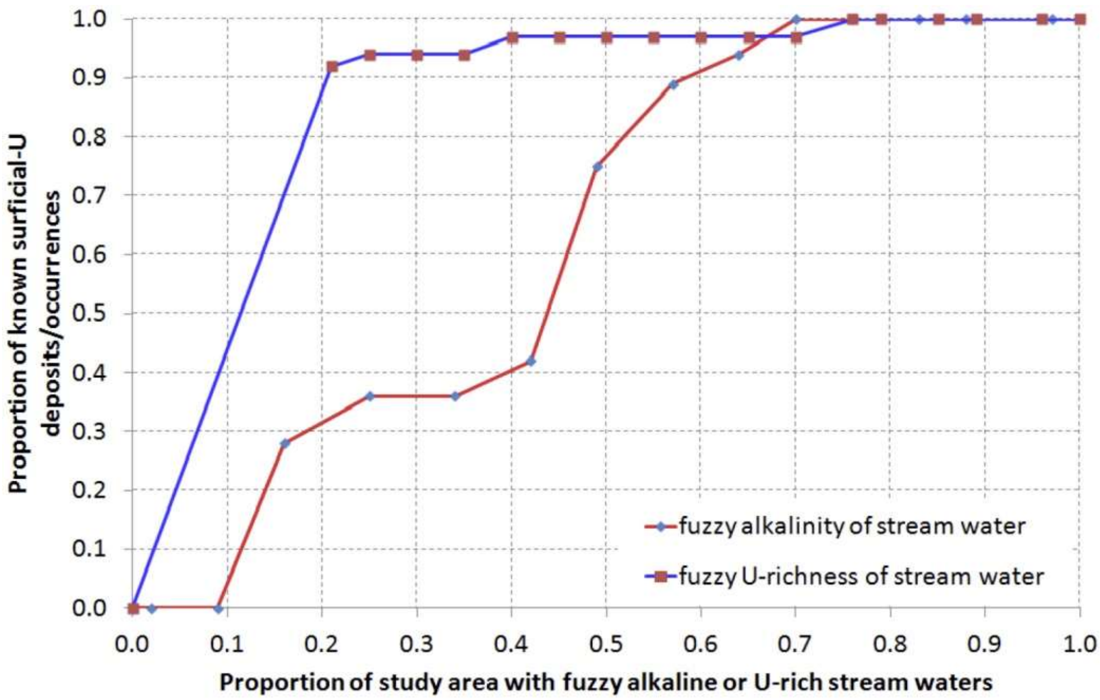

FIG. 13. Graphs depicting the spatial associations of the known surficial U deposits in the study region with the map of fuzzy alkalinity of stream waters (Fig. 11, right panel) and the map of fuzzy U-richness of stream waters (Fig. 12, right panel. The procedure for deriving these graphs is explained in Appendix II.

3.3.2. Physical traps

For regional-scale mapping of prospectivity for surficial U deposits in the study region, spatial proxies for two physical trap targeting criteria can be modeled considering the regional-scale data that are available (Table 6).

TABLE 6. REGIONAL-SCALE TARGETING CRITERIA AND SPATIAL PROXIES FOR PHYSICAL TRAPS IN SURFICIAL URANIUM MINERALIZATION, SOUTH-CENTRAL BRITISH COLUMBIA

Targeting criteria	Spatial proxy	Data source	Rationale
Near-stagnant water in channels [22]	Nearly-flat topographic depressions	SRTM DEM	U precipitates close to surface from near-stagnant water in channels [22], and therefore in topographic depressions with flat or nearly-flat slopes, because higher evaporation rate and fluid modification can be expected in such locations compared to locations with different topographic characteristics (e.g., ridges).
Size of source area [22]	Flow accumulation [22]	SRTM DEM	Locations that accumulate drainage water flow from large U-source rock areas are likely to collect, enrich, and concentrate more U. A flow accumulation map is a good spatial proxy that estimates sizes of areas that may be underlain by potential U-source rocks from which certain locations accumulates water.

The SRTM DEM with 90-m spatial resolution, compared the ASTER DEM with 30-m spatial resolution (Fig. 14, left panel), would be slightly more suitable for generating a regional-scale map of channel slopes as spatial proxy for near-stagnant water in channels. Topographic depression can be determined from an image of the second vertical derivative of the SRTM DEM (Fig. 14, right panel), in which positive and negative values represent terrains that are concave upward (i.e., depression) and concave downward (i.e., ridge), and terrains with values around and close to 0 are more-or-less flat. As can be seen in Fig. 14 (right panel), surficial U deposits/occurrences in the study region are situated mostly in areas with positive values or values around and close to 0 (i.e., depressions or flat areas).

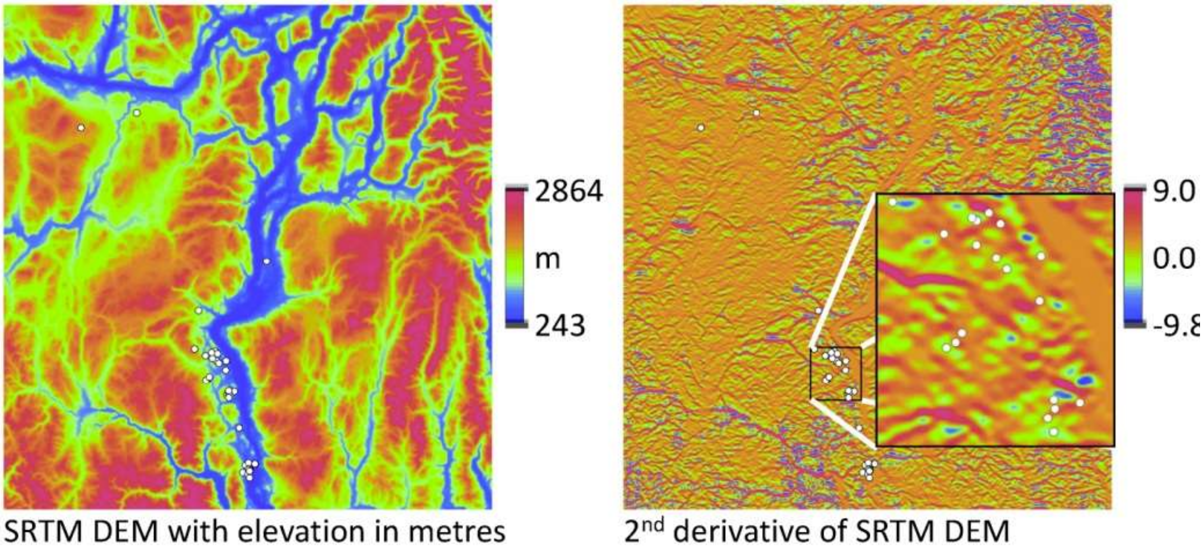

FIG. 14. SRTM DEM (left panel) and image of second derivative of the SRTM DEM (right panel). White dots are surficial U deposits/occurrences. For map coordinates, see Fig. 1 or 2.

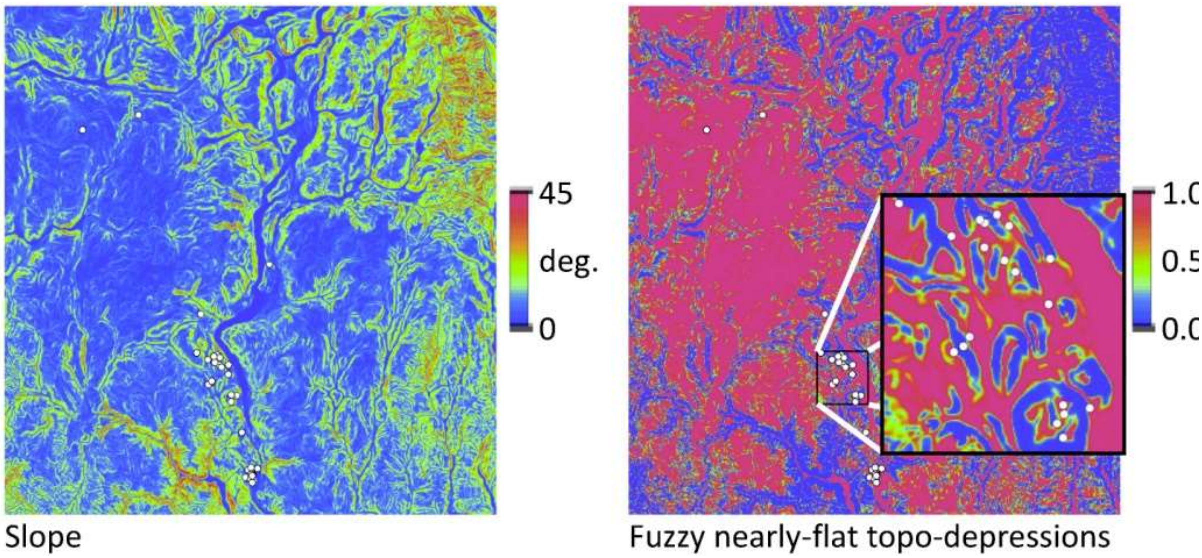

FIG. 15. Map of slopes derived from the SRTM DEM (left panel) and map of fuzzy nearly-flat topographic depressions (right panel). White dots are surficial U deposits/occurrences. For map coordinates, see Fig. 1 or 2.

To determine slopes in topographic depressions and flat areas, slope is derived from the SRTM DEM (Fig. 15, left panel). By studying the map of second derivative of the SRTM DEM (Fig.

14, right panel) and the slope map (Fig. 15, left panel), flat areas have values that vary from -2 to 2 in the former map whereas depressions have values greater than 2. This information is used to generate a map of fuzzy nearly-flat topographic depressions (Fig. 15, right panel), by assigning 0 to non-flat areas and non-depressions (i.e., with second derivative values less than or equal to -2) and by converting slopes in areas with second derivative values greater than -2 into the fuzzy range [0,1] using Equation 1 with a value of 10 degrees for m. Surficial U deposits/occurrences in the study region are situated mostly in areas with values of ~1 in the map of fuzzy nearly-flat topographic depressions (Fig. 15, right panel).

To calculate, from a given DEM, flow accumulation as spatial proxy for size of source area, there are a variety of GIS algorithms that can be used but the most popular one is that of [51], which can be implemented in several GIS software such as PCRaster, GRASS, IDRISI, ArcGIS. The main objective here to calculate flow accumulation is to generate a map of catchments which collect water flow from a source. This involves six steps, namely: (1) filling of sinks in a DEM, (2) calculation of flow direction, (3) calculation of flow accumulation based on flow direction, (4) extraction of streams based on flow accumulation, (5) labeling order of streams based on DEM and flow direction, and (6) extraction of catchments for the same highest stream order. The catchments extracted from the SRTM DEM of the study region are shown in Fig. 16 (left panel). No catchments are extracted along the edges of the study region, particularly the eastern parts, because no streams with the same highest order have been identified in those areas.

Subsequently, the sizes of the catchments were determined and then the minimum to maximum catchment areas were linearly re-scaled into a fuzzy range of 0.100 to 0.999. The choice of this range is arbitrary and, while expert knowledge is required in practice for the choice of a fuzzy range, it is meant for demonstrating the method here but not a submission of expert opinion. The linearly re-scaled fuzzy values were then attributed to the respective catchments, and locations outside the extracted catchments were assigned a value of 0.001. Likewise, the choice of this value here is arbitrary but not a submission of expert opinion. The generated map of fuzzy flow accumulation (or catchment area) is shown in Fig. 16 (right panel).

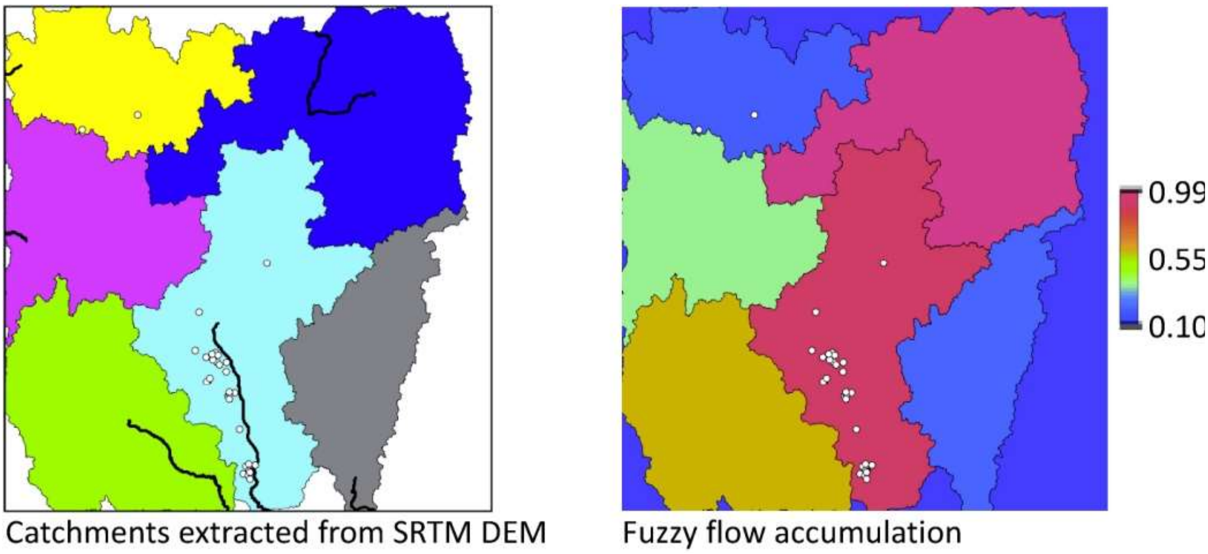

FIG. 16. Map of drainage catchments derived from the SRTM DEM (left panel) and map of fuzzy flow accumulation (right panel). Black lines are streams of the same highest order. White dots are surficial U deposits/occurrences. For map coordinates, see Fig. 1 or 2.

The largest catchment in the north-eastern part of the study has the highest fuzzy score of 0.999, whereas the second next largest catchment in the south-central part of the study region, which contains most of the known surficial U deposits/occurrences, has a fuzzy score of 0.883. The smallest catchment in the north-western part of the study region, which contains two known surficial U occurrences, has the lowest fuzzy score of 0.1.

According to Fig. 17, the map of fuzzy flow accumulation is a better spatial proxy of physical trap than the map of fuzzy nearly-flat depressions because 36% of the study region with the highest flow accumulation contains 94% of the known surficial U deposits/occurrences whereas 36% of the study region with the highest likelihood of being nearly-flat depression contains 60% of the known surficial U deposits/occurrences. This is rather intuitive because, in the study region, there are numerous areas with nearly-flat depression but it is unlikely that all or most of these areas have access to and collect groundwater whereas catchments with stream order of the same highest order certainly have direct access and collect to groundwater. It is probably better to confine slope calculations to paleo-channels; however, this would also require detailed and accurate demarcation of paleo-channels. Nevertheless, this initial evaluation of the efficiency of these physical trap spatial proxies for outlining of areas that are prospective surficial U deposits in the study region will be revisited in the next chapter wherein all the spatial proxies were integrated to map areas prospective for surficial U deposits.

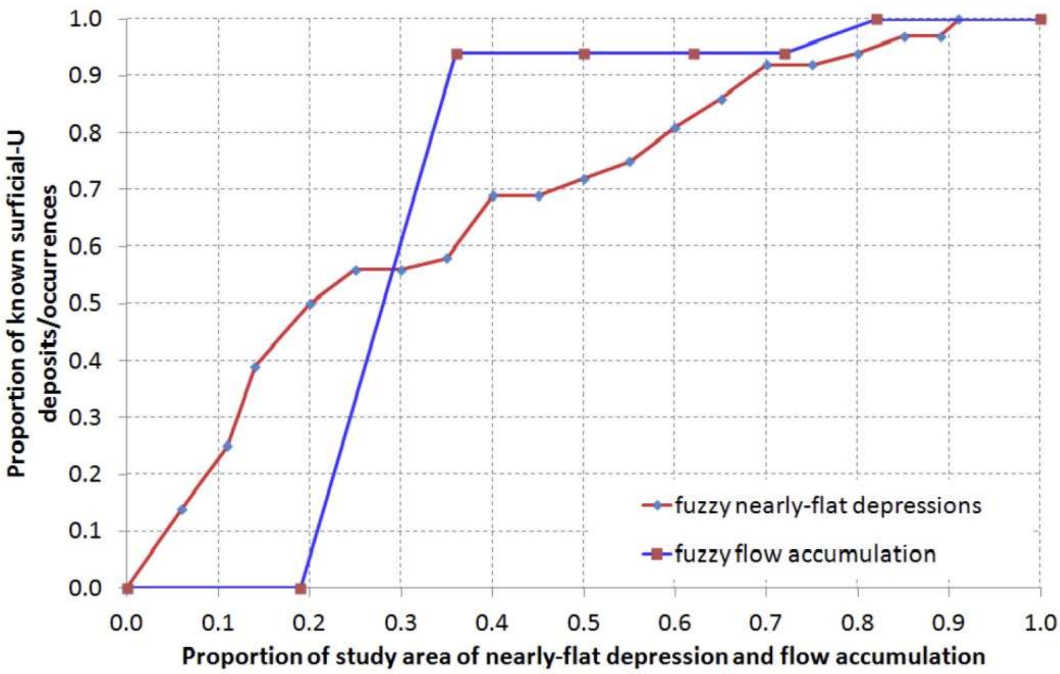

FIG. 17. Graphs depicting the spatial associations of the known surficial U deposits in the study region with the map of fuzzy nearly-flat topographic depressions (Fig. 15, right panel) and the map of fuzzy flow accumulation (Fig. 16, right panel). The procedure for deriving these graphs is explained in Appendix II.

4. REGIONAL-SCALE PROSPECTIVITY FOR SURFICIAL U DEPOSITS

As surficial U mineralization results from inter-play of processes involves sources, pathways and traps, the spatial proxies generated/described in the preceding section need to be combined systematically. To do so, it is useful to adapt an inference engine that reflects one's knowledge or hypotheses about the inter-relationships of the various processes linked to the formation of certain types of minerals deposits [22], [52]; hence, a mineral systems approach. Like in [22], we will use a fuzzy inference engine (Fig. 18) for regional-scale mapping of prospectivity for surficial U deposits in the study region based on the discussions in the preceding sections regarding the system of surficial U mineralization and regional-scale spatial proxies of targeting criteria for surficial U mineralization in the study region. We will apply the fuzzy set theory [53] because, as averred by [54], it is most appropriate for representation of geological processes due to its simplicity and flexibility.

Each step in a fuzzy inference engine, in which at least two spatial proxies were integrated using a suitable fuzzy operator, corresponds to a hypothesis regarding the inter-play of at least two processes linked to the formation of mineral deposits. A fuzzy inference engine and the fuzzy operators thus form a series of logical rules that sequentially integrates maps of fuzzy spatial proxies. A fuzzy inference engine also serves to cancel out the effect of uncertain spatial proxies. For example, nearly-flat topographic depressions are almost omnipresent in the study region (Fig. 15) but it is surely implausible that every nearly-flat topographic depression is linked with surficial U mineralization. Therefore, by logically integrating the fuzzy spatial proxy of nearly-flat depression with another fuzzy spatial proxy, say fuzzy flow accumulation, only the contributions of both or either of the two fuzzy spatial proxies are transmitted to the output depending on the hypothesis. No general guidelines exist for conceptualizing a fuzzy inference engine, except that as much as possible it must adequately represent one's knowledge of the relevant mineral system.

Accordingly, as discussed in the preceding section, the spatial proxies of potential U-source rocks (Figs 3–5) were combined into a single layer of integrated spatial proxies of U sources (Fig. 6, right panel) using the proposed weighted FAS operator (Equation 2) and here it is examined whether it is more efficient than a single layer of spatial proxy of U sources (Fig. 6, left panel) generated using the traditional FAS (see Appendix I). The fuzzy spatial proxies of alkalinity and U-richness of stream waters (Figs 11 and 12) were combined into a single layer of integrated spatial proxies of chemical traps (Fig. 19, left panel) using fuzzy AND operator (Fig. 18) operator because alkalinity and U-richness of stream waters are both required to precipitate and accumulate surficial U deposits.

The fuzzy spatial proxies of nearly-flat depressions (Fig. 15, right panel) and flow accumulation (Fig. 16, right panel) were combined into a single layer of integrated spatial proxies of physical traps (Fig. 19, right panel) using fuzzy OR operator because either nearly-flat depressions or catchments with large flow accumulation may be sufficient to constrain where surficial U deposits may form. However, nearly-flat depressions seem to be a more appropriate spatial proxy for physical traps on a local-scale rather than on a regional-scale. Therefore, it is examined whether it is more efficient to use a single layer of integrated spatial proxies of physical traps than to use spatial proxy of flow accumulation alone in regional-scale mapping of prospectivity for surficial U deposits in the study region. Finally, the integrated spatial proxies of U sources, chemical traps and physical traps were combined with the spatial proxy of pathways (Fig. 8, right panel) using fuzzy AND operator because the respective processes represented by these spatial proxies are all required for surficial U mineralization.

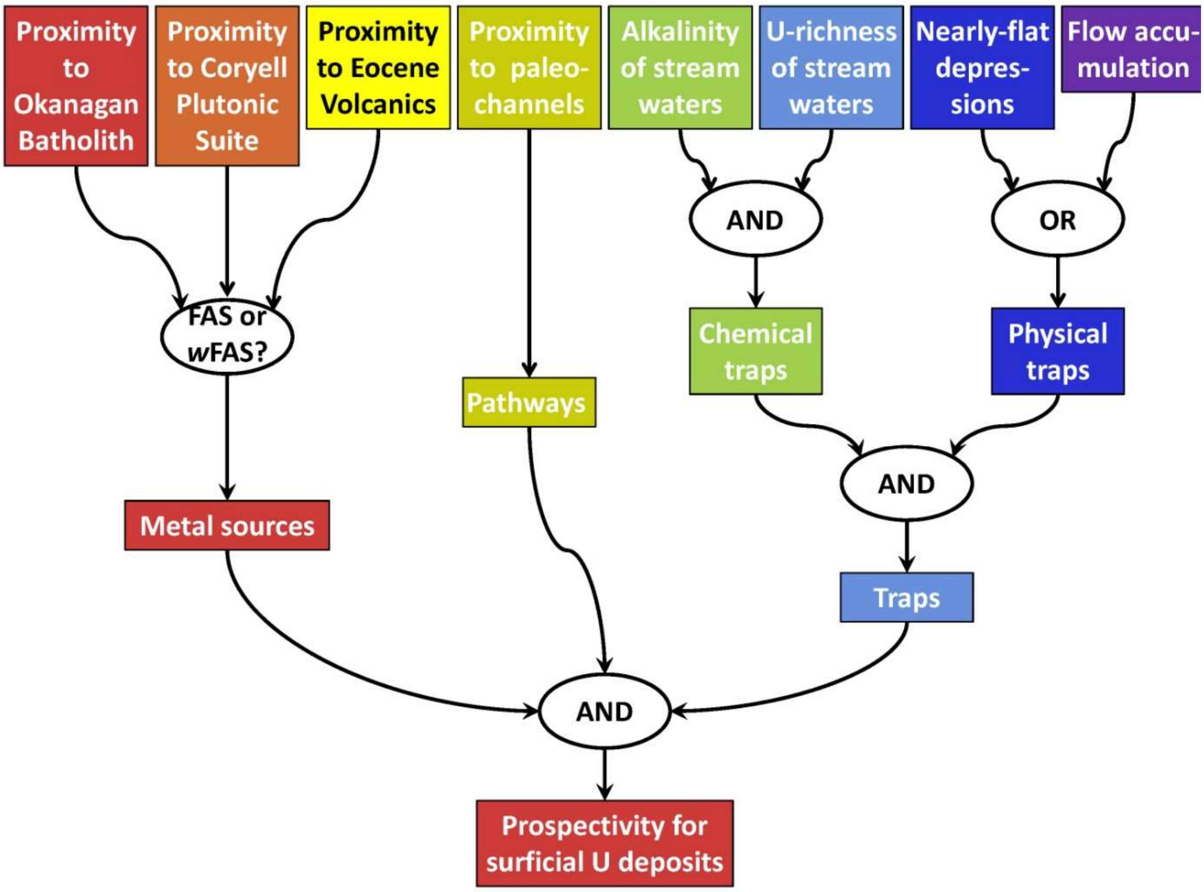

FIG. 18. Fuzzy inference engine as framework to integrate spatial proxies for mapping of regional-scale prospectivity for surficial U mineralization in the study region.

The result of combining the integrated spatial proxy of U sources derived using the proposed weighted *FAS* operator (Equation 1), spatial proxy of pathways, integrated fuzzy chemical traps and integrated fuzzy physical traps is shown in Fig. 20 (left panel), and hereafter referred to as fuzzy prospectivity model 1a. The result of combining the integrated spatial proxy of U sources derived using the traditional *FAS* operator (Appendix I), spatial proxy of pathways, integrated fuzzy chemical traps and integrated fuzzy physical traps is shown in Fig. 20 (right panel), and hereafter referred to as fuzzy prospectivity model 2a. Of these two prospectivity models, fuzzy prospectivity model 1a is better because its highest values covering 10% of the study region delineates 92% of the known surficial U deposits/occurrences whereas the highest values of fuzzy prospectivity model 2a covering 10% of the study region delineates only 36% of the known surficial U deposits/occurrences. Therefore, the integrated spatial proxy of U sources derived using the proposed weighted *FAS* operator (Equation 1) is more efficient than the integrated spatial proxy of U sources derived using the traditional FAS operator (Appendix I).

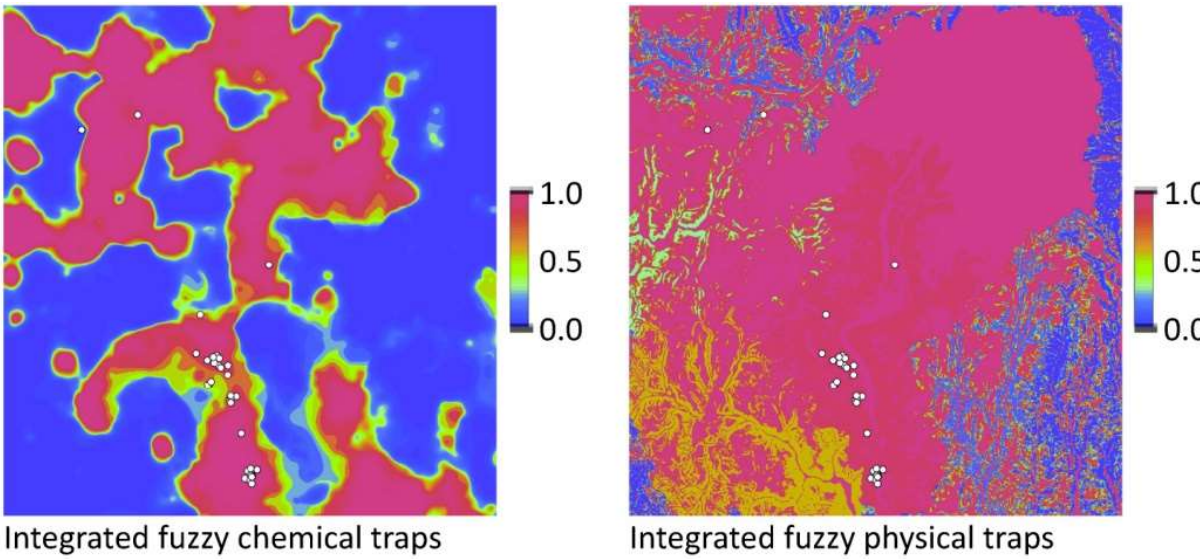

FIG. 19. Maps of integrated fuzzy chemical traps and integrated fuzzy physical traps. White dots are surficial U deposits/occurrences. For map coordinates, see Fig. 1 or 2.

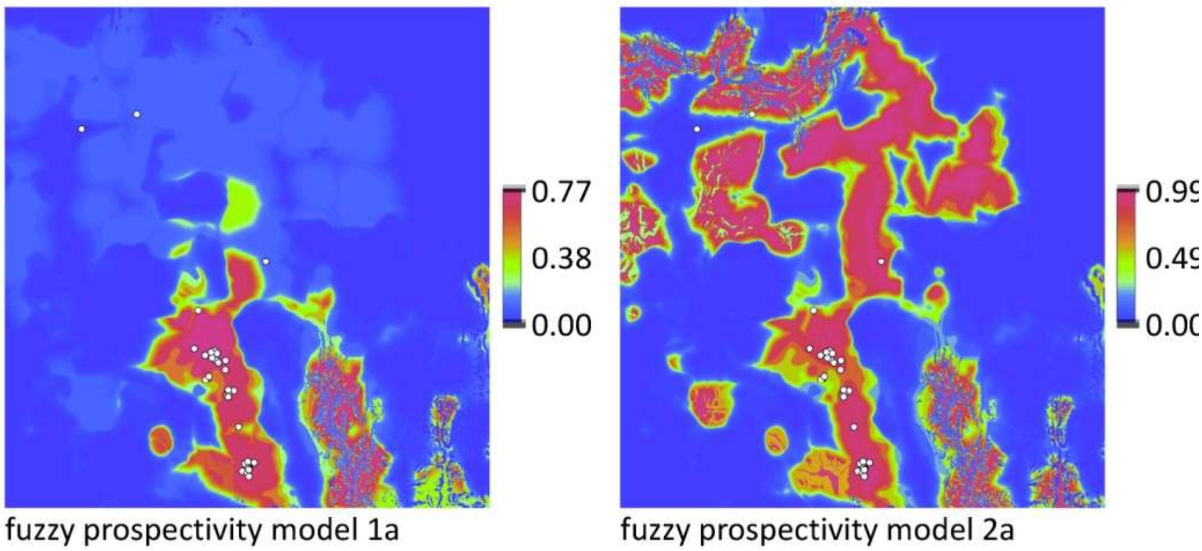

FIG. 20. Map of fuzzy prospectivity model 1a (left panel) obtained by combining the integrated spatial proxy of U sources derived using the proposed weighted FAS operator (Equation 1), spatial proxy of pathways, integrated fuzzy chemical traps and integrated fuzzy physical traps, and map of fuzzy prospectivity model 2a (right panel) obtained by combining the integrated spatial proxy of U sources derived using the traditional FAS operator (Appendix I), spatial proxy of pathways, integrated fuzzy chemical traps and integrated fuzzy physical traps. For map coordinates, see Fig. 1 or 2.

The result of combining the integrated spatial proxy of U sources derived using the proposed weighted FAS operator (Equation 1), spatial proxy of pathways, integrated fuzzy chemical traps and fuzzy flow accumulation is shown in Fig. 21 (left panel), and hereafter referred to as fuzzy prospectivity model 1b. The result of combining the integrated spatial proxy of U sources derived using the traditional FAS operator (Appendix I), spatial proxy of pathways, integrated fuzzy chemical traps and fuzzy flow accumulation is shown in Fig. 21 (right panel), and hereafter referred to as fuzzy prospectivity model 2b. Of these two prospectivity models, fuzzy prospectivity model 1b is better because its highest values covering 10% of the study region delineates 92% of the known surficial U deposits/occurrences whereas the highest values of fuzzy prospectivity model 2b covering 10% of the study region delineates only 83% of the known surficial U deposits/occurrences. These results further show that the integrated spatial proxy of U sources derived using the proposed weighted FAS operator (Equation 1) is more efficient than the integrated spatial proxy of U sources derived using the traditional FAS operator (Appendix I).

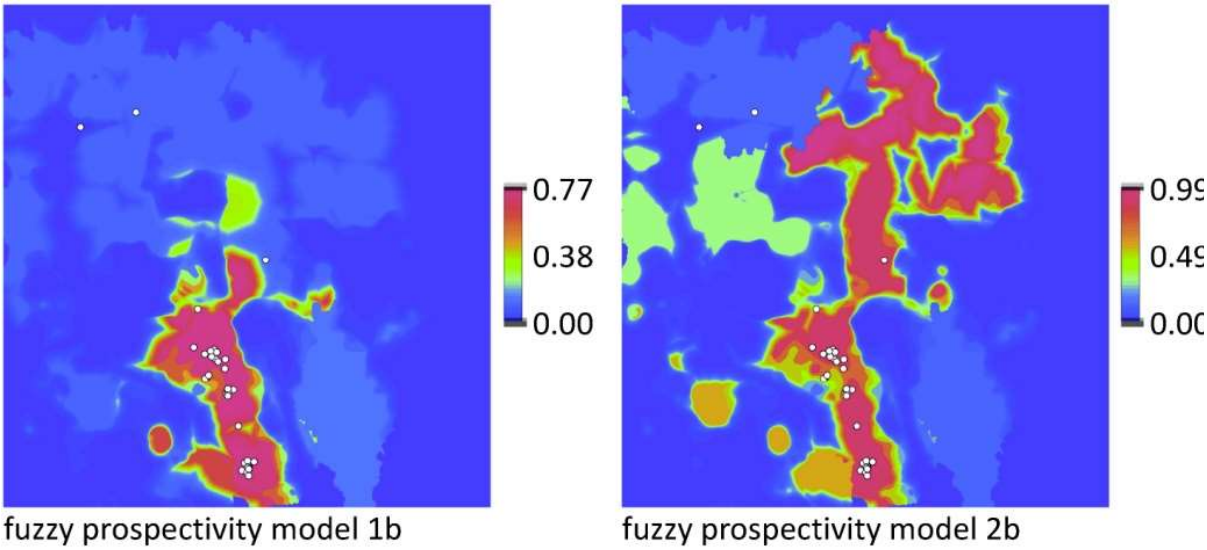

FIG. 21. Map of fuzzy prospectivity model 1b (left panel) obtained by combining the integrated spatial proxy of U sources derived using the proposed weighted FAS operator (Equation 1), spatial proxy of pathways, integrated fuzzy chemical traps and integrated fuzzy physical traps, and map of fuzzy prospectivity model 2b (right panel) obtained by combining the integrated spatial proxy of U sources derived using the traditional FAS operator (Appendix I), spatial proxy of pathways, integrated fuzzy chemical traps and integrated fuzzy physical traps. For map coordinates, see Fig. 1 or 2.

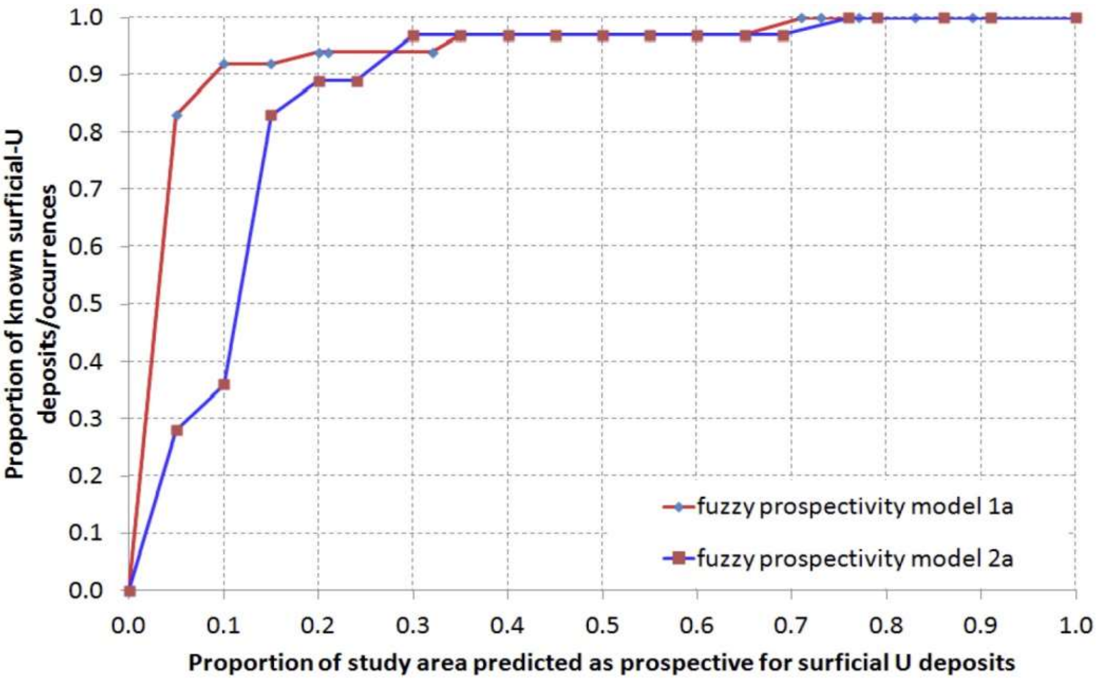

FIG. 22. Graphs depicting the spatial associations of the known surficial U deposits in the study region with the maps of fuzzy prospectivity models 1a and 2a (Fig. 20). The procedure for deriving these graphs is explained in Appendix II.

Between fuzzy prospectivity model 1a and fuzzy prospectivity model 1b, the latter is the better one because its highest values covering 5% of the study region delineates 89% of the known surficial U deposits/occurrences (Fig. 21) whereas the highest values of the former covering 5% of the study region delineates only 83% of the known surficial U deposits/occurrences (Fig. 22). Between fuzzy prospectivity model 2a and fuzzy prospectivity model 2b, the latter is the better one because its highest values covering 10% of the study region delineates 83% of the known surficial U deposits/occurrences (Fig. 23) whereas the highest values of the former covering 10% of the study region delineates only 36% of the known surficial U deposits/occurrences (Fig. 22). These results show that excluding the spatial proxy of nearly-flat depressions (Fig. 15, right panel) and using the spatial proxy of flow accumulation (Fig. 16, right panel) alone to represent physical trap does not degrade but improves mapping of prospectivity for surficial U deposits in this case study. This illustrates that the spatial proxy of flow accumulation is more efficient than the spatial proxy of nearly-flay depressions. The results suggest that nearly-flat depressions are likely more appropriate spatial proxy for physical traps of surficial U mineralization on a local-scale rather than on a regional-scale.

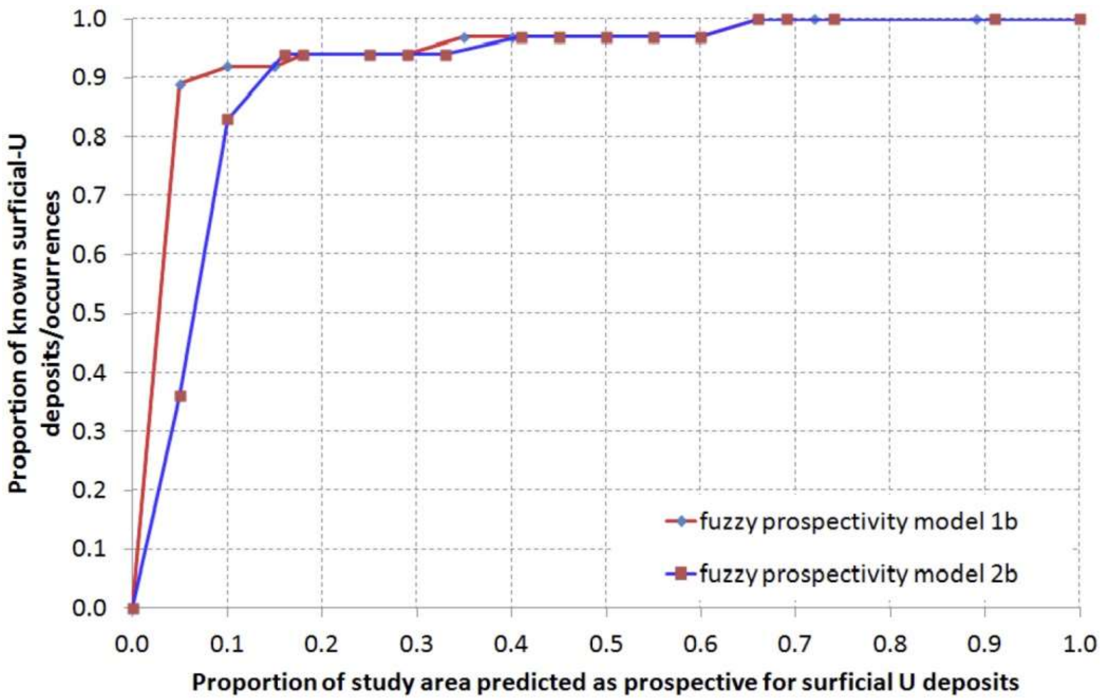

FIG. 23. Graphs depicting the spatial associations of the known surficial U deposits in the study region with the maps of fuzzy prospectivity models 1b and 2b (Fig. 21). The procedure for deriving these graphs is explained in Appendix II.

5. DISCUSSION AND CONCLUSIONS

The two best prospectivity maps generated in this case study – fuzzy prospectivity model 1a (Fig. 20 (left panel) and fuzzy prospectivity model 1b (Fig. 21, left panel) – include the spatial proxy weighted proximity to potential U-source rocks (Fig. 6, right panel), indicating: (a) the importance of labile U data in mapping of prospectivity for surficial U deposits, and (b) the usefulness of the proposed modification of the fuzzy algebraic sum operator (Equation 1) in order to incorporate the labile U data in the analysis. The two best prospectivity maps exclude the spatial proxy of nearly-flat depressions (Fig. 15, right panel), indicating: (a) the inefficiency and possibly inappropriateness of this spatial proxy in this present work of regional-scale mapping of prospectivity for surficial U deposits in the study region, or (b) the better efficiency of the spatial proxy of flow accumulation (Fig. 16, right panel). However, if, among the spatial proxies for traps, only the spatial proxy of U-richness of stream waters (Fig. 12, right panel) is used together with the spatial proxies of pathways (Fig. 8, right panel) and weighted potential U-source rocks, the resulting prospectivity map – fuzzy prospectivity model 3 (Fig. 24) – is only very slightly poorer than fuzzy prospectivity model 1a (Fig. 20 (left panel) and fuzzy prospectivity model 1b (Fig. 21, left panel). This illustrates that the spatial proxy of alkalinity of stream waters (Fig. 11, right panel) and the spatial proxy of flow accumulation only adds very little to improve the predictive capacity of prospectivity modeling despite their [conceptual] importance as targeting criteria for surficial U system in the study region. However, the result may reflect that alkalinity of stream waters is a better spatial proxy of U-carrying capability of surface waters (under oxidizing conditions) rather than U-trapping, and U-richness in stream waters could imply less U-trapping. These caveats would require updating of the prospectivity model as more suitable data become available.

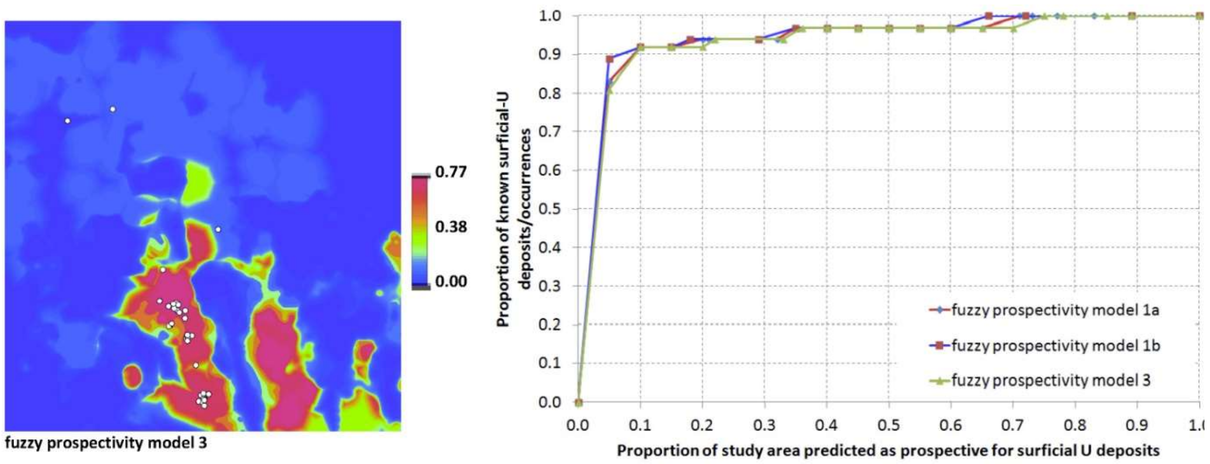

FIG. 24. Map of fuzzy prospectivity model 3 (left panel) obtained by combining the integrated spatial proxy of U sources derived using the proposed weighted FAS operator (Equation 1), spatial proxy of pathways, fuzzy U-richness of stream waters. For map coordinates, see Fig. 1 or 2. Graph depicting the spatial association of the known surficial U deposits in the study region with the maps of fuzzy prospectivity model 3, compared to those for fuzzy predictive models 1a (Fig. 20, left panel) and 1b (Fig. 22, left panel). The procedure for deriving these graphs is explained in Appendix II.

Nevertheless, based on the two best prospectivity maps generated in this case study (Figs 20 (left panel) and 21 (left panel)) there is still potential for undiscovered surficial U deposits in the south-central district of the study region. However, this is the same district where most of the known surficial U deposits/occurrences exist in the study region, and so these two best prospectivity maps also likely contain 'false-negative' bias with respect to undiscovered surficial U deposits that may possibly exist in other districts of the study region. In contrast, the two worst prospectivity maps generated in this case study (Figs 20 (right panel) and 21 (right panel)) contain significant 'false-positive' bias with respect to the known surficial U deposits/occurrences in the study region. Such 'false-negative' and 'false-positive' biases result in, respectively, systematic under- and over-estimation of prospectivity. However, between these two types of biases, it is better to avoid ‘false-positive’ bias because these will result in failure to discover new deposits and, thus, loss of financial investment on exploration whereas ‘false-negative’ bias will only result in missed opportunity for new deposit discovery. Porwal et al. [22] have used radiometric data to determine possibly "false-positive" prospective areas. However, the surficial U system in the study region is geologically too young to produce daughter products detectable by radiometrics. Alternatively, the reliability of the prospectivity maps generated in this case study may be analyzed further by using past exploration data, as this type of analysis has been demonstrated by [55] in the analysis of prospectivity for porphyry Cu-Au systems. Another possible alternative validation is to compare the results with a spatio-temporal analysis of changes in exploration/mining claims in this region [56]. However, these validation strategies are beyond the scope of this case study.

The work described here for regional-scale mapping of prospectivity for surficial U deposits in south-central British Columbia (Canada) can be implemented rather easily in a GIS. A more elaborate fuzzy inference system with if-then rules to represent expert reasoning for prospectivity mapping of surficial U system, described by [22] for regional-scale mapping of prospectivity for surficial U deposits in Yeelirrie (Western Australia), would probably be as useful for researchers who have deeper understanding or expert knowledge of the surficial U system south-central British Columbia (Canada).

ACKNOWLEDGEMENTS

The material discussed in this case study was presented by the author in the IAEA-USGS QURE (Quantitative Uranium Resource Evaluation) Workshop held in the Denver Federal Centre, USA, during 6–10 July 2015. The author appreciates the fruitful discussion with Dr. Subhash Jaireth regarding the critical elements and corresponding suitable spatial proxies of the surficial U system in the study area. The author is grateful to Dr. Alok Porwal and Dr. Vladimir Lisitsin for carefully reading the manuscript and for giving suggestions for revision, which greatly helped to improve presentation of the material discussed in this case study.

Appendix I

FUZZY SETS AND FUZZY OPERATORS

Fuzzy logic modeling is based on the fuzzy set theory [53]. The application of fuzzy logic modeling to knowledge-driven mineral prospectivity mapping typically entails three main feed-forward stages: (1) fuzzification (i.e., generating fuzzy sets) of spatial proxy; (2) logical integration of fuzzy spatial proxies with the aid of an inference engine and appropriate fuzzy set operations; and (3) defuzzification of fuzzy mineral prospectivity output in order to aid its interpretation.

Fuzzy sets are modeled by means of membership grades. If X is a set of object attributes commonly symbolized by x, then a fuzzy set A in X is a set of ordered pairs of object attributes and their grades of membership in A (x, $\mu_A(x)$):

$$A = \{(x, \mu_A(x) | x \in X)\} \tag{I.1}$$

where $\mu_A(x)$ is a membership grade function of x in A. A membership grade function, $\mu_A(x)$, is a classification of the fuzzy membership of x, in the unit interval [0,1], from a universe of discourse X to fuzzy set A; thus

$$\{(\boldsymbol{\mu_a(x)} | \boldsymbol{x} \in \boldsymbol{X})\} \rightarrow [\mathbf{0}, \mathbf{1}]. \tag{I.2}$$

An example of a universe of discourse X typically used in mineral prospectivity mapping is distance to geological structures.

Of the several types of fuzzy operators for integrating fuzzy sets [53], [57], [58], [59], [60], the five fuzzy operators that are commonly used for combining fuzzy sets of spatial proxies of targeting criteria for mineral prospectivity mapping are the fuzzy AND, fuzzy OR, fuzzy algebraic product, fuzzy algebraic sum and fuzzy gamma (γ) [4], [5], [61].

The fuzzy AND (FA) operator is defined as:

$$\boldsymbol{\mu_{FA}} = \mathbf{MIN}(\boldsymbol{\mu_1}, \boldsymbol{\mu_2}, \dots, \boldsymbol{\mu_n}) \tag{I.3}$$

where μ_{FA} is the output fuzzy score and μ_1, μ_2,…, μ_n are, respectively, the input fuzzy scores at a location in spatial proxy map 1, spatial proxy map 2,…, spatial proxy map n. The MIN is an arithmetic function that selects the smallest value among input values. The output of the FA operator is, therefore, controlled by the lowest fuzzy score at every location. The FA operator is appropriate for combining complementary sets of spatial proxies, meaning that the spatial proxies to be integrated with this operator are deemed all necessary to support the proposition of mineral prospectivity at every location.

The fuzzy OR (FO) operator is defined as:

$$\boldsymbol{\mu_{FO}} = \mathbf{MAX}(\boldsymbol{\mu_1}, \boldsymbol{\mu_2}, \dots, \boldsymbol{\mu_n}) \tag{I.4}$$

where μ_{FO} is the output fuzzy score and μ_1, μ_2,…, μ_n are, respectively, the input fuzzy scores at a location in spatial proxy map 1, spatial proxy map 2,…, spatial proxy map n. The MAX is an arithmetic function that selects the largest value among input values. The output of the FO operator is, therefore, controlled by the highest fuzzy score at every location. The FO operator is appropriate for combining supplementary sets of spatial proxies, meaning that at least one of any of the spatial proxies to be combined with this operator is deemed necessary to support the proposition of mineral prospectivity at every location.

The fuzzy algebraic product (FAP) operator is defined as:

$$\boldsymbol{\mu_{FAP}} = \prod_{\boldsymbol{i=1}}^{\boldsymbol{n}} \boldsymbol{\mu_i} \tag{I.5}$$

where μ_{FAP} is the output fuzzy score and μ_i represents the fuzzy scores at a location in i (=1, 2,…, n) spatial proxy maps. The output of the *FAP* is less than or equal to the lowest fuzzy score at every location. Like the *FA* operator, the *FAP* is appropriate for combining complementary sets of spatial proxies, meaning that all input fuzzy scores at a location must contribute to the output to support the proposition of mineral prospectivity, except in the case when at least one of the input fuzzy scores is 0.

The fuzzy algebraic sum (*FAS*) operator is defined as:

$$\boldsymbol{\mu_{FAS} = 1 - \prod_{i=1}^{n}(1 - \mu_i)} \tag{I.6}$$

where μ_{FAS} is the output fuzzy score and μ_i represents the input fuzzy scores at a location in i (=1, 2,…, n) spatial proxy maps. The *FAS* is, by definition, not actually an algebraic sum, whereas the *FAP* is consistent with its definition. The output of the *FAS* is greater than or equal to the highest fuzzy score at every location. Like the *FO* operator, the *FAS* is appropriate for combining supplementary sets of spatial proxies, meaning that all input fuzzy scores at a location must contribute to the output to support the proposition of mineral prospectivity, except in the case when at least one of the input fuzzy scores is 1.

The fuzzy γ (*FG*) operator is defined as [62]:

$$\boldsymbol{\mu_{FG} = \left(\prod_{i=1}^{n}\mu_i\right)^{1-\gamma} \times \left(1 - \prod_{i=1}^{n}(1 - \mu_i)\right)^{\gamma}} \tag{I.7}$$

where μ_{FG} is the output fuzzy score and μ_i represents the fuzzy scores at a location in i (=1, 2,…, n) spatial proxy maps. The value of γ varies in the range [0,1]. If $\gamma = 0$, then *FG* = *FAP*. If $\gamma = 1$, then *FG* = *FAS*.

Appendix II

MEASURING SPATIAL ASSOCIATION OF MINERAL DEPOSITS WITH SPATIAL PROXY OR MINERAL PROSPECTIVITY MAPS

The procedure described here for creating occurrence-area proportion plots is adopted from [63].

To derive area proportions, values in a map are discretized or classified using narrow equal-frequency (equal-proportion or equal-percentile) intervals, say 5-percentile intervals (if/when possible), following a cumulative increasing or cumulative decreasing approach depending on what the values in a map represent.

For example, a cumulative decreasing approach is followed for a map of pH of stream waters if the analysis is to determine whether mineral deposits/occurrences are spatially associated with (i.e., exist at or near) alkaline stream waters whereas a cumulative increasing approach is followed for a map of pH of stream waters if the analysis is to determine whether mineral deposits/occurrences are spatially associated with (i.e., exist at or near) acidic stream waters.

Therefore, in this case study, a cumulative decreasing approach was used for all fuzzy spatial proxy maps and integrated fuzzy maps because the analysis was to determine whether surficial U deposits/occurrences are spatially associated with high fuzzy scores. For any fuzzy score map, the highest fuzzy score results in minimum proportion [≅0] of the study region whereas the lowest fuzzy score results in maximum proportion [≅1] of the study region.

Then, to derive occurrence proportions, the proportions of mineral deposits/occurrences coinciding with the respective cumulative increasing area proportions are determined. Finally, occurrence proportions are plotted on the y-axis and area proportions on the x-axis.

The steeper the occurrence-area proportion curve is on the left-hand side of the graph, the stronger the spatial association is between mineral deposits/occurrences with the highest fuzzy scores on any fuzzy score map. For comparison of spatial associations of mineral deposits/occurrences with at least two fuzzy score maps, the occurrence-area proportion curve that plots [mostly] on top of another occurrence-area proportion curve means stronger spatial association.

REFERENCES

[1] IAEA, "Methods of exploitation of different types of uranium deposits", International Atomic Energy Agency (IAEA), Vienna, IAEA-TECDOC-1174, 75p. (2000).

[2] BOYLE, D.R., "The Formation of Basal-type Uranium Deposits in South Central British Columbia", Economic Geology 77, 1176-1209 (1982).

[3] CULBERT, R.R., BOYLE, D.R., LEVINSON, A.A., "Surficial Uranium Deposits in Canada", In: "Surficial Uranium Deposits", IAEA-TECDOC-322, IAEA, Vienna, pp. 179-191 (1984).

[4] BONHAM-CARTER, G.F., "Geographic Information Systems for Geoscientists, Modelling with GIS". Pergamon, Ontario, 398p. (1994).

[5] CARRANZA, E.J.M., "Geochemical Anomaly and Mineral Prospectivity Mapping in GIS". Handbook of Exploration and Environmental Geochemistry vol. 11. Elsevier, Amsterdam, 351p. (2009).

[6] CARRANZA, E.J.M., "Data-driven evidential belief modeling of mineral potential using few prospects and evidence with missing values", Natural Resources Research 24, 291-304 (2015).

[7] CARRANZA, E.J.M., LABORTE, A.G., "Data-driven predictive modeling of mineral prospectivity using Random Forests: a case study in Catanduanes Island (Philippines), Natural Resources Research 25, 35-50.

[8] YOUSEFI, M., CARRANZA, E.J.M., "Data-driven index overlay and Boolean logic mineral prospectivity modeling in greenfields exploration", Natural Resources Research 25, 3-18 (2016).

[9] LUSTY, P.A.J., SCHIEB, C., GUNN, A.G., WALKER, A.S.D., "Reconnaissance-scale prospectivity analysis for gold mineralisation in the southern Uplands-Down-Longford terrane, Northern Ireland", Natural Resources Research 21, 359-382 (2012).

[10] ASADI, H.H., SANSOLEIMANI, A., FATEHI, M., CARRANZA, E.J.M., "An AHP-TOPSIS predictive model for district-scale mapping of porphyry Cu-Au potential: a case study from Salafchegan area (Central Iran)", Natural Resources Research 25, 417-429 (2016).

[11] ELLIOTT, B.A., VERMA, R., KYLE, J.R., "Prospectivity modeling for Cambrian-Ordovician hydraulic fracturing sand resources around the Llano Uplift, central Texas", Natural Resources Research 25, 389-415 (2016).

[12] HARRIS, J.R., GRUNSKY, E., BEHNIA, P., CORRIGAN, D., "Data- and knowledge-driven mineral prospectivity maps for Canada's North", Ore Geology Reviews 71, 788-803 (2015).

[13] FORD, A., MILLER, J.M., MOL, A.G., "A comparative analysis of weights of evidence, evidential belief functions, and fuzzy logic for mineral potential mapping using incomplete data at the scale of investigation", Natural Resources Research 25, 19-33 (2016).

[14] MCKAY, G., HARRIS, J.R., "Comparison of the data-driven Random Forests model and a knowledge-driven method for mineral prospectivity mapping: a case study for gold deposits around the Huritz Group and Nueltin Suite, Nunavut, Canada", Natural Resources Research 25, 125-143 (2016).

[15] MCCUAIG, T.C., BERESFORD, S., HRONSKY, J., "Translating the mineral systems approach into an effective targeting system", Ore Geology Reviews 38, 128–138 (2010).

[16] PORWAL, A.K., KREUZER, O.P., "Introduction to the Special Issue: Mineral prospectivity analysis and quantitative resource estimation", Ore Geology Reviews 38, 121-127 (2010).
[17] LISITSIN, V.A., GONZÁLEZ-ÁLVAREZ, I., PORWAL, A., "Regional prospectivity analysis for hydrothermal-remobilised nickel mineral systems in western Victoria, Australia", Ore Geology Reviews 52, 100-112 (2013).
[18] KREUZER, O.P., MILLER, A.V.M., PETERS, K.J., PAYNE, C., WILDMAN, C., PARTINGTON, G.A., PUCCIONI, E., MCMAHON, M.E., ETHERIDGE, M.A., "Comparing prospectivity modelling results and past exploration data: a case study of porphyry Cu-Au mineral systems in the Macquarie Arc, Lachlan Fold Belt, New South Wales", Ore Geology Reviews 71, 516-544 (2015).
[19] JOLY, A., PORWAL, A., MCCUAG, T.C., CHUDASAMA, B., DENTITH, M.C., AITKEN, A.R.A., "Mineral systems approach applied to GIS-based 2D-prospectivity modelling of geological regions: insights from Western Australia", Ore Geology Reviews 71, 673-702 (2015).
[20] OCCHIPINTI, S.A., METELKA, V., LINDSAY, M.D., HOLLIS, J.A., AITKEN, A.R.A., TYLER, I.M., MILLER, J.M., MCCUAIG, T.C., "Multicommodity mineral systems analysis highlighting mineral prospectivity in the Halls Creek Orogen", Ore Geology Reviews 72, 86-113 (2016).
[21] KREUZER, O.P., MARKWITZ, V., PORWAL, A.K., MCCUAIG, T.C., "A continental-wide study of Australia's uranium potential. Part I: GIS-assisted manual prospectivity analysis", Ore Geology Reviews 38, 334-366 (2010).
[22] PORWAL, A., DAS, R.D., CHAUDHARY, B., GONZÁLEZ-ÁLVAREZ, I., KREUZER, O., "Fuzzy inference systems for prospectivity modeling of mineral systems and a case-study for prospectivity mapping of surficial uranium in Yeelirrie area, Western Australia", Ore Geology Reviews 71, 839-852 (2015).
[23] CAMERON, E., "The Yeelirrie calcrete uranium deposit, Western Australia", In: "Surficial Uranium Deposits", IAEA-TECDOC-322, IAEA, Vienna, pp. 157-164 (1984).
[24] MASSEY N.W.D., MACINTYRE D.G., DESJARDINS P.J., COONEY R.T., "Digital Geology Map of British Columbia: Whole Province". B.C. Ministry of Energy and Mines, Geofile 2005-1, scale 1:250,000 (2005).
[25] CULBERT, R.R., LEIGHTON, D.G., "Young uranium", Ore Geology Reviews 3, 313-330 (1988).
[26] TIXIER, K., BECKIE, R., "Uranium depositional controls at the Prairie Flats surficial uranium deposit, Summerland, British Columbia", Environmental Geology 40, 1242-1251 (2001).
[27] BOYLE, D.R., "The genesis of surficial uranium deposit", Report of the working group on uranium geology organized by the International Atomic Energy Agency, Vienna, IAEA-TECDOC-322, pp. 45-52 (1984).
[28] CULBERT, R.R., LEIGHTON, D.G., "Uranium in alkaline waters – Okanagan area, British Columbia", CIM (Canadian Institute of Mining & Metallurgy) Bulletin 71, 103-110 (1978).
[29] CARLISLE, D., "Surficial uranium occurrences in relation to climate and physical setting", IAEA-TECDOC-322, IAEA, Vienna, pp. 25-35 (1984).
[30] CAMERON, E., "The Yeelirrie calcrete uranium deposit, Western Australia", IAEA-TECDOC-322, IAEA, Vienna, pp. 157-164 (1984).

[31] MISRA, A., PANDE, D., KUMAR, K.R., NANDA, L.K., MAITHANI, P.B., CHAKI, A., "Calcrete-hosted surficial uranium occurrence in playa-lake environment at Lachari, Nagaur District, Rajasthan, India", Current Science 101, 84-88 (2011).

[32] KHOURY, H.N., "Geochemistry of surficial uranium deposits from Central Jordan", Jordan Journal of Earth and Environmental Sciences 6, 11-22 (2014).

[33] CUI, Y., KATAY, F., NELSON, J.L., HAN, T., DESJARDINS, P.J., SINCLAIR, L., "British Columbia Digital Geology", BCGS Open File 2013-04, British Columbia Geological Survey (http://www.empr.gov.bc.ca/ Mining/Geoscience/ PublicationsCatalogue/OpenFiles/2013/Pages/2013-4.aspx) (2013).

[34] PORWAL, A., CARRANZA, E.J.M., "Knowledge-driven and data-driven fuzzy models for predictive mineral potential mapping", Natural Resources Research 12, 1-25 (2003).

[35] PORWAL, A., CARRANZA, E.J.M., HALE, M., "A hybrid fuzzy weights-of-evidence model for mineral potential mapping", Natural Resources Research 15, 1-15 (2006).

[36] CARRANZA, E.J.M., "Improved wildcat modelling of mineral prospectivity", Resource Geology 60, 129-149 (2010).

[37] NYKÄNEN, V., GROVES, D.I., OJALA, V.J., EILU, P., GARDOLL, S.J., "Reconnaissance scale conceptual fuzzy-logic prospectivity modeling for iron oxide copper–gold deposits in the northern Fennoscandian Shield, Finland", Australian Journal of Earth Sciences 55, 25-38 (2008).

[38] YOUSEFI, M., CARRANZA, E.J.M., "Fuzzification of continuous-value spatial evidence for mineral prospectivity mapping", Computers & Geosciences 74, 97-109 (2015).

[39] KAZANSKIY, V.I., LAVEROV, N.P., TUGARINOV, A.I., "Sources of ore material in endogenic uranium deposits". International Geology Review 19, 283-294 (1977).

[40] ZIELINSKI, R.A., "Uranium abundances and distribution in associated glassy and crystalline rhyolites of the western United States". Geological Society of America Bulletin 89, 409-414 (1978).

[41] CUNNINGHAM, C.G., LUDWIG, K.R., NAESER, C.W., WEILAND, E.K., MEHNERT, H.H., STEVEN, T.A., RASMUSSEN, J.D., "Geochronology of hydrothermal uranium deposits and associated igneous rocks in the eastern source area of the Mount Belknap Volcanics, Marysvale, Utah". Economic Geology 77, 453-463 (1982).

[42] LINDSEY, D.A., Tertiary volcanic rocks and uranium in the Thomas Range and northern Drum Mountains, Juab County, Utah". U.S. Geological Survey Professional Paper No. 1221 (1982).

[43] PAGE, R.W., "Chronology of magmatism, skarn formation, and uranium mineralization, Mary Kathleen, Queensland, Australia". Economic Geology 78, 838-853 (1983).

[44] ZIELINSKI, R.A. "Tuffaceous sediments as source rocks for uranium: a case study of the White River Formation, Wyoming." Journal of Geochemical Exploration 18, 285-306 (1983).

[45] CHABIRON, A., CUNEY, M., POTY, B., "Possible uranium sources for the largest uranium district associated with volcanism: the Streltsovka caldera (Transbaikalia, Russia)". Mineralium Deposita 38, 127-140 (2003).

[46] BONNETTI, C., CUNEY, M., BOURLANGE, S., DELOULE, E., POUJOL, M., LIU, X., PENG, Y., YANG, J., "Primary uranium sources for sedimentary-hosted uranium deposits in NE China: insight from basement igneous rocks of the Erlian Basin". Mineralium Deposita 52, 297-315 (2017).

[47] STAMOULIS, V., "ASTER night-time thermal infrared data: interpreting subsurface features from high resolution data", MESA Journal 43, 36-39 (2006).

[48] THAKUR, S., CHUDASAMA, B., PORWAL, A., GONZÁLEZ-ÁLVAREZ, I., "Sub-surface paleochannel detection in DeGrussa area, Western Australia, using thermal infrared remote sensing", Proceedings SPIE 9877, Land Surface and Cryosphere Remote Sensing III, 98772C (May 5, 2016), doi:10.1117/12.2223626.

[49] JONES, L.D., "Uranium and Thorium Occurrences in British Columbia", Open File 1990-32, British Columbia Geological Survey, Victoria, B.C., Canada (1990).

[50] LETT, R., "Regional Geochemical Survey Database", GeoFile 2011-07, British Columbia Geological Survey (http://www.empr.gov.bc.ca/Mining/Geoscience/PublicationsCatalogue/GeoFiles/Pages/GF2011-7.aspx) (2011).

[51] O'CALLAGHAN, J.F., MARK, D.M., "The extraction of drainage networks from digital elevation data", Computer Vision, Graphics and Image Processing 28, 323-344 (1984).

[52] CARRANZA, E.J.M., HALE, M., "Geologically constrained fuzzy mapping of gold mineralization potential, Baguio district, Philippines", Natural Resources Research 10, 125-136 (2001).

[53] ZADEH, L.A., "Fuzzy sets", IEEE Information and Control 8, 338-353 (1965).

[54] BARDOSSY, G., FODOR, J., "Geological reasoning and the problem of uncertainty". In: Cubitt, J., Whalley, J., Henley, S. (Eds.), Modeling Geohazards: IAMG2003 Proceedings, Portsmouth UK. Portsmouth University, UK (2003).

[55] KREUZER, O.P., MILLER, A.V.M., PETERS, K.J., PAYNE, C., WILDMAN, C., PARTINGTON, G.A., PUCCIONI, E., MCMAHON, M.E., ETHERIDGE, M.A., "Comparing prospectivity modelling results and past exploration data: A case study of porphyry Cu–Au mineral systems in the Macquarie Arc, Lachlan Fold Belt, New South Wales", Ore Geology Reviews 71, 516-544 (2015).

[56] COYAN, J.A., ZIENTEK, M.L., MIHALASKY, M.J., "Spatiotemporal Analysis of Changes in Lode Mining Claims Around the McDermitt Caldera, Northern Nevada and Southern Oregon". Natural Resources Research, doi:10.1007/s11053-017-9324-9 (2017).

[57] ZADEH, L.A., "Outline of a new approach to the analysis of complex systems and decision processes", IEEE Transactions on Systems, Man and Cybernetics 3, 28-44 (1973).

[58] ZADEH, L.A., "The role of fuzzy logic in the management of uncertainty", Fuzzy Sets and Systems 11, 199-227 (1983).

[59] THOLE, U., ZIMMERMANN, H.-J., ZYSNO, P., "On the suitability of minimum and product operators for intersection of fuzzy sets", Fuzzy Sets and Systems 2, 167-180 (1979).

[60] ZIMMERMANN, H.-J., "Fuzzy Set Theory – and Its Applications", 2nd edn., Kluwer Academic Publisher, Dordrecht (1991).

[61] AN, P., MOON, W.M., RENCZ, A., "Application of fuzzy set theory for integration of geological, geophysical and remote sensing data", Canadian Journal of Exploration Geophysics 27, 1-11 (1991).

[62] ZIMMERMANN, H.-J., ZYSNO, P., "Latent connectives in human decision making", Fuzzy Sets and Systems 4, 37-51 (1980).

[63] AGTERBERG, F.P., BONHAM-CARTER, G.F., "Measuring performance of mineral-potential maps", Natural Resources Research 14, 1–17 (2005).

A CONTINENT-SCALE GIS-BASED ASSESSMENT OF THE DISTRIBUTION AND POTENTIAL FOR SANDSTONE-HOSTED URANIUM DEPOSITS

F.P. BIERLEIN
QMSD Mining Co Ltd,
Khartoum, Sudan

M.D. BRUCE
MDB Geoconsulting,
Blackwood, SA, 5051, Australia

Abstract

This chapter describes the steps required to design and construct a GIS-based fuzzy logic mineral prospectivity model for sandstone-hosted uranium deposits at a continental scale. The example of Australia (land mass ~7.69M km^2) is used, due to a relatively high density of pre-competitive data available for this continent, as well as its hosting a considerable number of economically significant deposits with >5,000 tonnes of contained U_3O_8 resources (e.g., Beverley, Four Mile, Manyingee, Oobagooma, Mulga Rock). The output generated from the fuzzy logic model documented in this study successfully 'rediscovers' proven sandstone-hosted uranium provinces and confirms the veracity of the current exploration targeting model for this type of uranium deposit. In addition, the result highlights several favorable geological regions within 'geologically-permissive tracts' that *should* be prospective for as yet undiscovered sandstone-hosted uranium deposits. We demonstrate the importance of suitable input layers (i.e., scale-dependence of mappable proxies, relevance to the formation of the deposit type sought), re-classification of pertinent data into appropriate groupings, and the development of a meaningful inference network that combines individual input layers to produce a realistic result. The methodology and approach employed herein is readily transferrable to other continents or geological provinces of interest, provided *a-priori* assessments of suitable input data and their limitations form an integral part of the development of the fuzzy logic mineral prospectivity model. If done correctly, GIS-based fuzzy logic mineral prospectivity modeling provides an extremely powerful visualization and decision-making tool for the explorationist.

1. INTRODUCTION

The last decade has seen a virtual 'explosion' of high-resolution digital data and the ability to collect, query and manipulate this information at unprecedented computing speeds. Almost as a logical consequence, Geographic Information Systems (GIS) have rapidly become an integral part of mineral exploration and are increasingly employed in the targeting and assessment of potentially prospective geological domains at all scales.

There is an increasing volume of work in the literature, which has demonstrated that the generation of GIS-based mineral prospectivity maps can aid significantly in the identification of areas that have high likelihood ('favorability') to contain economic concentrations of sought after commodities [1–8]. This is because statistical models enable accurate processing and interpretation of capacious geoscientific datasets. Moreover, the output from these can be reproduced and revised in a time-efficient manner while minimizing subjective bias. Additional data and newly gained knowledge can readily be incorporated and visualized as they become available without the need to completely re-build the targeting model.

The ultimate goal of this iterative process is to reduce complex conceptual models of ore deposit genesis to their most fundamental mappable components and reconstruct the targeting models in a way that imitates the geoscientist's thought process. Previous work and successful application of both statistical and expert-driven analysis methods to a range of mineral systems [9–11] have shown that prospectivity modeling provides not only a powerful visualization tool, but also a sound scientific basis for ground acquisition, and financial and tenement management decision-making. This GIS-based targeting approach forms the premise of the study documented here.

A key aspect of this chapter is to provide a basic guide on how to apply a GIS-based targeting approach to uranium deposits in sedimentary environments at the continental scale. For the purpose of this study, we focus on economically important sandstone-hosted uranium deposits and using the example of the continent of Australia (Figs. 1a, b), for which an adequate amount of publically available GIS data exists. The sandstone-hosted deposit group represented ~55% (33,090 t U from 25 deposits) of world production in 2013 (59,637 t U) [12] and occurs in a wide range of sedimentary basins across numerous geological domains worldwide [13].

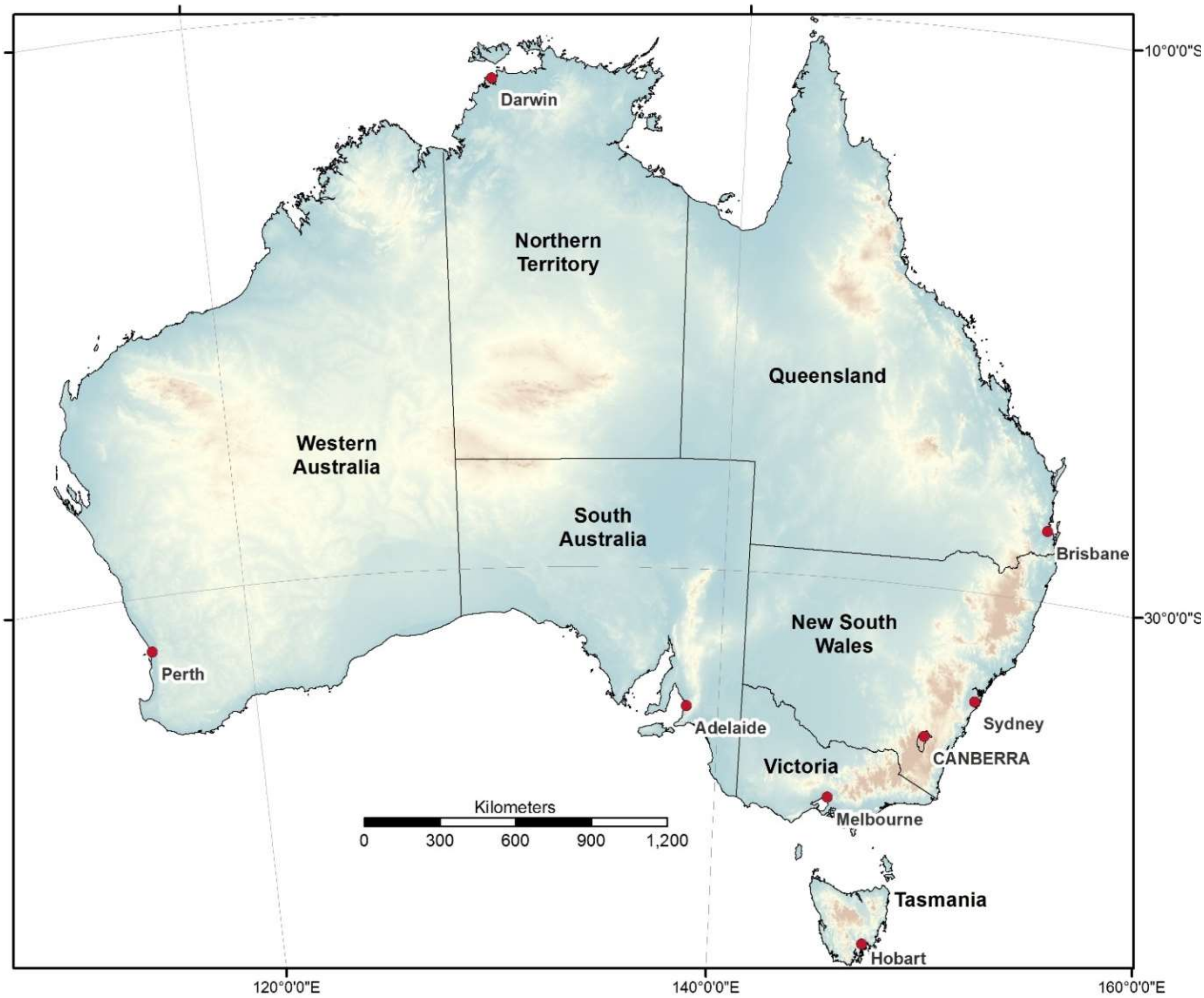

FIG. 1a. Map of Australia, showing state and territory borders and capital cities, superimposed on a digital terrain image (elevated relief indicated by warmer colors).

In addition to providing a practical example of using GIS-based statistical methods in the generation of exploration targets at a continental scale, the principal objective of this work is two-fold: (1) to delineate known provinces of sandstone-hosted uranium deposits (i.e., demonstrate that the output is geologically meaningful); and (2) to provide a framework for the definition of 'geologically-permissive' tracts, which have potential to host uranium deposits in a sedimentary environment. Implicit to the scale of the chosen approach is the use of suitable datasets, which, in our high-level example, can be sourced readily from public-domain repositories (see Section 3, References and Appendices). As we focus on processes that operate primarily at the scale of geological domains, the output from this work should by no means be considered exhaustive; neither is it intended to provide 'drill-ready' targets within any of the identified domains. For such to come to the fore, progressively more focused mineral prospectivity targeting models and using scale-appropriate GIS data sets (many of which might be proprietary) will be required.

2. FIRST-ORDER CONTROLS ON SANDSTONE-HOSTED URANIUM DEPOSITS

The following provides a brief summary of the parameters regarded as fundamental to controlling uranium mineralization in the sedimentary ore deposit setting considered herein (Table 1). As outlined further in the following section, recognition of these fundamental parameters, and their translation to quantifiable criteria form the basic premise of the GIS-based mineral prospectivity analysis conducted in this study. For more information on sandstone-hosted uranium deposits, the reader is referred to [13] and references therein.

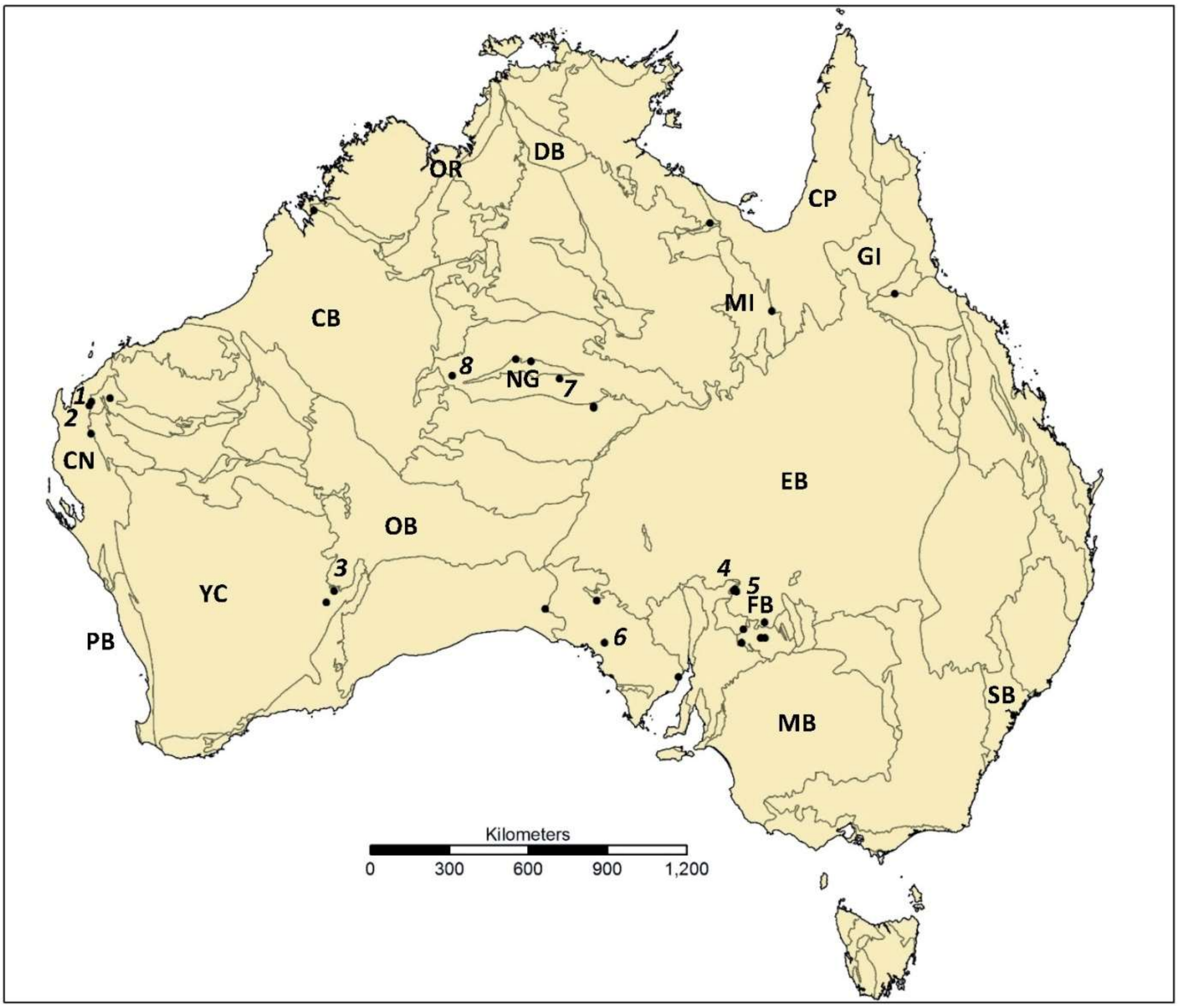

FIG 1b. Map of Australia showing principal sandstone-hosted deposits (black dots) and outlines of major geological provinces. Labels of selected deposits and key geological provinces cited in text are as follows: 1 = Manyingee; 2 = Bennett Well; 3 = Mulga Rock; 4 = Four Mile; 5 = Beverley; 6 = Warrior; 7 = Bigrlyi; 8 = Lake Mackay; 'CB' = Canning Basin; 'CN' = Carnarvon Basin; 'CP' = Carpentaria Basin; 'DB' = Daily River Basin; 'EB' = Eromanga Basin; 'FB' = Frome Basin; 'GI' = Georgetown Inlier; 'MI' = Mt Isa Inlier; 'MB' = Murray River Basin; 'NB' = Ngalia Basin; 'OB' = Officer Basin; 'OR' = Ord River Basin; 'PB' = Perth Basin; 'SB' = Sydney Basin; 'YC' = Yilgarn Craton.

The formation of major sandstone-hosted uranium systems requires a suitable depositional environment within an intra- to epi-cratonic sedimentary basin. The most favorable host rocks include first-cycle arkosic or feldspathic sandstone, which have retained their permeable and porous characteristics and are inter-layered with fine-grained, low permeability clastic sediments. The source of the uranium is typically provided by exposures of acid volcanic rocks and/or uranium-enriched crystalline basement upstream from the trap site. Groundwater chemistry and migration, either within paleo-channels or along a broad 'roll front', are instrumental in leaching oxidized uranium from source rocks and transporting it to a chemical interface commonly provided by adsorptive, reducing or complexing agents where the uranium is deposited. The hydraulic pressure head is driven by maintaining a dynamic topographic gradient between the source and the host rocks (i.e., via basin subsidence and/or basement uplift), with active or reactivated structures also exerting a certain degree of control over the transport and deposition of the ore in most cases.

The ideal conditions between dissolution, transport and precipitation of uranium appear to prevail in arid to semi-arid climates, with the resulting deposits typically restricted to young, undeformed Phanerozoic rocks mostly younger than 200 Ma at a global scale. However, the unique geological evolution of the Australian continent has resulted in the siting of at least some significant sandstone-hosted uranium deposits in significantly older sedimentary units, such as Bigrlyi in the intra-cratonic Neo-proterozoic to Late Paleozoic Ngalia Basin, and which is hosted in the Upper Devonian to Carboniferous Mt Eclipse Sandstone (Fig. 1b) [18].

TABLE 1. CRITICAL FEATURES OF SANDSTONE-HOSTED URANIUM SYSTEMS.

Deposit types (including synonyms): — Basal channel type; — Tabular type; — Roll-front type; — Tectonic-lithologic type.
Geological setting: — Sedimentary basins (intra-cratonic, epi-cratonic) in semi-arid environments; — Undeformed basin succession, typically Phanerozoic in age.
Source (fluid, metal, energy): *Fluids* — Low-temperature oxygenated, neutral to alkaline groundwater. *Uranium source* — Radiometrically anomalous granitoid intrusions and/or felsic volcanic rocks. *Energy drivers of fluid-flow* — Topographic relief and hydrological pressure heads.
Fluid pathway: — Groundwater migration within permeable and porous channel-ways and conduits (including permeable faults).
Trap: *Physical*

— First-cycle feldspathic or arkosic sandstones inter-bedded with layers of fine-grained, low-permeability clastic sediments.

Chemical

— Precipitation of pitchblende and coffinite under reducing conditions (or uranyl vanadates under oxidized conditions);

— Presence of suitable reductants such as coalified vegetal matter, woody fragments, structureless organic matter, petroleum, natural gas, hydrogen sulfides, pyrite, bacteria

Age and relative timing of mineralization:

— Most deposits are Mesozoic or younger, with some deposits occurring in Paleozoic sedimentary successions (e.g., Bigrlyi);

— Uranium typically emplaced paragenetically *after* deposition and sedimentation of host rocks (i.e., diagenetic to epigenetic).

Preservation:

— Deposits generally located within sedimentary successions and drainage pathways in stable cratonic environments with low erosion rates and high preservation potential.

Main references: [13−17]

Most of the Australian continent can be divided into three Archaean to Paleo-proterozoic basement cratons, which were amalgamated during several orogenic episodes between ~1,800 and ~1,200 Ma. These cratonized regions contain an abundance of relatively uranium-enriched felsic igneous units, which have the potential to provide fertile source regions for the accumulation of uraniferous detritus in sedimentary basins as they developed adjacent to exposed portions of these 'hot' basement terrains. Sandstone-hosted uranium deposits occur in sedimentary basins of Carboniferous, Cretaceous and Tertiary age [19]. Out of the four sub-types commonly recognized, tabular, roll-front, channel and fault/fracture-related [13], tabular, roll-front and channel types are well represented in Australian deposits. These deposits are associated with extensive intra-continental sedimentary basins that developed during the Neo-proterozoic – Paleozoic period, and flat-lying Mesozoic to early Tertiary sedimentary units that cover large areas of inland eastern Australia. The eastern third of Australia comprises Paleozoic to Mesozoic sequences, which were progressively accreted to the largely intact Neo-proterozoic Australian continent. Several sedimentary basins with potential for sandstone-hosted uranium occurrences developed along the margins on all sides of the continent during Late Paleozoic – Mesozoic extension and the break-up of Gondwana [20].

3. METHODOLOGY AND APPROACH

3.1. The minerals system approach

Of fundamental importance to the investigation carried out herein is the holistic mineral systems concept [21, 22], as it forms the basis for the selection of appropriate GIS data and the way these have been combined to generate meaningful output. This approach considers geological factors across all scales and which control the generation and preservation of mineral deposits. This includes the source of metals, ligands and energy, migration pathways, mechanical and structural focusing mechanisms, and the chemical and/or physical causes for precipitation at the trap site. From these, identifiable mappable criteria are derived and are then used within the framework of the GIS-based prospectivity analysis.

3.2. GIS-based mineral prospectivity analysis

In traditional approaches to mineral potential mapping, so-called 'predictor maps' are interpreted, either individually or conjunctively using manual overlay, to delineate potentially-mineralized zones. In recent years, the use of GIS (geographic information systems) for digital overlay of predictor maps has replaced these traditional approaches. However, unsophisticated applications of GIS involving, for example, Boolean operations or simple overlay to integrate predictor maps, are generally inappropriate for mineral potential mapping because they have a propensity to assign equal importance to every recognition criterion. Given the complexity of earth systems that form mineral deposits, it would be too naive to think that every earth process that was involved in the formation of the target mineral deposits contributed equally and, thus, all recognition criteria are given equal weight as predictors of the target mineral deposits (Porwal, 2006). The maps produced from the modeling software are commonly called "favorability maps" or "posterior probability maps" and are generally interpreted as a relative measure of the degree of prospectivity within the area of interest.

GIS-based prospectivity analyses can be broadly grouped into two principal types: (1) knowledge-driven approaches such as those that incorporate fuzzy-set theory (i.e., reasoning that is approximate rather than precise) and are based on exploration targeting models and expert opinion; and (2) data-driven approaches such as Bayesian probability, artificial neural networks and logistic regression that are based on statistical measures. Examples of these different approaches are briefly summarized below. Hybrid methods, such as the neuro-fuzzy approach use a mixture of both expert knowledge and statistics. The advantage of hybrid approaches over purely statistical methods is that they allow for a non-linear assessment of areas of interest in a way that is more akin to the way the human mind operates [10]. However, they were considered unsuitable for a continent-scale assessment as they (like purely statistical approaches) require a relatively high level of data density (i.e., a large number of known deposits).

The Weights-of-Evidence (WofE) method for mineral potential mapping uses the theory of conditional probability to quantify spatial associations between a set of predictor maps and a set of known mineral deposits [23]. The spatial association is expressed in terms of weights-of-evidence per predictor map. The weights-of-evidence of all predictor maps are combined with the prior probability of occurrence of mineral deposits using Bayes' rule in a log-linear form under an assumption of conditional independence of the predictor maps to derive posterior probability of occurrence of mineral deposits. The aim of the application of simple (i.e., using only binary predictor maps) and extended (i.e., using multi-class predictor maps) weights-of evidence models to a given area under study is the demarcation of high favorability, moderate favorability and low favorability zones, and by doing so result in a significant reduction of the search area and exploration risk. It is also possible to quantify the level of uncertainty in the favorability values using this type of analysis. The prerequisites for a meaningful WofE are that: (1) the number of known deposits (i.e., the training population) in an area under investigation is comparatively large relative to the number of undiscovered deposits; (2) the area is characterized by a high data density; and (3) the targeted mineralization style is analogous to that of the training population. In view of the relatively small number of factual, derived and conceptual input layers available at a continental scale, and the total number of known sandstone-hosted uranium deposits (<100, excluding minor occurrences and surface anomalies) comparative to the size of the study area (~7.69M km^2) meaningful spatial associations between one or more predictor layers and uranium mineralization are unlikely to be expressed in a data-driven MPA. As such, the WofE method was considered generally inappropriate and unsuitable for a continent-scale assessment of uranium resources and potential related to sedimentary environments.

In contrast to purely data-driven evaluations, the fuzzy logic approach requires expert input and the quantitative assessment of predictor maps and classes similar to those used for WofE analysis. Data preparation commonly requires some simplification (of, for example, lithological layers or fault orientation) so that each predictor map is made up of a manageable number of classes. This can have implications for output accuracy and error rate. Various fuzzy logic operators are used to infer relations between input predictor maps.

Solving these mathematical relationships results in a raster grid of numerical values that can be displayed as a colour-coded multi-class or binary prospectivity map. Such a map, in turn, can be used to increase the level of confidence in the decision-making process. Fuzzy logic analysis can be shown to be superior to the application of WofE in particular in areas that are characterized by low data density and do not have any or a very limited number of training populations (i.e., mineral deposits). As stated above, the reason for this is that fuzzy logic does not depend on statistical measures and instead relies largely on expert knowledge-driven input.

Regions of relatively high data density and/or an expert understanding of the parameters involved in the formation of a deposit type allow for a hierarchical classification of input maps into those that relate to each major component of the mineralizing system. ‘Source’ (e.g., basement, uranium-enriched felsic igneous rocks), ‘Transport’ (e.g., faults, drainage pathways) and ‘Trap’ (e.g., reduced sediments, morphological barriers) components are then combined using logical operators that enable a weighted, logical assessment of truly independent evidence.

Each approach (knowledge-driven, statistical or hybrid) involves the analysis of available spatial datasets to calculate the relative prospectivity of each unit cell (typically 0.01 to 1 km^2, depending on the scale of the study) in an area under investigation. The analysis presented herein was performed using ESRI ArcGIS™ software.

3.3. Review and selection of continent-scale datasets

The first step in undertaking any MPA is to acquire and assess spatial datasets that have the potential to be turned into useful proxies for components of the mineralization genetic model. This requires a thorough audit of all publically available data and their formats.

Scale-dependent and potentially usable datasets for the construction of an Australia-wide, continent-scale MPA include surface geology (1:1M, 1:5M and 1:2.5M scales), geological provinces, crustal elements, basic lithology, metamorphic grade and ages, structural elements, digital terrain models, images of radiometric U, Th and K content, drainage pathways, uranium occurrences, sedimentary basin thickness, and the distribution of paleo-channels.

By global standards, Australia is endowed with an extraordinary amount of pre-competitive multi-disciplinary datasets of very high quality. However, many of these data sets are not necessarily useful for their straightforward inclusion in a continent-scale GIS-based MPA. That is, they either lack sufficient resolution, or, conversely, are too data-rich to be practical at the scale of the proposed MPA. In addition, several datasets do not provide complete coverage of the continent.

Table 2 and Fig. 2 show the input datasets used in the current study, with additional information and links to individual source files (where relevant) provided in Section 3 and the References.

3.4. Input predictor maps

Having chosen appropriate spatial datasets for the analysis, the next step in constructing a MPA model is to turn those data into useful ‘predictor’ maps. Each input is constructed in such a way that it acts as a proxy for a single component of the genetic model under consideration. From the factual and derived layers identified in the previous section, a series of predictor maps (including appropriate buffer intervals where applicable; see below) was generated using ESRI ArcGIS (Version 10.4.1; Figs. 3, 4). Importantly, each input dataset was created using a common coordinate system (GDA 1994 Geoscience Australia Lambert) to ensure geographic integrity of the model.

A layer showing the location of 30 major sandstone-hosted uranium deposits (derived from the Australian Minerals Occurrences Collection database; available at http://www.ga.gov.au/metadata-gateway/metadata/record/73131) was not included in the construction of the model but to assess the geological relevance of the output.

TABLE 2: INPUT DATASETS UTILIZED IN THIS STUDY

Layer	Rationale/mappable criteria	Comments
Significant sandstone-hosted uranium deposits	Location of sandstone-hosted uranium deposits	Not included in the model but serves as a means to assess geological accuracy of MPA output (Fig 2a)
First-order crustal fractures	Principal faults controlling basin margins, movement, orientation of drainage pathways and potential trap sites	Considers 1st order structures only; regional and local fault control impossible to consider at continent-scale (Fig. 2b)
Hydrological data and maps based on SHuttle Elevation Derivatives at multiple Scales (‘HydroSHEDS’)	Drainage pathways and potential trap sites	Comprehensive stream network derived from hydrologically conditioned SRTM data; requires choice of appropriate cut-off to remove minor tributaries (Fig. 2c)
Surface geology of Australia (1:1,000,000 scale)	Potential source (i.e., felsic igneous units, volcanics, sediments) and trap (basin successions) rock lithologies	Reclassified/simplified to group and distinguish relevant rock types, stratigraphy and lithologies, and to differentiate ‘unprospective’ basement from ‘prospective’ basins (Fig. 2d)
Geoscientific thematic map of Australia's arid and semi-arid zone paleo-valley systems in WA, SA and the NT (‘WASANT paleo-valley map’)	Location and extent of paleo-channels (drainage pathways and potential trap sites)	Incomplete coverage (South Australia, Northern Territory and West Australia only; Fig. 2e)

Layer	Rationale/mappable criteria	Comments
Australian geological provinces	Outlines of all Australian geological provinces including sedimentary basins	Includes seven basin categories (grouped by age) considered prospective (Fig. 2f)
Australian crustal elements	Outline and extent of the basic 'building blocks' of Australia	Proxy for the presence of 'fertile' lithosphere to generate suitable source rocks (Fig. 2g)
Hydrogeology map of Australia	Porosity and permeability of sedimentary units in basins and drainage pathways	Proxy for permeable/porous lithologies capable of transporting uranium (Fig. 2h)
Radiometric map of Australia	Radiometric anomalies	Proxy for enriched sources and availability of leachable uranium using a 5ppm cut-off (Fig. 2i)
SRTM 90 m digital elevation data for Australia	Topographic relief; low-lying areas delineating potential drainage pathways	Reprocessed SRTM elevation data used for calculating local topographic 'lows' (Fig. 2j)

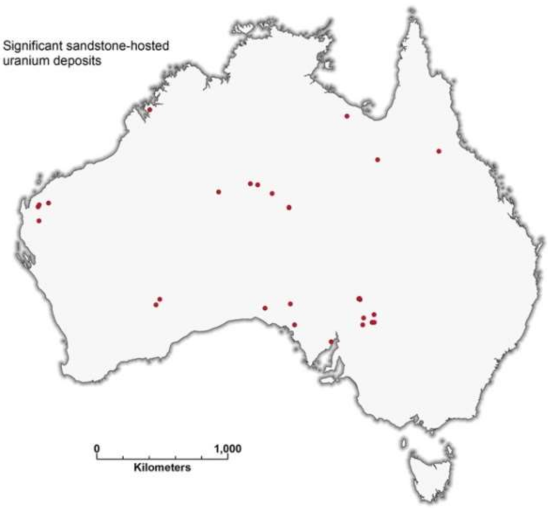

(a)

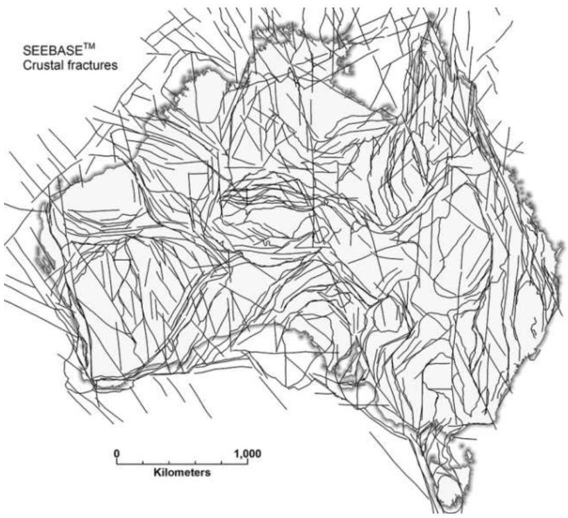

(b)

FIG. 2. Schematic illustration of input data sets utilized in this study (see Table 2 for description).

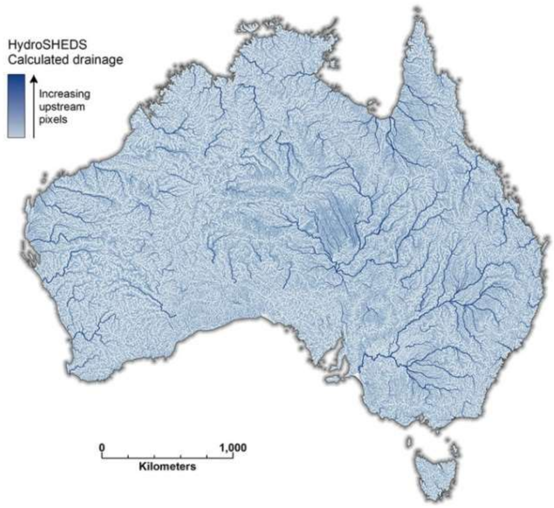

(c)

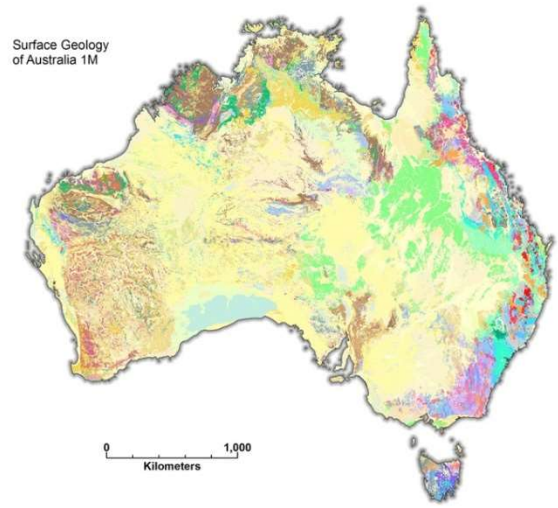

(d)

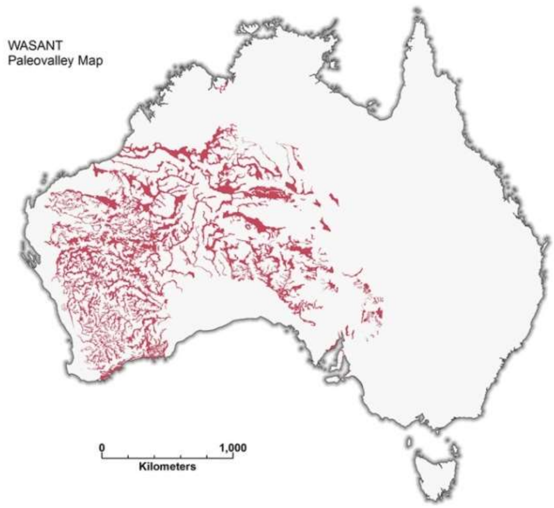

(e)

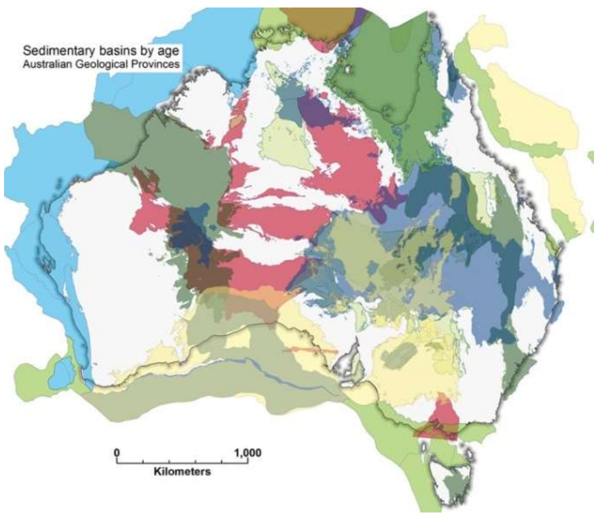

(f)

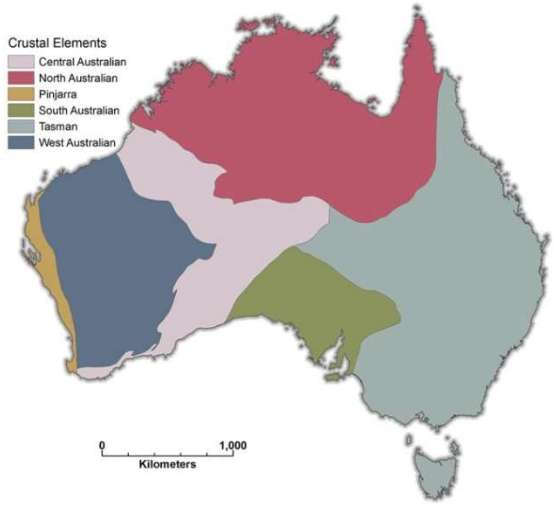

(g)

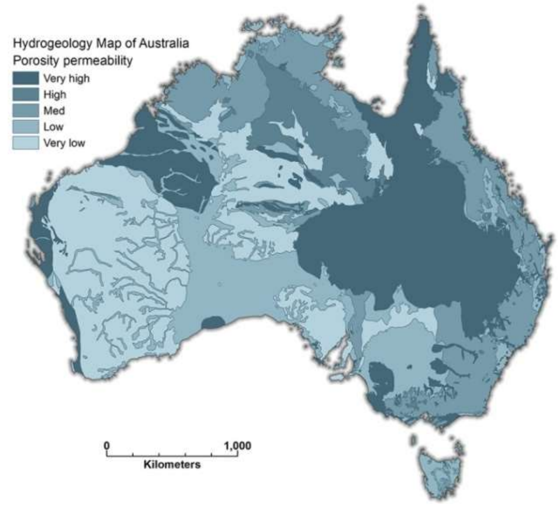

(h)

FIG. 2 (continued from preceding page).

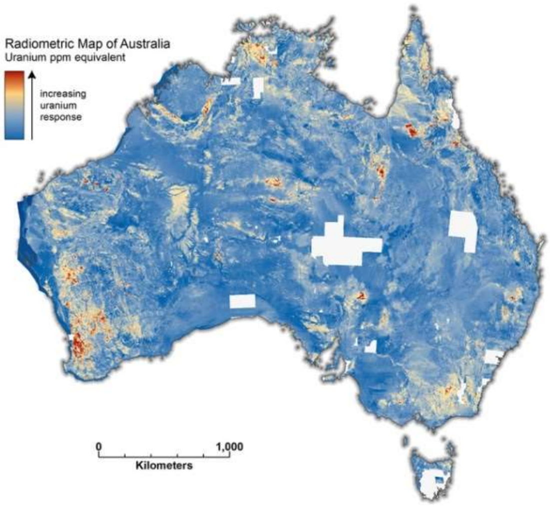

(i)

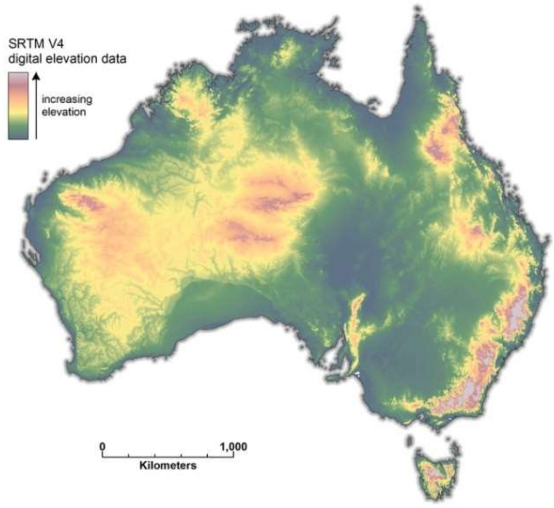

(j)

FIG. 2 (continued from preceding page).

3.4.1. Source

Several predictor maps were generated from the Australia-wide 1:1M scale surface geology data (from [24]; Fig. 2d). These data were initially re-classified and simplified into suitable groups of general lithology and stratigraphic successions. A basic distinction was made between generally more favorable (i.e., felsic plutonic and volcanic units) and less uraniferous (i.e., mafic successions, metamorphics) source rocks. In addition, the felsic igneous rock suites were re-classified into appropriate age groupings so as to account for Proterozoic (A-type) granites representing more favorable source rocks than their Phanerozoic and Archaean (I- and S-type) counterparts. Note that no predictor map was generated for the 'Cenozoic' age group, as it was considered irrelevant for the current model.

A further distinction was made between radiometrically anomalous felsic igneous rocks and those that display little or no anomalism. Uranium channel radiometric data for the Australian continent (Fig. 2i) taken from [25] were re-classified by using a 5-ppm cut-off to filter out areas characterized by less than 5 ppm U and converting the raster data into a binary vector shapefile. The output from this was then combined with the age-classified felsic igneous rocks from the 1:1M scale lithology map to give a derived layer that delineates 'hot' felsic igneous rock units that could have provided a suitable source of leached uranium. This approach was considered preferable to using the 'raw' radiometric data because it effectively removes 'false positive' signals such as those generated by the occurrence of calcrete expanses and organic-rich sedimentary units.

The genetic model favors areas proximal to these potential sources because uranium has the potential to be liberated directly from the source rocks during weathering, and also because the plume of detrital uraniferous material surrounding the exposed felsic rock can act as an additional uranium source. This potential decreases with distance from the exposed felsic rocks. To account for this in the MPA model, multiple concentric buffers (20 km intervals out to 100 km) were created around each potential felsic source. These buffer distances are considered reasonable, realistic and also appropriate at the scale of a continent-wide model. If a more regional targeting model or a different deposit type is considered, the user may wish to adjust buffer widths accordingly. The approach chosen in the current study results in a total of eight buffered 'Felsic Igneous' and 'Hot Felsic Igneous' predictor maps, separated into four age groups (Figs. 3a-h), thus providing a high degree of control as each buffer zone around the differently aged felsic igneous features can be treated and weighted separately.

A further potential source of uranium is represented by the sedimentary units themselves. It is recognized that roll-front systems operating over large areas in sedimentary rocks with even slightly elevated background uranium levels can result in significant economic accumulations of the metal. The combination of 'Simplified Lithology' and 'Simplified Stratigraphy' predictor maps (Figs. 3i, j) in the model was used to account for regions dominated by more permeable sedimentary units that may have acted as their own uranium sources.

Australia's three Precambrian building blocks (i.e., West, North and South Australian cratons) are exceptionally well-endowed with a range of mineral resources, as well as containing a significant amount of 'fertile' granite bodies and co-magmatic volcanics, when compared to the make-up of the intervening crustal elements of younger association [26, 27]. This discrepancy has been linked to systematic variations in the presence and abundance of metasomatized lithosphere underlying the Australian crust [21]. Therefore, it is reasonable to assume that the three cratons have a higher degree of 'fertility' in terms of their ability to generate uranium-enriched source rocks and, by inference, also possess greater sandstone-hosted uranium potential. This discrepancy is reflected by the weighting of the respective domains distinguished in the 'crustal element' input predictor map (Fig. 3k) which is based on data in [28].

3.4.2. Transport

One of the principal controls on sediment-hosted uranium mineralization is groundwater migration within permeable and porous channels and conduits. First-order structures (data taken from the Proterozoic OZ SEEBASE™ dataset [29]; Fig. 2b) were buffered (10 km intervals out to 50 km) to account for the enhanced fluid migration potential in zones proximal to structures (Fig. 3l). However, as discussed below, first-order structures are likely to have limited value in this continent-scale prospectivity model.

The WASANT paleo-valleys data show the interpreted distribution of paleo-valleys including those obscured of desert dune-fields in arid and semi-arid zones covering parts of three Australian states (data taken from the geoscientific thematic map of Australia's arid and semi-arid zone paleo-valley systems in West Australia, South Australia and Northern Territory [30]). These paleo-valleys represent obvious channel-ways for groundwater migration. A major drawback of this dataset is it covers only part of the continent (Figs. 2e, 3m).

HydroSHEDS [31] (Fig. 2c) data have been developed primarily by the Conservation Science Program of World Wildlife Fund (WWF). The data consist of stream networks calculated from shuttle radar topography mission (SRTM; available from http://www2.jpl.nasa.gov/srtm/) elevation data that have been hydrologically conditioned to force the digital elevation model (DEM) to produce correct river network topology, while preserving as much original SRTM information as possible (i.e., where necessary, minor changes have been made to the original SRTM elevation data to force the subsequently calculated drainage networks to conform to true drainage paths). The derived stream network corresponds to modern-day drainage but an assumption used in this model is that in relatively undeformed terranes, and where paleo-channels exist, they are more likely to be located close to current day drainage or low-lying areas than in elevated regions. The raw source data represent an extremely complex and comprehensive continent-wide drainage network. In order to make these data usable at the scale of this study, they were re-classified in such a way so as to use an arbitrarily chosen cut-off of upstream 8,500 pixels. Doing so removed minor tributaries and water ways that were considered inconsequential in their ability to contribute significant concentrations of dissolved uranium to a downstream trap site. Multiple ring buffers (10 km intervals out to 50 km) were constructed around each feature to highlight not just current day drainage but proximal zones (Fig. 3n). In areas where HydroSHEDS data are not available, modern-day drainage can be calculated from SRTM or other digital elevation data using the 'Hydrology' tools in the Spatial Analyst extension for ArcGIS.

The aforementioned SRTM elevation data (Fig. 2j) can also provide a very useful input parameter for the demarcation of low-lying areas that may be the focus of surficial fluid migration. However, the straightforward use of these data at a continental scale is rendered difficult as a locally low-lying area in one region can have the same absolute height above sea level as a locally elevated topographic region elsewhere. For example, a simple re-classification of the SRTM data displayed in Fig. 2j would achieve little more than differentiating between the generally lower south-eastern and more elevated north-western areas rather than identifying zones of potential fluid migration and uranium accumulation.

In order to identify 'Local Lows', the Australia-wide SRTM data (taken from [32]) were re-processed in ArcGIS using the Spatial Analyst extension. The steps involved in this procedure are outlined briefly in the following and illustrated in Fig. 4.

The 'Focal Statistics' tool calculates a statistic of the values within a user-defined neighborhood around each cell of a raster dataset. First, a 'local mean elevation' raster was created by calculating the mean SRTM value in a 5-km radius around each raster cell. In Fig. 4a, a single pixel is represented by the black dot at the centre of the two concentric circles. The 'local mean elevation' for that pixel is simply the mean value inside the illustrated "Local" zone. The 'Focal Statistics' tool was used to calculate this value for every cell in the raster, resulting in a continent-wide grid of 'local mean elevation' values. This was followed by a second iterative process in which the 'Focal Statistics' tool was again used to calculate the mean elevation values around each pixel. This time however, an annulus with a 5-km inner radius and 50 km outer radius was used. This results in a 'regional mean elevation' raster ('Regional" zone in Fig. 4a). A 'local low' is considered to occur anywhere the local mean elevation is lower than the regional mean elevation. The 'Less Than Equal' tool in Spatial Analyst was used to make this comparison (the process is summarized in Fig. 4c).

From this, an accurate assessment of local sinks and surficial fluid migration pathways can be made for the entire continent, irrespective of absolute elevation (Fig. 3o). The value of this technique lies in its ability to highlight broad, low-lying zones that have an increased likelihood of being a focus for surficial and shallow-level ground-water migration and uranium accumulation (Fig. 4b), rather than simply delineating modern-day drainages. The result compares favorably with the WASANT paleo-valley data. In general, the favorability of drainage pathways within these derived low-lying regions, as well as those highlighted in the paleo-valley layer, can be reflected in a simple 'yes'/'no' binary manner.

The data from [33] were reclassified into five distinct classes of porosity and permeability (i.e., 'very high', 'high', 'medium', 'low', and 'very low'; Fig. 3p).

3.4.3. Trap

The original classification scheme of Australian on-shore sedimentary basins used by [34] was kept and incorporated into the model. This classification groups the basins from the Australian Geological Provinces dataset into seven age categories (i.e., Cenozoic, Mesozoic – Cenozoic, Mesozoic, Paleozoic – Cenozoic, Paleozoic – Mesozoic, Paleozoic and Neo-proterozoic – Paleozoic) based on the age ranges of sedimentary succession within each basin. Basins older than Neo-proterozoic on the Australian continent generally have been deformed, metamorphosed and cratonized, and as such were not considered. In general terms, the porosity and permeability of Australian on-shore sedimentary basins decrease with increasing age but may vary widely as a function of the presence and thickness of specific rock units.

In the example of the Australian continent, numerous prospective sedimentary basins are bounded by – in some case, inverted – normal faults and the sandstone-hosted deposits tend to be situated within close proximity of these (epi- to intra-cratonic) basin margins. This is because the close interplay between uranium-enriched basement sources in the upstream portion of the drainage system, transport of dissolved uranium in oxidized near-surface fluids within the drainage network, and the development of a redox front within suitable sedimentary units in the subsiding basin-hosted downstream portion of the system. As mentioned above, however, this strongly positive spatial correlation cannot be emphasized by way of ‘filtering out’ basin-bounding faults from a structural layer appropriate to the continental scale as applied herein. Therefore, the sedimentary basin input predictor maps include appropriate buffer intervals to reflect this increased favorability along basin margins (Figs. 3q-w). Relatively rapidly growing Mesozoic to Cenozoic basins which developed in response to the break-up of Gondwana are considered most favorable as they contain thick units of both porous and permeable detritus, as well as substantial amounts of highly reduced material.

It is important to note that drainage pathways represented by the ‘HydroSHEDS’, ‘Local SRTM Lows’ and ‘WASANT Paleo-valleys’ data have been considered both from a ‘transport’ and a ‘trap’ viewpoint in the MPA discussed herein.

3.5. Fuzzy membership values

Once all suitable input layers have been assembled, appropriate class scores (i.e., relative prospectivity) and map weights (i.e., importance of, and confidence in the data layer) (Appendix 1) need to be assigned to each of the input predictor maps. As it is of absolutely vital importance to the output, the class scoring and map weighting should be based on expert input from collaborators familiar with the subject matter and an assessment of the quality and fidelity of each data set. In this example, a relatively simple method is used to calculate ‘Fuzzy Membership’ values. Multiplication of the class scores per feature and map weight per predictor map gives a class weight per feature. A ‘Fuzzy Membership’ value is then derived simply by dividing the class weight by 100 (Appendix 1). From these fuzzy membership values ‘Fuzzy predictor maps’ are then generated. These maps provide a graphic illustration of the perceived relative importance for each category within a given input layer considered in terms of their combined class and map weights (i.e., the ‘Fuzzy Membership’ value; Appendix 1).

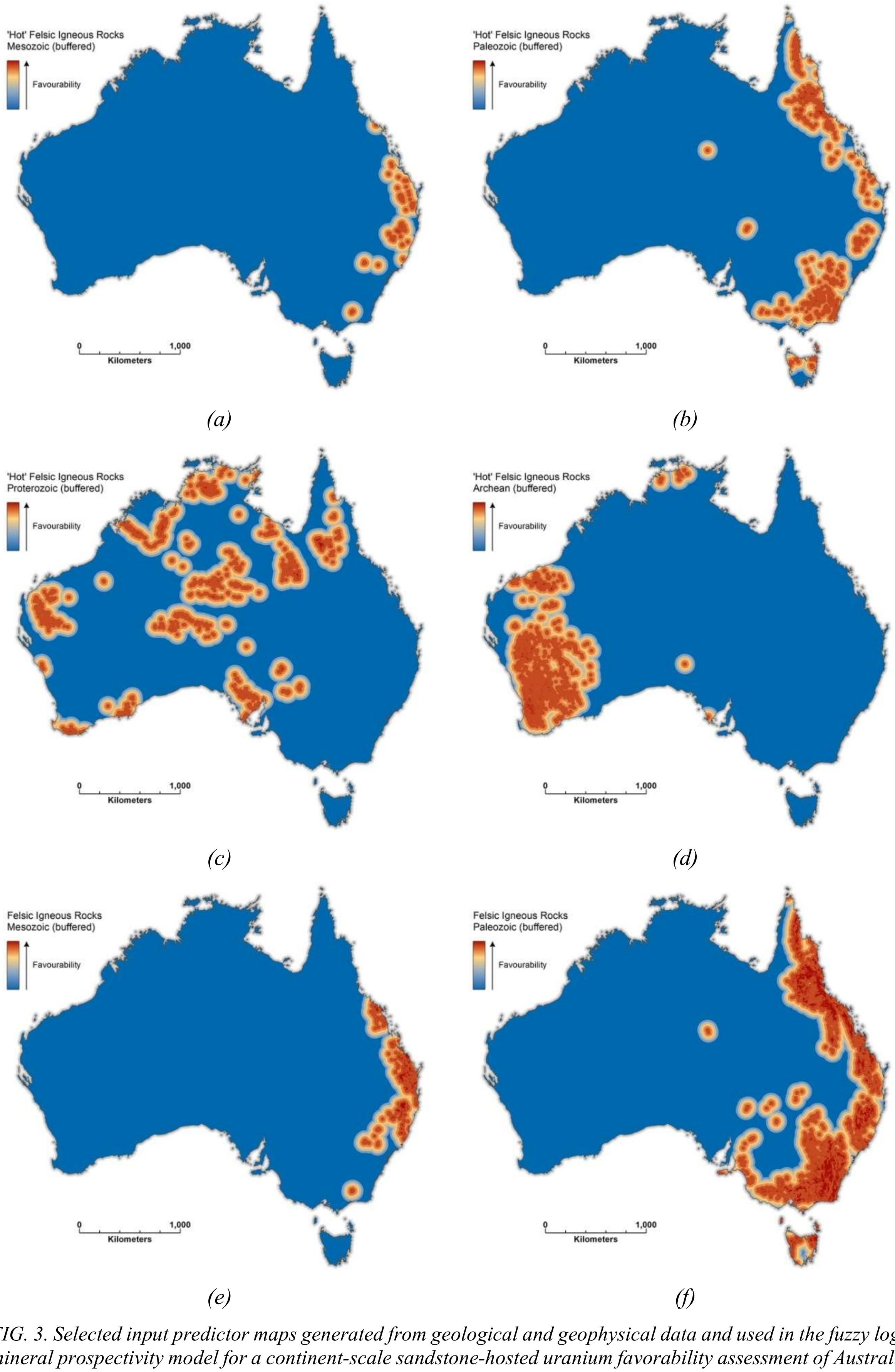

FIG. 3. Selected input predictor maps generated from geological and geophysical data and used in the fuzzy logic mineral prospectivity model for a continent-scale sandstone-hosted uranium favorability assessment of Australia. Warmer colors in each of the maps represent increased favorability. See text for explanation.

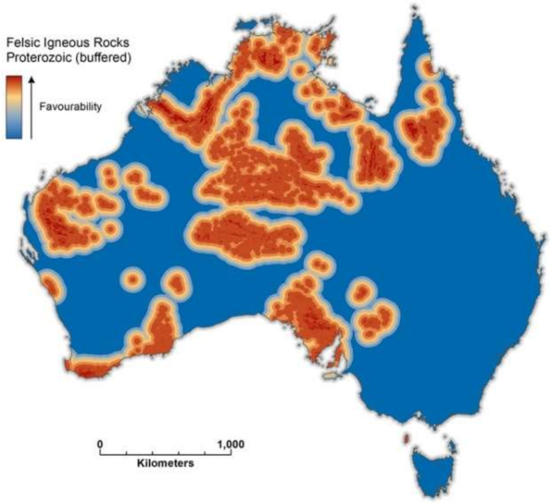

(g)

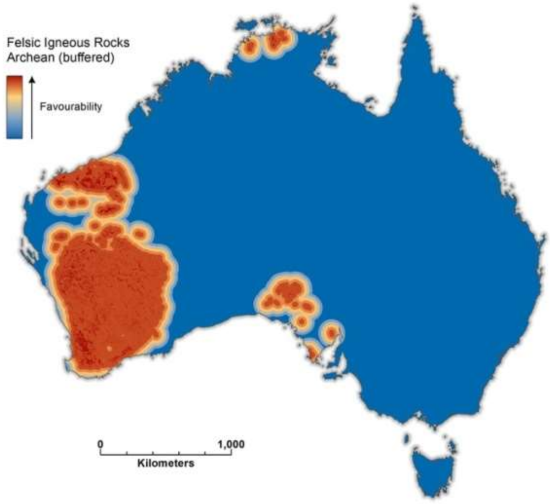

(h)

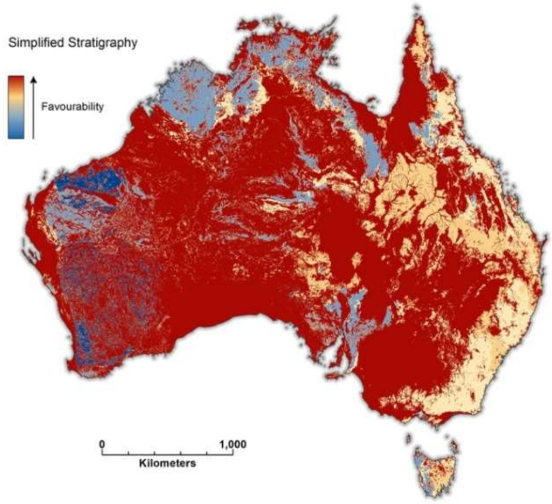

(i)

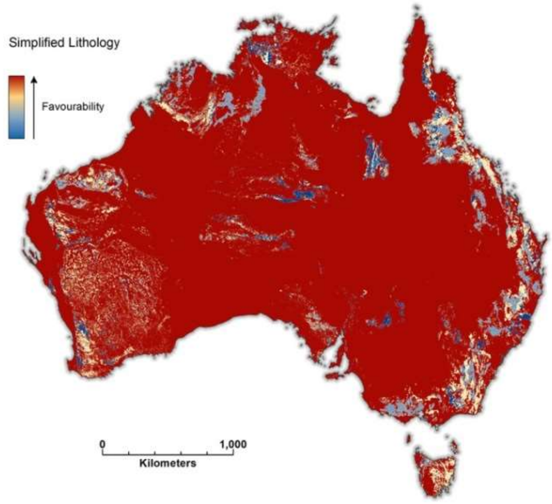

(j)

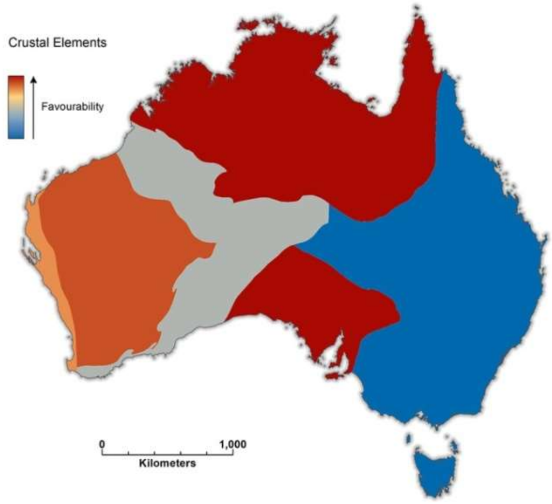

(k)

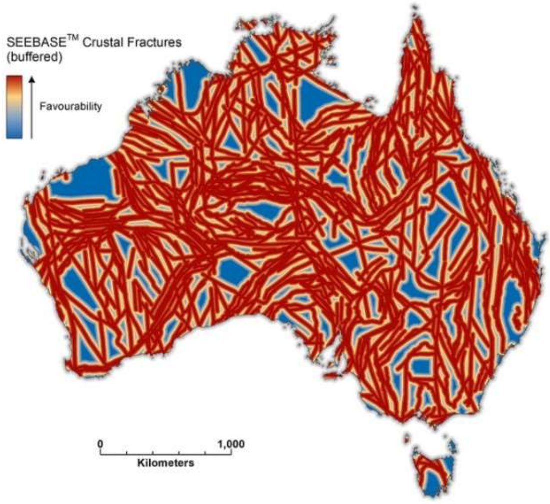

(l)

FIG. 3 (continued).

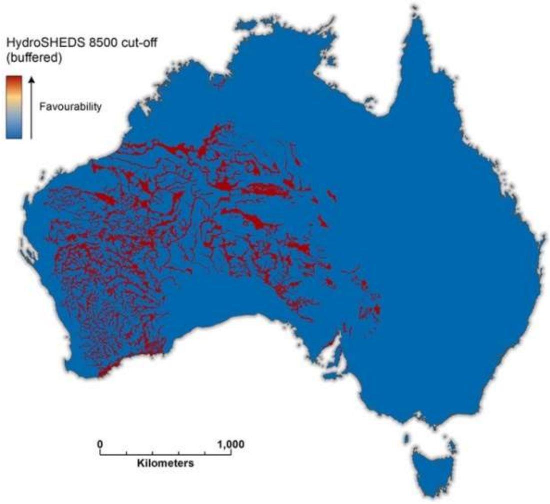

(m)

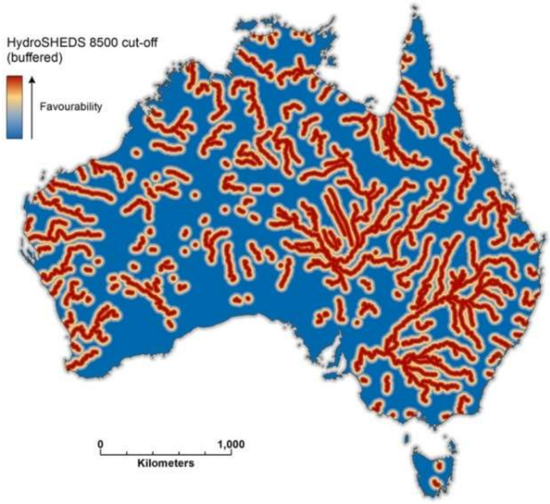

(n)

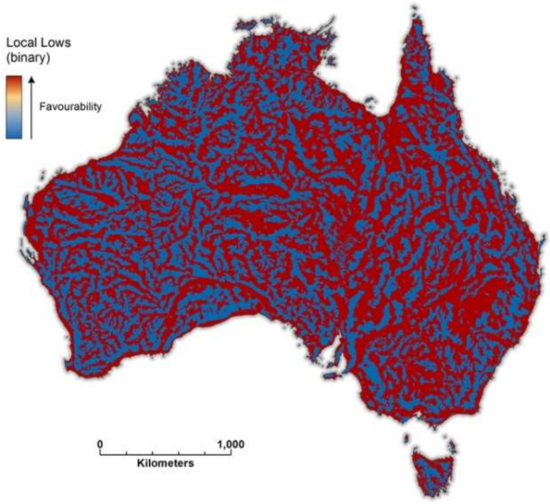

(o)

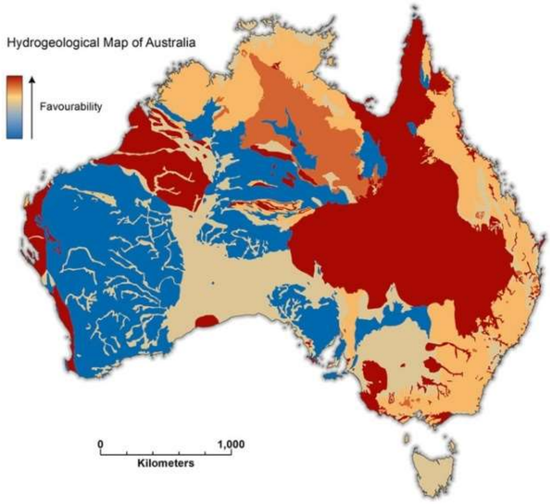

(p)

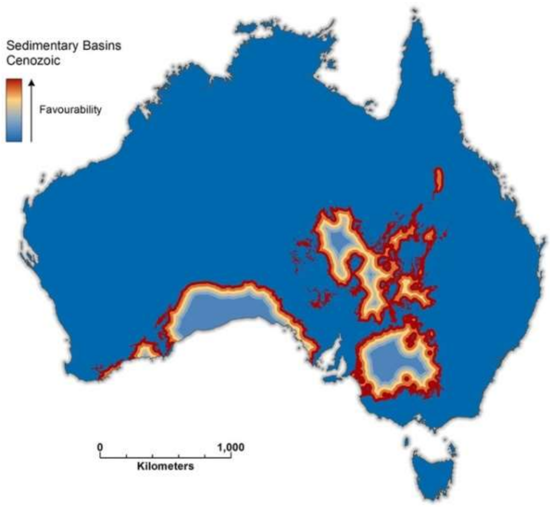

(q)

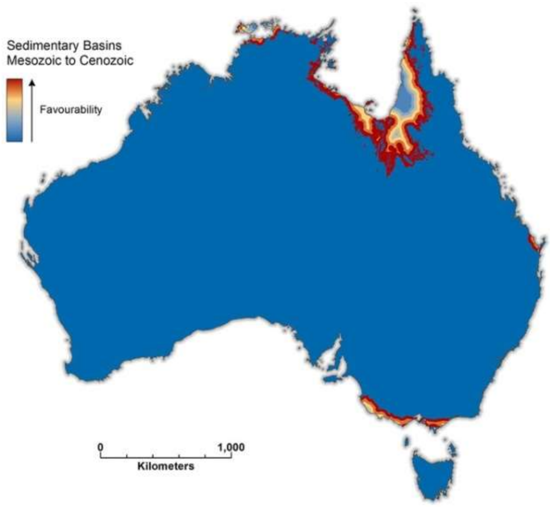

(r)

FIG. 3 (continued).

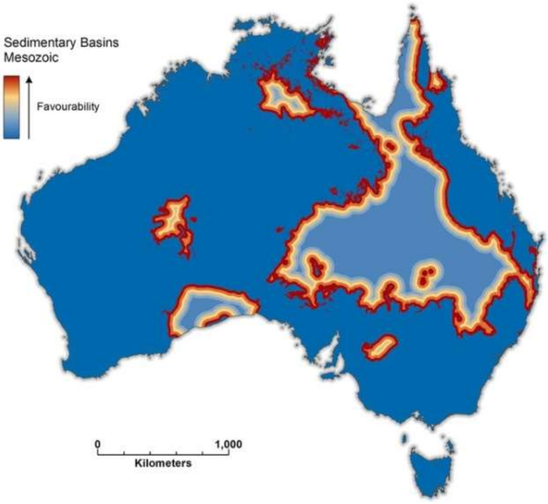

(s)

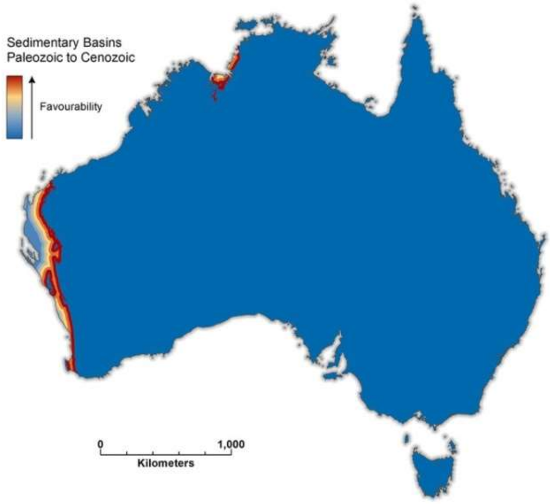

(t)

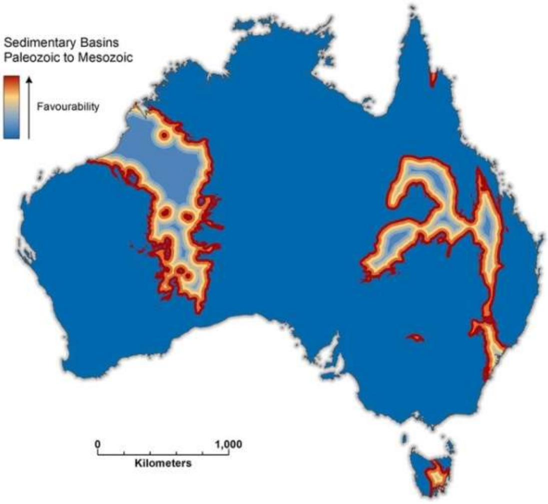

(u)

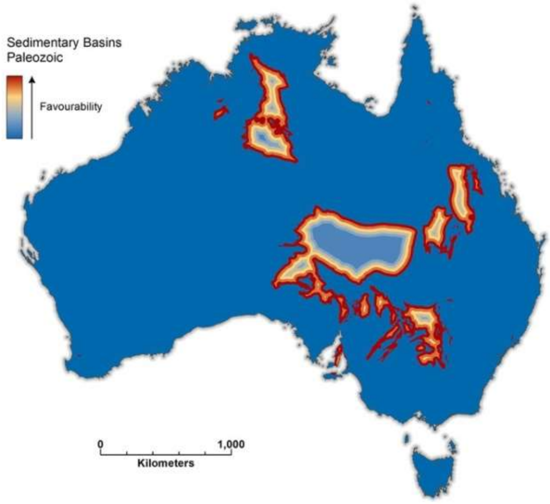

(w)

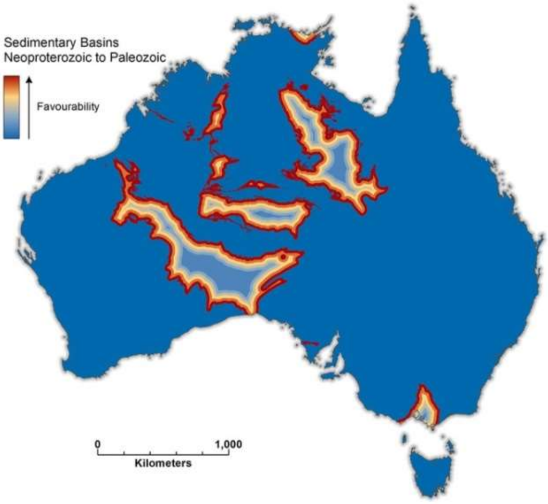

(w)

FIG. 3 (continued).

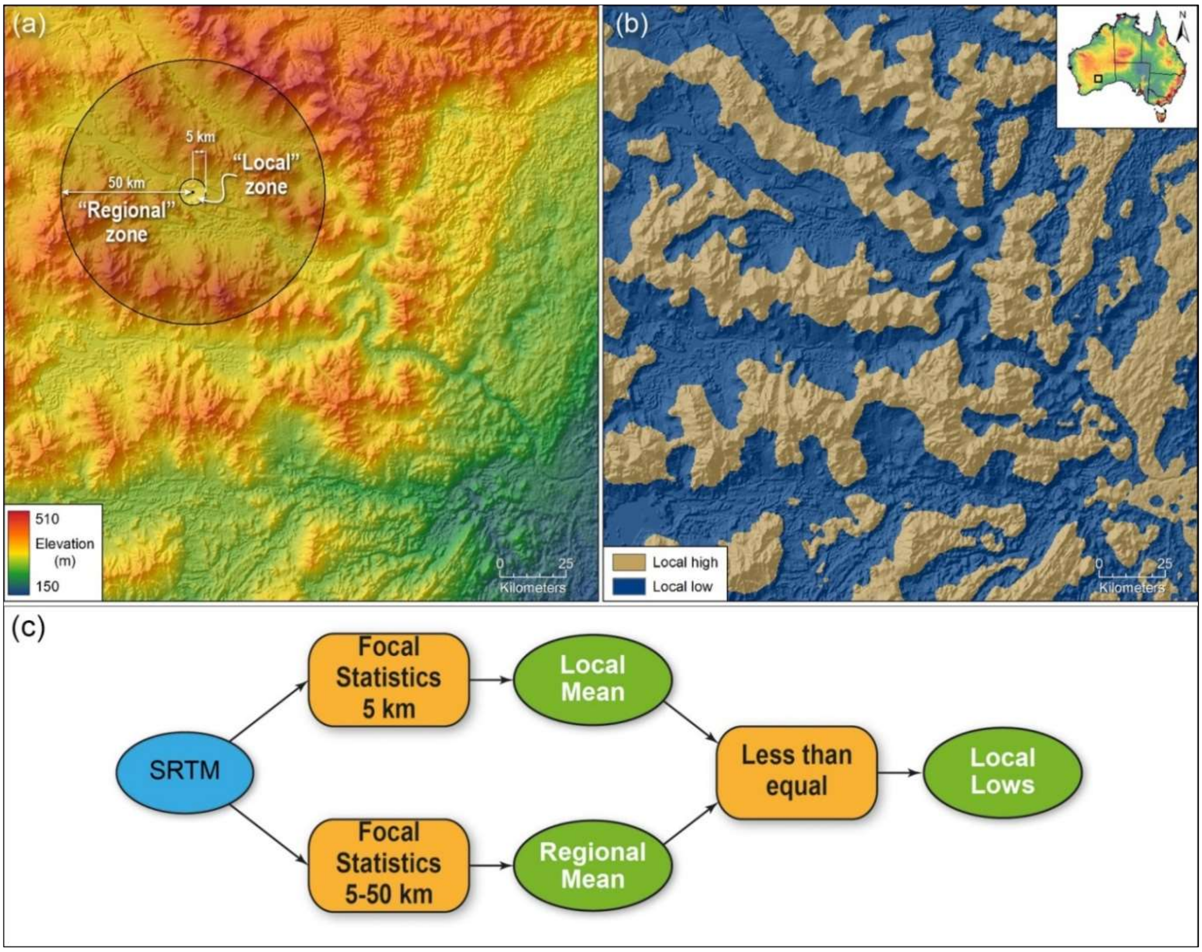

FIG. 4. Calculation of "Local Lows" from SRTM elevation data. See text for discussion.

Where proximity to a particular feature is being modeled through the use of multiple ring buffers, class scores are assigned such that they decrease with increasing distance. Using a scale from 0 to 10, each buffer interval surrounding the source rock lithology is assigned a class score that reflects its (perceived) importance from the viewpoint of contributing to the formation of a sandstone-hosted uranium deposit. As can be seen from Appendix 1, the assigned class scores are identical for each of the eight rock types considered. On the other hand, the respective map weights vary significantly across these input layers, as 'hot' felsic rocks of Proterozoic association are considered far more important in terms of representing a suitable source (i.e., map weight = '9') than, for example, their Mesozoic counterparts (map weight = '2'). Similarly and based on empirical knowledge (cf. Section 2), 'Proterozoic felsic igneous rocks' are considered to be far more important than their Paleozoic analogues (map weight of '8' versus '2'). Note that the map weights apply equally to all classes within the same predictor map.

The 'Simplified Lithology' and 'Simplified Stratigraphy' predictor maps were included in the model to account for regions where permeable sedimentary units may have acted as their own uranium sources. When considering the 'simplified stratigraphy' predictor map, it might seem somewhat counter-intuitive to assign the highest-class score (i.e., '9') to the Cenozoic. This is done to take into account the fact that, although much of the thin veneer of Cenozoic material that covers a large part of the continent is considered unprospective, it conceals older stratigraphic units of unknown prospectivity. Put in another way, if one were to assign a low-class score to the Cenozoic cover, large tracts of the Australian continent would be designated as unprospective in the final analysis, which is highly unrealistic. At the continental scale and due to the necessary use of highly simplified versions, uncertainties and spatial variations in the properties of the lithological units represented in these predictor maps remain quite large. Consequently, relatively low map weights have been assigned to both the ‘Simplified Lithology’ and ‘Simplified Stratigraphy’ predictor maps (map weight = ‘5’ in both cases). In regional or local studies, where tighter constraints can be placed on the various lithological units, it may be appropriate to use significantly higher map weights.

The majority of known sandstone-hosted uranium deposits in Australia are situated within close proximity to the margin of a sedimentary basin of Paleozoic to Cenozoic age. As such, class scores assigned to the buffers in each of the ‘Sedimentary Basins’ predictor maps are such that favorability decreases with distance from the basin margin. Younger basins are assigned the highest map weights (cf. Appendix 1).

Although many, if not most sediment-hosted uranium deposits display a strong spatial association with structural elements, these tend to be local- to regional-scale, rather than true first-order (i.e., terrane-bounding, trans-crustal) in nature. Buffered first-order structures are included in the model to reflect the potential importance of structure in the genetic model, but for the purpose of an MPA undertaken at the continent-scale it remains virtually impossible to account for this spatial association. The first-order structural layer is considered to be of rather limited value and this is reflected in the relatively low map weight (map weight = ‘4’) attributed to the predictor map.

Where a layer is considered in more than one category (i.e., ‘Source’, ‘Transport’, ‘Trap’) such as the ‘HydroSHEDS’ layer, it is legitimate to assign different class scores and map weights so as to reflect variations in its perceived significance as a ‘transport’ medium when compared to contributing to the provision of a ‘trap’.

In the case of the paleo-valley and ‘Local Lows’ input data, simple binary ‘yes’/’no’ (i.e., ‘favorable’ or ‘unfavorable’) classifications were used instead of buffer distances – and assigned ‘9’ and ‘0’ class scores, respectively. This arrangement reflects the geographical nature of these features whereby a specific location is either inside or outside an identified paleo-valley. This contrasts with the approach used for linear stream networks (e.g., ‘HydroSHEDS’) where multiple-ring buffers are used to reflect decreasing favorability with distance.

Vector predictor maps must be converted to raster grids before the mathematical fuzzy logic operations can be carried out. An appropriate raster cell size is specified by the analyst and will depend upon the scale of the data being considered and, to some extent, the computer processing power available. For the purpose of the current study, a cell size of 500 m was considered appropriate for balancing resolution and computing time. The use of high powered computer facilities would make a smaller raster cell size, and hence higher resolutions achievable but due to the scale of most input datasets, this would not significantly improve the quality of the final analysis. Predictor maps were rasterized as a numerical grid using the Fuzzy Membership value. In total, the sandstone-hosted uranium Fuzzy Logic prospectivity model constructed herein consists of 26 predictor maps. The unique rasterized predictor maps are shown in Fig. 4.

3.6. Inference network

A critical component of constructing mineral potential maps concerns the design of an appropriate inference network that combines possible conditionally-dependent maps, using operators like the fuzzy AND or the fuzzy OR. The choice of the fuzzy AND operator or the fuzzy OR operator depends upon whether the presence of only one of the two fuzzy predictor maps to be combined is sufficient or whether the presence of both fuzzy predictor maps is considered mandatory for the recognition of areas with elevated uranium potential. In the second-stage and subsequent steps intermediate predictor maps are combined to produce separate favorability maps for 'Source', 'Transport' and 'Trap'. The final stage is to combine these three critical components to create a synthesized favorability map.

Conditional dependence exists amongst maps due to one of the following two reasons: (1) the maps represent the same recognition criterion (e.g., drainage pathways are represented by the re-processed 'WASANT', 'Local Lows' and 'HydroSHEDS' input layers); or (2) there is possibly a genetic link between the recognition criteria represented by them (e.g., permeability and drainage pathways). Conditional dependence can create problems in complex fuzzy operations, such as combining maps using fuzzy algebraic product or fuzzy algebraic sum, where the additive effect of conditionally-dependent maps may result in erroneous values, either over- or under-emphasizing the relative importance of one or more predictor maps. For this reason, it is essential that the design of the inference network adheres to a geologically meaningful context and an appropriate targeting model. Several of the individually rasterized but related maps (e.g., sedimentary basins of different age groups; drainage pathways of different kinds; igneous sources & sedimentary sources) were combined via an intermediate step before generating rasterized fuzzy maps representing each of the three basic minerals system components (i.e., 'Source', 'Transport', 'Trap').

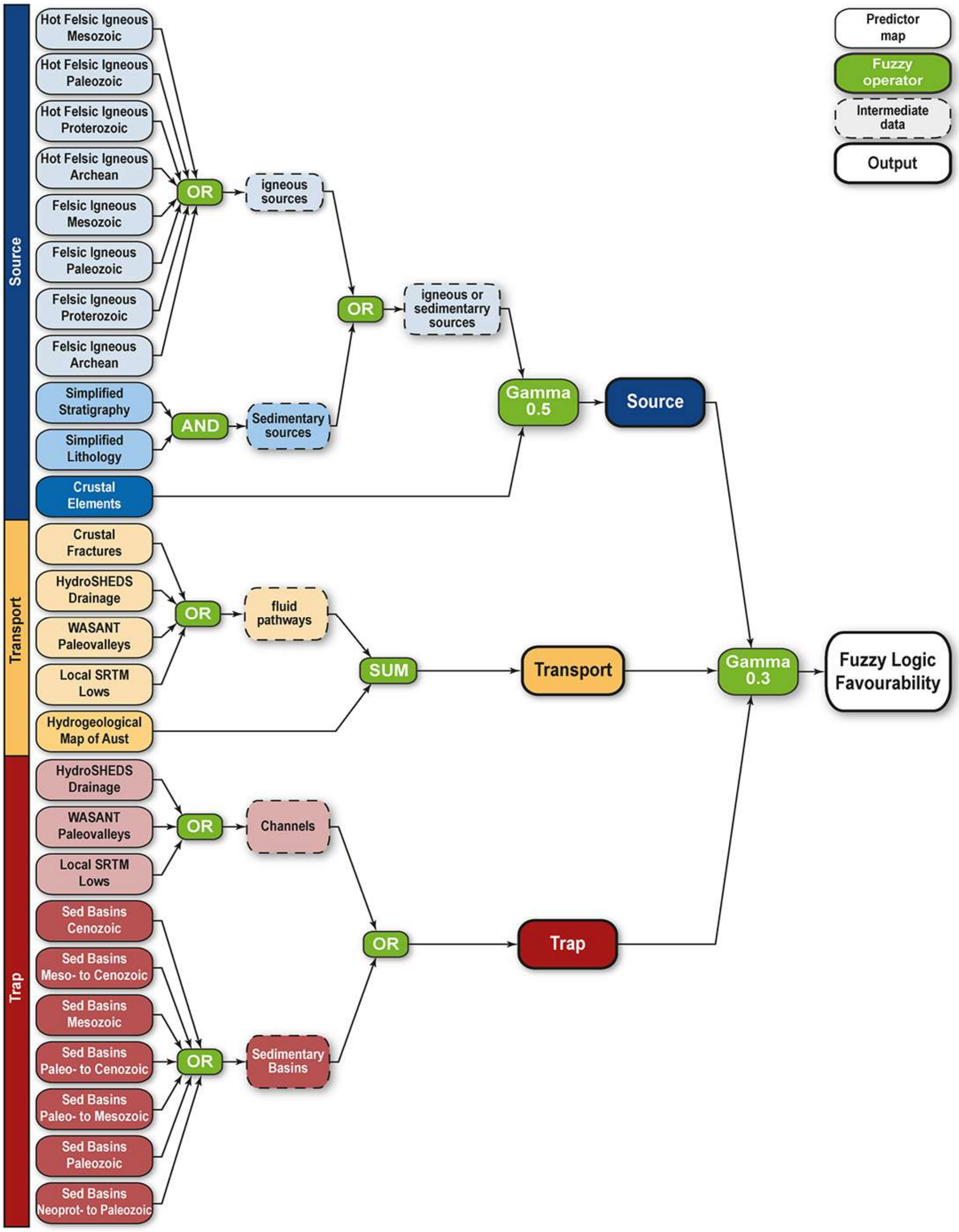

FIG. 5. Inference network for the continental-scale Fuzzy Logic mineral prospectivity analysis of sandstone-hosted uranium deposits in Australia constructed herein.

The work flow diagram for the fuzzy logic inference network is shown in Fig. 5, with the resulting favorability maps for the prospectivity model constructed in the current study presented in the following Section and in Figs 6a-c and7.

In terms of ‘source’, an area is considered prospective if it is near to one of the potential felsic igneous sources defined by the genetic model. As discussed above, the buffers and weights applied to each model component quantify the requirement to be near a source, while the ‘OR’ operator that links them together in the inference network specifies that any one of those sources is acceptable. Proximity to two or more effective sources does not further increase the prospectivity in this model; the ‘OR’ operator applies the highest value of the predictor maps to the cell under consideration. The combination of the ‘Simplified Stratigraphy’ and ‘Simplified Lithology’ predictor maps with an ‘AND’ operator accounts for the case where sedimentary units can potentially act as their own source of uranium if sedimentary rocks of the right age and type are present. The relatively low favorability attributed to these individual predictor maps (map weight = ‘5’ in both cases) and the use of the ‘AND’ operator result in the intermediate step ‘Sedimentary sources’ also having a relatively low overall favorability. An ‘OR’ operator is used to combine the ‘Igneous sources’ and ‘Sedimentary sources’ intermediates since the presence of either source type enhances prospectivity. However, the generally higher weights of the felsic igneous sources mean that these dominate over sedimentary sources.

The final stage is to incorporate the ‘Crustal Elements’ predictor map into the source component of the overall model via the use of the fuzzy gamma (FG) operator. This operator is a mix between the fuzzy algebraic sum (FAS) and the fuzzy algebraic product (FAP) operators. In contrast to using ‘OR’ or ‘AND’, when the FAS, FAP or FG operator is used, every output raster cell is influenced by all inputs. The use of the FG operator late in the inference network effectively turns the ‘Crustal Elements’ predictor map into a weighting factor, enhancing the favorability in areas where the crust is known to be more fertile in uranium (i.e., West, North and South Australian cratons) and reducing favorability elsewhere. The output from the Source section is shown in Fig. 6a.

The ‘Transport’ component of the inference network first combines all potential fluid pathway and conduits with an ‘OR’ operator. These are then combined with the Hydrogeological Map of Australia using the FAS operator. The result is shown in Fig. 6b.

The ‘Trap’ component simply states that an area will be considered prospective if it is proximal to the edge of a sedimentary basin (with the relative importance of the basins and buffered margins defined by the map weights applied earlier) ‘OR’ in a channel defined by the ‘HydroSHEDS’, ‘WASANT Paleo-valleys’ or ‘Local SRTM Lows’ predictor maps. The resultant Trap model is shown in Fig. 6c.

The final stage combines the ‘Source’, ‘Transport’ and ‘Trap’ components with the FG operator, using a low (gamma = ‘0.3’) value. The low gamma value means that this acts more like the FAP than the FAS and has a generally decreasive effect (since we are effectively multiplying numbers smaller than one). Consequently, areas where all three components of the model (Source, Transport and Trap) are high show up as favorable in the final result, whereas areas where one or more components are relatively low show up as generally unfavorable (Fig. 7).

4. RESULTS

Figs 6 and 7 show the output generated from the combination of all processed input layers and as defined by the inference network discussed in the previous section. For illustrative purposes, the intermediate output for each of the three basic mineral systems categories (i.e., ‘Source’, ‘Transport’ and ‘Trap’) are shown in Fig.s 6a, 6b and 6c, respectively.

From this, it becomes apparent that the general lack of more suitable (i.e., highly uranium-enriched, radiogenic) sources in the Phanerozoic of the Australian continent is largely responsible for the virtual absence of target regions considered favorable for sandstone-hosted uranium deposits in eastern Australia. Notable exceptions are the Carpentaria Basin in Far North Queensland and the margins of the Eromanga Basin, due to their proximity to radiogenic basement exposures in the Mt Isa and Georgetown inliers. By contrast, well-known exposures of Proterozoic (and to a lesser extent, Archaean) basement are portrayed strongly in the 'Source' map (Fig 6a). Conversely, metamorphosed basement is generally characterized by low to very low porosity and permeability, resulting in these areas representing least-favorable areas as far as the 'Transport' map (Fig. 6b); highly favorable regions are centered on young (i.e., Phanerozoic) sedimentary basins and Tertiary – Cenozoic drainage pathways. The latter also represent highly favorable 'Trap' regions (Fig. 6c), with the margins of all sedimentary basins also signifying ideal trap environments.

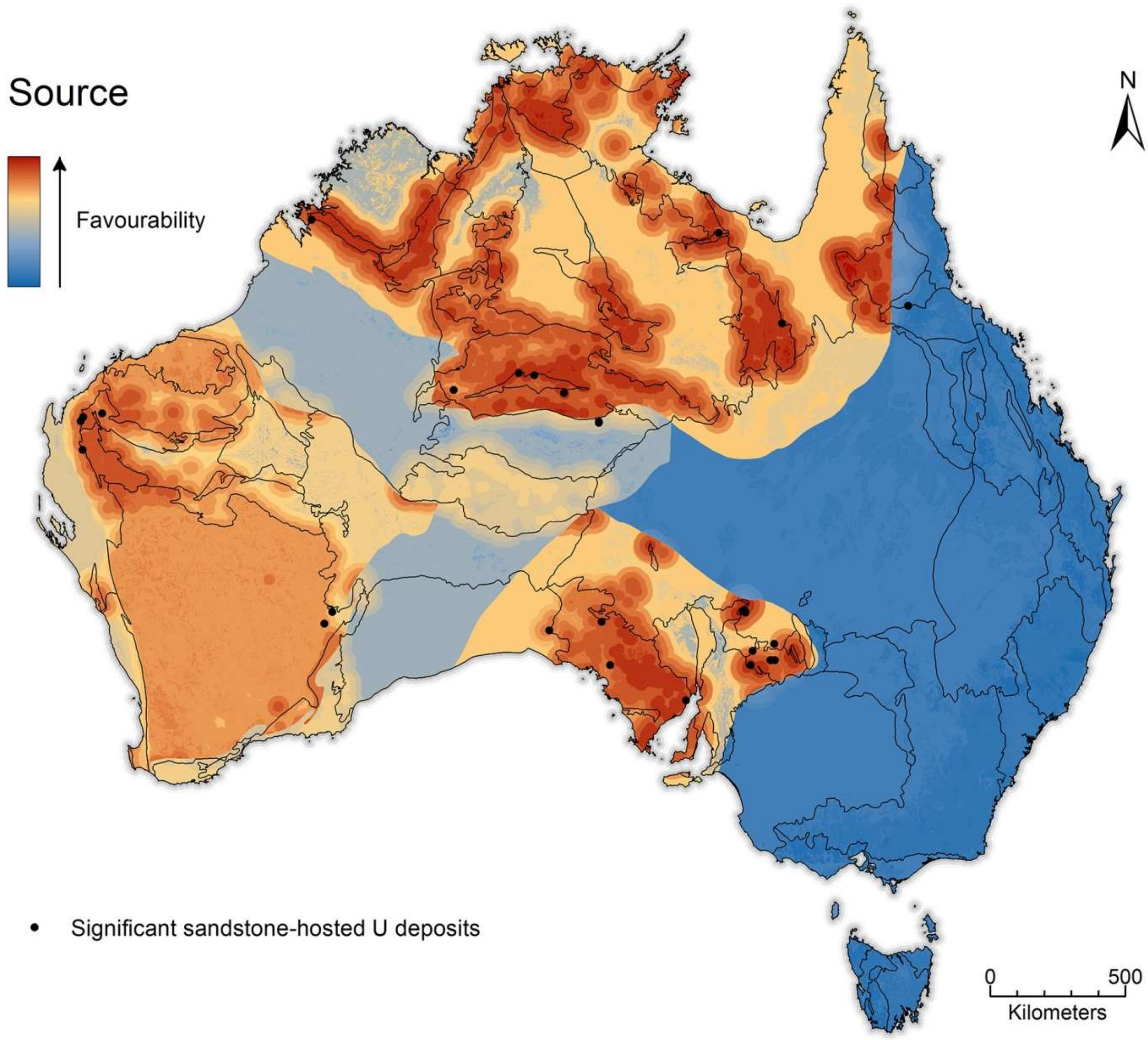

FIG. 6a. Rasterized fuzzy predictor map for favorable source rock regions (combining igneous and sedimentary sources, lithology, stratigraphy and crustal elements) superimposed on the outlines of principal geological regions on the Australian continent.

Fig. 7 illustrates the result of combining the three fuzzy predictor maps shown in Figs 6a - c, to produce the final output from a continent-scale fuzzy logic mineral prospectivity model for sandstone-hosted uranium occurrences in Australia. In this model, the majority of known sandstone-hosted uranium deposits that contain significant resources occur within areas of elevated to high favorability. Using these deposits as a 'control population', the close spatial correlation demonstrates that the output generated from the model constructed herein can be considered geologically meaningful. As such, the results of the fuzzy logic MPA for sandstone-hosted uranium occurrences on the Australian continent demonstrates the capability of a GIS-based targeting concept to objectively delineate and visualize zones of elevated uranium potential, reduce the search space, and assist in the area selection and decision-making process. Importantly, this example demonstrates the ability of a fuzzy logic MPA to combine multiple input layers via a carefully constructed inference network, thus enabling the efficient visualization of relative favorability for a specific mineral deposit type at the continent scale.

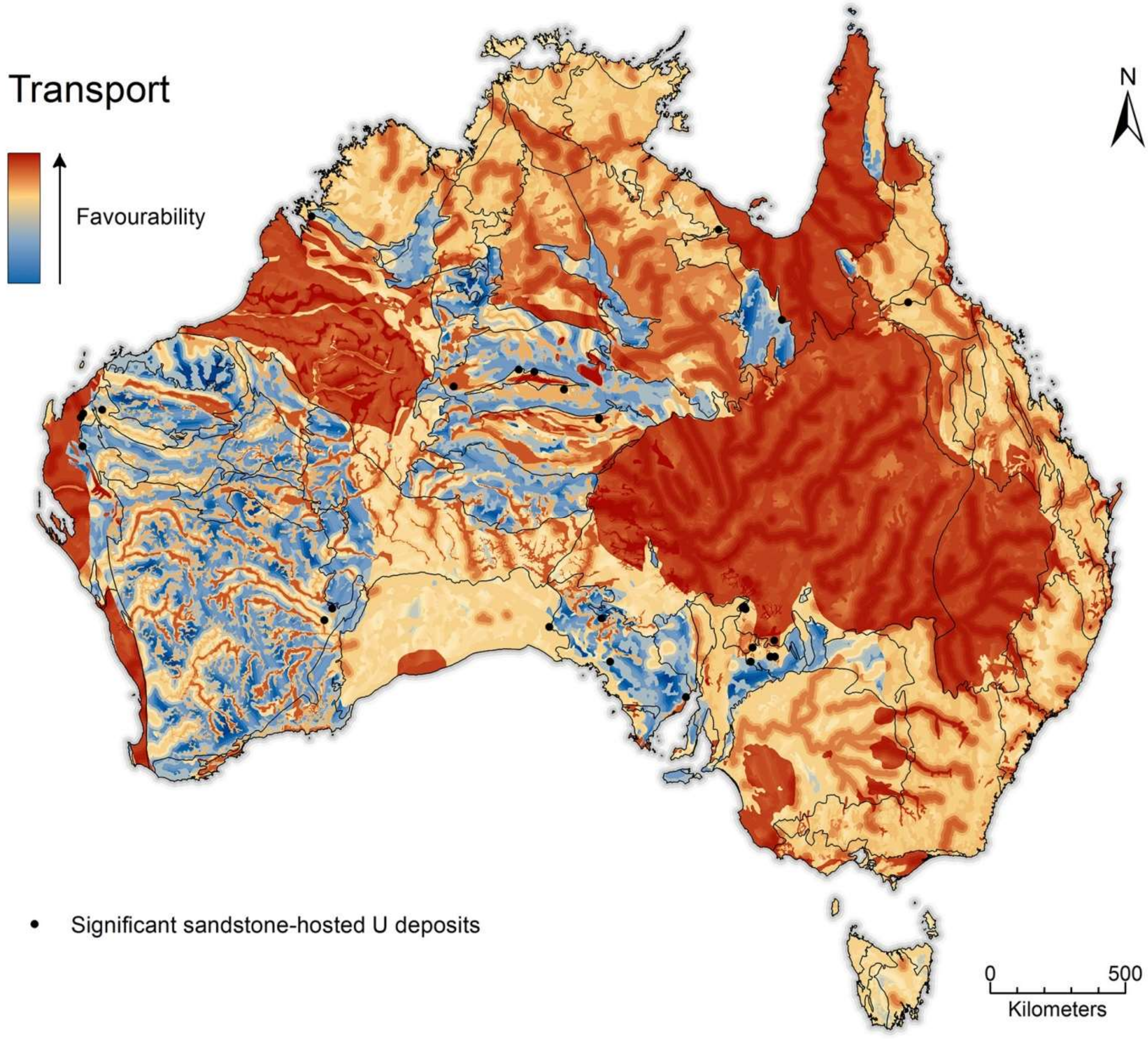

FIG. 6b. Rasterized fuzzy predictor map for favorable transport regions (combining crustral fractures, drainage pathways, and hydrogeology) superimposed on the outlines of principal geological regions on the Australian continent.

5. DISCUSSION

Given the relatively small size of the deposits targeted versus the continent-scale approach employed in the current study, it quickly becomes apparent that the methodology's strength lies in its ability to highlight specific zones of perceived mineral potential, and for the exploration geologist to prioritize and rank the targets generated by the MPA. At a continental scale, these target zones ideally correlate with, generally fall within, and delineate so-called 'geologically-permissive tracts' [35]. These tracts represent regions that are geologically-permissive for the occurrence of undiscovered mineral deposits, and which can be utilized in quantitative mineral resource assessments for the purpose of estimating numbers of undiscovered deposits in ways that allow these estimates to be used for a variety of applications in land, resource, economic, and environmental planning and decision-making [36, 37]. From Fig. 7, it is obvious that the output generated from our continental scale fuzzy logic model elucidates and successfully 're-discovers' a number of tracts on the Australian continent that are known to be geologically-permissive for sandstone-hosted uranium deposits. In addition, the output highlights several regions which should be geologically-permissive but may as yet have not been adequately considered, let alone explored for this type of uranium deposit (e.g., Ord and Murray basins).

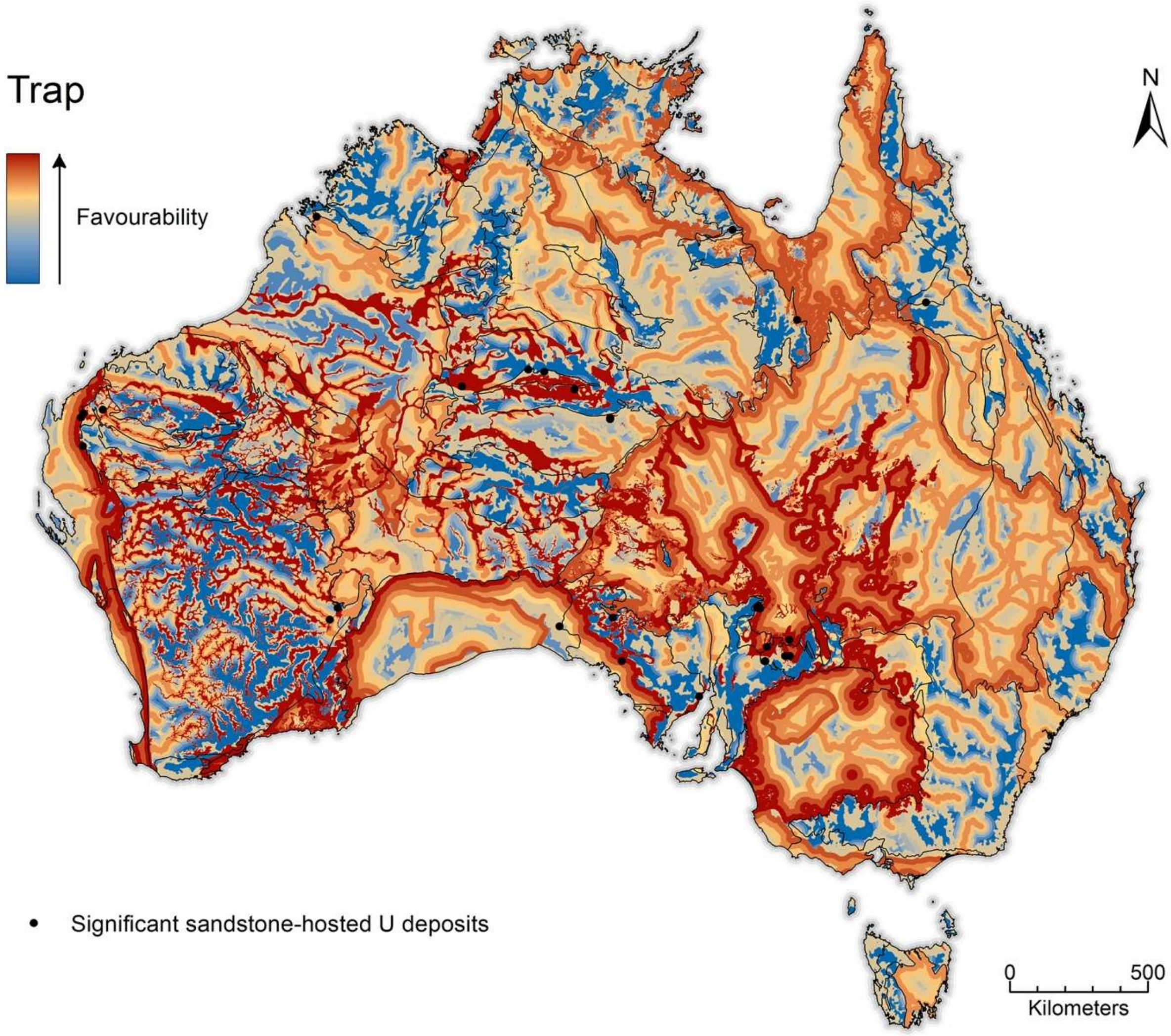

FIG. 6c. Rasterized fuzzy predictor map for favorable trap regions (combining basins of all age groupings and drainage pathways) superimposed on the outlines of principal geological regions on the Australian continent.

As has been stated earlier in this chapter, the most significant benefit of applying ArcGIS-based fuzzy logic approach to mineral prospectivity modeling lies in the technique's ability to assign varying degrees of importance to chosen input parameters and combine all predictor maps in a logical, as well as a visually concise and comprehensible manner. As such, the design of the deposit-type specific model constructed in this study 'honors' the parameters listed in Table 1, such as the importance of a highly uranium-enriched, exposed source within close proximity of a permeable and porous trap medium, and which are linked by a suitable transport mechanism such as a surface drainage system, structural conduit, and/or a permeable sedimentary unit. For this reason, the output from our model inherently favors the (buffered) margins of several sedimentary basins, rather than these basins in their entirety.

Empirically, the location of significant deposits such as Manyingee close to the eastern margin of the (fault-bounded) Carnarvon Basin and where the Ashburton River paleo-channel exits the uranium-enriched source region of the Pilbara Craton, justifies this approach. Similarly, the model emphasizes paleo-channel drainage systems and drainage systems as being highly favorable, which reflects the empirical observation that several of these host significant sandstone-hosted uranium deposits in South Australia (e.g., Four Mile, Beverley, Warrior), Western Australia (e.g., Mulga Rock, Bennett Well) and the Northern Territory (e.g., Lake Mackay, Bigrlyi; cf. Fig 1b; Fig. 7).

In the assignment of class scores to the input data, the ages of both the source and the trap were also considered highly important, with Proterozoic (radiogenic) igneous rocks regarded as the most favorable for the generation of dissolvable uranium. By contrast, Mesozoic to Cenozoic sedimentary successions and drainage pathways were deemed more favorable than their more ancient analogues, as the former were considered more likely to have retained their porosity/permeability. However, and as mentioned above, in the absence of a suitable source at the lithospheric scale, almost the entire Phanerozoic Tasman Fold Belt of eastern Australia was considered unfavorable for sandstone-hosted uranium deposit formation – and this notion is clearly reflected in the output from our model.

There are several cases on the Australian continent where fertile detritus from suitable source rocks situated along the edges of the Precambrian cratons unquestionably sheds into drainage systems that are underlain by Phanerozoic crust. Yet, the favorability of these potentially prospective fluid pathways is suppressed in the current model. To overcome this shortcoming, the 'Crustal element' input layer (comprising six classes) would have to be taken into consideration at the initial step in the 'Source' component of the inference diagram and in conjunction with each of the eight rock type input layers (cf. Fig. 3) – but doing so would result in 48 individual input layers for this aspect of the model alone! At the continental scale, we believe such a convoluted model framework to be of little use. We acknowledge that this view might be in some ways an over-simplification and potentially does injustice to regions such as the Mesozoic Sydney Basin (Fig. 1b), which is known to host thick units of permeable, in part conglomeratic sandstone that are inter-layered with coal seams and carbonaceous horizons. However, while both transport and trap criteria are fulfilled, at least in the case of the Sydney Basin, there is a noticeable dearth of suitable source rocks in the exposed basement on either side of the epi-cratonic rift basin.

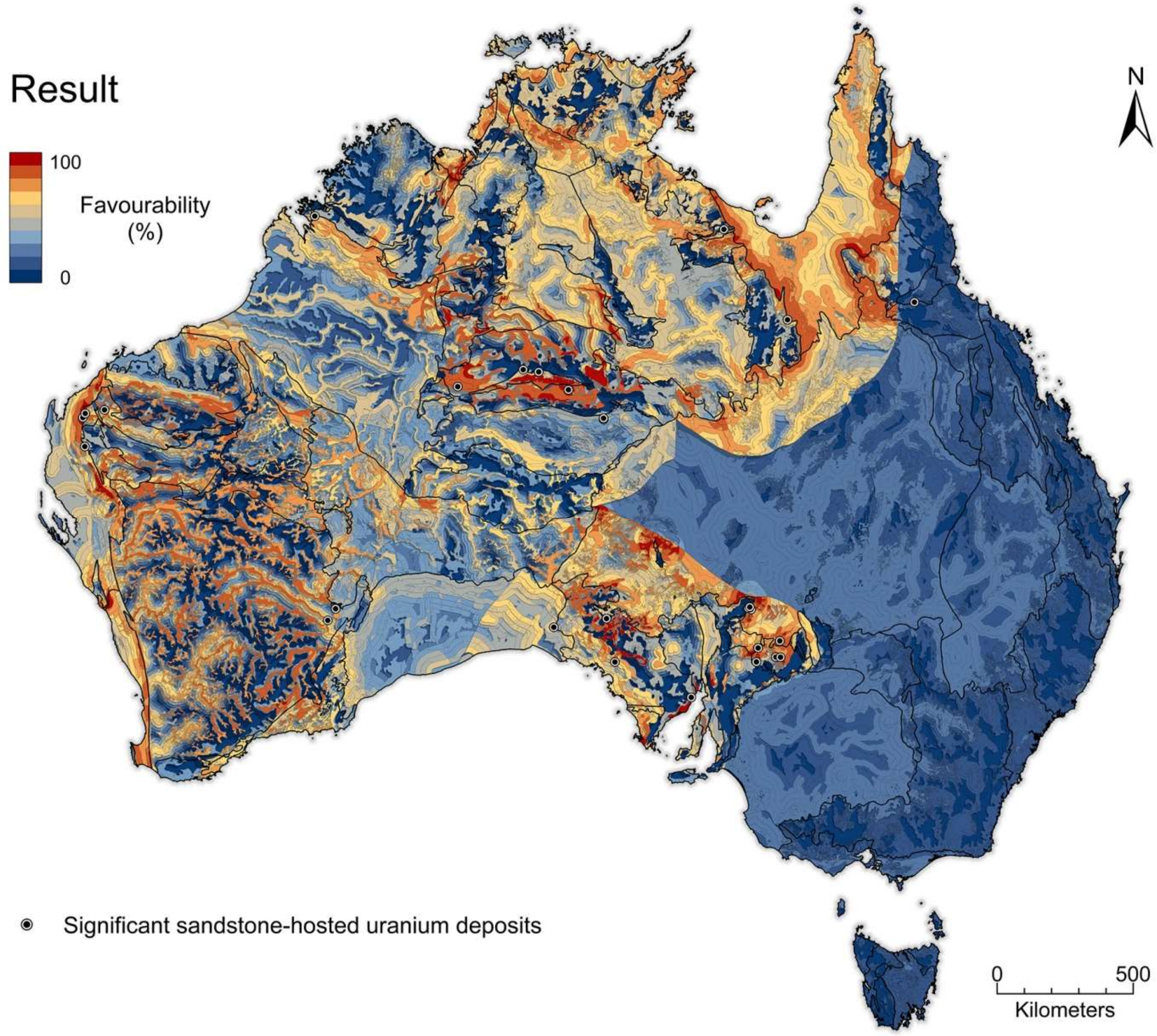

FIG. 7. Final output from the continental-scale fuzzy logic mineral prospectivity analysis for sandstone-hosted uranium on the Australian continent developed in this chapter. Also shown are the locations of significant sandstone-hosted uranium deposits and the outlines of principal geological regions.

On the other hand, the output from the model developed herein in particular highlights several broad regions within portions of Australia that are underlain by Precambrian basement, as well as the (typically fault-bounded) margins of undeformed sedimentary basins situated adjacent to uraniferous basement sources, such as the epi-cratonic Paleozoic – Mesozoic Perth, Carnarvon, Murray River, Carpentaria and Canning basins, and the intra-cratonic Ngalia and Frome basins (cf. Fig. 1b). Additionally, drainage pathways with uranium-enriched sources in their upstream regions are highlighted by the output from the mineral prospectivity model.

A key aspect of both the model's design and the interpretation of output from it alike concerns scale-dependence, resolution and choice of relevant and meaningful input data. For example, faults are undoubtedly important in controlling the location of sandstone-hosted uranium deposits via their influence on landscape development (i.e., neo-tectonics, juxtaposition of permeable units with reduced and/or impermeable rock units, etc.) and the evolution of ancient and present-day drainage pathways. However, and as was pointed out in Section 3, these controls tend to operate at the camp to regional, rather than the continental scale considered here. Moreover, the type of (first-order) structures represented in the crustal fractures input layer may act as an enhanced fluid conduit but globally is not known to provide an efficient trap site (with the possible exception of the tectonic-lithologic sub-type of sediment-hosted uranium deposits [13]). Consequently, the presence and orientation of major structures bears no apparent influence on the output from the mineral prospectivity model. Higher-order faults, where considered relevant, and in particular specific fault-bounding structures such as, for example, the Darling Fault which forms the eastern margin of the Perth and Carnarvon basins, are virtually impossible to 'filter out' for the purpose of the assessment undertaken in this Chapter. Similarly, felsic intrusions with highly anomalous concentrations of dissolvable uranium occur extensively throughout the Proterozoic basement of Australia. In many regions, however, their surface footprint may only reflect a very small portion of the overall extent of the intrusion. Using radiometric data and lithological information to identify each exposure, and generating a buffered input data layer from these has the undesired effect of potentially creating large false 'Source' positives.

Assigning distinct Fuzzy Membership values to specific sedimentary basins requires prior knowledge of the geological make-up of these basins, including information on, for example, the extent and thickness of first-cycle siliciclastic rock units and the presence and abundance of reducing agents (i.e., coal seams, hydrocarbons). At the continental scale, this sub-surface information is particularly relevant as more detailed consideration of lithologically discriminating criteria, and incorporating these in the construction of a fuzzy logic mineral prospectivity model is rendered virtually impossible. In the case of the Australian continent, the relatively high density of relevant pre-competitive data enables such distinction at the whole-of-basin scale. Where this information is lacking (e.g., in parts of Africa), meaningful output is nevertheless possible but the user may be required to adhere to a more simplistic approach and model design.

Incomplete coverage of data sets also exists in the case of Australia, as exemplified by the 'WASANT paleo-valleys' input layer utilized in this study. For this reason, we chose to include several conditionally co-dependent layers in our model, as these can provide at least some coverage for News South Wales, Tasmania and Queensland (which are not covered by the WASANT paleo-valley data). From the output shown in Fig. 7 it is quite apparent, however, that a significant gradient in the fidelity and density of the data exists when comparing drainage pathways in, for example, Far North Queensland with their counterparts in Western Australia.

At the opposite end of the spectrum, the unprocessed 1:1M surface geology of Australia input layer contains a large number of lithological sub-classes that had to be re-classified, as discussed in Section 3. This necessity has naturally resulted in some over-simplification, which, in turn, is likely to have fed into the final output from the model. Considering the scale of the analysis, however, we stand by the chosen approach and stress that any more detailed, regional-scale sub-model will require a reassessment of relevant and appropriate input data. As a matter of principle, the collation of suitable input layers for an area or region under consideration should also include a "gap analysis" of any desirable but unavailable data sets.

We note that the output generated from our model and discussed herein represents just one of several possible scenarios. A significant advantage of the computer-based methodology over traditional targeting approaches lies in the fact that it allows for iterative testing and time-effective adjustment of fuzzy membership values to suit a specific targeting concept or taking into account a set of parameters that may be considered of particular relevance in a specific region under investigation. Similarly, exploration paradigms constantly evolve as new knowledge becomes available, with fuzzy logic models capable of being adjusted accordingly by incorporating fresh expert input.

Finally, we cannot over-emphasize the importance of recognizing, and guarding against the limitations of an entirely heuristic approach, even if based on factual geological data and empirical knowledge. An equally important aspect is the ground-truthing of output generated from any GIS-based, computer-generated mineral prospectivity model. Doing so provides the ultimate test of these models and also represents the only means of truly validating what, to our minds, constitutes an extremely powerful decision-making tool in exploration.

6. CONCLUSIONS

The fuzzy logic mineral prospectivity model presented in this chapter exemplifies a successful illustration of a first-pass GIS-based analysis for sandstone-hosted uranium deposits on the Australian continent. The output generated from this model has positively identified proven uranium provinces, thus confirming the geological validity of both the current empirical exploration targeting model and the design of our computer-generated model. In addition, the output has identified several regions on the Australian continent that should be prospective for as yet unidentified sandstone-hosted uranium occurrences.

Due to its scale and the input data sets utilized, the computer-generated analysis cannot provide a realistic means to delineate actual drill targets. Rather, the modeled output is particularly effective for the purpose of identifying geologically-permissive tracts, as well as regions of elevated favorability within these tracts. As such, the methodology provides a powerful visualization and decision-making tool, though the value and geological meaningfulness of output from this, or any other GIS-based computer-generated prospectivity analysis for that matter, will heavily depend on the quality and availability of suitable input datasets.

Application of the approach discussed herein is transferrable to other regions, countries and continents, provided scale-dependence and the selection of relevant input data form an integral part of the fuzzy logic model's design.

ACKNOWLEDGEMENTS

We thank the International Atomic Energy Agency for financial support. The work documented herein was proposed and instigated by M. Fairclough.

Appendix

MAP AND CLASS WEIGHTS, AND FUZZY MEMBERSHIP VALUES FOR PREDICTOR MAPS USED IN THE CONSTRUCTION OF A CONTINENT-SCALE FUZZY LOGIC MINERAL PROSPECTIVITY MODEL FOR SANDSTONE-HOSTED URANIUM DEPOSITS

Predictor map	Criterion class	Class score	Map weight	Class weight	Fuzzy membership value
SOURCE					
Hot felsic igneous Mesozoic_Source	0.001 km	10	2	20	0.20
(Radiometric Map of Australia 2015 and	20 km	9	2	18	0.18
1M Surface Geology 2012)	40 km	8	2	16	0.16
	60 km	7	2	14	0.14
	80 km	5	2	10	0.10
	100 km	3	2	6	0.06
	100 km+	0	2	0	0.001
Hot felsic igneous Paleozoic_Source	0.001 km	10	3	30	0.30
(Radiometric Map of Australia 2015 and	20 km	9	3	27	0.27
1M Surface Geology 2012)	40 km	8	3	24	0.24
	60 km	7	3	21	0.21
	80 km	5	3	15	0.15
	100 km	3	3	9	0.09
	100 km+	0	3	0	0.001
Hot felsic igneous Proterozoic_Source	0.001 km	10	9	90	0.90
(Radiometric Map of Australia 2015 and	20 km	9	9	81	0.81
1M Surface Geology 2012)	40 km	8	9	72	0.72
	60 km	7	9	63	0.63
	80 km	5	9	45	0.45
	100 km	3	9	27	0.27
	100 km+	0	9	0	0.001
Hot felsic igneous Archean_Source	0.001 km	10	6	60	0.60
(Radiometric Map of Australia 2015 and	20 km	9	6	54	0.54
1M Surface Geology 2012)	40 km	8	6	48	0.48
	60 km	7	6	42	0.42
	80 km	5	6	30	0.30
	100 km	3	6	18	0.18
	100 km+	0	6	0	0.001
Felsic igneous Mesozoic_Source	0.001 km	10	1	10	0.10
(1M Surface Geology 2012)	20 km	9	1	9	0.09
	40 km	8	1	8	0.08
	60 km	7	1	7	0.07
	80 km	5	1	5	0.05
	100 km	3	1	3	0.03

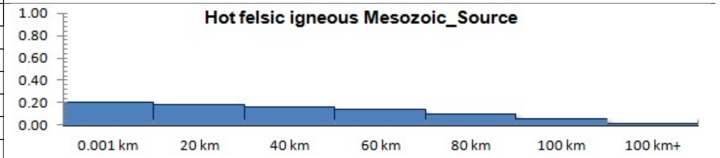

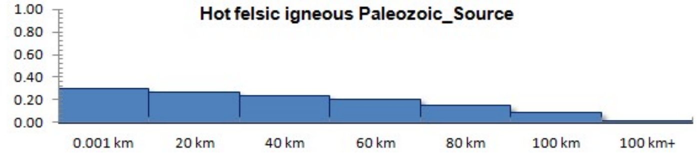

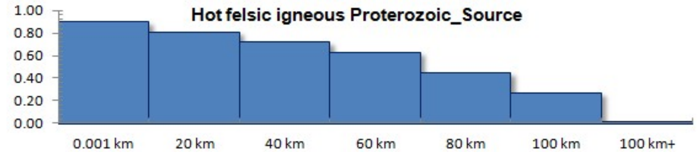

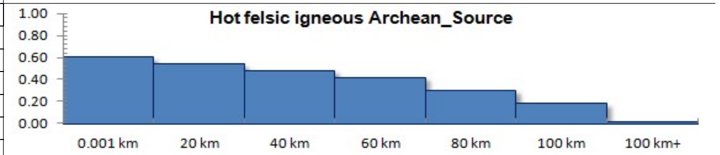

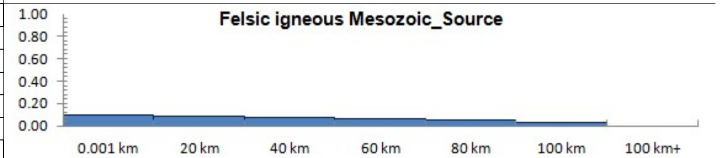

Predictor map	Criterion class	Class score	Map weight	Class weight	Fuzzy membership value
SOURCE					
Hot felsic igneous Mesozoic_Source	0.001 km	10	2	20	0.20
(Radiometric Map of Australia 2015 and	20 km	9	2	18	0.18
1M Surface Geology 2012)	40 km	8	2	16	0.16
	60 km	7	2	14	0.14
	80 km	5	2	10	0.10
	100 km	3	2	6	0.06
	100 km+	0	2	0	0.001
Hot felsic igneous Paleozoic_Source	0.001 km	10	3	30	0.30
(Radiometric Map of Australia 2015 and	20 km	9	3	27	0.27
1M Surface Geology 2012)	40 km	8	3	24	0.24
	60 km	7	3	21	0.21
	80 km	5	3	15	0.15
	100 km	3	3	9	0.09
	100 km+	0	3	0	0.001
Hot felsic igneous Proterozoic_Source	0.001 km	10	9	90	0.90
(Radiometric Map of Australia 2015 and	20 km	9	9	81	0.81
1M Surface Geology 2012)	40 km	8	9	72	0.72
	60 km	7	9	63	0.63
	80 km	5	9	45	0.45
	100 km	3	9	27	0.27
	100 km+	0	9	0	0.001
Hot felsic igneous Archean_Source	0.001 km	10	6	60	0.60
(Radiometric Map of Australia 2015 and	20 km	9	6	54	0.54
1M Surface Geology 2012)	40 km	8	6	48	0.48
	60 km	7	6	42	0.42
	80 km	5	6	30	0.30
	100 km	3	6	18	0.18
	100 km+	0	6	0	0.001
Felsic igneous Mesozoic_Source	0.001 km	10	1	10	0.10
(1M Surface Geology 2012)	20 km	9	1	9	0.09
	40 km	8	1	8	0.08
	60 km	7	1	7	0.07
	80 km	5	1	5	0.05
	100 km	3	1	3	0.03

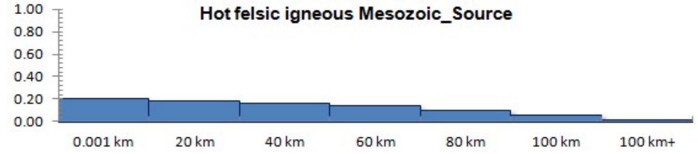

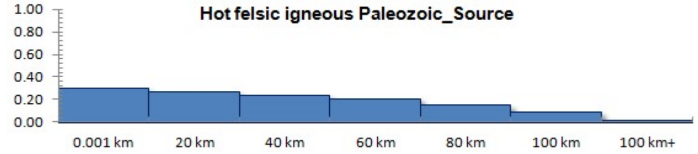

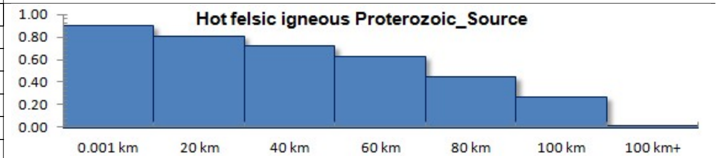

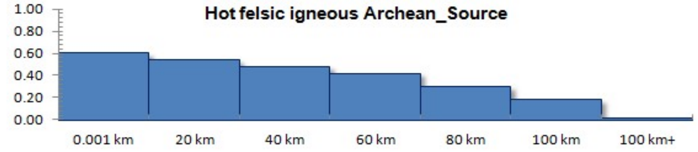

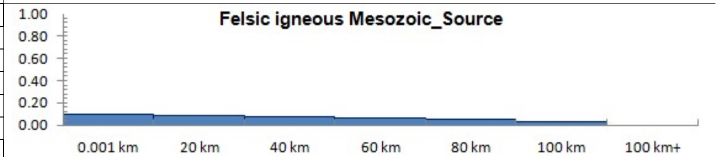

Predictor map	Criterion class	Class score	Map weight	Class weight	Fuzzy membership value
Felsic igneous Paleozoic Source	0.001 km	10	2	20	0.20
(1M Surface Geology 2012)	20 km	9	2	18	0.18
	40 km	8	2	16	0.16
	60 km	7	2	14	0.14
	80 km	5	2	10	0.10
	100 km	3	2	6	0.06
	100 km+	0	2	0	0.001
Felsic igneous Proterozoic Source	0.001 km	10	8	80	0.80
(1M Surface Geology 2012)	20 km	9	8	72	0.72
	40 km	8	8	64	0.64
	60 km	7	8	56	0.56
	80 km	5	8	40	0.40
	100 km	3	8	24	0.24
	100 km+	0	8	0	0.001
Felsic igneous Archean Source	0.001 km	10	7	70	0.70
(1M Surface Geology 2012)	20 km	9	7	63	0.63
	40 km	8	7	56	0.56
	60 km	7	7	49	0.49
	80 km	5	7	35	0.35
	100 km	3	7	21	0.21
	100 km+	0	7	0	0.001
Simplified stratigraphy Source	Cenozoic	9	5	45	0.45
(1M Surface Geology 2012)	Mesozoic	7	5	35	0.35
	Paleozoic	6	5	30	0.30
	Proterozoic	4	5	20	0.20
	Archean	1	5	5	0.05
Simplified lithology Source	Sedimentary	9	5	45	0.45
(1M Surface Geology 2012)	Volcanics	4	5	20	0.20
	Metamorphic	1	5	5	0.05
	Intrusive	6	5	30	0.30
Crustal elements Source	Central	5	9	45	0.45
(Australian Crustal Elements 1996 -	North	10	9	90	0.90
re-issued in 2011)	Pinjarra	8	9	72	0.72
	South	10	9	90	0.90
	Tasman	1	9	9	0.09
	West	9	9	81	0.81

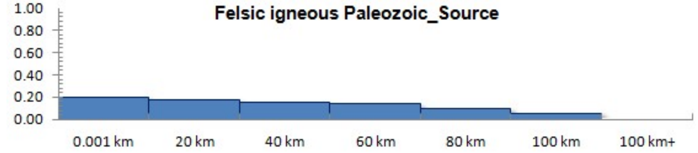

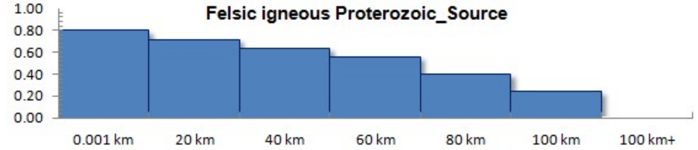

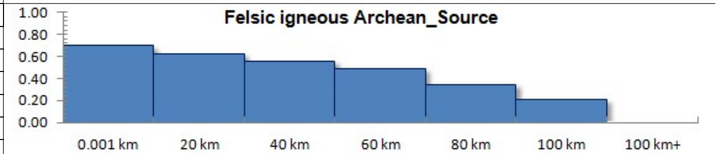

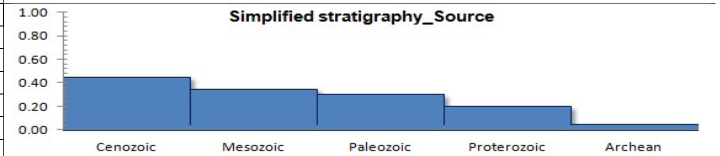

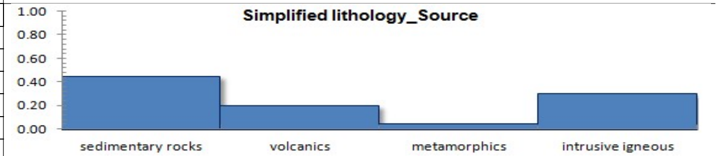

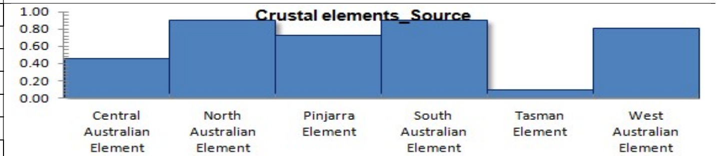

Predictor map	Criterion class	Class score	Map weight	Class weight	Fuzzy membership value
TRANSPORT					
SEEBASE crustal fractures_Trans	0-10 km	9	4	36	0.36
(OZSEEBASE Proterozoic)	10-20 km	8	4	32	0.32
	20-30 km	6	4	24	0.24
	30-40 km	4	4	16	0.16
	40-50 km	2	4	8	0.08
	50 km+	0	4	0	0.001
HydroSHEDS_Trans	0-10 km	9	8	72	0.72
Proximity to current major drainage channels	10-20 km	8	8	64	0.64
(HydroSHEDS 2006)	20-30 km	6	8	48	0.48
	30-40 km	4	8	32	0.32
	40-50 km	2	8	16	0.16
	50 km+	0	8	0	0.001
WASANT_Paleovalleys_Trans	No	0	9	0	0.001
(WASANT Paleovalley Map 2012)	Yes	9	9	81	0.81
Hydrogeology Map of Aust_Trans	Very high	9	9	81	0.81
(Hydrogeology Map of Australia 1987)	High	8	9	72	0.72
	Medium	7	9	63	0.63
	Low	6	9	54	0.54
	Very low	3	9	27	0.27
Local SRTM lows_Trans	No	0	5	0	0.001
(Derived from 90m Hole-filled SRTM 2008)	Yes	9	5	45	0.45
TRAP					
HydroSHEDS_Trap	0-10 km	9	7	63	0.63
Proximity to current major drainage channels	10-20 km	8	7	56	0.56
(HydroSHEDS 2006)	20-30 km	6	7	42	0.42
	30-40 km	4	7	28	0.28
	40-50 km	2	7	14	0.14
	50 km+	0	7	0	0.001

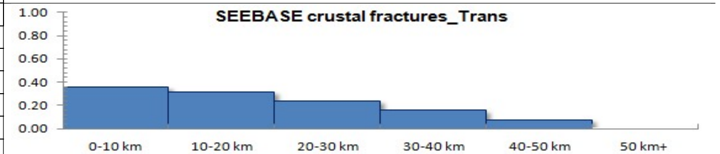

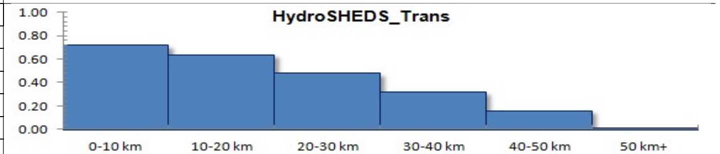

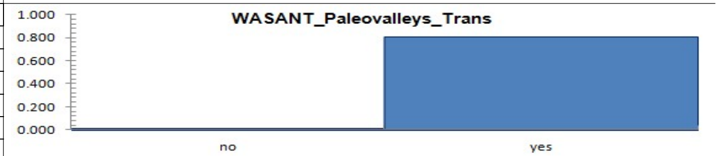

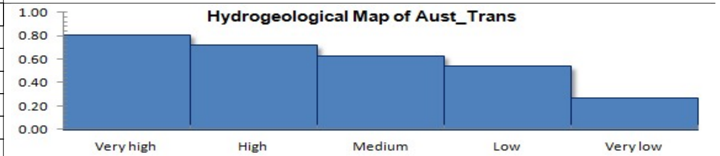

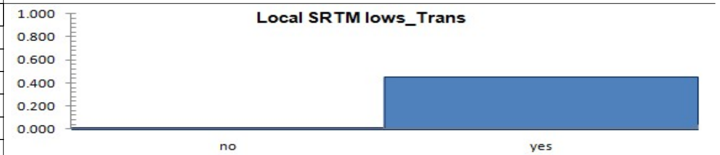

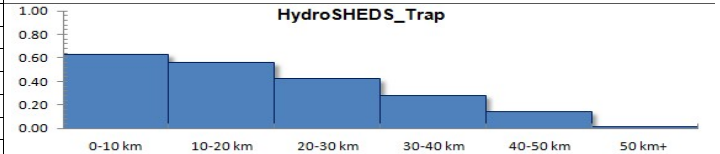

Predictor map	Criterion class	Class score	Map weight	Class weight	Fuzzy membership value
WASANT Paleovalleys Trap	No	0	9	0	0.001
(WASANT Paleovalley Map 2012)	Yes	9	9	81	0.81
Local SRTM lows Trap	No	0	5	0	0.001
(Derived from 90m Hole-filled SRTM 2008)	Yes	9	5	45	0.45
SedBasins Cenozoic Trap	non basin	0	9	0	0.001
Distance from basin margin	0 - 20 km	9	9	81	0.81
(Australian Geological Provinces 2013)	20 - 40 km	8	9	72	0.72
	40 - 60 km	7	9	63	0.63
	60 - 80 km	6	9	54	0.54
	80 -100 km	4	9	36	0.36
	100 km+	2	9	18	0.18
SedBasins Mesozoic to Cenozoic Trap	non basin	0	8	0	0.001
Distance from basin margin	0 - 20 km	9	8	72	0.72
(Australian Geological Provinces 2013)	20 - 40 km	8	8	64	0.64
	40 - 60 km	7	8	56	0.56
	60 - 80 km	6	8	48	0.48
	80 -100 km	4	8	32	0.32
	100 km+	2	8	16	0.16
SedBasins Mesozoic Trap	non basin	0	8	0	0.001
Distance from basin margin	0 - 20 km	9	8	72	0.72
(Australian Geological Provinces 2013)	20 - 40 km	8	8	64	0.64
	40 - 60 km	7	8	56	0.56
	60 - 80 km	6	8	48	0.48
	80 -100 km	4	8	32	0.32
	100 km+	2	8	16	0.16
SedBasins Paleozoic to Cenozoic Trap	non basin	0	9	0	0.001
Distance from basin margin	0 - 20 km	9	9	81	0.81
(Australian Geological Provinces 2013)	20 - 40 km	8	9	72	0.72
	40 - 60 km	7	9	63	0.63
	60 - 80 km	6	9	54	0.54
	80 -100 km	4	9	36	0.36
	100 km+	2	9	18	0.18

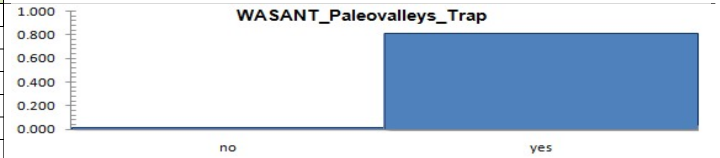

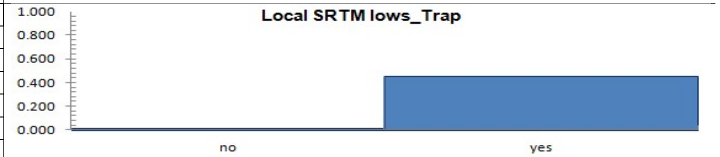

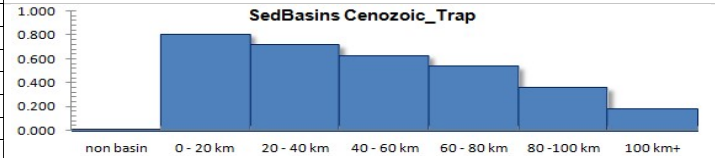

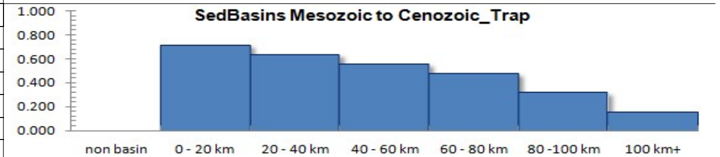

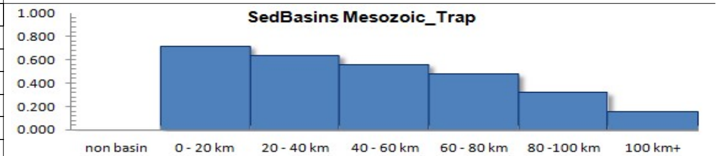

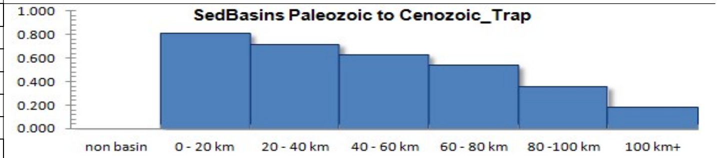

Predictor map	Criterion class	Class score	Map weight	Class weight	Fuzzy membership value
SedBasins Paleozoic to Mezozoic Trap	non basin	0	7	0	0.001
Distance from basin margin	0 - 20 km	9	7	63	0.63
(Australian Geological Provinces 2013)	20 - 40 km	8	7	56	0.56
	40 - 60 km	7	7	49	0.49
	60 - 80 km	6	7	42	0.42
	80 -100 km	4	7	28	0.28
	100 km+	2	7	14	0.14
SedBasins Paleozoic Trap	non basin	0	6	0	0.001
Distance from basin margin	0 - 20 km	9	6	54	0.54
(Australian Geological Provinces 2013)	20 - 40 km	8	6	48	0.48
	40 - 60 km	7	6	42	0.42
	60 - 80 km	6	6	36	0.36
	80 -100 km	4	6	24	0.24
	100 km+	2	6	12	0.12
SedBasins Neoproterozoic to Paleozoic Trap	non basin	0	5	0	0.001
Distance from basin margin	0 - 20 km	9	5	45	0.45
(Australian Geological Provinces 2013)	20 - 40 km	8	5	40	0.40
	40 - 60 km	7	5	35	0.35
	60 - 80 km	6	5	30	0.30
	80 -100 km	4	5	20	0.20
	100 km+	2	5	10	0.10

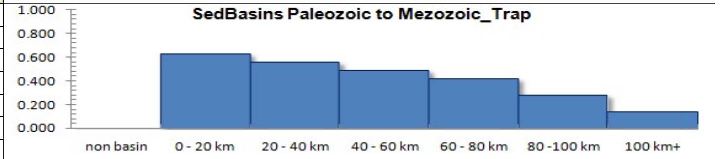

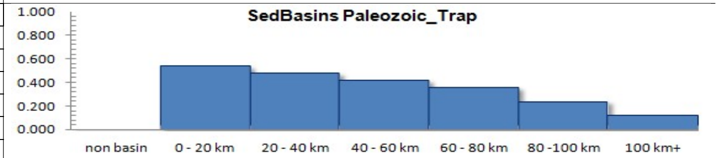

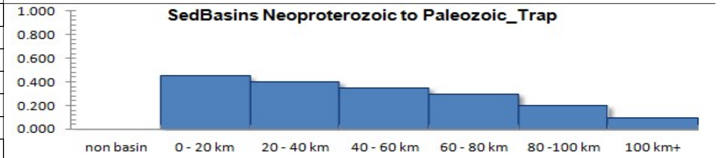

REFERENCES

[1] TURNER, D.D., Predictive GIS model for sediment-hosted gold deposits, North-Central Nevada, USA, Proceedings of Exploration 97: Fourth Decennial International Conference on Mineral Exploration, 115–126 (1997).

[2] HARRIS, J.R., WILKINSON, L., HEATHER, K., FUMERTON, S., BERNIER, M.A., AYER, J., DAHN, R., Application of GIS Processing Techniques for Producing Mineral Prospectivity Maps – A Case Study: Mesothermal Au in the Swayze Greenstone Belt, Ontario, Canada. Natural Resources Research 10, No. 2, 91–124 (2001).

[3] PORWAL, A., CARRANZA, E.J.M., HALE, M., Extended weights-of-evidence modelling for predictive mapping of base metal deposit potential in Aravalli Province, Western India, Exploration and Mineral Geology 10, 273–287 (2001).

[4] LUO, X., DIMITRAKOPOULOS, R., Data-driven fuzzy analysis in quantitative mineral resource assessment. Computers & Geosciences 29, 3–13 (2003).

[5] NYKÄNEN, V., SALMIRINNE, H., Prospectivity analysis of gold using regional geophysical and geochemical data from the Central Lapland Greenstone Belt, Finland Geological Survey of Finland, Special Paper 44, 251–269 (2007).

[6] JOLY, A., PORWAL, A., MCCUAIG, T.C., Exploration targeting for orogenic gold deposits in the Granites-Tanami Orogen: mineral system analysis, targeting model and prospectivity analysis, Ore Geology Reviews 48, 349–383 (2012).

[7] LISITSIN, V.A., GONZÁLEZ-ÁLVAREZ, I., PORWAL, A., Regional prospectivity analysis for hydrothermal-remobilised nickel mineral systems in western Victoria, Australia, Ore Geology Reviews 52, 100–112 (2013).

[8] LINDSAY, M., BETTS, P.G., AILLERES, L., Data fusion and porphyry copper prospectivity models, southeastern Arizona, Ore Geology Reviews 61, 120-140 (2014).

[9] CHENG, Q., AGTERBERG, F.P., Fuzzy weights of evidence and its application in mineral potential mapping, Natural Resources Research 8, 27-35 (1999).

[10] BROWN, W., GROVES, D.I., GEDEON, T., Use of fuzzy membership input layers to combine subjective geological knowledge and empirical data in a neural network method for mineral-potential mapping, Natural Resources Research 12, 183-200 (2003).

[11] PORWAL, A. K., Mineral Potential Mapping with Mathematical Geological Models: ITC PhD Dissertations 130 (2006).

[12] OECD-NEA & IAEA, Uranium 2014: resources, production and demand, NEA no. 7209, A joint report by the Organization for Economic Co-operation and Development Nuclear Energy Agency (OECD-NEA) and the International Atomic Energy Agency (IAEA), 508p (2014).

[13] IAEA, World Distribution of Uranium Deposits (UDEPO) with Uranium Deposit Classification, Vienna, IAEA-Tecdoc-1629, INTERNATIONAL ATOMIC ENERGY AGENCY (IAEA), 126p (2009).

[14] NASH, J.T., GRAINGER, H.C., ADAMS, S.S., Geology and concepts of genesis of important types of uranium deposits (SKINNER, B.J. Ed.) Economic Geology Seventy-Fifth Anniversary Volume 1905–1980, The Economic Geology Publishing Company, El Paso, TX, 63–116 (1981).

[15] DAHLKAMP, F.J., Uranium Ore Deposits, Heidelberg, Springer-Verlag, 460p (1993).

[16] DAHLKAMP, F.J., Uranium Deposits of the World: USA and Latin America. Springer-Verlag, Berlin, 520p (2009).

[17] JAIRETH, S., MCKAY, A., LAMBERT, I., Association of large sandstone uranium deposits with hydrocarbons, AusGeo News 89, 1–6 (2008).

[18] EDGOOSE, C.J., Chapter 24: Ngalia Basin: in AHMAD, M., MUNSON, T.J. (compilers), Geology and mineral resources of the Northern Territory', Northern Territory Geological Survey, Special Publication 5 (2013).
[19] PENNEY, R., Australian sandstone-hosted uranium deposits, Applied Earth Science IMM Transactions Section B 121-2, 65-75 (2012).
[20] BRAUN, J., DOOLEY, J., GOLEBY, B., VAN DER HILST, R., KLOOTWIJK, C. (Eds) Structure and Evolution of the Australian Plate, American Geophysical Union, Geodynamics Series Monographs 26, 186p (1998).
[21] WYBORN, L.A.I., HEINRICH, C. A., JAQUES, A.L., Australian Proterozoic mineral systems: essential ingredients and mappable criteria, Australasian Institute of Mining and Metallurgy Annual Conference Proceedings, 109–115 (1994).
[22] KNOX-ROBINSON, C.M., WYBORN, L.A.I., Towards a holistic exploration strategy: Using geographic information systems as tool to enhance exploration, Australian Journal of Earth Sciences 44, 453-463 (1997).
[23] BONHAM-CARTER, G.F., AGTERBERG, F.P., Application of a microcomputer based geographic information system to mineral-potential mapping (HANLEY, J.T., MERRIAM, D.F., Eds), Microcomputer-based Applications in Geology, II, Petroleum, Pergamon Press, New York, p. 49-74 (1990).
[24] RAYMOND, O.L., LIU, S., GALLAGHER, R., HIGHET, L.M., ZHANG, W., Surface Geology of Australia, 1:1 000 000 scale, 2012 edition [Digital Dataset]. Geoscience Australia, Commonwealth of Australia, Canberra, http://www.ga.gov.au (2012).
[25] MINTY, B.R.S., FRANKLIN, R., MILLIGAN, P.R., RICHARDSON, L.M., WILFORD, J., Radiometric Map of Australia (Second Edition), scale 1:15 000 000, Geoscience Australia, Canberra (2010).
[26] WYBORN, L.A.I., WYBORN, D., WARREN, R.G., DRUMMOND, B.J., Proterozoic granite types in Australia: implications for lower crust composition, structure and evolution, Transactions of the Royal Society of Edinburgh 83, 201– 210 (1992).
[27] CAWOOD, P.A., KORSCH, R.J., Assembling Australia: Proterozoic building of a continent, Precambrian Research 166, 1–38 (2008).
[28] SHAW, R.D., WELLMAN, P., GUNN, P., WHITAKER, A.J., TARLOWSKI, C., MORSE, M., Australian Crustal Elements based on the distribution of geophysical domains (1:5 000 000 scale map), Version 2.4 ArcGIS dataset, Geoscience Australia, Canberra (1996).
[29] FROGTECH, The Australian Proterozoic OZ SEEBASE™; available from http://www.frogtech.com.au/australia.html (2006).
[30] BELL, J.G., KILGOUR, P.L., ENGLISH, P.M., WOODGATE, M.F., LEWIS, S.J., WISCHUSEN, J.D.H. (compilers) WASANT Palaeovalley Map—Distribution of Palaeovalleys in Arid and Semi-arid WA-SA-NT (First edition), scale: 1:4 500 000, Geoscientific thematic map Geocat No 73980 (2012).
[31] LEHNER, B., VERDIN, K., JARVIS, A., HydroSHEDS, Technical Documentation Version 1.0, http://hydrosheds.cr.usgs.gov/HydroSHEDS_TechDoc_v10.doc (2006) (accessed 10 August 2016).
[32] JARVIS, A., REUTER, H.I., NELSON, A., GUEVARA, E., Hole-filled SRTM for the globe Version 4, available from the CGIAR-CSI SRTM 90m Database, http://srtm.csi.cgiar.org (2008).
[33] JACOBSON, G., LAU, J.E., Hydrogeology of Australia, 1:5,000,000 scale map, Bureau of Mineral Resources, Geology and Geophysics, Canberra, http://www.agso.gov.au/databases/catalog/agsocat.html (1987).

[34] STEWART, A.J., RAYMOND, O.L., TOTTERDELL, J.M., ZHANG, W., GALLAGHER, R., Australian Geological Provinces, 2013.01 edition [Digital Dataset]. Geoscience Australia, Commonwealth of Australia, Canberra, http://www.ga.gov.au (2013).

[35] SINGER, D.A., Basic concepts in three-part quantitative assessments of undiscovered mineral resources, Nonrenewable Resources 2, 69–81 (1993).

[36] CUNNINGHAM, C.G., ZAPPETTINI, E.O., VIVALLO S., WALDO, CELADA, C.M., QUISPE, JORGE, SINGER, D.A., BRISKEY, J.A, SUTPHIN, D.M., GAJARDO M., MARIANO, DIAZ, ALEJANDRO, PORTIGLIATI, CARLOS, BERGER, V.I., CARRASCO, RODRIGO, AND SCHULZ, K.J., Quantitative mineral resource assessment of copper, molybdenum, gold, and silver in undiscovered porphyry copper deposits in the Andes Mountains of South America, U.S. Geological Survey Open-File Report 2008-1253, 282p (2008).

[37] SINGER, D.A., JAIRETH, S., ROCHE, I., A three-part quantitative assessment of undiscovered unconformity-related uranium deposits in the Pine Creek Region of Australia, in this volume.

ARE WORLD URANIUM RESOURCES LOG-NORMALLY DISTRIBUTED?

J.-J. ROYER
Université de Lorraine UdL, CNRS-GeoRessources (UMR7359),
ENSG, gOcad-ASGA,
Vandoeuvre-les-Nancy Cedex
France

Abstract

Investigating uranium resources is a significant opportunity for the future energy policy. Uranium deposits are usually classified according to their host rocks, for instance, in the uranium database of the International Atomic Energy Agency (IAEA) in which the uranium deposits are re-grouped into 15 major types[18]. This work investigates uranium resources using a mineralogical and process-based approach. Emphasis is put on re-grouping the deposits into three main classes according to their geological types. The statistical study of more than 1,500 uranium ore deposits recorded in the IAEA database shows that their grades and tonnages are remarkably distributed according to a log-normal distribution, their median tonnages being linearly inversely correlated to their median grades into a log-log cross plot. The log-normal characteristic is attributed to overprints of successive concentration first-order processes. The log-normal grade-and-tonnage model seems to be applicable globally as well as per main type, making these models comprise useful for estimation of potential resources of under-explored areas. The 15 major types of uranium deposits can be re-grouped according to their median grades and into three main genetic families, namely superficial, syn-sedimentary and hydrothermal. Uranium, as sub-product of phosphate deposits, constitutes the largest world uranium potential resources with an estimated median tonnage[19] estimated as ~30,000 t U $_{[3,450 – 246,150]}$ but at the lowest median grade of 0.18‰ U $_{[0.06 – 0.6]}$. The following world uranium resources, in decreasing order, are: superficial 4,575 t U $_{[970 – 21,650]}$ @ 0.3‰ U $_{[0.1 – 0.8]}$, sedimentary 3,025 t U $_{[750 – 12,250]}$ @ 0.8‰ U $_{[0.3 – 1.9]}$, and hydrothermal deposits 2,350 t U $_{[680 – 8,130]}$ @ 1‰ U $_{[0.4 – 2.4]}$. The largest median grades, but also associated with the lowest tonnages, are observed in collapse breccia pipe (Colorado type) 780 t U $_{[385 – 1,575]}$ @ 4‰U $_{[2.1 – 8.1]}$, and Proterozoic unconformity (Saskatchewan) type deposits 4,550 t U $_{[900 – 22,750]}$ @ 7‰U $_{[1.5 – 29]}$, with average grade reaching maximum grades as high as 19.5% U with resources greater than 200,000 t U for unconformity deposits (McArthur River, Canada).

1. INTRODUCTION AND OVERVIEW

Uranium resource assessment is a significant opportunity for future energy policy. Uranium deposits are usually classified according to their host rocks, for instance, in the uranium database of the International Atomic Energy Agency (IAEA) in which uranium deposits are re-grouped into 15 major types[20]. In this work, uranium resources are investigated using a mineralogical and process-based approach, resulting in re-grouping of uranium deposits into three main classes according to their geological types. The statistical study of more than 1,500 uranium deposits recorded in the IAEA database indicates that their grades and tonnages are remarkably distributed according to a log-normal distribution, their median tonnages being linearly inversely correlated to their median grades into a log-log cross plot. This log-normal grade-and-tonnage model is used to estimate potential resources of under-explored areas, making these approaches a useful tool.

---

[18] The IAEA classifies uranium deposits into 15 types in increasing average grades as follows: phosphate, intrusive, surficial, polymetallic breccias complex, paleo-quartz pebble conglomerate, lignite coal, black shale, carbonate, metasomatite, sandstone, volcanite, granite-related, metamorphite, collapse breccia pipe, Proterozoic unconformity.

[19] The confidence band enclosed in brackets is reported as indices corresponding to the median plus or minus the log standard deviation [log med $\pm\sigma$] transformed into grade or tonnage.

[20] The IAEA classifies uranium ore deposits into 15 major types in increasing average grades as follows: phosphate, intrusive, surficial, polymetallic breccias complex, paleo-quartz pebble conglomerate, lignite coal, black shale, carbonate, metasomatite, sandstone, volcanite, granite-related, metamorphite, collapse breccia pipe, Proterozoic unconformity.

1.1. Database

The World Distribution of Uranium Deposits (UDEPO) is a database of uranium deposits in the world, containing information on the classification, geological characteristics, geographical distribution and resources of the deposits. It covers all geographical regions of the world from more than 70 countries. Currently, the database contains over 2,200 mineralized records and is constantly updated[21]. The UDEPO IAEA database is accessible via Internet at: https://infcis.iaea.org/UDEPO/About.cshtml. The database contains the name of the deposit, its location, the uranium grade (in % U), the total metal content (in t U), and the ore tonnage (in Mt) for each deposit. A copy of the database was extracted into an Excel sheet according to the procedure illustrated in Fig. 1. For each region, the deposits have been ranked in increasing order according to their metal content in order to build the metal content frequency cumulative distribution. Not all the records are fully informed, and a lot of missing values make some records not useful. Only ~1,490 records were used to carry out this statistical study. Other limits are that the data are public and provided by governments, agencies or company on voluntary bases, which make some records only indicative (possible bias, errors, not up-dated data, voluntary or not). However, the UDEPO provides a good overview of the uranium sector.

FIG. 1. Schematic diagram showing the access to the UDEPO uranium database via Internet allowing the user to extract Excel sheet. Website of the UDEPO database https://infcis.iaea.org/UDEPO/About.cshtml

1.2. Background and objectives

Uranium was a strategic metal globally in the 1950's. Early production went first into military inventories and then, in the early 1980s, into civil stockpiles. This early production led to the shortfall in mining supply since the mid-1980s, which was diminishing towards the level of continuing secondary supplies. Currently, the uranium market has reached a more classical demand-supply commodities model allowing resource prognostic as for the other commodities (Fig. 2). Installed nuclear capacity and military uses (much of which being confidential) are two factors that drive demand for uranium. Uranium cannot be substituted in the atomic sector[22] unlike other mineral resources sectors (i.e., steel can be substituted by aluminum) [1]. Demand estimates are complicated by the choice of fuel cycle technology of a country or firm; in case of a once-through fuel cycle, demand is proportional to the electricity produced.

[21] Some records are incomplete (absence of grade or indicated tonnage), so only 1,490 records were used in this study.
[22] Except in future possibly by thorium if this technology is becoming mature.

The world total uranium production in 2014 reached 56,217 t U (a slight decrease compared to 59,370 t U in 2013). Fig. 3 illustrates the largest corporate producers (Fig. 3a) and the total world uranium resources (in t U) (Fig. 3b). The total resources are estimated at 55.334 Mt U, indicating enough resources for a period of more than 500 years based on the U consumed in 2014[23].

Several emerging countries (e.g., China and India) are currently developing long term policies for producing electricity from nuclear power plants, while others (e.g., Germany, France) following the tragic nuclear accident of Fukushima are actively decreasing their national electricity production from nuclear power by substituting them with renewable technologies. Despite these opposing policies, experts forecast an increase in uranium demand in the next coming decades. Therefore, it is important to investigate the available future uranium resources per deposit type and to try to evaluate potential exploration targets based on existing ones. This work aims at drawing a dynamic picture of uranium resources, their evolution through time, and location per continent based on information recorded in the UDEPO database.

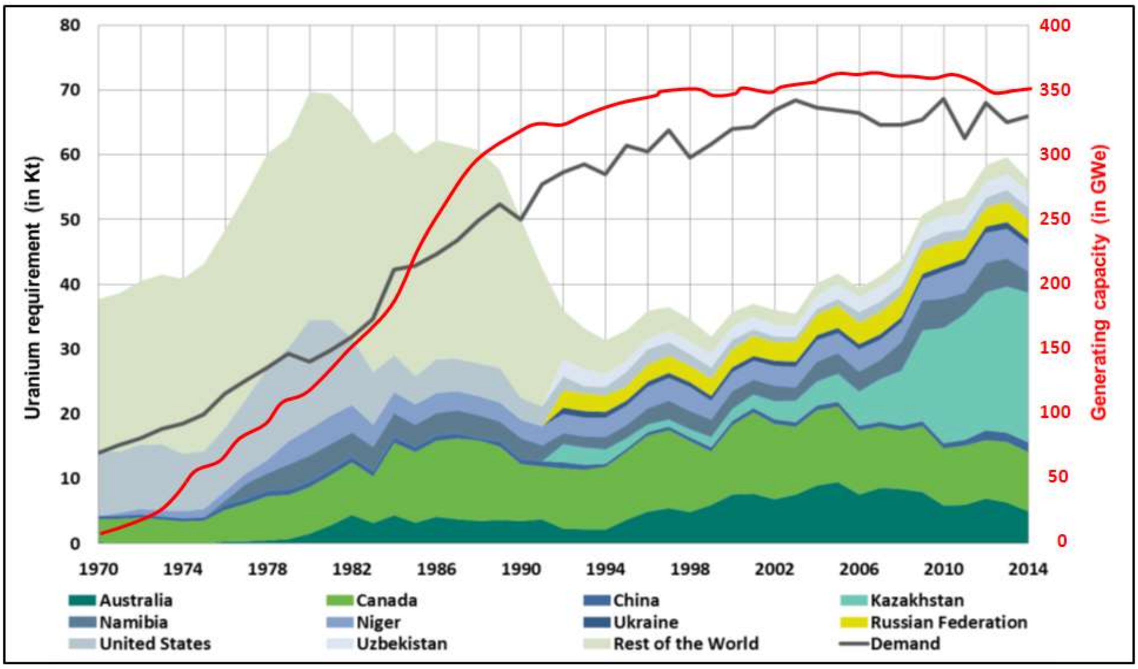

FIG. 2. World uranium supply and demand over the 50 last years (modified after [1] and merged with data from the Red Book 2014 ([2], [3]); source: own illustration based on [4] sec. Appendix 7.1) and OECD data 2004-2014).

[23] Given the many nuclear power programs in construction in several countries in the World, this figure is certainly overestimated as one can expected an increase in World uranium consumption in the next coming decades.

Company	tonnes U	%
KazAtomProm	13,801	25
Cameco	8,956	16
ARMZ - Uranium One	6,944	12
Areva	6,496	12
BHP Billiton	3,351	6
CNNC & CGN	2,684	5
Navoi	2,400	4
Rio Tinto	2,316	4
Rio Tinto	2,296	4
Other	6,973	12
Total	**56,217**	**100%**

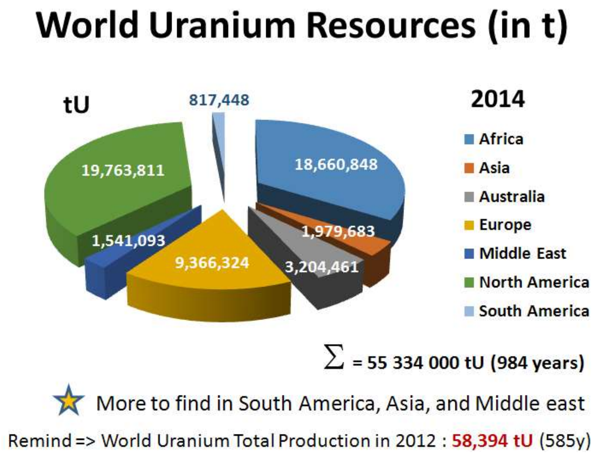

(a) *(b)*

FIG. 3. (a) Major companies producing uranium (in t U) in 2014[24]; (b) Main world uranium resources (in t) per continent based on declarations in the UDEPO database. Total resources are estimated at 55.334 Mt U, indicating enough resources for a period of more than 500 years based on the U consumed in 2014[25].

2. STATISTICAL STUDY OF URANIUM RESOURCES REPORTED IN THE UDEPO DATABASE

2.1. Does the 2008 economic crisis impact uranium exploration?

Figs 4a and 4b illustrate, respectively, the number and cumulative number of deposits discoveries vs. time since the 1950's, together with their corresponding (cumulative) tonnage (Fig. 4c and 4d). The figures come from the declared values in the UDEPO database. Major economical crises and nuclear accidents are superposed on the time diagram (Fig. 4a) and uranium prices for comparison. Details of Fig. 4b over the period 1950-2000 are reported in Figs 5a-d.

[24] The figures in this table are liable to change as new data become available. The first uranium producer in the World is Kazakhstan with 23,127 t U in 2014, more than half produced by KazAtomprom, followed by Canada (9,134 t U), Australia (5,001 t U) and Niger (4,057 t U) (see at http://www.world-nuclear.org/information-library/facts-and-figures/uranium-production-figures.aspx).

[25] Given the many nuclear power programs in construction in several countries in the World, this figure is certainly overestimated as one can expected an increase in World uranium consumption in the next coming decades.

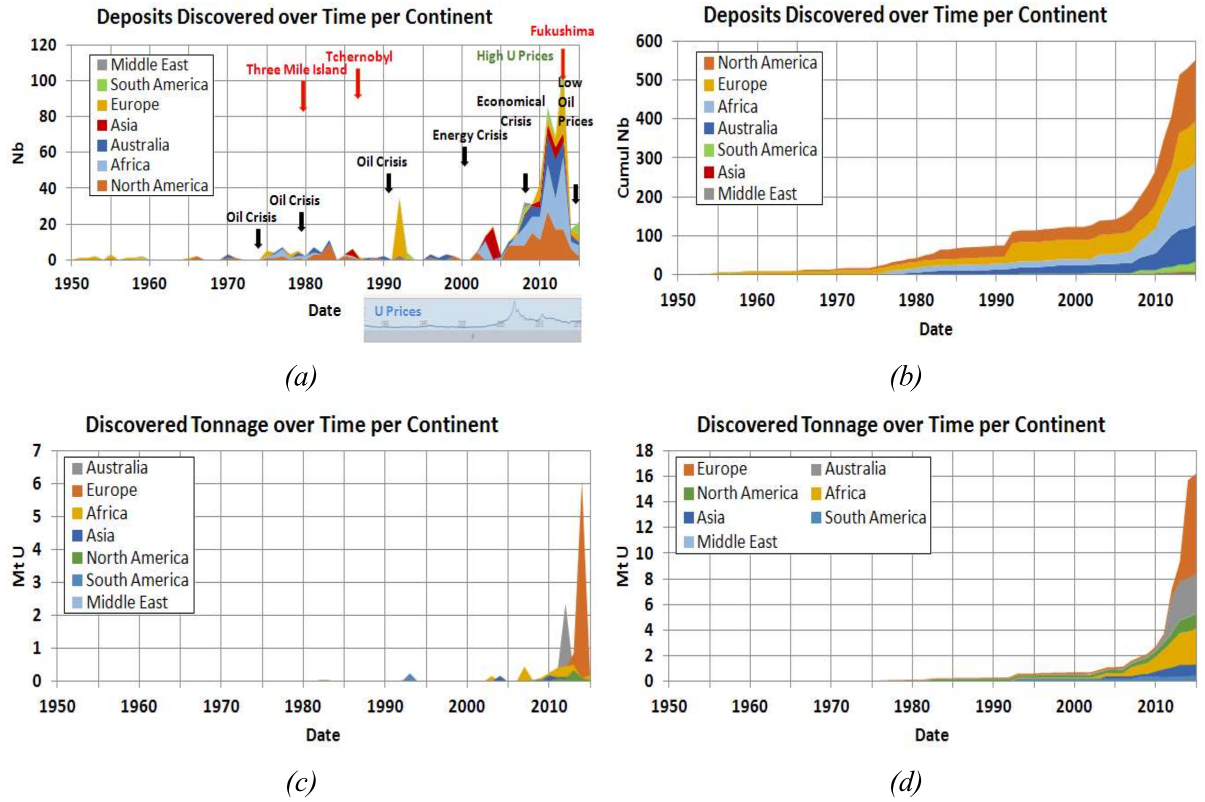

Fig. 4. (a) Number of deposits discovered against time recorded in the UDEPO database since the 1950's. Oil crisis and nuclear accidents seemed to have been a great impact. U prices remained to drive exploration before 2008. (b) Cumulated number of deposits. (c) U (in Mt U) tonnage discovered against time since the 1950's (d) Cumulative tonnage.

As indicated in Fig. 4, the number of uranium deposits discovered has decreased after major nuclear accidents (Three Miles Island, Chernobyl, Fukushima), indicating that exploration activity was significantly reduced shortly after these incidents. On the contrary, every oil or energy crises were followed by a reassessment in exploration activity leading to the discovery of new oil deposits some years after (Fig. 5a). Uranium prices seem to have relatively less impact in uranium exploration activities in the past, but high uranium prices seem to have driven the exploration before the 2008 crisis and the Fukushima accident. However, recent studies on U price changes related to exploration delays show that exploration tends to increase during times of high uranium prices, but the time lag between exploration success and production of uranium plays a significant role in influencing price volatility [5, 6]. This is probably explained why the recent 2008 crisis had no impact on the number of uranium deposit discoveries (the highest numbers of discoveries were registered just after the crisis) probably due to the emergence of new exploration areas such as Asia. In conclusion, exploration was very active the past 10 years with major discoveries (or reported discoveries) in regions like Africa, Asia, Middle East, and South America (Fig. 6), but recently decreased following the Fukushima accident. Major turning points (in 1975, 1983, and 1992) can be observed on the cumulative curves (Fig. 5b, d), indicating significant discoveries in terms of numbers and tonnages (some of them due to new explored areas or discoveries such as Africa in 1975, Canada in 1982, and Asia in 1992).

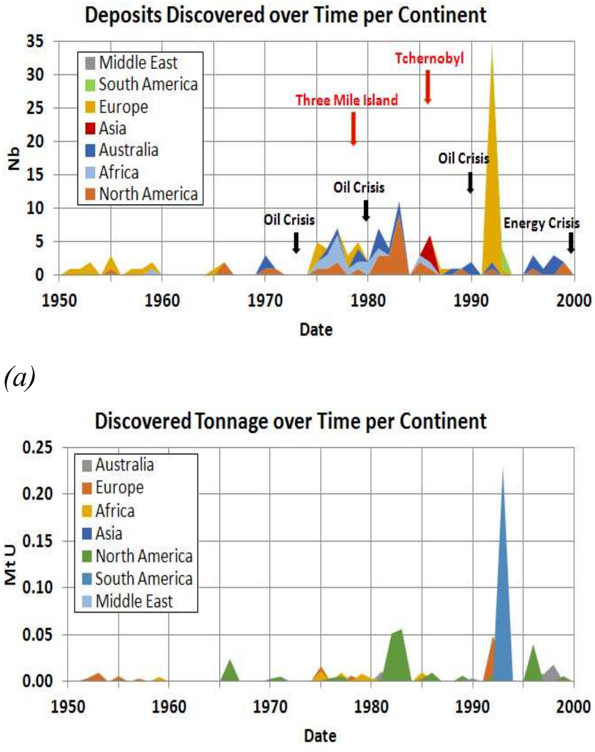

(a) (b)

(c) (d)

FIG. 5. Data for period before the 2000's. (a) Number of deposits discovered against time recorded in the UDEPO database since the 1950's. (b) The same as (a) but with cumulated number of deposits. (c) U (in Mt U) tonnage discovered against time over the same period (d) with cumulative tonnage.

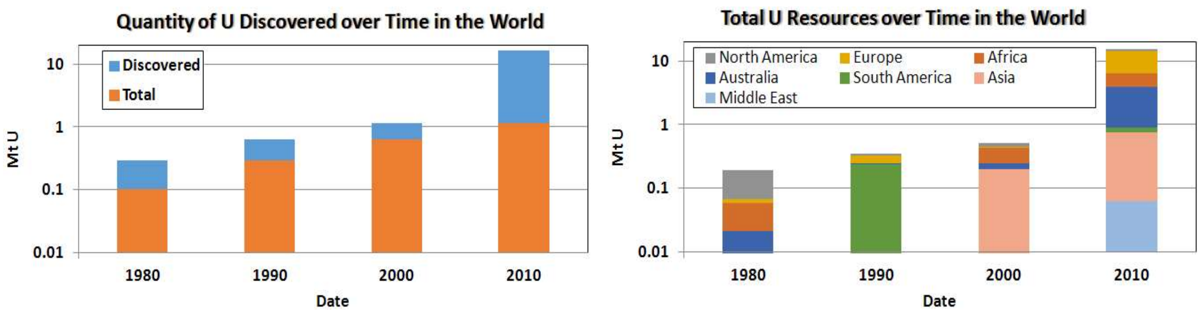

(a) (b)

FIG. 6. (a) Quantity (in Mt) of uranium discovered compared to known resources vs. decades as recorded in the UDEPO database since the 1980's. (b) The same as (a) but detailed per continent indicating the emergence of South America in the 1990's, Asia in the 2000's, and Middle East in the 2010's.

What next? It is hard to say and be prognostic if the uranium prices will increase again or not in the next few years, but given the long term on-going nuclear programs in India and China there are signals that U spot prices will increase in the near term. More precisely, a recent study by [1] suggests that increase in use of civil atomic power in some emerging economies, such as South Korea and China, would question the availability in uranium resources and may lead to a supply shortage for the forthcoming decade, despite the fact that global uranium resources are more than sufficient to supply reactor-related demand for the rest of the century, especially if the super regenerators technology is started in operation.

2.2. Identifying new target areas

Geology plays a major role in identifying potential resources for natural commodities. However, global multivariate indicators based on past discoveries can help in pointing out lacking or unexplored prospective areas. This approach is used in oil and gas exploration assessment for identifying geologically-permissive prospective areas [7] and in mineral exploration for locating undiscovered mineral resources in large tracts [8], [9]. Keeping this in mind, the amount of uranium per square kilometer (in U kg/km^2) (referred as Exploration Index EI, Fig. 7) has been introduced. It has been calculated per continent in order to identify the exploration degree of a region. The ranking of continents in order of increasing EI is: Europe (EI = 920), North America (800), Africa (617), Australia (417), World (382), Middle East (176), South America (46), and Asia (43). In short, regardless of geological endowment (which is certainly wrong, if compared with other metals such as gold) but given their vast areas, the higher the EI is, the better the region is for exploration. Or, in geological context, the higher the EI, the better the chance a country has for successful exploration.

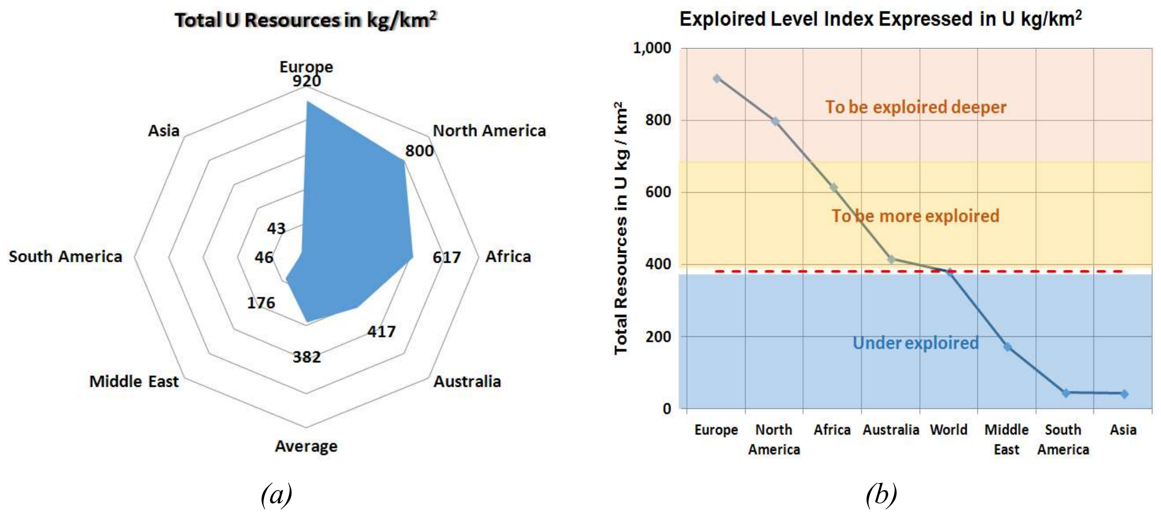

FIG. 7. (a) Radar diagram of exploration index (values indicated) calculated per continent. (b) Continents are ranked in decreasing exploration index showing the best to the least explored area. Regardless of geological context, it is indicated that there are more uranium deposits to be found in the Middle East, South America and Asia, given their vast areas compared to Europe, North America and Africa[26].

2.3. Discussion

Several other approaches including geological indicators have been used in the past for estimating potential undiscovered mineral resources, country by country, such as the work by [10] for estimating potential uranium resources in the USA, including 700 areas and 1,022 files

[26] Kazakhstan is included in Middle East.

accounting for economical constraints on the uranium price, assuming log-normal distribution of grade and resources. More recently, based on a cumulative distribution curves approach (called endowment curves), Jaireth and Huston [11] discussed the spatial distribution of gold, uranium, and base metal (copper, lead and zinc) on mineralized regions of several cratonic terranes and districts in the world (including Canada, Australia, Chile, Poland, Uzbekistan, and Ghana). They concluded that mineral districts with a single giant or super-giant deposit represent areas with higher fertility but also highly focused or concentrated mineral system, reflecting more intense and duration of metal accumulation caused by larger systems of energy and mass flux. This index does not pretend to be a universal key to identify new deposits; it is only a global indicator (in the UNEP sense) to point out eventually unexplored areas. It must be cross-validated with some other geological and exploration indicators to best identify the most potential targets. Keeping in mind these limitations, it appears that Europe is the best explored (920) while significant potentiality seems to exist in Asia, which presents some similar geological contexts as the Europe (such as Hercynian complexes). Several types of such indices can be derived, such as the number of deposits per square kilometer. This approach is global and valid only on large areas containing a collection of different geological formations of different ages, so that the geological context is assumed to be significantly represented.

The global aspect is one of the weaknesses of the methodology. It is suited to uranium, which is very mobile in oxidizing contexts and precipitates in reducing conditions, unlike some other commodities, such as gold, that occurs in very specific geological settings. This explains the diversity of geological settings in which uranium deposits can occur, varying from phosphate, sedimentary, plutonic to volcanic-related deposit-types (see Fig. 8). In order to account for their geological setting, uranium deposits have been grouped according to the classification recommended by the IEAE, which comprises 15 main types. Then, a statistical study was carried out to try to build a grade-and-tonnage model.

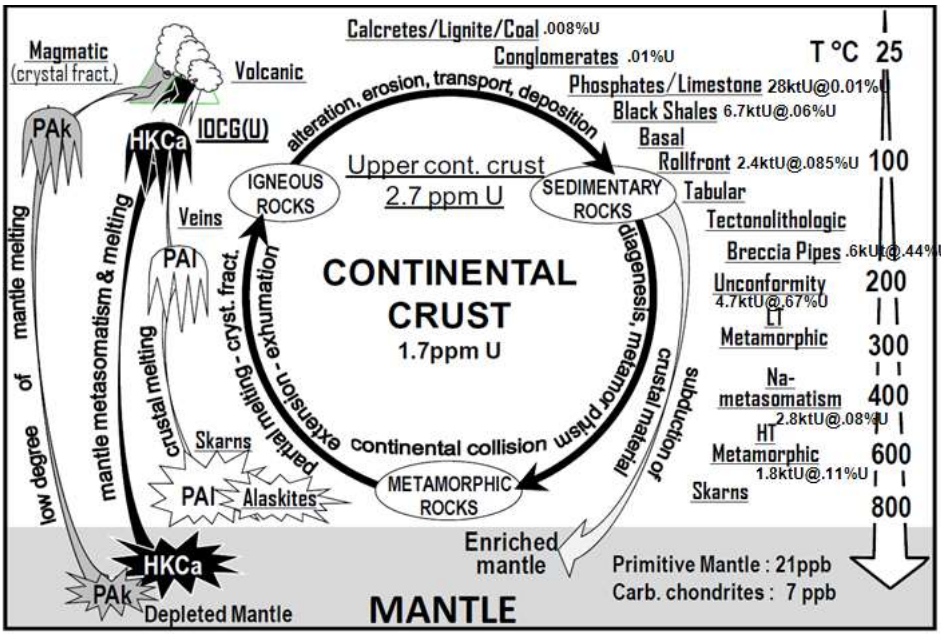

(After Cuney, 2009) Pak peralkaline, KCa High-K calcalkaline, Pal peralumineux

FIG. 8. Classification of uranium deposits into 15 main types according to their geological cycle. The median graded and tonnages are indicated per deposit type (modified after [12, 13]).

3. URANIUM DEPOSITS STATISTICS ACCOUNTING FOR THEIR GEOLOGICAL TYPES

Uranium is a lithophile element with an upper crustal abundance of 2.7 ppm. This results from the incompatible[27] behavior of uranium during magmatic processes. As uranyl ions form a large variety of complexes, uranium is very mobile under oxidizing conditions. Uranium deposits can be formed at every step of the geological cycle from high grade metamorphism (up to 800°C, 5 to 7 bars) to sedimentary or surficial conditions (Fig. 8). The age of uranium deposits ranges from Neo-Archaean to the Quaternary [12]. This important diversity in uranium deposits leads many authors to constitute a classification of uranium deposits since the early 1970's [14].

3.1. Uranium deposit main type as defined by the iaea classification

A new classification of uranium deposits, with 15 main types and 39 subtypes, has been proposed by the IAEA ([15, 16]) (Table 1). It is based on host rock lithology, ranked from very high temperature deposits (mainly related to magmatic processes) to very low temperature ones (related to surficial processes). It is officially used by the mining industry since 2009.

However, according to the geological cycles of uranium, it can be simplified into three main types and two outliers a suggested by Cuney (2009) (Table 2):

- Low grade: phosphate;
- Superficial: intrusive, surficial;
- Syn-sedimentary: paleo-quartz pebble conglomerate, lignite coal, black shale, carbonate, metasomatite, sandstone;
- Hydrothermal: volcanite, granite-related, polymetallic breccia complex, metamorphite;
- High grade: collapse breccia pipe, Proterozoic unconformity;

A systematic statistical study of the grade and tonnage distribution was carried out on each of the 15 types, and then re-grouped into the three above main types for simplification. The aim is to try to identify a grade-and-tonnage model per type [18, 21].

[27] Uranium tends to be concentrated in the early liquids during partial melting, and in the last melt fraction during crystal fractionation.

TABLE 1. IAEA URANIUM DEPOSITS CLASSIFICATION WITH GEOLOGICAL DESCRIPTION (AFTER [15])

IAEA uranium deposits classification[28]

The most common deposits are grouped into 15 types, mainly defined on the nature of host rock lithology, and 39 sub-types	1	Intrusives	Deposits associated with intrusive rocks of various type and chemical composition (alaskite, granite, syenite, carbonatite…) indicating different uranium concentration genetic processes. Intrusive rocks typically emplace in sedimentary rocks (sandstone) or quartzite, metamorphosed to upper amphibolite facies. Typical example: Rössing (Namibia) ([12]; [16]).
	2	Granite-related	Vein type found in a disseminated form in leucogranite plutons or in the granite metamorphic host rocks, either associated to de-quartzified granite, or as massive veins or stockworks formed in the contact metamorphic rocks or in the meta-sediments.
	3	Polymetallic iron-oxide breccia complex	Complexes occurring in hematite-rich breccias associated with uranium, copper, gold and rare earths (also referred as IOCG[29]). Typical example: Olympic Dam (Australia). Metallogenesis quite complicated and not fully understood, can occur in several tectonic settings such as rift, subduction zones or basin collapse ([16]).
	4	Volcanic-related	Occurring within large calderas filled by mafic to felsic volcanic rocks (peralkaline) complex and intercalated by clastic sediments (sub-types: strata-bound, veins, stockworks, pyroclastic units...). Ore genesis mainly formed by mixing saline magmatic fluid containing the metallic ions with oxidized meteoric water. Typical example: Streltsovskoye(Russia), Dornot complex (Mongolia).
	5	Metasomatite	Related to alkaline metasomatism (Na or K series) and to skarns with various origin for the weathering fluid (from exsolved fluid from granite to high-salinity and low temperature basin fluid). Albitization and associated uranium mineralization often epigenetic affecting both plutonic and metamorphic rocks. On the opposite, skarns synchronous with the magmatic event and the metamorphism.
	6	Metamorphite	Result from a regional metamorphism affecting uraniferous sediments or volcanites leading to a partial recrystallization of uranium-bearing minerals and thus an increase in U grade content.
	7	Proterozoic unconformity	Associated to lithological changes occurring close to major Proterozoic unconformities. Below the unconformity, the metamorphic rocks of the basement rocks which may host the mineralization are usually faulted and brecciated and are constituted of Archaean to Paleo-proterozoic lithologies. The overlying younger Paleo–Meso-Proterozoic clastic basin (usually sandstones) is generally undeformed. The exceptional enrichment of uranium is due to a combination of several uranium fractionation mechanisms: at first the basement is well pre-enriched in uranium and then the hydrothermal alteration is so important that it enables a very efficient uranium extraction. At last, exceptional trapping conditions are present. They result from the strong redox gradient developed between the oxidized Paleo- to Meso-Proterozoic sediments and the epi-continental Paleo-proterozoic organic-rich meta-sediments of the basement. But also from the creation of large openings due to faulting in the basement and intensive hydrothermal quartz dissolution in the overlying sandstone ([12]). So this category regroups some of the largest and the richest uranium deposit in the Athabasca Basin with, for instance, the mine of Cigar Lake in Canada. They provide more than a third of the world consumption of uranium.
	8	Collapse-breccia pipe	Occurring in vertical collapse structures such as chimney (or pipes) of 30 to 200m in diameter and up to 1000m in height, filled with coarse fragments and fine penetrated sediments. Uranium transported in pipe by ascending basinal brines and deposited where temperature, pressure or chemical environment change, often in interstices between breccias fragments or fractures surrounding the chimney structure and the unaffected rocks.
	9	Sandstone-hosted	Occurring in carbon and/or pyrite-bearing fluvial (less commonly marine), arkosic sandstones bounded by less permeable horizons (clays). Uranium precipitated

[28] See also the Red Book, OECD-NEA and IAEA (2014).

[29] IOCG = Iron Oxide Copper Gold complex.

IAEA uranium deposits classification[28]

			under reducing conditions caused by a variety of reducing agents (i.e., carbonaceous material, sulfides, hydrocarbons and iron/magnesium minerals as chlorite). Age ranges from Paleozoic to Tertiary, with also small Precambrian sandstone-hosted deposits associated with carbonaceous matter of probable algal origin. Most important type of uranium deposit in the World (representing 2/5 of total uranium deposits). Four major subtypes: roll-front type, tectonic-lithologic, basal channel and tabular. Roll-front is of major economic importance in Kazakhstan, Uzbekistan, USA and Niger providing a great part of the uranium world production by low cost in-situ leaching.
	10	Paleo-quartz-pebble conglomerate	Formed during Neo-Archaean and Paleo-proterozoic basins (> 2.3 Ga) in intra-craton consisting of fluviatile or lacustrian paleo-channel trapping detrital uranium oxides. Host rock formed by quartz-pebble conglomerate with quartz-rich matrix showing also presence of pyrite, gold, uranium oxide and other detrital oxide or sulfide minerals. Amount of uranium in those ‘placers’ depends on the geological sources. Fluviatile transport favored by poor oxygen atmosphere at this period. Diagenetic processes could also modify the mineralogy with, for instance, appearance of rutile, anatase and brannerite. Typical example: Witwatersrand basin (South Africa).
	11	Surficial	Youngest near-surface uranium deposits aged from Tertiary to today, including uranium mineralization in soils and sediments, such as calcretes formed in arid to semi-arid climatic conditions by alteration of pre-enriched granite. Uranium is only deposited as UO_2^{2+} minerals with presence of important amounts of vanadium due to its low solubility. Typical example: calcretes (Australia, Namibia).
	12	Lignite and coal	Concentration of uranium occurring in lignite/coal, and in clay and sandstone immediately adjacent to lignite. Uranium is concentrated by adsorption on organic matter, forming a reducing environment, or by the activity of anaerobic bacteria which can reduce UO_2.
	13	Carbonate	Hosted in limestone or dolomites, often related to karsts, fractures, faults and folds, controlled by various factors (i.e., stratigraphic lithofacies, tectonics, topography, hydrography and paleo-climate). Ore bodies developed mainly in oxidation-reduction transition zones of lagoonal lithofacies cut by structures in fault-depression basins. Mineralization closely related to clay minerals and organic matter where adsorbed uranium is the most present species ([17]).
	14	Phosphate	Uraniferous phosphorite deposits consist of syn-sedimentary, stratiform, dissemi-nated uranium in marine phosphate-rich rocks or phosphorite deposits that formed in continental shelf environments. Uranium substituted Ca in the apatite minerals, uranium grade are very low (25-150 ppm) and is a by-product of phosphates produced by the chemical fertilizer industry.
	15	Black shale	Consisting of marine organic-rich shale or coal-rich pyritic shale, containing syn-sedimentary disseminated uranium adsorbed onto organic material and clays. Uranium enrichment often due to the reducing conditions and biogenic processes characteristics of the black shales.

TABLE 2. SIMPLIFIED URANIUM DEPOSITS CLASSIFICATION BASED ON GEOLOGICAL CYCLES

Simplified grade-based uranium deposits classification[1]			
The deposits are regrouped in 3 main types (1, 2, 3), and outliers (0, 4) based on the natural uranium cycle	0	Low grade	Phosphate
	1	Superficial	Intrusive, surficial, polymetallic breccia complex
	2	Syn- or sedimentary	Paleo-quartz pebble conglomerate, lignite coal, black shale, carbonate, metasomatite, sandstone.
	3	Hydrothermal	Volcanite, granite-related, metamorphite
	4	High grade	collapse breccia pipe, Proterozoic unconformity

[1] For sake of commodities, this classification is based on average grade and resources distribution curves and NOT on genetic concepts. For instance, the metasomatite type deposits have high temperature hydrothermal origin; sandstone-hosted deposits may have various origins such as meteoric fluid infiltration for roll types, diagenetic fluids for tabulars, etc. The same for the superficial ones, intrusives, IOCG and calcrete are very different in terms of origin.

3.2. Statistical study of grade and tonnage of uranium deposit per types

3.2.1. Available data and procedure

Available tonnage and grade values for uranium deposits declared in the UDEPO database (n ≈ 2,200) were exported to an Excel™ sheet and gOcad to calculate a cumulative frequency curve for each of the 15 main types according to the IAEA classification. Estimated statistical parameters (mean, standard deviation, 1st and 3rd quartiles, inter-quartile range, log-normal parameters) for grades and tonnages are given in Appendix Tables A1 and A2. For the all 15 (and simplified three) types, the tonnage and grade cumulative distributions are log-normal as shown in Fig. 9.

3.2.2. Discussion and interpretation

Uranium grades of all types of deposits seem to follow log-normal distribution. This can be explained by a multi-step geological formation process, during which the metal is concentrated by successive over-printing of enrichment processes. Let us consider a multi-concentration natural process (e.g., partial melting, exsolution, concentration, etc.) comprising i=1, ..., s steps, and U_i be the concentration in uranium observed at step i. Assuming that the increase δU_i in concentration of uranium at step i is proportional[30], with parameter α_i, to the initial uranium concentration at step U_i–1, the governing equations describing the evolution in uranium concentration after s processes are:

[30] This is the general conceptual model for partial melting, chemical reaction, diffusion, etc.

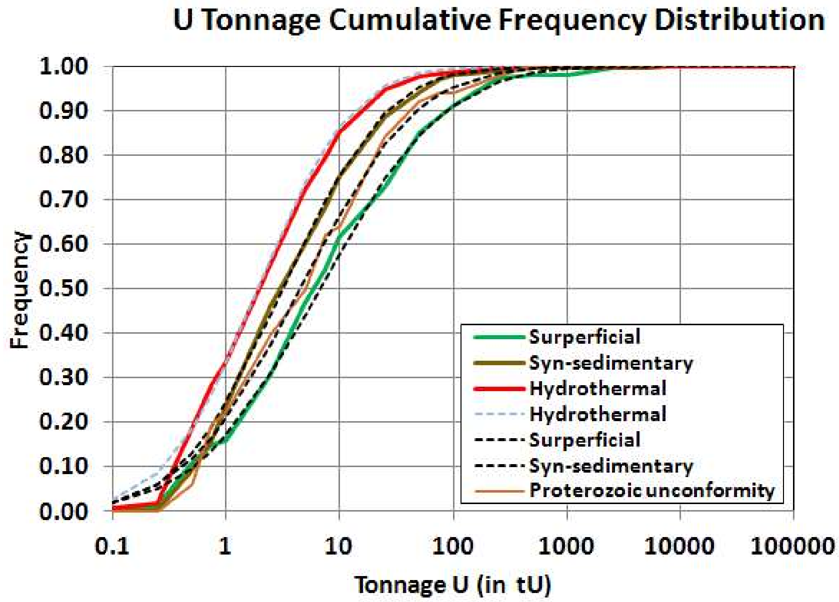

FIG. 9. Frequency distributions (on log-plot) calculated for tonnages of the simplified 3 main types of uranium deposits showing a log-normal distributed. The fitted log-normal model distribution is shown as dotted curves.

$$\delta U_i = \alpha_i U_{i-1} \Rightarrow U_i = \left(\prod_{i=1}^{s}(1+\alpha_i)\right) U_0 \Rightarrow \log U_i = \log U_0 + \sum_{i=1}^{s}\log(1+\alpha_i) \qquad (1)$$

If the parameters α_i are randomly distributed, the sum $\sum_{i=1}^{s}\log(1+\alpha_i)$converges to a Gaussian distribution, so does log U_i, and thus, the uranium concentration U_i and the corresponding tonnage are log-normally distributed [22]. This is an often-observed behavior for several mineral commodities (e.g., Au, Pb, Zn, Cu, etc.), which can be explained by a multi-stage concentration model in some situations given some assumption [23].

When observed carefully, it can be noticed that uranium deposits of similar types have quite the same log-normal cumulative distributions of grade and tonnage (Fig. 10a). This is why it was decided to re-group the 15 types into only three simplified types, regardless of their geological structural setting or control, but accounting for their mean uranium grades. The new groups are reported in Table 2, referred as superficial, syn-sedimentary, and hydrothermal (some outliers have been kept such as the lowest grade phosphate and the highest grades breccias pipes and Proterozoic unconformity types). Their corresponding cumulative distribution curves of uranium grade (in %) are reported in Fig. 10b, and their statistical parameters for grades and tonnages in Tables 6 and 7 (see Annex) and in Table 3. The experimental cumulative distributions of uranium grades were fitted with a log-normal distribution in Fig. 10.

TABLE 3. AVERAGE TONNAGES AND GRADES WITH INTERVAL VARIATION RANGE FOR SOME MAIN URANIUM TYPE DEPOSITS CALCULATED FROM THE DECLARED VALUES IN THE UDEPO IAEA DATABASE*

Type	Tonnage (in UMt)	Grade	Comments
Phosphates	30.000 [3.450, 246.150]	0.18 ‰ U [0.06; 0.6]	Greatest potential resources
Surficial	4.575 [0.970, 21.650]	0.3 ‰ U [0.1; 0.8]	Low grade deposits
Sedimentary	3.025 [0.750, 12.250]	0.8 ‰ U [0.3; 1.9]	Greatest resources
Hydrothermal	2.350 [0.680, 8.130]	1 ‰ U [0.4; 2.4]	Small size deposits
Collapse Breccia Pipe	0.780 [0.385, 1.575]	4 ‰ U [2.1; 8.5]	Up to 8.5‰ at Hermit (USA)
Proterozoic unconformity	4.550 [0.900, 22.750]	7 ‰ U [1.5; 195]	Monsters up to 19.5% with resources > 200,000 t U at McArthur River (Canada)

* In brackets, ranges defined as 10m ± σ where m and σ are, respectively, the mean and standard deviation of the log10 of the values; e.g., the tonnages of Proterozoic unconformity deposits vary between 0.9 to 22.750 Mt U, while their grades vary between 0.15 and 19.5% U.

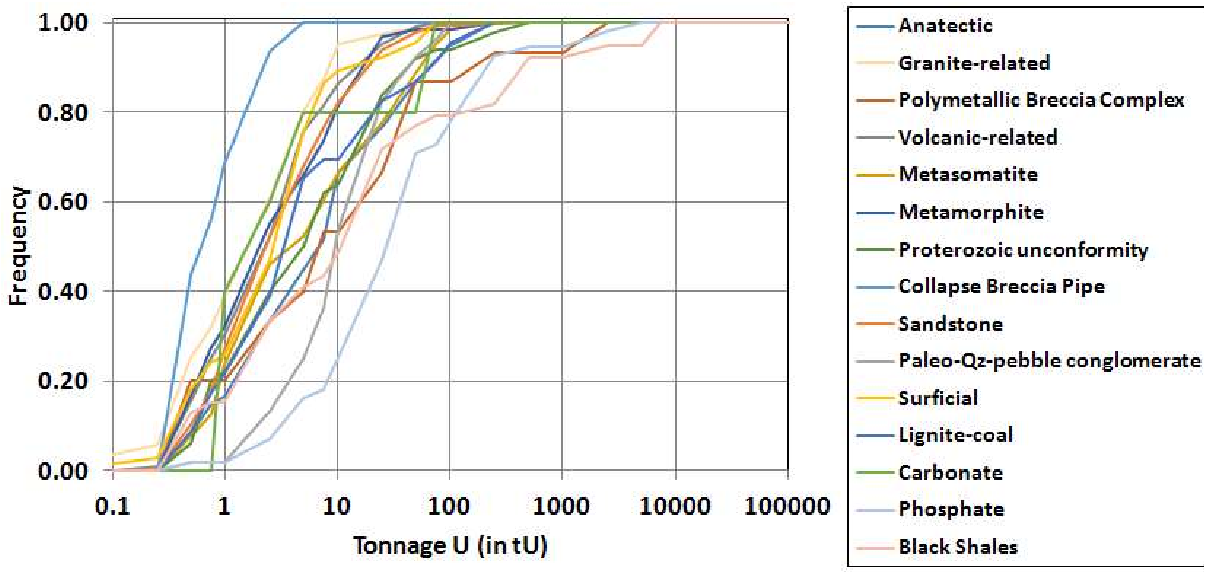

(a)

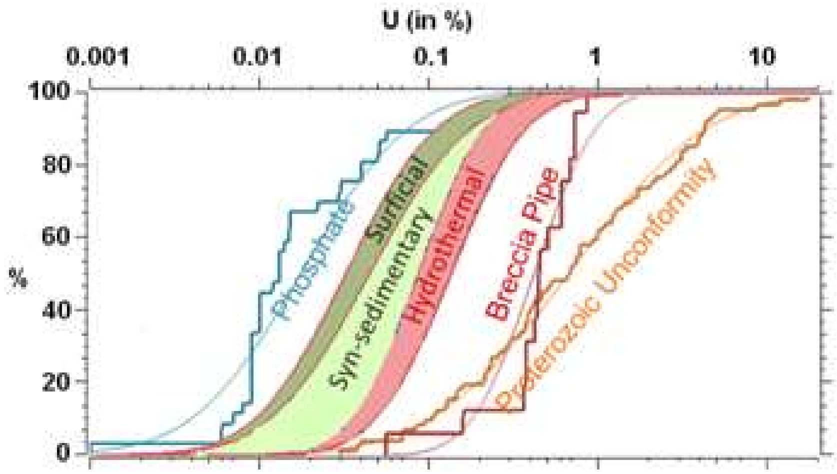

(b)

FIG. 10. (a) Frequency distributions (on log-plot) of tonnages for the 15 main types of uranium deposits. (b) Frequency distributions of grades of uranium deposits simplified into three main types and two outliers (Table 2). Frequency distributions show that all types seem to have log-normal distributions. Solid lines are the fitted theoretical log-normal distributions.

In order to build a grade-and-tonnage model, the median grade and tonnage values per uranium deposit type were represented in a log-log plot accounting for their variation range (± quartile) (Fig. 11). Tonnages, like grades, are log-normally distributed and inversely correlated with each other. This diagram clearly shows that:

- Tonnage decrease with increasing average uranium grade per deposit type according to a linear tendency in log-log plot (except for very unique huge deposits such as McArthur River and Olympic Dam, collapse breccias pipes being the richer but with the smaller tonnage, while phosphates having the lower grades but with huge tonnages);
- The log-log plot allows classifying deposit types in increasing average grades;

— For a given uranium deposit type, grade and tonnage are highly variable as indicated by variation bars (-1st qt + 3rd qt);
— Major deposit types follow a remarkable line in the log-log plot with a slope equal to about ½.

This grade/tonnage log-log linear model can be used to:

— Evaluate potential resources: in under-explored areas, if some uranium deposits of a given type are discovered, and if their representation in this diagram is not similar to those of the same type in other regions, this may indicate under-estimation of the estimate tonnage-grade values;
— Compare uranium deposits of different types, or two deposits of the same types in under-explored regions.

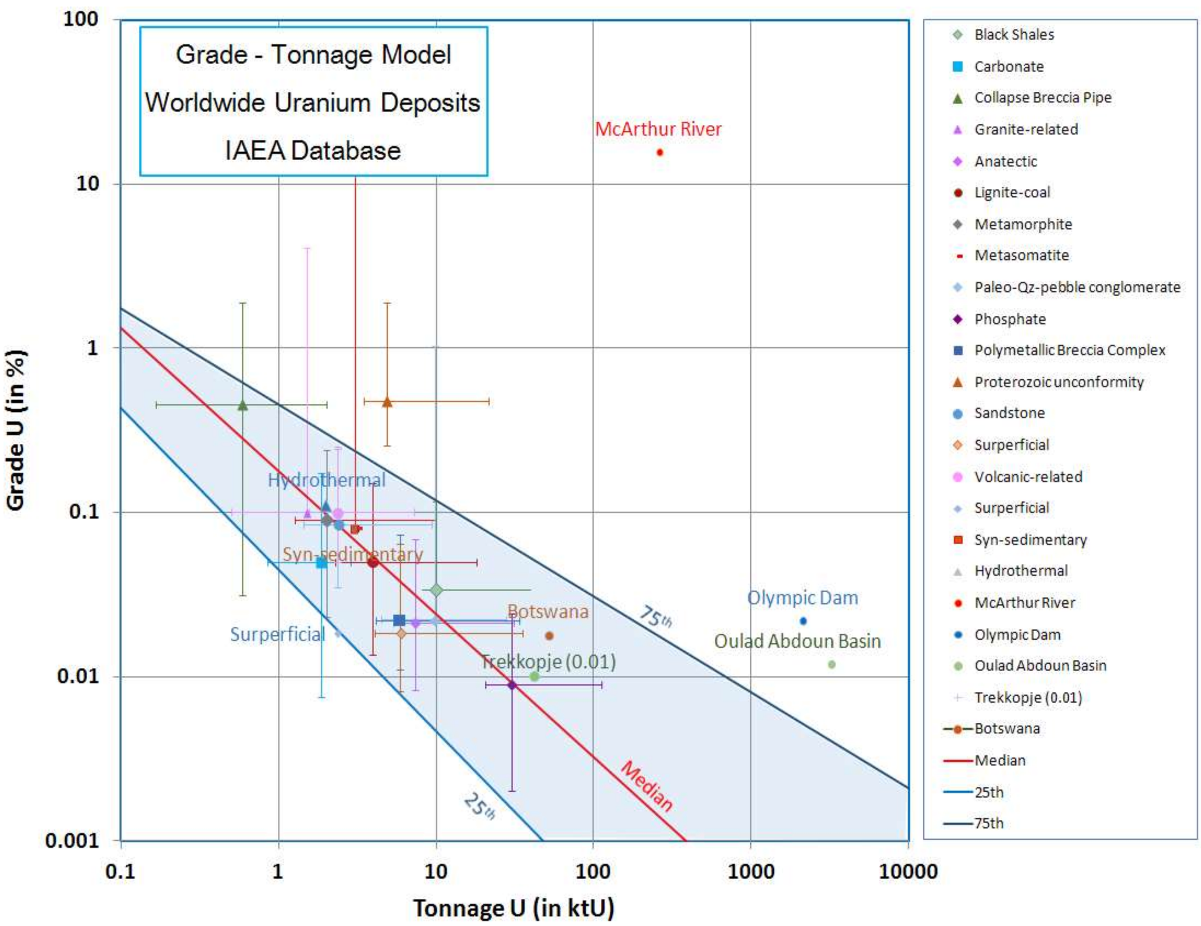

FIG. 11. Median grades vs. median tonnages, with range of variation, calculated for the 15 main types of uranium deposits showing a decreasing linear trend in a log-log plot, indicating that tonnages increase when grade decrease and vice versa. Biggest deposits like Mc Arthur River, Olympic Dam, and Oulad Abdoun Basin do not fit this general trend.

3.2.3. Interpretation of the log-log linear grade-and-tonnage model

Let Q_U be the tonnage (in t U) and U the uranium grade content (in %), the above log-log linear grade tonnage model means that there exists a linear relationship between the logarithm of these two quantities:

$$\log_{10} U + \alpha \log_{10} Q_U = \beta \quad (2)$$

where α is the negative slope of the regression line in a log-log plot (≈0.872), β=log10 U0 (≈ -0.75; U_0 = 0.178%) for a minimum tonnage of Q_0 = 1t U ($\log_{10} Q_U = 0$). This corresponds to a hypothetic small uranium deposit of 1 t U @ 0.178% U. Eq. (2) indicates that, on average, there is a relationship between the grade and the tonnage according to:

$$UQ_U^{\alpha} = U_0 Q_0^{\alpha} = 10^{\beta} \Rightarrow UQ_U^{0.872} = U_0 Q_0^{0.872} = 0.178 \Rightarrow Q_U(in\ tU) = 7.23\ U^{-1.147} \quad (3)$$

indicating that the product of grade and tonnage power 0.872 is, on average, about equal to a constant for a large number of uranium deposit types.

3.2.4. Discussion and perspectives

The grade-and-tonnage model is only valid, on average, for a collection of deposits of the same type. It was not verified if it is valid at the deposit scale. Given the very high variability of both grades and tonnages for a given type, the relationship is only approximate, but can give some indication for characterizing newly discovered deposits. The negative correlation between grades and tonnages is documented and reported by [24], [25], who suggest that this results from mixing deposit types, and seems to disappear when the relationship is tested within deposit types (i.e., within a type class). When plotting the all database in log-log grades vs. tonnages with respect to types, this negative correlation pattern seems to disappear and is highly blurred (or masked) by the number of samples that are highly variable from one type to the other (Fig. 12).

3.2.5. Most common extraction technique

Table 4 reports the yearly quantity of uranium mined according to various mining techniques including underground, in-situ leaching (ISL), open pits and by-product. ISL is the most commonly used extraction method especially for roll-front uranium types, representing 45% of the world total uranium production (Kazakhstan, Uzbekistan, Australia, US), followed by conventional underground mining (27%) and open pit (20%), by-product is only 6.6% (phosphate, coals).

TABLE 4. PRINCIPAL MODE OF PRODUCING URANIUM IN THE WORLD. IN-SITU LEACH (ISL) IS THE MOST USED EXTRACTION TECHNIQUE (MAINLY IN KAZAKHSTAN, AUSTRALIA AND US) FOLLOWED BY UNDERGROUND MINING AND OPEN-PITS

Method	tonnes U	%
Conventional underground (except Olympic Dam)*	16,324	27.9%
Conventional open pit	11,906	20.4%
In situ leach (ISL)	26,263	45.0%
By-product*	3,851	6.6%

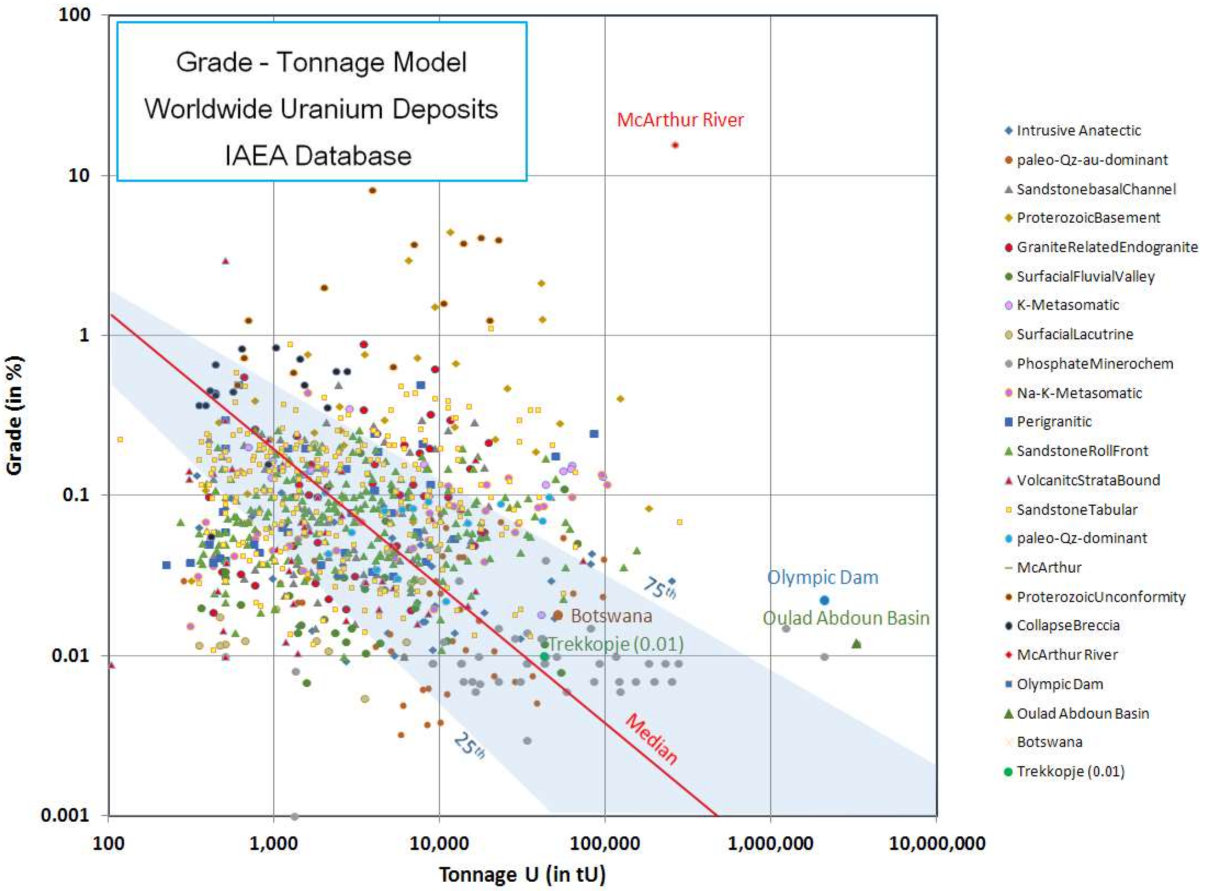

FIG. 12. Grades vs. tonnages in a log-log plot (with range of variation defined in Fig. 11) with respect to the types of uranium deposits as defined in the UDEPO database. The negative correlations between grades and tonnages are less clear on individual plot than on the average by types. Biggest deposits like Mc Arthur River, Olympic Dam, and Oulad Abdoun Basin are also plotted.

4. POTENTIAL RESOURCES EVALUATION

4.2. Methodology

Percentages (in number) of uranium deposits per type and region have been systematically calculated (Appendix Table A3), and compared to the percentage in each type of the world uranium deposits. If a region[31] presented a deficit in a given type, it can mean that (i) the regional geology is not favorable; (ii) some types are missing because not explored; or (iii) the region is under-explored. Similar frequencies are then calculated for tonnage of uranium (Appendix Table A4).

4.3. Results and discussion

Results are plotted as bar charts in order to simplify the interpretation. Bar charts showing the number of uranium deposits per region and type in percentage of the total (Fig. 13) indicate that sandstone-hosted type is mostly present in North America while granite type is more frequent in Europe than in other regions, volcanic-related is more frequent in South America, etc. The sandstone-hosted type being frequently observed in North America can be explained by the fact that huge sedimentary basins constitute a significant part of the North American geology; however, such formations are also present in other part of world not represented in these statistics. So, probably, especially in South America, Middle East, Siberia, more sandstone-hosted type uranium deposits are probably present and could be explored. The same conclusion can be accorded to Hercynian granite-related type, which is frequently observed and extensively explored in Europe but not in other parts of the world. The same conclusions can be derived from the bar charts representing the tonnage of uranium deposits per region and type in percentage of the total (Fig. 14) and number of deposits per type and continent (Fig. 15): black shale types represent huge tonnage mostly in Europe, sandstone-hosted in Asia, polymetallic breccia complex in Australia, etc.

5. CONCLUSIONS

The grade-and-tonnage model seems useful to estimate potential resources for a given deposit type but it is needed to better understand the underlying processes that led to the log-normal law (multi-stages processes?). Statistics per region and type indicate some regions with abnormal low number of deposits in some given types or missing tonnages, including brownfields with mining tradition (such as Europe) indicating that exploration should focus on this type of uranium deposits if the geological and structural settings are favorable. Currently, commodities are explored at depth. For instance, uranium has been exploited at a depth greater than 1,000 m at Beaverlodge (1,800 m) (Canada), Schwarzwalder (USA), Pribram (Check Republic), and Niederschema (in former East Germany). Presently, metasomatites are exploited at about 900 m at Streltsovka (Ukraine) and more than 1,000 m in Athabasca (Canada). In Europe, the Pyhasalmy underground polymetallic mine exploits ore from as deep as 1,400m, the same for Kupfershiefer in Poland. This is true for other commodities such as Cu-Zn at the Kidd Creek mine, which extends down to 2,927m beneath the surface in Ontario (Canada), and Ni at Sudbury (Creighton mine extending down to 2.5km). Gold is exploited in several mines at depths greater than 4,000 m in the Rand Basin in South Africa (2.4 km to more than 3.9 km below the surface by the end of 2012 at Mponeng). Most of uranium deposits in Western Europe have been exploited at a depth less than 200 m, while in the former East Germany for the same

[31] The first column is the number of deposits per region, the second column (ratio) is the ratio of the number of deposits in the region divided by the number of those observed in the World in the same type; the third column (%) is the percentage per region. If the percentage per region in one type is very different from that observed globally in the World, it may mean that the geology is not favorable, the type of deposit is unexplored in the region, the region is globally unexplored, i.e., only 6.2% of the total number of uranium deposits are located in South America; given it superficies, it may be concluded that they are more to find in South America despite it peculiar geological context.

type of deposits they have been exploited at more than 1,000 m deep. This means that from 200 m to 1000 m, there are likely significant quantities of ore remaining underground within continental Europe as demonstrated by the recent ProMine EC Project ([26], [27]). Another track for extending operational uranium extraction would be to develop advanced processing methods together with selective extractive methods (geometallurgy) to co-valorize uranium contained in polymetallic ores including phosphates (the greatest potential source of uranium as by-product), black-shales, and peralkaline polymetallic ore deposit as it has been done at Olympic Dam.

ACKNOWLEDGEMENTS

The authors of this contribution would like to express their thanks to the gOcad consortium, the ASGA and to the Centre National de Recherche Scientifique CNRS-GeoResources (UMR7359) for their support.

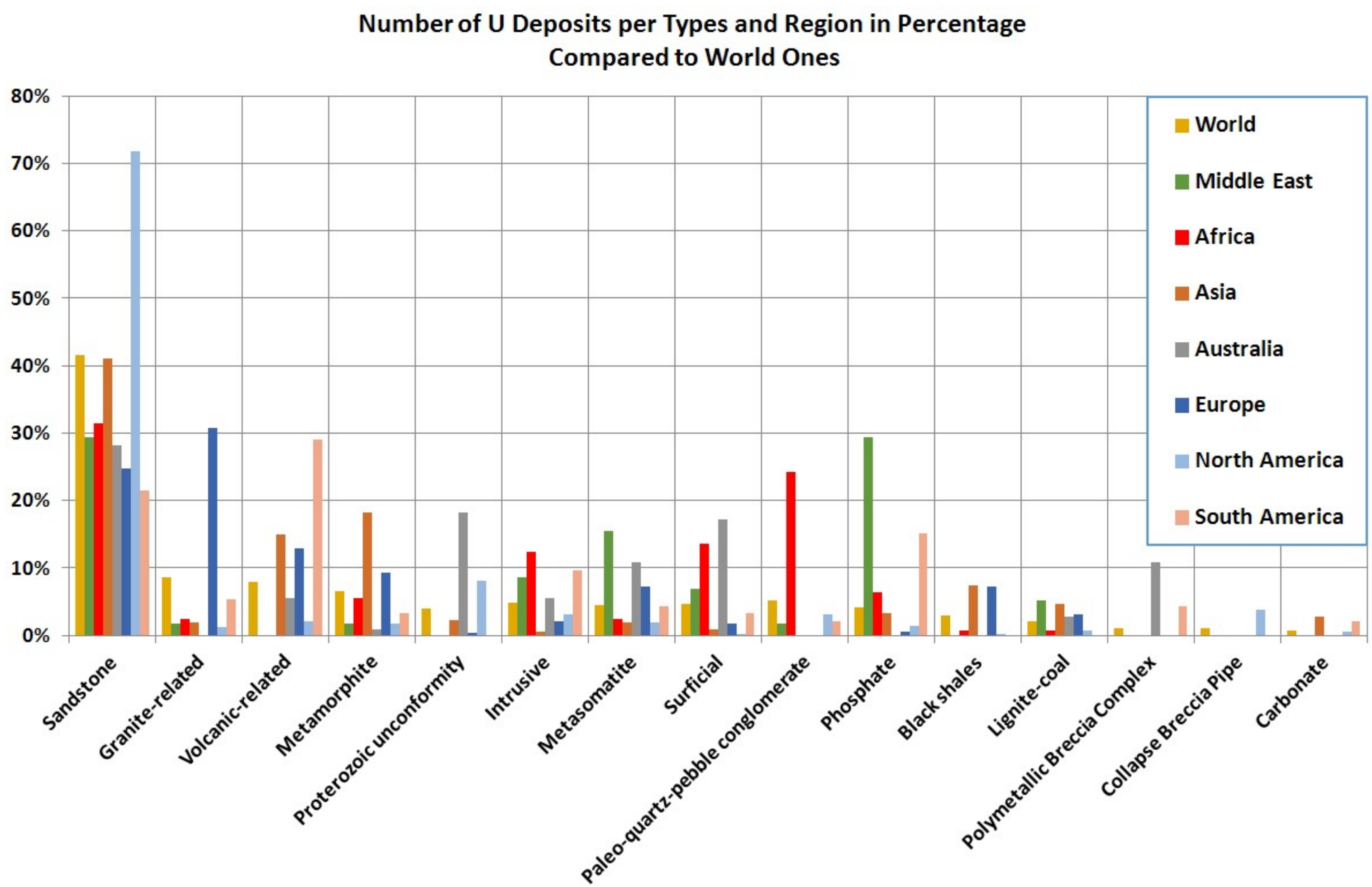

FIG. 13. Bar chart diagram showing the number of uranium deposits per region and types in percentage of the total. This shows that sandstone-hosted types are mostly present in North America, while granite-related in Europe, volcanic-related in South America, etc.

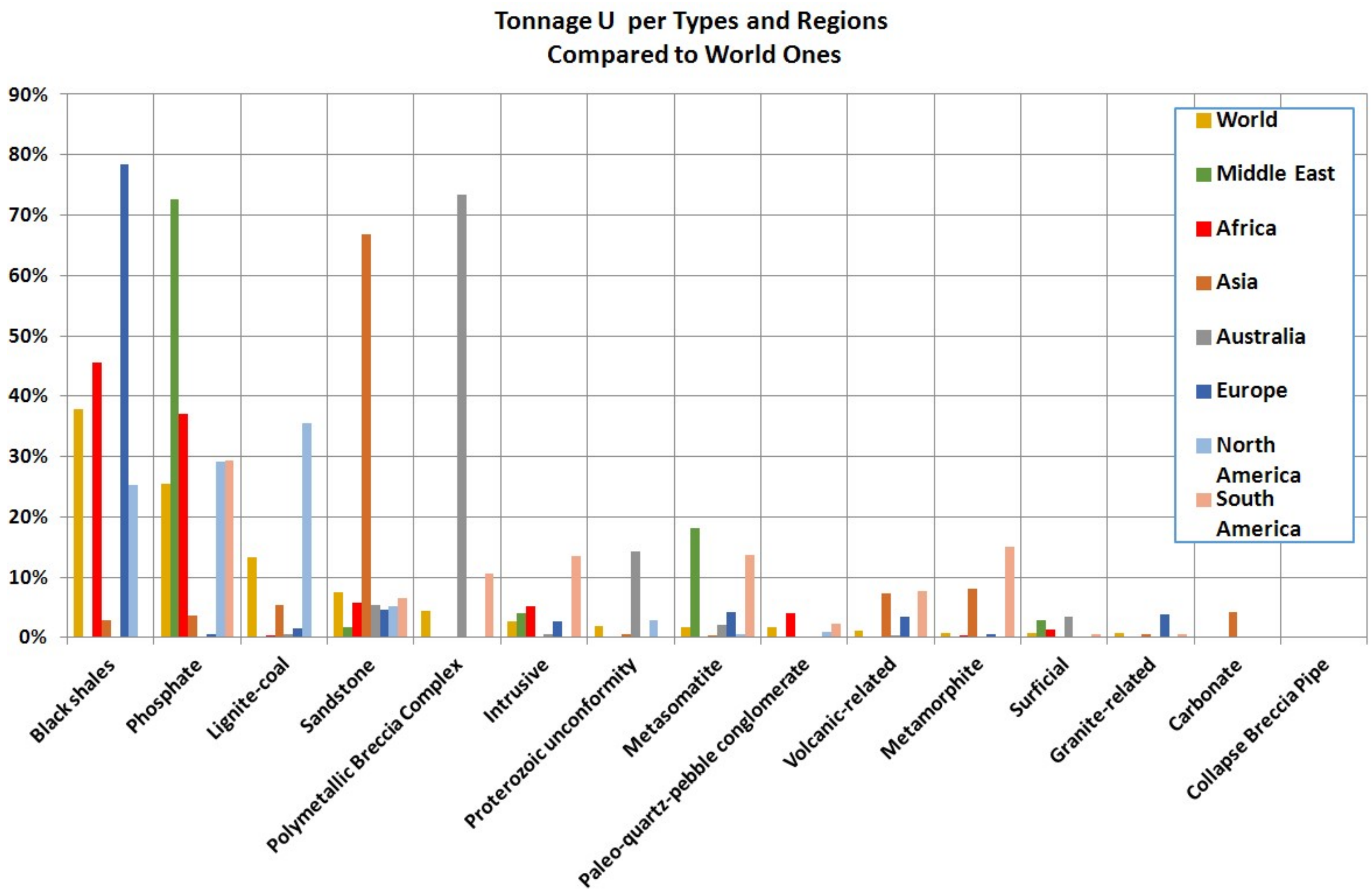

FIG. 14. Bar chart diagram showing the tonnage of uranium deposits per region and types in percentage of the total. This shows that black shales types represent huge tonnage mostly in Europe, sandstone-hosted in Asia, polymetallic breccia complex in Australia, etc.

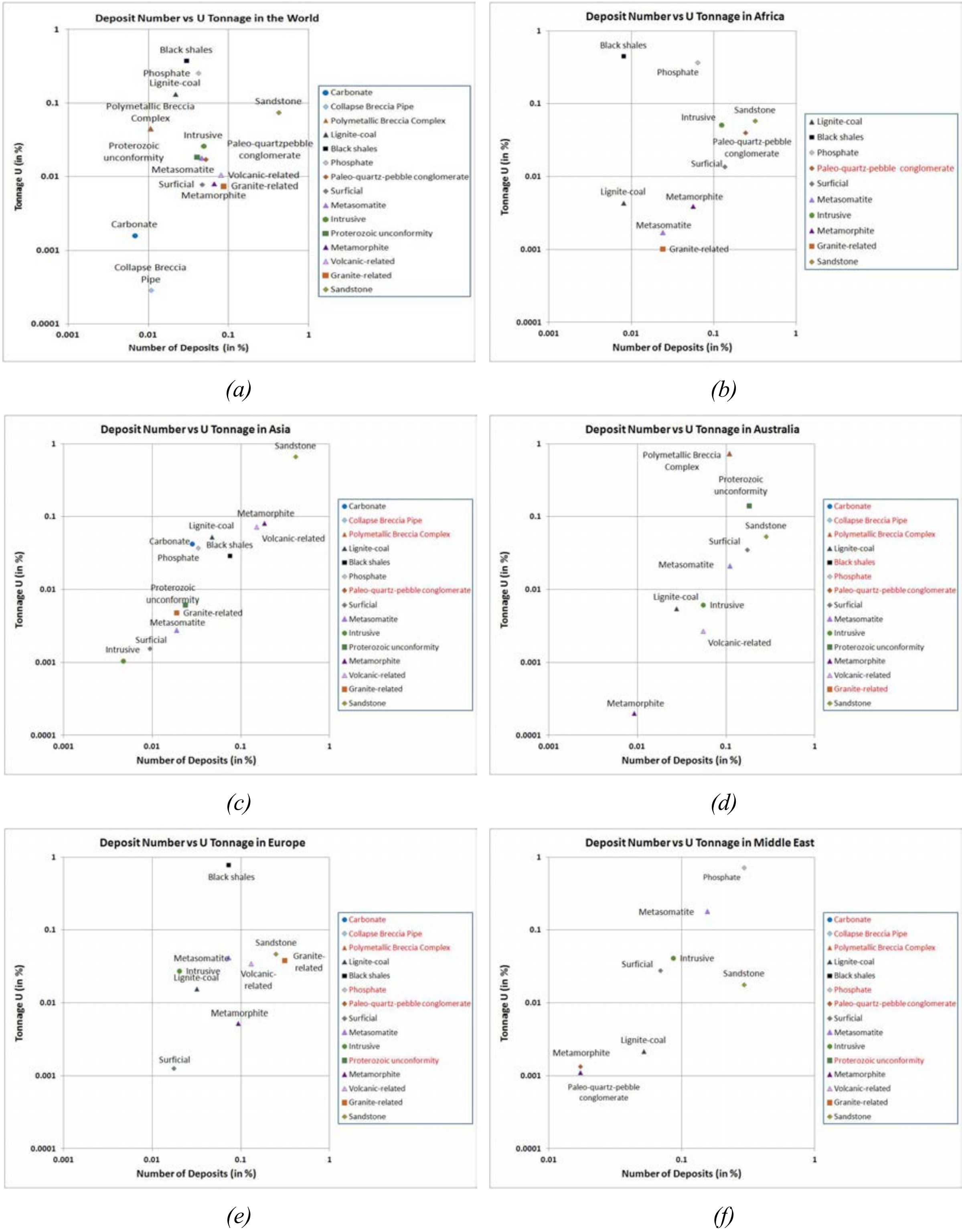

FIG. 15. Cross-plots tonnage vs. deposits number per types and continents showing under-explored or non- favorable geological contexts.

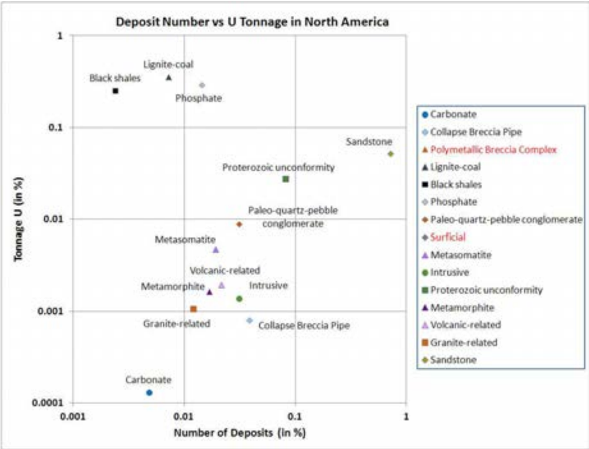

(g)

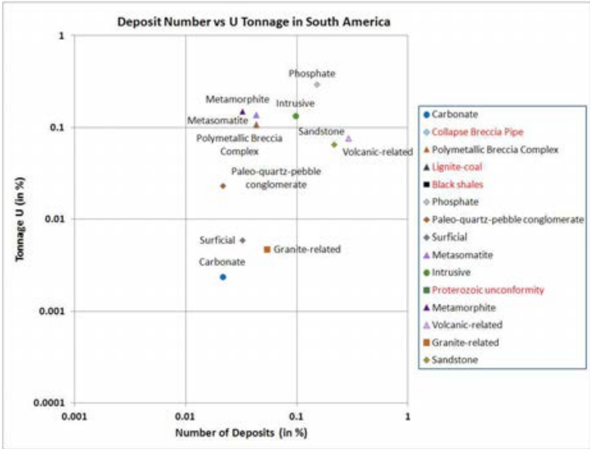

(h)

FIG. 15 (continued).

Appendix

TABLE A1. SOME BASIC STATISTIC PARAMETERS CALCULATED ON GRADE (IN %U) FOR THE 15 MAIN (AND SIMPLIFIED 3) TYPES DEPOSITS

	U Grade (in %)									
Type	*m*	*s*	*med*	*1qt*	*3qt*	*IQR*	μ	σ	med*	*n*
Anatectic	0.0443	0.0831	0.0212	0.0130	0.0475	0.0345	-3.869	1.228	0.021	60
Granite-related	0.1362	0.1413	0.1000	0.0500	0.1650	0.1150	-2.359	0.855	0.095	87
Polymetallic Breccia Complex	0.0422	0.0529	0.0220	0.0110	0.0513	0.0403	-3.636	0.971	0.026	15
Volcanic-related	0.1368	0.2903	0.1000	0.0500	0.1508	0.1008	-2.843	1.306	*0.058*	197
Metasomatite	0.0996	0.0724	0.0810	0.0530	0.1348	0.0818	-2.518	0.651	0.081	63
Metamorphite	0.1425	0.1506	0.0900	0.0670	0.1500	0.0830	-2.324	0.866	0.098	65
Proterozoic unconformity	1.6882	3.3107	0.4770	0.2205	1.4075	1.1870	-0.265	1.256	*0.767*	50
Collapse Breccia Pipe	0.4916	0.2170	0.4550	0.3700	0.6175	0.2475	-0.799	0.422	0.450	16
Sandstone	0.1183	0.1067	0.0850	0.0500	0.1600	0.1100	-2.432	0.771	0.088	540
Paleo-quartz-pebble conglomerate	0.0325	0.0275	0.0222	0.0116	0.0428	0.0312	-3.698	0.735	0.025	52
Surficial	0.0408	0.0397	0.0290	0.0145	0.0493	0.0348	-3.533	0.816	0.029	66
Lignite-coal	0.0726	0.0524	0.0500	0.0365	0.1015	0.0650	-2.833	0.648	0.059	23
Carbonate	0.0830	0.0739	0.0500	0.0425	0.1235	0.0810	-2.780	0.764	0.062	5
Phosphate	0.0295	0.0556	0.0090	0.0070	0.0150	0.0080	-4.278	1.230	*0.014*	55
Black Shales	0.0507	0.0372	0.0340	0.0188	0.0825	0.0638	-3.196	0.656	0.041	39
Superficial (14+11+3+1)[1]	**0.0389**	**0.0609**	**0.0184**	**0.0103**	**0.0455**	**0.0353**	**-3.868**	**1.114**	**0.021**	**196**
Syn-sedimentary (15+13+12+10+9+5)	**0.1035**	**0.0991**	**0.0790**	**0.0400**	**0.1400**	**0.1000**	**-2.593**	**0.807**	**0.075**	**757**
Hydrothermal (2+4+6+7+8)	**0.3872**	**1.4002**	**0.1100**	**0.0600**	**0.2293**	**0.1693**	**-2.271**	**1.626**	**0.103**	**321**

m, s, med, 1qt, 3qt, IQR are, respectively average, standard deviation, median, first and third quartile and inter quartile range calculated on grades; μ, σ are, respectively, mean and standard deviation on the adjusted log-normal distribution; ***n*** = number of samples. 1 Numbers in brackets correspond to the type of deposits defined in Table 1. In column med*, the median is recalculated as **med*** = exp(μ) from the mean μ of the log-normal distribution. It can be observed a good agreement between the experimental median and med* on quite all types (with some reserves for volcanic-related, Proterozoic unconformity, and phosphate), indicating that grades distribution can be approximated by a log-normal distribution.

TABLE A2. SOME BASIC STATISTIC PARAMETERS CALCULATED ON TONNAGE (KT U) FOR THE 15 MAIN (AND SIMPLIFIED THREE) TYPES DEPOSITS

	Tonnage U (in kt U)									
Type	*m*	*s*	*med*	*1qt*	*3qt*	*IQR*	μ	σ	med*	*n*
Anatectic	23.007	41.754	7.345	1.960	23.914	21.954	2.407	1.207	*11.1*	60
Granite-related	4.181	10.460	1.500	0.505	3.989	3.484	0.439	1.408	1.55	87
Polymetallic Breccia Complex	162.493	541.091	5.850	1.692	28.044	26.352	3.845	1.579	*46.76*	15
Volcanic-related	5.577	9.744	2.350	0.797	4.925	4.128	1.019	1.183	2.77	197
Metasomatite	15.581	24.838	3.070	1.115	18.313	17.198	2.114	1.125	*8.28*	63
Metamorphite	6.623	15.646	2.000	0.735	7.890	7.155	0.948	1.373	2.58	65
Proterozoic unconformity	20.253	46.475	4.861	1.415	16.588	15.173	2.091	1.355	*8.09*	50
Collapse Breccia Pipe	0.991	0.771	0.589	0.424	1.425	1.001	-0.246	0.688	0.78	16
Sandstone	7.147	17.279	2.382	0.950	6.939	5.989	1.005	1.387	2.73	540
Paleo-quartz-pebble conglomerate	16.820	20.980	9.858	5.401	17.971	12.571	2.353	0.969	10.51	52
Surficial	6.541	13.123	2.624	1.005	4.698	3.693	1.071	1.271	2.92	66
Lignite-coal	15.998	27.881	3.977	1.670	14.026	12.356	2.075	1.181	*7.96*	23
Carbonate	15.674	31.494	1.850	0.975	2.570	1.595	1.944	1.272	*6.99*	5
Phosphate	165.993	524.309	30.000	9.585	81.500	71.915	3.914	1.548	*50.1*	55
Black Shales	407.598	1,371.341	10.010	1.919	29.373	27.454	4.755	1.585	*116.2*	39
Superficial (14+11+3+1)[1]	**68.261**	**320.979**	**5.925**	**1.827**	**29.625**	**27.798**	**2.653**	**1.772**	***14.2***	**196**
Syn-sedimentary (15+13+12+10+9+5)	**31.128**	**321.993**	**3.000**	**1.094**	**10.033**	**8.939**	**1.097**	**2.164**	**3.00**	**757**
Hydrothermal (2+4+6+7+8)	**7.468**	**21.708**	**2.000**	**0.654**	**6.000**	**5.346**	**0.888**	**1.499**	**2.4**	**321**

m, s, med, 1qt, 3qt, IQR are, respectively average, standard deviation, median, first and third quartile and inter quartile range calculated on grades; μ, σ are, respectively, mean and standard deviation on the adjusted log-normal distribution; ***n*** = number of samples. 1 Numbers in brackets correspond to the type of deposits defined in Table 1. In column med*, the median is recalculated as **med*** = exp(μ) from the mean μ of the log-normal distribution. It can be observed a good agreement between the experimental median and med* on quite all types (with some reserves for volcanic-related, Proterozoic unconformity, and phosphate), indicating that grades distribution can be approximated by a log-normal distribution.

TABLE A3. PERCENTAGES IN UMBER OF U DEPOSITS EVALUATED PER REGIONS AND TYPES

	World		Africa			Asia			Australia			Europe			Middle East			North America			South America		
Type	**World**	**%**	**Africa**	**Ratio**	**%**	**Asia**	**Ratio**	**%**	**Australia**	**Ratio**	**%**	**Europe**	**Ratio**	**%**	**Middle East**	**Ratio**	**%**	**orth Americ**	**Ratio**	**%**	**uth Ameri**	**Ratio**	**%**
Sandstone	621	41.6%	79	12.7%	31.5%	88	14.2%	41.1%	31	5.0%	28.2%	86	13.8%	24.8%	17	2.7%	29.3%	300	48.3%	71.8%	20	3.2%	21.5%
Granite-related	128	8.6%	6	4.7%	2.4%	4	3.1%	1.9%	-	-	-	107	83.6%	30.8%	1	0.8%	1.7%	5	3.9%	1.2%	5	3.9%	5.4%
Volcanic-related	119	8.0%	-	-	-	32	26.9%	15.0%	6	5.0%	5.5%	45	37.8%	13.0%	-	-	-	9	7.6%	2.2%	27	22.7%	29.0%
Metamorphite	97	6.5%	14	14.4%	5.6%	39	40.2%	18.2%	1	1.0%	0.9%	32	33.0%	9.2%	1	1.0%	1.7%	7	7.2%	1.7%	3	3.1%	3.2%
Proterozoic unconformity	60	4.0%	-	-	-	5	8.3%	2.3%	20	33.3%	18.2%	1	1.7%	0.3%	-	-	-	34	56.7%	8.1%	-	-	-
Intrusive	72	4.8%	31	43.1%	12.4%	1	1.4%	0.5%	6	8.3%	5.5%	7	9.7%	2.0%	5	6.9%	8.6%	13	18.1%	3.1%	9	12.5%	9.7%
Metasomatite	68	4.6%	6	8.8%	2.4%	4	5.9%	1.9%	12	17.6%	10.9%	25	36.8%	7.2%	9	13.2%	15.5%	8	11.8%	1.9%	4	5.9%	4.3%
Surficial	69	4.6%	34	49.3%	13.5%	2	2.9%	0.9%	19	27.5%	17.3%	6	8.7%	1.7%	4	5.8%	6.9%	1	1.4%	0.2%	3	4.3%	3.2%
Paleo-quartz-pebble conglomerate	77	5.2%	61	79.2%	24.3%	-	-	-	-	-	-	-	-	-	1	1.3%	1.7%	13	16.9%	3.1%	2	2.6%	2.2%
Phosphate	62	4.2%	16	25.8%	6.4%	7	11.3%	3.3%	-	-	-	2	3.2%	0.6%	17	27.4%	29.3%	6	9.7%	1.4%	14	22.6%	15.1%
Black shales	44	3.0%	2	4.5%	0.8%	16	36.4%	7.5%	-	-	-	25	56.8%	7.2%	-	-	-	1	2.3%	0.2%	-	-	-
Lignite-coal	32	2.1%	2	6.3%	0.8%	10	31.3%	4.7%	3	9.4%	2.7%	11	34.4%	3.2%	3	9.4%	5.2%	3	9.4%	0.7%	-	-	-
Polymetallic Breccia Complex	16	1.1%	-	-	-	-	-	-	12	75.0%	10.9%	-	-	-	-	-	-	-	-	-	4	25.0%	4.3%
Collapse Breccia Pipe	16	1.1%	-	-	-	-	-	-	-	-	-	-	-	-	-	-	-	16	100.0%	3.8%	-	-	-
Carbonate	10	0.7%	-	-	-	6	60.0%	2.8%	-	-	-	-	-	-	-	-	-	2	20.0%	0.5%	2	20.0%	2.2%
Total	**1,491**		**251**	**16.8%**		**214**	**14.4%**		**110**	**7.4%**		**347**	**23.3%**		**58**	**3.9%**		**418**	**28.0%**		**93**	**6.2%**	

TABLE A4. PERCENTAGES IN TONNAGE OF U DEPOSITS EVALUATED PER REGIONS AND TYPES

Tonnage	**World**		**Africa**			**Asia**			**Australia**			**Europe**			**Middle East**			**North America**			**South America**		
Type	**tU**	**%**	**tU**	**Ratio**	**%**	**tU**	**Ratio**	**%**	**tU**	**Ratio**	**%**	**tU**	**Ratio**	**%**	**tU**	**Ratio**	**%**	**tU**	**Ratio**	**%**	**tU**	**Ratio**	**%**
Black shales	20,898,573	37.8%	8,500,000	40.7%	**45.5%**	57,673	0.3%	**2.9%**	-	-	-	7,340,900	35.1%	**78.4%**	-	-	-	5,000,000	23.9%	**25.3%**	-	-	-
Phosphate	14,145,585	25.6%	6,904,400	48.8%	**37.0%**	73,400	0.5%	**3.7%**	-	-	-	42,800	0.3%	**0.5%**	1,119,740	7.9%	**72.7%**	5,765,000	40.8%	**29.2%**	240,245	1.7%	**29.4%**
Lignite-coal	7,367,944	13.3%	81,920	1.1%	**0.4%**	105,000	1.4%	**5.3%**	17,842	0.2%	**0.6%**	145,857	2.0%	**1.6%**	3,380	0.0%	**0.2%**	7,013,945	95.2%	**35.5%**	-	-	-
Sandstone	4,128,498	7.5%	1,085,209	26.3%	**5.8%**	1,322,317	32.0%	**66.8%**	170,556	4.1%	**5.3%**	440,265	10.7%	**4.7%**	27,392	0.7%	**1.8%**	1,029,172	24.9%	**5.2%**	53,587	1.3%	**6.6%**
Polymetallic Breccia Complex	2,438,773	4.4%	-	-	-	-	-	-	2,351,398	96.4%	**73.4%**	-	-	-	-	-	-	-	-	-	87,375	3.6%	**10.7%**
Intrusive	1,433,057	2.6%	954,831	66.6%	**5.1%**	2,100	0.1%	**0.1%**	19,908	1.4%	**0.6%**	256,057	17.9%	**2.7%**	63,155	4.4%	**4.1%**	27,478	1.9%	**0.1%**	109,528	7.6%	**13.4%**
Proterozoic unconformity	1,016,165	1.8%	-	-	-	12,320	1.2%	**0.6%**	455,375	44.8%	**14.2%**	-	-	-	-	-	-	548,470	54.0%	**2.8%**	-	-	-
Metasomatite	984,474	1.8%	32,450	3.3%	**0.2%**	5,566	0.6%	**0.3%**	67,396	6.8%	**2.1%**	392,253	39.8%	**4.2%**	280,747	28.5%	**18.2%**	93,912	9.5%	**0.5%**	112,150	11.4%	**13.7%**
Paleo-quartz-pebble conglomerate	948,598	1.7%	753,053	79.4%	**4.0%**	-	-	-	-	-	-	-	-	-	2,090	0.2%	**0.1%**	174,455	18.4%	**0.9%**	19,000	2.0%	**2.3%**
Volcanic-related	578,937	1.0%	-	-	-	142,975	24.7%	**7.2%**	8,767	1.5%	**0.3%**	325,887	56.3%	**3.5%**	-	-	-	38,752	6.7%	**0.2%**	62,556	10.8%	**7.7%**
Metamorphite	442,893	0.8%	73,812	16.7%	**0.4%**	161,777	36.5%	**8.2%**	650	0.1%	**0.0%**	49,990	11.3%	**0.5%**	1,729	0.4%	**0.1%**	32,705	7.4%	**0.2%**	122,230	27.6%	**15.0%**
Surficial	432,029	0.8%	256,099	59.3%	**1.4%**	3,114	0.7%	**0.2%**	112,569	26.1%	**3.5%**	12,010	2.8%	**0.1%**	42,860	9.9%	**2.8%**	450	0.1%	**0.0%**	4,927	1.1%	**0.6%**
Granite-related	413,922	0.7%	19,074	4.6%	**0.1%**	9,591	2.3%	**0.5%**	-	-	-	360,305	87.0%	**3.8%**	-	-	-	21,052	5.1%	**0.1%**	3,900	0.9%	**0.5%**
Carbonate	88,370	0.2%	-	-	-	83,850	94.9%	**4.2%**	-	-	-	-	-	-	-	-	-	2,570	2.9%	**0.0%**	1,950	2.2%	**0.2%**
Collapse Breccia Pipe	15,850	0.0%	-	-	-	-	-	-	-	-	-	-	-	-	-	-	-	15,850	100.0%	**0.1%**	-	-	-
Total	**55,333,668**		**18,660,848**	**33.7%**		**1,979,683**			**3,204,461**			**9,366,324**			**1,541,093**			**19,763,811**			**817,448**		

REFERENCES

[1] MENDELEVITCH, R., DANG, T.T., Nuclear Power and the Uranium Market: Are reserves and resources sufficient? Deutsches Institut für Wirtschaftsforschung, Berlin, Diw Roundup, 98, 15p (2016).

[2] IAEA, Uranium 2014: Resources, Production and Demand. Nuclear Energy Agency (NEA) Report nº 7209, OECD, Vienna, 508p (2014).

[3] OECD-NEA and IAEA, Uranium 2014: resources, Production and Demand. NEA No. 7209, OECD Nuclear Energy Agency, Paris, France. 508p (https://www.oecdnea.org/ndd/pubs/2014/7209-uranium-2014.pdf) (2014).

[4] OECD-NEA, "Forty Years of Uranium Resources, Production and Demand in Perspective." Paris (https://www.oecd-nea.org/ndd/pubs/2006/6096-40-years-uranium.pdf) (2006).

[5] ROONEY, M., NUTTALL, W.J., KAZANTZIS, N., A dynamic model of the global uranium market and the nuclear fuel cycle, Resources Policy. 43, 50-60 (2015).

[6] MONNET, A., GABRIEL, S, PERCEBOIS, J., Statistical model of global uranium resources and long-term availability. Proc. of Global 2015, Sep. 20-24, Paris (France), paper 5309, 12p (2015).

[7] HARBAUGH, J.W., DAVIS, J.C., WENDEBOURG, J., Computing risk for oil prospects: Principles and programs. Computer Methods in the Geosciences, vol. 14, 452p (1995).

[8] BONHAM-CARTER, G.F., Geographic Information Systems for Geoscientists: modeling with GIS. Computer Methods in the Geosciences. Pergamon, New York, 414p (1994).

[9] SINGER, D.A., Progress in integrated quantitative mineral resource assessments. Ore Geology Reviews 38, 242-250 (2010).

[10] DAS, S., LEE, R., A computerized system to estimate potential uranium resources. Resources and Energy, 13, 201-215 (1991).

[11] JAIRETH, S., HUSTON, D., Metal endowment of craton, terranes and districts: insights from a quantitative analysis of regions with giant and super-giant deposits. Ore Geology Reviews, 38, 288-303 (2010).

[12] CUNEY, M., The extreme diversity of uranium deposits. Mineralium Deposita, 44, 3-9 (2009).

[13] CUNEY, M., Chapter 15: Uranium and thorium resources and the sustainability of nuclear energy. Mineralogical Association of Canada Short Course 43, Winnipeg MB, May 2013, 417-437 (2013).

[14] DAHLKAMP, F.J., Classification of uranium deposits. Miner. Deposita, 13, 83-104 (1978).

[15] BRUNETON, P., CUNEY M., DAHLKAMP, F., ZALUSKI, G., IAEA geological classification of uranium deposits. URAM 2014, IAEA Vienna (2014).

[16] IAEA, World Distribution of Uranium Deposits (UDEPO) with Uranium Deposit Classification, Vienna, IAEA-Tecdoc-1629, INTERNATIONAL ATOMIC ENERGY AGENCY (IAEA), 126p (2009).

[17] YUHUI, P., Metallogenesis of Devonian-Carboniferous strata-bound carbonate-type uranium deposits in south China. Chinese Journal of Geochemistry, 9 (3), 264-274 (1990).

[18] MOSIER, D.L., Grade and tonnage model of unconformity U-Au, in "Mineral Deposit Models" (Cox, D.P. and Singer, D.A., Eds.), U.S. Geological Survey Bulletin 1693, 249-250 (1986).

[19] MCCAMMON, R.B., BRISKEY, Jr. J.A., A proposed national mineral-resource assessment. Nonrenewable Resources 1(4), 259-266 (1992).

[20] MCCAMMON, R.B., FINCH, W., The deposit size frequency method for estimating undiscovered uranium deposits. Nonrenewable Resources 2(2), 106-112 (1993).
[21] FINCH, W.I., SHEN, F., CHEN, Z., MCCAMMON, R.B., Descriptive models of major Uranium deposits in China. Nonrenewable Resources. 2(l), 39-48 (1993).
[22] AITCHISON, J., BROWN, J.A.C., The lognormal distribution with special reference to its use in economic. Cambridge University Press, London, 194p (1957).
[23] SINGER, D.A., The lognormal distribution of metal resources in mineral deposits. Ore Geology Reviews, 55, 80-86 (2013).
[24] SINGER, D.A., MENZIE, W.D., Quantitative Mineral Resource Assessments – An Integrated Approach, Oxford University Press, New York, 219p (2010).
[25] CHENG, Q., Non-linear theory and power-law models for information integration and mineral resources quantitative assessments. in Bonham-Carter, G.F., Cheng, Q. (eds.), Progress in Geomathematics, Springer-Verlag Berlin Heidelberg, 1995-225 (2008).
[26] ROYER, J.J., MEJÍA, P., CAUMON, G., COLLON, P., 3 and 4D Geomodeling Applied to Mineral Resources Exploration – An Introduction. Ch 4, in P. Weihed (ed.), 3D, 4D and Predictive Modeling of Major Mineral Belts in Europe, Mineral Resource Reviews, Springer Int. Pub. Switzerland, 73-89 (2015).
[27] MEJÍA, P., ROYER, J.-J., FRABOULET, J.-G., ZIELIŃSKA, A., 4D Geomodeling: A Tool for Exploration – The Kupferschiefer in the Lubin Region, Poland. Springer Int. Pub., Switzerland, in Weihed, P. (ed.), 3D, 4D and Predictive Modeling of Major Mineral Belts in Europe, Mineral Resource Reviews, Ch. 8, 163-187 (2015).

STATISTICAL DISTRIBUTION OF THE URANIUM RESOURCES IN THE VARISCAN HYDROTHERMAL URANIUM DEPOSITS OF WESTERN EUROPE

J.-J. ROYER
Université de Lorraine,
CNRS-GeoRessources (UMR7359),
ENSG, gOcad-ASGA,

M. CUNEY
Université de Lorraine,
CNRS-GéoRessources (UMR 7359),
CREGU,

Vandoeuvre-lès-Nancy, France

Abstract

A database of European granite-related uranium deposits containing the average grade and resources for individual ore deposits has been constituted from the resources declared by the countries available in the literature and in the UDEPO website of the IAEA. This database was used to evaluate the statistical distribution of deposit size and grade and of the total uranium resources per region. It is shown that most deposits sizes expressed as their uranium content (in t U) are distributed according to a log-uniform distribution. However, the smallest deposits in France and Spain/Portugal fall off this general pattern, together with the largest uranium deposit known in Europe, the Niederschlema deposit, located in south-eastern Germany. These smallest outliers correspond to near surface or skimmed deposits, while the biggest Niederschlema deposit was mined down to a depth of up to five times deeper than most other uranium deposits known in Europe because their mining was not driven by the same economic constraints. It is observed that the total resources defined as the cumulative resources of deposits ranked in increasing size are also log-uniform distributed. Experimental distributions are fit to theoretical log- uniform laws in order to predict the expected largest deposit and the expected total resources in Europe. This statistical approach shows that additional undiscovered uranium resources estimated to be over 40,000 t U can be expected in Europe, and probably more if deposits are mined to depths greater than 400 m.

1. INTRODUCTION

The European Variscan belt, which extends from the south-western part of the Iberian Peninsula to central Europe, resulted from the collision between the Gondwana and Eurasian continents [1]. During the late stage of the collision, the crustal thickening led to partial melting of the crust and the generation of a series of uranium-enriched peraluminous leucogranites. A large part of the uranium resources within Europe occur as granite-related uranium deposits, occurring as veins or disseminations (the so called “epi-syenites”) hosted by either these granites, especially in France, or the surrounding metamorphic rocks, especially in the south-eastern part of Germany and the Czech Republic, as well as a major part of the deposits of Spain and Portugal (Fig. 1) [2]. These deposits resulted from hydrothermal circulations related to the post-orogenic Permian extension [3, 4]), although other hypotheses have been proposed especially for the Spanish and Portuguese deposits.

The database used for the European granite-related uranium deposits containing the average grade and the uranium content was derived from the UDEPO website developed by the IAEA (http://www-nfcis.iaea.org). This database has been constituted from the resources declared by countries and available in the literature and websites. The database was used in this study to analyze the statistical distribution of the uranium resources and grades in the different European ore districts and to predict the undiscovered potential uranium resources in Europe for granite-related uranium deposits.

2. DATABASE

The database was constituted from a collection of more than 275 granite-related uranium deposits of Europe, mainly from the Iberian Peninsula (Portugal and Spain), France, Germany, and Bulgaria to the Czech Republic. The database contains per deposit its name, location, uranium grade (in % U), total metal content (in t U), and ore tonnage (in Mt).

For each country, the deposits have been ranked in increasing order according to their metal content in order to build the metal content frequency cumulative distribution $F_Q(q)$. Similarly, the cumulative metal content, (also referred as the "cumulative total ore resources (in t U)") frequency distribution curve $F_R(r)$ has been estimated. This $F_R(r)$ is useful to estimate the probability $P(R>r)$ for a given region to have metal resources greater than a given cut-off value r as $P(R>r) = 1- F_R(r)$.

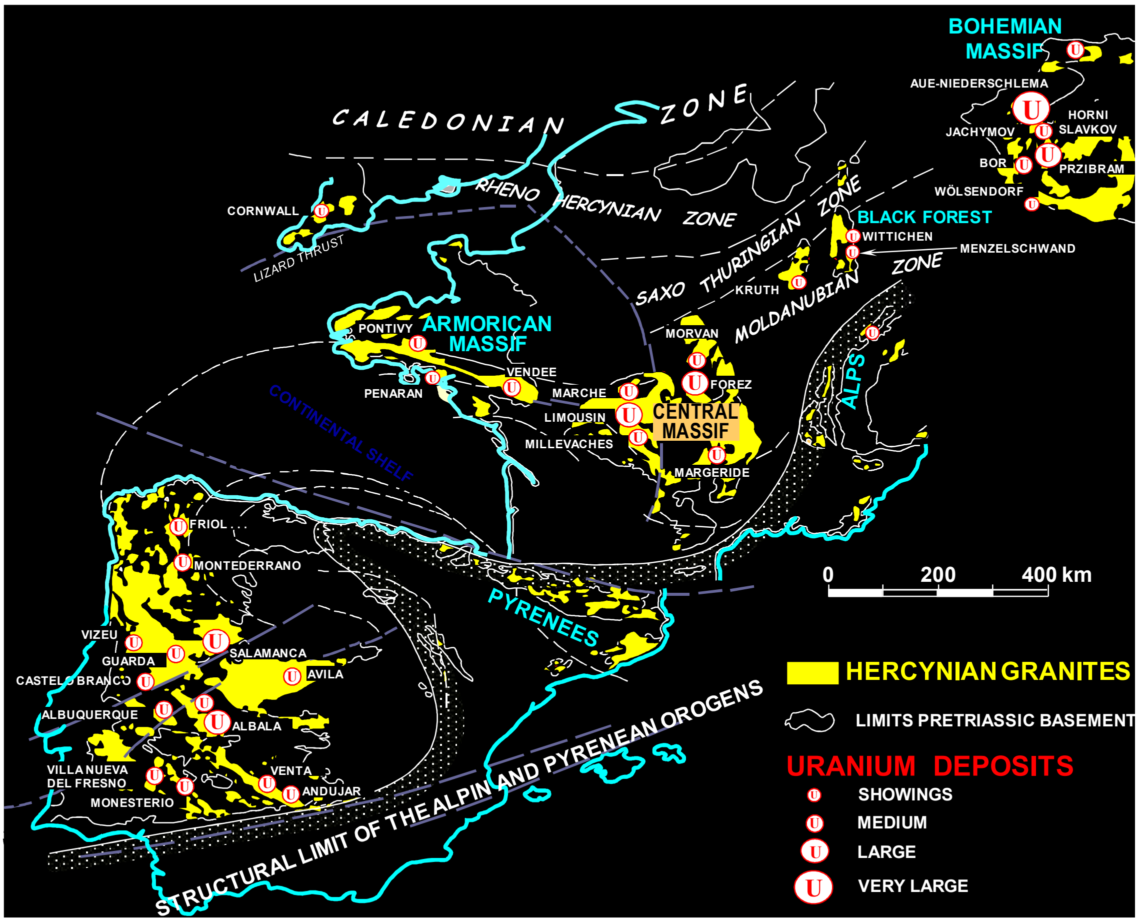

FIG. 1. Distribution of granite-related uranium deposits and the Variscan granites in the European Variscan Belt (modified from [2]).

The data on uranium resources from granite-related deposits, which were used in this work, correspond to previously mined deposits[32]. Most of the Variscan hydrothermal uranium

[32] Mainly extracted from the UDEPO which is constantly updated; thus, some values on resources in UDEPO might have been changed since the end of this study.

deposits have grades ranging from 0.1 to 0.5 % U and tonnages from 1,000 to 10,000 t U (Fig. 2). The Spanish deposits tend to have the lowest grades, as in Bulgaria, whereas deposits of the Czech Republic and France have the highest grades. The smallest deposits (below 1,000 t U) are mostly found in France, Bulgaria (except the Bukhovo District with 10,000 t U), Spain and Portugal. The Niederschlema deposit in East Germany, which has been mined down to a depth of 2,000 m, is one order of magnitude larger than other deposits, like Rozna and Pribram in the Czech Republic (exploited down to over 1,000 m). In Spain and Portugal, the deposits have been mined at shallower levels (less than 100 m for most of them) corresponding to the oxidized weathering zone and possibly explaining the observed lower grades. In France, mining has not exceeded 400 m despite the occurrence of deeper resources as shown by drillings, for example at the Bernardan deposit.

Germany has the largest already mined resources of uranium (144,000 t U) associated with granites followed by the Czech Republic (98,500 t U), France (64,500 t U), Iberian Peninsula (43,680 t U) and finally Bulgaria (14,600 t U). However, the uranium resources from Germany and the Czech Republic (242,500 t U cumulated) have been mined from a much smaller area (Erzgebirge + Northern part of the Bohemian Massif) compared to the area covered by the French Massif Central, Morvan and Brittany in France, and the western part of Spain and Portugal in the Iberian Peninsula.

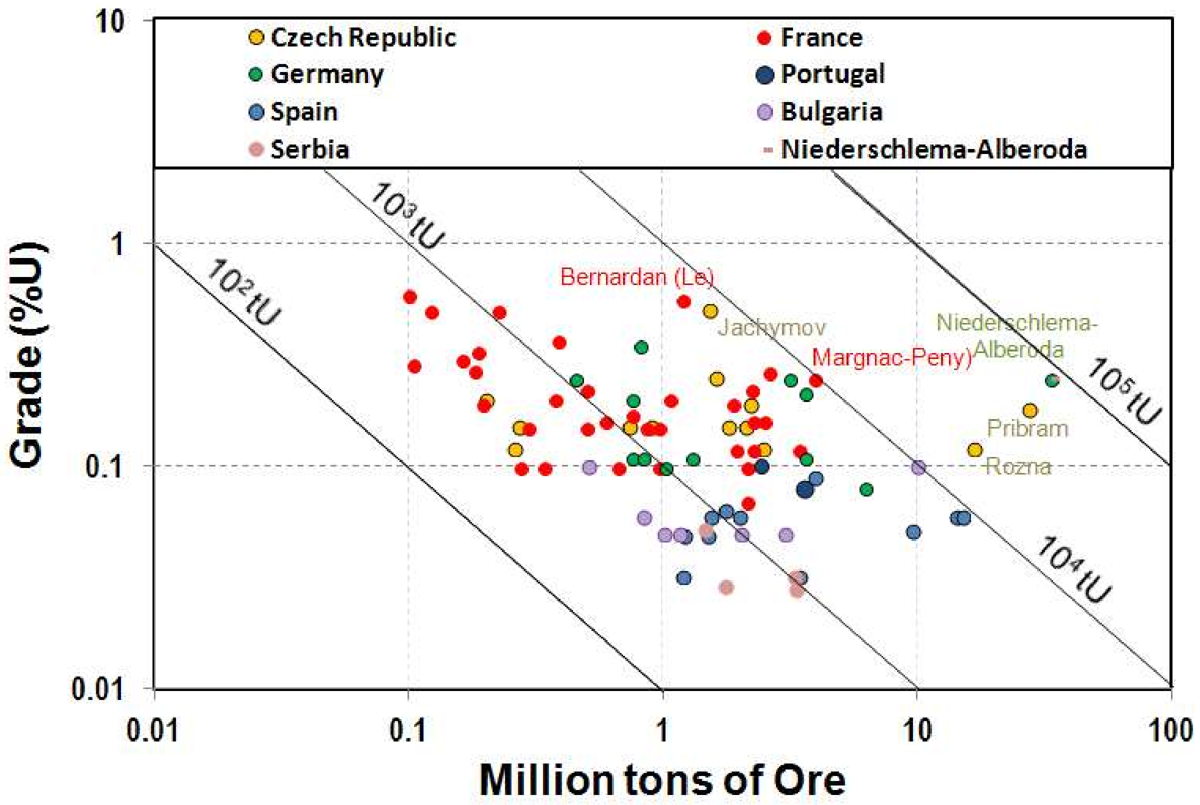

FIG. 2. Distribution of ore tonnage versus ore grade for the European granite-related uranium deposits.

3. DEPOSIT SIZE DISTRIBUTION

The cumulative frequency curves of the uranium content have been calculated and displayed in a log-uniform plot per mineral district, mainly France, German Erzgebirge, Iberian Peninsula, and for the total (Fig. 3). The curves exhibit a remarkable linear trend in a log-uniform plot except for the extraordinary large deposit of Niederschlema-Alberoda in Germany, and Pribram and Rozna in the Czech Republic (see details in Table 1). This linear trend observed for all districts shows that the cumulative distribution function $F_Q(q)$ of the deposit size expressed as metal uranium content q can be fit to a log-uniform cumulative distribution function given by:

$$F_Q(q,a,b) = \begin{cases} 0 & if\ q < q_{min} \\ \frac{\ln(q)-\ln(q_{min})}{\ln(q_{max})-\ln(q_{min})} = a \times ln(q) - b; \ln(q_{min})\frac{b}{a}; \ln(q_{max}) = \frac{b+1}{a} & ; if\ q_{min} \leq q \leq q_{max} \\ 1 & if\ q > q_{max} \end{cases} \quad (1)$$

where q_{min} and q_{max} are the uranium metal content in the smallest and largest deposits, respectively. Note that as Eq. (1) is function of the logarithm of the uranium metal content; it does not depend on the unit used for expressing the resources *r* (i.e., t, kg, pounds), nor on the coefficients *a* and *b* defined by:

$$a = \frac{1}{\ln(q_{max})-\ln(a_{min})}; b = \frac{\ln(q_{min})}{\ln(q_{max})-\ln(a_{min})} \quad (2)$$

The log-uniform distribution is a distribution whose logarithm is uniformly distributed. It is used in modeling when "inputs cover a large range of values (e.g., multiple orders of magnitude), but nothing else is known about the shape of the underlying distribution" [5].

TABLE 1: ESTIMATION OF THE MINIMUM AND MAXIMUM DEPOSIT SIZES (IN T U) ON VARIOUS EUROPEAN REGIONS USING THE GRAPHIC AND THE UMVU ESTIMATORS

	Sample size	Observed		Graphic		UMVUE[4]	
	n	Q_{min}	Q_{max}	Q_{min}	Q_{max}	Q_{min}	Q_{max}
Czech Republic	13	380	49,225	200 ± 380	21,815 *(34,570)*[1]	265	31,190
France[2]	34	280	9,900	230 ± 50	7,330 *(9,800)*	535	11,075
Germany	17	800	84,660	250 ± 525	30,400 *(82,300)*	685	9,330
Iberian District	16	395	9,000	290 ± 210	10,480 *(15,110)*	485	11,085
Bulgaria[3]	7	500	10,000	260 ± 200	2,440 (8,900)	400	1,870
Total	87	275	95,600	200 ± 250	15,550 *(23,190)*	560	23,205

[1]Values in brackets give the expected largest deposit size defined as $q_{max} + \sigma_q$.
[2]French deposits in the UDEPO database were recently updated with small resources, and so, to be relevant with records of other countries, deposits with resources < 250 t U were excluded from the above statistics.
[3]Most of uranium deposits in Bulgaria are volcanic-related, but only those related to granitoids were considered here.
[4]UMVU = uniformly minimum-variance unbiased estimator.

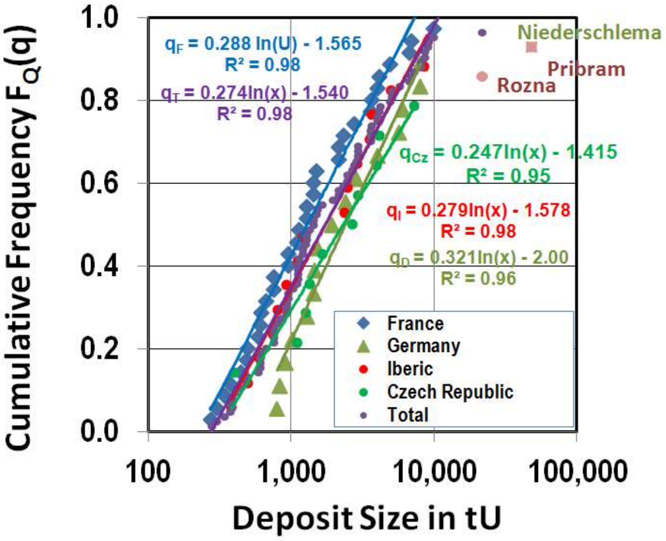

FIG. 3. Cumulative frequency plot of the metal content for the granite-related European uranium deposits. For most regions, the cumulative tonnage curves fit remarkably to a log-uniform distribution.

3.1. Properties of log-uniform distribution

Density distribution f(q,a,b)

The density function of a log-uniform distribution is given by:

$$f_Q(q,a,b) = \begin{cases} 0 & if\ q < q_{min}\ or\ q > q_{max} \\ \frac{1}{q[\ln(q_{max}) - \ln(q_{min})]} = \frac{a}{q}; & if\ q_{min} \leq q \leq q_{max} \end{cases} \quad (3)$$

The moments of a log-uniform random distribution Q are given below [Warning $E(Q) \neq E(e^{ln[Q]})$. See Appendix for details (e.g., Fig. A1)].

First moment or *mean*: $E(Q) = m$

$$m = E(Q) = \frac{q_{max} - q_{min}}{\ln(q_{max}) - \ln(q_{min})} = a\Delta q\ with\ \Delta q = q_{max} - q_{min} \quad (4)$$

Variance (second centered moment): $\sigma^2 = E(X^2)–m^2$ and *variation coefficient*: $\rho = \sigma/m$

$$\sigma = m(m_u - m) \qquad \rho = \frac{\sigma}{m} = \sqrt{\frac{m_u}{m} - 1} \quad (5)$$

where m_u is the mean of the uniform distribution defined on the interval $[q_{min}, q_{max}]$. Additional statistical properties of the log-uniform distribution are given in Annex I. Moments of log-uniform distribution can be estimated graphically by fitting a line on experimental values using linear regression (called graphic in Table 1) or using an uniformly *minimum-variance unbiased* *estimator* (UMVUE) or *minimum-variance unbiased estimator* (MVUE). The UMVUE is an *unbiased estimator* that has the lowest variance than any other unbiased estimator for all possible values of the parameter [6].

Recently, French deposits in the UDEPO database were updated to include resources as small as 1 t U (212 records in total). It seems that this is not yet the case for all the other European countries. In order to have a representative sampling, French deposits with resources lower than 250 t U (n = 178) were excluded in the estimations of Table 1.

3.2. Estimating extremes values Q_{MIN} and Q_{MAX}

Several methods can be used to estimate the continuous uniform distribution parameters. Three methods have been compared here:

(i) *GM*: *the graphic method*: the estimators are calculated according to Eq. (1) from the best linear fit regression coefficients calculated on the cumulative distribution curve plotted in a log-linear scale:

$$\ln(\hat{q}_{min}) = \frac{\hat{b}}{\hat{a}}; \qquad \ln(\hat{q}_{max}) = \frac{\hat{b}+1}{\hat{a}} \tag{6}$$

This method consists in extending the regression line for the frequencies 0 and 1, respectively, and to read the corresponding tonnages on log-scale. A confidence band for q_{min} and q_{max}, respectively, can be estimated from the confidence band of a, and b. Results are reported in Table 1.

(ii) *ML*: the *maximum likelihood* (ML) estimate of $\hat{q}_{min} = q_{(1)}$ is the smallest value $q_{(1)}$ observed over a sample data of size *n*, and the ML estimate of $\hat{q}_{max} = q_{(n)}$ is the largest one:

$$\hat{q}_{min} = q_{(1)} \qquad \hat{q}_{max} = q_{(n)} \tag{7}$$

This method is conservative as sampling under-estimates the "true" minimum and maximum of a distribution. It may lead to under-estimation depending on situations and on the sample size.

(iii) *UMVU*: the *uniformly minimum variance unbiased* (UMVU) estimates of the continuous uniform distribution are defined by [7]: (i) the MS estimator of q_{min} is the minimal value minus the sample range divided by $n-1$ with *n* being the sample size; the MS estimator of q_{max} is the maximal value plus the sample range divided by n−1:

$$\hat{q}_{min} = \frac{nq_{(1)} - q_{(n)}}{n-1} \qquad \hat{q}_{max} = \frac{nq_{(n)} - q_{(1)}}{n-1} \tag{8}$$

In contrast, the ML estimates are biased and have higher mean-squared error [8].

In all cases, the *additional potential resources* of a country are defined as the predicted q_{max} reads or calculated from the log-uniform cumulative distribution curves (Fig. 3). The total *additional potential resources* are the sum of those of the considered countries.

3.3. Results and discussion

Despite that the uranium resource estimations in some countries (e.g., Czech Republic) seem to be less well defined than for the rest of Europe, their statistical distributions are similar (Fig. 4). Results of resources estimation are reported in Table 1 per country and for all countries[33]. The log-uniform distribution seems inefficient to predict "exceptional" deposits such as Rozna, Pribram (Czech Republic), Niederschlema (Germany) or Bukhovo District (Bulgaria), suggesting that the "true" underlying distribution of deposit sizes would be more complicated than log-uniform.

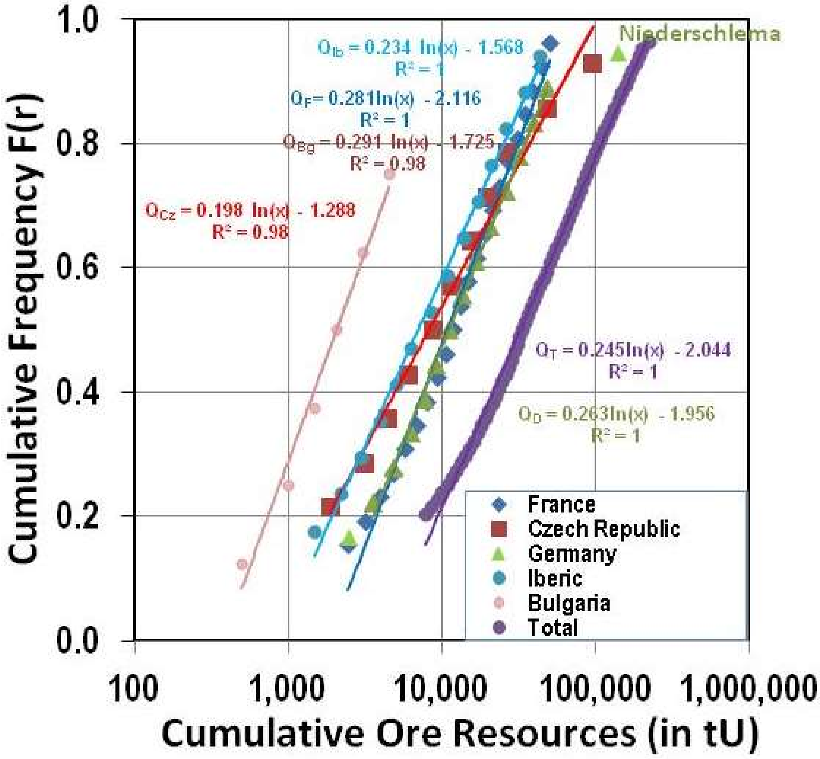

FIG. 4. Cumulative frequency plot of the cumulative tonnage for the granite-related European uranium deposits. For most regions, the cumulative tonnage fits remarkably to a log-uniform distribution.

However, the log-uniform distribution provides good estimates for France and the Iberian District, which lead to the question of why there are no undiscovered giant deposits in these districts compared to Germany. The largest German and Iberian Peninsula deposits are predicted to have sizes of ~30,400 t U (up to 82,300 t U), and ~10,500 t U (up to 15,100 t U), respectively, whereas there is smaller uncertainty on the estimates of the largest deposits in France and the whole Europe (up to 9,800 t U and 23,200 t U, respectively).

The Bukhovo District (with up to 10,000 t U) seems to be the biggest one in Bulgaria whereas the average sizes of the other deposits are smaller (from 1,000 to 1,500 t U). The UMVU estimates predict similar biggest deposits about 31,200 t U in size in all regions.

The graphic method predicts relatively higher potential total uranium resources than observed for all countries, except for Germany (and Bulgaria) for which the Niederschlema deposit

[33] Excluding deposits whose metal content is less than 250 t U for French deposits.

appears to be an outlier (like the Bukhovo District), and of course for the resources in Europe. The estimates of the smallest and largest deposits are highly uncertain due to the log-uniform nature of the underlying law and mainly depend on the sample set size.

4. PREDICTING THE TOTAL RESOURCES

A similar prediction technique has been applied on the cumulative ore resources (in t U) R per region obtained by summing the uranium metal content of deposits ranked in increasing sizes, the maximum being the observed total resources. The total ore resources R are also log-uniform distributed over a large range (including Czech Republic, Fig. 4) like the deposit sizes as shown in Fig. 3. The maximum potential resources are estimated using a similar approach as for the deposit size (i.e. using graphic and UMVU estimates). Results are reported in Tables 2 and 3. Table 2 accounts for the whole dataset in estimating the log-uniform distribution parameters (i.e., r_{min} and r_{max}) whereas Table 3 excludes the smallest and the largest deposits. The last columns of each table give, per predicting method, the difference between the predicted maximum resources and the observed one.

TABLE 2. POTENTIAL RESOURCES *R* (IN T U) ESTIMATED ON VARIOUS EUROPEAN REGIONS USING THE GRAPHIC AND THE UMVU ESTIMATORS FIT ON THE WHOLE DATASET

	Sample size	Observed		Graphic		UMVU		Potential additional resources	
	n	q_{min}	R_{max}	q_{min}	R_{max}	q_{min}	R_{max}	*Graphic*	*UMVU*
Czech Republic	13	385	97,050	380	118,825	245	153,850	21,775	56,800
France	34	275	70,550	740	114,140	230	83,450	12,915	43,590
Germany	17	800	143,800	975	119,475	580	198,920	-	55,120
Iberian Belt	16	395	43,500	540	76,140	290	59,525	16,025	32,640
Bulgaria	7	500	14,550	290	18,080	285	25,520	3,530	10,970
Total[1]	87	275	369,400	3,630	274,740	250	403,335	-	33,935
			(368,060)		*(446,660)*		*(521,285)*	*(78,600)*	(*153,225*)

[1]Figures in brackets are the total resources of the whole area estimated as the sum of the predicted resources calculated on each sub-area, while the first line are the total resources predicted from the statistical model.

TABLE 3. SAME AS TABLE 2 BUT EXCLUDING OUTLIERS SUCH AS THE NIEDERSCHLEMA DEPOSIT IN GERMANY, AND THE SMALLEST DEPOSITS IN CZECH-REPUBLIC, FRANCE, BULGARIA, AND IBERIC BELT

	Sample size	Observed		Graphic		UMVU		Potential additional resources	
	N	q_{min}	R_{max}	q_{min}	R_{max}	q_{min}	R_{max}	*Graphic*	*UMVU*
Czech Republic	9	4,500	97,050	630	104,975	3,065	142,485	7,925	45,425
France	27	3,280	70,550	1,510	76,400	2,915	79,400	5,850	8,840
Germany	16	1,630	48,200[34]	1,360	84,170	1,300	60,410	35,970	12,210
Iberic Belt	14	1,480	43,680	830	59,930	1,140	56,670	3,890	12,990
Bulgaria	6	1,000	14,580	270	18,440	585	24,920	16,430	10,340
Total[1]	64	10,000	273,060	4,370	248,500	9,490	287,780	-	14,720
					(343,905)		*(363,870)*	*(70,055)*	(*89,800*)

[1]Figures in brackets are the total resources of the whole area estimated as the sum of the predicted resources calculated on each sub-area, while the first line are the total resources predicted from the statistical model.

4.1. Results

The plot of uranium deposit cumulative tonnage versus their frequency (Fig. 4) shows a log-uniform distribution fitting quite perfectly to a linear trend ($R^2 = 0.97$ to 0.99) for the four main European uranium districts, including Portugal with only two deposits being re-grouped with Spain under the Iberian Belt group. In Germany, the largest deposit (Niederschlema) plots well above the correlation; it contains much larger resources than any other European granite-related deposits.

The cumulative tonnage/cumulative frequency curve of the granite-related deposits from France is the closest to the one defined by the Czech Republic (Fig. 4). The Spanish deposits, mined at the shallowest level, tend to have lower resources, whereas the ones from the Czech Republic mined at much greater depths tend to have the largest resources. Assuming a similar genetic model for these deposits, and given the fact that deposits in the Iberian Peninsula have been mined only close to the surface, and in France the mining has been limited to less than 400 m, it can be speculated that there are still large uranium resources to be discovered in Spain, Portugal and France by exploring at deeper levels.

The graphic method predicts relatively higher potential total uranium content resources than observed for all countries, excepted for Germany (and for the total resources) for which the Niederschlema deposit appears to be an outlier (Table 2). An addition potential resource estimated at ~78,600 t U is predicted by the graphic method. The additional potential resource

[34] Excluding the Niederschlema deposit.

reaches from 70,000 to 90,000 t U when excluding outliers, and skyrocketed to 153,225 t U using outliers and the UMVU estimates (Tables 2 and 3).

By construction, the UMVU estimator always predicts lower size for small deposits and greater resources than observed, leading to unrealistic fit of the cumulative function, especially in case of outliers. This method seems to work realistically for all countries, but over-estimates the resources for Germany as it predicts double resources than observed. An additional potential of ~30,000 t U seems to be more realistic for Germany. The UMVU estimator gives an estimated additional resource of ~34,000 t U for the total, while the potential resources summed on all regions are ~90,000 t U (excluding outliers).

4.2. Discussion

As the Niederschlema deposit in Germany appears to be an outlier, it has been excluded from the dataset, in keeping with the smallest deposits of France, in order to reassess the UMVU estimators. The new estimates are reported in Table 3. The graphic estimator is repeated in columns 5 and 6 for sake of comparison, but is identical as in the previous case of Table 2. As the extreme values for the sample set have changed, the UMVU estimates of the minimum and maximum differ. The new estimates are reported in Table 3 columns 7 and 8. For all countries, the suggested estimation methods, with and without outliers, give very similar predictions for the maximum resources.

However, the estimates using the methods and excluding the outliers (2nd method) under-estimate the total resources of Germany (the predicted resource is ~60,000 t U while the observed one is 144,000 t U). This demonstrates that excluding one outlier sample may drastically change the prediction. This also shows that the Niederschlema deposit could not have been found by applying only a static model. This last method predicts an additional U resource estimated at ~90,000 t U. An update of the UDEPO database was made recently including some small uranium occurrences (lower than 300 t U), especially in some countries like France and in the Iberian Peninsula. Including these new small uranium occurrences, the cumulative metal resource distribution is log-normal (Fig. 5) rather than log-uniform distributed as observed in the previous versions of the UDEPO. This demonstrates that the log-uniform distribution is an approximation of the log-normal one when neglecting small and large extremes. This new dataset allows a more accurate description of the statistical distribution, but does not change much the estimation of the additional potential resources.

5. DISCUSSION AND CONCLUSIONS

The reasons that the Niederschlema deposit has larger resources than the other deposits in Germany are probably mainly because it has been mined and exploited at greater depths (down to a depth of ~2,000 m), at a lower cut-off grade than the other deposits of similar type, whereas the other deposits have been recognized at depths no greater than 400 m. An additional reason for the particularity of the Niederschlema deposit is the economic constrains as this deposit was located in the former East Germany and has been mined during the Soviet time during which the economic conditions were very different from those controlling uranium mining in the Western countries. The Bernadan uranium deposit in Limousin, France, for example, is known by drillings to extend at least down to 800 m, and still totally open at this depth, but has been mined (and estimated) only down to 400 m. This disseminated type deposit (epi-syenite type), mined in the Marche Occidentale two-mica granite, was discovered in 1970 and mined by open pit exploited until the early 1990s. At that time, because of the stripping ratio was becoming too large, it was decided to stop the exploitation. However, before closing, a 3D model was built in order to investigate possible undiscovered mining zones. The 3D model revealed two side unexploited vertical pipes confirmed by drillings. Given this new potential, additional drilling revealed an extension of the mineralization as an open structure down at least to a depth greater than 800 m. The company in charge of the mine decided to sell the deposit (instead of closing it as planned before the 3D modeling) to Cogema. The Bernardan exploitation turned to be operated underground during 10 years more, and closed in 2001. These two case studies demonstrate that more mineral resources exist at depth even in mature mining fields. Of course, it is highly speculative to assume that all uranium deposits in Europe extend at depth, but the Niederschlema and Bernardan deposits tend to demonstrate that additional mineral potential resources may have remained unexplored in Europe. This suggests that depths (minimum, average, and maximum) at which mineralization occurs, even if difficult to find, should be recorded in the UDEPO database, and might help to progress in this discussion. The same is probably true for other commodities, particularly base and strategic metals.

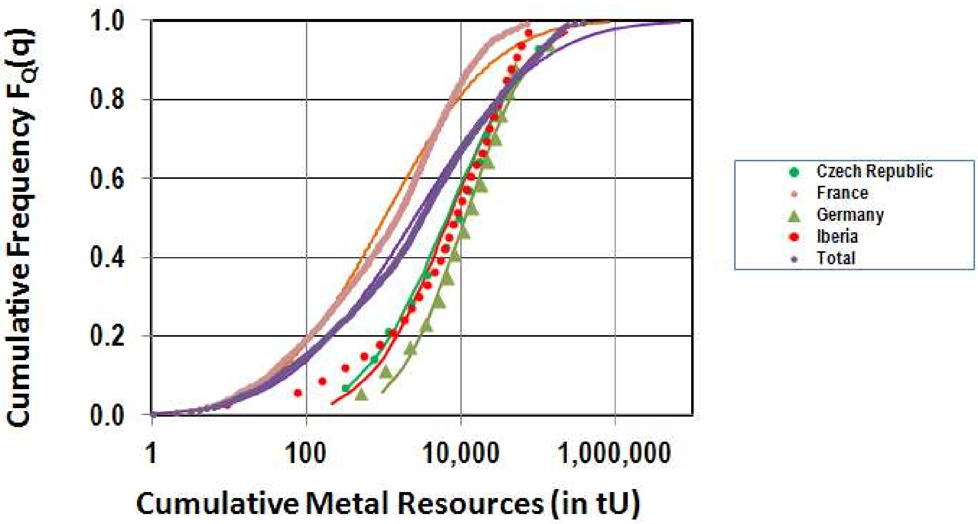

FIG. 5. Cumulative resources tonnage distribution for the granite-related European uranium deposits. Accounting for small size occurrences, the cumulative metal tonnage distributions are log-normal.

Appendix

Characteristic function: $\Phi_Q(iu)$

$$\Phi_Q(iu) = E(e^{iuQ}) = \int_{q_{min}}^{q_{max}} e^{iuq} f_Q(q)dq = a\int_{iuq_{min}}^{iuq_{max}} \frac{e^t}{t}dt = a[Ei(iuq_{max}) - Ei(iuq_{min})] \tag{A1}$$

Using a series representation for the exponential integral $Ei(x)$, it can be derived as a series of representation for the characteristic function $\Phi_Q(iu)$; after some arithmetic, it becomes:

$$\Phi_Q(iu) = 1 + a\sum_{k=1}^{\infty} \frac{(iu)^k}{k!}\frac{q_{max}^k - q_{min}^k}{k} \qquad u \neq 0 \tag{A2}$$

This formula is useful to compute the *i*th moment of Q by derivation of $\Phi_Q(iu)$ against u.

Mean $E(X)$:

$$E(X) = \frac{q_{max}-q_{min}}{\ln(q_{max})-l\ (q_{min})} = m_u m \qquad \text{with} \qquad m_u = \frac{q_{max}+q_{min}}{2} \tag{A3}$$

Second moment: $E(X^2)$

$$E(X^2) = \frac{1}{2}\frac{(q_{max}-q_{min})(q_{max}+q_{min})}{\ln(q_{max})-\ln(q_{min})} = m_u m \qquad \text{with} \qquad m_u = \frac{q_{max}+q_{min}}{2} \tag{A4}$$

where m_u is the mean of the uniform distribution defined on the interval $[q_{min}, q_{max}]$.

Warning: A log-uniform distribution X means that $Y = \ln(X)$ is uniformly distributed within the interval $[\ln(x_{min}), \ln(x_{max})]$ so the mean and variance of Y are $E(Y) = \ln(\ln(\sqrt{x_{min}x_{max}})$ and $\sigma^2_Y = [\ln(x_{max}) - \ln(x_{min})]^2/12$, but the mean and variance of X are more tricky and given by Eqs. (4) and (5), respectively, after derivation of Eq. (A2).

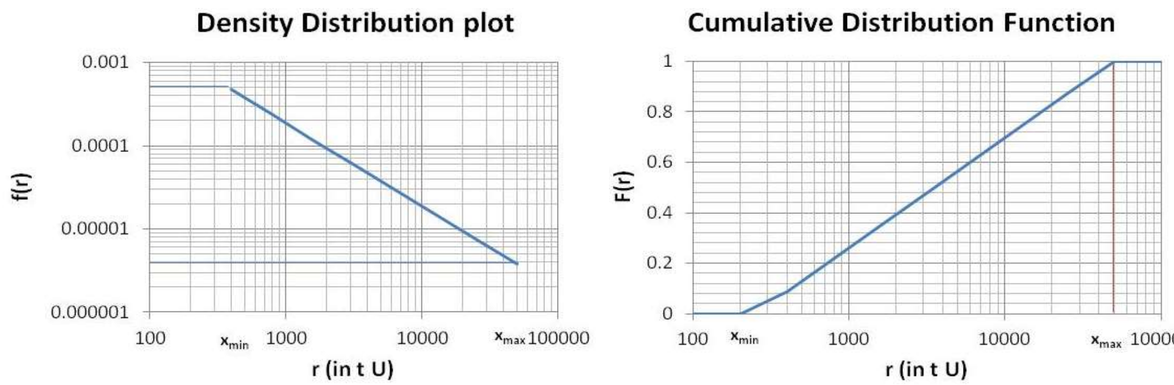

FIG. A1. Density and cumulative plots of a log-uniform distribution.

Confidence band on estimates

The confidence bands of a and b are estimated like the coefficients a and b from the best regression linear fit of $F_Q(q)$ vs. $\ln(Q)$. The errors are propagated onto the estimates of $\ln(q_{min})$ and $\ln(q_{max})$, and q_{min} and q_{max} using Eq. (7) and the classical ratio [9] and exponential [10] uncertainty formulas:

$$f = \frac{b}{a}; \qquad \left(\frac{\sigma_f}{f}\right)^2 = \left(\frac{\sigma_b}{b}\right)^2 + \left(\frac{\sigma_a}{a}\right)^2 \qquad f = e^a \qquad \sigma_f = f\sigma_a \tag{A5}$$

Results are reported in Table 1.

Effect of truncation on log-normal distribution plot

Fig. A2 shows the effect of truncation on a log-normal distribution. Log-normal values are simulated and represented in green on Fig. A2a. Then, 15% and 10% of extreme low and high values were excluded, and their experimental cumulative distributions plotted in red and black on Fig. A2a. The log-normality aspect is lost when applying the truncation, and the experimental truncated log-normal distributions appear to be log-uniformly distributed. This truncation has little effects on the cumulative plot of the cumulative values distribution, excepted on the left part of the curve corresponding to small occurrences. In conclusion, when a database is partially constituted, not including small occurrences of a log-normal distribution property, one can erroneously conclude that the distribution of that property is log-uniformly distributed; but when studying the cumulative distribution of that property is not so much affected as shown on Fig. A2.

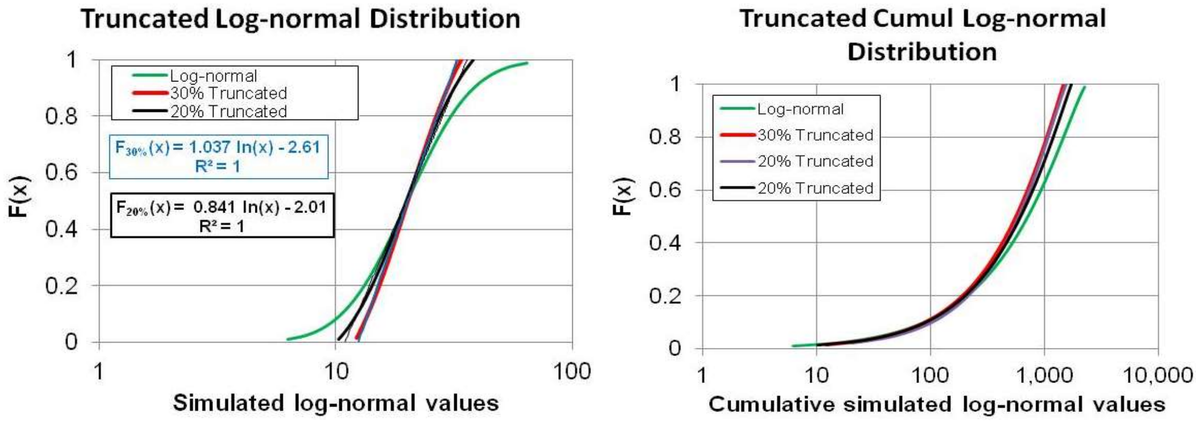

(a) *(b)*

FIG. A2. (a) Cumulative plots of a log-normal, and "truncated" log-normal distributions. (b) Cumulative plot of simulated values.

REFERENCES

[1] LEDRU P., PHARAOH T.C., ZEDLER H., ZEH A., ZULAUF, G., Variscan tectonics. In: McCann T (ed.): The Geology of Central Europe. Volume 1: Precambrian and Palaeozoic. Geol. Soc. London, 599-664 (2008).

[2] CUNEY, M., Geologic environment, mineralogy and fluid inclusions of the Bois Noirs Limousin uranium vein, Forez, France, Economic Geology, 73, 1576-1610 (1978).

[3] CUNEY, M., Contrôles magmatiques et structuraux sur la métallogenèse tardi hercynienne de l'uranium. Chron. Rech. Min., 499, 9-17 (1990).

[4] CUNEY, M., The extreme diversity of uranium deposits. Mineralium Deposita, 44, 3-9 (2009).

[5] MISHRA, S., Assigning probability distributions to input parameters of performance assessment models. INTERA Inc. USA, SKB, Swedish Nuclear Fuel and Waste Management Co, Stockholm Sweden, Technical report TR-02-11, 45p (2002).

[6] VOINOV, V. G., NIKULIN, M.S., Unbiased estimators and their applications, Vol.1: Univariate case. Kluwer Academic Publishers, 521p (1993).

[7] KOSENOK, A. S., An alternative to maximum likelihood based on spacings. Econometric Theory, 21 (2), 472–476 (2005).

[8] WONG, T.S.T., LI, W.K., A note on the estimation of extreme value distributions using maximum product of spacings. Time series and related topics: in memory of Ching-Zong Wei. Beachwood, Ohio: Institute of Mathematical Statistic. 272-283 (2006).
[9] FORNASINI, P., The uncertainty in physical measurements: an introduction to data analysis in the physics laboratory, Springer, 161p (2008).
[10] HARRIS, D. C., Quantitative Chemical Analysis, (6th ed.), Macmillan, 56p (2003).

GLOBAL GRADE-AND-TONNAGE MODELING OF URANIUM DEPOSITS

S. THAKUR
University of Trento,
Trento, Italy

B. CHUDASAMA, A. PORWAL
Indian Institute of Technology Bombay,
Mumbai, India

A. PORWAL
Centre of Exploration Targetting,
University of Western Australia,
Perth, WA, Australia

Abstract

This contribution presents models of grade and tonnage distribution of various uranium deposit types and sub-types. A *p*-value derived from the Kolmogorov-Smirnov test is used for evaluating the goodness-of-fit of the frequency-grade and frequency-tonnage distributions to the log-normal distribution. The results indicate that both frequency-grade and frequency-tonnage distributions of most deposit types and sub-types conform to the log-normal distribution at the 95% confidence level. Models created by dividing deposits into sub-types show significant improvement in the goodness-of-fit. The *t*-tests reveal that the grade and tonnage distributions of sub-types of the sandstone-hosted type (namely, roll-front, tabular, basal channel and tectonic-lithologic sub-types) are significantly different from each other. Furthermore, country-wise models of the roll-front deposits in different countries do not necessarily correlate, which explains the lower goodness-of-fit for the global frequency-grade and frequency-tonnage models for sandstone-hosted deposits. This implies that sandstone-hosted deposits may differ in their geological settings from country to country, thus requiring some reclassification. The same applies to basement-hosted and unconformity contact deposits in Canada and Australia. Some modifications in the current classification scheme are suggested.

1. INTRODUCTION

According to the IAEA deposit classifications, there are 15 different uranium deposit types based on geological attributes and genetic processes. These deposit-types have varying costs of production depending on grade and tonnage. Grade-and-tonnage models provide comprehensive information about the pattern in which different deposit types occur across the globe. In addition, these models provide insights into differences in the exploration condition in which the deposits were discovered and the geological conditions in which they formed [1]. Moreover, frequency distributions of grades and tonnages derived from well-explored deposits serve as an input to quantitative resources assessment algorithms that are used for estimating the number and amount of undiscovered deposits formed in similar geological settings [1].

Grade-and-tonnage models, which have been developed at the global scale for 87 different metallic and non-metallic minerals [2], are used as inputs for an economic mineral resource simulator (EMINERS) [3]. Currently, descriptive models for uranium deposits are available for only two uranium deposit types but they are quite dated [2]. In this contribution, grade-and-tonnage models for different uranium deposit types, sub-types and geological locations are presented. Grades, tonnages, and contained metals in deposits belonging to the same global population of uranium deposit types should conform to the expected log-normal frequency distribution based on experience documented in [1, 4]. Therefore, goodness-of-fit statistics of the distribution have been used to draw inferences about the geological similarities and differences among deposit types and sub-types and their country-wise locations. This analysis could throw light on the justification behind the current deposit classification and the need to revise the classification scheme.

2. DESCRIPTION OF THE DATASET

The database of world distribution of uranium deposits (UDEPO) contains records of uranium deposits across the globe. Information regarding the classification of these deposits, their geological characteristics and resources was published by [5]. The database is being regularly updated by the member states with information regarding status of deposits (dormant, permitted or operating), the country and district where they are located, the resources and grade of the deposits.

For this analysis, detailed data were obtained from the IAEA. The data comprise records for 1556 deposits across the world, with ancillary information about each deposit, as available in the online database (http://www-nfcis.iaea.org/). In addition, information about the resources, grades and the coordinates of the deposits were provided. This dataset consists of reasonably assured resources. These are known uranium deposits of delineated size, grade and configuration. The tonnages indicate the total amount of naturally occurring or pre-mining resources in tons of uranium metal. The grades are reported as percentage of uranium metal in the ore. The tonnages and grades are the sum of past production and remaining resources. However, grades from past production represent recovered grades, so non-recovered uranium has not been included.

2.1. Deposit classification

The uranium deposit classification used in the UDEPO database [6] was decided upon by experts from six countries with the IAEA. Inputs from expert geologists from across the globe were used to update the classification scheme. Deposits were classified into a particular type and sub-type based on the geological setting of their formation and occurrence. Table 1 shows the current classification scheme of the 15 uranium deposit types (in order of their economic significance) and their sub-types.

TABLE 1. IAEA DEPOSIT CLASSIFICATION WITH EXAMPLES

Deposit type	Deposit sub-type	Examples of deposits
Proterozoic unconformity	Basement hosted	Jabiluka, Ranger (Australia); Rabbit Lake (Canada)
	Stratiform fracture controlled	Koppunuru, Peddagattu (India)
	Unconformity contact	McClean, Cluff Lake D (Canada)
Sandstone	Roll-front	Moynkum (Kazakhstan); Crow Butte, Smith Ranch (USA)
	Tabular	Westmoreland (Australia); Imouraren (Niger)
	Basal channel	Dalmatovskoye (Transural Region); Beverley (Australia)
	Tectonic-lithologic	Mas Laveyre (France); Mikouloungou (Gabon)
Polymetallic breccia complex		Olympic Dam (South Australia)
Paleo-quartz-pebble conglomerate	U-dominant	Denison Mine, Banana Lake (Canada)
	Au-dominant	Ezulwini, Potchefstroom Goldfield (South Africa)
	Mono-metal	Buckels (Canada)
Granite-related	Endogranitic	Timgaouinek (Algeria)
	Endo-perigranitic	Gambuta (Spain)
	Perigranitic	Niederschlema-Alberoda (Germany)
Intrusive	Anatectic	Rössing, Namibplass (Namibia)
	Carbonatite	Catalao (Brazil)
	Peralkaline complex	Ilimaussaq (Greenland)
	Quartz monzonite	Bingham Canyon, Twin Butte (USA)
Volcanic- and caldera-related	Strata-bound	Olovskoye (Russia)
	Strata-structure bound	Dornod, Gurvanbulak (Mongolia)
	Structure-bound	Xiangshan District (China)
	Volcano sedimentary	Sierra Pintada District (Argentina)
Metasomatite	Na-metasomatite	Centralnoe, Novokonstantinovskoe (Ukraine)
	Na-K-metasomatite	Tsarevskoye (Russia)
	K-metasomatite	Druzhnoye, Elkonskoe Plateau (Russia)
	Skarn	Mary Kathleen (Australia)
Surficial	Fluvial valley	Yeelirrie (Australia); Tubas Red Sand, Tumas (Namibia)
	Lacustrine-playa	Lake Maitland (Australia)
	Paleo-karst	Tyuya-Muyum (Kyrgyzstan)
	Peat bog	Kamushanovskoye (Kyrgyzstan)
	Pedogenic-structure fill	Igralishte, Senokos, Beslet (Bulgaria)
Collapse breccia pipe		Arizona Strip north of the Grand Canyon (USA)
Phosphate	Continental	Fosse-Pamela (Central African Republic)
	Minerochemical phosphorite	Phosphoria Formation (USA)
	Organic phosphorite	Melovoye, Taybagarskoye (Kazakhstan)
Metamorphite	Marble-hosted phosphate	Itataia-Santa Quiteria District (Brazil)
	Strata-bound	Kvarnan (Sweden)
	Structure-bound	Shinkolobwe-Kasolo (Democratic Republic of Congo)
Lignite-coal	Stratiform	East Ebro Valley (Spain)
	Fracture-controlled	Badyelskoye (Russia)
	Stratabound	Northern Great Plains (USA)
Black shale	Stockwork	Schmirchau - Reust (Germany)
	Stratiform	Chattanooga Shale Formation (USA)
Carbonate	Cataclastic	Mailuu-Suu (Kyrgyzstan)
	Karst	Pryor Mountains-Little Mountains District (USA)
	Stratabound	Tummalapalle - Rachakuntapalle (India)

2.2. Descriptive statistics

The database consists of 1,393 deposits with reported tonnage values and 1,323 deposits with reported grades – these were used for frequency modeling of grade and tonnage. There were 1,290 deposits with both grade and tonnage values reported – these were used for generating the grade vs. tonnage plots.

Fig. 1 shows the number of deposits per type. The largest number of deposits is sandstone-hosted, followed by granite-related, volcanic-related, and metamorphite deposit types. Fig. 2 shows a comparison among total pre-mining uranium content resources for the different deposit types. Phosphate, lignite coal and black shale deposit types hold the largest resource tonnage of uranium. However, they are low-grade deposits and it is profitably uneconomical to extract uranium from them. Uranium is extracted from these deposits as a by-product of mining of other basic minerals, if at all.

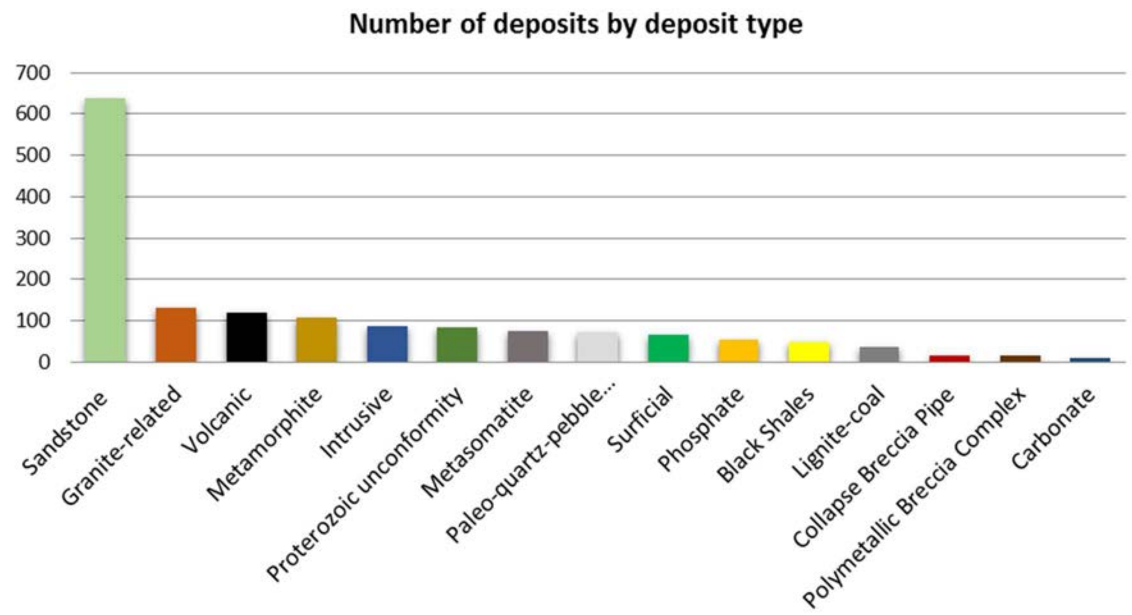

FIG. 1. Number of deposits per deposit type.

Fig. 3 shows the distribution of uranium content per deposit type excluding phosphate, lignite-coal and black shale types. From this pie chart, it can be seen that sandstone-hosted uranium has the largest resources among all the deposit types. It is noteworthy that the number of deposits of the polymetallic breccia type is small, but tonnage is very large. This is because of the large uranium mine Olympic Dam in Australia, which is the single major contributor to this large value of tonnage for this particular deposit type.

The distribution of uranium content per country is shown in Fig. 4. Thirteen countries contribute to ~70% of the world's uranium. In fact, the original uranium resources from USA alone are greater than ~45% of the world's total uranium known endowment. This is because the USA has the largest number of deposits of the phosphate, lignite coal and black shale types, which, as discussed above, form the major tonnage of world uranium but are not economically extractable as a single commodity.

Fig. 5 shows the uranium resource distribution by country with contributions from phosphate, lignite coal and black shale deposit-types excluded. Here, we can see that Australia is leading with the largest uranium producing mine in the world – Olympic Dam. The original resource distributions in leading uranium-producing countries such as Australia, Canada, USA and Kazakhstan by deposit type are plotted separately (Figs 6–9).

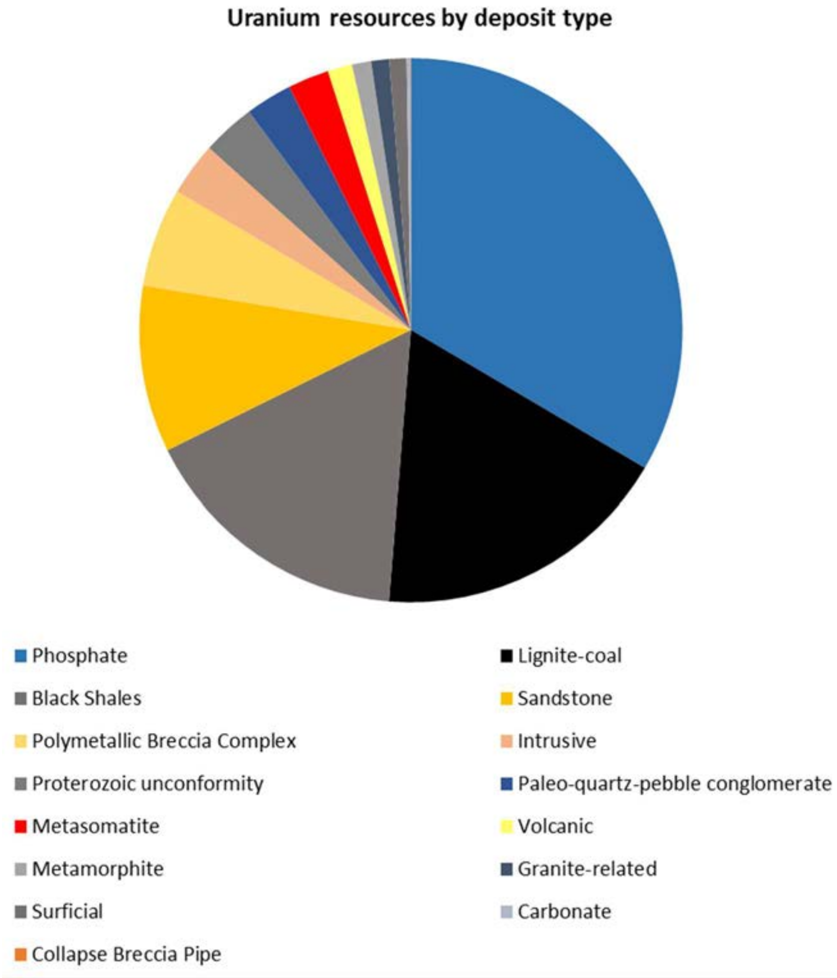

FIG. 2. Uranium resources per deposit type.

Australia has its primary contribution from a polymetallic breccia complex type deposit (Fig. 6). As mentioned above, Olympic Dam in Australia, which is the largest uranium mine in the world, is of polymetallic breccia type. However, ~70% of the mine's revenue comes from copper, ~25% from uranium, and the remainder from silver and gold [6]. A uranium deposit of polymetallic breccia type is not profitable if mined only for uranium. In Canada, the McArthur River uranium mine in Saskatchewan province is the world’s largest high-grade uranium deposit. All the deposits in Saskatchewan region – Key Lake, Cluff Lake, Rabbit Lake, McClean Lake, McArthur River and Cigar Lake deposits – are unconformity-related (Fig. 7).

Kazakhstan has its major contribution from low-medium grade sandstone deposits. These are roll-front type deposits cross-cutting sandstone beds often in paleo-channels. They are found in Budenovskoye, Tortkuduk, Moynkum, Inkai and Mynkuduk mines [5].

It is interesting to note that the majority of the resources in USA – phosphate, lignite and black shale type of deposits – have very low uranium grade. Sandstone deposits have low–medium grades of uranium. Thus, although USA has abundance of uranium resources, it is not very economical to mine most of them. Recent uranium production is from one mill (White Mesa, Utah) fed by four or five underground mines and several in-situ leach (ISL) operations [5].

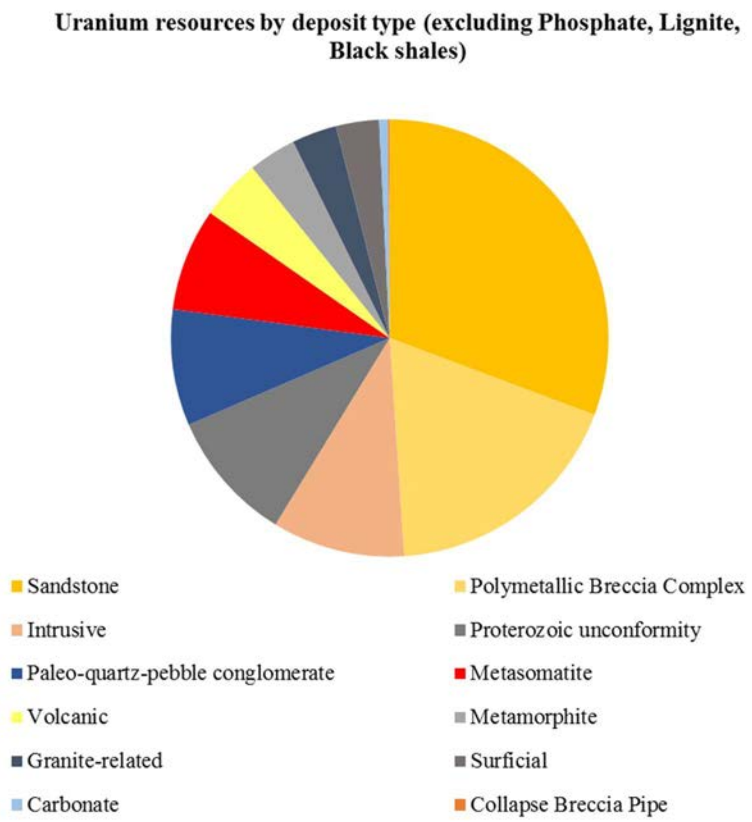

FIG. 3. Uranium resources per deposit type (excluding phosphate, lignite and black shale-hosted deposit types).

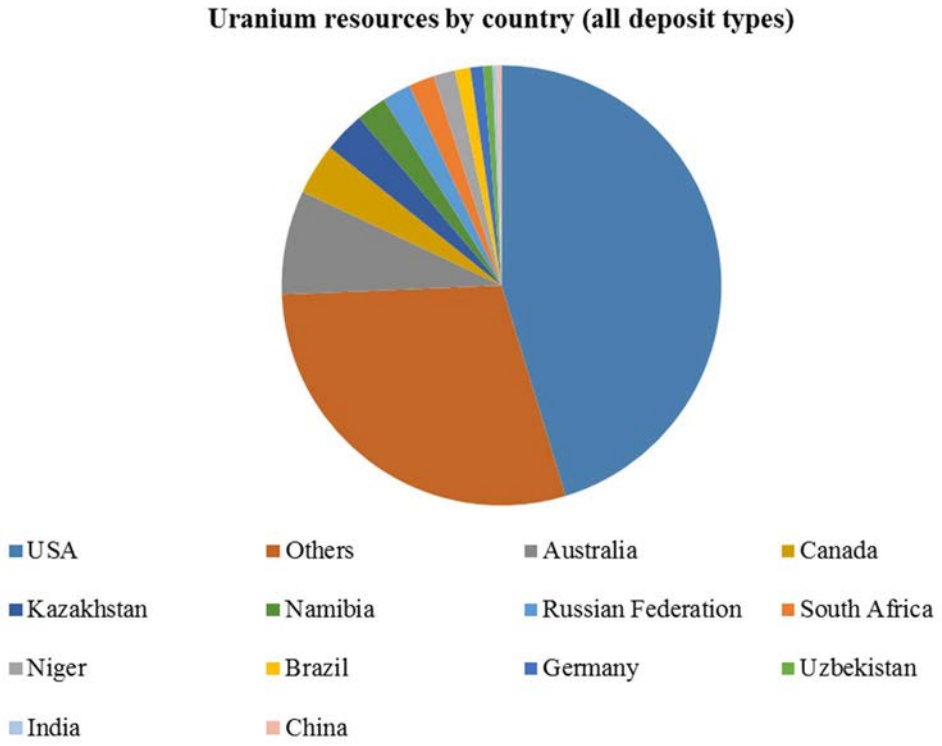

FIG. 4. Uranium resources per country for all deposit types.

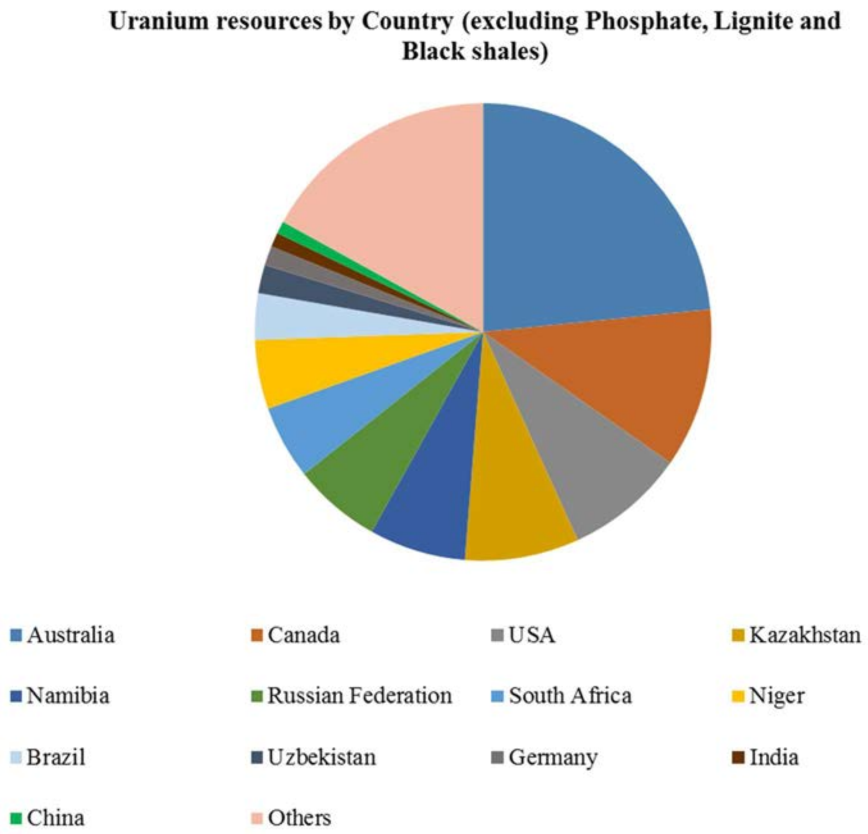

FIG. 5. Uranium resources per country excluding contribution from phosphate, lignite and black shale deposit types.

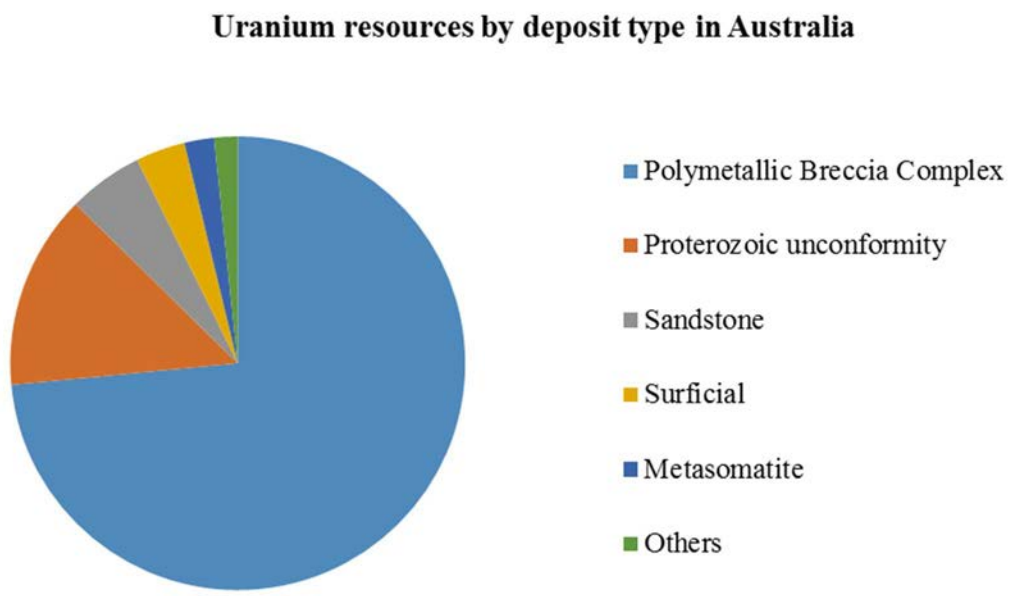

FIG. 6. Uranium resources per deposit-type in Australia.

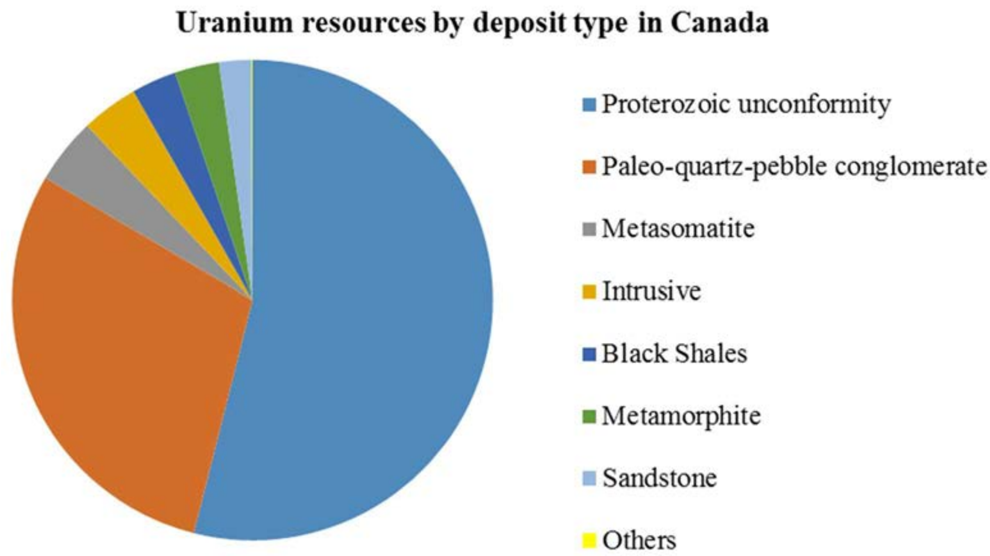

FIG. 7. Uranium resources per deposit type in Canada.

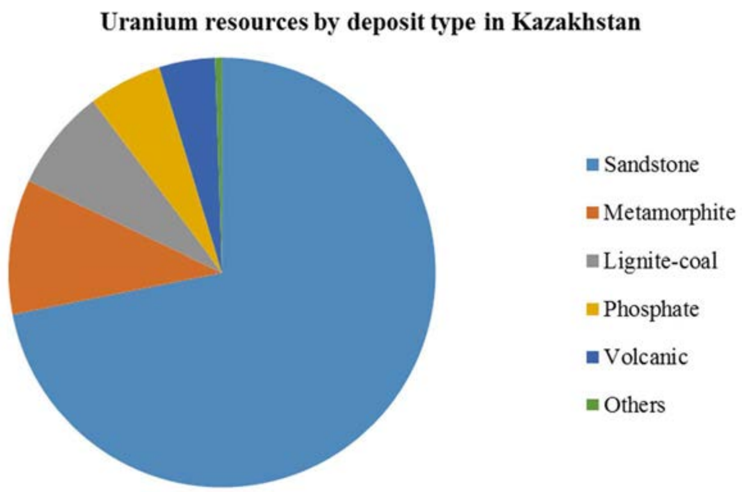

FIG. 8. Uranium resources per deposit type in Kazakhstan.

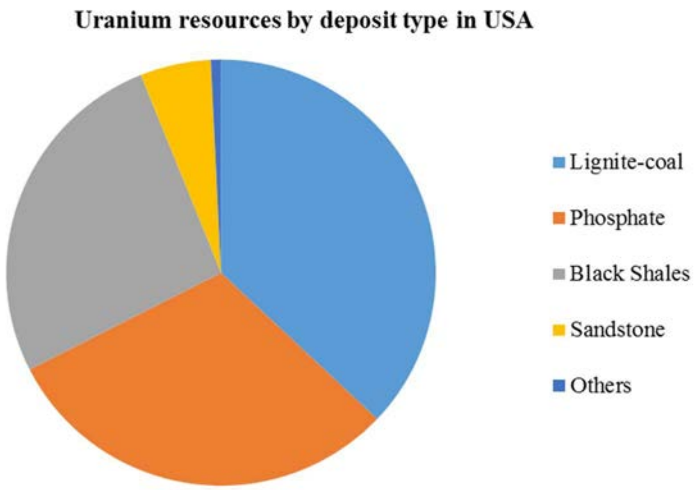

FIG. 9. Uranium resources per deposit type in the USA.

3. METHODOLOGY

Information regarding the amount of economically extractable uranium resource is critical for making decisions at different tiers of the nuclear fuel cycle. The long-term benefits of a nuclear power plant depend on the supply of uranium from the mines. Thus, estimation of the number of undiscovered deposits, the expected total amount of uranium in the earth’s crust and the quality or grade of the uranium ore in these deposits are vital inputs in energy planning.

Our knowledge regarding the undiscovered resources comes from past exploration history. There are two fundamental issues to be addressed: (1) the total amount of undiscovered uranium resources in terms of their number and tonnage; and (2) the probable locations of these deposits to guide exploration geologists to successful drilling. The former is addressed by methods of quantitative resources assessment. The latter comes under the purview of mineral potential modeling, which requires spatial information about existing deposits and spatial proxies for geological processes that lead to the formation of uranium deposits. Mineral potential modeling is closely related to genetic modeling of mineral resources.

One of the most widely used approach to quantitative mineral resources assessment is the USGS three-part assessment [1]. Developed and used by the USGS since 1975, this approach formed a key part of the GMRAP (Global Mineral Resource Assessment Project) for the purpose of translating a geologist's exploration concepts to a decision support system and allowing an economic analysis. The three parts in this form of assessment are:

1) Delineation of tracts that are geologically-permissive for the existence of a particular type of deposit;
2) Estimation of the number of undiscovered deposits per type per geologically-permissive tract;
3) Construction of frequency distributions of grades and tonnages of well-explored deposits to serve as models of, respectively, grades and tonnages of undiscovered deposits.

Grade-and-tonnage models form critical inputs to the USGS three-part quantitative resources assessments. In this section, we outline the statistical concepts used in the grade-and-tonnage models described in this contribution.

For frequency-grade and frequency-tonnage modeling, log-normal distribution is fitted to the observed cumulative distribution of grades and tonnages, which follows from the fundamental law of elemental distribution based on experience documented in [1] and on experience and tests in [4]. The goodness-of-fit of log-normal distribution is assessed using the Lilliefors test, which is a special case of the Kolmogorov-Smirnov (K-S) test [7, 8]. First, the maximum likelihood [9] estimates of the parameters of log-normal distribution (i.e., the log mean and the log standard deviation) are obtained from the observed distributions. These estimated parameters are used to generate the theoretical cumulative frequency distribution for the given values of the random variable (in this case, the grades and the tonnages). The K-S test compares the maximum difference between the observed and the theoretical cumulative distributions to test the null hypothesis that the data follow log-normal distribution. The Lilliefors test is used when the theoretical cumulative distribution parameters are derived from the observed data, as in this case. Table 2 explains some of the terms used for statistically explaining the goodness-of-fit.

For a comparison of deposit grades and tonnages by their sub-types, the t-test was also used in conjugation with the goodness-of-fit test for studying homogeneity between sub-types and statistical differences between different deposit sub-types [10]. In this analysis, two-sample t-test is carried out for selected pairs of deposit sub-types belonging to the same deposit type. There are two types of t-test – a one-tailed t-test and a two-tailed t-test. When it is known a priori that one of the deposit sub-types definitely has higher grades or tonnages than the other, one-tailed t-test can be used. Since, in this case, such assumptions cannot be made with a proper scientific basis, the two-tailed t-test is appropriate and was used. For each sample, the mean, variance, t-statistic, critical t-value (as a function of level of significance (α) and number of observations) and the *p*-value were calculated. The null hypothesis is that there is no difference between the two populations. Table 3 shows the inferences that can be drawn from the t-test results for the samples.

TABLE 2. COMMON STATISTICAL TERMS USED IN THE K-S GOODNESS-OF-FIT TEST

p-value	It is the calculated or estimated probability of rejecting the null hypothesis when the null hypothesis is true. It indicates the statistical significance of the assumed distribution for the grades or tonnages of the given deposits. If the *p*-value is higher than the level of significance (here 0.05 for 95% confidence), the assumption of the distribution is valid.
K-S Statistic	The K-S statistic is the maximum difference between the actual grade or tonnage value and the value estimated from log-normal distribution. The smaller the K-S statistic, the better is the goodness-of-fit.
Confidence interval	It is a range of values for the estimated parameters of the log-normal distribution (i.e., the log mean and the log standard deviation), within which there is 95% probability of the true population parameter values to occur.
Critical K-S value	The value for the maximum absolute difference between the observed and the theoretical distribution obtained from the limiting cumulative distribution function of the maximum difference. This value can be obtained from K-S tables [11[11].
Null hypothesis	It is accepted when the K-S statistic does not exceed the critical K-S value. In that case, it can be assumed at a certain level of confidence (here 95%) that the deposit grades or tonnages follow log-normal distribution.

TABLE 3. INTERPRETATION OF T-TEST RESULTS

t-statistic	*p*-value	Sample means	Inference
t-statistic > t-critical	*p*-value < α	Mean 1 > Mean 2	Samples are from different populations. Sample 1 is larger than Sample 2
t-statistic < t-critical	*p*-value > α		Samples are from same population

* For information on how to calculate t-statistic and t-critical refer to [10]

4. ANALYSIS

4.1. Objective of the analysis

Information on existing uranium deposits, their resource contents and average grades can be useful in modeling the grades and tonnages of the undiscovered deposits from the same geological setting [1]. It is important to note that different deposit types have significantly different grades and tonnages, which are a key value to three-part assessment [1]. It is thus necessary to classify uranium deposits into types such that all deposits of the same type have characteristic geological similarities, but are distinctly different from other deposit types. This is the first step in grade-and-tonnage modeling – identification of deposits that belong to one particular deposit type. Interestingly, looking from a different perspective, the grade-and-tonnage model can be used to classify deposits and to search for possible sub-classification.

The present study aims at developing grade-and-tonnage models for different uranium deposit types. As seen from Zipf's law, natural systems follow power law relationships [12] and likewise characteristic properties of mineral deposits such as grade or tonnage tend to follow log-normal frequency distribution [1]. Frequency grade-and-tonnage modeling involves fitting log-normal distributions to the tonnages and grades of existing uranium deposits of each particular type and determining their statistical significance.

In the current analysis, the log-normal distribution is modeled for the grades and tonnages of each deposit type. Further, to study the effect of deposit classification and sub-classification on grade-and-tonnage modeling, the sub-types of each of the deposit types were extracted from the UDEPO dataset. The log-normal distribution fitting and goodness-of-fit statistics estimation was applied to each major sub-type (with at least more than 20 deposits) of the deposit types.

This exercise was carried out to see if the sub-types are significantly similar within themselves (indicated by high p-value) and significantly different from each other. For this, the Student's t-test was carried out to test the hypothesis that deposits classified into different sub-types actually belong to different populations. All possible pairs of sub-types of each deposit type were taken into consideration and the t-statistic and p-values were determined.

4.2. Frequency grade and frequency tonnage modeling by deposit types

The analysis described here is carried out in Microsoft Excel and Matlab. However, any database management tool and mathematical programming software can be used. First, the deposits belonging to the same deposit type were extracted from the UDEPO dataset. Now, for frequency-tonnage modeling, all the tonnage data were extracted from this reduced dataset and further analysis was carried out on this subset of tonnages. Similarly, for frequency-grade modeling, all the grade data for each deposit type are extracted [1].

The next step was to model the frequency distributions of the tonnages and grades of deposits of each type. For frequency tonnage modeling, tonnages are sorted in ascending order. The observed cumulative frequency $F(X)$ for a deposit is defined as the proportion of deposits with tonnage less than the tonnage of that deposit for grade-and-tonnage modeling. The cumulative frequencies of all deposits of that type are determined by simple counting.

The next step was to fit log-normal distribution to the tonnage and grade values. The maximum likelihood estimates of the parameters of the best fit log-normal distribution were determined. These are the log mean and the log standard deviation. In addition, the 95% confidence interval estimates of these parameters were calculated using the chi-square test. In this analysis, the Lilliefors test was used to quantify the degree to which the deposit grade- and tonnage-frequency distributions follow log-normal distribution. The following statistics were calculated as a measure of degree of log-normality in the data: the 95% confidence interval of the log mean and log standard deviation, the p-value, the K-S statistic, and the critical K-S value. Each of these is described in the previous section (Table 2). The smaller the confidence interval, the greater is the degree of certainty in estimated distribution parameters. Thus, a smaller confidence interval is an indirect indicator of the goodness-of-fit. The p-value is used as a direct indicator of the goodness-of-fit. The higher the p-value, the better is the fit. A poor fit could reflect mixed extent of exploration among the deposits of a particular deposit type, although it is not necessary that a good fit can only exist if all deposits are well explored. A good fit could be an indication that the deposits tend to have similar geological characteristics and it is less likely for significantly different sub-types to exist within this deposit type. Similar analysis is done for frequency-grade modeling.

4.3. Grade vs tonnage plots by deposit types

Economic planning of uranium exploration would require the mining firms to identify deposits from which uranium can be extracted profitably. Different deposit types and their sub-types require different production methods for extracting uranium from the ore. In general, tonnage can be used as an indicator of the production capacity of a deposit. The capacity of mines is based on tonnage. High grade and high tonnage deposits are targets for production companies. These deposits can be located easily on a grade vs. tonnage plot. The principle behind such a plot and the diagonal lines of constant metal has been described in the previous section. High tonnage deposits where uranium is a by-product of the mining of other economic minerals like Olympic Dam in Australia are also of interest to mining companies. For these deposits, an equivalent grade versus tonnage plot is necessary.

4.4. Grade-and-tonnage modeling by deposit sub-type and country

The goodness-of-fit, as mentioned before, is a good indicator of the statistical similarity between the deposits of a given type. Anomalies in log-normal behavior of the observed grades and tonnages indicate differences between the sub-types of the deposit type, mixed mining methods, or data quality issues. There are two approaches to confirm this. First, the frequency grade and frequency tonnage model of the sub-types are generated. If the goodness-of-fit is found to improve for the sub-type models over the deposit super type, this suggests that the deposits of the sub-type belong to a population that is statistically different from the parent deposit type. The second approach is to sort out the deposit sub-types within each deposit type and to check for significant statistical differences between the two groups.

In the present study, the first approach was implemented using the Lilliefors goodness-of-fit test and the second approach was implemented using the t-test. The sub-types chosen for modeling are based on the constraint of minimum number of data-points required for the model. Only sub-types with at least 20 deposits were chosen for analysis. If the number of data points is less than 20, the sample may not be representative of the actual population of deposits of that type, and the estimated parameters would have considerable uncertainty. An analysis similar to the one carried out for frequency-grade and frequency-tonnage modeling of deposit types was followed for the sub-types.

The deposit sub-types of sandstone-hosted deposits that were modeled are shown in Table 4. Some of these deposit types and sub-types are predominantly found in particular countries. Although a country is defined by a political boundary, which has no bearing on the underlying geology, the geographical location of the deposits could be a deciding factor in discriminating them into different populations. In this analysis, geographical location of the deposits, inferred from the country to which they belong is considered as a crude approximation of the province boundaries. The second approach used the t-test to test the hypothesis that two groups belong to the same population.

TABLE 4. DEPOSIT SUB-TYPES USED FOR ANALYSIS

Deposit type	Sub-types modeled
Sandstone-hosted	Roll-front type
	Basal channel
	Tabular
	Tectonic-lithologic

5. RESULTS AND INTERPRETATIONS

5.1. Grade-and-tonnage modeling by deposit type

The grade vs. tonnage plots for all deposit types of uranium are presented in Fig.s 10 to 23. The diagonal lines of constant metal with negative slope are plotted on the grade-tonnage scatter plots. The legend indicating the constant metal value is given alongside.

5.2. Frequency grade models by deposit type

Figs 24 to 34 show the frequency-grade models for different deposit types. The blue line plot is the log-normal distribution fitted to the dataset. The red scatter points are the observed values of cumulative frequency corresponding to the deposit grade values expressed in logarithm base 10 on the x-axis. The numbers of deposits of the lignite coal, collapse breccia, carbonate-hosted and polymetallic breccia types were less than 20 and, hence, were not considered for the models.

The maximum likelihood fitted parameters of the log-normal distribution (i.e., the log mean and the log standard deviation, the 95% confidence interval of the estimated parameters obtained using the chi-squared test and the K-S goodness-of-fit statistics) for frequency-grade modeling are shown in Table 5.

It can be observed from the plots (Figs 24 to 34) that the deposits represented by the scatter plots are oriented along the fitted log-normal distribution curves. However, it is necessary to quantify how well the deposits conform to the assumption of log-normality. The estimated log means (base e) of grades is negative for all deposit types. This is because all uranium deposits have less than 1% uranium metal in the ore. In addition, the more negative the mean, the lower is the grade of that deposit type. Thus, these results indicate that phosphate deposits have the lowest ore grades (mean = -4.18) while Proterozoic unconformity deposits have the highest ore grades (mean = -0.55).

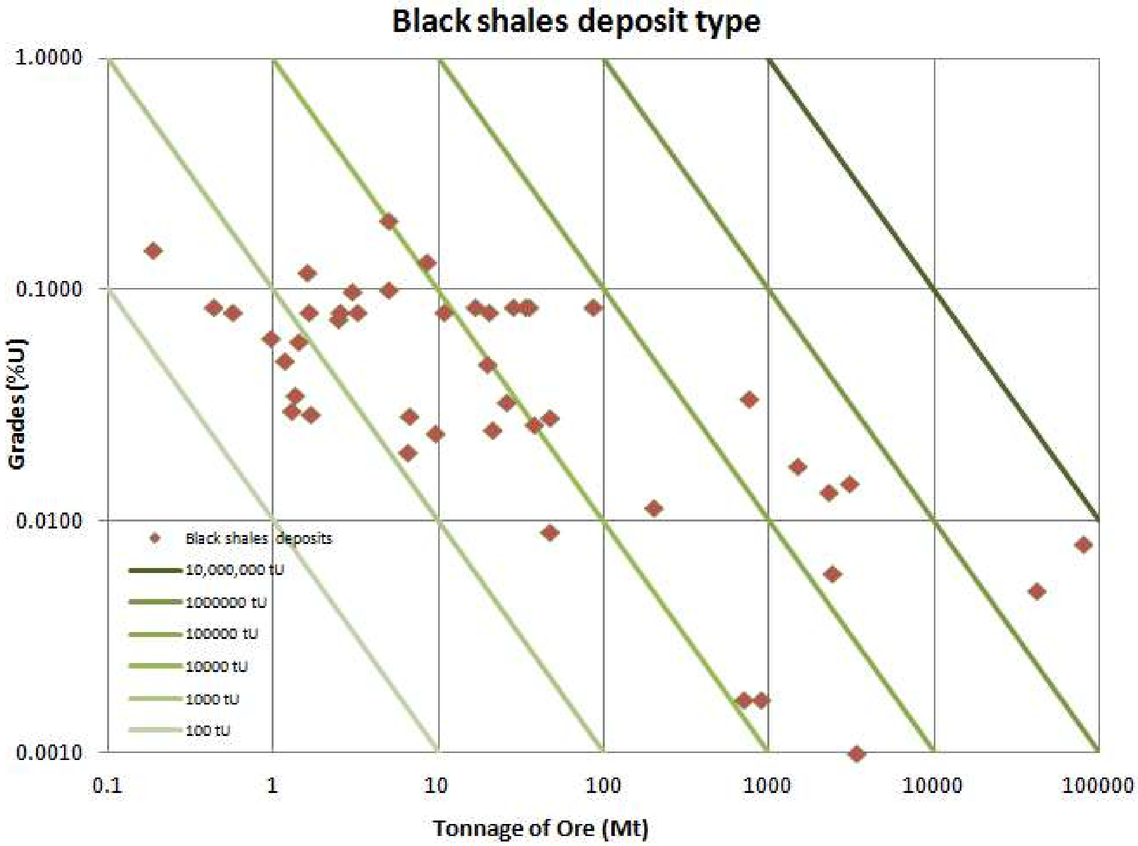

FIG. 10. Grade-tonnage plot for black shale type uranium deposits.

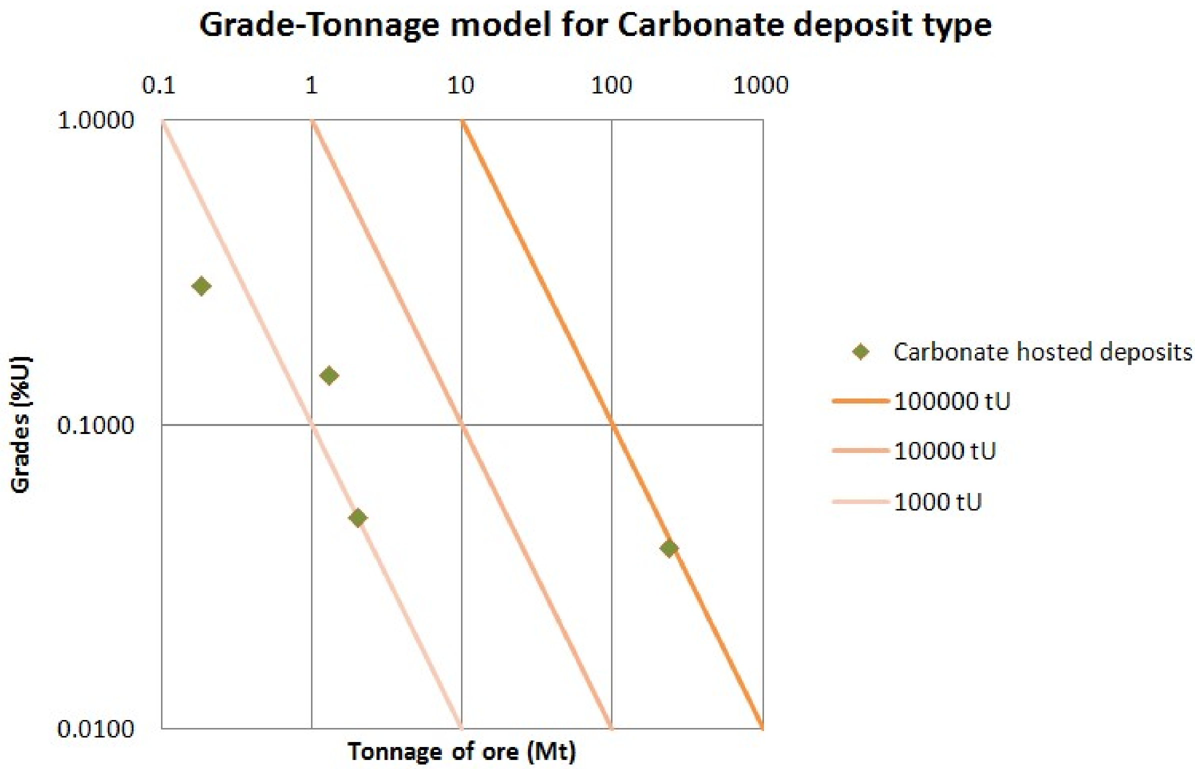

FIG. 11. Grade-tonnage plot for carbonate-hosted deposits.

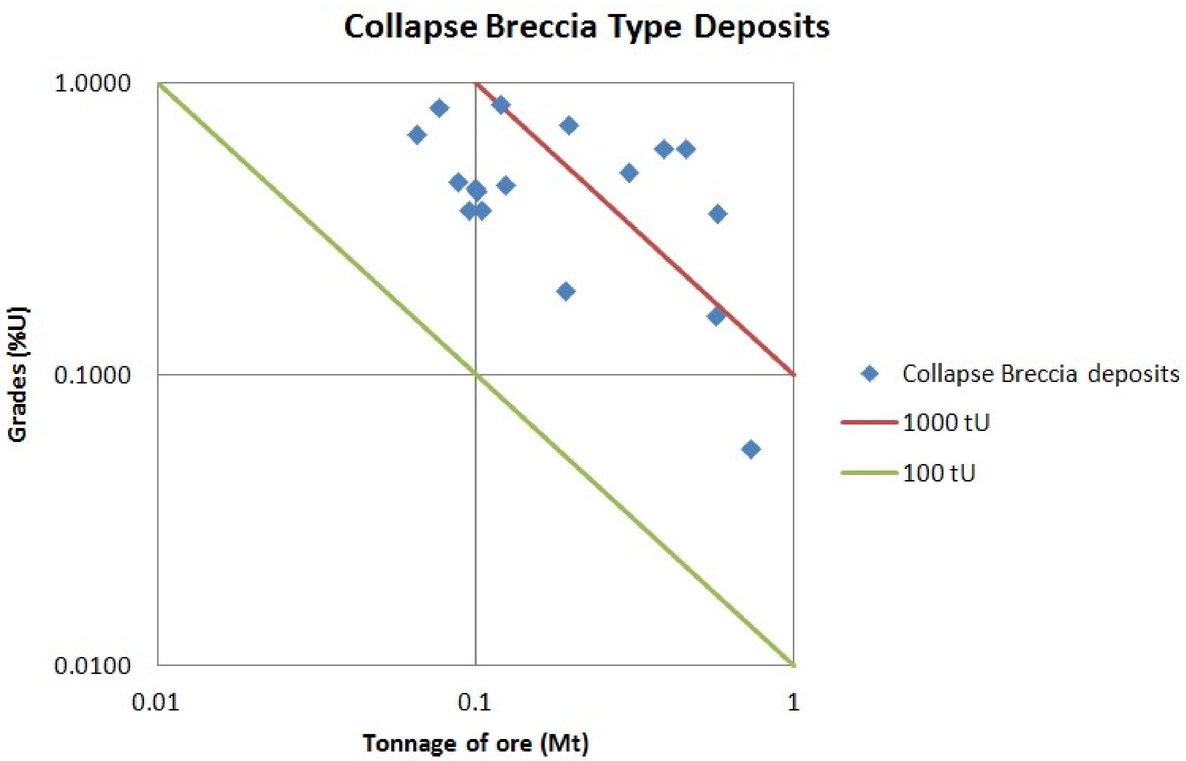

FIG. 12. Grade-tonnage plot for collapse breccia type deposits.

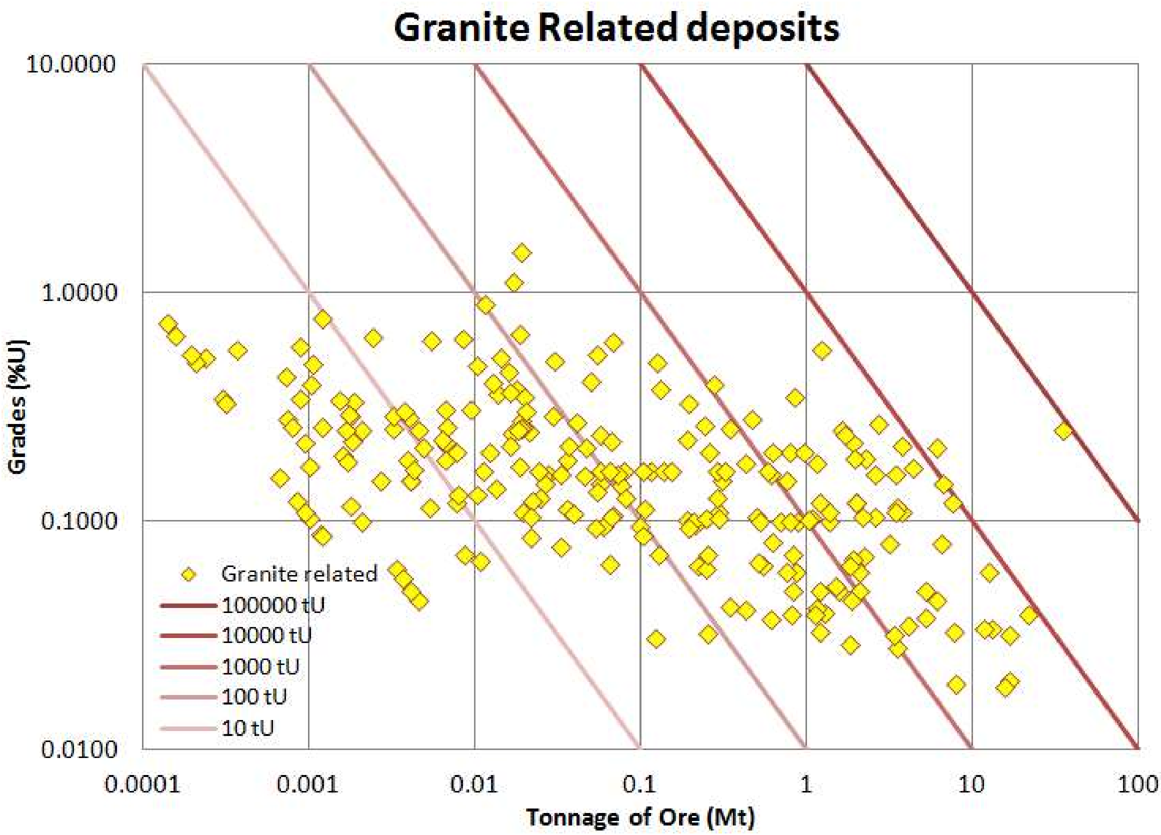

FIG. 13. Grade-tonnage plot for granite-related deposits.

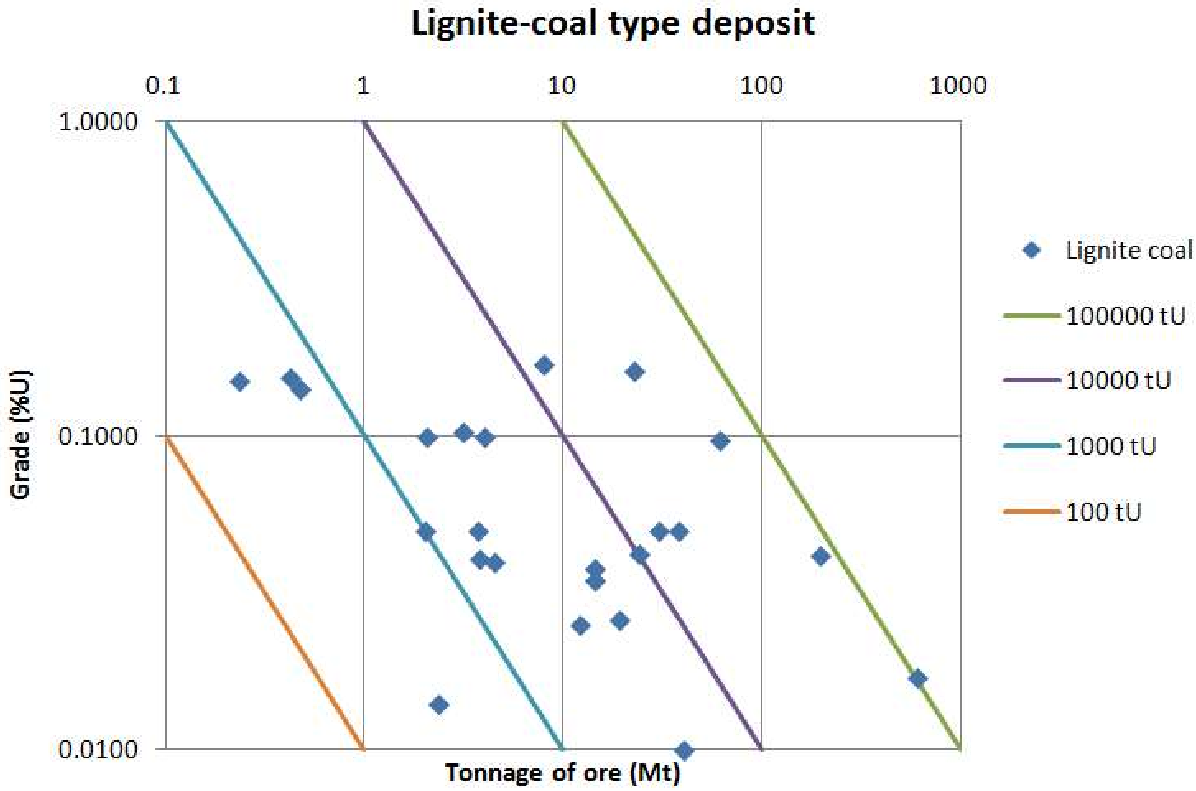

FIG. 14. Grade-tonnage plot for lignite coal type deposits.

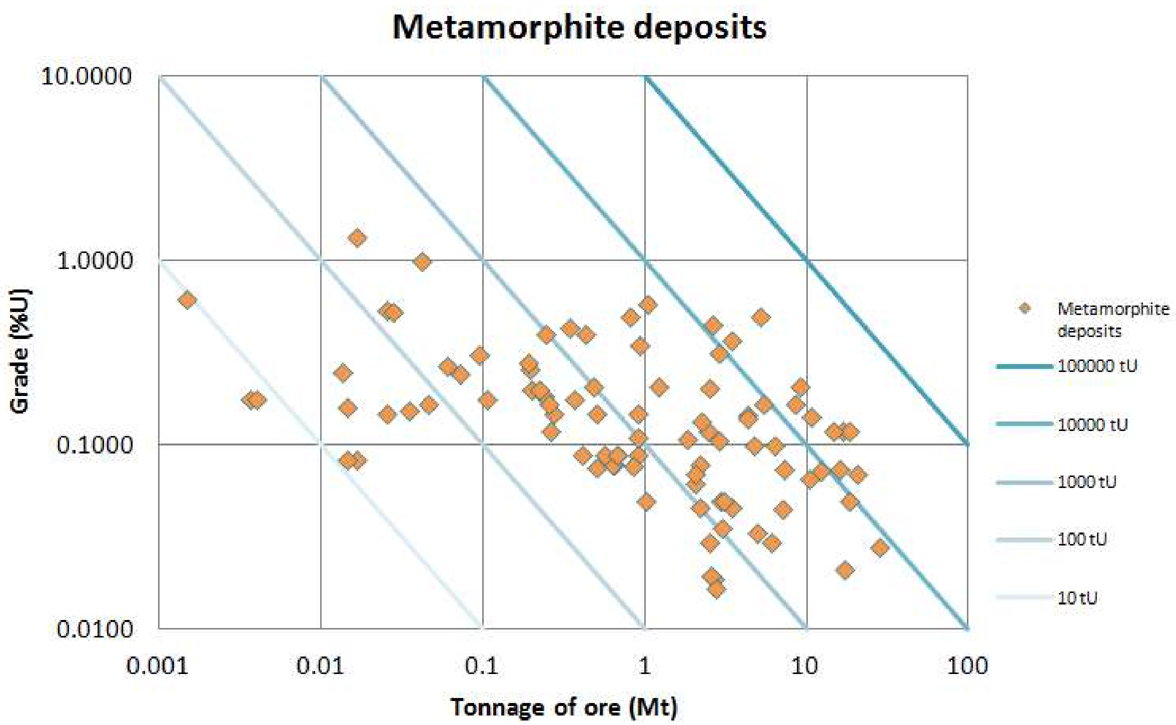

FIG. 15. Grade-tonnage plot for metamorphite type uranium deposits.

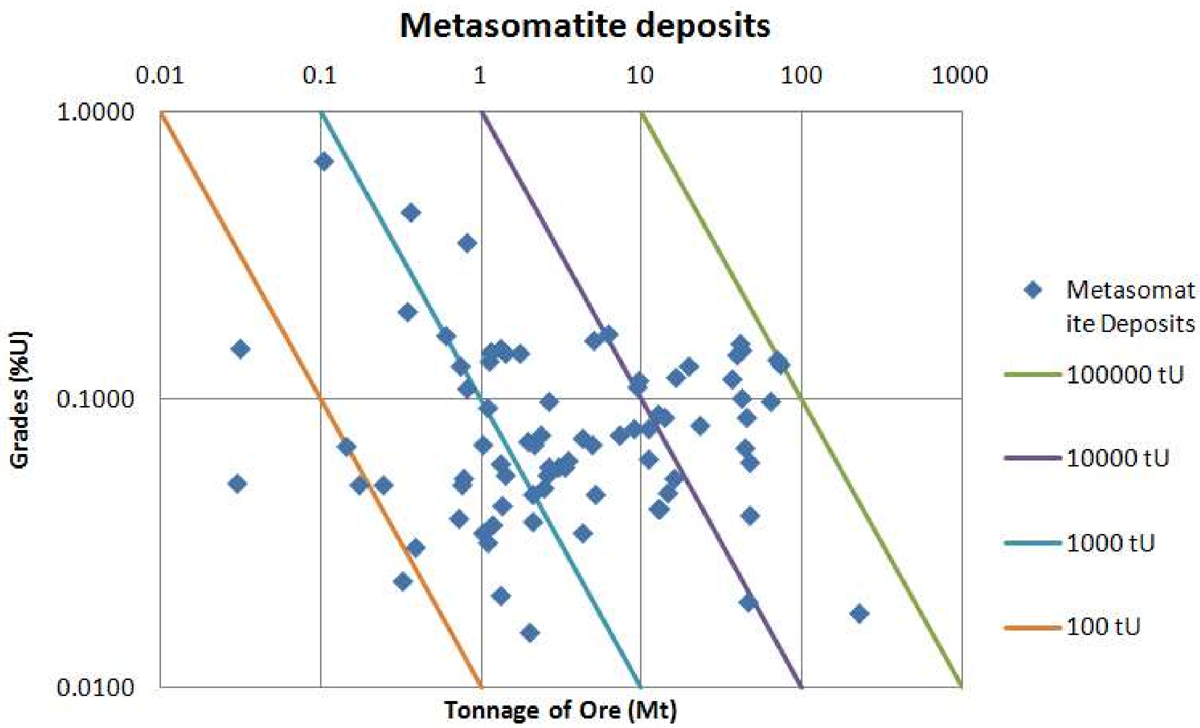

FIG. 16. Grade-tonnage plot for metasomatite type deposits.

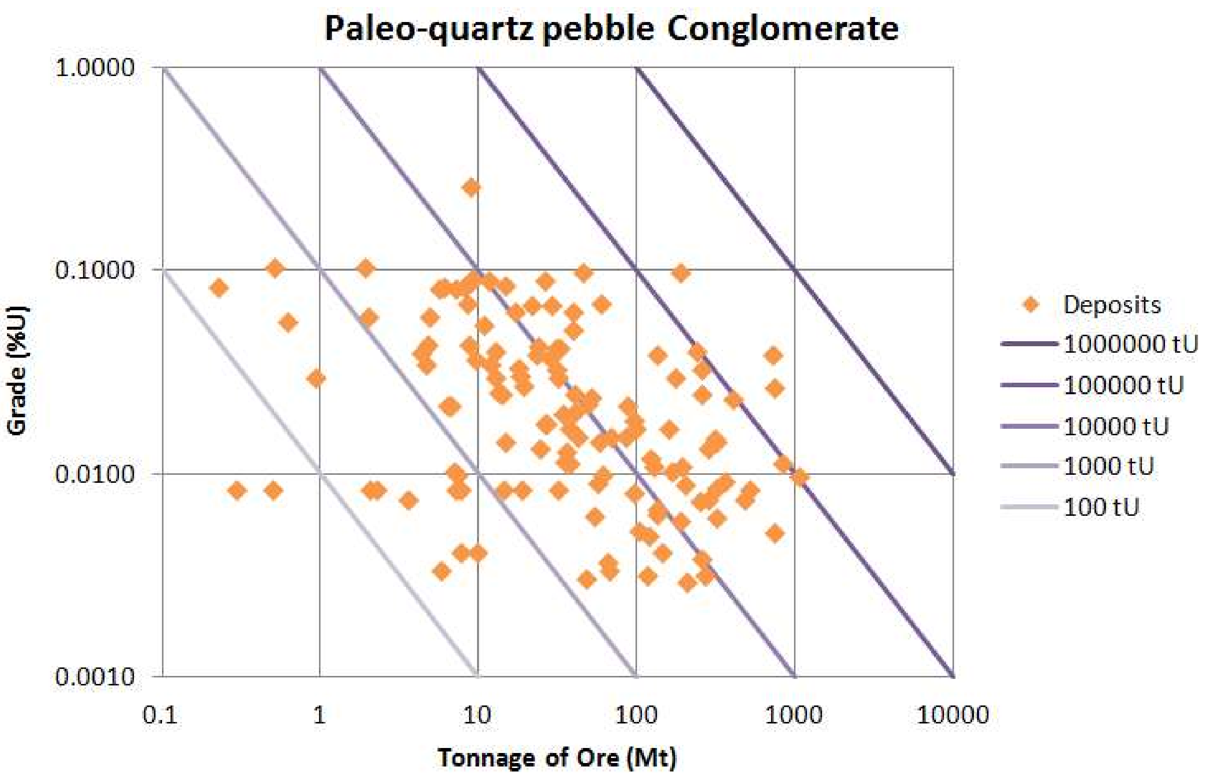

FIG. 17. Grade-tonnage plot for paleo-quartz pebble conglomerate type deposits.

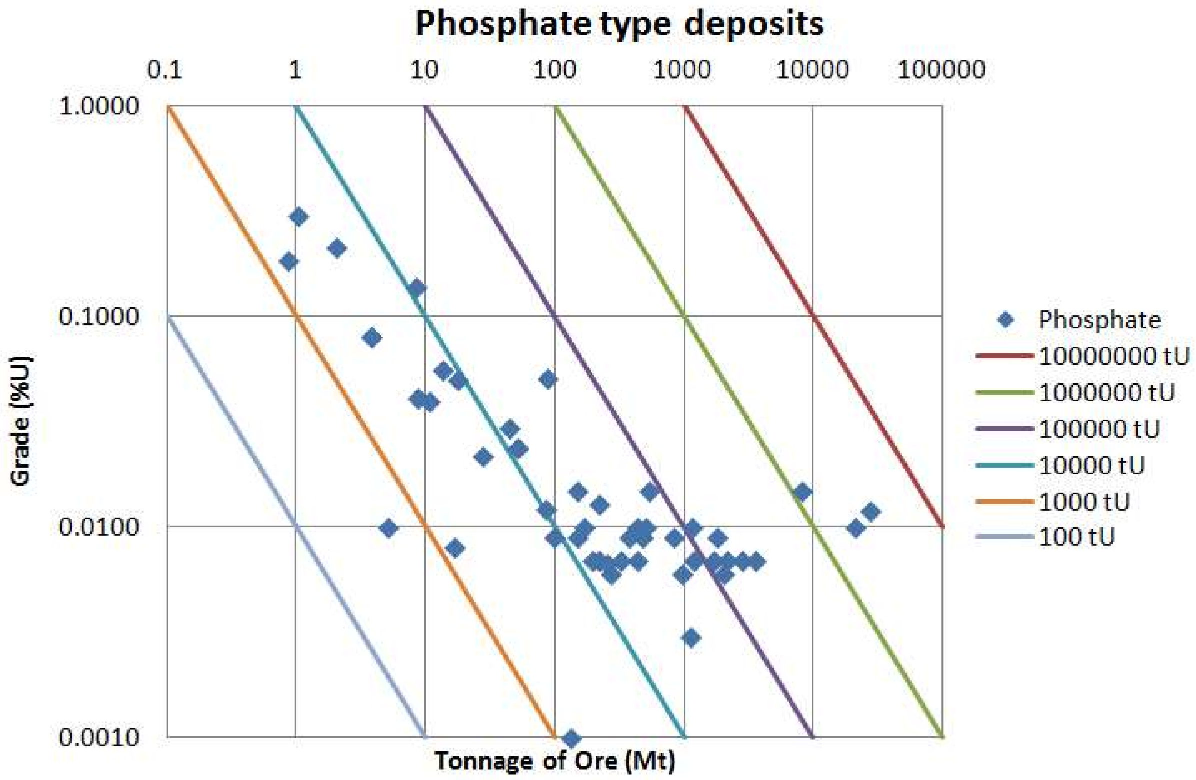

FIG. 18. Grade-tonnage plot for phosphate type deposits.

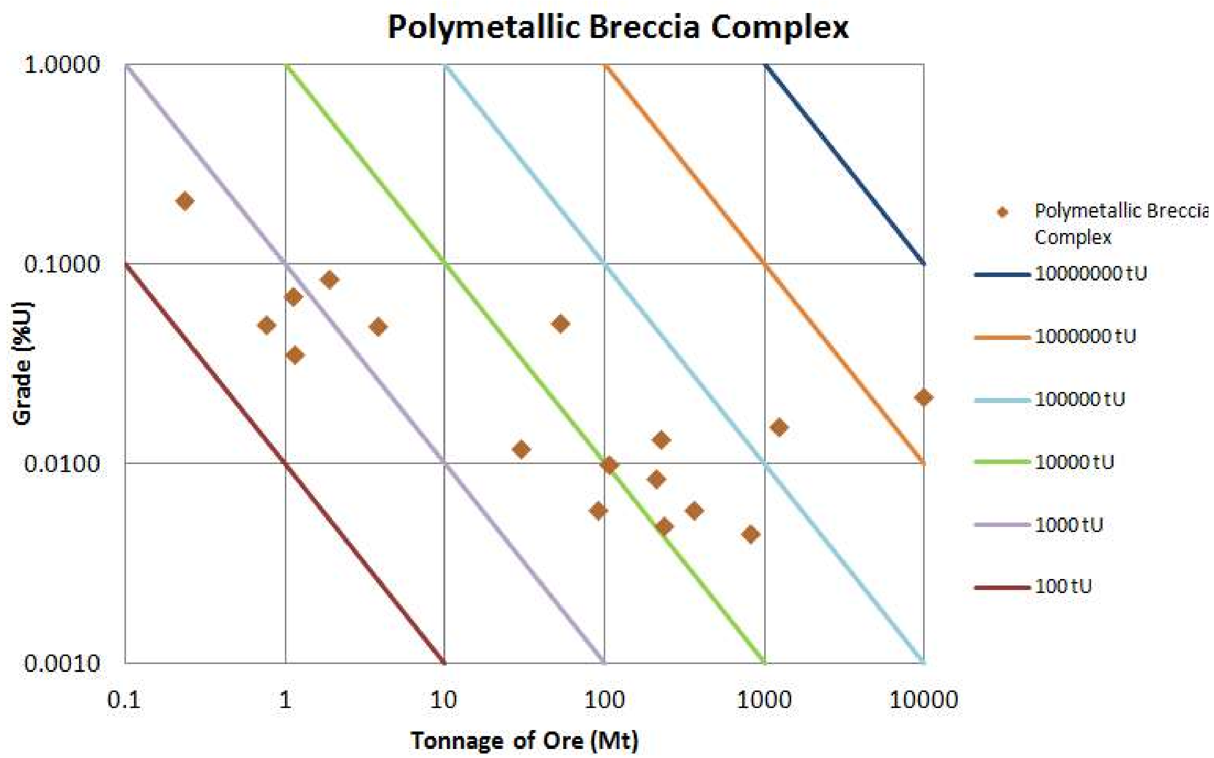

FIG. 19. Grade-tonnage plot for polymetallic breccia type deposits.

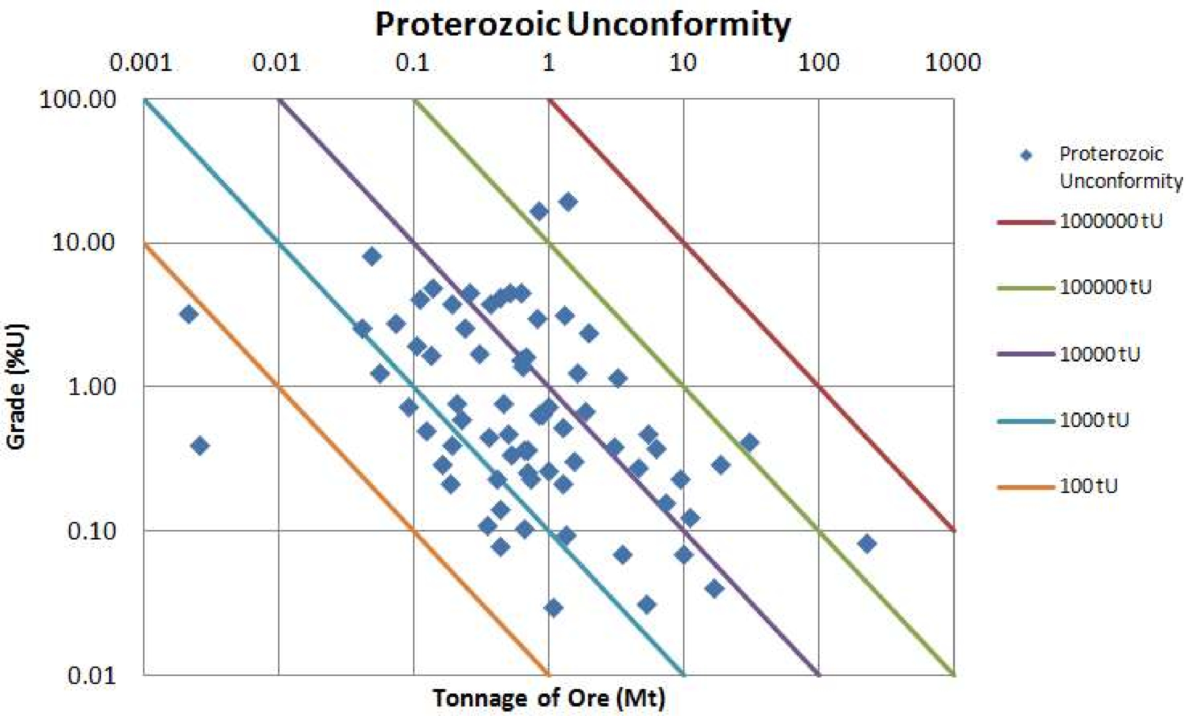

FIG. 20. Grade-tonnage plot for Proterozoic unconformity type deposits.

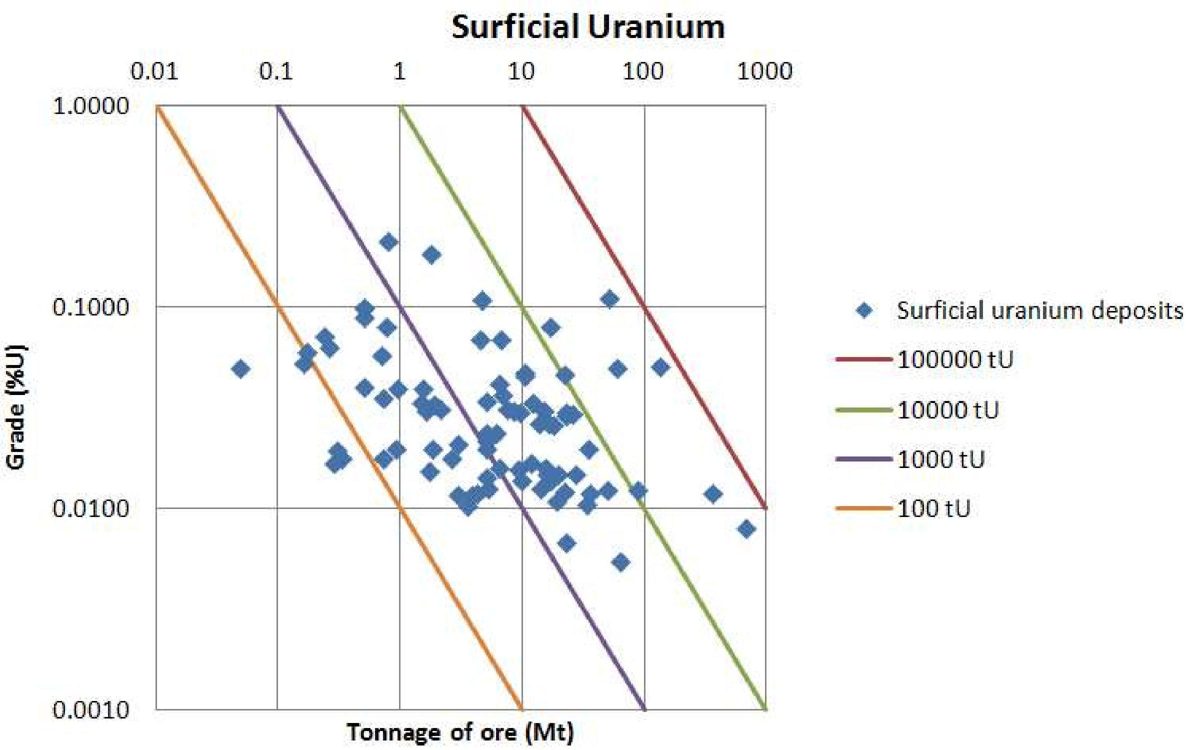

FIG. 21. Grade-tonnage plot for surficial uranium deposits.

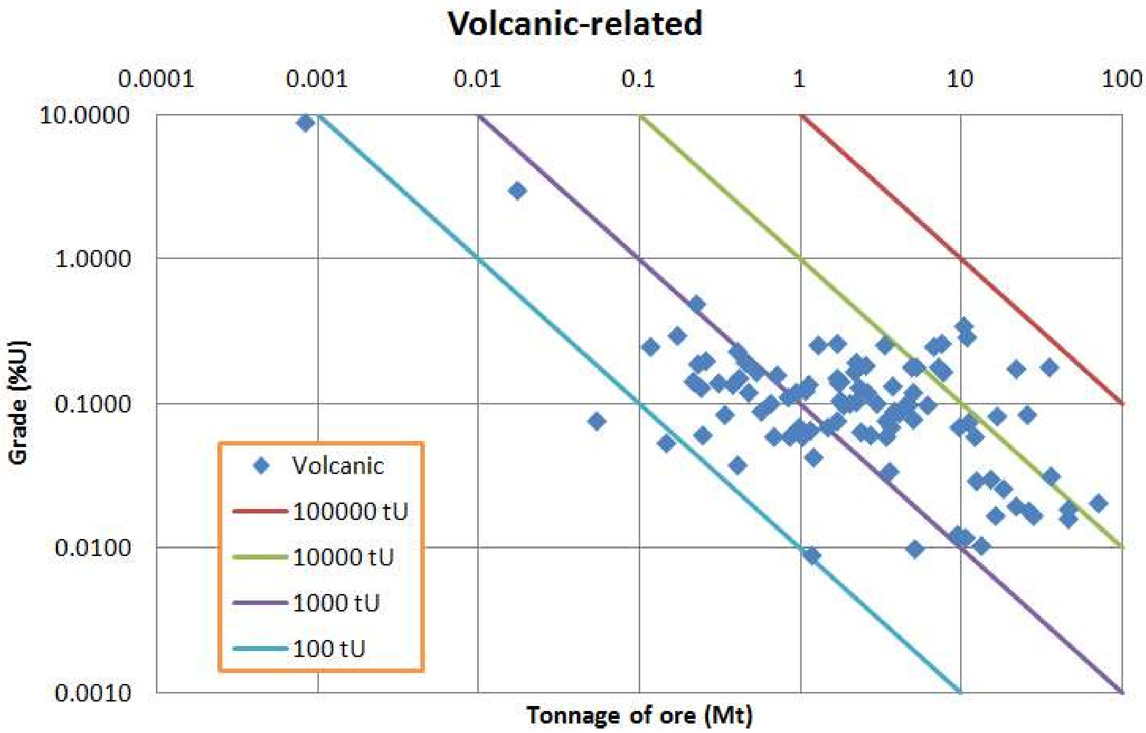

FIG. 22. Grade-tonnage plot for volcanic-related deposits.

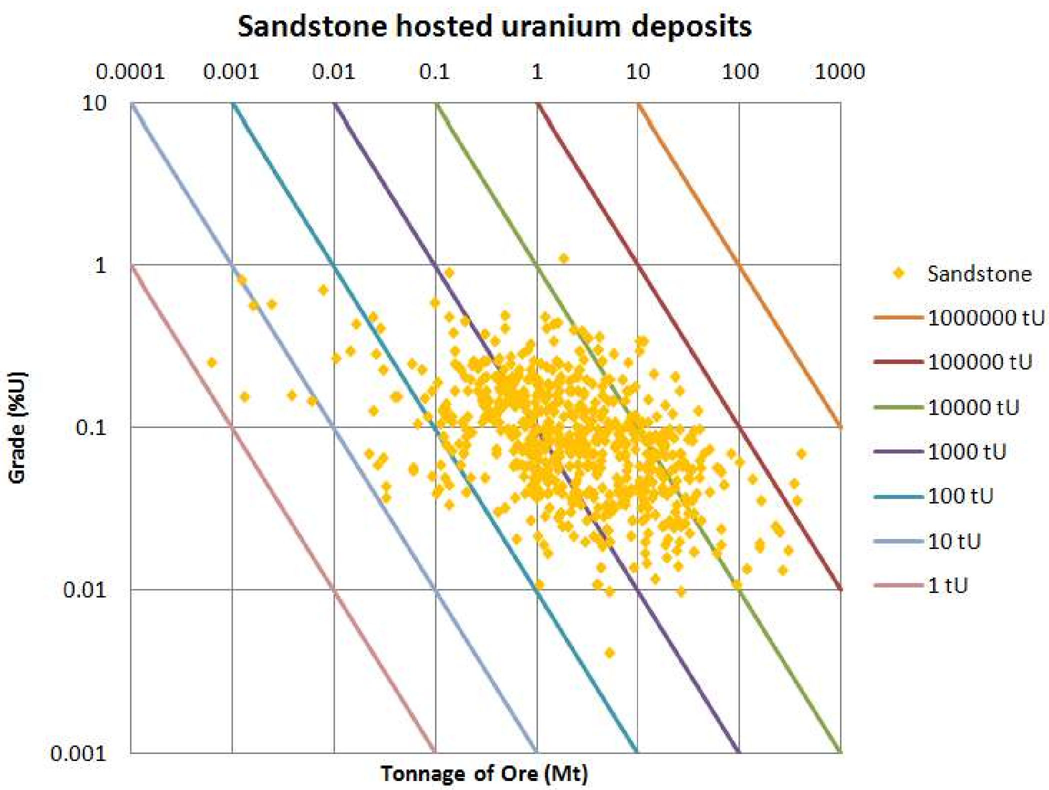

FIG. 23. Grade-tonnage plot for sandstone-hosted uranium deposits.

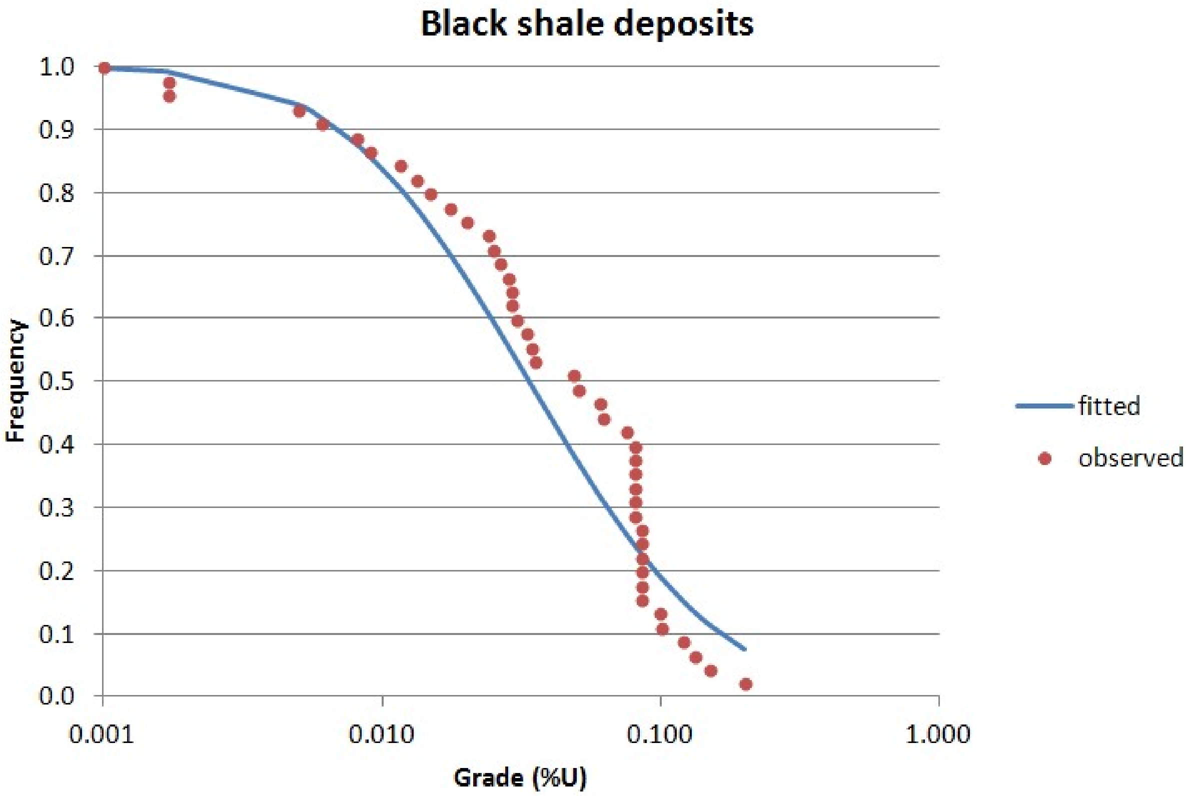

FIG. 24. Frequency-grade plot for black shale deposit type.

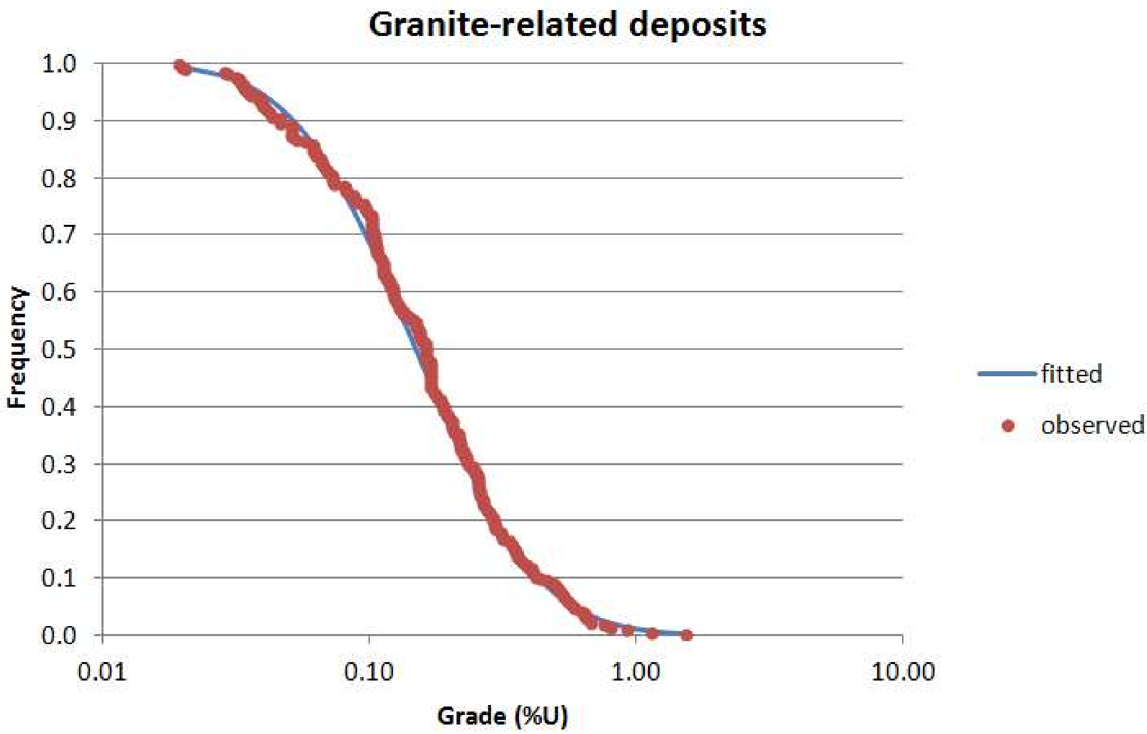

FIG. 25. Frequency-grade plot for granite-related deposits.

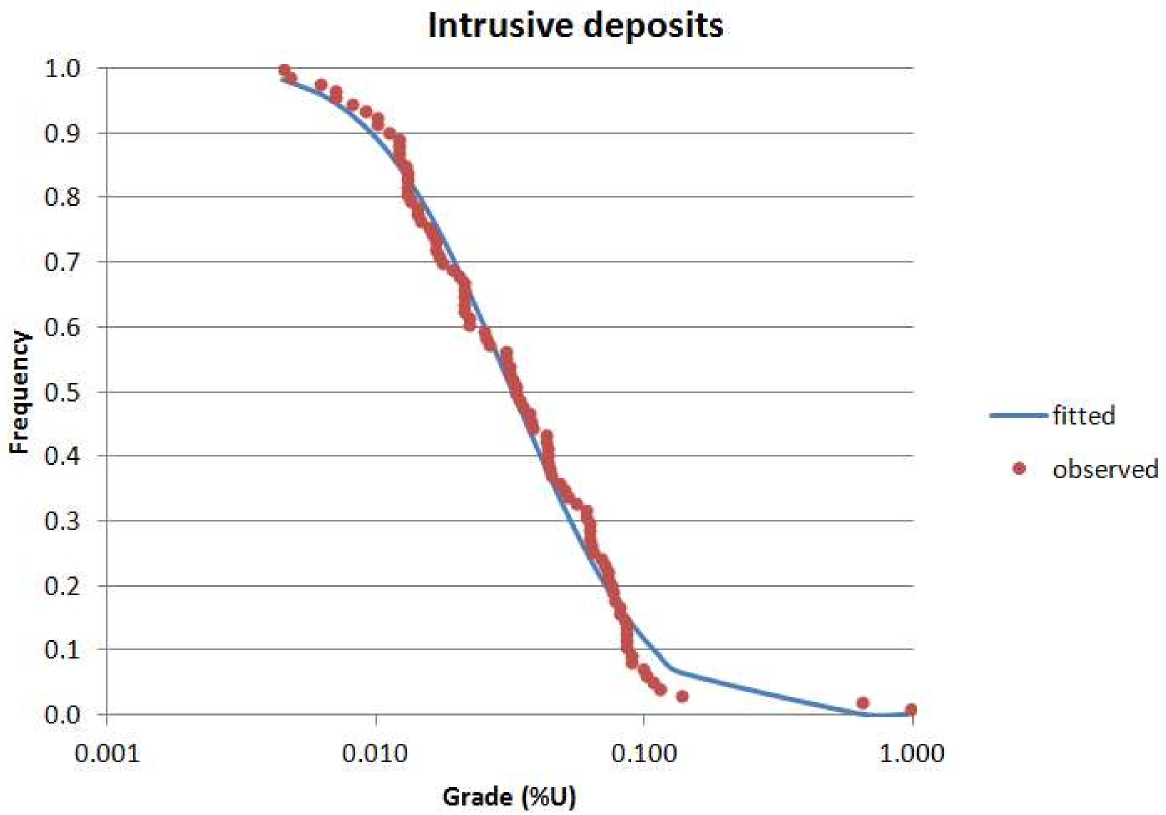

FIG. 26. Frequency-grade plot for intrusive deposit types.

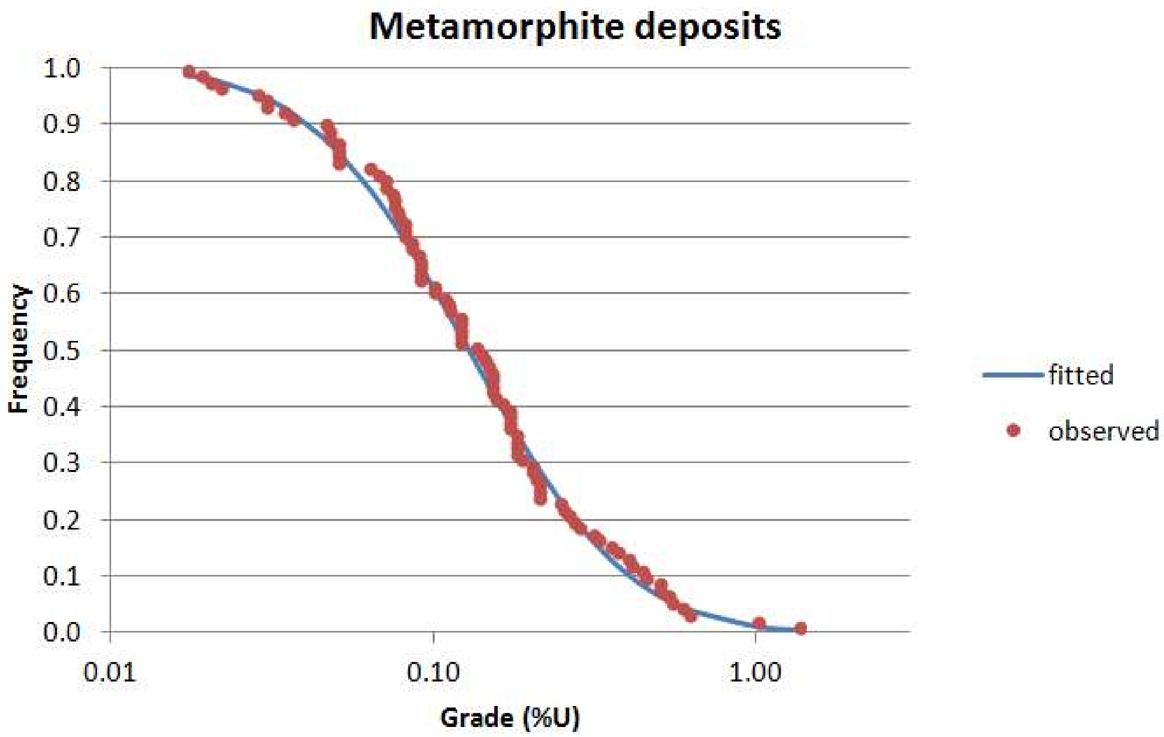

FIG. 27. Frequency-grade plot for metamorphite deposits.

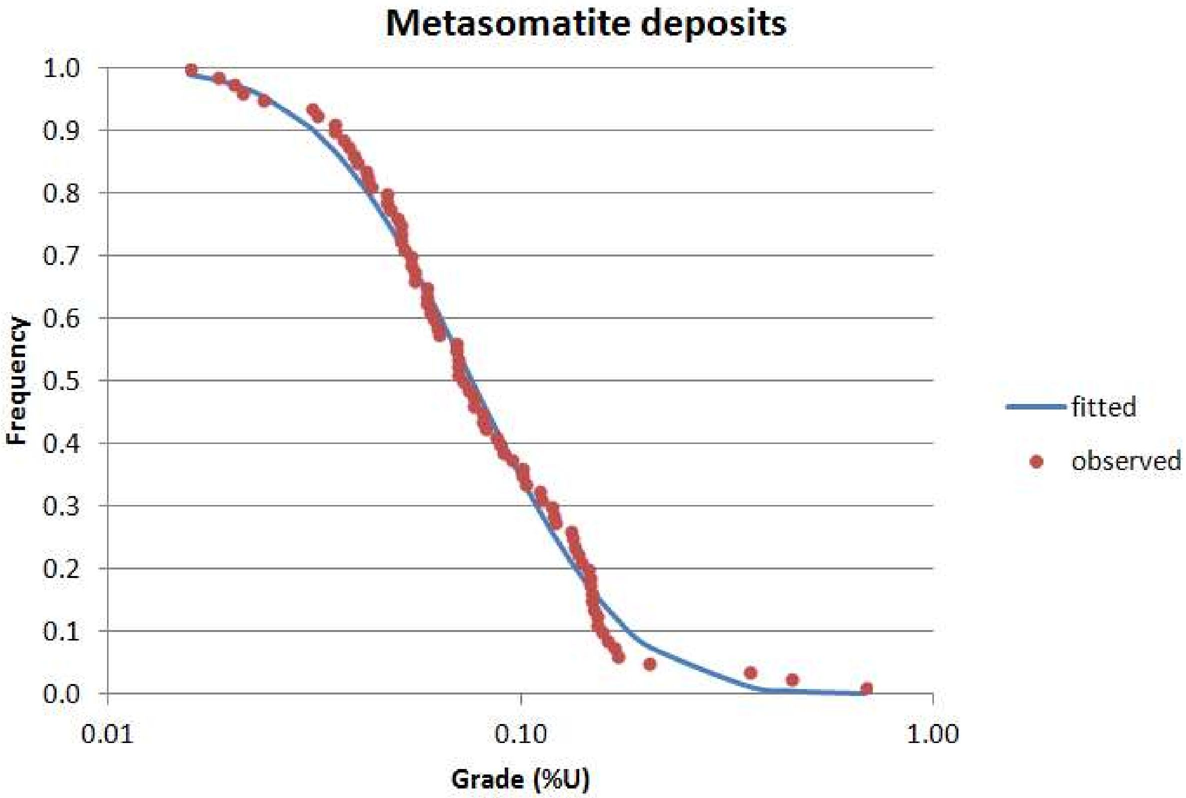

FIG. 28. Frequency-grade plot for metasomatite deposits.

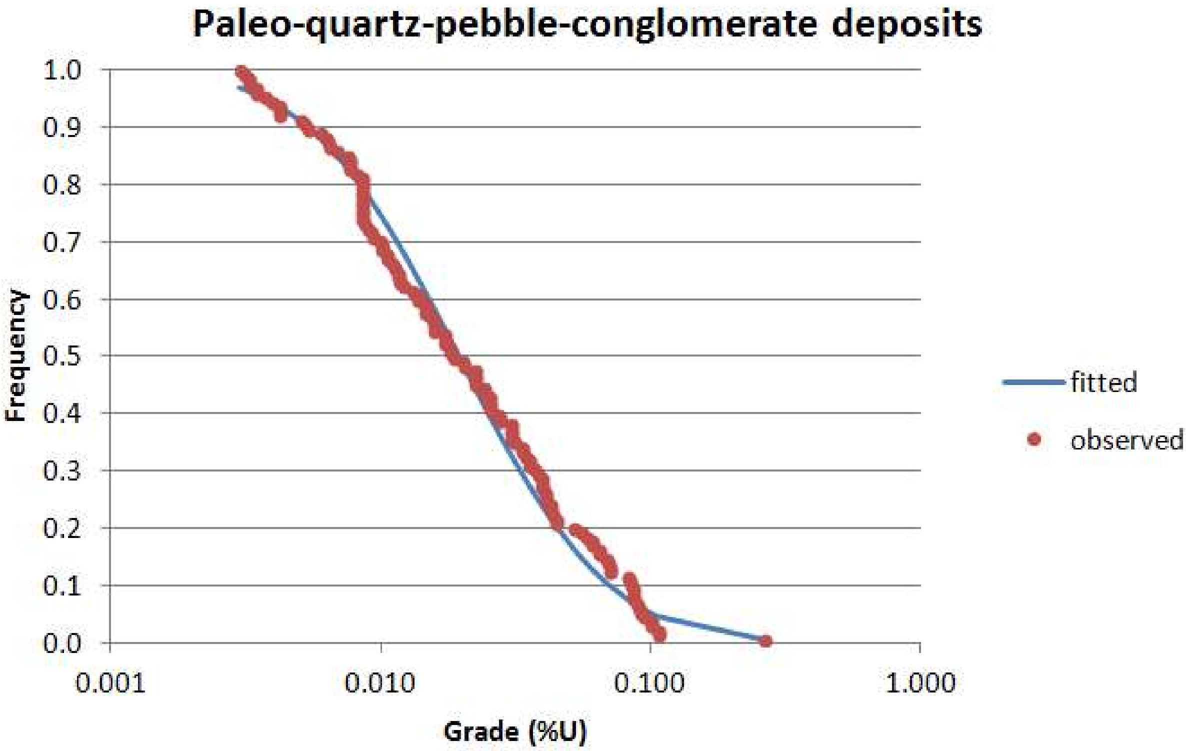

FIG. 29. Frequency-grade plot for paleo-quartz pebble conglomerate type deposits.

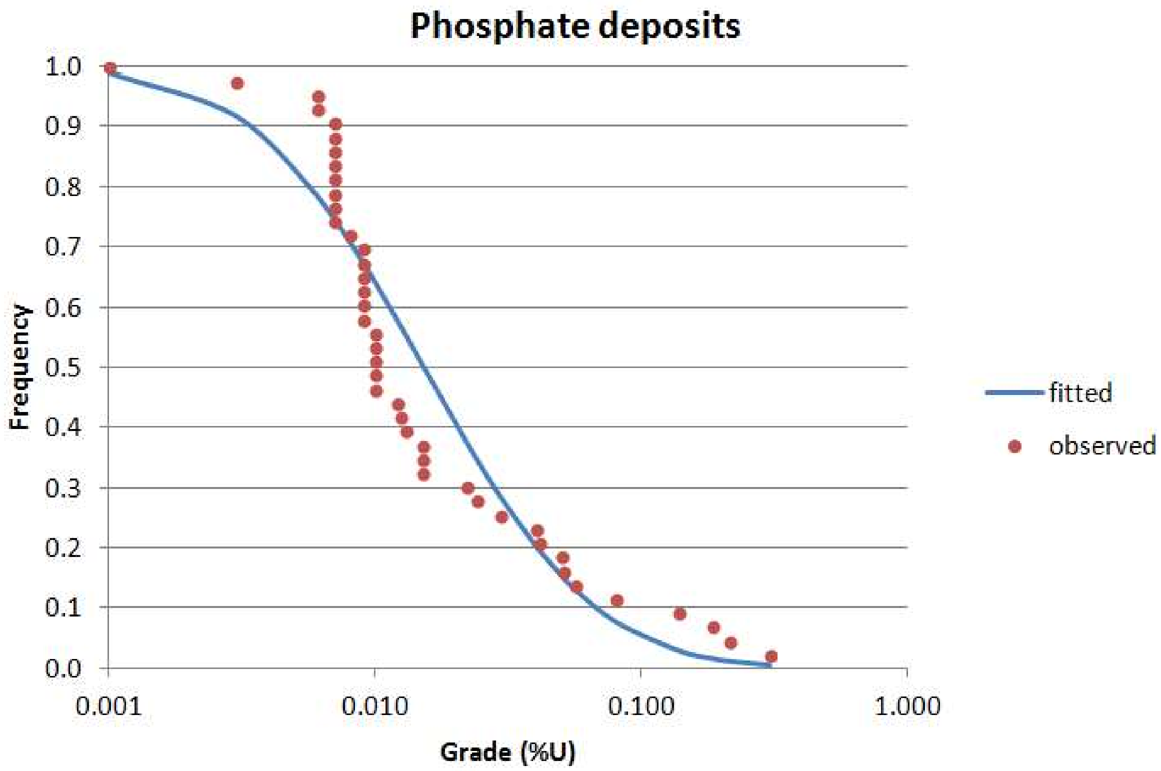

FIG. 30. Frequency-grade plot for phosphate type deposits.

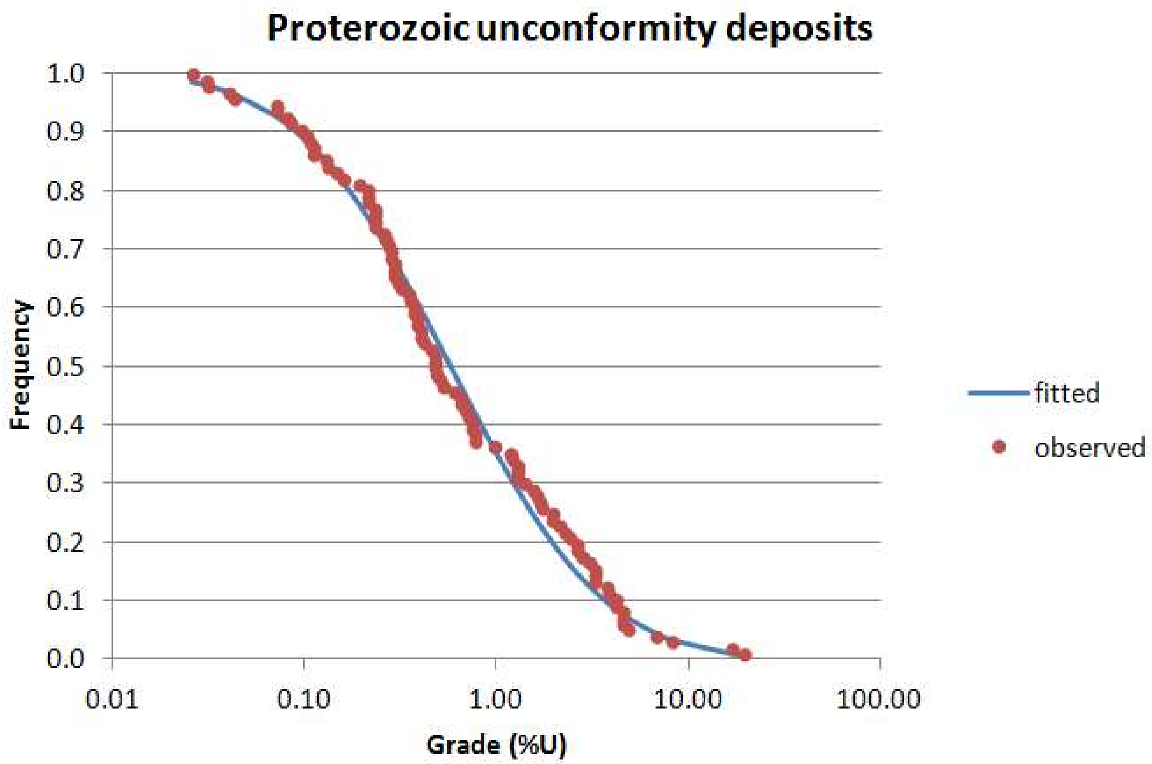

FIG. 31. Frequency-grade plot for Proterozoic unconformity type deposits.

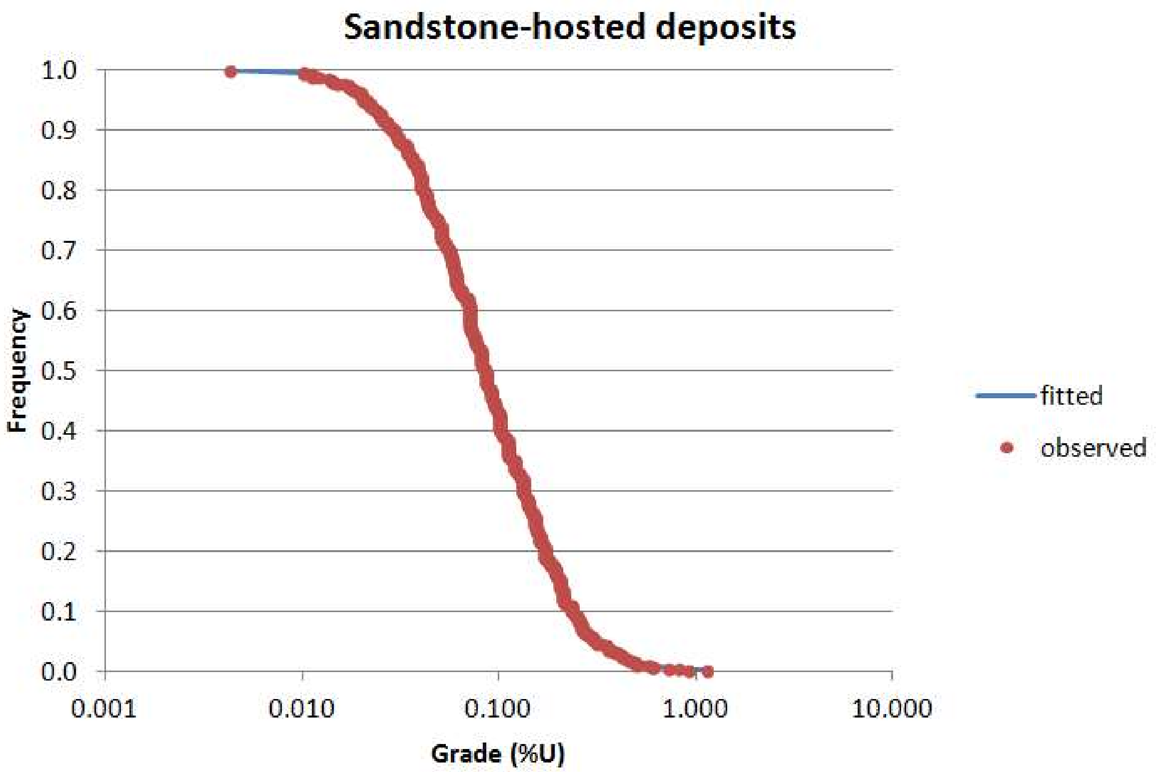

FIG. 32. Frequency-grade plot for sandstone-hosted deposits.

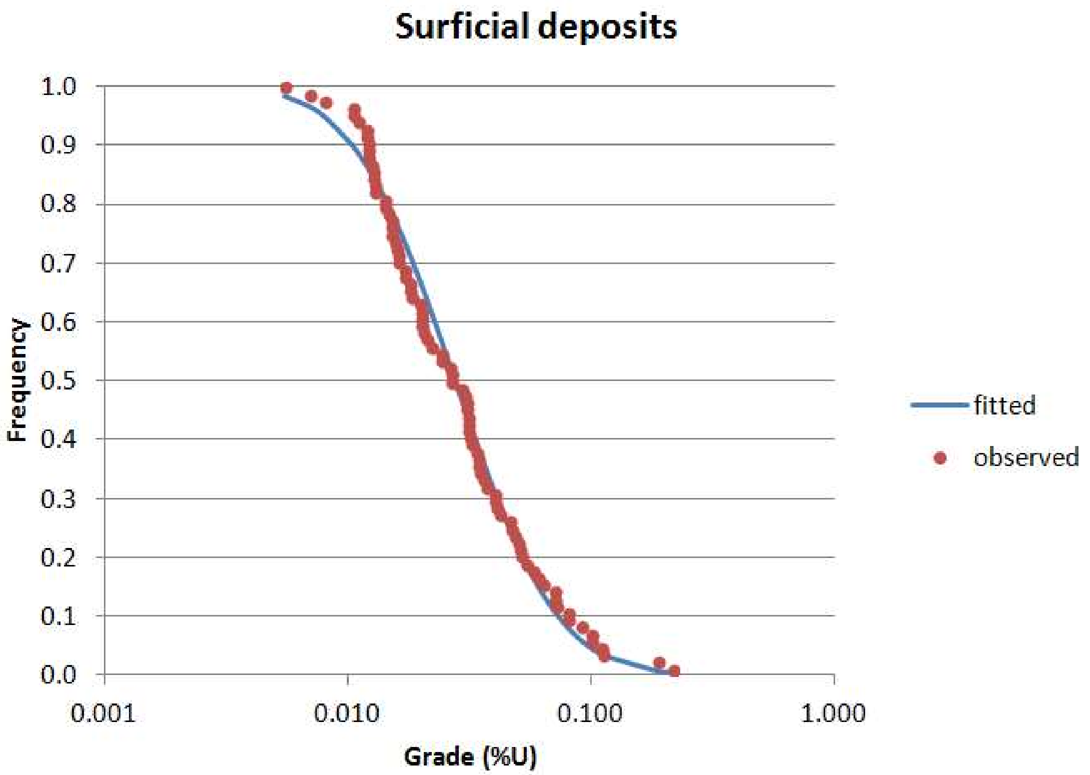

FIG. 33. Frequency-grade plot for surficial deposits.

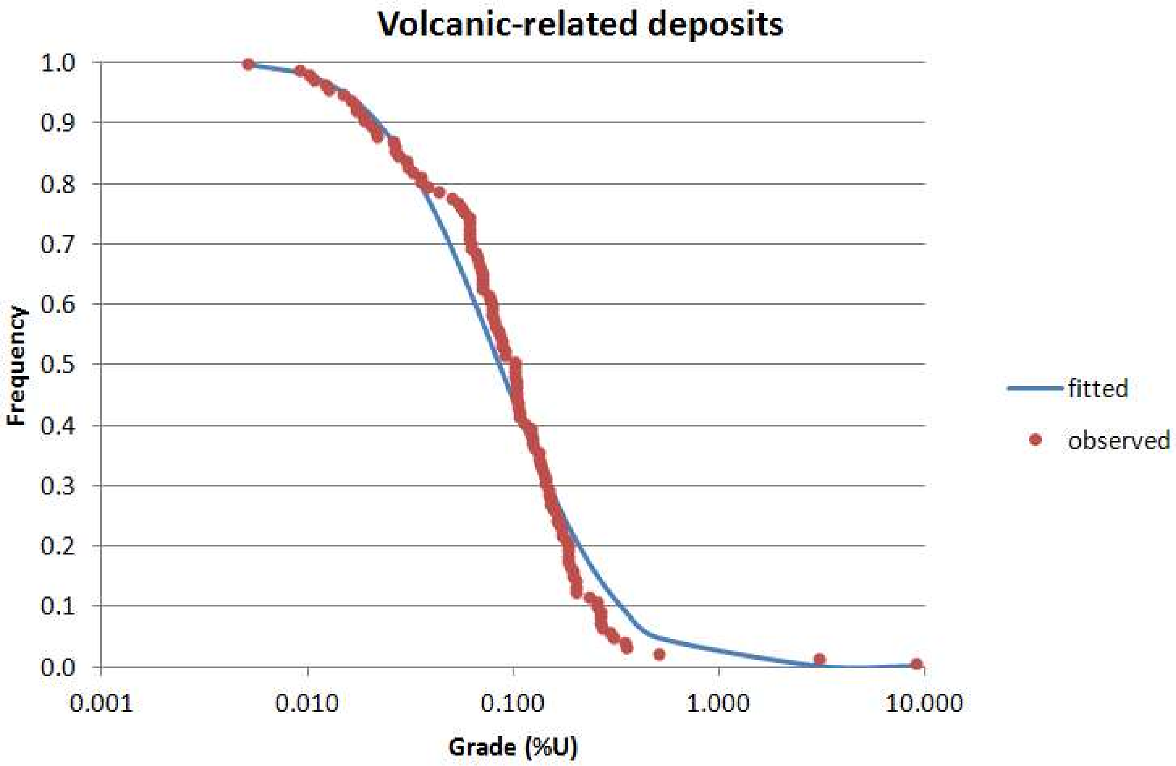

FIG. 34. Frequency-grade plot for volcanic-related deposits.

TABLE 5. LOG-NORMAL DISTRIBUTION PARAMETER ESTIMATION AND GOODNESS-OF-FIT STATISTICS FOR GRADES*

Deposit type	Mean	s.d.	95% CI of mean		95% CI of s.d.		N	*p*-value	K-S statistic	Critical K-S
Black shale	-3.39	1.23	-3.76	-3.02	1.02	1.56	45	**0.00**	0.16	0.13
Granite-related	-1.91	0.83	-2.02	-1.81	0.76	0.91	246	0.08	0.05	0.06
Intrusive	-3.43	0.95	-3.62	-3.24	0.83	1.11	94	0.28	0.01	0.09
Metamorphite	-2.05	0.90	-2.24	-1.86	0.78	1.05	91	***0.50***	0.06	0.09
Metasomatite	-2.58	0.69	-2.73	-2.42	0.60	0.81	80	0.39	0.07	0.10
Paleo-quartz pebble conglomerate	-3.94	1.00	-4.12	-3.76	0.89	1.14	128	0.14	0.07	0.08
Phosphate	-4.18	1.16	-4.54	-3.82	0.96	1.48	43	**0.00**	0.20	0.13
Proterozoic unconformity	-0.55	1.45	-0.84	-0.26	1.27	1.69	96	0.23	0.07	0.09
Sandstone	-2.48	0.83	-2.54	-2.42	0.78	0.88	643	0.47	0.02	0.04
Surficial	-3.59	0.76	-3.76	-3.43	0.66	0.89	84	0.10	0.09	0.10
Volcanic	-2.46	1.06	-2.65	-2.27	0.94	1.21	118	**0.00**	0.12	0.08

* The field names 'Mean' and 's.d.' refer to the estimated log (base e) mean and the log (base e) standard deviations, that are the parameters of the log-normal distribution fitted on the dataset. The field names '95% CI of mean' and '95% CI of s.d.' represent the chi-square 95% confidence intervals of the estimated parameters. The number of unique values of grades is represented by 'N'. The other fields '*p*-value', 'K-S statistic' and 'Critical K-S' represent the outputs of the Lilliefors goodness-of-fit test. The *p*-values in bold indicate those deposit types for which the hypothesis of log-normal distribution was rejected. The highest *p*-value for Lilliefors test is 0.5 and this is marked in italics bold.

The log standard deviation values are a measure of dispersion of the observed data. High standard deviations indicate that the grades in different deposits of a particular type would have large variations about the mean. Here it is observed that the standard deviations are close to 1, which is consistent with the values obtained for other mineral deposit models except for the high standard deviation of grades (1.45) in Proterozoic unconformity deposits, which suggests more than one population is present [1]. The confidence intervals are indicative of the degree of certainty in estimates of the distribution parameters. The closer the upper and the lower confidence interval to the estimated parameter, the better is the precision of estimates, which indirectly indicates that the log-normal distribution robustly describes the observed grades.

The goodness-of-fit test results show that the K-S statistic is less than the critical K-S value for all deposit types except black shale, phosphate and volcanic-related deposits. Hence, the hypothesis that a log-normal distribution is accepted at 95% level of confidence for most deposit types. It is observed that metamorphite and sandstone-hosted deposits have better goodness-of-fit and probabilities that they come from a homogenous population of grades, indicative of similar geological characteristics within the deposit type [13].

5.3. Frequency tonnage models by deposit type

Figs 35 to 45 show the frequency-tonnage models for different deposit types. The tonnage values on the *x*-axis are expressed in log base 10. The lignite coal, polymetallic breccia, carbonate and collapse breccia pipe types of deposits have been excluded from the analysis since the number of deposits is less than 20. Similar to the frequency-grade models, the estimated parameters of the log-normal distribution, the 95% confidence intervals and the Lilliefors goodness-of-fit statistics for frequency – grade modeling are shown in Table 6. The estimated log mean (base *e*) values indicate that, on average, phosphate deposits have the largest average tonnage per deposit type while granite-related deposits are the smallest in size. This inference, in conjunction with the pie charts (Fig. 2), show that not only do the phosphate deposits have the highest total resources, but also that each individual phosphate type deposit has high resource content. Although phosphate deposits are low grade, development of technology for profitable extraction of low-grade uranium in the future may render phosphate-hosted deposits to be an important source of uranium.

TABLE 6. LOG-NORMAL DISTRIBUTION PARAMETER ESTIMATION AND GOODNESS-OF-FIT STATISTICS FOR TONNAGES*

Deposit type	Mean	s.d.	95% CI of mean		95% CI of s.d.		N	*p*-value	K-S statistic	Critical K-S
Black shale	9.04	2.36	8.33	9.75	1.95	2.98	45	0.25	0.10	0.13
Granite-related	4.67	2.54	4.35	4.99	2.33	2.79	246	**0.03**	0.06	0.06
Intrusive	7.92	2.07	7.50	8.34	1.81	2.42	94	***0.50***	0.06	0.09
Metamorphite	6.92	1.95	6.52	1.70	7.33	2.28	91	**0.02**	0.10	0.09
Metasomatite	7.82	1.94	7.39	8.26	1.67	2.29	80	0.31	0.08	0.10
Paleo-quartz pebble conglomerate	8.76	1.67	8.47	9.05	1.49	1.90	128	**0.00**	0.10	0.08
Phosphate	10.04	1.89	9.46	10.63	1.56	2.41	43	***0.50***	0.09	0.13
Proterozoic unconformity	7.69	2.50	7.18	8.20	2.19	2.91	96	**0.05**	0.09	0.09
Sandstone	7.44	1.72	7.30	7.57	1.63	1.82	643	**0.00**	0.06	0.04
Surficial	7.25	1.64	6.89	7.61	1.43	1.94	84	0.38	0.07	0.10
Volcanic	7.38	1.76	7.06	7.70	1.56	2.02	118	0.31	0.06	0.08

* The field names 'Mean' and 's.d.' refer to the estimated log (base e) mean and the log (base e) standard deviations, that are the parameters of the log-normal distribution fitted on the dataset. The field names '95% CI of mean' and '95% CI of s.d.' represent the chi-square 95% confidence intervals of the estimated parameters. The number of unique values of grades is represented by 'N'. The other fields '*p*-value', 'K-S statistic' and 'Critical K-S' represent the outputs of the Lilliefors goodness-of-fit test. The *p*-values in bold indicate those deposit types for which the hypothesis of log-normal distribution was rejected. The highest *p*-value for Lilliefors test is 0.5 and this is marked in italics bold.

For granite-related, metamorphite, paleo-quartz pebble conglomerate, Proterozoic unconformity and sandstone-hosted deposits, the hypothesis of log-normal distribution is rejected. Compared to grades, tonnages show poor fit with log-normal distribution. The reason could be attributed to the higher uncertainty in estimates of total endowment of a deposit compared to ore grade. Accurate estimation of the total endowment of a deposit requires it to be delineated fully in three-dimensions. Since the dataset here comes from regions across the globe with varied degrees of exploration, uncertainty in the reported values of tonnages can be expected. The consistently high standard deviations of tonnage that are over 1.0 in each of the types strongly suggest data issues that need to be addressed [1]. One of the possible explanations for the high standard deviations is that the spatial rules to combine adjacent deposits has not been applied to this data. It is likely also that many of the small tonnage deposits have not been thoroughly explored and should be excluded from analysis. An additional explanation is the existence of sub-types within these types. This recognition is based on experience in construction and examination of over 100 grade tonnage models [1], [2], [4].

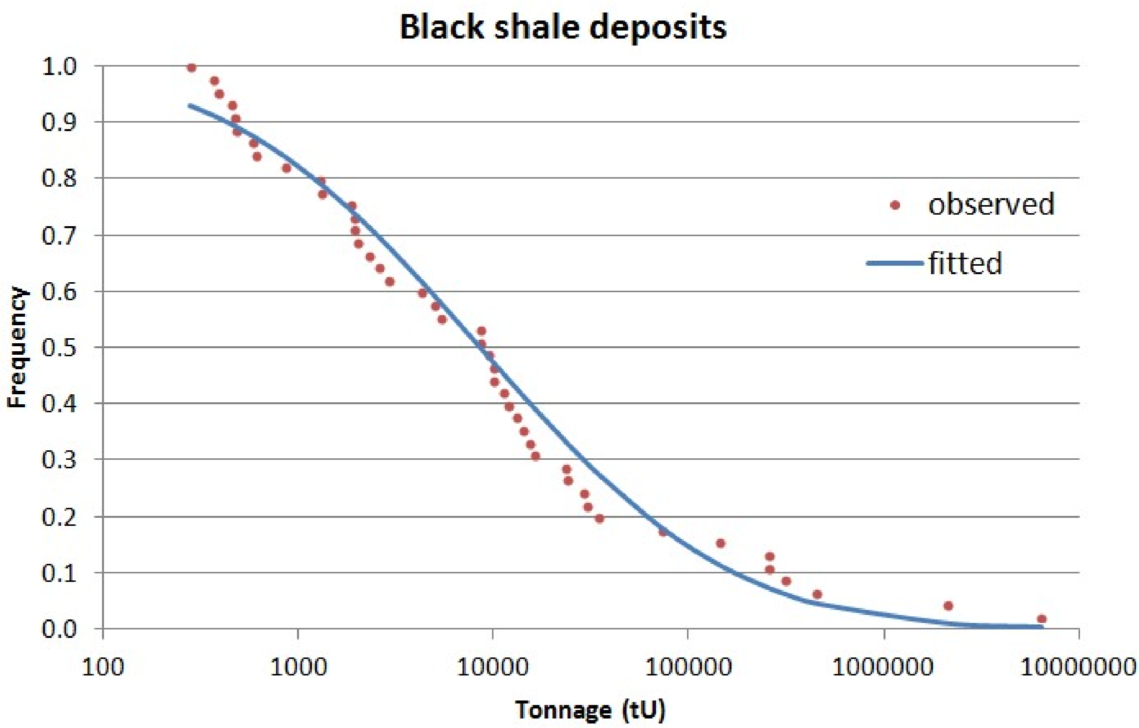

FIG. 35. Frequency-tonnage plot for black shale deposit type.

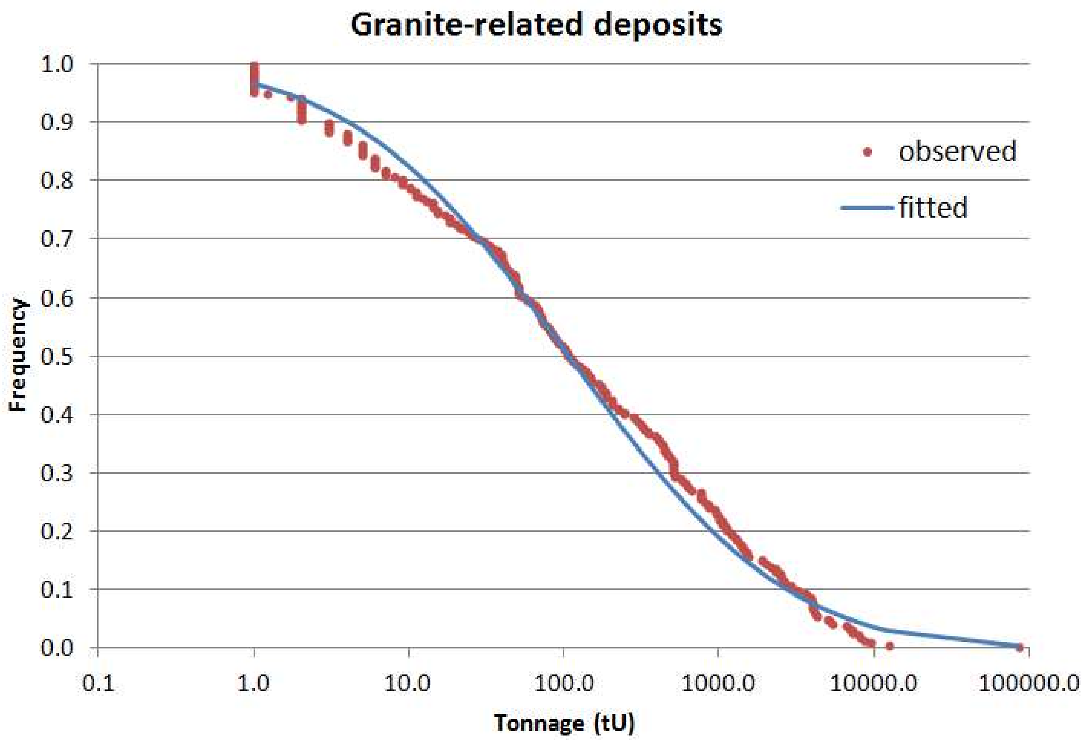

FIG. 36. Frequency-tonnage plot for granite-related deposits.

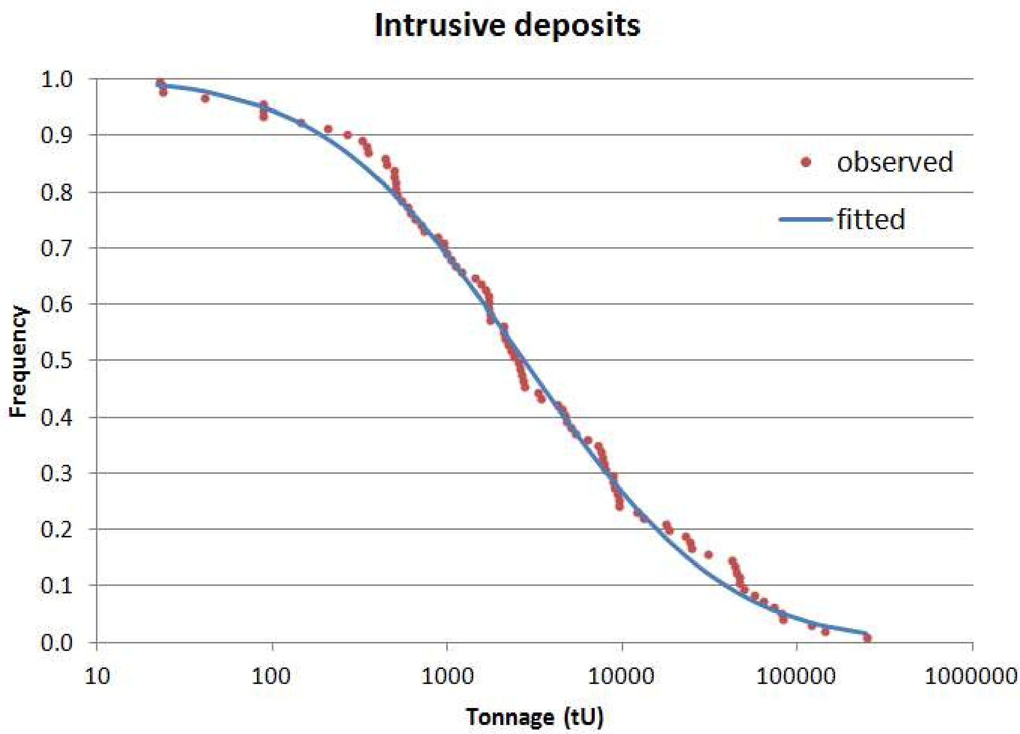

FIG. 37. Frequency-tonnage plot for intrusive deposits.

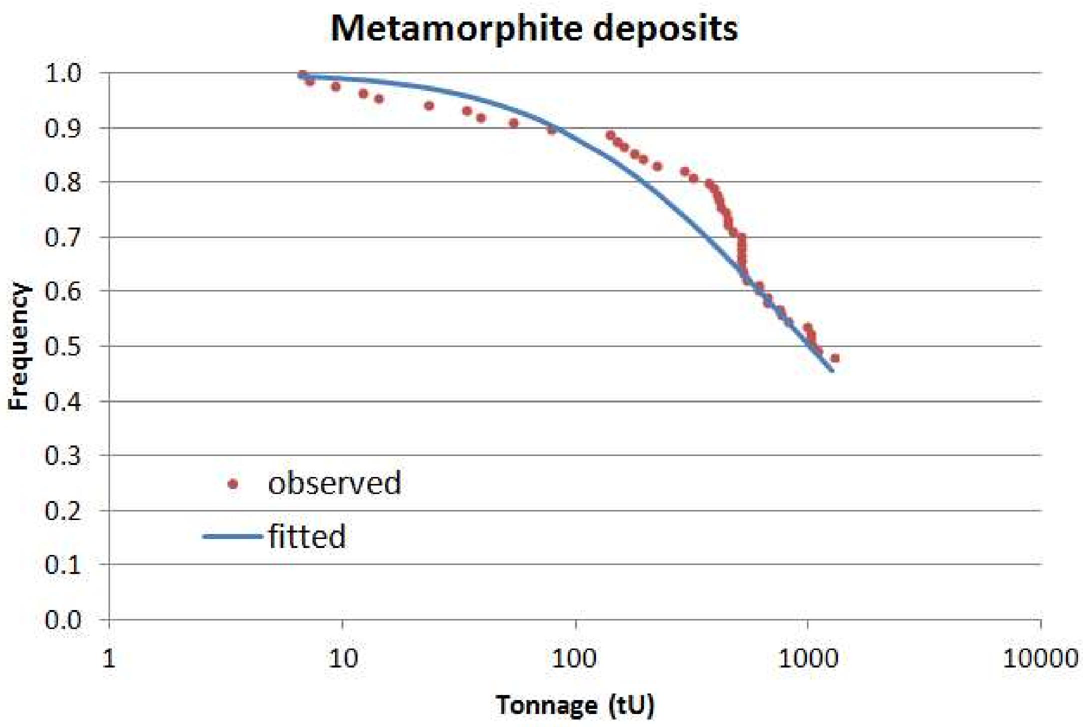

FIG. 38. Frequency-tonnage plot for metamorphite type deposits.

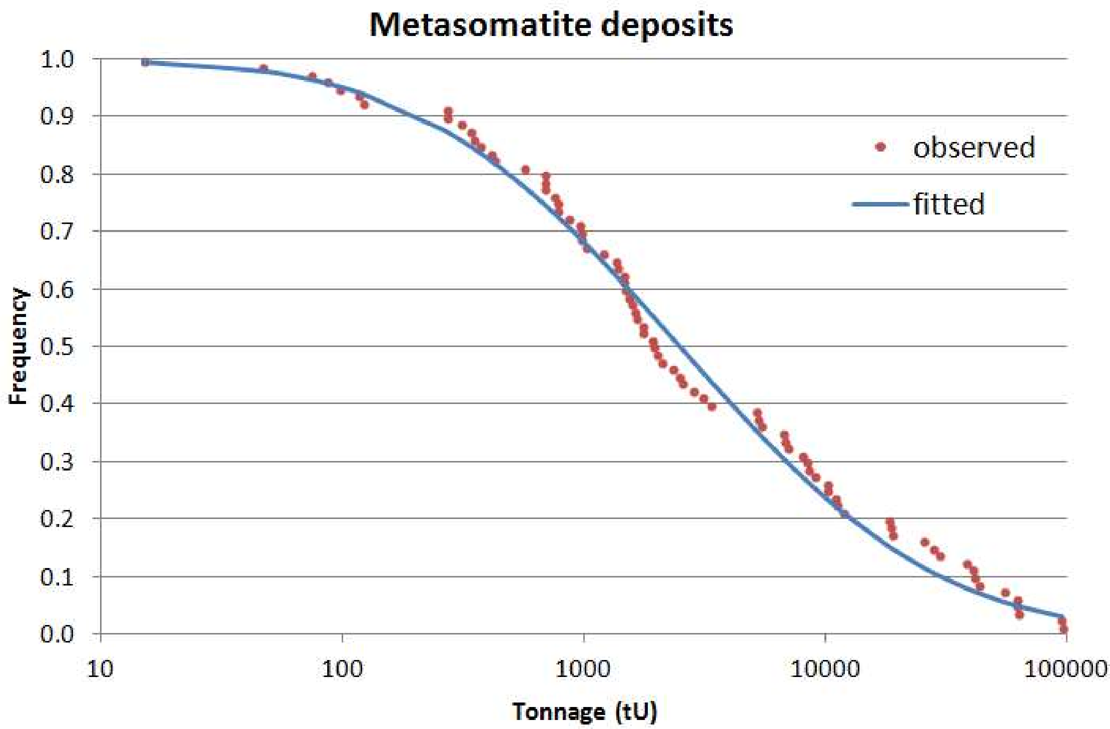

FIG. 39. Frequency-tonnage plot for metasomatite deposits.

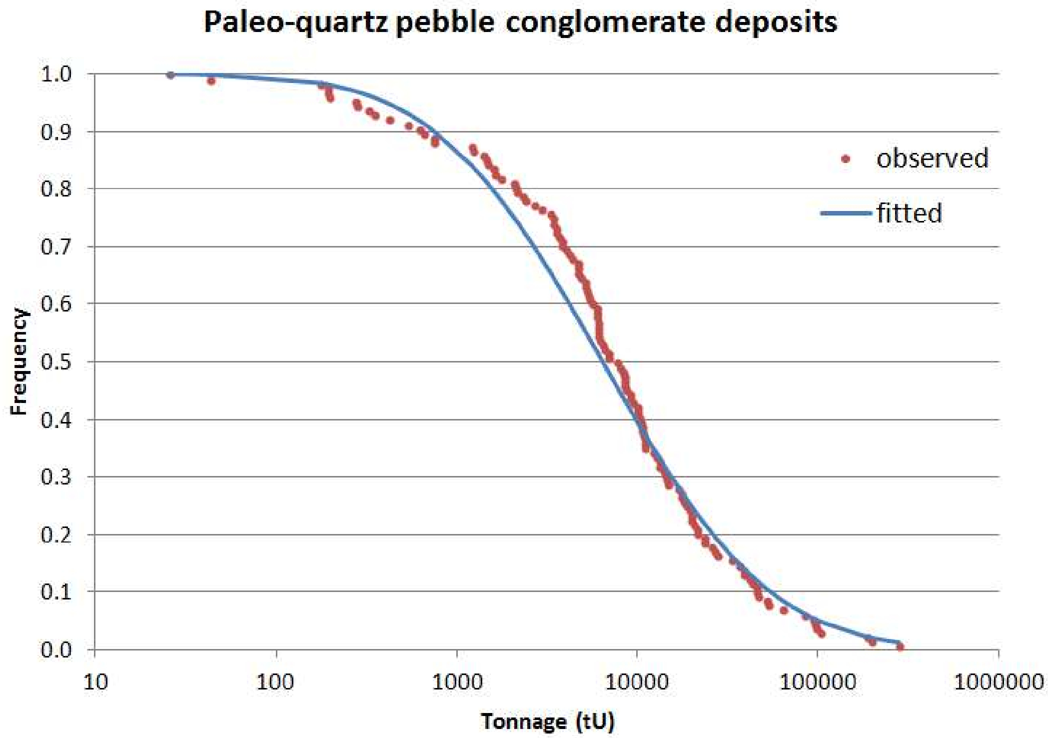

FIG. 40. Frequency-tonnage plot for paleo-quartz pebble conglomerate type deposits.

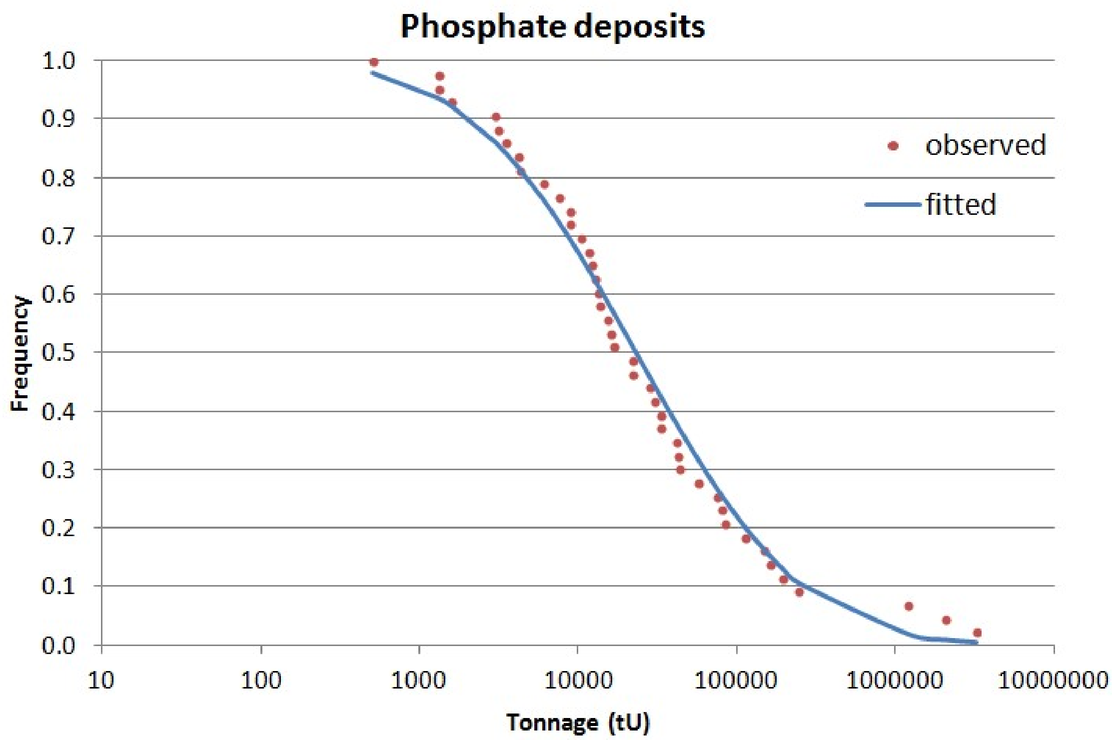

FIG. 41. Frequency-tonnage plot for phosphate type deposits.

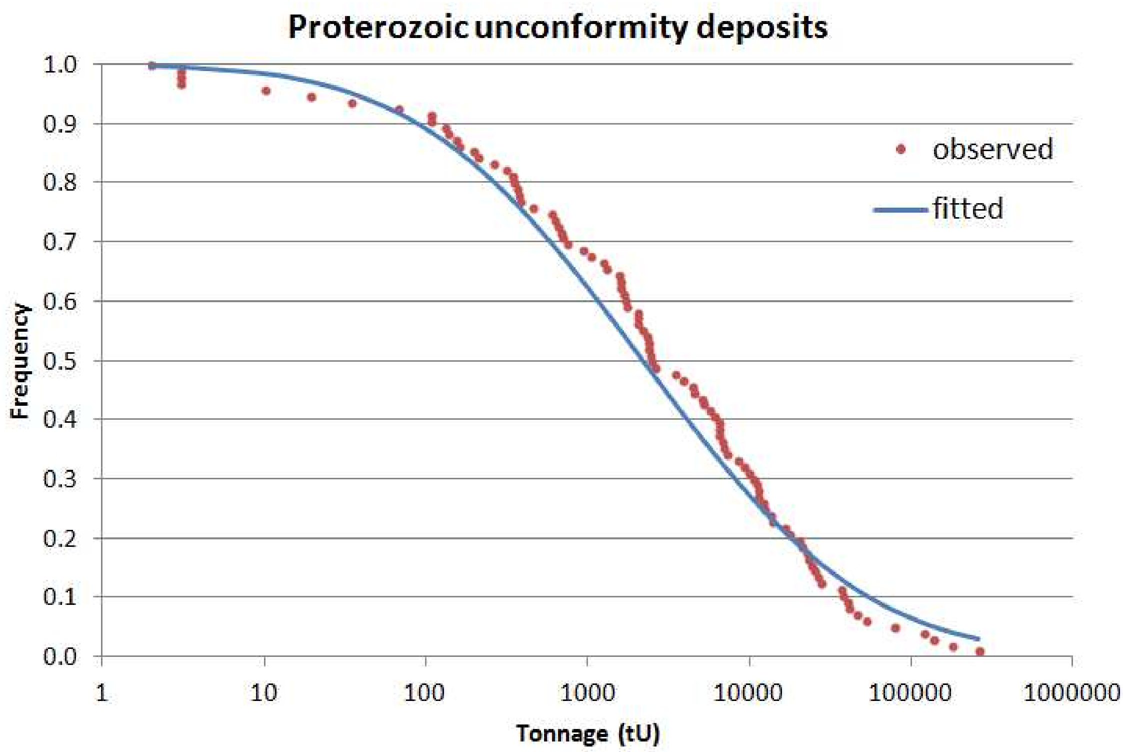

FIG. 42. Frequency-tonnage plot for Proterozoic unconformity deposits.

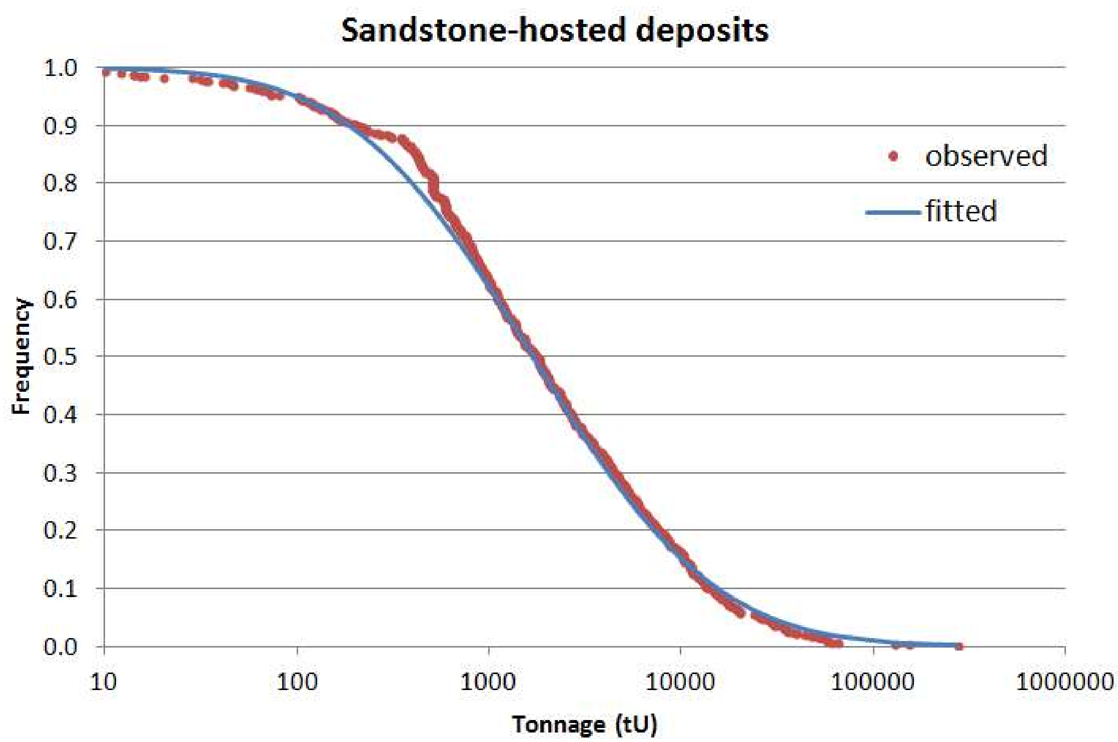

FIG. 43. Frequency-tonnage plot for sandstone-hosted deposits.

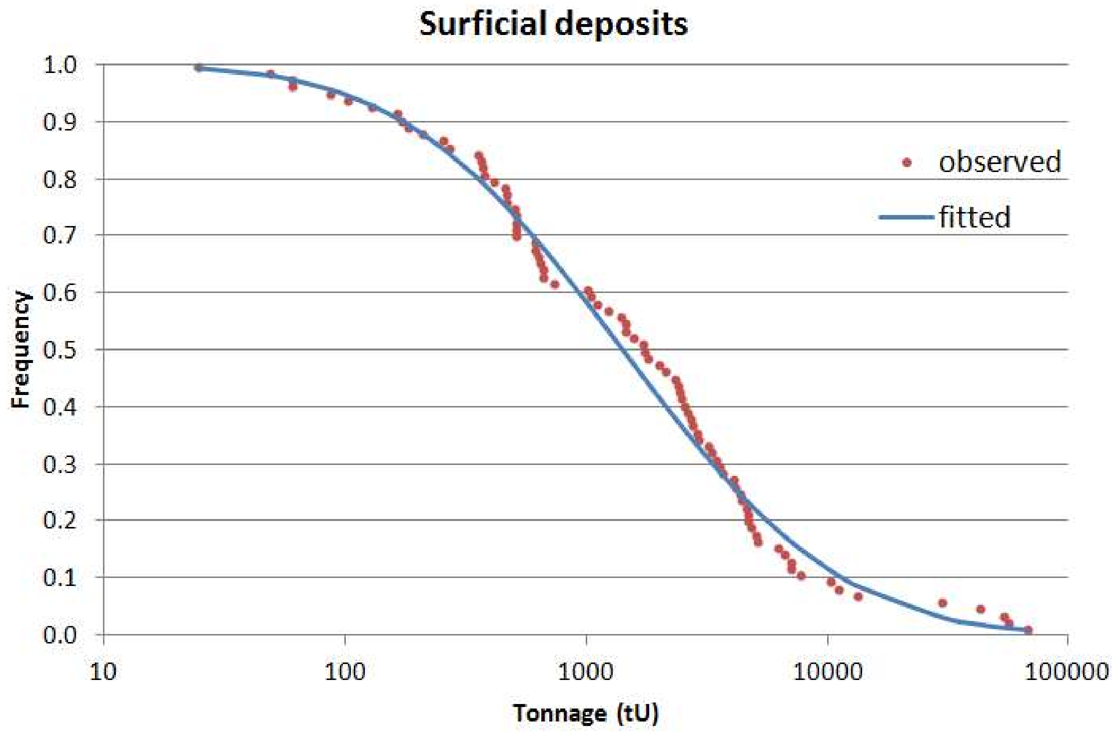

FIG. 44. Frequency-tonnage plots for surficial uranium deposits.

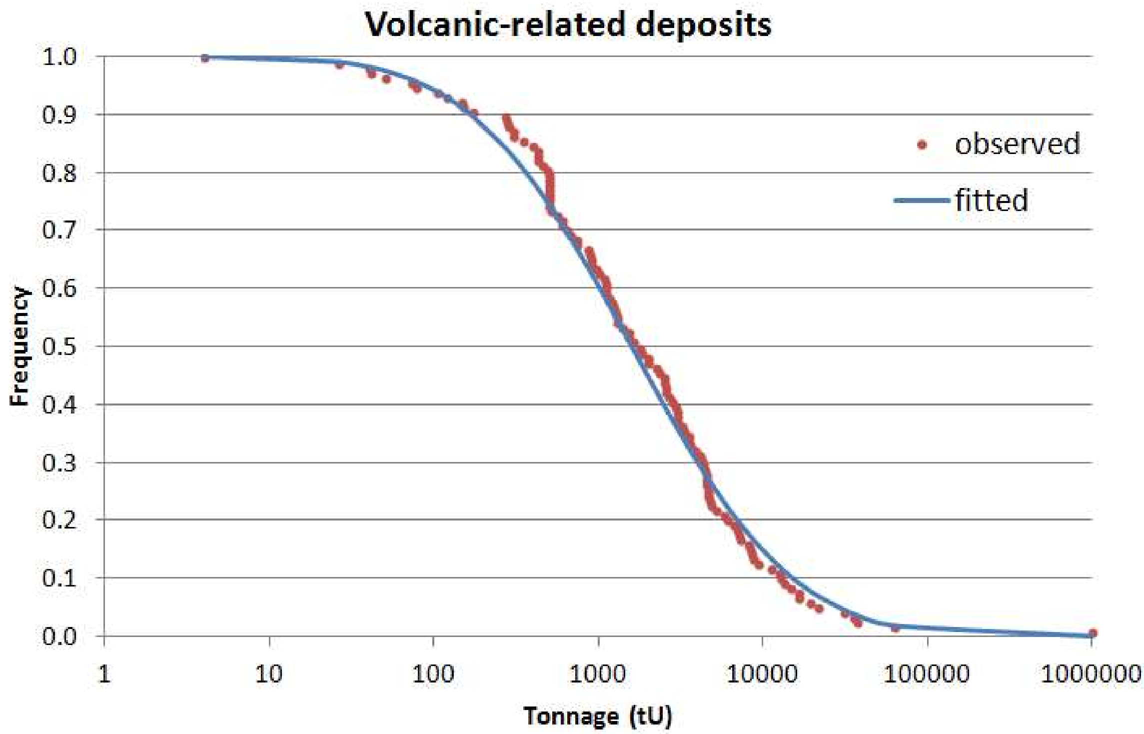

FIG. 45. Frequency-tonnage plot for volcanic-related deposits.

Intrusive and phosphate deposit types have very high probabilities of following log-normal distribution, indicating that the reported tonnages for these deposit types come from a homogenous population, possibly from similar geological settings. However, the high standard deviations suggest problems. Both grades and tonnages of intrusive, metasomatite and surficial deposit types conform to the log-normal distribution at the 0.05 significance level. The largest number of deposits belongs to sandstone-hosted type, which shows the lowest p-value for tonnages while highest p-value for grades. The internal inconsistency between grades and tonnages of sandstone-hosted type of deposits could possibly indicate presence of statistically different populations of sub-types among sandstone-hosted deposits.

5.4. Grade-and-tonnage modeling by deposit sub-types

There are four sub-types of sandstone-hosted deposits – roll-front, tabular, basal channel, and tectonic-lithologic. The sandstone-hosted deposits and their sub-types have different geographical locations. Majority of roll-front deposits are located in the USA, Uzbekistan and Kazakhstan. Tabular deposits are mostly located in Niger and the USA. The frequency grade-and-tonnage models of the sub-types of sandstone-hosted deposits and in different countries are presented here (Figs. 46–51) and compared with those of the global superset of all sandstone-hosted deposits. The statistics are presented in Tables 7 and 8.

The hypothesis that the deposits follow a log-normal distribution is rejected for the frequency-grade models of all tabular sandstone-hosted deposits – the global superset and those in the USA and Niger. The global model for grades of sandstone-hosted deposits shows a very good fit with log-normal distribution while tonnages of sandstone-hosted deposits do not fit with log-normal distribution at the 0.05 level of significance. Contrary to this, the frequency-tonnage model of basal channel sub-type of sandstone-hosted deposits shows very good fit with log-normal distribution, while the hypothesis of log-normality is rejected for its frequency-grade model.

Further, the frequency-tonnage models of all four sub-types of sandstone-hosted deposits show an improvement in the goodness-of-fit compared to the frequency-tonnage model of the global superset. For example, the frequency-tonnage models for roll-front deposits in the USA, Uzbekistan and Kazakhstan fit better to log-normal distribution than the global roll-front deposits. The very good log-normal distribution fit of the frequency-tonnage models of roll-front deposits in Kazakhstan and Uzbekistan could be an indication that these deposits in these countries are geologically similar.

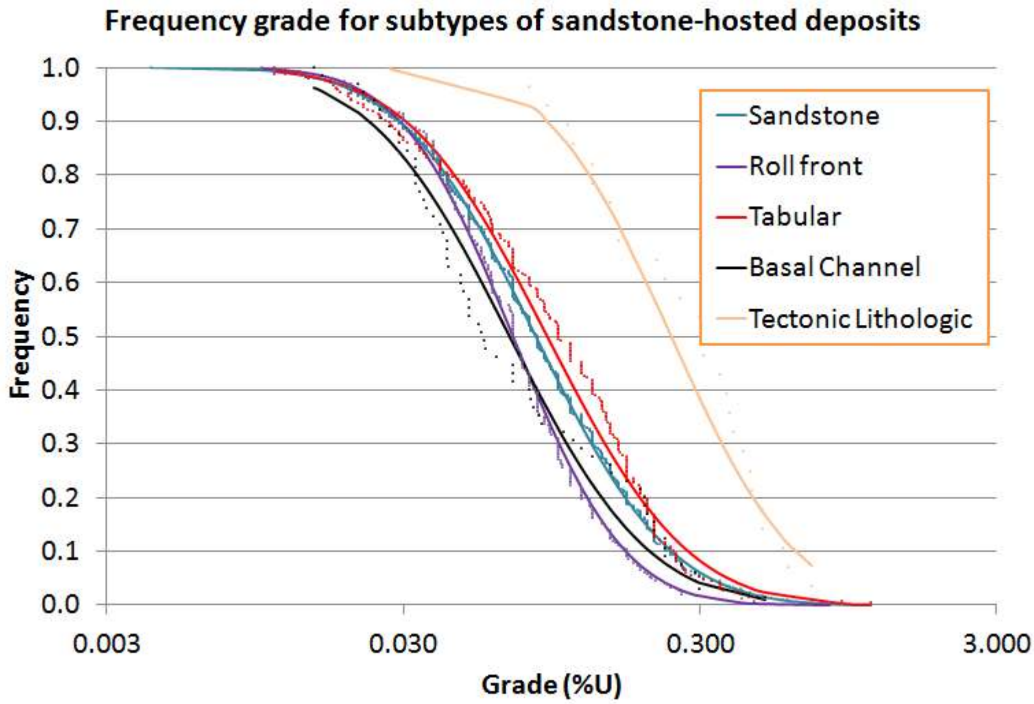

FIG. 46. Frequency-grade plots for sub-types of sandstone-hosted deposits.

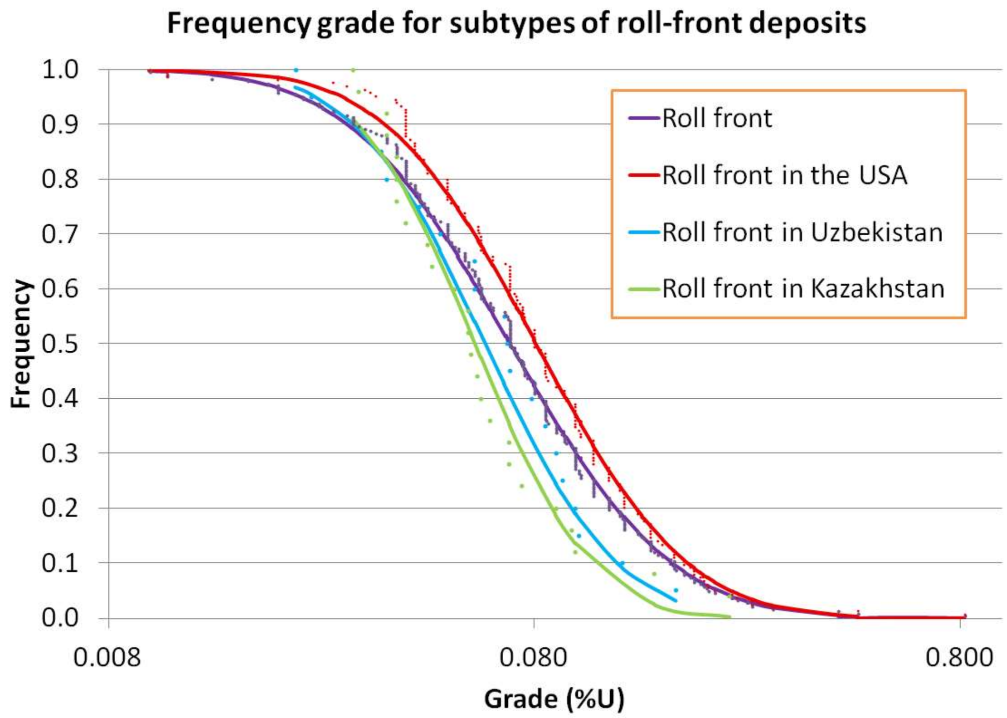

FIG. 47. Frequency-grade plots for roll-front sub-type of sandstone-hosted deposits grouped by country

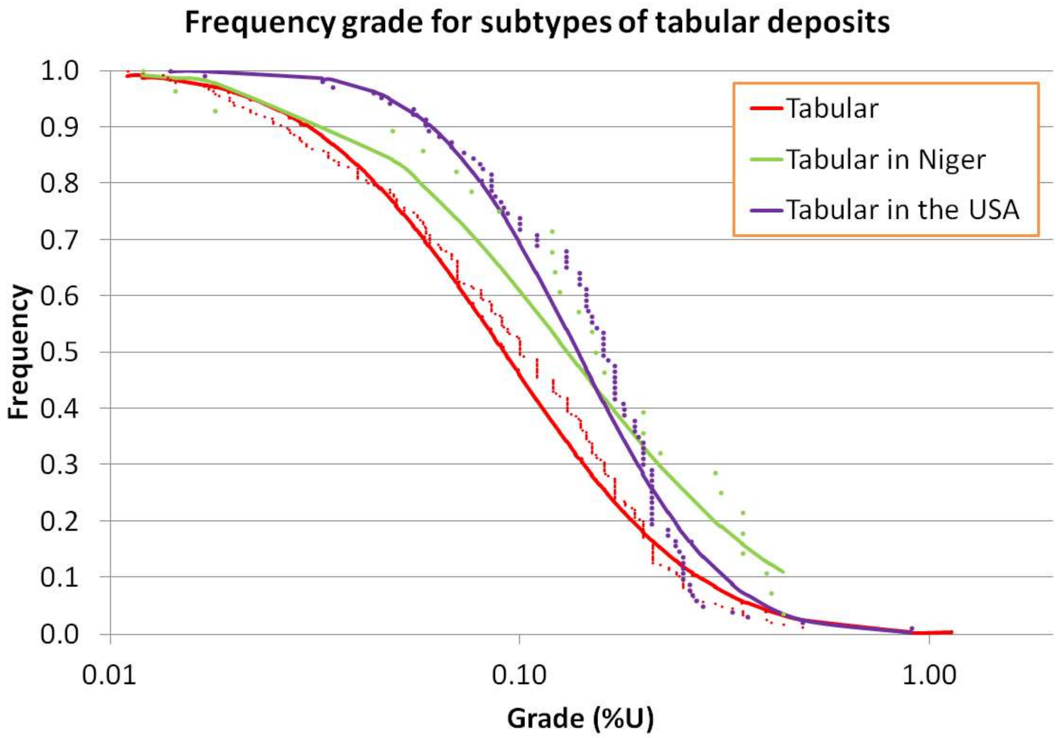

FIG. 48. Frequency-grade plots for tabular sub-types of sandstone-hosted deposits grouped by country

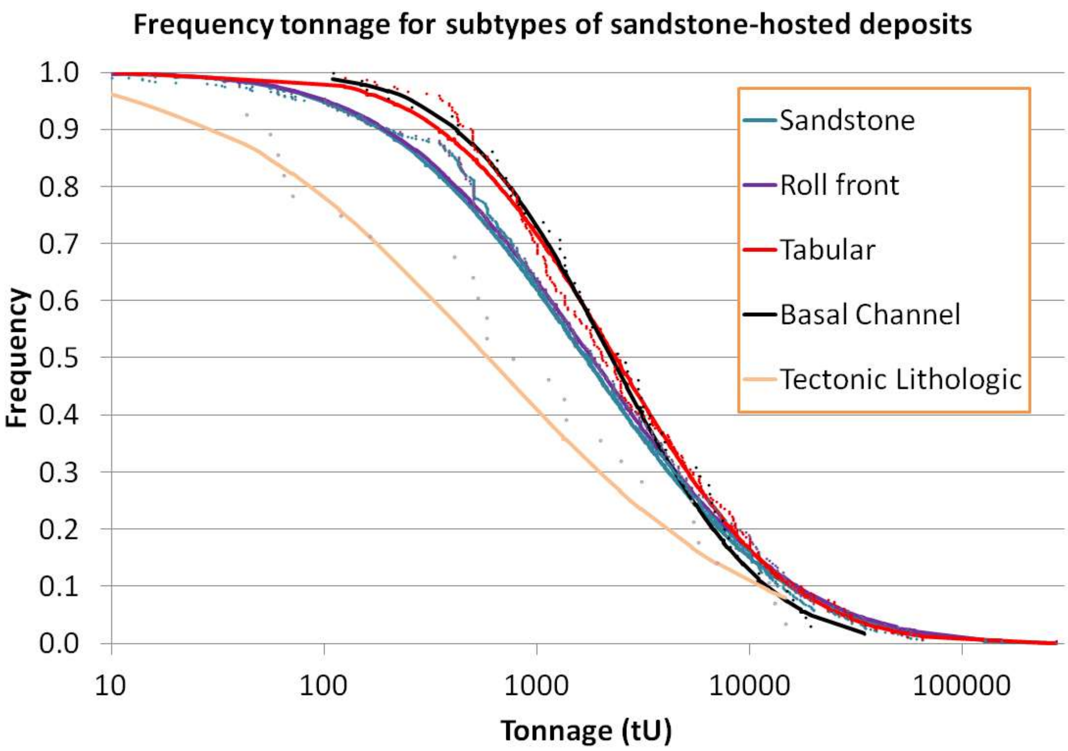

FIG. 49. Frequency-tonnage plots for sub-types of sandstone-hosted deposits.

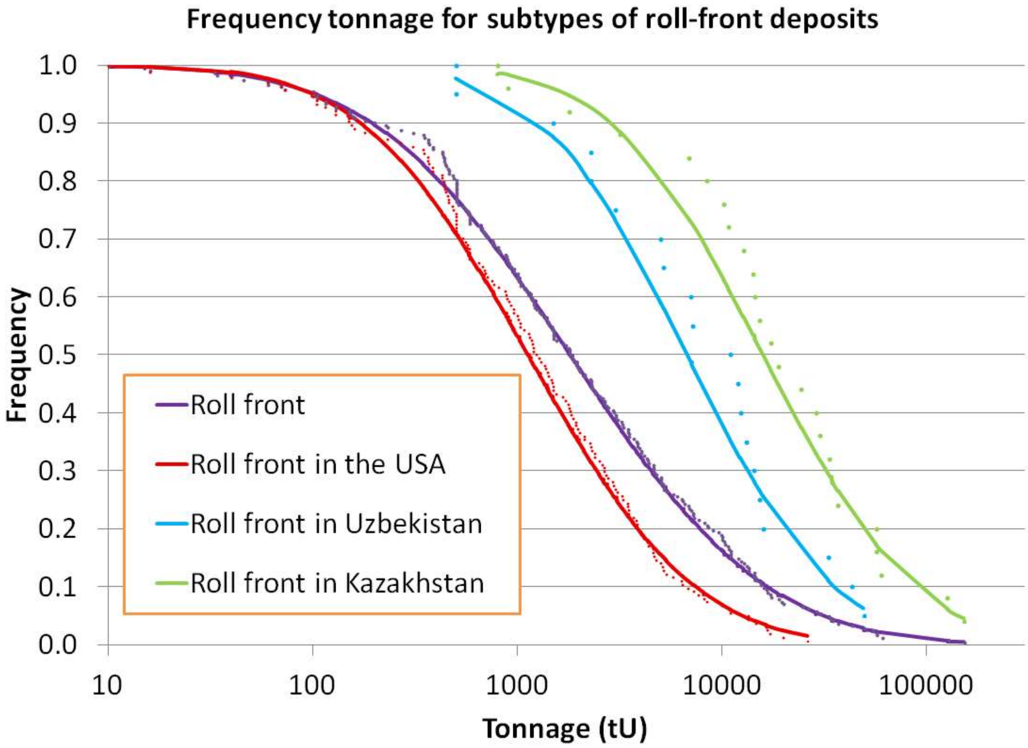

FIG. 50. Frequency-tonnage plots for roll-front sub-type of sandstone-hosted deposits grouped by country

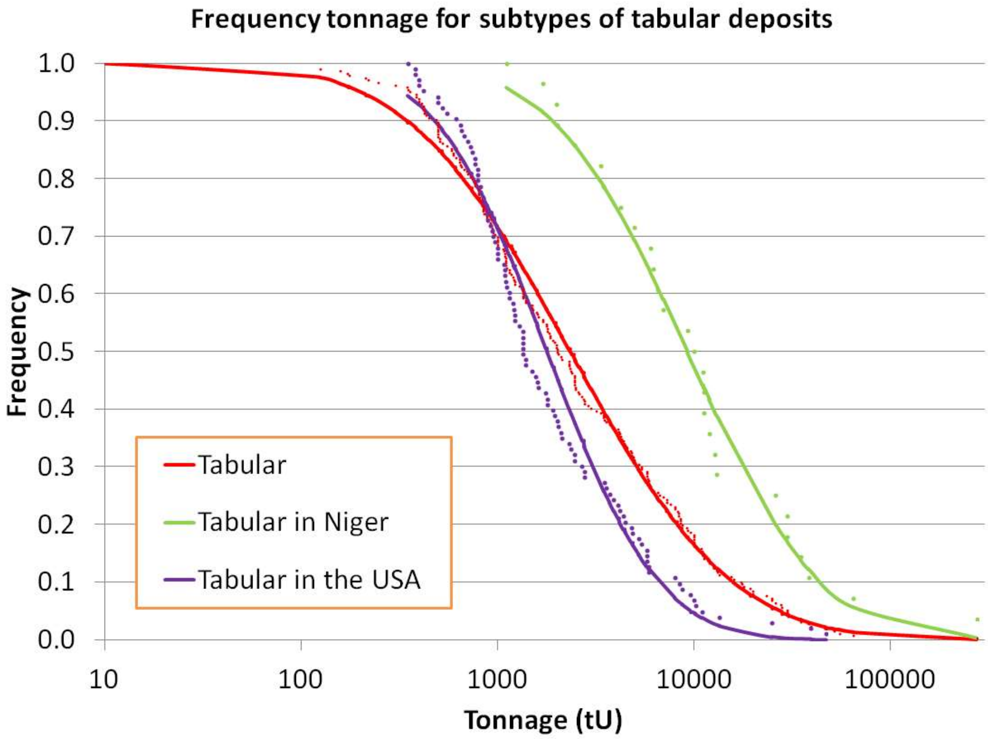

FIG. 51. Frequency-tonnage plots for tabular sub-type of sandstone-hosted deposits.

TABLE 7. STATISTICS FOR FREQUENCY-GRADE MODELING OF SUB-TYPES OF SANDSTONE-HOSTED DEPOSITS*

Sub-type	Mean	s.d.	95% CI of mean		95% CI of s.d.		N	*p*	K-S statistic	Critical K-S
Sandstone	-2.48	0.83	-2.54	-2.42	0.78	0.88	643	0.47	0.02	0.04
Roll-front	-2.66	0.68	-2.74	-2.57	0.63	0.75	242	0.23	0.05	0.06
Tabular	-2.39	0.86	-2.50	-2.28	0.79	0.94	246	**0.00**	0.08	0.06
Tectonic-lithologic	-1.42	0.75	-1.71	-1.13	0.60	1.03	28	0.11	0.15	0.16
Basal Channel	-2.68	0.85	-2.89	-2.47	0.72	1.03	65	**0.01**	0.12	0.11
Roll-front in USA	-2.51	0.64	-2.61	-2.42	0.58	0.72	164	0.13	0.06	0.07
Roll-front in Uzbekistan	-2.79	0.56	-3.05	-2.53	0.42	0.81	20	*0.50*	0.12	0.19
Roll-front in Kazakhstan	-2.84	0.49	-3.05	-2.64	0.39	0.69	25	*0.50*	0.12	0.17
Tabular in Niger	-2.03	0.98	-2.41	-1.65	0.78	1.34	28	**0.02**	0.18	0.16
Tabular in USA	-1.97	0.64	-2.10	-1.85	0.56	0.74	103	**0.00**	0.15	0.09

* The field names 'Mean' and 's.d.' refer to the estimated log (base e) mean and the log (base e) standard deviations, that are the parameters of the log-normal distribution fitted on the dataset. The field names '95% CI of mean' and '95% CI of s.d.' represent the chi-square 95% confidence intervals of the estimated parameters. The number of unique values of grades is represented by 'N'. The other fields '*p*-value', 'K-S statistic' and 'Critical K-S' represent the outputs of the Lilliefors goodness-of-fit test. The *p*-values in bold indicate those deposit types for which the hypothesis of log-normal distribution was rejected. The highest *p*-value for Lilliefors test is 0.5 and this is marked in italics bold.

TABLE 8. STATISTICS FOR FREQUENCY-TONNAGE MODELING OF SUB-TYPES OF SANDSTONE-HOSTED DEPOSITS*

Sub-type	Mean	s.d.	95% CI of mean		95% CI of s.d.		N	*p*	K-S statistic	Critical K-S
Sandstone	7.44	1.72	7.30	7.57	1.63	1.82	643	**0.00**	0.06	0.04
Roll-front	7.51	1.74	7.29	7.73	1.59	1.91	242	0.08	0.05	0.06
Tabular	7.76	1.49	7.58	7.95	1.37	1.63	246	**0.04**	0.06	0.06
Basal Channel	7.72	1.31	7.39	8.04	1.12	1.58	65	*0.50*	0.06	0.11
Tectonic-lithologic	6.39	2.29	5.50	7.28	1.81	3.12	28	0.46	0.11	0.16
Roll-front in USA	7.03	1.47	6.81	7.26	1.33	1.65	164	0.09	0.07	0.07
Roll-front in Uzbekistan	8.82	1.30	8.21	9.43	0.99	1.90	20	0.32	0.15	0.19
Roll-front in Kazakhstan	9.68	1.34	9.12	10.23	1.05	1.87	25	0.34	0.13	0.17
Tabular in Niger	9.13	1.23	8.66	9.61	0.97	1.67	28	0.17	0.14	0.16
Tabular in USA	7.49	1.03	7.29	7.69	0.90	1.19	103	**0.00**	0.13	0.09

* The field names 'Mean' and 's.d.' refer to the estimated log (base e) mean and the log (base e) standard deviations, that are the parameters of the log-normal distribution fitted on the dataset. The field names '95% CI of mean' and '95% CI of s.d.' represent the chi-square 95% confidence intervals of the estimated parameters. The number of unique values of grades is represented by 'N'. The other fields '*p*-value', 'K-S statistic' and 'Critical K-S' represent the outputs of the Lilliefors goodness-of-fit test. The *p*-values in bold indicate those deposit types for which the hypothesis of log-normal distribution was rejected. The highest *p*-value for Lilliefors test is 0.5 and this is marked in italics bold.

5.5. T-test for assessment of similarity between deposits by sub-type and country

The frequency-grade and frequency-tonnage models indicate that the deposit sub-types are more homogeneous and geologically similar within themselves when compared with the general deposit types. A two-sample Student's t-test was used here to understand and quantify the similarities and differences between deposit sub-types of the same deposit type. The results are shown in Tables 9 and 10. Group 1 and Group 2 are the two sub-classes of deposits being compared. These groups are either the geological sub-type (such as roll-front, tabular, etc.) or the location-based sub-types (such as the country where they are found – Kazakhstan or the USA).

Mean 1 and Mean 2 are the average tonnages or grades for the deposits in Group 1 and Group 2, respectively. 'n1' and 'n2' are the numbers of deposits with reported grades or tonnages for

Group 1 and Group 2 deposits, respectively. The statistical results of two-sample, two-tailed t-test are described in previous section. Here 't-stat' represents the t-statistic, which is a measure of the difference between the group means of the two groups taking into account the standard deviation or the spread of values within each group. The 't-crit' is the critical t-distribution value calculated for a significance level of 0.05. '*p*' represents the *p*-value. 'Inference' is the conclusion about the hypothesis that the samples come from the same population.

TABLE 9. T-TEST RESULTS FOR TONNAGES OF SUB-TYPES OF SANDSTONE-HOSTED DEPOSITS*

Group 1	Group 2	Mean Group 1	Mean Group 2	N_1	N_2	t-stat	t-crit	*p*	Inference
Sub-types of sandstone-hosted:									
Roll-front	Tabular	3.260	3.372	242	246	-1.761	1.965	0.079	Same
Roll-front	Basal channel	3.260	3.352	242	65	-1.080	1.978	0.282	Same
Roll-front	Tectonic-lithologic	3.260	2.774	242	28	2.498	2.040	0.018	Different
Tabular	Basal channel	3.372	3.352	246	65	0.240	1.981	0.811	Same
Tabular	Tectonic-lithologic	3.372	2.774	246	28	3.101	2.042	0.004	Different
Basal channel	Tectonic-lithologic	3.352	2.774	65	28	2.875	2.030	0.007	Different
Sub-types of roll-front grouped by country:									
Kazakhstan	USA	4.204	3.055	25	164	-9.055	2.035	0.000	Different
USA	Uzbekistan	3.055	3.831	164	20	-5.710	2.060	0.000	Different
Uzbekistan	Kazakhstan	3.831	4.204	20	25	-2.168	2.020	0.036	Different
Sub-types of tabular grouped by country:									
Niger	USA	3.967	3.254	28	103	6.482	2.024	0.000	Different

* The mean values are in log (base e).

TABLE 10. T-TEST RESULTS FOR GRADES OF SUB-TYPES OF SANDSTONE-HOSTED DEPOSITS*

Group 1	Group 2	Mean Group 1	Mean Group 2	N_1	N_2	t-stat	t-crit	*p*	Inference
Sub-types of Sandstone-hosted:									
Roll-front	Tabular	-1.154	-1.037	242	246	-3.816	1.965	0.000	Different
Roll-front	Basal channel	-1.154	-1.164	242	65	-0.202	1.987	0.840	Same
Roll-front	Tectonic-lithologic	-1.154	-0.617	242	28	-8.295	2.037	0.000	Different
Tabular	Basal channel	-1.037	-1.164	246	65	-2.450	1.984	0.016	Different
Tabular	Tectonic-lithologic	-1.037	-0.617	246	28	-6.351	2.030	0.000	Different
Basal channel	Tectonic-lithologic	-1.164	-0.617	65	28	-7.109	2.002	0.000	Different
Sub-types of Roll-front grouped by country:									
Kazakhstan	USA	-1.236	-1.092	25	164	2.992	2.024	0.005	Different
USA	Uzbekistan	-1.092	-1.212	164	20	2.061	2.056	0.049	Different
Uzbekistan	Kazakhstan	-1.212	-1.236	20	25	0.343	2.024	0.734	Same
Sub-types of Tabular grouped by country:									
Niger	USA	-0.882	-0.858	28	103	-0.285	2.035	0.777	Same

* The mean values are in log (base e).

As described in Table 3, if p is less than 0.05 and t-stat is less than t-crit, it is concluded here that the two groups are statistically significantly different. These groups have been highlighted. The group with a higher mean would belong to a population having higher tonnage or grade than the other group. These higher value group means are also highlighted. In some cases, it is seen that the t-statistic is negative. T-distribution is symmetric about the origin. Negative values of t-statistic indicate the group used as the first variable in t-test had a higher mean compared to the other group. In case of negative t-values, the negative of the t-critical value should be used for comparison. If the t-statistic is more negative than the negative t-critical value, the deposit groups are significantly different from each other.

Table 9 shows that tonnages of the tectonic-lithologic sub-type of sandstone-hosted deposits is significantly different from those of the other sub-types (i.e., roll-front, tabular and basal channel). The t-test for grades (Table 10) indicates that all the sub-types have significantly different grade-distribution except for the roll-front and the basal channel sub-types. The analysis by country indicates that the roll-front deposits in Kazakhstan, Uzbekistan and the USA are significantly different from each other, both in terms of grades and in terms of tonnages, although the grades of deposits in Uzbekistan and Kazakhstan are similar to each other. The tabular deposits in the USA and Niger have significantly different tonnages while having similar grades.

The analyses by country indicate that roll-front and tabular deposit sub-types may have further sub-types based on the geological setting in which they occur in different geographical locations. Further exploration and in-depth analysis for these sub-types is warranted. In addition, the differences could also highlight different exploration maturity of the deposit sub-types.

6. SUMMARY AND CONCLUSIONS

The analysis presented here shows the descriptive statistics of different uranium deposits across the globe. The grades and tonnages of these deposits are modeled with the log-normal distribution. For most of the deposit types and sub-types, the assumption of log-normality is valid at the 0.05 level of significance. Goodness-of-fit was used as a measure of homogeneity within the deposit types modeled and as an indicator of geological similarities within each deposit type and the exploration maturity.

The deposits were divided into smaller samples based on the sub-types and each sub-type was modeled separately. This analysis revealed that, for most of the deposit types, the goodness-of-fit increases when sub-types are considered compared to deposit types. The improvement is more characteristic for grades than for tonnages. In addition, the t-tests show more pronounced differences in grades of deposit sub-types against the differences in tonnages.

When subdivided into their respective sub-types, the goodness-of-fit for tonnages of the sub-types of sandstone-hosted deposits improved, while that for grades has declined. This demonstrates that tests of log-normality are insufficient to determine subgroups of deposits. For example, our goal in constructing many of these grade-and-tonnage models was to use them to provide an unbiased model of the grade-tonnage distributions of undiscovered deposits of the same type. In addition, the t-tests revealed that the sub-types of sandstone-hosted deposits (i.e., roll-front, tabular, basal channel and tectonic-lithologic sub-types) are statistically significantly different from each other. Moreover, roll-front deposits in different countries are also different. Due to presence of such heterogeneities in the sandstone-hosted deposits, there is lack of substantial goodness-of-fit in the global frequency-grade and frequency-tonnage models.

When analyzed by country, it is interesting to note that the roll-front deposits in Kazakhstan, Uzbekistan and the USA have significantly different grades and tonnages. This suggests questions about the mineralization processes and the geological setting(s) in which these deposits were formed. In conclusion, it can be said that further studies into the geological classification of the deposit types are necessary, particularly for sandstone-hosted deposits and the metamorphite deposits, which, in spite of sub-type classification, still show relatively lower goodness-of-fit with log-normal distribution compared to other deposit types. The mineral systems of roll-front deposits in Kazakhstan, Uzbekistan and the USA and the basement-hosted and unconformity contact deposits and Canada and Australia also need to be analyzed to justify the differences in the deposit formation in these countries. This analytical technique can find applications in improving the current classification scheme, such as merging the black shale and lignite type of deposits, discovering sub-types of roll-front and volcanic-related deposits in different countries and analyzing the classification of the basement-hosted and unconformity contact sub-types of Proterozoic unconformity deposits.

This study clearly demonstrates that the log-normal distribution fits the grade and tonnage data of each deposit type. However, the significant differences in sub-types of deposits is an important indicator that generating unbiased grade-and-tonnage models for estimating undiscovered deposits needs further work. It is clear that the high standard deviations of tonnages in every deposit type and most sub-types reflect unresolved data issues derived from including incompletely explored deposits in the data and by not applying spatial rules to combine adjacent (or even touching) deposits.

REFERENCES

[1] SINGER, D.A., MENZIE, W.D., Quantitative Mineral Resource Assessments—An Integrated Approach: Oxford University Press, New York, 219p (2010).

[2] COX, D.P., SINGER, D.A. (Eds.), Mineral deposit models: U.S. Geological Survey Bulletin 1693, 379p. (1986) (http://pubs.usgs.gov/bul/b1693/)

[3] BAWIEC, W.J., SPANSKI, G.T., Quick-start guide for version 3.0 of EMINERS – Economic Mineral Resources Simulator: US Geological Survey Open-File Report 2009-1057, 26p (2012), available only at http://pubs.usgs.gov/of/2009/1057. (This report supplements USGS OFR 2004-1344).

[4] SINGER, D.A., The lognormal distribution of metal resources in mineral deposits. Ore Geology Reviews, 55, 80-86 (2013).

[5] IAEA, World Distribution of Uranium Deposits (UDEPO) with Uranium Deposit Classification, INTERNATIONAL ATOMIC ENERGY AGENCY, IAEA TECHDOC No. 1629, 2009 Edition.

[6] OECD-NEA & IAEA, Uranium 2014: Resources, Production and Demand, OECD 2014, NEA No. 7209 (2014)

[7] MASSEY, F.J., Jr., "The Kolmogorov-Smirnov Test for Goodness of Fit", Journal of the American Statistical Association 46(253), 68-78 (1951) (http://dx.doi.org/10.1080/01621459.1951.10500769).

[8] LILLIEFORS, H.W., On the Kolmogorov-Smirnov test for normality with mean and variance unknown, Journal of the American Statistical Association 62, 399–402 (1967).

[9] SCHOLZ, F.W., "Maximum likelihood estimation", Encyclopedia of Statistical Sciences (1985).

[10] HAYNES. W., "Student's t-test", Encyclopedia of Systems Biology, 2023-2025 (2013).

[11] SMIRNOV, N., "Table for estimating the goodness of fit of empirical distributions", The annals of mathematical statistics 19(2), 279-281 (1948).

[12] ZIPF, G. K., Human Behavior and the Principle of Least Effort: An Introduction to Human Ecology. Reading, MA, Addison-Wesley (1949).

[13] SINGER, D.A., JAIRETH, S., "A three-part quantitative assessment of undiscovered unconformity-related uranium deposits in the Pine Creek region of Australia", this volume

QUANTITATIVE METHODS OF ASSESSMENT OF UNDISCOVERED URANIUM RESOURCES: A REVIEW

S. JAIRETH
Aranda, ACT 2614
Australia

A. PORWAL
Indian Institute of Technology Bombay, Powai,
Mumbai, India
Centre of Exploration Targetting,
University of Western Australia,
Perth, WA, Australia

Abstract

In 1992 IAEA published in TECDOC 344 a comprehensive review and an instruction manual of quantitative methods of mineral resource assessment. The TECDOC 344 presented material prepared between 1985 and 1989, which provides a comprehensive survey of statistical models and assessment methods useful in undertaking mineral potential assessment of uranium deposits. However, the focus of the 1992 review was on statistical framework at the expense of critical geological features of uranium deposits which underpin the robustness of mineral resource assessment. The 1992 review also not on GIS-based techniques, as these had not been developed when the review was published. This was partially overcome by a new IAEA guidebook (IAEA, 1994), which focused on techniques of spatial data integration (including GIS) for mineral exploration and, resource assessment and environmental studies. The present review only briefly discusses methods described in the previous two publications but focuses predominantly on GIS-based methods/models of assessment. The main objective of the review is to describe methods of quantitative mineral resource assessment, but as most quantitative methods rely on delineating permissive or favorable tracts. It also provides a brief review of qualitative methods for delineating tracts with different levels of mineral potential (prospectivity or favorability). In its scope the review is not extensive but aims to produce a critical review of most common methods. The main purpose is to provide guidelines, which can assist in selecting method(s) suitable for specific regions and/or specific tasks. The review only includes a few case studies. This is principally because it is intended to be an introduction to a series of separate contributions dealing with case studies. References to important case studies are included in this review. The main focus of the review is to provide sufficient information to the end users so that they can select one or the other methods based on their specific needs and objectives. The principal features of a number of important methods are summarized in a table, the aim of which is to assist in the selection of the suitable method(s). The review also includes a number of important recommendations that could be useful for conducting systematic quantitative resource assessment of yet to be discovered uranium deposits. These include: (1) compiling and updating of descriptive models or uranium deposit style and making them compatible with a process based mineral-system approach; (2) compiling grade-tonnage models of deposits styles; (2) preparing deposit-density models of deposit styles; and (4) identifying mappable signatures associated with critical features of uranium deposits styles and mineral systems.

1. INTRODUCTION

This review focuses on quantitative methods, but because most methods of quantitative assessment rely on delineating geologically-permissive or favorable areas, it also provides a brief review of qualitative methods, the principle goal of which is to delineate tracts with different levels of potential/prospectivity/favorability for mineral deposit occurrence. In its scope, the review is not extensive but aims to produce a critical review of the most common methods to provide guidelines that can assist in selecting method(s) suitable for specific regions and/or specific tasks.

A comprehensive review of quantitative methods, published by IAEA in 1992 (TECDOC 344), provided a good summary of mathematical and statistical models used for quantitative assessment of undiscovered uranium resources. The present review does not aim to revisit those methods in great detail but aims to add discussions of new, predominantly GIS-based methods/models of assessment. The present review does not discuss specific examples (case histories) of assessments, as these are published separately as individual contributions in the final TECDOC. However, it provides a comprehensive list of bibliographic references of benchmark studies, both methodological as well as case studies. The focus of the present review is on practical information that can help in selecting methods that can be appropriately and effectively used in a particular region and/or to accomplish a particular task.

Quantitative mineral resource assessment (QMRA) of undiscovered uranium resources are generally conducted to serve different objectives, which include: (a) compilation of global resource inventory of uranium to assist informed analysis of global supply and demand issues; (b) estimation of mineral values as inputs in decision support systems to resolve conflicting land-use issues in a region; (c) stimulation of mineral exploration by delineating prospective areas with estimated endowment of undiscovered resources in them; and (d) uranium mine rehabilitation and other related environmental impact assessments.

Modern quantitative resource assessment is considered to have initiated by [1]. One of the principle aims of his assessment was to design a system capable of responding to the needs of decision makers [2]. He used Poisson distribution model for quantitative assessment in the region of Algerian Sahara. The use of the Poisson distribution model was justified by the results of a study of the number of mineral deposits exceeding a certain value in 89 French administrative divisions [2]. The method of [1] was further developed by [3], who introduced the use of multivariate methods. Harris [3] also produced a comprehensive review and discussion of various methods of QMRA in a book that summarized mathematical and statistical models of quantitative resource assessments and discussed results of a large number of assessments conducted in various regions. The book also contains a number of assessments of undiscovered uranium resources such as world uranium resource estimates, uranium resources in USA by a bivariate log-normal deposit model of PAU (Program Analysis Unit of Great Britain), and uranium endowment estimates by NURE (National Uranium Resource Evaluation of the United States). Harris [3] also described a number of uranium endowment appraisal systems. The system of [4], described as implicit subjective, was employed to assess uranium resources in the San Juan Basin (USA). The appraisal system developed by [5], on the other hand, was based on a sequential scheme of eight processes/stages critical for sandstone-hosted uranium deposits.

Comprehensive reviews of quantitative methods for resource assessment were also provided by [6] and [7]. In 1975, a team in the USGS (US Geological Survey) published estimates of the number of undiscovered deposits in a 1:250,000-scale quadrangle in Alaska [2]. This was followed by an assessment of a larger area (1:1,000,000 scale assessment of ~80% of Alaska) in which grade-and-tonnage models and geologically-permissive tracts were used to produce 85 estimates of number of deposits [2]. Although these assessments did not estimate undiscovered uranium resources, they became the basis of the three-part assessment method developed by the USGS.

A detailed quantitative assessment of uranium resources was undertaken in Australia in the Kakadu Conservation Zone, Northern Territory, by a team of experts in the Bureau of Mineral Resources, Geology and Geophysics (now Geoscience Australia) [8]. The method used by the team was a variation on the three-part assessment method developed by the USGS. Quantitative estimates did not make use of existing grade-and-tonnage model of unconformity-related uranium deposits, but experts were asked to submit estimates of tonnage of uranium based on their knowledge of these deposits in the area. Cumulative probabilistic curves obtained from these estimates were then used to assess uranium resources at three different levels of probability.

A smaller scale quantitative assessment of undiscovered uranium resources was also carried out in 1996 in the Lake Eyre Basin area in South Australia by a team in ABARE (Australian Bureau of Agriculture and Resource Economics) and BMR, Australia [9]. Uranium resources associated with the Olympic Dam-type deposits were assessed using Zipf's law [10, 11]. The Zipf's law curve was computed from resource data of geologically similar deposits inside as well as outside of Australia.

In parallel with the above-mentioned quantitative mineral resource assessments, several qualitative assessments were being carried out in the USA and Australia. Various teams in the USGS have developed qualitative methods of mineral potential assessment conducted as inputs into land-use decisions in forest areas (e.g., [12−14]. The methods relied on the definitions of mineral potential and certainty proposed by [24]. Geological, geophysical and geochemical datasets were used to delineate mineral potential tract maps of a number of mineral deposit models (types) and levels of mineral potential and certainty were assigned to the tract maps.

Similar qualitative mineral potential assessments were also conducted in Australia jointly by the BRS (Bureau of Resource Sciences), AGSO (Australian Geological Survey Organization now Geoscience Australia), and state Geological Surveys between 1996 and 2001 in regional forest areas in New South Wales, Queensland, Victoria, Tasmania and Western Australia [15]. In these assessments, GIS (Geographic Information System) techniques were employed to combine mineral potential tract maps of individual deposit models to produce composite mineral potential maps of the study areas [16].

The emergence of relational databases and GIS in the 1980s provided a catalyst to develop new GIS-based techniques for mineral potential assessments (or prospectivity and favorability analysis). These new developments are briefly described by [17]. A comprehensive description of various GIS-based techniques with case studies can be found in [18].

A national-scale qualitative assessment of uranium deposits in Australia helped to produce a uranium mineral potential map of Australia [19]. This map was later refined by [20], who used a probabilistic framework to produce national-scale mineral potential maps of uranium deposits in Australia.

Development of comprehensive geoscientific databases in GIS accelerated regional- and district-scale mineral potential assessments in many geological surveys and agencies world-wide. New approaches combining GIS-based prospectivity analysis and quantitative mineral resource assessments are being developed (e.g., [21]. These new developments and methods will be the focus of this review.

In 1992, IAEA produced an instruction manual on methods and techniques of mineral potential assessment [22]. The manual presented material prepared between 1985 and 1989. It provided a comprehensive survey of statistical models and assessment methods that are useful for undertaking mineral potential assessment of uranium deposits. However, the focus of that survey was on statistical framework at the expense of critical geological features of uranium deposits, which underpin the robustness of mineral potential assessment. The 1992 manual also did not describe GIS-based techniques, as they had not been developed when the manual was compiled. This shortcoming was partially overcome by a new IAEA guidebook [23] that focused on techniques of spatial data integration (including GIS) for mineral exploration and, resource assessment and environmental studies.

As mentioned earlier, this review aims to highlight new methods, methodologies and techniques of qualitative and quantitative mineral resource assessments developed in the last twenty years. Therefore, this review is an extension of the previous two documents produced by IAEA.

2. THEORETICAL FRAMEWORK

This contribution presents a brief summary of basic concepts that are useful for qualitative and quantitative mineral resource assessments. Some of these concepts have been discussed in several published papers and reviews (e.g., [3, 6, 17, 22–25].

2.1. Mineral deposit

As most methods of quantitative assessments of undiscovered resources are based on estimating number of undiscovered mineral deposits of a particular type, it is important to underline what we mean by the term mineral deposit. The most common definition of a mineral deposit states that it is a natural concentration of minerals in such form and concentration that it was either economically extracted in the past or its economic extraction is feasible at present or in the near future. Taylor and Steven [24] cite a similar definition of the term 'mineral resource' put forward in a circular by the USGS. A similar definition has also been put forward by [2] with the qualification that the concentration of minerals might, 'under the most favorable of circumstances, be considered to have economic potential'. For quantitative assessment of undiscovered resources this is an important qualification. It suggests that the grade and tonnage data of known deposits, used for quantitative assessments need to be compiled using lowest cut-off grades. In IAEA's UDEPO database, such resources data are defined as initial resources (IAEA, UDEPO TECDOC). Cox et al. [26] distinguish an ore deposit from a mineral deposit, defining an ore deposit as a mineral deposit that has been tested and is known to be of sufficient size, grade, and accessibility to be producible to yield profit. In this review, the terms ore deposit and mineral deposits are used as synonyms.

In contrast, a mineral occurrence (or showing) is generally understood as a concentration of a mineral that is considered valuable by someone somewhere, or that is of scientific or technical interest [26]. The term mineral prospect is also commonly used in literature. It is generally defined as a mineral occurrence that has been drilled or investigated in some detail and is believed to have a chance of becoming a mineral deposit [2].

Distinguishing between mineral occurrence, mineral prospect and mineral deposit is significant for any QMRA because only mineral deposits with reliable grade and tonnage data can be used to produce a robust quantitative assessment of undiscovered uranium resources.

Mineral deposits result from fertile mineralizing processes intimately associated with the geological evolution of an area. Studies of mineral deposits undertaken by economic and ore geologists are focused on explaining the nature and intensity of mineralizing geological processes. These studies often produce cause-and-effect relations between processes and the formation of mineral deposits. A deterministic view of such relationships generates deterministic models of mineral deposits [3] in which the relationships are understood as fixed and certain. However, the formation of a mineral deposit can be also conceptualized as a statistical or probabilistic event so that the relation between a particular geological process and the formation of a mineral deposit is understood and quantified as probabilities of an event. Such probabilistic approaches underpin mineral potential and quantitative mineral resource assessments [3].

2.2. Mineral potential

QMRA relies on assessing mineral potential of an area to host a mineral deposit. Taylor and Steven [24] define mineral deposit/resource potential of an area as a measure of the likelihood of occurrence of valuable minerals or minerals that may become valuable within the foreseeable future. They noted that the likelihood of occurrence is not a measure of the resources themselves and thus cannot be classified according to the two-dimensional McKelvey diagram [27], which categorizes undiscovered resources. Taylor et al. [14] defined a matrix of levels of mineral potential and levels of certainty. The matrix has been widely used in mineral resource/potential assessments in public lands in the USA and Australia [12, 14, 16].

Harris and Carrigan [4] presented a probabilistic framework for understanding mineral potential more directly relevant to QMRA. Mineral potential is understood as conditional probability based on a number of mineral deposits, $P(N=n|\ X=x)$, in which N, the number of deposits, is a random variable, the probability of which depends on the state of geological process, X, in a region. Thus, for each value of X, there exists a distribution of probabilities for the random variable N. However, the state of a geological process in a region depends on geological features observable and observed in it. The uncertainty involved in the observation of geological features is expressed through another probability concept, the probability for the state of a geological process X, conditional upon the geological observation (g_1, ….., g_m) recorded by a geologist, $P(X=x1|\ g_1, g_2, \ldots.., g_m)$. This probabilities can be represented by another function Φ, $P(X=x_1|\ g_1, g_2, \ldots.., g_m) = \Phi(x|g_1, \ldots., g_m)$.

To compute the probability for the joint occurrence of N (number of deposits) and X (geological process), given geological observations g_1, …., g_m, the two functions can be combined as:

$P(X=x_1|\ g_1, g_2, \ldots.., g_m) = P(N=n_1|X=x_1) \times P(X=x_1|g_1, \ldots.., g_m)$.

For example, the probability of forming a sandstone-hosted uranium deposit in a region depends on whether the region has experienced a geological process such as transportation of uranium in oxidized shallow groundwater. The probability of this process in turn depends on a number of geological features observed in the region, which may include presence of leachable sources of uranium, presence of permeable sandstones and presence of hydrogeological head driving groundwater flow.

The probabilities in the conceptual model presented above can be estimated either objectively (objective probability) or can be assigned by experts (subjective probability). These methods of estimating objective and subjective probabilities will be discussed in the following sections of the review.

2.3. Undiscovered resources

Taylor and Steven [24] warned that undiscovered resources cannot be classified according to the two-dimensional McKelvey diagram. They described these resources as hypothetical or speculative. The 1992 review presented in IAEA's report [22] includes a table that shows correlation of uranium resources, including undiscovered resources, used by various agencies. The most common terms used to describe undiscovered resources include potential resources, hypothetical resources, and prognosticated resources. The undiscovered resources estimated in an area can be put through a number of different economic filters on the basis of various cost models to classify them into cost categories. These economic filters are described in [22].

3. CLASSIFICATION OF METHODS

Since the publication of Allais's groundbreaking work on quantitative assessment of mineral resources in the Algerian Sahara [1], several methods of assessments have been developed, applied, and discussed. These methods have been reviewed and summarized in many papers that include [3, 6 and 22]. Most reviews are dominated by statistical and probabilistic focus. This present review provides a brief classification and summary of methods, focusing on the needs of geologists who are interested in conducting QMRA of undiscovered uranium. This classification forms the basis of description summarized in the following sections of this review.

3.1. Qualitative and quantitative methods

QMRA of undiscovered resources are in principle methods of mineral potential assessment, which are commonly classified into qualitative and quantitative methods. Qualitative methods of assessment involve delineation of prospective tracts and ranking areas within the tracts in terms of their relative levels of mineral potential. The scale used to assign levels of mineral potential can be either non-numerical (low, moderate, high) or numerical (ordinal or cardinal) scales. Qualitative methods have been used in many assessments for both prospectivity analysis and for inputs into advice on conflicting land-use issues in Australia and USA [12, 14, 16]. Ordinal (numbers representing ranking) and cardinal (counting numbers) scales are often used to assist in combining mineral potential maps of different deposit types in an area [16].

Quantitative methods of assessment estimate tonnage of a commodity (uranium) in an area deemed to be geologically-permissive for mineral deposits. The tonnage is either estimated directly (e.g., [1, 28–31] independent of deposit types or indirectly by first estimating number of deposit per type and then using grade and tonnage data of known deposit types of that commodity (e.g., [2, 8].

3.2. Deterministic and probabilistic methods

QMRA can be either deterministic or probabilistic [3, 22]. Deterministic methods rely on one-to-one, cause-and-effect relationship between the numbers of deposits or tonnages of a commodity and one or more geological features deemed critical for the presence of that type of deposit and/or commodity. For example, crustal abundance methods are deterministic because they are based on the relationship between the crustal abundance of an element and its resources as a commodity in an area [22]. Similarly, deterministic methods may rely on the concentration of leachable uranium in a source rock to estimate resources of undiscovered uranium in a basin. Harris [3] describes the NURE method of assessment of uranium resources developed by the

US Energy Research and Development Administration (ERDA) as a deterministic geological method.

Probabilistic methods conceptualize the relationship between resources (e.g., number of deposits or tonnage of a commodity) and critical geological features in probabilistic terms. The probabilities attached to estimated resources can be either calculated by objective methods or estimated subjectively by expert-geologists or with the help of expert systems [3, 22]. Some QMRA combine deterministic and probabilistic approaches. For example, in the 3-part USGS method of assessment geologically-permissive tracts are delineated using deterministic approach but number of deposits and probabilities assigned to them are estimated by members of an expert panel. However, the numbers estimated by the experts have to be in agreement with the grade-and-tonnage model of the assessed deposit type. This method will be described more comprehensively in the latter sections of this review. The NURE method also combines deterministic and probabilistic approaches.

3.3. Data- and knowledge-driven methods

QMRA are also classified as either data- or knowledge-driven methods. In data-driven methods, assessments are based on geoscientific data available in the study area. The relationship between the deposits/resources and geological features is established through spatial analysis. The Weights-of-Evidence (WofE) method [18, 23] is commonly used data-driven method for prospectivity analysis and resource assessment. Similarly, many other data-driven methods that use objective probabilities are based on relationships established in a control area to estimate resources in data-rich study areas that are geologically analogous [3]. On the other hand, knowledge-driven methods are based on conceptual geological models of deposit types that list critical geological features essential for the formation of economic deposits. All qualitative methods of mineral resource assessments are predominantly knowledge-driven. Delineation of geologically-permissive tracts in many QMRA is based on deposit-type models or on the analysis of fertile mineral systems. It needs to be emphasized that there are no purely data- or knowledge-driven methods. Most QMRA combine these approaches.

3.4. Choice of methods

QMRA are carried out to meet different objectives, which include inventory (supply and demand of a commodity) studies, for input into resolving conflicting and multiple land-use decisions, for environmental planning in a region, and for guiding mineral exploration (regional and deposit-scale targeting). The choice of an appropriate method depends on the principal objective of the assessment. The appropriateness or suitability of a method also depends on the quality and extent of geoscientific information/data in the target region. Methods suitable for data-rich regions (also described as ‘brownfield’) may not be fully applicable to data-poor (‘greenfield’) regions and may have to be modified. Hence, methods that can be successfully altered to meet the needs of both data-poor and data-rich regions hold more promise.

As the quality of geoscientific data varies within a region and from region to region, the choice of an appropriate method will also be guided by the scale (global, crustal, continental, national, district, deposit), at which undiscovered resources are being assessed. Most commonly, QMRA have been conducted at continental, national and district scales. Crustal-abundance methods allow generating estimates at national as well as global scales. Harris [3] describes estimates of world uranium resources conducted by OECD/IAEA and published in 1975. In several studies, QMRA that has been conducted at regional scales within various countries were combined to produce global assessments (e.g., [32].

3.5. Requirements of methods

As mineral deposits and mineral resources are fundamentally spatial categories, it is essential that undiscovered resources estimated by QMRAs are spatial and can be visualized in the form of map. The development of GISs in the 1980s, which provide tools for quick spatial data analysis, integration and visualization, has helped in producing map-based assessments of undiscovered resources. Many resource inventories and multiple land-use decision require that undiscovered resources are spatially defined within geologically-permissive tracts. QMRA undertaken for exploration targeting is by its nature need to be map-based.

Although QMRA of a commodity can be carried out independent of a particular deposit type, assessments of resources based on deposit types have a distinct advantage. Firstly, because deposit-type models and associated critical geological features assist in more reliable delineation of geologically-permissive tracts in a region. Knowledge of deposit types can be critical in providing economic filters to categorize undiscovered resources in different cost categories. This is primarily because mining and processing depends on the nature and quantity of ore minerals in an ore deposit.

QMRAs that can be applied with little or no modification to both data-rich (brown-fields) and data-poor (green-fields) regions have a distinct advantage over methods suitable for only one type of region according to data availability. Methods that combine knowledge- and data-driven approaches can be readily modified to achieve the objective.

The reliability of estimates derived by different QMRA depends largely on our knowledge of mineralizing processes (as conceptualized in deposit types) and on geoscientific data (quantity and quality) in a study area. Hence, methods that can document levels of certainty attached to the estimates are more useful. For example, qualitative methods of resource assessment follow a definite matrix in which levels mineral potential in a tract is also assigned a corresponding level of certainty [14]. The GIS-based Dempster-Shafer method produces two predictive maps of the study area, one showing the lower bound (of the belief function) and the other the upper bound (of the belief function), thereby showing uncertainty associated with the results [23]. The one-level prediction method developed by [33] also computes errors associated with the assessments. The 3-part USGS method emphasizes the need for assessments to be unbiased. It includes techniques that can be used to reduce the chances of introducing bias in the estimates of undiscovered resources [2].

Methods of QMRA described in this review are assessed in terms of four main requirements discussed in this section. These requirements are: (a) capability to produce map-based estimates; (b) capability to estimate resources associated with specific deposit types; (c) applicability to both data-rich and data-poor regions; and (d) capability to compute levels of certainties associated with the estimates. These four main requirements assist in grouping methods that can be used to assess undiscovered resources for specific regions and for specific tasks.

4. MINERAL SYSTEM APPORACH AND URANIUM MINERAL SYSTEMS

4.1. What is a mineral system?

Mineral deposits develop via the happenstance of favorable geological processes within a certain spatial setting and at a particular geological time. In comparison with the notion of a petroleum system [34], processes that generate a mineral deposit can jointly be referred to as a mineral system. Therefore, a mineral system is defined as ‘all geological factors that control the generation and preservation of mineral deposits', and there are seven important geological factors that define the characteristics of a hydrothermal mineral system, namely [35]: (1) source of the mineralizing fluids and transporting legends; (2) source of metals and other ore components; (3) migration pathways that may include inflow as well as outflow zones; (4) thermal gradients; (5) source of energy to mobilized fluids; (6) mechanical and structural focusing mechanism at the trap site; and (7) chemical and/or physical cause for precipitation of ore minerals at the trap site. The principal components of a mineral system are shown in Fig. 1 [36].

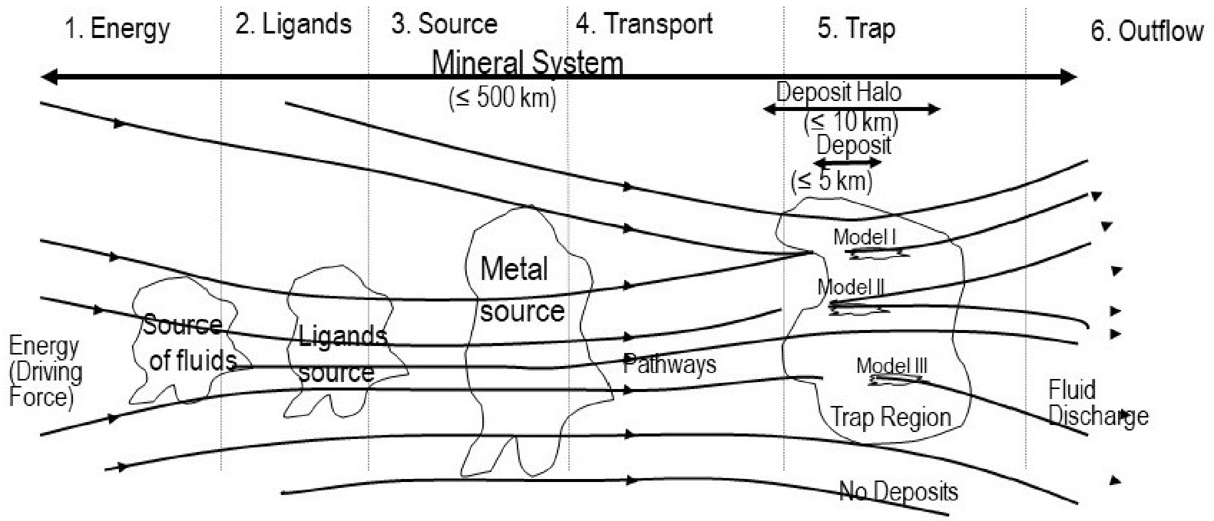

FIG. 1. Schematic diagram representing major components of a mineral system. It has to be noted that deposit-style models often concentrate on mappable features observable at the deposit-scale. These features often represent footprints of physical and chemical processes happening at the trap-site. Modified after [36].

The notion of a mineral system is also known as the source-transport-trap paradigm, as re-defined by [37], who raised the following five questions as a basis for understanding the spatio-temporal evolution of a mineral system at all scales (regional to deposit): (1) What is the architecture and size of the system? (2) What is P–T and geodynamic history of the system? (3) What is the nature of the fluids and fluid reservoirs in the system? (4) What is the nature of fluid pathways? (5) What is the chemistry of metal transport and deposition in space as well as time? The notion of a mineral system has been used to develop process-based conceptual models of ore systems (e.g., [38] and to define flexible probabilistic frameworks for quantitative risk analysis in mineral exploration [20]. It has also been used to map critical ingredients of fertile mineral systems and to map mineral prospectivity (e.g., [16, 35, 36, 39]. A similar mineral-system approach was applied to describe ore-forming processes in Archean lode–gold deposits [40, 41] and volcanic-associated massive sulfide deposits [42].

An important aspect of the concept of mineral system is the scale-dependent nature of its constitutive elements. The system as a whole functions on a regional scale but the features that are generally observable at the camp- or deposit-scale are controlled by processes occurring at or near physical and chemical traps. Some of these processes leave their footprints in wall-rock alterations, and revealed by several physical (density, magnetic, conductivity) and chemical (geochemical vectors of major and minor elements) gradients. A deposit- and camp-scale focus can in many cases miss important signatures of fertile mineral systems. It can also miss important information left as footprints by fluids and melts passing through the outflow zone. Therefore, prospectivity analysis and mineral potential modeling based on the concept of mineral system can provide important additional mappable features useful at both regional and deposit scales.

4.2. Diversity and classification of uranium mineral systems

Several global and regional classification schemes for uranium deposits have been proposed and used [43]. All classifications serve a purpose. One of the most detailed classification schemes was developed by [43, 44]. This classification is a mixture of descriptive and genetic approaches. Cuney [45] proposed a dominantly genetic classification of uranium deposits relating types of uranium deposits to a general geochemical cycle of uranium.

Expert panels in IAEA have developed their own classification of uranium deposit types. The scheme produced by IAEA in 1991 identified 15 major deposit types [46]. A modified version of the classification defined the basic structure of IAEA's UDEPO database [47]. This classification scheme will become the principal classification of uranium deposits to be used in the description of uranium deposits and for maintaining IAEA's uranium resource database (UDEPO).

A mineral-system-based classification of uranium deposits was proposed by [38]. In this predominantly genetic classification, uranium deposits were classified as part of uranium mineral systems, which in turn were classified based on the nature of fluid or melt responsible for their formation.

The mineral-system classification included in this review is a modification of the genetic, process-based, classification proposed by [45]. The classification is hierarchal in structure, with the most general grouping of deposit called 'mineral-system clan' (Table 1). This high-level category is divided into Regolith, Basinal, Magmatic and Metamorphic clans. These clans are divided into groups, and groups are subdivided into subgroups and deposit types. Deposit types have the same names as those proposed in IAEA's classification [46, 47].

Figs 2 and 3 show the classification of uranium mineral systems conceptualized as part of the global mantle-crust-surface geochemical cycle of uranium. A similar scheme of classification was proposed earlier for rare-earth-element mineral systems and deposits [48]. The figure also shows average concentrations of uranium and thorium/uranium ratios in the Earth's mantle and crust. Both uranium and thorium belong to the group of high-field strength elements (high ionic charge and high ionic radius), which make them behave incompatibly during partial melting of mantle and crustal rocks and also during crystallization of felsic magmas. The incompatibility of uranium and thorium controls their gradual accumulation into crust. In the mantle-crustal cycle, the thorium/uranium ratio of ~4 is maintained. The only exceptions are the carbonatites and some peralkaline rocks, which tend to be relatively enriched in uranium. The diversity of magmatic uranium mineral systems and deposit types is principally controlled by the degree of partial melting of the mantle and crustal material and by temperature and depth at which the partial melting occurs. These issues have been discussed comprehensively by [45, 49, 50 and 51].

The diversity of uranium mineral systems and associated deposit types in the surficial and shallow-crustal-level environments is predominantly controlled by the fact that uranium forms stable complexes and minerals containing hexavalent uranium. Its behavior is in turn determined by the oxidation-reduction process occurring in these environments.

TABLE 1: CLASSIFICATION OF URANIUM MINERAL SYSTEMS[1]

1. BASINAL (Clan)
    - 1.1. Sedimentary (Group)
        - 1.1.1. Mechanical (subgroup)
            - 1.1.1.1. Paleo-proterozoic quartz-pebble conglomerate (deposit style)
        - 1.1.2. Chemical and biochemical
            - 1.1.2.1. Coal-lignite
            - 1.1.2.2. Black shale
            - 1.1.2.3. Phosphate
    - 1.2. Diagenetic hydrothermal
        - 1.2.1. Unconformity-related
            - 1.2.1.1. Basement-hosted
            - 1.2.1.2. Unconformity-contact
            - 1.2.1.3. Stratiform fracture-controlled
            - 1.2.1.4. Mafic dikes/sills in Proterozoic sandstones
            - 1.2.1.5. Stratabound carbonate hosted
    - 1.3. Epi-sedimentary
        - 1.3.1. Sandstone uranium
            - 1.3.1.1. Roll-front
            - 1.3.1.2. Tabular
            - 1.3.1.3. Basal channel
            - 1.3.1.4. Tectonic-lithologic
            - 1.3.1.5. Collapse breccia-pipe
        - 1.3.2. Calcrete uranium
            - 1.3.2.1. Fluvial valley-fill
            - 1.3.2.2. Lacustrine-playa
2. MAGMATIC
    - 2.1. Orthomagmatic
        - 2.1.1. Deposits related to partial melting (intrusive anatectic)
        - 2.1.2. Deposits related to magmatic differentiation (intrusive-magmatic)
    - 2.2. Magmatic hydrothermal
        - 2.2.1. Metasomatic
            - 2.2.1.1. Na-metasomatite

2.2.1.2. K-metasomatite
2.2.1.3. Skarn
2.2.2. Intrusive-related
2.2.2.1. Intra-granitic
2.2.2.2. Peri-granitic
2.2.3. Volcanic-related
2.2.3.1. Structure-bound
2.2.3.2. Stratabound
2.2.3.3. Volcano-sedimentary
2.3. Hybrid hydrothermal
2.3.1.1. Polymetallic hematite breccia complex
3. METAMORPHIC
3.1.1.1. Stratabound
3.1.1.2. Structure-bound
3.1.1.3. Marble-hosted phosphate
4. REGOLITH
4.1. Zones of secondary uranium minerals formed from exogenic and supergene processes. Some uranium mineralization reported in British Columbia may have resulted from regolith-related processes

---

[1] The classification is hierarchical. Clans of mineral systems are subdivided into groups and groups are subdivided into subgroups. Uranium deposit styles described in IAEA's classification belong to either mineral system groups or to deposit styles in this classification. These names are shown in blue italics. Mineral system templates (Tables 2, 3, and 4) are compiled for mineral system subgroups.

Basinal uranium mineral systems include uranium deposits formed during various stages of basin evolution (sedimentation, diagenesis and post-sedimentation fluid-flow), and account for a significant proportion of uranium resources worldwide. In the UDEPO database of the IAEA, uranium resource data (from 1,140 deposits worldwide) account for ~74% of resources, almost 3× greater than resources in the magmatic-related uranium systems (Fig. 4). Of the basin-related uranium mineral systems, ~59% of world's uranium resources are related with various types of phosphorites (Fig. 5). In general, phosphorite-related deposits are low grade (200–600 ppm U) [43]. Sandstone-hosted uranium deposits account for ~23% of the known world's uranium resources (Fig. 5) and, at present, represent the largest economically extractable resources of uranium of any type. Amongst sandstone-hosted deposits, ~54% of known uranium resources are accounted for by the roll-front type of deposit (Fig. 6) followed by tabular (~37%) and basal-channel types (~7%). Although only ~8% of the world's uranium resources are accounted for by unconformity-related uranium deposits, some of the world's highest-grade deposits are of this type. Nearly 2% of the world's uranium resources are accounted for by calcrete-hosted uranium deposits (termed surficial in the UDEPO database).

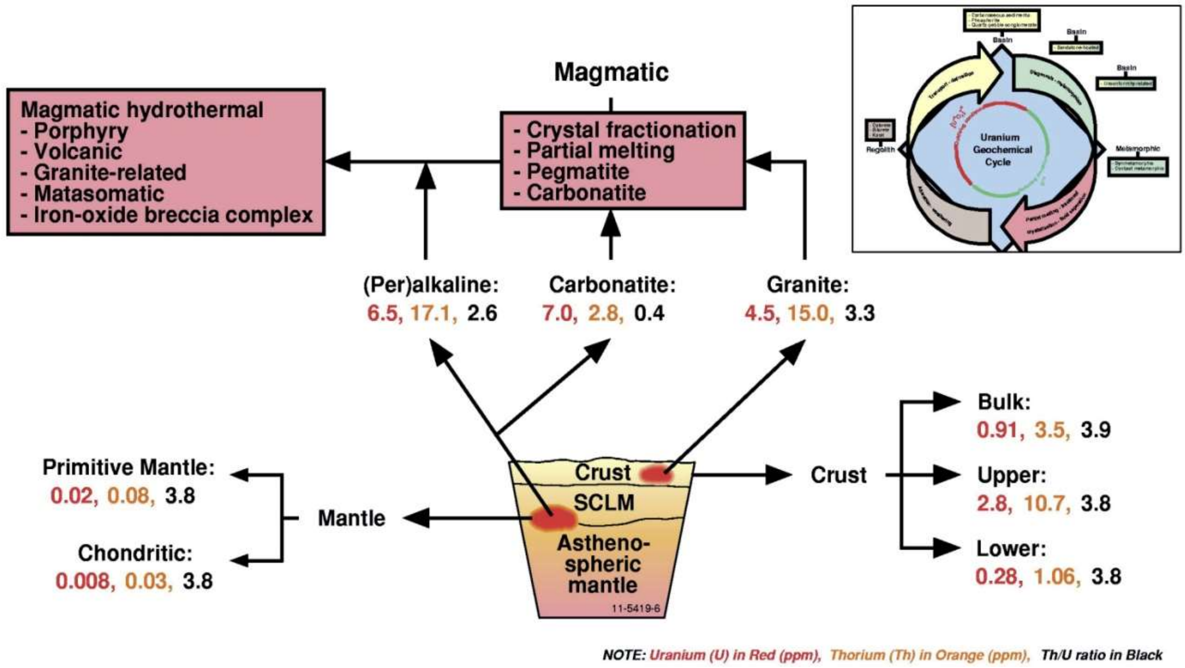

FIG. 2. Classification of major uranium mineral system based on geochemical cycle of uranium. Concentration of uranium (number in red) and thorium (numbers in orange) represent average concentration. This figure represents the mantle-crustal part of the geochemical cycle.

Oxidation-reduction reactions, which control transport (in oxidized conditions) and deposition (in reduced conditions) of uranium, is the reason for the high proportion of basin-related uranium systems in the global metallogeny of uranium. Intensive removal of uranium from rocks and its transport in oxidized fluids is due to variations in the oxygenation level of Earth's atmosphere, which occurred in a number of stages [52].

During Stage 1 (3.85–2.45 Ga), the atmosphere as well as the oceans were largely or entirely anoxic. This condition favored accumulation of detrital uraninite and formation of uraniferous quartz-pebble conglomerates (e.g., the Blind-River and Elliot Lake area in Canada and the Witwatersrand Basin in South Africa; [43].

During Stage 2 (2.45–1.85 Ga), the oxygen level in the Earth's atmosphere increased to 0.02–0.04 atm and shallow regions of oceans were mildly oxygenated. Proterozoic unconformity-related uranium deposits formed predominantly during 1.75–1.60 Ga in Australia [53] and during 1.60–1.30 Ga in Canada (the Athabasca and Thelon basins; [54]. These time periods overlap with Stage 3 of oxygenation (1.85–0.85 Ga), when the Earth's atmospheric oxygen levels were not significantly different from those in Stage 2 (2.45–1.85 Ga) levels. The Earth's atmospheric oxygen levels during Stage 4 (0.85–0.54 Ga) increased 10 times to reach values of ~0.2 atm. The Earth's atmospheric oxygen levels most likely rose to a maximum value of ~0.3 atm during Stage 5 (0.54 Ga to present), which was when most large sandstone-hosted uranium deposits in the world have been formed.

Aside from oxygenation of the atmosphere, as the most critical factor that has controlled the formation of basin-related uranium deposits, the other most critical factor was the presence of vascular plants in sedimentary basins. After the emergence of vascular plants on the Earth (in the Late Silurian or even as early as the Late Ordovician [45]), the deposition of continental siliciclastic sediments did not lead to the development of thick strata of uniformly oxidized 'red sandstones', which are typical features of basins hosting Proterozoic unconformity-related deposits, but it favored the formation of strata comprising alternating series of oxidized and reduced carbonaceous-rich sediments [45]. The generation of intra-formational redox gradients bestowed ideal conditions for the formation of sandstone-hosted uranium deposits.

In the Cenozoic, when valley calcretes were formed in areas of relatively arid climate conditions, calcrete-uranium deposits appeared. In these mineral systems, uranium and vanadium are transported in oxidized groundwater and carnotite is deposited, not because of changes in redox conditions, but because of variations in pH and CO_2 concentration in groundwater due to seasonal fluctuation of groundwater levels.

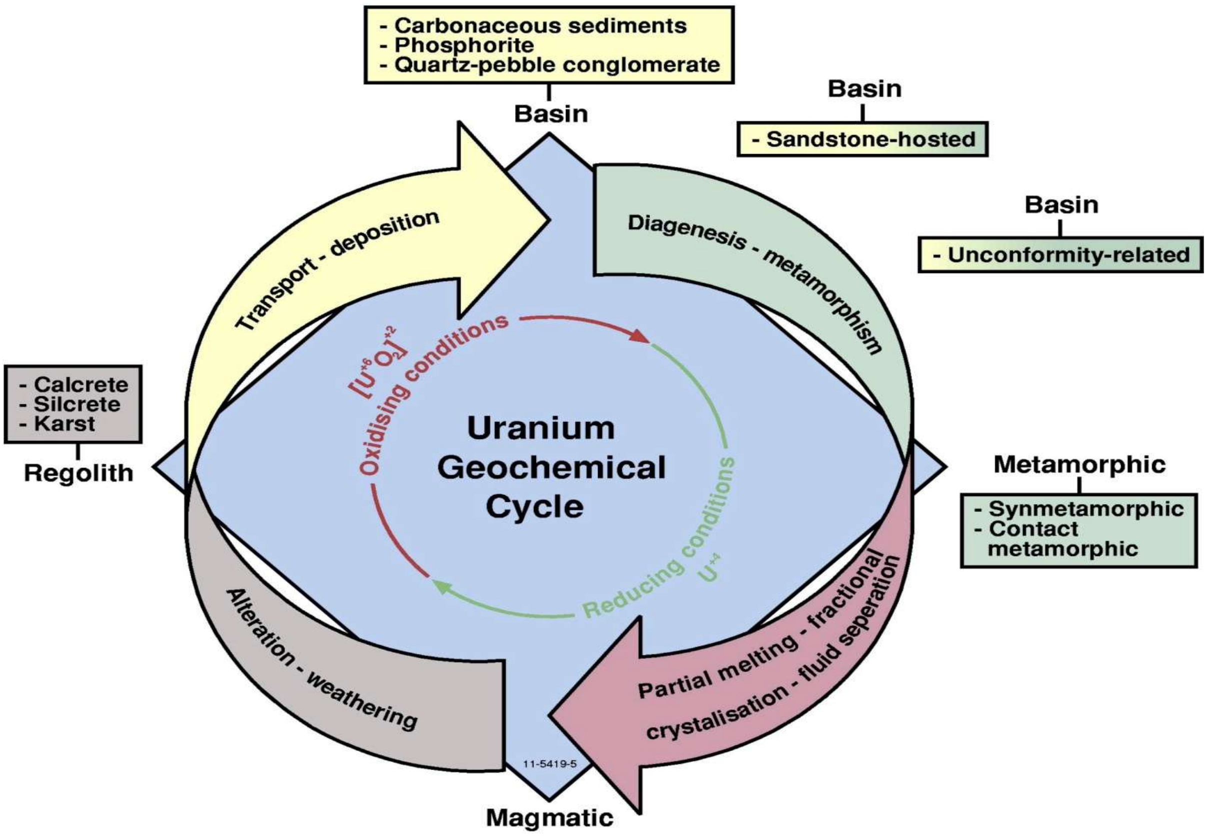

FIG. 3. The geochemical cycle of uranium and associated major uranium mineral systems.

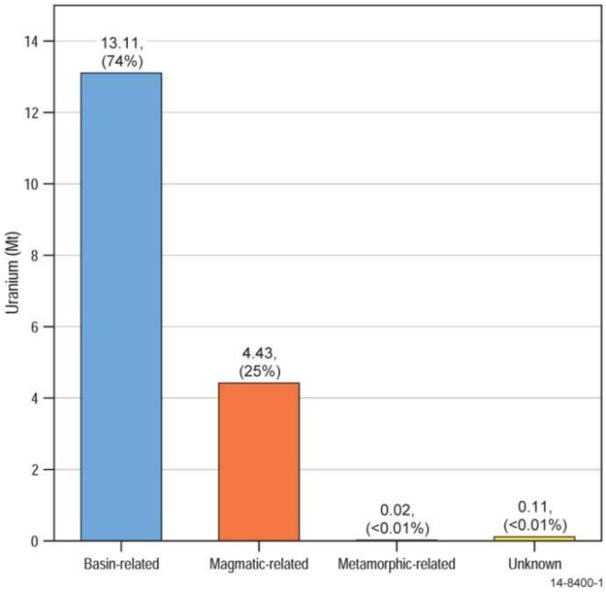

FIG. 4. Uranium resources of four major classes of uranium deposits. Data are sourced from the IAEA's UDEPO database [47]. Data accessed in January 2014 (https://infcis.iaea.org/UDEPO/About.cshtml).

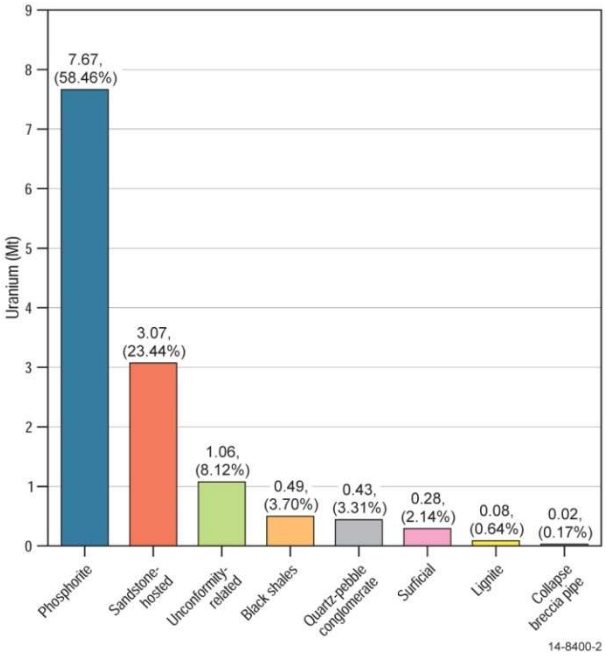

FIG. 5. Uranium resources of basin-related uranium deposits. Data are sourced from the IAEA's UDEPO database [47]. Data accessed in January 2014 (https://infcis.iaea.org/UDEPO/About.cshtml).

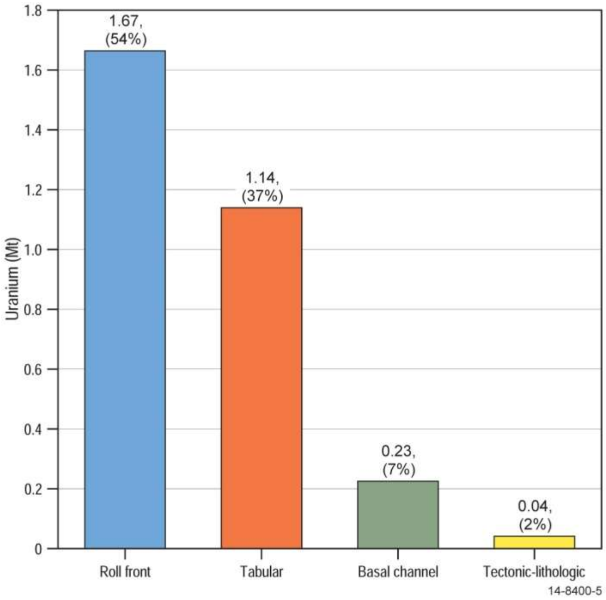

FIG. 6. Uranium resources of sandstone-hosted uranium deposits. Data are sourced from the IAEA's UDEPO database [47]. Data accessed in January 2014 (https://infcis.iaea.org/UDEPO/About.cshtml).

4.3. Examples of mineral system templates

This review used the so-called 'source-pathway-trap' paradigm to summarize critical features of fertile mineral systems (Tables 2, 3, and 4). However, it is extended to take account of information on the geological setting, age and relative timing of mineralization, and preservation of mineral systems. These features can afford the basis for mineral potential analysis in an area, which needs recognition of mappable signatures of above-mentioned critical features in geological, geochemical and geophysical datasets.

These mineral-system templates are more comprehensive and diagnostic than the descriptive models used in three-part USGS method of quantitative resource assessment [61]. Their main purpose is to assist in delineation of geologically-permissive tracts and prospectivity and favorability maps, which form the first step in the quantitative resource assessments in a study area. Similar templates can be compiled for other types of mineral systems listed in the classification.

TABLE 2. CRITICAL FEATURES OF UNCONFORMITY-RELATED URANIUM MINERAL SYSTEMS

Deposit types (including synonyms):

- Ingress-type, Egress-type; Unconformity-contact (fracture-bound, clay-bound) Proterozoic sub-unconformity – epi-metamorphic.

Geological setting:

- Unconformity between Paleoproterozoic metasedimentary rocks and Paleo- to Mesoproterozoic sandstones;
- Basement of Archean domes/inliers flanked by Paleoproterozoic metasedimentary rocks.
- Metasediments formed in shallow marine conditions rather than turbiditic, containing units enriched in carbonaceous material;
- Thick (> ~ 5 km) package of Paleoproterozoic to Mesoproterozoic sediments containing sandstones formed in braided, fluvial conditions. Flat-lying at the time of mineralization (often foreland basin). Often partially or fully eroded.

Source (fluid, metal, energy):

Fluids

- Fluid 1: Diagenesis of sedimentary package overlying the unconformity. High salinity fluids formed from dissolution of evaporite;
- Fluid 2: Evolved from Fluid 1 after reacting with metasedimentary rocks below the unconformity. High salinity but higher Ca/Na ratio than Fluid 1;
- Fluid 3: Hydrocarbon-rich fluid formed from hydrogenation of carbonaceous material in metasediments below the unconformity.

Uranium

- Uranium-bearing detrital minerals in the sandstone such as monazite and/or zircon. Felsic volcanics or their fragments in the sandstone package overlying the unconformity;
- Uraninite and or uranium-bearing minerals (monazite and/or zircon) in the granites and/or metasediments below the unconformity;
- ‘Paleo-regolith’, often altered by reaction with fluids.

Energy drivers of fluid-flow

- Compaction of sediments in the basin;
- Heat (radio-thermal, produced by granitoids and Archean rocks in the basement, and by intrusives emplaced in the sandstone overlying the unconformity). Compaction and heat can initiate basin-scale convection of fluid;
- Tectonic activity along faults and shear zone.

Fluid pathway:

- Unconformity surface with or without paleo-regolith;
- Aquifers in the sandstone package overlying the unconformity;
- Faults and breccia zones leading up to and/or cutting the unconformity.

Trap:

Physical

- Unconformity surface;

- Breccia zones and faults (in the basement rocks and in the sandstones overlying the unconformity).

Chemical
- Carbonaceous (graphite) rocks below the unconformity;
- Rocks with Fe^{+2}-bearing silicates such as chlorite either below the unconformity or in the sandstone package above the unconformity;
- Reduced fluid resulting from the hydrogenation of carbonaceous material;
- Presence of calcareous rocks (affecting pH, not fully clear).

Age and relative timing of mineralization:
- Proterozoic age important for world-class deposits;
- Mineralization closely linked with the timing of diagenesis in the sandstone package overlying the unconformity;
- Mineralization linked to compression during basin inversion in the basin overlying unconformity;
- During extension diagenetic fluids accumulate, during inversion the fluids move outward from the basin.

Preservation:
- Presence of sandstone above the unconformity indicates high probability of preservation of unconformity type uranium deposits.
- Most known deposits show remnants of the sandstone package overlying unconformity in close proximity.

Main references: [43, 53−56].

TABLE 3. CRITICAL FEATURES OF SANDSTONE-HOSTED URANIUM MINERAL SYSTEMS

Deposit types (including synonyms):

- Roll-front, tabular, basal channel, tectonic/lithologic, epigenetic strata-infiltration.

Geological setting:

- Intra-cratonic basin, continental margin basin, inter-montane basin;
- Embayment of basins rimmed by uranium-rich felsic rocks;
- Permeable sands in channels in paleo-valleys;
- Shallow dipping (normally between 5 to 10°) basin sequences;
- Often basin sequences tilted in the direction of a major reservoir (outflow zone): lake or sea;
- Sandstone aquifers sealed by over- and under-lying impermeable layers (mudstone, etc.).

Source (fluid, metal, energy):

Fluids

- Meteoric water. Locally diagenetic. Salinity variable but mostly not very saline (can locally reach ~5 wt. % NaCl). Oxidized. Neutral to moderately acidic;
- In rock sequence devoid of organic material a second reduced fluid sourced from hydrocarbon or coal-bearing basins may be involved.

Uranium

- Peraluminous felsic rocks (intrusive and volcanic), especially two-mica leucocratic granites. Peralkaline volcanics. Uranium either derived from volcanic glass or from uraninite. Minerals such as zircon, monazite and uranium-bearing thorite become leachable sources after metamictization (100 to 150 Ma after emplacement of felsic rocks). Locally uranium can be sourced from the lithic material in the sandstone, volcanic ash in overlying or underlying beds;
- Presence of orthomagmatic and/or magmatic-hydrothermal uranium mineralization in the source area is important in forming bigger deposits.

Energy drivers of fluid-flow

- Dominantly gravity-driven fluid-flow. Reactivation of faults at the basin margin (causing tilting and doming of the basin) can trigger groundwater flow.

Fluid pathway:

- Lithified and/or unlithified immature and permeable sands;
- If a second reduced fluid (mobile reductant) is involved, faults within the basin sequence can be important;
- In paleo-channels, groundwater flows occurs both along the channel as well as across the channel.

Trap:

Physical

- Contact with carbonaceous shales underlying sandstone. In paleo-channel systems mineralization can be found in basement scours, at meandering bends, at sites of channel widening and at sites of confluence with tributaries;

Chemical

- Carbonaceous material in the sands is the most common reductant (biogenic reduction in the presence of anaerobic and sulfate-reducing bacteria). Locally Fe^{+2}- and vanadium-bearing clays and silicates can be important. In some regions Fe^{+2}-bearing silicates, especially chlorite in mafic rocks, can serve as effective reductants. Mobile reductants, such as CH_4, CO, H_2S, N_2 and H_2, and other hydrocarbons derived from hydrocarbon and coal basins, can also cause reduction.

Age and relative timing of mineralization:

- Generally Paleozoic and younger. In older basins, mineralization can form if the sandstones contain algal material and/or Fe^{+2}-bearing silicates and sulfides;
- Mineralization often occurs in unconsolidated and semi-consolidated sands soon after the deposition of overlying shales. In many basins with significant resources mineralization is formed in more than one episode of groundwater flow, closely related to uplift history of sediment provenance areas. The uplift is caused by reactivation of faults.

Preservation:

- Critical. As mineralization often occurs in good aquifers, it can be easily dissolved and re-deposited or completely destroyed. Preservation requires physical isolation of mineralization from the flow of oxidized groundwater. Slowing down of groundwater or its cession can also promote preservation.

Main references: [43, 55, 57].

TABLE 4. CRITICAL FEATURES OF CALCRETE-HOSTED URANIUM SYSTEMS

Deposit types (including synonyms):

- Fluvial valley-fill or valley-type, lacustrine or playa-type.

Geological setting:

- Cenozoic paleo-valleys and channels in arid zones;
- Paleo-channels filled with sediments containing non-pedogenic calcrete. Formation of non-pedogenic calcrete is controlled by climate (arid) and by the soil-type (neutral to acid soils);
- Playa lakes with evaporitic sediments.

Source (fluid, metal, energy):

Fluids

- Meteoric water, lake water, shallow to deep (~400 m) ground water;
- Salinity (chloride): variable ranging between 136 mg/L and 95 160 mg/L. High salinity waters can transport more uranium and vanadium; pH varies between 6.0 and 8.2. pH is not considered important for the transport of uranium and vanadium.

Potassium, uranium, and vanadium source

- Felsic rocks for uranium (rocks with > ~20 ppm U);
- Mafic rocks and banded iron formations for vanadium. Average abundance (in ppm) of vanadium in major rock types [58]: Basalt (250); Shale (130); Granite (50);
- Potassium from felsic rocks.

Energy drivers of fluid-flow

- Dominantly gravity-driven fluid-flow. Seasonal variation of the groundwater table is considered important. Hydrological gradients are low (~ 0.12% and lower).

Fluid pathway:

- Permeable sands in paleo-channels;
- Efficient hydrological system involves a good connection between aquifers in paleo-channels and salt lakes (discharge areas).

Trap:

Physical

- Changes in the shape of paleo-channels and subsurface barriers in paleo-channels can restrict flow of groundwater causing its ponding and upwelling.

Chemical

- For valley-type calcrete deposits: changes in pH and concentration of potassium, vanadium and uranium, and dissolved CO_2 due to evaporation of upwelling groundwater;
- For playa-type deposits: mixing of groundwater with saline lake water and changes in the concentration of K, Ca, CO_3 and SO_4;
- Less frequently: mixing of relatively reduced waters carrying vanadium with more oxidized waters carrying uranium.

Age and relative timing of mineralization:

- Cenozoic age;

- Paragenetically, carnotite mineralization is late and replaces carbonate minerals in the calcrete. Activation of the mineral system depends on the hydrogeological connection between aquifers in the paleo-channels and playa lakes.

Preservation:

- Critical. As mineralization is formed in relatively shallow paleo-channels with good aquifers, it can be dissolved, re-precipitated and enriched or completely destroyed. Mineralization can also be destroyed by changes in the climate.

Main references: [43, 59–61].

5. QUALITATIVE METHODS

Qualitative assessment of mineral potential is an essential first step of any map-based QMRA. Qualitative assessment of mineral potential involves delineation of areas that are favorable to host mineral deposit and to assign and/or compute levels of mineral potential to a whole geologically-permissive tract or to areas within a geologically-permissive tract. Qualitative methods of mineral potential assessment were first used in forest areas in the USA and Australia, most often for input into decisions regarding conflicting multiple land-uses in a region (e.g., [12, 14 and 16]). The development of GIS and relational datasets led to techniques that allowed rapid spatial data analysis, integration and visualization. This paved way for the emergence of new GIS-based methods of mineral potential assessments commonly described as favorability and/or prospectivity analysis [18, 23].

All pre-GIS- and GIS-methods are predominantly knowledge-driven relying on the study of known deposit types. The WofE is one of the few GIS-methods that are predominantly data-driven. In this method, mineral potential (as probabilities) is computed based on spatial association between the known deposits and geological features in the region.

Qualitative assessment of mineral potential is generally carried out in the following steps:

— Preparation of geological models of deposit types deemed to be permissive in the study region;
— Listing of features considered to be critical for the formation of that deposit type;
— Identifying mappable signatures of critical features in available geoscientific datasets;
— Delineating favorable areas within geologically-permissive tracts and assigning or computing levels of mineral potential (on a nominal scale or as probabilities) based on the presence or absence of critical features. In some methods levels of mineral potential are also assigned levels of certainty based on the quality and extent of available geological information in the study region. Description of geologically-permissive tract maps contains information used to justify assessed levels of potential and certainty.

5.1. Qualitative assessment of mineral potential in public lands

The method was developed and used by assessment teams in the US Geological Survey (e.g., [12, 14] to conduct mineral potential assessment in several forest areas. A slightly modified version of the same method was used in Australia as part of comprehensive regional assessments in forest areas for input into regional forest agreement [16].

5.1.1. Qualitative assessment in Forest regions, USA

Basic concepts and methodology are described in [14] and [24]. A brief description is also available in [63]. In this method, the mineral potential of an area is assessed by identifying the types of mineral deposits likely to be found under the geological settings known or believed to exist there. An assessment of the potential mineral of a region involves integration of knowledge of the region's mineral deposits and occurrences, geology, geochemistry, and geophysics with current theories of mineral deposit formation and results of mineral exploration. The assessment requires analysis of available geoscientific data – from a region to a small area, as required – to understand the history of geological processes and environments. Geological settings that are typically known to be linked with specific types of mineral deposits are then determined. The assessment particularly considers regional and local characteristics described by mineral deposit models to establish whether or not specific types of mineral deposits are likely to occur.

The assessment is conducted for specific deposit types that can occur in the study area. Geological characteristics of these deposit types are summarized for assessment purposes. The summary is similar to descriptive models [62] used in the three-part USGS method of QMRA. The description of deposit types also lists criteria used for the assessment of mineral potential (e.g., [14]. The 'assessment' section in the description provides justification for the assessed level of mineral potential and certainty shown on a mineral potential map of that deposit type. An interesting aspect of the description of deposit type is a brief discussion on the economic significance of the deposit type in the study area.

The mineral potential of an area is assessed for specific types of mineral deposits. For each type of deposit considered in a given area, the mineral potential is ranked in qualitative terms as 'high', 'moderate', 'low', 'no' or 'unknown', based upon professional judgments of geoscientists involved in the assessment. The levels of mineral potential are defined as follows (Table 5):

H (high): An area is regarded to have high mineral potential if the geological, geochemical or geophysical evidence indicates a strong likelihood that mineral concentration has taken place and that there is a strong possibility of specific type(s) of mineral deposit(s) being present. The area has features providing strong evidence for the presence of specific types of mineral deposits. The assignment of high mineral potential does not require that the specific mineral deposit types have already been identified in the area being assessed.

M (moderate): An area is regarded to have a moderate mineral potential if the available evidence indicates reasonable possibility of specific type(s) of mineral deposit(s) being present. Evidence of mineral occurrences or deposits may or may not be available. The features for the presence of specific types of mineral deposits are less clear.

L (low): An area is regarded to have a low mineral potential if there is a low possibility of specific types of mineral deposit(s) being present. Geological, geochemical and geophysical features in such an area indicate that mineral concentrations are unlikely, and evidence for specific mineral deposit models is lacking. The assignment of low potential requires positive knowledge and cannot be used as a valid description for areas where adequate data are lacking.

N (no): The term ‘no’ mineral potential can be used for specific types of mineral deposits in areas where there is detailed understanding of the geological setting and geoscientific evidence indicates that such deposits are not present.

U (unknown): If there are insufficient data to regard an area as having high, moderate, low or no potential, then the mineral potential is unknown.

To reflect the varying amount of information available, the assessment of mineral potential is also categorized according to levels of certainty, denoted by letters A to D (Table 5);

A: The available data are inadequate to determine the level of mineral potential. This level is used with an assignment of unknown mineral potential.

B: The available data are adequate to suggest the geological setting and the level of mineral potential, but either the evidence is insufficient to establish precisely the likelihood of resource occurrence or the occurrence and/or genetic models are not well enough known for predictive resource assessment.

C: The available data give good indication of the geological setting and the level of mineral potential. D: The available data clearly define the geological setting and the level of mineral potential.

Qualitative mineral potential assessment in forest regions involved assessment of a number of deposit types of uranium, such as, sediment-hosted syn-genetic deposits (copper and uranium; uranium deposits in sandstones [14].

TABLE 5: RELATIONSHIP BETWEEN LEVELS OF MINERAL POTENTIAL AND CERTAINTY (AFTER [14]

Level of potential	Unknown potential	H/B High potential	H/C High potential	H/D High potential
		M/B Moderate potential	M/C Moderate potential	M/D Moderate potential
		L/B Low potential	L/C Low potential	L/D Low potential
	A	B	C	D
	Level of certainty			

5.1.2. Qualitative assessment in forest regions, Australia

In the period 1996–2000, assessment teams in the Geoscience Australia Bureau of Mineral Resources and State Geological Surveys in Australia conducted mineral potential assessments in forest regions as part of Comprehensive Resource Assessments as input into Regional Forest

Agreement. The teams used a modified version of qualitative assessment method employed by teams in the USGS as described in section 5.1.1. The method has been described in [16]. The mineral potential assessment was conducted for more than 40 deposit types in each of the forest regions. For each deposit type, descriptive models [62] were modified to meet geological settings specific to the region. Each model listed criteria applied to assess mineral potential and levels of certainty. The model also included description of mineral potential areas with summary of geological information in support of assessed level of mineral potential and certainty. To add more resolution to the mineral potential maps, the three levels of mineral potential (Low, Moderate, and High) were expanded to five levels (Low, Low–Moderate, Moderate, Moderate–High, and High).

As regions were deemed to have potential to host a number of different deposit types in the same area, numerical techniques were developed to combine maps of different types to produce a number of composite mineral potential maps [16]. A simple composite mineral potential map showed the highest level of mineral potential of deposit types for an area in which mineral potential for different types overlapped. In cumulative mineral potential maps, numerical scores (High = 18; Moderate to High = 12; Moderate = 6; Low to Moderate = 2; and Low = 1) corresponding to different levels of potential were added to differentiate areas that had potential to host more than one deposit type. Numerical weightings were employed to provide some perspective to the relative economic significance of different types of deposits. In general, the weightings reflect the in-ground dollar value of extractable commodity associated with a particular deposit type. To estimate in-ground dollar values, grade-and-tonnage models developed by [62] were found to be useful. Cumulative grade-and-tonnage curves [62] provide estimates of the tonnage of the commodity at different quantiles (10th, 50th, and 90th). The weighted mineral potential (mineral potential score multiplied by the weighting index) were used to produce weighted composite and weighted cumulative mineral potential maps [16].

Mineral potential maps and assessment reports for forest regions are archived and can be accessed on the website maintained by Geoscience Australia (http://www.ga.gov.au/about/what-we-do/projects/minerals/concluded/mineral-potential/products).

5.1.3. Qualitative assessment, Woomera Prohibited Area (WPA), South Australia

A qualitative method has been used to assess mineral potential in the Woomera Prohibited Area in South Australia (http://www.ga.gov.au/metadata-gateway/metadata/record/gcat_71239). The main aim of the assessment was to provide advice on multiple land-use issues in the area.

Geologically, WPA is located in the Gawler Craton/Region that is known to host several uranium deposits and occurrences belonging to a number of significant deposit types of uranium such as, uranium-bearing iron-oxide copper-gold (the world-class Olympic Dam deposit is located in close proximity to the area), unconformity-related uranium, sandstone-hosted uranium, and calcrete-hosted uranium deposits.

The method followed four steps outlined in the introduction to section 5. The assessment of unconformity-related uranium deposits illustrates the method (Fig. 7). At this stage no unconformity-related uranium deposits have been reported in the Gawler Region (including WPA).

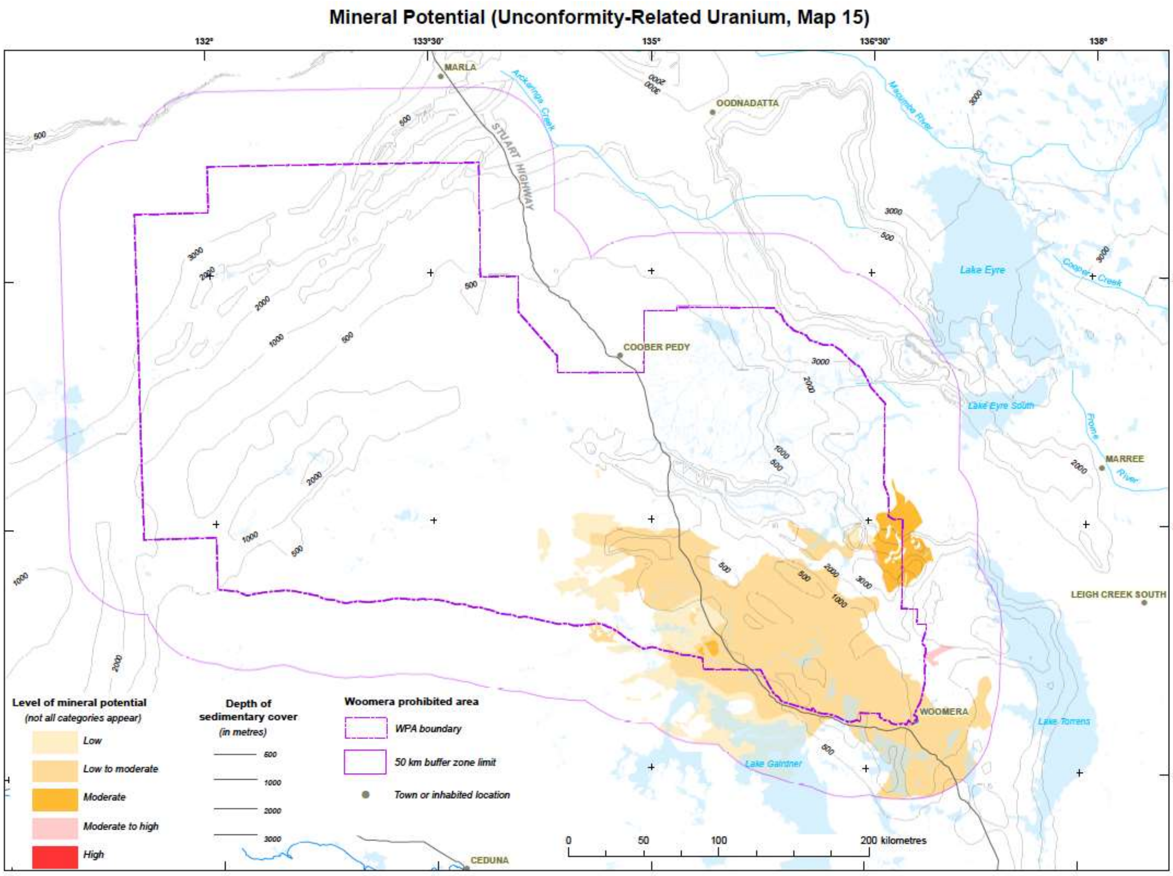

FIG. 7. Mineral potential map of unconformity-related uranium deposits in the Woomera Prohibited Area, Australia. An example of qualitative method of mineral potential assessment (see text for discussion).

Major deposits and prospects in WPA: There are no known deposits of this type in the WPA.

Assessment Criteria (critical geological features): No unconformity-related deposits or prospects have yet been found in the WPA. However, geological similarities to the Gawler Craton and the Pine Creek Inlier (hosting large uranium deposits of this type; for, example, Jabiluka and Ranger in the latter) are of great interest for exploration companies prospecting for uranium deposits of this type. The main assessment criteria for this type of deposits are:

- Unconformity between Archean and/ or Paleo-proterozoic and younger preferably Proterozoic rocks;
- A thick (at least 5–7 km) sequence of highly permeable siliciclastic sandstone formed preferably in fluvial conditions above the unconformity;
- Rocks with reductants (graphite, Fe+2-bearing silicates) below the unconformity;
- Major structures as pathways of fluid and/or as traps.

Assessment: The presence of a regional unconformity between rocks of the Pandurra Formation (Meso-proterozoic age) and older rocks of Paleo-proterozoic age is revealed by geological studies. Deposited within the Cariewerloo Basin is the Pandurra Formation, which is a thick series of flat-lying, arenaceous redbed sedimentary rocks [64]. A similar regional unconformity has been mapped between the Paleo-proterozoic rocks and the overlying fluvial to moderately deep marine sedimentary rocks of the Corunna Conglomerate (Meso-proterozoic age) [65]. Volcanic rocks of the McGregor Volcanics and coarse-grained sedimentary rocks of the Moonabie Formation are unconformably overlain by the Corunna Conglomerate [65]. Another prospective series of rocks belongs to the Blue Range Beds (coarse-grained sandstone and shale) of the Itiledoo Basin. This thick series (up to 2,500 m) was deposited in braided stream-alluvial fan environment. The Paleo-proterozoic sediments of the Hutchison Group are unconformably overlain by basal sedimentary rocks. The Blue Range Beds are located outside WPA.

In many areas with world-class unconformity-related uranium deposits such as the Pine Creek Orogen in Australia, the series of rocks overlying the unconformity is often eroded exposing mineralization hosted in the basement rocks. Most known deposits in the Pine Creek area are situated within 40–50 km of the present-day margin of the basin wherein the sandstone series was deposited. In the Gawler Craton, the Cariewerloo Basin, which has been filled by the sediments of the Pandurra Formation, was more extensive than its present-day boundary. Therefore, a buffer of 40 km around the mapped boundary of the Pandurra Formation was represented for the assessment of the potential of deposits, which might have been formed in the basement rock but from which the cover of the Pandurra Formation has been eroded.

The Hutchison Group comprises most favorable basement rocks, which are composed of various types of schists locally containing graphite and graphitic schists. Thus, areas with the Hutchison Group overlain by the Pandurra Formation is considered to have moderate to high potential with C (moderate) level of certainty. The laminated carbonaceous and pyritic siltstone and shale in the Tarcoola Formation can also serve as good reductants. Thus, areas underlain by the Tarcoola Formation are considered to have moderate potential with a moderate certainty (level C). Although not as effective as carbonaceous material or graphite, the Fe^{+2}-bearing silicates in the lower member of the Gawler Range Volcanics and Lake Harris Komatiites can also provide effective reductants. These rocks are considered to have low to moderate potential with moderate certainty (level C). Silicate reductants are also present in the rocks of the Broadview Schist, Wandearah Formation and the Wallaroo Group. These rocks, which are located within the 40-km buffer around the Pandurra Formation, were considered to have low potential with low certainty (level B).

For many rock-units, geological information is not sufficient to judge the presence of effective reductants in them. Their potential is considered as unknown. Mineral potential of all rock units within the 40-km buffer zone around the Pandurra Formation was reduced by one level relative to the level of potential of the same units in areas underlain by the Pandurra Formation because of uncertainty in the estimate of its original extent.

5.1.4. National-scale assessment of mineral potential of Australia

Qualitative assessments can be carried out at scales varying from national-scale to more detailed district- or deposit-scale. A good example of a national-scale assessment is the mineral potential assessment conducted by a team in Geoscience Australia (http://www.australianminesatlas.gov.au/build/common/minpot.html). The main objective of the assessment was to create a national-scale mineral potential dataset that was equivalent to other national-scale datasets such as, bioregions, forest-types, and the wilderness index, and that was useful for policy advice on national-scale land-use issues. The methodology and results of the assessment are summarized in a GIS package (Ozpot GIS). In this methodology, mineral potential has been assessed for individual geological provinces delineated on a map of

Australian geological provinces. Mineral potential assessment was carried out for 17 significant deposit types of gold, base metals and uranium.

An assessment matrix (Table 6) summarizes regional-scale critical features of deposit types. Mineral potential was assessed by recording presence or absence of critical features in a geological province. Geological information is tabulated in assessment sheets (Table 7). Levels of certainty reflect the reliability of geological information available to assess the presence or absence of critical features of a deposit type in a geological province. Certainty level is high if the critical features can be identified using available geological information. It is low if the information suggests that the presence of critical features is unlikely. It is of intermediate level if the available information is such that it indicates that the critical features are likely to be identified (Table 7).

TABLE 6: ASSESSMENT MATRIX FOR UNCONFORMITY-RELATED URANIUM DEPOSITS

Province potential	Certainty			
Critical elements (assessment criteria)	Identified	Not identified, but likely	Unlikely	Weighting
Setting				
• Intra-cratonic basin; • A basement of Archean domes/inliers flanked by Paleo-proterozoic metasediments; • Flat lying oxidized late Paleo-proterozoic to Meso-proterozoic sandstones in the intra-cratonic basin unconformably overlying the crystalline Archean/Paleo-proterozoic basement.				
Source (fluid, metal, energy)				
Fluids • Oxidized sediments in the basin (source for oxidized fluids); • Archean/Paleo-proterozoic reduced basement (for reduced fluids). Metals • Archean/Paleo-proterozoic igneous and metamorphic				

rocks (the Archean metasediments may have contained detrital uranium in non- oxidizing atmosphere);

- Volcanics in the cover sandstone (for Uranium).

Energy

- Depth of burial in intra-cratonic basin;
- High radioactive decay in granitoids;
- Several phases of igneous intrusives.

Fluid pathway

- Unconformity surface;
- Oxidized permeable sedimentary cover;
- Extensional Faults and breccia zones leading up to and/or cutting the unconformity.

Trap (any of the following)

Structural

- Unconformity surface;
- Breccia zones and faults.

Chemical

- Reduced pelitic rocks below the unconformity;
- Presence of calcareous rocks (pH).

Signs of mineralizing process (any of the following, but if occurrences have been identified the level of certainty increases)

- Alteration extends over 1 km from mineralization and is characterized by
- sericite/chlorite±kaolinite ±hematite;
- sericite/chlorite±kaolinite ±hematite;
- Mg metasomatism and formation of late stage Mg-rich chlorite common;

• Strong desilicification and loss of Na, Ca, Fe^{2+}, Th; • Geochemical anomalies and radiometric anomalies; • Known occurrences of uranium ± gold.	
Age	
• Proterozoic age of mineralization but presence of Archean rocks appears to be important.	
Preservation	
• Presence of unconformity indicates high probability of preservation of unconformity type uranium deposits.	

Mineral potential assessment helped to rank geological provinces in terms of their potential to host mineral deposits of a particular deposit type. The GIS-dataset includes mineral potential and certainty-level maps of 17 deposits types and composite mineral potential (see section 5.1.1 for definition) and certainty-level maps of gold, base metals and uranium. Fig. 8 shows a composite mineral potential map of uranium based on the assessment of three important types of uranium deposits: unconformity-related uranium; sandstone-hosted uranium and iron-oxide copper, gold and uranium.

Kreuzer et al. [20] also conducted a national-scale assessment/ranking of geological regions by assessing their potential to host 14 principal deposit types in Australia. The authors used a GIS-based automated prospectivity analysis based on linking mineral systems concept (see for discussion) to a semi-quantitative probabilistic matrix.

TABLE 7. ASSESSMENT SHEET FOR UNCONFORMITY-RELATED DEPOSITS (GRANITES-TANAMI REGION)

Province Granites-Tanami
Potential: 4 Certainty: 3

Critical elements (assessment criteria)	Identified	Not identified, but likely	Unlikely	Weighting
Setting				
• Intra-cratonic basin;		Paleo-proterozoic McFarlane Peak Fm in rift setting; the Birrindudu Group deposited in a large shallow marine shelf.		
• A basement of Archean domes flanked by Paleo-proterozoic metasediments;	Yes; Billabong complex, Browns Range Metamorphics			
• Flat lying oxidized Paleo-proterozoic/Meso-proterozoic sandstones in the intra-cratonic basin unconformably overlying the crystalline Archean/Paleo-proterozoic basement.	Birrindudu Group is about 1.9 km thick; the basal unit (Gardiner Sandstone) of 1 km is mainly lithic arenites and quartz arenites.			
Source (fluid, metal, energy)				
Fluids				
• Oxidized sediments in the basin (source for oxidized fluids);	Basal Gardiner Sandstone of Birrindudu Group range in colour from white and grey to pink, maroon and purple and may have provided an oxidizing environment.			
• Archean/Paleo-proterozoic reduced basement (for reduced fluids).	Billabong complex and Browns Range Metamorphics; the McFarlane Peak Fm has mafic volcanics; the Dead Bullock Fm of the Tanami Gp has carbonaceous siltstone and minor BIF.			
Metals				
• Archean/Paleo-proterozoic igneous and metamorphic rocks (the Archean metasediments may have contained detrital uranium in non- oxidizing atmosphere);	Xenotime in Gardiner Sandstone and anomalous radioactivity along Gardiner Ss/Killi Killi contact for 1350 m.			

• Volcanics in the cover sandstone (For Uranium).			Not in Birrindud u
Energy			
• Considerable depth of burial in intra-cratonic basin;		Birrindudu up to 1900 m, deposited in large shallow marine shelf	
• High radioactive decay in granitoids;		Uranium content not known	
• Several phases of igneous intrusives.	1830-1810 Ma three phases of granitic intrusion and two phases of volcanism; another intrusion of granitic suite during 1800 Ma. No intrusives after deposition of the Birrindudu		
Fluid pathway			
• Unconformity surface;	Yes; Birrindudu/Tanami Group		
• Oxidized permeable sedimentary cover;		Some sediments may be oxidized in Birrindudu	
• Extensional Faults and breccia zones leading up to and/or cutting the unconformity.	The Birrindudu/Tanami group unconformity has been faulted.		
Trap (any of the following)			
Structural			
• Unconformity surface;	Yes	Probably possible	
• Breccia zones and faults.			
Chemical			
• Reduced pelitic rocks below the unconformity;	Yes; carbonaceous siltstones		
• Presence of calcareous rocks (pH).	Yes; carbonaceous siltstones in Tanami Group		
Signs of mineralizing process (any of the following, but if occurrences have been identified the level of certainty increases)			
• Alteration extends over 1km from mineralization and is characterized by:			
• sericite/chlorite±kaolinite±h ematite;		Not recorded	
• sericite/chlorite±kaolinite±h ematite;		Not recorded	

• Mg metasomatism and formation of late stage Mg-rich chlorite common;		Not recorded
• Strong desilicification and loss of Na, Ca, Fe^{2+}, Th;		Not recorded
• geochemical anomalies and radiometric anomalies;	Yes; along the contact	
• Known occurrences of uranium ± gold.	Killi Killi (xenotime in basal 6 m of Gardiner Sandstone), Don (uranium, gold), Mount Junction (uranium, copper in ferruginous chert of Tanami Group) and four other uranium prospects (Hassan, 2000).	
Age		
• Proterozoic age of mineralization but presence of Archean rocks appears to be important.	Archean rocks are present	
Preservation		
• Presence of unconformity indicates high probability of preservation of unconformity type uranium deposits. Preservation for Cigar type unconformity deposits which occur at/above unconformity more important than for Jabiluka, Ranger, Rabbit Lake deposits which are below the unconformity.	Major Birrindudu/Archaean – Paleo-proterozoic basement unconformity present	

5.2. GIS-methods of qualitative assessment of mineral potential

The development of GIS and of relational datasets in the 1980s provided tools suitable for rapid analysis and integration of geospatial information. This triggered emergence of new data- and knowledge-driven methods of mineral potential assessment and prospectivity analysis of geological regions at different scales. A detailed description of these methods and of their mathematical and probabilistic framework can be found in [18] and [23]. It needs to be emphasized that mathematical and probabilistic framework of these methods emerged well before the development of GISs (e.g., [3, 6]. However, GISs help to combine spatial data to make predictions. The analysis and combination is described as spatial modeling and it produces different models based on the probabilistic framework used to combine them. The resulting maps are called favorability or prospectivity maps.

In data-driven methods, model parameters reflecting relationship between geological features and deposits are derived from training datasets (deposits, prospects, occurrences) in an area. These methods include: logistic regression, WofE, and neural network [18]. In knowledge-driven methods, model parameters are largely derived from the knowledge base of experts who define the relationship between geological features and deposits in the description of deposit models. The two most common knowledge-driven methods are fuzzy logic and Dempster-Shafer belief theory [18].

This review presents a very brief summary of each of these methods, firstly because more detailed description of these methods with case studies can be accessed in [18, 23 and 66], and secondly because there are very few case studies focused on the assessment of uranium deposits.

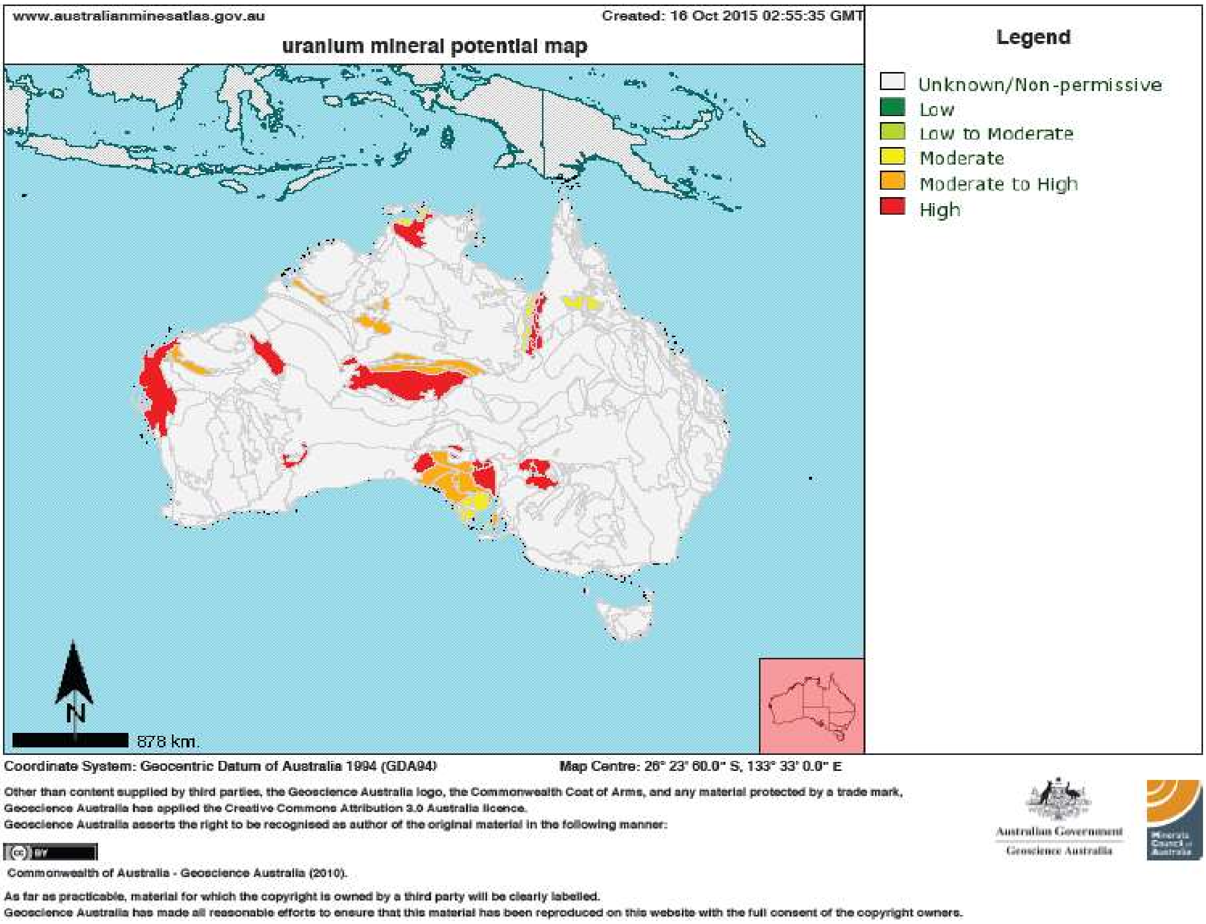

FIG. 8. National-scale uranium mineral potential map of Australia. This a composite mineral potential map derived from the mineral potential assessment of only three types of mineral systems: sandstone-hosted, unconformity-related and iron-oxide copper-gold-uranium. The map generated in October 2015 from datasets available at: http://www.australianminesatlas.gov.au/build/common/minpot.html

5.2.1. Knowledge-driven methods/models

5.2.1.1. Boolean logic

The Boolean logic method of combining spatial datasets for mineral potential assessment is one of the simplest and intuitive methods. The method involves two simple steps: (a) converting geological datasets or maps into binary maps encapsulating: (1) TRUE or (0) FALSE relationship between a geological feature and the presence of a deposit; and (b) combining binary maps by using Boolean operators AND, OR, and NOT.

Bonham-Carter [18] applied this method to assess mineral potential map of gold deposits in the Meguma terrane, southeast Nova Scotia (Canada). A literature search shows that this method has not been used to conduct an assessment of uranium deposits. However, prescriptive guidelines based on critical features of uranium deposits can easily be used to create binary maps. For instance, a geology map of an area can be converted into a number of binary maps for assessing mineral potential of sandstone-hosted deposits. The areas occupied by permeable sands/sandstone will have a value of 1 (TRUE) whereas those where such sandstones are absent will have a value of 0 (FALSE). Similar binary maps can also be produced using the presence of felsic rocks with leachable uranium or by using the presence of rocks containing organic and/or inorganic reductant. The three binary maps can then be combined using Boolean operator AND to produce a map that shows the presence of three features critical for the formation of a sandstone-hosted deposit.

Although the method is simple and practical, its major limitation is its inability to give different weighting (degree of importance) to different assessment criteria and geological features associated with them [18]. For instance, for many uranium deposits the presence of a leachable source of uranium is far more critical than the hydrogeological gradient driving the flow of oxidized waters in the sandstone.

The method is knowledge-driven but in some cases the presence of known deposits and prospects in the study area can assist in refining spatial relationships between geological features and mineral deposits/prospects.

5.2.1.2. Index overlay method

Like the Boolean logic method, this method is also based on the creation of binary maps and combining them to produce a mineral potential or prospectivity map. However, in this method binary maps can be assigned different scores/weightings reflecting the degree of their importance. Often, different classes on the same input map can be given different scores or weightings. For example, the map of leachable source rocks can have a score different from that of a binary map derived from favorable structures. In fact, different classes on the binary map of leachable source rocks can be identified using uranium concentration of felsic rocks and each class can be assigned different scores. The index overlay method allows this type of differentiation and classification.

Thus, the method allows more flexible combination of input binary maps (also known as evidence maps). The scores and weights of maps and classes on maps can be adjusted to reflect the judgment of experts [18]. The scores can be positive integers or real numbers, with no limit on numerical range. However, the range needs to be compatible between maps [18]. One of the main disadvantages of the method according to [18] is its linear additive nature.

5.2.1.3. Fuzzy logic method

The fuzzy logic method has become the most commonly used method for prospectivity analysis and mineral potential assessment. Details of the method and case studies are described by [18, 66 and 67].

In the Boolean logic method, the membership value of 1 in a set (i.e., geological feature indicative of the presence of a mineral deposit) or 0 (i.e., geological feature indicative that a mineral deposit is not present) is fixed. It can only be either 1 (i.e., TRUE) or 0 (i.e., FALSE). In fuzzy logic, the membership in a set is expressed on a continuous scale from 1 (full membership) to 0 (full non-membership). For example, concentrations of uranium in groundwater can be used to define the degree of membership of a set called "uranium anomaly". Very high values (above a particular threshold) of uranium can be given a fuzzy membership of 1 and very low values (below a particular threshold) can be given a fuzzy membership of 0. Values lying between the two thresholds are given fuzzy membership values varying between 0 and 1.

Using the same approach, other geoscientific datasets can be used to create a number of input maps/datasets with fuzzy membership values. These maps are then combined by using a variety of combination rules and operators [68], [69]. The five most commonly used fuzzy operators are fuzzy AND, fuzzy OR, fuzzy algebraic sum, fuzzy algebraic product and fuzzy gamma [18]. A combined map shows areas with combined fuzzy membership scores, which are proxies of the prospectivity/favorability of an area to host a mineral deposit.

The effectiveness of different fuzzy operators has been discussed in many works (e.g., [18, 66, 67]. In practice, evidence maps with fuzzy membership values are combined in a series of steps, commonly depicted as an inference network. The inference network shows the workflow and logic of combining different maps [18]. A fuzzy inference system for prospectivity modeling of calcrete-uranium mineral system is described by [70]. Prospectivity map of calcrete uranium deposits in the Yilgarn Craton, Australia produced by this study is shown in Fig. 9.

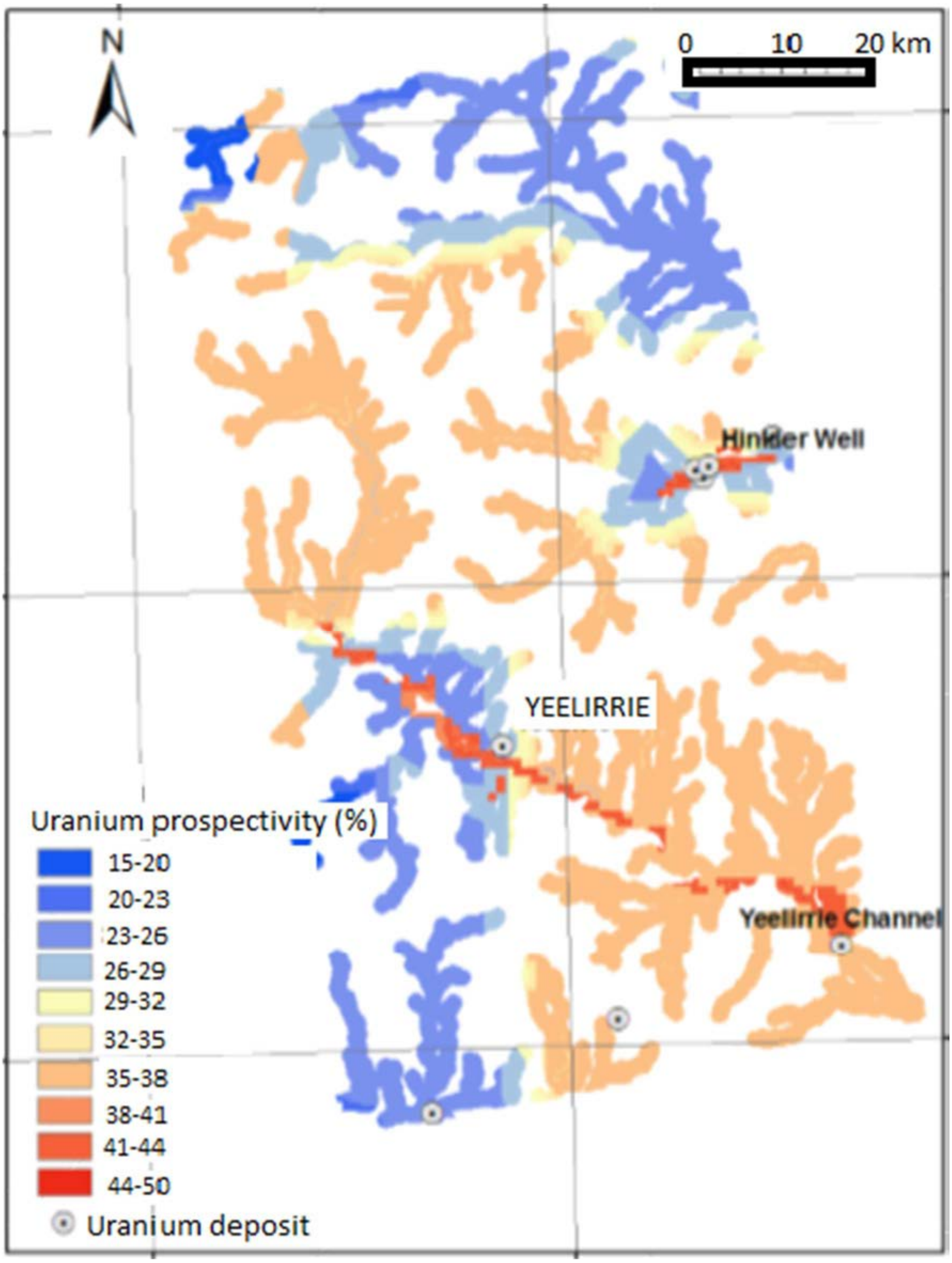

FIG. 9. Prospectivity map of calcrete-uranium deposits in the Yilgarn Craton, derived by using fuzzy-logic or fuzzy-inference system. Map was modified from [70].

5.2.1.4. Mineral potential mapping of magmatic-related uranium mineral systems in Australia using fuzzy logic method

A mineral potential assessment of magmatic-related uranium mineral systems in Australia was conducted by [71]. Geoscience Australia's Ozchem database was one of the major datasets used in the assessment. The national-scale database contains geochemical analysis of rocks. The assessment was carried out for both intrusive- and volcanic-related uranium mineral systems. This section summarizes assessment for intrusive-related uranium systems only. The assessment method used a number of geochemical assessment criteria identifiable in the database. For each assessment criterion, appropriate geochemical indicators were identified and used to assign fuzzy membership values. The list of important assessment criteria and their geochemical indicators were:

- Intrusive composition (ultramafic to mafic; intermediate to mafic; intermediate; mixed (felsic to mafic); felsic to intermediate; felsic; unknown);
- Magmatic affinity (agapaitic index based on the assumption that peralkaline rocks are more favorable);
- Type of felsic magma (a-, i-, and s-type);
- Degree of fractional crystallization (rb/sr ratio and concentration of f, u and other high field strength elements such as zr, nb, and y);
- High uranium radiometric anomalies (u^2/th ratio derived from radiometric map of australia.

Fuzzy membership values of each of the input layers were combined using several fuzzy operators shown on the inference network (Fig. 10). Prospectivity maps not only matched regions with proven prospectivity (areas with known uranium mineralization) but also identified several new prospective areas, one of which is shown in Fig. 11.

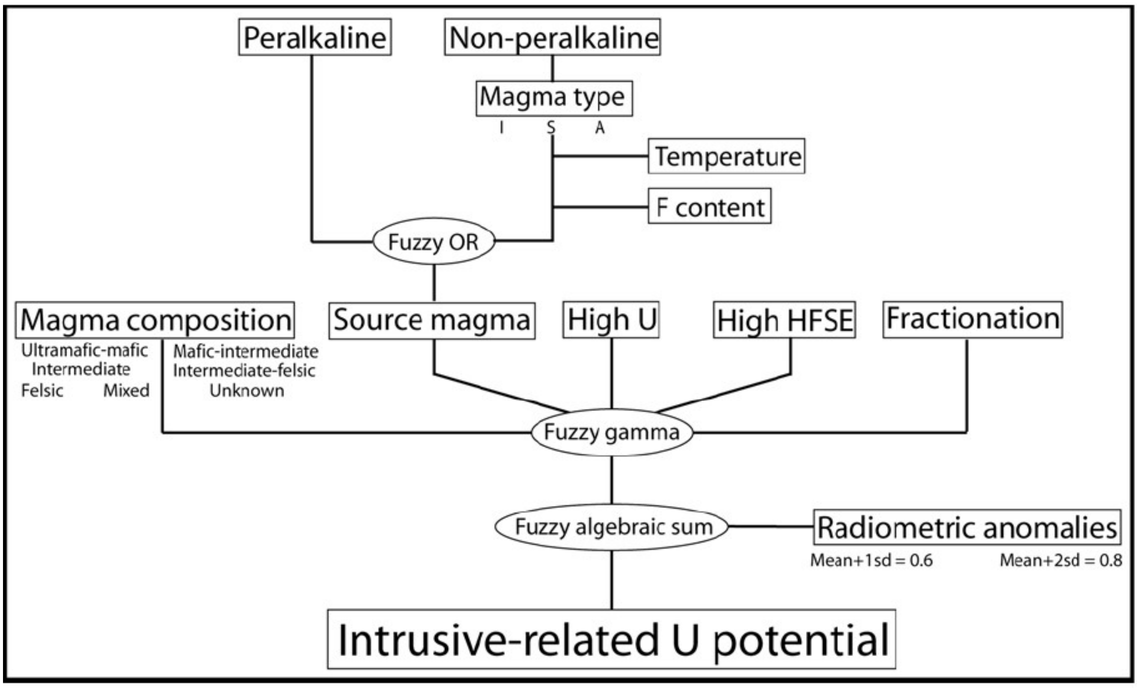

FIG. 10. Fuzzy-inference network used to model mineral potential of intrusive-related uranium deposits in Australia [72]. Figure is © Commonwealth of Australia (Geoscience Australia) 2017; it is released under the Creative Commons Attribution 4.0 International Licence. http://creativecommons.org/licenses/by/4.0/legalcode.

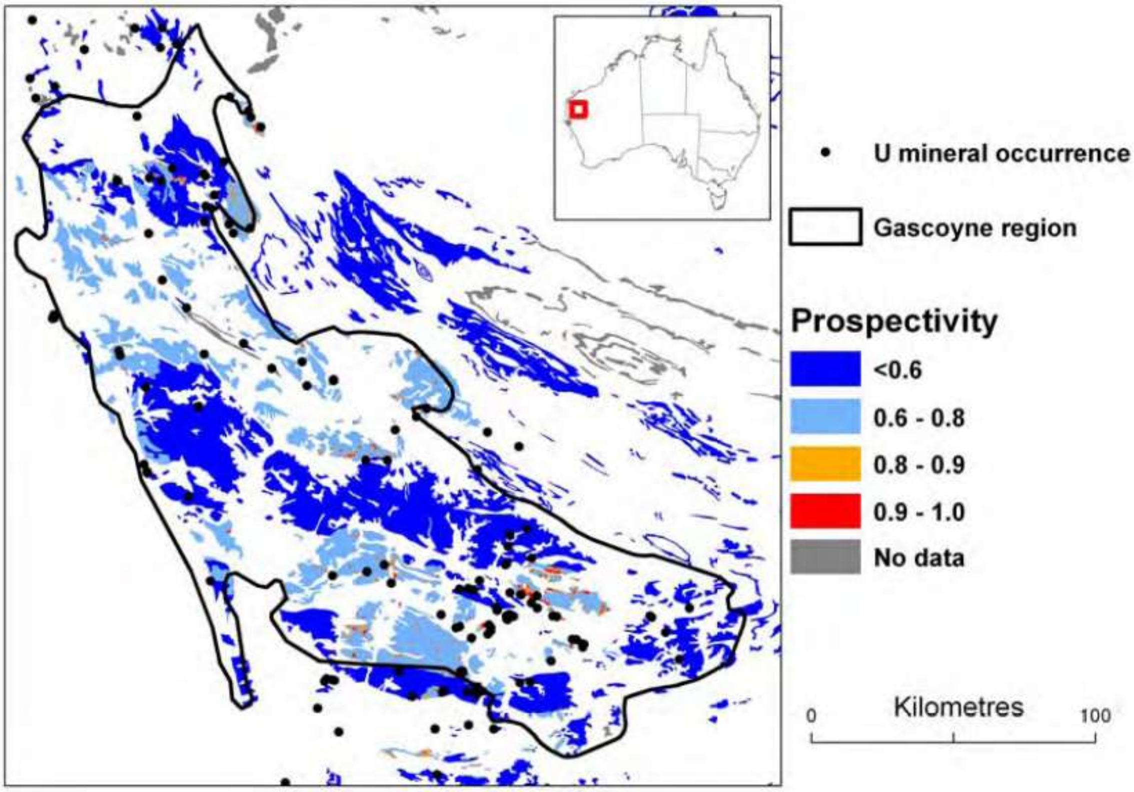

FIG. 11. Prospectivity map of intrusive-related uranium deposits in the Gascoyne Provinces, Western Australia, Australia. Map was produced using fuzzy-logic method and fuzzy-inference network shown in Fig. 9 [72]. Figure is © Commonwealth of Australia (Geoscience Australia) 2017; it is released under the Creative Commons Attribution 4.0 International Licence. http://creativecommons.org/licenses/by/4.0/legalcode.

5.2.1.5. Dempster-Shafer method

This knowledge-driven method uses the idea of belief functions and the Dempster-Shafer rule of combining map evidence [23, 73, 74]. One of the main advantages of the method is that it allows representation of uncertainty. The uncertainty is represented by the interval between the value of support function (lower belief function or a conservative estimate of a proposition) and the value of plausibility function (an optimistic assessment that the evidence supports a proposition). The interval can be considered as a confidence band.

Whereas in the fuzzy logic method fuzzy membership values are assigned to map classes, in the Dempster-Shafer method each class on a map is assigned a pair of belief functions: support and plausibility. The uncertainty is calculated from these two functions and is represented by the difference between the values of plausibility and support functions. The fourth, disbelief, function is obtained from the value of plausibility function, and is denoted by 1- (value of plausibility function). Hence, the sum of the three values (support, uncertainty and disbelief functions) is 1 [75]. Another important advantage of the method is its ability to deal with areas on maps with no data. Missing data can be defined to have the plausibility function value of 1 and the support function value of 0.

Like fuzzy membership values in the fuzzy logic method, the values of belief function are usually estimated and assigned subjectively by experts. Maps with assigned values of belief functions for map classes are combined by a model described by [76]. The combination model is able to produce three different maps, one each for support, plausibility and uncertainty values [75]. A relatively recent description of the method can be found in [75], which summarizes results of mineral potential mapping of porphyry copper deposits in Iran (Figs. 12 and 13).

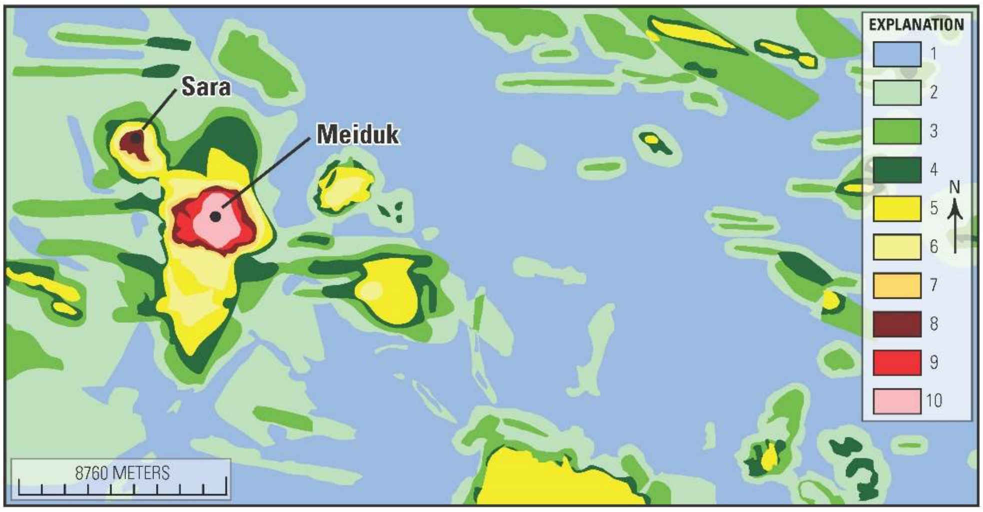

FIG. 12. Plausibility (prospectivity) map of porphyry copper deposits in the north of Shahr-e-Babak, derived by using Dempster-Shafer belief system. The legend shows increasing levels of plausibility (prospectivity). The map was modified from [75].

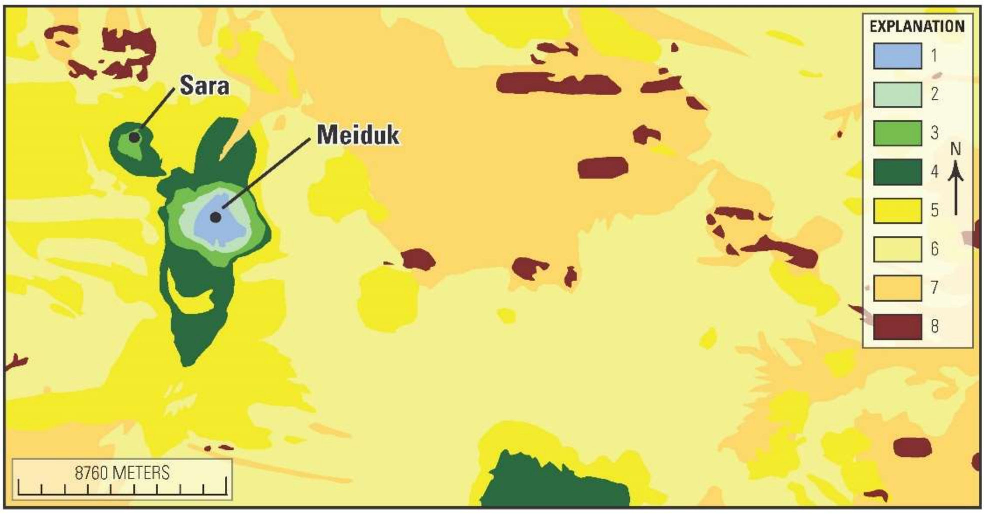

FIG. 13. Uncertainty map of prospectivity for porphyry copper deposits in the north of Shahr-e-Babak, derived by using Dempster-Shafer belief system. The legend shows increasing levels of uncertainty. The map was modified from [75].

5.2.1.6. PROSPECTOR system

PROSPECTOR is the name of a computer software program that captured and imitated the decision process of expert geologist to assess the prospectivity of an area [3]. It was originally developed by Stanford Research Institute International [77] and was later modified and expanded at the US Geological Survey [78]. The system was defined by a set of rules that guided geologists through a series of questions, answers to which led to a decision about the relative chances of finding an undiscovered deposit of a particular type [23]. The set of rules formed an inference network.

The general inference rule used by the system has a form:

If E, then H (to degree LS, LN)

The statement is read as, "the observed evidence E suggest the assertion H (hypothesis)". The two parameters, LS (sufficiency measure) and LN (necessity measure) represent the 'strength' of the rule. They define the way the probability of H is to be updated given the existence of evidence E. If for an inference rule, LS is large, it means that the evidence E is encouraging for the hypothesis H. Similarly, if LN for the rule is much less than unity, the known absence of evidence E diminishes the chance of H happening [23].

The PROSPECTOR system has been used to create a regional-scale mineral potential assessment model of Western States Sandstone Uranium (RWSSU; [79]. Examples of inference network of the model for sandstone-hosted uranium can be found in [3, 23]. The model was tested by a team of geologists and results of testing are summarized in [3].

5.2.2. Data-driven methods/models

5.2.2.1. Weights-of-Evidence (WofE)

The WofE method utilizes a log-linear form of Bayesian model to the problem of combining datasets [18]. The main concept behind the Bayesian approach is the notion of prior and posterior probability. The mathematical and probabilistic framework of the method is described among many others by [18, 80, 81 and 82]. A number of interesting examples of this method can also be found in these works.

In prospectivity analysis, mineral deposits are considered as small area objects within a small unit cell (often 1 km × 1 km) and are treated as binary (either present or absent). An estimate of the prior probability of deposits in an area can be obtained by counting number of known deposits of that type in the area. The method can be illustrated by a hypothetical example. Let us suppose that the study area of 10,000 km^2 is known to contain 50 deposits of sandstone-hosted uranium. The prior probability of uranium deposits in the study area will be equal to 50/10000 (i.e., 0.005). This prior probability can be updated by calculating the effect of geological evidence provides by spatial relationship between known deposits in the area and geological features. The influence of the evidence is estimated from maps or datasets available in the area. However, most multi-scale maps (e.g., geological maps with several different geological rock types) have to be converted into binary maps, i.e., maps showing positive and negative patterns or relationships with the known deposits. For example, the maps can be reclassified into two types of areas: areas occupied by carbonaceous sandstones (positive pattern) and areas where the sandstones are absent (negative pattern).

The influence of the evidence in this binary map on the prior probability can be estimated by counting number of uranium deposits located within areas of positive pattern (areas containing sandstones). Let us assume that 48 known deposits are hosted in areas occupied by sandstones. The influence of the evidence is estimated in the form of conditional or posterior probability, which represents prior probability multiplied by a factor that measures the influence. The multiplying factor can be calculated from two ratios: A = (number of deposits on a positive pattern)/(number of deposits in the whole study area); and B = (size in km^2 of the positive pattern)/(size in km^2 of the whole study area).

In the above example, the ratio A is 48/50 (i.e., 0.96) and the ratio B is 5000/10000 (i.e., 0.5). Hence, the multiplying factor is (0.96/0.5), i.e., 1.92. The resulting posterior probability is equal to 0.005 (prior probability) $\times$ 1.92 (multiplying factor), or 0.0096. Thus, as a result of the influence of one binary evidence map, the posterior probability in one part of the study area (i.e., occupied by sandstones) has increased from 0.005 to 0.0096 (i.e., 1.92 times), whereas the posterior probability in the rest of the study area (i.e., areas not occupied by sandstones) decreased from 0.005 to 0.0004.

Thus, the WofE method involves estimating posterior probabilities conditional to evidence provided by a number of different geological datasets and combining them to estimate a map of combined posterior probabilities. The method also estimates natural logarithm of odds (logits), likelihood ratios (sufficiency and likelihood), and positive (W+) and negative (W-) weights-of-evidence [18].

One of the basic assumptions of the Bayesian approach when combining two or more maps is that there exists conditional independence (CI) between them [18]. In practice, this condition is always violated to some extent because geological datasets and binary maps produced from them are often inter-dependent. Hence, there is a need to assess and mitigate the effects of violation of CI. This is the reason why positive and negative weights (W+ and W-) for each layer are also calculated. These weights are checked with statistical tests to show the magnitude of violation and to identify binary maps contributing to it [18].

Bonham-Carter [18] outlines following steps in applying the WofE method:

— Select a series of maps that are likely to provide useful evidence for predicting mineral deposits. This information can derive from descriptive and/or conceptual models of that deposits type. For example, for calcrete-uranium deposits these maps may include a map of calcretes in an area; a map showing paleo-channels and a map showing U^2/Th ratio derived from radiometric surveys;
— If a map is multi-class (such as a geological map showing distribution of various rock types), convert the multi-class map into a binary map showing spatial association between the deposit points a specific geological feature on the map;
— Check that CI exists between the binary maps. The check is made between pairs of maps and if there is a problem of violation of CI, the problematic map is either deleted or the maps are combined to produce a new binary map;
— Combine binary maps with their weights. The combination can be carried out either with a modeling language internal to GIS (as e.g., in ArcSDM available for download at http://www.ige.unicamp.br/sdm/), or with an external modeling program;
— Produce a combined posterior probability map. Some modeling packages allow calculations of the effects of uncertainty in the weights, and uncertainty due to missing

information. This provides information to generate an uncertainty map.

Although there are several examples of the application of this method for mineral potential mapping and prospectivity analysis for several different deposit types and commodities, the method has yet to be applied for the assessment of uranium deposits. Bonham-Carter [18] presents a detailed description of a case study focused on the prospectivity analysis of gold deposits in Nova Scotia, Canada. A more relatively recent case study is summarized by [83]. In this study, WofE method was employed to map prospectivity of nickel sulfide deposits in the Yilgarn Craton (Fig. 14).

5.2.2.2. Logistic regressions

Regression is a mathematic tool that allows analysis of the relationship between mineral deposits (dependent variable) and geological features (independent variable). In the past 20 to 30 years, a number of regression models have been developed and applied to assess prospectivity of mineral deposits (e.g., [84–89]. The popularity of logistic regression over linear and other methods of regression can be explained by a number of distinct advantages of logistic regression. One such advantage is that it allows estimation of probabilities within the unit interval of zero and one. The dependent variable in mineral potential modeling is mineral deposit occurrence, which can have only two categories or values (dichotomous variable), 1 (present) and 0 (absent). However, the independent variables (geological features on maps) can be a mixture of dichotomous (variables which can have only two categories), nominal (variables with more than two categories), and/or ratio variables [89]. Logistic regression permits mathematical analysis of relationships between different types of variables but treating them as a non-linear function.

Agterberg [90] and Agterberg et al. [91] have demonstrated that the results of weighted logistic regression are similar to those obtained from WofE method. This overcomes a major limitation of the WofE method, which requires adherence to the assumption of CI [89].

In general, the method involves the following steps (as illustrated by [89]: (a) identification of positive geological features in an area (geological features showing positive relationship with known mineral deposits; (b) quantification of spatial relationship for input into the logistic regression model; (c) forced and backward stepwise regression modeling (see [89] for details); and (d) preparation of probability maps (forced regression, backward stepwise regression) and binary favorability maps (derived from probability maps).

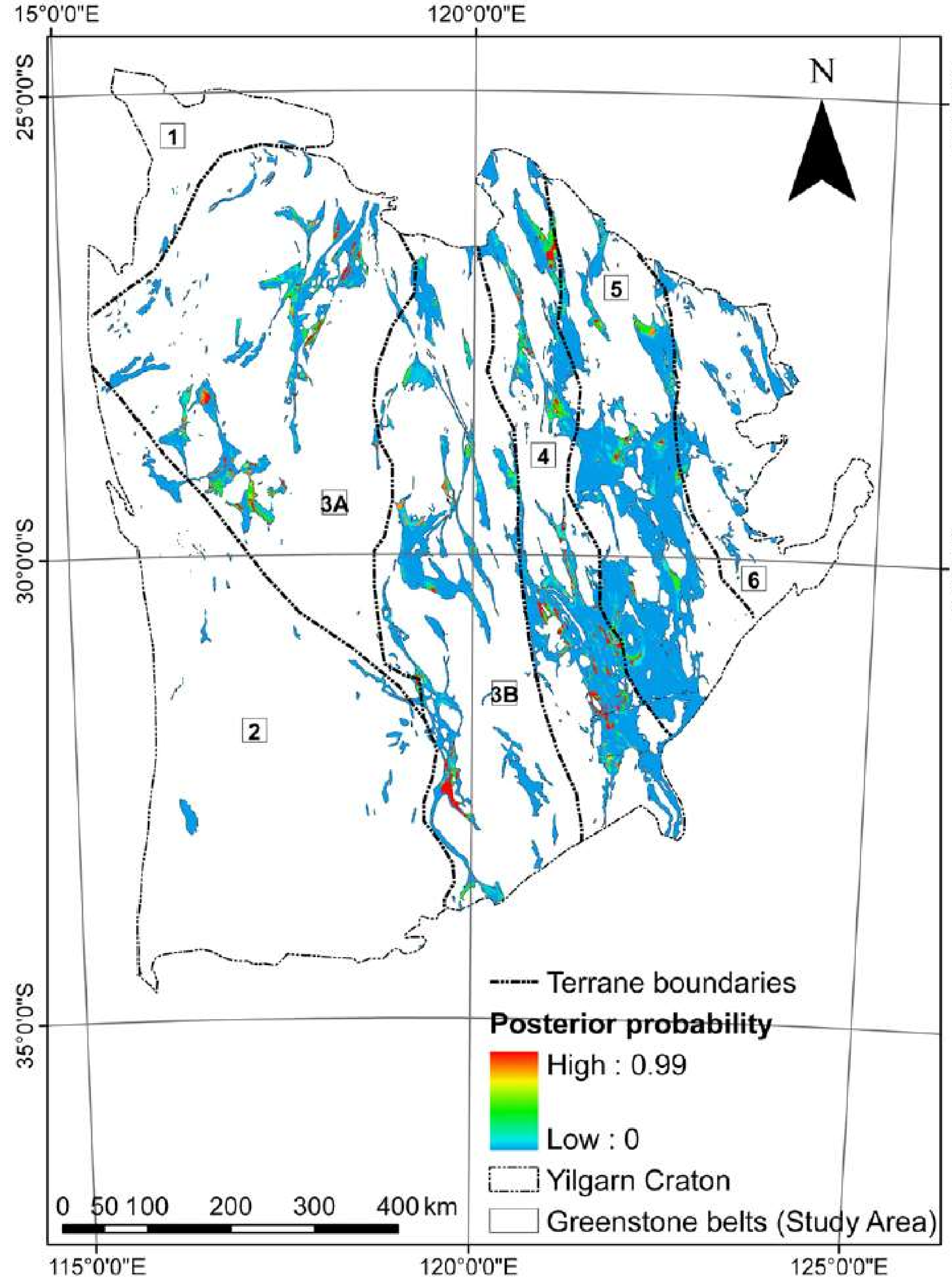

FIG. 14. Prospectivity map of nickel sulphide deposits in the Yilgarn Craton, Australia. Map was produced by WofE method [83].

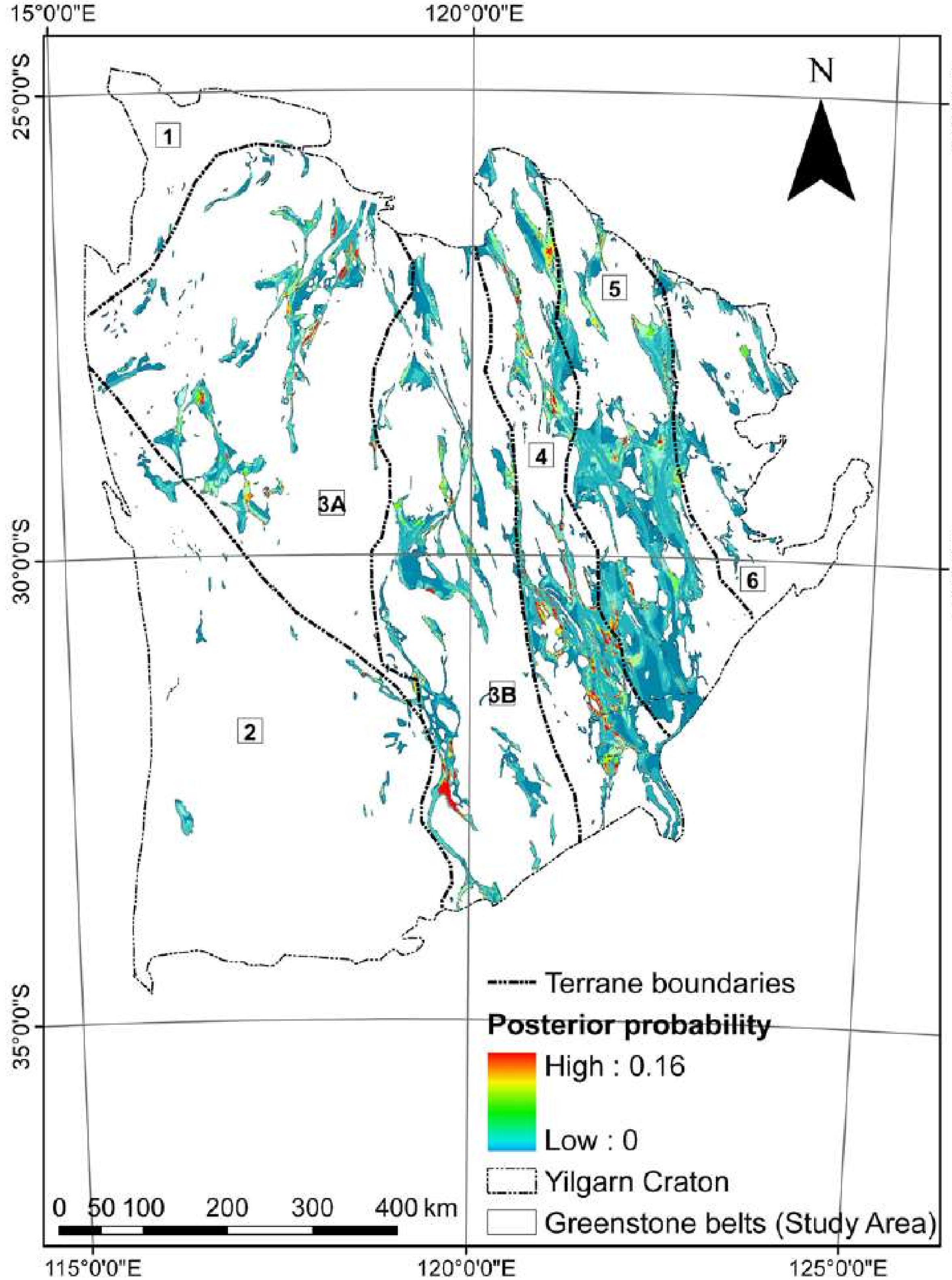

FIG. 15. Prospectivity map of nickel sulphide deposits in the Yilgarn Craton, Australia (the same study area as in Fig. 14). Map was produced by logistic regression modeling [83].

A detailed description of the method and of output maps can be found in [89] focused on the mineral potential modeling of epithermal gold deposits in the Baguio district, Philippines. Porwal et al. [83] have applied this method to produce a prospectivity map of nickel sulfide deposits in the Yilgarn Craton (Fig. 15). A comparison of this map with the map produced by using the WofE method for the same area provides a good analysis of the usefulness of the two methods. Although two methods generally delineate similar areas of prospectivity, there are some notable differences in a number of terranes (Figs. 14 and 15).

5.2.2.3. Artificial neural network

Artificial neural networks (ANNs) represent a type of adaptive computing system that can learn from the data [92]. In this way, they are based on machine-learning acquired from training on the known deposits of assessed type present in the study area. Brown et al. [92] underlined a number of special features of ANNs, which include their ability to: (a) extract patterns in a dataset otherwise imperceptible to standard statistical techniques; (b) operate without a-priori knowledge (e.g., deposit-type models); (c) function at acceptable accuracy when the data are noisy or contain outliers; (d) perform well when the input parameters are inter-dependent and exhibit significant non-linearity; (e) be flexible and retrained when new data become available; and (f) be used on large mixed datasets.

ANNs have been used to solve geological problems associated with prediction and classification. Singer and Kouda [93] used a three-layer feed-forward neural network to predict/estimate distances to the nearest Kuroko-type volcanic-hosted massive sulfide deposits. The same predictive capability of ANN is used for mineral potential modeling and prospectivity analysis (e.g., [92, 94–99]. Singer and Kouda [100, 101] explored the classificatory capability of probabilistic neural network when they used it to classify mineral deposits into types based on mineralogy and their grade and tonnage data.

The method of feed-forward ANN for prospectivity mapping has been described in a number of papers [92], [95–100]. In general, the method involves the following steps:

Creation of evidential maps or GIS thematic layers (in raster format) using geological recognition criteria (critical features) of a deposit type assessed in the area. Often, this also involves data encoding (one-of-n) to simplify complex datasets.

Generation of vectors (feature, training and validation) for input into neural network. Feature vectors are generated by combining GIS thematic layers which also includes the mineral deposit layer (Fig. 16). In order to create training and validation vectors, the deposit dataset is randomly divided into training and validation sets. In some studies, they are divided into three sets: (1) training dataset, used to train the network and to learn the network weights; (2) training-stop set, used in a cross-validation procedure with early stopping in order to avoid over-fitting the data; and (3) the test set which does not play role in training but is used as a guide to the ability of the trained network to generalize when new data are processed [95].

Network training/learning and processing. Neural network of selected architecture (defined by number of input, hidden and output layers) is used for learning/training the network (Fig. 17). Learning is achieved by adjusting the connection of weights while a set of training examples is processed iteratively. The difference between the expected output and the output generated by the network represents an error, which is minimized iteratively. This process of learning progresses by applying a learning algorithm, which iteratively adjusts the weight values to achieve error minimization (Fig. 18).

Production of mineral prospectivity maps showing neural network values as a measure of prospectivity (Fig. 19). It is instructive to compare this map (Fig. 19) with the prospectivity map of the same area using WofE method (Fig. 20). The maps show that the two methods produce largely similar results but neural network produce a map with slightly better resolution [92].

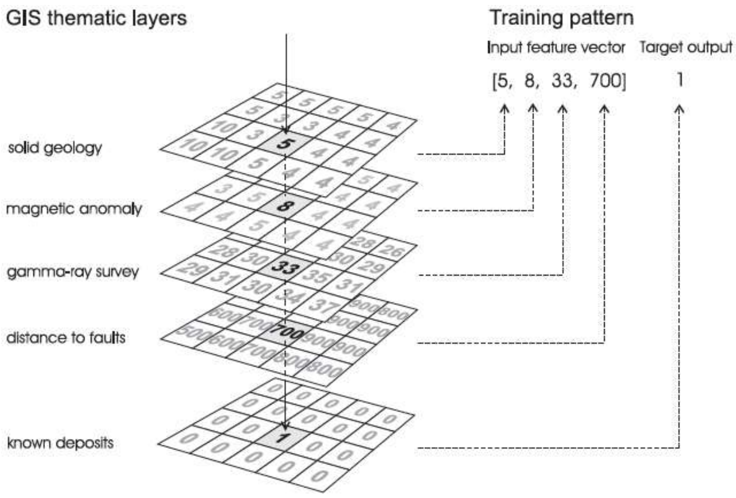

FIG. 16. Schematic diagram showing generation of feature vectors by combining raster datasets (thematic layers). These feature vectors are uses as input to the neural network. Each pattern in the dataset used to train the network consists of an input feature vector paired with the desired output (i.e., 1: the value indicating the presence of a deposits and 0: indicating the absence of a deposit, [92]. Figure is reproduced with permission from the copyright owner Geological Society of Australia.

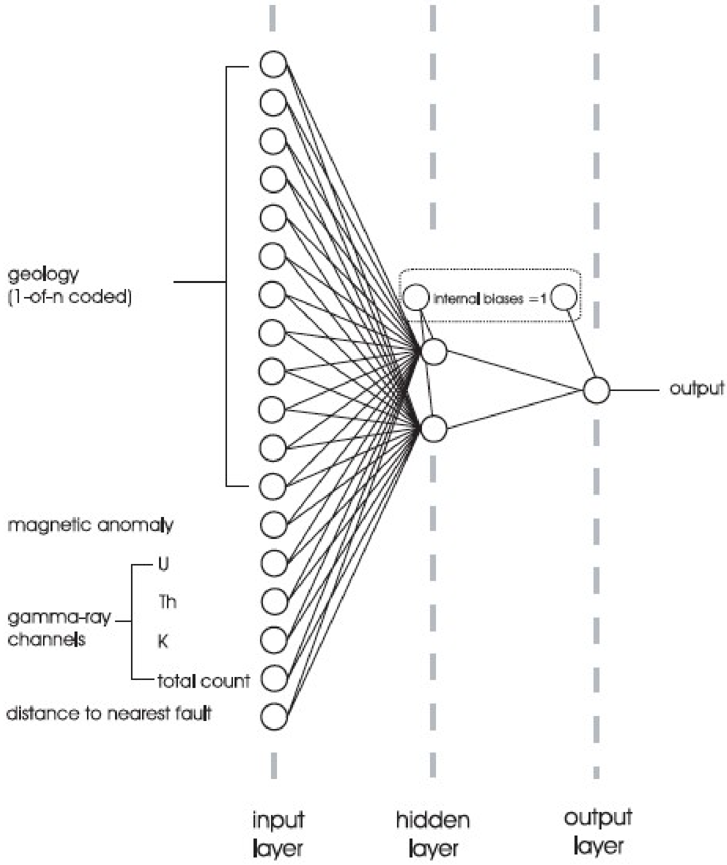

FIG. 17. Schematic diagram showing architecture of the multilayer neural network used in the study [92]. The network has an 18-2-1 topology (where the numbers refer to input, hidden and output layers, respectively). Each layer consists of units connected by links that are associated with a weight. Figure is reproduced with permission from the copyright owner Geological Society of Australia.

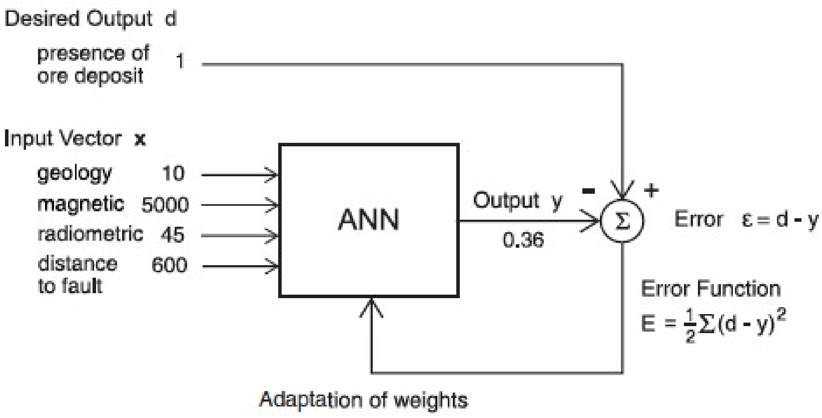

FIG. 18. Block diagram showing the training process in a multilayer neural network. The difference between actual output (y) produced by the network in response to response to an input vector and desired output (d), supplied as part of the training data, represents the network error. The error back-propagation algorithm is used to iteratively modify the connection of weights in order to minimize the network error function [92]. Figure is reproduced with permission from the copyright owner Geological Society of Australia.

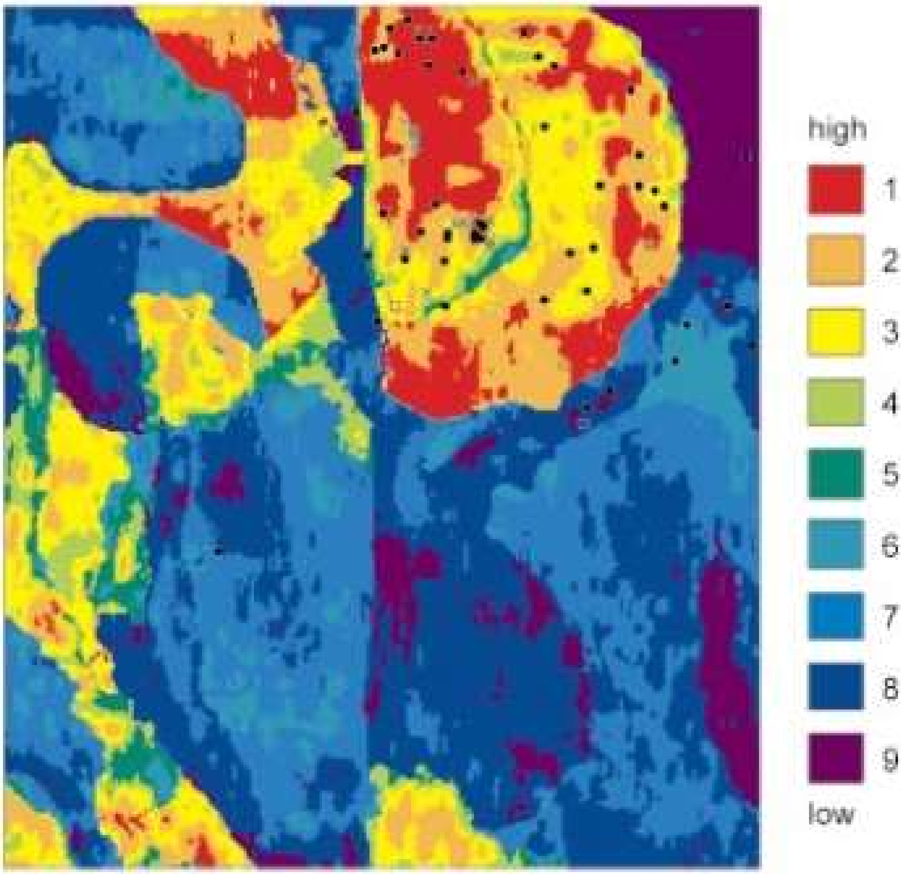

FIG. 19. Prospectivity map for the Tenterfield 1: 100,000 area. Map is produced by neural network method; x, primary gold deposits and occurrences; dark filled circles show alluvial gold deposits and occurrences; blank squares represent undifferentiated gold deposits and occurrences [92]. Figure is reproduced with permission from the copyright owner Geological Society of Australia.

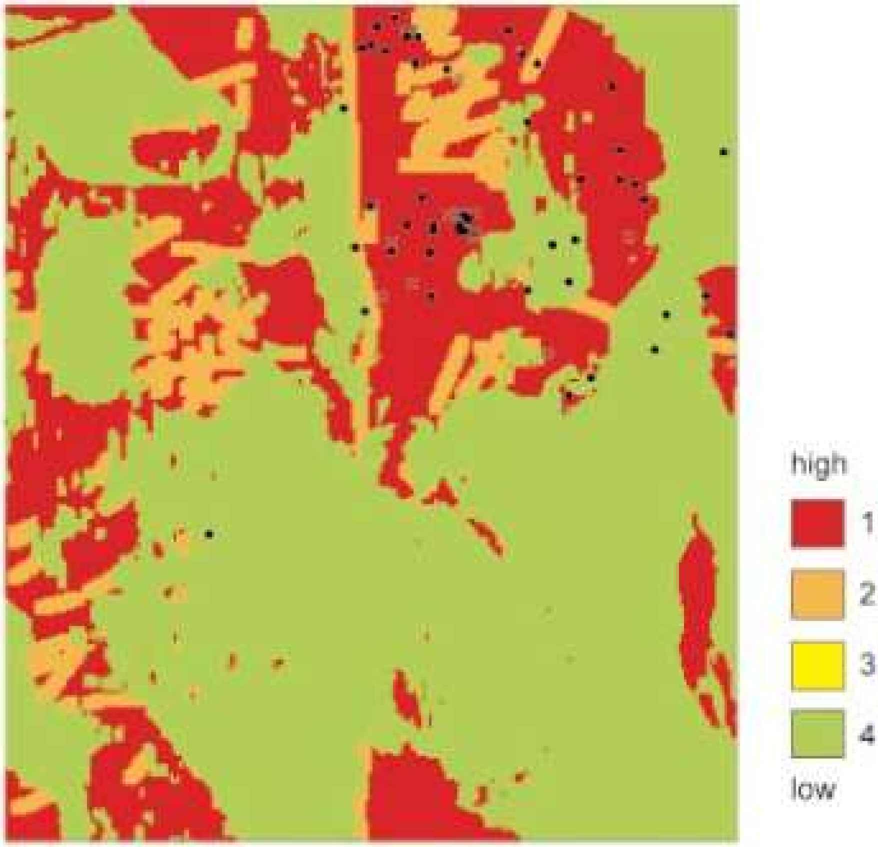

FIG. 20. Prospectivity map for the Tenterfield 1: 100 000 area. Map is produced by WofE method; x, primary gold deposits and occurrences; dark filled circles show alluvial gold deposits and occurrences; blank squares represent undifferentiated gold deposits and occurrences [92]. Figure is reproduced with permission from the copyright owner Geological Society of Australia.

Singer and Kouda [93] used a three-layer feed-forward network to estimate distances to the nearest Kuroko-type volcanic-hosted massive sulfide deposit. They also compared the performance of probabilistic neural network with that of the WofE method and found that the neural network was more effective in classifying locations of mineral deposit and mineral non-deposits for an ore district in Manitoba, Canada [94]. Brown et al. [92] used feed-forward neural network to undertake prospectivity analysis of gold deposits in the Tenterfield area, Australia. They compared results of neural network and fuzzy-logic method and found the results showed a close match. The maps from the two methods were broadly similar to those obtained from the WofE method. Porwal et al. [96] have applied an ANN to model mineral potential of base-metal sulfide deposits in the Aravalli Province, India (2003). Results of prospectivity modeling of gold-silver deposits in the Tabaeksan district, Korea can be found in a paper by [98]. Wang et al. [99] have used 3D modeling and nonlinear methods (fractal, multifractal and probabilistic neural network) for regional-scale mineral potential mapping and quantitative assessment of porphyry, skarn-type molybdenum deposits and hydrothermal vein-type poly-metallic deposit in Luanchuan region, China. A back-propagation ANN was employed by [97] to conduct mineral potential mapping of gold deposits in the Rodalquilar goldfield, Spain. All these studies contain detailed description of the method and prospectivity maps resulting from these studies.

By its nature, neural network methods represent a data-driven or empirical approach [95]. Therefore, they are more applicable in data-rich or brownfield areas. Knowledge-driven fuzzy-logic method, on the other hand, is useful in areas where deposits of the type assessed are not present. In recent years, hybrid methods such fuzzy-WofE and fuzzy-neural network have been developed. These methods enable combination of conceptual and empirical approaches. A fuzzy-neural network hybrid system has been described by [95], in which fuzzy membership layers are used as input layers in the neural network (Fig. 21). The system has been used to model prospectivity of orogenic lode gold deposits in the Kalgoorlie Terrane, Australia (Fig. 22).

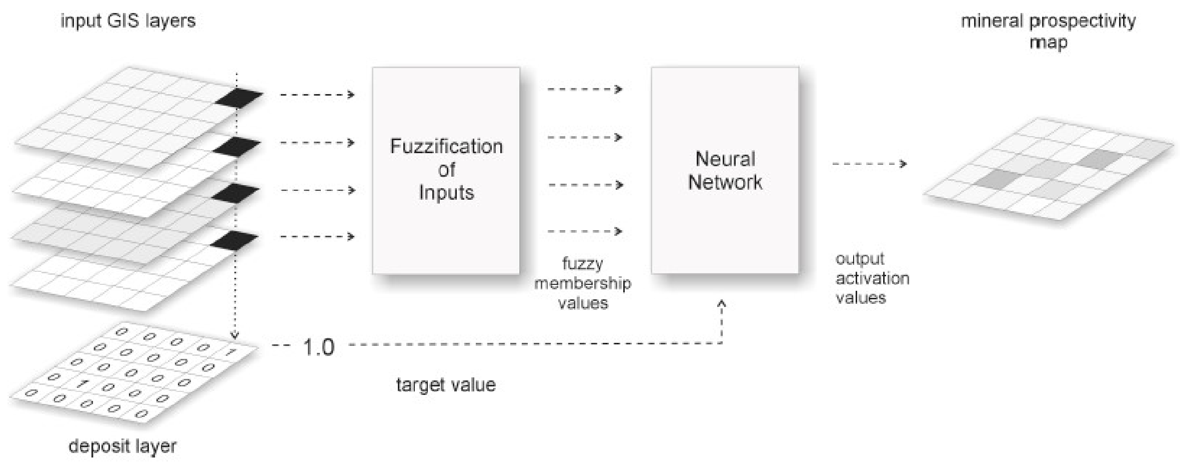

FIG. 21. Schematic diagram showing hybrid, fuzzy-neural network system. Some or all network inputs may be fuzzy membership variables [95]. Figure is reproduced with permission from the copyright owner International Association of Mathematical Geosciences.

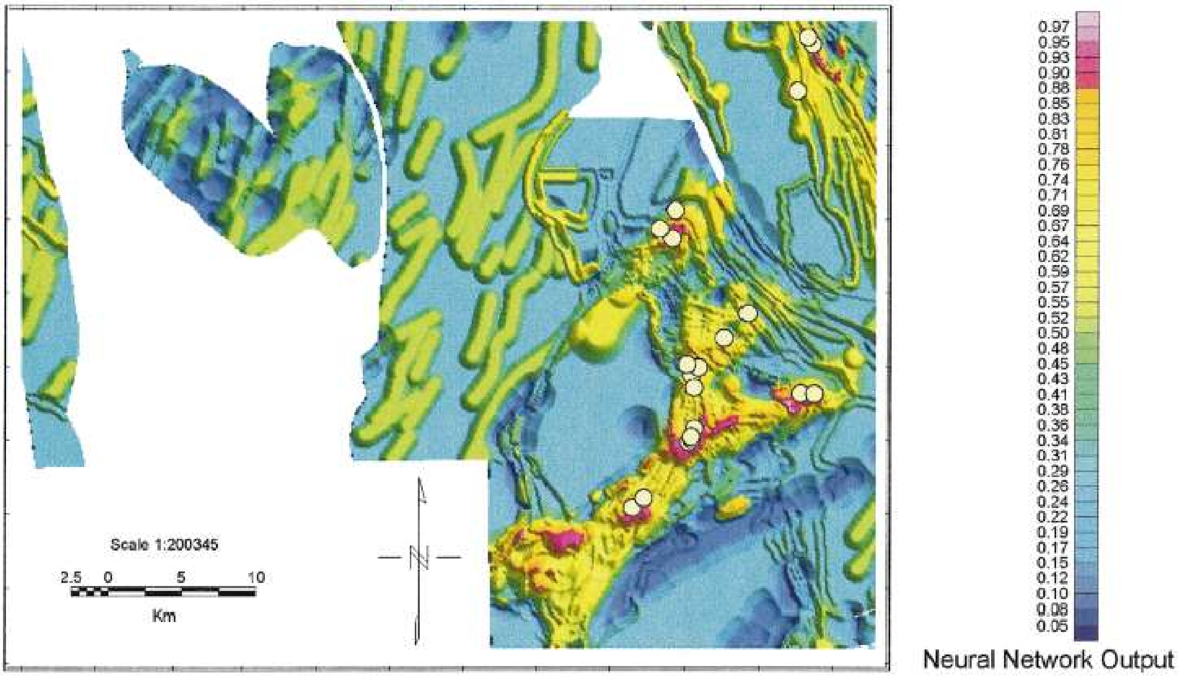

FIG. 22. Mineral-prospectivity map produced by hybrid fuzzy-neural network, showing potential for orogenic lode-gold deposits in part of Kalgoorlie Terrane, Western Australia. Map was created using 10-20-1 hybrid fuzzy-neural network in which all ten inputs were converted to fuzzy membership values before being processed by network. Yellow circles indicate deposits containing resource of 1000 kg total contained gold [95]. Figure is reproduced with permission from the copyright owner International Association of Mathematical Geosciences.

6. QUANTITATIVE METHODS

Quantitative methods of mineral resource assessment of undiscovered deposits estimate tonnage of a commodity in the study area. The assessments are either carried out directly of the commodity (e.g., uranium) or indirectly by first estimating number of deposits of a particular deposit type and them calculating tonnage of ore, ore grade and total tonnage of the commodity. This section presents a brief review of deterministic and probabilistic methods of quantitative assessment.

6.1. Deterministic methods of quantitative assessment

6.1.1. Methods based on crustal abundance of elements

McKelvey [28] described crustal abundance method for making a rough estimate of recoverable reserves of metals from crustal abundance data. For this, he plotted recoverable reserves in the USA from various metals against their crustal abundance. The plot of reserves versus crustal abundance followed a general relationship: R (reserve) = ($A \times 10^k$), where A is the crustal abundance and k is a number between 9 and 10. The plot also includes estimates for uranium. The relationship shows that the more abundant the elements are in the Earth's crust, the greater are the recoverable reserves of that element [3]. Harris [3] notes that the variation in the value of 'k' is in fact between 6 and 10 (and not 9 and 10) when all points plotted on the diagram are included in the calculation. Thus, a variation of 10,000 times means that when examined across all metals, the relationship is very weak. The empirical equation was later modified by [29].

Both [28] and [29] were aware that these plots only provided a very rough estimate of reserves or resources.

6.1.2. Method based on tectonic-diffusion of metals

Kesler and Wilkinson [30] and Wilkinson and Kesler [31] describe a method based on tectonic-diffusion of gold and copper to produce very rough estimates of global resources of gold (orogenic gold) and copper (porphyry copper). The tectonic-diffusion approach assumes that the vertical tectonic displacement of rock bodies (including ore deposits) relative to the Earth's surface is effectively random at global and geological scales of consideration [31]. After a deposit has been formed at any crustal level, tectonic processes can move it upward by exhumation and erosion, downward by subsidence and burial, or can cause it to stay at the same level in the crust as time passes. Wilkinson and Kesler [31] termed this movement tectonic diffusion and suggest that data from a large number of deposits of any specific type that form at some characteristic level in the crust can be simulated numerically by continuously emplacing the deposits at a specific depth and then allowing them to undergo random vertical displacement.

The method requires information on the age-frequency distribution and metal content of known deposits, as well as the average crustal depth at which they formed. The age-frequency distribution, which is obtained from ages of dated deposits, is used along with the average depth of formation to estimate the number of deposits in the subsurface; this number can then be multiplied by the average metal content of known deposits to determine the total metal content of all deposits. The calculations produced by [31] show that of the 4,554 deposits containing 706,439 t of estimated gold in crustal rocks, the resource down to a depth of 3 km is about 112,653 t or ~16% of the total orogenic gold endowment. The tectonic-diffusion method is less empirical than that proposed by [28] and [29] and, therefore, its use for quantitative assessment of uranium resources appears speculative.

6.1.3. Methods based simple and compound density

These methods are based on the concept of analogy, which assumes that the distribution densities of deposits and of contained commodities are, in general, similar between control and study areas. Harris [3] briefly describes the estimates produced by Nolan (1950) for a number of mining districts in the USA. Lowell [102] conducted resource appraisal of copper using the principle of analogy.

6.1.4. Estimates of world uranium resources

In 1975, a rough estimate of the world uranium resources was published by the OECD/IAEA. The assessment was made by first determining the ratio of 1978 US total (reserves + potential + cumulative production) resources to the 1975 reasonable reserves reported by the OECD/IAEA. It was assumed that the same ratio was true for other similar regions, and undiscovered resources were estimated for Canada + Australia + Western Europe, and for the rest of the world [3]. The concept of mineral density, combined with the principle of geographical analogy, was also employed to conduct a second estimate of world uranium resources (Table 4.6 in [3].

6.1.5. *NURE assessment method*

The NURE method developed and employed by the US Energy Research and Development Administration (ERDA) also uses the concepts of analogy and deposit and resource density. However, the method also relies on assigning probabilities by experts' geologists, and it will be described in the section dealing with probabilistic methods of quantitative assessment.

6.1.6. *Zipf's law*

Zipf's law was proposed originally as a guide to study statistical distributions in social studies. It describes a relationship between rank and size of discrete entities and phenomena [11]. The law suggests that many phenomena/entities are arranged in a succession of order in such a way that the largest is followed by half the size for the next largest, which in turn, is followed by the half of that size, and so on. The application of the law has been tested for geological entities and the law has been used in resource assessment in petroleum, and, to a limited extent, in mineral deposits. In the 1970s and 1980s, the method was applied for a number of resource assessment studies (e.g., [103].

Merriam et al. [11] discussed the application of the law for geological problems (oil and gas field sizes, earthquake size, anticline size) and concluded that it is applicable in describing size and rank of oil and gas fields according to their respective cumulative productions. They also suggested that the law can be used for predicting the occurrence of oil and gas fields according to their sizes and, therefore, for predicting the amount of undiscovered resources in large structural entities (e.g., sedimentary basins).

The law can be applied by plotting the rank and size of deposits or oil and gas fields to estimate how many deposits still remain undiscovered in a province or a basin [11]. Fallon et al. [104] used the Zipf's law to estimate that the Plutonic Marymia Greenstone Belt in the Yilgarn Craton, Western Australia, may contain an undiscovered gold resource of 5.5–5.7 Moz (156–160 t). A similar assessment of nickel sulfide resources was conducted by [105] in the Norseman-Wiluna Greenstone Belt, Western Australia. The analysis suggests that about 3–10 Mt of nickel sulfide resources are yet to be discovered in the greenstone belt.

It is important to emphasize that the Zipf's law can be successfully applied only in areas with known mineralization (brownfield areas), and that the resource assessment is non-spatial (no map output). The assessments are generally carried out at the scale of a belt, sedimentary basin or a province and the method does not provide any measure of uncertainty associated with the assessment.

6.2. Objective probabilistic methods of quantitative assessment

Probabilistic methods of quantitative assessment of resource are classified into types: objective probabilistic and subjective probabilistic methods. In objective probabilistic methods, assessment of resources and endowment are estimated using probabilistic models derived from controls areas which are then applied to the study areas. Harris [3] provides a comprehensive discussion of geostatistical and probabilistic framework of several methods. The discussion also summarizes important case studies. These methods are:

— Crustal abundance models, which include crustal abundance geostatistical approach (CAG) of Brinck; univariate log-normal crustal abundance models of mineral

endowment; bivariate log-normal deposit model of PAU (Programmes Analysis Unit of Great Britain);
— Occurrence models;
— Multivariate model for wealth (Harris model and model of for Grenville Province of the Canadian Shield).

A common feature of these methods is that they can be used to estimate resources of metals or commodities directly (without any consideration of deposit types) from the crustal abundance of these metals. Models of wealth estimate in-ground values of commodities. The methods estimate metal endowment, which does not represent resources or potential supply [3]. This limits the use of these methods to conduct geology based quantitative resource assessments of undiscovered deposits. Another major drawback of these methods is that they are non-spatial (no map outputs). This section will briefly discuss a method used by [1] to conduct an assessment of mineral resources in the Algerian Sahara.

6.2.1. Spatial occurrence model of Allais (Poisson probability)

In 1957, Allais published results of quantitative assessment of resource values in the Algerian Sahara. The main objective of the assessment was to comment on the economic merits of conducting mineral exploration the Algerian Sahara. The method Allais used is described as a spatial occurrence model [3] of mineral of mining districts. As there was no or limited information about the geology in the Sahara, information from other geologically analogous regions has been used [1]. The basic assumption of the approach was that regions that had received sufficient quantum of exploration, the number of mining districts known to be present in the region would provide a reasonable approximation of the mining districts geologically possible in them.

Information from a number of control regions, such as, the western part of the USA, France and North Africa, has been used [1]. The study on the number of mining districts per unit cell in these regions showed that the data could be described by the Poisson distribution function: $P(n) = ((m^{-n})(e^{m}))/n!$ where P represents the Poisson probability, n is the number of mining districts, e is a constant and $n = 0, 1, 2, \ldots.$

The conclusion that the Poisson distribution function could describe the distribution of mining districts in a unit cell, had a number of significant implications. It showed that the probability of mining districts in a unit cell is small; that this probability is constant across cells (i.e., no one cell has a higher probability than any other cell for hosting a mining district), and the probability that a unit cell contains two mining districts is extremely small [3]. The assessment by [1] concluded that the expected number of deposits, each worth between 1 and 1,000 billion francs, was of the order of 20, and that in the Sahara, a region of the size of 1,000,000 km^2, the expected number of deposits lies between 4 and 50. It has also been showed by [1] that the probability of net gain of exploration in the Sahara is only 0.35. In other words, there is about one chance out of three that exploitation of mineral resources in the Sahara will prove profitable.

The assessment conducted by [1] was considered pioneering [2, 3]. One of its major drawbacks is that the study lumped together many different kinds of deposits [2]. However, the frequency distribution of deposit sizes revealed by the study emphasized the point that only the largest deposits are important for global supply. It also showed that the expected financial return from exploration investment was positive, but the probability of economic failure was 0.65 [2].

6.3. Subjective probabilistic methods of quantitative assessment

In these methods, probabilities associated with the estimates are assigned by expert geologists. Although these methods are predominantly knowledge-driven, they are based on robust datasets that assist expert geologist to make the assessments. The question of bias associated with subjective approach is discussed by [2, 3] and [22].

6.3.1. NURE assessment method

The NURE programme conducted quantitative assessments of undiscovered uranium resources in the USA in a six-year period between 1974 and 1980. The final report of the assessment was published in 1980. It is one of the largest and most intensive single efforts undertaken to estimate undiscovered uranium resources [3]. A comprehensive description of the methodology and results are covered in [3, 22], and [106].

The assessment programme consisted of the following major activities [3]:

- Geological investigation and evaluation of NURE regions and preparation of multi-map folio for each 2-degree quadrangle;
- Support analysis to be used for the selection of favorable areas and in the estimation of resources. This involved selection of the control areas, identification of recognition criteria per geological setting and construction of quantitative estimates of appraisal factors on each control area;
- Selection of favorable areas for resource evaluation;
- Elicitation of subjective probabilities from expert appraisers for the component of endowment and of P0, the probability for at least one deposit of at least 10 t of U_3O_8 (given a cut-off grated of 0.01% U_3O_8);
- Statistical analysis of subjective estimates.

The standard NURE endowment assessment equation is based on five components [106]:

$$U = A \times F \times T \times G \times P$$

where:

U = unconditional uranium endowment in tonnes of U_3O_8 above a cut-off grade of 0.01 % U_3O_8;
A = projected surface area of favorable ground in square miles;
F = fraction of A that is underlain by endowment;
T = tonnes of endowed rock per square mile within ($A \times F$);
G = average grade of endowment, in decimal form;
P = probability of occurrence, a factor that expresses likelihood that one or more deposits actually exist within the favorable area.

The project surface area A is the size of the favorable area measured on a map, most commonly on a quadrangle map at a scale of 1:250,000. Factor F is a variable, and for it three values are estimated: lower (at 5% probability), most likely (mode), and upper (at 95% probability). Factor T (tonnes per square mile) is obtained by multiplying average thickness of the endowed portion of the host rock by the average density of the rock. The average thickness is estimated by comparing the favorable area with the analogous control area. For it, three values are estimated: lower, most likely and upper values. Factor G (average grade in % U_3O_8) is determined either based on known deposits near the favorable area or based on the average grade for an analogous control area. The value of factor P varies between 0 and 1, and expresses the likelihood of occurrences of a deposit. The highest value of 1 denotes that the favorable area is identical to the control area. The factors are recorded in an assessment form for the quadrangle [3]. The data from the assessment forms are subjected to statistical analyses which involves fitting of there-parameter log-normal distributions, combining of variable, computing of moments, and aggregation across regions. A number of cumulative probability distributions for endowment and for various categories of resources for the aggregate of all areas and of the continental USA can be seen in [3].

Harris [3] discusses several shortcomings in the elicitation of subjective estimates in the assessment. Finch and McCammon [106] noted that the estimation of factor F (fraction of favorable area underlain by endowment) was the most difficult factor to estimate. It was also the most commonly adjusted factor in the iterative process of elicitation. The difficulties in estimating this factor led to the development of the DSF (Deposit-Size Frequency) method [106].

6.3.2. Deposit-Size Frequency (DSF) method: modification of standard NURE method

Finch and McCammon [106] note that the difficulty in factor F (fraction of favorable area underlain by endowment) in the original NURE method arose from a number of considerations which include, the kind and quality of the available data, the state of knowledge about the mode of occurrences of the type of deposit being assessed, and the size of the area being assessed.

The DSF (modified NURE) method consists of a sequence of seven steps [22], [106]:

1) Delineation of favorable area and determination of geological favorability of the area.
2) Selection of control area;
3) Development of grade-tonnage data;
4) Development of DSF data;
5) Selection of the option for calculating endowment and for estimating necessary factors through elicitation;
6) Calculation of endowment and review of results with re-evaluation as necessary;
7) Expert peer review.

Finch and McCammon [106] also modified the standard NURE equation first by replacing factors F and T by a single factor, and second, by replacing P with an optional factor L. The modified equation is:

$U = A \ \{\sum(n_{ic}/A_c) \times T_i\} \times G \times L$

where:

U = unconditional uranium endowment in tonnes of U_3O_8 above a cut-off grade of 0.01% U_3O_8;
A = favorable area in square miles;
$\sum$ = sum of k deposit-size classes;
k = number of deposit-size classes;
n_{ic}/A_c = spatial density (number of deposits/unit area) of deposits of size T_i (tonnes of endowed rock) in the ith deposit-size class within a control area. The ratio n_{ic}/A_c is a measure of the spatial density.

T_i = tonnes of endowed rock;
A_c = control area from which the spatial density is obtained;
G = average grade of endowment, in decimal fraction form;
L = optional scaling factor that expresses the relation between the endowment in the favorable area and that in either the control area or some designated subarea for which estimates of the number of deposits in different size classes have been made.

The DSF method is described as more flexible than the NURE method because the assessors can use any of the three following options for estimating number of deposits [106]:

— Option A: In cases where the favorable area has been examined in sufficient details (L = 1), and where estimating the number and size of deposits that may occur is possible. In this case, factors A, and nic/Ac are not included in the equation;
— Option B: In case where the favorable area has been examined cursorily but sufficiently so that spatial densities of deposits of different sizes can be estimated with reference to a control area (L = 1). In this case all factors of the equation are used;
— Option C: In cases where the favorable area can be delineated but has been examined in detail only for some portion (i.e., the proto-control area Ac), so that the number and size of deposits within that portion can be estimated. In such cases, the factor L can take any positive value between 0 and 1.

One of the most critical tasks in the assessment is the development of a DSF (deposit size frequency) distribution. This is achieved by compiling the number of known deposits of various sizes within a control or proto-control areas. An appropriate form to assist in this task is included in [22].

6.3.3. Three-part USGS method

The first assessment using an earlier version of this method was conducted in the early 1970s in a 1:250,000 quadrangle in Alaska with results of the assessment published in 1975 [107], [108]. Since then several quantitative assessments of undiscovered resources of various types of commodities at various scales have been published. The method has been developed, modified and perfected by assessment teams in the USGS. Some of the most recent quantitative assessments have been published by [109, 110], and [111]. There are several papers that describe the method [7, 25, 112] but a more comprehensive description of the method can be found in [2].

The three parts in the method refer to the three following activities (Fig. 23):

1) Preparation of resource maps showing tracts geologically-permissive for deposit types;
2) Preparation of grade-and-tonnage models of deposit types;
3) Estimation of number of undiscovered deposits of the assessed deposit types.

The three parts or activities are followed by an equally important exercise that involves probabilistic analysis (using Monte-Carlo simulation techniques) of the estimated number of deposits culminating in the assessment of tonnage of the commodity at three or more levels of probabilities. The method is based on the following three types of models (Fig. 24):

1) Descriptive models of deposit types;
2) Grade-and-tonnage models of deposit types;

3) Deposit-density models.

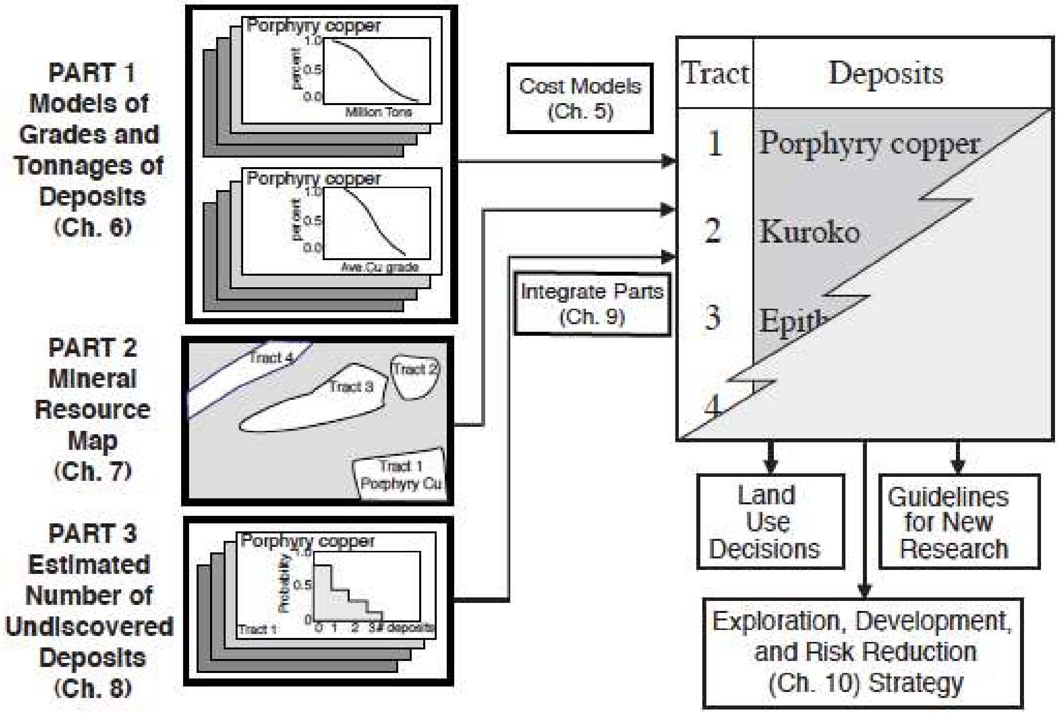

FIG. 23. Three parts of the three-part U.S.G.S method of assessment. Chapter numbers in the figure refer to chapters in [2].

6.3.3.1. Descriptive models of deposit types

The main focus of descriptive models of deposit types is on observations and on the use of theories of genesis of a deposit type to guide what to observe in order to outline a number of critical features that can assist in the delineation of a geologically-permissive tract [2]. Descriptive models compiled in [62] have two parts. The first part describes the geological setting in which the deposit type is often found. The second part summarizes distinguishing features of deposit types.

In mineral potential assessments carried out in the forest regions in Australia, the descriptive models in [62] were modified and adjusted to accommodate geological features specific to the deposits in the region [16]. An interesting feature of these descriptive models of was the listing of geological features thought to be critical for their formation. These critical features were then identified in various types of geoscientific datasets to enable delineation of geologically-permissive tracts.

In recent years, a number of assessment projects have used mineral-systems approach to modify descriptive models to help in the delineation of geologically-permissive tracts (e.g., [70, 113].

6.3.3.2. Grade-and-tonnage models of deposit types

The grade-and-tonnage models used in the three-part method show frequency distributions of average grades and tonnages of well-explored deposits of each type, which are employed as models for estimating grades and tonnages of undiscovered deposits of the same type in the study area [2]. These models are based on data collected from a large number of well-explored deposits from around the world [62, 114–118]. Grade and tonnage data for deposits are based on the total production, reserves, and resources at the lowest possible cut-off grade and, thus, represent an estimate to the total endowment of the deposits [2].

Grade and tonnage data of deposit types are presented in the forms of cumulated frequency curves (Figs. 24 and 25). The grade and tonnage are plotted (on two separate plots) on the horizontal axis and the cumulative proportions of deposits are plotted on the vertical axis (Figs. 24 and 25). A logarithmic scale is used for both values. The first step in making such plots is to arrange the data from the smallest to the largest. On these plots, each dot represents a deposit. A smoothed curve, representing percentiles of a log-normal distribution that has the same mean and standard deviation as the observed data, is also shown on these plots (Figs. 24 and 25). The plots are commonly described as 'greater-than' diagrams. The median of the data (50th percentile) separates the data into two groups showing that 50% deposits have grades and tonnages greater than the median value and the other 50% have values smaller than the median value. In addition to the median values, the values for 10th and 90th percentiles are also shown. For example, the 10th percentile value shows that 10% deposits of that model have grades and tonnages greater than the value of the 10th percentile. Thus, the plot can very quickly and clearly show the grades and tonnages of the largest 10% deposits of that type. This information is particularly important because for many deposit types, bulk of the resources seem to be associated with the largest 10% deposits of that type, and that the contribution of the rest 90% deposits is significantly lower [2].

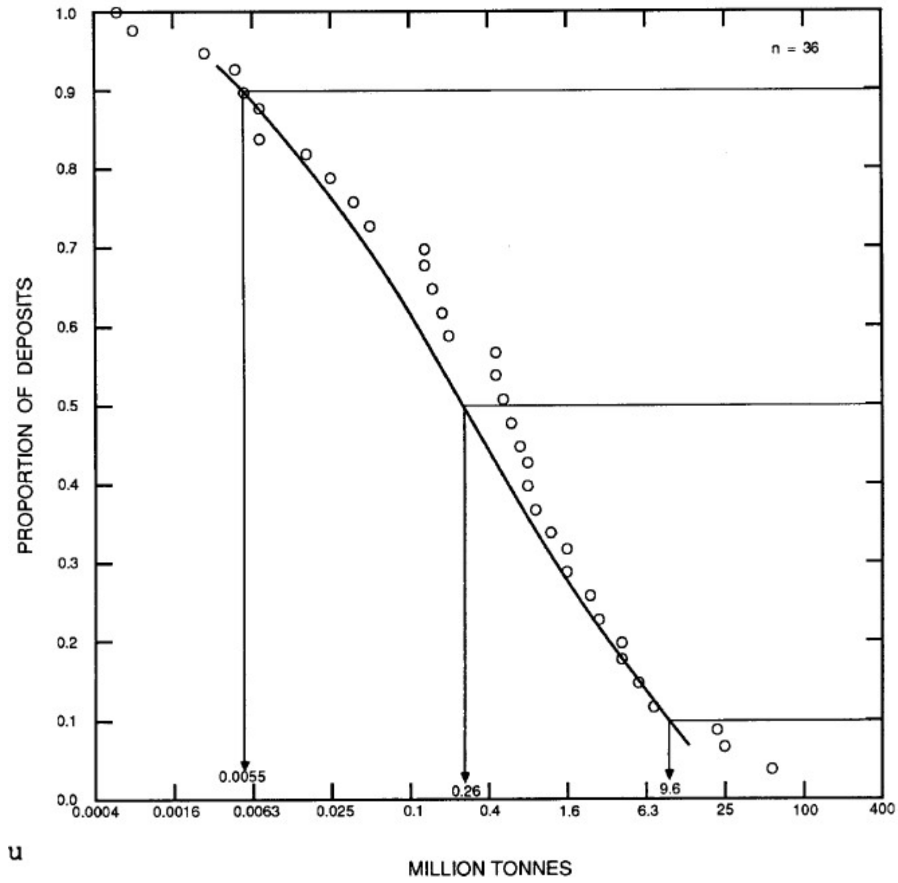

FIG. 24. Cumulative frequency curve showing tonnage of unconformity related uranium deposits. The figure represents the tonnage part of the grade-tonnage model of unconformity-related uranium deposits [62].

In preparing grade-and-tonnage models of deposits types it is important to distinguish between ore zones, ore bodies and deposits. In many databases, resources are recorded for not only individual deposits but for ore zones and ore bodies. In many cases, resources are available for ore fields and districts rather than individual deposits. One of the simplest methods used in three-part methods is to aggregate and disaggregate data using a uniform spatial proximity rule. For example, for the grade-and-tonnage model of low-sulfide Au-quartz veins (also described as orogenic lode gold), all deposits within 1.6 km were combined [62].

Cox and Singer [62] summarize grade-and-tonnage models (also known as 'global' models) of many deposits types using data from well-explored deposits from around the world. In many cases, it is essential to check if the grade and tonnage data of local deposits matches the distribution of global grade-and-tonnage model. Several examples have been discussed by [2] for statistical testing of local and global models. The simplest of these tests is t-test [2].

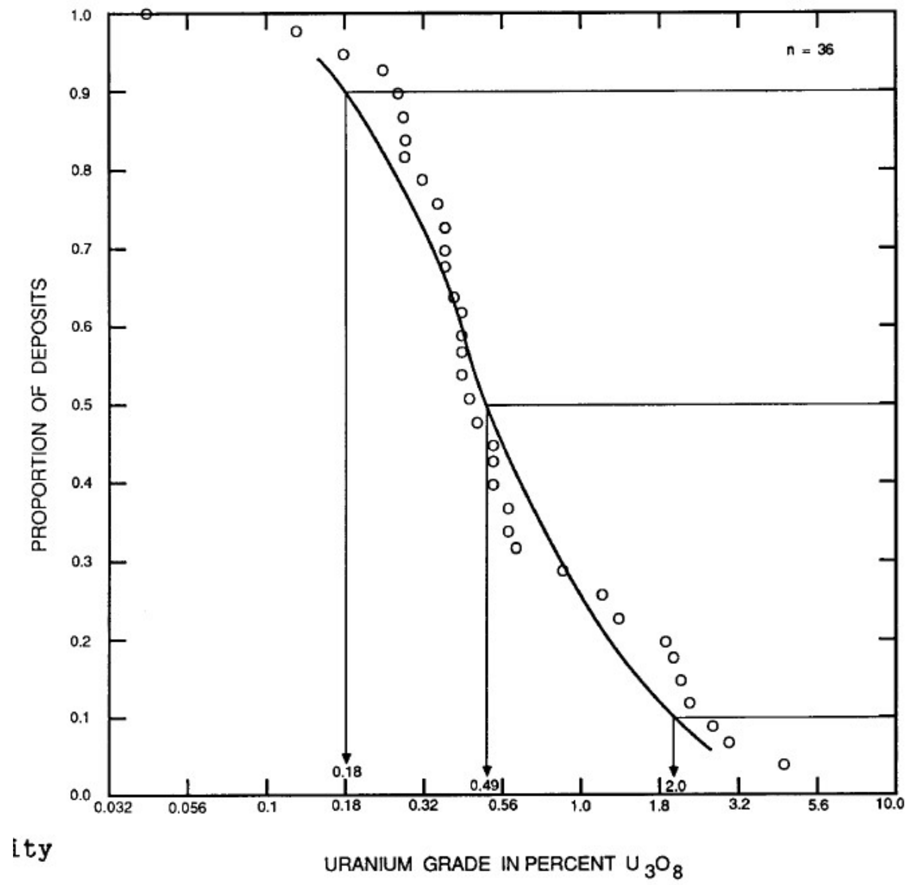

FIG. 25. Cumulative frequency curve showing tonnage of unconformity related uranium deposits. The figure represents the grade part of the grade-tonnage model of unconformity-related uranium deposits [62].

In regions where no well-explored deposits are known, the use of the global model is thought to be the best representative of undiscovered deposits. If the well-explored deposits are significantly different in grade and tonnage, it is recommended that the local deposit be tested to see if they belong to a geologically homogeneous subset of the global model [2].

6.3.3.3. Deposit density models

Deposit density data are critical for quantitative resource assessment of undiscovered data. They can be used directly to estimate number of undiscovered deposits and they also provide the most critical information to expert geologist to judge their estimates of number of undiscovered deposits.

Deposit density (number of deposits per unit area) can be determined by counting the number of deposits per unit area in well-explored control regions. Deposit densities are often plotted in histograms to show variations of densities [2]. Singer et al. [119] summarize deposit densities of several deposit types. A detailed discussion on deposit densities of porphyry copper deposits world-wide is available in [117]. One of such density plots is shown in Fig. 26. On this plot, the log10 values of number of deposits (y-axis) are plotted against the log10 values of geologically-permissive area. The thick black line represents the linear regression fit of the point data.

The study of deposit densities of different deposit type reveals an interesting relationship between the median size of a deposit and the size of the geologically-permissive area (Fig. 27). In general, for a given size of geologically-permissive area, an increase in the median size of the deposit decreases the number of deposit per unit area of the geologically-permissive tract. In other words, the number of giant and super giant deposits that can be found in a geologically-permissive tract of a given size is generally low (Figs. 27 and 28).

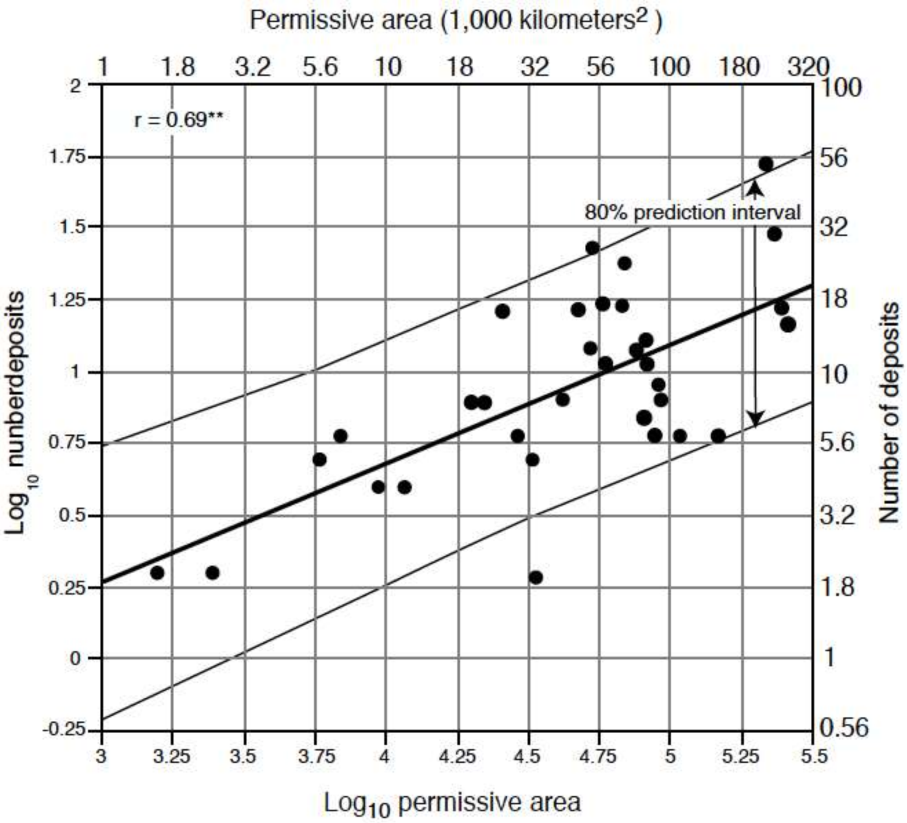

FIG. 26. Figure showing density model of porphyry copper deposits. In this figure permissive areas (Log10 values) on the x-axis are plotted against number of deposits (Log10 values). The figure also shows 80% prediction interval for deposits [2].

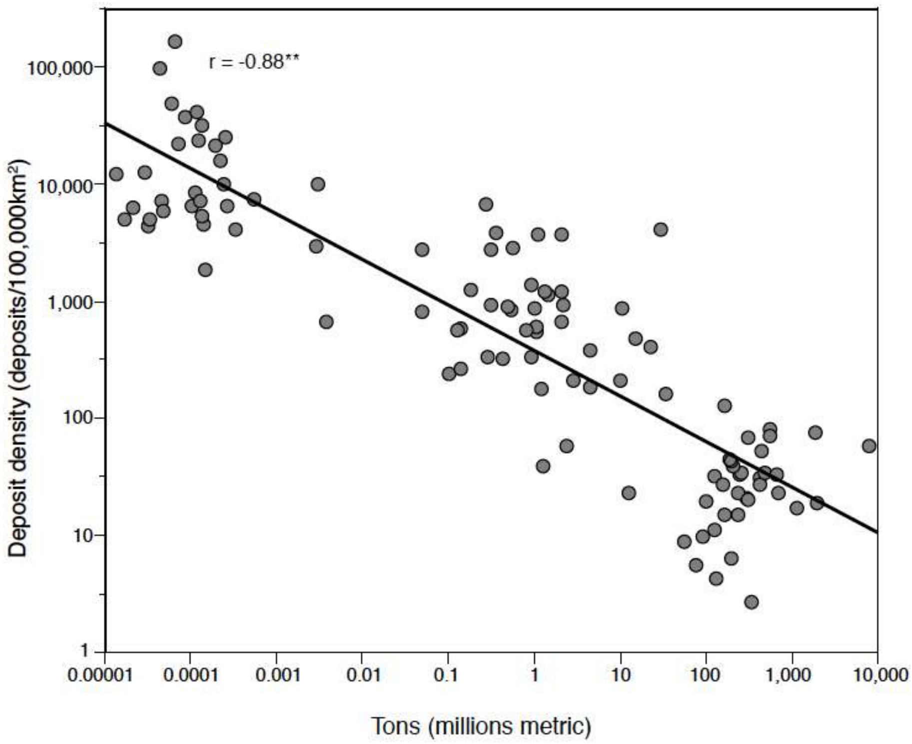

FIG. 27. Figure showing median deposit size (in million tonnes) for all deposit types plotted against deposit density (number of deposits/100 000 km^2). As median deposit size increases, the density of deposit in the area decreases [2].

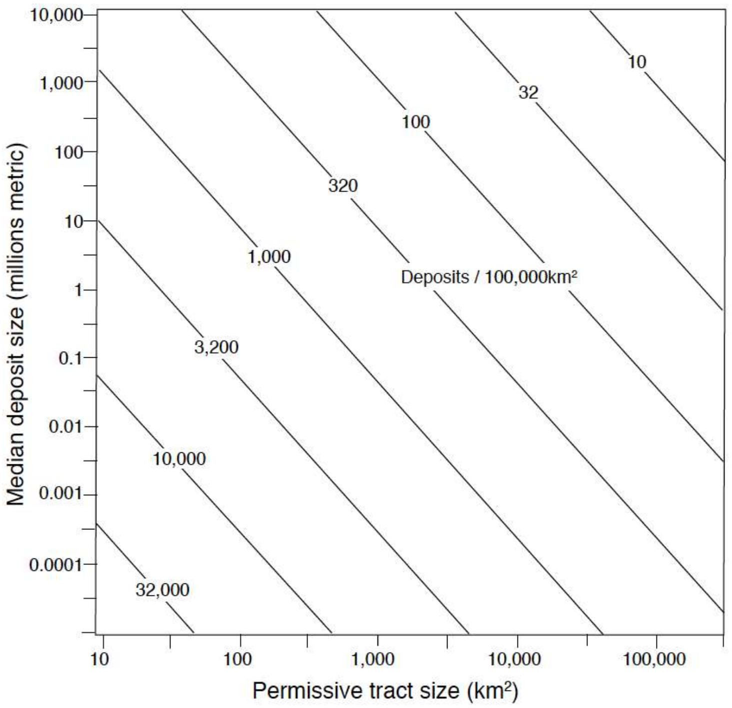

FIG. 28. Figure showing relation between the size of a permissive tract (x-axis) and median deposit size (million tonnes, y-axis). Diagonal lines with numbers show deposit density (number of deposits/100 000 km^2 [2].

6.3.3.4. Delineation of geologically-permissive tract

Descriptive models of deposit types include geological information deemed critical for the formation of that deposit type. This information is used to delineate areas that are geologically favorable to host deposits of a particular type. These favorable areas are called geologically-permissive tracts. Their boundaries are delineated in such a way that the probability that these deposits occur outside the delineated areas age negligible, that is less than 1 in 100,000 [2]. The geologically-permissive tracts are in a way more generalized than favorability or prospectivity maps, which can be drawn by using more sophisticated GIS-modeling techniques described in section 4 of this review. GIS-modeling techniques allow delineation of areas of differing favorability or prospectivity within a geologically-permissive tract. The usefulness of this approach and its combination with the three-part method will be discussed in more detail in the following sections of this review.

An important feature of geologically-permissive tracts as delineated in the three-part method is the separation of outcropping and under-cover parts in a geologically-permissive tract [2].

6.3.3.5. Estimating the number of undiscovered deposits

Grade and tonnage and deposit density models provide the basis to estimate number of undiscovered deposits in a geologically-permissive tract. The geologically-permissive tract is delineated using geological features deemed to be critical for the formation of deposits of that type. This information is summarized in descriptive models. The number of deposits estimated represents the probability that some specific number of undiscovered deposits could have been formed within the geologically-permissive tract [2]. Estimates of number of deposits are provided for three or more quantiles (probabilities), namely 90th, 50th and 10th percentiles. The spread in the number of deposits for these three quantiles provides a measure of the uncertainty associated with the assessment. A large difference in the number of deposit estimates reflects a great level of uncertainty [2].

Estimates of number of undiscovered deposit can be derived either subjectively (by a panel of experts) or objectively by using deposit density models. In cases where estimates are made by a panel of experts, deposit density and grade-and-tonnage models are used to check the validity and consistency of estimated number of deposits. Several case studies illustrating this process have been cited by [2].

A method based on global deposit density model of porphyry copper deposits has been described by [2]. This method allows robust estimates of discovered plus undiscovered deposits. The global deposit density data for porphyry copper deposit are shown in Fig. 26 discussed in section 5.3.3.3. In this figure, the regression line represents the estimate for the 50 percent quantile. Using the size of the geologically-permissive area (plotted on the x-axis), it is possible to estimate number of deposits (plotted on the y-axis). The lower prediction line on Fig. 26 shows estimates for the 90th percentile, whereas the upper prediction line on the same figure shows estimates for the 10th percentile [2]. The estimate requires calculation of a number of statistical parameters of the deposit-density distribution. These are: t = Student-t value, $Sy|x$ = standard error of predicted y values; Sx^2 = variance of x values. Estimates of deposits at the 90th, 50th and 10th percentiles can then be used to estimate the expected number of deposit from the equation [2]: $\log_{10} E(N) = \log_{10} (N_{50}) + (((\log_{10} (N_{10}) - \log_{10} (N_{50}))/t)^2)/2$, where $E(N)$ is the expected number of deposits and N_{50} and N_{10} are number of deposits estimated for the 50th and 10th percentiles, respectively. The above equation can be used for any deposit type for which the deposit-density model is available and for which the regression equations of the type shown in Fig. 26 are available [2].

Lisitsin et al. [110] describe a similar method to estimate number of undiscovered orogenic lode gold deposits in Northern Victoria. A calculated ore field density of 3.3 per 1,000 km^2 (Bendigo Zone) was used to estimate number of undiscovered deposits in the under-cover part of the geologically-permissive tract. This number represented the estimate at the 50th percentile. Estimates for the 10th and 90th percentiles were obtained by assuming the Poisson probability distribution with a mean of 25 (number of deposit estimated from deposit density equation). These estimates were moderated by the expert panel taking into account geological information available for the area. The final estimates for the number of undiscovered ore fields in the Bendigo Zone were 15 (90th percentile), 25 (50th percentile) and 32 (10th percentile).

6.3.3.6. Tonnage of undiscovered resources (Monte Carlo simulation)

Estimates of number of deposits are generally made at three (90th, 50th and 10th percentiles) quantiles or probabilities. The level of uncertainty associated with these estimates is reflected in the spread between numbers of deposits estimated at each quantile. For example, in the Bendigo Zone, the estimates show that there is 90% probability that there are 15 or more undiscovered ore fields in the zone, 50% probability that there are 25 or more ore fields and 10% probability that there are 32 or more ore fields (Lisitsin et al., 2010). However, these estimates do not show the probabilities associated with intermediate number of deposits (e.g., 10, 22 or 31) that may occur in the Bendigo Zone. This task of determining probabilities of each possible number of deposits that may occur in a geologically-permissive tract requires sophisticated mathematical tools. The Poisson distribution function can be used to estimate these probabilities but this distribution cannot account for the clustering of deposits, which is commonly observed in mineralized regions [2].

The MARK3 Monte Carlo simulation program [120] provides a tool to calculate probabilities associated with the intermediate number of deposits. The algorithm for allocating the total probability among all possible number of deposits used in the simulation program can be found in [2]. The MARK3 program also simulates the process of combining estimates of numbers of deposits at different probabilities with the grade and tonnage data of deposits of that type to produce probability estimates of tonnages of commodities (metals) and of mineralized rock (tonnage of ore). The simulation program draws random numbers between 0 and 1. For each of the 4,999 draws, a number of deposits is selected (Fig. 29) and for that number of times, the program selects grade and tonnage data stored in it for that particular deposit type. The output is typically displayed in the form a table of frequencies of number of deposits, tonnages of ore and of contained metal. The table is accompanied with plots of cumulative frequencies of tonnages of ore and contained metal (Fig. 29). Tonnages on these plots are shown on the x-axis, and probabilities plotted on the y-axis (Fig. 29).

Several useful case studies of three-part method are described in [2]. Lisitsin et al. [110] applied the same method to estimate number of undiscovered orogenic lode gold ore fields in Victoria. The assessment shows that in the northern part of the Bendigo Zone under-cover (10,000 km^2) the mean estimate of undiscovered gold is ~1,000 t, with a 90% probability of at least 290 t, of gold in undiscovered mesozonal orogenic gold deposits. In the northern, covered area of the Stawell Zone (30,000 km^2), the mean estimate is ~1,200 t, with a 90% probability of at least 200 t, of undiscovered gold and in the northern part of the Melbourne Zone (4,400 km^2) the mean estimate is ~90 t, with a 90% probability of at least 10 t, of gold.

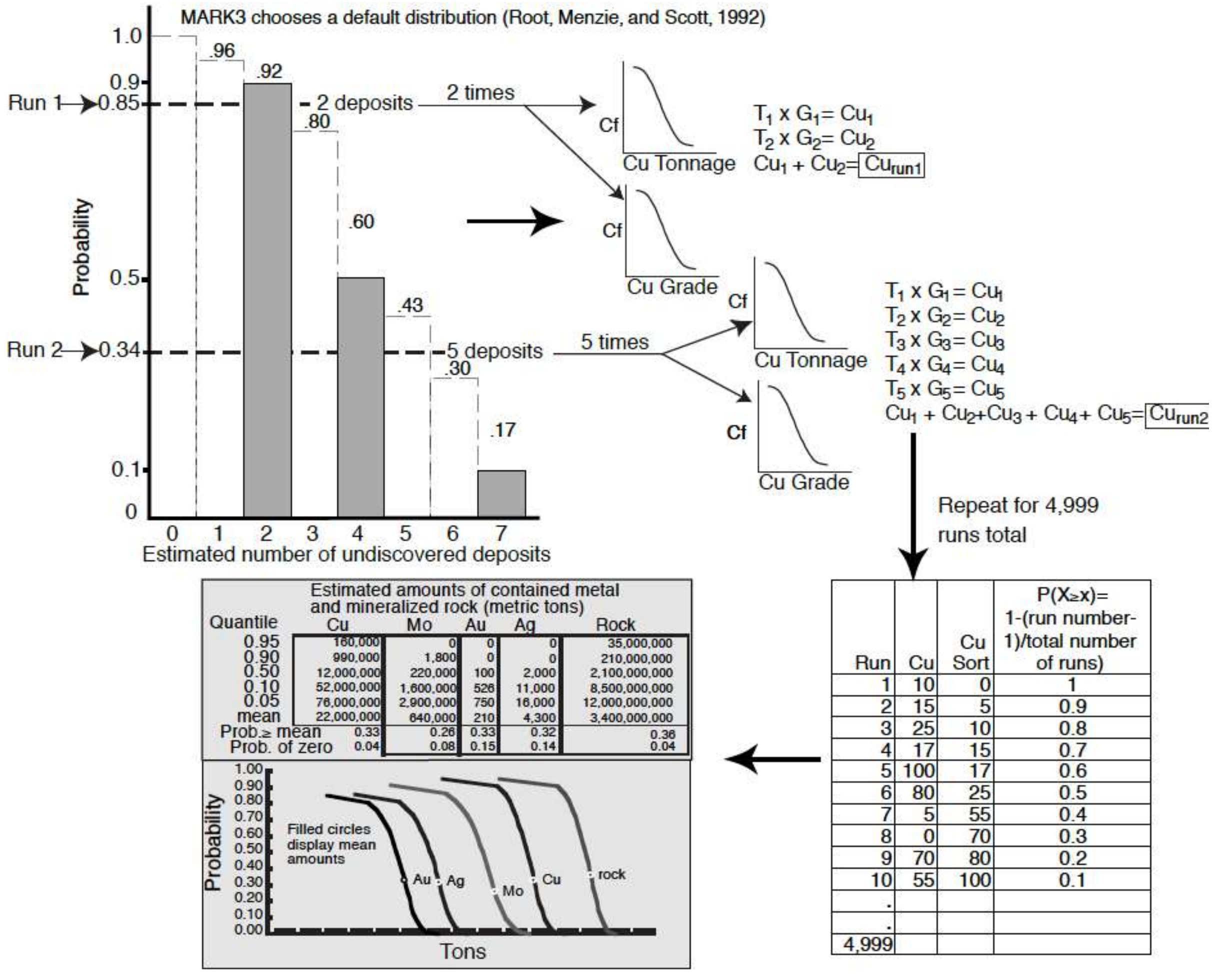

FIG. 29. Schematic diagram showing Monte-Carlo simulation by MARK3. The simulation is for a scenario in which estimated number of deposits is 2 at 90% level, 4 at 50% level, and 7 at 10% level. The deposit type estimated is porphyry copper. Cf stands for cumulative frequency [2].

6.3.4. One-level prediction method

The method was developed as a numerical technique for estimating undiscovered metal endowment within large areas [33]. It is based on a presumed relationship between quantified geological favorability of an area to contain a deposit and spatial distribution of metal endowment. The method of one-level prediction aims to estimate total undiscovered endowment in a region using information that is neither precise enough nor extensive enough to assess potential for mineral deposits [33]. However, it is also assumed that the geological information is sufficient to calculate: (a) a numerical measure of favorability; (b) the extent of exploration in the area; and (c) the known endowment for a suitably defined grid of an equal area cell. The method was first demonstrated for estimating undiscovered uranium endowment in the San Juan basin, New Mexico, USA [121] as part of the NURE program.

The method relies on analogy with a control region in which the known endowment or metal density is used to estimate endowment in the study area. The metal density (defined as constant of proportionality) is the ratio of the known endowment in the well-explored control region to the size (area) of the control region. The basic assumption is that the study area is geologically similar to the well-explored control region.

Resource assessment is conducted in the following four steps [33]:

1) Classification of study area into cells of different favorability using a numerical measure of favorability;
2) Reclassification of cells into two categories (favorable and unfavorable) based on a selected threshold favorability value;
3) Calculation of endowment in a favorable cell using constant of proportionality (metal density) estimated from a suitably selected control region;
4) Calculation of total undiscovered endowment in the study area by summing endowment in each of the favorable cell.

Although the method is capable of producing favorability maps of the study area showing favorable and unfavorable cells, the total endowment estimated by this method does not apply to individual cells but to the whole favorable area [33].

The method also helps to define a measure of errors in estimating total endowment of the study area. The main source of error is the uncertainty in identifying endowed (favorable) versus unendowed (unfavorable) portions based on selected favorability threshold value. If the threshold value is too high the method will under-estimate the true endowment; whereas if the threshold is too low the method will over-estimate true endowment. A trial-and-error method is employed to select a threshold value to minimize the two errors. As a result, the method produces an area normalized measure of error [33]. A hypothetical example of an assessment is discussed by [33], who also note that the one-level prediction method was applied to estimate total uranium endowment for the main host rock unit, the Westwater Canyon Member. The estimated values of 2.6 Mt U_3O_8 with an estimated error of 0.25 Mt U_3O_8 was roughly twice that obtained by the NURE method but was similar to the values assessed by [4].

McCammon and Kork [33] emphasize that the amount of data required to apply this method is far greater than the data usually collected in most regional resource assessments. As a result, this method is more limited in application than the three-part USGS method.

6.3.5. Method combining mineral prospectivity mapping (MPA) and mineral resource assessment (MRA)

In recent years, attempts have been made to combine methods of mineral prospectivity mapping (MPA) and mineral resource assessment (e.g., [122–124]. A number of different GIS-based methods can be used to map prospectivity/favorability in a study area. The prospectivity maps are then combined with either one-level prediction method or with three-part USGS method to estimate mineral resources in undiscovered deposits.

6.3.5.1. Mineral prospectivity mapping combined with one-level prediction method

This approach was developed by [123] and [124]. The approach employs data-driven evidential belief functions for prospectivity mapping [124]. Therefore, the method is applicable to areas with known deposits and/or prospects of the assessed type. The presence of these deposits and prospects in an area is used to establish spatial relations between them and geological features extracted from geological, geophysical and geochemical datasets. The assessment is generally carried out in a number of discrete steps [123, 124]:

Analysis of spatial relations between known deposits and prospects in the area with geological, geophysical and geochemical features. This results in the recognition of spatial criteria for prospectivity mapping. Carranza and Sadeghi [124] used fractal and Fry analyses to study spatial relations, which are described as indices of prospectivity.

Calculations and integration of indices of prospectivity to produce a mineral prospectivity map of the study area (Fig. 30). Carranza and Sadeghi [124] used the Dempster-Shafer theory of evidence to develop their method of employing evidential belief functions. This is because the methods allow explicit representation of both evidence uncertainty and of missing data (Fig. 30).

Estimation of number of undiscovered deposits and of resources associated with them. A modified one-level prediction method is used for this purpose.

As discussed earlier, one-level prediction method requires a unit cell by which a study area and the control region are divided and have sufficient information to estimate: (a) favorability of deposits to occur; (b) degree of exploration; and (c) known endowment in order to derive mineral deposit or resource density. The one-level prediction method used by [124] proceeds in a number of discrete steps:

- Reclassification of the prospectivity map into a binary favorability map based on a threshold favorability factor. This map shows two types of areas: favorable and unfavorable;
- Representation and measuring of degree of exploration in the area. The degree of exploration is estimated from the number of known deposits, prospects, occurrences and drill holes in the control area;
- Calibration of estimate parameters for one-level prediction. The calibration is conducted by first selecting control cells for calibration. The control cells can be selected either subjectively by experts or objectively based on the presence known deposits, prospects and occurrences;
- Estimation of undiscovered endowment/resources.

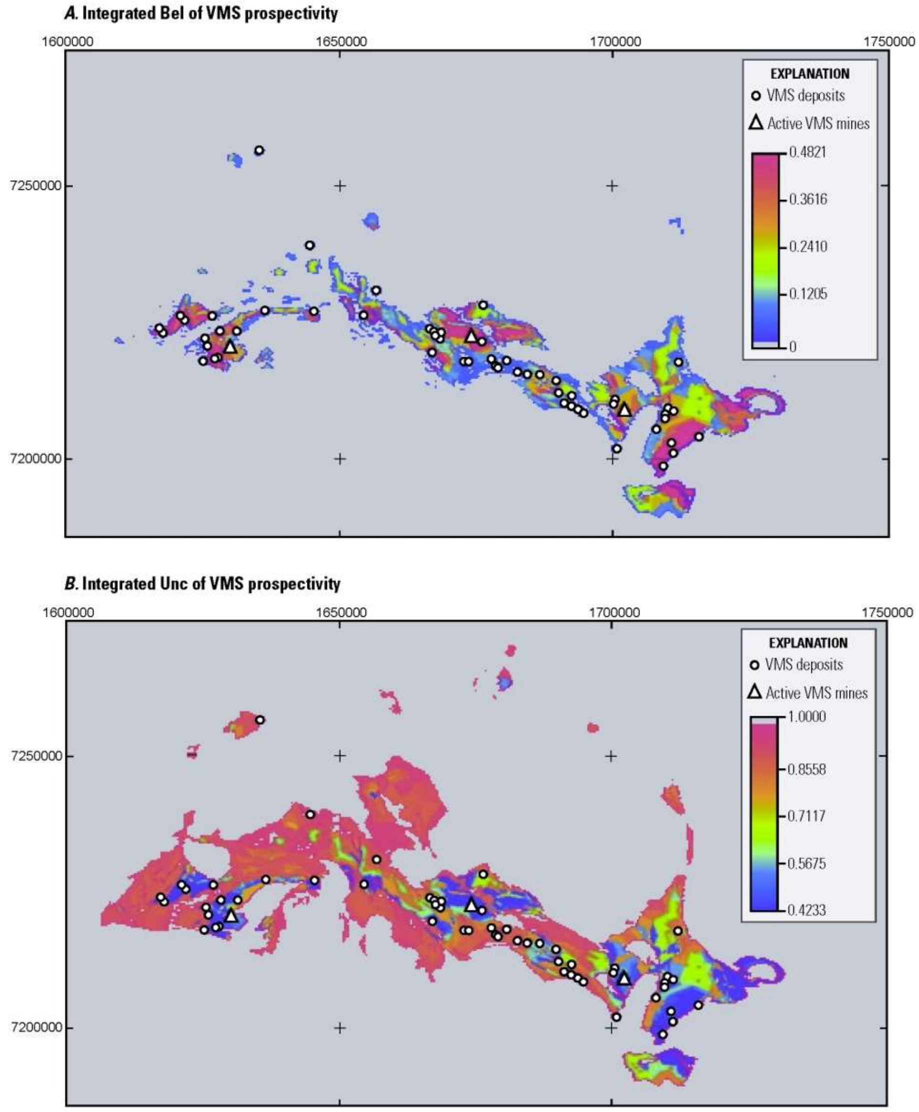

FIG. 30. Maps showing indices of prospectivity for volcanic associated massive sulfide deposits in the Skellefte District, Sweden (modified from [124]). A: integrated Bel (belief function) and, B: integrated Unc (uncertainty).

Each unit area cell is classified as either endowed (contains a deposit or a prospect) and unendowed (does not contain a deposit or a prospect). Each endowed cell is then allocated a score equal to the metal endowment (i.e., product of grade and ore tonnage). As a result, the unendowed cells get a score of zero. The map of endowed and unendowed cell is combined with the binary prospectivity map (map showing prospective and unprospective cells). The combination produces four types of cells: (a) prospective-endowed (*pm*); (b) prospective-unendowed (*pum*); (c) unprospective-endowed (*upm*); and (d) unprospective-unendowed (*upum*).

One-level prediction method defines total metal endowments of the area as the sum of known and undiscovered endowment. The known endowment is the sum of metal endowment of each of endowed cell (*pm*). The unknown endowment is calculated by totaling resources in the prospective-unendowed cells (*pum*). This is obtained by first estimating a proportionality constant C, which represents resource density in the control area. The method computes fractions of unexplored area in each of the prospective-unendowed (*pum*) cells. This fraction is multiplied by the prospectivity score of that cell. The product the two is summed for all prospective-unendowed cells in the study area. The unknown endowment is obtained by multiplying this total with the proportionality constant (resource density).

Mathematical equations and other details of the method are described in [124], which presents a good case study that summarizes assessments of undiscovered resources in the volcanic massive sulfide deposits in Skellefte district, Sweden. The study showed that the district contains an average unknown endowment of 0.709 Mt of Cu and ~3.19 Mt Zn. The method also estimated unknown endowments of ore tonnages (~95 Mt).

6.3.5.2. Mineral prospectivity mapping combined with three-part USGS method

As mentioned in section 5.3.3, the first step in the three-part method of quantitative resources assessment is to delineate geologically-permissive tracts. Scott and Dimitrakopoulos [122] used the WofE method to prepare a prospectivity map of porphyry copper deposits in the Yarrol Province, Queensland, Australia.

The quantitative assessment used global grade and tonnage data of porphyry copper deposits [119]. The estimates of the number of undiscovered deposits at three quantiles (90th, 50th, and 10th) were produced on the basis of three models (approaches). The first approach used exploration and geological information available in the Mount Morgan control area. The second approach relied on: (a) estimates based on the government regional scientific information available over the entire study area; and (b) results of earlier prospectivity modeling. The third approach used base-rate estimates from areas both favorable for the occurrence and well explored for porphyry copper deposits [122].

The estimates of undiscovered deposits showed no deposits at the 90th percentile, and a relatively high number (more than 3 and 4) between the 50th and 10th percentiles. This suggested that, whereas there was limited confidence based on current knowledge of a deposit being present, there was evidence that potential remains for undiscovered deposits in the area. It needs to be emphasized that the estimates of the numbers undiscovered deposits is valid for the whole study area and not for separate highly prospective areas delineated on the prospectivity map produced from the WofE modeling.

Mihalasky [125] reports the use a similar combination of methods to conduct quantitative assessment of undiscovered uranium resources of roll-front uranium deposit in the Texas Coastal Plain. The assessment used WofE modeling to produce prospectivity maps of roll-front deposits in the study area. The evidence maps for the assessment were generated from the analysis of spatial relations between known deposits and prospects (254 points) and several geological, geochemical and geophysical features. Out of 18 evidence maps, 10 maps were found useful to delineate three different tract maps. Each tract map was classified into prospective, favorable and geologically-permissive areas. Quantitative assessment used a robust local grade-and-tonnage model of roll-front deposits. A panel of expert geologists estimated number of deposits in each of the tracts at five different quantiles (90th, 50th, 10th, 5th, and 1st). Monte-Carol simulation was used to produce cumulative frequency values of undiscovered uranium resources.

7. CONCLUSIONS AND REC0MMENDATIONS

This review aimed to present a ‘geologist-friendly’ summary of basic concepts and methods of qualitative and quantitative assessment of undiscovered resources. Therefore, the focus is more on simple description of methods and their usefulness without going into details of the mathematical and probabilistic frameworks underpinning these methods. Comprehensive discussion of this theoretical framework can be found in several benchmark papers that have been referred to in the review.

The review only includes a few case studies. This is principally because it is intended to be an introduction to a series of separate contributions dealing with case studies. References to important case studies are included in this review and details are provided in the bibliography. The main aim of the review was to provide sufficient information to the end users so that they can select one or the other methods based on their specific needs and objectives.

7.1. Conclusions

The main conclusions of the review are:

Quantitative assessment of undiscovered mineral resources begins with and relies on effective methods of qualitative assessment of mineral potential or prospectivity of target areas. The main task of this assessment is to produce a map of that shows areas prospective for or favorable to form an economic-grade mineralization. Such maps are called geologically-permissive tracts or prospectivity maps. GIS-based techniques allow production of more detailed prospectivity and favorability maps. In the 3-part USGS method of assessment, delineation of geologically-permissive tract (with or without classification into areas ranked on some scale of prospectivity or favorability) is an important step because estimates of number of undiscovered deposits and, therefore, of undiscovered resources depends on the size of the geologically-permissive tract.

The selection of an appropriate method depends on the principal objective of the assessment. However, methods that are spatial (i.e., produce a map to show the results of assessment) are more useful than non-spatial methods. Similarly, methods that first estimate number of undiscovered deposits followed by estimates of resources are preferable than methods that directly estimate tonnage of the commodity. Although deterministic methods can be useful, probabilistic methods can provide some measure of the certainty associated with the assessment. However, availability of geological information in the study area is one the main factors that determine which method will be more appropriate for that area. The principal features of a number of important methods are summarized in Table 8, the aim of which is to assist in the selection of an appropriate method.

No clear definition of brownfield and greenfield areas exists in the literature. For mineral potential modeling, areas with known deposits (mineral occurrences with known resources) can be considered as brownfield areas, whereas those with and without known mineral occurrences of the assessed deposit type can be called greenfield areas. Therefore, in brownfield areas both three-part USGS and one-level prediction methods are thought to be useful. Both these methods can be combined with any of the several methods of qualitative mineral potential assessment (e.g., WofE, neural network, fuzzy logic, Dempster-Shafer). However, for greenfield areas, only three-part USGS method is able to provide robust and reproducible estimates. This is based on the assumption that global grade-and-tonnage and deposit-density models of the assessed deposit type are applicable in the study area.

A number of data- and knowledge-driven methods can be applied to delineate geologically-permissive and prospective tracts. In brownfield or well-explored areas, which are generally data-rich, so-called empirical methods (e.g., WofE, neural network) are often more useful. However, in greenfield or less explored area, which are generally data-poor, so-called conceptual methods (e.g., fuzzy-logic, Dempster-Shafer) are more effective (Fig. 31). In recent years, new hybrid (empirical-conceptual) methods have been developed (Fig. 31). Fuzzy-neural network and fuzzy weight of evidence approaches may provide tools to conduct prospectivity analysis in areas that straddle the divide between brownfield and greenfield areas [95].

Geologically-permissive tracts (or prospective/favorability maps) are delineated using critical features of well-studied deposit types. This information is summarized in descriptive models of deposit type. A process based mineral system approach provides a better strategy to delineate critical features of deposit types. This is principally because deposit-type models generally focus on physical and chemical processes happening at the scale of a deposit. A mineral system approach has been shown to be even more effective for mineral resources assessment at regional and basinal scales.

TABLE 8. METHODS OF QUALITATIVE AND QUANTITATIVE ASSESSMENT AND THEIR MAIN FEATURES

Method\feature	Qualitative/ Quantitative[1]	Deterministic/ probabilistic	Objective/ subjective probabilistic	Data-/ knowledge-driven	Brown/green-fields[2]	Spatial/non-spatial	Certainty	Useful for
Boolean logic	Qualitative	Probabilistic	Subjective	Hybrid	Both	Spatial	Defined	Exploration targeting, land-use decision
Index overlay	Qualitative	Probabilistic	Subjective	Hybrid	Both	Spatial	Undefined	Exploration targeting, land-use decision
Fuzzy logic	Qualitative	Probabilistic	Subjective	Hybrid	Both	Spatial	Undefined	Exploration targeting, land-use decision
Dempster-shafer	Qualitative	Probabilistic	Subjective	Hybrid	Both	Spatial	Defined	Exploration targeting, land-use decision
PRSOPECTOR/ expert systems	Qualitative	Probabilistic	Subjective	Hybrid	Both	Spatial	Undefined	Exploration targeting, land-use decisions
WofE	Qualitative	Probabilistic	Objective	Hybrid	Brown	Spatial	Undefined	Exploration targeting, land-use decision
Logistic regression	Qualitative	Probabilistic	Objective	Hybrid	Brown	Spatial	Undefined	Exploration targeting, land-use decision
Neural network	Qualitative	Probabilistic	Objective	Hybrid	Brown	Spatial	Undefined	Exploration targeting, land-use decisions
Zipf's law	Quantitative	Deterministic	Objective	Data	Brown	Non-spatial	Undefined	Resource inventory, exploration risk, land-use decision

Method\feature	Qualitative/ Quantitative[1]	Deterministic/ probabilistic	Objective/ subjective probabilistic	Data-/ knowledge-driven	Brown/green-fields[2]	Spatial/non-spatial	Certainty	Useful for
Spatial occurrence model of Allais (1957)	Quantitative	Probabilistic (Poisson)	Objective	Data	Green	Non- spatial	Undefined	Resource inventory, exploration risk, land-use decision
NURE	Quantitative	Probabilistic	Subjective	Hybrid	Both	Spatial	Undefined	Resource inventory, exploration targeting, land-use decision
DSF (deposit-size frequency)	Quantitative	Probabilistic	Subjective	Hybrid	Both	Spatial	Undefined	Resource inventory, exploration targeting, land-use decision
3 Part USGS	Quantitative	Probabilistic	Both	Hybrid	Both	Spatial	Undefined	Resource inventory, exploration risk, land-use decision
One-level prediction	Quantitative	Probabilistic	Both	Hybrid	Brown	Spatial	Defined	Exploration targeting, resource inventory, land-use decision
Combination of MPA and 3 Part USGS[3]	Quantitative	Probabilistic	Both	Hybrid	Both	Spatial	Undefined	Exploration targeting, resource inventory, land-use decision
Combination of MPA and one-level prediction[2]	Quantitative	Probabilistic	Both	Hybrid	Brown	Spatial	Defined	Exploration targeting, resource inventory, land-use decision

[1]Quantitative methods rely on delineation of prospective tracts (or prospectivity/favorability zones) which represent qualitative assessment.
[2]There no clear definition of brownfield and greenfield areas. For mineral potential modeling areas with known deposits (mineral occurrences with resources can be considered as brownfield areas, whereas those with and without known mineral occurrences of the assessed deposit style can be called greenfield areas.
[3]MPA (mineral potential assessment or qualitative assessment) employing any one of the many GIS-based methods of prospectivity analysis.

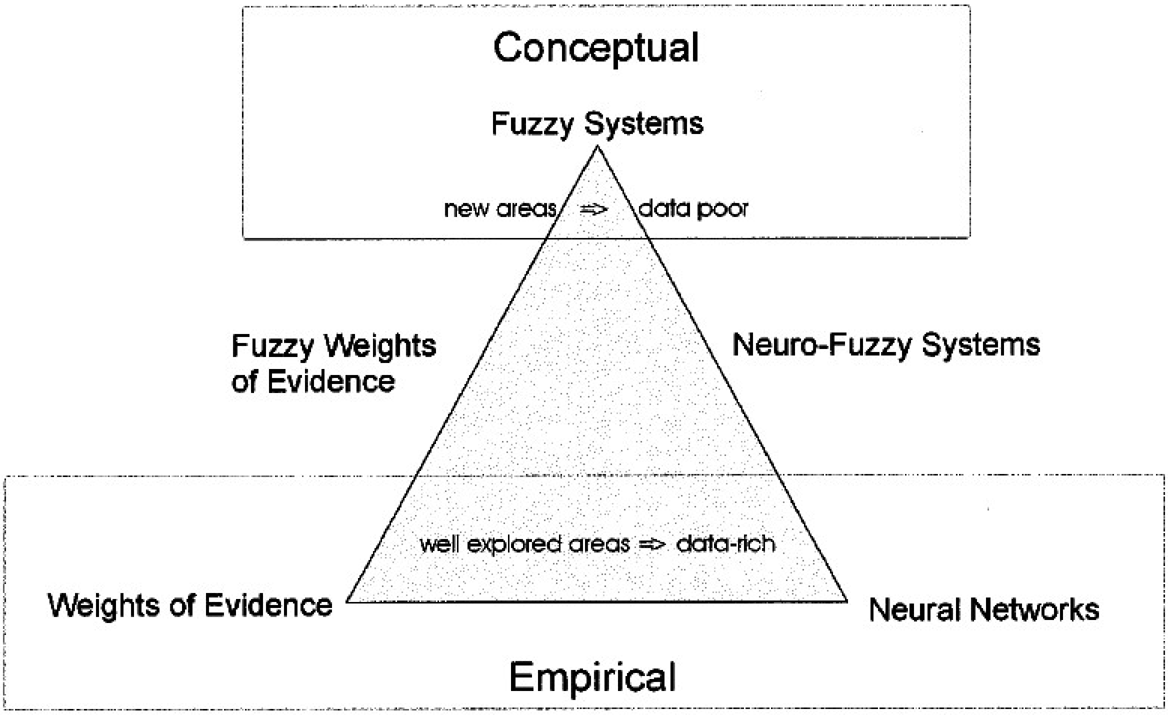

FIG. 31. Figure showing relationship of hybrid fuzzy-neural network systems and fuzzy WofE approaches to main empirical and conceptual methods of mineral potential modeling. Both WofE and neural network approaches require large amount of data, generally available in well-explored or brown-field area. However, fuzzy systems which are dominantly knowledge-driven, can be more successfully applied in not so well-explored or green-field areas where generally data are not so widely available [95]. Figure is reproduced with permission from the copyright owner International Association of Mathematical Geosciences.

7.2. Recommendations

The main recommendations of the review are:

Descriptive models of deposit types require updating to make them compatible with a process based mineral-system approach. This review includes a preliminary mineral-system classification of uranium mineral systems (Table 1). In this classification, clans of uranium mineral systems are subdivided into groups and groups are subdivided into subgroups. This classification is identical with IAEA's classification of uranium deposit type at the subgroup and deposit-type levels (Table 1). It will be useful to develop templates of uranium mineral systems for each of the mineral-system subgroup. Three examples of templates (unconformity-related, sandstone- and calcrete-hosted uranium) are included in this review. Similar templates can be produced for other mineral systems (e.g., intrusive anatectic, intrusive magmatic, metasomatic, intrusive-related, volcanic-related mineral systems). It is believed that a mineral-system approach will assist in producing more robust geologically-permissive tracts for quantitative assessments.

Grade-and-tonnage models of deposits types are one of the most critical components of any quantitative mineral resource assessment. It is essential that such models are developed for all uranium deposit types. This exercise can be undertaken by using grade and tonnage data stored in IAEA's UDEPO database. However, before undertaking this exercise, it is important to conduct a thorough QC (quality control) and QA (quality assurance) of the stored data. The exercise also requires that a uniform proximity rule is applied to aggregate and disaggregate resource data. Such proximity rules have been used for other deposit types. For instance, a distance of 1.6 km was used to aggregate and disaggregate data for Au-quartz veins [62]. Recently, Singer et al. [126] (this volume), used a distance of 250 m to reassess resource data for unconformity-related uranium deposits in the Pine Creek Orogen, Australia.

Deposit-density models are equally critical for quantitative assessment of undiscovered resources. Unfortunately, no such models exist for uranium deposits. It is important that this task is prioritized. Density of deposits can be estimated either for geologically-permissive areas or for geologically-permissive basins and sub-basins. As sandstone-uranium and unconformity-related uranium deposits are the most common types of uranium deposit, it is recommended that deposit-density models for these types could be developed first.

Delineation of geologically-permissive tracts and prospective area requires, identifying mappable signatures of critical features of uranium deposits types and mineral systems. It will be useful to initiate workshops to produce matrices of mappable signatures of uranium deposit types and mineral systems useful at different scales (regional, basinal and district).

REFERENCES

[1] ALLAIS, M., Method of Appraising Economic Prospects of Mining Exploration over Large Territories: Algerian Sahara Case Study. Management Science, 3(4), 285-347 (1957).

[2] SINGER, D.A., MENZIE, W.D., Quantitative Mineral Resource Assessments – An Integrated Approach, Oxford University Press, New York, 219p (2010).

[3] HARRIS, D.P., Mineral resource appraisal: mineral endowment, resources, and potential supply: concepts, methods and cases, Oxford, Oxford University Press (1984).

[4] HARRIS, D. P., CARRIGAN, F. J., Estimation of uranium endowment by subjective analysis- a comparison of methods and estimates for the San Juan Basin, New Mexico: Economic Geology, 76, 1032-1055 (1981).

[5] FINCH, W. I., GRANGER, H. C., LUPE, R., MCCAMMON, R. B., Genetic-geological models - a systematic approach to evaluate geologic favorability for undiscovered uranium resources, Part I, Research on uranium resource models, a progress report: US Geological Survey (1980).

[6] HARRIS, D. P., AGTERBERG, F. P., The appraisal of mineral resources: Economic Geology, 75th anniversary volume, 897-938 (1981).

[7] SINGER, D. A., MOSIER, D. L., A review of regional mineral resource assessment methods: Economic Geology, 76, 1006-1015 (1981).

[8] MIEZITIS, Y., BATTEY, G. C., Subjective quantitative assessment of the mineral potential of the Conservation Zone: (excluding gold-platinum-palladium resource at Coronation Hill), Canberra, Bureau of Mineral Resources, Geology and Geophysics, 17 p (1990).

[9] ABARE, Lake Eyre Basin: an economic and resource profile of the South Australian portion, Canberra, ABARE (Australian Bureau of Agriculture and Resource Economics), ABARE research report, 96.1 (1996).

[10] ZIPF, G. K., Human Behavior and the Principle of Least Effort: An Introduction to Human Ecology. Reading, MA, Addison-Wesley (1949).

[11] MERRIAM, D. F., DREW, L. J., SCHUENEMEYER, J. H., Zipf's Law: A viable geological paradigm? Natural Resources Research, 13, 265-271 (2004).
[12] BANKEY, V., SOULLIERE, J., TOTH, M. I., DERSCH, J. S., Mineral resource potential and geology of the Routt National Forest and the Middle Park Ranger District of the Arapaho National Forest, Colorado, Volume U.S. Geological Survey Professional Paper 1610: Washington, U.S. Geological Survey, 124 (2000).
[13] DUBRAY, E. A., BLANK (JR), J. R., WOOD, R. H., Mineral resources, geology, and geophysics of the Worthington Mountains Wilderness Study Area, Lincoln County, Nevada, Volume U.S. Geological Survey Bulletin 1728-A: Washington, U.S. Geological Survey, 20 (1986).
[14] TAYLOR, R. B., STONEMAN, R. J., MARSH, S. P., An assessment of the mineral resource potential of the San Isabel National Forrest, South-Central Colorado, U.S. Geological Survey Bulletin, Volume 1638, U.S. Geological Survey, 48 (1984).
[15] BUREAU OF RESOURCE SCIENCES, NEW SOUTH WALES GEOLOGICAL SURVEY, Assessment of mineral resources in the Eden CRA study area (1998).
[16] BARNES, R. G., JAIRETH, S., MIEZITIS, Y., SUPPEL, D. W., Regional mineral potential assessment for land use planning: GIS-based examples from Eastern Australia, Volume 4-99, Australasian Institute of Mining and Metallurgy, 601-605 (1999).
[17] PORWAL, A.K., KREUZER, O.P., "Introduction to the Special Issue: Mineral prospectivity analysis and quantitative resource estimation", Ore Geology Reviews 38, 121-127 (2010).
[18] BONHAM-CARTER, G.F., "Geographic Information Systems for Geoscientists, Modelling with GIS". Pergamon, Ontario, 398p. (1994).
[19] JAIRETH, S., MIEZITIS, Y., OZPOT GIS: geoprovince-scale assessment of mineral potential, Volume 2015: Canberra, Geoscience Australia (2004).
[20] KREUZER, O.P., MARKWITZ, V., PORWAL, A.K., MCCUAIG, T.C., "A continental-wide study of Australia's uranium potential. Part I: GIS-assisted manual prospectivity analysis", Ore Geology Reviews 38, 334-366 (2010).
[21] CARRANZA, E.J.M., "Data-driven evidential belief modeling of mineral potential using few prospects and evidence with missing values", Natural Resources Research 24, 291-304 (2015).
[22] IAEA, Methods for the estimation and economic evaluation of undiscovered uranium endowment and resources: an instruction manual, Volume Technical Report Series 344: Vienna, IAEA, 145p (1992).
[23] IAEA, Spatial data integration for mineral exploration, resource assessment and environmental studies: a guidebook, Volume IAEA-TECDOC-782: Vienna, IAEA, 190p (1994).
[24] TAYLOR, R. B., STEVEN, T. A., Definitions of mineral resource potential: Economic Geology, 78, 1268-1270 (1983).
[25] SINGER, D.A., Progress in integrated quantitative mineral resource assessments. Ore Geology Reviews 38, 242-250 (2010).
[26] COX, D. P., BARTON, R., SINGER, D. A., Introduction, in Cox, D. P., Singer, D. A., eds., Mineral Deposit Models, Volume U.S. Geological Survey Bulletin 1693, U.S. Geological Survey, 1-10 (1986).
[27] MCKELVEY, V.E., Mineral resource estimates and public policy. American Scientist, 60, 3240 (1967).
[28] MCKELVEY, E., Relations of reserves of the elements to their crustal abundance: American Journal of Science, 258-A, 234-241 (1960).

[29] ERICKSON, R. L., Crustal abundance of elements, and mineral resources, in Brobst, D. A., Pratt, W. P., eds., United States Mineral Resources, Volume Geological Survey Professional Paper 820: Washington DC, U.S. Geological Survey, 21-25 (1973).
[30] KESLER, S. E., WILKINSON, B. H., Earth's copper resources estimated from tectonic diffusion of porphyry copper deposits: Geology, 36, 255-258 (2008).
[31] WILKINSON, B. H., KESLER, S. E., Tectonic-diffusion estimate of orogenic gold resources: Economic Geology, 105, 1321-1334 (2010).
[32] JOHNSON, K. M., HAMMARSTROM, J. M., ZIENTEK, M. L., DICKE, C. L., Estimate of undiscovered copper resources of the world, 2013, Volume U.S. Geological Survey Fact Sheet 2014-3004, 3 (2014).
[33] MCCAMMON, R. B., KORK, J. O., One-level prediction - a numerical method of estimating undiscovered metal endowment: Nonrenewable Resources, 1, 139-147 (1992).
[34] MAGOON, L. B., DOW, W. G., The petroleum system: AAPG Memoir, 60, 3-24 (1991).
[35] WYBORN, L.A.I., HEINRICH, C. A., JAQUES, A.L., Australian Proterozoic mineral systems: essential ingredients and mappable criteria, Australasian Institute of Mining and Metallurgy Annual Conference Proceedings, 109–115 (1994).
[36] KNOX-ROBINSON, C.M., WYBORN, L.A.I., Towards a holistic exploration strategy: Using geographic information systems as tool to enhance exploration, Australian Journal of Earth Sciences 44, 453-463 (1997).
[37] WALSHE, J. D., COOKE, D. R., NEUMAYR, P., Five questions for fun and profit: a mineral system perspective on metallogenic epochs, provinces, and magmatic hydrothermal Cu and Au deposits, in Mao, J., Bierlein, F., eds., Mineral deposit research: meeting the global challenge: Berlin, Springer, 477-480 (2005).
[38] SKIRROW, R. G., JAIRETH, S., HUSTON, D. L., BASTRAKOV, E. N., SCHOFIELD, A., VAN DER WIELEN, S. E., BARNICOAT, A. C., Uranium Mineral Systems: processes, exploration and a new deposit framework, Volume Geoscience Australia Record 2009/20: Canberra, Geoscience Australia, 45 (2009).
[39] JAQUES, A. L., JAIRETH, S., WALSHE, J. D., Mineral systems of Australia: an overview of resources, settings and processes: Australian Journal of Earth Sciences, 49, 623-660 (2002).
[40] PHILLIPS, G. N., GROVES, D. I., KERRICH, R., Factors in the formation of the giant Kalgoorlie gold deposit: Ore Geology Reviews, 10, 295-317 (1996).
[41] HAGEMANN, S. G., CASSIDY, K. F., Archean orogenic lode gold deposits: Reviews Economic Geology, 13, 9-68 (2000).
[42] HUSTON, D.L., BRAUHART, C.W., FOLKERT, S., DAVIDSON, G.J., GROVES, D.I., Metal leaching and inorganic sulfate reduction in volcanic-hosted massive sulfide mineral systems: evidence from the Paleo-Archean Panorama district, Western Australia. Geology 29:687–690 ((2001).
[43] DAHLKAMP, F.J., Uranium Deposits of the World: USA and Latin America. Springer-Verlag, Berlin, 520p (2009).
[44] DAHLKAMP, F.J., Uranium Ore Deposits, Heidelberg, Springer-Verlag, 460p (1993).
[45] CUNEY, M., Evolution of uranium fractionation processes through time: driving the secular variation of uranium deposit types. Economic Geology, 105, 553-569 (2010).
[46] BRUNETON, P., CUNEY, M., DAHLKAMP, F. J., ZALUSKI, G., IAEA geological classification of uranium deposits, URAM-2014: Vienna, IAEA, 12-13 (2014).
[47] IAEA, 2009, World distribution of uranium deposits (UDEPO) with uranium deposit classification, Volume IAEA-TECDOC-1629: Vienna, IAEA, 118.

[48] JAIRETH, S., HOATSON, D. M., MIEZITIS, Y., Geological setting and resources of the major rare-earth-element deposits in Australia: Ore Geology Reviews, 62, 72-128 (2014).
[49] CUNEY, M., KYSER, K., Deposits related to magmatic differentiation, in Cuney, M., Kyser, K., eds., Recent and not-so-recent developments in uranium deposits and implications for exploration, Volume Short Course Series Volume 39: Quebec, Mineralogical Association of Canada, 57-77 (2009).
[50] CUNEY, M., KYSER, K., Deposits related to partial melting, in Cuney, M., Kyser, K., eds., Recent and not-so-recent developments in uranium deposits and implications for exploration, Volume Short Course Series Volume 39: Quebec, Mineralogical Association of Canada, 79-95 (2009).
[51] CUNEY, M., KYSER, K., Hydrothermal uranium deposits related to igneous rocks, in Cuney, M., Kyser, K., eds., Recent and not-so-recent developments in uranium deposits and implications for exploration, Volume Short Course Series Volume 39: Quebec, Mineralogical Association of Canada, 117-160 (2009).
[52] HOLLAND, H. D., The oxygenation of the atmosphere and oceans: Philosophical Transactions of the Royal Society of London Series B Biological Sciences, 361, 903-915 (2006).
[53] LALLY, J. H., BAJWAH, Z. U., Uranium deposits of the Northern Territory, Volume Northern Territory Geological Survey Report 20: Darwin, Northern Territory Geological Survey, 87p (2006).
[54] JEFFERSON, C. W., THOMAS, D. J., GANDHI, S. S., RAMAEKERS, P., DELANEY, G., BRISBIN, D., CUTTS, C., PORTELLA, P., OLSON, R. A., Unconformity-associated uranium deposits of the Athabasca Basin, Saskatchewan and Alberta, in Goodfellow, W. D., ed., Mineral deposits of Canada. Geological Association of Canada: Newfoundland, Geological Association of Canada, 273-306 (2007).
[55] KYSER, K., CUNEY, M., Unconformity-related uranium deposits, in Cuney, M., Kyser, K., eds., Recent and not-so-recent developments in uranium deposits and implications for exploration, Volume Short Course Series Volume 39: Quebec, Mineralogical Association of Canada, 161-220 (2009).
[56] MCKAY, A., MIEZITIS, Y., Australia's uranium resources, geology and development of deposits, Volume AGSO-Geoscience Australia Mineral Resource Report 1: Canberra, Geoscience Australia, 195 (2001).
[57] JAIRETH, S., MCKAY, A., LAMBERT, I., Association of large sandstone uranium deposits with hydrocarbons: AusGeo News, 89, 8-12 (2008).
[58] KRAUSKOPF, K.B., Introduction to Geochemistry. McGraw-Hill, New York, 721p (1967).
[59] BASTRAKOV, E. N., JAIRETH, S., T.P., M., Solubility of uranium in hydrothermal fluids at 25¬∞-300¬∞: Implications for the formation of uranium deposits, Volume Geoscience Australia Record 2010/20: Canberra, Geoscience Australia, 86p (2009).
[60] BOYLE, D.R., "The genesis of surficial uranium deposit", Report of the working group on uranium geology organized by the International Atomic Energy Agency, Vienna, IAEA-TECDOC-322, pp. 45-52 (1984).
[61] BUTT, C. R. M., MANN, A. W., HOROWITZ, R. C., Regional setting, distribution and genesis of surficial uranium deposits in calcretes and associates sediments in Western Australia, Surficial Uranium Deposits, Volume IAEA TECDOC-322: Vienna, IAEA, 121-127 (1984).
[62] COX, D. P., SINGER, D. A., Mineral Deposit Models, U.S. Geological Survey Bulletin Volume 1693, U.S. Geological Survey, 400 (1986).

[63] DREW, L. J., Undiscovered petroleum and mineral resources: assessment and controversy, New York, Plenum Press, 210p. (1997).
[64] COWLEY, W. M., Pandurra Formation, in DREXEL, J. F., PREISS, W. V., PARKER, A. J. (eds.), The Geology of South Australia, Volume 1, The Precambrian: Adelaide, 139-142 (1993).
[65] DALY, S., Corunna Conglomerate, in DREXEL, J. F., PREISS, W. V., PARKER, A. J. (eds.), The Geology of South Australia, Volume 1, The Precambrian: Adelaide, 124-126 (1993).
[66] CARRANZA, E. J. M., Geologically-constrained mineral potential mapping [Ph.D.: Delft University of Technology, The Netherlands, 480p (2002).
[67] PORWAL, A. K., Mineral potential mapping with mathematical geological models: ITC PhD Dissertations 130 (2006).
[68] ZIMMERMANN, H. J., Fuzzy set theory and its applications, Boston-Dordrecht-Lancaster, Kluwer-Nijhoff Publishing (1985).
[69] AN, P., MOON, W. M., RENCZ, A., Application of fuzzy set theory for integration of geological, geophysical and remote sensing data: Canadian Journal of Exploration Geophysics, 27, 1-11 (1991).
[70] PORWAL, A., D.R., D., CHAUDHARY, B., GONZALEZ-ÅLVAREZ, I., KREUZER, O. P., Fuzzy inference systems for prospectivity modelling of mineral systems and a case-study for prospectivity mapping of surficial uranium in Yeelirrie area, Western Australia: Ore Geology Reviews, 71, 839-852 (2015).
[71] SCHOFIELD, A., Uranium content of igneous rocks of Australia 1:5 000 000 maps , Explanatory notes and discussion, Volume Geoscience Australia Record 2009/17: Canberra, Geoscience Australia, 20p (2009).
[72] SCHOFIELD, A., Potential for magmatic-related uranium mineral systems in Australia, Volume Geoscience Australia Record 2010/20: Canberra, Geoscience Australia, 56p (2010).
[73] CHUNG, C. F., MOON, W. M., Combination rules of spatial geoscience data for mineral exploration: Geoinformatics, 2, 159-169 (1991).
[74] AN, P., MOON, W. M., BONHAM-CARTER, G. F., Uncertainty management integration of exploration data using the belief function: Nonrenewable Resources, 3, 60-71 (1994).
[75] TANGESTANI, M. H., MOORE, F., The use of Dempster-Shafer model and GIS in integration of geoscientific data for porphyry copper potential mapping, north of Shahr-e-Babak, Iran: International Journal of Applied Earth Observation and Geoinformation, 4, 65-74 (2002).
[76] WRIGHT, D. F., BONHAM-CARTER, G. F., VHMS favourability mapping with GIS-based integration models, Chisel Lake, Anderson Lake area, in Bonham-Carter, G. F., Galley, H., eds., EXTECHI: A Multidisciplinary Approach to Massive Sulfide Research in the Rusty Lake, Snow Lake Greenstone Belts, Manitoba, Volume Bulletin 426, Geol. Survey Canada, 339-376 (1996).
[77] DUDA, R. O., The Prospector system for mineral exploration: Final Report SRI Project 8172, SRI International, Menlo Park, California (1980).
[78] MCCAMMON, R.B., Prospector II, The Annual AI Systems in Government Conference Proceedings, March 27-31: Washington, D.C., 88-92 (1989).
[79] GASCHNIG, J., Development of uranium exploration models for the Prospector consultant system for mineral exploration. Final Report, SRI Project 7856: Stanford Research Institute International, Menlo Park, California (1980).

[80] BONHAM-CARTER, G. F., AGTERBERG, F. P., WRIGHT, D. F., Integration of geological datasets for gold exploration in Nova Scotia: Photogrammetric Engineering and Remote Sensing, 54, 1585-1592 (1988).
[81] WATSON, G. P., RENCZ, A. N., BONHAM-CARTER, G. F., Computers assist prospecting: Geos, 18, 8-15 (1989).
[82] AGTERBERG, F. P., BONHAM-CARTER, G. F., WRIGHT, D. F., Statistical pattern integration for mineral exploration, in Gaal, G., Merriam, D. F., eds., Computer applications in resource estimation prediction and assessment for metals and petroleum: Oxford-New York, Pergamon Press, 1-21 (1990).
[83] PORWAL, A., GONZALEZ-ALVAREZ, I., MARKWITZ, V., MCCUAIG, T., MAMUSE, A., Weights-of-evidence and logistic regression modeling of magmatic nickel sulfide prospectivity in the Yilgarn Craton, Western Australia: Ore Geology Reviews, 38, 184-196 (2010).
[84] AGTERBERG, F. P., Application of recent developments of regression analysis in regional mineral resource evaluation, in Chung, C. F., Fabbri, A. G., Sinding-Larsen, R., eds., Quantitative Analysis of Mineral and Energy Resources: Dordrecht, D. Reidel Publishing Company, 1-28 (1988).
[85] CHUNG, C. F., AGTERBERG, F. P., Regression models for estimating mineral resources from geological map data: Mathematical Geology, 12, 472-488 (1980).
[86] CHUNG, C. F., AGTERBERG, F. P., Poisson regression analysis and its application, in Chung, C. F., Fabbri, A. G., Sinding-Larsen, R., eds., Quantitative Analysis of Mineral and Energy Resources: Dordrecht, D. Reidel Publishing Company, 29-36 (1988).
[87] REDDY, R. K. T., BONHAM-CARTER, G. F., WRIGHT, D. F., GIS for mapping mineral resource potential: Preliminary results of base-metal study, Snow Lake area, Manitoba, Proceedings, GIS for the 1990s Conference, 384-400 (1990).
[88] REDDY, R. K. T., AGTERBERG, F. P., BONHAM-CARTER, G. F., Application of GIS-based logistic models to base-metal potential mapping in Snow Lake area, Manitoba, Proceedings, Canadian Conference on GIS, 607-618 (1991).
[89] CARRANZA, E. J. M., HALE, M., Logistic regression for geologically-constrained mapping of gold mineralization potential, Baguio district, Philippines. Exploration and Mining Geology, 10 (3), 165-175 (2001).
[90] AGTERBERG, F. P., Combining indicator patterns in weights of evidence modeling for resource evaluation: Nonrenewable Resources, 1, 39-50 (1992).
[91] AGTERBERG, F. P., BONHAM-CARTER, G. F., CHENG, Q., WRIGHT, D. F., Weights of evidence modeling and weighted logistic regression in mineral potential mapping, in DAVIS, J. S., HERZFELD, U. C. (eds.), Computers in Geology: New York, Oxford University Press, 13-32 (1993).
[92] BROWN, W. M., GEDEON, T., GROVES, D., BARNES, R., Artificial neural networks: a new method for mineral prospectivity mapping: Australian Journal of Earth Sciences, 47, 757-770 (2000).
[93] SINGER, D. A., KOUDA, R., Application of feedforward neural network in the search of Kuroko deposits in the Hokoruku district, Japan: Mathematical Geology, 28, 1017-1023 (1996).
[94] SINGER, D. A., KOUDA, R., A comparison of the weights-of-evidence methods and probabilistic neural networks: Natural Resources Research, 8, 287-298 (1999).
[95] BROWN, W., GROVES, D., GEDEON, T., Use of fuzzy membership input layers to combine subjective geological knowledge and empirical data in a neural network method for mineral-potential mapping: Natural Resources Research, 12, 183-200 (2003).

[96] PORWAL, A., CARRANZA, E., HALE, M., Artificial neural networks for mineral-potential mapping: a case study from Aravalli Province, Western India: Natural Resources Research, 12, 155-171 (2003).
[97] RIGOL-SANCHEZ, J., CHICA-OLMO, M., ABARCA-HERNANDEZ, F., Artificial neural networks as a tool for mineral potential mapping with GIS: International Journal of Remote Sensing, 24, 1151-1156 (2003).
[98] LEE, S., OH, H.-J., Application of artificial neural network for mineral potential mapping, in Hui, C. L. P., ed., Artificial Neural Networks - Applications: Shanghai, In Tech, 67-104 (2011).
[99] WANG, G., ZHANG, S., YAN, C., SONG, Y., SUN, Y., LI, D., XU, F., Mineral potential targeting and resource assessment based on 3D geological modeling in Luanchuan region, China: Computers & Geosciences, 37, 1976-1988 (2011).
[100] SINGER, D. A., KOUDA, R., Classification of mineral deposit types using mineralogy with a probabilistic neural network: Nonrenewable Resources, 6, 69-81 (1997).
[101] SINGER, D. A., KOUDA, R., Typing of mineral deposits using their grades and tonnages in an artificial neural network: Natural Resources Research, 12, 201-208 (2003).
[102] LOWELL, J.D., Copper resources: Mining Engineering, 22, 67-73 (1970).
[103] PALIWAL, H., BHATNAGAR, S., HALDAR, S., Lead-zinc resource prediction in India: An application of Zipf's law: Mathematical geology, 18, 539-549 (1986).
[104] FALLON, M., PORWAL, A., GUJ, P., Prospectivity analysis of the Plutonic Marymia Greenstone Belt, Western Australia. Ore Geology Reviews, 38(3), 208-218 (2010).
[105] MAMUSE, A., GUJ, P., Rank statistical analysis of nickel sulphide resources of the Norseman-Wiluna Greenstone Belt, Western Australia: Mineralium Deposita, 46, 305-318 (2011).
[106] FINCH, W.I., MCCAMMON, R.B., Uranium assessment by the Geological Survey: proposed methodology and a plan to update the national resource base. U.S. Geological Survey Circular 994, 31p (1987).
[107] RICHTER, D. H., SINGER, D. A., COX, D. P., Mineral resource map of the Nabesna Quadrangle, Alaska, Volume U.S. Geological Survey Miscellaneous Field Studies Map MF-655K, U.s. Geological Survey (1975).
[108] SINGER, D. A., Mineral resources models and the Alaskan Mineral Resource Assessment Program, in VOGELY, W. A. (ed.), Mineral material modelling: a state-of-the-art review: Baltimore, John Hopkins University Press, 370-382 (1975).
[109] CUNNINGHAM, C.G., ZAPPETTINI, E.O., VIVALLO S., WALDO, CELADA, C.M., QUISPE, JORGE, SINGER, D.A., BRISKEY, J.A, SUTPHIN, D.M., GAJARDO M., MARIANO, DIAZ, ALEJANDRO, PORTIGLIATI, CARLOS, BERGER, V.I., CARRASCO, RODRIGO, AND SCHULZ, K.J., Quantitative mineral resource assessment of copper, molybdenum, gold, and silver in undiscovered porphyry copper deposits in the Andes Mountains of South America, U.S. Geological Survey Open-File Report 2008-1253, 282p (2008).
[110] LISITSIN, V., MOORE, D., OLSHINA, A., WILLMAN, C., Undiscovered orogenic gold endowment in Northern Victoria, Australia: Ore Geology Reviews, 38, 251-269 (2010).
[111] HAMMARSTROM, J. M., LUNDINGTON, S., ROBINSON, G. R., BOOKSTROM, A., ZIENTEK, M. L., MIHALASKY, M. J., ZURCHER, L., BERGER, B. B., DICKEN, C. L., FLOYD, G. R., Undiscovered Phanerozoic porphyry copper deposits - a global assessment: Acta Geologica Sinica (English Edition), 88 (sup 2), 532-534 (2014).

[112] SINGER, D. A., Basic concepts in three-part quantitative assessments of undiscovered mineral resources: Nonrenewable Resources, 2, 69-81 (1993).
[113] JAIRETH, S., ROACH, I.C., BASTRAKOV, E., LIU, S., Basin-related uranium mineral systems in Australia: A review of critical features. Ore Geology Reviews, 76, 360-394 (2016).
[114] MOSIER, D. L., PAGE, N. J., Descriptive and grade-tonnage models of volcanogenic manganese deposits: a modification, Volume U.S. Geological Survey Bulletin 1811: Washington, D.C., U.S. Geological Survey (1988).
[115] BLISS, J. D., Grade-tonnage and other models for diamond kimberlite pipes: Nonrenewable Resources, 1, 214-230 (1992).
[116] COX, D.P., LINDSEY, D.A., SINGER, D.A., DIGGLES, M.F., Sediment-hosted copper deposits of the world—deposit models and database: US Geological Survey Open-File Report 03-107 (2003).
[117] SINGER, D. A., BERGER, I., MENZIE, W. D., BERGER, B. B., Porphyry copper deposit density: Economic Geology, 100, 491-514 (2005).
[118] SINGER, D.A., BERGER, V.I., MORING, B.C., Porphyry copper deposits of the world: database, map, and grade and tonnage models. US Geological Survey Open-File Report, 1060(9) (2005).
[119] SINGER, D. A., MENZIE, W. D., SUTPHIN, D. M., MOSIER, D. L., BLISS, J. D., Mineral deposit density: an update, in Schultz, K. J., ed., Contributions to global mineral resource assessment research, Volume U.S. Geological Survey Professional Paper 1640-A: Washington, D.C., U.S. Geological Survey, A1-A13 (2001).
[120] ROOT, D. H., MENZIE, W. D., SCOTT, W. A., Computer Monte Carlo simulation in quantitative resource estimation: Nonrenewable Resources, 1, 125-138 (1992).
[121] MCCAMMON, R. B., FINCH, W. I., KORK, J. O., BRIDGES, N., An integrated data-directed numerical method for estimating the undiscovered metal endowment in a region: Nonrenewable Resources, 3, 109-122 (1994).
[122] SCOTT, M., DIMITRAKOPOULOS, R., Quantitative analysis of mineral resources for strategic planning: implications for Australian Geological Surveys: Natural Resources Research, 10, 159-177 (2001).
[123] CARRANZA, E. J. M., OWUSU, E. A., HALE, M., Mapping of prospectivity and estimation of number of undiscovered prospects for lode gold, southwestern Ashanti Belt, Ghana: Mineralium Deposita, 44, 915-938 (2009).
[124] CARRANZA, E. J. M., SADEGHI, M., Predictive mapping of prospectivity and quantitative estimation of undiscovered VMS deposits in Skellefte district (Sweden): Ore Geology Reviews, 38, 219-241 (2010).
[125] MIHALASKY, M. J., Roll-front uranium Texas Coastal Plain: quantitative mineral resource assessment, IAEA-U.S. G.S workshop of quantitative mineral resource assessment: Denver (2015).
[126] SINGER, D.A., JAIRETH, S., ROACH, I., A three-part quantitative assessment of undiscovered unconformity-related uranium deposits in the Pine Creek region of Australia. This volume (2017).

A THREE-PART QUANTITATIVE ASSESSMENT OF UNDISCOVERED UNCONFORMITY-RELATED URANIUM DEPOSITS IN THE PINE CREEK REGION OF AUSTRALIA

D.A. Singer
Cupertino, CA 95014
United States

S. Jaireth
Aranda, ACT 2614

I. Roach
Watson, ACT 2602

Australia

Abstract

Information about long-term availability of uranium resources comes from resources in known mineral deposits and estimates of resources in yet-to-be discovered uranium-bearing deposits. Here, we document a proven way to estimate undiscovered uranium resources in unconformity-related deposits in an important region of Australia. The assessment starts with a new descriptive model of geologic settings used to guide delineation of where (geologically-permissive tract) deposits could occur. A grade-and-tonnage model is constructed following spatial rules to provide guidance on frequencies of grades, tonnages and contained uranium in undiscovered deposits. Number of undiscovered deposits is estimated probabilistically from geologically-permissive areas and median size of deposits is estimated using a generalized deposit density regression model. In the Pine Creek Region there is a 90% chance of 9 and a 50% chance of 25 or more undiscovered deposits. Using Monte Carlo simulation, probabilistic estimates of number of deposits are combined with the distribution of contained uranium in deposits to produce probabilistic estimates of tons of undiscovered uranium. There is a 90% chance of at least 0.095 Mt, a 50% chance of at least 0.53 Mt, and a 10% chance of at least 1.8 Mt of undiscovered uranium in the Pine Creek Region. The expected (mean) estimate is 0.8 Mt uranium.

1. INTRODUCTION

Exploration and interest in estimation of undiscovered uranium resources tends to increase during times of high uranium prices but the time lag between exploration success and production of uranium plays a significant role in formation of price volatility [1]. Providing resource estimates in a timely and relevant form could reduce price volatility and lead to more informed planning. Uranium resource information is available by country in [2] and, in many cases, by company and mine in company reports. For the most part, the resource estimates are timely and follow consistent documented procedures. However, because of the long-time lag between discovery and production of uranium, estimates of amounts of economically recoverable uranium in undiscovered deposits are also important in planning. Recently, reported estimates of undiscovered uranium resources were only updated for nine out of 37 countries that have resources [2]. Some larger producers of uranium such as Australia did not provide any estimates of undiscovered uranium. Even for countries where estimates of undiscovered uranium are reported, there is no indication of how the estimates were derived and there are reasons to find some estimates suspect due to impossibly large number of significant digits reported or to unchanging numbers over many years.

Decisions on how land that may contain undiscovered resources should be used, whether to invest in exploration for minerals or not, are made by mineral exploration experts, policy makers, and regional planners. Decisions are also made concerning the adequacy of mineral resources to meet future needs, national policy, and regional development. This contribution intends to demonstrate, by means of an example, how one might assess undiscovered uranium resources in a consistent, documented manner. Part of the assessment process results in making explicit the factors and their uncertainties, which can influence a mineral-related decision, letting decision-makers to visualize clearly the potential effects of their decisions.

The example of the integrated approach discussed here focuses on three assessment parts and models that bear on the parts as described in detail in [3]. Here, we first discuss three-part quantitative assessments in order to show how they differ from uranium resources assessments that have been performed in the past. This is followed by a descriptive model for unconformity-related uranium deposits that is appropriate for the Pine Creek Region of Australia, delineation of a geologically-permissive tract in the Pine Creek Region and, development of a grade-and-tonnage model that is appropriate for assessing unconformity-related uranium deposits in Australia. The grade-and-tonnage data used in the model are from [4]. Next is a discussion of a way to estimate the number of undiscovered unconformity uranium deposits in this geologically-permissive tract. The number of deposits estimates are combined with the estimated grades and tonnages to make probabilistic estimates of tons of uranium yet-to-be discovered in this part of Australia.

2. THREE PART ASSESSMENTS

Three-part resource assessments were designed to provide information for decision-making as regards undiscovered mineral resources under conditions of uncertainty [3, 5]. This form of assessment has been widely applied, including a global assessment of undiscovered copper [6]. The parts include delineated geologically-permissive tracts, where undiscovered deposits may exist based on the geologic setting of the mineral deposit type considered, the frequency distributions of grades and tonnages of well-explored deposits, which function as models of such attributes of undiscovered deposits, and the number of undiscovered deposits that were probabilistically estimated per mineral deposit type. These parts can be combined to provide probabilistic estimates of amounts of undiscovered metal and, if an economic filter is available, the values of economically recoverable metal. The probabilistic output conveys to assessment users the uncertainties of such estimates. The approach is based on internally consistent mineral deposit models, which guide the assessors in converting outputs into forms that are helpful to decision-makers. This synthesis of methods and models boosts the distinction of this form of assessment from others and reduces the chances of biased estimates. The designed integration of the parts is also a burden requiring both careful development of models and applications of methods.

In the delineation of geologically-permissive tracts – the first part of assessments – the primary sources of control for relating geoscience information to deposit types are descriptive mineral deposit models [7, 8]. The models serve this function properly by using theories of deposit origins and by focusing on observations only to suggest what should be observed and what model properties should be observable at the map scale of assessments. Boundaries of geologically-permissive tracts in three-part assessments are defined such that there is negligible probability of deposits of the type assessed occurring outside the geologically-permissive tracts.

Frequency distributions of tonnages and average grades of well-explored deposits per type are a kind of deposit model used in the second part of assessments. These are applied as models of the frequency distributions of grades and tonnages of undiscovered deposits of the same type in geologically similar settings [3]. Deposits suitable for a grade-and-tonnage model are described in published literature as well-explored in three dimensions (3D) and closed in any direction. In addition, by using a spatial rule for deciding which ore bodies should be combined, a consistent sampling unit is applied to undiscovered deposits. For example, a 500-m rule of adjacency has been applied to combine ore bodies of volcanic-hosted massive sulfides into single deposits [9]. This essential procedure influences the associated grade-and-tonnage and deposit density models and, as the parts are integrated, estimates of the number of undiscovered deposits [3].

The third part of an assessment involves estimation of some fixed, but unknown, number of undiscovered deposits per type that likely exist in the delineated geologically-permissive tracts. This number of deposits has significance only with regard to a grade-and-tonnage model. In many assessments, estimates of number of undiscovered deposits are made by experts [3]. A key guideline for these estimates is that they must be consistent with a grade-and-tonnage model and by deposit type. A second guideline is mineral deposit density, a robust method based on relationships of the numbers of well-explored deposits in well-explored control regions to the sizes of the geologically-permissive control regions [10, 11].

3. DESCRIPTIVE MODEL FOR UNCONFORMITY URANIUM DEPOSITS, PINE CREEK OROGEN, AUSTRALIA

Descriptive mineral deposit models are the chief source of control for relating geoscience information to deposit types in the delineation of geologically-permissive tracts and are crucial to the generation of grade-and-tonnage models. Descriptive mineral deposit models fulfill this function properly by focusing on observations and using theories of deposit origins to suggest what to observe, and by having properties that are observable at the scale suitable to the assessment.

There are two parts in a descriptive mineral deposit model, as in Cox and Singer [7]. The first part explains the geological settings where mineral deposits exist and is, therefore, useful for delineation of geologically-permissive tracts. The second part provides signature characteristics of deposits and is, therefore, useful in the classification of known deposits and prospects into types.

In the Pine Creek Orogen (PCO, uranium deposits are generally separated into three mineral fields (Table 1, Fig. 1): (1) the Alligator Rivers; (2) the South Alligator Valley; and (3) the Rum Jungles. Several new uranium prospects (e.g., Bella Rose, Corkscrew, and Thunderball) have been discovered in recent years in a new mineral field – Hayes Creek – between Emerald Springs and Adelaide River. This field also contains the Fleur De Lys deposit, which was discovered in the early 1960s. Details of uranium deposits in the PCO have been described in several publications (e.g., [12–15]).

TABLE 1. MAJOR UNCONFORMITY-RELATED URANIUM MINERAL FIELDS IN THE PINE CREEK OROGEN. INFORMATION SOURCED FROM LALLY AND BAJWAH [14]

Attribute\Uranium Field	Alligator Rivers	South Alligator Valley	Rum Jungle	Hayes Creek
Metal association	U, Au	U, Au, PGEs	U, Cu, Pb, Zn, Co, Ni	U, PGE
Host rocks	Cahill Formation	Koolpin Formation, Coronation Sandstone	Whites Formation	Mount Bonnie Formation, Gerowie Tuff
Age of host rock (Ma)	~1870	~1860, ~1829	~2019	`1860
Sandstone above unconformity	Mamadawerre Sandstone	Mamadawerre Sandstone	Depot Creek Sandstone, Geolsec Formation	Depot Creek Sandstone
Metamorphic grade of the host (facies)	Amphibolite	Greenschist	Greenschist	Greenschist
Nearby Archean complex	Annaba, Ararat Gneiss, Kuala Gneiss	Unknown	Rum Jungle	Unknown
Age of Archean complex (Ma)	2670, 2640, 2520		2545, 2520	Unknown
Associated mafic rocks (< 1800 Ma)	Oenpelli Dolerite (?), mafic volcanics in the Katherine River Group	Oenpelli Dolerite (?)	None mapped	None mapped
Mafic rocks (> 1800 Ma)	Zamu Dolerite present near Caramel	Zamu Dolerite, Goodparla Dolerite	Zamu Dolerite	Zamu Dolerite
Alteration in metasedimentary rocks	Chloritic, sericitic, hematitic, desilicification	Chloritic, sericitic, hematitic, desilicification	High-Mg chloritic, Fe-Mg Chloritic, sericitic, hematitic. In some deposits magnesite, dolomite and tourmaline present	Sericitic
Alteration in sandstone	Chloritic, sericitic hematitic, desilicification	Hematitic	Hematitic	Unknown

More than 95% of the known uranium resources are located in the Alligator Rivers Uranium Field, which hosts the largest uranium deposits in the PCO (Table 3). The Rum Jungle and South Alligator Valley Mineral fields account for 1.7% and 0.6%, respectively, of known resources and uranium deposits in these fields are much smaller [16].

A descriptive model for unconformity-related uranium deposits used in this contribution is based on the most recent information available from a large number of studies conducted in these deposits in Australia and Canada, as summarized in several benchmark papers and reports [15, 17–19]. This model (Table 2) is appropriate for unconformity-related permissive tracts in Australia and Canada and other parts of the world where the deposit type might exist.

TABLE 2. DESCRIPTIVE MODELS OF UNCONFORMITY-RELATED URANIUM-GOLD-PLATINUM GROUP ELEMENT DEPOSITS

DESCRIPTIVE MODEL OF UNCONFORMITY U-Au-PGE
Approximate synonym:
Veinlike type U [20]; Unconformity-Contact Uranium Deposits [21]. Subtypes include: Ingress- and Egress-type [19], Fracture-Bound, Clay-Bound and Proterozoic subunconformity-epimetamorphic [21].
Description:
Uranium mineralization exists as breccia- and fracture-filling in quartz arenites, metapsammites and metapelites situated above, below, or across an unconformity that separate Paleo- and Meso- and occasionally Neo-Proterozoic rocks.
General references: [14, 17, 19, 21, 22]
Geological setting:
Rock types Regionally metamorphosed carbonate rocks, psammites, carbonaceous pelites. Younger argillites and quartz arenites, conglomerates, and mafic and felsic volcanics. Older metamorphosed rocks intruded and inter-layered by mafic rocks and post-tectonic granitoids and felsic volcanics.
Textures Metamorphic foliation and later brecciation.
Age range In rocks of early, middle and late Proterozoic age (1,800–800 Ma), affected by Proterozoic regional metamorphism.
Depositional setting Metasediments underlying the unconformity are formed in shallow marine conditions rather than turbiditic and contain units enriched in carbonaceous material. Sediments forming a thick package (> ~ 5 km) and overlying the unconformity are formed in braided, fluvial conditions. They are generally more oxidized than the metasediments underlying the unconformity.

Sedimentary package overlying the unconformity is generally flat-lying at the time of mineralization. It is often partially or fully eroded. Mineralization results from complex processes including diagenesis of sediments overlying the unconformity and regional metamorphism of sediments underlying the unconformity. Primary uranium minerals are formed when oxidized fluids carrying uranium are reduced by organic and/or inorganic reductants in the host rock. Movement of fluids is thought to be triggered by proximal and/or distal tectonic reactivation. Age dating reveals that primary mineralization is younger than the age of deposition of sedimentary package overlying the unconformity. Weathering and supergene enrichment related to Proterozoic unconformity, can enrich and/or partially or fully erode mineralization.

Tectonic setting(s)
Intra-cratonic sedimentary basins on the flanks of Archean domes. Tectonically stable since middle Proterozoic. In some regions, the mineralization is overprinted by younger events of deformation (folding and faulting).

Associated deposit types
Gold-, nickel-, lead-zinc, copper, PGE-, and REE (rare-earth element)-rich ore zones in and/or in close proximity to known deposits may occur but are poorly understood.

Deposit description:

Mineralogy
Pitchblende + uraninite ± coffinite ± pyrite ± chalcopyrite ± galena ± sphalerite ± arsenopyrite ± niccolite. Chlorite + quartz + calcite + dolomite + hematite + siderite + sericite. Locally late quartz-chlorite veins contain gold or silver, uraninite, galena, and tellurides of Bi, Ni, Pb and Pd. Latest quartz-calcite veins contain pyrite, chalcopyrite, and bituminous matter. Locally quartz-carbonate-hematite veinlets with gold + electrum + clausthalite (PbSe) + stibiopalladinite with or without pyrite, marcasite, pyrrhotite, sphalerite, chalcopyrite, and galena.

Texture/structure
Disseminations, veins, and breccia filling. Coarse euhedral uraninite and fine colloform pitchblende. Latest quartz-calcite veins show colloform texture, open-space fillings. Locally gold and PGE mineralization along micro-fractures, micro-veinlets, disseminations and within the alteration matrix in altered intrusive rocks.

Alteration
Multistage chloritization is dominant. Local sericitization, dolomitization, hematitization, kaolinitization. Vuggy and incipient vuggy vein-type silicification exists all over the alteration envelope. Alteration envelope is enriched variably in Mg, P, REE, and various metals. Alkali elements are depleted.

Ore controls
Uranium mineralization is controlled by both physical and chemical traps. Physical traps are in the form of fractures, faults, breccia zones and the high permeable zones along or near the unconformity surface. Organic (graphite, methane) and inorganic reductants (chlorite, H2S) generate chemical traps. In all deposits mineralization is structurally controlled by structures

DESCRIPTIVE MODEL OF UNCONFORMITY U-Au-PGE

which cut across the unconformity surface. The movement of ore forming diagenetic fluids in the sedimentary rocks overlying the unconformity requires good permeability.

Weathering
Secondary U minerals uranyl-phosphate, metatorbernite, autunite, uranophane, gummite, skoldowskite.

Geochemical and geophysical Signature
Increase in U, Mg, P and locally in Ni, Cu, Pb, Zn, Co, As; decrease in SiO2. Locally Au, associated with Ag, Hg, Mo, Ni, Pd, Te, Rb, Re, REE and Y. Anomalous radioactivity. Presence of graphite and other sulfide minerals in the mineralized zone can create mappable contrast in electrical conductivity (or resistivity).

Examples:

Cigar Lake, Saskatchewan, Canada [23]
McArthur River, Saskatchewan, Canada [24]
Coronation Hill, Northern Territory, Australia [14]
Jabiluka, Northern Territory, Australia [25]
Ranger, Northern Territory, Australia [26]
Nabarlek, Northern Territory, Australia [27]
Key Lake, Saskatchewan, Canada [28]
Rabbit Lake, Saskatchewan, Canada [29]

4. DELINEATION OF GEOLOGICALLY-PERMISSIVE TRACT(S) IN PINE CREEK, AUSTRALIA

The geological setting in the descriptive mineral deposit model (Table 2) is the key to recognizing where the deposit type could exist. To assess consistently undiscovered mineral resources, tracts where geology is permissive for the occurrence of deposits of at least one specified type are delineated according to geological criteria based on descriptive mineral deposit models, which are also based on studies of known deposits within and outside the study area. Thus, the descriptive mineral deposit model becomes the chief guide for delineation. Geologically-permissive tracts may or may not contain known deposits because of the extent and quality of previous exploration. Geologically-permissive tract margins are delineated in such a way that the probability of deposits of the type assessed existing outside the geologically-permissive tract is insignificant, for example, less than 1 in 100,000. A geologic map is the chief source of local information for defining geologically-permissive tracts and recognizing the ones that are geologically-permissive for individual deposit types. The nature and quality of information available for defining geologically-permissive tracts are influenced by map scales, which also affect the level to which geologic units are merged and how cover is depicted. Decisions to exclude areas from geologically-permissive tracts are based only on geology, knowledge of thorough but fruitless exploration, or the existence of barren overburden exceeding some predetermined thickness. In this study, the assessment was limited to deposits that could occur in the upper 1,000 m. Geophysical tools contribute to recognition of extensions of geologically-permissive rock units under cover and to identification of rock units in poorly mapped areas. Boundaries of geologically-permissive tracts are reduced only where it can be strongly proven that a deposit type could not exist or the depth boundary is exceeded.

Geological settings of unconformity-related uranium systems in the PCO can be identified by three essential components: (1) major unconformity; (2) reduced Paleo-proterozoic metasedimentary rocks below the unconformity; and (3) a relatively thick (> ~5 km) package of Paleo-proterozoic coarse-grained, dominantly fluvial sedimentary rocks overlying the unconformity [17]. Presence of these features is deemed essential to delineate the geologically-permissive area in the PCO. An important feature that distinguishes uranium deposits in the PCO from similar deposits in the Athabasca Basin, Canada is that almost all known deposits in the PCO are hosted by metasedimentary rocks underlying the unconformity. Such deposits in Canada are classified as 'Ingress-style' [19]. In the PCO, sedimentary rocks overlying the unconformity (Katherine River Group and Tolmer Group) have been preserved only in and near a few deposits.

The geologically-permissive tract (Fig. 1) in the PCO has been delineated using geological features critical for the formation of unconformity-related uranium deposits. The distribution of known deposits and mineral occurrences and information on the exploration for these deposits reinforces the identification of geologic settings. The critical geological features include: (1) presence of Archean granites and gneisses; (2) presence graphite bearing reduced Paleo-proterozoic metasediments which underlie the unconformity; and (3) presence Paleo-proterozoic sedimentary rocks of the Katherine River and Tolmer Groups. Rocks of the Katherine River Group (McArthur Basin) are confined to the eastern and south-eastern part of the PCO (Fig. 1) and geological information suggests that the basin deepens in the south-eastern direction [14]. A large part of these rocks has been eroded in the Alligator Rivers Uranium and South Alligator Mineral fields. For example, only minor remnants of these rocks are found in proximity to major uranium deposits. Similarly, rocks of the Tolmer Groups have been partially or completely removed from areas in proximity to the Rum Jungle Mineral Field (Fig. 1). There is very little information on the distribution of these rocks in the central part of the PCO. This area has been excluded from the geologically-permissive tract. The central part of the PCO hosts several lode-gold deposits (e.g., Goodall and Toms Gully), which, based on fluid inclusion data, could have been formed at depths of ~6 km and more [12]. Geochronological studies show that gold mineralization could have occurred between 1820 and 1800 Ma [12], which is less than 20 million years before deposition of Katherine River and Tolmer Groups began (estimated to be ~1800 Ma [30]). Therefore, it is likely that these rocks were either not deposited in the central part of the PCO or they (and much of the underlying Paleo-proterozoic metasediments, which host uranium mineralization) have been eroded.

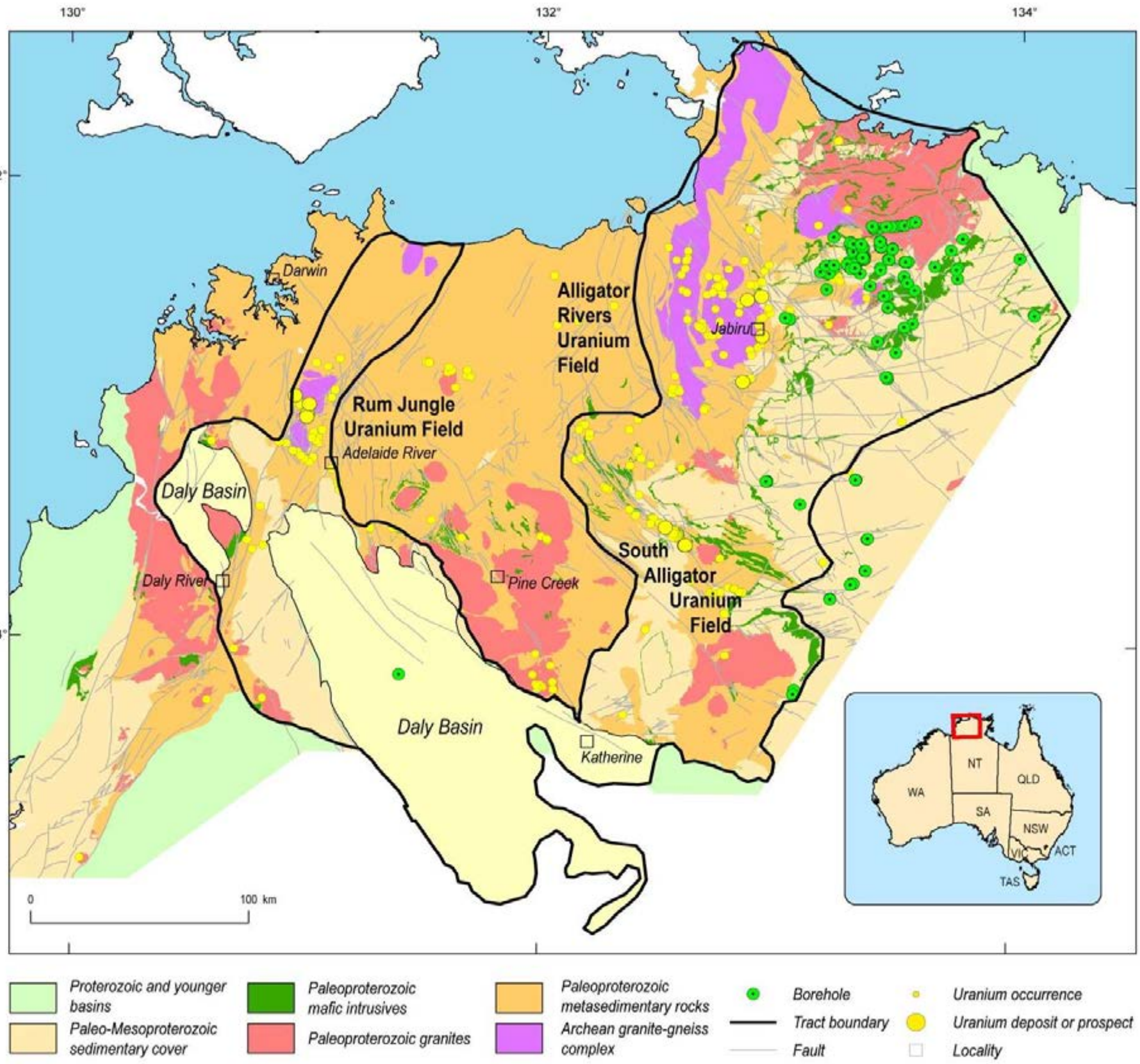

FIG. 1. Delineated geologically-permissive tract for unconformity-related uranium deposits in Pine Creek Australia.

The geologically-permissive tract includes the Daly Basin (Fig. 1) because rocks of the Tolmer Group have been mapped below the unconformity with the Paleozoic rocks of the Daly Basin [31]. Presence of these rocks is supported by drilling in the Daly Basin [32]. Recent exploration also suggests presence of uranium and REE mineralization in the Paleo-proterozoic rocks [31].

The eastern and south-eastern boundary of the geologically-permissive tract has been drawn to include areas where the unconformity between Paleo-proterozoic reduced metasediments and sedimentary rocks of the Katherine River Group is interpreted is to be less than ~1000 m [31], which is the depth limit of this assessment. A report on exploration drilling by Cameco Pty Ltd. in the area suggests that the company was not interested in targets in areas where the Paleo-proterozoic basements rocks were located at depths greater ~700 m [33].

The eastern boundary of the geologically-permissive tract is tentative and based on only a few drill holes in which the unconformity has been intersected. For example, the unconformity is intersected in drill hole DAD0008 at depth of 993 m (unpublished report). However, in hole

DAD006 (~50 km southwest of DAD008), which was drilled to a depth of 1,436 m, the unconformity was not intersected [34].

Modeling of gravity data (unconstrained inversion) has been used to map basement of the McArthur Basin in the study area [35]. The modeling delineates several sub-basins and deposition centers in the basin. However, a comparison of depth estimates by the model and the depths observed in drill-hole data reveals major inconsistencies. Therefore, in this study, the boundary of the geologically-permissive tract is based solely on drillhole data. It is quite likely that the boundary will have to be modified after new data from drilling and geophysical surveys are made available.

5. GRADE-AND-TONNAGE MODEL

Grade-and-tonnage models of mineral deposits are an essential component of quantitative mineral resource assessments and mineral exploration planning. Having an idea of the likely tonnages and grades of deposits that might exist is crucial to good planning for exploration. Different kinds of deposits typically have significantly different grades, tonnages or amounts of metals. Grade-and-tonnage models play two roles in quantitative mineral resource assessments: first, they can assist in grouping the known deposits in a region into types and thus aid in delineation of geologically-permissive tracts per deposit type [36]; second, they present information about the potential value of undiscovered deposits in geologically-permissive tracts and are vital to economic analysis of these resources. Frequency distributions of tonnages and average grades of well-explored deposits per type are models of the tonnages and grades of undiscovered deposits per the same type in geologically similar settings. To ensure that the tonnages and grades of undiscovered deposits are properly represented, considerable care must be exercised in constructing the models.

Mosier [37] prepared a grade-and-tonnage model for unconformity-related uranium deposits, but with the passage of 30 years, additional information allows improvement in the original model. For example, it is now known that the unconformity uranium deposits in Canada have average grades higher than those in Australia and are, therefore, a poor model of grades of undiscovered deposits in Australia. Also, the value of using spatial rules to combine adjacent deposits is now clear [3] and such a rule was here applied to the Australian deposits.

Multiple steps are involved in the construction of grade-and-tonnage models. First, a group of well-explored deposits considered to belong to the deposit type being modeled is identified and must be consistent with the descriptive mineral deposit model. In this case well-explored means completely drilled in 3D. Then, from each well-explored deposit included in the group, data consisting of average grade per metal or mineral commodity of potential economic interest and tonnages based on resources, reserves, and the total production at the lowest available cut-off grade are compiled. Here, total resource (t U) includes all resource categories and past production. If a deposit was estimated at several cut-off grades, the resources at the lowest cut-off grade are adopted. All content data are in metric tons of uranium [4]. It is not possible to guarantee that the grade or tonnage will not change upon further mining or drilling, but using estimates associated with the lowest available cut-off grade and determining that there are no statements about the mineralization being open in some direction are the best ways to reduce the chances of using biased estimates.

For deposit models, it is imperative to use a spatial rule to decide which ore bodies must be merged in order to have a consistent sampling unit that can be applied to the undiscovered deposits. The consequence of not using spatial rules are models that are dependent on the stage of exploration, local legal rules affecting mining boundaries and on the detail and scale of reporting that typically vary over time and place. For unconformity-related uranium deposits, a 250-m rule was applied. This is somewhat arbitrary, but it is consistent with the level of information available about the spatial distribution of uranium mineralization and can be applied to the undiscovered deposits. Among the consequence of using this rule in the Pine Creek region is the merging of the grades and tonnages of El Sherana and El Sherana West, Koongarra and Koongarra 2, and Ranger 1 no3 and Ranger Deeps (Table 3). Several deposits with reported grades and tonnages in the Pine Creek region of Australia were not included in this study because they were believed to be incompletely explored (Beatrice, Koolpin Creek, Mount Burton, Rockhole, O'Dwyers, Palette, Saddle Ridge, Skull, Scinto 5 and 6, and Sleisbeck, Twin). The standard applied was deposits (mines) with total reported uranium content of less than 150 t were excluded.

TABLE 3. DEPOSITS USED TO CONSTRUCT THE GRADE-AND-TONNAGE MODELS FOR UNCONFORMITY-RELATED URANIUM DEPOSITS, PINE CREEK, AUSTRALIA

Deposit name	Country	Ore tons metric (millions)	Grade U %	U content (t)
Caramal	Australia	0.955	0.26	2482
Coronation Hill	Australia	0.363	0.455	1,567
Dam	Australia	0.34	0.11	375
Dyson's	Australia	0.157	0.288	453
El Sherana + El Sherana West	Australia	0.0631	0.56	351
Hades Flat	Australia	0.363	0.17	612
Jabiluka 1	Australia	1.3	0.212	2,860
Jabiluka 2	Australia	29.09	0.412	119,884
Koongarra 1 + Koongarra 2	Australia	2.5	0.56	13,992
Mount Fitch	Australia	5.05	0.031	1,567
Angularli	Australia	1.0	0.75	7500
Nabarlek	Australia	0.59	1.535	9,208
Ranger 1 n°1	Australia	19.78	0.272	53,800
Ranger 1 n°3 + Ranger Deeps	Australia	214	0.084	179,792
Ranger 68	Australia	1.5	0.303	4,540
Rum Jungle Creek South	Australia	0.665	0.365	2,425
White's	Australia	0.779	0.2076	2,481

Frequency distributions of the uranium grades, uranium contents and tonnages of the 17 well-explored unconformity-related uranium deposits in the Pine Creek region of Australia (Figs. 2–4; Table 4) can be used as grade-and-tonnage models of undiscovered deposits (Table 3). The grade-and-tonnage plots depict the cumulative proportion of deposits versus the deposits' grade or tonnage. Different symbols portray the deposits and intercepts for the 10th, 50th, and 90th percentiles are shown.

TABLE 4. GRADE-AND-TONNAGE MODELS OF UNCONFORMITY-RELATED URANIUM DEPOSITS PINE CREEK REGION

	Number of deposits	10th percentile of deposits	50th percentile of deposits	90th percentile of deposits	Mean $\log_{10}$	Standard deviation $\log_{10}$	Probability [4] log-normal
Tons [1]	17	66	0.955	0.138	6.1526	0.8783	0.14
U grade [2]	17	0.907	0.288	0.073	-0.5579	0.3896	0.75
U content [3]	17	132,000	2,480	370	3.6054	0.8256	0.18

(1) Tonnage reported in millions of metric tons
(2) Uranium grades in percent
(3) Uranium content in metric tons of uranium
(4) Probability of log-normal distribution (Shapiro-Wilk test for normality)

Inter-variable relationships are important as they affect: (a) our understanding of how deposits form; (b) simulations of resources; and (c) our hypotheses regarding resource availability. The plot of average grade of uranium versus ore tonnage (Fig. 5) shows a low negative correlation ($r = -0.35$), which is not significantly different from zero at 1% level of significance.

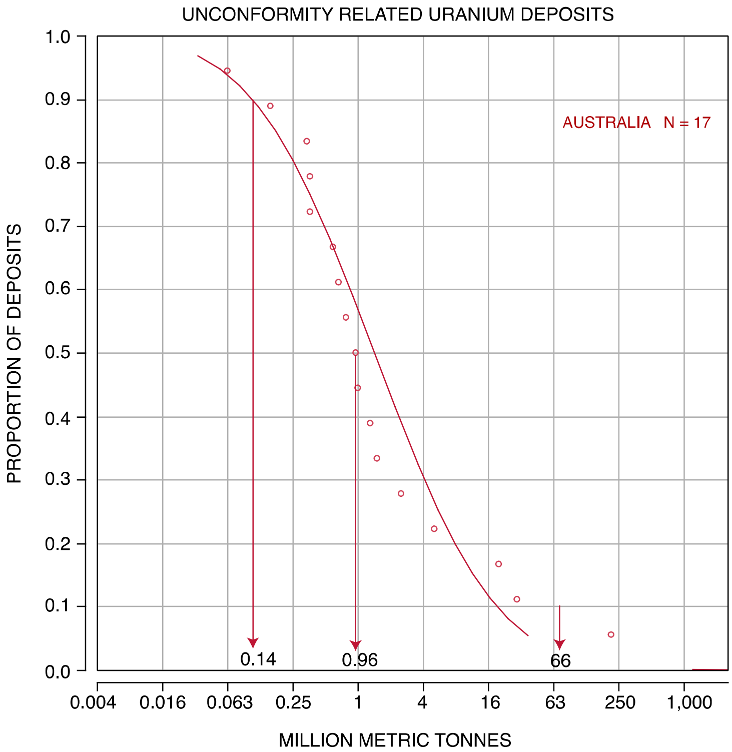

FIG. 2. Cumulative frequency of ore tonnage of unconformity-related uranium deposits located in Pine Creek, Australia (red circles). Every circle depicts a single deposit. Intercepts for the 10th, 50th, and 90th percentiles of the observed distributions are provided. Solid line is best fit log-normal curve.

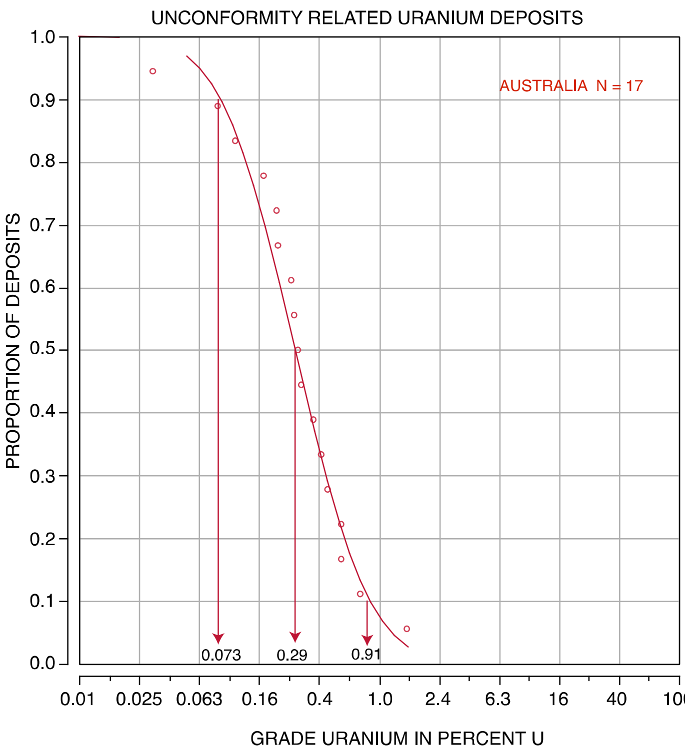

FIG. 3. Cumulative frequency of average uranium grade of unconformity-related uranium deposits located in Pine Creek, Australia (red circles). Every circle depicts a single deposit. Intercepts for the 10th, 50th, and 90th percentiles of the observed distributions are provided. Solid line is best fit log-normal curve.

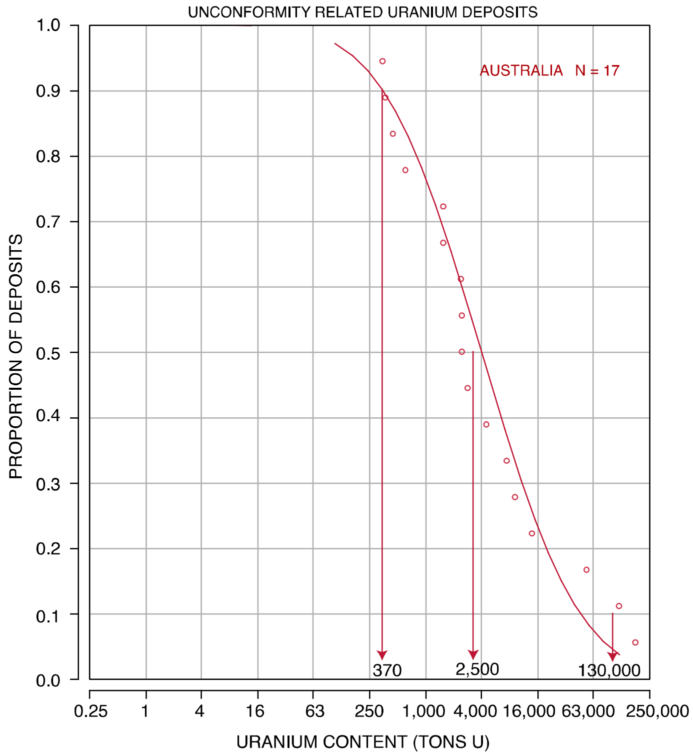

FIG. 4. Cumulative frequency of uranium content of unconformity-related uranium deposits located in Pine Creek, Australia (red circles). Every circle depicts a single deposit. Intercepts for the 10th, 50th, and 90th percentiles of the observed distributions are provided. Solid line is best fit log-normal curve.

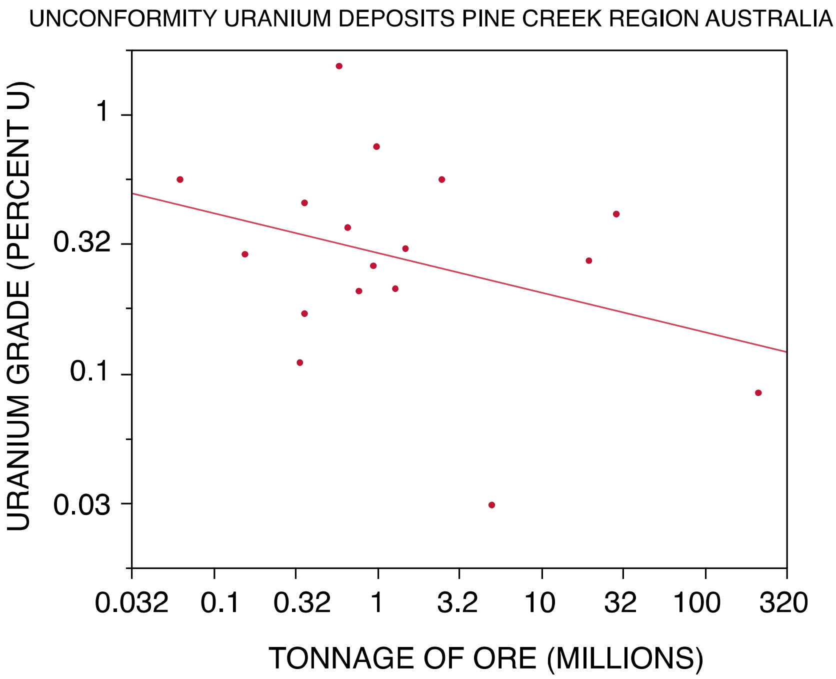

FIG. 5. Plot of versus average uranium grade versus ore tonnage of Pine Creek, Australia unconformity-related deposits. Line is best fit regression.

6. DEPOSIT DENSITY MODELS

Just as grade-and-tonnage models of well-explored deposits provide a proxy of the frequencies of grades and tonnages of undiscovered deposits, the number of well-explored deposits in well-explored control tracts provides a proxy of the frequencies of number of deposits in geologically-permissive tracts. Mineral deposit density models were designed to work within three-part assessments, which affect how such models should be constructed. For consistency with three-part assessments, such models portray areas of well-explored control tracts wherein the known number of deposits is consistent with the grade-and-tonnage model (Fig. 6). To avoid biased estimates of number of undiscovered deposits in assessments, the deposits counted in density estimates generated from control tracts should be consistent with the well-explored deposits in grade-and-tonnage models. Prospects are not counted in the densities of control tracts. In control tracts, only the areas that are well-explored parts are counted. These typically are the parts of the tracts that are exposed and covered areas are excluded because in most cases they are not well-explored. Incompletely explored deposits are also not counted. In Fig. 6, number of deposits counted would be the three completely explored deposits and the geologically-permissive area would be the total geologically-permissive tract area minus the area covered.

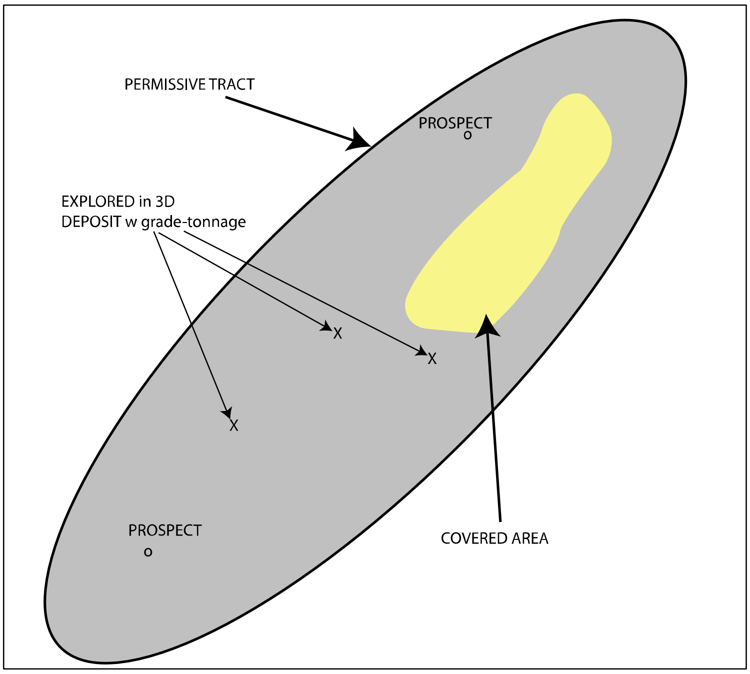

FIG. 6. One hypothetical control area for density estimate. Total area of geologically-permissive tract minus area of cover is area of control tract. Only the three well-explored deposits used in grade-and-tonnage model are counted.

Deposit densities were studied using three deposit types with large numbers of well-explored control tracts and deposits from around the world; podiform chromite [38], porphyry copper [39], and volcanogenic massive sulfide [40]. In each deposit type, mineral deposit densities were not constant across all sized control tracts as might be expected. That is, if a tract of 20,000 km^2 contained 10 deposits, one might expect that a tract of twice the area would contain twice the number of deposits. But for each deposit type, the number of deposits is less than expected if one assumes constant density of deposits per unit area (deposits/area). Fortunately for each deposit type, the area that is geologically-permissive can be used to make a good estimate of number of deposits using linear regression.

The slope of the regression lines relating area of control geologically-permissive tracts to deposit density were almost the same for each of the three deposit types [10]. For a given sized geologically-permissive tract, the density of the relatively small podiform chromite deposits was much higher than the density of the intermediate sized volcanogenic massive sulfide deposits which was larger than the density for the quite large porphyry copper deposits—that is the density is related to the size of deposits. When all of the data from control tracts of these three types were combined with well-explored control tracts for seven other deposit types, tonnage was found to be a good predictor of density. So, when the area of geologically-permissive tracts and median deposit size (tonnage) are both used in a multiple regression equation, over 90% of the variation in density could be predicted [10]. In other words, the area of the geologically-permissive tract and the median tonnage of the deposits being estimated from the grade-and-tonnage model could be used to predict the number of deposits quite well, regardless of deposit type. According to empirical evidence, processes that influence the amount of resources in various geologic settings are very similar for almost all deposit types. Sizes of geologically geologically-permissive tracts per deposit type are excellent predictors of total numbers of deposits. Geologically-permissive tracts, not arbitrary cells, are natural sampling control areas for specific deposit types.

Regressions using the above-mentioned variables present a method for estimating the number and total tonnages of deposits in a geologically-permissive tract [11]. Robust estimators were derived from analysis of 10 different deposit types from 109 control geologically-permissive tracts worldwide, generalizing across deposit types [10]. Estimates of mineral deposit density were derived by regressing median tons of deposits (s) and geologically-permissive area (a) against density of deposits for the 50th percentile estimate. The data were logged (base 10) so that requirements of statistical tests were not violated. The following equations [11] can be used regardless of deposit type ($R^2 = 0.91$):

$$\log_{10}(Density_{50}) = 4.21 - 0.499 \log_{10}(a) - 0.225 \log_{10}(s) \quad (1)$$

where $Density_{50}$ is the 50th percentile estimate in the number of deposits per 100,000 km^2, a is geologically-permissive area in km^2, s is mean tonnage in millions of metric tons.

For density estimate at a 90% confidence level and an upper density estimate limit at a 10% confidence level:

$$\log_{10}(Density_{90}, Density_{10}) = (\log_{10}(Density_{50}) \pm 1.290 \cdot 0.3484 \cdot \surd\ (1+(1/109) + (3.173 - \log_{10}(a))^2 \cdot (-0.3292 - \log_{10}(t))^2 /(109-1) \cdot 2.615 \cdot 1.188) \quad (2)$$

where 1.290 is Student's t at the 10% confidence level with 106 degrees of freedom, $t_{10,106df}$, 0.3484 is standard deviation (s.d.) of deposit density | tons, area, 109 is number control tracts, 3.173 is mean log area [km^2] of control tracts, -0.3292 is mean log tons [millions] in control tracts, 2.615 is s.d. of log tons in control tracts, and 1.188 is s.d. of log areas of control tracts. For conversion of density estimates to number of deposit estimates at the 10th, 50th, and 90th confidence levels, log density per 100,000 km^2 should be adjusted for geologically-permissive tract size and scale:

$$N\%\text{ile} = a / 100{,}000 * 10^{\wedge}(\log_{10}(Density_{\%\text{ile}})) \quad (3)$$

$$\log_{10} E(N) = \log_{10}(N_{50}) + (((\log_{10}(N_{10}) - \log_{10}(N_{50}))/t)^2)/2 \quad (4)$$

The expected number of deposits can then be estimated as 10 to the power of $\log_{10}E(N)$. Estimates made using these density equations are for the total number of deposits in geologically-permissive tracts because they were based on the total number of deposits in the control tracts. The expected total number of deposits in a geologically-permissive tract is the sum of the known number of deposits plus the estimate of expected number of undiscovered deposits. For estimation of the number of undiscovered deposits, the known number of deposits in a geologically-permissive tract must be subtracted from the expected total number of deposits [Eq. 4]. To maintain the property of expected numbers being additive and to estimate the number undiscovered requires revising the total expected number by subtracting the known number of deposits to make a new expected number. The new expected number and the variance are used to estimate a new median and 10th and 90th percentiles. The regression variance is calculated as

$$\text{var}_N = ((\log_{10}(N_{10}) - \log_{10}(N_{50}))/ t)^2 \quad (5)$$

Estimates of median number of deposits adjusted for number of known deposits are 10 to the power of

$$\log_{10}(N_{50}) = \log_{10}(E(N) - \text{known number}) - \text{var}_N /2 \quad (6)$$

$\log_{10}(N_{50})$ is used instead of $Density_{50}$ in Equation (2) to make probabilistic estimates of the number of undiscovered deposits while taking into account known deposits.

A comparison of number of undiscovered deposit estimates made by expert panels with the generalized density method for porphyry copper, orogenic gold, and sediment-volcanic iron deposits provides confidence in the quality of density estimates for various deposit types [37].

7. NUMBER OF UNDISCOVERED DEPOSITS

The third part of an assessment involves the estimation of some fixed, but unknown, number of undiscovered deposits per type existing in the delineated geologically-permissive tracts. This fixed number of undiscovered deposits, which could be any number including 0, will not be known with certainty until a geologically-permissive tract being assessed is completely drilled. The probability (or degree of belief) that some fixed but unknown number of undiscovered deposits is present in a geologically-permissive tract is explicitly portrayed by estimates of the number of undiscovered deposits, which represent both the uncertainty of the number that may be present and the measure of favorableness of the occurrence of the deposit type in the geologically-permissive tract. Uncertainty is depicted by the spread of the number-of-deposit estimates (quantiles) from the 90 to 10 or 1% quantile — a large relative difference in the numbers suggests great uncertainty. A measure of favorability can be portrayed by the estimated number of undiscovered deposits at a certain probability level or by the expected (that is, mean) number of deposits.

Estimates of the number of undiscovered deposits are only meaningful with respect to a grade-and-tonnage model. Without this constraint, any cluster of mineral grains could be deemed worthy of estimation, and even in small geologically-permissive tracts, we would have to estimate millions of ‘deposits’. In three-part assessments, there is internal consistency among the assessment parts and estimates: delineated geologically-permissive tracts are consistent with descriptive mineral deposit models, grade-and-tonnage models with descriptive mineral deposit models and with the known deposits in the geologically-permissive tract, and estimates of the number of undiscovered deposits with grade-and-tonnage models. This is what is meant by integration of the parts and models in the three-part assessments. Care should be taken in quantitative mineral resource assessments to avert the introduction of biased estimates of undiscovered mineral resources [3]. Therefore, the most important guideline for quantitative mineral resource assessments is the consistency of estimates of the number of undiscovered deposits with the grade-and-tonnage models.

In a quantitative mineral resource assessment, an essential factor influencing estimates of the number of undiscovered deposits in a geologically-permissive tract is a clear distinction between known deposits and prospects. In the published literature, deposits considered “known” or “discovered” are described as well-explored in 3D and not open in any part, and have published grades and tonnages. Explored metal/mineral occurrences that do not meet these criteria are considered prospects even if they are, or have been, mined because of evidence that more resources are expected. Examples of some known and in some cases mined uranium deposits in the Pine Creek region that must be counted as prospects are listed in the grade-and-tonnage section above. Such a distinction is needed to prevent either missing some resources or double counting. Commonly, some of these prospects may represent some of the estimated undiscovered resources.

In several cases of three-part assessments, estimates of number of deposits are made by experts [3, 6]. The goal is to provide unbiased estimates of the number of undiscovered deposits by using methods that produce the minimum variance. Typically, expert judgment is used because of the need to capture the knowledge of the experts and uncertainty of such estimates. More importantly, the various relevant data upon which such estimates must be based are normally of different types and have different quality and coverage. A proper elicitation procedure is followed whereby certain criteria are applied, experts are chosen, the method is designed, and the response mode is specified [41–43]. An important guide when experts estimate the number of undiscovered deposits is the internally consistent deposit density estimates.

8. ESTIMATED NUMBER OF DEPOSITS IN PINE CREEK REGION

In this section we estimate the number of undiscovered unconformity uranium deposits in the Pine Creek Region using only the deposit density method. In this study, the median tonnage of the well-explored Australian deposits used in the grade-and-tonnage model is 0.96 Mt (Table 4) and the total area geologically-permissive (Fig. 1) in the Pine Creek Region is 67,028 km^2. These estimates are used in the above equations (EQ. 1-6), along with accounting for the 17 known discovered deposits leading to the following estimates of number of undiscovered unconformity-related deposits in the Pine Creek Region: 90% of 9, 50% of 25, and 10% of 72 or more deposits. The expected number of undiscovered deposits is 29. Although the estimated number of undiscovered deposits is similar to the number of known deposits (17), some of the prospects not used in the grade-and-tonnage model may represent some of the undiscovered deposits estimated.

The mean of the log number of deposits from EQ. 6 (log10(N50) = 1.4056) and the standard deviation of the log number (= 0.34841) were used to simulate possible numbers of undiscovered deposits 2,000 times with the results shown in the histogram in Fig. 7. The histogram demonstrates that numbers of undiscovered deposits is increasingly less likely as the number increases beyond 25 deposits. For purposes of simulation and to understand how commonly different numbers of undiscovered deposits might exist, it is useful to see the same simulated data plotted as the cumulative number of deposits (Fig. 8). In Monte Carlo, simulation equally likely random numbers between 0 and 1 are selected many times for the 'Y' axis in Fig. 8 and each associated number of undiscovered deposits from the 'X' axis is used. Multiple selections from Fig. 8 will lead to the number of deposits being properly weighted by their likelihood of occurrence using this method.

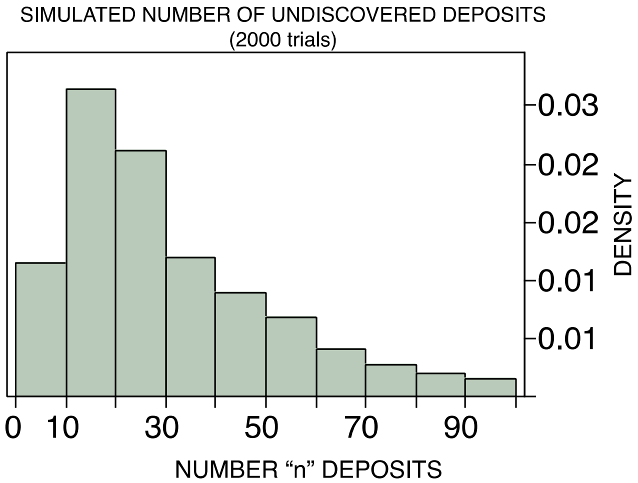

FIG. 7. Histogram of number of undiscovered unconformity-related deposits in Pine Creek, Australia simulated based on deposit density equations.

9. ESTIMATING THE AMOUNT OF UNDISCOVERED URANIUM

It is possible to multiply the mean amount of uranium in the grade-and-tonnage model by the mean number of undiscovered deposits, but doing so would hide the considerable uncertainty in the underlying estimate. Part of the goal of three-part assessments is to fully convey to decision-makers not just the expected estimates, but also information about the uncertainty of the estimates. Using Monte Carlo simulation, probabilistic estimates of the number of deposits can be combined with the simulated grades and tonnages of the deposits to produce probabilistic estimates of tons of undiscovered uranium. In Monte Carlo simulation a random number between 0 and 1 is selected so that its value on the 'Y' axis of Fig. 8 is used to select a corresponding number of deposits on the 'X' axis and this number of simulated deposits determines the number of deposits needing simulated tonnages of uranium content from Fig. 4. This process is repeated hundreds of times. If we were including economic filters of the amounts of economically recoverable uranium we need to use number of deposits, grades and tonnages and possibly depths of the undiscovered deposits.

Here, we are not explicitly considering economics and only attempt to estimate amounts of undiscovered uranium. To estimate the amounts and the uncertainty of the estimated amounts, it is necessary to simulate the number of deposits as discussed above and, for each simulated number, simulate the amount of uranium in each of the simulated deposits. The mean and standard deviation of the log-normally distributed contained uranium in the deposits used in the grade-and-tonnage model and the mean and standard deviation of the number of undiscovered deposits are used for this simulation. From the simulation results there is a 90% chance of at least 0.095 Mt, a 50% chance of at least 0.53 Mt, and a 10% chance of at least 1.8 Mt of undiscovered uranium in the Pine Creek Region of Australia (Fig. 9). The expected (mean) estimate is 0.8 Mt uranium. This method produces a probabilistic estimate uranium in undiscovered deposits that explicitly shows the associated uncertainty of the estimate. There seem to be no quantitative estimates available for comparison with these estimates.

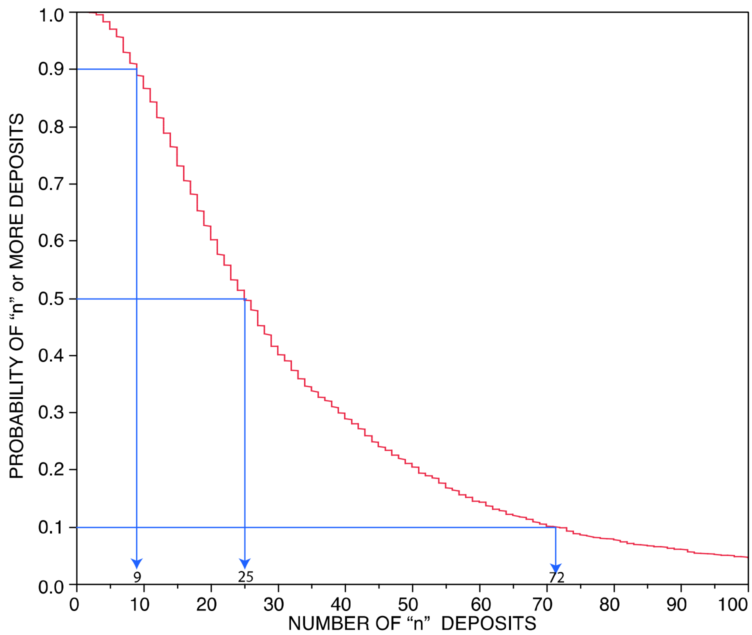

FIG. 8. Plot of cumulative number of undiscovered unconformity-related deposits in Pine Creek, Australia simulated based on deposit density equations.

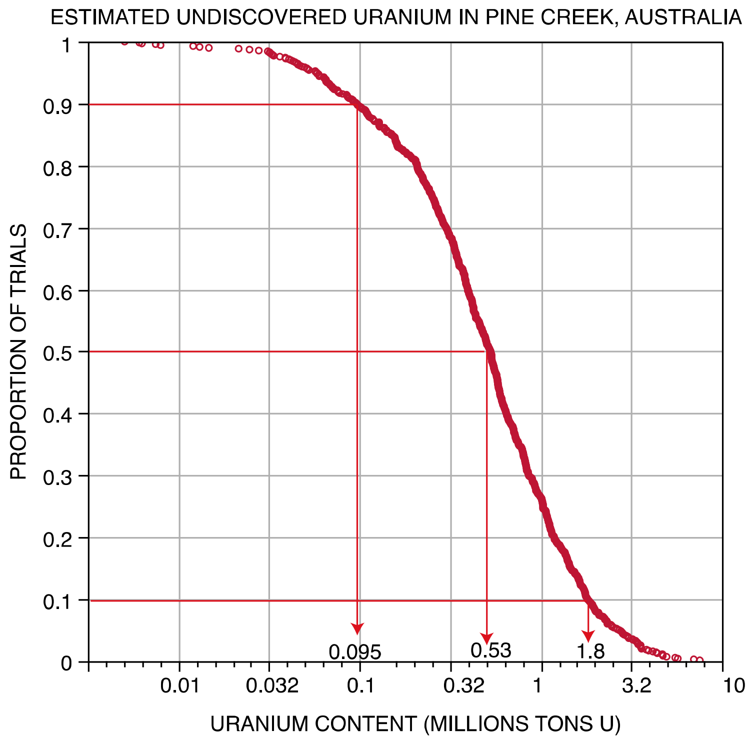

FIG. 9. Cumulative frequency of uranium content of undiscovered unconformity-related uranium deposits located in the Pine Creek region, Australia (red circles). Each circle represents a Monte Carlo simulated trail combining number of undiscovered deposits with uranium content per deposit.

10. CONCLUSIONS

An example of a three-part quantitative assessment of undiscovered uranium deposits has been provided here for unconformity-related uranium deposits in the Pine Creek Region of Australia. The assessment demonstrates that the Pine Creek Region contains a substantial amount of undiscovered uranium in deposits similar to those already discovered. The probabilistic nature of the estimated amount of uranium explicitly demonstrates the uncertainty associated with such estimates of undiscovered resources. Based on this assessment, there is considerable uncertainty in the estimated amount of undiscovered uranium with probability of 0.8 that the amount is between 0.095 and 1.8 Mt. Ideally, a further step would be to take into consideration the economics of the undiscovered deposits by including depth and appropriate mining/processing methods.

ACKNOWLEDGMENT

The authors of this contribution gratefully acknowledge the support and advice of Patrice Bruneton on deposits in the Pine Creek region.

REFERENCES

[1] ROONEY, M., NUTTALL, W.J., KAZANTZIS, N., A dynamic model of the global uranium market and the nuclear fuel cycle, Resources Policy. 43, 50-60 (2015).

[2] OECD-NEA & IAEA, Uranium 2014: resources, production and demand, NEA no. 7209, A joint report by the Organization for Economic Co-operation and Development Nuclear Energy Agency (OECD-NEA) and the International Atomic Energy Agency (IAEA), 508p (2014).

[3] SINGER, D.A., MENZIE, W.D., Quantitative Mineral Resource Assessments—An Integrated Approach: Oxford University Press, New York, 219p (2010).

[4] International Atomic Energy Agency, IAEA-TECDOC-1629, World distribution of uranium deposits (UDEPO) with uranium deposit classification, 2009 edition, Vienna, p. 15–21. UDEPO v208-2015Mod (2009).

[5] SINGER, D.A., Basic concepts in three-part quantitative assessments of undiscovered mineral resources, Nonrenewable Resources 2(2), 69–81 (1993).

[6] JOHNSON, K.M., HAMMARSTROM, J.M., ZIENTEK, M.L., DICKEN, C.L., Estimate Of Undiscovered Copper Resources Of The World, 2013; U.S. Geological Survey Fact Sheet 2014-3004 (2014).

[7] COX, D., SINGER, D., Mineral Deposit Models, U.S. Geological Survey Bulletin 1693, United States Government Printing Office, Washington (1986).

[8] BLISS, J.D., Ed., Developments in mineral deposit modeling, U. S. Geological Survey Bulletin 2004, 168p (1992).

[9] MOSIER, D.L., BERGER, V.I, SINGER, D.A., Volcanogenic massive sulfide deposits of the world—Database and grade and tonnage models, U.S. Geological Survey Scientific Investigations Report 2009–1034 (2009). http://pubs.usgs.gov/of/2009/1034/

[10] SINGER, D.A., Mineral deposit densities for estimating mineral resources, Mathematical Geosciences 40(1), 33–46 (2008).

[11] SINGER, D.A., KOUDA, R., Probabilistic estimates of number of undiscovered deposits and their total tonnages in permissive tracts using deposit densities. Natural Resources Research 20, 89–93 (2011).

[12] AHMAD, M., HOLLIS, J. A., "Chapter 5: Pine Creek Orogen", Geology and Mineral Resources Of The Northern Territory (AHMAD, M., MUNSON, T. J., Eds.), Volume Special publication 5, Darwin, Northern Territory Geological Survey, 134p (2013).

[13] AHMAD M., LALLY JH, MCCREADY A.J., Geology and mineral deposits of the Rum Jungle Mineral Field, Northern Territory, Northern Territory Geological Survey, Report 19 (2006).

[14] LALLY, J. H., BAJWAH, Z. U., Uranium deposits of the Northern Territory, Volume Northern Territory Geological Survey Report 20: Darwin, Northern Territory Geological Survey, 87p (2006).

[15] MCKAY, A.D., MIEZITIS, Y., Australia's Uranium Resources, Geology and Development Of Deposits: AGSO – Geoscience Australia, Mineral Resource Report 1, 184p (2001).

[16] JAIRETH, S., HUSTON, D., Metal endowment of cratons, terranes and districts: Insights from a quantitative analysis of regions with giant and super-giant deposits, Ore Geology Reviews 38(3), 288–303 (2010).

[17] JAIRETH, S., ROACH, I. C., BASTRAKOV, E. N., LIU, S., Basin-related uranium mineral systems in Australia: a review of critical features, Ore Geology Reviews 76, 360–394 (2016).

[18] GRAUCH, R.T., MOSIER, D.L., "Descriptive model of unconformity U-Au", Mineral Deposit Models (COX, D.P. AND SINGER, D.A., Eds.), U.S. Geological Survey Bulletin 1693, 248p (1986).
[19] JEFFERSON, C.W., THOMAS, D.J., GANDHI, S.S., RAMAEKERS, P., DELANEY, G., BRISBIN, D., CUTTS, C., QUIRT, D., PORTELLA, P., OLSON, R.A., "Unconformity- associated uranium deposits of the Athabasca Basin, Saskatchewan and Alberta", Mineral Deposits Of Canada A Synthesis Of Major Deposit-Types, District Metallogeny, The Evolution Of Geological Provinces, And Exploration Methods (GOODFELLOW, W.D., Ed.), Geological Association of Canada, Mineral Deposits Division, Special Publication No. 5, 273–305 (2007).
[20] DAHLKAMP, F. J., ADAMS, S. S., Geology and Recognition Criteria For Veinlike Uranium Deposits Of The Lower To Middle Proterozoic Unconformity And Strata-Related Types, U.S. Department of Energy, National Resource Evaluation GJBX-5(81), 253p (1981).
[21] DAHLKAMP, F.J., Uranium Deposits of The World: Asia. Springer-Verlag, Berlin, 493p (2009).
[22] KYSER, K., CUNEY, M., "Unconformity-related uranium deposits", Recent and Not-So-Recent Developments in Uranium Deposits and Implications for Exploration (CUNEY, M., KYSER, K. Eds.), Mineralogical Association of Canada and Society for Geology Applied to Mineral Deposits, Quebec, 161–219 (2009).
[23] BRUNETON, P., Geological environment of the Cigar Lake uranium deposit, Canadian Journal of Earth Sciences 30(4), 653–673 (1993).
[24] DEROME, D., CATHELINEAU, M., CUNEY, M., FABRE, C., LHOMME, T., BANKS, D. A., Mixing of sodic and calcic brines and uranium deposition at McArthur River, Saskatchewan, Canada: a Raman and laser-induced breakdown spectroscopic study of fluid inclusions, Economic Geology 100(8), 1529–1545 (2005).
[25] POLITO, P.A., KYSER, T.K., THOMAS, D., MARLATT, J., DREVER, G. Re-evaluation of the petrogenesis of the Proterozoic Jabiluka unconformity-related uranium deposit, Northern Territory, Australia, Mineralium Deposita 40, 257–288 (2005).
[26] HEIN, K.A.A., Geology of the Ranger uranium mine, Northern Territory, Australia; structural constraints on the timing of uranium emplacement, Ore Geology Reviews 20, 83–108 (2002).
[27] WILDE, A., AND WALL, V., Geology of the Nabarlek uranium deposit, Northern Territory, Australia, Economic Geology 82(5), 1152–1168 (1987).
[28] CARL, C., PECHMANN, E. V., HÖHNDORF, A., RUHRMANN, G., Mineralogy and U/Pb, Pb/Pb, and Sm/Nd geochronology of the Key Lake uranium deposit, Athabasca Basin, Saskatchewan, Canada, Canadian Journal of Earth Sciences 29(5), 879–895 (1992).
[29] HOEVE, J., SIBBALD, T. I. I., On the genesis of Rabbit Lake and other unconformity-type uranium deposits in northern Saskatchewan, Canada, Economic Geology 73, 1450–1473 (1978).
[30] WORDEN, K., CARSON, C., SCRIMGEOUR, I., LALLY, J., DOYLE, N., A revised Palaeoproterozoic chronostratigraphy for the Pine Creek Orogen, northern Australia: evidence from SHRIMP U–Pb zircon geochronology, Precambrian Research 166(1), 122–144 (2008).
[31] CRAIG, M., Ed., Geological and energy implications of the Pine Creek region airborne electromagnetic (AEM) survey, Northern Territory, Australia, Volume Geoscience Australia Record 2011/18, Geoscience Australia, Canberra, 292p (2011).

[32] TERRITORY URANIUM COMPANY LTD., Daly river uranium exploration, ‘targeted drilling in covered terrain’ (EL 25222-EL 25223), Unpublished report (CR2010-0736) downloaded from the website of Northern Territory Geological Survey, Darwin, 10p (2010).

[33] Cameco Australia Pty Ltd., Detailed diamond drill report for Plateau Project. Unpublished report (CR2007-0563) downloaded from the website of Northern Territory Geological Survey, Darwin, 19p (2007).

[34] Cameco Australia Pty Ltd., Annual report for period 27th May 1999 to 26th May 2000, Deaf Adder Project. Unpublished report (CR2001-0199) downloaded from the website of Northern Territory Geological Survey, Darwin, 21p (2000).

[35] Geophysical and structural interpretation of the greater McArthur Basin. Northern Territory Geological Survey, Digital Information Package DIP 015. (2015).

[36] SINGER, D.A., Typing mineral deposits using their associated rocks and grades and tonnages in a probabilistic neural network, Mathematical Geology 38(4), 465–475 (2006).

[37] MOSIER, D.L., “Grade and tonnage model of unconformity U-Au”, Mineral Deposit Models (COX, D.P., SINGER, D.A., Eds.), U.S. Geological Survey Bulletin 1693, 249–250 (1986).

[38] SINGER, D.A., Conditional estimates of the number of podiform chromite deposits, Nonrenewable Resources 3(3), 200–204 (1994).

[39] SINGER, D.A., BERGER, V.I., MENZIE, W.D., BERGER, B.R., Porphyry copper density, Economic Geology 100(3), 491–514 (2005).

[40] MOSIER, D.L., SINGER, D.A., BERGER, V.I., Volcanogenic massive sulfide deposit density: U.S. Geological Survey Scientific Investigations Report 2007–5082, 21p (2007). [http://pubs.usgs.gov/sir/2007/5082/]

[41] SINGER, D.A., Do we still need experts to make estimates of undiscovered mineral deposits? (Proceedings of the 34th International Geologic Congress), Brisbane, Australia (2012).

[42] MEYER, M.A., BOOKER, J.M., Eliciting And Analyzing Expert Judgment: A Practical Guide: American Statistical Association and Society for Industrial and Applied Mathematics, Philadelphia, PA, USA, 459p (2001).

[43] LISITSIN, V.A. MOORE, D.H., OLSHINA, A., WILLMAN, C.E., Undiscovered orogenic gold endowment in Northern Victoria, Australia, Ore Geology Reviews 38, 252–269 (2010).

UNDISCOVERED URANIUM RESOURCE ASSESSMENT OF ARGENTINA

C. BELLO, L. LÓPEZ, P. FERREYRA
National Atomic Energy Commission (CNEA),
Buenos Aires
Argentina

Abstract

Quantitative approaches have been used for the assessment of undiscovered uranium resources in geological investigation units of Argentina with the highest uranium potential at the current knowledge level. Applications of the McCammon and Deposit Size Frequency (DSF) methods are described in detail using the San Rafael basin investigation unit as example, but are applied as well to Paganzo basin, Pampean Ranges, Salta Group basin and Chubut basin.

1. INTRODUCTION

The International Atomic Energy Agency (IAEA) [1] specified the various reasons for the need to estimate undiscovered uranium resources. For individual countries, knowledge of uranium resources can play an important role in establishing energy policies and optimizing the use of natural resources. For an exploration project, an initial estimate of undiscovered resources can be useful in guiding the collection of new data and the direction of exploration; subsequent estimates can aid in focusing exploration on areas best suited for future discovery of resources.

However, the evaluation of potential or undiscovered resources can be considered controversial, as it is based on speculative concepts and on more or less incomplete data on the geological environments of uranium deposits. In spite of the uncertainty these issues bring, it is worthwhile to evaluate the potential of yet-to-be discovered resources that can be progressively refined as knowledge of uranium deposits and their geologic settings becomes more complete [2].

2. METHODOLOGY

To evaluate uranium favorability and to estimate undiscovered uranium resources in Argentina, the United States National Uranium Resource Evaluation (NURE) quantitative approach has been applied [1–3]. The implementation of this approach was supported by the IAEA Technical Cooperation Project 'Uranium Favorability and Exploration in Argentina (ARG 3/007)' during 1993–1997 [4, 5]. In this general context, the National Atomic Energy Commission (CNEA) has set up the 'Uranium Favorability Program' to estimate both geological (endowment) and potential (economic endowment) uranium resources using a quantitative systematic methodology to establish in a comprehensive manner the uranium resources of the country.

Conceptually, the methodology involves comparing the geological characteristics of an Investigation Unit (IU) whose favorability has been determined with those of a Control Area (CA) where the mineralization, the geological characteristics and parameters of the deposits, notably resources and average grades, have been well studied. These data constitute the base of a 'geological model'. Both active and defunct mines provide technical records such as extraction methods, dilution, mining-milling recovery factor, working days per year, annual production modules, which constitute a 'technical model'. When historical production costs, historical market values and the projection of economic variables during the life of the deposit are provided, it is also possible to define an 'economic model'. The geological, technical and economic models are established in a CA and together they constitute the 'model'.

The study of uranium favorability was developed in two main phases (Fig. 1). One was the elaboration of the geological base and the classification of the IU as favorable, unfavorable or uncertain, and the second involved the development of the CA and the estimation of both geological and potential resources. These resources evaluated for different Favorable Areas (FA) within IUs are 'Undiscovered Resources', which are expected to be present according to indirect evidence or geological extrapolations and that can be discovered by existing exploration techniques [6].

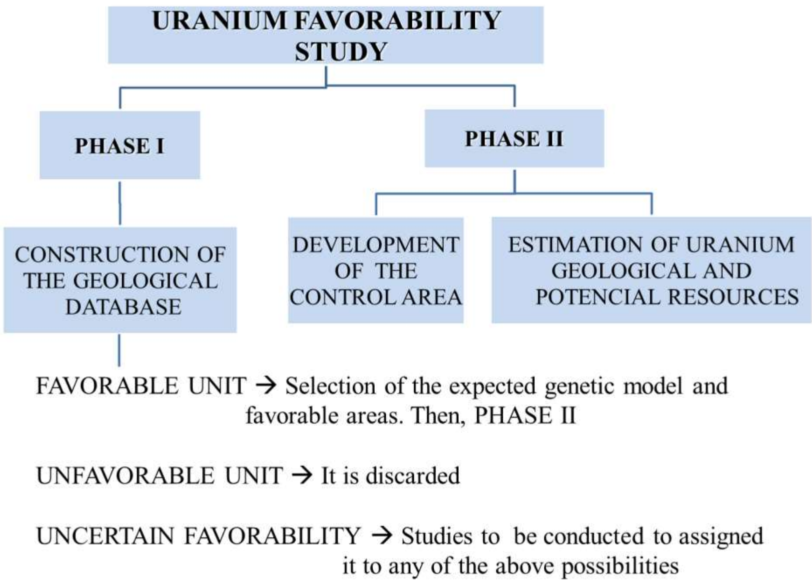

FIG. 1. Phases of the quantitative methodology for uranium favorability study.

3. URANIUM FAVORABILITY PROGRAM OF ARGENTINA

3.1. Phase I: construction of the geological database

To assess uranium favorability and to estimate potential uranium resources by the application of quantitative methods, the country was divided into 61 IUs (Fig. 2). Covering ~1,450,000 km^2 of the country, these areas were delineated on the basis of geotectonic setting and petrological, mineralogical and geochemical features. The assessment of undiscovered uranium resource has been completed in five of the 61 IUs, namely: Salta Group Basin, Pampean Ranges, Paganzo Basin, San Rafael Basin and Chubut Group Basin (Fig. 3).

3.1.1. Geological databases

The construction of different Geological Bases included the tasks of gathering, analyzing and synthesizing existing geological information from complementary geological reconnaissance studies. This information reflects the chronology of processes involved in the formation of uranium deposits, which include the following:

— Precursor processes (tectonic setting, regional geology, regional structure);
— Host rock formation (age, lithology, genesis);
— Host rock preparation (physical changes, chemical alteration, tramps);
— Uranium source development;
— Transport of uranium (potential solution pathways, timing conditions);
— Primary uranium mineral deposition (occurrence of uranium, precipitation conditions, age of mineralization);
— Post primary redistribution of uranium (geological history);
— Preservation (tectonic, erosional).

The final conclusion of the geological database report consists of the qualification of an IU as favorable, unfavorable or of uncertain geological favorability to contain uranium deposits of a determined typology and the possible geological formations to host them. The locations of FAs with the most uranium potential, which reflect the main characteristics of an IU, are also included in the report.

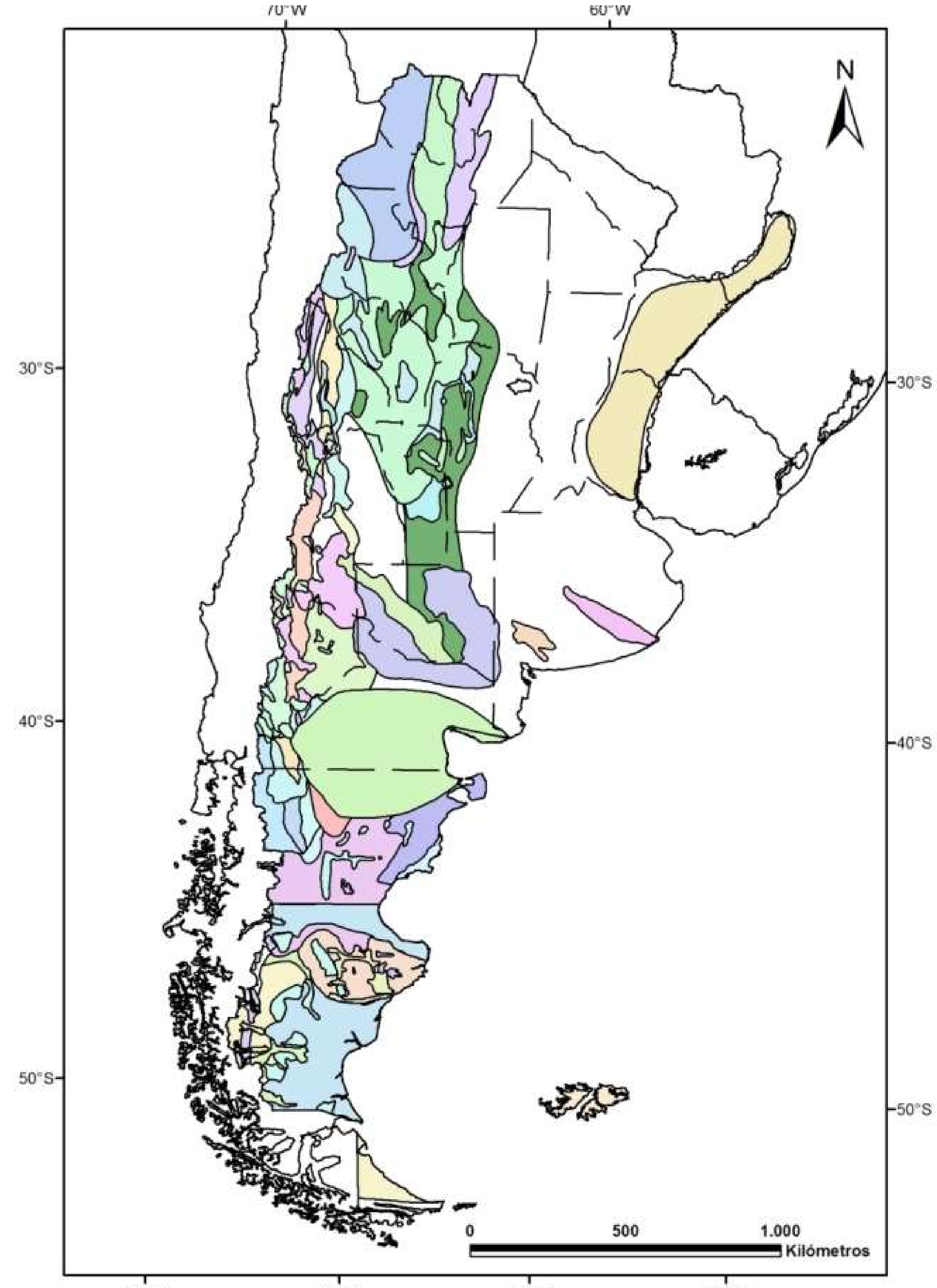

FIG. 2. Investigations units (IUs) for the assessment of uranium favorability and undiscovered uranium resource in Argentina.

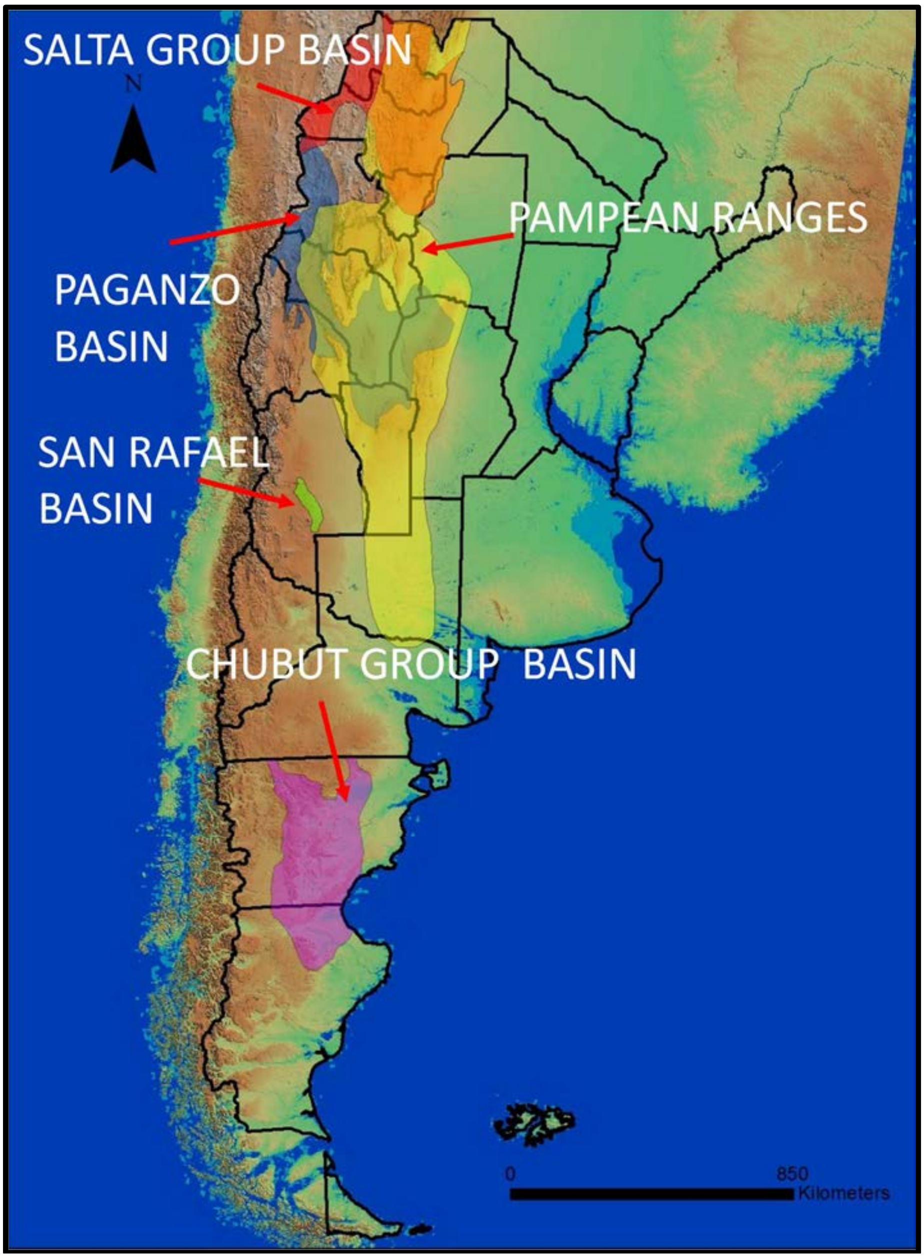

FIG. 3. IUs where assessment for undiscovered uranium resource has been completed.

3.1.2. Investigation units and favorable areas

The main features of the IUs studied, the geological types of expected uranium deposits and the FAs outlined for the assessment of undiscovered uranium resource, are presented below.

3.1.2.1. Salta group basin

The Cretaceous Salta Group Basin belongs to an extensive intra-continental geotectonic setting and extends into the northwestern part of Argentina. It is characterized by fluvial – lacustrine sediments, with a little transgressive marine influence, which lie over the Proterozoic igneous-metamorphic basement and under the Tertiary continental sedimentary rocks. The sedimentary sequence presents reducing environment associated to pelitic facies, which were favorable for the syngenetic formation of sandstone type uranium deposits [7]. In this IU, five FAs have been defined (Fig. 4).

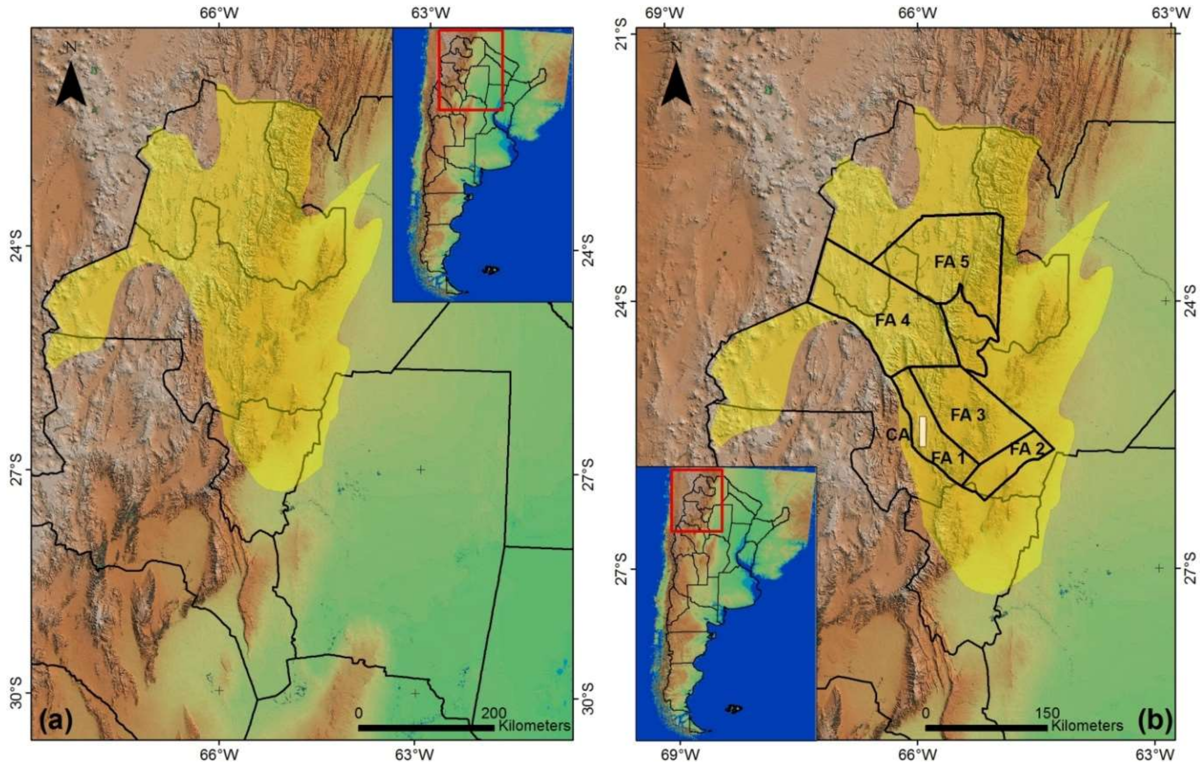

FIG. 4. Salta Group Basin: (a) location of the IU; (b) detail of FAs and CA. IU is indicated as a yellow-shaded area. Insets indicate the location at country scale.

3.1.2.2. Pampean Ranges

The Pampean Ranges belong to a Precambrian–Paleozoic peri-cratonic orogenic basin made of poly-metamorphic rocks intruded by magmatic rocks with a wide compositional spectrum. This IU exhibits a block faulting structure whose valleys have been covered by the Upper Paleozoic, Mesozoic and Cenozoic sediments. Uranium mineralization is linked to magmatic and hydrothermal processes, and the granite-related type is the main model considered [8]. In this IU, six FAs have been identified (Fig. 5).

3.1.2.3. Paganzo Basin

It is constituted by sedimentary rocks of Carboniferous and Permian age and covers ~150,000 km². The sedimentary rocks are assembled in diverse isolated sub-basins and unconformably overlie the main basement. The basin is dominantly fluvial – lacustrine and described as an extensive back-arc basin with marine influence. The origin of the uranium deposits is directly related to the circulation of dispersed acid solutions in groundwater and to the contribution and concentration of CO_2 accompanying the vulcanite effusions. Sandstone type of uranium deposits, both roll front and tabular, can be found [9, 10]. Five FAs have been studied (Fig. 6).

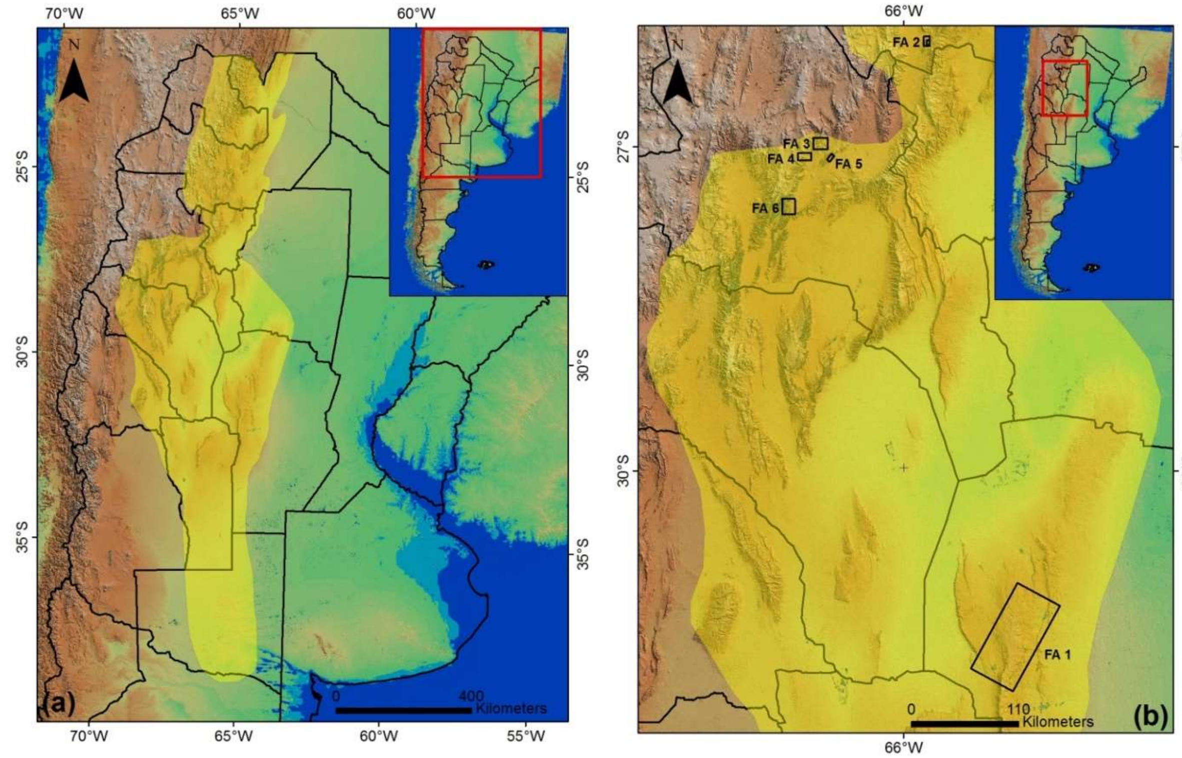

FIG. 5. Pampean Ranges: (a) location of the IU; (b) detail of FAs and CA. IU is indicated as a yellow-shaded area. Insets indicate the location at country scale.

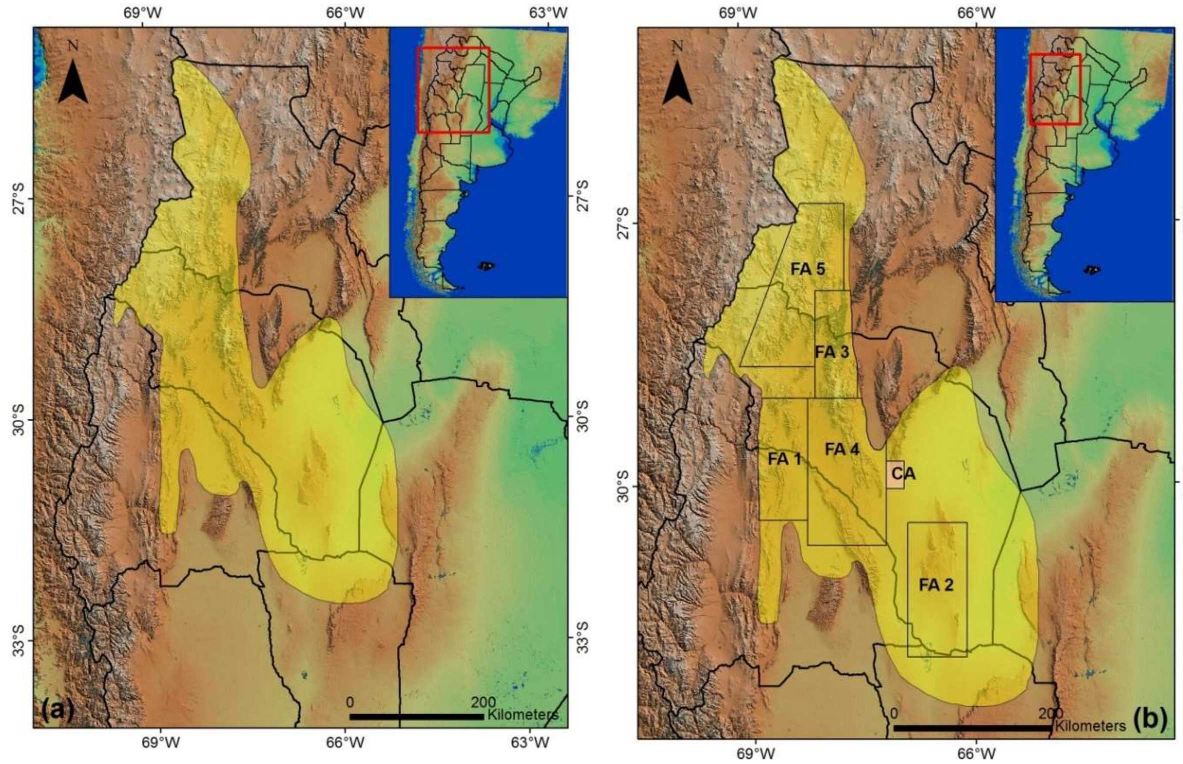

FIG. 6. Paganzo Basin: (a) location of the IU; (b) detail of FAs and CA. IU is indicated as a yellow-shaded area. Insets indicate the location at country scale.

3.1.2.4. San Rafael Basin

This is a back-arc basin filled with marine and continental sediments during late Carboniferous and then by volcanic and sedimentary rocks during Permian. The volcanic rocks are part of a wide extended rhyolitic province, the Choiyoi province. The sequence ends up with Lower – Middle Triassic continental sediments, rhyolitic ignimbrites and basaltic extrusions. Uranium deposits belong to the volcanic-related type (syn-sedimentary subtype), hosted by eolian sandstones with abundant pyroclastic material [11, 12] (Fig. 7).

3.1.2.5. Chubut Group Basin

The Cretaceous Chubut Group is an intra-cratonic basin related to rifting and extensional structures. The basin filling consists of continental sedimentary rocks, with some marine sequences. Uranium deposits are either sandstone-type (paleo-channel, tabular, roll-front?) or volcanic-related (syn-sedimentary). Seven FAs have been identified [13] (Fig. 8).

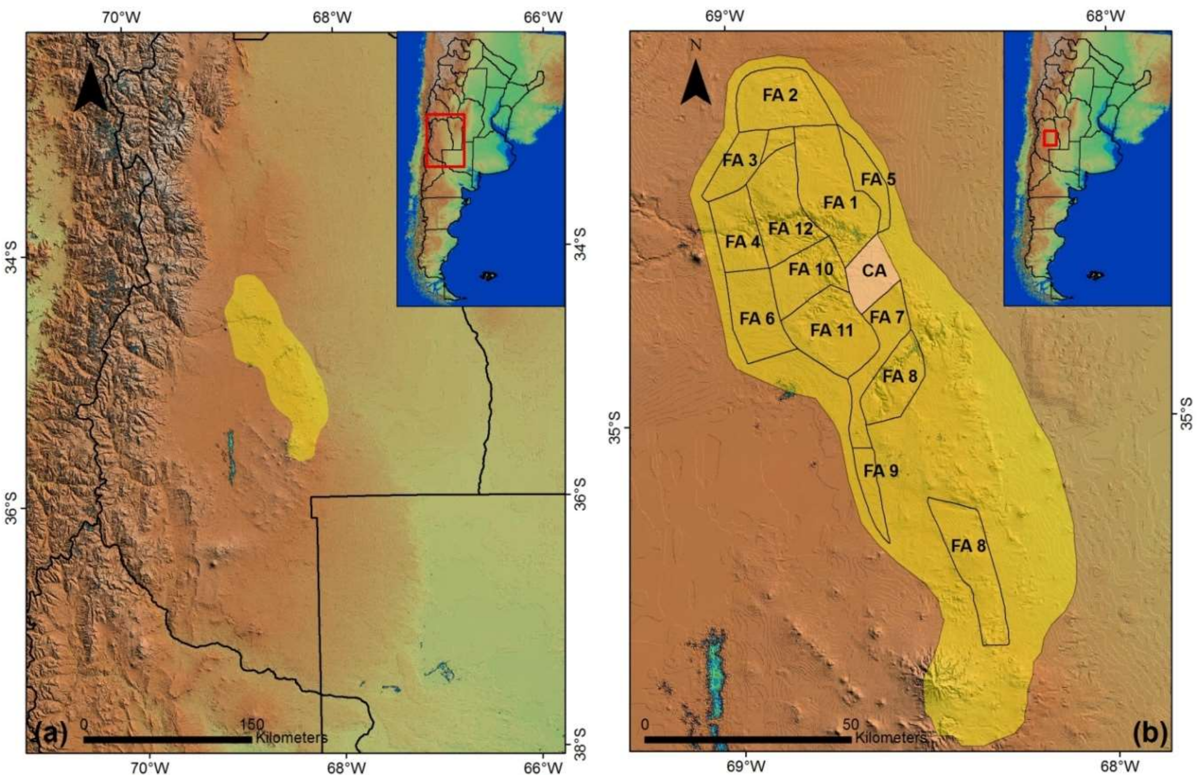

FIG. 7. San Rafael Basin (a) location of the IU; (b) detail of FAs and CA. IU is indicated as a yellow-shaded area. Insets indicate the location at country scale.

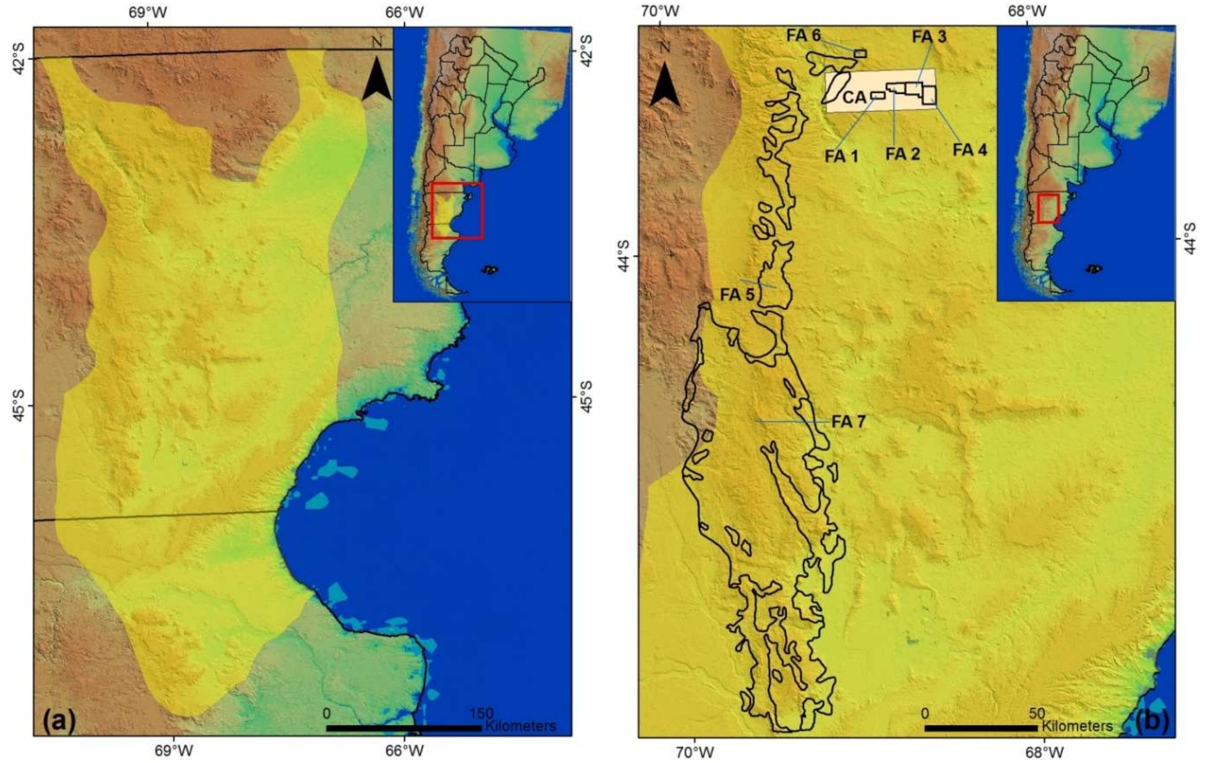

FIG. 8. Chubut Group Basin: (a) location of the IU; (b) detail of FAs and CA. IU is indicated as a yellow-shaded area. Insets indicate the location at country scale.

3.2. Phase II: development of the control area

A CA is a chosen geographical area, for which geological characteristics, potential resources, identified uranium resources and production are known. It is distinctive for each genetic mineralization model of a potential deposit and their geologic setting, and it should ideally occur in the same geologic context; in it defect, it can be developed on the available databases (e.g., UDEPO [14]) of the main deposits of the same mineralization model for other areas with similar geological characteristics [15].

The principal purpose of the development of the CA is to support the estimation of uranium geological resources or endowment in a FA, at a cut-off grade of 0.010% U, and uranium potential resources, or economic endowment, at a given economic cut-off grade.

3.2.1. Grade-tonnage distributions

Uranium grade-and-tonnage distributions developed from the sets of deposits in a CA are extremely important for the estimation of undiscovered resources. These distributions are referred to as tonnage-grade curves. Usually, these curves are developed from ore in a single deposit, but sometimes they are developed from ores in a set of deposits. There are three different relations that are collectively referred to as grade-tonnage curves: cut-off grade versus cumulative ore, average grade versus cut-off grade, and cumulative average grade versus cumulative ore.

The development of the CA is explained here in detail using the IU of the San Rafael Basin as example. In this IU, the CA defined for the volcanic-related syn-sedimentary type of uranium deposit measures131 km^2 and includes the Sierra Pintada mine, which records the highest historical production in the country consisting of 1,600 t of U. Fig. 7b shows the location of this CA, which is bounded by FAs 1, 7, 10 and 11 [16].

Data are available from 12 uranium deposits, whose in situ resources and grades have been determined mostly from drilling and underground works (Table 1). By processing historical production data from the Los Reyunos deposit, the average grade and tonnages of uranium at selected cut-off grades are derived (Table 2), from which a grade-tonnage curve was constructed (Fig. 9).

TABLE 1. ORIGINAL DATA OF TONNAGES AND GRADES OF THE 12 DEPOSITS IN THE CA IN THE SAN RAFAEL BASIN

Nº	Deposits	t ore	U%	t U	Cut-off U%
1	Tigre I	5,545,229	0.1187	6,583	0.0339
2	La Terraza	3,847,605	0.0933	3,589	0.0339
3	Terraza Norte	3,838,673	0.0746	2,865	0.0254
4	Media Luna I-II	1,619,835	0.0628	1,016	0.0339
5	Tigre III	1,343,882	0.0678	912	0.0339
6	Media Luna III-IV	557,769	0.0585	326	0.0339
7	La Caverna	337,913	0.0424	143	0.0254
8	Los Reyunos	261,434	0.1003	262	0.0339
9	Gauchos I-II	188,760	0.0729	138	0.0339
10	Los Chañares	113,185	0.0653	74	0.0339
11	La Pintada	52,128	0.0763	40	0.0254
12	Sondeo XCIII	21,068	0.1187	25	0.0254
	Total	17,727,481	0.0793	15,973	0.0311

The mathematical relations obtained from the grade-tonnage curve allowed standardization of the relative values of extractable ore (t Ore), recoverable uranium (t U) and average grades (% U) as a function of different cut-off grades. Therefore, as the final step of the development of the CA, the model was applied to recalculate tonnages and grades of all the deposits in the CA at a cut-off grade of 0.010% U and at a determined economic cut-off grade of 0.050% U as shown in Tables 3 and 4, respectively.

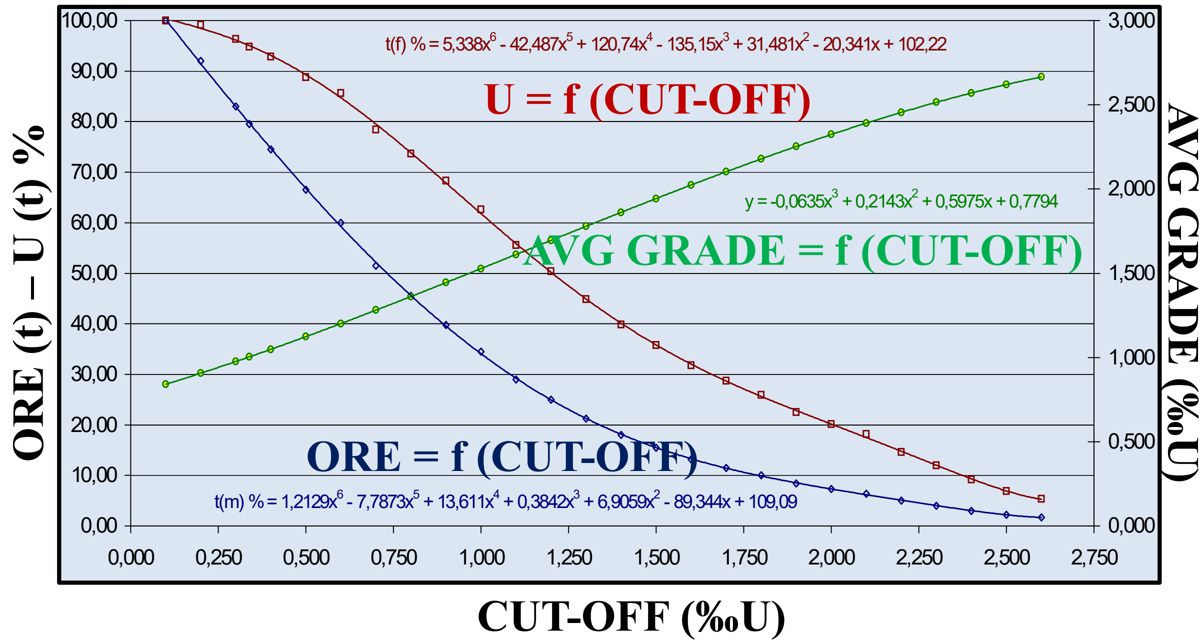

FIG. 9. Grade-tonnage curve of the CA in the San Rafael Basin.

TABLE 2. TONNAGES AND AVERAGE GRADES AT VARIOUS CUT-OFF GRADES

Cut-off U%	U%	t ore	t U
0.010	0.084	328,593	276
0.020	0.091	302,305	274
0.030	0.098	272,732	266
0.040	0.105	244,801	257
0.050	0.112	218,514	246
0.060	0.120	197,156	237
0.070	0.128	169,225	217
0.080	0.136	149,510	204
0.090	0.144	130,780	189
0.100	0.153	113,364	173
0.110	0.161	95,292	154
0.120	0.170	82,148	139
0.130	0.178	69,662	124
0.140	0.186	59,147	110
0.150	0.194	50,932	99
0.160	0.202	43,374	88
0.170	0.210	37,788	79

Cut-off U%	U%	t ore	t U
0.180	0.218	32,859	72
0.190	0.225	27,602	62
0.200	0.232	23,987	56
0.210	0.239	21,030	50
0.220	0.245	16,430	40
0.230	0.251	13,144	33
0.240	0.257	9,858	25
0.250	0.262	7,229	19
0.260	0.267	5,586	15

TABLE 3. TONNAGES AND GRADES OF THE DEPOSITS CONTAINED IN THE SAN RAFAEL BASIN CA AT A CUT-OFF GRADE OF 0.010% U

Nº	Deposits	t Ore	U%	t U	Cut-off U%
1	Tigre I	6,969,721	0.100	6,949	0.010
2	La Terraza	4,836,001	0.078	3,787	0.010
3	Terraza Norte	4,429,194	0.067	2,954	0.010
4	Media Luna I-II	2,035,948	0.053	1,073	0.010
5	Tigre III	1,689,107	0.057	963	0.010
6	Media Luna III-IV	701,052	0.049	344	0.010
7	La Caverna	389,896	0.038	148	0.010
8	Los Reyunos	328,593	0.084	277	0.010
9	Gauchos I-II	237,250	0.061	145	0.010
10	Los Chañares	142,261	0.055	78	0.010
11	La Pintada	60,147	0.068	41	0.010
12	Sondeo XCIII	24,309	0.106	26	0.010
12	Total	21,843,479	0.068	16,785	0.010

TABLE 4. TONNAGES AND GRADES OF THE DEPOSITS CONTAINED IN THE SAN RAFAEL BASIN CA AT THE ECONOMIC CUT-OFF GRADE OF 0.050% U

Nº	Deposits	t Ore	U%	t U	Cut-off U%
1	Tigre I	4,646,567	0.133	618	0.050
2	La Terraza	3,224,060	0.105	337	0.050
3	Terraza Norte	2,952,850	0.089	263	0.050
4	Media Luna I-II	1,357,324	0.070	96	0.050
5	Tigre III	1,126,092	0.076	86	0.050
6	Media Luna III-IV	467,377	0.066	31	0.050
7	La Caverna	259,935	0.051	13	0.050
8	Los Reyunos	219,066	0.113	25	0.050
9	Gauchos I-II	158,169	0.082	13	0.050
10	Los Chañares	94,842	0.073	7	0.050
11	La Pintada	40,099	0.091	4	0.050
12	Sondeo XCIII	16,206	0.142	2	0.050
12	Total	14,562,587	0.091	1,494	0.050

3.2.2. Calibration of the control area

The calibration of the CA, to estimate the uranium grade and tonnage distributions for the contained set of known deposits, is adopted from the 'McCammon step–by-step' and 'Deposit Size Frequency (DSF)' methods.

3.2.2.1. McCammon method

This method considers the combined probability of occurrence of the number of deposits and the ore tonnages by size class and grade intervals. It is specific for a given geological setting and metallogenic model, and applied in a particular target area. Assessments of geological and potential uranium resources in the FAs are performed taking into account both size classes and grade ranges determined with this method.

The different steps of the method are as follows:

- Analysis of the distribution of the deposits in the CA in size classes (Tables 5 and 6);
- Analysis of the distribution of the total tonnage of U in size classes for a given average grade (Tables 7 and 8);
- Analysis of the distribution of the total tonnage of U both in size classes and average grade intervals (Tables 9 and 10).

TABLE 5. DISTRIBUTION OF DEPOSITS IN THE CA IN SIZE CLASSES AT A CUT-OFF OF 0.010% U

Geological resources			Cut-off= 0.010% U	
Size classes	t Ore		Deposits	Probability%
1	18,000	90,000	2	0.167
2	90,000	450,000	4	0.333
3	450,000	2,250,000	3	0.250
4	2,250,000	11,250,000	3	0.250
5	11,250,000	56,250,000	0	0.000
			12	1.000

TABLE 6. DISTRIBUTION OF THE DEPOSITS IN THE CA IN SIZE CLASSES AT THE ECONOMIC CUT-OFF OF 0.050%

Potential uranium resources			Cut-off= 0.050 %U	
Size classes	t Ore		Deposits	Probability %
1	12,500	62,500	2	0.167
2	62,500	312,500	4	0.333
3	312,500	1,562,500	3	0.250
4	1,562,500	7,812,500	3	0.250
5	7,812,500	39,062,500	0	0.000
			12	1.000

TABLE 7. DISTRIBUTION OF TOTAL TONNAGE OF U OF THE DEPOSITS IN THE CA IN SIZE CLASSES FOR A GIVEN AVERAGE GRADE AT A CUT-OFF OF 0.010 %U

Nº	Control area deposits	t Ore	U%	t U	Cut-off grade= 0.010% U P(t U)		Avg U%	Nº deposits	Size classes
1	Tigre I	6,969,721	0.100	6,950	0.4140				
2	La Terraza	4,836,001	0.078	3,789	0.2257				
3	Terraza Norte	4,429,194	0.067	2,955	0.1760	0.8157	0.087	3	4
4	Media Luna I-II	2,035,948	0.053	1,073	0.0639				
5	Tigre III	1,689,107	0.057	962	0.0573				
6	Media Luna III-IV	701,052	0.049	345	0.0205	0.1418	0.054	3	3
7	La Caverna	389,896	0.038	148	0.0088				
8	Los Reyunos	328,593	0.084	277	0.0165				
9	Gauchos I-II	237,250	0.061	145	0.0087				
10	Los Chañares	142,261	0.055	78	0.0046	0.0386	0.065	4	2
11	La Pintada	60,147	0.068	41	0.0024				
12	Sondeo XCIII	24,309	0.106	26	0.0015	0.0040	0.083	2	1
	Total	21,843,479	0.077	16,788	1.0000	1.0000			

TABLE 8. DISTRIBUTION OF THE TOTAL TONNAGE OF U OF THE DEPOSITS IN THE CA IN SIZE CLASSES FOR A GIVEN AVERAGE GRADE AT A CUT-OFF GRADE OF 0.050%U

Nº	Control area deposits	t Ore	U%	t U	Cut-off grade= 0.050% U P(t U)		Avg U%	Nº deposits	Size classes
1	Tigre I	4,646,567	0.1331	6,185	0.4140				
2	La Terraza	3,224,060	0.1046	3,372	0.2257				
3	Terraza Norte	2,952,850	0.0890	2,629	0.1760	0.8157	0.116	3	4
4	Media Luna I-II	1,357,324	0.0704	955	0.0639				
5	Tigre III	1,126,092	0.0761	856	0.0573				
6	Media Luna III-IV	467,377	0.0656	307	0.0205	0.1418	0.072	3	3
7	La Caverna	259,935	0.0506	132	0.0088				
8	Los Reyunos	219,066	0.1125	246	0.0165				
9	Gauchos I-II	158,169	0.0818	129	0.0087				
10	Los Chañares	94,842	0.0732	69	0.0046	0.0386	0.087	4	2
11	La Pintada	40,099	0.0911	37	0.0024				
12	Sondeo XCIII	16,206	0.1417	23	0.0015	0.0040	0.111	2	1
	Total	14,562,588	0.1026	14,940	1.0000	1.0000			

TABLE 9. DISTRIBUTION OF TOTAL TONNAGE OF U BOTH IN SIZE CLASSES AND AVERAGE GRADE INTERVALS AT A CUT-OFF GRADE OF 0.010% U

Geological resources			Grade intervals U%		Cut-off 0.010			
Range of size classes t ore			1		2		3	
			0.04	0.075	0.075	0.086	0.086	0.113
1	18,000	90,000	0		0.0004		0	
2	90,000	450,000	0		0.0039		0	
3	450,000	2,250,000	0.0142		0		0.0816	
4	2,250,000	11,250,000	0		0		0	
5	11,250,000	56,250,000	0		0		0	

TABLE 10. DISTRIBUTION OF TOTAL TONNAGE OF U BOTH IN SIZE CLASSES AND AVERAGE GRADE INTERVALS AT A CUT-OFF GRADE OF 0.050% U

Potential resources			Grade intervals U%		cut-off 0.050			
Range of size classes t ore			1		2		3	
			0.05	0.1	0.1	0.15	0.15	0.22
1	12,500	62,500	0		0.0004		0	
2	62,500	312,500	0		0.0039		0	
3	312,500	1,562,500	0.0142		0		0	
4	1,562,500	7,812,500	0		0.0816		0	
5	7,812,500	39,062,500	0		0		0	

3.2.2.2. Deposit Size Frequency (DSF) Method

This method considers both statistical and geological concepts, and allows to estimate the calculation of the global geological resources and potential uranium resources based on deposit density by size classes and the factor $F = L \times P$ [3], where F is a weighting factor of the resource quantities expressed in tons of uranium, L is the degree of likeness between a FA and its CA according to a geological criterion (it varies from 0 to 1); and P is the probability of discovering at least one deposit (i.e., with 10 t U or more) based on the level of knowledge of the favorable geological criteria (it varies from 0 to 1). The $L \times P$ is optional scaling factor F that, on the whole expresses, the conformity between the endowment in the FA and that in the CA, for which estimates of the number of deposits in different size classes have been made. The L and P parameters are established in a subjective manner through an elicitation process, which involves formalized discussion between the principal geoscientist and the team of experts in order to review the investigation and to derive these factors for estimation of uranium resources in the FAs.

The application of the DSF method for estimating resources is processed using the same size classes and average grade intervals defined by the McCammon method.

The mathematical formula that links the different parameters for the estimation of resources (t U) in a CA or in a FA is (adapted from [3]):

$$U = A[\sum_{i=1}^{k=n} (n_{ic}/A_c)T_{ic}G_i]L \times P$$

where U stands for geological resources or uranium potential resources expressed in t U, A is surface of the FA in the same unit as for the CA (e.g., km^2), T is size class, K is number of deposit size classes, n_{ic}/A_c is the spatial density (number of deposit/unit area) of deposits of size T_i in the i-th deposit size class within a CA (A_c), n is number of deposit for a size class, ic is size class, A_c is surface of the FA in the same unit as for the CA (e.g., km^2), T_{ic} is average value of T, G_i is average grade of the size class.

The computer program TENDOWG [17], which consists of a DOS application, was used to calculate resources according to the DSF method. Table 11 lists the data used for the calculation of geological resources in the CA and FA 1 'Carrizalito – Agua de la Nieves' of the San Rafael Basin, whereas Table 12 lists the output tonnages and Pearson´s percentiles for the calculations in the mentioned CA.

TABLE 11: DATA INPUT FOR THE TENDOWG SCRIPT. EXAMPLE ESTIMATION OF GEOLOGICAL RESOURCES FOR THE CA AND FA 1 'CARRIZALITO – AGUA DE LA NIEVES' IN THE SAN RAFAEL BASIN. EXPLANATION OF PARAMETERS ARE GIVEN IN PARENTHESIS.

Geological Resources
Control Area – San Rafael Basin – 0.010% U (cut-off grade)
A (surface of the Control Area)
131 (km^2)
F (L.P, scaling factor)
0.5, 0.708, 1 (minimum, medium, maximum of L.T)
T (size class)
5 (number of size classes)
18000, 90000 (interval t ore of class T1)
0.01525, 0.01526, 0.01527 (min. med. and max. probabilities of finding deposits of class T1)
90000, 450000 (interval t ore of class T2)
0.03051, 0.030523, 0.03053 (min. med. and max. probabilities of finding deposits of class T2)
450000, 2250000 (interval t ore of class T3)
0.02288, 0.02289, 0.02290 (min. med. and max. probabilities of finding deposits of class T3)
2250000, 11250000 (interval t ore of class T4)
0.02288, 0.02289, 0.02290 (min. med. and max. probabilities of finding deposits of class T4)
11250000, 56250000 (interval t ore of class T5)
0.00000, 0.00000, 0.00000 (min. med. and max. probabilities of finding deposits of class T5)
G (average grade of the Control Area)
0.0678, 0.0949, 0.1173 (min. med. and max. average grades in %U)
U (code of continuation)
R (code of Geological Resources)
Geological Resources
Favorable Area 1 "Carrizalito – Agua de las Liebres" – 0.010% U (cut-off grade)
A (surface of Favorable Area 1)
412 (km2)
F (L.P, scaling factor)
0, 0, 0.541 (minimum, medium, maximum of L.T)
U (code of continuation)
R (code of Geological Resources)
Favorable Area 2 …
…
S (code of data entry ending)

TABLE 12: OUTPUT FROM THE TENDOWG SCRIPT. EXAMPLE ESTIMATION OF GEOLOGICAL RESOURCES FOR THE CA IN SAN RAFAEL BASIN. TONNAGES CORRESPONDING TO PEARSON´S PERCENTILES 0.95 ARE HIGHLIGHTED.

---------- PEARSON PERCENTILES FOR ENDOWMENT ---------

In t U
TONS PROBABILITY
U COND UNCOND

t U	Percentile
0.64019E+03	.05
0.68566E+03	.10
0.73113E+03	.15
0.77659E+03	.20
0.82206E+03	.25
0.08675E+04	.30
0.09130E+04	.35
0.10034E+04	.40
0.11689E+04	.45
0.13640E+04	.50
0.16350E+04	.55
0.20172E+04	.60
0.25323E+04	.65
0.32243E+04	.70
0.41786E+04	.75
0.55280E+04	.80
0.75187E+04	.85
0.10705E+05	.90
0.16809E+05	**.95**

3.2.3. Fine tuning

The final adjustment of the model that will be applied for the calculation of undiscovered resources in all the favorable areas is verified by comparing the estimates obtained by the McCammon and DSF methods with the identified resources mined and/or existing in the Control Area. As shown in Table 13 the different estimates are considered equivalent and, therefore, the adequate combination of parameters of the model is suitable to be applied in the 12 FAs of the San Rafael Basin for the final assessment of undiscovered resources.

TABLE 13. COMPARISON BETWEEN UNDISCOVERED URANIUM RESOURCES ESTIMATED BY THE MC CAMMON AND DSF METHODS AND THE IDENTIFIED RESOURCES (IR) OF THE CA

		Uranium Resources		
Estimates		McCammon	DSF	IR
Cut-off	0.01% U	16,788 t U	16,809 t U	16,830 t U
	0.05% U	14,940 t U	14,941 t U	14,980 t U

3.3. Phase III: assessment of geological and potential uranium resources

The San Rafael basin occupies 7,176 km^2, of which 4,306 km^2 have been considered as unfavorable areas and discarded. Therefore, by applying the parameters defined for the CA, geological and potential uranium resources have been estimated in the remaining 2,739 km^2 occupied by 12 FAs with diverse geological prospectivity for the volcanic-related deposit model.

Table 14 shows measured areas, degree of likeness (*L*), geological knowledge (*P*) and factor *F* (*L*×*P*) of the FAs defined for the San Rafael Basin, which have been used in the DSF method to estimate both geological and potential uranium resources. Mean values of 7,204 t U and 3,020 t U, obtained respectively, are considered the most reliable estimates. According to the results obtained by McCammon method and already discussed, these estimated resources are expected to come from the size class between 1,562,500 and 7,812,500 t ore at average grades between 0.10 and 0.15% U, with a probability of occurrence of 8.16% (see Table 10).

TABLE 14. GEOLOGICAL AND POTENTIAL URANIUM RESOURCES FOR THE 12 FAVORABLE AREAS OF THE SAN RAFAEL BASIN BY PROCESSING THE DEPOSIT SIZE FREQUENCY (DSF) METHOD

Favorable area	DSF				Geological resources			Potential uranium resources		
					t U (cut-off % U = 0.001)			t U (cut-off % U = 0.001)		
	Area (km^2)	L	P	F	Min	Median	Max	Min	Median	Max
FA1-Carrizalito-Agua de las Liebres	412	0.744	0.727	0.541	855	2,348	23,565	446	973	18,993
FA2- Las Peñas	285	0.244	0.518	0.126	248	525	6,470	108	242	5,197
FA3-Mina Santa Elena-Pto. López	140	0.672	0.620	0.417	269	679	7,274	133	291	5,843
FA4-Agua del Toro-Pantanito	193	0.637	0.598	0.381	360	884	9,675	174	383	7,767
FA5-Las Vertientes-La Hedionda	114	0.424	0.472	0.200	158	336	4,108	69	154	3,300
FA6-Pampa del Diamante	246	0.453	0.303	0.137	233	496	6,072	102	227	4,878
FA7-Puesto Cochicó-El Nihuil	206	0.520	0.502	0.261	462	1,029	12,167	150	334	7,033
FA8-Valle Grande-Los Leones	199	0.300	0.554	0.167	230	488	5,988	100	224	4,810
FA9-Subcc. del Nihuil	85	0.118	0.293	0.034	20	42	521	9	20	418
FA10-Agua del Infierno	209	0.084	0.359	0.030	43	92	1,130	19	42	907
FA11-Caldera del Potrerito	290	0.103	0.362	0.037	75	158	1,933	32	72	1,553
FA12-Cerro Rodeo	360	0.095	0.239	0.023	58	123	1,492	25	56	1,198
Total	2,739	0.366	0.462	0.169	3,010	7,204	80,393	1,367	3,020	61,898

TABLE 15: GEOLOGICAL URANIUM RESOURCES OF THE INVESTIGATION UNITS AT 0.01 %U CUT-OFF GRADE

Investigation units	Geological resources t U		
	Control area	Favorable areas	Total
San Rafael Basin	16,800	7,200	24,000
Paganzo Basin	500	2,200	2,700
Pampean Ranges	External area	24,000	24,000
Salta Group Basin	4,800	193,200	198,000
Chubut Group Basin	10,200	20,200	30,400
Total	32,300	246,800	279,100

TABLE 16: POTENTIAL URANIUM RESOURCES OF THE INVESTIGATION UNITS AT A SPECIFIC CUT-OFF GRADE FOR EACH STUDY CASE (E.G., 0.05 %U FOR SAN RAFAEL BASIN)

Investigation units	Potential resources t U		
	Control area	Favorable areas	Total
San Rafael Basin	15,000	3,050	18,050
Paganzo Basin	350	1,350	1,700
Pampean Ranges	External area	14,300	14,300
Salta Group Basin	1,000	29,100	30,100
Chubut Group Basin	7,000	8,300	15,300
Total	23,350	56,100	79,450

The same methodology described for the San Rafael basin case study has been applied to estimate the undiscovered uranium resources of the Paganzo Basin [18], Pampean Ranges [19], Salta Group Basin [20] and Chubut Basin [21, 22]. Tables 15 and 16 summarize the geological and potential uranium resources for the five IUs studied, which have been estimated as 279,100 t U and 79,450 t U, respectively [23].

4. CONCLUSIONS

The estimation of undiscovered uranium resources constitutes a valuable tool to sustain the state policy on planning exploration and eventual production projects, in accordance with the adopted nuclear supply strategy, independent of uranium immediate requirements.

The results of the quantitative methodology used depend on the fidelity of the available data and would allow defining appropriate criteria in formulating exploration programs and assessing uranium resources. Therefore, additional efforts should be made to improve the quantity and quality of geoscientific data pursuing the aim of increasing the degree of confidence in the estimates.

The assessment of Argentina's uranium potential is far from complete, as only a part of the territory has been considered so far. Nevertheless, the obtained results reflect the existing resources at the level of the current geological knowledge of the most interesting uranium investigation units.

It can be pointed out that the existence of favorable basins and different models of mineralization configure promising conditions to define and develop new uranium resources in Argentina.

REFERENCES

[1] IAEA, Methods for the estimation and economic evaluation of undiscovered uranium endowment and resources: an instruction manual, Volume Technical Report Series 344: Vienna, IAEA, 145p (1992).

[2] MCCAMMON, R., Uranium Resources/ Reserves Lecture, United States of the Interior, Geological Survey, Open File Report 97-701, 38p (1997).

[3] FINCH, W.I., MCCAMMON, R.B., Uranium assessment by the Geological Survey: proposed methodology and a plan to update the national resource base. U.S. Geological Survey Circular 994, 31p (1987).

[4] INTERNATIONAL ATOMIC ENERGY AGENCY, http://www.iaea.org/technicalcooperation/ Home/index.html (2017).

[5] LOPEZ, L., FERREYRA, R., Overview of the IAEA national technical cooperation projects on uranium exploration in Argentina, Uranium raw material for the nuclear fuel cycle: exploration, mining, production, supply and demand, economics and environmental issues (URAM-2009): proceedings of an international symposium, IAEA, Vienna, Appendix, TC workshop (2014).

[6] OECD-NEA & IAEA, Uranium 2016: Resources, Production and Demand. OECD Report No. 7301, Organization for Economic Co-operation and Development (OECD), Nuclear Energy Agency (NEA), and the International Atomic Energy Agency (IAEA), 548p (2016). Available at http://www.oecd-nea.org/pub/.

[7] GORUSTOVICH, S., Estudio de la Favorabilidad Geológico-Uranífera del Territorio Nacional, Unidad de Investigación N° 7, Cuenca Cretácico-Eoterciaria del Grupo Salta, Parte I: Base Geológica, Versión B, CNEA internal report (2006).

[8] ZARCO, J., Geología estructural y petrología estructural del complejo granítico peraluminoso de Achala en relación con la génesis y localización de mineralizaciones de uranio (Sierras Pampeanas – Argentina), Doctoral Thesis, Universidad Nacional de Salta, Argentina (2006).

[9] BELLUCO, A., NORIEGA, J., BRAGANTINI, J., Yacimiento Los Mogotes Colorados, distrito uranífero Los Colorados, La Rioja, (E. ZAPPETTINI, E. Ed.), Recursos Minerales de la República Argentina, Anales Nº 35 SEGEMAR: 767-772 (1999).

[10] BELLO, F. C., BLASON, R., QUER, J., Favorabilidad geológico-uranífera de la cuenca neopaleozoica de Paganzo, Estimación de recursos uraníferos potenciales, XVIII Congreso Geológico Argentino, Proceedings, 1p. (2011).

[11] KLEIMAN, L., JAPAS, M., The Choiyoi volcanic province at 34ºS-36ºS (San Rafael, Mendoza, Argentina): Implications for the Late Paleozoic evolution of the southwestern margin of Gondwana. Tectonophysics (473) 473: 283-299 (2009).

[12] KLEIMAN, L., Geologic setting and mineralization controls at the Sierra Pintada uranium district, Mendoza, Argentina, International Atomic Energy Agency Technical Meeting on “Origin of Sandstone Type Uranium Deposits: A Global Perspective”, IAEA, Vienna, Austria (2012).

[13] FUENTE, A., GAYONE, M., Estudio de la Favorabilidad Geológico-Uranífera del Territorio Nacional, Unidad de Investigación N° 46, Cuenca Cretácica del Grupo Chubut, CNEA internal report (2006).

[14] IAEA, World Distribution of Uranium Deposits (UDEPO) with Uranium Deposit Classification, Vienna, IAEA-Tecdoc-1629, INTERNATIONAL ATOMIC ENERGY AGENCY (IAEA), 126p (2009).

[15] BLASÓN, R., Estimación de recursos minerales. Desarrollo del Área de Control. VII Congreso Argentino de Geología Económica, Salta, Argentina, Proceedings (2001).

[16] BLASÓN, R., QUER, J. C., BELLO, C., Estudio de la Favorabilidad Geológico-Uranífera del Territorio Nacional, Unidad de Investigación N° 23, Magmatismo neopaleozoico-triásico del Bloque de San Rafael, Desarrollo del Área de Control - Estimación de los RUP – Yacimientos vulcaniclásticos tipo “Dr Baulíes”, Versión “A”, CNEA internal report (2008).

[17] MCCAMMON, R.C., FINCH, W.I., PIERSON, C.T., BRIDGES, N.J., The micro-computer program TENDOWG for estimating undiscovered uranium endowment, United States Department of the Interior – Geological Survey, Open File Report 88-653 (1988).

[18] BLASÓN, R., QUER, J.C., BELLO C., Estudio de la Favorabilidad Geológico-Uranífera del Territorio Nacional, Unidad de Investigación N° 12, Cuenca neopaleozoica de Paganzo, Desarrollo del Área de Control – Estimación de los RUP, CNEA internal report (2007).

[19] BLASÓN, R., ALDANA, V., QUER J.C., Estudio de la favorabilidad geológico-uranífera del territorio nacional, Estimación de Recursos Uraníferos Potenciales – UIFGU 1-2, Yacimientos intragraníticos: fisurales y de impregnación tipo “Bernardan” y “Fanay”. Versión “A”, CNEA internal report (2002).

[20] BLASÓN, R., ALDANA, V., QUER J.C., Favorabilidad uranífera de la Unidad 7, Cuenca Cretácico – Eoterciaria del Grupo Salta, Estimación de Recursos Uraníferos Potenciales UIFGU 7, Depósitos en arenisca, Yacimiento Tipo: Don Otto, CNEA internal report (2003).

[21] BLASÓN, R., FUENTE, A., GAYONE, M.R., Estudio de la Favorabilidad Geológico-Uranífera del Territorio Nacional, Desarrollo del AC: “Laguna Colorada” – Estimación de los RUP. UIFGU 52 – Magmatismo cenozoico de Somuncurá, Yacimiento tipo: “Laguna Colorada”, Versión “B”, CNEA internal report (2005).
[22] BLASÓN, R., FUENTE, A., GAYONE, M.R., Estudio de la Favorabilidad Geológico-Uranífera del Territorio Nacional, Unidad de Investigación N° 46 – Sedimentitas Cretácicas del Grupo Chubut y Sedimentitas Senonianas, Estimación de los Recursos Geológicos y los Recursos Uraníferos Potenciales de los depósitos en areniscas controlados por canales de la formación Los Adobes, Yacimiento Tipo Cerro Solo, Versión “A”, CNEA internal report (2000).
[23] BELLO, C., LÓPEZ, L., FERREYRA, P., BLASÓN, R., Uranium potential assessment of Argentina using qualitative and quantitative approaches, International Atomic Energy Agency Technical Meeting on “Spatial and Quantitative Uranium Resources Assessment”, IAEA, Vienna, Austria (2015).

FUZZY LOGIC MINERAL PROSPECTIVITY ANALYSIS OF THE MOUNT ISA REGION (QUEENSLAND, AUSTRALIA) FOR METASOMATITE-TYPE (ALBITITE-TYPE) URANIUM

A.R. WILDE
Centre of Exploration Targetting,
University of Western Australia,
Perth, WA

M. BRUCE
MDB Geoconsulting,
Blackwood, SA

C. KNOX-ROBINSON
ProspectivityMapping.com,
Maylands, WA

Australia

F.P. BIERLEIN
QMSD Mining Co Ltd,
Khartoum, Sudan

V. LISITSIN
Geological Survey of Queensland,
Brisbane, QLD, Australia

Abstract

In this report, we use a fuzzy logic approach to generate mineral prospectivity maps for metasomatite-type (albitite-type) uranium deposits in the Proterozoic western succession of the Mount Isa region (Queensland, Australia). We provide two examples: an assessment of the entire Western Succession and a more detailed study of an area north of Mount Isa where the majority of significant uranium deposits of the region are present. Prospectivity maps generated by the fuzzy gamma and vectorial fuzzy logic techniques are similar. The latter technique, however, provides better discrimination of areas prospective for larger deposits and there is no need for intermediate combinations of input layers or a gamma parameter. This results in a simplified process and makes subsequent applications of the technique more repeatable and comparable. The prospectivity map of the Western Succession is then used to define the boundaries of a tract that is geologically-permissive for the discovery of presently unknown albitite-type uranium deposits. Using this tract as a basis, we discuss the application of quantitative mineral resource assessment.

1. INTRODUCTION

This contribution presents the results of quantitative mineral resource assessment (QMRA) and mineral prospectivity analysis (MPA) for metasomatite-type (albitite-type) uranium deposits in the Mount Isa region of Queensland, Australia. Two sets of MPA are presented, one incorporating the entire western part of the region, with a second focusing on a much smaller area north of the township of Mount Isa and which contains most of the albitite-type resources of the region. The MPA covering the entire area of interest is used to define the boundaries of a geologically-permissive tract, which forms the basis for quantitative mineral resource assessment. It is intended that the reader should become acquainted with the processes of MPA and QMRA and some of the key inputs. It is assumed that the reader has a basic understanding of creating and manipulating vector and raster spatial data.

2. GEOLOGY OF THE MOUNT ISA REGION

2.1. URANIUM ENDOWMENT

The Mount Isa region is part of a major Proterozoic terrane that extends from Darwin in the Northern Territory of Australia to south-east of Mount Isa, in Queensland, a distance of over 1,500 km (Fig. 1). There are several well-known uranium districts within this terrane, notably East Alligator, South Alligator, Westmoreland and Rum Jungle (Fig. 1). The Mount Isa region contains 14 significant albitite-type uranium deposits, which account for over 58,800 t U [1] (Table 1). In addition, the Mary Kathleen U-REE skarn-hosted deposit was mined intermittently during 1950–1982 and yielded 7,500 t U at a grade of 0.1% U. This rare type of deposit is not considered further in this report.

TABLE 1. ALBITITE-TYPE URANIUM RESOURCES OF THE MOUNT ISA REGION [1]

Deposit	Ore (Mt)	Grade %U	Tonnes U
Valhalla	43.8	0.067	29,349
Skal	15.7	0.053	8,384
Odin	14.0	0.048	6,755
Bikini	12.5	0.042	5,252
Anderson's Lode	1.5	0.129	1,936
Watta	5.6	0.034	1,917
Honey Pot	2.6	0.059	1,527
Mirrioola	2.0	0.048	960
Queen's Gift	4.4	0.017	915
Duke Batman	0.8	0.116	893
Slance	1.1	0.042	424
Citation/Mighty Glare	0.8	0.034	271
Eldorado North	0.4	0.042	144
Warawai	0.4	0.028	114

Mary Kathleen and Elaine Dorothy are excluded because they represent skarn-hosted variants distinct from the other albitite-type deposits. Also, the Mary Kathleen resource equals production to 1982.

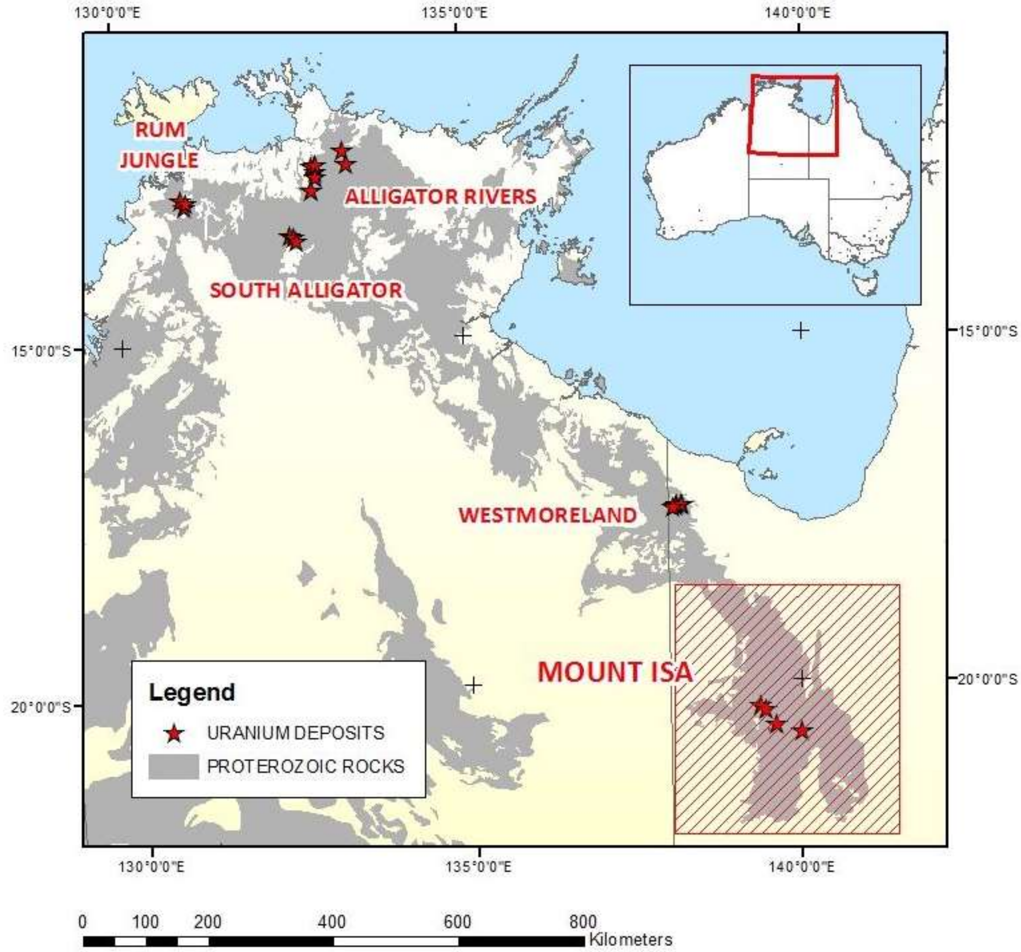

FIG. 1. Location of the Mount Isa region (red cross-hatched box) within the Northern Australian Proterozoic terrane and significant uranium deposits.

2.2. MAIN GEOLOGICAL UNITS

The Mount Isa region has been divided into three main geological units (inset Fig. 2): Western Succession, Kalkadoon-Leichhardt Belt, and Eastern Succession. The most significant uranium deposits of the Mount Isa uranium district occur within the Western Succession, and most are hosted by the Eastern Creek Volcanics (ECV) – a 7-km thick sequence of up to 100-m thick extrusive meta-basalt layers with inter-bedded meta-sedimentary units (Fig. 2) [2]. Re-Os dating of weakly metamorphosed ECV meta-basalt returned an isochron of 1.83 ± 0.05 Ga, probably the best estimate of extrusion age [3].

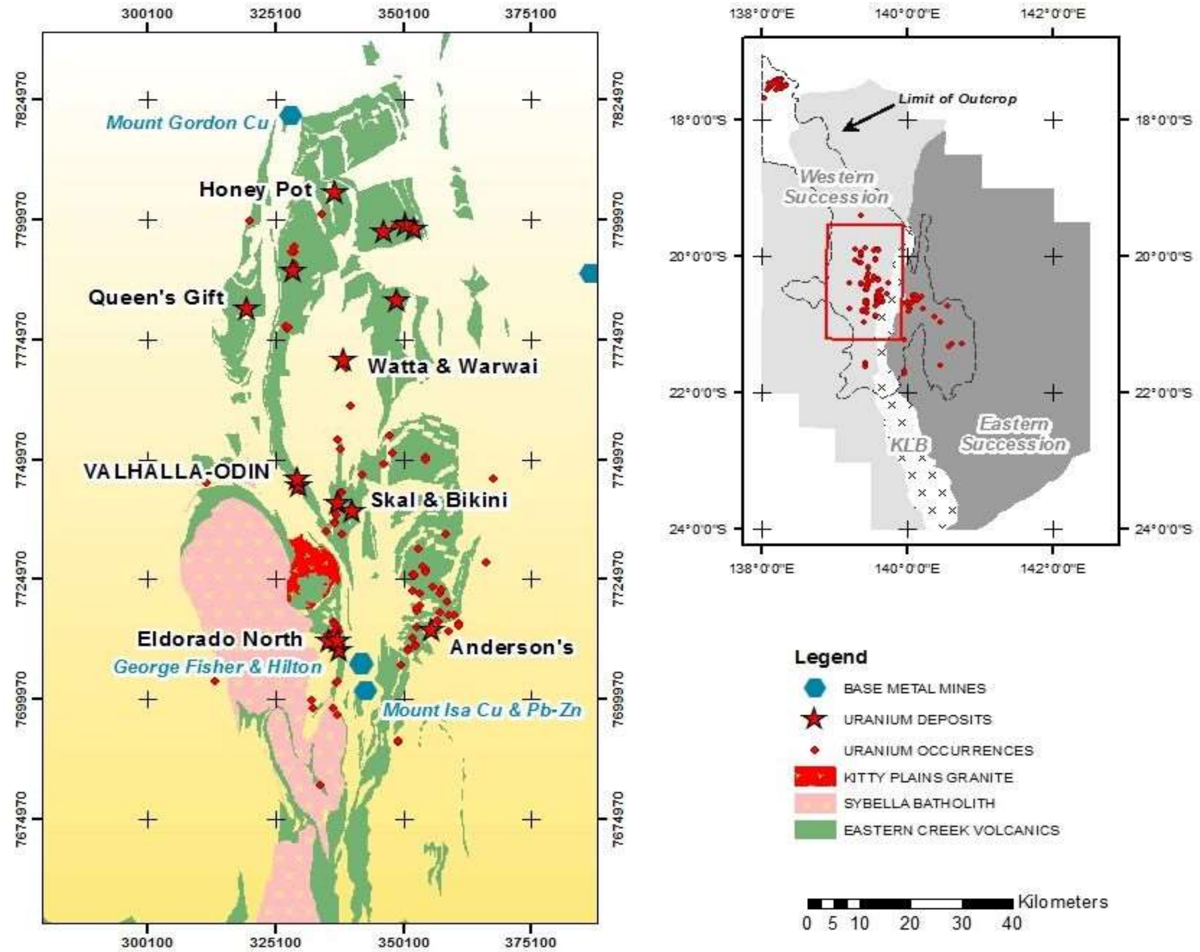

FIG. 2: Simplified geology of part of the Western Succession north of Mount Isa. Geology from Queensland Geological Survey. "KLB" = Kalkadoon-Leichhardt Belt. Red box is approximate area of detailed MPA.

Rocks of the ECV are intruded by the A-type Sybella Batholith, dated by U-Pb zircon at 1657 ± 7 Ma [4–6]. The batholith ranges in composition from granite to granodiorite to quartz diorite and gabbro [6]. Granites of the Sybella batholith average 7 ppm U (81 analyses) whereas granitic pegmatites are significantly more enriched in uranium with an average of 28 ppm U (5 analyses). The Kitty Plains Microgranite, which forms the north-eastern part of the Sybella Batholith (Fig. 2), is radiometrically anomalous and has been cited as a possible source of uranium [5]. Dating using the U-Pb zircon technique has yielded an age of 1670 ± 9 Ma with a later disturbance at 1589 ± 29 Ma [5]. The latter age overlaps the age of uranium deposition inferred from U-Pb dating of brannerite from the Valhalla deposit [7].

Among the rocks overlying the ECV are weakly metamorphosed dolomitic mudstones and siltstones of the Urquhart Shale. This unit is of great economic significance to the region as it hosts giant sedimentary-exhalative Pb-Zn deposits at Mount Isa, George Fisher and Hilton as well as the Cu-Co deposits at Mount Isa (Fig. 2). The Urquhart Shale, however, hosts no significant uranium occurrences.

2.3. DEFORMATION AND REGIONAL HYDROTHERMAL ALTERATION

The architecture of the Western Succession is largely a product of E–W compression during the regional Isan orogeny (D2), which has imposed a N–S grain (Fig. 2) and is estimated to have peaked at 1.59 Ga [8]. Rocks of the ECV are steeply dipping but, except in high strain zones that host uranium deposits, it is rare to observe fold closures in the field. Regional metamorphism accompanying the Isan orogeny generally reached greenschist facies but amphibolite and higher-grade rocks occur close to the Sybella Batholith [8].

Later ductile events had negligible impact on the overall architecture of the district. Of specific importance to uranium deposits are NW–SE-trending shear zones characterized by chlorite schist. These structures cut and displace uranium deposits but are suggested to be coeval with formation of sediment-hosted copper deposits at Mount Isa [9].

Regional hydrothermal alteration of rocks within the ECV in the locality of Mount Isa township has been documented extensively, mostly in the context of tracing flow paths for oxidized brines that formed the Mount Isa copper deposits [10–12]. Albitite is rare, but most known occurrences of albitite in the Western Succession are associated with uranium mineralization.

3. METASOMATITE-TYPE URANIUM DEPOSITS

3.1. GENERAL CHARACTERISTICS OF ALBITITE-TYPE URANIUM DEPOSITS

The IAEA metasomatite-type uranium deposit classification includes several distinct deposit styles. Most of the uranium deposits in the Mount Isa region can be assigned to the albitite-type sub-type [1, 15]. Albitite-type uranium deposits are quite common and major examples occur in the Brazil (Lagoa Real), Canada (Michelin), Guyana (Kurupung), Ukraine (Novokonstantinovskoe), and the USA (Coles Hill). Collectively, these deposits contain over 1 million t U but at relatively low grade (<0.1% U) [1]. Table 2 presents some of the key characteristics of the deposit type.

TABLE 2. KEY CHARACTERISTICS OF THE ALBITITE-TYPE URANIUM DEPOSIT TYPE [1, 13–15]

Deposit types:

- Sodic end-member. U spatially associated with transgressive, linear albitite bodies;
- Potassic end-member. U spatially associated with transgressive, linear K-feldspar-rich bodies. Notably Elkon, Russia.

Geological setting:

- Poly-deformed Paleo-proterozoic, Meso-proterozoic, Neo-proterozoic–Cambrian and Silurian metamorphic terranes intruded by radiometrically anomalous post-tectonic granitoids;
- Wide variety of host rock lithologies, but commonly granitoid gneisses or meta-volcanic rocks;
- Host rocks show ductile deformation and later brittle deformation during temperature decrease.

Source (fluid, metal, energy):

Fluids

- Temperature was probably >450°C in hottest (albitic) part of zoned systems at a depth of ~9-10 km but cooled in later (calcic and potassic) stages of alteration and mineralization;
- Alkaline during early stages of mineralization (e.g., riebeckite, aegirine, albite assemblage);
- F-rich as evidenced by significant masses of fluor-apatite in many deposits. Explains mobility of high field strength elements, though relative paucity of Th and REE is inconsistent;
- Stable isotopic data hint at involvement of meteoric or formation water origin for albitizing fluids, but equivocal. Some magmatic input is likely.

Uranium, titanium and zirconium source

- The source of key elements is not always well defined, but may be radiometrically anomalous (K-, U- and Th-rich) granitoid intrusions and/or felsic meta-volcanic rocks;
- U-Ti phases due to inheritance from primary Ti-bearing minerals and/or hydrothermal Ti addition.

Possible energy drivers of fluid-flow

- Thermal gradients established during regional metamorphism;
- Mantle plume hypothesized as fluid driver in Ukrainian deposits;
- Less probably, contact metamorphism and intrusion of hot felsic magmas.

Fluid pathway:

- Steeply dipping, narrow (<250m) mylonites associated with pervasive hydrothermal alteration;
- Host tectonic structures typically correspond to major gravity gradients that penetrate deeply into the crust and possibly into the upper mantle.

Trap:

Physical

- Association with local veining and brecciation implies mechanical processes are important.

Chemical

- Poorly defined. High alkalinity fluids imply U transport as hydroxyl or carbonate complexes.

Age and relative timing of mineralization:

- Absolute ages of uranium crystallization vary from 1.8 to 0.14 billion years.

Preservation:

- Deposits are generally located in stable cratonic environments with low erosion rates and high preservation potential.

Main references: [1], [13], [15], [16], [17]

Globally, albitite-type uranium is hosted in a wide range of mylonitized and albitized metamorphic rocks. Ore minerals are generally fine-grained (< 50µm) and disseminated in and adjacent to albitized mylonites. There is widespread evidence of hydrothermal titanium and zirconium mobility, and uranium commonly occurs in association with a variety of Ti-rich phases as well as unusual and as yet unnamed Zr-rich phases [1, 15]. The ore does not contain economic concentrations of metals apart from uranium although positive correlations are noted between uranium and various high field strength elements. Gangue minerals include albite, calcite, dolomite, sodic pyroxene, sodic amphibole, magnetite and hematite.

The Eastern Succession contains two skarn-hosted U-REE deposits, including the region's only productive uranium mine at Mary Kathleen (Table 1). Skarn-hosted uranium deposits such as Mary Kathleen are quite rare. No skarn-hosted deposits are present in the Western Succession and they are not considered further herein. The Kalkadoon-Leichhardt belt contains no significant uranium deposits.

3.2. ALBITITE-TYPE URANIUM DEPOSITS OF THE WESTERN SUCCESSION

The Western Succession hosts 14 significant albitite-type resources including the major deposit at Valhalla-Odin and satellite deposits at Skal and Bikini (Table 1; Fig. 2) [6, 15]. Most of these deposits were discovered during the 1950s but have not been developed due to relatively low grades (<0.1% U) and metallurgical issues such as high carbonate content and the perceived refractory nature of the uranium minerals.

The albitite-type deposits occur within NNE-striking transgressive, magnetite-bearing albititized shear zones developed in meta-basalt of the Eastern Creek Volcanics [2, 6, 21]. Thus, areas that are proximal to N–S-trending mapped faults are regarded as prospective. Larger deposits show an association with deep-penetrating faults as evidenced by the association of deposits with major gravity gradients. A correlation has also been noted between the occurrence of albitite-type deposits and areas of high fault density.

Another feature regarded as crucial in the development of the larger deposits is the angle between prospective structures and bedding in the meta-basalt [2, 15]. The relationship between albitite bodies and bedding is well illustrated at Skal (Fig. 3). Here bedding dips consistently at 80°NW whereas albitite bodies are clearly oblique but parallel the regional S2 foliation (Fig. 3). Evidence for this geometric control of higher grade uranium is that ore shoots typically plunge parallel to the intersection lineation of bedding and albitite bodies [2, 15].

The Skal albitites have been dismembered and offset by ~600 m by ~250 m wide D3 deformation (shear) zones trending WNW (Fig. 3). Thus, faults with this orientation are considered to have much lower prospectivity.

The presence of hydrothermal magnetite means that albitites developed in Fe-rich meta-basalts are detectable using airborne magnetic imagery. Indeed, albitized shear zones display some of the most intense magnetic responses of the Western Succession [15].

Radiometrically anomalous granites such as the Kitty Plains micro-granite (Fig. 2) have been suggested to be a source of uranium for the albitite-type deposits of the Western Succession [5]. Certainly, the largest deposits Valhalla, Odin, Skal, and Bikini, in addition to several sub-economic deposits, are arrayed around the periphery of the Kitty Plains intrusion (Fig. 2). Proximity to radiometrically anomalous granitoids is therefore another potential layer of a regional prospectivity analysis.

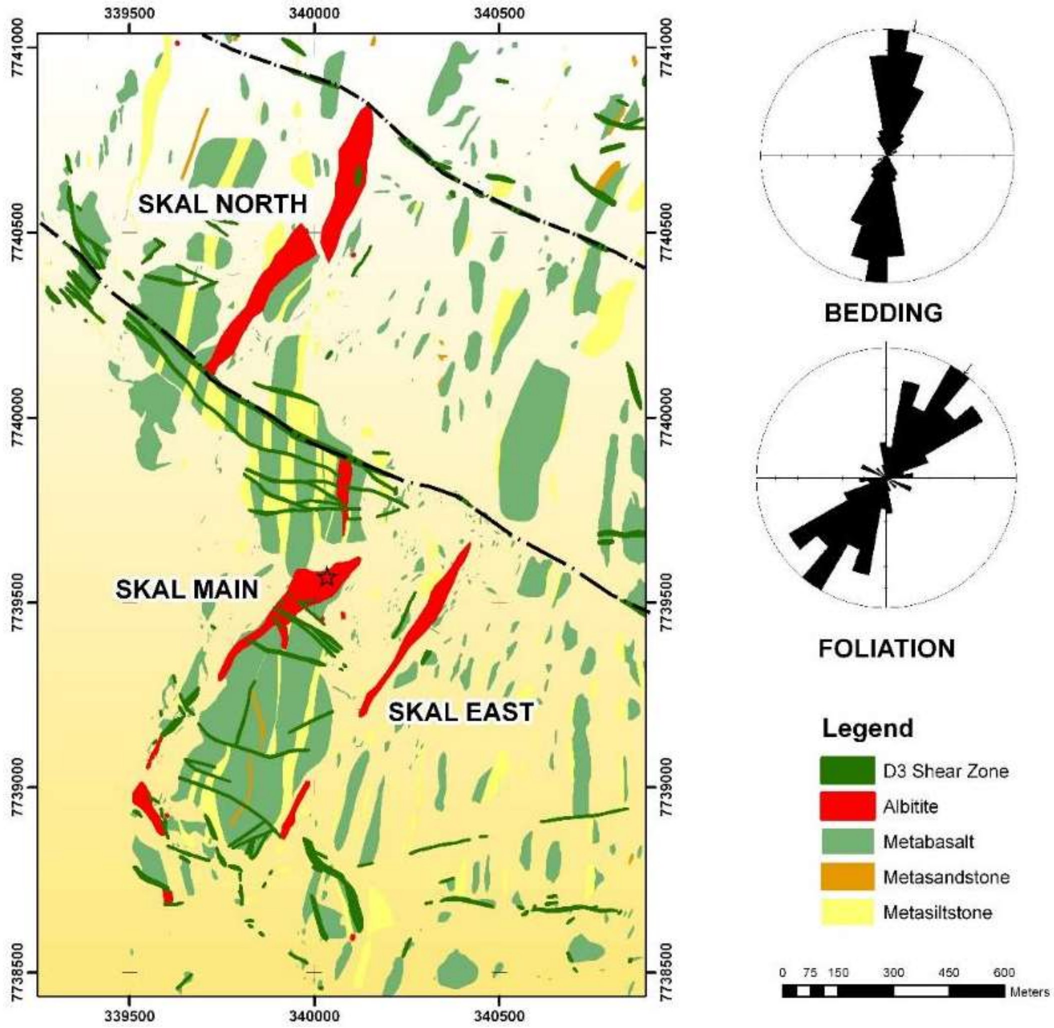

FIG. 3. Mapped geology of the Skal deposits [15]. Dashed black lines are D3 fault zones. The pale yellow colour represents Cenozoic cover.

4. METHODOLOGY

4.1. MINERAL PROSPECTIVITY ANALYSIS (MPA)

The definition of areas prospective for various mineral commodities including uranium has traditionally involved empirical techniques such as prospecting or geochemical and/or geophysical surveys. Geoscientists have also employed with limited success hardcopy ‘predictor’ maps, sometimes combined using manual overlay. Computerized geographic information systems (GIS) introduced in the late 1980s have largely replaced the use of hardcopy maps. Furthermore, the widespread adoption of GIS has paved the way for computer-based MPA. MPA describes the process of defining prospective areas by combining a number of digital input data layers or ‘predictor maps’ to produce ‘favorability’, ‘mineral potential’ or ‘prospectivity’ maps [18–20].

There are several different approaches to MPA. Prospectivity can be determined by simply adding input layers together to generate a digital image (or map) in which each pixel is attributed with a prospectivity value representing the sum of all input pixel values. This approach assumes all inputs are of equal importance, which is generally unlikely to be the case [18]. Several methods have been developed to combine the input layers in a more rigorous fashion. These methods can be characterized as either data-driven or knowledge-driven.

Data-driven methods seek to predict the occurrence of deposits with respect to the input layers using Bayesian probabilistic models, artificial neural networks or logistic regression models, and require the existence of a substantial population of known deposits as a training set [18, 19, 20]. Data-driven methods typically employ Boolean logic. In other words, a given area is either prospective or it is not, and the boundary between areas of high and low prospectivity is considered to be infinitely narrow [19]. This approach cannot deal effectively with the inaccuracies and uncertainties that are inherent in most geoscientific datasets, and which can introduce misleading artifacts into data-driven prospectivity maps [19].

4.2. FUZZY LOGIC AND MPA

The fuzzy logic approach recognizes that reasoning is approximate rather than precise and specifically deals with uncertainty [19]. Fuzzy variables can have one of an infinite number of states ranging from 0 (complete dissociation or unprospective) to 1 (complete association or prospective) [19]. The fuzzy logic approach is based on expert knowledge and does not require mineral deposits to be present in the area of interest.

It is this latter approach that is adopted here, applied using the software ArcInfo and ArcGIS 9.2 with the SDM spatial data modeler extension [21]. Input layers were either in vector or raster format, but each vector input layer was first converted to a raster grid prior to analysis. All raster grids were then populated with fuzzy membership values between 0 and 1, reflecting the degree to which each individual pixel is spatially associated or dissociated with mineral deposits. The last step involved combining the input datasets to produce a prospectivity map.

In combining the input layers, we considered the possibility that some of the input layers were not conditionally independent. That is to say, different input layers may represent the same geological feature. For example, granites may be represented by a mapped geology layer and by a gravity low. Additionally, there may be a genetic link between the layers; for example, metamorphic grade may be linked to stratigraphic age. Failure to recognize and deal with conditional dependence can lead to over- or under-emphasizing the relative importance of one or more predictor maps.

4.3. COMBINING DATA LAYERS USING FUZZY OPERATORS

In fuzzy logic MPA, individual input layers or predictor maps are combined using a number of different operators. The fuzzy AND operator takes the minimum of all the input layers. The fuzzy OR operator takes the maximum of all the input layers. The fuzzy gamma operator is a combination of fuzzy algebraic sum or *FAS* (i.e., sum of all input pixels) and fuzzy algebraic product or *FAP* (i.e., product of all input pixels) [20].

When using the *FAP* operator, output integrated fuzzy membership values tend to be very small. Due to the effect of multiplying several numbers less than 1, the output is always smaller than, or equal to, the smallest contributing membership value, and is therefore ‘decreasive’. For example, the *FAP* of [0.5, 0.75] is 0.375. However, all the input membership values have a contributing effect on the output, unlike the fuzzy AND or fuzzy OR operators [20]. Note, however, that if any pixel in the input data has a value of 0 then the output will also be 0 using this operator.

The *FAS* operator has an 'increasive' effect because its output is always larger (or equal to) the largest input fuzzy membership value. Two pieces of evidence that both favor a hypothesis reinforce each other and the integrated evidence is more supportive of the proposition than either piece of evidence taken individually. For example, the *FAS* of [0.5, 0.75] is 1–(1–0.75)×(1–0.5), which equals 0.875. The increasive effect of combining several favorable pieces of evidence is automatically limited by the maximum value of 1.0, which can never be exceeded.

The fuzzy gamma value is calculated as follows: fuzzy gamma = $(FAS)^{\gamma} \times (FAP)^{1-\gamma}$. The γ parameter is chosen to be within the range 0 to 1. When γ is 1, the combination is the same as the *FAS*; when γ is 0, the combination is the same as the *FAP*. The γ parameter is chosen by trial and error.

4.4. VECTORIAL FUZZY LOGIC

Another approach has been termed vectorial fuzzy logic [19]. In this approach inputs are treated as unit vectors and combined using vector arithmetic. The traditional 0–1 scores of conventional fuzzy logic are linearly converted to polar coordinates with values between 0 and pi/2. These inputs are combined using conventional resolution of vector maths. The final result, which also lies within 0 and pi/2, is then converted back to the range of 0 and 1. This approach has some benefits over the fuzzy gamma method. First, related datasets do not tend to overly bias the result and as such layers are combined in a single process. Second, a value of 0 for a pixel in one input does not automatically render that pixel with a value of 0 in the prospectivity map. Third, the length of the resultant vector is useful in the further analysis of areas of intermediate prospectivity and can be mapped and analyzed in its own right. If the input vectors are similar to one another, then a longer resultant vector length will be derived compared to the case where the input vectors vary greatly. Finally, there are no parameters, such as gamma, to define; thus, simplifying the process and making subsequent applications of the technique more repeatable and comparable.

5. REGIONAL MINERAL PROSPECTIVITY ANALYSIS

5.1. INPUT LAYERS

The Mount Isa Western Succession is particularly suited to MPA given availability of a large number of high quality geoscience datasets and good understanding of the albitite-type uranium geological model. Seventeen predictor layers were prepared for a region-wide analysis. These were grouped into three categories using a systems-based model [1, 9, 15]. Intermediate layers were created for source, transport and trap categories (Table 3) and a prospectivity map constructed by combining these three intermediate layers.

TABLE 3. INPUT LAYERS USED IN CREATING THE REGIONAL PROSPECTIVITY MAP, GROUPED INTO SOURCE, TRANSPORT AND TRAP. THE WEIGHTS REFLECT THE IMPORTANCE OF THE INDIVIDUAL LAYER IN THE OVERALL GENETIC MODEL

Category	Layer (predictor map)	Layer (map) type	Layer (map) weight
SOURCE	Coincident Magnetic/Gravity lows	Vector	7
	Granites	Vector	7
	Hot Granites	Vector	8
TRANSPORT	Fault Density	Vector	9
	1st Vertical Derivative Magnetic Image 1VD	Vector	4
	Major Faults	Vector	9
	Medium Faults	Vector	4
	Minor Faults	Vector	2
	E–W-trending Faults (045–105°)	Vector	3
	NNE-trending Faults (345–045°)	Vector	9
	NW-trending Faults (285–345°)	Vector	4
TRAP	Lithology	Vector	9
	Median Proterozoic Stratigraphic Age	Vector	9
	Metamorphic Grade	Vector	9
	Radiometric U (ppm) Image	Raster	6
	U/Th Radiometric Image	Raster	6
	U^2/Th Radiometric Image	Raster	6

5.2. SOURCE LAYER

The intermediate source layer encapsulates the idea that a specific source of uranium is required for deposit formation and that prospectivity declines with distance from source. It has been proposed that uranium in albitite-type deposits of Mount Isa is sourced in uranium-enriched granitoids such as the Kitty Plains micro-granite [5]. Source input layers therefore included granitoids as defined in surface mapping and airborne radiometric imagery and also as inferred from geophysical datasets such as gravity and airborne magnetics (Table 1).

Source (granitoid) polygons in the Hot Granite layer were buffered at 5 km intervals (Fig. 4). Each buffer interval was assigned a ‘class score’ based on expert opinion on prospectivity with regard to distance from the contacts. The class score multiplied by the map weight (reflecting the relative importance of this layer with respect to the other layers and the perceived quality of the data it contains) and divided by 100 gave the fuzzy membership value (Fig. 4; Appendix). It can be seen from Fig. 4 that areas within 10 km of the granitoid boundaries score most highly, but that the largest deposits fall outside of the highest score areas. An alternative approach would be to weight the 10–15 km buffer more highly than 0–10 km buffers because most of the larger deposits fall within the 10–15 km buffer (Fig. 4).

The Hot Granite buffer layer was then converted to a raster grid with a cell size of 50 m. The choice of cell size was a compromise between the scale (i.e., spatial complexity and size of the search space) of the input data and the computer processing power available. Each cell was attributed with a fuzzy membership value (listed in the Appendix). It is important to note that once rasterized in this way, each input predictor map is effectively a single component measure of prospectivity for the area under investigation.

A similar process was followed for the other two layers.

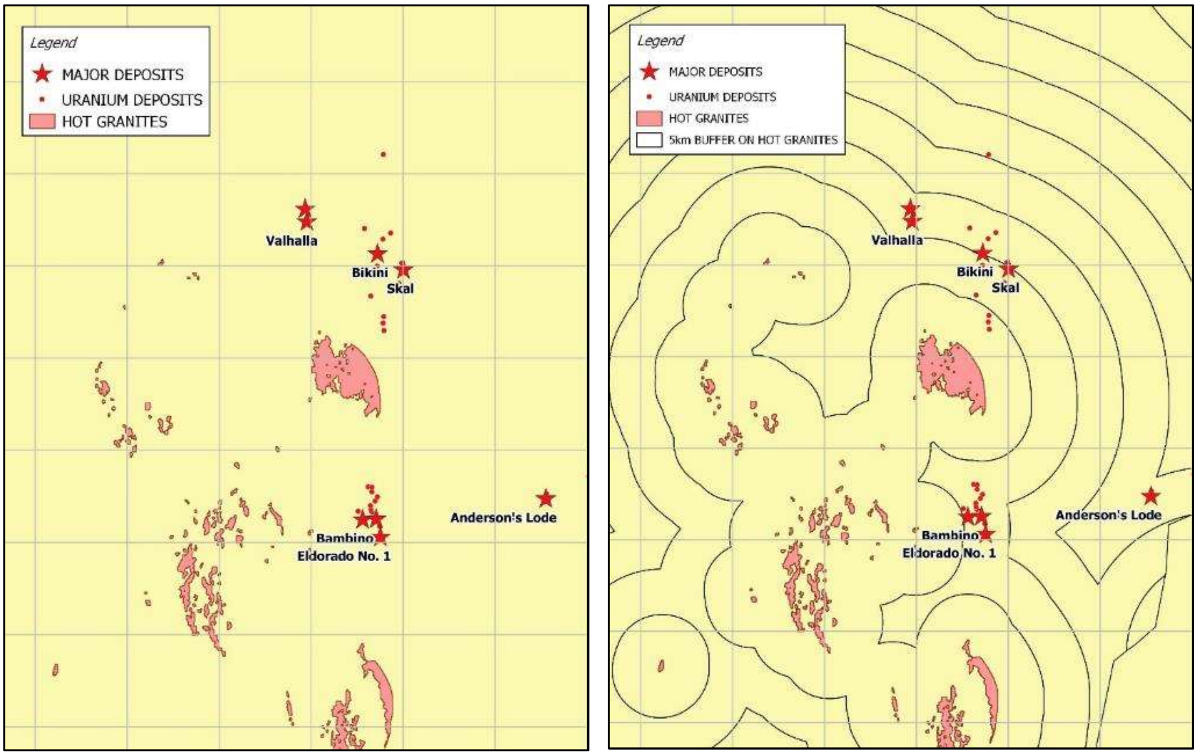

(a) *(b)*

FIG. 4. (a) Distribution of 'hot' granite intrusions. (b) Series of 5 km buffers around the granite outcrops. (c) Buffers attributed with fuzzy membership values (see Appendix). (d) Map in (c) converted from vector to raster. Gray grid lines are spaced at 10 km.

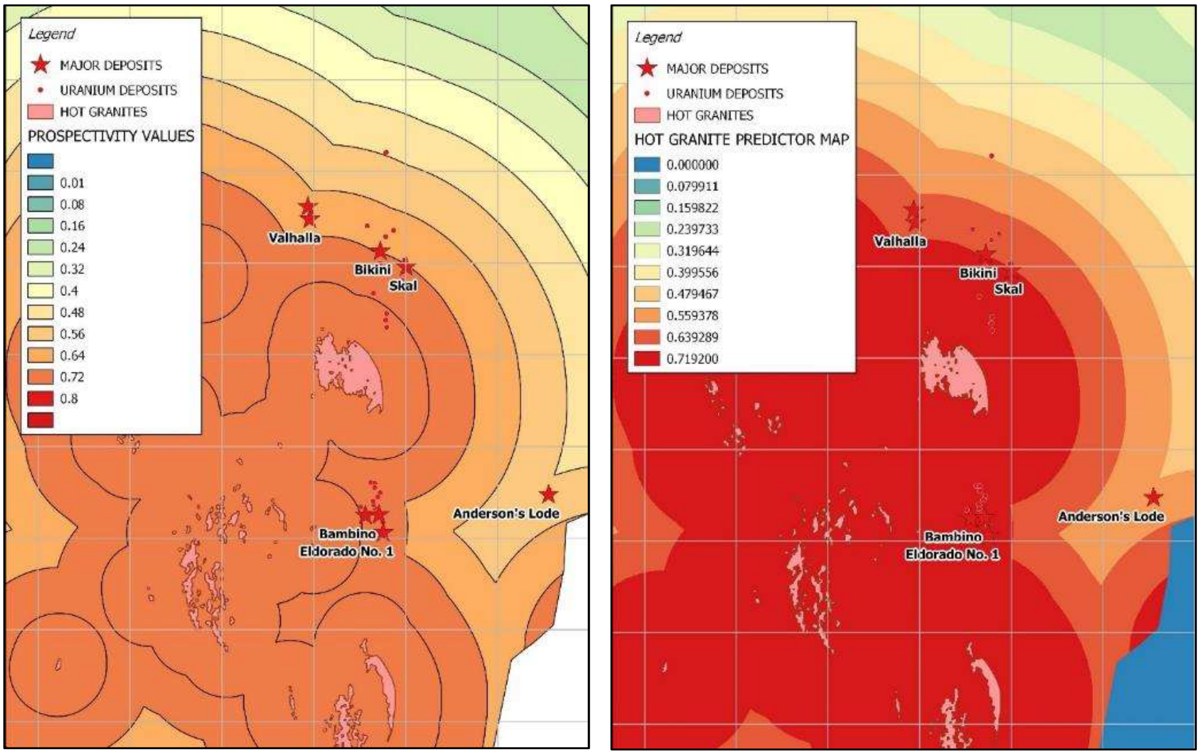

(c) *(d)*

FIG. 4. (continued).

5.3. TRANSPORT LAYER

The transport layer identifies possible fluid pathways that connect source to trap site. Eight layers were used for this purpose and six of these were based on mapped faults split into different orientations (Table 2). One layer portrays fault density, which is considered to be a proxy for zones of high permeability and porosity. The other layer used the first vertical derivative of magnetic intensity as a proxy for albitic alteration, which defines zones of hydrothermal fluid flow [15].

Fig. 5 shows the example of the subset of NW-trending faults with a series of 1 km interval buffers. NW-trending faults are thought to be less prospective than NNE-trending structures [15] and this is reflected in poor correspondence between presence of mineral occurrences and proximal buffers shown in Fig. 5. This layer has a low overall weighting of 4 (Table 2) and thus has only minimal impact on the final result.

5.4. TRAP LAYER

The third aspect (or layer) of the mineral systems approach concerns potential trap sites, or rock masses that are more likely to have caused precipitation of uranium from hydrothermal fluids. There is an empirical relationship between the Mount Isa albitite-type deposits and metamorphic grade with approximately two thirds of deposits falling within areas deemed to have undergone greenschist facies metamorphism. There is, however, no conceptual basis for thinking that depositional processes were more efficient in greenschist facies rocks. Nevertheless, this analysis accorded a higher weighting to greenschist facies rocks.

The empirical approach was again adopted in creating the lithology and stratigraphic age layers, with mafic extrusive rocks between 1,757 and 1,800 Ma (i.e., Eastern Creek Volcanics) being assigned maximum prospectivity values.

In order to generate the metamorphic grade predictor, map polygons representing the distribution of metamorphic grade (Fig. 6) were first converted to a grid (i.e., the vector dataset was rasterized) with cell size 50 m and individual pixels assigned a value based, again, on expert opinion (the values are listed in the Appendix).

The process by which the three predictor maps based on radiometric imagery were created was similar, except of course that the rasterization stage was not required. These three layers were given a relatively low weighting (i.e., 6), reflecting that fact that some deposits are likely to be concealed under cover and lack a radiometric response.

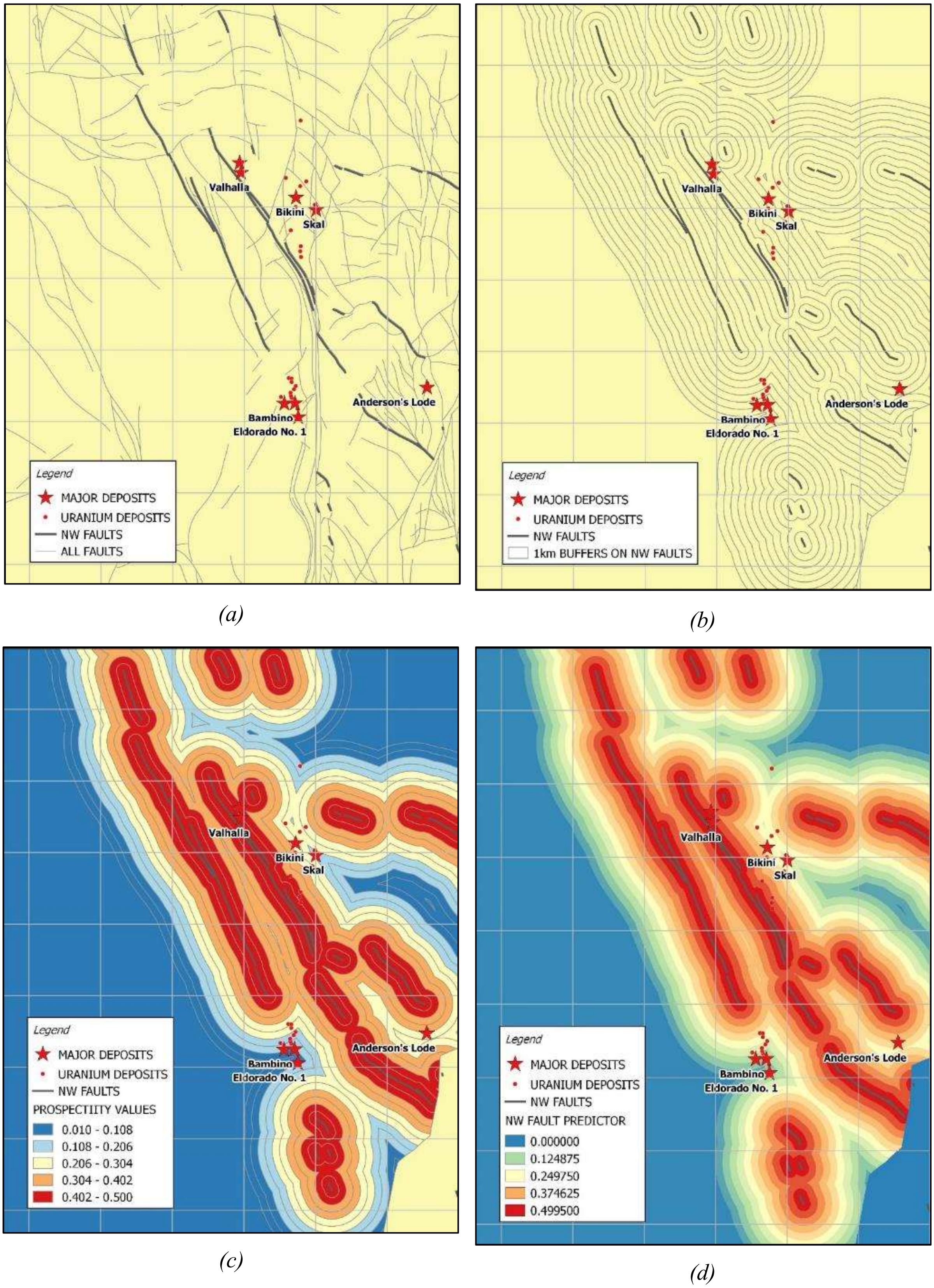

FIG. 5. (a) Mapped faults in pale gray with selected subset of NW-trending faults in bold gray. (b) Series of 1 km wide buffers around selected fault subset. (c) Buffers attributed with fuzzy membership values (see Appendix). (d) Map in (c) converted from vector to raster. Gray grid lines are spaced at 10 km.

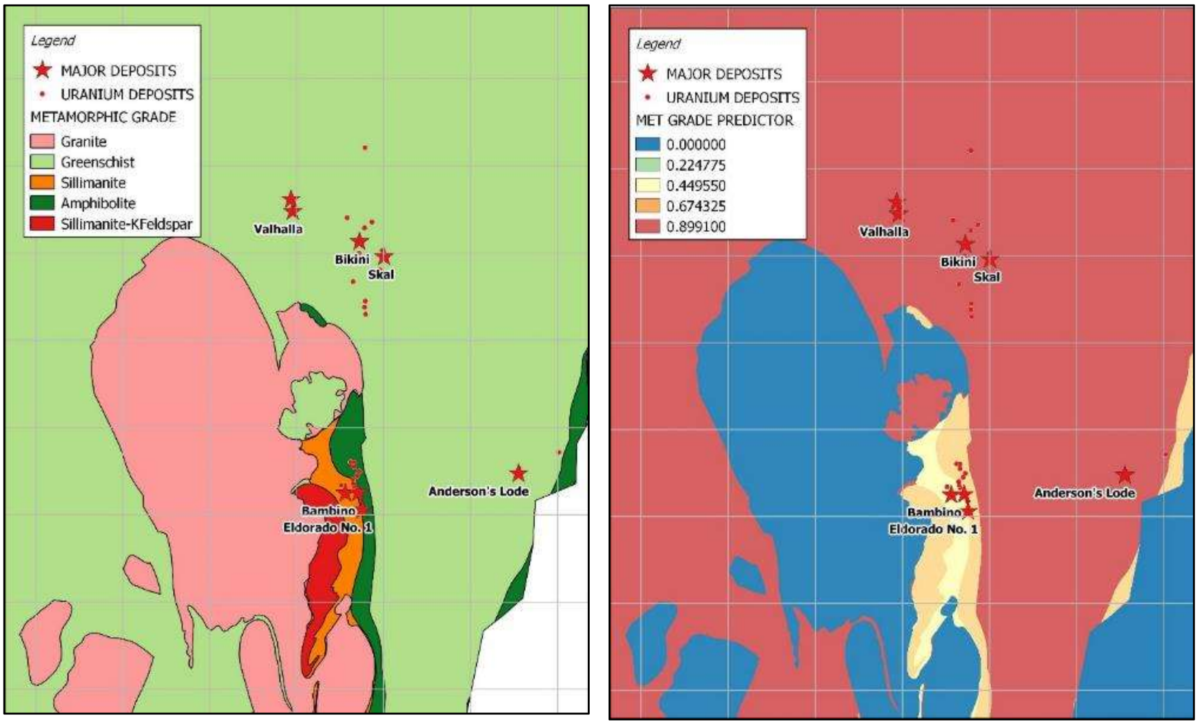

(a) *(b)*

FIG. 6. (a) Metamorphic grade map. (b) Grid of metamorphic grade predictor; granites are not considered to be prospective (see Appendix). Gray grid lines are spaced at 10 km.

5.5. COMBINING THE LAYERS

The next stage was to combine the input layers into three intermediate layers (Fig. 7) representing source, transport or trap as depicted in Fig. 8. The choice of the fuzzy OR operator or the fuzzy AND operator depended upon whether the presence of either of the predictor (input) maps to be combined was considered important (fuzzy OR) or mandatory for the recognition of areas with elevated uranium potential (fuzzy AND).

Thus, in creating the source layer, the highest value of three predictor map inputs was used. In other words, an area can be considered prospective if it is near to only one of the potential uranium sources such as granitic intrusions, radiometrically anomalous intrusions and gravity or magnetic lows (implying buried intrusions). Conversely, if all three inputs were required, the importance of this layer would be exaggerated.

The transport layer identifies areas of enhanced dilation potential by combining all faults and zones of albitization (represented by the first vertical derivative of the magnetics) with an 'OR' operator. These are then combined with the weighted and combined major faults with an 'AND' operator to identify potential zones of dilation near major structures. An acceptable level of structural complexity (fault density) must also be present for a cell to be considered prospective.

The trap layer requires that an area must have the correct lithology, age and metamorphic grade to be considered prospective. This is accomplished by combining three input layers with an 'AND' operator. Uranium radiometric anomalies are also combined with an 'AND' operator meaning that only uranium anomalies with corresponding U/Th and U^2/Th anomalies will be highlighted. The 'SUM' operator and the relatively low weights assigned to the radiometric anomaly components mean that these have only a slight enhancing effect on the trap layer.

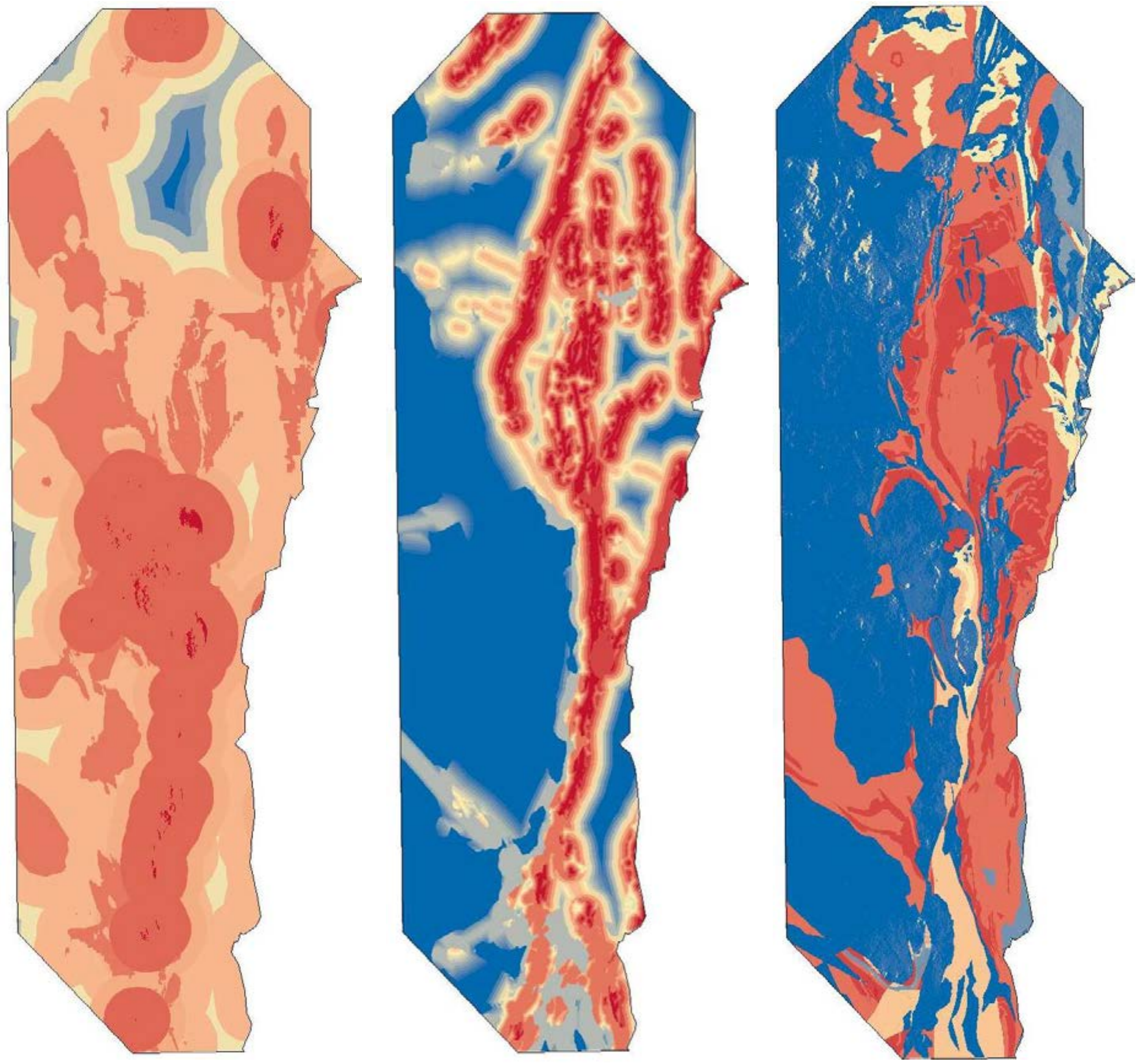

(a) (b) (c)

FIG. 7. Three intermediate images representing (a) source, (b) transport and (c) trap. These were combined using the fuzzy gamma operator to form the prospectivity map.

5.6. PROSPECTIVITY MAP

The final stage combined the source, transport and trap layers with a fuzzy gamma operator, using a low gamma value of 0.2. The resultant prospectivity map is shown as Fig. 9. It can be seen that there is good correlation between highly prospective zones in the map produced and known mineral deposits. This prospectivity map could also be the basis for defining a geologically-permissive tract for albitite-type deposits by selecting an appropriate threshold value such that the probability of a discovery outside the threshold zone is negligible.

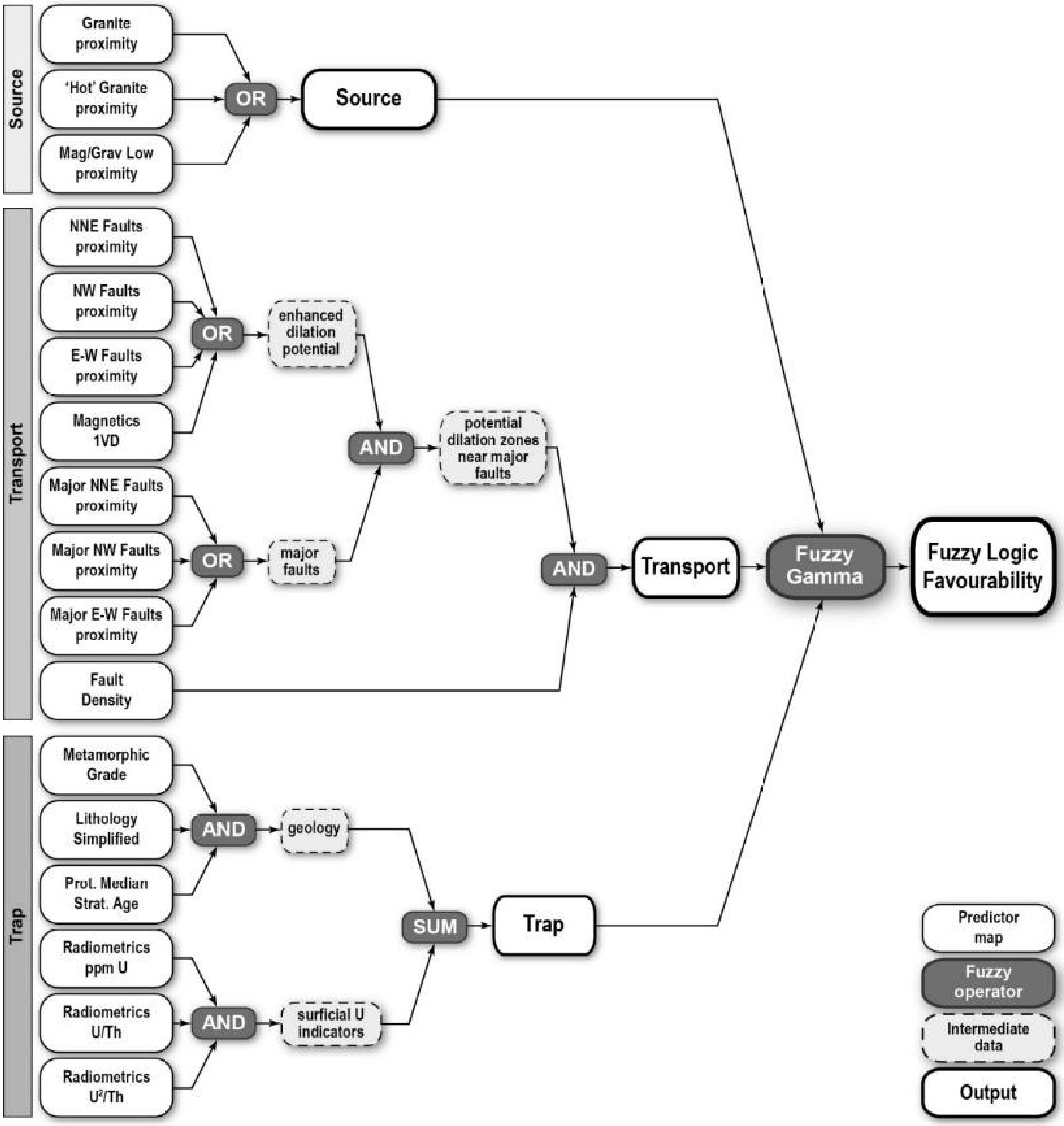

FIG. 8. Inference network, showing how input layers were combined to generate the regional prospectivity map.

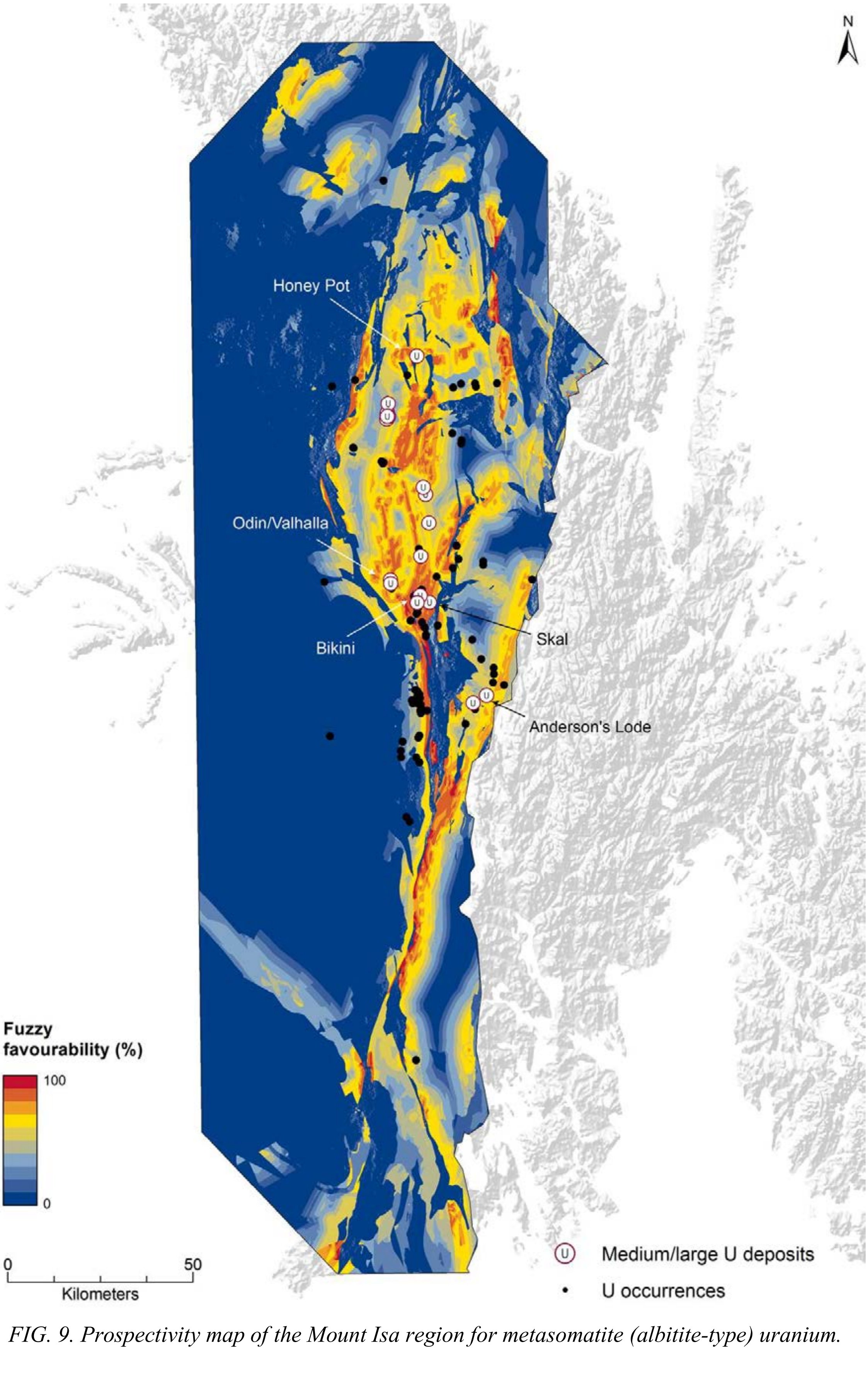

FIG. 9. *Prospectivity map of the Mount Isa region for metasomatite (albitite-type) uranium.*

6. MT ISA NORTH MINERAL PROSPECTIVITY ANALYSIS

6.1. METHOD

A different approach was adopted for an MPA of the smaller Mount Isa North area. This area hosts all of the significant albitite-type U deposits of the Mount Isa region and a further 44 uranium occurrences (Fig. 2). Some of the input layers used in the regional analysis are of limited value in the smaller area; for example, metamorphic grade and stratigraphic age exhibit only minimal variation in the smaller area and are therefore irrelevant at this scale. Conversely, we were able to create a layer representing the spatial relationship between prospective faults and bedding that would have been impossible at the scale of the entire Western Succession. A combined source layer was not used in this analysis as the abundance of significant uranium deposits and the relatively small size of the study area meant that it was also of lesser relevance at this scale. Another point of difference was that fuzzy gamma and vectorial fuzzy logic [19] were employed to combine the input layers allowing us to compare the results of using these different approaches

6.2. INPUT LAYERS

Seven layers were selected for the more detailed analysis. Owing to some conditional dependence, the seven layers were first combined into four using the fuzzy gamma operator and a gamma value of 0.98 (Table 4; Fig. 10). The gamma value of 0.98 means that the output is similar to that using the *FAS* operator, as highs in one or more of the inputs will be transferred into the single output layer. The four intermediate layers (Z1 to Z4) were combined to form the prospectivity map using the fuzzy gamma operator and a gamma value of 0.1 (Fig. 10). The output of using a gamma value of 0.10 is similar to that using the *FAP* operator.

TABLE 4: DATA LAYERS USED IN PREPARATION OF MPA OF THE MOUNT ISA NORTH AREA. EACH LAYER WAS AN ARCINFO FORMAT GRID WITH 100M CELL (PIXEL) SIZE

Initial data layer	Data type	Combined layer (grid)	Comments
Proximity to prospective fault (orientation between 350° and 040°)	Vector	Z4	Fuzzy gamma combination using gamma value of 0.98
Discordance (i.e., areas of favorable fault and bedding intersection angle)	Raster		
Areas of high fault density	Raster	Z2	Fuzzy gamma combination using gamma value of 0.98
Areas of high fault intersection density	Raster		
Proximity to magnetic high (indicative of albitization)	Vector	Z1	
Areas of negative gravity curvature	Raster	Z3	Fuzzy gamma combination using gamma value of 0.98
Proximity to gravity gradient (indicative of major structural breaks and/or zones of major mechanical contrast)	Vector		

As mentioned above, total magnetic intensity (TMI) from airborne survey data can be used to map albitite bodies (Fig. 11). Ten percent of deposits fall within the top 1% of TMI values and 50% within the top 10%, confirming a strong spatial relationship between highly magnetic rocks and uranium deposits. The optimum buffer distance around magnetic highs was determined by maximizing the contrast in known deposit density across the buffer boundary [20]. The maximum contrast of 3.67 is achieved using the 3rd percentile TMI bin to determine buffer distance. Put another way, the boundary of the most magnetic 3% of the region represents the ideal cut-off for exploration purposes. This buffer captures over 27% of known uranium deposits. The contrast then falls off steeply with increasing buffer width. Pixels were assigned a value of between 0.01 (distal) and 1 (proximal) depending on distance to the top 1% of magnetic anomalies polygon (Fig. 11).

The fault occurrence layer (Fig. 12) is based on a combination of Geoscience Australia 1:100,000 scale geological mapping augmented by interpretation of airborne magnetic and other imagery. After interpretation was completed, the faults were split into 300 m segments and each segment attributed with orientation. This was in order to focus on fault segments that fell within the range deemed to be most prospective, namely between 350° and 040°. It is acknowledged that this approach probably includes multiple generations of faults, and that it is likely that many of these faults moved more than once and some could have changed orientation as a result of later deformation. This simplification is forced upon us by the prohibitive amount of time required to effectively attribute each fault with movement timing and displacement vectors and in reconstructing fault geometry at the time of mineralization. Since mineralization was contemporaneous with, or later than, the main D2 deformation relatively minor displacement of N–S-trending faults along NW–SE-trending structures should be anticipated.

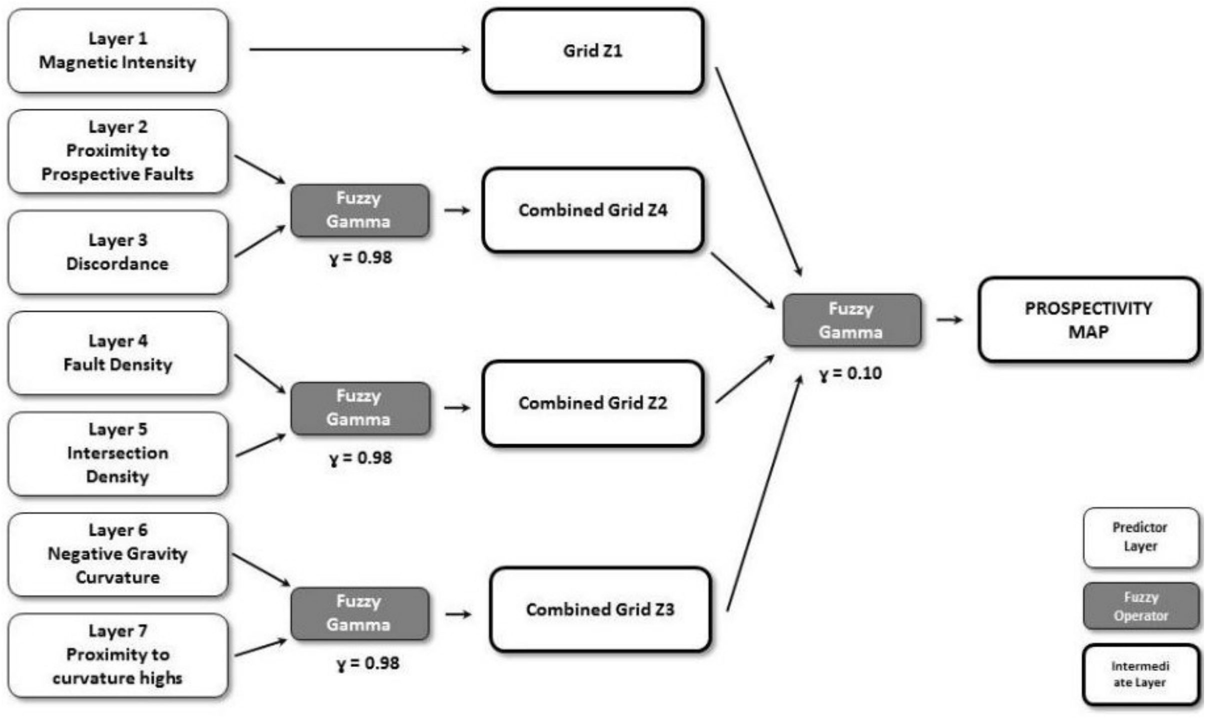

FIG. 10. Inference network for the Mount Isa North MPA.

As previously stated, it has been hypothesized that a crucial control on deposit location is the angle between bedding and prospective structures [15]. A significant problem, however, is the absence of a data layer that adequately expresses bedding orientations. To remedy this situation, strike and dip symbols from Geoscience Australia published 1: 100,000 scale geology maps were extracted and the strike of each bedding surface calculated by the GIS software. Large areas, however, are devoid of any bedding trend information, which is a significant problem for rigorous analysis.

A grid was generated that shows average 'fabric' (bedding and/or main foliation) direction using a 100-m cell size and search radius of 2,000 m (Fig. 13). These values were considered appropriate given the extent of the area to be analyzed, the abundance of structural information and the likely size of uranium deposit footprints. This layer was binned into five equal area categories and the category into which each of the 44 prospects occurs was determined. These data were tabulated and a chi-square analysis was conducted to determine if angular deviation has a significant control on mineralization. The chi-square value of 8.67 at 4 degrees of freedom is not considered significant at 95% confidence level; hence, we are not able to show a relationship between the two. This lack of support for a relationship is thought to reflect the poor quality of input data rather than the actual lack of a spatial relationship.

Fault density images were created using a coarse hexagonal grid (2 km sides; Fig. 13). The hexagonal grid was employed because it avoided artifacts due to preferred orientation of faults. For each hexagonal cell the total length of faults was measured and normalized to the cell area. The relationship between deposits and the density image was then examined using a chi-squared test, which proved a statistically significant association between deposits and areas of high fault density.

Fault intersections can also influence the location of mineral deposits. Therefore, a fault intersection grid was created that represented all intersections, triple-point intersections and quad-point intersections from the input data in Fig. 12. Triple point intersections are where one fault terminates at a point along another fault. Quad-point intersections highlight where faults physically cross one another or where several faults terminate at the same location. Density maps were created for these three cases using the same hexagonal mesh as for the fault abundance analysis. For each density map, two analyses were attempted: one using all points and the other using only small to large uranium deposits. Unfortunately, the counting statistics were too poor to generate results for the small to large uranium deposit group. Both triple- and quad-point intersections share a similar positive statistical relationship to uranium mineralization.

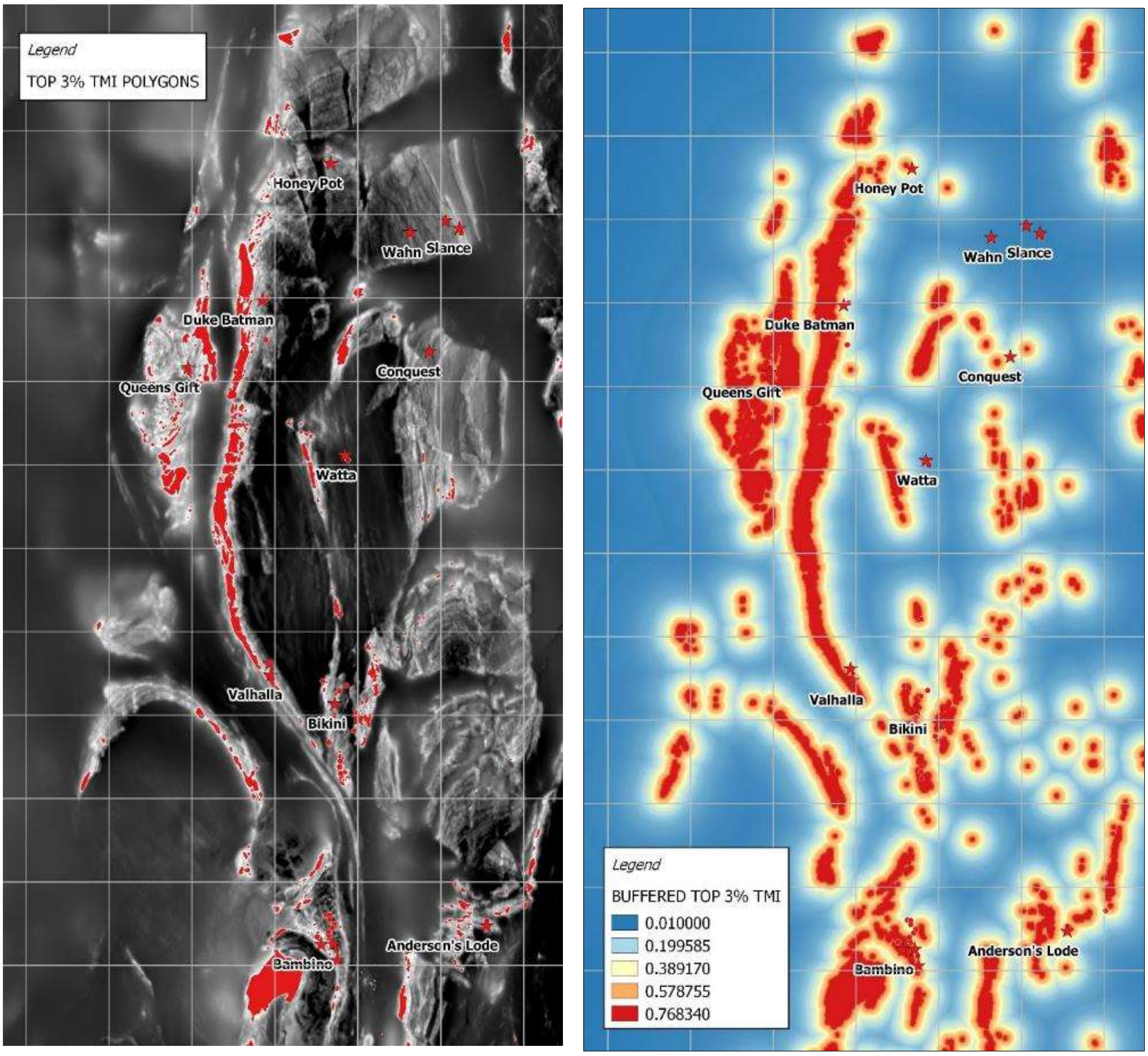

(a) *(b)*

FIG. 11. (a) Total magnetic intensity image with red polygons representing top 1% of TMI values, inferred to be albitite bodies. (b) Buffers around top 3% TMI polygons, with fuzzy membership values reflecting high prospectivity within or proximal to highly magnetic areas.

Visual inspection of uranium deposit distribution and a Bouguer gravity image (Fig. 14) suggests a good relationship between deposit occurrence and areas of high gravity gradient (curvature) inferred to represent deeply penetrating, crustal-scale faults (Fig. 14). There is also a relationship between deposit occurrence and areas of negative gravity curvature (shown blue in Fig. 14). This can probably be best explained as while deposits favor axes of high gravity gradient, they are more likely to occur where a zone of negative gradient occurs adjacent to a gradient maximum.

Four intermediate layers were created from these seven input layers (Figs. 10 and 15; Table 3) using the fuzzy gamma operator and a gamma value of 0.98. Grid Z1 (Fig. 10) represents the inferred presence of albitic alteration based entirely on magnetic patterns and can be related to the 'transport' layer of the previous study. Grid Z2 (Table 3, Fig. 15) represents structural orientation, that is to say it defines structures with the most prospective orientation and with a favorable angular relationship to bedding. It therefore represents a measure of trap favorability. Grid Z3 (Table 3, Fig. 15) represents a different facet of structural preparation, namely fault density and intersection density. Grid Z4 (Table 3, Fig. 15) is a combination of two datasets derived from Bouguer gravity and represents transport, namely deep crust-penetrating structures.

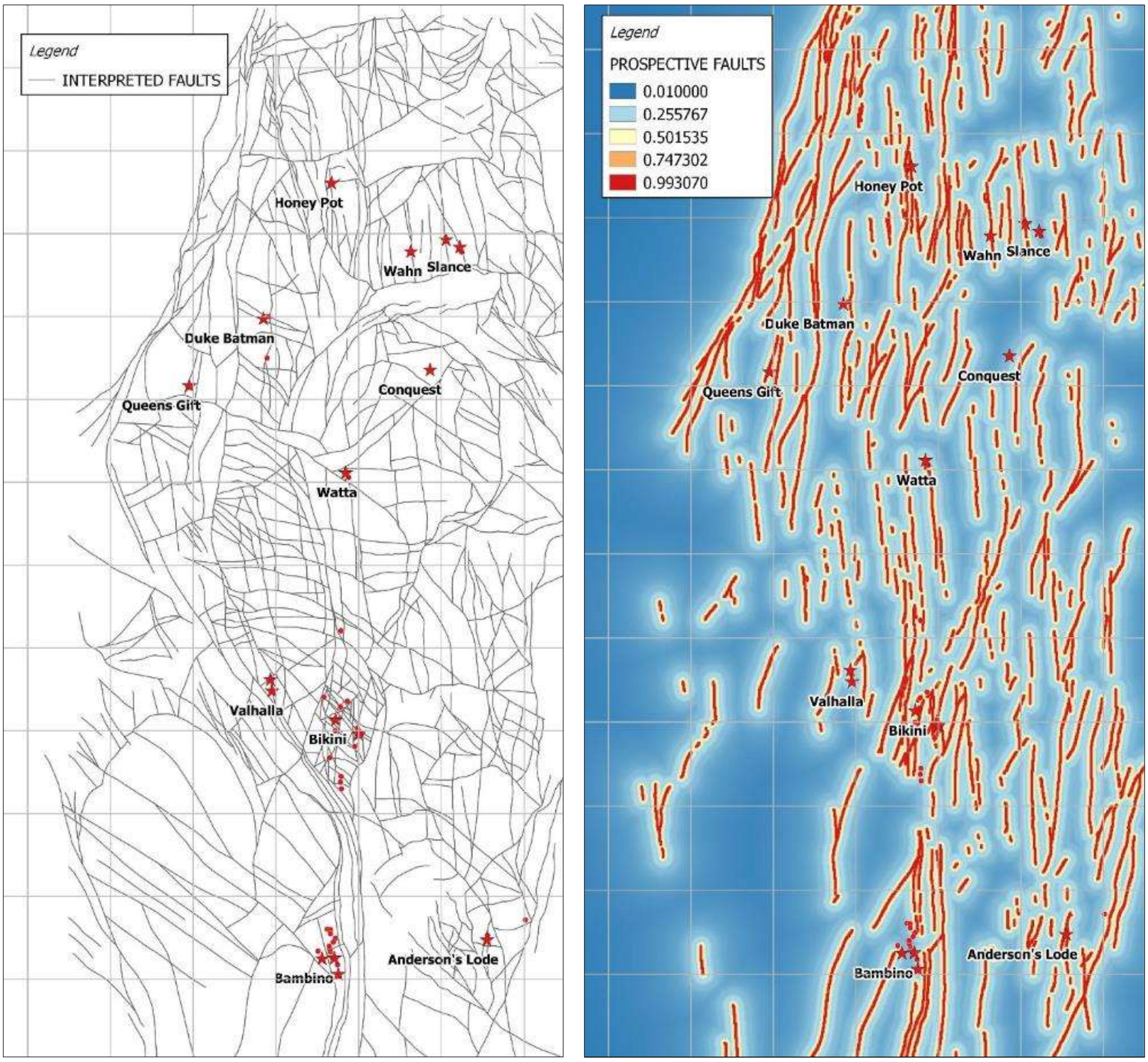

(a) *(b)*

FIG. 12. (a) Map of faults from Queensland Geological Survey mapping supplemented by interpretation of airborne magnetic data and aerial photography. (b) Buffered prospective faults. Grid cells are 10 km.

6.3. PROSPECTIVITY MAPS

Both fuzzy gamma and vectorial fuzzy logic techniques were used to generate prospectivity maps (Fig 16). In the former case, the intermediate grids were combined using the fuzzy gamma function with a gamma value of 0.1. This value was derived through a number of trials and found to best fit the observed distribution of known uranium mineralization.

The two prospectivity maps are very similar and assign high prospectivity values to the same broad areas (Fig. 16). The fuzzy gamma map better defines areas of intermediate prospectivity. The vectorial fuzzy logic map shows greater detail in the lower prospectivity areas. The vectorial fuzzy logic map also places greater emphasis on the high fault-density area to the south.

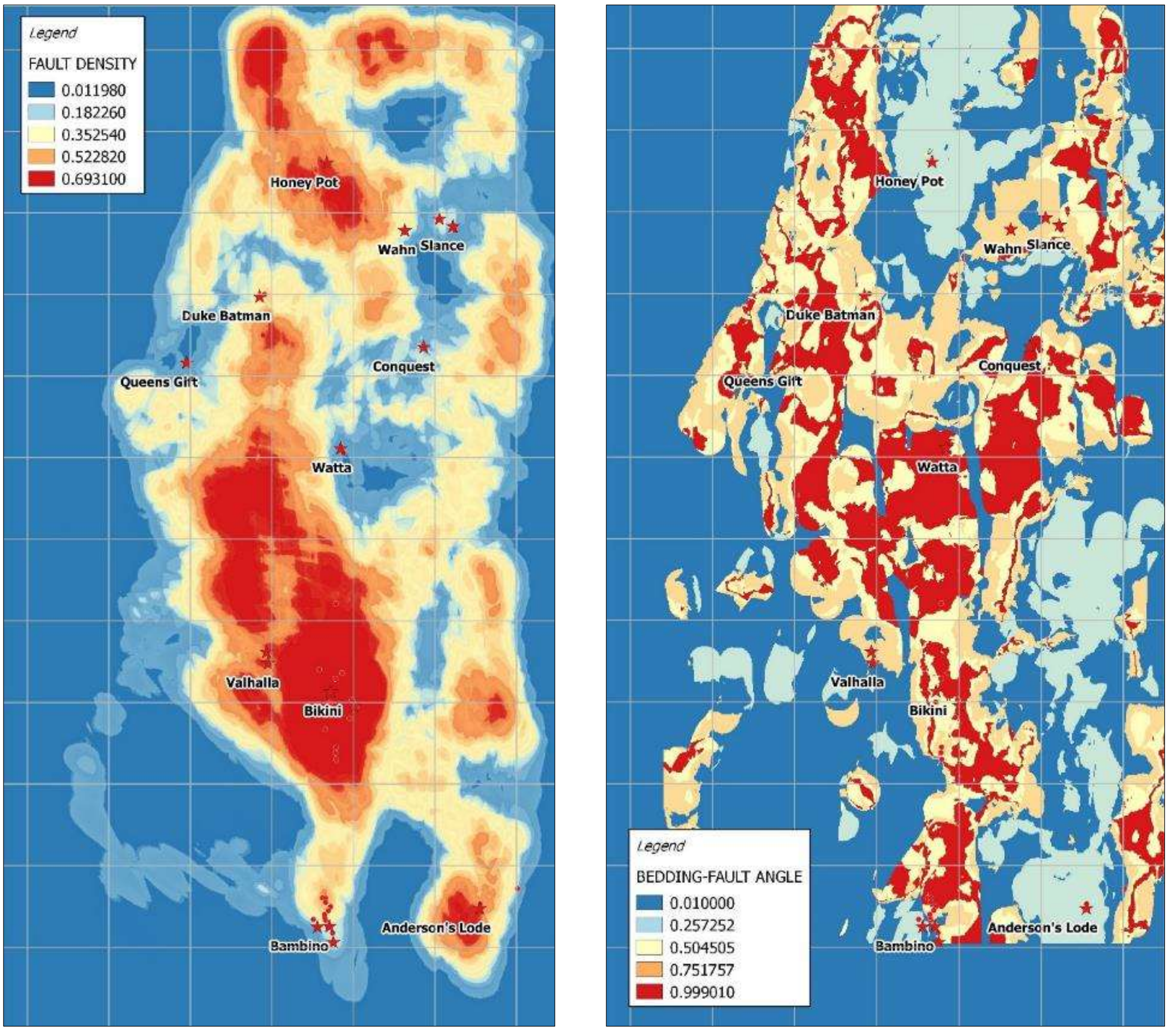

(a) *(b)*

FIG. 13. (a) Grid of fault density. (b) Image showing favorability of the angle between bedding and prospective faults. Grid cells are 10 km.

6.4. FUZZY GAMMA VS. VECTORIAL FUZZY LOGIC

The percentile prospectivity value corresponding to each deposit was determined in order to identify which technique was more successful at predicting the existence of uranium deposits (Table 4). The fuzzy gamma map captures 8 of the 44 uranium deposits (18%) in the top 1%

prospective percentile. The vectorial fuzzy logic map captures 10 out of 44 (23%). Table 5 suggests that both prospectivity maps accord higher prospectivities to large and medium deposits. The largest deposit, Valhalla, lies within the most prospective 9% of gamma fuzzy logic cells and 6% of vectorial fuzzy logic cells. In both maps, 3 of the 5 medium sized deposits occur within the top 1% of cells and all 5 medium sized deposits lie within the most prospective 4% of gamma fuzzy logic cells and 3% vectorial fuzzy logic cells.

For the most prospective 1% of the ground encompassed within the search space, the vectorial fuzzy logic approach provides a more powerful result; however, when averaging the percentiles over all 14 small and larger deposits, the two prospectivity maps share an almost identical predictive capability. An interesting aspect is that the medium sized deposits all fall in areas marked highly prospective, yet there is great variability in the smaller deposits. This is an indication that the maps have a notable predictive capability and that some of the input factors control not only the location of uranium mineralization but also the size of the body.

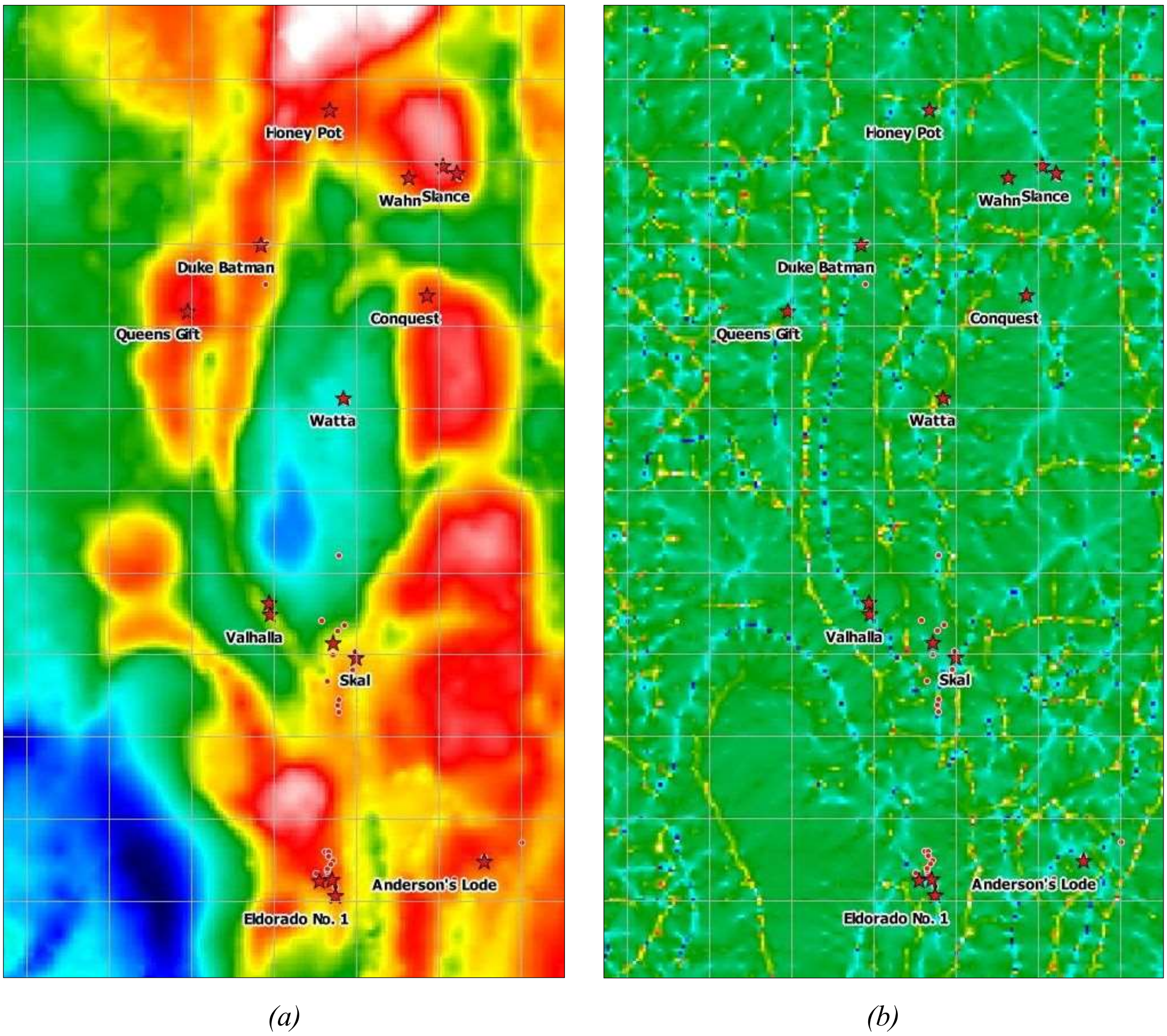

FIG. 14. (a) Bouguer gravity image. (b) Gravity curvature image derived from the Bouguer gravity data. Gray gridlines at 10 km intervals.

TABLE 5. COMPARISON OF VECTORIAL FUZZY LOGIC, GAMMA FUZZY LOGIC PROSPECTIVITY MAPS IN PREDICTING THE OCCURRENCE OF KNOWN DEPOSITS

Deposit size	Deposit name	Prospectivity percentile	
		Vectorial fuzzy logic	Fuzzy gamma
Large	Valhalla	6	9
Medium	Skal	1	1
	Bikini	1	1
	Anderson's Lode	2	2
	Skal East	1	1
	Odin	3	4
Small	Bambino	25	8
	Duke Batman	4	10
	Eldorado	16	11
	Queen's Gift	2	10
	Skal North	1	1
	Slance	38	56
	Thanksgiving	27	23
	Watta	57	48
Average		13.1	13.2

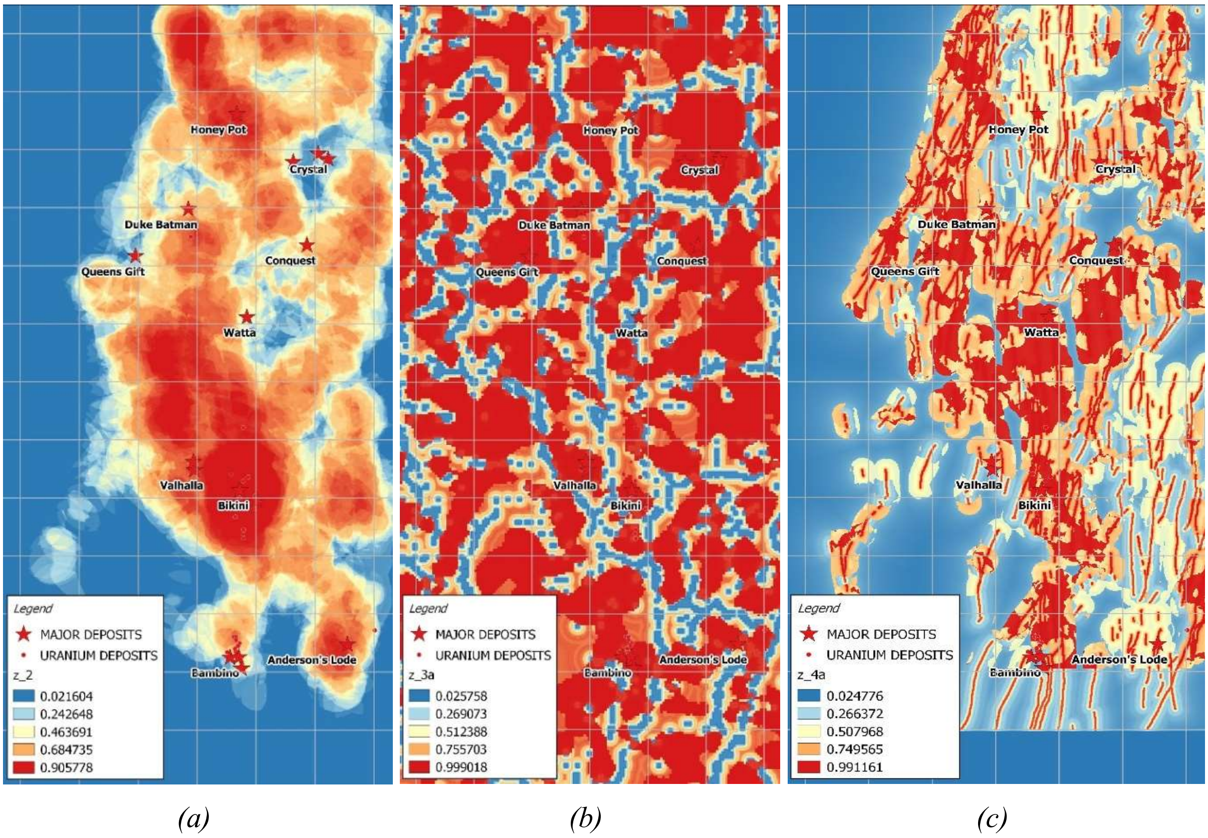

FIG. 15. Three of the four intermediate images used in construction of the prospectivity maps shown in Fig. 16. (a) Combined grid Z2. (b) Combined grid Z3. (c) Combined grid Z4. Grid Z1 is similar to that in Fig. 11.

7. QUANTITATIVE MINERAL RESOURCE ASSESSMENT

The undiscovered uranium endowment of the Mt Isa North region was estimated using two quantitative statistical approaches: firstly, the three-part assessment, which employs regression estimates of the number of undiscovered deposits and total ore tonnage [22, 23, 26], and, secondly, rank-size statistical analysis ('Zipf's law').

7.1. QUANTITATIVE ASSESSMENT FOLLOWING THE THREE-PART APPROACH

The three-part assessment was originally developed by the USGS and is the most commonly used approach to quantitative mineral resource assessment [22, 23]. It involves the following three parts:

- Definition of areas (geologically-permissive tracts) that may contain mineral deposits of a particular type;
- Estimation of likely grade and tonnage characteristics of undiscovered deposits by an appropriate grade-and-tonnage model (based on geologically similar known deposits);
- Estimation of the number of undiscovered deposits (as percentiles of a probability distribution) consistent with the selected grade-and-tonnage model.

The total endowment of undiscovered deposits can then be estimated either through a Monte Carlo simulation [24, 25] or regression modeling using the area of geologically-permissive tract and the median ore tonnage of the grade-and-tonnage model [26].

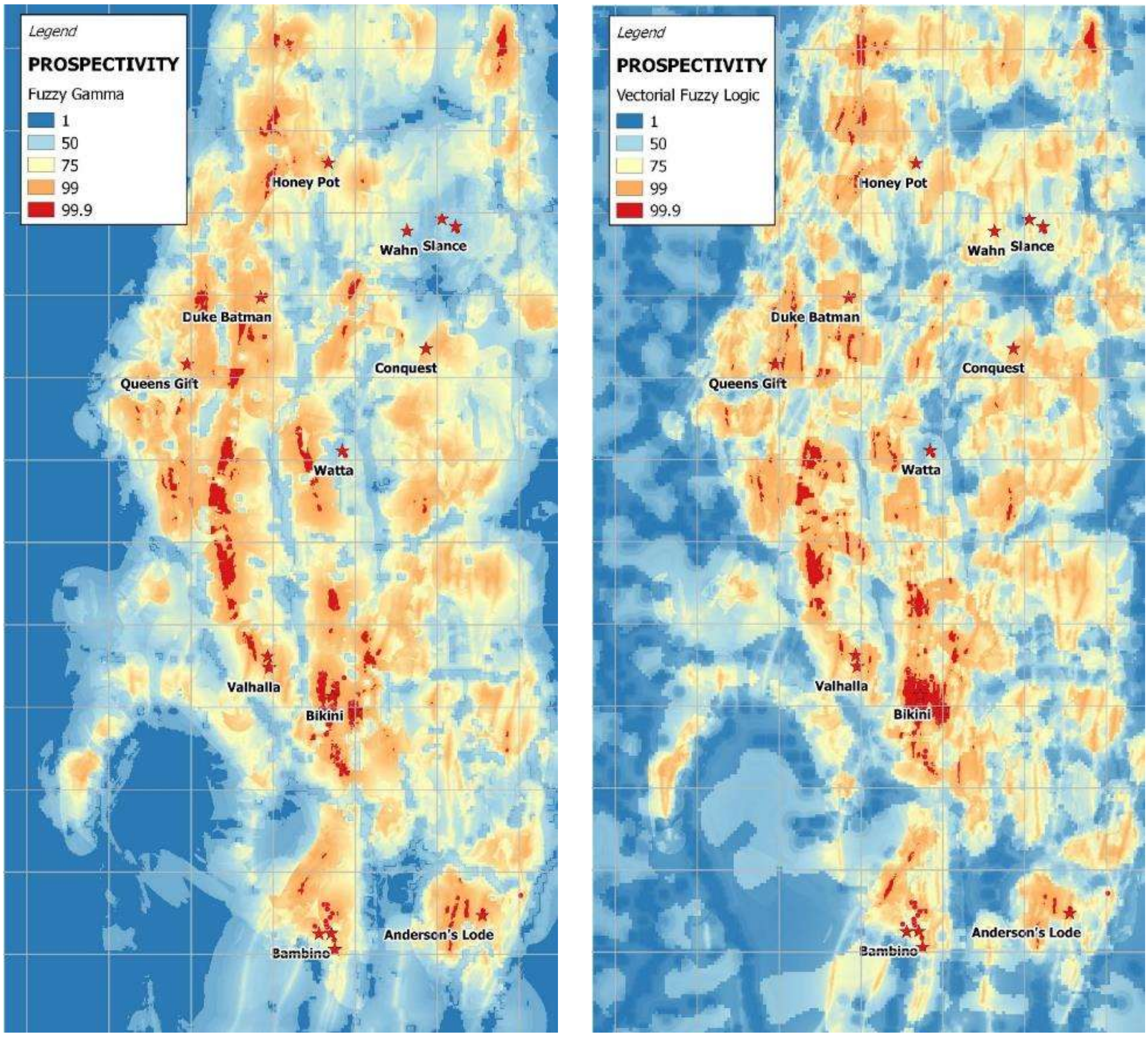

FIG. 16. (a) Fuzzy gamma prospectivity map. (b) Vectorial fuzzy gamma prospectivity map. Colour-coded by various percentile cut-offs of prospectivity value, e.g. red values exceed the 99.9 percentile value of prospectivity. Gray gridlines at 10 km intervals.

7.1.1. Definition of geologically-permissive tract and sub-tract boundaries

A geologically-permissive tract is an area where the presence of mineral deposits of a particular type is geologically possible, and the probability of a deposit occurring outside the tract boundaries is negligible [22, 23]. The spatial limits of a tract that is geologically-permissive for albitite-type uranium deposits in the Mt Isa North region were defined as a generalized outline including the areas with an estimated fuzzy favorability above 5% (Fig. 9). The probability of a significant albitite-type uranium discovery outside this tract (Fig. 17) is deemed to be negligible. The total area of the geologically-permissive tract is ~15,700 km^2.The density of albitite-type uranium occurrences (occurrences per 1,000 km^2, estimated using the isotropic quadratic kernel function in ArcGIS 10.3 with 30 km bandwidth) highlights strong regional heterogeneity (Fig. 17). All documented deposits and occurrences occur in the central part of the tract. This distribution could be the product of more effective exploration in the central part of the tract compared to the north and south portions. All deposits except Odin were discovered by anomalous levels of radiation at the surface. Since the entire tract has been covered by high resolution airborne radiometric surveys it is improbable that outcropping deposits are present in the northern and southern portions. Thus, the spatial heterogeneity of uranium mineralization is believed to be due to regional-scale metallogenic factors rendering the central part of the geologically-permissive tract significantly more prospective. Consequently, a central sub-tract was delineated as a continuous area within 30 km from any documented albitite-type uranium deposit or occurrence (red outline in Fig. 17). The area of the central sub-tract is ~7,900 km^2.

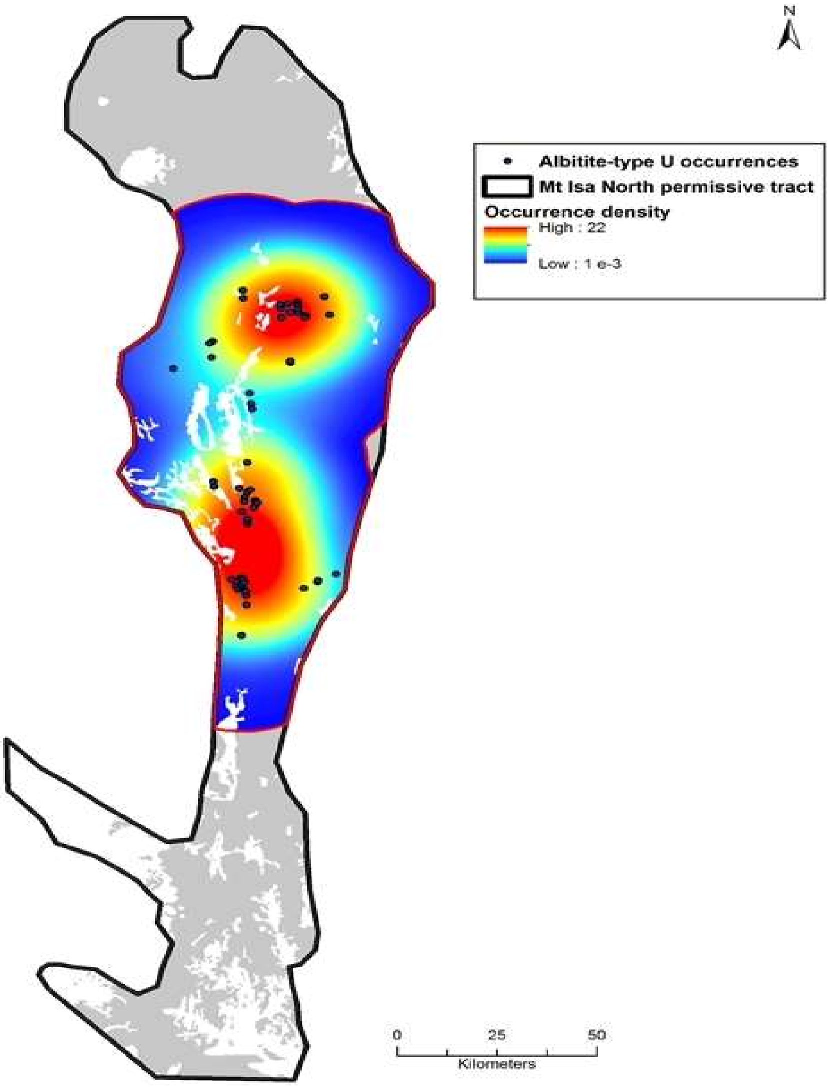

FIG. 17. The Mt Isa North geologically-permissive tract (black outline) and its central well-endowed sub-tract (red outline). The gray color shows the Proterozoic outcrop with areas under cover in white.

7.1.2. Grade-and-tonnage model of Albitite-type uranium deposits in the Mt Isa North Region

Grades and tonnages of the total population of albitite-type uranium deposits in the region, including any undiscovered deposits, can be statistically characterized by grade and tonnage frequency distributions of the known deposits. It is important to ensure that the grade and tonnage data were estimated in a consistent manner. All the deposit grades and tonnages listed in Table 1 are total in situ resources, mostly estimated by the same company using comparable methods and the same cut-off grades, thus ensuring internal consistency of endowment estimates. Furthermore, if two or more adjacent deposits are sufficiently close to each other that they can be considered to be parts of the same deposit, then their endowments should be aggregated. Each decision on deposit aggregation will affect the statistical properties of the deposit group and, consequently, the results of statistical quantitative mineral resource assessment. Typically, if deposits are within 500 m to 2 km of each other their endowment is aggregated [27]. In practice, subjective expert judgment is often used to define spatial extents of deposits and mineral fields.

Most of the uranium deposits listed in Table 1 occur at relatively large distances from each other (often >10 km). Four deposit groups or pairs, however, are less than 2 km apart and occur along the same mineralized structures: Citation, Mighty Glare and Eldorado North, Bikini and Mirrioola, Valhalla and Odin and Watta and Warawai. Considering that individual ore bodies of the albitite type commonly have a strike length of several hundred meters and that zones of uranium mineralization can extend several kilometers along mineralized structures; these four pairs of deposits can be considered parts of the same deposits and were aggregated for this assessment. The grade and tonnage distributions for the spatially aggregated albitite-type uranium deposits in the Mt Isa North region are illustrated in Fig. 18.

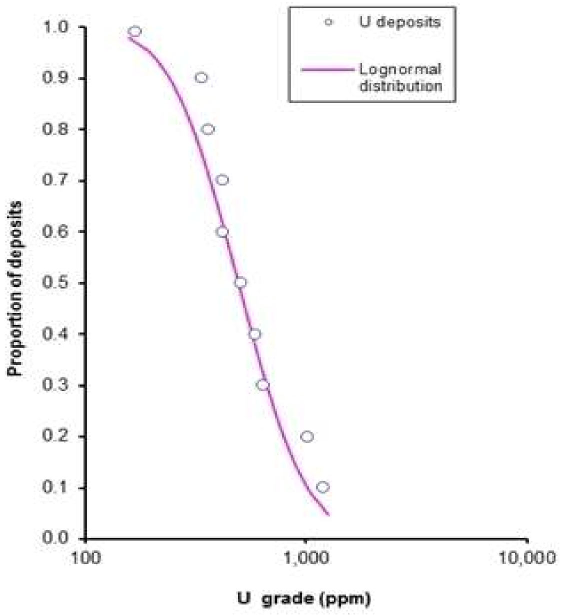

(a)

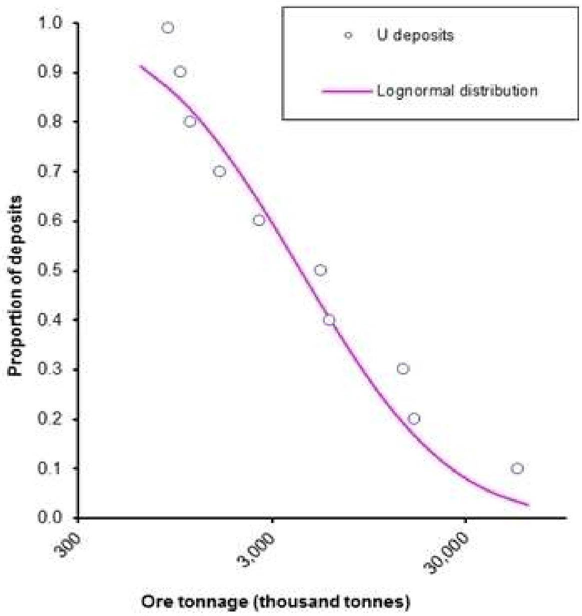

(b)

FIG. 18. (a) Probability plot of uranium grade in albitite-type deposits of Mount Isa. (b) Probability plot of contained uranium in albitite-type deposits of Mount Isa.

Deposit grades and tonnages are not significantly different from corresponding log-normal (base 10) distributions (as indicated by results of the Kolmogorov-Smirnov test, with $p > 0.15$) and are not significantly correlated (with Pearson's product-moment correlation coefficient for log-transformed grades and tonnages of -0.19, P(t) = 0.49). The mean of the log-transformed ore tonnage distribution is 4.15 Mt, the median is 3.74 Mt, and the mean and median uranium grades are both 0.05% U.

7.1.3. Estimating the number of undiscovered deposits

In three-part assessments, the number of undiscovered deposits, consistent with a selected grade-and-tonnage model, is commonly subjectively estimated by a group of experts, either by consensus [22] or by mathematical aggregation of individual assessment results [28]. At this potentially controversial stage of assessment, subjective expert judgment can also be complemented, or even substituted, by the statistical global deposit density model [26, 27]. This statistical model, applicable to any deposit type characterized by a grade-and-tonnage model, evaluates the spatial deposit density (the average number of deposits per 100,000 km^2) for any geologically-permissive tract through regression using the tract size and the median ore tonnage of the grade-and-tonnage model:

$$log_{10}(D_{50}) = 4.2096 - 0.4987 \text{ x } log_{10}(A) - 0.2252 \text{ x } log_{10}(T) \quad (1)$$

$$log_{10}(D_{90}, D_{10}) \cong$$

$$log_{10}(D_{50}) \pm 0.449 \times \sqrt{1.009 + 0.003 \times (3.173 - log_{10}(A))^2 \times (-0.329 - log_{10}(T))^2} \quad (2)$$

where A is geologically-permissive area in square kilometers, T is the mean of the log-transformed (base $_{10}$) tonnage distribution (in million tonnes) of the deposit model under consideration and D_{90}, D_{50} and D_{10} are deposit densities (per 100,000 km^2) at the 90, 50 and 10% certainty levels, respectively.

The total number of deposits (known and undiscovered) at those certainty levels can then be estimated as:

$$N_{10(50,90)} = \text{A}/100{,}000 \times 10^{\log10(D10(50,90))} \quad (3)$$

The regression model applied only to the central sub-tract and using the aggregated grade-and-tonnage model (with the mean of the log-transformed ore tonnage distribution of 4.15 Mt) estimates the total expected (mean) number of deposits (both discovered and undiscovered) to be 12, with 90% certainty of at least 3 deposits, 50% certainty of at least 10 undiscovered deposit, and 10% certainty of 30 deposits or more. Adjusting the estimates for the 10 deposits with identified resources [26] the expected number of undiscovered deposits in the central sub-tract is estimated to be 2, with 50% certainty of at least 1 undiscovered deposit, and 10% certainty of 4 deposits or more. For comparison, the regression model based on the original grade-and-tonnage model of 14 individual deposits without any spatial aggregation of adjacent deposits (Table 1), with the mean of the log-transformed ore tonnage distribution of 2.86 Mt, estimates the total expected number of uranium deposits (both discovered and undiscovered) in the central sub-tract to be 13. This mean estimate is smaller than the number of individual deposits already known within the central sub-tract and no undiscovered deposits are expected in the area.

For the entire Mt Isa North geologically-permissive tract (Fig. 17) the expected number of undiscovered deposits consistent with the aggregated grade-and-tonnage model is estimated by the regression model as 6, with 90% certainty of at least 2 undiscovered deposits, 50% certainty of at least 5 deposits, and 10% certainty of 16 deposits or more. This statistical estimate implies that the northern and southern parts of the region likely contain several undiscovered uranium deposits, with an upside possibility that those parts of the geologically-permissive tract can be as well endowed as the central sub-tract.

7.1.4. Estimating total ore tonnage of all uranium deposits in the region

In addition to the number of undiscovered deposits, total ore tonnage (including tonnages of both known and undiscovered deposits) can also be estimated by a global regression model [26]:

$$log_{10}(T_{50}) = -1.096 + 0.7039 \times log_{10}(A) + 0.6202 \times log_{10}(T) \quad (4)$$

$$log_{10}(T_{90}, T_{10}) \cong$$

$$log_{10}(T_{50}) \pm 0.664 \times \sqrt{1.009 + 0.003 \times (3.175 - log_{10}(A))^2 \times (-0.329 - log_{10}(T))^2} \quad (5)$$

where T_{90}, T_{50} and T_{10} are the estimates (at the 90, 50 and 10 % confidence levels, respectively) of total ore tonnage of all deposits belonging to a chosen deposit model with the mean of the log-transformed (base 10) tonnage distribution of T, within an assessment tract of size A. The regression estimates of the total ore tonnage only for the central sub-tract are: 90% certainty of 23.2 Mt or more total ore tonnage, 50% of 107.4 Mt or more and 10% of 503.4 Mt ore. The logarithm of the total expected tonnage of undiscovered deposits can be then estimated as the logarithm of (the mean of the log-normal distribution consistent with the above percentile estimates, minus the total tonnage of the known deposits) minus half of the variance of that log-normal distribution with 106 degrees of freedom [26].

The corresponding regression estimates of the ore tonnage of the undiscovered deposits in the central sub-tract are: 90% certainty of 6 Mt or more total ore tonnage, 50% of 30 Mt or more and 10% of at least 138 Mt ore.

7.2. QUANTITATIVE ASSESSMENT BASED ON THE RANK-SIZE STATISTICAL MODEL

Rank-size statistical analysis based on 'Zipf's law' has been often used as an easy to implement way to assess residual endowment and a degree of exploration maturity of a mineral province [29–31]. Zipf's law is basically a discrete version of the continuous Pareto distribution, a power-law distribution with the cumulative distribution function represented as a rank-frequency or rank-size plot [32]. The Zipf's law can be expressed in general form as:

$A_r = A_1 r^k \mid k < 0$
(6)

where r is rank of an object in a set of objects arranged in descending order of sizes, A_1 is size of the largest object in the set, A_r is size of the rth object and k is a constant. The application of Zipf's law to estimate amounts of contained metal (endowment) of mineral deposits implies that endowments of all the deposits that are present in a mineral province, and thus its total endowment, can be sufficiently estimated based on only two parameters, namely the endowment of the largest deposit present in the province and the value of k. Total metal endowment of the province M can then be estimated as:

$$M = \sum_{r=1}^{n} M_r \times r^k \tag{7}$$

where M_r is metal endowment of the rth deposit in a descending rank-ordered series and n is the number of deposits used in the analysis, which can be defined by setting the minimum individual deposit endowment used in an analysis. Previous studies applying Zipf's law to analyze endowments of mineral provinces suggest that in relatively mature provinces k is very close to -1 [30, 33].

The distribution of contained uranium between the 10 known spatially aggregated deposits in the Mount Isa North region, with the combined Valhalla-Odin deposit being the largest known deposit in the region containing 36,104 t U, can be modeled by a best-fit negative power function of the relative ore field ranks (Fig. 19). The power coefficient of -1.9 is significantly different from -1, the coefficient typically used to characterize deposit endowments by Zipf's law in most previous studies [30, 33], but it is similar to k = -1.991 in a case study for a province estimated to contain many large undiscovered deposits [31]. Adjusting ranks of the known deposits so that they fit a standard Zipf distribution with A_1 = 36,104 indicate the absence of several relatively large deposits, including the second and third largest (Fig. 19). This can be considered an indication (and a measure) of the relative exploration immaturity of the Mt Isa North region and implies that there are significant additional uranium resources still to be discovered in the region.

Total residual uranium endowment of the Mt Isa North region (including the total endowment of undiscovered deposits and any extensions of known deposits) can be estimated using Equation 2, deducting the combined identified endowment of all the known deposits from the total 'natural' endowment as estimated by the standard Zipf function. The Zipf function is likely to be adequately applicable to characterize sizes and frequencies of only relatively large deposits, often grossly over-estimating the number of smaller deposits [31, 32]. Consequently, only deposits with more than 1,500 t U were considered. These deposits jointly contain >95% of the total uranium endowment identified to date in the Mt Isa North region. The total residual uranium endowment of the region, contained in deposits with at least 1,500 t U, is thus estimated to be approximately 80,000 t U, compared to 58,800 t U of total current resources of the known deposits. For comparison, a standard Zipf function assuming that the largest deposit in the region is Valhalla excluding Odin (as per the original deposit list in Table 1) implies a significantly smaller residual endowment of 49,000 t U.

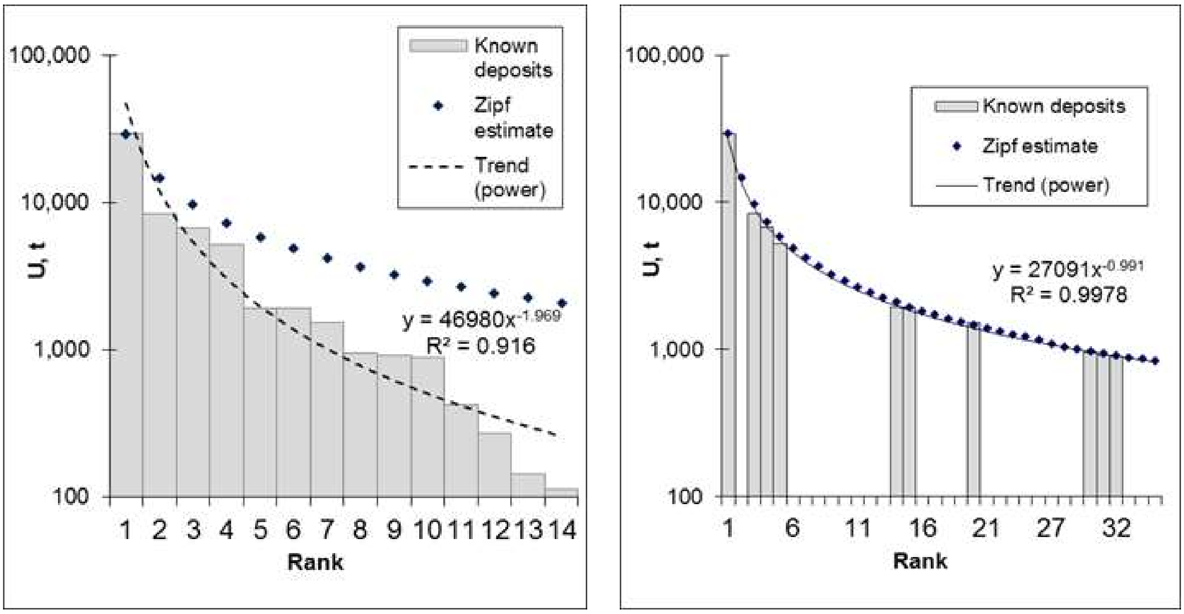

(a) *(b)*

FIG. 19. (A) Rank-size distribution illustrating identified uranium resources of known deposits, plotted in the descending order of their relative ranks. (b) Rank-size plot with ranks of known deposits fitted to the standard Zipf function.

8. DISCUSSION AND CONCLUSIONS

8.1. MINERAL PROSPECTIVITY MAPPING

These two studies illustrate the process of using a geological model and various input data to define areas prospective for undiscovered uranium resources. The approach was fundamentally knowledge-driven and required use of geological judgment in choosing appropriate input layers, in assigning fuzzy membership values and in deciding the most appropriate methods of combining the input layers. All three prospectivity maps were successful in that known deposits, particularly the larger examples, fall within pixels categorized as highly prospective. Ultimately, however, the success of the approach will need to be judged by the success of ongoing mineral exploration in areas deemed to have prospectivity.

A comparison of the regional and detailed studies shows the scale dependency of the input parameters, with some input layers being appropriate for the regional analysis but not for the more detailed one. Prospectivity maps generated by the fuzzy gamma and vectorial fuzzy logic techniques are similar. The latter technique may, however, provide better discrimination of areas prospective for large (rather than medium or small) deposits. A further benefit of this technique is that there is no need to produce intermediate combinations of input layers and no necessity for a gamma parameter. This results in a simplified process and makes subsequent applications of the technique more repeatable and comparable [19].

8.2. QUANTITATIVE ASSESSMENT RESULTS

Both the global regression and rank-size ('Zipf's law') models used in this study suggest that the Mt Isa North region contains significant undiscovered uranium resources. The rank-size model suggests that the total residual endowment of the region is comparable to, or larger than, the current uranium resource. The rank-size model estimates are particularly sensitive to the spatial definition of the largest uranium deposit in the region, i.e., whether Valhalla and Odin are considered parts of the same deposit or two separate deposits. This sensitivity can be used to provide a measure of uncertainty of the estimates of residual endowment in the region.

The spatial distribution of known albitite-type uranium deposits and occurrences suggests that the central part of the region may be significantly better endowed than the rest of the region. The global regression model of the number of deposits applied only to that central sub-tract indicates that an area of that size can contain only a few additional deposits similar in grades and tonnages to the known deposits. However, if the entire region is considered geologically-permissive for albitite-type uranium deposits (as suggested by our mineral prospectivity modeling), the global regression model of the number of deposits indicates that the region can still contain more undiscovered uranium deposits than the total number of deposits discovered to date. For the spatially aggregated grade-and-tonnage model, the regression estimates are the expected number of 6 undiscovered deposits and 10% probability of 16 deposits or more. The global regression model of total ore tonnage estimates the expected undiscovered ore tonnage for the entire Mt Isa North geologically-permissive tract as 83 Mt using the original deposit model and 132 Mt ore using the aggregated deposit model. The upside regression model scenarios, which imply a relatively high prospectivity of the northern and southern parts which do not have any significant documented albitite-type uranium mineralization, are generally consistent with implications of the rank-size endowment models.

The application of global regression and district rank-size models to albitite-type uranium deposits in the Mount Isa North area reveals the inherent uncertainty of such estimates. Possible scenarios range from the presence of only a few or even no undiscovered deposits in the region to a significant residual endowment comparable to that identified to date in all the known deposits. Such uncertainty is a feature of any quantitative mineral resource assessment for a region which yet to be exhaustively explored.

Appendix

FUZZY MEMBERSHIP CALCULATIONS FOR REGIONAL MPA

Predictor map	Criterion	Class score	Map weight	Class weight	Fuzzy membership value
SOURCE					
Granites	0.001 km	10	7	70	0.70
	05 km	9	7	63	0.63
	10 km	9	7	63	0.63
	15 km	8	7	56	0.56
	20 km	7	7	49	0.49
	25 km	6	7	42	0.42
	30 km	5	7	35	0.35
	35 km	4	7	28	0.28
	40 km	3	7	21	0.21
	45 km	2	7	14	0.14
	50 km	1	7	7	0.07
	50 km+	0	7	1	0.01
Hot granites	0.001 km	10	8	80	0.80
	05 km	9	8	72	0.72
	10 km	9	8	72	0.72
	15 km	8	8	64	0.64
	20 km	7	8	56	0.56
	25 km	6	8	48	0.48
	30 km	5	8	40	0.40
	35 km	4	8	32	0.32
	40 km	3	8	24	0.24
	45 km	2	8	16	0.16
	50 km	1	8	8	0.08
	50 km+	0	8	1	0.01
Coincident mag/grav lows buff	0.001 km	10	7	70	0.70
	05 km	9	7	63	0.63
	10 km	9	7	63	0.63
	15 km	8	7	56	0.56
	20 km	7	7	49	0.49
	25 km	6	7	42	0.42
	30 km	5	7	35	0.35
	35 km	4	7	28	0.28
	40 km	3	7	21	0.21
	45 km	2	7	14	0.14
	50 km	1	7	7	0.07
	50 km+	0	7	1	0.01
TRANSPORT					
NNE faults (345° - 045°)	500 m	10	9	90	0.90
	1000 m	9	9	81	0.81
	1500 m	8	9	72	0.72
	2000 m	7	9	63	0.63
	2500 m	6	9	54	0.54
	3000 m	5	9	45	0.45

Predictor map	Criterion	Class score	Map weight	Class weight	Fuzzy membership value
	3500 m	4	9	36	0.36
	4000 m	3	9	27	0.27
	4500 m	2	9	18	0.18
	5000 m	1	9	9	0.09
	5000 m+	0	9	1	0.01
NW Faults	500 m	10	4	40	0.40
(285º - 345º)	1000 m	9	4	36	0.36
	1500 m	8	4	32	0.32
	2000 m	7	4	28	0.28
	2500 m	6	4	24	0.24
	3000 m	5	4	20	0.20
	3500 m	4	4	16	0.16
	4000 m	3	4	12	0.12
	4500 m	2	4	8	0.08
	5000 m	1	4	4	0.04
	5000 m+	0	4	1	0.01
E-W faults	500 m	10	3	30	0.30
(045º - 105º)	1000 m	9	3	27	0.27
	1500 m	8	3	24	0.24
	2000 m	7	3	21	0.21
	2500 m	6	3	18	0.18
	3000 m	5	3	15	0.15
	3500 m	4	3	12	0.12
	4000 m	3	3	9	0.09
	4500 m	2	3	6	0.06
	5000 m	1	3	3	0.03
	5000 m+	0	3	1	0.01
Major faults	01 km	10	9	90	0.90
	02 km	9	9	81	0.81
	03 km	8	9	72	0.72
	04 km	7	9	63	0.63
	05 km	6	9	54	0.54
	06 km	5	9	45	0.45
	07 km	4	9	36	0.36
	08 km	3	9	27	0.27
	09 km	2	9	18	0.18
	10 km	1	9	9	0.09
	10 km+	0	9	1	0.01
Medium faults	01 km	10	4	40	0.40
	02 km	9	4	36	0.36
	03 km	8	4	32	0.32
	04 km	7	4	28	0.28
	05 km	6	4	24	0.24
	06 km	5	4	20	0.20
	07 km	4	4	16	0.16
	08 km	3	4	12	0.12
	09 km	2	4	8	0.08
	10 km	1	4	4	0.04
	10 km+	0	4	1	0.01
Minor faults	01 km	10	2	20	0.20
	02 km	9	2	18	0.18
	03 km	8	2	16	0.16

Predictor map	Criterion	Class score	Map weight	Class weight	Fuzzy membership value
	04 km	7	2	14	0.14
	05 km	6	2	12	0.12
	06 km	5	2	10	0.10
	07 km	4	2	8	0.08
	08 km	3	2	6	0.06
	09 km	2	2	4	0.04
	10 km	1	2	2	0.02
	10 km+	0	2	1	0.01
Fault density	v. low (<0.1 km/km^2)	0	9	1	0.01
	low (0.1 - 0.3 km/km^2)	3	9	27	0.27
	med (0.3 - 0.6 km/km^2)	7	9	63	0.63
	high (0.6 - 1.75 km/km^2)	9	9	81	0.81
	v. high (>1.75 km/km^2)	8	9	72	0.72
Mag 1VD	Low	0	4	1	0.01
	High	9	4	36	0.36
TRAP					
Metamorphic grade	Amphibolite	6	9	54	0.54
	Granite	0	9	1	0.01
	Greenschist	10	9	90	0.90
	Sillimanite	5	9	45	0.45
	SillimaniteKspar	6	9	54	0.54
Lithology simplified	Calcarenite	4	9	36	0.36
	Carbonates	1	9	9	0.09
	Chert	0	9	1	0.01
	Extrusive – felsic	2	9	18	0.18
	Extrusive – mafic	10	9	90	0.90
	Intrusive – felsic	3	9	27	0.27
	Intrusive – mafic	2	9	18	0.18
	Metamorphics	6	9	54	0.54
	Sandstone	8	9	72	0.72
Prot median strat age	1,657 (1,590-1,724 Ma)	0	9	1	0.01
	1,749 (1,742-1,756 Ma)	5	9	45	0.45
	1,778 (1,757-1,800 Ma)	9	9	81	0.81
	1,814 (1,802-1,825 Ma)	5	9	45	0.45
	1,856 (1,844-1,867 Ma)	4	9	36	0.36
	1,880 Ma +	0	9	1	0.01
ppm U radiometrics	v. low (<2 ppm U equiv.)	0	6	1	0.01
	low (2 - 3 ppm U equiv.)	1	6	6	0.06

Predictor map	Criterion	Class score	Map weight	Class weight	Fuzzy membership value
	med (3 - 4 ppm U equiv.)	4	6	24	0.24
	high (4 - 5 ppm U equiv.)	7	6	42	0.42
	v. high (>5 ppm U equiv.)	9	6	54	0.54
U/Th radiometrics	v. low (<0.125.)	0	6	1	0.01
	low (0.125 - 0.25)	1	6	6	0.06
	med (0.25 - 0.33)	4	6	24	0.24
	high (0.33 - 1.00)	7	6	42	0.42
	v. high (>1.00)	9	6	54	0.54
U^2/Th radiometrics	v. low (<0.125.)	0	6	1	0.01
	low (0.125 - 0.25)	1	6	6	0.06
	med (0.25 - 0.33)	4	6	24	0.24
	high (0.33 - 1.00)	7	6	42	0.42
	v. high (>1.00)	9	6	54	0.54

REFERENCES

[1] WILDE, A.R., Towards a model for albitite-type uranium. Minerals 3, 36–48 (2013).

[2] BAIN, J.H.C.; HEINRICH, C.A.; HENDERSON, G.A.M., Stratigraphy, Structure and Metasomatism of the Haslingdon Group, East Moondarra Area, Mt Isa: A Deformed and Mineralised Proterozoic Multistage Rift-sag Sequence. In Detailed Studies of the Mount Isa Inlier; Australian Geological Survey Organisation Bulletin 243; Stewart, A.J., Blake, D.H., Eds.; Australian Geological Survey Organisation: Canberra, Australia; pp. 125–136 (1992).

[3] GREGORY, M.J.; SCHAEFER, B.F.; KEAYS, R.R., WILDE, A.R., Rhenium-Osmium systematics of the Mount Isa copper orebody and the Eastern Creek volcanics, Queensland: Implications for ore genesis. Mineralium Deposita 43, 553–573 (2008).

[4] CONNORS, K.A., PAGE, R.W., Relationship between magmatism, metamorphism and deformation in the western Mount Isa Inlier, Australia. Precambrian Research 71, 131–153 (1995).

[5] MCGLOIN, M., U-Pb Shrimp geochronology of the Sybella microgranite: Is there a link to U-Ree prospects at Mount Isa? AIG News 110, 29–30 (2012).

[6] HOADLEY E., Evolution of the Sybella Batholith: petrographic, geochemical and structural development of an A-type intrusive complex: PhD Thesis, James Cooke University (2003).

[7] POLITO, P.; KYSER, K.; STANLEY, C., The Proterozoic, albitite-type, Valhalla uranium deposit, Queensland, Australia: A description of the alteration assemblage associated with uranium mineralisation in diamond drill hole V39. Mineralium Deposita 44, 11–40 (2007).

[8] ABU SHARIB, A.S., SANISLAV, I.V., Polymetamorphism accompanied switching in horizontal shortening during Isan Orogeny: Example from the Eastern Fold Belt, Mount Isa Inlier, Australia. Tectonophysics 587, 146–167 (2012).

[9] WILDE, A.R., Mount Isa copper orebodies: Improving predictive discovery. Australian Journal of Earth Science 58, 937–951 (2011).

[10] WYBORN, L. The Petrology and Geochemistry of Alteration Assemblages in the Eastern Creek Volcanics, as a Guide to Copper and Uranium Mobility Associated with Regional Metamorphism and Deformation, Mt Isa, Queensland. In Geochemistry and Mineralization of Proterozoic Volcanic Suites; GS Special Publication No. 33; Pharaoh, T.C., Beckinsale, R.D., Rickard, D., Eds.; Institute of Mining and Metallurgy: London, UK, pp. 425–434 (1987).

[11] HANNAN, K.; GOLDING, S.D.; HERBERT, H.K.; KROUSE, H.R. Contrasting alteration assemblages in metabasites from Mount Isa, Queensland: Implications for copper ore genesis. Economic Geology 88, 1135–1175 (1993).

[12] HEINRICH, C.A., BAIN, J.H.C., MERNAGH, T.P., WYBORN, L.A.I., ANDREW, A.S., WARING, C.L. Fluid and mass transfer during metabasalt alteration and copper mineralization. Economic Geology 90, 705–730 (1995).

[13] CUNEY M., EMETZ A., MERCADIER J., MYKCHAYLOV V., SHUNKO V., YUSLENKO A., Uranium deposits associated with Na-metasomatism from central Ukraine: A review of some of the major deposits and genetic constraints: Ore Geology Reviews 44, 82-106 (2012).

[14] LOBATO L., FYFE W., Metamorphism, metasomatism and mineralization at Lagoa Real, Bahia, Brazil: Economic Geology 85, 968-989 (1990).

[15] WILDE A.R., OTTO A., JORY J., MACRAE C., POWNCEBY M., WILSON N., TORPY A., Geology and Mineralogy of Uranium Deposits from Mount Isa, Australia: Implications for Albitite Uranium Deposit Models: Minerals (online open access) 3, 258-283 (2013).
[16] ALEXANDRE, P., Mineralogy and geochemistry of the sodium metasomatism-related uranium occurrence of Aricheng South, Guyana. Mineralium Deposita 45(4), 351-367 (2010).
[17] CUNEY, M., KYSER, T.K., The Geology and Geochemistry of Uranium and Thorium Deposits. Mineralogical Association of Canada (MAC) (2015).
[18] PORWAL, A. K., Mineral Potential Mapping with Mathematical Geological Models: ITC PhD Dissertations 130 (2006).
[19] KNOX-ROBINSON C.M., Vectorial Fuzzy Logic: a Novel Technique for Enhanced Mineral Prospectivity Mapping, with Reference to the Orogenic Gold Mineralisation Potential of the Kalgoorlie terrane, Western Australia: Australian Journal of Earth Science 47, 929-941 (2000).
[20] BONHAM-CARTER G.F., Geographic Information Systems for Geoscientists: Modelling with GIS: Computer Methods in the Geosciences, 13, Pergamon, New York (1994).
[21] SAWATZKY, D., RAINES, G., BONHAM-CARTER, G., Spatial Data Modeller, http://www.ige.unicamp.br/sdm/ArcSDM10/source/ReadMe.pdf (2010).
[22] SINGER, D.A., Basic concepts in three-part quantitative assessments of undiscovered mineral resources. Nonrenewable Resources 2(2), 69–81 (1993).
[23] SINGER, D.A., MENZIE, W.D., Quantitative mineral resource assessments—an integrated approach. Oxford University Press, New York, 219 pp (2010).
[24] ROOT, D.H., MENZIE, W.D., SCOTT, W.A., Computer Monte Carlo simulation in quantitative mineral resource assessment. Nonrenewable Resources 1(2), 125–138 (1992).
[25] BAWIEC, W.J., SPANSKI, G.T., Quick-start guide for version 3.0 of EMINERS – Economic Mineral Resources Simulator: US Geological Survey Open-File Report 2009-1057, 26p (2012), available only at http://pubs.usgs.gov/of/2009/1057. (This report supplements USGS OFR 2004-1344).
[26] SINGER, D.A., KOUDA, R., Probabilistic estimates of number of undiscovered deposits and their total tonnages in permissive tracts using deposit densities. Natural Resources Research 20(2), 89–93 (2011).
[27] SINGER, D.A., JAIRETH, S., ROCHE, I., A three-part quantitative assessment of undiscovered unconformity-related uranium deposits in the Pine Creek Region of Australia, in this volume.
[28] LISITSIN, V.A., Methods of three-part quantitative assessments of undiscovered resources: examples from Victoria (Australia): Mathematical Geosciences 42, 571–582 (2010).
[29] MERRIAM, D.F., DREW, L.J., SCHUENEMEYER, J.H., Zipf's Law: A viable geological paradigm? Natural Resources Research 13(4), 265-271 (2004).
[30] GUJ, P., FALLON, M., MCCUAIG, T. C., FAGAN, R., A timeseries audit of Zipf's law as a measure of terrane endowment and maturity in mineral exploration. Economic Geology 106, 241–259 (2011).
[31] LISITSIN, V.A., Rank-size statistical assessments of undiscovered gold endowment in the Bendigo and Stawell Zones (Victoria) and the Mossman Orogen (Queensland), Australia: Comparison with three-part assessment results. Natural Resources Research 25(3), 269–282 (2015).

[32] NEWMAN, M.E.G., Power laws, Pareto distributions and Zipf's law. Contemporary Physics 46(5), 323–351 (2005).
[33] MAMUSE, A., GUJ, P., Rank statistical analysis of nickel sulphide resources of the Norseman-Wiluna Greenstone Belt, Western Australia: Mineralium Deposita, 46, 305-318 (2011).

SURFICIAL URANIUM MINERAL SYSTEMS IN WESTERN AUSTRALIA: GEOLOGICALLY-PERMISSIVE TRACTS AND UNDISCOVERED ENDOWMENT

B. CHUDASAMA,
Centre of Studies for Resources Engineering,
Indian Institute of Technology Bombay,
Mumbai, India

O.P. KREUZER
Corporate Geoscience Group,
Perth

Economic Geology Research Centre,
James Cook University,
Townsville

Australia

S. THAKUR
Centre of Studies for Resources Engineering,
Indian Institute of Technology Bombay,
Mumbai, India

A.K. PORWAL
Centre of Studies for Resources Engineering,
Indian Institute of Technology Bombay,
Mumbai, India

Centre for Exploration Targeting,
University of Western Australia,
Perth, Australia

A.J. BUCKINGHAM
Fathom Geophysics Australia,
Yallingup

Centre for Exploration Targeting,
University of Western Australia,
Perth

Australia

Abstract

This contribution describes a novel, integrated approach to prospectivity analysis and quantitative resource assessment of surficial uranium deposits in Western Australia that may serve as a universal, best practice template for the estimation and the planning and managing of undiscovered uranium resources elsewhere. The key objectives of and principal steps taken in this study were: (1) development of a process-based, mineral systems-type targeting model for surficial uranium deposits; (2) delineation of areas where the geology is permissive for the existence of surficial uranium deposits (i.e., geologically-permissive tracts) using mineral prospectivity analysis and employing a combination of knowledge-driven fuzzy inference systems (FIS) and data-driven weights-of-evidence and artificial neural networks; and (3) estimation of the number of undiscovered surficial uranium deposits and total amount of undiscovered uranium endowment utilizing regression models of deposit density and endowment density, the USGS three-part assessment and Zipf's Law analysis. The approach described in this contribution is a world first in that it is the first published quantitative mineral resource assessment employing three different methods and building upon the results of a systematic, multi-pronged knowledge- and data-driven prospectivity analyses. The results of these analyses indicate that the study area (the ~1,700,000 km^2 deserts and xeric shrublands region of Western Australia) contains a total undiscovered endowment (i.e., speculative resources) of >180,000 t U, contained in identified and up to 145 additional, undiscovered deposits. Based on the prospectivity analysis, undiscovered surficial uranium deposits are most likely to be found within geologically-permissive tracts in the remote, commonly sand dune-covered northern and eastern parts of the study area, which to date have recorded little, if any, uranium exploration.

1. INTRODUCTION

1.1. Aims and objectives

The main aim of this contribution is to present a detailed case study of how to assess uranium prospectivity and to estimate undiscovered uranium endowment in order to assist Member States of the IAEA with identifying and planning and managing for undiscovered uranium resources. The key objectives of, and steps taken in, this case study were:

— Development of a targeting model for calcrete-hosted uranium deposits;
— Delineation of geologically-permissive tracts for this type of uranium deposit;
— Quantitative estimation of undiscovered calcrete-hosted uranium resources.

The overall goal was to develop and showcase a holistic, methodical, mineral systems approach to mineral prospectivity analysis and quantitative resource assessment that may serve as a universal, best practice template underpinning similar studies elsewhere.

1.2. Study area

For the purpose of this case study, it was important to select a uranium deposit type that is relatively well defined and understood, and whose expressions are relatively easy to recognize and map in the available geoscience datasets. Surficial uranium deposits [1–3] in calcrete, dolocrete and associated alluvial and playa lake sediments fit these criteria well. Given that consideration, an area in Western Australia was chosen as a case study because this jurisdiction:

— Has been explored for surficial uranium deposits since 1968;
— Is well endowed with surficial uranium deposits that have combined resources in excess of 100,000 t U;
— Offers high-quality precompetitive geoscience data that are readily available from the online servers of the Western Australian Department of Mines and Petroleum [4] and Geoscience Australia.

The study area (Fig. 1) in Western Australia covers over ~1.7 million square kilometers, or more than one fifth of the total land area of the Australian continent. Its boundary was designed to capture the entire surficial uranium system that is spatially or genetically limited, or defined, by:

— The deserts and xeric (i.e., drought resistant) shrublands region [5];
— The subtropical dry arid desert (BWh) category of the Köppen-Geiger climate classification scheme [6];
— The known groundwater calcretes and dolocretes in Western Australia [7].

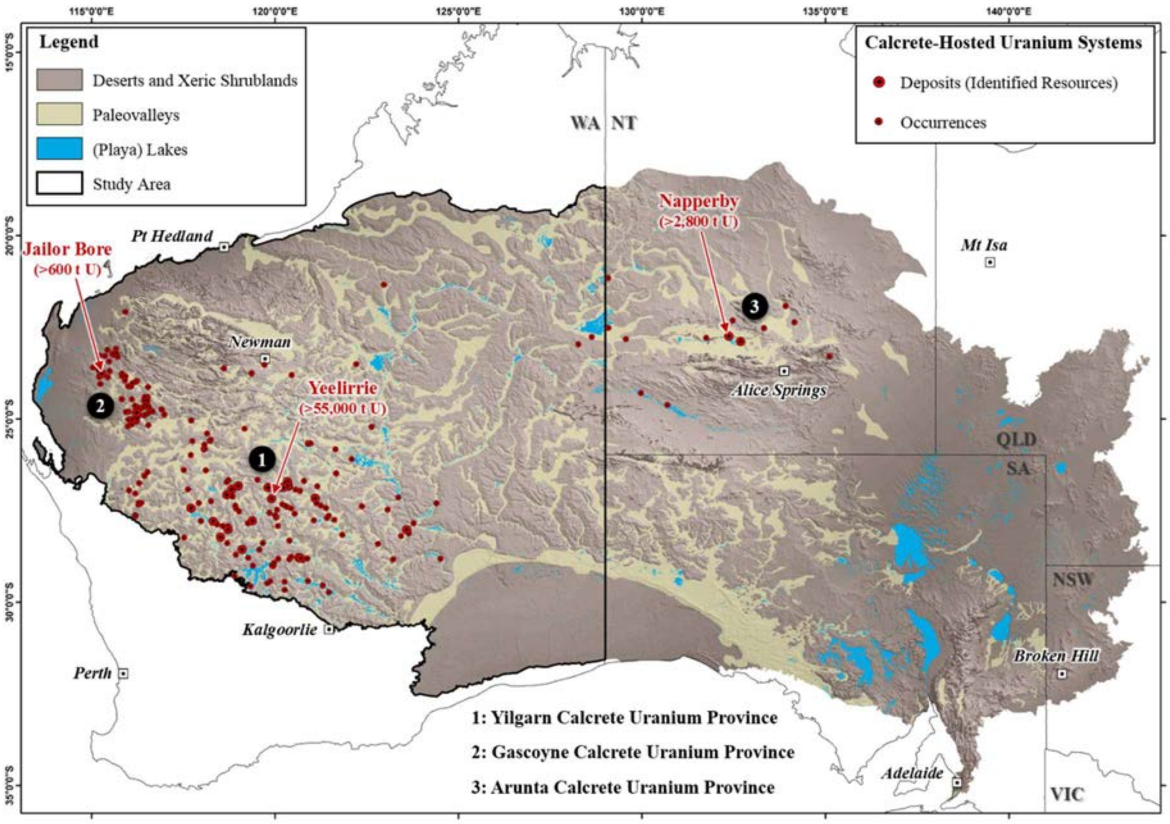

FIG. 1. Map of the study area, illustrating the distribution of calcrete-hosted uranium deposits across the Australian continent [8]. These deposits occur in three clusters, here termed as the Yilgarn, Gascoyne and Arunta calcrete uranium provinces. All known deposits are located within the deserts and xeric shrublands region of Australia.

Other Australian states and territories were excluded from this case study, not because of lack of potential for calcrete-hosted uranium deposits but to avoid cross-border data integration, consistency and compatibility issues.

1.3. Methods

1.3.1. Data compilation

Data compiled for and utilized in this study were mainly sourced from the websites and online repositories of:

- The International Atomic Energy Agency (IAEA);
- The Geological Survey of Western Australia (GSWA);
- Geoscience Australia (GA);
- The Australian Government's Geoscience Portal, in particular the Geophysical Archive Data Delivery System (GADDS).

A summary of key data employed in this study and data sources is provided in Table 1. Further data and information were compiled from the literature and company reports referenced in this contribution.

1.3.2. *Mineral systems approach*

This study adopted a mineral systems approach [9–15] to generating a targeting model for calcrete-hosted uranium deposits, and for guiding the work flow of the prospectivity analysis (Fig. 2).

The formal adaptation of the petroleum systems approach [16] to mineral deposits by [9] in the 1990s occurred on the back of the successful application of a systems approach to understanding and discovering hydrocarbons. As summarized in [15], the "mineral systems approach is based on the premise that mineral deposits are focal points of much larger earth process systems that operate on a variety of scales to focus mass and energy flux. Being process-based, the application of the mineral systems approach is neither restricted to a particular geological setting nor limited to a specific mineral deposit type. Rather, the flexibility of this concept allows for multiple mineral deposit types to be realized within a single mineral system, thereby acknowledging the inherent natural variability among mineral deposits. In this approach, the critical processes acting together to form mineral deposits are:

- Source – all geological processes required for extraction of necessary ore components (melts or fluids, metals and ligands) from crustal and/or mantle sources;
- Transport – all geological processes required for melt- or fluid-assisted transfer of ore components from sources to traps (i.e., effective, active melt or fluid pathways);
- Trap – all geological processes required to focus melt or fluid migration into channels that can accommodate metal deposition;
- Deposition – all geological processes required for extraction of metals from melts or fluids passing through the traps;
- Preservation – all geological processes required to preserve the accumulated metals through time.

While none of these processes can be directly observed or mapped, we can observe and map in our geoscience datasets the expressions of these processes (i.e., the targeting elements). The GIS environment is ideally suited for this task and for using this information to create derivative predictor maps, spatial maps that serve as spatial proxies for these mappable targeting criteria and, thus, for the critical ore-forming processes. The mineral systems approach is essentially a probabilistic concept in that if the probability of occurrence of any of the critical processes becomes zero, then no deposit will be present. By integrating mineral systems models into a probabilistic framework, a prior probability of success can be calculated for discovery of a potentially economic mineral deposit in an area. This thinking has been applied to valuation of exploration programs, development of targeting decision and ranking tools, economic risk analysis, and prospectivity analysis."

The key benefits of the mineral systems approach are that it is a predictive, flexible concept that is relevant at all scales, and that it provides a conceptual framework for integrating, organizing and interrogating multi-disciplinary data. In summary, the mineral systems approach:

- Regards ore deposits as focal points of much larger earth process systems that operate on a variety of scales to focus mass and energy flux;
- Is neither restricted to a particular geological setting nor limited to a specific mineral deposit type in that it accepts that different ore deposit types or styles may be created by

the same mineral system depending on, for example, depth level, host rocks or mixing agents;

- Aims to define the common, unifying processes that control ore deposit formation at all scales;
- Aims to define the common, unifying processes that control ore deposit formation at all scales;
- Focuses on identifying the critical processes of ore deposit formation and their mappable expressions (i.e., proxies, targeting elements, or targeting criteria);
- Integrates geodynamic setting, geological and P-T histories, structural and lithological architecture, metal sources and fluid reservoirs, fluid drivers and pathways, and geologic time;
- Provides a basis for target ranking and economic risk and expected value analysis.

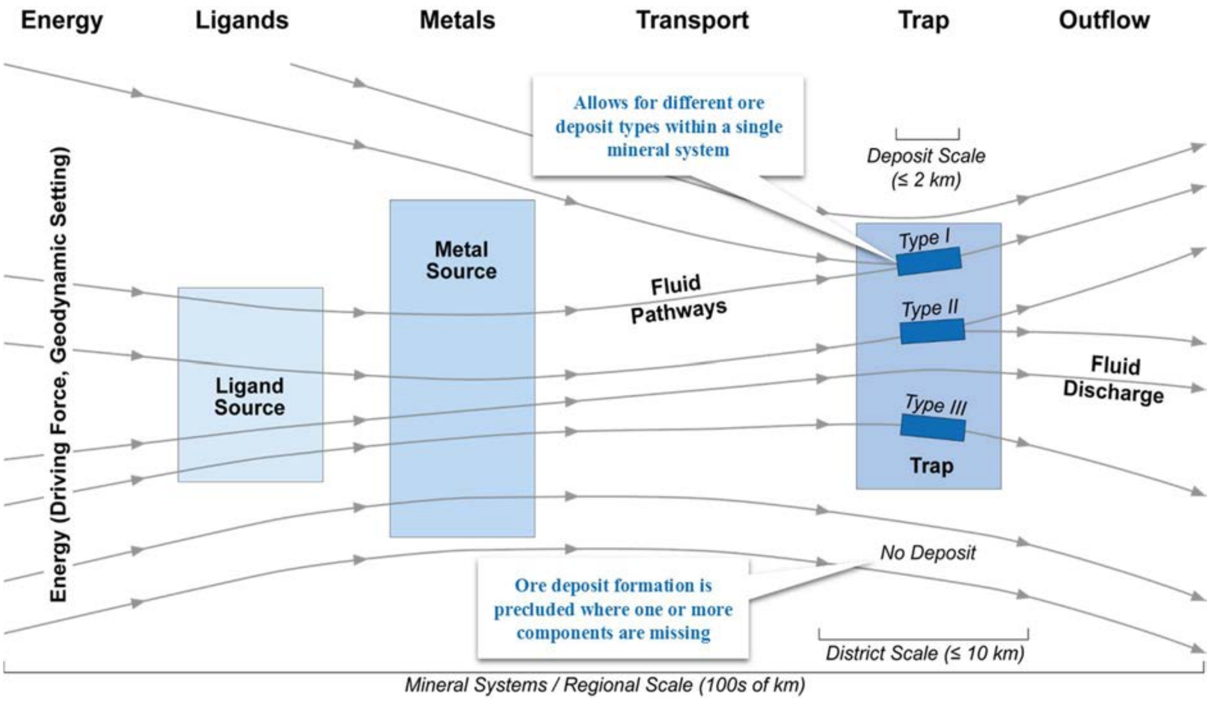

(a)

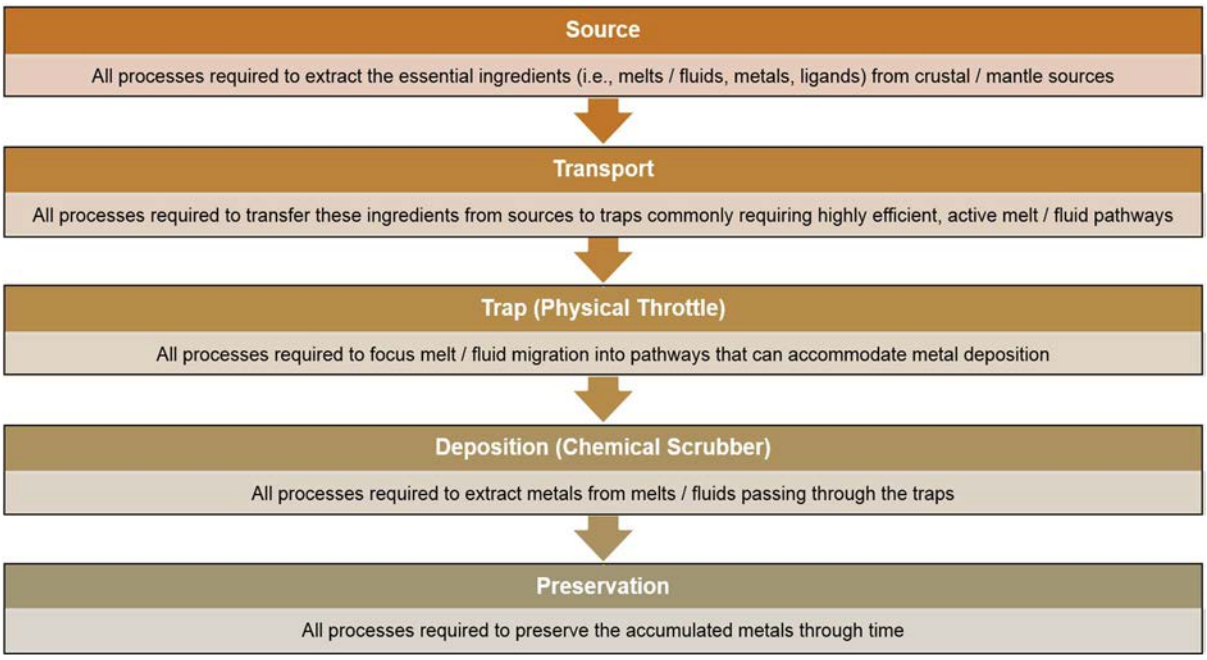

(b)

FIG. 2. (a) Schematic representation of important features and processes in mineral systems (modified from [10]). (b) Flow diagram detailing and defining features and processes in mineral systems.

TABLE 1. DATA SOURCES

Type	Item	Overarching dataset	Format	Source	Brief description
Mineral occurrences	Calcrete-hosted uranium occurrences	Mines and Mineral Deposits (MINEDEX)	Vector	GSWA: http://geodownloads.dmp.wa.gov.au/datacentre/datacentreDb.asp	Uranium occurrence data for Western Australia; no genetic classifications
	Calcrete-hosted uranium occurrences	Kreuzer et al. (2010)	Vector	Appendix	Uranium occurrence data for Australia with genetic classifications
	Calcrete-hosted uranium occurrences	World Distribution of Uranium Deposits (UDEPO)	Online repository	IAEA: https://infcis.iaea.org/UDEPO/About.cshtml	Global uranium occurrence data with genetic classifications; information limited to deposits >300 t U
Geology	Geological regions	1:5,000,000 Geological Regions of Australia	Vector	GA: http://www.ga.gov.au/	Geographical areas with cohesive geological assemblages significantly different in overall geology from adjoining regions
	Surface geology	1:1,000,000 Surface Geology of Western Australia	Vector	GSWA: http://geodownloads.dmp.wa.gov.au/datacentre/datacentreDb.asp	Map of Western Australian outcrop and surficial geology
	Solid geology	1:500,000 Interpreted Bedrock Geology, 2016	Vector	GSWA: http://geodownloads.dmp.wa.gov.au/datacentre/datacentreDb.asp	Map of Western Australian interpreted bedrock geology
	Structure	1:500,000 Interpreted Bedrock Geology - Structural Lines, 2016	Vector	GSWA: http://geodownloads.dmp.wa.gov.au/datacentre/datacentreDb.asp	Map of Western Australian interpreted structure
	Paleo-valleys	WASANT Paleo-valley Map	Vector	GA: http://www.ga.gov.au/	Geoscientific thematic map of Australia's arid and semi-arid zone paleo-valley systems in WA, SA and the NT
	Calcretes	1:500,000 State Regolith 500m grid	Vector	GSWA: http://geodownloads.dmp.wa.gov.au/datacentre/datacentreDb.asp	Map of Western Australia calcrete bodies
	Lacustrine sediments	1:500,000 State Regolith 500m grid	Vector	GSWA: http://geodownloads.dmp.wa.gov.au/datacentre/datacentreDb.asp	Map of Western Australia lacustrine sediments

Type	Item	Overarching dataset	Format	Source	Brief description
	Outcrops	1:500,000 State Regolith 500m grid	Vector	GSWA: http://geodownloads.dmp.wa.gov.au/datacentre/datacentreDb.asp	Map of Western Australia rock outcrops
Exploration	Current tenure over uranium occurrences	Tenements - Current (Live and Pending)	Vector	GSWA: http://geodownloads.dmp.wa.gov.au/datacentre/datacentreDb.asp	All current tenure in WA with holder information
	Past tenure over uranium occurrences	Tenements - Dead	Vector	GSWA: http://geodownloads.dmp.wa.gov.au/datacentre/datacentreDb.asp	All historic tenure in WA with holder information
	Historical exploration activity	Historical exploration activity (EXACT)	Vector	GSWA: http://geodownloads.dmp.wa.gov.au/datacentre/datacentreDb.asp	Detailed albeit incomplete compilation of past exploration activities (e.g., areas of drilling, geochemical sampling, geophysics)
	Mineral exploration reports	Mineral Exploration Reports (WAMEX)	Vector	GSWA: http://geodownloads.dmp.wa.gov.au/datacentre/datacentreDb.asp	Facilitates extraction and plotting of historic tenure that was subject to uranium exploration
Climate	Köppen-Geiger climate classification	Köppen-Geiger GIS	Grid	VUW: http://koeppen-geiger.vu-wien.ac.at/present.htm	Desert climates in Australia and worldwide
	Deserts and xeric shrublands	Terrestrial Ecoregions	Vector	The Nature Conservancy: http://maps.tnc.org/gis_data.html	Desert climates in Australia and worldwide
	Average pan evaporation, annual	Climate Data Online	Georeferenced Map	BOM: http://www.bom.gov.au/	Maps of climatic averages / maxima recorded over 10 to 30-year periods
	Maximum temperature, annual	Climate Data Online	Georeferenced Map	BOM: http://www.bom.gov.au/	Maps of climatic averages / maxima recorded over 10 to 30-year periods
	Average point potential evapo-transpiration, annual	Climate Data Online	Georeferenced Map	BOM: http://www.bom.gov.au/	Maps of climatic averages / maxima recorded over 10 to 30-year periods
	Average rainfall, annual	Climate Data Online	Georeferenced Map	BOM: http://www.bom.gov.au/	Maps of climatic averages / maxima recorded over 10 to 30-year periods
	Tropical Cyclones 1906-2006	Climate Data Online	Georeferenced Map	BOM: http://www.bom.gov.au/	Map of cyclone pathways recorded over a 100-year period

Type	Item	Overarching dataset	Format	Source	Brief description
Topography & hydrology	Relevant topographic datasets	GEODATA TOPO 250K Series 3	Vector	GA: http://www.ga.gov.au/	Detailed compilation of Australian topographic features (e.g., lakes, streams, dunes)
	DEM	GTOPO30	Grid	USGS: https://lta.cr.usgs.gov/GTOPO30	USGS global DEM formed the basis for enhancement filtering and feature extraction (e.g., ridges and valleys) (this study)
	Drainage basins	National Drainage Basins	Vector	GA: http://www.ga.gov.au/	Major drainage basins and divisions
Geophysics	Total magnetic intensity data	Total Magnetic Intensity (TMI) Anomaly Grid of Australia (6th Edition)	Grid	GADDS: http://www.geoscience.gov.au/	Original grid served as the basis for enhancement filtering and feature extraction (this study)
	Filtered and unfiltered radiometric data and ratios	Radiometric Map of Australia (3rd Edition)	Grid	GADDS: http://www.geoscience.gov.au/	Original grid served as the basis for enhancement filtering, feature extraction and ratio generation (this study)
	Weathering index	Weathering Intensity Map of Australia	Grid	GADDS: http://www.geoscience.gov.au/	Degree of surface bedrock and sediment weathering

Key to abbreviations: BOM = Bureau of Meteorology; DEM = Digital elevation model; GA = Geoscience Australia; GSWA = Geological Survey of Western Australia; IAEA = International Atomic Energy Agency; NT = Northern Territory; SA = South Australia; USGS: United States Geological Survey; VUW = Veterinärmedizinische Universität Wien (VetMedUni Vienna); WA = Western Australia.

1.3.3. *Mineral prospectivity analysis*

Prospectivity modeling employs GIS software for exploration targeting. A mineral prospectivity model is an empirical mathematical function for mapping geospatial features (explanatory variables) specific to the targeted mineral deposit type (dependent variables). The modeling is undertaken as a series of sequential steps (Fig. 3), commonly incorporating:

- Construction of a conceptual model of the targeted mineral system based on the current understanding and available geoscience information;
- Translation of the geospatial expressions of the critical mineral systems (i.e., genetic) processes into targeting criteria;
- Mapping of the targeting criteria in the available geoscience and exploration data and creation of thematic input GIS layers (i.e., predictor or evidential maps) that are used as proxies for the critical mineral systems processes;
- Combination of the predictor maps through empirical functions from simplistic arithmetic, or logical, operators to complex non-linear functions;
- Generation of unique condition grids, and training and validation datasets (if required by the chosen modeling technique);
- Processing of the unique conditions grids with mathematical models that are applied either inside or outside the GIS environment;
- Mapping of the outputs of the mathematical models to generate continuous-scale favorability maps;
- Segregation of the prospective, potentially mineralized population from the non-prospective background population by way of their fractal dimensions;
- Creation and validation of binary favorability maps to derive prospectivity maps.

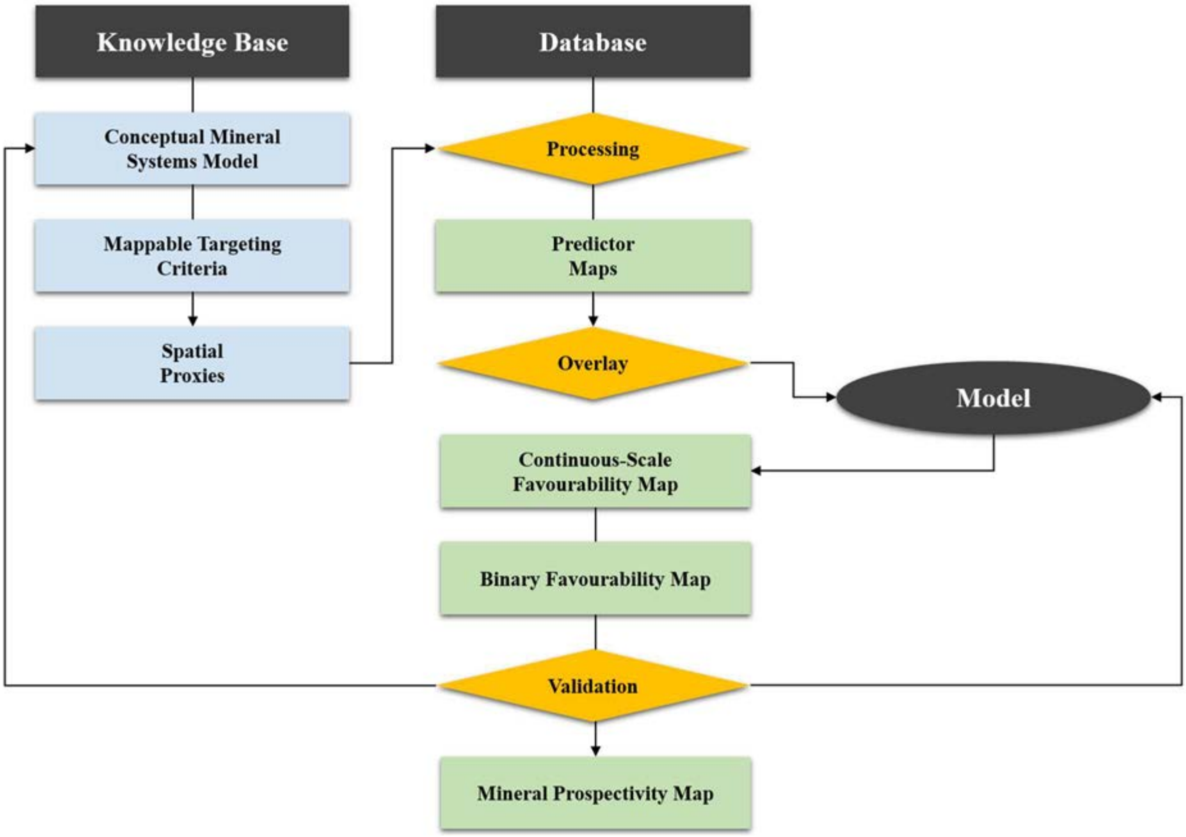

FIG. 3. Generalized flow chart of procedures commonly used in mineral prospectivity modeling.

Prospectivity models can be classified as either data- or knowledge-driven, depending on whether the model parameters are estimated empirically based on the available training data or heuristically based on expert knowledge, respectively. There are four main approaches to prospectivity modeling: (a) probabilistic; (b) regression-based; (c) machine-learning; and (d) expert systems. Approaches (a) to (c) are data-driven while approach (d) is knowledge-driven.

Probabilistic approaches use Bayes' theory for estimating a posterior probability of the occurrence of the targeted mineral deposit type within a certain unit area given the presence, or absence, of input predictor maps. The most widely used probabilistic method is the Weights-of-Evidence (WofE) model [17–20], whereby Bayes' equation is used in a log-linear form to combine the likelihood ratios of the input predictor maps, which are assumed to be conditionally independent. This assumption allows for modular estimations of the likelihood ratios of the input predictor maps.

Regression-based approaches are based on estimation of a line of best fit between the binary dependent variable (targeted deposit type) and explanatory variables (input predictor maps) in an n-dimensional feature space. Regression coefficients are measures of the spatial association of identified mineral deposits with input predictor maps. Regression models can be either linear or generalized linear. The most widely applied model of this approach is logistic regression [20–25], which is an example of a generalized linear model. In logistic regression, the dependent variable is binary with regression values constrained between 0 and 1. Thus, the output of logistic regression for any given unit area is interpreted as the probability of occurrence of a deposit in that unit area.

Machine learning approaches are a suite of soft-computation algorithms developed by computer scientists mainly for pattern recognition and classification tasks. These algorithms use activation and transfer functions for mapping in a non-linear fashion the combinations of input predictor maps to the targeted deposit types. Most machine-learning algorithms are black boxes in that the model parameters cannot be interpreted geologically. However, these models, if properly trained, have good prediction capabilities. Some of the most widely used machine learning algorithms in prospectivity modeling are artificial neural networks (ANN) [27–29], decision trees [30], support vector machines [31–33], and random forests [34–37].

Expert systems include a variety of soft-computation techniques aimed at capturing the cognitive reasoning of the exploration geologist. These techniques include fuzzy inference systems (FIS) [38–45] and Dempster-Shafer belief functions [46–51].

1.3.4. Quantitative mineral resource assessment

The primary objectives of quantitative mineral resource assessments (QMRA) are to estimate: (a) the number of undiscovered deposits that may exist in the delineated geologically-permissive tracts; and (b) the total amount of undiscovered mineral resources, or endowment. Proven methods commonly applied to QMRA include:

— Deposit density and endowment density models [52];
— Rank-size distribution, or Zipf's Law, analysis [53];
— The USGS three-part QMRA [54].

Deposit density and endowment density models described a simple and intuitive method in which regression-based models of deposit and endowment density serve to determine the number and amount of undiscovered resources [52]. These models require data from well-explored, or control, area where the recorded number of mineral deposits and identified endowment are close to the actual values and where this assumption can be made with high confidence.

Mineral deposit density is defined as the number of mineral deposits per unit area of geologically-permissive host rock; that is, the area of rock beyond which the probability of finding a mineral deposit is negligible [54]. A power law relationship exists between mineral deposit density and the area of geologically-permissive host rock [52, 55]. In other words, a linear relationship is present between the logarithm of mineral deposit density and that of the area of geologically-permissive host rock. Regression modeling is employed to obtain a least square linear fit for the control areas between the logarithm of the geologically-permissive areas and that of the deposit densities. The resultant relationship can be used for determining the deposit density of any geologically-permissive, geologically similar area, whether it encompasses any known mineral deposits, or not. The deposit density multiplied by the area gives an estimate of total number of deposits, including both identified and undiscovered deposits [52].

Endowment density models are used to estimate the undiscovered endowment, or the total amount of mineral resources, thought to be present in a geologically-permissive tract. Endowment density is defined as the ratio of the total amount of metal contained within the geologically-permissive host rock to the area of the geologically-permissive rock. As described above, a best fit linear regression between the logarithm of endowment density and logarithm of area applied over data from control areas can be used to estimate the total endowment of any given, geologically similar host rock [52].

The rank-size distribution or Zipf's Law analysis for estimating the number of undiscovered deposits is based on Zipf's Law [53]. Many natural variables show a log-normal distribution, or power law relation, with their frequency of occurrence. Mathematically, this law can be written as:

$$y = c.r^{-k} \quad (1)$$

where y is the size (i.e., tonnage) of the mineral deposit, c is the size of the largest deposit (rank = 1), r is the rank of deposits of size y, sorted in descending order of their respective sizes, k is a constant to be estimated. Previous mineral resource assessments utilizing Zipf's Law [56–66] illustrated that areas that had attained exploration maturity have $k = 1$.

The basic assumption in the application of Zipf's Law to QMRA is that the largest deposit present in a particular area has been discovered, thoroughly explored, and delineated with respect to its total endowment. This assumption commonly holds because the largest deposits have the largest footprints and, generally, are discovered early in the exploration history of an area [54]. A best fit power law regression applied to a selected area will yield the parameter c (i.e., the size of the largest deposit) and aid in estimating the value of the parameter k. If $k \neq 1$, a possible explanation could be the presence of undiscovered resources of intermediate size. If c is greater than the size of the largest existing deposit, it could allude to the largest deposit not having been discovered yet [66, 67]. The total undiscovered endowment above a certain minimum cut-off can be estimated as the difference between the total endowment as per the rank-modified Zipf's Law equation and total endowment.

The USGS three-part assessment was developed in 1975 [54], and forms an integral component of the Global Mineral Resource Assessments Project (GMRAP). The three-part assessment has been designed for converting geoscientific models and concepts into a format appropriate for use in a decision support system and cost-benefit analysis. The three steps in this QMRA are:

1) Delineation of tracts that are geologically-permissive for a particular mineral deposit type;
2) Estimation of the number of undiscovered deposits in each geologically-permissive tract;
3) Estimation of the amount of metal contained in the undiscovered deposits.

Geologically-permissive tracts are areas where the geology is permissive for the existence of mineral deposits of a specified type. The boundaries of geologically-permissive tracts are drawn such that the probability of the targeted mineral deposits type occurring outside the tract is negligible (i.e., <1 in 100,000 or <0.00001). The delineation of geologically-permissive tracts is mainly informed by geological criteria derived from descriptive or conceptual mineral deposit models and geological maps. Additional information such as mineral occurrence, geochemical and geophysical data may improve the accuracy of the demarcation [54].

The estimation of the number of undiscovered deposits is subjective in that it is based on the experience and judgment of the geoscientist(s) tasked with the assessment. However, guidelines are in place to help to reduce this human bias [54]. Alternatively, any of the methods described above can be used to estimate the number of undiscovered deposits.

The estimation of the amount of metal contained in the undiscovered deposits relies on grade and tonnage models. The fundamental strength of this approach is its internal consistency; that is, estimates of the number of undiscovered deposits must be consistent with the grade-and-tonnage models and the mineral deposit model used to delineate the geologically-permissive tracts.

The numerical analysis of the three steps is implemented in EMINERS, a Monte Carlo mineral resource simulator developed by the USGS [68, 69]. By combining probabilistic estimates of undiscovered mineral deposits with grade-and-tonnage models to estimate mineral resources, this simulator returns the total amount of undiscovered mineral resources and their probability distribution. EMINERS also supports basic economic filtering of quantitative mineral resource simulations [70].

2. SURFICIAL URANIUM DEPOSITS

2.3. Deposit classification and terminology

The IAEA defines surficial uranium deposits [1–3] as “young (Tertiary to Recent) near-surface uranium concentrations in sediments or soils. These deposits usually have secondary cementing minerals including calcite, gypsum, dolomite, ferric oxide and halite. Uranium deposits in calcrete (calcium and magnesium carbonates) are the largest of the surficial deposits. The calcrete bodies are interbedded with Tertiary sand and clay, which are usually cemented by calcium and magnesium carbonates. Calcrete deposits form in regions where uranium-rich granites were deeply weathered in a semi-arid to arid climate. Surficial uranium deposits also occur in peat bogs and karst caverns”.

For the purpose of this study, surficial uranium deposits in calcrete, dolocrete and associated sediments were referred to as calcrete-hosted uranium deposits, a popular umbrella term for this deposit type, previously utilized in the Red Book [71–72], and widely adopted and utilized in the pertinent scientific literature and in industry and government publications [7, 73–84], in particular in the Western Australian context.

The term calcrete, an amalgamation of the words ‘calcareous’ and ‘concrete’, was introduced by [85] for carbonate-cemented gravels. Since its introduction, the use of the term has been broadened to include a much wider range of authigenic, non-marine carbonates that form in-situ by precipitation or recrystallization, and are characterized by a minimum carbonate content in the range from 10 to 15% $CaCO_3$, although a much higher value equal to, or greater than, 40 to 50% $CaCO_3$ is commonly expected [86]. The most common definition of the term calcrete in use today was formulated by [87] who described calcrete as a “near surface, terrestrial, accumulation of predominantly calcium carbonate, which occurs in a variety of forms from powdery to nodular to highly indurated. It results from the cementation and displacive and replacive introduction of calcium carbonate into soil profiles, bedrock and sediments, in areas where vadose and shallow phreatic groundwater become saturated with respect to calcium carbonate. Tufa, travertine, beach rock, lake carbonate and calcareous soil are excluded from this classification scheme.

Calcrete classification systems in use today range from purely descriptive (e.g., based on mineralogy or morphology) to genetic (e.g., based on hydrological setting or degree of maturity), with the diversity and abundance of classification schemes [86–88] reflecting our still poor understanding of calcrete formation. However, a fundamental distinction is evident between two end-members of a continuum that varies according to landscape setting and origin [87, 89, 90]:

- Pedogenic (or vadose) calcretes that form in soil profiles in the vadose zone;
- Groundwater (or phreatic, valley, channel) calcretes that form in shallow aquifer systems, mainly in the capillary fringe directly above moving groundwater or at, or slightly below, the local water table (Fig. 4).

As discussed by [86], "it is commonly agreed that for calcrete, calcium carbonate should be the dominant carbonate mineral and the dolomite-dominant type should be referred to as dolocrete." However, thus far no standard $CaCO_3/MgCO_3$ ratio has been determined, making the discrimination between calcrete and dolocrete somewhat arbitrary. Based on the classification system of [92] calcrete should contain less than 5% dolomite by mass of total carbonate. Dolocrete, on the other hand, requires a dolomite content of at least 50%. As stated by [86], "this system is straightforward, but laboratory analysis is needed to determine calcite and dolomite contents and so is not suitable for field usage". This statement goes straight to the core of the problem:

- Evidence exists that at least some Western Australian groundwater carbonates are indeed dolocretes (i.e., at Yeelirrie, Lake Austin and Pogo Pool; [93]). However, insufficient laboratory data exist to determine whether dolocretes are more widely distributed both at the deposit and regional scales. Seminal reviews by [90] and [94] indicate the presence in Western Australia of both calcrete and dolocrete groundwater carbonates;
- Western Australian groundwater carbonates have historically been mapped as calcrete only, which is not surprising given that prior to the advent of portable XRF and SWIR spectrometers it was virtually impossible to accurately discriminate between calcrete and dolocrete in the field.

Given the shortcomings and uncertainties described above, this study adopted an approach similar to that of [94] who used the term calcrete as an umbrella term, including calcrete, dolocrete and gypcrete.

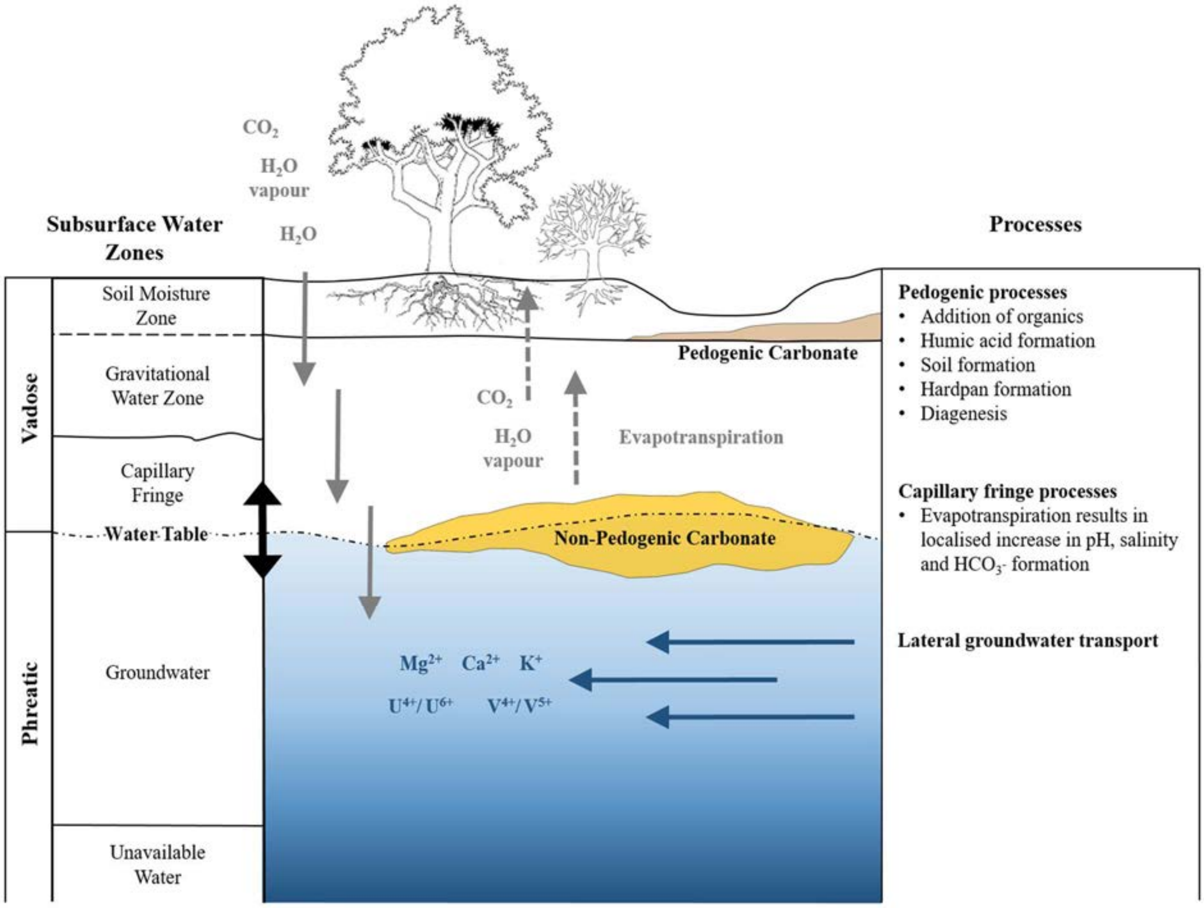

FIG. 4. Genetic classification of calcretes by hydrological setting. Non-pedogenic groundwater calcretes develop within the capillary fringe at or immediately above a shallow groundwater table [90, 91].

2.4. Deposit morphology

The largest surficial uranium deposits and best endowed provinces of this kind are located in the Republic of Namibia and Western Australia (Fig. 5). In the Republic of Namibia, most surficial uranium deposits take the form of carnotite ($K_2(UO_2)_2(VO_4)_2 \times 3H_2O$) hosted by [95–98]:

— Calcrete-cemented and non-calcareous conglomerates, silts and sands associated with Tertiary paleo-drainage systems, and with carnotite occurring as disseminations in the (± calcretized) sediment matrix, veneers lining cavities and fracture planes, and as coatings on pebbles and boulders (e.g., Langer Heinrich, Klein Trekkopje, Aussinanis);
— Gypsiferous red sands and underlying calcretized conglomerates associated with Tertiary paleo-drainage systems with carnotite occurring interstitial to clastic sand grains, in worm burrows and in shrinkage cracks (e.g., Tubas).

Importantly, Langer Heinrich, and perhaps other Namibian calcrete-hosted uranium deposits, may represent fossil systems. At Langer Heinrich, for example, the uranium mineralization is buried underneath barren Quaternary sands of the Gawib River, and occurs below the current Gawib shallow alluvial aquifer. However, U-Th dating by [99] returned a mineralization age for Langer Heinrich of 68,000 years suggesting that at least part of the uranium mineralization process is very recent.

In Western Australia, most surficial uranium deposits take the form of carnotite-hosted by [1, 79, 100]:

— Groundwater calcretes, dolocretes and associated fine-grained alluvial sediments in Tertiary paleo-drainage systems (e.g., Yeelirrie), or deltaic platforms and chemical deltas that developed where these paleo-valleys enter into playa lakes (e.g., Centipede/Millipede);
— Near-surface evaporitic and alluvial playa lake sediments (e.g., Lake Maitland);
— Fossil terrace calcretes in dissected paleo-valleys cut by modern drainage systems (e.g., Jailor Bore).

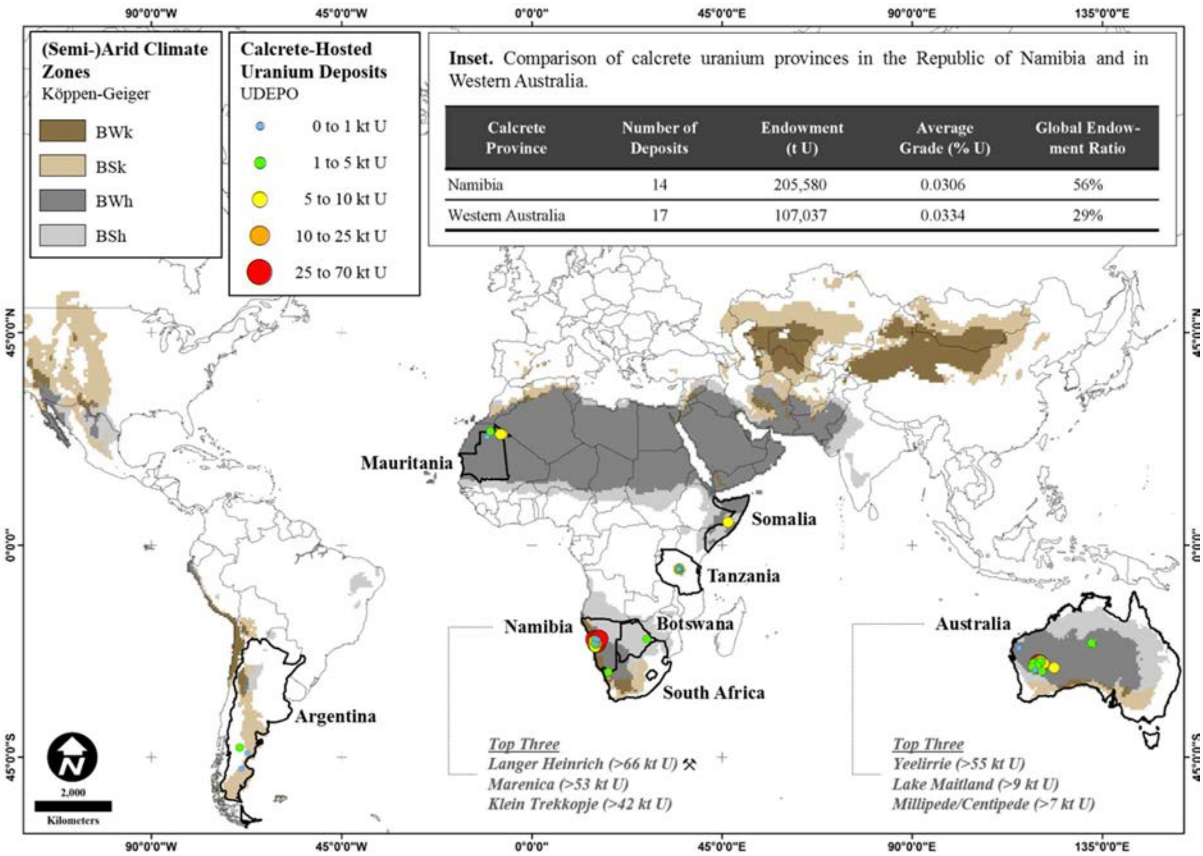

FIG. 5. Global distribution of calcrete-hosted uranium deposits and spatially and genetically associated (semi)arid climate zones. Inset: Comparison of the globally most significant calcrete uranium provinces in Australia and the Republic of Namibia. Deposit locations and sizes are based on UDEPO [3].

Fig. 6 illustrates the footprints of selected calcrete-hosted uranium deposits in the Republic of Namibia and Western Australia based on published resource outlines. Three-dimensional representations of calcrete-hosted uranium deposits are rarely available in the public domain. Exceptions are cross-sections and geological slices through the three-dimensional resource models of the Centipede/Millipede and Lake Way deposits owned by Toro Energy Limited. These models, which are shown at 20× vertical exaggeration, clearly illustrate the planar nature of the Centipede/Millipede and Lake Way deposits and the lateral continuity of the respective grade shells across the sand, clay, calcrete and silcrete host lithologies.

2.5. Global distribution and endowment

Calcrete-hosted uranium deposits are spatially and genetically associated with semi-arid to arid climate regimes [1–3]. As illustrated in Fig. 5, most deposits (n = 47, or 92%) captured in the UDEPO database [3] are located in sub-tropical dry arid desert zones (Köppen-Geiger climate category BWh: [6]) of Australia and Africa. These low-latitude deserts record precipitation of less than 50% of potential evapo-transpiration and high annual average temperatures greater than 18°C. Only four calcrete-hosted uranium deposits captured in the UDEPO database [3] are located outside the BWh zone, in regions characterized by semi-arid low- and mid-latitude steppe climates (i.e., BSk and BSh).

In terms of endowment, the largest and globally most important calcrete uranium provinces are found in the Republic of Namibia and in Australia, particularly in Western Australia (Figs. 5 and 7). According to the UDEPO [3], the 14 Namibian calcrete-hosted uranium deposits with defined resources greater 300 t U contain a total of 205,580 t U, or 56%, of the entire global calcrete uranium endowment. The Republic of Namibia not only contains the largest endowment but also contains the largest number of top-tier calcrete-hosted uranium deposits with defined resources in the range from 10,000 to 50,000 t U (Klein Trekkopje and Tubas) and greater than 50,000 t U (Langer Heinrich and Marenica).

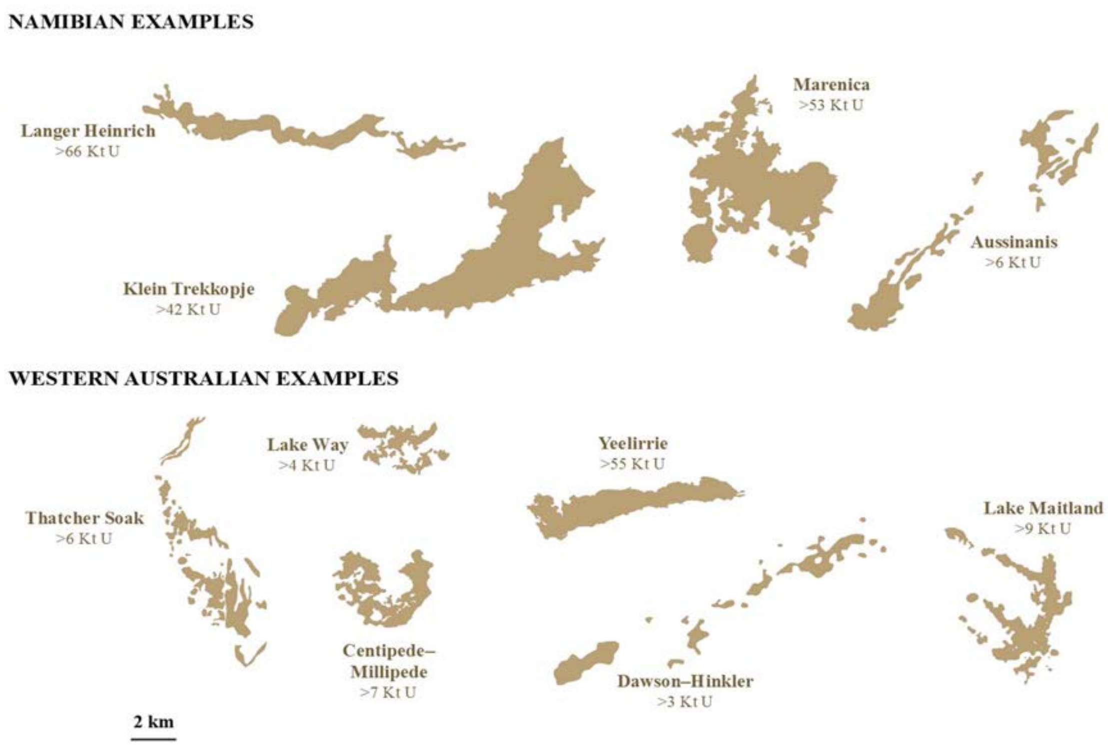

FIG. 6. Two-dimensional (surface) footprints of selected calcrete-hosted uranium deposits in the Republic of Namibia and Western Australia. Uranium deposit outlines were digitized from figures presented in company reports and announcements.

The 19 calcrete-hosted uranium deposits in Australia recorded in the UDEPO database [3] contain a total of 112,569 t U, or 31% of the global endowment. Most of the Australian endowment is captured by the 17 Western Australian calcrete-hosted uranium deposits with defined resources greater than 300 t U. These account for 29% of the global endowment, or 107,037 t U. Most of this is contained in Yeelirrie [101, 102], the only Australian top-tier calcrete-hosted uranium deposit with identified resources greater 50,000 t U.

The Republic of Namibia and Australia combined capture 87% of the current global calcrete-hosted uranium inventory. There would be few, if any, other mineral deposit types for which the distribution of the identified resources is so highly skewed towards only two countries, capturing almost the entire global endowment. The Islamic Republic of Mauritania (5%), the United Republic of Tanzania (3%), Somalia (2%) and Argentina (1%) have small calcrete-hosted uranium resource inventories that may further grow in the future as knowledge of these systems increases and exploration progresses.

The central part of the Hashemite Kingdom of Jordan is home to unusual surficial uranium accumulations of tyuyamunite, metatyuyamunite and strelkinite (uranium vanadates) hosted by travertine and caliche linked to fracture-controlled ascent of highly alkaline artesian groundwater feeding large lakes that developed in structurally controlled topographic depressions [103]. An example of this type of surficial uranium deposit is Khan Azzabib [104]. Given the unusual and low-grade (~0.0100% U) nature of the uranium accumulations, and lack of any assured uranium resource estimates [104] this type of surficial uranium deposit was not considered here.

2.6. Grade-tonnage characteristics

Calcrete-hosted uranium deposits can have medium (5,000 to 25,000 t U) to large (>25,000 t U) tonnages but commonly have low (<0.0500% U) or very low (<0.0250% U) grades (Fig. 7) compared to other uranium deposit types. Based on statistical data derived from the UDEPO database [3], the median tonnage of calcrete-hosted uranium deposit is 2,766 t U. Their median average grade is 0.0225% U. Most of the larger calcrete-hosted uranium deposits (>5,000 t U) are located in the Republic of Namibia (n = 7) and in Australia (n = 4), with additional occurrences being located in the Islamic Republic of Mauritania (n = 2), Somalia (n = 1), and the United Republic of Tanzania (n = 1).

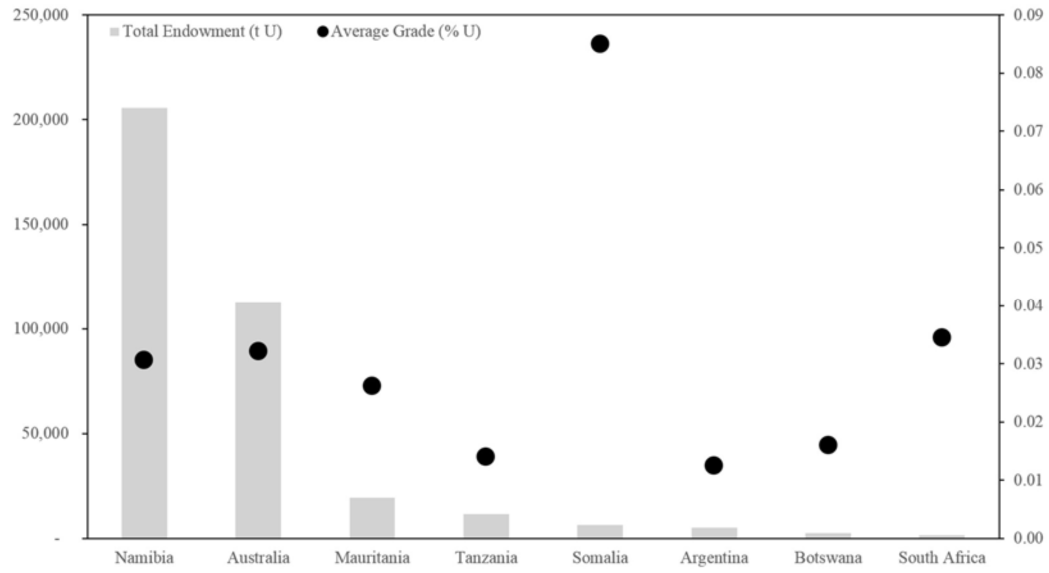

FIG. 7. Comparison of average grades and total endowment of calcrete-hosted uranium deposits in the world's top eight jurisdictions for this deposit type. Data source: UDEPO [3].

There is no obvious correlation between deposit sizes (i.e., tonnages) and uranium concentrations (i.e., grades), in that many of the larger deposits have grades well below the median (e.g., Klein Trekkopje or Marenica in the Republic of Namibia), while some very small deposits have grades well above the median (e.g., Jailor Bore or Yuinmery in Western Australia). The median grade of the Namibian deposits is 0.0235% U, which is slightly above the global median grade for calcrete-hosted uranium deposits of 0.0225% U. The median grade of the Australian calcrete-hosted uranium deposits is 0.0290% U, thus exceeding both the Namibian and the global median grades. The higher-grade nature of the Australian deposits is even more pronounced when comparing average grades, which are 0.0318% U globally, 0.0306% U for the Namibian deposits, 0.0306% U for the Australian deposits, and 0.0334% U when considering the Western Australian calcrete-hosted uranium deposits only. Much of this grade superiority of the Australian deposits, and the Western Australian ones in particular, can be attributed to Yeelirrie (Fig. 8). This exceptional deposit not only has a large tonnage (>55,000 t U) but it also has the highest grade (0.1110% U) amongst the larger calcrete-hosted uranium deposits. In the apt words of [79], Yeelirrie "has higher reserves than all other known deposits in the [north Yilgarn Craton] region combined, at higher grades and higher cut-off values".

2.7. Importance

According to figures presented in the latest Red Book [72], surficial uranium deposits account for only 3% (110,108 t U) of the total world's reasonably assured resources (<US$130/kg U) (Fig. 9). In comparison, sandstone-hosted, IOCG and unconformity-related uranium deposits capture 70% of the resources in this cost category. Intrusive, quartz-pebble conglomerate and volcanic-related uranium deposits also rank higher than surficial deposits with respect to reasonably assured resources (<US$130/kg U) attributable to these deposits types worldwide.

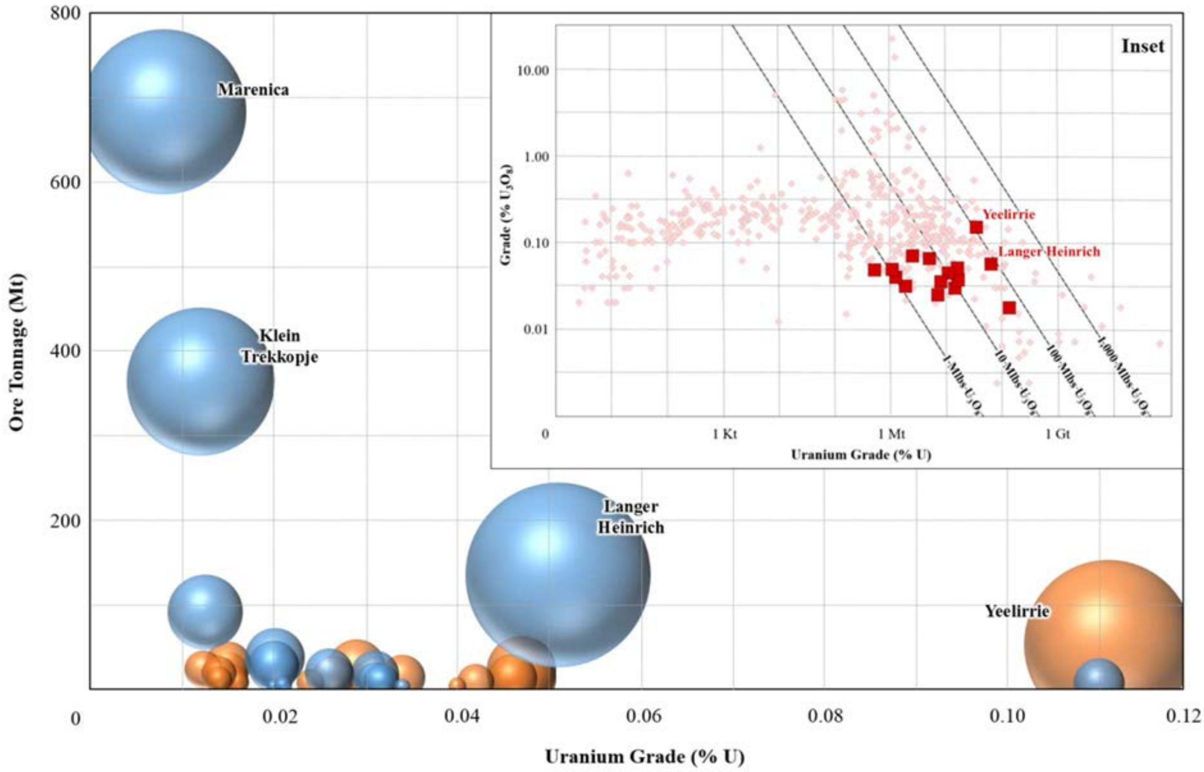

FIG. 8. Bubble diagram illustrating grade and ore tonnage of Namibian (orange) and Australian (blue) calcrete-hosted uranium deposits. The bubble size is proportional to the amount of contained uranium in each deposit. Data source: UDEPO [3]. Inset: Grade-tonnage plot for calcrete-hosted uranium deposits (red squares) after [105]. Faint red diamond symbols represent the overall grade-tonnage distribution of uranium deposits of other types.

This situation is very different when only considering the Republic of Namibia. Surficial uranium deposits rank second with respect to and account for 20% (49,200 t U) of the country's reasonably assured resources (<US$130/kg U). In the Australian context, surficial uranium deposits account for 5% (58,500 t U) of the country's reasonably assured resources (<US$130/kg U), ranking third after IOCG and unconformity-related but higher than sandstone-hosted deposits.

Despite the importance of surficial uranium deposits in the Republic of Namibia and Australia, there is currently only one operating mine in the world that exploits a calcrete-hosted uranium deposit: The Langer Heinrich [106, 107] mine in the Republic of Namibia. As emphasized by [108], the main technical issues holding back development and mining of calcrete-hosted deposits in Australia are:

— Difficult and complex metallurgy;
— High capital and operating expenditures;
— Project economics hypersensitive to uranium price;
— Groundwater control issues.

3. WESTERN AUSTRALIAN CALCRETE URANIUM PROVINCE

For the purpose of this study, the Western Australian calcrete uranium province is defined as the region that captures the geographic distribution of:

— Identified and inferred calcrete-hosted uranium deposits;
— Identified and inferred groundwater calcretes;
— The climatic conditions and geological and hydrological ingredients required to form calcrete-hosted uranium deposits.

The study area (Figs. 1 and 10) encapsulates all of the above.

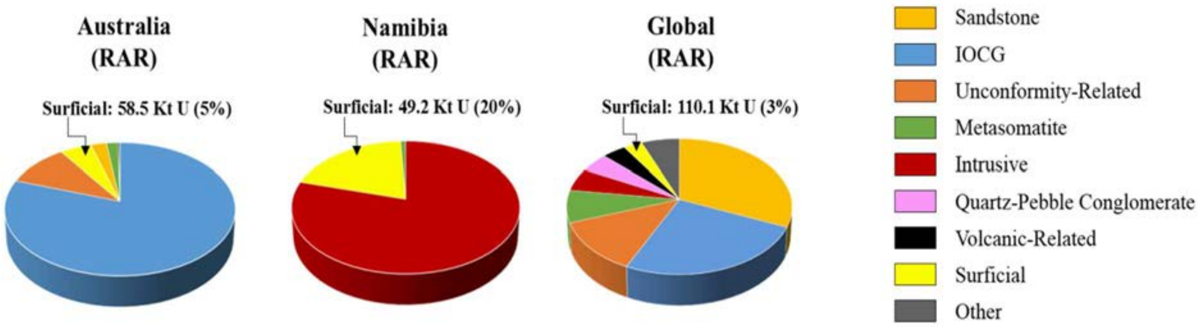

FIG. 9. Importance of calcrete-hosted uranium deposits in Australia, the Republic of Namibia and worldwide, based on reasonable assured resources (RAR) figures published in [72].

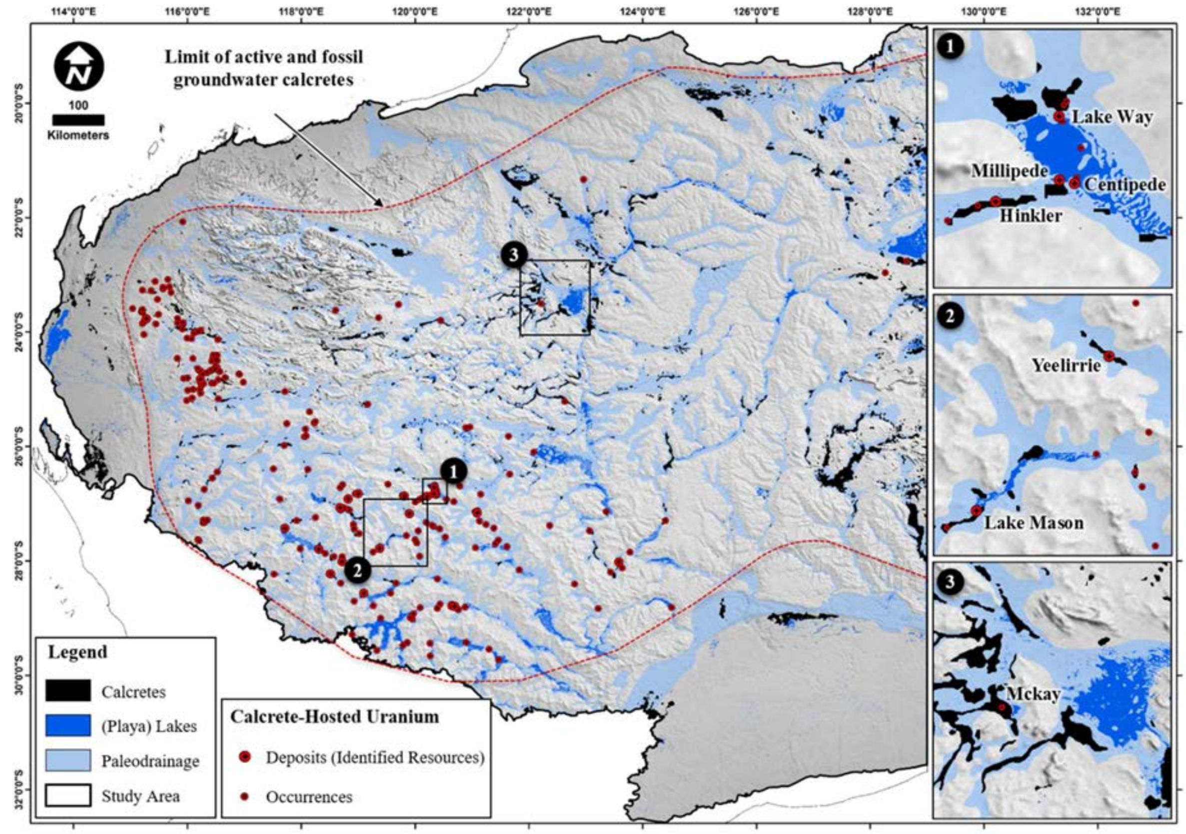

FIG. 10. Map of the study area illustrating the distribution and approximate geographic limit of active and fossil groundwater calcretes. Also shown are the locations of calcrete-hosted uranium deposits, and playa lakes and paleo-valleys as mapped by [109].

3.3. Deposit types

Calcrete-hosted uranium deposits in Western Australia can be subdivided into three broad classes [1, 100] that may be regarded as end-members, or parts of a continuum:

- Valley-type;
- Playa-type;
- Terrace-type.

Most of the larger calcrete-hosted uranium deposits in Western Australia are either valley- or playa-type deposits. Carnotite ($K_2(UO_2)_2(VO_4)_2{\times}3H_2O$) is commonly the only, or major, uranium mineral recorded in calcrete-hosted uranium deposits. The uranium mineralization in these systems is very young, ranging in age from Pleistocene (<700,000 years) to Recent. Their groundwater calcrete hosts are still actively forming today [94, 110, 111].

3.3.1. Valley-type deposits

Of the five largest surficial uranium accumulations in Western Australia, four are valley-type deposits: Yeelirrie (~49,000 t U), Centipede/Millipede (>7,600 t U), Thatcher Soak (>5,800 t U) and Lake Way (>4,700 t U) (Table 2). Valley-type deposits are hosted by either groundwater calcretes developed in paleo-river valleys (Fig. 11a), or deltaic platform calcretes that formed where paleo-valleys enter into playa lakes (Fig. 11b).

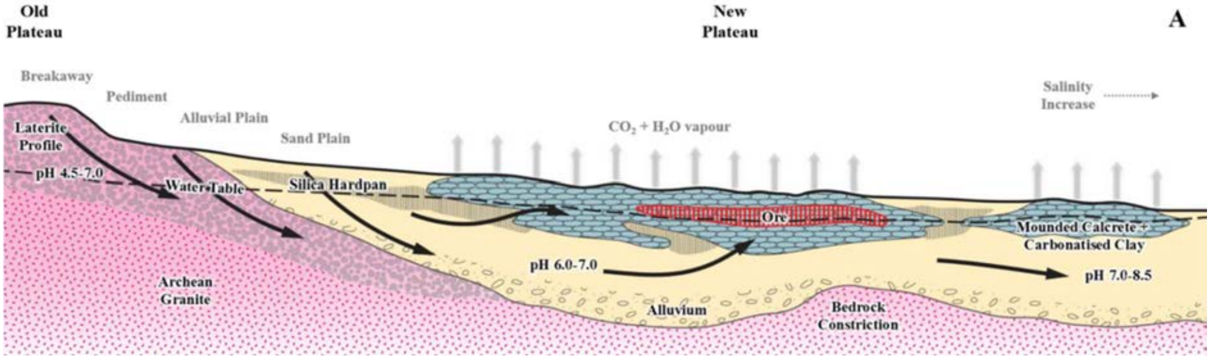

(a)

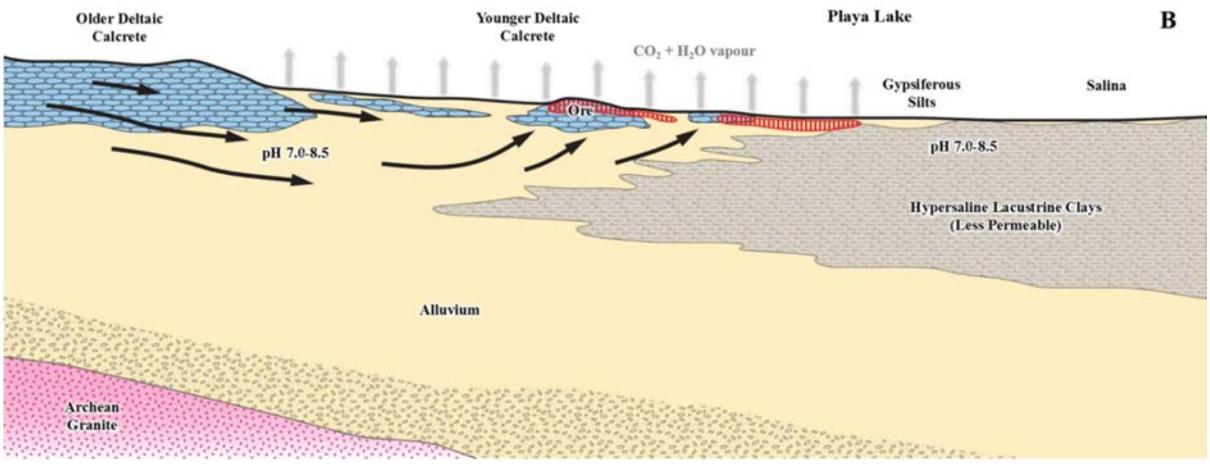

(b)

FIG. 11. Schematic models illustrating genetic factors in the formation of calcrete-hosted uranium deposits in Western Australia [91]. A. Valley-type deposits. B. Playa-type deposits.

Western Australian groundwater calcretes are composed of both calcite and dolomite in varying proportions. Most calcretes sampled to date actually represent high magnesium carbonates with most mineralized calcrete samples representing calcitic dolocrete or dolocrete [86, 93]. At the local scale, groundwater calcretes are developed as mounds, domes or elongated lenses (Fig. 12) that often form positive relief features in the paleo-valleys that contain them, marking zones of groundwater upwelling and active carbonate precipitation. The largest, most continuous and thickest calcretes develop within the capillary fringe (Fig. 4), or spatially coincident vadose zone, above a shallow groundwater table, and because of their permeability can be important aquifers. At the larger scale, individual calcretes may coalesce into elongate, semi-continuous carbonate sheets occupying the central tracts of the host paleo-valleys. These sheets can be up to 100 km long, 10 km wide and 30 m thick (Figs. 6 and 10). However, most groundwater calcretes have smaller surface dimensions and vary in thickness from 5 to 10 m [79, 91, 89, 90, 93].

According to [100], zones of uranium enrichment are often very large, and can extend for several kilometers along the drainage. Uranium concentrations within these zones are commonly relatively low with higher-grade mineralization patchily distributed within the overall anomaly. Importantly, zones of uranium enrichment are not only associated with the calcrete aquifers but transgress into all permeable units present, including fine-grained alluvial sediment underlying the calcretes. The greatest uranium enrichment is commonly found in the vicinity of the water table.

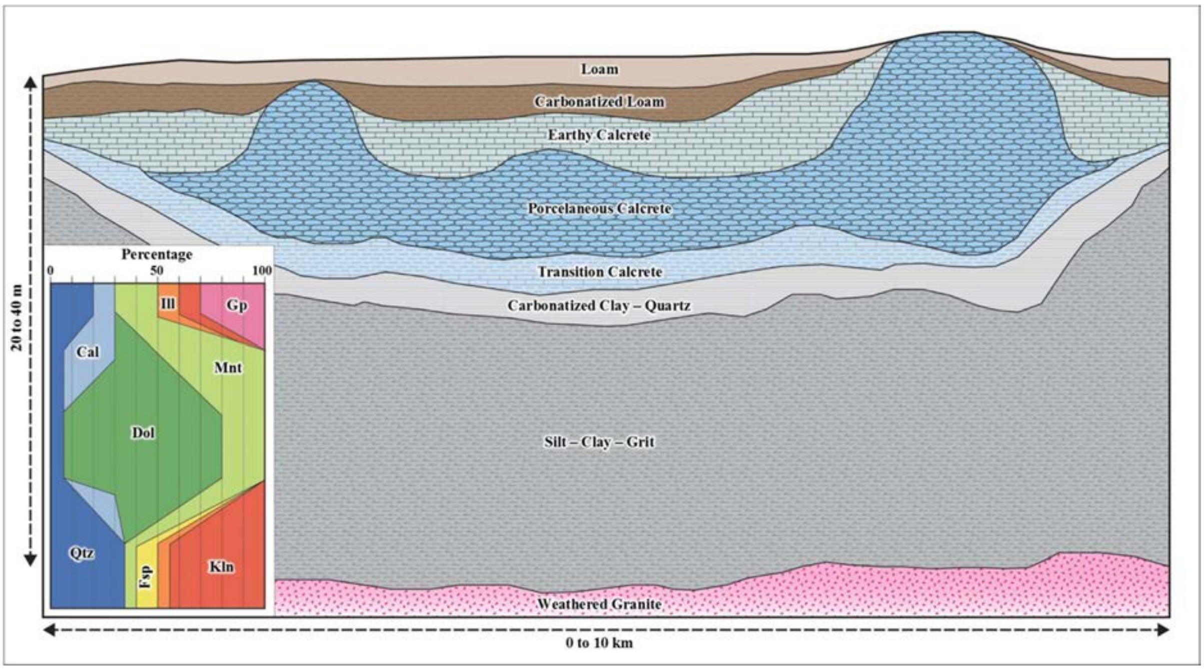

FIG. 12. Diagrammatic cross-section of a typical, uranium-mineralized groundwater calcrete in Western Australia [91].

3.3.2. Playa-type deposits

Playa-type deposits such as Lake Maitland (>9,300 t U) or Lakeside (>1,000 t U) are spatially associated with near-surface evaporitic and alluvial sediments that accumulated in playa lakes. These lakes represent local base levels for erosion and drainage sumps with little or no outflow. Playas are an important component of the groundwater flow system, being a major site of groundwater discharge from paleo-valley aquifers promoted by evaporative pumping due to high evaporation rates. Calcretes at the margins of, or near, playas act as principal aquifers to the playas. Groundwater systems within the lake environment are commonly shallow and dominated by sodium and chloride brines interacting with the landscape surface. Playa-type uranium mineralization is commonly hosted by gypsiferous clays and muds with sporadic calcareous nodules, and occurs at or near the groundwater. Uranium mineralization also occurs in thin soft calcrete horizons [78], such as observed at Lake Maitland, the largest known playa-type deposit in Western Australia [7, 100, 112].

TABLE 2. RESOURCE ESTIMATES FOR CALCRETE-HOSTED URANIUM DEPOSITS, WESTERN AUSTRALIA

Name	Latitude (decimal degrees)	Longitude (decimal degrees)	Deposit type	Ore (tons)	Grade (% U)	Uranium (tons U)	*Grade (% U_3O_8)*	*Uranium (Lbs U_3O_8)*	*Cut-Off (% U_3O_8)*	Resource date	Resource type	Source
Yeelirrie	119.902	-27.176	Surficial: Groundwater / Valley Calcrete	36,640,000	0.1357	48,966	*0.1600*	*27,300,000*	*Unknown*	Dec-14	Measured & Indicated Resources (NI 43-101)	Cameco Corp
Lake Maitland	121.094	-27.161	Surficial: Playa Lake	19,900,000	0.0471	9,347	*0.0555*	*24,300,000*	*0.0200*	Nov-13	Indicated Resource (JORC 2012)	Toro Energy Ltd
Thatcher Soak	123.584	-28.018	Surficial: Groundwater / Valley Calcrete	21,600,000	0.0267	5,885	*0.0315*	*15,300,000*	*0.0150*	Jun-12	Inferred Resource (JORC)	Uranex NL, Eleckra Mines Ltd
Centipede	120.368	-26.835	Surficial: Playa Lake	10,400,000	0.0480	5,000	*0.0566*	*13,000,000*	*0.0200*	Nov-13	Measured & Indicated Resources (JORC 2012)	Toro Energy Ltd
Lake Way	120.338	-26.707	Surficial: Delta Calcrete	10,300,000	0.0462	4,731	*0.0545*	*12,300,000*	*0.0200*	Nov-13	Indicated Resource (JORC 2012)	Toro Energy Ltd
Hillview	118.826	-26.918	Surficial: Groundwater / Valley Calcrete	27,600,000	0.0148	4,077	*0.0174*	*10,600,000*	*0.0100*	Jul-08	Inferred Resource (JORC)	Encounter Resources Ltd
Nowthanna	118.679	-27.071	Surficial: Delta Calcrete	11,900,000	0.0338	4,039	*0.0399*	*10,500,000*	*0.0200*	Nov-13	Inferred Resource (JORC 2012)	Toro Energy Ltd
Windimurra	118.516	-28.226	Surficial: Groundwater / Valley Calcrete	19,000,000	0.0153	2,885	*0.0180*	*7,500,000*	*0.0100*	Dec-07	Inferred Resource (JORC)	Maximus Resources Ltd

Name	Latitude (decimal degrees)	Longitude (decimal degrees)	Deposit type	Ore (tons)	Grade (% U)	Uranium (tons U)	*Grade (% U_3O_8)*	*Uranium (Lbs U_3O_8)*	*Cut-Off (% U_3O_8)*	Resource date	Resource type	Source
Millipede	120.339	-26.828	Surficial: Delta Calcrete	6,400,000	0.0412	2,654	*0.0486*	*6,900,000*	*0.0200*	Nov-13	Indicated & Inferred Resources (JORC 2012)	Toro Energy Ltd
Anketell	118.720	-28.014	Surficial: Groundwater / Valley Calcrete	16,300,000	0.0142	2,308	*0.0167*	*6,000,000*	*Unknown*	Jul-09	Inferred Resource (JORC)	Energy Metals Ltd
Lake Mason	119.380	-27.779	Surficial: Groundwater / Valley Calcrete	9,100,000	0.0157	1,423	*0.0185*	*3,700,000*	*0.0100*	Dec-10	Indicated & Inferred Resources (JORC)	Energy Metals Ltd
Peninsula	120.698	-28.797	Surficial: Groundwater / Valley Calcrete	9,751,000	0.0140	1,365	*0.0165*	*3,550,000*	*0.0100*	Jul-14	Inferred Resource (JORC)	Energy Metals Ltd
Dawson-Hinkler	120.218	-26.869	Surficial: Groundwater / Valley Calcrete	5,200,000	0.0239	1,231	*0.0282*	*3,200,000*	*0.0200*	Nov-13	Inferred Resource (JORC 2012)	Toro Energy Ltd
Lakeside	117.711	-27.432	Surficial: Groundwater / Valley Calcrete	5,020,000	0.0218	1,092	*0.0257*	*2,840,000*	*0.0100*	Jun-14	Inferred Resource (JORC)	Energy Metals Ltd
Wondinong	118.310	-27.795	Surficial: Groundwater / Valley Calcrete	6,500,000	0.0157	1,000	*0.0185*	*2,600,000*	*0.0150*	Apr-08	Inferred Resource (JORC)	Aura Energy Ltd
Jailor Bore	115.279	-23.765	Surficial: Terrace Calcrete	1,400,000	0.0424	615	*0.0500*	*1,600,000*	*Unknown*	Unknown	Unclassified Resource (Historic)	GSWA
Yuinmery	119.100	-28.564	Surficial: Playa Lake	1,580,000	0.0321	481	*0.0379*	*1,250,000*	*Unknown*	Unknown	Unclassified Resource (Historic)	Resource Star Ltd

Name	Latitude (decimal degrees)	Longitude (decimal degrees)	Deposit type	Ore (tons)	Grade (% U)	Uranium (tons U)	*Grade (% U_3O_8)*	*Uranium (Lbs U_3O_8)*	*Cut-Off (% U_3O_8)*	Resource date	Resource type	Source
Minindi Creek	116.225	-24.825	Surficial: Terrace Calcrete	3,500,000	0.0104	346	*0.0123*	*900,000*	*Unknown*	Unknown	Unclassified Resource (Historic)	GSWA
Murchison Downs	119.001	-26.824	Surficial: Delta Calcrete	300,000	0.0537	154	*0.0633*	*400,000*	*Unknown*	Unknown	Unclassified Resource (Historic)	GSWA
Bellah Bore East	119.812	-26.867	Surficial: Groundwater / Valley Calcrete	400,000	0.0178	28	*0.0210*	*73,500*	*0.0100*	Unknown	Inferred Resource (JORC)	Encounter Resources Ltd
Ore (tons), Total:				222,791,000								
Grade (% U), Average:					0.0335							
Grade (% U), Median:					0.0253							
Uranium (Tons U), Total:						97,629						

3.3.3. *Terrance-type deposits*

Terrace-type deposits, typified by Jailor Bore (615 t U) and Minindi Creek (346 t U), mainly occur in what is termed here as the Gascoyne calcrete uranium sub-province (Fig. 1), straddling the northwestern-most Archean Yilgarn Craton and Paleo-proterozoic Gascoyne Complex (Fig. 13). The Gascoyne calcrete uranium sub-province is located to the west of the Meckering Line (Fig. 14), a major drainage divide separating streams that drain to the base level of the Indian Ocean to the west and those that drain to the base level of inland playa lakes to the east. Post Eocene uplift and rejuvenation of the drainage to the west of the Meckering Line resulted in a more dissected terrain as evident in the area occupied by the Gascoyne calcrete uranium sub-province. Here, rejuvenated stream valleys cut into and expose calcretes developed on river terraces. These calcretes are detached from the local water table and, thus, are fossil. Calcretes in the lower terraces are commonly thin (1 to 3 m), whereas those in the upper terraces can be up to 8 m thick and overlain by up to 5 m thick silcrete and silicified calcrete. In lower terraces, moderately high uranium grades have been recorded in some calcretes and underlying sediments whereas only minor uranium concentrations are present in calcretes in the upper terraces. Most terrace calcrete-hosted uranium occurrences are too small to be economic [100] [112].

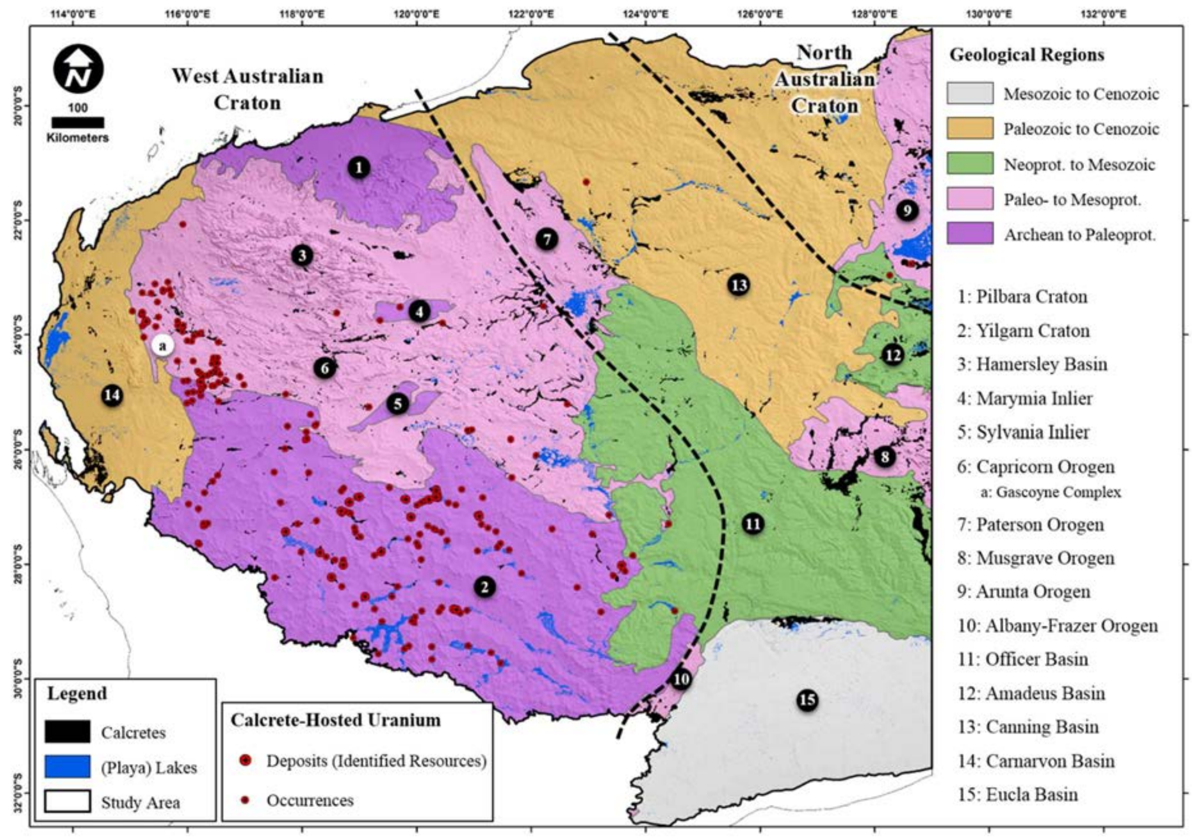

FIG. 13. Map of the study area illustrating the main geological regions (or elements), ranging in age from Archean to Phanerozoic. Dashed lines indicate the approximate boundaries of the West Australian and North Australian cratons, respectively. Most known calcrete-hosted uranium deposits (215 out of 240, or 90%) are located in paleo-valleys and playa lakes developed on the northern Yilgarn Craton and the Gascoyne Complex.

3.4. Mineral occurrence and resource data

There are 240 surficial uranium occurrences in the study area (Appendix), of which 219 are genuine calcrete-hosted uranium occurrences and 21 are likely to belong to this category but have not yet been classified beyond doubt. Of the 219 identified calcrete-hosted uranium occurrences, 28 are valley-type (including deltaic platforms), 14 are playa-type, and nine are terrace-type. The remaining 168 occurrences have not been classified as little information is available about these generally small, or very small, deposits. Given their respective settings, most of the unclassified calcrete-hosted uranium occurrences are either valley- or terrace-type.

Resources have been defined for 20 of the 240 known occurrences (Table 2). The figures were compiled from the most recent mineral resource estimates published by the current or former project owners and the Western Australian Department of Mines and Petroleum [82]. It is important to note that the total Western Australian calcrete-hosted uranium resource in Table 2 differs from that given in UDEPO [3], with the UDEPO figure exceeding our total by about 6,600 t U. The main reason for this large discrepancy may be that our figures were taken from the most recent resource estimates, most of which (12 out of 20, or 60%) were published between 2009 and 2014, whereas the UDEPO data date back to pre-2009. It is possible that, given the ongoing uranium commodity price decline since the 2007 price peak, forced the project owners to recalculate resources using more sustainable uranium prices and, therefore, higher cut-off grades resulting in reduction of resources. Another reason for the discrepancy may lie in historic estimates having over-stated actual resources. For example, [81] cautioned that the historic resource estimate for Yeelirrie may be over-stated by ~10% given that part of the postulated historic resource was not supported by sufficient drilling density and geochemical assays.

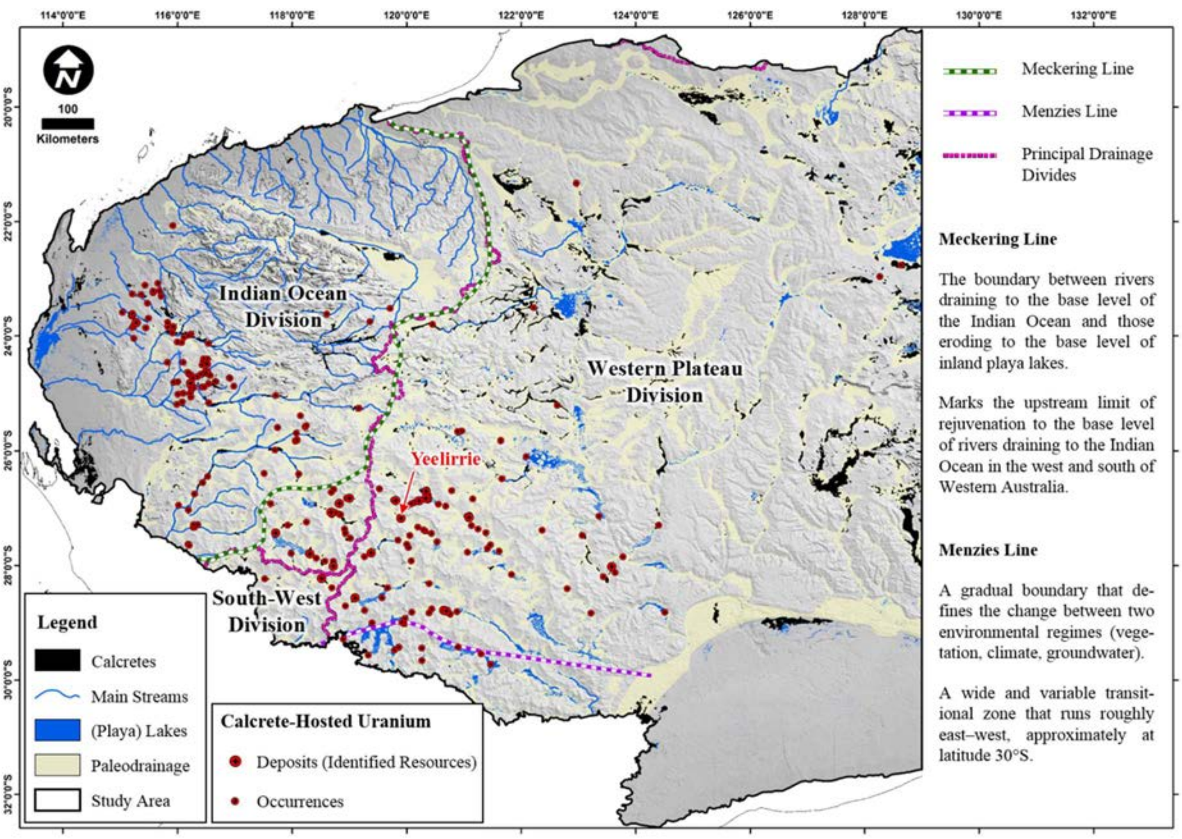

FIG. 14. Map of the study area illustrating the major catchments: The Indian Ocean, Western Plateau and South-West drainage divisions. Also illustrated and explain are the Meckering and Menzies lines.

3.5. Geology and geomorphology

3.5.1. Archean to Paleozoic basement elements

The geology of the study area is diverse, ranging in age from Archean to Cenozoic (Fig. 13). Roughly 468,000 km^2, or 27%, of the study area are on Archean terrain, including the northern Yilgarn Craton, the Pilbara Craton, and the Marymia and Sylvania inliers. These crustal elements, which contain some of the oldest known pieces of early Archean crust on Earth, are mainly composed of Archean granite-greenstone belts and have essentially been stable for the past 2,400 million years. The same is true for the Hamersley Basin that comprises a late Archean to early Paleo-proterozoic volcano-sedimentary succession, unconformably overlying the southern Pilbara Craton [113].

Paleo- to Meso-proterozoic crust is present over ~378,000 km^2, or 22%, of the study area. Much of this crust belongs to the Capricorn Orogen, a 1000 km-long and 500 km-wide mobile belt that formed between the Pilbara and the Yilgarn cratons during assembly of the Nuna supercontinent between 2,500 and 1,700 Ma. The main elements of the Capricorn Orogen are the Gascoyne Complex, which is characterized by high-grade metamorphic rocks, orthogneisses and voluminous granitoids, and a series of inverted intra-cratonic basins. These mainly contain sedimentary and minor volcanic rocks of generally low metamorphic grade [113, 114]. The remainder of the Paleo- to Meso-proterozoic crust within the study area can be attributed to the Paterson, Musgrave and Arunta orogens. The Paterson Orogen, a poorly known mobile belt separating the West Australian Craton (Pilbara and Yilgarn cratons, Capricorn Orogen) from the North Australian Craton, consists of multiply deformed and metamorphosed sedimentary and igneous rocks. The Musgrave Orogen is a Meso-proterozoic basement inlier, exposed in a window through Neo-proterozoic sedimentary rocks of the Centralian Superbasin. In Western Australia, the orogen is composed felsic gneisses of amphibolite to granulite facies metamorphic grade and voluminous plutonic and volcano-sedimentary rocks. The Giles Complex in the western Musgrave Orogen is one of the world's largest mafic to ultramafic layered intrusions. The Arunta Orogen only has a small footprint and is poorly exposed in Western Australia. It comprises a thick succession of polydefomed Paleo-proterozoic metasedimentary rocks intruded by granitoids of the same period [114−116].

The Officer and Amadeus basins in eastern Western Australia occupy ~278,000 km^2, or 16%, of the study area. These basins formed part of the Centralian Superbasin, a Neo-proterozoic intra-cratonic basin (or basin cluster?) that covered much of central Australia [117]. As outlined by [114, 115, 118], the Centralian Superbasin was tectonically disrupted by the Miles, Paterson and Peterman orogenies between ~750 and ~550 Ma. These disruptions resulted in progressive compartmentalization of the Centralian Superbasin and subsequent development of several discrete basins. According to [119], Neo-proterozoic basin formation was mainly related to the break-up of the supercontinent Rodinia, and was terminated in the late Neo-proterozoic due to compression linked to the amalgamation of the Gondwana supercontinent.

Three large Phanerozoic epi-cratonic basins are developed within the study area covering ~615,000 km^2, or 36%. These are the Early Ordovician to Cenozoic Canning Basin and Carnarvon basins, and the Jurassic(?) to Cenozoic Eucla Basin. The Canning Basin, the largest sedimentary basin in Western Australia, is a faulted and folded rift-sag basin containing Ordovician to recent marine and non-marine siliciclastics and marine carbonates. The basin has a maximum sediment thickness of over 15 km concentrated in two depo-centers. The Carnarvon Basin is a faulted and folded rift basin containing up to 15 km of Paleozoic to recent sediment infill. The Eucla Basin comprises a thin passive margin succession of marine clastic and carbonate sedimentary rocks that were deposited during the final stages of separation between the Australia and Antarctica plates. Minor regional tectonic tilting in the Miocene (Fig. 15) caused exposure of the northern Eucla Basin, limiting Neogene sedimentation to the modern-day outer-shelf and upper-slope [113, 120].

Considering the study area as a whole, most calcrete-hosted uranium deposits (215 out of 240, or 90%) are located in paleo-valleys and playa lakes etched into the northern Yilgarn Craton and Gascoyne Complex. Only three deposits are located outside these geological regions, and none have been recorded in the Pilbara Craton, even though geologically the latter shares many similarities with the Yilgarn Craton.

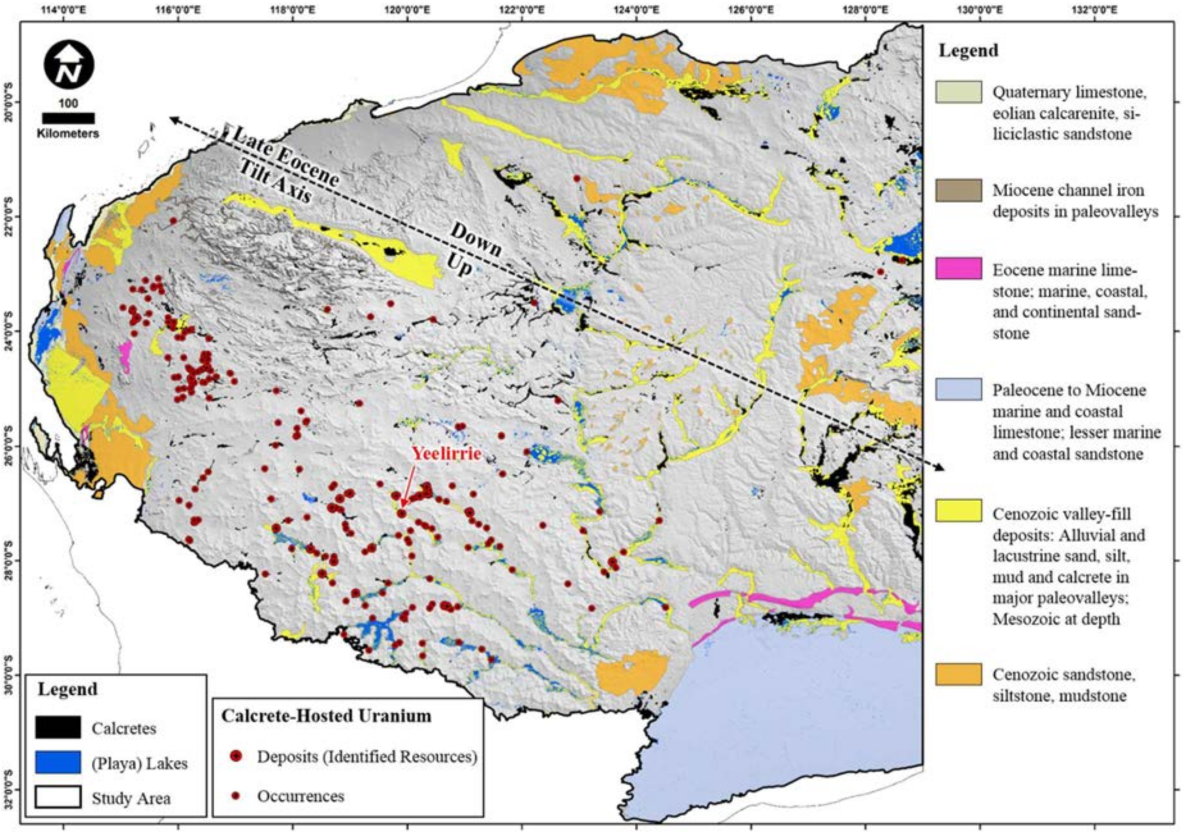

FIG. 15. Cenozoic geological elements of the study area. Also shown is the approximate location of the late Eocene tilt axis. Continent-scale tilting about this NW–SE-oriented axis resulted in uplift in southwestern Western Australia, and thus much of the study area.

3.5.2. Cenozoic Elements

The amount of Cenozoic strata (other than regolith) present within the study area is limited (Fig. 15). This situation is not surprising given:

— The remarkable tectonic stability of the study area during the Cenozoic [121] and long periods of tectonic quiescence since the Permian that facilitated deep weathering and allowed a variety of climatic conditions and landscape forces to interact and develop various types of regolith and landscape [90];
— That large parts of the study area have been exposed to weathering since the Proterozoic, with most of the study area having been exposed to subaerial conditions since the Cretaceous (Fig. 16).

Of particular importance for this study is the Cenozoic paleo-valley system etched into the Archean to Paleozoic basement, as these paleo-river valleys are the host environment of the calcrete-hosted uranium deposits within the study area. This system of broad, shallow drainage channels, one of the largest paleo-valley systems known worldwide, most likely was established in the Cretaceous when a then humid climate promoted fluviatile erosion. Continent-scale tilting about an approximately NW–SE-oriented tilt axis (Fig. 15) resulted in uplift in the late Eocene of southwestern Western Australia, and thus much of the study area. This tilting is the result of a dynamic topography response to the progressive northward movement of the

Australian Plate toward the subduction zones of Indonesia and Southeast Asia since the break-up of Gondwana. The resultant uplift promoted further drainage incision along the pre-existing paleo-valleys [90, 122], and active erosion of previously formed terrace calcretes to the west of the Meckering Line (Fig. 14) [112].

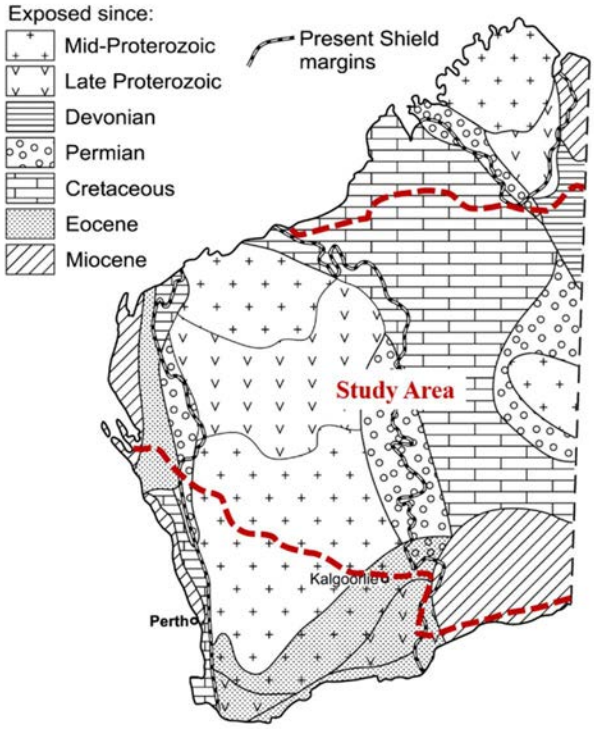

FIG. 16. Map of Western Australia illustrating periods of exposure to subaerial weathering of outcropping bedrock. The boundaries of the study area are superimposed. Figure modified from [90] and published with the permission of the Geological Society of Australia.

The WASANT paleo-valley map of [109] provides an excellent overview of the paleo-valley systems in Western Australia, including two cross sections illustrating the complex, composite nature of these paleo-rivers using the Murchison River and Kintyre paleo-valleys as examples. Both are characterized by wide (4 to 16 km) primary valleys of Mesozoic age and two or three smaller (0.25 to 4 km) Tertiary inset valleys that are up to 200 m deep.

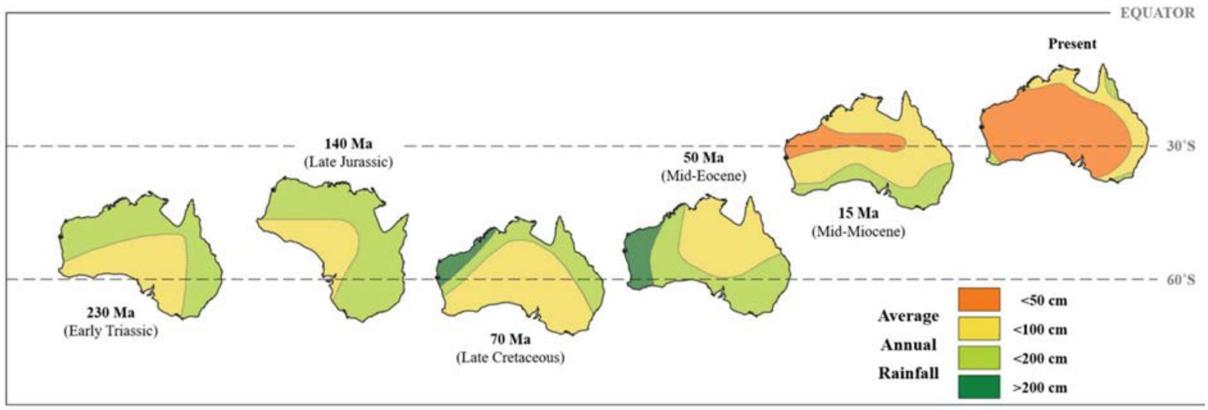

FIG. 17. Paleo-climate history of Australia showing changes in latitude and distribution of climate zones as Australia moved north into its present-day position. Today's arid climate took hold as early as the middle Miocene [125].

Due to an increasingly arid climate since the middle Miocene (Fig. 17), caused by Australia's progressive northward movement, the fluvial systems became defunct and river valleys were choked by sediments, ultimately transforming into the sites of chains of playa, lakes. Despite these significant changes, the paleo-valleys remained active groundwater systems [90, 123].

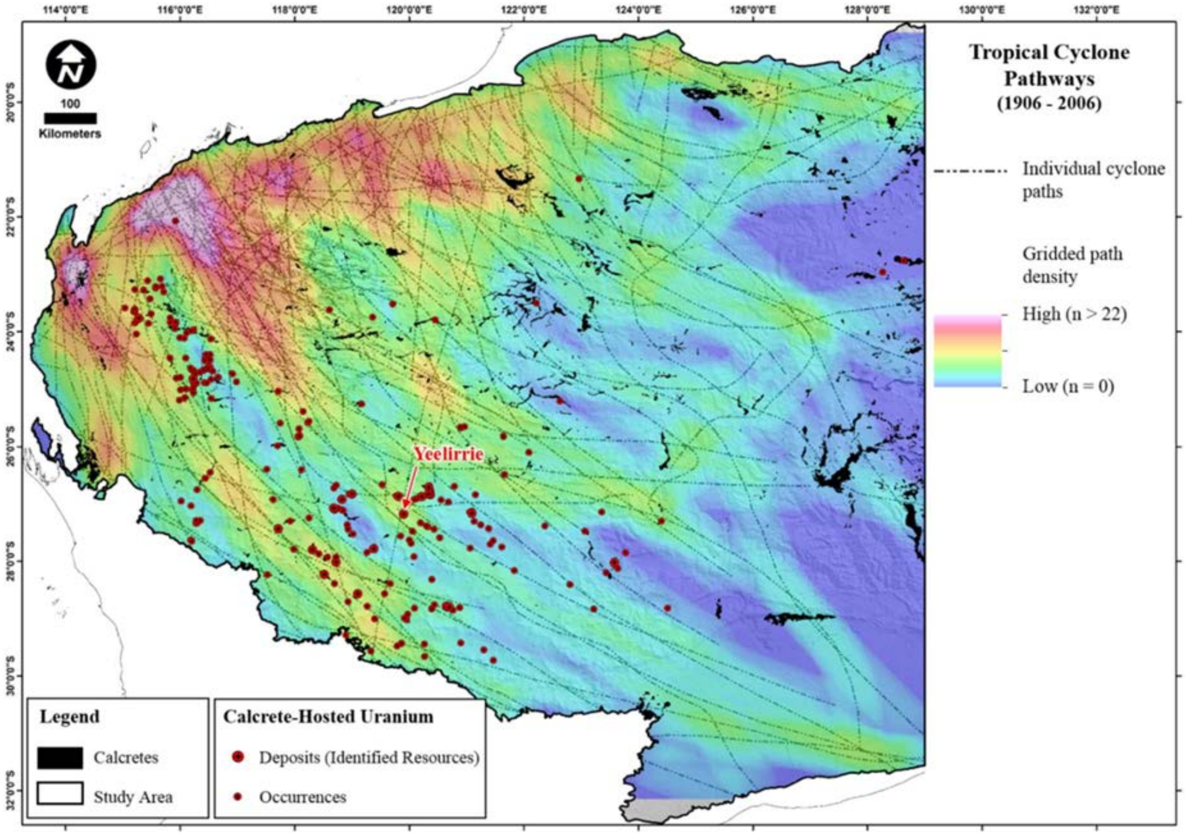

FIG. 18. Map of the study area illustrating tropical cyclone pathways recorded by the Australian Bureau of Meteorology over a 100-year period. The gridded path density highlights those areas that are passed by cyclones more frequently. Cyclones that cross the coast and weaken over land may continue to produce heavy rain a considerable distance inland. The Australian cyclone season runs from November to April. The cyclone path data may be taken to imply that the Gascoyne and Yilgarn calcrete uranium receive more rainfall from tropical cyclones than most other areas in the desert climate zone away from the coastline. This potential cyclone alley was previously suggested by [89, 108].

3.6. Climate regime

A marked change in climate occurred in Australia from about middle Miocene times (~15 Ma). Prior to this point in time Australia had recorded long periods characterized by temperate to warm (Mesozoic) and sub-tropical to tropical (Paleocene to middle Miocene) climates (Table 3). However, the Australian plate's progressive northward movement since the break-up of Gondwana saw the continent become more arid as it moved into the zone of sub-tropical high pressure, characterized by mid-latitude deserts. However, desert conditions were not fully established until the late Pliocene (~3 Ma).

TABLE 3. PRINCIPAL CLIMATIC EPISODES IN THE SOUTHERN YILGARN CRATON (MODIFIED FROM [87])

Period /Epoch	Age (Ma)	Climate
Quaternary	1.8 – 0	Temperate to warm; semiarid to arid (25,000 – 13,000 peak aridity, glacial maximum)
Middle Miocene – Pliocene	15 – 1.8	Subtropical; aridity increasing; cooler after 2.5 Ma
Paleocene – Middle Miocene	65 – 15	Subtropical to tropical; humid; probably seasonal (savanna)
Mesozoic	230 – 65	Temperate to warm; humid

For the study area, the climatic shift from temperate to arid resulted in [7, 90, 94, 123]:

— The nature and distribution of the vegetation becoming similar to that currently prevailing;
— The ancient river system becoming sluggish due to limited availability of surface water and fluvial sediment blocking the drainage;
— The pre-middle Miocene fluvial systems becoming defunct whereas the groundwater systems centered upon the paleo-valleys remained active;
— Groundwater levels dropping and waters becoming saline;
— The ancient river valleys and lakes becoming the sites of chains of playa lakes.

According to [7, 123], the paleo-valley-hosted groundwater systems further evolved since commencement of the Quaternary glacial cycles ~2.6 million years ago. Episodic groundwater recharge has been most effective during warmer and wetter interglacial periods while discharge has been dominant during the drier glacial periods by way of evaporative pumping and evaporation through playas and salt lakes.

The present-day climate of much of the study area can be described as semi-arid to arid. Rainfall is irregular with heavy but infrequent rainfalls originating in tropical low-pressure systems and cyclonic storms (Fig. 18), mainly between January and June. Smaller amounts of rain, mainly derived from local thunderstorms in October and November, contribute to the annual total. The annual average maximum temperature is over 30°C for most of the area [124]. Average climate data for the study area are given in Fig. 19.

The Menzies Line (Fig. 14), a gradational boundary at approximately 30ºS, marks a change in interrelated climatic, vegetation, regolith and groundwater characteristics. North of the Menzies Line [7]:

— Rainfall is influenced by sporadic cyclonic storms as described above;
— Groundwater calcretes form in paleo-valleys whereas pedogenic carbonates are less common;
— There is generally more topographic relief;

— Groundwater is of commonly potable or stock quality.

3.7. Three-stage genetic model

According to [77, 79, 105], the formation of calcrete-hosted uranium deposits in Western Australia can be illustrated by a three-stage model, including critical processes and ingredients that partly overlap in time and space (Fig. 20):

1) Climatic shift from humid to arid and filling of paleo-valleys (stage 1): The climatic shift from humid to arid as described above was essential in terms of ground preparation. A progressively more arid climate resulted in lesser surface water availability, and reduced water flow within and clogging of the previously formed river systems. In essence, the pre-middle Miocene fluvial systems became defunct although the groundwater systems centered upon these paleo-valleys remained active promoted by the permeability of the valley fill sediments;
2) Initiation of an active groundwater drainage system and calcrete deposition (stage 2): Episodic recharge of the paleo-valley aquifers is achieved by rainfall, up-gradient aquifers in tributary valleys, or weathered bedrock aquifers. Discharge is principally by way of evaporation at playa lakes promoting deposition of evaporates. Given the availability of calcium and magnesium carbonate, the intensive evaporation also promoted deposition of groundwater calcrete (see below for further detail) at, or immediately above, the groundwater table within the defunct drainages, or where paleo-valleys enter into playa lakes. Once formed, the calcrete began to act as an aquifer affected by and responding to evaporation and a fluctuating water table.

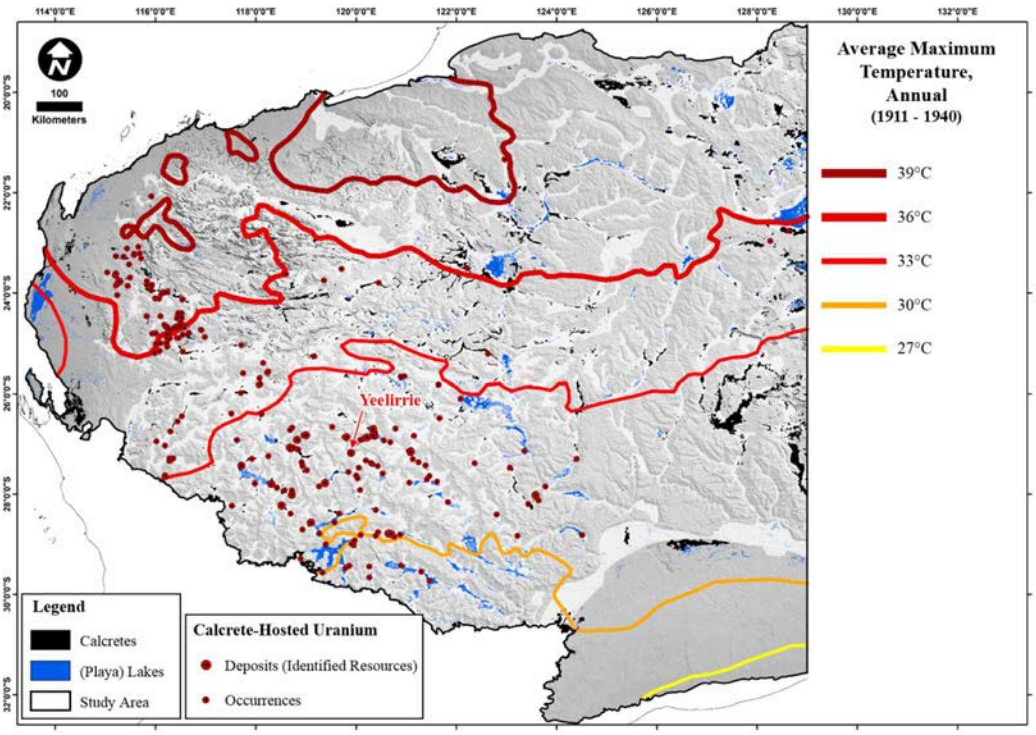

(a)

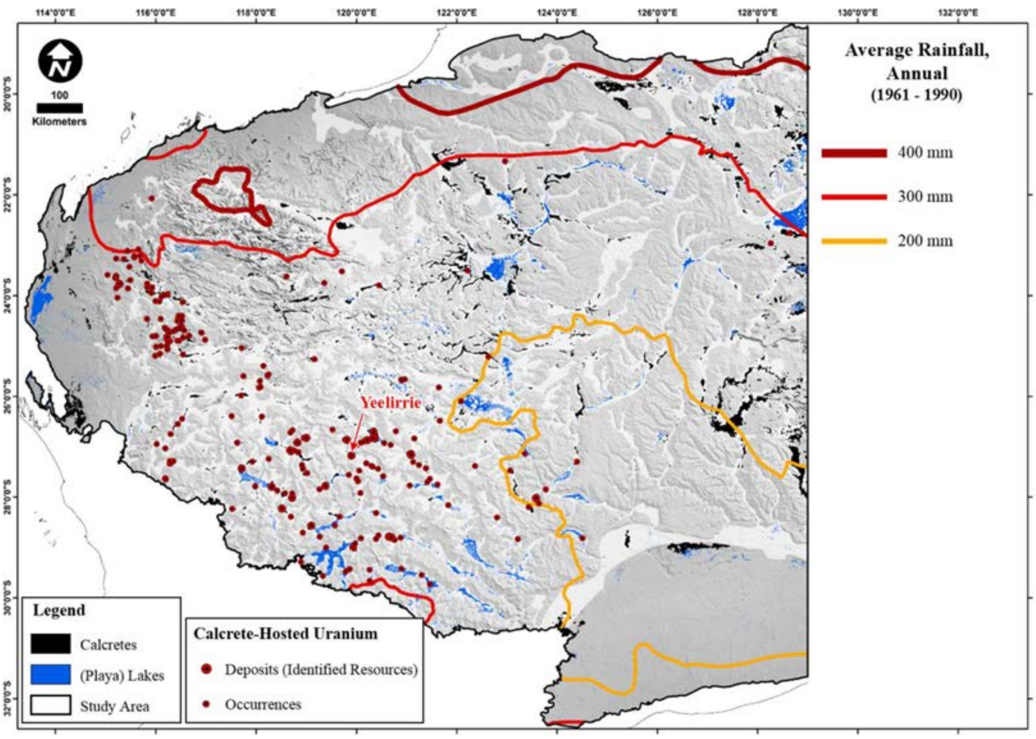

(b)

FIG. 19. Map of the study area illustrating long term climate patterns recorded by the Australian Bureau of Meteorology. (a) Average annual maximum temperatures recorded over a 30-year period from 1911 to 1940. (b) Average annual rainfall recorded over a 30-year period from 1961 to 1990. Only very few of the known calcrete-hosted uranium deposits are located in areas receiving more than 300 mm of average annual rainfall.

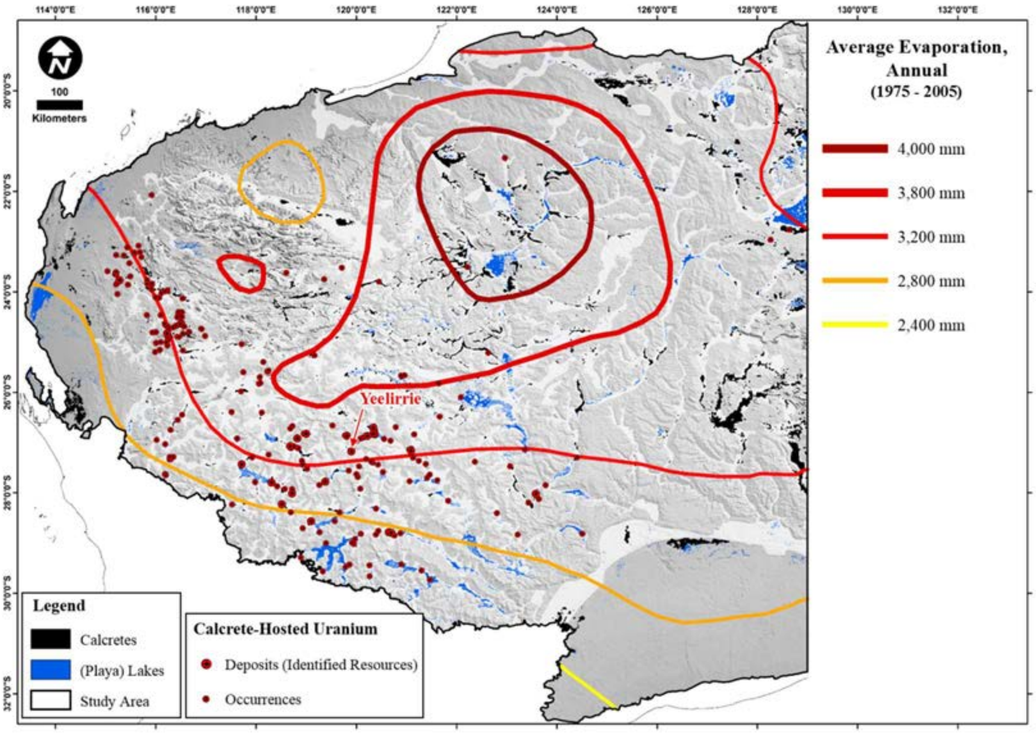

(b)

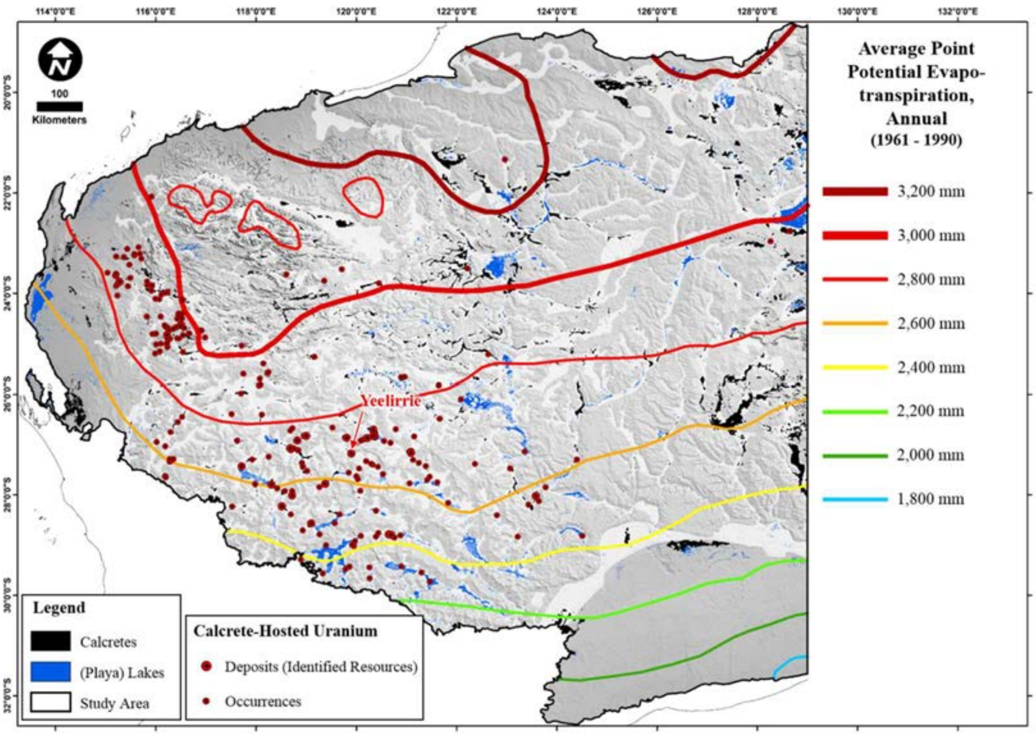

(c)

FIG. 19 (continued). (c) Average annual evaporation recorded over a 30-year period from 1975 to 2005. Only few of the known calcrete-hosted uranium deposits are located in areas where evaporation exceeds 3,800 mm.

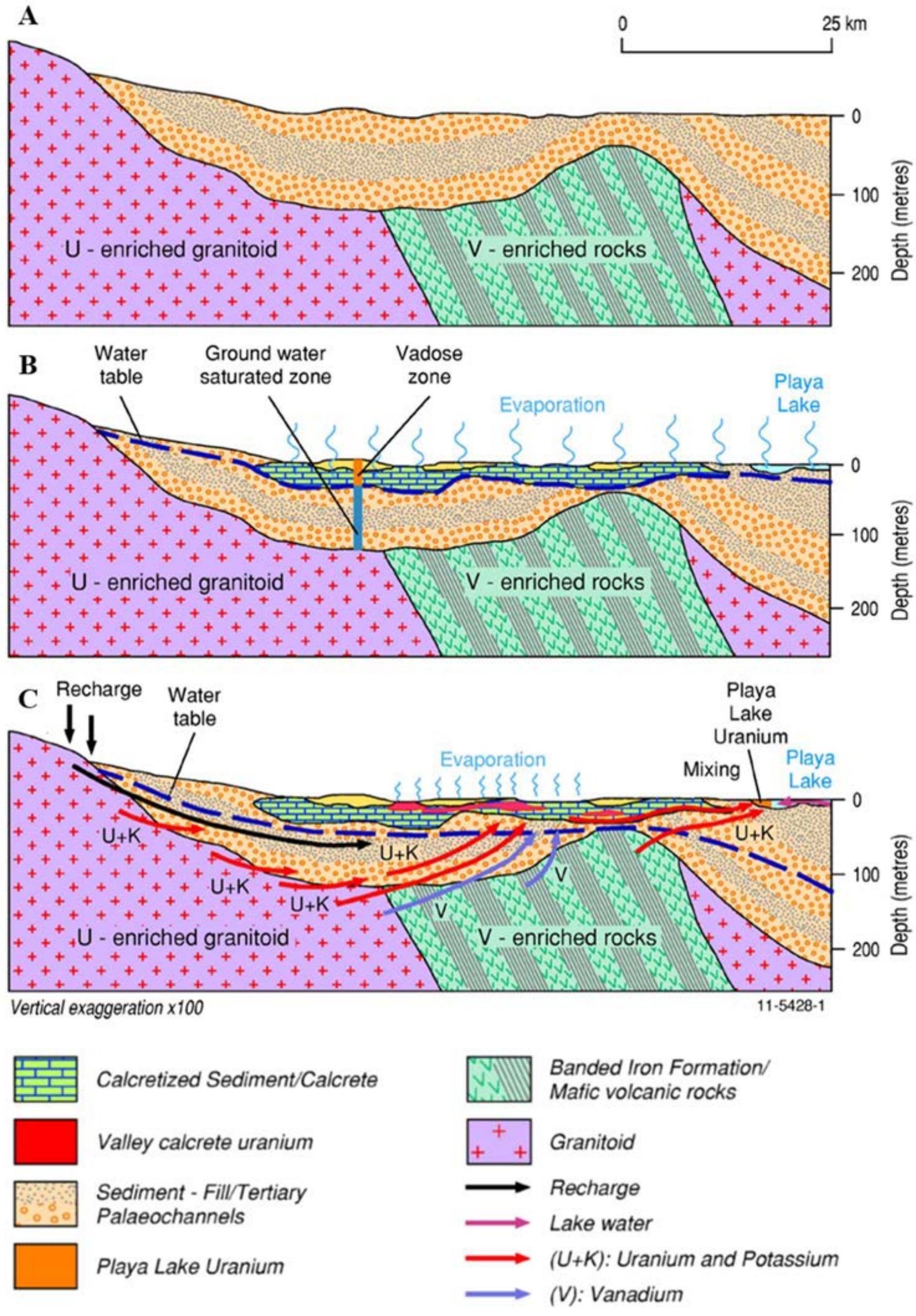

FIG. 20. Schematic representation of the three-stage genetic model for the formation of calcrete-hosted uranium deposits as synthesized by [77, 105]. See text for details. Figure taken from [77] and reproduced here under the Creative Commons Attribution 3.0 Australia (CC BY 3.0 AU) (https://creativecommons.org/licenses/by/3.0/au/legalcode).

3) Leaching and transport of ore components, and precipitation of carnotite (stage 3): Potassium and uranium were leached from weathered felsic rocks (in particular granite) either by surface waters washing over exposed bedrock, or by groundwater percolating through fractured and / or highly weathered bedrock. Vanadium, on the other hand, is commonly thought to be sourced from mafic to ultramafic igneous, or iron-rich

(meta)sedimentary, rocks. Physico-chemical changes in the groundwater, for example through evaporation at sites of groundwater pooling, or upwelling, (a) caused precipitation of carbonate and apatite, (b) which in turn resulted in the loss of phosphorous and bicarbonate from the groundwater, (c) thereby forcing a reaction of the aqueous species of uranium, vanadium and potassium to form carnotite. Alternatively, in the vicinity of playa lakes, carnotite precipitation may have been triggered by mixing of valley-derived groundwater with potassium-rich saline lake water. Because uranium precipitates as uranyl mineral species in the surficial, oxidizing environment, a change in redox potential was not required.

3.8. Targeting elements

3.8.1. Mappable source processes

A form of energy is required for driving and sustaining a mineral system (Table 4). In terms of Western Australian calcrete-hosted uranium province, the main sources of energy are gravity, which drives lateral water movement down slope, and evaporation, which promotes vertical water movement. Given the generally relatively flat topography within the study area gravity is most likely not a strong driver of groundwater flow. For example, the Yeelirrie paleo-valley has an elevation of 549 m above sea level at the highest point of its headwaters whereas Lake Well, a playa lake downstream from Yeelirrie, sits at an elevation of 474 m above sea level. The difference in elevation between the high and low point is a mere 75 m over a distance of almost 100 km giving an average slope of less than 0.1%. The maximum slope is 0.3% but those numbers are restricted to the uppermost reaches of the paleo-valley. No information is readily available regarding fluid pressure, another possible energy gradient affecting groundwater flow. However, another very effective force that is in play in this arid climatic zone is evaporation whereby water that is discharged through evaporation at playa lakes is replaced by inflowing groundwater from further upstream.

Most authors (e.g., [3, 13, 77, 100, 126, 127]) agree on weathered granite as the main source of uranium in calcrete-hosted uranium deposits (Figs. 11, 20, 21). Key arguments in support of this hypothesis are the spatial distribution of the known calcrete-hosted uranium deposits coinciding with that of outcropping and concealed granitoids, and the commonly elevated uranium concentrations of the granitic rocks (average of Yilgarn Craton granites = 3 to 8 ppm U; range = 1 to 80 ppm U: [100]). However, the actual uranium content of a suitable source rock may not be as important as the ease with which this rock releases the uranium [45, 127, 128]. Factors promoting the leachability of uranium from granitic rocks [45] include:

- High fluid-rock ratio (higher for rocks that are more fractured and more weathered, and mappable from structural, topographic and remote sensing data);
- Granite geochemistry (both peraluminous and peralkaline igneous are commonly enriched in uranium but peraluminous intrusions make better uranium source rocks than peralkaline intrusions because they contain more readily leachable uraninite whereas in peralkaline rocks uranium occurs in complex mineral phases: [129, 130];
- Oxidizing environment (a common situation due to the abundance of O_2 in the vadose zone, the depositional environment of calcrete-hosted uranium deposits).

Greater than 346,000 km^2 (20%) of the study area are underlain by granitic rocks (Fig. 22), including ~61,000 km^2 of outcropping granitoids (<4%). When buffered to 2 km, outcropping and subsurface granitoids capture 209 out of 240 (or 87%) of the known calcrete-hosted uranium occurrences. This spatial relationship offers strong empirical evidence in support of granitoids as the main sources of uranium in the Western Australian calcrete-hosted uranium province. The strong spatial relationship between uranium-enriched granitoids and calcrete-hosted uranium deposits is also evident at the local scale. Fig. 23 provides an example of the Yeelirrie catchment where uranium-enriched granitoids are exposed along erosion scarps (breakaways) above the paleo-valley, shedding uranium-enriched debris down-slope. The importance of granitoids as uranium source rocks was also demonstrated by [131], who found that over 2,700 of the ~22,000 samples in Geoscience Australia's OZCHEM national whole rock geochemistry database have uranium concentrations of at least 10 ppm U, and that most of these uranium-enriched samples are from granitic and felsic volcanic rocks.

TABLE 4. MINERAL SYSTEMS APPROACH TO TARGETING CALCRETE-HOSTED URANIUM DEPOSITS

Critical processes	Constituent processes	Targeting elements	Mappable features	Available supporting data[#]	GIS processing steps	Derived predictor maps*
Source	Energy to drive and sustain the system	Hydraulic gradient (gravity); Evaporation (discharge via playa lakes and recharge via water inflow from upstream); Fluid pressure	Topographic gradient (as proxy for hydraulic gradient)	GTOPO30 DEM (topography)	Present-day topography served as a proxy for paleo-topography and paleo-geomorphology, which were "reconstructed" using GTOPO30 DEM data.	
	Active, shallow groundwater aquifers	Paleo-valley - playa lake groundwater systems	Paleo-valleys; Playa lakes	Paleo-valley map; Playa lake map		
	Availability of ligands	Carbonate source rocks / sediments; Calcium carbonate (calcite) in regolith; Sulfur-bearing rocks	Rocks / sediments / regolith with elevated / readily releasable CO3 and S	Surface (fact) and solid (interpretative) geology maps; Structural geology map; Weathering intensity index map	Proximity to sources of U complexing ligands: (a) Extraction of carbonate and S-bearing rocks from solid geology map; (b) Calculation of the proximity to U complexing ligands within each paleo-valley catchment using Euclidean distances. Proximity to sources of V complexing ligands: (a) Extraction of S-bearing rocks from solid geology map; (b) Calculation of the proximity to U complexing ligands within each paleo-valley catchment using Euclidean distances.	Proximity to sources of U complexing ligands; Proximity to sources of V complexing ligands
	Availability of ore components - U from deeply	U, V, K, Ca and Mg sources that coincide with:	Rock units with elevated U, V, K, Ca and Mg, in particular	Surface (fact) and solid (interpretative) geology maps;	U source rocks: (a) Extraction of granitic and felsic volcanic rocks from solid geology map; (b) Calculation of	Proximity to U sources; Proximity to V

Critical processes	Constituent processes	Targeting elements	Mappable features	Available supporting data#	GIS processing steps	Derived predictor maps*
	oxidized / intensively weathered and / or fractured U-rich country rocks (e.g., Archean or Proterozoic granitoids) - V from deeply weathered and / or fractured V-rich country rocks (e.g., Archean or Proterozoic mafic- ultramafic igneous rocks) - K from deeply oxidized / intensively weathered and / or fractured K-rich country rocks (e.g., Archean or Proterozoic granitoids) - Ca and Mg from deeply oxidized / intensively weathered and / or fractured Ca-	- domains of deep oxidation / intense weathering; - domains of high fault-fracture density; - paleo-valley catchments; - V-enriched valley-fill sediments	felsic or mafic-ultramafic igneous rocks, and mafic schist and gneiss of Archean to Proterozoic age; Spatial union of such rock units and paleo-valley catchments; Spatial union of such rock units and areas of intense weathering; Spatial union of such rock units and areas of high fault-fracture density	Radiometric (U, U/Th, U^2/Th, K) data; Magnetic, electromagnetic and gravity data; ASTER and Landsat data; Geochemical soil, stream sediment, rock chip and groundwater assay data; Drill hole and assay data; Weathering intensity index map; GTOPO30 DEM (topography)	the proximity to U source rocks within each paleo-valley catchment using Euclidean distances (note: Present-day catchments served as proxies for paleo-valley catchments). Proximity to V source rocks: (a) Extraction of BIFs and mafic-ultramafic volcanic and igneous rocks from solid geology map; (b) Calculation of the proximity to V source rocks within each paleo-valley catchment using Euclidean distances. Domains of intense weathering: (a) Reclassification of the weathering intensity map into two classes (high, low) using suitable statistically derived thresholds; (b) Extraction of intense weathering domains; (c) Calculation of the proximity to domains of intense weathering within each paleo-valley catchment using Euclidean distances. Domains of high fault-fracture density: (a) Extraction of structures from solid geology map; (b) Calculation of structure density; (c) Reclassification of the density map using statistically derived thresholds for identification of domains of high structure density; (d) Calculation of the proximity to areas of high fault-fracture density within each paleo-valley catchment using Euclidean distances.	sources; Proximity to domains of intense weathering and high fault-fracture density

Critical processes	Constituent processes	Targeting elements	Mappable features	Available supporting data[#]	GIS processing steps	Derived predictor maps*
	and Mg-rich country rocks (e.g., Archean or Proterozoic mafic-ultramafic igneous rocks); Alternatively V may be (pre-)concentrated in valley-fill sediments in shallow groundwater aquifers					
Transport	Transport of ore components by rainwater run-off and groundwater Focusing of rainwater run-off and groundwater flow into shallow phreatic aquifers Channeling of groundwater flow toward playa lakes	Paleo-valley systems in (semi-)arid regions marked by chains of playa lakes; Negligible surface water flow in a (semi-)arid climate; Low hydraulic gradient; Peneplain with near-flat relief	Paleo-valleys; Groundwater calcretes; Lacustrine sediments; Playa lakes (in particular deltas where paleo-valleys enter the playas); Topography (hydraulic gradient)	WASANT paleo-valley map; Calcrete map; Lacustrine sediment map; Playa lake map; GTOPO30 DEM (topography); ASTER thermal map (concealed river valleys); Climate data; Hydrological data	Amendment and augmentation of the WASANT paleo-valley map based on our own interpretations of remote sensing and GTOPO30 DEM data (note: The paleo-valley boundaries were used to constrain the spatial analyses to the area (i.e., pixels) within the paleo-valleys, rendering the areas (or pixels) outside the paleo-valleys as unprospective for calcrete-hosted uranium deposits).	Paleo-valley drainage systems
Trap	Locations within the paleo-valleys or at playa lake entries that promote pooling,	Playa lake deltas ("chemical deltas"); Mounded calcrete with complex internal mineralogy, texture	Playa lakes; Groundwater calcretes and spatially associated clay and clay-quartz horizons;	Calcrete map; Lacustrine sediment map; Playa lake map; GTOPO30 DEM;	Paleo-valley slopes: (a) Creation of a drainage map based on GTOPO30 DEM; (b) Calculation of the drainage slopes in ArcGIS interface with low values considered more favorable	Paleo-valley slopes; Proximity to paleo-valley bends and confluences; Proximity to favorable

Critical processes	Constituent processes	Targeting elements	Mappable features	Available supporting data#	GIS processing steps	Derived predictor maps*
	upwelling, evaporation and subsequent chemical modification of uranium-bearing groundwater	and structure is regarded as a marker for areas of groundwater upwelling; High evaporation and evapo-transpiration rates; Locations within the paleo-drainage system that promote fluid mixing; Subsurface barriers (or bars) restricting groundwater flow and causing upwelling and ponding of groundwater	Topography (hydraulic gradient); Playa lakes; Climate records (e.g., temperature, evaporation rates, evapo-transpiration rates); Paleo-valley morphology; Barriers to groundwater flow	ASTER thermal map; Surface (fact) geology maps; Climate records	because of slower groundwater flow promoting greater evaporation. Proximity to paleo-valley bends and confluences: (a) Generation of a flow accumulation raster from the GTOPO30 DEM; (b) Identification of points of maximum water accumulation within each paleo-valley (in particular at stream undulations and sharp bends, and channel confluences); (c) Calculation of the proximity to paleo-valley bends and confluences within each paleo-valley catchment using Euclidean distances.	carnotite host media; Annual evapo-transpiration; Annual precipitation; Annual temperature
	Locations within the drainage or at playa lake entries that promote fluid mixing				Proximity to carnotite host environments: (a) Extraction of calcretes and lacustrine (playa lake) deposits from regolith map; (b) Calculation of the proximity to calcretes and lacustrine (playa lake) deposits within each paleo-valley catchment using Euclidean distances.	
	Locations within the drainage or at playa lake entries that promote active formation of calcrete bodies (limestone deposits that formed as chemical precipitates of calcium and					

Critical processes	Constituent processes	Targeting elements	Mappable features	Available supporting data[#]	GIS processing steps	Derived predictor maps*
	magnesium carbonates from carbonate-bearing groundwater)					
	Areas of high evapo-transpiration, evaporation and temperature				Annual evapo-transpiration, precipitation and temperature: (a) Digitization of evapo-transpiration, rainfall and temperature contours from available climate maps (image files); (b) Interpolation of climate data across the entire study area using the natural neighbor's interpolation method	
Deposition	Interaction between uranium-, vanadium- and potassium-bearing fluids and calcium carbonate in the calcretized horizons Adsorption of uranium onto clays at or immediately below the water table Chemical reduction in anoxic paleo-valley and playa	Playa lake deltas ("chemical deltas"); Mounded calcrete with complex internal mineralogy, texture and structure is regarded as a marker for areas of groundwater upwelling; Locations within the paleo-drainage system that promote fluid mixing; Highly saline groundwater; Subsurface barriers (or bars) restricting groundwater flow and causing upwelling and	Uranium anomalism (U, U/Th, U^2/Th radiometric anomalies, carnotite occurrences) spatially associated with groundwater calcretes, deltaic platforms and chemical deltas; Uranium anomalism (U, U/Th, U^2/Th radiometric anomalies, carnotite occurrences) spatially associated with playa (salt) lakes with surface or subsurface uranium enrichment, mainly in clay and mud horizons;	Radiometric data; Geochemical assay data (e.g., soils, streams sediments, water, rock chips); Drill hole assay data; Groundwater salinity maps		None

Critical processes	Constituent processes	Targeting elements	Mappable features	Available supporting data#	GIS processing steps	Derived predictor maps*
	lake environments (e.g., rotting vegetation zones below the sediment/water boundary) Absorption of uranyl and uranous ions by organic and inorganic materials Dissociation of complexes as a result of changes in pH, Eh and partial pressure of carbon dioxide Evaporation of surface and ground waters Mixing of surficial uranium- and potassium-bearing waters with deeper groundwater that had access to a source of vanadium Colloidal precipitation	ponding of groundwater	Uranium anomalism (U, U/Th, U^2/Th radiometric anomalies, carnotite occurrences) spatially associated with terrace calcretes; Geochemical anomalism; Hydro-geochemical anomalism; Highly elevated groundwater salinities			

Critical processes	Constituent processes	Targeting elements	Mappable features	Available supporting data#	GIS processing steps	Derived predictor maps*
Preservation	Preservation is counteracted by erosional forces in areas of uplift and / or recent re-adjustments in drainage and / or catchment parameters (in particular the hydraulic gradient) Calcrete-carnotite systems are dynamic systems that are prone to remobilization and redeposition Young(er) actively forming systems have better preservation potential than older fossil systems	Regions characterized by low relief, low hydraulic gradient and active and ongoing calcrete formation (lesser chance to erode uranium deposits); Regions where calcretes are dissected or truncated have much lower, or no, preservation potential with respect to surficial uranium mineralization; Calcretes are well preserved and / or actively being formed across much of the study area except for the Gascoyne region where calcretes are mainly fossil and actively being eroded	Topography; Hydraulic gradient; Paleo-valley morphology; Dissected or truncated, fossil calcretes	Calcrete map; WASANT paleo-valley map; GTOPO30 DEM		None

See Table 1 for details.

* Data represented by the predictor maps must: (a) be an unbiased sample of the area of interest; and (b) have uniform coverage of this area. Any departure from these ideal criteria inevitably results in a biased data set and all the inherent problems that stem from such bias.

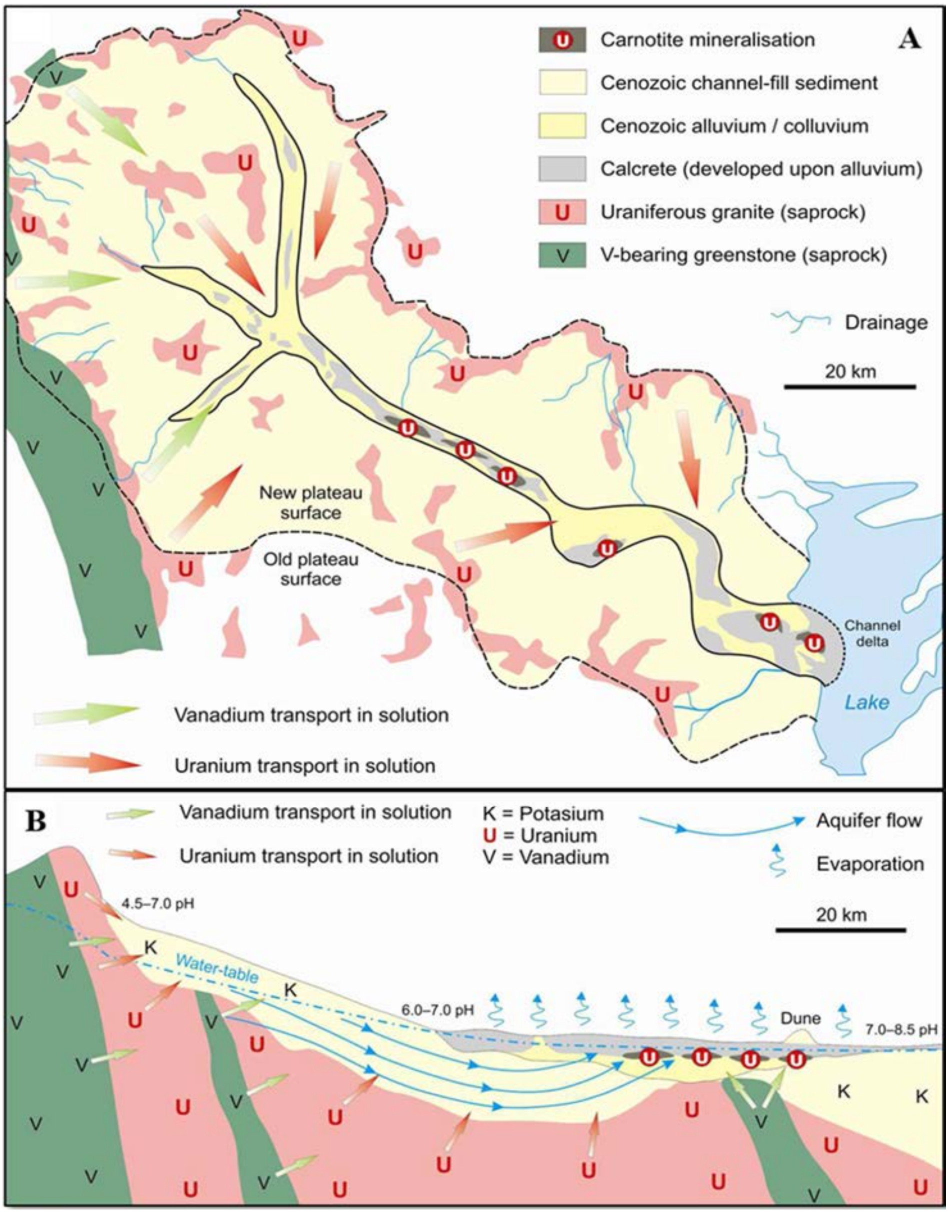

FIG. 21. Generalized model illustrating potential sources of and transport pathways for uranium and vanadium in calcrete-hosted valley-type uranium deposits of Western Australia, using elements of the Yeelirrie and Centipede/Millipede uranium deposits [111, 124]. A. Plan view. B. Cross-section. This figure is reproduced here with the permission of the International Union of Geological Sciences (IUGS) Publications Committee.

A weathering intensity index map (Fig. 24) developed by Geoscience Australia [132] provides more information about the degree of weathering of the regolith, and clearly delineates a series of retreating erosional scarps (Fig. 24: Inset Maps 1 and 2) characterized by low to moderate weathering intensity (green to yellow colors) and an older, more intensively weathered land surface (red and orange colors) above the scarps. The paleo-valleys lie below the scarps, receiving the erosional debris from up slope. The weathering intensity of the granitoids pictured in Fig. 24 is mixed, ranging from low to high.

The source of vanadium is more cryptic [133]. Most authors (e.g., [3, 77, 100, 124]) proposed that vanadium is extracted from pyroxene, hornblende and biotite contained in mafic to ultramafic igneous rocks such as present in Archean greenstone belts. In contrast to the strong spatial relationship between calcrete-hosted uranium occurrences and inferred granitic source rocks, the spatial relationship between the uranium occurrences and mafic to ultramafic igneous rocks is weak. When buffered to 2 km, outcropping and subsurface mafic to ultramafic igneous rocks only capture 51 out of 240 (or 21%) of the known calcrete-hosted uranium occurrences (Fig. 25). More importantly, some paleo-valleys and their catchments, most notably the one hosting Yeelirrie, do not contain any, or only small volumes of, mafic to ultramafic igneous rocks (Fig. 26). Given that the mafic to ultramafic greenstone belt successions commonly stand out very well in gravity and magnetic data and are of great interest to gold and nickel explorers it is unlikely that the area pictured in Fig. 26 contains any sizeable, hidden belts. The question then becomes whether the known volumes of mafic to ultramafic igneous rocks are sufficiently abundant and viable as a vanadium source. Alternative vanadium sources may be:

- Pyroxene, hornblende and biotite contained in granitoids [133];
- (Meta-)sedimentary rocks rich in magnetite, ilmenite or hematite, such as banded iron formations [77, 127];
- Ferruginous concretions in lateritic regolith [127]; or
- Sediment deposited within paleo-valleys and playa lakes [79]. For example, vanadium concentrations in valley-fill sediment at the Centipede/Millipede calcrete-hosted uranium deposit are sufficiently high to explain the vanadium content of the carnotite ore contained in this deposit (Dr. Greg Shirtliff, Toro Energy Limited, personal communication, 2015).

Based on the evidence presented by the authors listed above, we consider iron-rich rocks (e.g., mafic to ultramafic volcanic rocks or BIFs) in weathered greenstone belt successions as the main source of vanadium in uranium deposits of the Western Australian calcrete-hosted uranium province, with proximity to greenstone belts employed in our models as the predictor map for vanadium source potential.

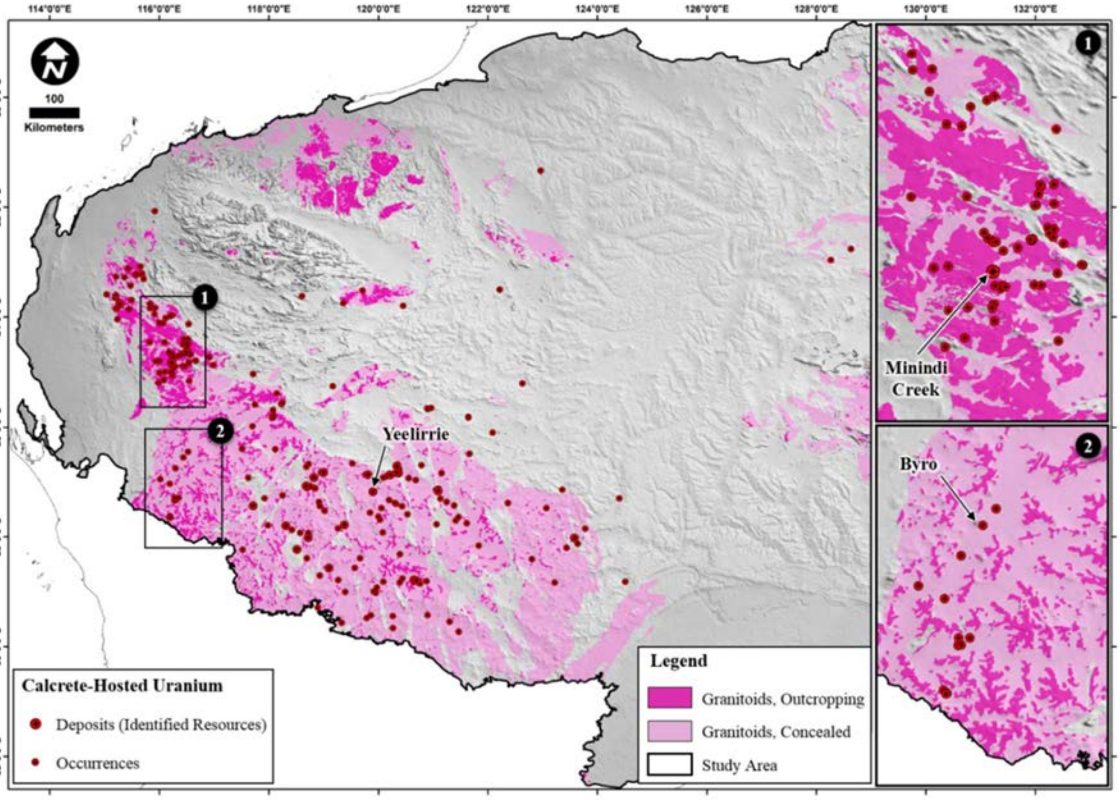

(a)

FIG. 22. Map of the study area illustrating (a) the distribution of outcropping and concealed granitoids, (b) the radiometric response of the outcropping granitoids, and (c) areas characterized by high to very high U^2/Th anomalism. Inset maps (labeled 1 and 2) show particular areas in greater detail. Overall, the maps serve to illustrate the strong spatial relationship that exists between the known calcrete-hosted uranium deposits and exposed or concealed granitoids. The maps also serve to illustrate that many of the granitoids are enriched with respect to uranium. Sand dunes in the central and western parts of the study area mask bedrock or regolith radiometric responses in many areas

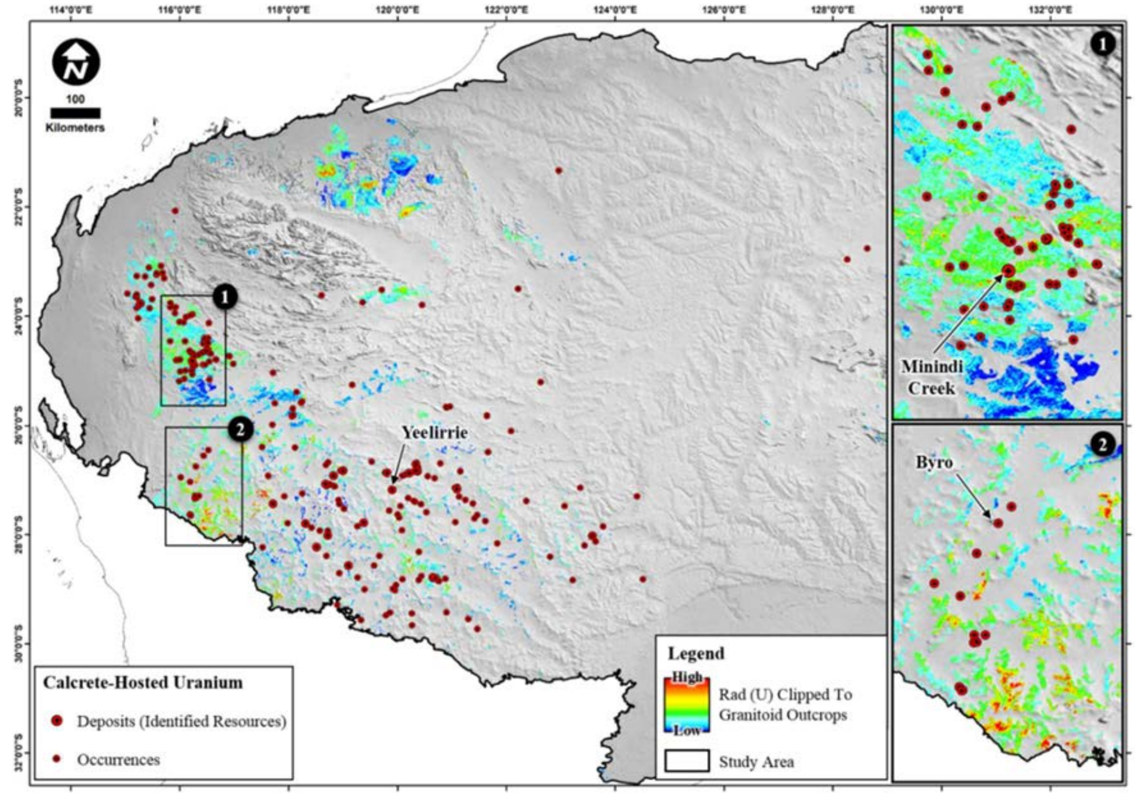

(b)

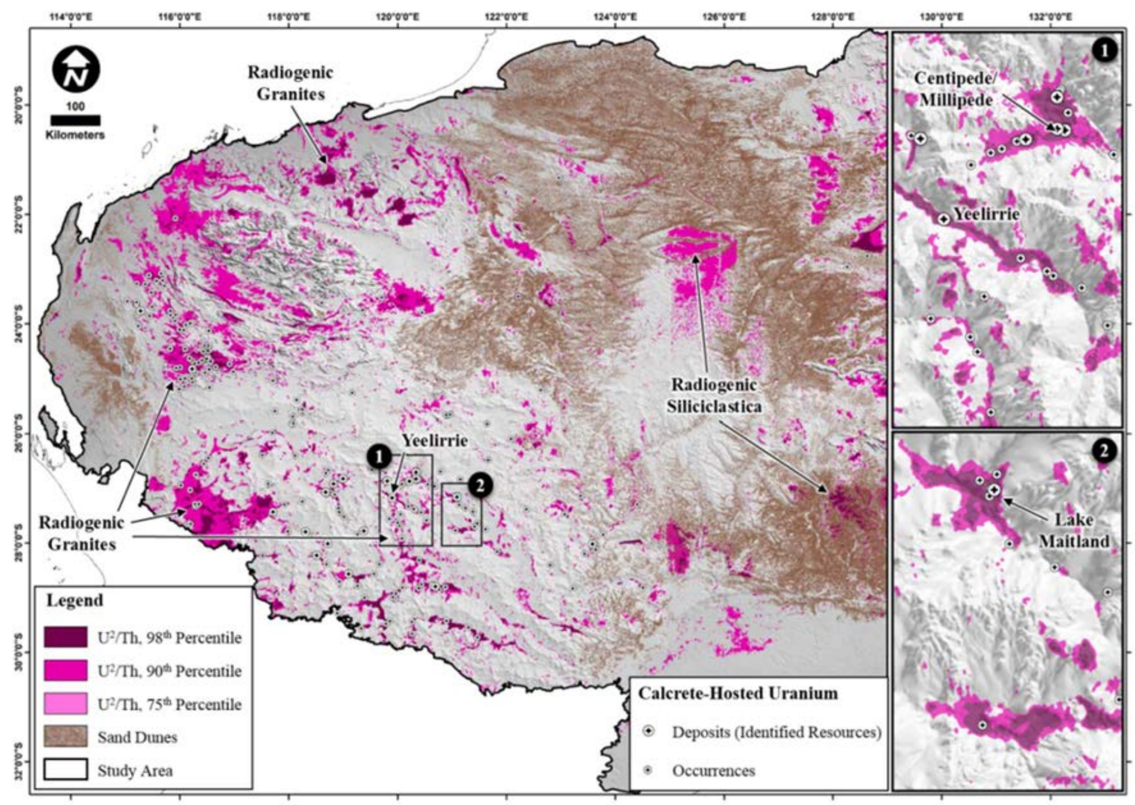

(c)

FIG. 22 (continued).

The most likely and widely available source of potassium in Western Australian calcrete-hosted uranium mineral systems are weathered granitoids. The Yeelirrie catchment is an excellent example of this relationship. Fig. 27 illustrates the location of the Yeelirrie uranium deposit and outcropping granitoids nearby. It also shows trails of potassium-enriched material emanating from the outcropping granitoids, which are also enriched in potassium compared to other geological and regolith units in the catchment area. This pattern can be interpreted in terms of potassium release from weathered granitoids exposed along erosion scarps (breakaways) and transport of the potassium-enriched debris down-slope and into the Yeelirrie drainage channel and paleo-valley-hosted groundwater system. Interestingly, the Yeelirrie deposit itself is marked by a prominent, 8 km-long potassium channel radiometric anomaly.

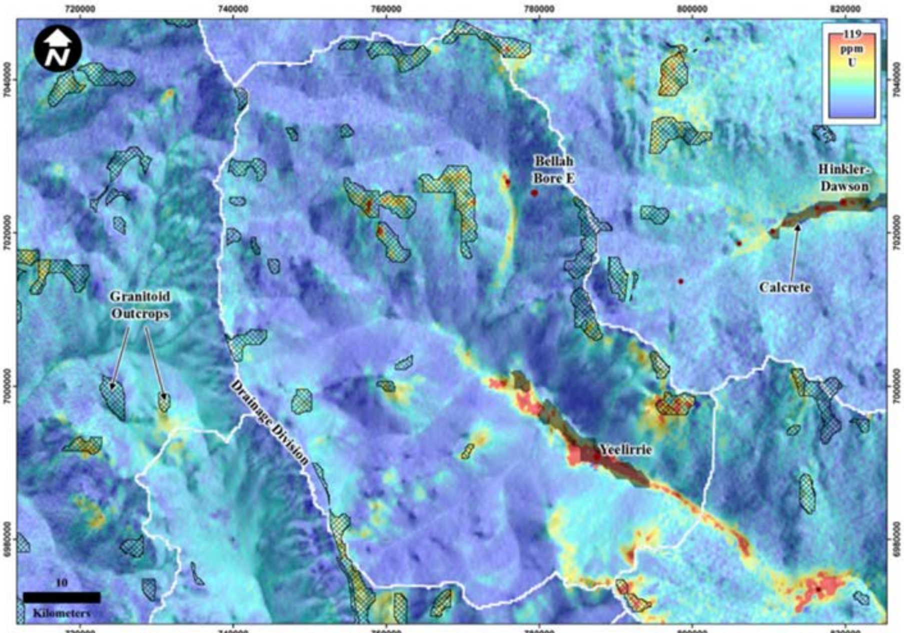

FIG. 23. Radiometric (uranium channel) map of the Yeelirrie area draped over a digital elevation model. The map also shows drainage divisions, granite outcrops and mapped calcretes. Some of the granitoids exposed upstream from the Yeelirrie calcrete-hosted uranium deposit, or in breakaways (erosional scarps) above the deposit, coincide with strong radiometric uranium channel anomalies indicating that they are enriched in uranium.

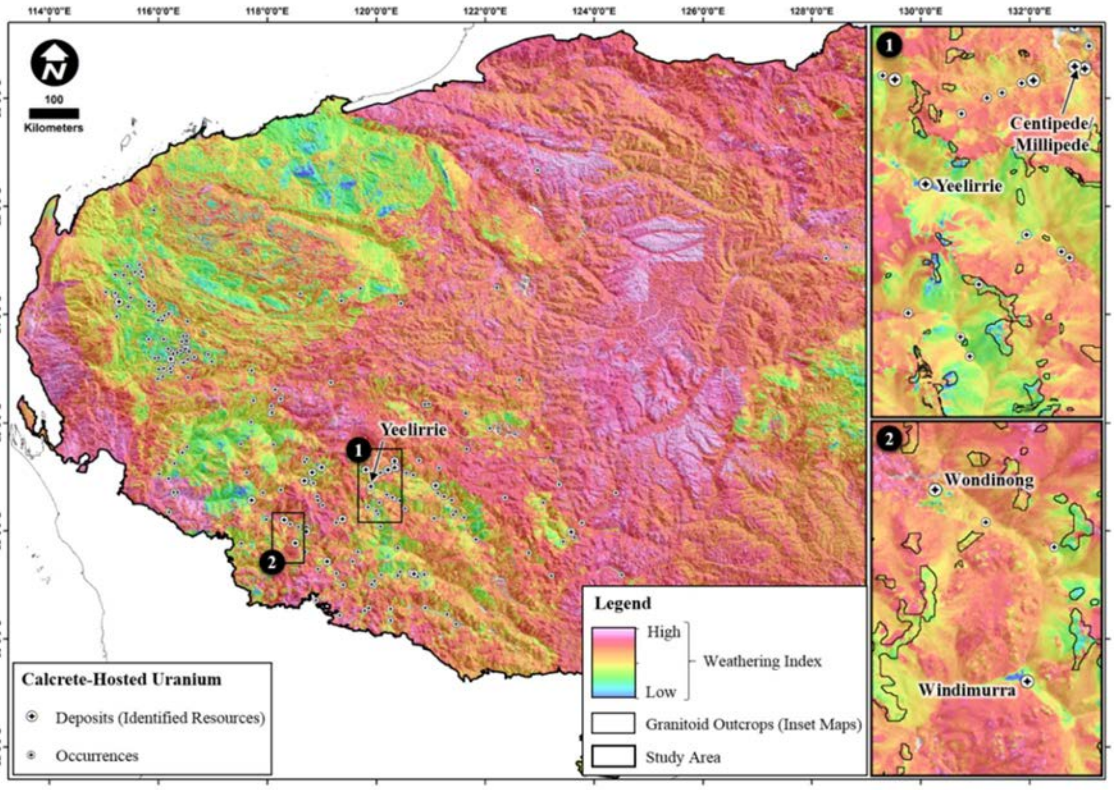

FIG. 24. Weathering intensity index map of Australia [132] clipped to the study area and draped over a digital elevation model. Inset maps 1 and 2 clearly illustrate granitoids outcrops along erosional scarps above paleo-valley systems in the Yeelirrie and Windimurra areas. Areas shown in Inset maps 1 and 2 that are dominated by red colors represent more weathered regolith of the 'old plateau' illustrated in Fig.s 10 and 20. Areas dominated by green and blue colors represent the least weathered materials exposed at the base of erosional scarps along the flanks of paleo-valleys.

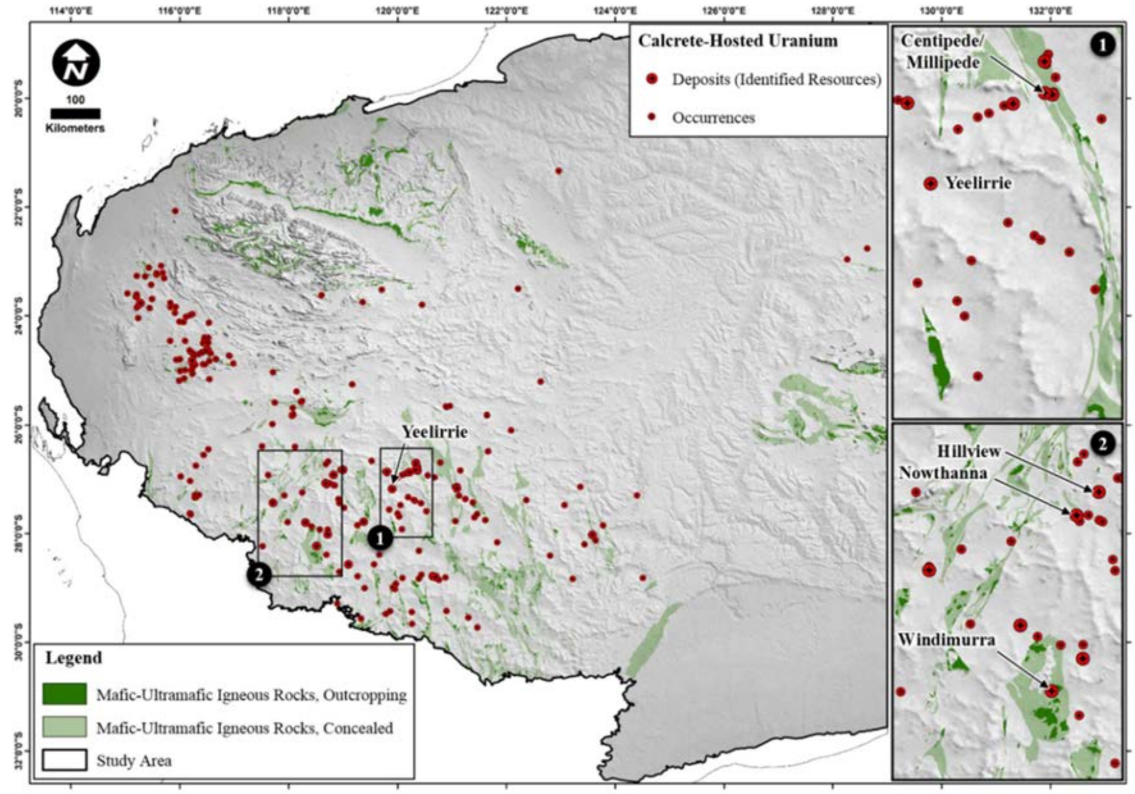

FIG. 25. Map of the study area showing the distribution of mafic- to ultramafic igneous rocks, both outcropping and concealed. Inset maps 1 and 2 provide more detailed representations of certain areas. Mafic- to ultramafic igneous rocks are considered potential vanadium source rocks.

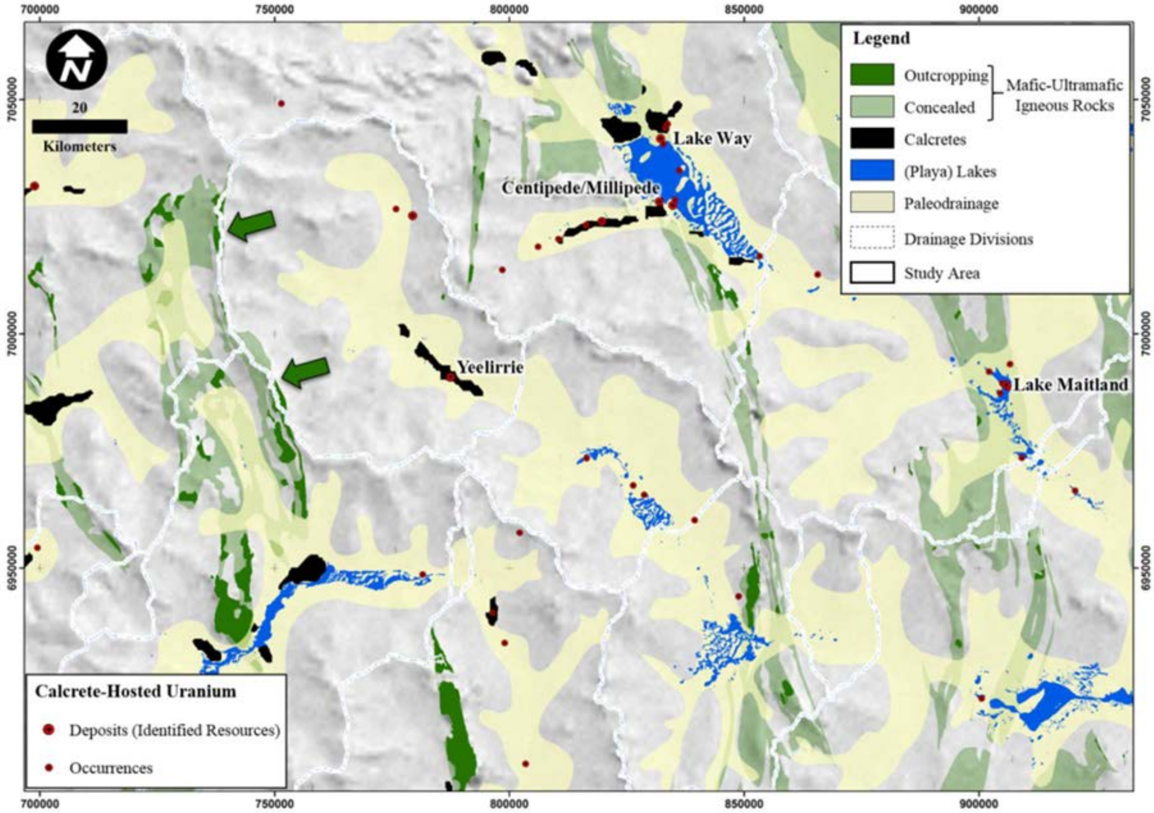

FIG. 26. Map of the greater Yeelirrie area illustrating the distribution of mafic- to ultramafic igneous rocks with respect to calcrete-hosted uranium deposits, calcretes, paleo-valleys and playa lakes. Some of the calcrete-hosted uranium deposits, such as Centipede/Millipede, Lake Way and Lake Maitland, illustrate a strong spatial association with linear belts of mafic- to ultramafic igneous rocks (i.e., Archean greenstone belts). However, no such relationship is obvious at Yeelirrie, the largest known deposit of its kind in Australia. Indeed, only a very small volume of mafic- to ultramafic igneous rock (green arrows) is contained within the Yeelirrie drainage compartment.

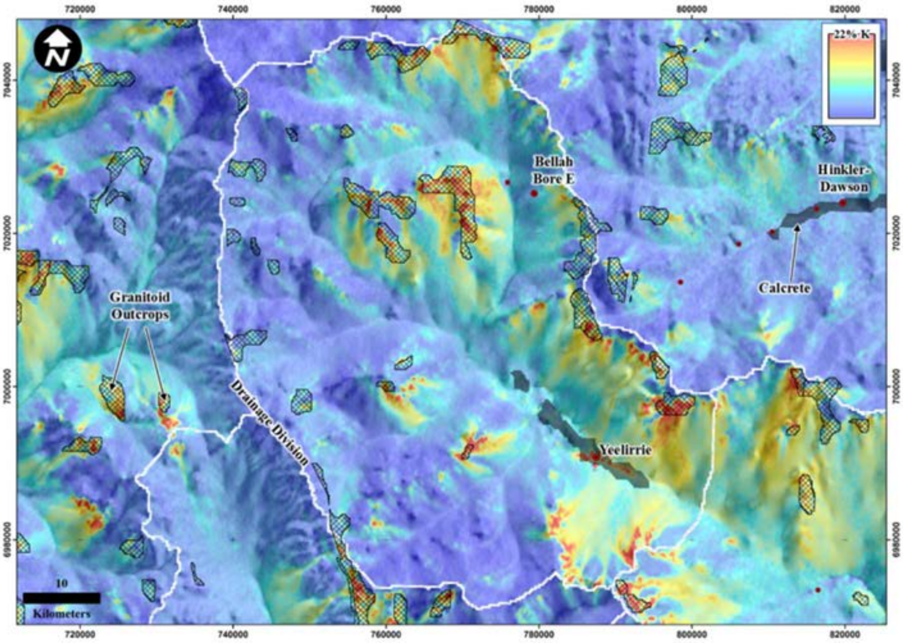

FIG. 27. Radiometric (potassium channel) map of the Yeelirrie area draped over a digital elevation model. The map also shows drainage divisions, granite outcrops and mapped calcretes. Most of the granitoids exposed in the catchment containing the Yeelirrie calcrete-hosted uranium deposit, or in breakaways (erosional scarps) above the deposit, coincide with strong radiometric potassium channel anomalies. Clearly evident in this map is what we interpret as potassium-rich erosional debris emanating from the granitoids and migrating down slope towards the paleo-valley. Also of interest is the potassium anomaly coincident with the Yeelirrie deposit. With carnotite, the main uranium ore mineral at Yeelirrie, being a potassium uranium vanadate, the strong potassium anomalism is not surprising but a geophysical signature of the deposit.

Metals are transported in oxidized groundwater as soluble complexes with their solubility depending on water pH and the availability of complexing ligands. Uranium is transported as either uranyl-carbonate complexes in alkaline, or uranyl-sulfate complexes in acidic fluids. Similarly, vanadium is transported in the form of vanadium-sulfate complexes. The availability of carbonate and sulfate anions for complexing uranium and vanadium was captured by calculating proximity to carbonate- and gypsum-bearing rocks and sediments.

3.8.2. *Mappable transport processes*

The main carnotite ore components (uranium, vanadium, potassium) are extracted from their sources (particular rock types, valley-fill sediment, or the regolith) by:

- Abundant surface water available after occasional rainfall (e.g., during the Western Australian cyclone season from November to April) running off into paleo-valleys, and taking up uranium, potassium, or vanadium from weathered granitic or mafic- to ultramafic igneous rocks in its path (e.g., rocks exposed in erosion scarps above paleo-valleys, or rock debris trails emanating from scarps); or
- Groundwater interacting with fractured, deeply oxidized rock.

In both cases, the leached ore components end up in shallow aquifers centered upon the paleo-river systems, and ultimately in aquifers associated with the playa lakes these river systems enter. They are the main pathways for the transport of the dissolved ore components by groundwater, with the playa lakes representing regional sinks. Detailed compilations exist of all mapped and interpreted paleo-valley and playa lake systems in Western Australia (Figs. 1 and 10), South Australia and the Northern Territory [109].

The characteristics and geochemistry of the groundwater and playa lake aquifers are complex, and the compositions of these waters play a major role in how the various ore components remain in solution [79]. While the geochemistry of the groundwater can be determined at the local scale, there are currently insufficient data available at the regional scale.

3.8.3. Mappable trap processes

Carnotite precipitation is caused by physico-chemical changes (e.g., Eh, pH, and pCO_2) affecting groundwater chemistry, and as a consequence the solubility of the uranyl and vanadium complexes carried by these waters. As outlined below, physico-chemical changes are strongly climatically controlled, although physical factors such as paleo-valley architecture (e.g., basement constrictions, drainage confluences) are also important.

As indicated by their name, calcrete bodies are typical components of calcrete-hosted uranium deposits. According to [87] and [89], groundwater calcretes form in shallow aquifer systems in predominantly arid to semi-arid climate zones where large volumes of sediments within these aquifers may be cemented, displaced or replaced by non-pedogenic carbonates. Precipitation of calcium carbonate ($CaCO_3$) in such environments is promoted by any processes affecting $CaCO_3$ solubility, which can be disturbed by the addition of carbon dioxide (CO_2) or calcium (Ca^{2+}), or the removal of hydrogen oxide (H_2O), as triggered by [86, 87]:

- Evaporation (removal of H_2O due to groundwater vaporization);
- Evapo-transpiration (removal of H_2O due to evaporation and plant transpiration);
- CO_2 degassing (removal of CO_2 due to increasing water temperature or pH);
- Common ion effect (addition of Ca^{2+} to the original solution due to fluid mixing, gypsum dissolution or fluid interaction with calcareous matter);
- Organic activity (removal of CO_2 by microorganisms).

Carbonate precipitation can be triggered by a range of mechanisms with the degree of evaporation, evapo-transpiration, biological activity, and to a lesser extent the degree of degassing, all being strongly climatically controlled [87], and most intense in arid climate zones such as encapsulated by the study area. Recent climatic expressions can be mapped. Australian climate records are readily available from the Bureau of Meteorology (Figs. 18–19) and other sources (Table 1). The main limitation of these data is that they reflect the climate of the last couple of decades rather than the past climate at the time of carnotite deposition. However, the uranium mineralization in Western Australian calcrete-hosted uranium mineral systems is very young ranging in age from Pleistocene (<700,000 years) to Recent, and both the carnotite and host groundwater calcretes are still actively forming, dissolving and re-precipitating today [79, [94, 110, 111]. Hence, the present climate may serve as an acceptable proxy for the climate of the recent geological past.

According to [87], the main controls on the location of groundwater calcrete formation are:

- Groundwater upwelling at basement highs brings this groundwater closer to the surface, facilitating increased degassing, evaporation and evapo-transpiration bringing about changes in the partial pressure of dissolved CO_2, groundwater pH, oxidation potential (Eh) of groundwater and redox state of soluble vanadium (V^{4+} oxidizes to V^{5+}) [134];
- Mixing of calcium or magnesium bicarbonate-bearing waters with calcium or magnesium sulfate-bearing, or chlorite-rich, playa groundwater, promoting precipitation due to the common ion effect; or
- Where drainages converge, flow gradients decrease, saline waters mix, or permeability is low.

Apart from the locations where paleo-valleys enter into playa lakes, or where drainages converge (Fig. 10), none of the above controls are readily mappable at the regional scale and/or in two dimensions. However, at the local scale, and given the availability of relevant, more detailed datasets (e.g., high resolution magnetic or electromagnetic, LIDAR, ASTER, hydro-geochemical assay, or regolith mapping data), it should be possible to map at least some of the controls listed above.

3.8.4. Mappable deposition processes

As is the case for most mineral systems, depositional processes are commonly not mappable at the district to regional scales, which typically are the scales at which prospectivity modeling (and predictive targeting) is undertaken.

Radiometric data analysis would be an obvious tool for identifying potential sites of carnotite deposition (e.g., U^2/Th ratio anomalies coincident with mapped calcrete) but, in the context of prospectivity modeling, radiometric data are generally more useful for defining and assigning weights to fertile source rocks. In addition, the relatively high false positive rate (proportion of radiometric uranium channel anomalies that do not coincide with uranium deposits) of this analysis may introduce significant bias.

Another obvious tool is groundwater geochemistry. For example, [79] demonstrated that hydro-geochemistry and particularly the calculation of a carnotite saturation index (a direct measure of the potential for the formation of calcrete-hosted uranium deposits) are effective tools for uranium exploration. The carnotite saturation index (SI) can be defined as (e.g., [79, 124, 134]):

$$SI = \frac{[K^+][UO_2^{+2}][H_2VO_4^-]}{[H^+]^2 K_{S.P.}} \qquad (2)$$

where $K_{S.P.}$ is the solubility product of carnotite, and [124] used a value of $10^{-6.85}$. This index would be highly relevant to prospectivity modeling if sample data existed at relatively even spacing for the entire study area. Unfortunately, the data are clustered and currently only available for ~150,000 km^2 area of the northern Yilgarn Craton.

3.8.5. Mappable preservation processes

The paleo-river system within the study area is well developed and well preserved with dynamic groundwater systems being active in the central part of the study area. The uranium mineralization in Western Australian calcrete-hosted uranium mineral systems is very young ranging in age from Pleistocene (<700,000 years) to Recent, and both the carnotite and host groundwater calcretes are still actively forming, dissolving and re-precipitating today [79]. As such, there are no obvious problems regarding the preservation of these systems, at least not to the east of the Meckering Line (Fig. 14). To the west of this line, paleo-river systems have been rejuvenated [112], which resulted in the fossilization of the groundwater calcretes in this region as they are now positioned well above the groundwater aquifers, and active erosion of previously formed calcrete-hosted uranium deposits. Fig. 28 illustrates how the rejuvenated river valley at Minindi Creek cuts mineralized terrace calcrete bodies exposed in the valley shoulders.

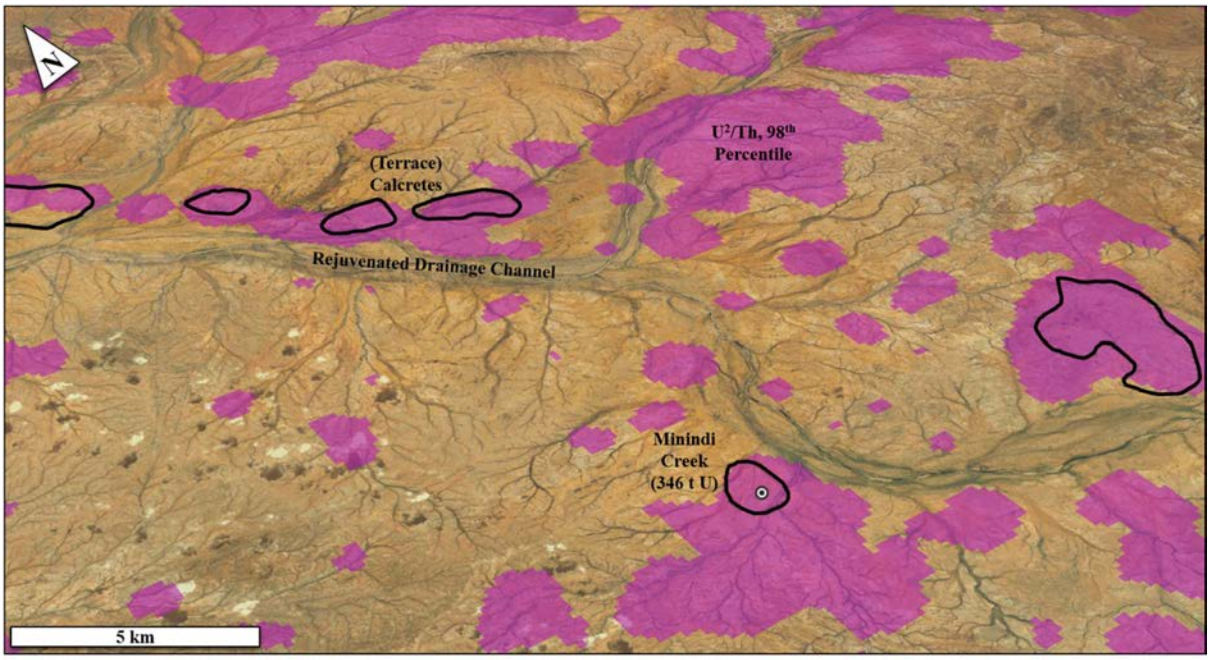

FIG. 28. Oblique Google Earth view of the Minindi Creek area, looking to the northeast. Minindi Creek is a fossil calcrete-hosted uranium deposit hosted by terrace calcretes. These calcretes are now well above the current groundwater table and dissected by the current, rejuvenated drainage. Pink domains represent 98th percentile U^2/Th ratio radiometric anomalies that are spatially coincident with both mineralized calcretes and radiogenic basement rocks.

3.9. Exploration

3.9.1. Discovery history

In February 1972, Western Mining Corporation Limited announced the discovery at Yeelirrie of the first and highest-grade calcrete-hosted uranium deposit worldwide. Subsequent resource definition drilling confirmed the discovery and formed the basis of an initial resource estimate of ~46,000 t U_3O_8 @ 0.15% U_3O_8 [101, 135].

The Yeelirrie discovery was the culmination of an exploration program by Western Mining Corporation Limited targeting sandstone-hosted uranium deposits in the extensive Tertiary paleo-valley systems of Western Australia. The program commenced in 1968 utilizing new regional airborne radiometric total count data acquired by the Australian Bureau of Mineral Resources over parts of the Yilgarn Craton. In 1969, Western Mining Corporation Limited detected a strong uranium anomaly at Nowthanna that was drilled in 1970, identifying traces of carnotite and pointing toward a near-surface mechanism for concentrating uranium in calcrete. Also in 1970, Western Mining Corporation Limited followed up total count anomalies in the Yeelirrie area. It was at that stage that the exploration team discovered outcropping ore-grade mineralization at what is now known as the Yeelirrie calcrete-hosted uranium deposit. The first auger holes into the Yeelirrie deposit were drilled in 1971. The subsequent announcement in 1972 of the Yeelirrie discovery triggered intensive exploration activity across the Yilgarn Craton and beyond, and resulted in the discovery of many additional calcrete-hosted uranium occurrences [73, 135]. Permission to mine Yeelirrie was refused in 1983 under the Australian Government's 'Three Mines Policy' that limited Australian uranium production for much of the 1980s and 1990s (Fig. 29).

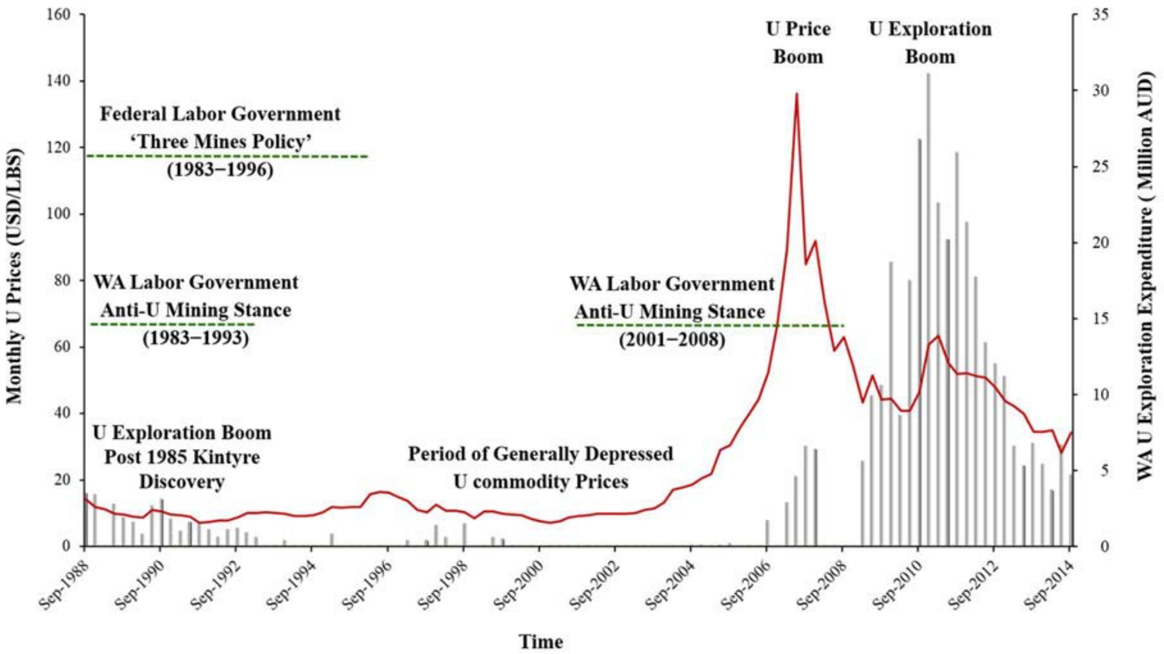

FIG. 29. Graph illustrating uranium commodity prices and Western Australian uranium exploration expenditures for a 26-year period from September 1988 to 2014. See text for a more detailed discussion. Western Australian exploration expenditures were sourced from the Australian Bureau of Statistics (http://www.abs.gov.au/); monthly uranium commodity prices were taken from IndexMundi (http://www.indexmundi.com/).

3.9.2. Uranium exploration and development activities in the study area

Little exploration was undertaken in Western Australia for calcrete-hosted uranium deposits between 1984 and the uranium commodity price boom of the mid- to late 2000s. The surge in uranium commodity prices triggered renewed exploration interest and investment, a situation that accelerated in the late 2000s after a change in state government saw the end of the uranium mining ban in Western Australia (Fig. 29). However, most of the attention was on re-evaluating historic and defining JORC-compliant [136] resources with no new calcrete-hosted uranium deposits of note having been discovered since.

None of Western Australia's calcrete-hosted uranium deposits have been mined. The main reasons for this situation have their roots in issues related to technical aspects [83, 108], politics and investor sentiment (Fig. 29), including:

- Project economics being hypersensitive to uranium commodity prices, which have been generally depressed, or falling, for most of the 1990s and early 2000s, and again since 2011;
- The metallurgy of Australian calcrete-hosted uranium deposits being difficult and complex;
- The projected costs of developing (CAPEX) and processing (OPEX) Australian calcrete-hosted uranium deposits being high;
- A 25-year period from 1983 to 2008 of recurring uranium mining bans imposed by the Western Australian and Federal Labor governments.

The only Australian calcrete-hosted uranium projects of sufficient size and grade that are likely to be developed in the medium-term are Yeelirrie (currently owned by Cameco Corporation) and Wiluna (currently owned by Toro Energy Limited). The latter is an aggregate of deposits, including Centipede/Millipede, Lake Maitland, Lake Way and others (Fig. 30).

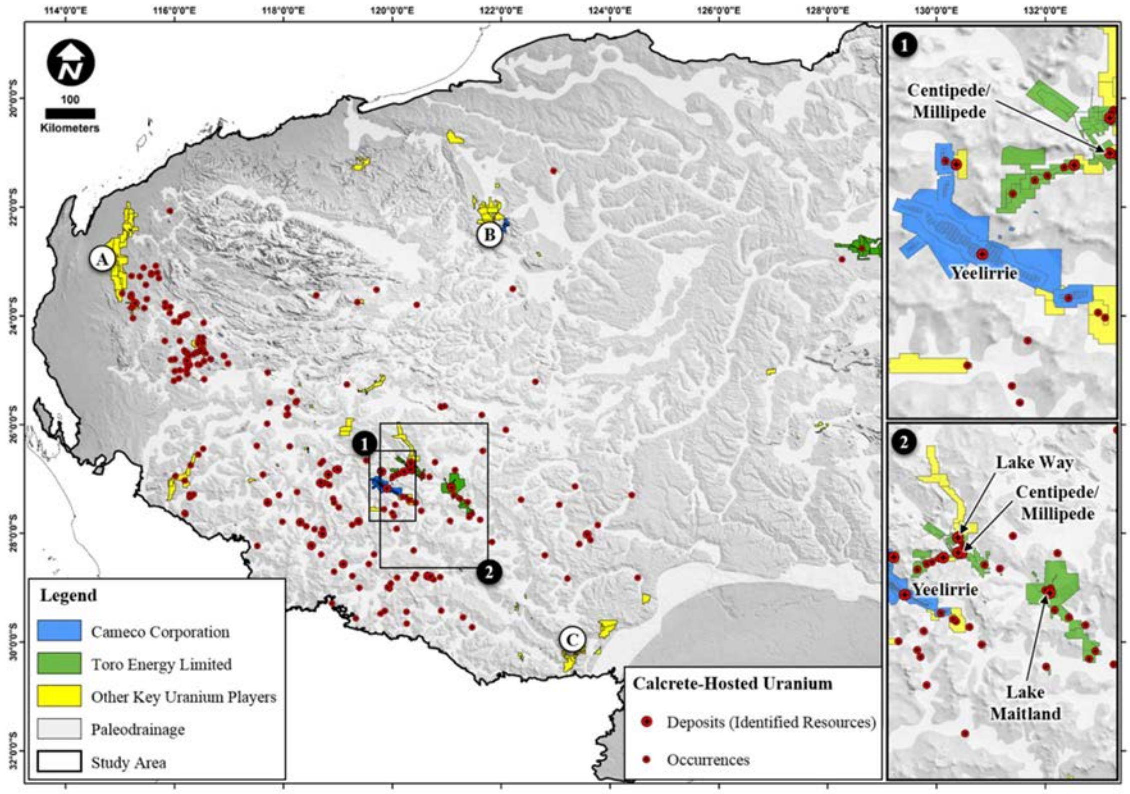

FIG. 30. Map of the study area illustrating current tenement blocks held by the main uranium players. The two largest projects covering calcrete-hosted uranium deposits are the Yeelirrie project (Cameco Corporation) and the Wiluna project (Toro Energy Limited). The latter includes a cluster of deposits, containing Centipede/Millipede, Lake Maitland and Lake Way. Other significant uranium projects are marked A to C and include the Manyingee sandstone-hosted uranium deposit (A) held by Paladin Energy Limited, the vein-hosted or unconformity-related Kintyre uranium deposit (B) held by Cameco Corporation, and the sandstone- and lignite-hosted Mulga Rock uranium deposit (C) held by Vimy Resources Limited.

3.9.3. Historic exploration activities recorded in the study area

Compilation of historic exploration activities is a very important step in developing a better understanding of the spatial distribution of such activities and helping to identify areas that appear to be under-explored. As discussed by [15], the distribution of exploration activities and related expenditures essentially serve as a spatial measure of prospectivity as perceived by mineral exploration companies.

The study area encapsulates a region of Western Australia that is extremely well endowed with respect to gold (e.g., Telfer, Sunrise Dam), nickel (e.g., Mount Keith, Leinster), copper (e.g., Nifty, DeGrussa), iron ore (e.g., Tom Price, Mount Whaleback) and uranium (e.g., Yeelirrie, Kintyre), and contains hundreds of operating mines. As expected in such an environment, the region has had a long history of mining and exploration with certain areas having been explored in great detail. At present (October 2015), ~446,000 km^2 (or 26%) of the study area are under tenure (Fig. 31), held by various mining exploration companies. Considering both active and relinquished ('dead') tenements, ~1,328,000 km^2 (or 77%) of the study area have been under tenure in the past.

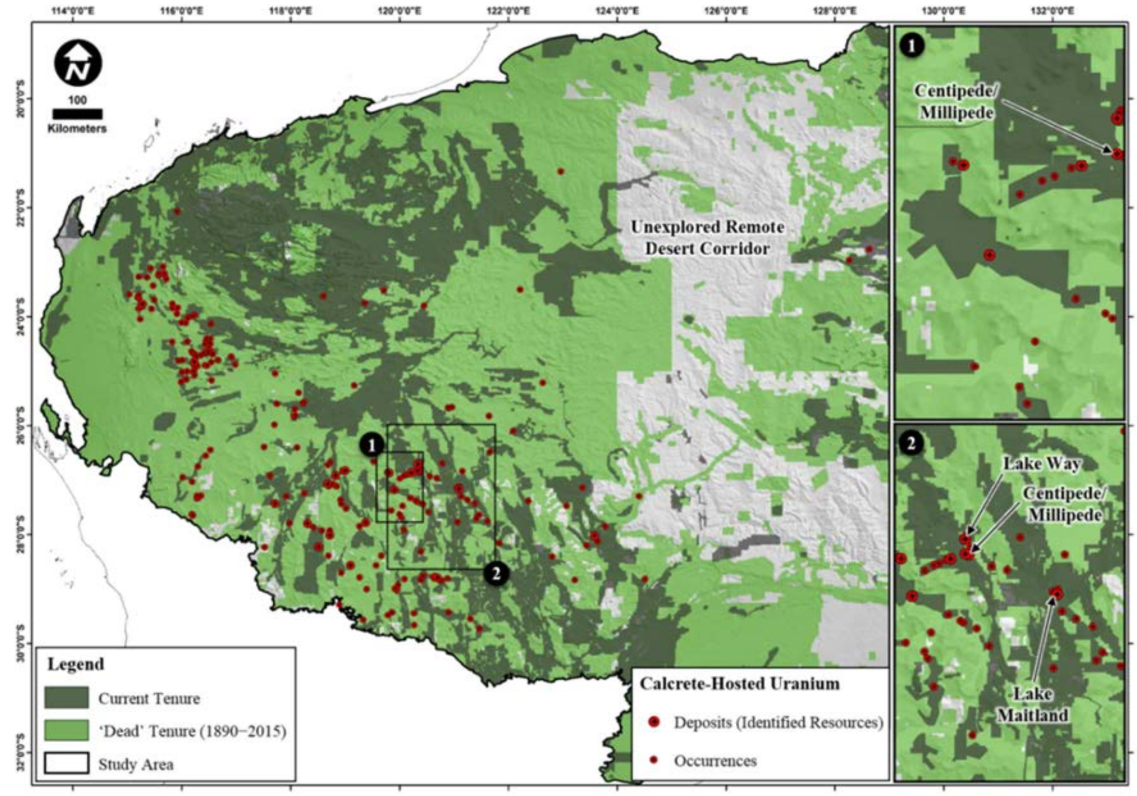

FIG. 31. Map of the study area illustrating the current tenure plus all historic ('dead') tenure for the period 1890 to 2015. Dead tenure includes tenements that have been relinquished or forfeited and tenement applications that have been withdrawn or rejected. Most of the study area was under tenure in the past or was deemed interesting enough as to warrant lodgment of an application. The exception is a narrow remote desert corridor in the western part of the study area that to date remains largely unexplored.

Fig. 32 is a representation of the relinquished tenure clipped to the Tertiary paleo-valleys and categorized according the number of overlapping dead tenements. In a crude way, the map illustrates that the number of overlapping dead tenements is generally greater at and/or in the vicinity of the known deposits. However, using Yeelirrie as an example (Fig. 32: Inset Map 1), this relationship does not necessarily hold for the entire study area as the Yeelirrie tenement block had no turnover because it was never relinquished. More importantly, the map clearly highlights that parts of the extensive paleo-drainage system have never been subjected to any exploration at all, and thus can be considered virgin greenfields territory.

Fig. 33 shows all tenements within the study area where uranium was reported as a target commodity. The underlying information, which was compiled by the Geological Survey of Western Australia, is based on open-file reports lodged with the survey between 1960 and 2013 that stated uranium as a target commodity. It is important to note, however, that this list of tenements with a uranium focus may be incomplete due to ongoing data compilation by the Geological Survey of Western Australia. The ~584,000 km^2 covered by the tenements shown in Fig. 33 account for 34% of the study area and capture 232 (or 97%) of the 240 identified calcrete-hosted uranium occurrences (Appendix). Importantly, the entire eastern part of the study area has only received minor attention from uranium explorers.

Fig. 34 illustrates the location of selected exploration activities as compiled by the Geological Survey of Western Australia from open-file reports, clipped to the Tertiary paleo-drainage system. Unfortunately, this compilation is by no means complete yet given the sheer amount of data to be gathered and verified. However, the Geological Survey of Western Australia's exploration activity database serves as an excellent tool for a first pass evaluation of what types of exploration activities have been undertaken and where.

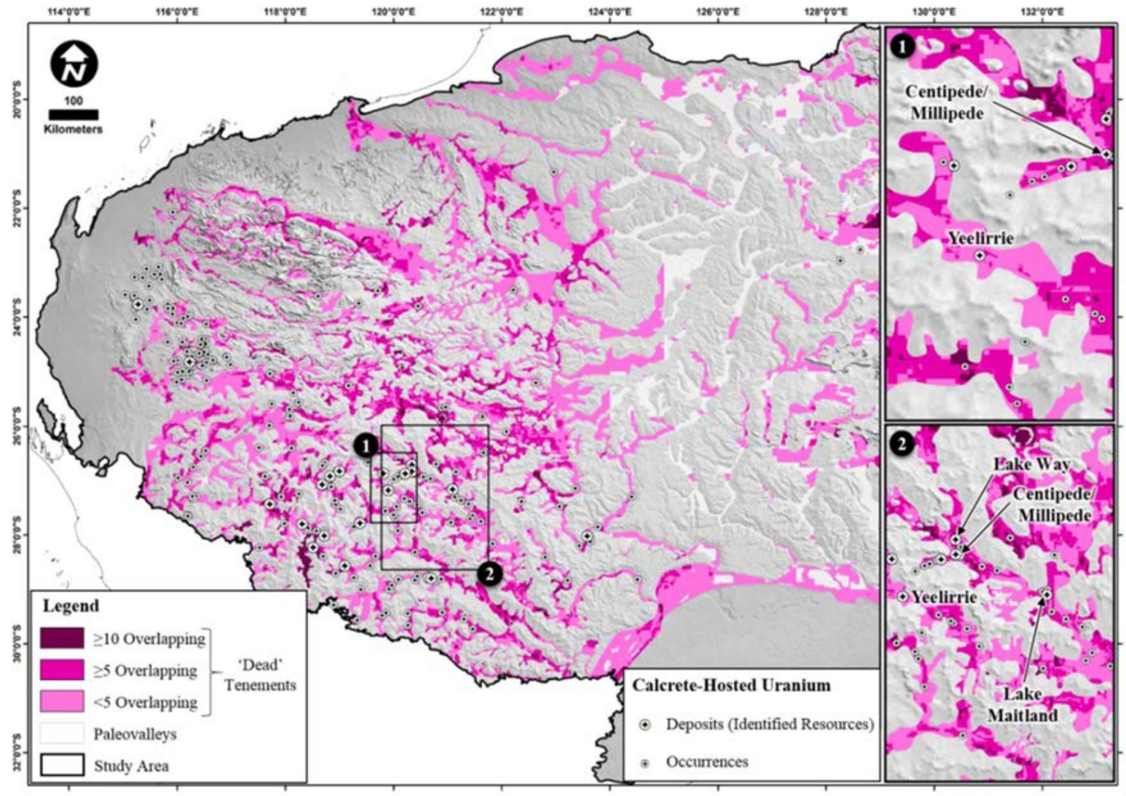

FIG. 32. Map of the study area illustrating the historic ('dead') tenure clipped to the paleo-valleys and categorized by number of overlapping tenements. This map highlights paleo-valley sections that, for example, have never been explored or that have been under tenure many times.

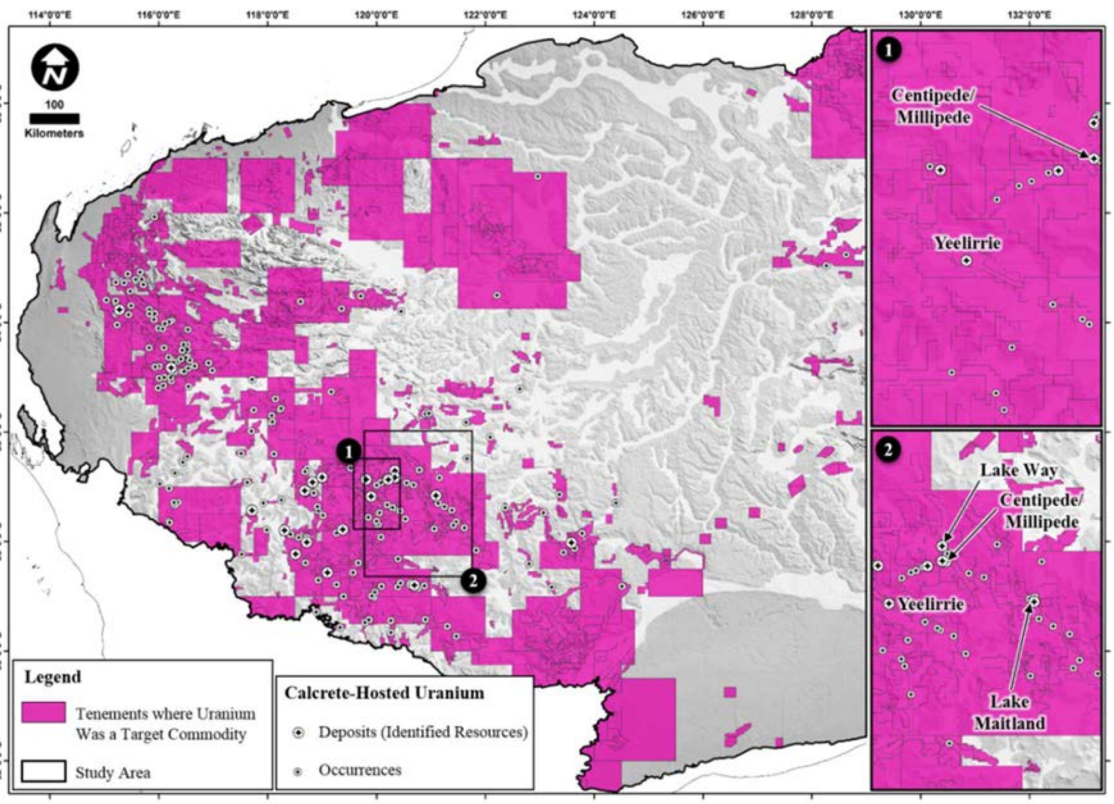

FIG. 33. Map of the study area illustrating all tenements where uranium was reported as a target commodity. The underlying information, which was compiled by the Geological Survey of Western Australia, is based on open-file reports lodged with the survey between 1960 and 2013 that stated uranium as a target commodity. As illustrated by inset maps 1 and 2, the very well-endowed Yeelirrie and Wiluna areas have been covered comprehensively. The eastern part of the study area, however, has not received much interest at all from uranium explorers with large tracts being virgin territory with respect to uranium exploration.

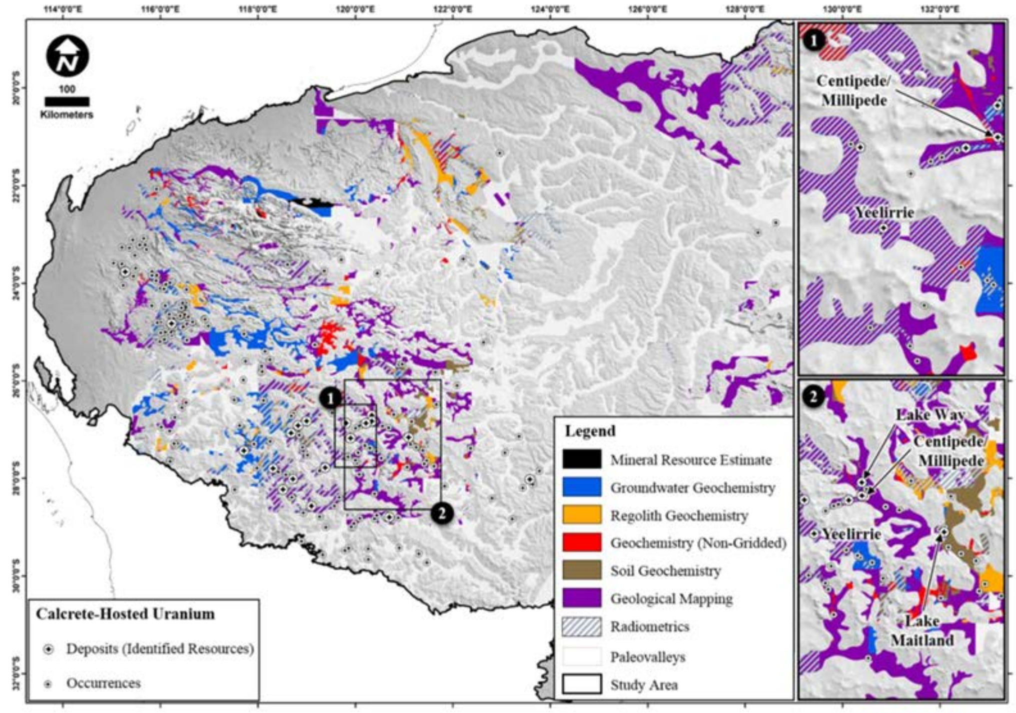

(a)

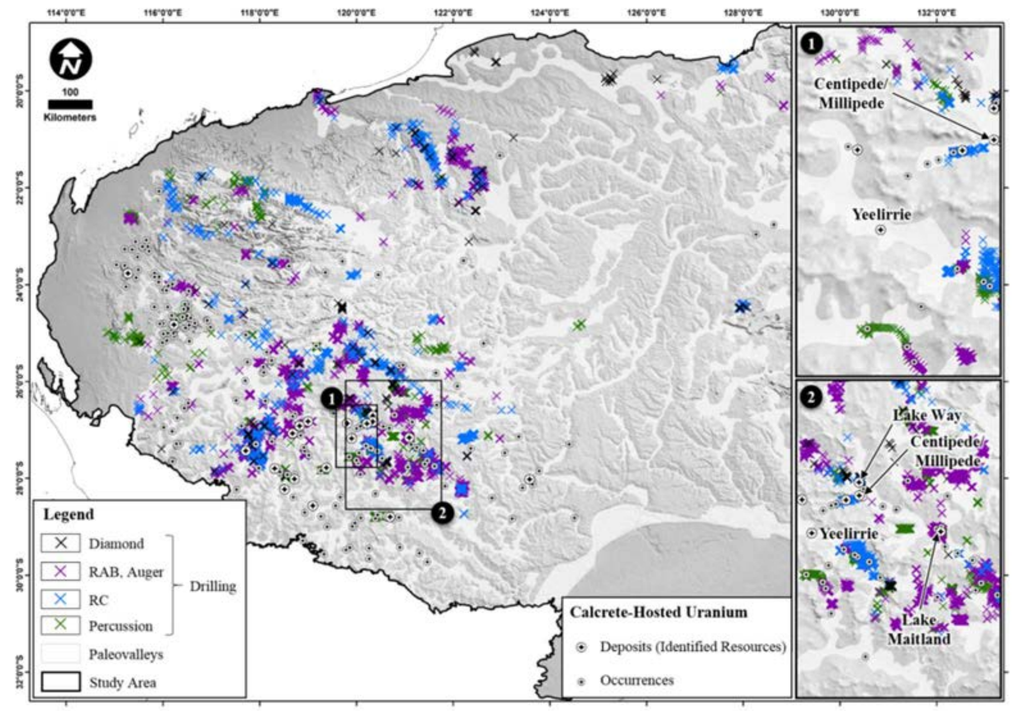

(b)

FIG. 34. Map of the study area illustrating selected exploration activities in areas overlapping with the paleo-valleys. A. Areas of mineral resource estimates, geological mapping and geochemical and geophysical activities. B. Areas of drilling activities. It is important to note though that these datasets are incomplete due to ongoing data compilation by the Geological Survey of Western Australia. Nevertheless, the map serves as an excellent tool for a first pass evaluating of what types of exploration activities have been undertaken and where.

4. MINERAL PROSPECTIVITY ANALYSIS

This study adopted a three-pronged approach to prospectivity modeling of surficial uranium mineral systems, employing a knowledge-driven FIS model and data-driven WofE and ANN models. These approaches are mutually exclusive because the model parameters are estimated using fundamentally different algorithms. In the three-pronged approach developed and tested in this study, the knowledge-driven FIS model was implemented first so as to avoid bias that may be introduced by learning the outcomes of the data-driven WofE and ANN models. The rationale for employing a three-pronged approach was not only to guarantee most advantageous utilization of the available conceptual and empirical information but also to investigate and understand possible consequences of stochastic and systemic uncertainties in the derived prospectivity maps and to employ this understanding to formulate informed decisions regarding the relative importance of exploration targets.

4.3. Theoretical background

4.3.1. Fuzzy Inference Systems (FIS)

As described by [45], at the core of a FIS sits the theory of fuzzy sets [137]. Unlike the membership of a binary set, the membership of a fuzzy set varies from 0 to 1. A key feature of the FIS approach is that the underlying fuzzy sets are labeled by way of a linguistic value. 'Proximity to granite', for example, is a fuzzy set of all pixels in a GIS-based model that are 'close' to granite. All pixels in a given image dataset are members of this fuzzy set, although the level of membership vary in the range [0, 1]. The fuzzy membership value portrays the level of truth that a given pixel is 'proximal to a granite' or not. A pixel encapsulating granite would have a membership value of 1 (definitely proximal) while a pixel that is located, say, 100 km from the nearest granite body would have a membership value of 0 (definitely not proximal). A fuzzy membership function is used to convert a certain pixel value to a fuzzy score bound by 0 and 1.

Formally, if X is a set whose elements are x then a fuzzy set $A^{\sim}$in X is a set of ordered pairs:

$$A^{\sim} = \{(x, \mu\_A^{\sim}(x) | x \in X)\} \tag{3}$$

where $\mu\_A^{\sim}$ is the membership function (degree of truth, or degree of compatibility) of x in $A^{\sim}$. The fuzzy set $A^{\sim}$ becomes a classical set if its membership value is constrained to either 0 or 1.

A FIS consists of a set of if-then rules in a natural language depicting an expert's conceptual logic for predicting the state of a system according to a mixture of conditions portrayed in terms of linguistic variables. A FIS can be employed to encapsulate an exploration geologist's deductive logic of predicting mineral prospectivity from a synthesis of linguistic predictor variables. Each of the linguistic values in an if-then rule is the label of a fuzzy set in which the degree of membership of relevant data is assessed according to a predefined membership function. Several sets of such fuzzy if-then rules portraying mineral prospectivity of the input spatial proxies in linguistic terms (e.g., low, moderate, high) are integrated in a FIS. The application of individual rules results in fuzzy values that are synthesized using a suitable fuzzy aggregation technique to obtain the FIS output. This output is a fuzzy area under the curve that is, however, defuzzified to facilitate its interpretation. This output is an estimate of the mineral prospectivity represented by a single number between 0 and 1 [45].

4.3.2. Weights-of-Evidence (WofE)

Bayes' equation provides the basis for estimating the a-posteriori belief in a hypothesis *H* regarding the occurrence of an event given the evidence *E* [138]. The equation relates the probability of the hypothesis *H* given the evidence *E* to the likelihood of the occurrence of *E* given that *H* is true. Bayes' model is, therefore, a generative model in the sense that it updates the a-priori probability of a hypothesis to its a-posteriori probability based on the likelihood of the hypothesis generating the given evidence. More formally,

$$p(H|E) = p(H) \times p(E|H)/p(E) \tag{4}$$

where: $p(H|E)$ is the posterior probability, $p(H)$ is the prior probability of *H* (i.e., the belief in H before the evidence E is considered), $p(E|H)$ is the likelihood of the evidence given the hypothesis, and $p(E)$, which is independent of H, is the marginal probability of the normalizing factor E.

Bayes' equation derives from the generalized product rule of conditionally dependent events. In its general form, it can be used to update the a-priori probability of a hypothesis sequentially as additional new evidences become available:

$$p(H|E) = \frac{p(H)\times p(E_1|H)\times\cdots\times p(E_n|E_n-1,\cdots,E_2,E_1)}{p(E_1)\times p(E_2|E_1)\times\cdots\times p(E_n|E_n-1,\cdots,E_2,E_1)} \tag{5}$$

However, the influence of each new evidence is conditional on all previously available evidence, which makes the problem non-deterministic in polynomial-time (or np hard). We can overcome this difficulty by assuming that all evidences are conditionally independent, in which case the multiple updating of a-priori probability using Bayes' equation reduces to:

$$p(H\Big|E_1, E_2, \cdots\cdots, E_n) = p(H)\prod_{i=1}^{n}\frac{p(E_i|H)}{p(E_i)} \tag{6}$$

For a spatial probabilistic modeling of the potential of a deposit-type D, probability in expressed in terms of odds:

$$O(D\Big|E_1, E_n, \cdots\cdots, E_n) = O(D)\prod_{i=1}^{n}\frac{O(E_i|D)}{O(E_i|\bar{D})} \tag{7}$$

where *D* and $\bar{D}$ indicate presence and absence, respectively, of the targeted deposit-type *D*. Taking the natural logarithms of both sides,

$$log_e O(D\Big|E_1, E_n, \cdots\cdots, E_n) = log_e O(D) + \prod_{i=1}^{n} log_e\frac{O(E_i|D)}{O(E_i|\bar{D})} \tag{8}$$

The posterior log of odds (or logit) of *D* is estimated from the prior logit of *D* modified by the presence of binary evidential maps E_i (i = 1 to n). A similar equation is used to estimate posterior log of odds of the targeted deposits, given the absence of E_i:

$$log_e O(D \left| \overline{E_1}, \overline{E_n}, \cdots\cdots, \overline{E_n} \right.) = log_e O(D) + \prod_{i=1}^{n} log_e \frac{O(\bar{E_i}|D)}{O(\bar{E_i}|\bar{D})}$$
(9)

The terms $log_e \frac{O(E_i|D)}{O(E_i|\bar{D})}$ and $log_e \frac{O(\bar{E_i}|D)}{O(\bar{E_i}|\bar{D})}$ are called, respectively, positive and negative weights-of-evidence, W^+ and W^-. The strength of spatial association of the targeted deposit-type and the evidential map E is quantified by Contrast (C), which is estimated as:

$$C = W^+ - W^-$$
(10)

A high positive contrast implies positive spatial association, while a high negative contrast implies negative spatial association. The Bayesian probabilistic model f for prospectivity modeling can be summarized as:

$$log_e O(D \left| E_1, E_n, \cdots\cdots, E_n \right.) = log_e O(D) + \prod_{i=1}^{n} W^{+/-}$$
(11)

In the above equation, the sign of W indicates the presence (+) or absence (–) of the predictor map. Finally, the updated posterior probability of the occurrence of the targeted deposits is calculated as:

$$p(D \left| E_1, E_2, \cdots, E_n \right.) = \frac{e^{loge[O(D|E_1,E_2,\cdots,E_n)]}}{1+e^{loge[O(D|E_1,E_2,\cdots,E_n)]}}$$
(12)

4.3.3. Artificial Neural Networks (ANN)

A type of nature-inspired machine learning algorithm, ANN obtains knowledge about diagnostic features of a data population by iteratively processing its samples (e.g., [28] [138]). Architecturally, ANN consists of several inter-connected computational layers of mathematical functions called neurons that functions to map every sample of an input feature vector in the training data to its output. The output may be a categorical class label (classification), or a continuous number (regression). Inter-neuron connection strengths known as synaptic weights control the mapping [139], and the synaptic weights are modified dynamically until every input feature vector is correctly mapped to its known output target vector. Therefore, synaptic weights are repositories of knowledge applied by a trained neural network for generalization beyond training data [139].

In the present study, we used a radial basis function based ANN, also known as radial basis functional link nets (RBFLN: [140]. A radial basis function centered on an N-dimensional feature vector v is defined on N-dimensional feature vectors x as follows:

$$y = e^{[-\frac{\|x-v\|^2}{2\sigma^2}]} \tag{13}$$

The response of a single radial unit represents a Gaussian function, peaked at the center of the feature vector and descending outwards. The term radial means that every point x equidistant from v returns the same value of y. A number M of radial basis functions can be centered on M feature vectors such that their circular disks occupy a delimited region of interest in the feature space. The values of a radial basis function comply with the constrain that $0 < y \leq 1$. A RBFLN (Fig. 35) is a three-layer feed-forward network comprising the following layers [140]:

— An input layer of N (number of variables or dimensions of feature vectors) neurons, each of which receives a component of input feature vector;
— A hidden layer of M neurons, each containing a radial basis function;
— An output layer of J (number of target vectors) neurons, which return the output for each input feature vector.

It implements the following composite mapping:

$$x \to y \to z \to t \tag{14}$$

where z and t are the output and target vectors, respectively.

For a training dataset with Q vectors, an incoming vector x from the input layer activates a neuron (radial basis function) in the hidden layer, which returns a unique value of y [141]:

$$y_m^q = e^{[-\frac{\|x^q - v^m\|^2}{2\sigma^2 m}]} \tag{15}$$

where v and σ are the center vector and spread parameter of the radial basis function and x is the training vector. The values of y are multiplied by synaptic weights along the lines connecting the neurons of the hidden layer to the neurons of the output layer and summed in the neurons of the output layer [141]:

$$z_j^q = \left(\frac{1}{M}\right) [\sum_{m=1}^{M} u_{mj} \times y_m^q + b_j] \leftarrow t \tag{16}$$

The synaptic weights, u, are modified dynamically to force the outputs z to match the targets t as closely as possible. The bias, b, is included at each neuron in the output layer.

A RBFLN was derived by [140] by extending the radial basis function ANN architecture to random vector functional link nets described by [142]. A RBFLN is a near-replica of radial basis function neural network but its main difference is that it has more lines of propagation that connect neurons in the input layer directly to neurons in the output layer (Fig. 35). Thus, A RBFLN realizes a composite mapping as follows:

$$\begin{tikzcd} & y \arrow[dr] & & \\ x \arrow[ur] \arrow[rr] & & z & t \arrow[l] \end{tikzcd} \tag{17}$$

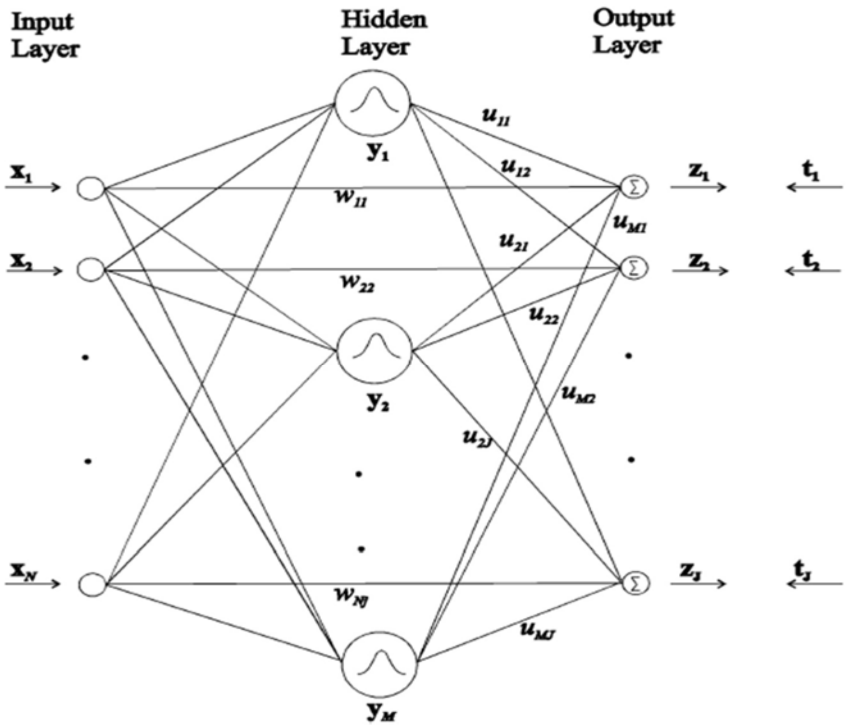

FIG. 35. Architecture of a radial basis function link net for mineral prospectivity modeling.

The lines that connect the *N* neurons in the input layer to the *J* neurons in the output layer bear an extra set of synaptic weights, *w* (Fig. 35). Evidently, RBFLNs are a generalization of radial basis function neural networks. When the extra weights, *w*, are set to zero, the two are the same. A radial basis function neural network is a nonlinear model whereas an RBFLN comprises that nonlinear model and a linear model (the direct lines from the input to the output nodes) as well so that the linear parts of a mapping do not need to be approximated by the nonlinear model. The RBFLN is therefore a more complete model of a general nonlinear mapping. The output of RBFLNs differs from that of radial basis function neural network, thus [141]:

$$z_j^q = \left(\frac{1}{M}\right)\left[\sum_{m=1}^{M} u_{mj} \times y_m^q + b_j + \sum_{n=1}^{N} w_{nj} \times y_n^q + b_j\right] \leftarrow t \tag{18}$$

where is$y_m^q = e^{[-\|x^q - v^m\|^2/2\sigma^2 m]}$.

For a training dataset with Q feature vectors and Q associated output target vectors, namely:

$$\{x_q : q{=}1,2,\ldots\ldots\ldots\ldots Q\} \text{ and } \{t_q : q{=}1,2,\ldots\ldots\ldots\ldots Q\} \tag{19}$$

a RBFLN is trained in the following stages [140, 141]:

— Centers, spread parameters and synaptic weights are initialized;
— Synaptic weights and spread parameter are adjusted to minimize the output total sum-squared error, which is the sum of partial sum-squared errors defined as:

$$E = \sum_{q=1}^{Q} E^q = \sum_{q=1}^{Q} \sum_{j=1}^{J} (t_j^q - z_j^q)^2 \quad (20)$$

The training on synaptic weights is via steepest descent iteration:

$$u_{mj} \leftarrow u_{mj} - \eta_1 \left(\frac{\delta E}{\delta u_{mj}}\right) = u_{mj} + (\eta_1/(M+N)) \sum_{q=1}^{Q} (t_j^q - z_j^q) y_m^q \quad (21)$$

and

$$w_{mj} \leftarrow w_{mj} - \eta_1 \left(\frac{\delta E}{\delta w_{mj}}\right) = w_{mj} + (\eta_1/(M+N)) \sum_{q=1}^{Q} (t_j^q - z_j^q) x \quad (22)$$

Every center and spread parameter is likewise updated with steepest descent iteration [141]:

$$v_n^m \leftarrow v_n^m - \eta_3 \left(\frac{\delta E}{\delta v_n^m}\right) = v_n^m + [\eta_3/\sigma_m^2] \sum_{q=1}^{Q} \{\sum_{j=1}^{J} (t_j^q - z_j^q) m_{mj}\} y_m^q (x_n^q - v_n^m) \quad (23)$$

and

$$\sigma_m^2 \leftarrow \sigma_m^2 - \eta_4 \left(\frac{\delta E}{\delta \sigma_m^2}\right) = \sigma_m^2 + [\eta_4/\sigma_m^4] \sum_{q=1}^{Q} \{\sum_{j=1}^{J} (t_j^q - z_j^q) m_{mj}\} [y_m^q \left\| x_n^q - v_n^m \right\|^2] \quad (24)$$

In the above equations, η are the learning rates. Using the full propagation method described by [143], the ANN is trained with the steepest descent iteration on the total sum-squared error, for all Q input feature vectors per iteration, so that individual adjustments per synaptic weight are affected by all Q input feature vectors.

The modeling of ANN is far more intricate than WofE. However, a well-trained ANN generally returns better results than WofE because it does not assume conditional independence of the input predictor maps. Training an ANN involves optimizing the network architecture, and estimating the optimal network parameters. The former involves estimating the optimal number, centers and spread parameters of the radial basis functions, while the latter involves estimation of optimal synaptic weights. The performance of a neural network is evaluated by the error in the classification of the training samples.

The training error reduces exponentially as the number of training iterations and hidden neurons increases [29]. However, as the number of training iterations increases, a specialized learning on the specific characteristics of the training samples sets in that leads to an over-trained network that is highly effective in classifying training samples, but fails to classify unseen samples. Therefore, it is imperative that an ANN should be trained only to the extent that they learn the general characters of the mineralized and barren population and not the specific traits of the training samples of the mineralized and barren populations.

For optimal performance, the number of radial basis functions in the hidden layer of a neural network must be sufficient enough to cover the entire feature space. This needs a large number of training samples, because each training sample forms the center of a radial basis function in the feature space. However, in practice, the number of training samples can never be large enough to cover the entire feature space. Extra radial basis functions are, therefore, drawn and centered randomly in the feature space, providing higher resolution and stronger non-linearity and, thus, improves the performance of an ANN. However, too many extra radial basis functions can induce the network to focus on specific characters of individual training samples and thereby reduce its ability to generalize. Thus, tuning the number of training iterations and hidden neurons is crucial such that generalized training is maximized on the one hand and specialized training is avoided on the other hand. A set of validation samples can be employed to establish the onset of specialized training, which is denoted by a reversal in the decreasing trend of the error for the validation samples.

In the context of ANN, feature vectors in a prospectivity model are defined as unique combinations of spatially coincident input predictor features mapped using GIS 'spatial overlay and combine' tools. Target vectors mark out the output vectors to which the input feature vectors are mapped by an ANN. In prospectivity mapping, there is just one single-dimensional binary target vector, encoded as 1 (deposit) or 0 (non-deposit), representing presence or absence, respectively, of a deposit of the targeted type. Input feature vectors with known targets (deposit or non-deposit locations) constitute training samples. Validation samples also have known target vectors but are employed only for validating the training of the ANN. The feature vectors representing presence of a mineral deposit are referred to as deposit training or validation samples and those representing absence of mineral deposits are referred to as non-deposit training or validation samples. It is straightforward to select the former as they comprise the feature vectors that coincide spatially with the locations of known deposits. However, selecting non-deposit training samples can be difficult. Both data-driven and knowledge-driven approaches can be used for this purpose. In the data-driven approach, non-deposit locations are picked at random from locations (i.e., pixels) identified to have a very low probability of containing the targeted mineral deposit type. Feature vectors that coincide spatially with such locations can then be selected as non-deposit training or validation samples. Otherwise, feature vectors can be selected according to some expert knowledge of the target mineral deposit type [29].

4.4. Model inputs

4.4.1. Spatial proxies

The spatial proxies (or targeting elements) for calcrete-hosted uranium mineral systems outlined in Section 3.6 represent the mappable expressions of processes deemed critical in the generation and preservation of these deposits (Table 4). Importantly, not all proxies can be visualized in and extracted from the available public domain data because the data:

- Are mainly regional in scope, meaning that while adequate for mapping the expressions of many source, transport and trap processes, their resolution is inadequate for mapping the expressions of depositional processes that occurred at the mineral deposit scale;
- Are two-dimensional in nature preventing us from interrogating the crucial third dimension;
- Do not uniformly cover the entire study area.

4.4.2. *Predictor maps*

The predictor maps prepared for and utilized in this study are illustrated in Fig. 36; the GIS procedures used to generate them are listed in Table 4.

4.5. Prospectivity analysis

As described above, we adopted a three-pronged approach to prospectivity modeling of surficial uranium mineral systems, employing an initial, knowledge-driven FIS model and subsequent, data-driven WofE and ANN models. A uniform unit cell size of 1 km^2 was used in all three models.

4.5.1. *Fuzzy Inference Systems (FIS) model*

The FIS model was implemented using MATLAB™ and following the methodology of [45]. As a knowledge-based approach, the FIS model does not require the use of mineral occurrence training and verification data. A multi-stage FIS model was designed for the purpose of this study. In the first stage, separate FIS were generated to model the potential for source and trap processes for each paleo-valley (i.e., pathway) unit cell within the study area:

- The potential for source components was modeled by firstly evaluating the potential for uranium (Fig. 37a) and vanadium (Fig. 37b) sources individually, and then combining the two (Fig. 38) using a fuzzy AND operator;
- The potential for trap components was modeled by firstly evaluating the individual potential for favorable climate conditions (temperature, rainfall, and evapo-transpiration: Fig. 39a), water ponding (Fig. 39b) and environments favorable for carnotite deposition (Fig. 39c) individually, and then combining the three (Fig. 40) using a fuzzy AND operator.

In the second stage, the potential for sources and traps in the same unit cell was calculated by combining the various FIS using a fuzzy PRODUCT operator, thereby generating the FIS prospectivity model. Last but not least, and because there is higher probability of preservation of deposits in landward flowing drainage compared to the seaward flowing channels, we applied a preservation filter to generate the final FIS prospectivity map (Fig. 41). The purpose of this filter was to downgrade the prospectivity of the areas to the east of the Meckering Line (characterized by small, fossil terrace-type deposits: Fig. 14) by a factor of 0.25, while upgrading the prospectivity of areas to the east of the Meckering Line by a factor of 0.75.

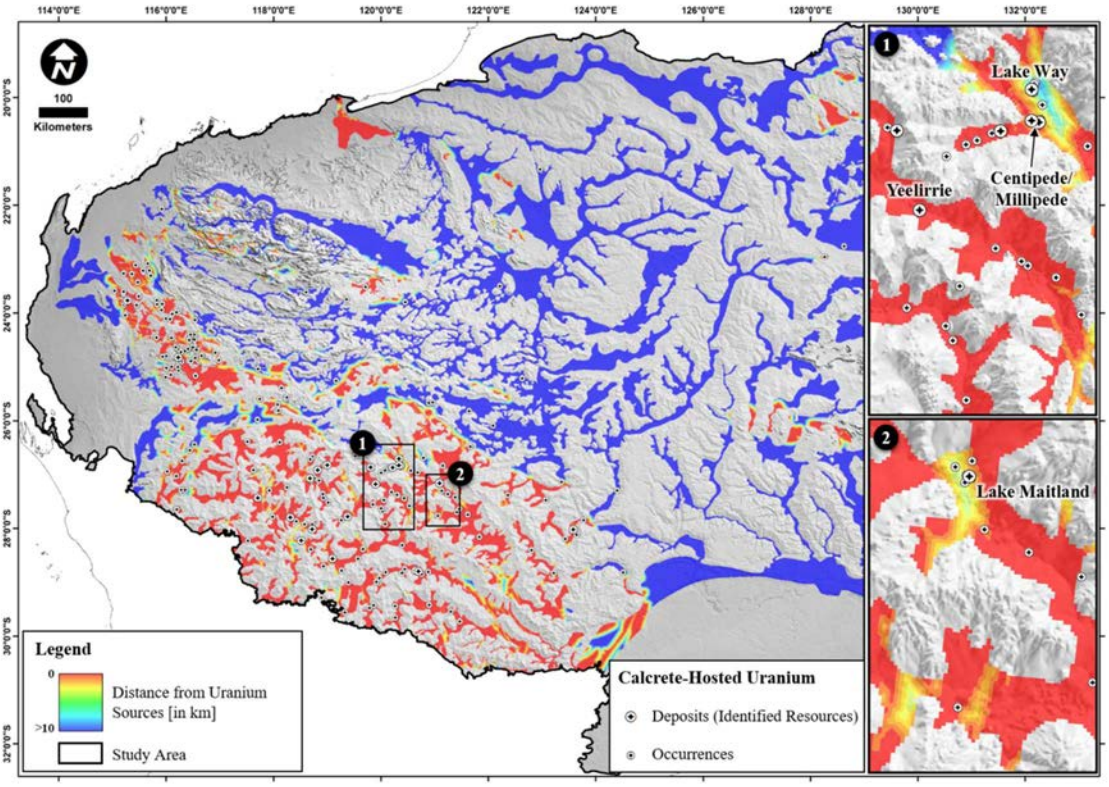

(a)

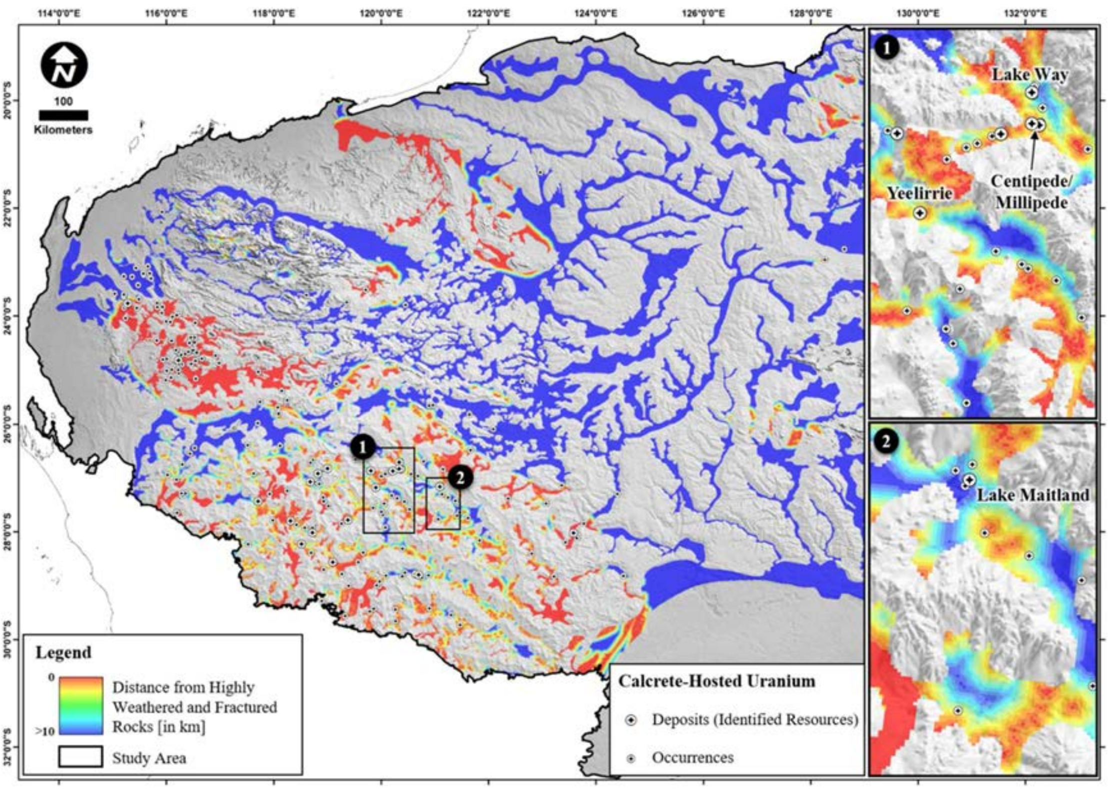

(b)

FIG. 36. Predictor maps (see Table 4 for more detail). (a) Proximity to potential uranium source rocks. (b) Proximity to sources of readily leachable uranium (highly weathered and fractured rocks).

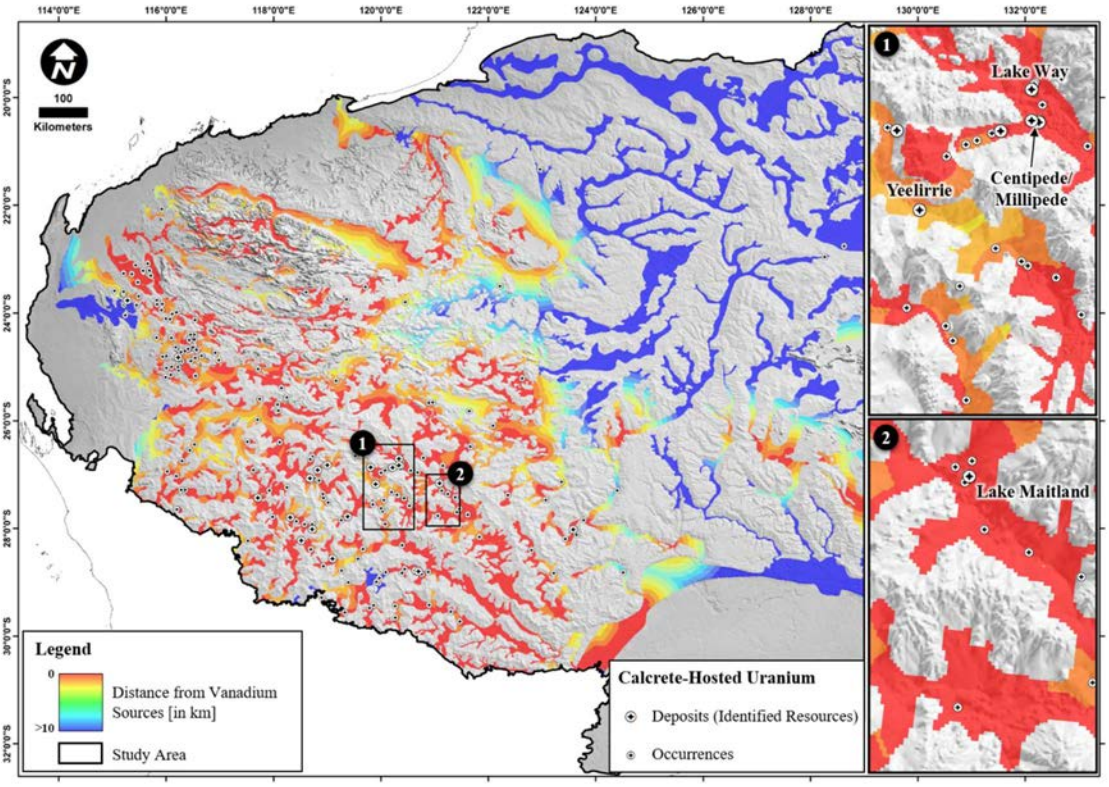

(c)

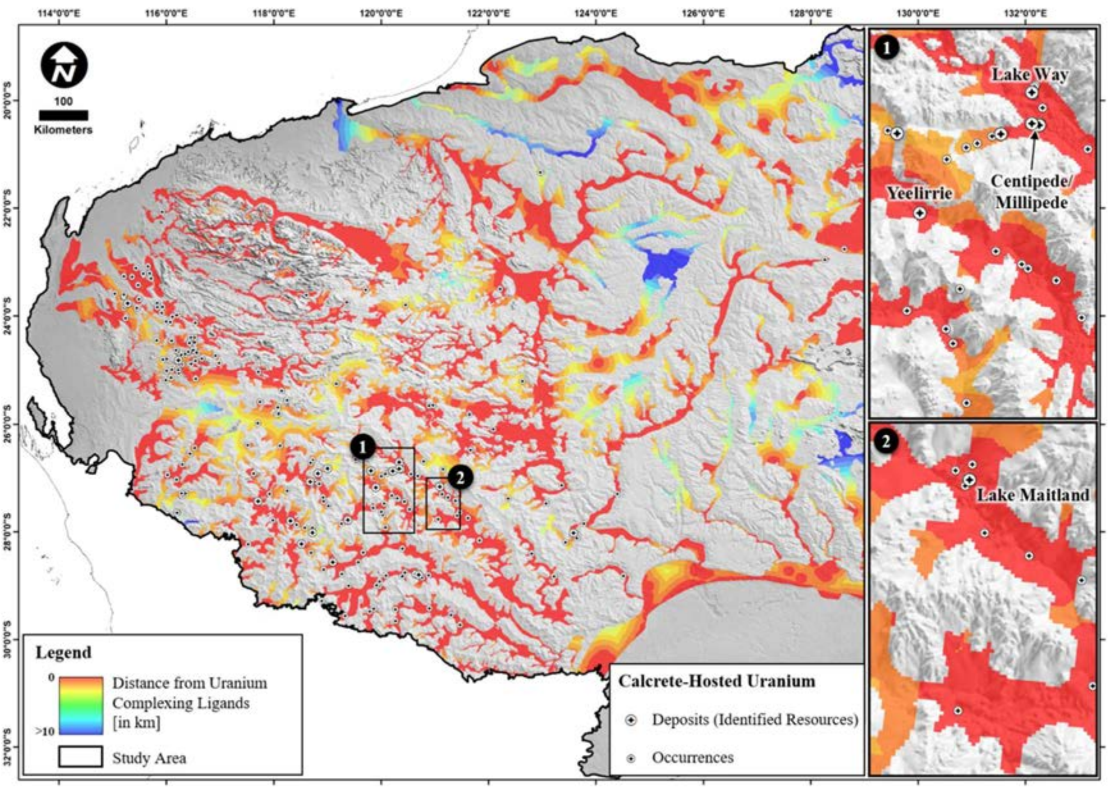

(d)

FIG. 36 (continued). (c) Proximity to potential vanadium source rocks. (d) Proximity to potential source rocks for uranium complexing ligands.

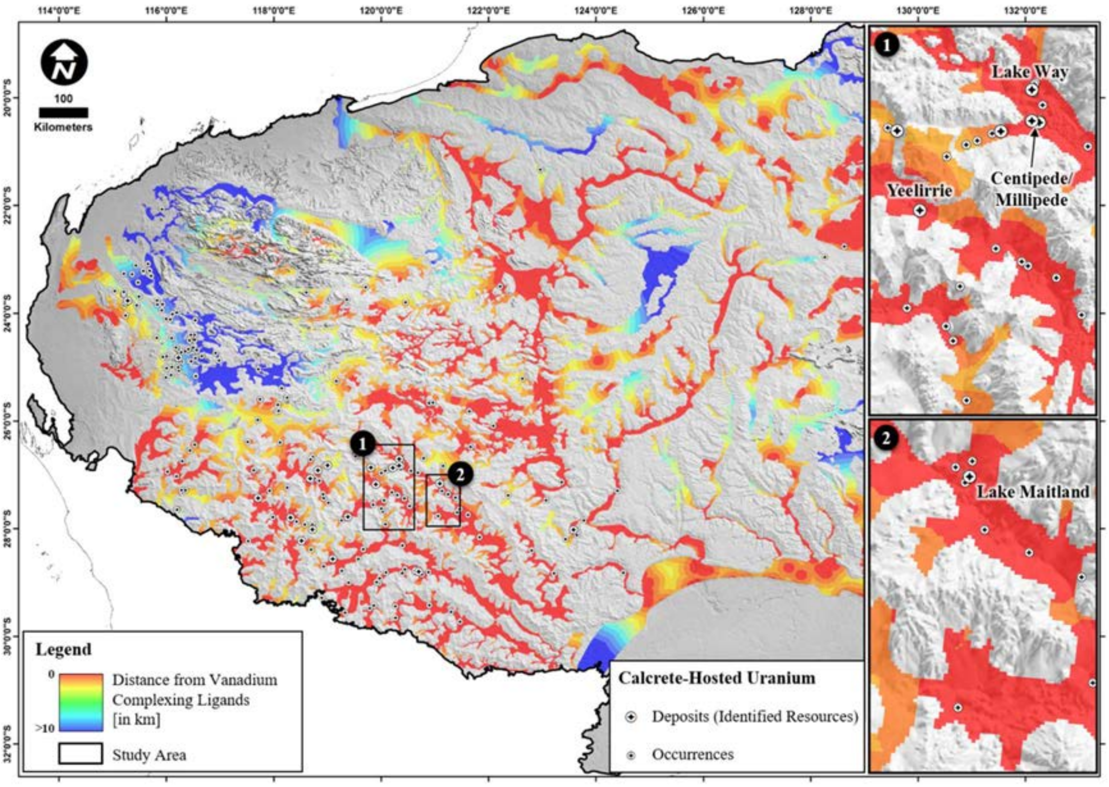

(e)

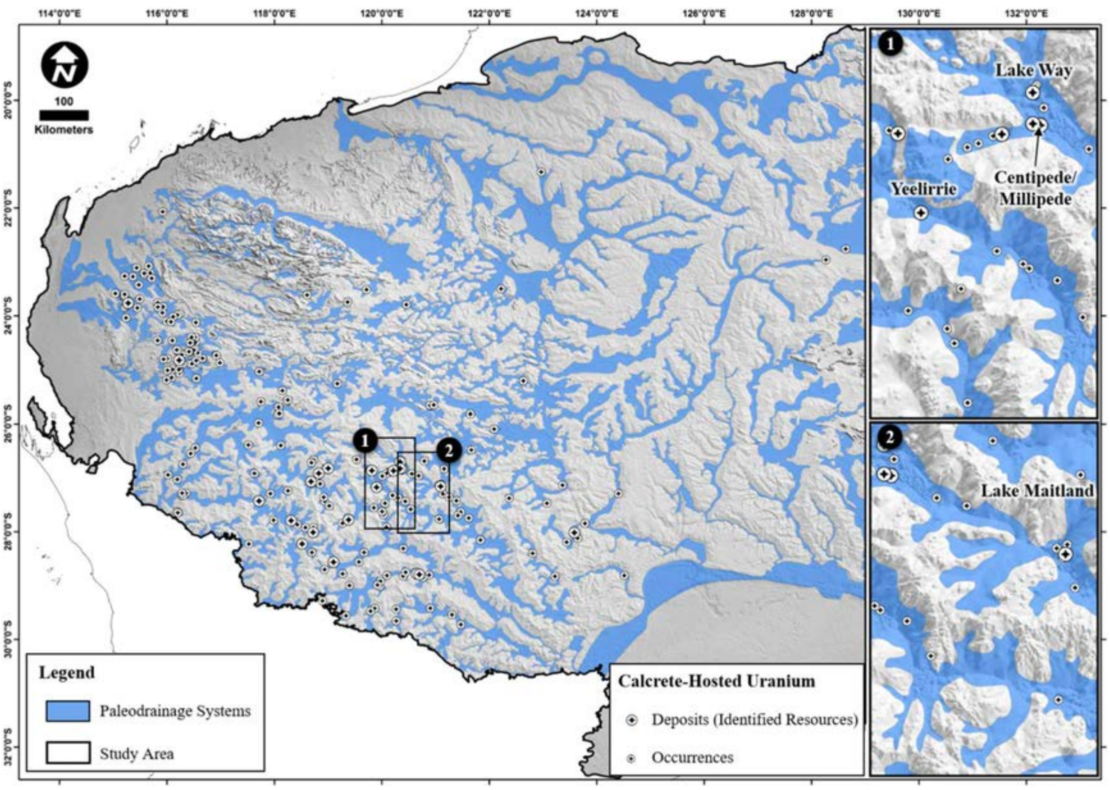

(f)

FIG. 36 (continued)). (e) Proximity to potential source rocks for vanadium complexing ligands. (f) Paleo-drainage systems (modified after [109]).

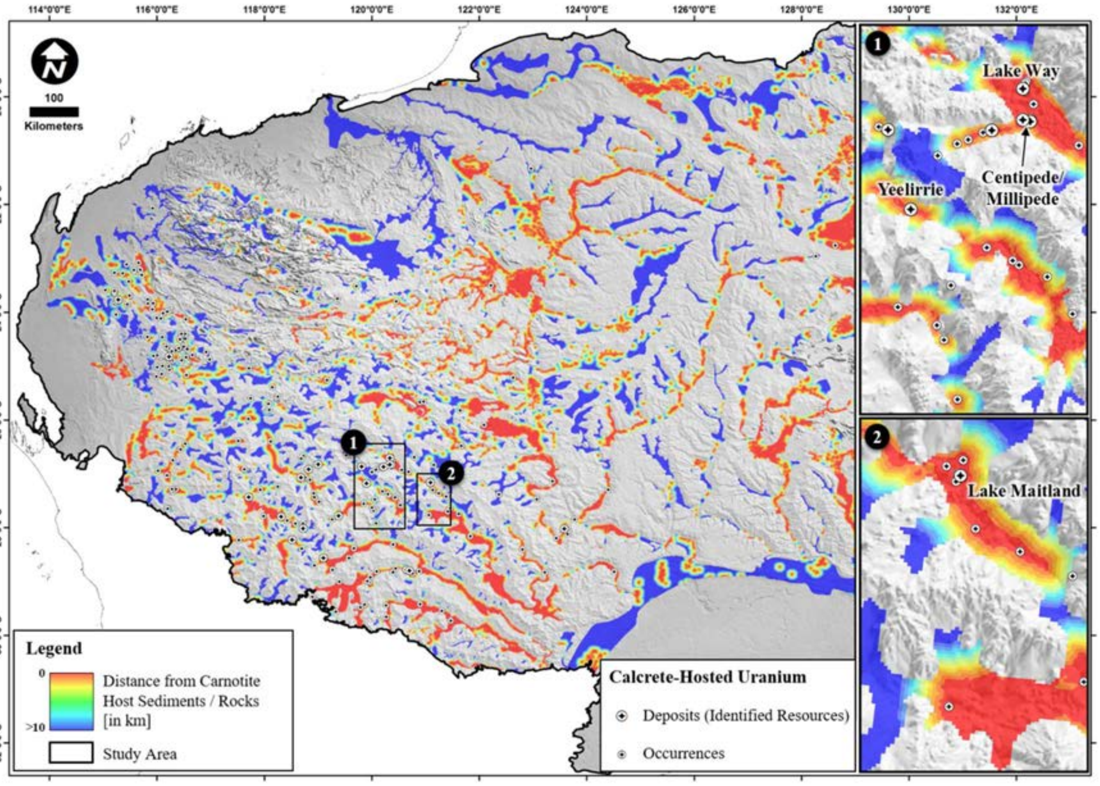

(g)

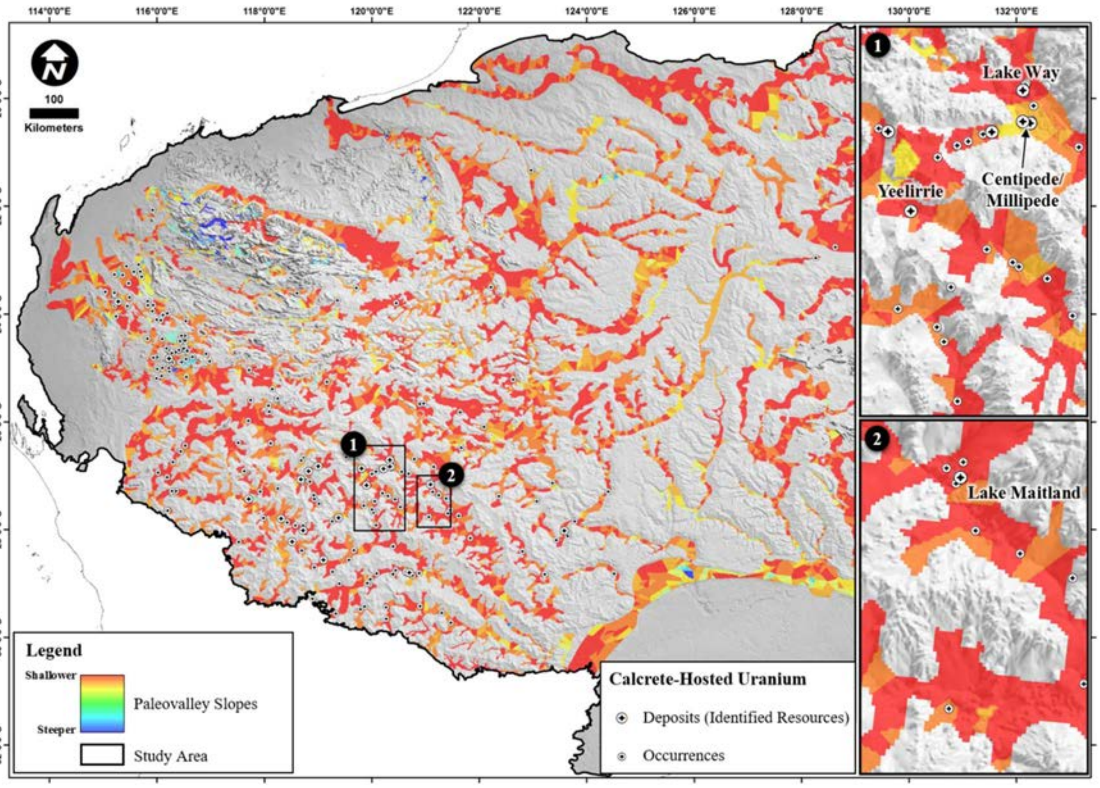

(h)

FIG. 36 (continued). (g) Proximity to favorable carnotite host media (e.g., calcrete bodies, playa lake sediments). (h) Proximity to gently paleo-valley slopes.

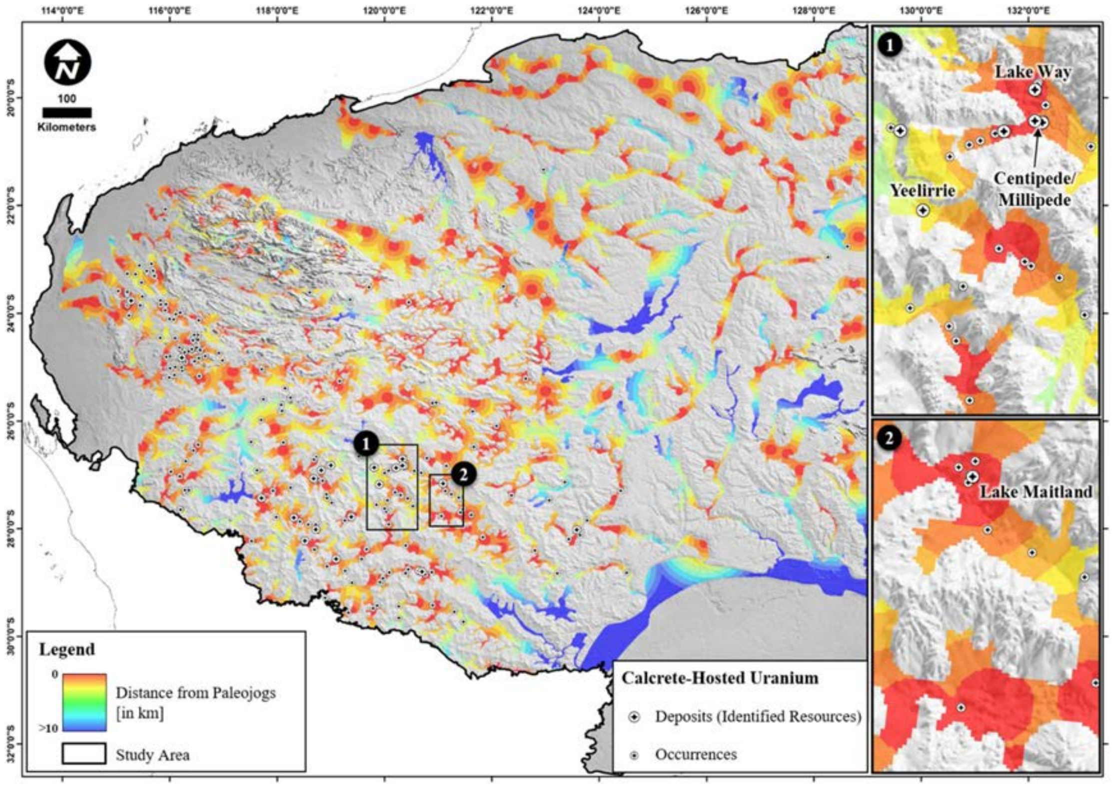

(i)

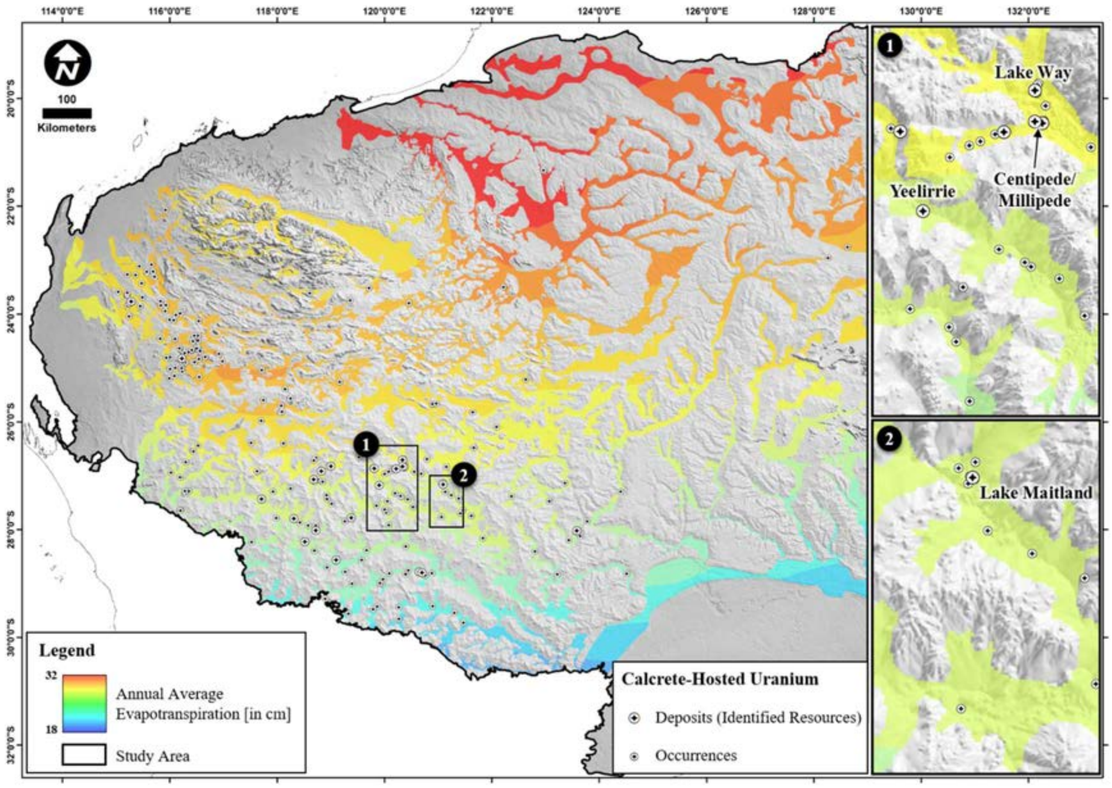

(j)

FIG. 36 (continued). (i). Proximity to paleo-valley bends and confluences. (j) Average annual evapotranspiration.

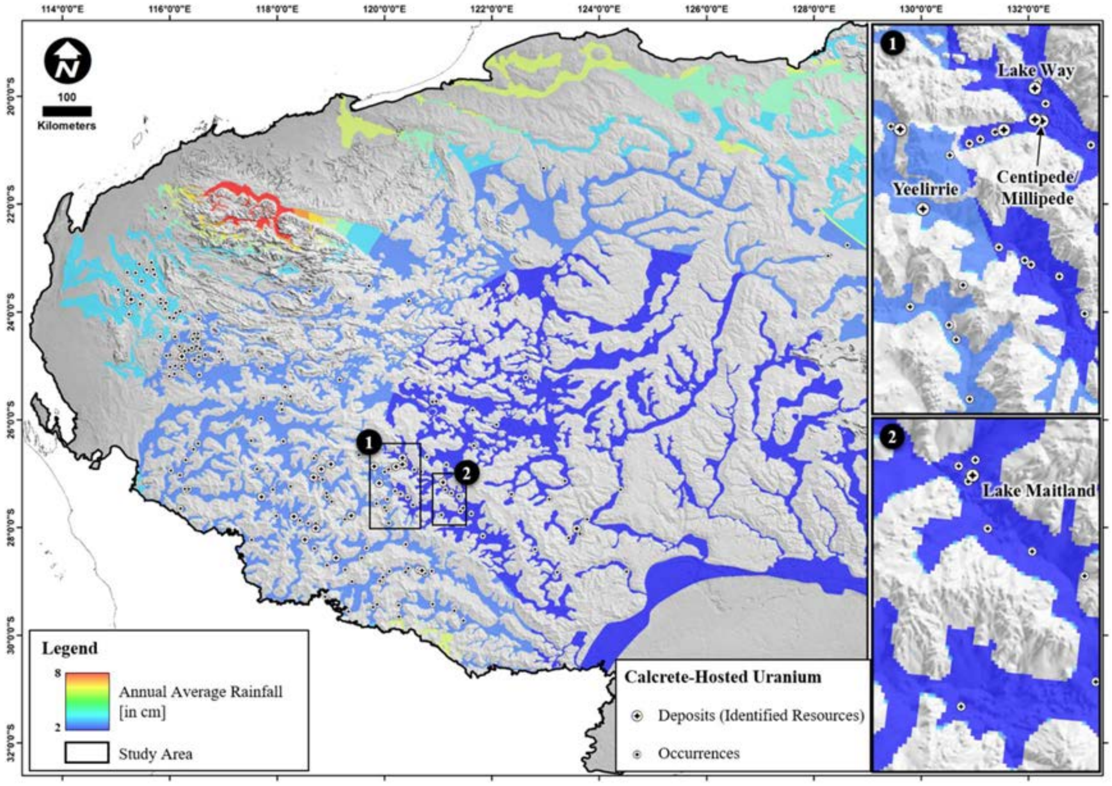

(k)

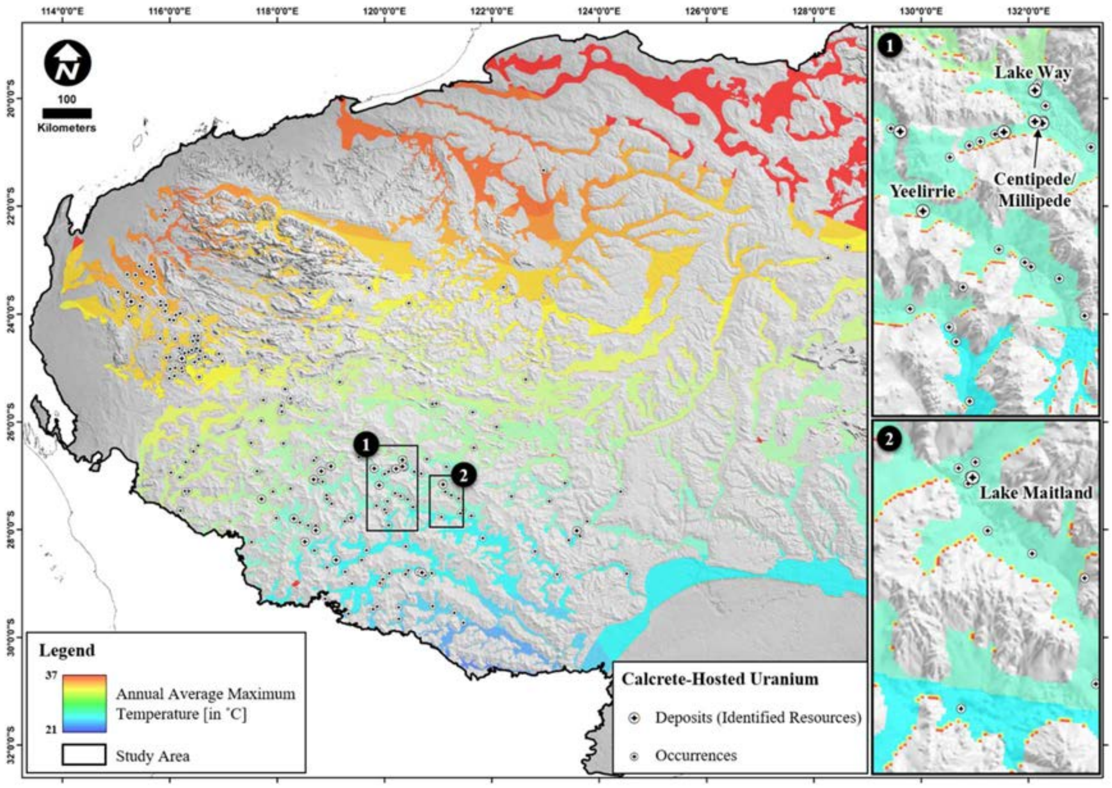

(l)

FIG. 36 (continued). (k) Average annual rainfall. (l) Average maximum annual temperature.

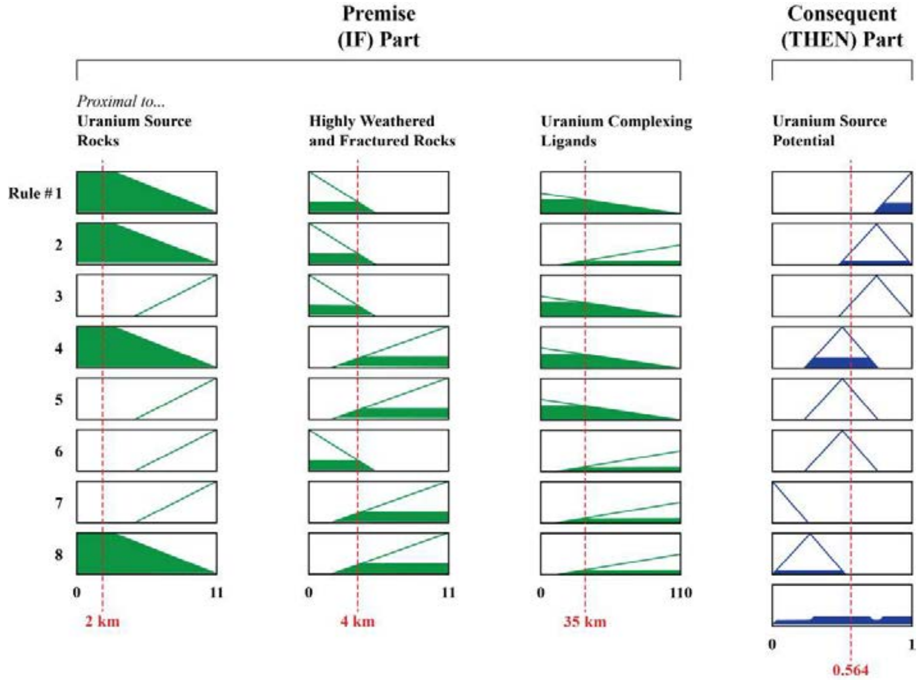

(a)

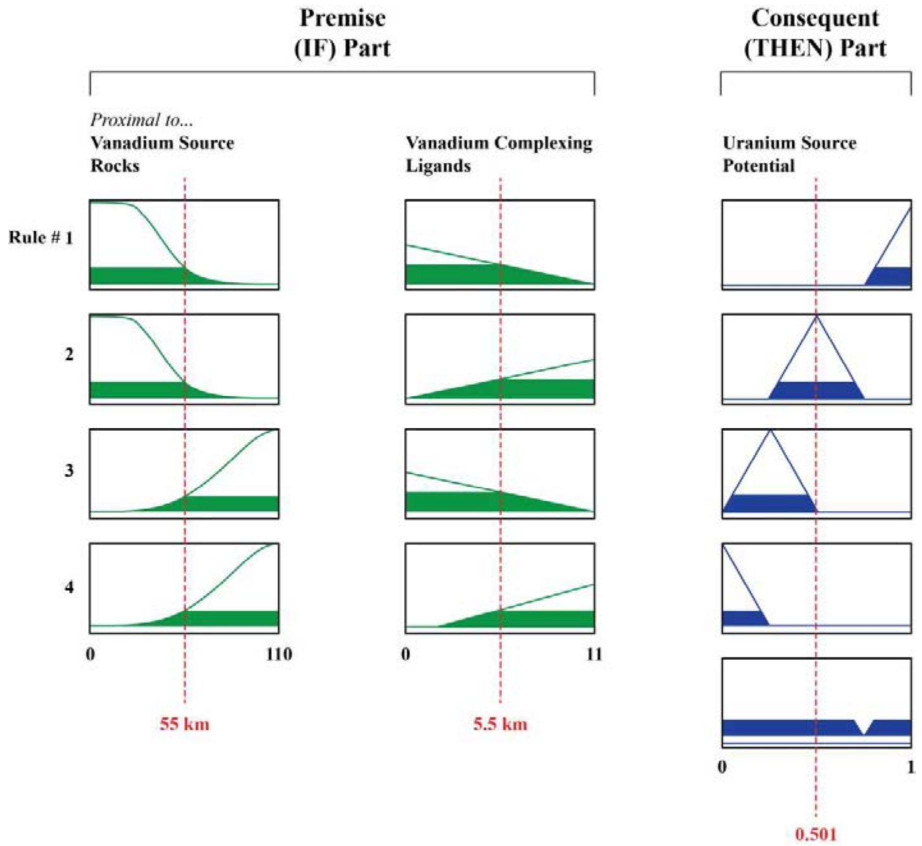

(b)

FIG. 37. Fuzzy Inference Systems (FIS) architecture. (a) For mapping uranium source potential. (b) For mapping vanadium source potential.

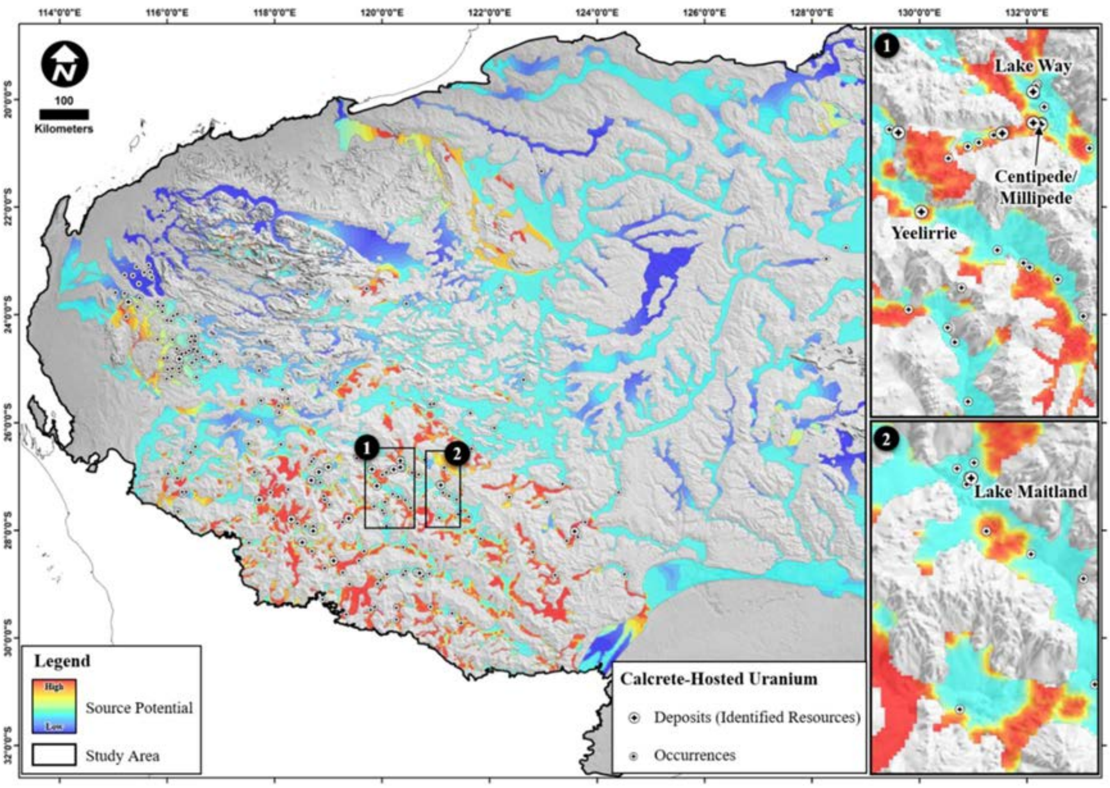

FIG. 38. Fuzzy Inference Systems (FIS) predictor map illustrating combined source potential.

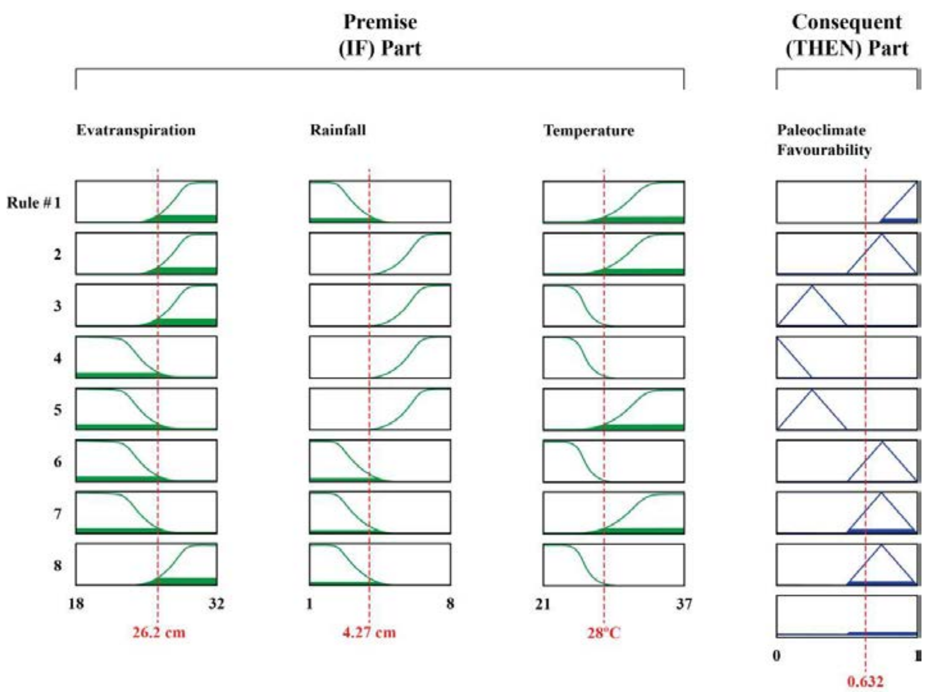

(a)

FIG. 39. Fuzzy Inference Systems (FIS) architecture. (a) For mapping paleo-climate favorability. (b) For mapping paleo-drainage favorability. (c) For mapping favorable carnotite host media.

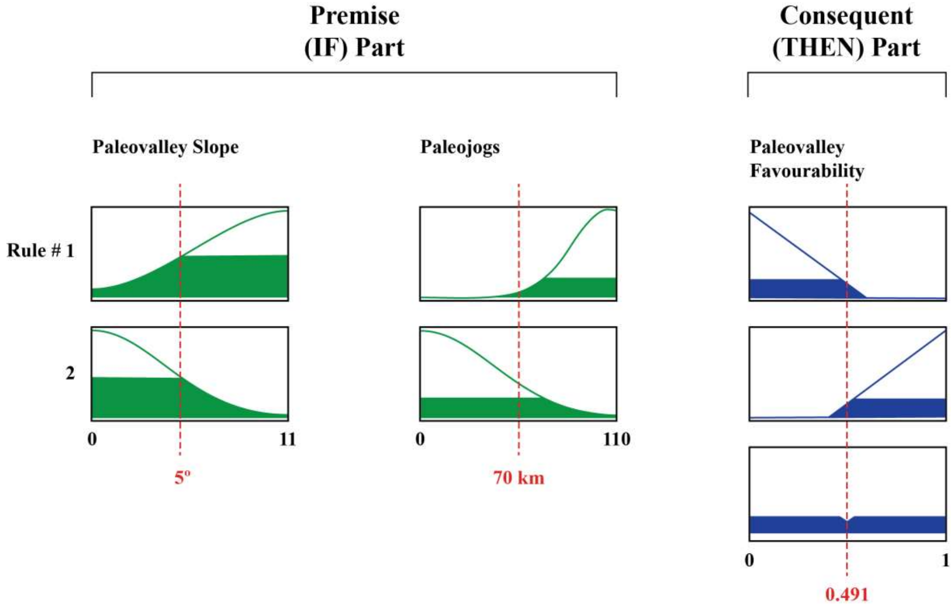

(b)

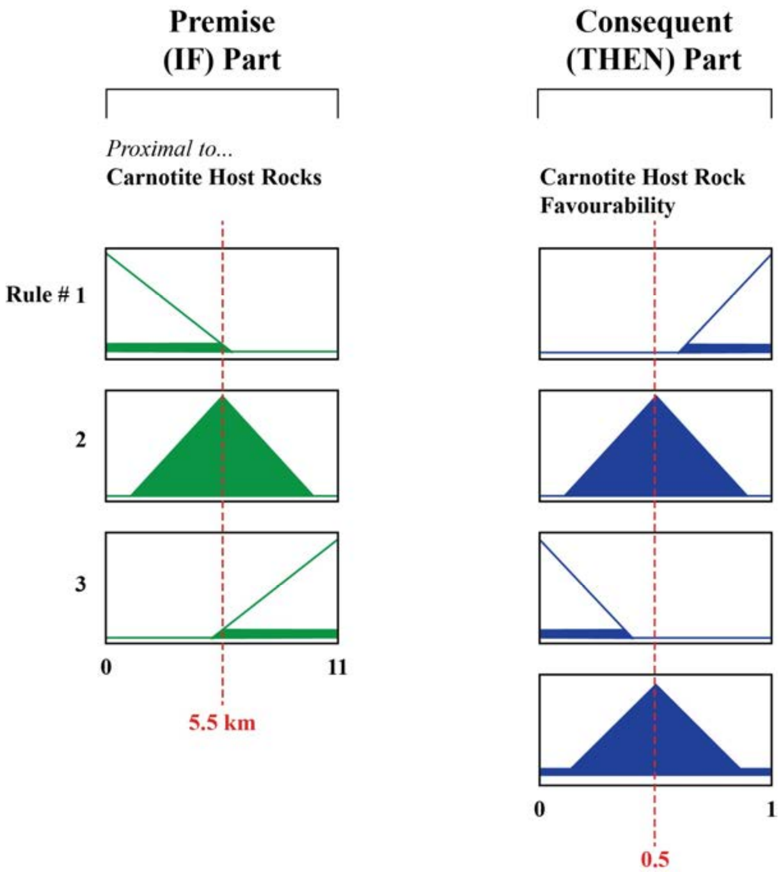

(c)

FIG. 39 (continued). (b) For mapping paleo-drainage favorability. (c) For mapping favorable carnotite host media.

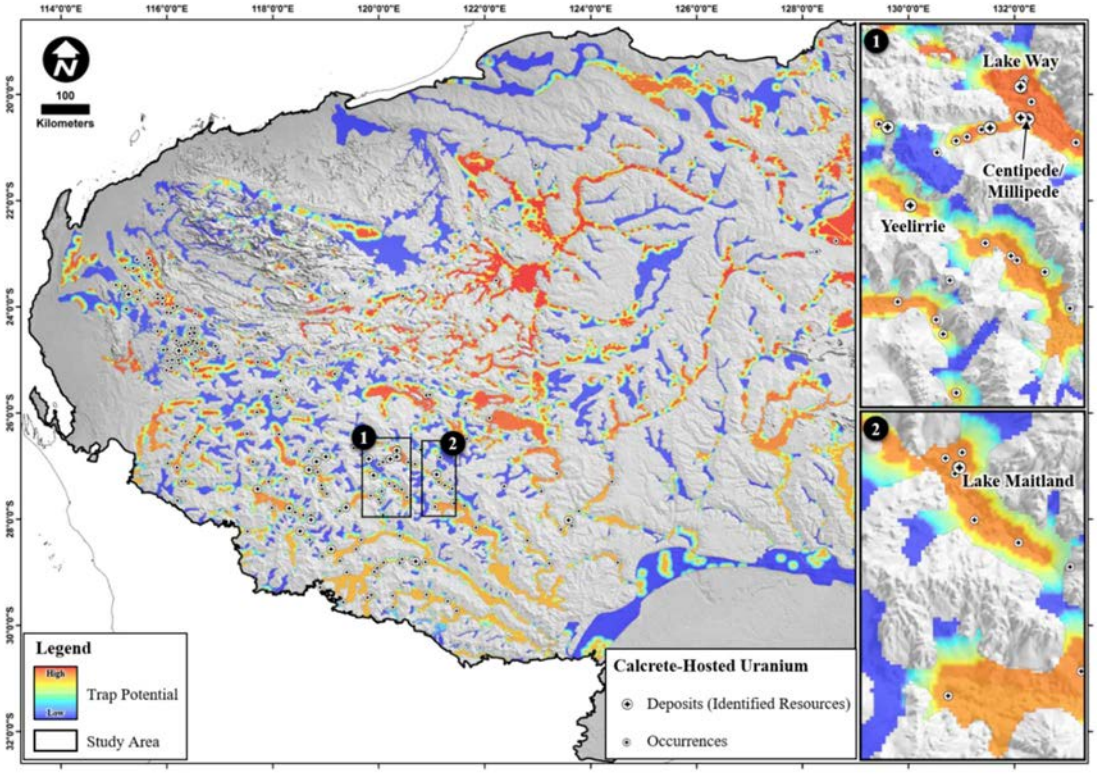

FIG. 40. Fuzzy Inference Systems (FIS) predictor map illustrating combined trap potential.

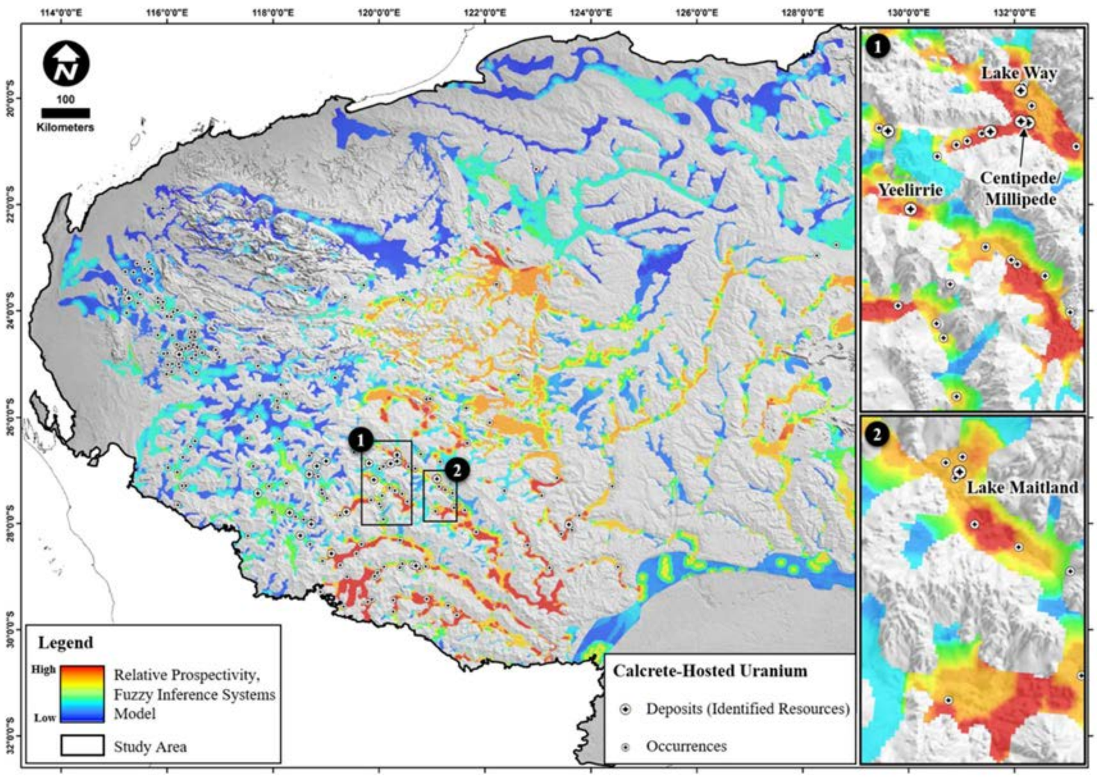

FIG. 41. Continuous-scale Fuzzy Inference Systems (FIS)-based prospectivity map of calcrete-hosted uranium potential.

4.5.2. *Weights-of-Evidence (WofE) model*

The WofE model was implemented within the GIS using the software tools and procedures described by [144]. For the purpose of the statistical analysis, all calcrete-hosted uranium occurrences outside the identified paleo-valleys (n = 10 of a total of 240) were excluded and not used as model input. As such, the training data comprised 230 calcrete-hosted uranium occurrences, of which 145 were used for training and 85 for validating the model.

The WofE modeling process involved two key steps:

— Estimation of likelihood ratios (i.e., weights-of-evidence) for each predictor map, including of a negative and positive weight of evidence and a contrast value (Table 5);
— Estimation of the posterior probability of occurrence of a calcrete-hosted uranium deposit for each unit cell of paleo-valley drainage in the study area, achieved by combining the weights-of-evidence of the for individual predictor maps under the assumption of conditional independence.

The resulting WofE prospectivity map is shown in Fig. 42.

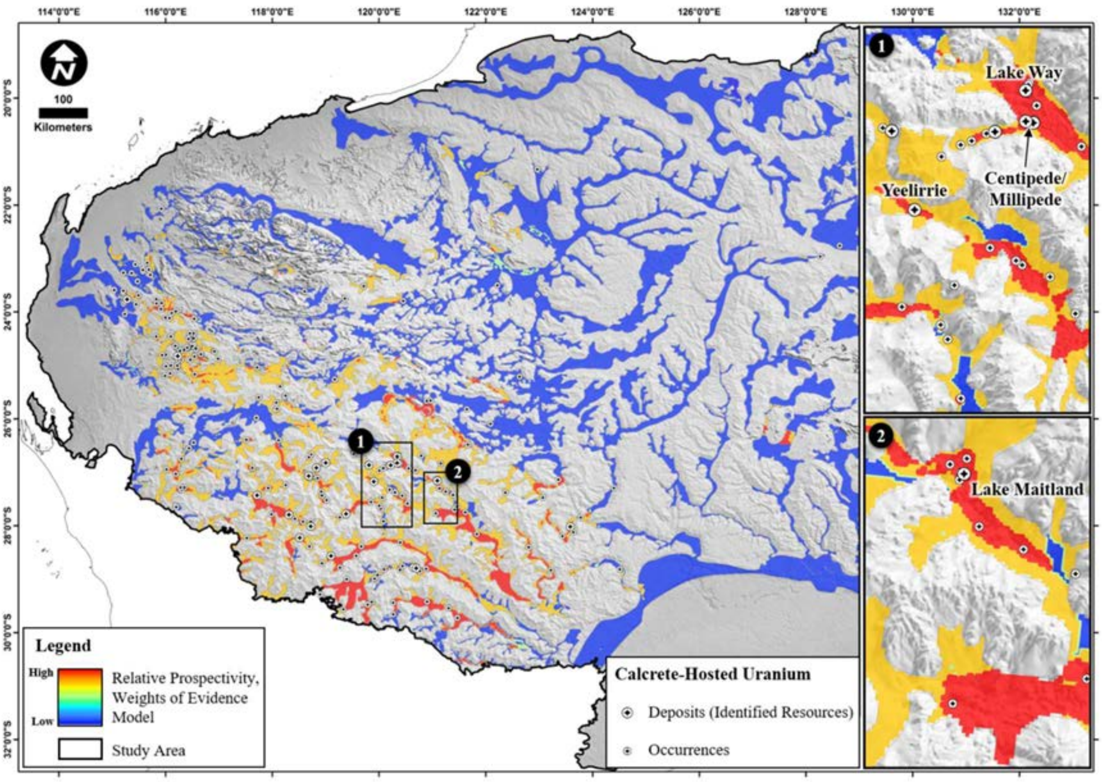

FIG. 42. Continuous-scale WofE-based prospectivity map of calcrete-hosted uranium potential.

4.5.3. *Artificial Neural Networks (ANN) Model*

While the inputs to the ANN model were generated within the GIS environment, the modeling was implemented outside the GIS, using the software and procedure described by [140]. Upon completion of this process, the ANN output was imported into the GIS and mapped to produce the ANN prospectivity model. The ANN training data included both deposit and non-deposit samples. With respect to the deposit samples, we selected 145 of the 230 calcrete-hosted uranium occurrences in the study area for training and 85 for validation. Regarding the non-deposit samples, we randomly extracted 236-point locations identified by the WofE prospectivity model as having negligible probability of containing a calcrete-hosted uranium deposit. Of these, 142 were used for training the ANN and 94 for validation.

TABLE 5. WEIGHTS-OF-EVIDENCE (WOFE) STATISTICS

Predictor map	Values	Area (km^2)	Training points	W+	s(W+)	W-	s(W-)	C	s(C)	StudC	Generalized class	W	s(W)
Distance [km] from: U source rocks	0 - 1	101,911	95	1.0288	0.1026	-0.8205	0.1443	1.8493	0.1771	10.4407	2	0.9175	0.0867
	1 - 2	115,598	110	1.0494	0.0954	-1.1525	0.1741	2.2019	0.1985	11.0920	2	0.9175	0.0867
	2 - 3	125,175	117	1.0314	0.0925	-1.3599	0.1961	2.3913	0.2168	11.0281	2	0.9175	0.0867
	3 - 4	130,877	121	1.0205	0.0910	-1.5080	0.2132	2.5285	0.2318	10.9083	2	0.9175	0.0867
	4 - 5	135,640	123	1.0011	0.0902	-1.5872	0.2236	2.5883	0.2411	10.7345	2	0.9175	0.0867
	5 - 6	141,204	126	0.9850	0.0891	-1.7306	0.2425	2.7156	0.2584	10.5093	2	0.9175	0.0867
	6 - 7	144,813	127	0.9677	0.0888	-1.7786	0.2500	2.7462	0.2653	10.3515	2	0.9175	0.0867
	7 - 8	148,892	130	0.9632	0.0877	-1.9718	0.2774	2.9350	0.2909	10.0892	2	0.9175	0.0867
	8 - 9	152,862	132	0.9522	0.0871	-2.1246	0.3015	3.0767	0.3138	9.8035	2	0.9175	0.0867
	9 - 10	156,228	132	0.9304	0.0871	-2.1123	0.3015	3.0427	0.3138	9.6950	2	0.9175	0.0867
	10 - 11	159,445	133	0.9175	0.0867	-2.1957	0.3162	3.1133	0.3279	9.4941	2	0.9175	0.0867
	>11	428,898	143	-0.0001	0.0836	8.0058	14.1421	-8.0059	14.1424	-0.5661	1	-2.1957	0.3162
Distance [km] from: domains of intense weathering & high fault-fracture density	0 - 1	67,073	53	0.8624	0.1374	-0.2929	0.1054	1.1553	0.1732	6.6706	2	0.8400	0.0906
	1 - 2	85,978	66	0.8335	0.1231	-0.3952	0.1140	1.2287	0.1678	7.3226	2	0.8400	0.0906
	2 - 3	99,942	81	0.8878	0.1112	-0.5703	0.1270	1.4581	0.1688	8.6388	2	0.8400	0.0906
	3 - 4	109,601	86	0.8554	0.1079	-0.6245	0.1325	1.4799	0.1708	8.6631	2	0.8400	0.0906
	4 - 5	117,848	91	0.8394	0.1049	-0.6902	0.1387	1.5295	0.1739	8.7968	2	0.8400	0.0906
	5 - 6	127,838	95	0.8010	0.1026	-0.7375	0.1443	1.5385	0.1771	8.6863	2	0.8400	0.0906
	6 - 7	134,385	96	0.7615	0.1021	-0.7366	0.1459	1.4980	0.1781	8.4133	2	0.8400	0.0906
	7 - 8	141,374	108	0.8286	0.0963	-1.0073	0.1690	1.8360	0.1945	9.4380	2	0.8400	0.0906
	8 - 9	147,959	117	0.8632	0.0925	-1.2814	0.1961	2.1446	0.2168	9.8902	2	0.8400	0.0906

Predictor map	Values	Area (km^2)	Training points	W+	s(W+)	W-	s(W-)	C	s(C)	StudC	Generalized class	W	s(W)
	9 - 10	153,069	120	0.8545	0.0913	-1.3857	0.2085	2.2402	0.2276	9.8407	2	0.8400	0.0906
	10 - 11	157,892	122	0.8400	0.0906	-1.4590	0.2182	2.2990	0.2363	9.7301	2	0.8400	0.0906
	>11	428,506	143	-0.0001	0.0836	8.0049	14.1421	-8.0050	14.1424	-0.5660	1	-1.4590	0.2182
Distance [km] from: U complexing ligands	0 - 100	215,258	87	0.1925	0.1072	-0.2406	0.1336	0.4332	0.1713	2.5279	2	0.0700	0.0839
	100 - 200	290,743	104	0.0703	0.0981	-0.1665	0.1602	0.2368	0.1878	1.2612	2	0.0700	0.0839
	200 - 300	336,976	133	0.1688	0.0867	-1.1202	0.3162	1.2890	0.3279	3.9308	2	0.0700	0.0839
	300 - 400	367,376	138	0.1193	0.0851	-1.4118	0.4472	1.5311	0.4553	3.3631	2	0.0700	0.0839
	400 - 500	386,273	139	0.0763	0.0848	-1.2680	0.5000	1.3443	0.5072	2.6507	2	0.0700	0.0839
	500 - 600	397,106	142	0.0700	0.0839	-2.3611	1.0000	2.4312	1.0035	2.4226	2	0.0700	0.0839
	600 - 700	404,213	143	0.0592	0.0836	-6.7133	10.0000	6.7726	10.0004	0.6772	1	-2.3611	1.0000
	700 - 800	408,748	143	0.0481	0.0836	-6.5103	10.0000	6.5584	10.0004	0.6558	1	-2.3611	1.0000
	800 - 900	412,618	143	0.0386	0.0836	-6.2971	10.0000	6.3357	10.0004	0.6335	1	-2.3611	1.0000
	900 - 1000	416,660	143	0.0289	0.0836	-6.0117	10.0000	6.0406	10.0004	0.6040	1	-2.3611	1.0000
	1000 - 1100	420,558	143	0.0196	0.0836	-5.6282	10.0000	5.6478	10.0004	0.5648	1	-2.3611	1.0000
	>1100	428,898	143	-0.0001	0.0836	8.0058	14.1421	-8.0059	14.1424	-0.5661	1	-2.3611	1.0000
Distance [km] from: V source rocks	0 - 10	118,047	86	0.7817	0.1079	-0.5979	0.1325	1.3797	0.1708	8.0762	2	0.5385	0.0864
	10 - 20	174,530	112	0.6548	0.0945	-1.0064	0.1796	1.6612	0.2030	8.1846	2	0.5385	0.0864
	20 - 30	210,974	126	0.5829	0.0891	-1.4525	0.2425	2.0354	0.2584	7.8771	2	0.5385	0.0864
	30 - 40	234,542	134	0.5385	0.0864	-1.9740	0.3333	2.5125	0.3444	7.2963	2	0.5385	0.0864
	40 - 50	250,834	134	0.4713	0.0864	-1.8864	0.3333	2.3577	0.3444	6.8467	1	-1.9740	0.3333
	50 - 60	263,244	134	0.4230	0.0864	-1.8141	0.3333	2.2371	0.3444	6.4965	1	-1.9740	0.3333

Predictor map	Values	Area (km^2)	Training points	W+	s(W+)	W-	s(W-)	C	s(C)	StudC	Generalized class	W	s(W)
	60 - 70	273,726	134	0.3839	0.0864	-1.7487	0.3333	2.1326	0.3444	6.1931	1	-1.9740	0.3333
	70 - 80	282,275	135	0.3606	0.0861	-1.8098	0.3536	2.1704	0.3639	5.9643	1	-1.9740	0.3333
	80 - 90	289,126	136	0.3440	0.0858	-1.8954	0.3780	2.2394	0.3876	5.7779	1	-1.9740	0.3333
	90 - 100	294,165	136	0.3267	0.0858	-1.8587	0.3780	2.1854	0.3876	5.6385	1	-1.9740	0.3333
	>100	428,772	143	-0.0001	0.0836	8.0055	14.1421	-8.0056	14.1424	-0.5661	1	-1.9740	0.3333
Distance [km] from: paleo-valley bends & confluences	0 - 10	67,496	77	1.1863	0.1140	-0.5936	0.1231	1.7799	0.1678	10.6073	2	0.0985	0.0839
	10 - 20	155,553	99	0.6022	0.1005	-0.7021	0.1508	1.3043	0.1812	7.1975	2	0.0985	0.0839
	20 - 30	225,197	117	0.3992	0.0925	-0.9087	0.1961	1.3078	0.2168	6.0315	2	0.0985	0.0839
	30 - 40	273,594	131	0.3175	0.0874	-1.3786	0.2887	1.6961	0.3016	5.6233	2	0.0985	0.0839
	40 - 50	304,825	134	0.2320	0.0864	-1.4068	0.3333	1.6387	0.3444	4.7588	2	0.0985	0.0839
	50 - 60	326,699	137	0.1848	0.0855	-1.5796	0.4083	1.7644	0.4171	4.2300	2	0.0985	0.0839
	60 - 70	343,609	140	0.1560	0.0845	-2.0464	0.5774	2.2024	0.5835	3.7744	2	0.0985	0.0839
	70 - 80	358,780	141	0.1199	0.0842	-2.1934	0.7071	2.3133	0.7121	3.2484	2	0.0985	0.0839
	80 - 90	369,130	142	0.0985	0.0839	-2.6618	1.0000	2.7603	1.0035	2.7506	2	0.0985	0.0839
	90 - 100	376,675	142	0.0783	0.0839	-2.4588	1.0000	2.5371	1.0035	2.5281	1	-2.6618	1.0000
	>100	410,199	143	-0.0001	0.0836	7.9612	14.1421	-7.9613	14.1424	-0.5629	1	-2.6618	1.0000
Distance [km] from: favorable carnotite host media	0 - 1	75,201	110	1.4410	0.0954	-1.2654	0.1741	2.7064	0.1985	13.6330	2	1.4410	0.0954
	1 - 2	118,662	122	1.0880	0.0906	-1.5795	0.2182	2.6675	0.2363	11.2897	1	-1.2654	0.1741
	2 - 3	153,463	123	0.8388	0.0902	-1.5022	0.2236	2.3410	0.2411	9.7089	1	-1.2654	0.1741
	3 - 4	176,500	124	0.7069	0.0898	-1.4604	0.2294	2.1674	0.2464	8.7966	1	-1.2654	0.1741
	4 - 5	195,438	126	0.6210	0.0891	-1.4880	0.2425	2.1090	0.2584	8.1618	1	-1.2654	0.1741
	5 - 6	216,878	127	0.5247	0.0888	-1.4447	0.2500	1.9694	0.2653	7.4234	1	-1.2654	0.1741

Predictor map	Values	Area (km^2)	Training points	W+	s(W+)	W-	s(W-)	C	s(C)	StudC	Generalized class	W	s(W)
	6 - 7	230,560	130	0.4869	0.0877	-1.5799	0.2774	2.0667	0.2909	7.1046	1	-1.2654	0.1741
	7 - 8	244,559	132	0.4432	0.0871	-1.6669	0.3015	2.1101	0.3138	6.7235	1	-1.2654	0.1741
	8 - 9	257,150	136	0.4228	0.0858	-2.0410	0.3780	2.4638	0.3876	6.3569	1	-1.2654	0.1741
	9 - 10	267,510	137	0.3906	0.0855	-2.1262	0.4083	2.5168	0.4171	6.0341	1	-1.2654	0.1741
	10 - 11	277,698	137	0.3532	0.0855	-2.0534	0.4083	2.4066	0.4171	5.7698	1	-1.2654	0.1741
	>11	412,592	143	-0.0001	0.0836	7.9670	14.1421	-7.9671	14.1424	-0.5633	1	-1.2654	0.1741
Amount [cm] of: evapo-transpiration	32	33,330	1	-2.4508	1.0000	0.0776	0.0839	-2.5284	1.0035	-2.5195	2	0.0454	0.0839
	31	73,353	1	-3.2396	1.0000	0.1896	0.0839	-3.4292	1.0035	-3.4172	2	0.0454	0.0839
	30	108,246	1	-3.6288	1.0000	0.2987	0.0839	-3.9275	1.0035	-3.9137	2	0.0454	0.0839
	29	164,388	47	-0.1962	0.1459	0.1122	0.1021	-0.3083	0.1781	-1.7317	2	0.0454	0.0839
	28	236,342	65	-0.2350	0.1241	0.2494	0.1133	-0.4844	0.1680	-2.8838	2	0.0454	0.0839
	27	284,964	90	-0.0966	0.1054	0.1890	0.1374	-0.2856	0.1732	-1.6493	2	0.0454	0.0839
	26	321,032	117	0.0466	0.0925	-0.1865	0.1961	0.2331	0.2168	1.0751	2	0.0454	0.0839
	25	343,601	128	0.0686	0.0884	-0.4481	0.2582	0.5167	0.2729	1.8930	2	0.0454	0.0839
	24	370,620	138	0.0681	0.0851	-1.0355	0.4472	1.1036	0.4553	2.4240	2	0.0454	0.0839
	23	390,116	142	0.0454	0.0839	-1.9878	1.0000	2.0332	1.0035	2.0260	2	0.0454	0.0839
	22	407,777	143	0.0080	0.0836	-4.7489	10.0000	4.7569	10.0004	0.4757	1	-1.9878	1.0000
	21	411,078	143	0.0000	0.0836	0.5256	10.0029	-0.5256	10.0033	-0.0525	1	-1.9878	1.0000
	20	411,084	143	0.0000	0.0836	0.9612	10.0045	-0.9613	10.0049	-0.0961	1	-1.9878	1.0000
	19	411,090	143	-0.0001	0.0836	1.7508	10.0100	-1.7508	10.0104	-0.1749	1	-1.9878	1.0000
	18	411,095	143	-0.0001	0.0836	7.9634	14.1421	-7.9635	14.1424	-0.5631	1	-1.9878	1.0000

Predictor map	Values	Area (km^2)	Training points	W+	s(W+)	W-	s(W-)	C	s(C)	StudC	Generalized class	W	s(W)
Amount [cm] of: rainfall	2.0 - 2.5	154,524	33	-0.4462	0.1741	0.1848	0.0954	-0.6310	0.1985	-3.1788	2	0.1298	0.0839
	2.5 - 3.0	311,924	118	0.1257	0.0921	-0.4431	0.2000	0.5688	0.2202	2.5833	2	0.1298	0.0839
	3.0 - 3.5	373,823	142	0.1298	0.0839	-2.9063	1.0000	3.0361	1.0035	3.0255	2	0.1298	0.0839
	3.5 - 4.0	399,064	143	0.0714	0.0836	-6.8942	10.0000	6.9656	10.0004	0.6965	1	-2.9063	1.0000
	4.0 - 4.5	421,740	143	0.0161	0.0836	-5.4371	10.0000	5.4532	10.0004	0.5453	1	-2.9063	1.0000
	4.5 - 5.0	423,119	143	0.0129	0.0836	-5.2136	10.0000	5.2265	10.0004	0.5226	1	-2.9063	1.0000
	5.0 - 5.5	424,123	143	0.0105	0.0836	-5.0123	10.0000	5.0228	10.0004	0.5023	1	-2.9063	1.0000
	5.5 - 6.0	428,625	143	-0.0001	0.0836	8.0052	14.1421	-8.0052	14.1424	-0.5660	1	-2.9063	1.0000

Key to abbreviations: W+= Positive spatial correlation (prior probability of a (training set) feature being present); s(W+) = Standard deviation of W+; W- = Negative spatial correlation (prior probability of a (training set) feature being absent; s(W-) = standard deviation of W-; C = Contrast (difference between positive and negative weights); s(C) = Standard deviation of C; StudC = Studentized contrast; W = Weights; s(W) = Standard deviation of W.

Studentized contrast (C/s(C)) is also helpful for choosing the cutoff distance, because it shows the contrast relative to the uncertainty due to the weights (Bonham-Carter, 1994).

In general terms, absolute weights between 0 and 0.5 are mildly predictive; values between 0.5 and 1 are moderately predictive; values between 1 and 2 are strongly predictive, and greater than 2 are extremely predictive.

Generalized class: 1 = Unfavorable class (negative spatial association); 2 = Favorable class (positive spatial association).

The training was initiated, using a RBFLN with 100 hidden neurons. The network was trained for 50 iterations via a set of randomly initialized centers and weights, and the training error recorded. Then, the validation samples were processed through the network, again with the validation error recorded. This two-step process was repeated by stepping up the number of iterations in increments of 10 until the error converged to zero. The procedure was iterated five times, each iteration using a different set of randomly initialized weights and centers designed for selecting a set of initial weights and centers that returned the best performance with respect to the validation samples. The same training procedure was repeated by increasing the number of radial basis functions in steps of 20. The optimal performance indication was obtained in 210 iterations, with 200 functions in the hidden layers. This network was used to process all feature vectors (i.e., unique condition grids considering each unique combination of spatially coincident classes of input predictor maps) and the outputs were mapped to obtain the output prospectivity map shown in Fig. 43.

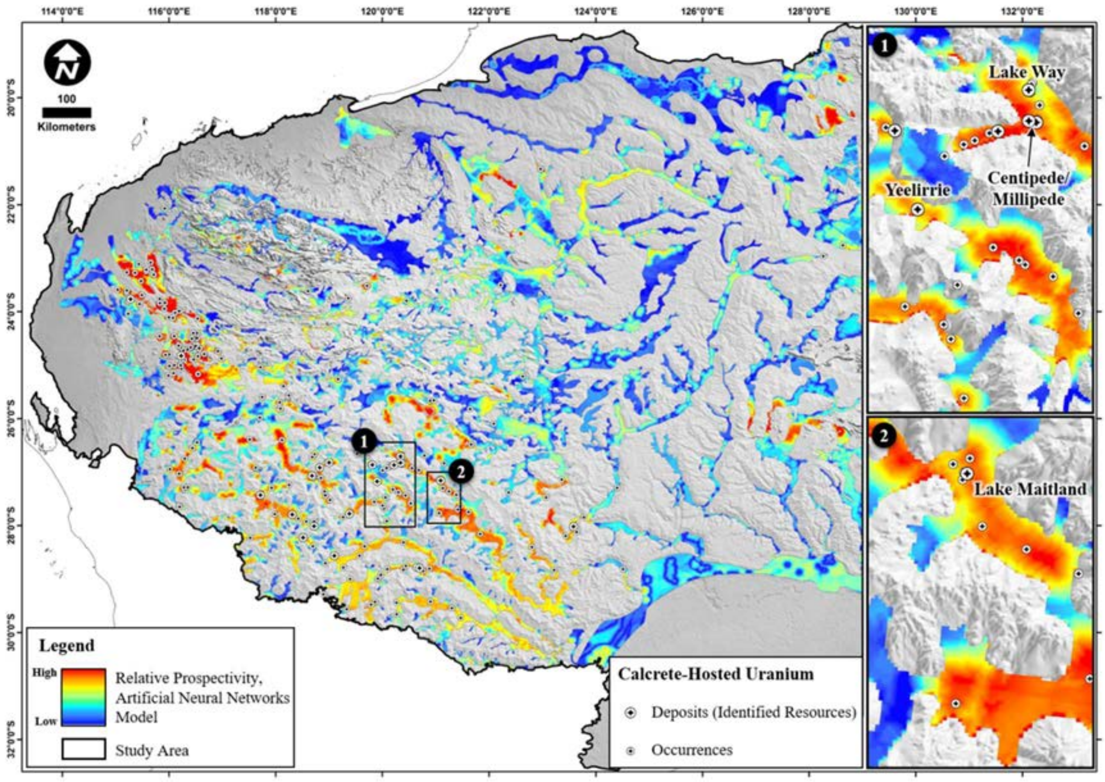

FIG. 43. Continuous-scale ANN-based prospectivity map of calcrete-hosted uranium potential.

4.6. Results

The prospectivity maps obtained from the FIS, WofE and ANN models (Figs. 41-43) are continuous-scale maps, showing relative prospectivity values ranging from 0 to 1. Reclassification of these continuous-scale prospectivity maps into ternary prospectivity maps is highly recommended as this step categorizes prospective domains in terms of high, moderate and low priority exploration targets. To reclassify the continuous-scale prospectivity maps into ternary prospectivity maps, we used cumulative area versus posterior probability (CAPP) curves. The slopes under the various segments of a CAPP curve represent the fractal dimensions of different spatial populations present in any given area [29]. If the entire study area comprised of a single population, the expected CAPP plot would be a straight line with a constant slope. However, if there were two populations, for example a mineralized and a barren one, the expected CAPP plot would be characterized by two segments with different slopes. The inflexion points at which the slopes change indicate changes in fractal dimension, and are used as thresholds for separating areas of different prospectivity and reclassifying continuous-scale prospectivity models as binary, or ternary, models.

We generated CAPP plots for FIS, WofE and ANN models (Fig. 44) to create ternary prospectivity maps for each model (Fig. 45). The performance of each model was validated using the known surficial uranium occurrences and deposits in the study area including the deposits with identified resources. All three models performed well (Table 6) and showed similar distribution of prospective ground

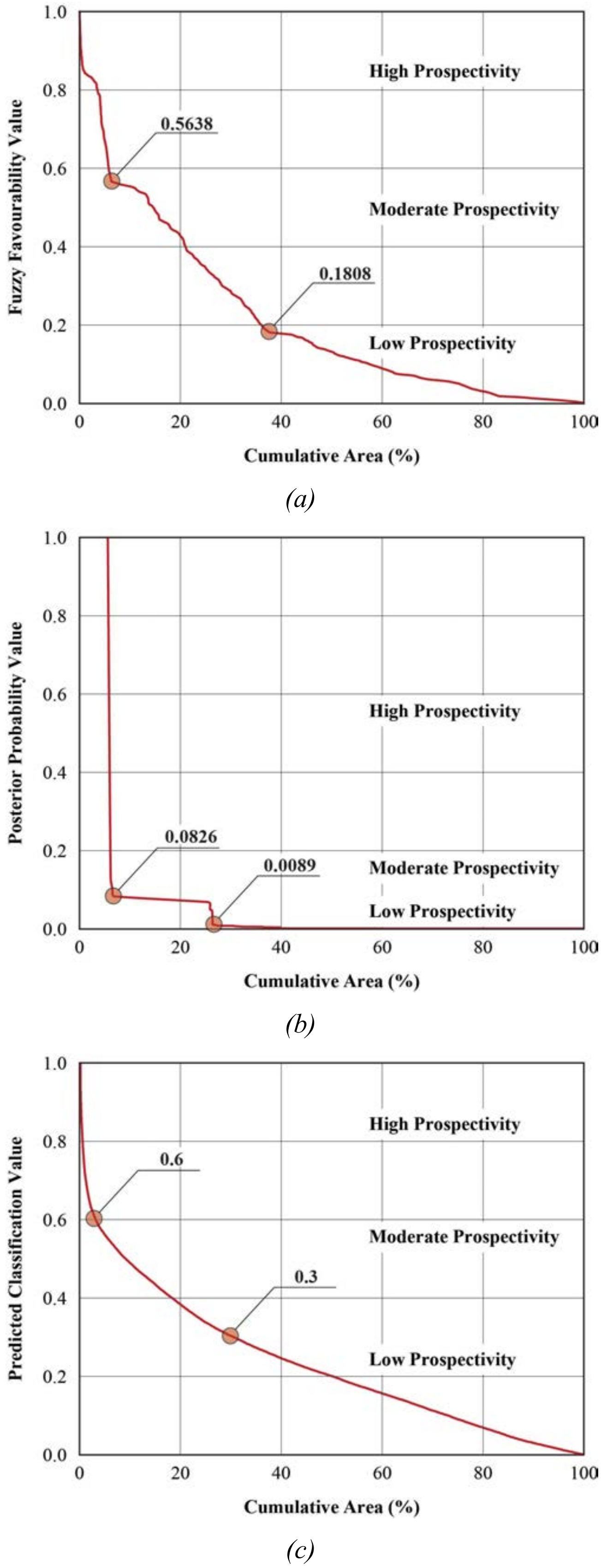

FIG. 44. Cumulative area versus posterior probability (CAPP) plots. (a) Fuzzy Inference Systems (FIS) model. (b) Weights-of-Evidence (WofE) model. (c) Artificial Neural Networks (ANN) model.

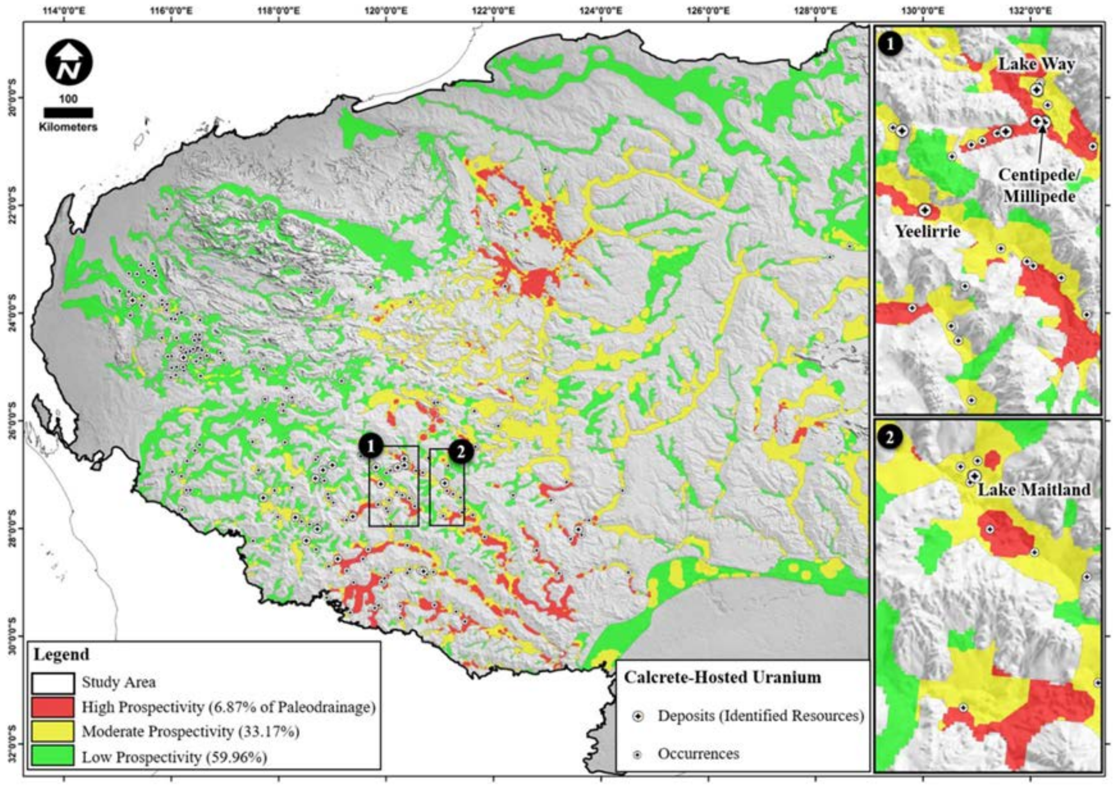

(a)

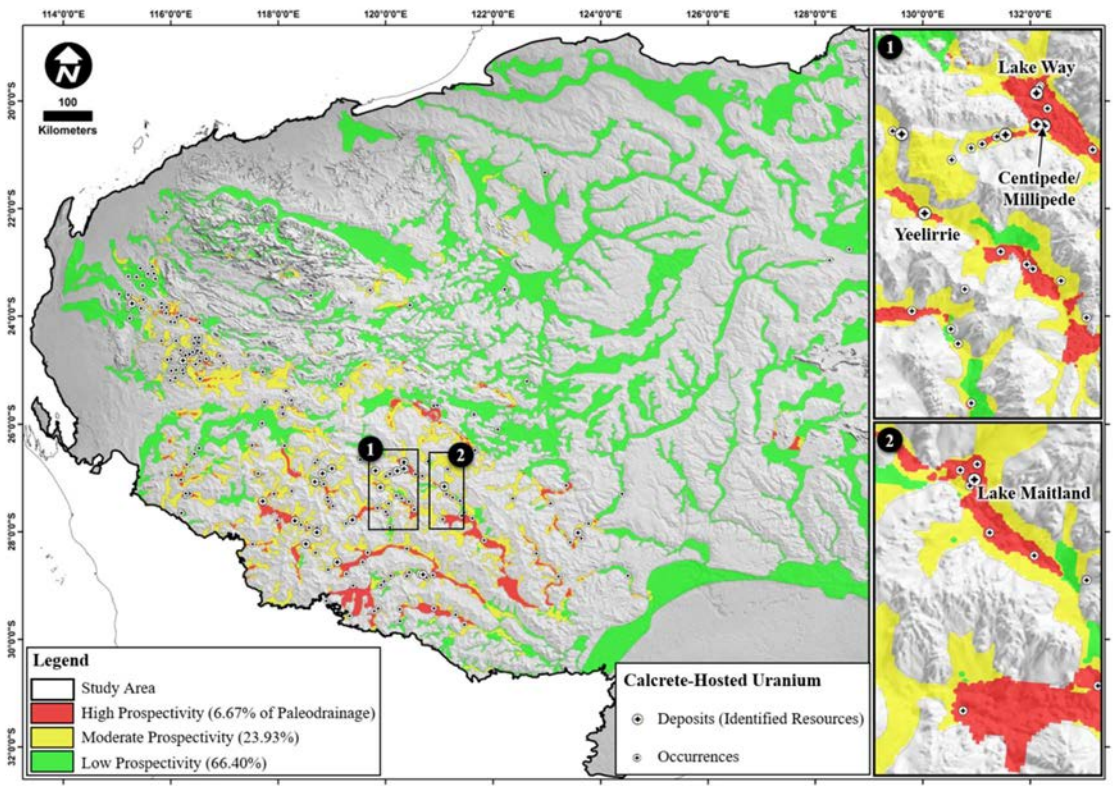

(b)

FIG. 45. Reclassified ternary prospectivity models. (a) Fuzzy Inference Systems (FIS). (b) Weights-of-Evidence (WofE).

TABLE 6A. PROSPECTIVITY MODELING RESULTS: FUZZY INFERENCE SYSTEMS (FIS) APPROACH

Study area + calcrete preservation filter[1]

Prospectivity class	Deposits [*n*]	%	Deposits with resources [*n*]	%	Paleo-valley area (%)	Study area (%)
High	40	17	8	31	7	1
Moderate	122	53	12	46	34	7
Low	68	30	6	23	59	92
Total	230	100	13	100	100	100

Inland drainage only[2]

Prospectivity class	Deposits [*n*]	%	Deposits with resources [*n*]	%	Paleo-valley area (%)	Study area (%)	Inland drainage area (%)
High	39	45	8	62	15	3	30
Moderate	44	50	5	38	28	6	56
Low	4	5	0	0	7	1	14
Total	87	100	13	100	50	10	100

[1]Total number of deposits = 236; total number of deposits outside mapped paleovalleys = 6; total number of deposits used in the modeling = 236 – 6 = 230; Total number of deposits with identified resources = 27; Total number of deposits with identified resources outside mapped paleovalleys = 1; total number of deposits with identified resources used in the modeling = 27 – 1 = 26. Result: Approximately 8% of the study area (or 41% of the paleo-valley area) was identified as highly to moderately prospective, capturing 70% of the known calcrete-hosted uranium occurrences and 77% of all deposits with identified resources. This is an impressive result given that in this model the prospectivity of the oceanward drainage was suppressed relative to the inland drainage inland, using a calcrete preservation filter that accounts for the active erosion of calcretes (and contained uranium deposits) the oceanward drainage.

[2]Total number of deposits = 87; Total number of deposits with identified resources = 13. Result: Inland draining paleovalleys constitute 50% of the total paleo-valley area and 10% of the study area. As illustrated by this model, the relative amount of prospective area captured by the inland drainage is six times that of the non-prospective area. Statistically, approximately 9% of the study area (or 43% paleo-valley area) was identified as highly to moderately prospective, capturing 95% of the known calcrete-hosted uranium occurrences and all deposits with identified resources.

TABLE 6B. PROSPECTIVITY MODELING RESULTS: WEIGHTS-OF-EVIDENCE (WOFE) APPROACH

Prospectivity class	Deposits [*n*]	%	Deposits with resources [*n*]	%	Paleo-valley Area (%)	Study Area (%)
High	158	69	26	100	6	1
Moderate	42	18	0	0	27	7
Low	30	13	0	0	67	92
Total	230	100	26	100	100	100

Total number of deposits = 236; total number of deposits outside mapped paleovalleys = 6; total number of deposits used in the modeling = 236 – 6 = 230; Total number of deposits with identified resources = 27; Total number of deposits with identified resources outside mapped paleovalleys = 1; total number of deposits with identified resources used in the modeling = 27 – 1 = 26.
Results: Approximately 8% of the study area (or 33% of the paleo-valley area) was identified as highly to moderately prospective, capturing 87% of the known calcrete-hosted uranium occurrences and all deposits with identified resources.

TABLE 6C. PROSPECTIVITY MODELING RESULTS: ARTIFICIAL NEURAL NETWORKS (ANN) APPROACH

Prospectivity class	Deposits (*n*0	%	Deposits with resources (*n*)	%	Validation deposits with resources (n)	%	Paleo-valley Area (%)	Study Area (%)
High	111	48	11	42	3	25	3	1
Moderate	101	44	15	48	9	75	27	6
Low	18	8	0	0	0	0	70	93
Total	230	100	26	100	12	100	100	100

Total number of deposits = 236; total number of deposits outside mapped paleovalleys = 6; total number of deposits used in the modeling = 236 – 6 = 230; Total number of deposits with identified resources = 27; Total number of deposits with identified resources outside mapped paleovalleys = 1; total number of deposits with identified resources used in the modeling = 27 – 1 = 26.
Result: Approximately 7% of the study area (or 30% of the paleo-valley area) was identified as highly to moderately prospective, capturing 92% of the known calcrete-hosted uranium occurrences and all deposits with identified resources. In addition, approximately 89% of the validation deposits not used for training are located within the prospective area.

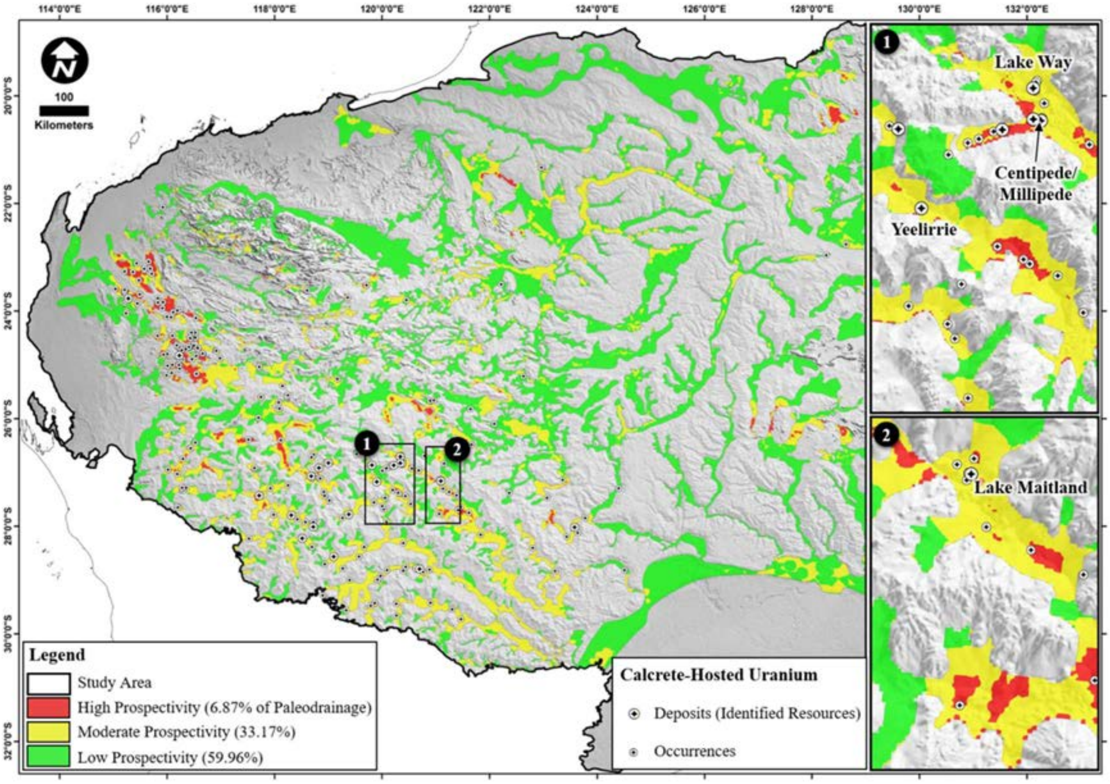

FIG. 45 (continued). (c) Artificial Neural Networks (ANN).

5. QUANTITATIVE URANIUM RESOURCE ASSESSMENT

5.3. Delineation of geologically-permissive tracts

As described in above, we used three complimentary approaches to quantitative resource assessment (Fig. 46) for estimating undiscovered calcrete-hosted uranium endowment in the deserts and xeric shrublands region of Western Australia:

— Regression models of deposit density and endowment density [52];
— Rank-size distribution, or Zipf's Law, analysis [53, 67];
— The USGS three-part quantitative mineral resource assessment [54].

The first step in any QMRA is the delineation of geologically-permissive tracts. Calcrete bodies that form the geologically-permissive tracts for calcrete-hosted uranium deposits were taken from the Geological Survey of Western Australia's digital 1:500,000 scale regolith map of Western Australia (Table 1). A total of 214 calcrete bodies were recorded in the study area (Fig. 10). However, as illustrated by the prospectivity models, not all of these bodies are permissive for the existence of calcrete-hosted uranium deposits. Based on the results of our prospectivity modeling (Fig. 45), only 85 (or ~40%) of these 214 calcrete bodies represent geologically-permissive tracts characterized by a greater than zero probability of hosting a uranium deposit. Given this result and to avoid over-estimating the total uranium endowment and number of undiscovered uranium deposits, only the 85 calcretes deemed prospective were considered in this QMRA (Fig. 47).

The next step involved the identification of control areas, a critical task for developing deposit density and endowment density models. Control areas are defined as those parts of the geologically-permissive tracts that are expected to have been thoroughly explored and, therefore, are unlikely to contain any undiscovered resources. In the deserts and xeric shrublands region of Western Australia, suitable control areas are those calcrete bodies containing known, well-explored deposits with Measured and Indicated JORC-compliant resources [136], such as Yeelirrie (Fig. 47; Table 2). The identification of control areas is a prerequisite for developing an empirical model describing the relationship between the size (in km^2) of a prospective area and associated deposit density and endowment density. The resulting deposit density and endowment density models can then be applied to estimating the number of undiscovered deposits and amount of undiscovered endowment for un- or underexplored, geologically similar geologically-permissive tracts. In case of the three-part QMRA, the empirical model of deposit density is used as an input in conjunction with grade-and-tonnage models for estimating undiscovered endowment and using Monte-Carlo simulation.

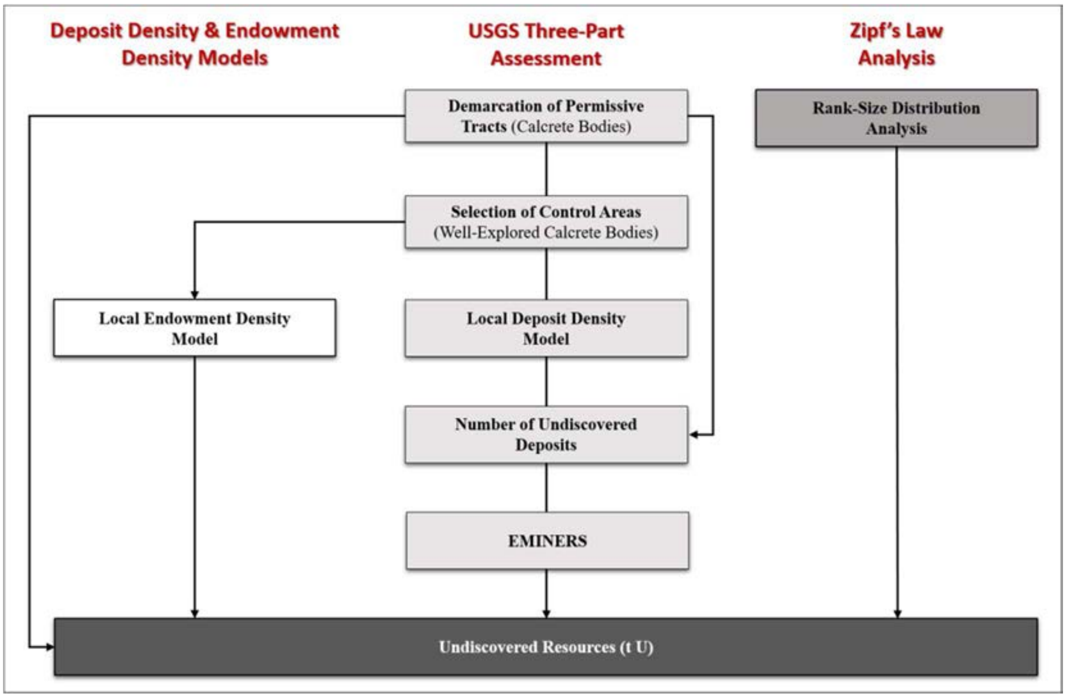

FIG. 46. Schematic representation of the workflow adopted in this Quantitative Resource Assessment.

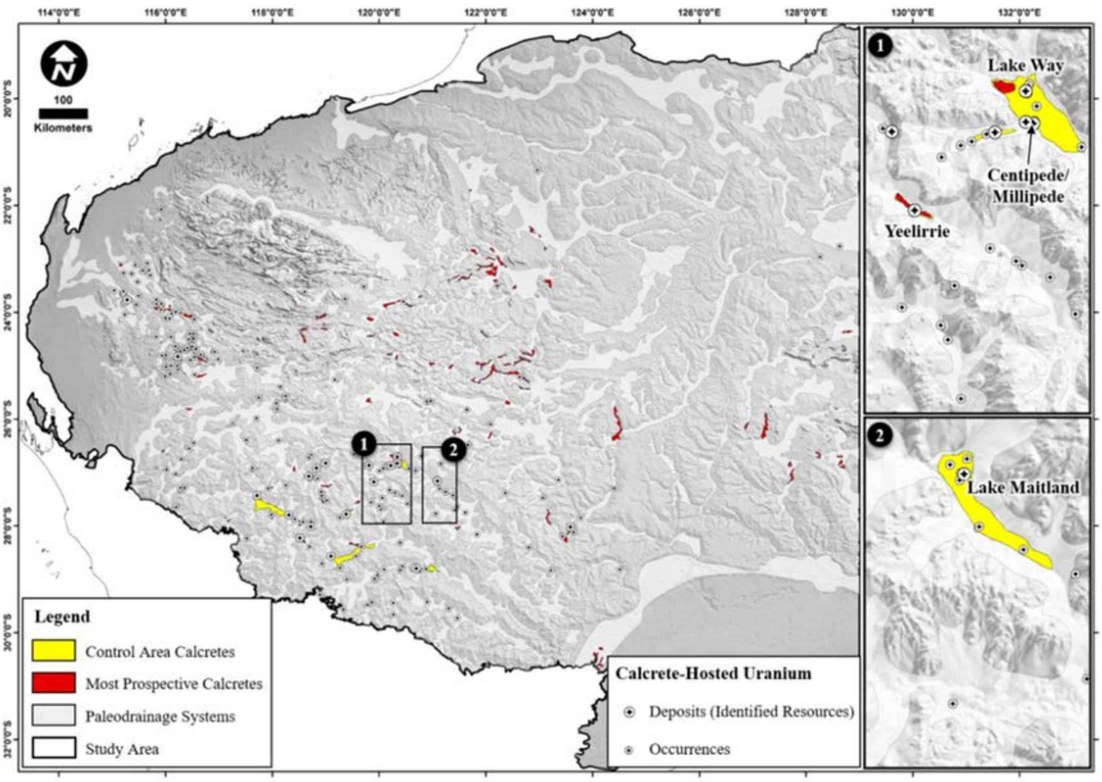

FIG. 47. Geologically-permissive tracts considered in this quantitative resource assessment. These tracts represent the 85 most prospective calcrete bodies out of a total of 240 calcrete bodies in the study area and were selected based on the results of the prospectivity analyses. Also shown are the nominated control areas (calcrete bodies with well-explored, identified resources).

In contrast to the above, Zipf's Law analysis is a non-spatial statistical approach that neither requires an understanding of the geological controls nor the delineation of geologically-permissive tracts or control areas. Only fully-delineated deposits and their pre-mining resource figures are necessary for modeling the undiscovered endowment and number of undiscovered deposits.

As outlined above, the study area contains more than 200 calcrete-hosted uranium occurrences, prospects and deposits. Of these, only 20 are well-explored with established grade and tonnage figures (Table 2). For the purpose of this study, the 18 calcrete bodies that host these 20 deposits served as the control areas for the QMRA models.

5.4. Regression models

5.4.1. Deposit density models

The deposit density for each control area was estimated by dividing the number of contained deposits by the size of the control area in square kilometers (Table 7).

TABLE 7. ESTIMATION OF DEPOSIT DENSITY FOR CONTROL AREA CALCRETE BODIES

Rank	Calcrete body (name)*	Surface area (km^2)	Deposits (per calcrete body)	Deposit density (deposits/surface area)	Log (area)	Log (density)
1	Bellah Bore East	0.0421	1	23.7452	-1.3756	1.3756
2	Jailor Bore	0.1555	1	6.4326	-0.8084	0.8084
3	Minindi Creek	4.0836	1	0.2449	0.6110	-0.6110
4	Anketell	7.6807	1	0.1302	0.8854	-0.8854
5	Murchison Downs	16.4440	1	0.0608	1.2160	-1.2160
6	Hillview	17.8510	1	0.0560	1.2517	-1.2517
7	Dawson-Hinkler	32.0647	1	0.0312	1.5060	-1.5060
8	Yeelirrie	33.6646	1	0.0297	1.5272	-1.5272
9	Thatcher Soak	43.0437	1	0.0232	1.6339	-1.6339
10	Windimurra	43.4449	1	0.0230	1.6379	-1.6379
11	Lake Mason	55.9799	1	0.0179	1.7480	-1.7480
12	Lakeside	65.0232	1	0.0154	1.8131	-1.8131
13	Nowthanna	70.0921	1	0.0143	1.8457	-1.8457
14	Lake Maitland	214.5020	1	0.0047	2.3314	-2.3314
15	Peninsula	339.2850	1	0.0029	2.5306	-2.5306
16	Centipede, Lake Way, Millipede	483.9240	3	0.0062	2.6848	-2.2077
17	Wondinong	897.5370	1	0.0011	2.9531	-2.9531
18	Yuinmery	929.4700	1	0.0011	2.9682	-2.9682

*The control area calcrete bodies were named after the deposits hosted by these bodies.

The deposit density model (Eq. 25) was generated by fitting a log-linear least-squares model to the plot of deposit density against the size (Fig. 48).

$$y = -0.975x - 0.0109 \; (R^2 = 0.9908) \qquad (25)$$

where x is the $\log_{10}$ of the size of the size of control area in square kilometers and y is the $\log_{10}$ of the deposit density. The prediction interval was estimated as:

$$PI(90\%) = t_{0.1}S_{yx}\sqrt{1 + \frac{1}{n} + [\frac{x_o - \bar{x}}{S_{xx}}]} \qquad (26)$$

where n is the number of observations (in this case n = 6 control area calcretes), $t_{0.1}$ is the two-tailed t-value at 0.9 probability level and with degrees of freedom = n–2($t_{0.1,4}$=2.1318), S_{yx} is the standard error of the predicted y-value for each x in the regression. It is the measure of the amount of error in the prediction of y for a given value of x. The latter is estimated by way of Equation 27:

$$S_{yx} = \sqrt{\frac{1}{n-2} \times \left[\sum(y-\bar{y}) - \frac{[\sum(x-\bar{x})\times(y-\bar{y})]^2}{\sum(x-\bar{x})^2}\right]}=0.1474 \quad (27)$$

$S_{xx} = \sum(x-\bar{x})^2 = 1.58$ is the sum of squares of the deviation from the mean, where x is the logarithm of area of the control calcretes, y is the logarithm of the deposit density calculated for the control calcretes, $\bar{x}$=2.15 is the mean of the logarithm of area of control calcretes, and x_o is the logarithm area value at which deposit density is to be estimated from the model.

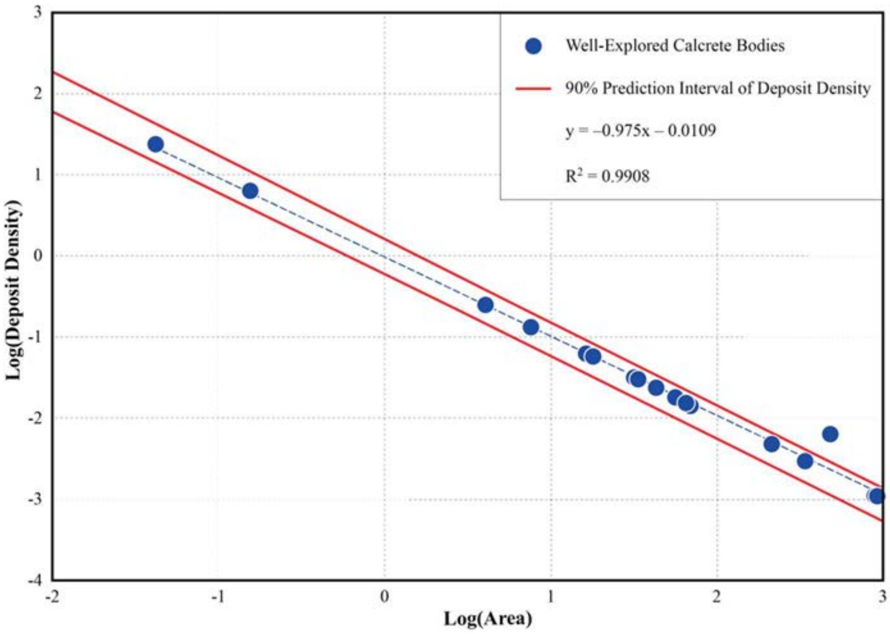

FIG. 48. Log-linear least squares regression model of deposit density in the control areas.

The log-linear correlation between the logarithm of deposit density and the logarithm of the calcrete areas is reasonably strong, meaning that this model is valid for estimating deposit densities of the un- and under-explored calcrete bodies in the study area. The upper and lower envelopes of the 90% prediction interval of y are given by Equation 28:

$$y - PI < y < y + PI \quad (28)$$

The deposit density of each prospective un- or under-explored calcrete body was obtained with Equation 25 using the size of the calcrete body in square kilometers. The number of deposits hosted by a calcrete body was estimated by multiplying the deposit density with the size of the calcrete area. The total number of undiscovered deposits in the study area was obtained by adding up the number of expected deposits for all prospective calcrete bodies and subtracting from this total the number of known deposits. The upper and lower envelopes provide the U10 and L90 estimates of the number of undiscovered deposits (Fig. 48; Table 8). The R50 band represents the mean number of undiscovered deposits derived from Equation 27.

The results suggest that at 90%, 50% and 10% confidence levels the number of undiscovered calcrete-hosted uranium deposits within the study areas is 29, 58, and 105, respectively.

5.4.2. Endowment density models

The endowment density for each control area calcrete body was estimated by dividing the endowment of the calcrete body in tonnes uranium (t U) by its size in square kilometers (Table 9). The endowment density model in Equation 27 was generated by fitting a log-linear least-squares model to the plot of endowment density against the size of the control area calcrete (Fig. 49):

$$y = -0.67x + 2.7072; R^2=0.5939 \qquad (27)$$

where x is the $\log_{10}$ of the size of the size of control area in square kilometers and y is the $\log_{10}$ of the endowment density. The 90% prediction interval and with the upper and lower envelopes of the predictions were estimated using Equations 24, 25 and 26.

TABLE 8. ESTIMATION OF THE TOTAL NUMBER OF DEPOSITS WITHIN PROSPECTIVE CALCRETE BODIES USING DEPOSIT DENSITY MODELS

Rank	Prospective calcrete body (km^2)	90% Prediction interval of log of deposit density					Estimate of number of deposits = 10^ (deposit density*area)		
		Log area	CL	Y+CL (U10)	Y-CL (L90)	Y (= R50)	U10	R50	L90
1	1.3436	0.1283	0.2087	0.0674	-0.3500	-0.1413	1.5692	0.9705	0.6002
2	7.3699	0.8675	0.2026	-0.6898	-1.0951	-0.8924	1.5054	0.9441	0.5921
3	60.6965	1.7832	0.2013	-1.6216	-2.0242	-1.8229	1.4505	0.9125	0.5740
4	15.2025	1.1819	0.2014	-1.0106	-1.4134	-1.2120	1.4836	0.9331	0.5869
5	27.5556	1.4402	0.2010	-1.2735	-1.6754	-1.4744	1.4681	0.9242	0.5818
6	51.6070	1.7127	0.2012	-1.5502	-1.9525	-1.7513	1.4539	0.9149	0.5757
7	86.8920	1.9390	0.2018	-1.7795	-2.1831	-1.9813	1.4437	0.9072	0.5701
8	29.7308	1.4732	0.2010	-1.3070	-1.7089	-1.5080	1.4662	0.9231	0.5811
9	277.3694	2.4431	0.2047	-2.2888	-2.6982	-2.4935	1.4264	0.8903	0.5557
10	22.0845	1.3441	0.2011	-1.1757	-1.5778	-1.3768	1.4736	0.9275	0.5838
11	92.7149	1.9671	0.2019	-1.8080	-2.2118	-2.0099	1.4426	0.9063	0.5693
12	22.1855	1.3461	0.2011	-1.1777	-1.5798	-1.3788	1.4735	0.9275	0.5838
13	92.8957	1.9680	0.2019	-1.8089	-2.2127	-2.0108	1.4425	0.9062	0.5693
14	27.4884	1.4391	0.2010	-1.2724	-1.6743	-1.4734	1.4681	0.9242	0.5818
15	10.5954	1.0251	0.2019	-0.8507	-1.2545	-1.0526	1.4941	0.9386	0.5896
16	171.6459	2.2346	0.2032	-2.0785	-2.4849	-2.2817	1.4327	0.8973	0.5619
17	0.7443	-0.1283	0.2118	0.3312	-0.0924	0.1194	1.5956	0.9798	0.6016
18	124.5118	2.0952	0.2025	-1.9376	-2.3425	-2.1400	1.4376	0.9019	0.5659
19	35.4061	1.5491	0.2010	-1.3841	-1.7860	-1.5851	1.4621	0.9205	0.5795
20	56.3926	1.7512	0.2012	-1.5892	-1.9917	-1.7905	1.4520	0.9136	0.5748
21	68.2791	1.8343	0.2014	-1.6735	-2.0763	-1.8749	1.4482	0.9107	0.5727
22	63.4687	1.8026	0.2014	-1.6413	-2.0440	-1.8426	1.4497	0.9118	0.5735
23	57.7638	1.7617	0.2013	-1.5998	-2.0023	-1.8011	1.4515	0.9132	0.5745
24	0.6817	-0.1664	0.2123	0.3704	-0.0541	0.1582	1.5997	0.9812	0.6018
25	47.4770	1.6765	0.2011	-1.5134	-1.9156	-1.7145	1.4556	0.9161	0.5766
26	56.3663	1.7510	0.2012	-1.5890	-1.9915	-1.7903	1.4520	0.9136	0.5748
27	4.5393	0.6570	0.2039	-0.4746	-0.8825	-0.6786	1.5218	0.9516	0.5950
28	45.0714	1.6539	0.2011	-1.4905	-1.8927	-1.6916	1.4567	0.9169	0.5771
29	21.6388	1.3352	0.2011	-1.1667	-1.5688	-1.3678	1.4741	0.9278	0.5840

Rank	Prospective calcrete body (km^2)	90% Prediction interval of log of deposit density					Estimate of number of deposits = 10^ (deposit density*area)		
		Log area	CL	Y+CL (U10)	Y-CL (L90)	Y (= R50)	U10	R50	L90
30	52.4078	1.7194	0.2012	-1.5570	-1.9593	-1.7581	1.4535	0.9147	0.5756
31	26.9205	1.4301	0.2010	-1.2632	-1.6651	-1.4642	1.4686	0.9246	0.5820
32	75.6206	1.8786	0.2016	-1.7184	-2.1215	-1.9200	1.4463	0.9092	0.5716
33	19.1602	1.2824	0.2012	-1.1129	-1.5152	-1.3141	1.4773	0.9297	0.5850
34	23.2647	1.3667	0.2010	-1.1987	-1.6008	-1.3997	1.4723	0.9267	0.5833
35	25.2518	1.4023	0.2010	-1.2349	-1.6369	-1.4359	1.4702	0.9255	0.5826
36	96.6980	1.9854	0.2020	-1.8265	-2.2304	-2.0285	1.4418	0.9056	0.5688
37	76.6804	1.8847	0.2016	-1.7245	-2.1277	-1.9261	1.4460	0.9090	0.5715
38	90.1097	1.9548	0.2018	-1.7955	-2.1992	-1.9973	1.4431	0.9067	0.5697
39	30.8791	1.4897	0.2010	-1.3237	-1.7257	-1.5247	1.4653	0.9225	0.5808
40	24.6210	1.3913	0.2010	-1.2237	-1.6258	-1.4247	1.4709	0.9259	0.5828
41	319.9666	2.5051	0.2052	-2.3514	-2.7617	-2.5566	1.4247	0.8883	0.5538
42	33.1410	1.5204	0.2010	-1.3549	-1.7569	-1.5559	1.4637	0.9215	0.5801
43	79.8950	1.9025	0.2017	-1.7426	-2.1459	-1.9442	1.4453	0.9084	0.5710
44	26.6248	1.4253	0.2010	-1.2583	-1.6603	-1.4593	1.4689	0.9247	0.5821
45	21.4964	1.3324	0.2011	-1.1638	-1.5659	-1.3649	1.4743	0.9279	0.5840
46	5.6493	0.7520	0.2033	-0.5718	-0.9784	-0.7751	1.5142	0.9482	0.5938
47	43.9204	1.6427	0.2011	-1.4791	-1.8812	-1.6802	1.4573	0.9173	0.5774
48	42.2590	1.6259	0.2010	-1.4621	-1.8642	-1.6632	1.4581	0.9178	0.5777
49	1.3493	0.1301	0.2087	0.0655	-0.3519	-0.1432	1.5690	0.9704	0.6002
50	322.4226	2.5084	0.2052	-2.3547	-2.7651	-2.5599	1.4247	0.8882	0.5537
51	23.9655	1.3796	0.2010	-1.2118	-1.6139	-1.4128	1.4715	0.9263	0.5831
52	223.1322	2.3486	0.2040	-2.1935	-2.6015	-2.3975	1.4291	0.8935	0.5586
53	41.0234	1.6130	0.2010	-1.4490	-1.8511	-1.6501	1.4588	0.9183	0.5780
54	23.5583	1.3721	0.2010	-1.2042	-1.6063	-1.4053	1.4720	0.9266	0.5832
55	27.0817	1.4327	0.2010	-1.2658	-1.6678	-1.4668	1.4685	0.9245	0.5820
56	30.7902	1.4884	0.2010	-1.3225	-1.7244	-1.5234	1.4654	0.9225	0.5808
57	68.7933	1.8375	0.2014	-1.6768	-2.0796	-1.8782	1.4481	0.9106	0.5727
58	13.7709	1.1390	0.2015	-0.9668	-1.3698	-1.1683	1.4864	0.9346	0.5877
59	43.3144	1.6366	0.2010	-1.4730	-1.8751	-1.6740	1.4576	0.9175	0.5775
60	63.1357	1.8003	0.2013	-1.6390	-2.0417	-1.8403	1.4498	0.9119	0.5736

Rank	Prospective calcrete body (km^2)	90% Prediction interval of log of deposit density					Estimate of number of deposits = 10^ (deposit density*area)		
		Log area	CL	Y+CL (U10)	Y-CL (L90)	Y (= R50)	U10	R50	L90
61	30.5459	1.4850	0.2010	-1.3189	-1.7209	-1.5199	1.4656	0.9227	0.5809
62	23.5845	1.3726	0.2010	-1.2047	-1.6068	-1.4058	1.4719	0.9265	0.5832
63	39.6372	1.5981	0.2010	-1.4339	-1.8359	-1.6349	1.4596	0.9188	0.5784
64	21.4801	1.3320	0.2011	-1.1634	-1.5656	-1.3645	1.4743	0.9279	0.5840
65	85.5669	1.9323	0.2018	-1.7727	-2.1762	-1.9745	1.4440	0.9074	0.5702
66	33.5407	1.5256	0.2010	-1.3602	-1.7622	-1.5612	1.4634	0.9213	0.5800
67	42.2812	1.6261	0.2010	-1.4624	-1.8644	-1.6634	1.4581	0.9178	0.5777
68	26.0193	1.4153	0.2010	-1.2481	-1.6501	-1.4491	1.4695	0.9251	0.5823
69	28.2568	1.4511	0.2010	-1.2846	-1.6865	-1.4855	1.4675	0.9238	0.5816
70	60.2077	1.7797	0.2013	-1.6181	-2.0207	-1.8194	1.4507	0.9126	0.5741
71	44.1485	1.6449	0.2011	-1.4814	-1.8835	-1.6825	1.4572	0.9172	0.5773
72	32.8656	1.5167	0.2010	-1.3512	-1.7532	-1.5522	1.4638	0.9216	0.5802
73	81.8749	1.9132	0.2017	-1.7533	-2.1567	-1.9550	1.4448	0.9081	0.5707
74	25.0319	1.3985	0.2010	-1.2310	-1.6331	-1.4320	1.4704	0.9256	0.5827
75	51.7124	1.7136	0.2012	-1.5511	-1.9534	-1.7522	1.4538	0.9148	0.5757
76	14.1001	1.1492	0.2015	-0.9773	-1.3802	-1.1787	1.4858	0.9343	0.5875
77	9.2038	0.9640	0.2022	-0.7883	-1.1927	-0.9905	1.4984	0.9407	0.5906
78	29.9456	1.4763	0.2010	-1.3102	-1.7121	-1.5111	1.4661	0.9230	0.5811
79	29.8880	1.4755	0.2010	-1.3093	-1.7113	-1.5103	1.4661	0.9230	0.5811
80	76.8657	1.8857	0.2016	-1.7256	-2.1288	-1.9272	1.4460	0.9090	0.5714
81	20.1853	1.3050	0.2011	-1.1360	-1.5382	-1.3371	1.4760	0.9289	0.5846
82	51.4256	1.7112	0.2012	-1.5486	-1.9509	-1.7498	1.4539	0.9149	0.5757
83	26.3543	1.4209	0.2010	-1.2538	-1.6558	-1.4548	1.4692	0.9249	0.5822
84	46.2204	1.6648	0.2011	-1.5016	-1.9038	-1.7027	1.4562	0.9165	0.5768
85	51.3805	1.7108	0.2012	-1.5483	-1.9506	-1.7494	1.4539	0.9149	0.5758
			Total				124.6997	78.3265	49.1998

Key to abbreviations: CL = Confidence limit; L90 = Estimate at lower 10% confidence limit (i.e., there is 90% probability of the actual number of deposits exceeding the L90 estimate); R50 = Mean estimate of the number of deposits, derived from Equation 27; U10 = Estimate at upper 10% confidence limit (i.e., there is 10% probability of the actual number of deposits exceeding the U10 estimate).

The endowment density of each prospective un- or under-explored calcrete body was estimated with Equation 27 by inputting the size of the calcrete body in square kilometers. The endowment in t U of each calcrete body was then estimated by multiplying the endowment density with the size of the respective calcrete areas. The total undiscovered endowment in the study area was calculated by summing up the expected endowment for all prospective calcrete bodies and subtracting the identified endowment. The upper and lower envelopes give the U10 and L90 estimates of the endowment (Fig. 49; Table 10).

The results illustrate that the total undiscovered endowment at the 90%, 50% and 10% confidence levels is nil, 48,000 t U and 2,150,000 t U, respectively.

5.5. USGS three-part assessment

For the purpose of this study, we utilized EMINERS [68] [69], a Monte Carlo mineral resource simulator developed by the USGS for estimating undiscovered endowment according to the USGS three-part assessment [54]. EMINERS requires input in form of (a) global or local grade and ore tonnage data for the deposit type under consideration, and (b) an estimate of the number of undiscovered deposits at 10%, 50% and 90% confidence levels. The undiscovered endowment is estimated by way of Monte Carlo simulation using the frequency distributions of the grade and the ore tonnage data. Uranium metal tonnages are estimated from the input grades.

Grade frequency and tonnage frequency models were generated using the calcrete-hosted uranium deposit data available for the study area (Table 2). A local model of deposit density developed for the study area (Eq. 25) was used to estimate the number of undiscovered deposits at the 90% (n = 29 undiscovered deposits), 50% (n = 58) and 10% (n = 105) confidence levels.

The results returned by EMINERS suggest a total undiscovered endowment at the 90%, 50% and 10% confidence levels of 102,000 t U, 387,000 t U and 908,000 t U, respectively.

TABLE 9. ESTIMATION OF ENDOWMENT DENSITY FOR CONTROL AREA CALCRETE BODIES

Rank	Calcrete body *[name]* *	Surface area *[km²]*	Identified endowment *[t U]*	Endowment density *[surface area / endowment]*	Log (area)	Log (endowment density)
1	Bellah Bore East	0.0421	28	664.8652	-1.3756	2.8227
2	Jailor Bore	0.1555	615	3,956.0524	-0.8084	3.5973
3	Minindi Creek	4.0836	346	84.7296	0.6110	1.9280
4	Anketell	7.6807	2,308	300.4938	0.8854	2.4778
5	Murchison Downs	16.4440	154	9.3651	1.2160	0.9715
6	Hillview	17.8510	4,077	228.3906	1.2517	2.3587
7	Dawson-Hinkler	32.0647	1,231	38.3911	1.5060	1.5842
8	Yeelirrie	33.6646	48,966	1,454.5249	1.5272	3.1627
9	Thatcher Soak	43.0437	5,885	136.7215	1.6339	2.1358
10	Windimurra	43.4449	2,885	66.4060	1.6379	1.8222
11	Lake Mason	55.9799	1,423	25.4198	1.7480	1.4052
12	Lakeside	65.0232	1,092	16.7940	1.8131	1.2252
13	Nowthanna	70.0921	4,039	57.6242	1.8457	1.7606
14	Lake Maitland	214.5020	9,347	43.5754	2.3314	1.6392
15	Peninsula	339.2850	1,365	4.0232	2.5306	0.6046
16	Centipede, Lake Way, Millipede	483.9240	12,385	25.5929	2.6848	1.4081
17	Wondinong	897.5370	1,000	1.1142	2.9531	0.0469
18	Yuinmery	929.4700	481	0.5175	2.9682	-0.2861

*The control area calcrete bodies were named after the deposits hosted by these bodies.

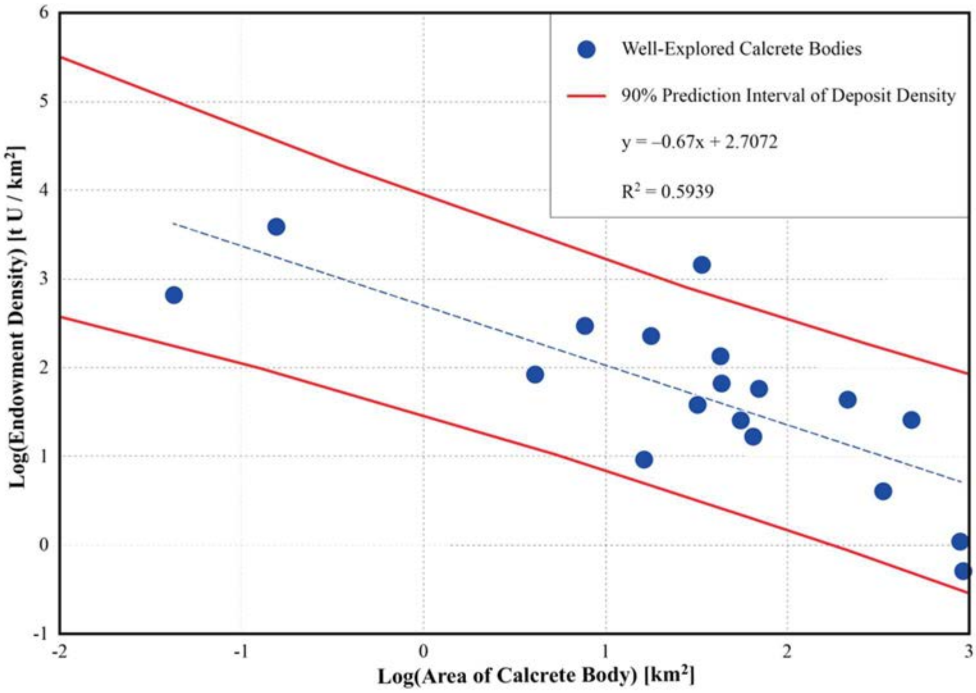

FIG. 49. Log-linear least squares regression model of endowment density in the control areas.

5.6. Zipf's law analysis

The third approach used in this study to estimate undiscovered endowment is the rank-size distribution, or Zipf's Law analysis. For the purpose of this analysis, the 20 deposits in the study area with existing resource estimates were arranged in ascending order of their respective ore tonnages, and then ranked and plotted (Fig. 50; Table 11). The best fit power law for tonnage versus rank was found to vary from the expected Zipf's Law (Eq. 28):

$$\textit{Tonnage}\ (\text{t U}) = 63{,}830 \times \textit{Rank}^{(-1.728)};\ (R^2 = 0.77) \tag{28}$$

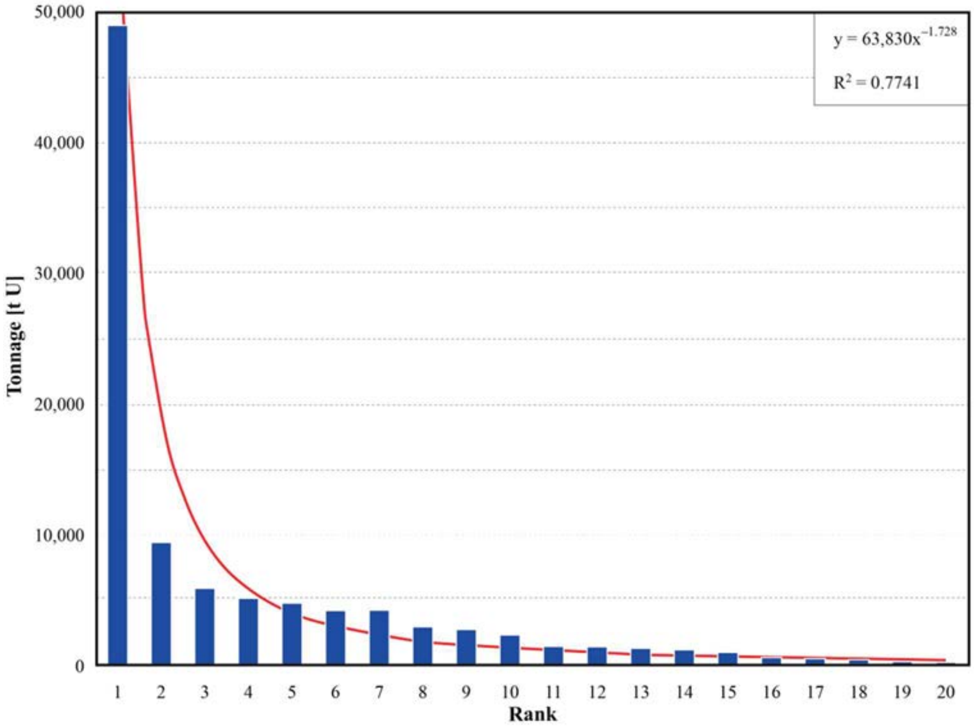

FIG. 50. Zipf's model of rank versus tonnage distribution of the 20 calcrete-hosted uranium deposits in the study area with identified resources.

TABLE 10. ESTIMATION OF TOTAL ENDOWMENT CONTAINED WITHIN PROSPECTIVE CALCRETE BODIES USING ENDOWMENT DENSITY MODELS

Rank	Prospective calcrete body (km^2)	90% Prediction interval of log of deposit density				Estimate of endowment = 10^ (endowment density*area)		
		Log area	CL	Y+CL (U10)	Y-CL (L90)	U10	R50	L90
1	1.3436	0.1283	1.2280	3.8492	1.3932	9,494.6437	561.6651	33.2259
2	7.3699	0.8675	1.1923	3.3182	0.9337	15,334.4427	984.8972	63.2578
3	60.6965	1.7832	1.1845	2.6969	0.3279	30,203.0384	1,974.9053	129.1344
4	15.2025	1.1819	1.1850	3.1002	0.7303	19,147.3560	1,250.6970	81.6950
5	27.5556	1.4402	1.1826	2.9247	0.5596	23,171.5554	1,521.8834	99.9557
6	51.6070	1.7127	1.1836	2.7432	0.3760	28,571.4173	1,871.9663	122.6491
7	86.8920	1.9390	1.1873	2.5953	0.2207	34,218.1956	2,223.1097	144.4324
8	29.7308	1.4732	1.1825	2.9026	0.5376	23,756.1513	1,560.5198	102.5091
9	277.3694	2.4431	1.2044	2.2746	- 0.1342	52,201.1353	3,260.5602	203.6594
10	22.0845	1.3441	1.1831	2.9897	0.6235	21,564.5196	1,414.6985	92.8086
11	92.7149	1.9671	1.1879	2.5770	0.2012	35,009.3464	2,271.2041	147.3426
12	22.1855	1.3461	1.1831	2.9883	0.6222	21,596.2665	1,416.8300	92.9516
13	92.8957	1.9680	1.1879	2.5765	0.2006	35,033.4334	2,272.6643	147.4307
14	27.4884	1.4391	1.1826	2.9255	0.5603	23,153.0621	1,520.6581	99.8745
15	10.5954	1.0251	1.1880	3.2083	0.8323	17,116.5965	1,110.2307	72.0127
16	171.6459	2.2346	1.1958	2.4057	0.0140	43,688.0202	2,783.0308	177.2857
17	0.7443	- 0.1283	1.2462	4.0393	1.5469	8,147.0461	462.2041	26.2221
18	124.5118	2.0952	1.1913	2.4946	0.1120	38,886.5007	2,503.2981	161.1485
19	35.4061	1.5491	1.1826	2.8518	0.4867	25,168.7485	1,653.1212	108.5795
20	56.3926	1.7512	1.1841	2.7179	0.3497	29,450.0324	1,927.5534	126.1616
21	68.2791	1.8343	1.1853	2.6634	0.2928	31,456.0918	2,053.1265	134.0067
22	63.4687	1.8026	1.1848	2.6842	0.3146	30,671.3778	2,004.2244	130.9663
23	57.7638	1.7617	1.1842	2.7110	0.3426	29,693.5250	1,942.8940	127.1266
24	0.6817	- 0.1664	1.2491	4.0678	1.5695	7,968.0831	448.9988	25.3009
25	47.4770	1.6765	1.1833	2.7671	0.4006	27,773.2188	1,821.1463	119.4163
26	56.3663	1.7510	1.1841	2.7180	0.3498	29,445.3293	1,927.2568	126.1429
27	4.5393	0.6570	1.1998	3.4668	1.0671	13,298.1225	839.3495	52.9780
28	45.0714	1.6539	1.1831	2.7821	0.4159	27,289.0028	1,790.1654	117.4353
29	21.6388	1.3352	1.1831	2.9957	0.6294	21,423.3419	1,405.2129	92.1716
30	52.4078	1.7194	1.1837	2.7388	0.3714	28,721.7281	1,881.5020	123.2534
31	26.9205	1.4301	1.1826	2.9316	0.5664	22,995.6300	1,510.2197	99.1825
32	75.6206	1.8786	1.1861	2.6345	0.2623	32,593.0067	2,123.4920	138.3493

Rank	Prospective calcrete body (km^2)	90% Prediction interval of log of deposit density				Estimate of endowment = 10^ (endowment density*area)		
		Log area	CL	Y+CL (U10)	Y-CL (L90)	U10	R50	L90
33	19.1602	1.2824	1.1836	3.0315	0.6643	20,603.7963	1,349.9221	88.4444
34	23.2647	1.3667	1.1829	2.9743	0.6085	21,930.1273	1,439.2109	94.4512
35	25.2518	1.4023	1.1827	2.9503	0.5849	22,520.9665	1,478.6647	97.0851
36	96.6980	1.9854	1.1884	2.5652	0.1885	35,533.8462	2,302.9477	149.2540
37	76.6804	1.8847	1.1862	2.6305	0.2582	32,751.6619	2,133.2665	138.9495
38	90.1097	1.9548	1.1876	2.5850	0.2098	34,659.1058	2,249.9446	146.0583
39	30.8791	1.4897	1.1825	2.8915	0.5265	24,054.3477	1,580.1565	103.8022
40	24.6210	1.3913	1.1828	2.9577	0.5922	22,336.5817	1,466.3732	96.2659
41	319.9666	2.5051	1.2073	2.2360	- 0.1787	55,092.3770	3,417.9493	212.0507
42	33.1410	1.5204	1.1825	2.8710	0.5060	24,622.6684	1,617.4492	106.2493
43	79.8950	1.9025	1.1865	2.6189	0.2459	33,225.1046	2,162.3704	140.7323
44	26.6248	1.4253	1.1826	2.9348	0.5695	22,912.8312	1,504.7243	98.8178
45	21.4964	1.3324	1.1832	2.9976	0.6313	21,377.8733	1,402.1554	91.9661
46	5.6493	0.7520	1.1962	3.3995	1.0071	14,172.8727	902.1727	57.4277
47	43.9204	1.6427	1.1830	2.7895	0.4235	27,051.8617	1,774.9505	116.4596
48	42.2590	1.6259	1.1829	2.8006	0.4348	26,702.8781	1,752.5088	115.0171
49	1.3493	0.1301	1.2279	3.8478	1.3921	9,505.4161	562.4593	33.2821
50	322.4226	2.5084	1.2075	2.2339	- 0.1811	55,252.2027	3,426.5841	212.5070
51	23.9655	1.3796	1.1828	2.9656	0.6000	22,141.9064	1,453.3751	95.3983
52	223.1322	2.3486	1.2003	2.3338	- 0.0667	48,125.0044	3,034.6682	191.3602
53	41.0234	1.6130	1.1828	2.8092	0.4436	26,437.9500	1,735.4315	113.9166
54	23.5583	1.3721	1.1829	2.9707	0.6049	22,019.3284	1,445.1799	94.8505
55	27.0817	1.4327	1.1826	2.9298	0.5646	23,040.5130	1,513.1970	99.3800
56	30.7902	1.4884	1.1825	2.8924	0.5274	24,031.5126	1,578.6545	103.7034
57	68.7933	1.8375	1.1853	2.6613	0.2906	31,538.0018	2,058.2151	134.3221
58	13.7709	1.1390	1.1857	3.1297	0.7583	18,563.0870	1,210.5382	78.9418
59	43.3144	1.6366	1.1830	2.7935	0.4276	26,925.4941	1,766.8314	115.9382
60	63.1357	1.8003	1.1848	2.6857	0.3162	30,615.7583	2,000.7478	130.7494
61	30.5459	1.4850	1.1825	2.8947	0.5297	23,968.5268	1,574.5100	103.4307
62	23.5845	1.3726	1.1829	2.9703	0.6046	22,027.2456	1,445.7095	94.8859
63	39.6372	1.5981	1.1827	2.8191	0.4536	26,134.9929	1,715.8592	112.6525
64	21.4801	1.3320	1.1832	2.9978	0.6315	21,372.6653	1,401.8051	91.9426
65	85.5669	1.9323	1.1872	2.5996	0.2253	34,033.8452	2,211.8658	143.7496
66	33.5407	1.5256	1.1825	2.8675	0.5025	24,720.6326	1,623.8601	106.6689

Rank	Prospective calcrete body (km^2)	90% Prediction interval of log of deposit density				Estimate of endowment = 10^ (endowment density*area)		
		Log area	CL	Y+CL (U10)	Y-CL (L90)	U10	R50	L90
67	42.2812	1.6261	1.1829	2.8005	0.4347	26,707.5831	1,752.8118	115.0366
68	26.0193	1.4153	1.1827	2.9415	0.5762	22,741.5644	1,493.3453	98.0619
69	28.2568	1.4511	1.1825	2.9174	0.5523	23,362.9744	1,534.5549	100.7945
70	60.2077	1.7797	1.1845	2.6992	0.3303	30,119.1452	1,969.6428	128.8049
71	44.1485	1.6449	1.1830	2.7880	0.4220	27,099.1454	1,777.9865	116.6544
72	32.8656	1.5167	1.1825	2.8734	0.5084	24,554.7448	1,613.0011	105.9580
73	81.8749	1.9132	1.1868	2.6120	0.2385	33,511.1407	2,179.9076	141.8035
74	25.0319	1.3985	1.1827	2.9529	0.5874	22,457.0044	1,474.4030	96.8012
75	51.7124	1.7136	1.1836	2.7426	0.3754	28,591.2807	1,873.2271	122.7290
76	14.1001	1.1492	1.1855	3.1226	0.7516	18,700.6483	1,220.0116	79.5923
77	9.2038	0.9640	1.1895	3.2508	0.8718	16,396.5698	1,059.8263	68.5041
78	29.9456	1.4763	1.1825	2.9005	0.5355	23,812.4575	1,564.2314	102.7538
79	29.8880	1.4755	1.1825	2.9010	0.5360	23,797.3997	1,563.2390	102.6884
80	76.8657	1.8857	1.1862	2.6299	0.2575	32,779.2671	2,134.9661	139.0538
81	20.1853	1.3050	1.1834	3.0162	0.6493	20,950.1902	1,373.3388	90.0259
82	51.4256	1.7112	1.1836	2.7442	0.3770	28,537.1878	1,869.7933	122.5113
83	26.3543	1.4209	1.1826	2.9378	0.5725	22,836.6151	1,499.6625	98.4817
84	46.2204	1.6648	1.1832	2.7748	0.4085	27,522.1661	1,805.0980	118.3911
85	51.3805	1.7108	1.1836	2.7445	0.3773	28,528.6611	1,869.2519	122.4769
Total						2,251,248.6950	146,215.8434	9,500.5003

Key to abbreviations: CL = Confidence limit; L90 = Estimate at lower 10% confidence limit (i.e., there is 90% probability of the actual number of deposits exceeding the L90 estimate); R50 = Mean estimate of the number of deposits, derived from Equation 27; U10 = Estimate at upper 10% confidence limit (i.e., there is 10% probability of the actual number of deposits exceeding the U10 estimate)

The Pearson correlation function (R^2) result of 0.77 suggests that the calcrete-hosted uranium deposits in the study area follow a power law relationship. However, the expected power of the rank (i.e., k) should be equal to -1 (Eq. 1), whereas the actual number is –1.728. In addition, the value of constant c of 63,830 t U is much larger than the resource of Yeelirrie (48,966 t U), the largest calcrete-hosted uranium deposit in the study area. These discrepancies between actual and expected results are indicative of either the presence of undiscovered deposits or systematic under-estimation of the known uranium endowment.

Assuming that the uranium endowment in the study area is distributed according to Zipf's Law, the number and endowment of the undiscovered deposits can be estimated by applying the standard form of Zipf's Law (Eq. 1) with c = 48,965 (representing the uranium tonnage contained in Yeelirrie) and $k = –1$ (Eq. 29):

$$Tonnage\ (\text{t U}) = 48{,}966 \times Rank^{(-1)} \quad (29)$$

TABLE 11. ZIPF RANKING OF DEPOSITS WITH IDENTIFIED RESOURCES

Name	t U	Rank
Yeelirrie	48,966	1
Lake Maitland	9,347	2
Thatcher Soak	5,885	3
Centipede	5,000	4
Lake Way	4,731	5
Hillview	4,077	6
Nowthanna	4,039	7
Windimurra	2,885	8
Millipede	2,654	9
Anketell	2,308	10
Lake Mason	1,423	11
Peninsula	1,365	12
Dawson-Hinkler	1,231	13
Lakeside	1,092	14
Wondinong	1,000	15
Jailor Bore	615	16
Yuinmery	481	17
Minindi Creek	346	18
Murchison Downs	154	19
Bellah Bore East	28	20

The identified resources were substituted in Equation 29 to calculate the expected ranks of the known deposits, and rounded off to the next highest integer to obtain their adjusted ranks. The application of such a ceiling function ensured that the Zipf's curve, or best fit power law relationship, would coincide with the upper envelope of the identified endowment. It also ensured that the identified endowment was less than the endowment predicted by Zipf's Law. Given that the identified endowment is based on robust mineral resource estimates using industry standard resource calculation techniques, a systematic overestimation of these figures is unlikely. Moreover, none of the calcrete-hosted uranium deposits in the study have, or are being, mined and, therefore, their contained resources are likely to increase once these deposits are being fully delineated [66, 67]. The adjusted ranks were plotted against the tonnages of deposits with an endowment greater than 300 t U (Fig. 51; Table 12).

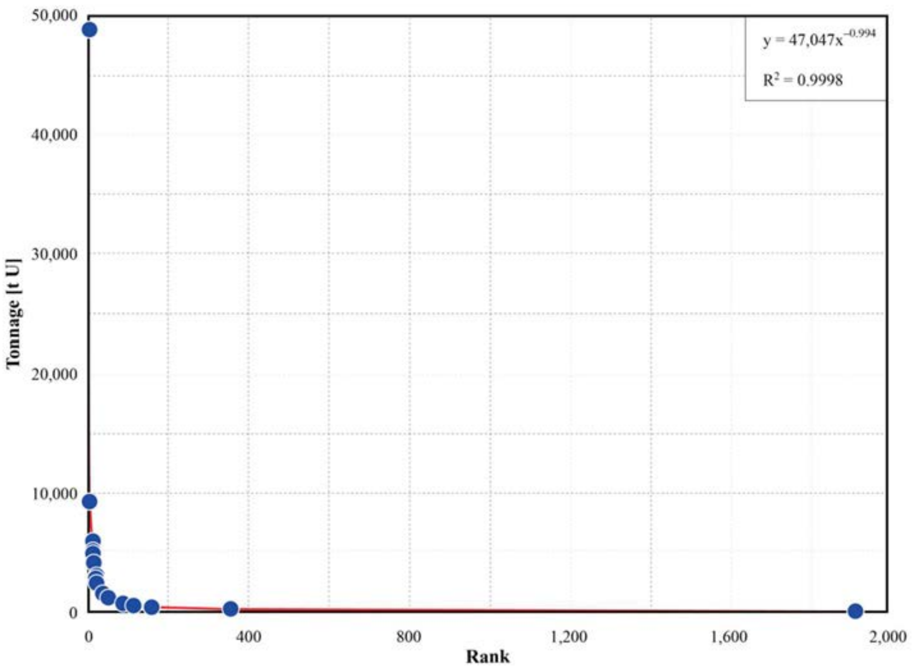

FIG. 51. Rank-adjusted Zipf's model of rank versus tonnage distribution of all calcrete-hosted uranium deposits in the study area that contain >300 t U.

TABLE 12. RANK ADJUSTED CALCRETE-HOSTED URANIUM DEPOSITS WITH IDENTIFIED RESOURCES

Deposits* (name)	Identified resources (t U)	Zipf's rank (adjusted)	Zipf's estimate (t U)	Undiscovered resources (t U)
Yeelirrie	48,966	1	48,966	-
Lake Maitland	9,347	5	9,793	446
Thatcher Soak	5,885	8	6,121	236
Centipede	5,000	9	5,441	440
Lake Way	4,731	10	4,897	165
Hillview	4,077	12	4,080	3
Nowthanna	4,039	12	4,080	42
Windimurra	2,885	16	3,060	175
Millipede	2,654	18	2,720	66
Anketell	2,308	21	2,332	24
Lake Mason	1,423	34	1,440	17
Peninsula	1,365	35	1,399	34
Dawson-Hinkler	1,231	39	1,256	25
Lakeside	1,092	44	1,113	20
Wondinong	1,000	48	1,020	20
Jailor Bore	615	79	620	4
Yuinmery	481	101	485	4
Minindi Creek	346	141	347	1
Total	97,447		99,169	1,723

*Using a minimum deposit size cut-off of >300 t U

Equation 30 gives the best fit power function for the rank adjusted size distribution:

$$\textit{Tonnage} \text{ (t U)} = 47{,}047\,\textit{Rank}^{(-0.9998)} \tag{30}$$

As evident from the rank-adjusted power law distribution above, the power is 0.9998 and, thus, very close to –1. This result indicates that the rank-adjusted deposit distribution follows Zipf's Law. In addition, the rank-adjusted value obtained for the constant c of 47,047 t U is much closer to the tonnage of Yeelirrie (48,966 t U) compared to the unadjusted value of 63,830 t U.

From the above rank-adjusted Zipf's Law model, two conclusions could be drawn:

1) Deposits at ranks 2, 3, 4, 6, 7 and at many of the higher ranks are missing (Table 12), indicating that the study area contains undiscovered deposits with a total endowment close to the standard Zipf's Law estimate of 277,832 t U for deposits with an endowment greater than 300 t U (Table 13);
2) The known deposits are likely to contain additional resources (Table 12).

TABLE 13. ESTIMATION OF UNDISCOVERED ENDOWMENT BASED ON ZIPF'S LAW[1]

Tonnes of Uranium	
Total endowment	277,832
Identified endowment	97,447
Undiscovered endowment	180,386
Number of deposits	
Total deposits	163
Identified deposits	18
Undiscovered deposits	145

[1]Using a deposit size cut-off of >300 t U

The number of undiscovered deposits can be obtained by counting the number of missing ranks. Zipf's Law also facilitates the estimation of the number of undiscovered deposits at different size ranges (Table 14). In this estimation procedure it is very important to specify the size threshold above which a deposit is considered significant. According to the power law, deposit size decreases dramatically with increasing rank. In other words, and as commonly observed in nature, while small deposits are abundant (represented by the tail of the curve) there are only few large ones.

TABLE 14. ESTIMATION OF UNDISCOVERD ENDOWMENT BASED ON ZIPF'S LAW[1]

Rank	'Expected' endowment (t U)	Comments
1	48,966	Yeelirrie
2	*24,483*	*Vacant*
3	*16,322*	*Vacant*
4	*12,241*	*Vacant*
5	9,793	Lake Maitland
6	*8,161*	*Vacant*
7	*6,995*	*Vacant*
8	6,121	Thatcher Soak
9	5,441	Centipede
10	4,897	Lake Way
11	*4,451*	*Vacant*
12	4,080	Hillview, Nowthanna[2]
13	*3,767*	*Vacant*
14	*3,498*	*Vacant*
15	*3,264*	*Vacant*
16	3,060	Windimurra
17	*2,880*	*Vacant*
18	2,720	Millipede
19 - 20	*2,448 - 2577*	*Vacant*
21	2,332	Anketell
22 - 33	*1,484 - 2226*	*Vacant*
34	1,440	Lake Mason
35	1,399	Peninsula
36 - 38	*1,289 - 1360*	*Vacant*
39	1,256	Dawson-Hinkler
40 - 43	*1,139 - 1224*	*Vacant*
44	1,113	Lakeside
45 - 47	*1,042 - 1088*	*Vacant*
48	1,020	Wondinong
49 - 78	*628 - 999*	*Vacant*
79	620	Jailor Bore
80 - 100	*490 - 612*	*Vacant*
101	485	Yuinmery
102 - 140	*350 - 480*	*Vacant*
141	347	Minindi Creek
142 - 163	*300 - 345*	*Vacant*

[1]Using a deposit size cut-off tonnage of >300 t U
[2] Hillview and Nowthanna have equal known endowment and thus share the same rank

The undiscovered endowment for the size category >300 t U was calculated using Equation 31.

$$T_u = \sum_{r=1}^{n} c \times r^{-1} - \sum_{j=1}^{m} T_m \qquad (31)$$

where T_u is the total undiscovered endowment in tonnes, c is the size of the largest deposit (i.e., Yeelirrie: 48,966 t U), r is the rank of deposits ranging from 1 to n, where n is the rank of the smallest deposit with >300 t U, T_j is the tonnage of the known deposits, where j ranges from 1 to 7, the number of known deposits with an endowment greater than 300 t U.

Using Equation 31 and only considering resource figures >300 t U, Zipf's Law predicts a total endowment of 277,832 t U. Given a total identified endowment of 97,446 t U the total undiscovered endowment expected within the study area is 180,385 t U, contained in the known deposits plus 145 yet-to-be discovered deposits.

6. DISCUSSION

6.3. Deposit model

The discovery of Yeelirrie in 1972 and subsequent delineation of two calcrete-hosted uranium provinces in Western Australia (Fig. 1) highlighted the importance of (near-) surface processes in the generation of uranium deposits, and triggered a wave of academic research into calcrete-hosted uranium deposits. However, this wave ebbed in the 1980s (in concert with falling uranium prices) with little or no research dedicated to calcrete-hosted uranium deposits in the last 25 years.

Overall, the controls on the genesis and location of Western Australian calcrete-hosted uranium deposits are relatively well-understood but some important questions remain. For example:

- Why is Yeelirrie so much larger and higher-grade than any other calcrete-hosted uranium deposits in Western Australia? And, is Yeelirrie unique or could the same conditions have existed elsewhere within the study area?
- How common is dolocrete as a carnotite host and what is its spatial distribution both at the deposit and regional scales? Are Western Australian valley-type deposits in fact mainly hosted by dolocrete rather than calcrete? And if so, what are the implications thereof?
- What is the source of the vanadium in Western Australian calcrete-hosted uranium deposits? Resolving this question is important because if the vanadium were mainly sourced from greenstone belt successions (i.e., mafic to ultramafic rocks, banded iron formations) vanadium sources would be localized. However, if vanadium were also extracted in sufficient quantities from mafic minerals contained in granitoids, ferruginous concretions in lateritic regolith, or sediment deposited within the network of paleo-valleys and playa lakes, vanadium sources would be ubiquitous;
- Is it possible to overcome, or offset, the geo-metallurgical issues of Western Australian calcrete-hosted uranium deposits so that these deposits could support viable uranium mines even during periods of low uranium prices?

There is no doubt that new research is required to gain a better understanding of the above, make Western Australian calcrete-hosted uranium deposits a more attractive exploration target and unlock their significant resource and production potential.

6.4. Prospectivity modeling

This study adopted and tested a three-pronged approach to prospectivity analysis using a knowledge-driven FIS model and data-driven WofE and ANN models designed to (1) make optimal use of the available information pertaining to calcrete-hosted uranium deposits, and (2) account for both the conceptual and empirical nature of this information.

In this context, the knowledge-driven FIS model served to represent our conceptual understanding of the mineralization processes based on the genetic deposit model constructed above. The FIS model was implemented first to avoid bias that may be introduced by us learning the outcomes of the data-driven WofE and ANN models. The WofE and ANN models, on the other hand, served to analyze and explore the empirical relationships between the mineral occurrence data and a set of predictor maps (Fig. 36).

Despite their fundamentally different nature and the model parameters being estimated by different algorithms, the models produced relatively similar prospectivity maps, highlighting similar geologically-permissive tracts (Fig. 45). We take this result as further confirmation that the input data were robust and the models performed well.

6.5. Quantitative resource assessment

The QMRA presented in this study is a world first in that it is the first published assessment utilizing three different approaches: (1) regression models of deposit density and endowment density modeling; (2) the USGS three-part assessment; and (3) Zipf's Law analysis. The combination of these methods delivered a well-constrained estimate of the number of undiscovered calcrete-hosted uranium deposits in the deserts and xeric shrublands region of Western Australia, and their endowment. The results obtained by the different methods are comparable at the scale of the study area and summarized in Table 15. Discrepancies in the results can be linked to the intricacies of the individual methods, each requiring different input parameters and employing distinctive estimation methods.

As noted by [145], the USGS three-part assessment is prone to over-estimation of undiscovered endowment, in particular if geologically-permissive tracts are not prospective. In the present study, undiscovered uranium endowment was estimated based on the USGS three-part and using the total area of the identified geologically-permissive tracts (i.e., 85 calcrete bodies).

TABLE 15. SUMMARY OF UNDISCOVERED ENDOWMENT ESTIMATES

Method	Type of estimate	10% probability	50% probability	90% probability
Deposit density model	Number of undiscovered deposits	105	58	29
Endowment density model	Undiscovered endowment (t U)	2,150,000	48,600	0
USGS three-part assessment	Undiscovered endowment (t U)	908,000	387,000	102,000
Zipf's law analysis	Number of undiscovered deposits (>1,000 t U)	50	N/A	N/A
Zipf's law analysis	Undiscovered endowment (>1,000 t U)	190,000	N/A	N/A

Key to abbreviations: N/A = Not applicable

The estimates of deposit density and endowment density are contingent upon the surface areas of the geologically-permissive tracts. Given that most calcrete bodies are relatively small (average = 0.011 km^2), human error in accurately determining the size of a calcrete body could be a factor contributing to inaccurate estimates. In addition, multiplication of the relatively small numbers representing calcrete body sizes resulted in fractional deposit numbers (e.g., 0.01 deposits). In this study, smaller fractions were cumulated to obtain the total number of undiscovered deposits and rounded to the nearest whole number.

Zipf's Law analysis is subjective in that the results vary according to the minimum cut-off grade selected for estimation of undiscovered resources. For example, larger cut-offs can curtail the long tail of small and insignificant deposits predicted by the power-law model. Despite this shortcoming, Zipf's Law analysis is a valid tool for estimating the number of large(r) undiscovered deposits and their endowment as the higher ranked deposits are fitted to the power law with greater accuracy. In addition, the robustness of the results depends on the degree to which the assumptions on which the method is based hold true (e.g., whether the largest deposit in a belt has been discovered and fully delineated). In the case of our study area and considering that calcrete-hosted uranium deposits form in the near-surface environment, it is very likely that Yeelirrie represents the largest deposit of its kind. In addition, Yeelirrie has been well explored and based on the data available in the public domain appears to be (close to) fully delineated. Overall, Zipf's Law appears to hold true for calcrete-hosted uranium deposits in our study area and given the goodness of fit to the power law.

In summary, the proven approaches to QMRA used in this study all indicated that a significant number of sizeable calcrete-hosted uranium deposits are yet to be discovered in the deserts and xeric shrublands region of Western Australia. Since calcrete-hosted uranium deposits occur at, or close to surface, and, thus, are relatively easy to discover and cheap to explore for, this well-endowed region may present an attractive target for future uranium exploration.

6.6. Exploration applications

As summarized in above, exploration activities targeting calcrete-hosted uranium deposits were mainly focused on the Yilgarn and Gascoyne calcrete-hosted uranium provinces (Figs. 1, 32-34). The prospectivity modeling undertaken as part of this study clearly identified these provinces (Fig. 43). However, the modeling also identified new areas of significant potential, including two areas that have received very little exploration attention with respect to calcrete-hosted uranium deposits (Fig. 52). One of these areas (Fig. 53a), located in Western Australia's Great Sandy Desert, is centered upon paleo-drainage systems etched into the Proterozoic Paterson Orogen (home to the large vein-hosted, or unconformity-related, Kintyre uranium deposit: Fig. 30) and Savory Basin, and the Paleozoic to Mesozoic Canning Basin. While some of the area is covered by the Karlamilyi National Park, most is open to mineral exploration. As illustrated in Fig. 53a, the area comprises several immediate targets characterized by the spatial coincidence of significant 98th percentile U^2/Th anomalism and (a) paleo-drainages, many of which are marked by outcropping valley calcretes, and (b) playa margins and deltas. It is important to note that the sand dune cover developed over much of the area may work to effectively conceal significant radiometric anomalies. Previous work by [77] on the potential for calcrete-hosted uranium deposits in the Paterson Orogen also concluded that the region is prospective, in particular the area to the south of Lake Waukarlycarly (Fig. 53a: Target 10). This conclusion was based on several critical ingredients being present or available in this particular area, including a substantial groundwater flow system, calcrete bodies with surface areas up to 20 by 60 km, sources of uranium and vanadium, and indications of uranium enrichment.

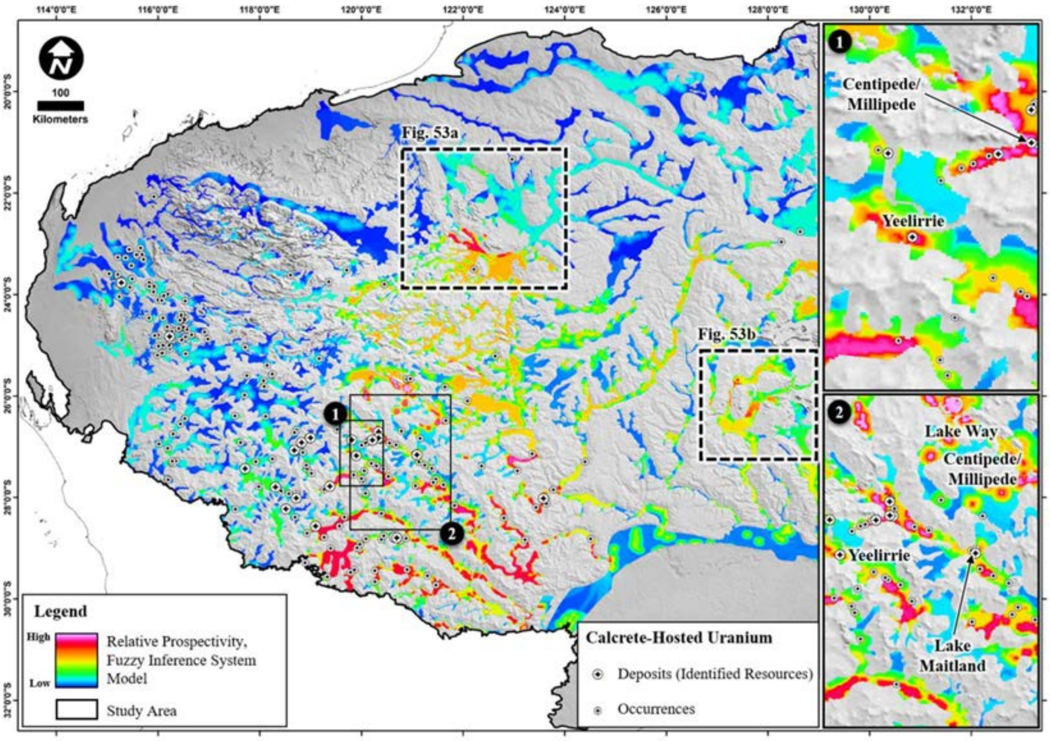

FIG. 52. Continuous-scale Fuzzy Inference Systems (FIS)-based prospectivity map of calcrete-hosted uranium potential illustrating large areas that are geologically-permissive for calcrete-hosted uranium deposits outside the known calcrete uranium provinces. Of particular interest are the two areas framed by thick dashed lines (boxes labeled Fig. 54a and Fig. 54b). These areas are identified as highly

prospective in all three prospectivity models, and they are un(der)explored.
The second prospective, yet under-explored area (Fig. 53b) is located in Western Australia's Great Victoria Desert, covering parts of the Proterozoic to Cretaceous Officer Basin and Proterozoic Musgrave Block. This remote area is one of Australia's last frontiers with vast swathes never having received any modern exploration. While there are no known calcrete-hosted uranium occurrences in the area, the critical ingredients appear to be present, at least with respect to the Musgrave Block and surrounds:

— A groundwater flow system [123];
— Calcrete bodies with surface areas up to 26 by 90 km;
— Sources of uranium (granitoids) and vanadium (mafic- to ultramafic volcanic and intrusive rocks);
— Indications of uranium enrichment coincident with or on the margins of calcrete bodies, paleo-valleys and playa lakes.

As for the area described above, abundant sand dune cover may work to effectively conceal significant radiometric anomalies.

6.7. Implications for economic valuations

Ideally, the undiscovered calcrete-hosted uranium endowment estimated in this study should be subjected to economic filtering as described by [146]. However, any meaningful economic filtering of the results is precluded here, mainly because of the scarcity of:

— Statistically robust mining and cost data (e.g., capital expenses, operating expenses, mine life and capacity) for Australian calcrete-hosted uranium deposits, none of which have been mined;
— Comparable global mining and cost data datasets with the Langer Heinrich mine in the Republic of Namibia still the only operation worldwide exploiting a calcrete-hosted uranium deposit, and the significant differences between Namibian and Australian deposits precluding the ready applicability of the Langer Heinrich mining and cost data in the Australian context;
— Calcrete-hosted uranium deposit grade and tonnage data that resulted in our grade-tonnage curves not being as statistically robust and defensible as expected for use in a sophisticated economic filtering model.

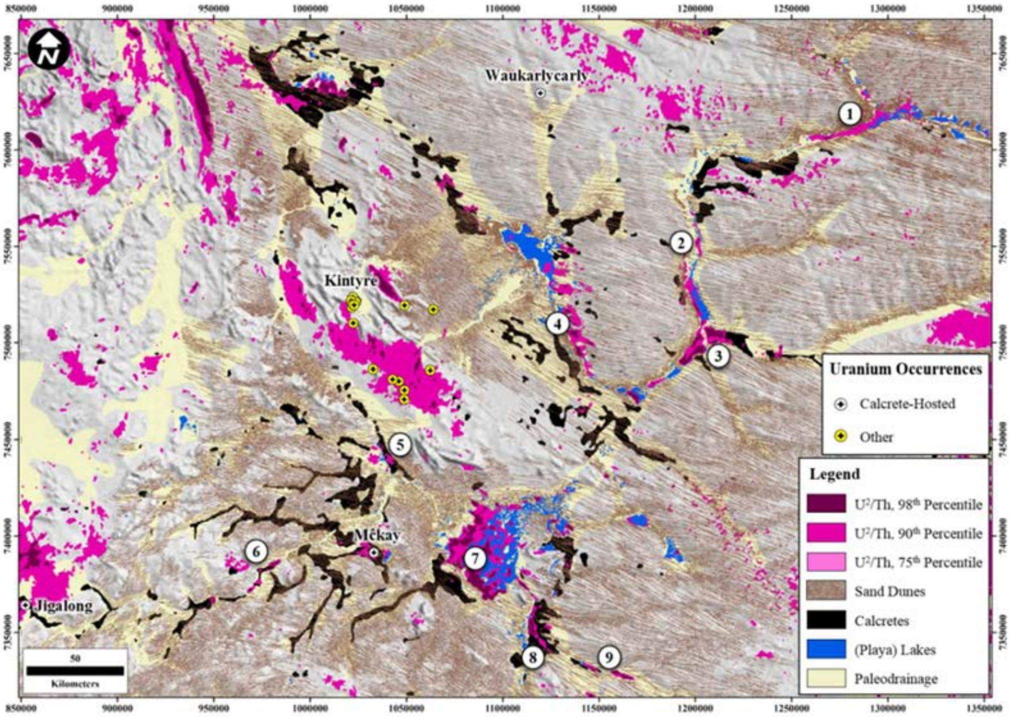

(a)

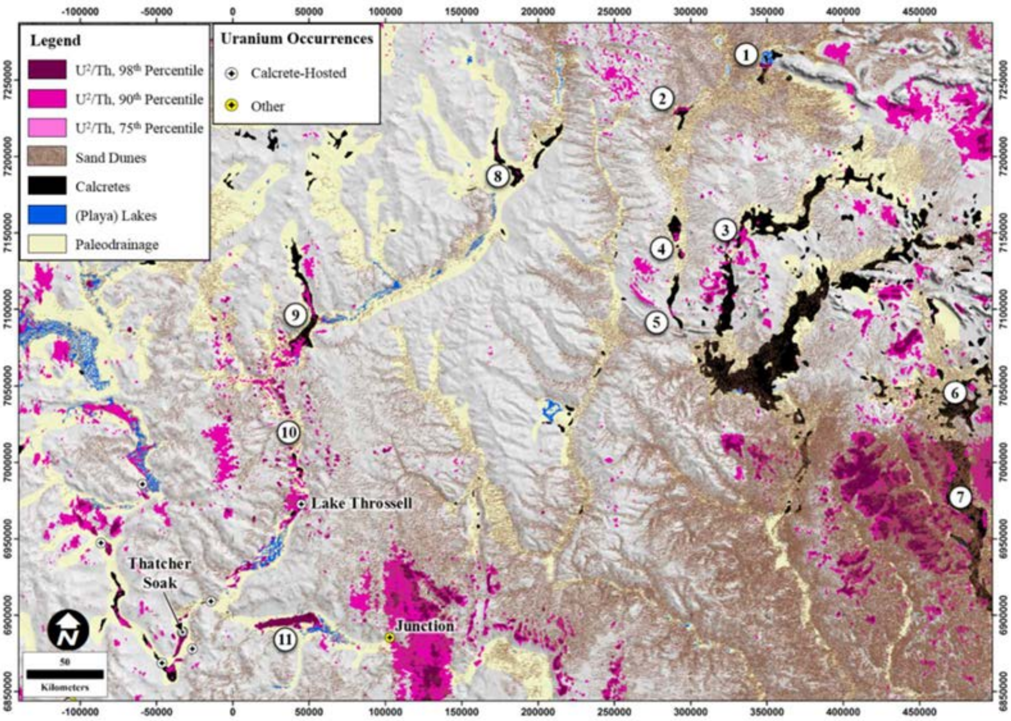

(b)

FIG. 53. Close-ups of the prospective, underexplored areas shown in Fig. 53, illustrating the location of the known uranium occurrences, paleo-drainages, mapped calcrete bodies, playa lakes, sand dune cover and domains of significant U^2/Th anomalism. See text for more detail. A. Great Sandy Desert region. B. Great Victoria Desert region.

6.7.1. *Surficial uranium cost categories*

With respect to global surficial uranium resources, the Red Book [72] reported total reasonably assured resources (RAR) and inferred resources (IR) of >260,000 t U (Table 16). Most of these (~81%) are contained in calcrete-hosted uranium deposits in Australia and the Republic of Namibia. According to the Red Book [72], nearly 80% of the combined global RAR and IR are recoverable at costs <US$130/kg U, while only 20% fall in the highest cost category of <US$260/kg U. The same ratio applies to the Australian context, where 78% of calcrete-hosted RAR and IR fall into the <US$130/kg U and 22% fall into <US$260/kg U cost categories.

TABLE 16. SURFICIAL URANIUM RESOURCES BY COST CATEGORY [72]

Jurisdiction	RAR (t U)		IR (t U)		RAR + IR (t U)
	<US$130/kg U	<US$260/kg U	<US$130/kg U	<US$260/kg U	
Global	110,108	140,154	97,140	123,695	263,849
Australia	58,500	58,500	14,100	35,100	93,600
Namibia, Republic of	49,245	78,964	34,987	40,355	119,319

Key to abbreviations: IR = Inferred resources; RAR = Reasonably assured resources.

6.7.2. *Economics of Western Australian calcrete-hosted uranium deposits*

Despite the more than 40-year period since the first Australian calcrete-hosted uranium discovery, none of the Australian deposits of this type have been mined. Moreover, very little information has been released into the public domain in the last 40 years regarding the economics and the intricacies of mining Australian calcrete-hosted uranium deposits. To a large degree, this deficiency can be ascribed to:

— Yeelirrie (Fig. 30), the largest and highest-grade Australian calcrete-hosted uranium deposit, having been continually owned by major mining houses (WMC Resources Limited, BHP Billiton Limited, Cameco Corporation) that are not required to publicly disclose immaterial information;

— Most other Australian calcrete-hosted uranium deposits being too small to warrant scoping, pre-feasibility or feasibility studies.

Toro Energy Limited, a junior company that consolidated the neighboring Centipede, Millipede, Lake Maitland, and Lake Way calcrete-hosted uranium deposits into the >32,000 t U Wiluna project (Fig. 30), was first to publicly disclose a mining scoping study and preliminary economic assessment for this type of deposit in Australia (Table 17). The project economics were modeled using a uranium price assumption of US$70 a pound [US$182/kg U] [147]. In October 2015, Toro Energy Limited stated that the Wiluna "project will require prices between US$60 and US$70 a pound [between US$156/kg U and US$182/kg U] to make money".

The fact is that none of the Australian calcrete-hosted uranium deposits are currently economically feasible. As emphasized by [108], the main technical issues holding back development and mining of calcrete-hosted deposits in Australia are (a) high capital and operating expenses, (b) extreme uranium price sensitivity, (c) difficult and complex metallurgy, and (d) groundwater control issues. Given the above, it seems unlikely that any of Australia's calcrete-hosted uranium deposits will be mined any time soon, unless the uranium price experienced a significant and sustained rise and / or new technological breakthroughs allowed Australian calcrete-hosted uranium ores to be exploited at much lower costs.

6.7.3. Economic considerations concerning the speculative resources

As illustrated by the outcomes of the mineral prospectivity analysis and quantitative resource assessment, the study area encompasses extensive tracts geologically-permissive for calcrete-hosted uranium deposits (Fig. 45) and may contain significant undiscovered calcrete-hosted uranium endowment (Table 15). While some of these speculative resources [72] would undoubtedly be contained in extensions to the identified deposits, our Zipf's Law analysis suggests that this portion of the undiscovered endowment is relatively minor (i.e., <1,800 t U: Table 12). As such, most of the speculative resources are likely to be contained in calcrete-hosted uranium deposits yet to be discovered.

TABLE 17. WILUNA URANIUM PROJECT HIGHLIGHTS AND ECONOMIC PARAMETERS [147]

Category	Details
Resources	79 Mt @ 482 ppm U_3O_8 (c. 409 ppm U) for 84 Mlb U_3O_8 (c. 32,310 t U) (200 ppm U_3O_8 / 170 ppm U cut-off) for 6 deposits, including
	23 Mt @ 916 ppm U_3O_8 (c. 777 ppm U) for 40 Mlb U_3O_8 (c. 15,386 t U) (500 ppm U_3O_8 / 424 ppm U cut-off) for 4 deposits
Deposits**	Centipede, Millipede, Lake Maitland, Lake Way, Dawson Hinkler, Nowthanna
Permits	Centipede and Lake Way approved for mining and processing facility and infrastructure at Centipede
	Mining of Millipede and Lake Maitland deposits under government assessment
Mine life	16 years from Centipede, Millipede, Lake Maitland and Lake Way
Mining	Open pit, to a depth of 10 m
Plant capacity	1.3 Mt per annum
Processing method	Alkaline leach with direct precipitation
Cost	Capital construction cost of US$180 to US$220M
	Average C1* cost for life of project of US$31.1/lb U_3O_8 (c. 0.4 kg U)
Tailings	In-pit tailings disposal
Average head grade	>800 ppm U_3O_8 (c. 678 ppm U), with a target of 1,000 ppm U_3O_8 (c. 848 ppm U)

Category	Details
Recovery	86%
Production	30.1 Mlb U_3O_8 (c. 11,578 t U)
Transport	Road transport to Port Adelaide for shipment

*C1 operating cost includes all mining, processing, site administration and transport costs but excludes royalties and any sales adjustments. Calculated by reference to the A$:US$ forward curve as at 16th January 2014.
**The Dawson Hinkler and Nowthanna deposits, which contain Indicated and Inferred Resources, have not been included in the mine plan at this stage.
Economic assumptions: Whittle pit optimizations were modeled using a long term U_3O_8 price of US$70/lb, a price considered by commodity price forecasters as being the incentive price required for new primary U_3O_8 production to be financed and brought to market. As the Wiluna Project moves toward project financing, Toro has applied the US$: A$ foreign currency forward curve to its financial model. The forward curve has been applied through to March 2024 then held constant through 2032 where required to show forecasts in US$. The economic model assumes first production at Wiluna in 4th quarter 2016, however this timetable is contingent upon a variety of tasks being successfully completed including, but not limited to, a final definitive feasibility study, full project financing, construction and any further necessary approvals.

At the 90% probability level, there may be scope for speculative resources of up to 102,000 t U contained within up to 29 undiscovered deposits (Table 15). As illustrated by Tables 13 and 14, some of these deposits could be very significant given that some of the top Zipf ranks, including ranks 2 to 4 (deposits containing between ~24,500 and ~12,250 t U) and 6 to 7 (deposits containing between ~8,200 and ~7,000 t U), are vacant. Two areas where such large deposits may be "hiding" are illustrated in Fig. 53. These areas are both under-explored compared to the known calcrete-hosted uranium provinces and covered by sand dunes abundant and extensive enough to potentially mask the radiometric response of a surficial uranium deposit. However, for any speculative resources outside the Yilgarn calcrete-hosted uranium province to be potentially economic, they would have to be significant not only in terms of their tonnages but also have high grades and occur as a cluster of deposits close to existing infrastructure. The latter is a problem in the prospective areas described above, and for much of the western part of the study area, where the lack of infrastructure (Fig. 54) may push any calcrete-hosted uranium deposits to be discovered there into the highest <US$260/kg U cost category and, thus, render them uneconomic, at least in the current low uranium price environment.

The Yilgarn calcrete-hosted uranium province, centered upon the Yeelirrie and Wiluna uranium projects, on the other hand, boosts significant infrastructure (mainly because of the existing gold and nickel mines) and may yield potentially important synergies linked to the clustering of identified calcrete-hosted uranium deposits, including the largest known deposits of this kind in Australia. Any new discoveries in this region, and preferably close to the identified deposits, would be significant in that they may enhance the economics of the existing projects. Any undiscovered endowment within the Yilgarn calcrete uranium province may thus fall into the <US$130/kg U cost category.

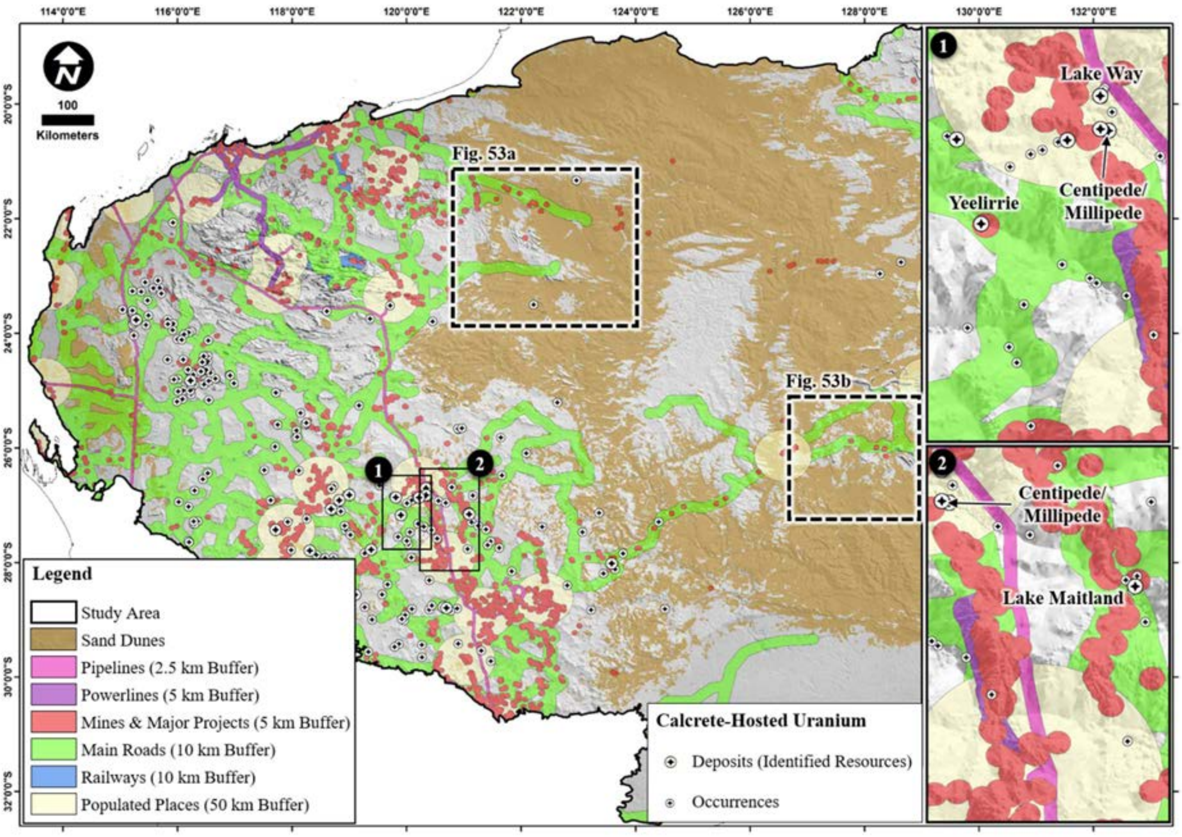

FIG. 54. Infrastructure map of the study area with buffers applied to key infrastructure categories such as populated places, main roads and operating mines. While the Yilgarn calcrete province centered upon Yeelirrie (Fig. 1) is situated in a region of relatively well-developed infrastructure, the newly identified high potential areas (marked by boxes labeled Fig. 54a and Fig. 54b) are not. Any new calcrete-hosted uranium discovers would have to be significant in terms of their grades and tonnages for such discoveries to be developed into future mines.

7. CONCLUSIONS

The following principal conclusions may be drawn from this study of calcrete-hosted (surficial) uranium deposits in the deserts and xeric shrublands region of Western Australia and this region's geologically-permissive tracts and undiscovered endowment:

— Western Australian calcrete-hosted uranium deposits are well understood in terms of the genetic processes critical in their formation, and thus lend themselves exceptionally well to a pilot study such as presented here. In addition, excellent spatial datasets are available for the study area, facilitating the generation of predictor maps representation mappable expressions of the processes critical in the formation of calcrete-hosted uranium deposits;

— This study adopted a three-pronged approach to prospectivity modeling, employing a knowledge-driven fuzzy inference systems (FIS) model and data-driven Weights-of-Evidence (WofE) and artificial neural networks (ANN) models. The results of these fundamentally different approaches to prospectivity modeling were remarkably similar.

In addition, all three models recorded high capture efficiencies (between 87% and 95%) with respect to the known uranium deposits and identified several new tracts geologically-permissive for calcrete-hosted uranium deposits, including two areas in the Great Sandy Desert and Great Victoria Desert that are remote, characterized by extensive sand dune cover and to date have recorded little, if any, uranium exploration;

— The approach to estimating the number of undiscovered deposits and total amount of undiscovered endowment described in this contribution is a world first in that it is the first published Quantitative Resource Assessment (QRA) employing three different yet complimentary methods: regression models of deposit density and endowment density, the USGS three-part assessment and Zipf's Law analysis. Moreover, in contrast to the published QRAs, our assessment was based on the results of a thorough, multi-pronged prospectivity analysis based on knowledge- and data-driven approaches. The results of our QRA indicate that the study area contains a total undiscovered endowment (or speculative resources) of >180,000 t U contained in the identified and up to 145 additional, undiscovered deposits.

ACKNOWLEDGEMENTS

B. Chudasama acknowledges Ph.D. research fellowship granted by the Council of Scientific and Industrial Research (CSIR), India. The authors are grateful to the Indian Institute of Technology (IIT) Bombay, Mumbai, India for providing technical and infrastructural facilities for completing this work. A. K. Porwal and O. P. Kreuzer were in receipt of IAEA Special Services Agreements to support the research, and additionally B. Chudasama and S. Thakur in receipt of IAEA travel grants.

Appendix

TABLE A-1. CALCRETE-HOSTED URANIUM OCCURRENCES (SORTED BY NAME)

Name	Alternative name	Latitude (decimal degrees)	Longitude (decimal degrees)	Status	Deposit type	Data source
Abercromby	-	-26.826	120.342	Occurrence	Surfical: Subtype Undefined	[84]
Albion Downs	-	-26.967	120.007	Occurrence	Surfical: Subtype Undefined	This Study
Alma Well	-	-23.759	115.827	Occurrence	Surfical: Subtype Undefined	GSWA
Altona	Puncture Well	-27.917	120.083	Occurrence	Surfical: Subtype Undefined	[84]
Andrew Bore	-	-24.673	116.415	Occurrence	Surfical: Subtype Undefined	GSWA
Anketell	-	-28.014	118.720	Deposit	Surfical: Groundwater / Valley Calcrete	GSWA
Anomaly P5	-	-24.493	116.526	Occurrence	Surfical: Subtype Undefined	GSWA
Anomaly PDH50	-	-23.213	115.574	Occurrence	Surfical: Subtype Undefined	GSWA
Bad Ass	-	-23.111	115.434	Occurrence	Surfical: Subtype Undefined	GSWA
Baltic Bore	-	-23.649	115.194	Occurrence	Surfical: Subtype Undefined	GSWA
Barlee S	-	-29.425	119.868	Occurrence	Surfical: Subtype Undefined	GSWA
Bellah Bore	-	-26.854	119.777	Deposit	Surfical: Groundwater / Valley Calcrete	This Study
Bellah Bore E	-	-26.867	119.812	Deposit	Surfical: Groundwater / Valley Calcrete	GSWA
Ben Hur	Jailor Bore Extended	-23.847	115.212	Occurrence	Surfical: Subtype Undefined	GSWA
Berragan Bore	-	-27.284	116.355	Occurrence	Surfical: Subtype Undefined	GSWA
Billara Bore	-	-25.589	118.230	Occurrence	Surfical: Subtype Undefined	GSWA
Billara Bore	-	-25.565	118.249	Occurrence	Surfical: Subtype Undefined	GSWA
Bolitho Bore	Lake Mason	-27.557	119.851	Deposit	Surfical: Groundwater / Valley Calcrete	GSWA
Boolardy	-	-26.442	116.526	Occurrence	Surfical: Subtype Undefined	[84]
Bordah Well	Bordah	-23.854	115.446	Occurrence	Surfical: Subtype Undefined	GSWA
Bruce Bore	Nowthanna	-27.102	118.829	Occurrence	Surfical: Subtype Undefined	GSWA
Bulga Downs N	Bulga Downs	-28.385	119.669	Occurrence	Surfical: Subtype Undefined	This Study
Bulga Downs S	-	-28.562	119.574	Occurrence	Surfical: Subtype Undefined	[84]
Bungalow Well	Beta	-28.314	120.398	Occurrence	Surfical: Subtype Undefined	[84]
Burgess Bore NW	-	-27.624	116.184	Occurrence	Surfical: Subtype Undefined	GSWA
Burgess Bore S	-	-27.645	116.205	Occurrence	Surfical: Subtype Undefined	GSWA
Burgess Bore SW	-	-27.649	116.200	Occurrence	Surfical: Subtype Undefined	GSWA
Bustler Well	-	-24.732	116.910	Occurrence	Surfical: Subtype Undefined	GSWA

Name	Alternative name	Latitude (decimal degrees)	Longitude (decimal degrees)	Status	Deposit type	Data source
Bustler Well	-	-24.737	116.915	Occurrence	Surfical: Subtype Undefined	GSWA
Byro	-	-26.550	116.440	Occurrence	Surfical: Subtype Undefined	GSWA
Byro Delta	Byro	-27.028	116.191	Occurrence	Surfical: Subtype Undefined	GSWA
Cahill	Holman, Baltic Bore	-23.614	115.202	Occurrence	Surfical: Subtype Undefined	GSWA
Carlo Creek	-	-25.149	116.087	Occurrence	Surfical: Subtype Undefined	GSWA
Cashmere Downs	Cashmere	-29.000	119.395	Occurrence	Surfical: Subtype Undefined	[84]
Cave Well	-	-27.636	121.467	Occurrence	Surfical: Subtype Undefined	[84]
Centipede	Wiluna	-26.835	120.368	Advanced Project; Test Pit	Surfical: Playa Lake	GSWA
Centipede N	Lake Way South	-26.824	120.373	Deposit	Surfical: Delta Calcrete	GSWA
Chalba Creek	-	-24.799	116.005	Occurrence	Surfical: Subtype Undefined	GSWA
Christmas Bore	-	-27.844	119.264	Occurrence	Surfical: Subtype Undefined	GSWA
Cogla Downs	Nowthanna, Murchison Downs, Two Mile	-27.433	118.933	Occurrence	Surfical: Subtype Undefined	[84]
Cosmo	-	-28.195	123.438	Occurrence	Surfical: Subtype Undefined	[84]
Curbaweeda	-	-27.785	117.983	Occurrence	Surfical: Subtype Undefined	[84]
Darawonga Well	-	-25.000	116.103	Occurrence	Inferred Surficial	GSWA
Dawson E	Dawson-Hinkler	-26.905	120.126	Deposit	Surfical: Groundwater / Valley Calcrete	GSWA
Dawson W	Dawson-Hinkler	-26.921	120.082	Deposit	Surfical: Groundwater / Valley Calcrete	GSWA
Downs East	-	-26.656	119.526	Occurrence	Surfical: Subtype Undefined	GSWA
Firestrike	-	-26.928	120.558	Occurrence	Surfical: Subtype Undefined	GSWA
Four Corners Bore	-	-27.333	116.279	Occurrence	Surfical: Subtype Undefined	GSWA
Four Corners Bore W	-	-27.329	116.299	Occurrence	Surfical: Subtype Undefined	GSWA
Fraser Creek	-	-23.965	116.235	Occurrence	Surfical: Subtype Undefined	GSWA
Fyfe Well	-	-25.678	120.905	Occurrence	Surfical: Subtype Undefined	GSWA
Fyfe Well	-	-25.667	120.894	Occurrence	Surfical: Subtype Undefined	GSWA
Galah Rocks	-	-29.659	120.270	Occurrence	Inferred Surficial	[84]
Giant's Prospect	-	-24.041	115.237	Occurrence	Surfical: Subtype Undefined	This Study
Gifford Creek	-	-23.986	116.196	Occurrence	Surfical: Subtype Undefined	GSWA
Glenburgh	-	-25.165	116.546	Occurrence	Surfical: Subtype Undefined	[84]
Gnaweeda	Glenburgh	-26.666	118.729	Occurrence	Inferred Surficial	[84]
Gum Well	Ida Valley	-28.827	120.392	Occurrence	Surfical: Subtype Undefined	[84]
Halfpenny Well	-	-27.700	121.417	Occurrence	Surfical: Subtype Undefined	[84]

Name	Alternative name	Latitude (decimal degrees)	Longitude (decimal degrees)	Status	Deposit type	Data source
Hazlett Cliffs	-	-28.830	123.222	Occurrence	Surfical: Subtype Undefined	[84]
Hectors Bore	Ti Tree Well	-25.067	116.233	Occurrence	Surfical: Subtype Undefined	[84]
Hillview	-	-26.918	118.826	Deposit	Surfical: Groundwater / Valley Calcrete	GSWA
Hinkler	Dawson-Hinkler	-26.869	120.218	Deposit	Surfical: Groundwater / Valley Calcrete	GSWA
Hinkler W	Dawson-Hinkler	-26.877	120.184	Deposit	Surfical: Groundwater / Valley Calcrete	GSWA
Holman	-	-23.604	115.208	Occurrence	Surfical: Subtype Undefined	This Study
Hope River	-	-26.400	118.117	Occurrence	Surfical: Subtype Undefined	[84]
Horse Well	-	-23.242	115.575	Occurrence	Surfical: Subtype Undefined	[84]
Ida Valley	-	-28.755	120.443	Occurrence	Surfical: Subtype Undefined	[84]
Jailor Bore	Cooper	-23.765	115.279	Deposit	Surfical: Terrace Calcrete	GSWA
Jamieson Well	-	-24.128	116.536	Occurrence	Surfical: Subtype Undefined	GSWA
Jigalong	-	-23.795	120.455	Occurrence	Surfical: Subtype Undefined	[84]
Jillary	-	-23.748	119.362	Occurrence	Surfical: Subtype Undefined	[84]
Jimmy Well	-	-23.689	115.492	Occurrence	Inferred Surficial	GSWA
Kaluwiri	-	-27.685	120.032	Occurrence	Surfical: Subtype Undefined	GSWA
Kaluwiri N	Kaluwiri	-27.628	120.004	Occurrence	Surfical: Subtype Undefined	GSWA
Kelly Bore	Nowthanna	-27.069	118.757	Occurrence	Surfical: Subtype Undefined	GSWA
Kendell Bore	-	-24.408	116.460	Occurrence	Surfical: Subtype Undefined	GSWA
Kendell Bore NE	-	-24.398	116.523	Occurrence	Surfical: Subtype Undefined	GSWA
Kendell Bore SW	-	-24.445	116.449	Occurrence	Surfical: Subtype Undefined	GSWA
Kewell	Quail Springs, Baltic Bore	-23.652	115.210	Occurrence	Surfical: Subtype Undefined	GSWA
Kitchener Bore	-	-26.388	117.513	Occurrence	Surfical: Subtype Undefined	[84]
Lake Barlee	-	-29.283	118.896	Occurrence	Surfical: Subtype Undefined	[84]
Lake Barlee	-	-29.015	119.957	Occurrence	Surfical: Subtype Undefined	GSWA
Lake Barlee	-	-29.562	119.332	Occurrence	Surfical: Subtype Undefined	[84]
Lake Barlee	-	-29.477	119.789	Occurrence	Surfical: Subtype Undefined	[84]
Lake Carnegie	-	-25.211	122.635	Occurrence	Surfical: Subtype Undefined	[84]
Lake Darlot	-	-27.747	121.618	Occurrence	Surfical: Subtype Undefined	[84]
Lake Irwin	-	-28.157	121.835	Occurrence	Surfical: Subtype Undefined	[84]
Lake Mackay	Far Out	-22.760	128.634	Occurrence	Surfical: Playa Lake	[84]
Lake Maitland	Mt Joel	-27.161	121.094	Advanced Project; Test Pit	Surfical: Playa Lake	[84]

Name	Alternative name	Latitude (decimal degrees)	Longitude (decimal degrees)	Status	Deposit type	Data source
Lake Maitland	-	-27.177	121.082	Advanced Project; Test Pit	Surfical: Playa Lake	GSWA
Lake Maitland	-	-27.166	121.099	Advanced Project; Test Pit	Surfical: Playa Lake	GSWA
Lake Maitland	-	-27.300	121.133	Occurrence	Surfical: Subtype Undefined	[84]
Lake Maitland Central	-	-27.137	121.057	Occurrence	Surfical: Subtype Undefined	GSWA
Lake Maitland N	-	-27.121	121.101	Occurrence	Surfical: Subtype Undefined	[84]
Lake Marmion	-	-29.726	121.472	Occurrence	Inferred Surficial	[84]
Lake Mason	-	-27.779	119.380	Deposit	Surfical: Groundwater / Valley Calcrete	GSWA
Lake Raeside	Red Oaks	-28.784	120.648	Deposit	Surfical: Playa Lake	GSWA
Lake Teague	Esso Anomaly	-25.659	120.966	Occurrence	Surfical: Subtype Undefined	[84]
Lake Throssell	-	-27.294	124.404	Occurrence	Surfical: Subtype Undefined	GSWA
Lake Throssell	-	-27.845	123.781	Occurrence	Surfical: Subtype Undefined	[84]
Lake Way	-	-26.707	120.338	Deposit	Surfical: Delta Calcrete	GSWA
Lake Way D	-	-26.717	120.345	Deposit	Surfical: Delta Calcrete	GSWA
Lake Way S	Yandal, Wiluna South	-26.767	120.381	Occurrence	Surfical: Subtype Undefined	[84]
Lake Wells	-	-27.138	123.363	Occurrence	Surfical: Subtype Undefined	GSWA
Lakeside Central	-	-27.432	117.711	Deposit	Surfical: Groundwater / Valley Calcrete	This Study
Lakeside N	Lake Austin, Austin Downs	-27.408	117.710	Deposit	Surfical: Groundwater / Valley Calcrete	GSWA
Lakeside S	-	-27.442	117.722	Deposit	Surfical: Groundwater / Valley Calcrete	GSWA
Lakeview	Lake Raeside	-28.806	120.882	Occurrence	Surfical: Subtype Undefined	[84]
Lyndon	Baltic Bore	-23.633	115.203	Occurrence	Surfical: Subtype Undefined	GSWA
Maitland	-	-27.158	121.086	Occurrence	Surfical: Subtype Undefined	[84]
Maitland Channel	Irwin, Devine	-27.424	121.387	Occurrence	Surfical: Subtype Undefined	[84]
Mckay	-	-23.500	122.217	Occurrence	Inferred Surficial	[84]
McPhersons Bore N	-	-28.815	120.092	Occurrence	Surfical: Subtype Undefined	GSWA
Meeberrie	-	-26.944	116.019	Occurrence	Surfical: Subtype Undefined	[84]
Meekatharra	-	-26.717	118.687	Occurrence	Surfical: Playa Lake	[84]
Melrose W	-	-26.832	121.156	Occurrence	Inferred Surficial	[84]
Middle Well	Minnie Creek	-23.834	115.927	Occurrence	Surfical: Subtype Undefined	GSWA
Millipede	-	-26.828	120.339	Deposit	Surfical: Delta Calcrete	GSWA
Mindoolah	-	-26.917	117.625	Occurrence	Surfical: Subtype Undefined	[84]
Minindi Creek	-	-24.825	116.225	Deposit	Surfical: Terrace Calcrete	GSWA

Name	Alternative name	Latitude (decimal degrees)	Longitude (decimal degrees)	Status	Deposit type	Data source
Minindi Creek	-	-24.827	116.229	Occurrence	Surfical: Terrace Calcrete	GSWA
Minindi Creek	-	-24.826	116.228	Occurrence	Surfical: Terrace Calcrete	GSWA
Minindi Creek	-	-24.825	116.223	Occurrence	Surfical: Terrace Calcrete	GSWA
Minindi Creek	-	-24.826	116.221	Occurrence	Surfical: Terrace Calcrete	GSWA
Minindi Creek	-	-24.824	116.229	Occurrence	Surfical: Terrace Calcrete	GSWA
Minindi Creek	-	-24.830	116.229	Occurrence	Surfical: Terrace Calcrete	GSWA
Minnawarra	-	-26.748	116.298	Occurrence	Surfical: Subtype Undefined	[84]
Minnie Creek	-	-24.104	115.998	Occurrence	Surfical: Subtype Undefined	GSWA
Minnie Creek	-	-23.943	115.914	Occurrence	Surfical: Subtype Undefined	[84]
Minniearra	-	-24.657	116.520	Occurrence	Inferred Surficial	GSWA
Minnieritchie Well	-	-24.708	116.347	Occurrence	Surfical: Subtype Undefined	GSWA
Mombo Bore	Mickey's Well	-24.807	115.935	Occurrence	Surfical: Subtype Undefined	[84]
Mt Alfred	-	-28.920	119.975	Occurrence	Surfical: Subtype Undefined	[84]
Mt Dalgety	-	-25.017	116.008	Occurrence	Inferred Surficial	[84]
Mt Dalgety South	-	-25.194	115.991	Occurrence	Inferred Surficial	GSWA
Mt James	-	-24.890	116.428	Occurrence	Surfical: Subtype Undefined	GSWA
Mt James	-	-24.892	116.461	Occurrence	Surfical: Subtype Undefined	GSWA
Mt James Creek	-	-24.833	116.542	Occurrence	Surfical: Subtype Undefined	GSWA
Mt James Creek	-	-24.793	116.666	Occurrence	Surfical: Subtype Undefined	GSWA
Mt James Creek NW	-	-24.792	116.660	Occurrence	Surfical: Subtype Undefined	GSWA
Mt Padbury	Homestead Pit	-25.697	118.076	Occurrence	Surfical: Subtype Undefined	This Study
Mt Padbury	Discovery Pit 1	-25.811	118.090	Occurrence	Surfical: Subtype Undefined	This Study
Mt Padbury	Discovery Pit 2	-25.827	118.060	Occurrence	Surfical: Subtype Undefined	[84]
Mt Phillips	-	-24.398	116.456	Occurrence	Surfical: Subtype Undefined	[84]
Mt Phillips	-	-24.670	116.215	Occurrence	Surfical: Subtype Undefined	[84]
Mt Phillips	-	-24.610	116.495	Occurrence	Surfical: Subtype Undefined	[84]
Mt Phillips	-	-24.661	116.199	Occurrence	Surfical: Terrace Calcrete	[84]
Mt Webb	Buck Hills, Uamari, Pokali, Mantati	-22.959	128.269	Occurrence	Surfical: Subtype Undefined	[84]
Murchison Downs	-	-26.824	119.001	Deposit	Surfical: Delta Calcrete	GSWA
Myamin	-	-29.543	121.303	Occurrence	Inferred Surficial	[84]
Nallan W	-	-27.293	117.924	Occurrence	Surfical: Subtype Undefined	GSWA

Name	Alternative name	Latitude (decimal degrees)	Longitude (decimal degrees)	Status	Deposit type	Data source
Nambi	-	-26.095	122.091	Occurrence	Surfical: Playa Lake	[84]
Nardoo Well	31 River	-24.459	116.097	Occurrence	Surfical: Subtype Undefined	GSWA
Neale	-	-28.816	124.513	Occurrence	Surfical: Subtype Undefined	[84]
Neil Bore	-	-27.922	118.723	Occurrence	Inferred Surficial	[84]
Nelson Well	Nelson	-27.520	119.020	Occurrence	Surfical: Subtype Undefined	[84]
Nichols	-	-27.472	123.071	Occurrence	Surfical: Subtype Undefined	[84]
Noondie	Cundeelee	-28.782	119.267	Occurrence	Surfical: Playa Lake	[84]
Nowthanna	Quinns Lake	-27.071	118.679	Deposit	Surfical: Delta Calcrete	GSWA
Nowthanna Hill	Nowthanna	-27.060	118.681	Deposit	Surfical: Delta Calcrete	GSWA
Nowthanna S	-	-27.109	118.700	Deposit	Surfical: Delta Calcrete	GSWA
Onslow Creek	-	-24.459	115.824	Occurrence	Inferred Surficial	GSWA
Oui Creek	-	-24.689	116.571	Occurrence	Inferred Surficial	GSWA
Panhandle	Gladys, Lesley, Charlotte	-28.990	119.918	Occurrence	Surfical: Subtype Undefined	[84]
Peninsula	Lake Raeside, Mopoke Well	-28.797	120.698	Occurrence	Surfical: Groundwater / Valley Calcrete	GSWA
Polly Well	-	-24.984	116.230	Occurrence	Surfical: Subtype Undefined	[84]
Pongo Pool	-	-23.274	115.363	Occurrence	Surfical: Subtype Undefined	GSWA
Poorinoo Well	-	-23.838	115.831	Occurrence	Surfical: Subtype Undefined	GSWA
Porcupine Well	-	-26.960	120.683	Occurrence	Surfical: Playa Lake	[84]
Quandong Well	-	-27.380	122.367	Occurrence	Surfical: Subtype Undefined	GSWA
Rabbit Well	-	-27.924	118.576	Occurrence	Inferred Surficial	[84]
Range Bore	-	-25.002	116.221	Occurrence	Inferred Surficial	GSWA
Relief Well	Jailor Bore Extended	-23.588	115.038	Occurrence	Inferred Surficial	GSWA
Robinson Range	-	-25.038	117.714	Occurrence	Surfical: Subtype Undefined	[84]
Salt Dam	Salt Dam	-29.421	120.900	Occurrence	Inferred Surficial	[84]
Scottie Well	Cogla Downs, Yarrabubba	-27.361	118.919	Deposit	Surfical: Subtype Undefined	GSWA
Shark Hill	-	-24.500	116.436	Occurrence	Surfical: Subtype Undefined	GSWA
Shark Hill	-	-24.502	116.431	Occurrence	Surfical: Subtype Undefined	GSWA
Shaws Bore	-	-28.702	118.933	Occurrence	Surfical: Subtype Undefined	[84]
Shepherd Well	-	-24.875	116.985	Occurrence	Surfical: Subtype Undefined	[84]
South Yeelirrie	-	-27.472	120.058	Occurrence	Surfical: Subtype Undefined	[84]
Stakeyard Well	Mopoke Well, Lake Raeside	-28.849	120.763	Deposit	Surfical: Subtype Undefined	GSWA
Stanley	Nabberu	-25.820	121.646	Occurrence	Surfical: Playa Lake	[84]
Stevies	-	-23.614	118.608	Occurrence	Surfical: Subtype Undefined	GSWA

Name	Alternative name	Latitude (decimal degrees)	Longitude (decimal degrees)	Status	Deposit type	Data source
Stirling	-	-27.360	121.250	Occurrence	Surfical: Playa Lake	[84]
Stone Tank Well	-	-24.018	116.115	Occurrence	Surfical: Subtype Undefined	GSWA
Sylvania	-	-23.516	119.712	Occurrence	Surfical: Subtype Undefined	[84]
Taincrow E	-	-27.241	118.251	Occurrence	Surfical: Subtype Undefined	GSWA
Tank Well	-	-23.208	115.687	Occurrence	Inferred Surficial	[84]
Telfer River	Chain Pool	-23.079	115.659	Occurrence	Surfical: Subtype Undefined	GSWA
Telfer S	-	-23.305	115.716	Occurrence	Surfical: Subtype Undefined	GSWA
Thatcher Soak	-	-28.018	123.584	Deposit	Surfical: Groundwater / Valley Calcrete	GSWA
Thomas River	-	-24.637	116.502	Occurrence	Surfical: Subtype Undefined	GSWA
Thomas River	-	-24.683	116.227	Occurrence	Surfical: Subtype Undefined	GSWA
Thomas River	-	-24.681	116.240	Occurrence	Surfical: Subtype Undefined	GSWA
Thomas River	-	-24.617	116.525	Occurrence	Surfical: Subtype Undefined	GSWA
Thomas River S	-	-24.724	116.276	Occurrence	Surfical: Subtype Undefined	GSWA
Three Rivers	-	-25.261	119.169	Occurrence	Surfical: Subtype Undefined	GSWA
Trillbar	-	-25.598	117.747	Occurrence	Surfical: Subtype Undefined	[84]
Two Mile	Murchison Downs	-26.825	118.951	Deposit	Surfical: Subtype Undefined	GSWA
Uramurdah Well	Lake Way	-26.678	120.353	Occurrence	Surfical: Subtype Undefined	GSWA
Uramurdah Well Extended	Lake Way	-26.686	120.348	Occurrence	Surfical: Subtype Undefined	GSWA
Wabli Creek	Yinnietharra, Minindi Creek	-24.899	116.287	Deposit	Surfical: Subtype Undefined	GSWA
Wabli Creek	Yinnietharra, Minindi Creek	-24.908	116.266	Occurrence	Surfical: Subtype Undefined	GSWA
Wabli Creek	Yinnietharra, Minindi Creek	-24.895	116.235	Occurrence	Surfical: Subtype Undefined	GSWA
Wabli Creek	Yinnietharra, Minindi Creek	-24.895	116.270	Occurrence	Surfical: Subtype Undefined	GSWA
Walling Rock	-	-29.440	120.265	Occurrence	Inferred Surficial	[84]
Wangannue	-	-27.284	116.282	Occurrence	Surfical: Subtype Undefined	GSWA
Warramboo	-	-22.070	115.920	Occurrence	Inferred Surficial	[84]
Waukarlycarly	Lamil Hills	-21.331	122.967	Occurrence	Surfical: Subtype Undefined	[84]
White Cliffs	White Cliffs	-28.404	122.806	Occurrence	Surfical: Subtype Undefined	[84]
Willi Creek	Jailor Bore Extended	-23.809	115.243	Occurrence	Surfical: Subtype Undefined	GSWA
Windimurra	-	-28.226	118.516	Deposit	Surfical: Groundwater / Valley Calcrete	GSWA
Winmar Creek	-	-24.113	116.073	Occurrence	Surfical: Subtype Undefined	GSWA
Wondinong	-	-27.795	118.310	Deposit	Surfical: Groundwater / Valley Calcrete	GSWA
Wondinong SE	-	-27.868	118.424	Deposit	Surfical: Groundwater / Valley Calcrete	GSWA

Name	Alternative name	Latitude (decimal degrees)	Longitude (decimal degrees)	Status	Deposit type	Data source
Yakabindie	-	-27.583	120.533	Occurrence	Surfical: Subtype Undefined	[84]
Yalgar	-	-25.979	117.704	Occurrence	Surfical: Subtype Undefined	[84]
Yalinga Bore	-	-28.386	118.698	Occurrence	Surfical: Subtype Undefined	[84]
Yamarna N	-	-28.120	123.644	Occurrence	Surfical: Subtype Undefined	[84]
Yandal N	-	-26.691	120.791	Occurrence	Surfical: Subtype Undefined	This Study
Yandal S	-	-27.765	121.064	Occurrence	Surfical: Subtype Undefined	[84]
Yannarie	Yannarie River	-23.263	115.210	Occurrence	Surfical: Subtype Undefined	GSWA
Yannarie	Yannarie River	-23.428	115.476	Occurrence	Surfical: Subtype Undefined	[84]
Yarlaweelor	Robinson Range, Billara Bore, Ann Prospect	-25.392	118.148	Occurrence	Surfical: Subtype Undefined	[84]
Yarrabubba	Nowthanna	-27.112	118.851	Occurrence	Surfical: Subtype Undefined	GSWA
Yeelirrie	-	-27.176	119.902	Advanced Project; Test Pit	Surfical: Groundwater / Valley Calcrete	GSWA
Yeelirrie Channel	Middle Bore, Bellah Bore	-27.393	120.324	Occurrence	Surfical: Subtype Undefined	[84]
Yeelirrie E	-	-27.375	120.300	Occurrence	Surfical: Subtype Undefined	GSWA
Yeelirrie S	Little Well	-27.325	120.198	Deposit	Surfical: Groundwater / Valley Calcrete	This Study
Yeelirrie SE	-	-27.439	120.434	Occurrence	Surfical: Subtype Undefined	[84]
Yelma	-	-26.482	121.666	Occurrence	Surfical: Playa Lake	[84]
Yinnietharra	-	-24.634	116.182	Occurrence	Surfical: Subtype Undefined	GSWA
Yinnietharra	-	-24.666	116.420	Occurrence	Surfical: Subtype Undefined	GSWA
Yinnietharra	-	-24.664	116.421	Occurrence	Surfical: Subtype Undefined	GSWA
Yinnietharra	-	-24.670	116.411	Occurrence	Surfical: Subtype Undefined	GSWA
Yinnietharra	-	-24.667	116.409	Occurrence	Surfical: Subtype Undefined	GSWA
Yoweragabbie	Munbinia	-28.231	117.525	Occurrence	Surfical: Subtype Undefined	GSWA
Yuinmery	-	-28.564	119.100	Deposit	Surfical: Playa Lake	GSWA

TABLE A-2. CALCRETE-HOSTED URANIUM OCCURRENCES (SORTED BY STATUS)

Name	Alternative name	Latitude (decimal degrees)	Longitude (decimal degrees)	Status	Deposit type	Data source
Centipede	Wiluna	-26.835	120.368	Advanced Project; Test Pit	Surfical: Playa Lake	GSWA
Lake Maitland	Mt Joel	-27.161	121.094	Advanced Project; Test Pit	Surfical: Playa Lake	CET
Lake Maitland	-	-27.177	121.082	Advanced Project; Test Pit	Surfical: Playa Lake	GSWA
Lake Maitland	-	-27.166	121.099	Advanced Project; Test Pit	Surfical: Playa Lake	GSWA
Yeelirrie	-	-27.176	119.902	Advanced Project; Test Pit	Surfical: Groundwater / Valley Calcrete	GSWA
Anketell	-	-28.014	118.720	Deposit	Surfical: Groundwater / Valley Calcrete	GSWA
Bellah Bore	-	-26.854	119.777	Deposit	Surfical: Groundwater / Valley Calcrete	CGSG
Bellah Bore E	-	-26.867	119.812	Deposit	Surfical: Groundwater / Valley Calcrete	GSWA
Bolitho Bore	Lake Mason	-27.557	119.851	Deposit	Surfical: Groundwater / Valley Calcrete	GSWA
Centipede N	Lake Way South	-26.824	120.373	Deposit	Surfical: Delta Calcrete	GSWA
Dawson E	Dawson-Hinkler	-26.905	120.126	Deposit	Surfical: Groundwater / Valley Calcrete	GSWA
Dawson W	Dawson-Hinkler	-26.921	120.082	Deposit	Surfical: Groundwater / Valley Calcrete	GSWA
Hillview	-	-26.918	118.826	Deposit	Surfical: Groundwater / Valley Calcrete	GSWA
Hinkler	Dawson-Hinkler	-26.869	120.218	Deposit	Surfical: Groundwater / Valley Calcrete	GSWA
Hinkler W	Dawson-Hinkler	-26.877	120.184	Deposit	Surfical: Groundwater / Valley Calcrete	GSWA
Jailor Bore	Cooper	-23.765	115.279	Deposit	Surfical: Terrace Calcrete	GSWA

Name	Alternative name	Latitude (decimal degrees)	Longitude (decimal degrees)	Status	Deposit type	Data source
Lake Mason	-	-27.779	119.380	Deposit	Surfical: Groundwater / Valley Calcrete	GSWA
Lake Raeside	Red Oaks	-28.784	120.648	Deposit	Surfical: Playa Lake	GSWA
Lake Way	-	-26.707	120.338	Deposit	Surfical: Delta Calcrete	GSWA
Lake Way D	-	-26.717	120.345	Deposit	Surfical: Delta Calcrete	GSWA
Lakeside Central	-	-27.432	117.711	Deposit	Surfical: Groundwater / Valley Calcrete	CGSG
Lakeside N	Lake Austin, Austin Downs	-27.408	117.710	Deposit	Surfical: Groundwater / Valley Calcrete	GSWA
Lakeside S	-	-27.442	117.722	Deposit	Surfical: Groundwater / Valley Calcrete	GSWA
Millipede	-	-26.828	120.339	Deposit	Surfical: Delta Calcrete	GSWA
Minindi Creek	-	-24.825	116.225	Deposit	Surfical: Terrace Calcrete	GSWA
Murchison Downs	-	-26.824	119.001	Deposit	Surfical: Delta Calcrete	GSWA
Nowthanna	Quinns Lake	-27.071	118.679	Deposit	Surfical: Delta Calcrete	GSWA
Nowthanna Hill	Nowthanna	-27.060	118.681	Deposit	Surfical: Delta Calcrete	GSWA
Nowthanna S	-	-27.109	118.700	Deposit	Surfical: Delta Calcrete	GSWA
Scottie Well	Cogla Downs, Yarrabubba	-27.361	118.919	Deposit	Surfical: Subtype Undefined	GSWA
Stakeyard Well	Mopoke Well, Lake Raeside	-28.849	120.763	Deposit	Surfical: Subtype Undefined	GSWA
Thatcher Soak	-	-28.018	123.584	Deposit	Surfical: Groundwater / Valley Calcrete	GSWA
Two Mile	Murchison Downs	-26.825	118.951	Deposit	Surfical: Subtype Undefined	GSWA
Wabli Creek	Yinnietharra, Minindi Creek	-24.899	116.287	Deposit	Surfical: Subtype Undefined	GSWA
Windimurra	-	-28.226	118.516	Deposit	Surfical: Groundwater / Valley Calcrete	GSWA
Wondinong	-	-27.795	118.310	Deposit	Surfical: Groundwater / Valley Calcrete	GSWA
Wondinong SE	-	-27.868	118.424	Deposit	Surfical: Groundwater / Valley Calcrete	GSWA
Yeelirrie S	Little Well	-27.325	120.198	Deposit	Surfical: Groundwater / Valley Calcrete	CGSG
Yuinmery	-	-28.564	119.100	Deposit	Surfical: Playa Lake	GSWA
Albion Downs	-	-26.967	120.007	Occurrence	Surfical: Subtype Undefined	CGSG

Name	Alternative name	Latitude (decimal degrees)	Longitude (decimal degrees)	Status	Deposit type	Data source
Byro	-	-26.550	116.440	Occurrence	Surfical: Subtype Undefined	GSWA
Byro Delta	Byro	-27.028	116.191	Occurrence	Surfical: Subtype Undefined	GSWA
Kaluwiri N	Kaluwiri	-27.628	120.004	Occurrence	Surfical: Subtype Undefined	GSWA
Lake Barlee	-	-29.283	118.896	Occurrence	Surfical: Subtype Undefined	CET
Lake Mackay	Far Out	-22.760	128.634	Occurrence	Surfical: Playa Lake	CET
Lake Teague	Esso Anomaly	-25.659	120.966	Occurrence	Surfical: Subtype Undefined	CET
Lake Wells	-	-27.138	123.363	Occurrence	Surfical: Subtype Undefined	GSWA
Noondie	Cundeelee	-28.782	119.267	Occurrence	Surfical: Playa Lake	CET
Quandong Well	-	-27.380	122.367	Occurrence	Surfical: Subtype Undefined	GSWA
Stanley	Nabberu	-25.820	121.646	Occurrence	Surfical: Playa Lake	CET
White Cliffs	White Cliffs	-28.404	122.806	Occurrence	Surfical: Subtype Undefined	CET
Yandal N	-	-26.691	120.791	Occurrence	Surfical: Subtype Undefined	CGSG
Yandal S	-	-27.765	121.064	Occurrence	Surfical: Subtype Undefined	CET
Yarlaweelor	Robinson Range, Billara Bore, Ann Prospect	-25.392	118.148	Occurrence	Surfical: Subtype Undefined	CET
Yeelirrie E	-	-27.375	120.300	Occurrence	Surfical: Subtype Undefined	GSWA
Alma Well	-	-23.759	115.827	Occurrence	Surfical: Subtype Undefined	GSWA
Anomaly P5	-	-24.493	116.526	Occurrence	Surfical: Subtype Undefined	GSWA
Anomaly PDH50	-	-23.213	115.574	Occurrence	Surfical: Subtype Undefined	GSWA
Baltic Bore	-	-23.649	115.194	Occurrence	Surfical: Subtype Undefined	GSWA
Barlee S	-	-29.425	119.868	Occurrence	Surfical: Subtype Undefined	GSWA
Ben Hur	Jailor Bore Extended	-23.847	115.212	Occurrence	Surfical: Subtype Undefined	GSWA
Berragan Bore	-	-27.284	116.355	Occurrence	Surfical: Subtype Undefined	GSWA
Burgess Bore NW	-	-27.624	116.184	Occurrence	Surfical: Subtype Undefined	GSWA
Burgess Bore S	-	-27.645	116.205	Occurrence	Surfical: Subtype Undefined	GSWA
Burgess Bore SW	-	-27.649	116.200	Occurrence	Surfical: Subtype Undefined	GSWA
Chalba Creek	Chalba Creek	-24.799	116.005	Occurrence	Surfical: Subtype Undefined	GSWA
Christmas Bore	Christmas Bore	-27.844	119.264	Occurrence	Surfical: Subtype Undefined	GSWA
Darawonga Well	-	-25.000	116.103	Occurrence	Inferred Surficial	GSWA
Four Corners Bore	-	-27.333	116.279	Occurrence	Surfical: Subtype Undefined	GSWA
Four Corners Bore W	-	-27.329	116.299	Occurrence	Surfical: Subtype Undefined	GSWA
Fraser Creek	-	-23.965	116.235	Occurrence	Surfical: Subtype Undefined	GSWA

Name	Alternative name	Latitude (decimal degrees)	Longitude (decimal degrees)	Status	Deposit type	Data source
Fyfe Well	-	-25.678	120.905	Occurrence	Surfical: Subtype Undefined	GSWA
Fyfe Well	-	-25.667	120.894	Occurrence	Surfical: Subtype Undefined	GSWA
Gifford Creek	-	-23.986	116.196	Occurrence	Surfical: Subtype Undefined	GSWA
Jamieson Well	-	-24.128	116.536	Occurrence	Surfical: Subtype Undefined	GSWA
Kaluwiri	-	-27.685	120.032	Occurrence	Surfical: Subtype Undefined	GSWA
Kendell Bore	-	-24.408	116.460	Occurrence	Surfical: Subtype Undefined	GSWA
Kendell Bore NE	-	-24.398	116.523	Occurrence	Surfical: Subtype Undefined	GSWA
Kendell Bore SW	-	-24.445	116.449	Occurrence	Surfical: Subtype Undefined	GSWA
Kewell	Quail Springs, Baltic Bore	-23.652	115.210	Occurrence	Surfical: Subtype Undefined	GSWA
Lake Throssell	-	-27.294	124.404	Occurrence	Surfical: Subtype Undefined	GSWA
Minindi Creek	-	-24.827	116.229	Occurrence	Surfical: Terrace Calcrete	GSWA
Minindi Creek	-	-24.826	116.228	Occurrence	Surfical: Terrace Calcrete	GSWA
Minindi Creek	-	-24.825	116.223	Occurrence	Surfical: Terrace Calcrete	GSWA
Minindi Creek	-	-24.826	116.221	Occurrence	Surfical: Terrace Calcrete	GSWA
Minindi Creek	-	-24.824	116.229	Occurrence	Surfical: Terrace Calcrete	GSWA
Minindi Creek	-	-24.830	116.229	Occurrence	Surfical: Terrace Calcrete	GSWA
Minnie Creek	-	-24.104	115.998	Occurrence	Surfical: Subtype Undefined	GSWA
Minnieritchie Well	-	-24.708	116.347	Occurrence	Surfical: Subtype Undefined	GSWA
Mt Dalgety South	-	-25.194	115.991	Occurrence	Inferred Surficial	GSWA
Mt James Creek	-	-24.833	116.542	Occurrence	Surfical: Subtype Undefined	GSWA
Nallan W	-	-27.293	117.924	Occurrence	Surfical: Subtype Undefined	GSWA
Nardoo Well	31 River	-24.459	116.097	Occurrence	Surfical: Subtype Undefined	GSWA
Onslow Creek	-	-24.459	115.824	Occurrence	Inferred Surficial	GSWA
Poorinoo Well	-	-23.838	115.831	Occurrence	Surfical: Subtype Undefined	GSWA
Range Bore	-	-25.002	116.221	Occurrence	Inferred Surficial	GSWA
Stevies	-	-23.614	118.608	Occurrence	Surfical: Subtype Undefined	GSWA
Taincrow E	-	-27.241	118.251	Occurrence	Surfical: Subtype Undefined	GSWA
Telfer River	Chain Pool	-23.079	115.659	Occurrence	Surfical: Subtype Undefined	GSWA
Thomas River	-	-24.637	116.502	Occurrence	Surfical: Subtype Undefined	GSWA
Three Rivers	-	-25.261	119.169	Occurrence	Surfical: Subtype Undefined	GSWA
Wabli Creek	Yinnietharra, Minindi Creek	-24.908	116.266	Occurrence	Surfical: Subtype Undefined	GSWA
Wabli Creek	Yinnietharra, Minindi Creek	-24.895	116.235	Occurrence	Surfical: Subtype Undefined	GSWA
Wangannue	-	-27.284	116.282	Occurrence	Surfical: Subtype Undefined	GSWA

Name	Alternative name	Latitude (decimal degrees)	Longitude (decimal degrees)	Status	Deposit type	Data source
Willi Creek	Jailor Bore Extended	-23.809	115.243	Occurrence	Surfical: Subtype Undefined	GSWA
Yarrabubba	Nowthanna	-27.112	118.851	Occurrence	Surfical: Subtype Undefined	GSWA
Yinnietharra	-	-24.634	116.182	Occurrence	Surfical: Subtype Undefined	GSWA
Cogla Downs	Nowthanna, Murchison Downs, Two Mile	-27.433	118.933	Occurrence	Surfical: Subtype Undefined	CET
Peninsula	Lake Raeside, Mopoke Well	-28.797	120.698	Occurrence	Surfical: Groundwater / Valley Calcrete	GSWA
Trillbar	-	-25.598	117.747	Occurrence	Surfical: Subtype Undefined	CET
Yamarna N	-	-28.120	123.644	Occurrence	Surfical: Subtype Undefined	CET
Abercromby	-	-26.826	120.342	Occurrence	Surfical: Subtype Undefined	CET
Altona	Puncture Well	-27.917	120.083	Occurrence	Surfical: Subtype Undefined	CET
Andrew Bore	-	-24.673	116.415	Occurrence	Surfical: Subtype Undefined	GSWA
Bad Ass	-	-23.111	115.434	Occurrence	Surfical: Subtype Undefined	GSWA
Billara Bore	-	-25.589	118.230	Occurrence	Surfical: Subtype Undefined	GSWA
Billara Bore	-	-25.565	118.249	Occurrence	Surfical: Subtype Undefined	GSWA
Boolardy	-	-26.442	116.526	Occurrence	Surfical: Subtype Undefined	CET
Bordah Well	Bordah	-23.854	115.446	Occurrence	Surfical: Subtype Undefined	GSWA
Bruce Bore	Nowthanna	-27.102	118.829	Occurrence	Surfical: Subtype Undefined	GSWA
Bulga Downs N	Bulga Downs	-28.385	119.669	Occurrence	Surfical: Subtype Undefined	CGSG
Bulga Downs S	-	-28.562	119.574	Occurrence	Surfical: Subtype Undefined	CET
Bungalow Well	Beta	-28.314	120.398	Occurrence	Surfical: Subtype Undefined	CET
Bustler Well	-	-24.732	116.910	Occurrence	Surfical: Subtype Undefined	GSWA
Bustler Well	-	-24.737	116.915	Occurrence	Surfical: Subtype Undefined	GSWA
Cahill	Holman, Baltic Bore	-23.614	115.202	Occurrence	Surfical: Subtype Undefined	GSWA
Carlo Creek	-	-25.149	116.087	Occurrence	Surfical: Subtype Undefined	GSWA
Cashmere Downs	Cashmere	-29.000	119.395	Occurrence	Surfical: Subtype Undefined	CET
Cave Well	-	-27.636	121.467	Occurrence	Surfical: Subtype Undefined	CET
Cosmo	-	-28.195	123.438	Occurrence	Surfical: Subtype Undefined	CET
Curbaweeda	-	-27.785	117.983	Occurrence	Surfical: Subtype Undefined	CET
Downs East	-	-26.656	119.526	Occurrence	Surfical: Subtype Undefined	GSWA
Firestrike	-	-26.928	120.558	Occurrence	Surfical: Subtype Undefined	GSWA
Galah Rocks	-	-29.659	120.270	Occurrence	Inferred Surficial	CET

Name	Alternative name	Latitude (decimal degrees)	Longitude (decimal degrees)	Status	Deposit type	Data source
Giant's Prospect	-	-24.041	115.237	Occurrence	Surfical: Subtype Undefined	CGSG
Glenburgh	-	-25.165	116.546	Occurrence	Surfical: Subtype Undefined	CET
Gnaweeda	Glenburgh	-26.666	118.729	Occurrence	Inferred Surficial	CET
Gum Well	Ida Valley	-28.827	120.392	Occurrence	Surfical: Subtype Undefined	CET
Halfpenny Well	-	-27.700	121.417	Occurrence	Surfical: Subtype Undefined	CET
Hazlett Cliffs	-	-28.830	123.222	Occurrence	Surfical: Subtype Undefined	CET
Hectors Bore	Ti Tree Well	-25.067	116.233	Occurrence	Surfical: Subtype Undefined	CET
Holman	-	-23.604	115.208	Occurrence	Surfical: Subtype Undefined	CGSG
Hope River	-	-26.400	118.117	Occurrence	Surfical: Subtype Undefined	CET
Horse Well	-	-23.242	115.575	Occurrence	Surfical: Subtype Undefined	CET
Ida Valley	-	-28.755	120.443	Occurrence	Surfical: Subtype Undefined	CET
Jigalong	-	-23.795	120.455	Occurrence	Surfical: Subtype Undefined	CET
Jillary	-	-23.748	119.362	Occurrence	Surfical: Subtype Undefined	CET
Jimmy Well	-	-23.689	115.492	Occurrence	Inferred Surficial	GSWA
Kelly Bore	Nowthanna	-27.069	118.757	Occurrence	Surfical: Subtype Undefined	GSWA
Kitchener Bore	-	-26.388	117.513	Occurrence	Surfical: Subtype Undefined	CET
Lake Barlee	-	-29.015	119.957	Occurrence	Surfical: Subtype Undefined	GSWA
Lake Barlee	-	-29.562	119.332	Occurrence	Surfical: Subtype Undefined	CET
Lake Barlee	-	-29.477	119.789	Occurrence	Surfical: Subtype Undefined	CET
Lake Carnegie	-	-25.211	122.635	Occurrence	Surfical: Subtype Undefined	CET
Lake Darlot	-	-27.747	121.618	Occurrence	Surfical: Subtype Undefined	CET
Lake Irwin	-	-28.157	121.835	Occurrence	Surfical: Subtype Undefined	CET
Lake Maitland	-	-27.300	121.133	Occurrence	Surfical: Subtype Undefined	CET
Lake Maitland Central	-	-27.137	121.057	Occurrence	Surfical: Subtype Undefined	GSWA
Lake Maitland N	-	-27.121	121.101	Occurrence	Surfical: Subtype Undefined	CET
Lake Marmion	-	-29.726	121.472	Occurrence	Inferred Surficial	CET
Lake Throssell	-	-27.845	123.781	Occurrence	Surfical: Subtype Undefined	CET
Lake Way S	Yandal, Wiluna South	-26.767	120.381	Occurrence	Surfical: Subtype Undefined	CET
Lakeview	Lake Raeside	-28.806	120.882	Occurrence	Surfical: Subtype Undefined	CET
Lyndon	Baltic Bore	-23.633	115.203	Occurrence	Surfical: Subtype Undefined	GSWA
Maitland	-	-27.158	121.086	Occurrence	Surfical: Subtype Undefined	CET
Maitland Channel	Irwin, Devine	-27.424	121.387	Occurrence	Surfical: Subtype Undefined	CET
Mckay	-	-23.500	122.217	Occurrence	Inferred Surficial	CET

Name	Alternative name	Latitude (decimal degrees)	Longitude (decimal degrees)	Status	Deposit type	Data source
McPhersons Bore N	-	-28.815	120.092	Occurrence	Surfical: Subtype Undefined	GSWA
Meeberrie	-	-26.944	116.019	Occurrence	Surfical: Subtype Undefined	CET
Meekatharra	-	-26.717	118.687	Occurrence	Surfical: Playa Lake	CET
Melrose W	-	-26.832	121.156	Occurrence	Inferred Surficial	CET
Middle Well	Minnie Creek	-23.834	115.927	Occurrence	Surfical: Subtype Undefined	GSWA
Mindoolah	-	-26.917	117.625	Occurrence	Surfical: Subtype Undefined	CET
Minnawarra	-	-26.748	116.298	Occurrence	Surfical: Subtype Undefined	CET
Minnie Creek	-	-23.943	115.914	Occurrence	Surfical: Subtype Undefined	CET
Minniearra	-	-24.657	116.520	Occurrence	Inferred Surficial	GSWA
Mombo Bore	Mickey's Well	-24.807	115.935	Occurrence	Surfical: Subtype Undefined	CET
Mt Alfred	-	-28.920	119.975	Occurrence	Surfical: Subtype Undefined	CET
Mt Dalgety	-	-25.017	116.008	Occurrence	Inferred Surficial	CET
Mt James	-	-24.890	116.428	Occurrence	Surfical: Subtype Undefined	GSWA
Mt James	-	-24.892	116.461	Occurrence	Surfical: Subtype Undefined	GSWA
Mt James Creek	-	-24.793	116.666	Occurrence	Surfical: Subtype Undefined	GSWA
Mt James Creek NW	-	-24.792	116.660	Occurrence	Surfical: Subtype Undefined	GSWA
Mt Padbury	Homestead Pit	-25.697	118.076	Occurrence	Surfical: Subtype Undefined	CGSG
Mt Padbury	Discovery Pit 1	-25.811	118.090	Occurrence	Surfical: Subtype Undefined	CGSG
Mt Padbury	Discovery Pit 2	-25.827	118.060	Occurrence	Surfical: Subtype Undefined	CET
Mt Phillips	-	-24.398	116.456	Occurrence	Surfical: Subtype Undefined	CET
Mt Phillips	-	-24.670	116.215	Occurrence	Surfical: Subtype Undefined	CET
Mt Phillips	-	-24.610	116.495	Occurrence	Surfical: Subtype Undefined	CET
Mt Phillips	-	-24.661	116.199	Occurrence	Surfical: Terrace Calcrete	CET
Mt Webb	Buck Hills, Uamari, Pokali, Mantati	-22.959	128.269	Occurrence	Surfical: Subtype Undefined	CET
Myamin	-	-29.543	121.303	Occurrence	Inferred Surficial	CET
Nambi	-	-26.095	122.091	Occurrence	Surfical: Playa Lake	CET
Neale	-	-28.816	124.513	Occurrence	Surfical: Subtype Undefined	CET
Neil Bore	-	-27.922	118.723	Occurrence	Inferred Surficial	CET
Nelson Well	Nelson	-27.520	119.020	Occurrence	Surfical: Subtype Undefined	CET
Nichols	-	-27.472	123.071	Occurrence	Surfical: Subtype Undefined	CET
Oui Creek	-	-24.689	116.571	Occurrence	Inferred Surficial	GSWA

Name	Alternative name	Latitude (decimal degrees)	Longitude (decimal degrees)	Status	Deposit type	Data source
Panhandle	Gladys, Lesley, Charlotte	-28.990	119.918	Occurrence	Surfical: Subtype Undefined	CET
Polly Well	-	-24.984	116.230	Occurrence	Surfical: Subtype Undefined	CET
Pongo Pool	-	-23.274	115.363	Occurrence	Surfical: Subtype Undefined	GSWA
Porcupine Well	-	-26.960	120.683	Occurrence	Surfical: Playa Lake	CET
Rabbit Well	-	-27.924	118.576	Occurrence	Inferred Surficial	CET
Relief Well	Jailor Bore Extended	-23.588	115.038	Occurrence	Inferred Surficial	GSWA
Robinson Range	-	-25.038	117.714	Occurrence	Surfical: Subtype Undefined	CET
Salt Dam	Salt Dam	-29.421	120.900	Occurrence	Inferred Surficial	CET
Shark Hill	-	-24.500	116.436	Occurrence	Surfical: Subtype Undefined	GSWA
Shark Hill	-	-24.502	116.431	Occurrence	Surfical: Subtype Undefined	GSWA
Shaws Bore	-	-28.702	118.933	Occurrence	Surfical: Subtype Undefined	CET
South Yeelirrie	-	-27.472	120.058	Occurrence	Surfical: Subtype Undefined	CET
Stirling	-	-27.360	121.250	Occurrence	Surfical: Playa Lake	CET
Stone Tank Well	-	-24.018	116.115	Occurrence	Surfical: Subtype Undefined	GSWA
Sylvania	-	-23.516	119.712	Occurrence	Surfical: Subtype Undefined	CET
Tank Well	-	-23.208	115.687	Occurrence	Inferred Surficial	CET
Telfer S	-	-23.305	115.716	Occurrence	Surfical: Subtype Undefined	GSWA
Thomas River	-	-24.683	116.227	Occurrence	Surfical: Subtype Undefined	GSWA
Thomas River	-	-24.681	116.240	Occurrence	Surfical: Subtype Undefined	GSWA
Thomas River	-	-24.617	116.525	Occurrence	Surfical: Subtype Undefined	GSWA
Thomas River S	-	-24.724	116.276	Occurrence	Surfical: Subtype Undefined	GSWA
Uramurdah Well	Lake Way	-26.678	120.353	Occurrence	Surfical: Subtype Undefined	GSWA
Uramurdah Well Extended	Lake Way	-26.686	120.348	Occurrence	Surfical: Subtype Undefined	GSWA
Wabli Creek	Yinnietharra, Minindi Creek	-24.895	116.270	Occurrence	Surfical: Subtype Undefined	GSWA
Walling Rock	-	-29.440	120.265	Occurrence	Inferred Surficial	CET
Warramboo	-	-22.070	115.920	Occurrence	Inferred Surficial	CET
Waukarlycarly	Lamil Hills	-21.331	122.967	Occurrence	Surfical: Subtype Undefined	CET
Winmar Creek	-	-24.113	116.073	Occurrence	Surfical: Subtype Undefined	GSWA
Yakabindie	-	-27.583	120.533	Occurrence	Surfical: Subtype Undefined	CET
Yalgar	-	-25.979	117.704	Occurrence	Surfical: Subtype Undefined	CET
Yalinga Bore	-	-28.386	118.698	Occurrence	Surfical: Subtype Undefined	CET
Yannarie	Yannarie River	-23.263	115.210	Occurrence	Surfical: Subtype Undefined	GSWA

Name	Alternative name	Latitude (decimal degrees)	Longitude (decimal degrees)	Status	Deposit type	Data source
Yannarie	Yannarie River	-23.428	115.476	Occurrence	Surfical: Subtype Undefined	CET
Yeelirrie Channel	Middle Bore, Bellah Bore	-27.393	120.324	Occurrence	Surfical: Subtype Undefined	CET
Yeelirrie SE	-	-27.439	120.434	Occurrence	Surfical: Subtype Undefined	CET
Yelma	-	-26.482	121.666	Occurrence	Surfical: Playa Lake	CET
Yinnietharra	-	-24.666	116.420	Occurrence	Surfical: Subtype Undefined	GSWA
Yinnietharra	-	-24.664	116.421	Occurrence	Surfical: Subtype Undefined	GSWA
Yinnietharra	-	-24.670	116.411	Occurrence	Surfical: Subtype Undefined	GSWA
Yinnietharra	-	-24.667	116.409	Occurrence	Surfical: Subtype Undefined	GSWA
Yoweragabbie	Munbinia	-28.231	117.525	Occurrence	Surfical: Subtype Undefined	GSWA
Shepherd Well	-	-24.875	116.985	Occurrence	Surfical: Subtype Undefined	CET

TABLE A-3. CALCRETE-HOSTED URANIUM OCCURRENCES (SORTED BY DEPOSIT SUB-TYPE)

Name	Alternative name	Latitude (decimal degrees)	Longitude (decimal degrees)	Status	Deposit type	Data source
Darawonga Well	-	-25.000	116.103	Occurrence	Inferred Surficial	GSWA
Mt Dalgety South	-	-25.194	115.991	Occurrence	Inferred Surficial	GSWA
Onslow Creek	-	-24.459	115.824	Occurrence	Inferred Surficial	GSWA
Range Bore	-	-25.002	116.221	Occurrence	Inferred Surficial	GSWA
Galah Rocks	-	-29.659	120.270	Occurrence	Inferred Surficial	CET
Gnaweeda	Glenburgh	-26.666	118.729	Occurrence	Inferred Surficial	CET
Jimmy Well	-	-23.689	115.492	Occurrence	Inferred Surficial	GSWA
Lake Marmion	-	-29.726	121.472	Occurrence	Inferred Surficial	CET
Mckay	-	-23.500	122.217	Occurrence	Inferred Surficial	CET
Melrose W	-	-26.832	121.156	Occurrence	Inferred Surficial	CET
Minniearra	-	-24.657	116.520	Occurrence	Inferred Surficial	GSWA
Mt Dalgety	-	-25.017	116.008	Occurrence	Inferred Surficial	CET
Myamin	-	-29.543	121.303	Occurrence	Inferred Surficial	CET
Neil Bore	-	-27.922	118.723	Occurrence	Inferred Surficial	CET
Oui Creek	-	-24.689	116.571	Occurrence	Inferred Surficial	GSWA
Rabbit Well	-	-27.924	118.576	Occurrence	Inferred Surficial	CET
Relief Well	Jailor Bore Extended	-23.588	115.038	Occurrence	Inferred Surficial	GSWA
Salt Dam	Salt Dam	-29.421	120.900	Occurrence	Inferred Surficial	CET
Tank Well	-	-23.208	115.687	Occurrence	Inferred Surficial	CET
Walling Rock	-	-29.440	120.265	Occurrence	Inferred Surficial	CET
Warramboo	-	-22.070	115.920	Occurrence	Inferred Surficial	CET
Centipede N	Lake Way South	-26.824	120.373	Deposit	Surfical: Delta Calcrete	GSWA
Lake Way	-	-26.707	120.338	Deposit	Surfical: Delta Calcrete	GSWA
Lake Way D	-	-26.717	120.345	Deposit	Surfical: Delta Calcrete	GSWA
Millipede	-	-26.828	120.339	Deposit	Surfical: Delta Calcrete	GSWA
Murchison Downs	-	-26.824	119.001	Deposit	Surfical: Delta Calcrete	GSWA
Nowthanna	Quinns Lake	-27.071	118.679	Deposit	Surfical: Delta Calcrete	GSWA
Nowthanna Hill	Nowthanna	-27.060	118.681	Deposit	Surfical: Delta Calcrete	GSWA
Nowthanna S	-	-27.109	118.700	Deposit	Surfical: Delta Calcrete	GSWA
Centipede	Wiluna	-26.835	120.368	Advanced Project; Test Pit	Surfical: Playa Lake	GSWA

Name	Alternative name	Latitude (decimal degrees)	Longitude (decimal degrees)	Status	Deposit type	Data source
Lake Maitland	Mt Joel	-27.161	121.094	Advanced Project; Test Pit	Surfical: Playa Lake	CET
Lake Maitland	-	-27.177	121.082	Advanced Project; Test Pit	Surfical: Playa Lake	GSWA
Lake Maitland	-	-27.166	121.099	Advanced Project; Test Pit	Surfical: Playa Lake	GSWA
Lake Raeside	Red Oaks	-28.784	120.648	Deposit	Surfical: Playa Lake	GSWA
Yuinmery	-	-28.564	119.100	Deposit	Surfical: Playa Lake	GSWA
Lake Mackay	Far Out	-22.760	128.634	Occurrence	Surfical: Playa Lake	CET
Noondie	Cundeelee	-28.782	119.267	Occurrence	Surfical: Playa Lake	CET
Stanley	Nabberu	-25.820	121.646	Occurrence	Surfical: Playa Lake	CET
Meekatharra	-	-26.717	118.687	Occurrence	Surfical: Playa Lake	CET
Nambi	-	-26.095	122.091	Occurrence	Surfical: Playa Lake	CET
Porcupine Well	-	-26.960	120.683	Occurrence	Surfical: Playa Lake	CET
Stirling	-	-27.360	121.250	Occurrence	Surfical: Playa Lake	CET
Yelma	-	-26.482	121.666	Occurrence	Surfical: Playa Lake	CET
Scottie Well	Cogla Downs, Yarrabubba	-27.361	118.919	Deposit	Surfical: Subtype Undefined	GSWA
Stakeyard Well	Mopoke Well, Lake Raeside	-28.849	120.763	Deposit	Surfical: Subtype Undefined	GSWA
Two Mile	Murchison Downs	-26.825	118.951	Deposit	Surfical: Subtype Undefined	GSWA
Wabli Creek	Yinnietharra, Minindi Creek	-24.899	116.287	Deposit	Surfical: Subtype Undefined	GSWA
Albion Downs	-	-26.967	120.007	Occurrence	Surfical: Subtype Undefined	CGSG
Byro	-	-26.550	116.440	Occurrence	Surfical: Subtype Undefined	GSWA
Byro Delta	Byro	-27.028	116.191	Occurrence	Surfical: Subtype Undefined	GSWA
Kaluwiri N	Kaluwiri	-27.628	120.004	Occurrence	Surfical: Subtype Undefined	GSWA
Lake Barlee	-	-29.283	118.896	Occurrence	Surfical: Subtype Undefined	CET
Lake Teague	Esso Anomaly	-25.659	120.966	Occurrence	Surfical: Subtype Undefined	CET
Lake Wells	-	-27.138	123.363	Occurrence	Surfical: Subtype Undefined	GSWA
Quandong Well	-	-27.380	122.367	Occurrence	Surfical: Subtype Undefined	GSWA
White Cliffs	White Cliffs	-28.404	122.806	Occurrence	Surfical: Subtype Undefined	CET
Yandal N	-	-26.691	120.791	Occurrence	Surfical: Subtype Undefined	CGSG
Yandal S	-	-27.765	121.064	Occurrence	Surfical: Subtype Undefined	CET

Name	Alternative name	Latitude (decimal degrees)	Longitude (decimal degrees)	Status	Deposit type	Data source
Yarlaweelor	Robinson Range, Billara Bore, Ann Prospect	-25.392	118.148	Occurrence	Surfical: Subtype Undefined	CET
Yeelirrie E	-	-27.375	120.300	Occurrence	Surfical: Subtype Undefined	GSWA
Alma Well	-	-23.759	115.827	Occurrence	Surfical: Subtype Undefined	GSWA
Anomaly P5	-	-24.493	116.526	Occurrence	Surfical: Subtype Undefined	GSWA
Anomaly PDH50	-	-23.213	115.574	Occurrence	Surfical: Subtype Undefined	GSWA
Baltic Bore	-	-23.649	115.194	Occurrence	Surfical: Subtype Undefined	GSWA
Barlee S	-	-29.425	119.868	Occurrence	Surfical: Subtype Undefined	GSWA
Ben Hur	Jailor Bore Extended	-23.847	115.212	Occurrence	Surfical: Subtype Undefined	GSWA
Berragan Bore	-	-27.284	116.355	Occurrence	Surfical: Subtype Undefined	GSWA
Burgess Bore NW	-	-27.624	116.184	Occurrence	Surfical: Subtype Undefined	GSWA
Burgess Bore S	-	-27.645	116.205	Occurrence	Surfical: Subtype Undefined	GSWA
Burgess Bore SW	-	-27.649	116.200	Occurrence	Surfical: Subtype Undefined	GSWA
Chalba Creek	Chalba Creek	-24.799	116.005	Occurrence	Surfical: Subtype Undefined	GSWA
Christmas Bore	Christmas Bore	-27.844	119.264	Occurrence	Surfical: Subtype Undefined	GSWA
Four Corners Bore	-	-27.333	116.279	Occurrence	Surfical: Subtype Undefined	GSWA
Four Corners Bore W	-	-27.329	116.299	Occurrence	Surfical: Subtype Undefined	GSWA
Fraser Creek	-	-23.965	116.235	Occurrence	Surfical: Subtype Undefined	GSWA
Fyfe Well	-	-25.678	120.905	Occurrence	Surfical: Subtype Undefined	GSWA
Fyfe Well	-	-25.667	120.894	Occurrence	Surfical: Subtype Undefined	GSWA
Gifford Creek	-	-23.986	116.196	Occurrence	Surfical: Subtype Undefined	GSWA
Jamieson Well	-	-24.128	116.536	Occurrence	Surfical: Subtype Undefined	GSWA
Kaluwiri	-	-27.685	120.032	Occurrence	Surfical: Subtype Undefined	GSWA
Kendell Bore	-	-24.408	116.460	Occurrence	Surfical: Subtype Undefined	GSWA
Kendell Bore NE	-	-24.398	116.523	Occurrence	Surfical: Subtype Undefined	GSWA
Kendell Bore SW	-	-24.445	116.449	Occurrence	Surfical: Subtype Undefined	GSWA
Kewell	Quail Springs, Baltic Bore	-23.652	115.210	Occurrence	Surfical: Subtype Undefined	GSWA
Lake Throssell	-	-27.294	124.404	Occurrence	Surfical: Subtype Undefined	GSWA
Minnie Creek	-	-24.104	115.998	Occurrence	Surfical: Subtype Undefined	GSWA
Minnieritchie Well	-	-24.708	116.347	Occurrence	Surfical: Subtype Undefined	GSWA
Mt James Creek	-	-24.833	116.542	Occurrence	Surfical: Subtype Undefined	GSWA
Nallan W	-	-27.293	117.924	Occurrence	Surfical: Subtype Undefined	GSWA
Nardoo Well	31 River	-24.459	116.097	Occurrence	Surfical: Subtype Undefined	GSWA

Name	Alternative name	Latitude (decimal degrees)	Longitude (decimal degrees)	Status	Deposit type	Data source
Poorinoo Well	-	-23.838	115.831	Occurrence	Surfical: Subtype Undefined	GSWA
Stevies	-	-23.614	118.608	Occurrence	Surfical: Subtype Undefined	GSWA
Taincrow E	-	-27.241	118.251	Occurrence	Surfical: Subtype Undefined	GSWA
Telfer River	Chain Pool	-23.079	115.659	Occurrence	Surfical: Subtype Undefined	GSWA
Thomas River	-	-24.637	116.502	Occurrence	Surfical: Subtype Undefined	GSWA
Three Rivers	-	-25.261	119.169	Occurrence	Surfical: Subtype Undefined	GSWA
Wabli Creek	Yinnietharra, Minindi Creek	-24.908	116.266	Occurrence	Surfical: Subtype Undefined	GSWA
Wabli Creek	Yinnietharra, Minindi Creek	-24.895	116.235	Occurrence	Surfical: Subtype Undefined	GSWA
Wangannue	-	-27.284	116.282	Occurrence	Surfical: Subtype Undefined	GSWA
Willi Creek	Jailor Bore Extended	-23.809	115.243	Occurrence	Surfical: Subtype Undefined	GSWA
Yarrabubba	Nowthanna	-27.112	118.851	Occurrence	Surfical: Subtype Undefined	GSWA
Yinnietharra	-	-24.634	116.182	Occurrence	Surfical: Subtype Undefined	GSWA
Cogla Downs	Nowthanna, Murchison Downs, Two Mile	-27.433	118.933	Occurrence	Surfical: Subtype Undefined	CET
Trillbar	-	-25.598	117.747	Occurrence	Surfical: Subtype Undefined	CET
Yamarna N	-	-28.120	123.644	Occurrence	Surfical: Subtype Undefined	CET
Abercromby	-	-26.826	120.342	Occurrence	Surfical: Subtype Undefined	CET
Altona	Puncture Well	-27.917	120.083	Occurrence	Surfical: Subtype Undefined	CET
Andrew Bore	-	-24.673	116.415	Occurrence	Surfical: Subtype Undefined	GSWA
Bad Ass	-	-23.111	115.434	Occurrence	Surfical: Subtype Undefined	GSWA
Billara Bore	-	-25.589	118.230	Occurrence	Surfical: Subtype Undefined	GSWA
Billara Bore	-	-25.565	118.249	Occurrence	Surfical: Subtype Undefined	GSWA
Boolardy	-	-26.442	116.526	Occurrence	Surfical: Subtype Undefined	CET
Bordah Well	Bordah	-23.854	115.446	Occurrence	Surfical: Subtype Undefined	GSWA
Bruce Bore	Nowthanna	-27.102	118.829	Occurrence	Surfical: Subtype Undefined	GSWA
Bulga Downs N	Bulga Downs	-28.385	119.669	Occurrence	Surfical: Subtype Undefined	CGSG
Bulga Downs S	-	-28.562	119.574	Occurrence	Surfical: Subtype Undefined	CET
Bungalow Well	Beta	-28.314	120.398	Occurrence	Surfical: Subtype Undefined	CET
Bustler Well	-	-24.732	116.910	Occurrence	Surfical: Subtype Undefined	GSWA
Bustler Well	-	-24.737	116.915	Occurrence	Surfical: Subtype Undefined	GSWA
Cahill	Holman, Baltic Bore	-23.614	115.202	Occurrence	Surfical: Subtype Undefined	GSWA
Carlo Creek	-	-25.149	116.087	Occurrence	Surfical: Subtype Undefined	GSWA

Name	Alternative name	Latitude (decimal degrees)	Longitude (decimal degrees)	Status	Deposit type	Data source
Cashmere Downs	Cashmere	-29.000	119.395	Occurrence	Surfical: Subtype Undefined	CET
Cave Well	-	-27.636	121.467	Occurrence	Surfical: Subtype Undefined	CET
Cosmo	-	-28.195	123.438	Occurrence	Surfical: Subtype Undefined	CET
Curbaweeda	-	-27.785	117.983	Occurrence	Surfical: Subtype Undefined	CET
Downs East	-	-26.656	119.526	Occurrence	Surfical: Subtype Undefined	GSWA
Firestrike	-	-26.928	120.558	Occurrence	Surfical: Subtype Undefined	GSWA
Giant's Prospect	-	-24.041	115.237	Occurrence	Surfical: Subtype Undefined	CGSG
Glenburgh	-	-25.165	116.546	Occurrence	Surfical: Subtype Undefined	CET
Gum Well	Ida Valley	-28.827	120.392	Occurrence	Surfical: Subtype Undefined	CET
Halfpenny Well	-	-27.700	121.417	Occurrence	Surfical: Subtype Undefined	CET
Hazlett Cliffs	-	-28.830	123.222	Occurrence	Surfical: Subtype Undefined	CET
Hectors Bore	Ti Tree Well	-25.067	116.233	Occurrence	Surfical: Subtype Undefined	CET
Holman	-	-23.604	115.208	Occurrence	Surfical: Subtype Undefined	CGSG
Hope River	-	-26.400	118.117	Occurrence	Surfical: Subtype Undefined	CET
Horse Well	-	-23.242	115.575	Occurrence	Surfical: Subtype Undefined	CET
Ida Valley	-	-28.755	120.443	Occurrence	Surfical: Subtype Undefined	CET
Jigalong	-	-23.795	120.455	Occurrence	Surfical: Subtype Undefined	CET
Jillary	-	-23.748	119.362	Occurrence	Surfical: Subtype Undefined	CET
Kelly Bore	Nowthanna	-27.069	118.757	Occurrence	Surfical: Subtype Undefined	GSWA
Kitchener Bore	-	-26.388	117.513	Occurrence	Surfical: Subtype Undefined	CET
Lake Barlee	-	-29.015	119.957	Occurrence	Surfical: Subtype Undefined	GSWA
Lake Barlee	-	-29.562	119.332	Occurrence	Surfical: Subtype Undefined	CET
Lake Barlee	-	-29.477	119.789	Occurrence	Surfical: Subtype Undefined	CET
Lake Carnegie	-	-25.211	122.635	Occurrence	Surfical: Subtype Undefined	CET
Lake Darlot	-	-27.747	121.618	Occurrence	Surfical: Subtype Undefined	CET
Lake Irwin	-	-28.157	121.835	Occurrence	Surfical: Subtype Undefined	CET
Lake Maitland	-	-27.300	121.133	Occurrence	Surfical: Subtype Undefined	CET
Lake Maitland Central	-	-27.137	121.057	Occurrence	Surfical: Subtype Undefined	GSWA
Lake Maitland N	-	-27.121	121.101	Occurrence	Surfical: Subtype Undefined	CET
Lake Throssell	-	-27.845	123.781	Occurrence	Surfical: Subtype Undefined	CET
Lake Way S	Yandal, Wiluna South	-26.767	120.381	Occurrence	Surfical: Subtype Undefined	CET
Lakeview	Lake Raeside	-28.806	120.882	Occurrence	Surfical: Subtype Undefined	CET
Lyndon	Baltic Bore	-23.633	115.203	Occurrence	Surfical: Subtype Undefined	GSWA

Name	Alternative name	Latitude (decimal degrees)	Longitude (decimal degrees)	Status	Deposit type	Data source
Maitland	-	-27.158	121.086	Occurrence	Surfical: Subtype Undefined	CET
Maitland Channel	Irwin, Devine	-27.424	121.387	Occurrence	Surfical: Subtype Undefined	CET
McPhersons Bore N	-	-28.815	120.092	Occurrence	Surfical: Subtype Undefined	GSWA
Meeberrie	-	-26.944	116.019	Occurrence	Surfical: Subtype Undefined	CET
Middle Well	Minnie Creek	-23.834	115.927	Occurrence	Surfical: Subtype Undefined	GSWA
Mindoolah	-	-26.917	117.625	Occurrence	Surfical: Subtype Undefined	CET
Minnawarra	-	-26.748	116.298	Occurrence	Surfical: Subtype Undefined	CET
Minnie Creek	-	-23.943	115.914	Occurrence	Surfical: Subtype Undefined	CET
Mombo Bore	Mickey's Well	-24.807	115.935	Occurrence	Surfical: Subtype Undefined	CET
Mt Alfred	-	-28.920	119.975	Occurrence	Surfical: Subtype Undefined	CET
Mt James	-	-24.890	116.428	Occurrence	Surfical: Subtype Undefined	GSWA
Mt James	-	-24.892	116.461	Occurrence	Surfical: Subtype Undefined	GSWA
Mt James Creek	-	-24.793	116.666	Occurrence	Surfical: Subtype Undefined	GSWA
Mt James Creek NW	-	-24.792	116.660	Occurrence	Surfical: Subtype Undefined	GSWA
Mt Padbury	Homestead Pit	-25.697	118.076	Occurrence	Surfical: Subtype Undefined	CGSG
Mt Padbury	Discovery Pit 1	-25.811	118.090	Occurrence	Surfical: Subtype Undefined	CGSG
Mt Padbury	Discovery Pit 2	-25.827	118.060	Occurrence	Surfical: Subtype Undefined	CET
Mt Phillips	-	-24.398	116.456	Occurrence	Surfical: Subtype Undefined	CET
Mt Phillips	-	-24.670	116.215	Occurrence	Surfical: Subtype Undefined	CET
Mt Phillips	-	-24.610	116.495	Occurrence	Surfical: Subtype Undefined	CET
Mt Webb	Buck Hills, Uamari, Pokali, Mantati	-22.959	128.269	Occurrence	Surfical: Subtype Undefined	CET
Neale	-	-28.816	124.513	Occurrence	Surfical: Subtype Undefined	CET
Nelson Well	Nelson	-27.520	119.020	Occurrence	Surfical: Subtype Undefined	CET
Nichols	-	-27.472	123.071	Occurrence	Surfical: Subtype Undefined	CET
Panhandle	Gladys, Lesley, Charlotte	-28.990	119.918	Occurrence	Surfical: Subtype Undefined	CET
Polly Well	-	-24.984	116.230	Occurrence	Surfical: Subtype Undefined	CET
Pongo Pool	-	-23.274	115.363	Occurrence	Surfical: Subtype Undefined	GSWA
Robinson Range	-	-25.038	117.714	Occurrence	Surfical: Subtype Undefined	CET
Shark Hill	-	-24.500	116.436	Occurrence	Surfical: Subtype Undefined	GSWA
Shark Hill	-	-24.502	116.431	Occurrence	Surfical: Subtype Undefined	GSWA
Shaws Bore	-	-28.702	118.933	Occurrence	Surfical: Subtype Undefined	CET

Name	Alternative name	Latitude (decimal degrees)	Longitude (decimal degrees)	Status	Deposit type	Data source
South Yeelirrie	-	-27.472	120.058	Occurrence	Surfical: Subtype Undefined	CET
Stone Tank Well	-	-24.018	116.115	Occurrence	Surfical: Subtype Undefined	GSWA
Sylvania	-	-23.516	119.712	Occurrence	Surfical: Subtype Undefined	CET
Telfer S	-	-23.305	115.716	Occurrence	Surfical: Subtype Undefined	GSWA
Thomas River	-	-24.683	116.227	Occurrence	Surfical: Subtype Undefined	GSWA
Thomas River	-	-24.681	116.240	Occurrence	Surfical: Subtype Undefined	GSWA
Thomas River	-	-24.617	116.525	Occurrence	Surfical: Subtype Undefined	GSWA
Thomas River S	-	-24.724	116.276	Occurrence	Surfical: Subtype Undefined	GSWA
Uramurdah Well	Lake Way	-26.678	120.353	Occurrence	Surfical: Subtype Undefined	GSWA
Uramurdah Well Extended	Lake Way	-26.686	120.348	Occurrence	Surfical: Subtype Undefined	GSWA
Wabli Creek	Yinnietharra, Minindi Creek	-24.895	116.270	Occurrence	Surfical: Subtype Undefined	GSWA
Waukarlycarly	Lamil Hills	-21.331	122.967	Occurrence	Surfical: Subtype Undefined	CET
Winmar Creek	-	-24.113	116.073	Occurrence	Surfical: Subtype Undefined	GSWA
Yakabindie	-	-27.583	120.533	Occurrence	Surfical: Subtype Undefined	CET
Yalgar	-	-25.979	117.704	Occurrence	Surfical: Subtype Undefined	CET
Yalinga Bore	-	-28.386	118.698	Occurrence	Surfical: Subtype Undefined	CET
Yannarie	Yannarie River	-23.263	115.210	Occurrence	Surfical: Subtype Undefined	GSWA
Yannarie	Yannarie River	-23.428	115.476	Occurrence	Surfical: Subtype Undefined	CET
Yeelirrie Channel	Middle Bore, Bellah Bore	-27.393	120.324	Occurrence	Surfical: Subtype Undefined	CET
Yeelirrie SE	-	-27.439	120.434	Occurrence	Surfical: Subtype Undefined	CET
Yinnietharra	-	-24.666	116.420	Occurrence	Surfical: Subtype Undefined	GSWA
Yinnietharra	-	-24.664	116.421	Occurrence	Surfical: Subtype Undefined	GSWA
Yinnietharra	-	-24.670	116.411	Occurrence	Surfical: Subtype Undefined	GSWA
Yinnietharra	-	-24.667	116.409	Occurrence	Surfical: Subtype Undefined	GSWA
Yoweragabbie	Munbinia	-28.231	117.525	Occurrence	Surfical: Subtype Undefined	GSWA
Shepherd Well	-	-24.875	116.985	Occurrence	Surfical: Subtype Undefined	CET
Jailor Bore	Cooper	-23.765	115.279	Deposit	Surfical: Terrace Calcrete	GSWA
Minindi Creek	-	-24.825	116.225	Deposit	Surfical: Terrace Calcrete	GSWA
Minindi Creek	-	-24.827	116.229	Occurrence	Surfical: Terrace Calcrete	GSWA
Minindi Creek	-	-24.826	116.228	Occurrence	Surfical: Terrace Calcrete	GSWA
Minindi Creek	-	-24.825	116.223	Occurrence	Surfical: Terrace Calcrete	GSWA
Minindi Creek	-	-24.826	116.221	Occurrence	Surfical: Terrace Calcrete	GSWA

Name	Alternative name	Latitude (decimal degrees)	Longitude (decimal degrees)	Status	Deposit type	Data source
Minindi Creek	-	-24.824	116.229	Occurrence	Surfical: Terrace Calcrete	GSWA
Minindi Creek	-	-24.830	116.229	Occurrence	Surfical: Terrace Calcrete	GSWA
Mt Phillips	-	-24.661	116.199	Occurrence	Surfical: Terrace Calcrete	CET
Yeelirrie	-	-27.176	119.902	Advanced Project; Test Pit	Surfical: Groundwater / Valley Calcrete	GSWA
Anketell	-	-28.014	118.720	Deposit	Surfical: Groundwater / Valley Calcrete	GSWA
Bellah Bore	-	-26.854	119.777	Deposit	Surfical: Groundwater / Valley Calcrete	CGSG
Bellah Bore E	-	-26.867	119.812	Deposit	Surfical: Groundwater / Valley Calcrete	GSWA
Bolitho Bore	Lake Mason	-27.557	119.851	Deposit	Surfical: Groundwater / Valley Calcrete	GSWA
Dawson E	Dawson-Hinkler	-26.905	120.126	Deposit	Surfical: Groundwater / Valley Calcrete	GSWA
Dawson W	Dawson-Hinkler	-26.921	120.082	Deposit	Surfical: Groundwater / Valley Calcrete	GSWA
Hillview	-	-26.918	118.826	Deposit	Surfical: Groundwater / Valley Calcrete	GSWA
Hinkler	Dawson-Hinkler	-26.869	120.218	Deposit	Surfical: Groundwater / Valley Calcrete	GSWA
Hinkler W	Dawson-Hinkler	-26.877	120.184	Deposit	Surfical: Groundwater / Valley Calcrete	GSWA
Lake Mason	-	-27.779	119.380	Deposit	Surfical: Groundwater / Valley Calcrete	GSWA
Lakeside Central	-	-27.432	117.711	Deposit	Surfical: Groundwater / Valley Calcrete	CGSG
Lakeside N	Lake Austin, Austin Downs	-27.408	117.710	Deposit	Surfical: Groundwater / Valley Calcrete	GSWA
Lakeside S	-	-27.442	117.722	Deposit	Surfical: Groundwater / Valley Calcrete	GSWA

Name	Alternative name	Latitude (decimal degrees)	Longitude (decimal degrees)	Status	Deposit type	Data source
Thatcher Soak	-	-28.018	123.584	Deposit	Surfical: Groundwater / Valley Calcrete	GSWA
Windimurra	-	-28.226	118.516	Deposit	Surfical: Groundwater / Valley Calcrete	GSWA
Wondinong	-	-27.795	118.310	Deposit	Surfical: Groundwater / Valley Calcrete	GSWA
Wondinong SE	-	-27.868	118.424	Deposit	Surfical: Groundwater / Valley Calcrete	GSWA
Yeelirrie S	Little Well	-27.325	120.198	Deposit	Surfical: Groundwater / Valley Calcrete	CGSG
Peninsula	Lake Raeside, Mopoke Well	-28.797	120.698	Occurrence	Surfical: Groundwater / Valley Calcrete	GSWA

REFERENCES

[1] BUTT, C. R. M., HORWITZ, R. C., MANN, A. W., Uranium occurrences in calcrete and associated sediments in Western Australia. Report FP 16, Commonwealth Scientific and Industrial Research Organization (CSIRO), Minerals Research Laboratories, Division of Mineralogy Floreat Park, Australia, 67p (1977).

[2] INTERNATIONAL ATOMIC ENERGY AGENCY, Surficial uranium deposits. IAEA-TECDOC 322, Vienna, Austria, 252p (1984).

[3] INTERNATIONAL ATOMIC ENERGY AGENCY, World distribution of uranium deposits (UDEPO) with uranium deposit classification. IAEA-TECDOC 1629, Vienna, Austria, 117p (2009).

[4] RIGANTI, A., FARRELL, T. R., ELLIS, M. J., IRIMIES, F., STRICKLAND, C. D., MARTIN, S. K., WALLACE, D. J., 125 years of legacy data at the Geological Survey of Western Australia: Capture and delivery. GeoResJ, 6, 175-194 (2015).

[5] OLSON, D. M., DINERSTEIN, E., WIKRAMANAYAKE, E. D., BURGESS, N. D., POWELL, G. V., UNDERWOOD, E. C., D'AMICO, J. A., ITOUA, I., STRAND, H. E., MORRISON, J. C., LOUCKS, C. J., ALLNUTT, T. F., RICKETTS, T. H., KURA, Y., LAMOREUX, J. F., WETTENGEL, W. W., HEDAO, P., KASSEM, K. R., Terrestrial Ecoregions of the World: A New Map of Life on Earth A new global map of terrestrial ecoregions provides an innovative tool for conserving biodiversity. BioScience, 51(11), 933-938 (2001).

[6] KOTTEK, M., GRIESER, J., BECK, C., RUDOLF, B., RUBEL, F., World map of the Köppen-Geiger climate classification updated. Meteorologische Zeitschrift, 15(3), 259-263 (2006).

[7] MERNAGH, T. P. (Ed.), A review of Australian salt lakes and assessment of their potential for strategic resources. Record 2013/39, Geoscience Australia, Canberra, 243p (2013).

[8] KREUZER, O. P., MARKWITZ, V., PORWAL, A. K., MCCUAIG, T. C., A continent-wide study of Australia's uranium potential: Part I: GIS-assisted manual prospectivity analysis. Ore Geology Reviews, 38(4), 334-366 (2010).

[9] WYBORN, L. A. I., HEINRICH, C. A., JAQUES, A. L., Australian Proterozoic mineral systems: essential ingredients and mappable criteria. The AusIMM Annual Conference, v. 1994, pp. 109-115 (1994).

[10] KNOX-ROBINSON, C. M., WYBORN, L. A. I., Towards a holistic exploration strategy: using geographic information systems as a tool to enhance exploration. Australian journal of earth sciences, 44(4), 453-463 (1997).

[11] HRONSKY, J. M. A., The science of exploration targeting. SEG 2004 Conference, Centre for Global Metallogeny, University of Western Australia Publication, Perth, v. 33, pp. 129-133 (2004).

[12] KREUZER, O. P., ETHERIDGE, M. A., GUJ, P., MCMAHON, M. E., HOLDEN, D. J., Linking mineral deposit models to quantitative risk analysis and decision-making in exploration. Economic Geology, 103(4), 829-850 (2008).

[13] PORWAL, A. K., KREUZER, O. P., Introduction to the special issue: Mineral prospectivity analysis and quantitative resource estimation. Ore Geology Reviews, 38(3), 121-127 (2010).

[14] MCCUAIG, T. C., BERESFORD, S., HRONSKY, J., Translating the mineral systems approach into an effective exploration targeting system. Ore Geology Reviews, 38(3), 128-138 (2010).
[15] KREUZER, O. P., MILLER, A. V., PETERS, K. J., PAYNE, C., WILDMAN, C., PARTINGTON, G. A., PUCCIONI, E., MCMAHON, M. E., ETHERIDGE, M. A., Comparing prospectivity modelling results and past exploration data: A case study of porphyry Cu–Au mineral systems in the Macquarie Arc, Lachlan Fold Belt, New South Wales. Ore Geology Reviews, 71, 516-544 (2015).
[16] MAGOON, L. B., DOW, W. G., The petroleum system. The petroleum system - from source to trap. AAPG Memoir, 60, 3-24 (1994).
[17] AGTERBERG, F. P., Systematic approach to dealing with uncertainty of geoscience information in mineral exploration. Chapter 18, Proceedings of the 21st APCOM Symposium, Las Vegas, USA, pp. 165-178 (1989).
[18] AGTERBERG, F. P., BONHAM-CARTER, G. F., Deriving weights-of-evidence from geoscience contour maps for prediction of discrete events. Proceedings of the 22nd APCOM Symposium, Berlin, Germany, 2, pp. 381-395 (1990).
[19] AGTERBERG, F. P., BONHAM-CARTER, G. F., CHENG, Q. M., WRIGHT, D. F., Weights of evidence modeling and weighted logistic regression for mineral potential mapping. Computers in Geology, 25, 13-32 (1993).
[20] AGTERBERG, F. P., Automatic contouring of geological maps to detect target areas for mineral exploration. Mathematical Geology, 6(4), 373-395 (1974).
[21] AGTERBERG, F. P., Combining indicator patterns in weights of evidence modeling for resource evaluation. Nonrenewable Resources, 1(1), 39-50 (1992).
[22] AGTERBERG, F. P., Estimating the probability of occurrence of mineral deposits from multiple map patterns. In: MERRIAM, D. F., KURZL, H. (Eds.), Microcomputers in Geology. Plenum Press, New York, pp. 73-92 (1992).
[23] CHUNG, C. F., AGTERBERG, F. P., Regression models for estimating mineral resources from geological map data. Mathematical Geology, 12(5), 472-488 (1980).
[24] CARRANZA, E. J. M., HALE, M., Logistic regression for geologically-constrained mapping of gold mineralization potential, Baguio district, Philippines. Exploration and Mining Geology, 10 (3), 165-175 (2001).
[25] PORWAL, A. K., GONZALEZ-ALVAREZ, I., MARKWITZ, V., MCCUAIG, T. C., MAMUSE, A., Weights-of-evidence and logistic regression modeling of magmatic nickel sulfide prospectivity in the Yilgarn Craton, Western Australia. Ore Geology Reviews, 38(3), 184-196 (2010).
[26] BONHAM-CARTER, G. F., Geographic information systems for geoscientists: Modeling with GIS. Computer Methods in the Geosciences, 13. Pergamon-Elsevier, Kidlington, UK, 398p (1994).
[27] SINGER, D. A., KOUDA, R., A comparison of the weights of evidence method and probabilistic neural networks. Natural Resources Research, 8(4), 287-298 (1999).
[28] BROWN, W. M., GEDEON, T. D., GROVES, D. I., BARNES, R. G., Artificial neural networks: A new method for mineral prospectivity mapping. Australian Journal of Earth Sciences, 47(4), 757-770 (2000).
[29] PORWAL, A. K., CARRANZA, E. J. M., HALE, M., Artificial neural networks for mineral potential mapping: A case study from Aravalli province, western India. Natural Resources Research, 12(3), 155-177 (2003).
[30] BREIMAN, L., FRIEDMAN, J., STONE, C. J., OLSHEN, R. A., Classification and regression trees. Chapman and Hall/CRC Press, 368p (1984).

[31] BOSER, B. E., GUYON, I. M., VAPNIK, V. N., A training algorithm for optimal margin classifiers. Proceedings of the Fifth ACM Annual Workshop on Computational Learning, Pittsburgh, PA, USA, pp. 144-152 (1992).
[32] CORTES, C., VAPNIK, V., Support-vector networks. Machine Learning, 20, 273-297 (1995).
[33] ZUO, R., CARRANZA, E. J. M., Support vector machine: A tool for mapping mineral prospectivity. Computers & Geosciences, 37(12), 1967-1975 (2011).
[34] BREIMAN, L., Random forests. Machine Learning, 45, 5-32 (2001).
[35] RODRIGUEZ-GALIANO, V. F., CHICA-OLMO, M., CHICA-RIVAS, M., Predictive modelling of gold potential with the integration of multisource information based on random forest: A case study on the Rodalquilar area, Southern Spain. International Journal of Geographical Information Science, 28(7), 1336-1354 (2014).
[36] CARRANZA, E. J. M., Data-driven evidential belief modelling of mineral potential using few prospects and evidence with missing values. Natural Resources Research, 24(3), 291-304 (2015).
[37] RODRIGUEZ-GALIANO, V. F., SANCHEZ-CASTILLO, M., CHICA-OLMO, M., CHICA-RIVAS, M., Machine learning predictive models for mineral prospectivity: An evaluation of neural networks, random forest, regression trees and support vector machines. Ore Geology Reviews, 71, 804-818 (2015).
[38] DUDA, R. O., HART, P. E., NILSSON, N. J., SUTHERLAND, G. L., Semantic network representations in rule-based interference systems. In: WATERMAN, D. A., HAYES-ROTH, F. (Eds.), Pattern-directed inference systems. Academic Press, pp. 203-221 (1978).
[39] DUDA, R. O., HART, P. E., BARRETT, P., GASCHING, J. G., KONOLIGE, K., REBOH, R., SLOCUM, J., Final Report, Development of the Prospector consultation system for mineral exploration, SRI Projects 5821 and 6415, Artificial Intelligence Center, SRI International, Menlo Park, 193p (1978).
[40] CAMPBELL, A. N., HOLLISTER, V. F., DUDA, R. O., Recognition of a hidden mineral deposit by an artificial intelligence program. Science 217, 927-929 (1982).
[41] KATZ, S. S., Emulating the Prospector expert system with a raster GIS. Computers & Geosciences, 17, 1033-1050 (1991).
[42] REDDY, R. K. T., BONHAM-CARTER, G. F., GALLEY, A. G., Developing a geographic expert system for regional mapping of volcanogenic massive sulphide (VMS) deposit potential. Nonrenewable Resources, 2, 112-124 (1992).
[43] AN, P., MOON, W. M., RENCZ, A., Application of fuzzy set theory for integration of geological, geophysical and remote sensing data. Canadian Journal of Exploration Geophysics, 27, 1-11 (1991).
[44] LUO, X., DIMITRAKOPOULOS, R., Data-driven fuzzy analysis in quantitative mineral resource assessment. Computers & Geosciences, 29(1), 3-13 (2003).
[45] PORWAL, A. K., DAS, R. D., CHAUDHARY, B., GONZALEZ-ALVAREZ, I., KREUZER, O. P., Fuzzy inference systems for prospectivity modeling of mineral systems and a case-study for prospectivity mapping of surficial uranium in Yeelirrie area, Western Australia. Ore Geology Reviews, 71, 839-852 (2015).
[46] MOON, W. M., Integration of geophysical and geological data using evidential belief function. IEEE Transactions on Geoscience and Remote Sensing, 28(4), 711-720 (1990).
[47] MOON, W. M., Mathematical basis for geophysical information representation and integration. Canadian Journal of Remote Sensing, 19, 63-67 (1993).
[48] MOON, W. M., CHUNG, C. F., AN, P., Representation and integration of geological, geophysical and remote sensing data. Geoinformatics, 2, 177-188 (1991).

[49] AN, P., MOON, W. M., BONHAM-CARTER, G. F., Uncertainty management in integration of exploration data using the belief function. Nonrenewable Resources, 3, 60-71 (1994).
[50] AN, P., MOON, W. M., BONHAM-CARTER, G. F., An object-oriented knowledge representation structure for exploration data integration. Nonrenewable Resources, 3, 132-145 (1994).
[51] CHUNG, C. F., FABBRI, A. G., The representation of geoscience information for data integration. Nonrenewable Resources, 2, 122-139 (1993).
[52] MAMUSE, A., BERESFORD, S., PORWAL, A. K., KREUZER, O. P., Assessment of undiscovered nickel sulphide resources, Kalgoorlie Terrane, Western Australia: Part 1. Deposit and endowment density models. Ore Geology Reviews, 37(3), 141-157 (2010).
[53] ZIPF, G. K., Human behaviour and the principle of least effort. Addison-Wesley, Cambridge, MA, 573p (1949).
[54] SINGER, D. A., Basic concepts in three-part quantitative assessments of undiscovered mineral resources. Nonrenewable Resources, 2(2), 69-81 (1993).
[55] SINGER, D. A., BERGER, V. I., MENZIE, W. D., BERGER, B. R., Porphyry copper deposit density. Economic Geology, 100(3), 491-514 (2005).
[56] FOLINSBEE, R. E., World's view-from Alph to Zipf. Geological Society of America Bulletin, 88, 897-907 (1977).
[57] ROWLANDS, N. J., SAMPEY, D., Zipf's law – an aid to resource inventory prediction in partially explored areas. Mathematical Geology, 9, 383-391 (1977).
[58] SCHUENEMEYER, J. H., DREW, L. J., A procedure to estimate the parent population of the size of oil and gas fields as revealed by a study of economic truncation. Mathematical Geology, 15, 145-161 (1983).
[59] PALIWAL, H. V., BHATNAGAR, S. N., HALDAR, S. K., Lead-zinc resource prediction in India: An application of Zipf's law. Mathematical Geology, 18, 539-549 (1986).
[60] BARKER, R., Recent exploration in the Hauraki Goldfield, Coromandel Peninsula. New Zealand Mining, 13, 9-15 (1994).
[61] MERRIAM, D. F., DREW, L. J., SCHUENEMEYER, J. H., Zipf's Law: A viable geological paradigm? Natural Resources Research, 13, 265-271 (2004).
[62] FAGAN, R. K., Modelling how much gold is left to be found in the Eastern Goldfields of W.A. Proceedings of the Kalgoorlie 2006 Conference, 30 April to 4 May 2006. Institute of Geoscientists Bulletin, 44, 23-25 (2006).
[63] MCCUAIG, T. C., GUJ, P., Balancing risk and reward in the face of increasing global exploration maturity. Proceedings of the Kalgoorlie 2006 Conference, 30 April to 4 May 2006. Institute of Geoscientists Bulletin, 44, 3-8 (2006).
[64] GUJ, P., MCCUAIG, T. C., GARZON, R., Can the petroleum industry's probabilistic approach to targeting and resources definition be applied in predicting mineral discoveries? In: Mineral Exploration and Research: Digging Deeper. Proceedings of the 9th Biennial Meeting of the Society for Geology Applied to Mineral Deposits (SGA), Dublin, Ireland, pp. 1467-1470 (2007).
[65] MAMUSE, A., GUJ, P., Rank statistical analysis of nickel sulphide resources of the Norseman-Wiluna Greenstone Belt, Western Australia. Mineralium Deposita, 46(3), 305-318 (2011).
[66] LISITSIN, V. A., Rank-size statistical assessments of undiscovered gold endowment in the Bendigo and Stawell Zones (Victoria) and the Mossman Orogen (Queensland), Australia: Comparison with three-part assessment results. Natural Resources Research, 25(3), 269-282 (2016).

[67] LYSYTSYN, V., Mineral prospectivity analysis and quantitative resource assessment for regional exploration targeting: Development of effective integration models and practical applications. PhD Thesis, The University of Western Australia, 403p (2015). Available online from: http://research-repository.uwa.edu.au/files/5263287/Lysytsyn_Volodymyr_2015.pdf [last accessed: 21 July 2016].
[68] DUVAL, J. S., Version 3.0 of EMINERS – Economic Mineral Resource Simulator. U.S. Geological Survey Open-File Report 2004–1344 (2012). Available online from: http://pubs.usgs.gov/of/2004/1344 [last accessed: 21 July 2016].
[69] BAWIEC, W. J., SPANSKI, G. T., Quick-start guide for version 3.0 of EMINERS – Economic Mineral Resources Simulator. U.S. Geological Survey Open-File Report 2009-1057, 26p (2012). Available online from: http://pubs.usgs.gov/of/2009/1057 [last accessed: 16 July 2016].
[70] DUVAL, J. S., Economic filters applied to quantitative mineral resource simulations. Natural Resources Research, 12(2), 121-126 (2003).
[71] OECD-NEA & IAEA, Uranium 2009: Resources, production and demand (the Red Book). A Joint Report by the OECD Nuclear Energy Agency and the International Atomic Energy Agency, Vienna, Austria, 456p (2010).
[72] OECD-NEA & IAEA, Uranium 2014: resources, production and demand, NEA no. 7209, A joint report by the Organization for Economic Co-operation and Development Nuclear Energy Agency (OECD-NEA) and the International Atomic Energy Agency (IAEA), 508p (2014).
[73] MCKAY, A. D., MIEZITIS, Y., Australia's uranium resources, geology and development of deposits. AGSO-Geoscience Australia, Mineral Resources Report 1. Australian Department of Industry, Science and Resources, Canberra, Australia, 184p (2001).
[74] CUNEY, M., AND KYSER, K., Recent and not-so-recent developments in uranium deposits and implications for exploration. Mineral Association of Canada Short Course Series, 39, 257p (2008).
[75] SKIRROW, R. G., JAIRETH, S., HUSTON, D. L., BASTRAKOV, E. N., SCHOFIELD, A., VAN DER WIELEN, S. E., BARNICOAT, A. C., Uranium mineral systems: Processes, exploration criteria and a new deposit framework. Geoscience Australia Record 2009/20, 44p (2009).
[76] ARAL, H., Mineralogical characteristics of low-grade uranium ores in Western Australia. IAEA Meeting, Vienna, 29 to 31 March 2010, 43p (2010). Available online from: https://www.iaea.org/OurWork/ST/NE/NEFW/documents/RawMaterials/TM_LGUO/1e%20Aral%20West%20Australia%20Mineralogy.pdf [last accessed: 21 July 2016].
[77] LIU, S., JAIRETH, S., Exploring for calcrete-hosted uranium deposits in the Paterson region, Western Australia. AusGeo News, September 2011, 103, 1-5 (2011).
[78] MISRA, A., PANDE, D., KUMAR, K. R., NANDA, L. K., MAITHANI, P. B., CHAKI, A., Calcrete-hosted surficial uranium occurrence in playa-lake environment at Lachhri, Nagaur District, Rajasthan, India. Current Science, 101(1), 84-88 (2011).
[79] NOBLE, R. R. P., GRAY, D. J., REID, N., Regional exploration for channel and playa uranium deposits in Western Australia using groundwater. Applied Geochemistry, 26(12), 1956-1974 (2011).

[80] GUTHRIE, V., Wiluna uranium project: Feasibility, development and approvals. IAEA Training Meeting, Darwin, 14 August 2012, 34p (2012). Available online from: https://www.iaea.org/OurWork/ST/NE/NEFW/Technical-Areas/NFC/documents/uranium/tr-darwin-2012/Presentations/16and17.Gutherie_(Toro)_-_Wiluna_Uranium_Project.pdf [last accessed: 21 July 2016].
[81] CAMECO CORPORATION, Cameco acquires Yeelirrie uranium project in Western Australia. TSX and NYSE Announcement, 26 August 2012, 3p (2012). Available online from: https://www.cameco.com/media/news/cameco-acquires-yeelirrie-uranium-project-in-western-australia [last accessed: 21 July 2016].
[82] DEPARTMENT OF MINES AND PETROLEUM, Guide to uranium in Western Australia. Government of Western Australia, 41p (2013).
[83] POWNCEBY, M. I., JOHNSON, C., Geometallurgy of Australian uranium deposits. Ore Geology Reviews, 56, 25-44 (2014).
[84] JAIRETH, S., ROACH, I. C., BASTRAKOV, E., LIU, S., Basin-related uranium mineral systems in Australia: A review of critical features. Ore Geology Reviews, 76, 360-394 (2016).
[85] LAMPLUGH, G. W., Calcrete. Geological Magazine (Decade IV), 9(12), 575-575 (1902).
[86] CHEN, X. Y., LINTERN, M. J., ROACH, I. C. (Eds.), Calcrete: characteristics, distribution and use in mineral exploration. Cooperative Research Centre for Landscape Environments and Mineral Exploration, CSIRO Exploration and Mining, Kensington, Western Australia, Australia and The University of Canberra, Division of Science and Design, Australian Capital Territory, Australia, 160p (2002).
[87] WRIGHT, V. P., TUCKER, M. E. (Eds.), Calcretes. Blackwell Scientific Publications, (1991).
[88] ALONSO-ZARZA, A. M., WRIGHT, V. P., Calcretes. Developments in Sedimentology, 61, 225-267 (2010).
[89] CARLISLE, D., Handbook on surficial uranium deposits; Chapter 3: World distribution relative to climate and physical setting. Report DOE/ER/10119-T3, United Nations International Atomic Energy Agency, Vienna, Austria, 108p (1983).
[90] ANAND, R. R., PAINE, M., Regolith geology of the Yilgarn Craton, Western Australia: implications for exploration. Australian Journal of Earth Sciences, 49(1), 3-162 (2002).
[91] CARLISLE, D., Possible variations on the calcrete-gypcrete uranium model. United States Department of Energy Subcontract Number 76-022-E, 38p (1980).
[92] NETTERBERG, F., Geology of southern African calcretes, I. Terminology, description, macrofeatures and classification. Transactions of the Geological Society of South Africa, 83, 255-283 (1980).
[93] GOODE, A., The geochemistry and mineralogy of Tertiary uraniferous carbonates, Western Australia. Unpublished Report, Data Metallogenica (http://www.datametallogenica.com), 10p (1977).
[94] CARLISLE, D., Surficial uranium occurrences in relation to climate and physical setting. In: Surficial uranium deposits. IAEA-TECDOC 322, International Atomic Energy Agency, Vienna, Austria, pp. 25-35 (1984).
[95] HAMBLETON-JONES, B. B., LEVIN, M., WAGENER, G. F., Uraniferous surficial deposits in southern Africa. In Mineral deposits of Southern Africa, 1-2 (1986).
[96] ROESENER, H., SCHREUDER, C. P., Uranium. Mineral resources of Namibia: Nuclear and fossil fuels: Geological Survey of Namibia, 7-1 (1992).

[97] TRITTSCHACK, R., Geological identification and mineralogical characterisation of palaeosurfaces and channel fills at the Langer Heinrich uranium deposit, Namibia. Diploma Thesis, Institute for Geosciences, Martin-Luther-University Halle Wittenberg, Germany, 143p (2008).
[98] KÄRNER, K., BECKER, E., Geological setting of the Langer Heinrich uranium mine, Namibia. In: Proceedings of the AusIMM International Uranium Conference 2009, 10-11 June 2009, Darwin, Australia, pp. 97-98 (2009).
[99] FLEURANCE, S., CUNEY, M., KINNAIRD, J., Mineralogical, geochemical and isotopic study of 6 samples from the Langer Heinrich calcrete deposit (Namibia). Unpublished Report, Henri Poincaré University, Nancy, and University of the Witwatersrand, Johannesburg, South Africa, 16p (2011).
[100] BUTT, C. R. M., MANN, A. W., HORWITZ, R. C., Regional setting, distribution and genesis of surficial uranium deposits in calcretes and associated sediments in Western Australia. In: Surficial uranium deposits. IAEA-TECDOC 322, International Atomic Energy Agency, Vienna, Austria, pp. 121-127 (1984).
[101] WESTERN MINING CORPORATION LIMITED, A general account of the Yeelirrie uranium deposit. Prepared by the staff of the Western Mining Corporation (Exploration Division). Privately published and distributed to the 25th International Geological Congress, April 1975, 14p (1975).
[102] CAMERON, E., The Yeelirrie calcrete uranium deposit, Western Australia. In: Surficial uranium deposits. IAEA-TECDOC 322, International Atomic Energy Agency, Vienna, Austria, pp. 157-163 (1984).
[103] KHOURY, H. N., CLARK, I. D., Mineralogy and origin of surficial uranium deposits hosted in travertine and calcrete from central Jordan. Applied Geochemistry, 43, 49-65 (2014).
[104] XOUBI, N., Evaluation of uranium concentration in soil samples of Central Jordan. Minerals, 5(2), 133-141 (2015).
[105] THOMAS, D., ZALUSKI, G., BRISBIN, D., DREVER, G., Uranium deposit models, with an emphasis on sedimentary-associated types. Presentation by Cameco Corporation at the Centre for Exploration Targeting, University of Western Australia, Perth, Australia, 29 November 2006 (2006).
[106] HARTLEB, J. W. O., The Langer Heinrich uranium deposit: Southwest Africa/Namibia. Ore Geology Reviews, 3(1), 277-287 (1988).
[107] IILENDE, A., The source of uranium and vanadium at the Langer Heinrich and Klein Trekkopje uranium deposits – genesis and controlling factors for uranium mineralization. Master of Science Thesis, Department of Geology, University of Namibia, 220p (2012).
[108] RAWLINGS, D., MCGEOUGH, M., The geology of Australian surficial calcrete deposits. U2011 Uranium Symposium, Casper, Wyoming, September 2011 (2011).
[109] BELL, J. G., KILGOUR, P. L., ENGLISH, P. M., WOODGATE, M. F., LEWIS, S. J., WISCHUSEN, J. D. H. (Comps.), WASANT palaeovalley map - distribution of palaeovalleys in arid and semi-arid WA-SA-NT, scale 1:4,500,000. Geoscience Australia Thematic Map, (2012). Available online from: https://d28rz98at9flks.cloudfront.net/73980/73980_update2.pdf [last accessed: 24 July 2016].
[110] MANN, A. W., HORWITZ, R. C., Groundwater calcrete deposits in Australia some observations from Western Australia. Journal of the Geological Society of Australia, 26(5-6), 293-303 (1979).

[111] HOU, B., MICHAELSEN, B. H., LI, Z., KEELING, J. L., FABRIS, A. J., Paleovalley-related uranium: exploration criteria and case-studies from Australia and China. Episodes, 37(3), 150-171 (2014).
[112] ANAND, R. R., BUTT, C. R. M., A guide for mineral exploration through the regolith in the Yilgarn Craton, Western Australia. Australian Journal of Earth Sciences, 57(8), 1015-1114 (2010).
[113] GEOLOGICAL SURVEY OF WESTERN AUSTRALIA, Geology and mineral resources of Western Australia. Memoir 3, Department of Mines, Western Australia, 827p (1990).
[114] JOHNSON, S. P., The birth of supercontinents and the Proterozoic assembly of Western Australia. Geological Survey of Western Australia, 78p (2013).
[115] BAGAS, L., Proterozoic evolution and tectonic setting of the northwest Paterson Orogen, Western Australia. Precambrian Research, 128(3), 475-496 (2004).
[116] CAWOOD, P. A., KORSCH, R. J., Assembling Australia: Proterozoic building of a continent. Precambrian Research, 166(1), 1-35 (2008).
[117] WALTER, M. R., VEEVERS, J. J., CALVER, C. R., GREY, K., Neoproterozoic stratigraphy of the Centralian Superbasin, Australia. Precambrian Research, 73(1), 173-195 (1995).
[118] GREY, K., HOCKING, R. M., STEVENS, M. K., BAGAS, L., CARLSEN, G. M., IRIMIES, F., PIRAJNO, F., HAINES, P. W., APAK, S. N., Lithostratigraphic nomenclature of the Officer Basin and correlative parts of the Paterson Orogen, Western Australia. Western Australia Geological Survey, Report 93, 89p (2005).
[119] DE VRIES, S. T., PRYER, L. L., FRY, N., Evolution of Neoarchaean and Proterozoic basins of Australia. Precambrian Research, 166(1), 39-53 (2008).
[120] BAILLIE, P. W., POWELL, C. M., LI, Z. X., RYALL, A. M., The tectonic framework of Western Australia's Neoproterozoic to Recent sedimentary basins. In The Sedimentary Basins of Western Australia, Proceedings of the Petroleum Exploration Society of Australia Symposium, Perth (pp. 45-62) (1994).
[121] BARNETT-MOORE, N., FLAMENT, N., HEINE, C., BUTTERWORTH, N., MÜLLER, R. D., Cenozoic uplift of south Western Australia as constrained by river profiles. Tectonophysics, 622, 186-197 (2014).
[122] COCKBAIN, A. E., Australia goes it alone - the emerging island continent 100 Ma to present. Geological Survey of Western Australia, 63p (2014).
[123] MAGEE, J. W., Palaeovalley groundwater resources in arid and semi-arid Australia – a literature review. Geoscience Australia Record 2009/03, 224p (2009).
[124] MANN, A. W., DEUTSCHER, R. L., Genesis principles for the precipitation of carnotite in calcrete drainages in Western Australia. Economic Geology, 73(8), 1724-1737 (1978).
[125] ANAND, R. R., Weathering history, landscape evolution and implications for exploration. In: BUTT, C. R. M., CORNELIUS, M., SCOTT, K. M., ROBERTSON, I. D. M. (Eds.), Regolith expression of Australian ore systems. Cooperative Research Centre for Landscape Environments and Mineral Exploration (CRCleme), Perth, Australia, pp. 15-45 (2005).
[126] MANN, A. W., Chemical ore genesis models for the precipitation of carnotite in calcrete. Commonwealth Scientific and Industrial Research Organisation (CSIRO), Minerals Research Laboratories, Division of Mineralogy Floreat Park, Australia (1974).
[127] BOYLE, D. R., The genesis of surficial uranium deposits. In: Surficial uranium deposits. IAEA-TECDOC 322, International Atomic Energy Agency, Vienna, Austria, pp. 45-52 (1984).

[128] PORWAL, A. K., CHUDASAMA, B., DAS, R. D., KREUZER, O. P., Surficial uranium targeting model and prospectivity mapping of the Yeelirrie area, Western Australia. In: Proceedings of the 13th Biennial SGA Meeting, Nancy, France, 5, 1871-1874 (2015).
[129] CUNEY, M., FRIEDRICH, M., Physicochemical and crystal-chemical controls on accessory mineral paragenesis in granitoids: implications for uranium metallogenesis. Bulletin de Mineralogie, 110(2-3), 235-247 (1987).
[130] CUNEY, M., Evolution of uranium fractionation processes through time: driving the secular variation of uranium deposit types. Economic Geology, 105(3), 553-569, (2010).
[131] LAMBERT, I., JAIRETH, S., MCKAY, A., MIEZITIS, Y., Why has Australia so much uranium? AusGeo News, December 2005, 80, 1-4 (2005).
[132] WILFORD, J., A weathering intensity index for the Australian continent using airborne gamma-ray spectrometry and digital terrain analysis. Geoderma, 183, 124-142 (2012).
[133] DAHLKAMP, F. J., Uranium ore deposits. Springer-Verlag Berlin Heidelberg, 460p (1993).
[134] SINCLAIR, P., Surficial uranium deposits. Uranium Geology Short Course, Society of Economic Geologists (SEG) 2015 Conference, Hobart, 26 to 27 September 2015, 31p (2015).
[135] WOODALL, R., Empiricism and concept in successful mineral exploration. Australian Journal of Earth Sciences, 41(1), 1-10 (1994).
[136] JORC, The Australasian code for reporting of exploration results, minerals resources and ore reserves, 2012 Edition. Prepared by the Joint Ore Reserves Committee of the Australasian Institute of Mining and Metallurgy, Australian Institute of Geoscientists and Minerals Council of Australia, JOINT ORE RESERVES COMMITTEE (JORC) (2012). Available online from: http://www.jorc.org/docs/jorc_code2012.pdf [last accessed: 15 October 2015].
[137] ZADEH, L. A., Outline of a new approach to the analysis of complex systems and decision processes. IEEE Transactions on Systems, Man, and Cybernetics, 1, 28-44 (1973).
[138] PORWAL, A. K., Mineral potential mapping with mathematical geological models. University of Utrecht, ITC Dissertation, 130, 289p (2006).
[139] HAYKIN, S., Neural networks: A comprehensive foundation. Mac-Millan, New York (1994).
[140] LOONEY, C. G., Radial basis functional link nets and fuzzy reasoning. Neurocomputing, 48(1), 489-509 (2002).
[141] LOONEY, C. G., YU, H., Special software development for neural network and fuzzy clustering analysis in geological information systems. Geological Survey of Canada, 34 (2000). Available online from: http://www.ige.unicamp.br/sdm/ArcSDM31/documentation/dataxplore.pdf [last accessed: 15 October 2015].
[142] PAO, Y. H., PARK, G. H., SOBAJIC, D. J., Learning and generalization characteristics of the random vector functional-link net. Neurocomputing, 6(2), 163-180 (1994).
[143] LOONEY, C. G., Pattern recognition using neural networks: Theory and algorithms for engineers and scientists. Oxford University Press, New York, 458p (1997).
[144] SAWATZKY, D., RAINES, G., BONHAM-CARTER, G., Spatial Data Modeller, http://www.ige.unicamp.br/sdm/ArcSDM10/source/ReadMe.pdf (2010).
[145] NELSON, S. W., MILLER, M. L., GOLDFARB, R. J., SNEE, L. W., SHERMAN, G. E., ROE, C. H., BALEN M. D., Mineral resource assessment of the Chugach National Forest special study area in northern Prince William Sound, Alaska. US Geological Survey Open-File Report 94-272, 20p (1994).

[146] SINGER, D. A., MENZIE, W. D., LONG, K. R., A simplified economic filter for open-pit gold-silver mining in the United States. U.S. Geological Survey Open-File Report 98-207, 13p (1998).
[147] TORO ENERGY LIMITED, Studies confirm combined Wiluna uranium project improvements. Australian Securities Exchange Release, 30 January 2014 (2014). Available online from: http://www.toroenergy.com.au/wp-content/uploads/2014/01/140131-Wiluna-Project-Update-and-Plans.pdf [last accessed: 21 July 2016].

LIST OF MEETINGS

Training Meeting on Uranium Deposit Modelling, Fuzhou, China, 3–7 November 2014.

Consultancy Meeting on Uranium Mineral Economics and Strategy, Regina, Canada, 18–21 May 2015. T1-CS-50227.

Consultancy Meeting on Uranium Mineral Economics and Strategy. 27-29th June 2016 Vienna. T1-CS-53266.

Consultancy Meeting on Quantitative Uranium Resource Assessments, Denver, United States of America, 6–10 July 2015. T1-CS-50223.

Technical Meeting and Consultancy Meeting on Spatial and Quantitative Uranium Resource, Vienna, Austria, 9–11 November 2015. T1-TM-50222.

Consultancy Meeting to Prepare a Report on Undiscovered Uranium Resource Calculations Vienna, Austria, 20–24 June 2016. T1-CS-53243.

Training Meeting on Evaluation of Undiscovered Uranium Resources, Buenos Aires, Argentina, 24–28 October 2016. T1-TR-52374 And T1-CS-53250.

LIST OF PARTICIPANTS

Agustin, M.	Comisión Nacional de Energía Atómica Presbitero Juan Gonzalez y Aragon Nº 15 B1802AYA Ezeiza Argentina
Aish, R. A.	King Abdulla Citry for Atomic and Renewable Energy PO Box 2022 Riyadh 11751 Saudia Arabia
Al-Fouad, S. A.	Iraq Geological Survey Al-Nedhal Street PO Box 968 Alwiya Near Iben Al-Nafees Hospital Baghdad Iraq
Altangerel, T.	Ministry of Foreign Affairs National Registration Center Central Post Box 954, Sukhbaatar, Chingeltei Ulaanbaatar 15170 Mongolia
Asiedu, D.	Department of Earth Science University of Ghana PO Box LG58 Accra Ghana
Bello, C.	National Atomic Energy Commission (CNEA) Espinel 902, Alta Cordoba X5001BKW Cordoba Argentina
Benni, T. J.	Iraq Geological Survey Al-Nedhal Street PO Box 968 Alwiya Near Iben Al-Nafees Hospital Baghdad Iraq
Bierlein, F.	24th Floor Tornado Tower West Bay, PO Box 20405 Doha Qatar

Bizhanov, A.	JV Inkai Yuzhnaya 4 Taikonur Kazakhstan
Bruneton, P.	4 Place de la Wantzenau 87500 Le Chalard France
Bianchi, R.	Comisión Nacional de Energía Atómica (CNEA) Avenida del Libertador 8250 C1429BNP Buenos Aires Argentina
Bruce, M.	21 Jackson Avenue Coromandel Valley Adelaide, South Australia, 5051 Australia
Canaj, E.	Geological Survey of Albania Street Panarama Building 4 Entry II Ap 43 Tirana 1016 Albania
Carlos, J.	Servicio Geológico Minero Argentino Avenida General Paz 5445, Edificio 25 San Martín Argentina
Carranaza, E.J M.	Economic Geology Research Centre James Cook University Townsville, Queensland, 4814 Australia
Ceballos, E.	Comisión Nacional de Energía Atómica (CNEA) Avenida Bolivia 4400 Salta Argentina
Changkrueng, K.	Office of Atoms for Peace 16 Vibhavadi Rangsit Road Lardyao, Jatujak 10900 Bangkok Thailand

Chirtes, A. P.	Ministry of Energy Small and Medium Enterprises and Business Environment 202 E Splaiul Independentei, Sector 6 060021 Bucharest Romania
Chualaowanich, T.	Department of Mineral Resources 75/10 Rama VI Road Ratchathewee 10400 Bangkok Thailand
Chudasama, B.	Indian Institute of Technology Bombay Powai, 400076, Mumbai India
Comito, E.	Comisión Nacional de Energía Atómica (CNEA) Avenida del Libertador 8250 C1429BNP Buenos Aires Argentina
Comlekciler, F.	General Directorate of Mineral Research and Exploration Universiteler Mahallesi Dumlupinar Bulvari Nº 139 Ankara 06800 Turkey
Cross, A.	Geoscience Australia Cnr Jerrabomberra Avenue and Hindmarsh Drive Symonston Australian Capital Territory 2601 Australia
Da Silva, L. F.	Industrias Nucleares Do Brasil/SA Av. Joao Cabral De Melo Neto 400 Brazil
Diwa, R.	Philippine Nuclear Research Institute Commonwealth Avenue 1101 Quezon City Philippines
Donbon, U.	Mineral Resources Authority of Mongolia Government Building 12, Bareilgachdyn Tolbi 3 Chingeltei District, Ulaanbaatar Mongolia

Ellefsen, K. United States Geological Survey
Southwest Region, West 6th Avenue & Kipling Street
DFC Building 20
Lakewood, Colorado, 80225-0046
Unites States of America

Ferreyra, P. Comisión Nacional de Energía Atómica (CNEA)
Espinel 902, Alta Cordoba
X5001BKW Cordoba
Argentina

Ferri, F. Comisión Nacional de Energía Atómica (CNEA)
Figueroa Alcorta 122
5501 Godoy Cruz, Mendoza
Argentina

Filip, D. National Uranium Company S. A.
68 Dionijie Lupa Street, Sector 1
030167 Bucharest
Romania

Fleming, P. Nuclear Energy Chilean Commission
Amunategui
Santiago 095
Chile

Franzoni, L. Comisión Nacional de Energía Atómica (CNEA)
Presbitero Juan Gonzalez y Aragon Nº 15
B1802AYA Ezeiza
Argentina

Garba, A. A. Nigerian Geological Survey Agency
Bhn Berger Yard, Litako District
PMB 616
Abuja
Nigeria

Gayone, M. Comisión Nacional de Energía Atómica (CNEA)
Avenida del Libertador 8250
C1429BNP Buenos Aires
Argentina

Grancea, L. OECD Nuclear Energy Agency (NEA)
12, boulevard des Îles
92130 Issy-Les-Moulineaux
France

<table>
<tr><td>Hall, S.</td><td>United States Geological Survey
Southwest Region, West 6th Avenue & Kipling Street
DFC Building 25
Lakewood, Colorado, 80225-0046
United States of America</td></tr>
<tr><td>Hannon, M.</td><td>United States Geological Survey
Southwest Region, West 6th Avenue & Kipling Street
DFC Building 25
Lakewood, Colorado, 80225-0046
United States of America</td></tr>
<tr><td>Higa, L.</td><td>Comisión Nacional de Energía Atómica (CNEA)
Avenida del Libertador 8250
C1429BNP Buenos Aires
Argentina</td></tr>
<tr><td>Jaireth, S.</td><td>45 Noala Street, Aranda
Australian Capital Territory, 2614
Australia</td></tr>
<tr><td>Irvine, J.</td><td>Geological Survey of South Australia
4/101 Grenfell Street
Adelaide 5001
Australia</td></tr>
<tr><td>Katona, L.</td><td>Geological Survey of South Australia
4/101 Grenfell Street
Adelaide 5001
Australia</td></tr>
<tr><td>Karkanis, C.</td><td>Comisión Nacional de Energía Atómica (CNEA)
Avenida del Libertador 8250
C1429BNP Buenos Aires
Argentina</td></tr>
<tr><td>Kenan, A.</td><td>Council for Geoscience
280 Pretoria Street
Silverton, Pretoria
South Africa</td></tr>
<tr><td>Khamies, A. A.</td><td>Nuclear Materials Authority
PO Box 530
Katamia Cairo
Egypt</td></tr>
</table>

Laowattanabandit, P.	Department of Mining and Petroleum Engineering 14th Floor, Building Nº 4, Faculty of Engineering Chulalongkorn University Pathumwan, Bangkok 10330 Thailand
Lisitsin, V.	Level 12 61 Mary Street Brisbane, QLD 4000 Australia
Lopez, L.	National Atomic Energy Commission (CNEA) Avenida del Libertador 8250 C1429BNP Buenos Aires Argentina
Mandshir, M.	Ministry of Foreign Affairs National Registration Center Central Post Box 954, Sukhbaatar, Chingeltei Ulaanbaatar 15170 Mongolia
Manrique, C. J.	Universidad Tecnica Particular de Loja San Cayetano Alto, Calle París Loja 11-01-608 Ecuador
Marquez, M. A.	Mexican Geological Survey Blvd. Felipe Angeles Km. 93.50-4 Pachuca De Soto 42083 Mexico
Marino, M.	Comisión Nacional de Energía Atómica (CNEA) Avenida del Libertador 8250 C1429BNP Buenos Aires Argentina
Marlatt, J.	648 Woodland Place Kingston, Ontario, K7L 4V1 Canada
Martin, R.	Servicio Geológico Minero Argentino Avenida General Paz 5445, Edificio 25 San Martín Argentina
Melgarejo, F.	Viceministerio de Minas y Energía Los Rosales y Ñangapiry, Barrio San Miguel San Lorenzo Paraguay

Mendoza, C. F.	Mexican Geological Survey Blvd. Felipe Angeles Km. 93.50-4 42083 Pachuca De Soto Mexico
Menyen, M. G.	Ministry of Mines, Industry and Technological Development P.O. Box 70, Nkolbison Yaounde Cameroon
Mihalasky, F.	18702 North Sands Road Green Bluff Washington 99005 United States of America
Mihalasky, M.	United States Geological Survey Pacific Region W. 904 Riverside Avenue Spokane, WA 99201-1011 United States of America
Monnet, A.	CEA DEN/DANS/l-tese, Bat 524 91191 Gif Sur Yvette France
Naiga, S. E.	Directorate of Geological Survey and Mines Plot 21-29 Johnstone Road PO Box 9 Entebbe Uganda
Niavas, H.	Comisión Nacional de Energía Atómica (CNEA) Avenida del Libertador 8250 C1429BNP Buenos Aires Argentina
Ninci, M.	Comisión Nacional de Energía Atómica (CNEA) Presbitero Juan González y Aragón Nº 15 B1802AYA Ezeiza Argentina
Oddino, H	Comisión Nacional de Energía Atómica (CNEA) 26 de Noviembre s/n, Parque Industrial Pesado 9100 Trelew Chabut Argentina

Osmolovskiy, A.	KATCO 282 Dostyk Avenue Almaty 050020 Republic of Kazahkstan
Oyedeji, O.	Nigerian Geological Survey Agency P.M.B. 616, 31 Shettima Monguno Crescent Abuja Nigeria
Ozituosauka, M. O.	Department of Mines Ministry of Energy and Mines P.O. Box 251 Lilongwe Malawi
Penalva, G.	Comisión Nacional de Energía Atómica (CNEA) Avenida del Libertador 8250 C1429BNP Buenos Aires Argentina
Pizzio, M.	Comisión Nacional de Energía Atómica (CNEA) Presbitero Juan González y Aragón Nº 15 B1802AYA Ezeiza Argentina
Polak, C.	Areva Mines Tour Areva – 1 place Jean Millier 924000 Courbevoie France
Pop, L.	National Commission of Nuclear Activities Control 14 Libertatii Blvd PO Box 4 050707 Bucharest Romania
Posa, A.	National Uranium Company S. A. 68 Dionijie Lupa Street, Sector 1 030167 Bucharest Romania
Paulo, F.	Comisión Nacional de Energía Atómica (CNEA) Presbitero Juan González y Aragón Nº 15 B1802AYA Ezeiza Argentina

Perayra, V.	Comisión Nacional de Energía Atómica Presbitero Juan González y Aragón Nº 15 B1802AYA Ezeiza Argentina
Porwal, A.	Indian Institute of Technology Bombay Powai, 400076, Mumbai India
Purohit, R. K.	Atomic Minerals Directorate for Exploration and Research Department of Atomic Energy AMD Complex – V Extension Pratap Nagar, Sanganer Jaipur 302033 India
Rai, A. K.	Atomic Minerals Directorate for Exploration and Research (AMD) Department of Atomic Energy 1-10-153-156 – AMD Complex Begumpet Hyderabad 500016 India
Rehman, M.	In Situ Leach Project, Qubul Khel NMC-II Qubul Khel, PO Box Nº 1 Isa Khel District Mianwali Pakistan
Rattanaphra, D.	Thailand Institute of Nuclear Technology 9/9 Moo 7, Sai Moon Ongkharak, Nakron 26120 Thailand
Reyes, R.	Philippine Nuclear Research Institute Commonwealth Avenue, Diliman Quezon City 1101 Philippines
Robinson, G.	United States Geological Survey Midwest Region 12201 Sunrise Valley Drive Reston, VA 20192-0002 United States of America

Royer, J. J.	Université de Lorraine UdL CNRS-GeoRessources (UMR7359) ENSG, gOcad-ASGA 2 Rue du Doyen Marcel Roubault – TSA 70605 54518 Vandoeuvre-les-Nancy Cedex France
Sakala, E.	Council for Geoscience 280 Pretoria Street Silverton Pretoria South Africa
Sambo, C. D.	Ministry of Mines and Industrial Development Niamey 11700 Niger
Sardin, P.	Comisión Nacional de Energía Atómica (CNEA) Figueroa Alcorta 122 5501 Godoy Cruz, Mendoza Argentina
Schodde, R.	MinEx Consulting 49 Surrey Road South Yarra, Victoria, 3141 Australia
Selezneva, V.	KATCO 282 Dostyk Avenue Almaty 050020 Republic of Kazahkstan
Setiawan, A.	Centre for Nuclear Mineral Technology Jl. Lebak Bulus Raya Nº 9 Jakarta Selatan Indonesia
Shumlianska, L.	15 Bogdan Khmelnitsky Kiev 01030 Ukraine
Singer, D.	10191 N. Blaney Avenue Cupertino, CA, 95014 United States of America
Slimmon. W.	Saskatchewan Geological Survey Regina, Saskatoon Canada

Sukadana, I. G.	Center for Nuclear Mineral Technology Jl Lebak Bulus Raya Nº 9 Cilandak 12440 Jakarta Indonesia
Tarasova, I.	Ministry of Energy and Coal Industry of Ukraine 30, Kreschatik Kyiv Ukraine
Tarkhanov, A.	Scientific Research Institute of Chemical Technology Kashirskoye Schosse 33 Moscow 115409 Russian Federation
Thakur, S.	University of Trento Via Calepina, 14 38122 Trento Italy
Top, G.	Istanbul Technical University Istanbul Turkey
Underhill, D.	829 S. 16 1/2 Road Glade Park, Colorado, 81523 United States of America
Van Gosen, B.	United States Geological Survey Southwest Region West 6th Avenue & Kipling Street DFC Bldg. 20 Lakewood, Colorado, 80225-0046 United States of America
Virshylo, I.	Taras Shevchenko National University of Kyiv 90 Vasylkivska street Kyiv Ukraine
Watcharamai, T.	Department of Mineral Resources 75/10 Rama VI Road Ratchatwee Bangkok 10400 Thailand

Wilde, A.	18 Mofflin Avenue Claremont Perth 6010 Australia
Wollenberg, P.	County Road 13 Picton, Ontario K0K2T0 Canada
Yousef, R. M.	Nuclear Materials Authority PO Box 530 Katamia, Cairo Egypt
Yaccup, R.	Malaysian Nuclear Energy Agency Komplex, Nuclear Malaysia Kajang, Selangor 43000 Malaysia
Zhang, Z.	East China Institute of Technology 418 Guanglan Avenue Nanchang City 330013, Jiangxi China
Zhu, P.	Beijing Research Institute of Uranium Geology PO Box 9818 Beijing China
Zurcher, L.	United States Geological Survey Pacific Region 520 N. Park Avenue, Suite 221 Tucson, AZ 85719 United States of America

ORDERING LOCALLY

In the following countries, IAEA priced publications may be purchased from the sources listed below or from major local booksellers.

Orders for unpriced publications should be made directly to the IAEA. The contact details are given at the end of this list.

CANADA

Renouf Publishing Co. Ltd

22-1010 Polytek Street, Ottawa, ON K1J 9J1, CANADA

Telephone: +1 613 745 2665 • Fax: +1 643 745 7660

Email: order@renoufbooks.com • Web site: www.renoufbooks.com

Bernan / Rowman & Littlefield

15200 NBN Way, Blue Ridge Summit, PA 17214, USA

Tel: +1 800 462 6420 • Fax: +1 800 338 4550

Email: orders@rowman.com Web site: www.rowman.com/bernan

CZECH REPUBLIC

Suweco CZ, s.r.o.

Sestupná 153/11, 162 00 Prague 6, CZECH REPUBLIC

Telephone: +420 242 459 205 • Fax: +420 284 821 646

Email: nakup@suweco.cz • Web site: www.suweco.cz

FRANCE

Form-Edit

5 rue Janssen, PO Box 25, 75921 Paris CEDEX, FRANCE

Telephone: +33 1 42 01 49 49 • Fax: +33 1 42 01 90 90

Email: formedit@formedit.fr • Web site: www.form-edit.com

GERMANY

Goethe Buchhandlung Teubig GmbH

Schweitzer Fachinformationen

Willstätterstrasse 15, 40549 Düsseldorf, GERMANY

Telephone: +49 (0) 211 49 874 015 • Fax: +49 (0) 211 49 874 28

Email: kundenbetreuung.goethe@schweitzer-online.de • Web site: www.goethebuch.de

INDIA

Allied Publishers

1st Floor, Dubash House, 15, J.N. Heredi Marg, Ballard Estate, Mumbai 400001, INDIA

Telephone: +91 22 4212 6930/31/69 • Fax: +91 22 2261 7928

Email: alliedpl@vsnl.com • Web site: www.alliedpublishers.com

Bookwell

3/79 Nirankari, Delhi 110009, INDIA

Telephone: +91 11 2760 1283/4536

Email: bkwell@nde.vsnl.net.in • Web site: www.bookwellindia.com

ITALY

Libreria Scientifica "AEIOU"

Via Vincenzo Maria Coronelli 6, 20146 Milan, ITALY
Telephone: +39 02 48 95 45 52 • Fax: +39 02 48 95 45 48
Email: info@libreriaaeiou.eu • Web site: www.libreriaaeiou.eu

JAPAN

Maruzen-Yushodo Co., Ltd

10-10 Yotsuyasakamachi, Shinjuku-ku, Tokyo 160-0002, JAPAN
Telephone: +81 3 4335 9312 • Fax: +81 3 4335 9364
Email: bookimport@maruzen.co.jp • Web site: www.maruzen.co.jp

RUSSIAN FEDERATION

Scientific and Engineering Centre for Nuclear and Radiation Safety

107140, Moscow, Malaya Krasnoselskaya st. 2/8, bld. 5, RUSSIAN FEDERATION
Telephone: +7 499 264 00 03 • Fax: +7 499 264 28 59
Email: secnrs@secnrs.ru • Web site: www.secnrs.ru

UNITED STATES OF AMERICA

Bernan / Rowman & Littlefield

15200 NBN Way, Blue Ridge Summit, PA 17214, USA
Tel: +1 800 462 6420 • Fax: +1 800 338 4550
Email: orders@rowman.com • Web site: www.rowman.com/bernan

Renouf Publishing Co. Ltd

812 Proctor Avenue, Ogdensburg, NY 13669-2205, USA
Telephone: +1 888 551 7470 • Fax: +1 888 551 7471
Email: orders@renoufbooks.com • Web site: www.renoufbooks.com

Orders for both priced and unpriced publications may be addressed directly to:

Marketing and Sales Unit
International Atomic Energy Agency
Vienna International Centre, PO Box 100, 1400 Vienna, Austria
Telephone: +43 1 2600 22529 or 22530 • Fax: +43 1 2600 29302 or +43 1 26007 22529
Email: sales.publications@iaea.org • Web site: www.iaea.org/books

18-04241

International Atomic Energy Agency
Vienna
ISBN 978–92–0–109518–3
ISSN 1011–4289